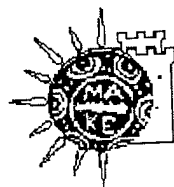


# 12<sup>th</sup> International Conference on Solid State Ionics



Kassandra, Halkidiki  
Thessaloniki, Greece  
June 6-12, 1999

## Extended Abstracts

**DISTRIBUTION STATEMENT A**  
Approved for Public Release  
Distribution Unlimited

Copyright © 1999

**ISSI**

International Society for Solid-State Ionics

DTIC QUALITY INSPECTED 4

20001106 060

# REPORT DOCUMENTATION PAGE

AFRL-SR-BL-TR-00-

0578

ie  
ig  
ntly

Public reporting burden for this collection of information is estimated to average 1 hour per response, including the time for reviewing instructions, searching existing data sources, gathering the required data, completing and reviewing this collection of information. Send comments regarding this burden estimate or any other aspect of this collection of information, including suggestions for reducing this burden to Washington Headquarters Services, Directorate for Information Operations and Reports (0704-0188). Respondents should be aware that notwithstanding any other provision of law, no person shall be subject to a penalty for failing to comply with a collection of information if it does not have a valid OMB control number. PLEASE DO NOT RETURN YOUR FORM TO THE ABOVE ADDRESS.

<b>1. REPORT DATE (DD-MM-YYYY)</b> 10/13/00		<b>2. REPORT TYPE</b> Special Final Technical Report		<b>3. DATES COVERED (From - To)</b> 04/15/99 - 10/15/99	
<b>4. TITLE AND SUBTITLE</b> 12 <sup>th</sup> International Conference on Solid State Ionics, Extended Abstracts  <b>6. AUTHOR(S)</b> International Society for Solid-State Ionics  Worrell, Wayne L.; , Vayenas, Stoukides, Iwahara, Bebelis				<b>5a. CONTRACT NUMBER</b>	
				<b>5b. GRANT NUMBER</b> F49620-99-1-0227	
				<b>5c. PROGRAM ELEMENT NUMBER</b>	
				<b>5d. PROJECT NUMBER</b>	
				<b>5e. TASK NUMBER</b> 2303/BX	
				<b>5f. WORK UNIT NUMBER</b>	
<b>7. PERFORMING ORGANIZATION NAME(S) AND ADDRESS(ES)</b>  Trustees of the University of Pennsylvania 133 S. 36 <sup>th</sup> Street Philadelphia, PA 19104-3246				<b>8. PERFORMING ORGANIZATION REPORT NUMBER</b>  533799	
<b>9. SPONSORING / MONITORING AGENCY NAME(S) AND ADDRESS(ES)</b> AFOSR/NL 801 N. Randolph St., Room 732 Arlington, VA 22203-1977				<b>10. SPONSOR/MONITOR'S ACRONYM(S)</b> AFOSR/NL	
				<b>11. SPONSOR/MONITOR'S REPORT NUMBER(S)</b>	
<b>12. DISTRIBUTION / AVAILABILITY STATEMENT</b>  APPROVED FOR PUBLIC RELEASE: DISTRIBUTION UNLIMITED					
<b>13. SUPPLEMENTARY NOTES</b>					
<b>14. ABSTRACT</b> The document is a compilation of Extended Abstracts from the 12 <sup>th</sup> International Conference on Solid State Ionics, held in Halkidiki, Greece, June 6-12, 1999.					
<b>15. SUBJECT TERMS</b> Solid State Ionics					
<b>16. SECURITY CLASSIFICATION OF:</b>			<b>17. LIMITATION OF ABSTRACT</b>  UU	<b>18. NUMBER OF PAGES</b>	<b>19a. NAME OF RESPONSIBLE PERSON</b> Wayne L. Worrell
<b>a. REPORT</b> UU	<b>b. ABSTRACT</b> UU	<b>c. THIS PAGE</b> UU			<b>19b. TELEPHONE NUMBER (include area code)</b> 215-898-8592



## **Solid State Ionic Conferences**

- SSI-1 Organized by Bruno Scrosatti, 1976, Rome, Italy**
- SSI-2 Organized by Collin Vincent, 1978, St. Andrews, Scotland**
- SSI-3 Organized by Takehiko Takahashi, 1980, Tokyo, Japan**
- SSI-4 Organized by Michel Kleitz, 1983, Grenoble, France**
- SSI-5 Organized by Robert Huggins, 1985, Lake Tahoe, CA, USA**
- SSI-6 Organized by Werner Weppner, 1987, Garmisch-Partenkirchen, Germany**
- SSI-7 Organized by Osamu Yamamoto, 1989, Hokone, Japan**
- SSI-8 Organized by Paul S. Nicholson, 1991, Lake Louise, Canada**
- SSI-9 Organized by Joop Schoonman, 1993, The Hague, Netherlands**
- SSI-10 Organized by B.V.P. Chowdari, 1995, Singapore**
- SSI-11 Organized by Bruce Liebert, 1997, Honolulu, HI, USA**

**Presidents of the International Society for Solid State Ionics (ISSI)**  
**(Established on Tuesday, September 8, 1987 at SSI-6)**

- |           |   |                   |
|-----------|---|-------------------|
| <b>1.</b> | <b>Robert A Huggins, Palo Alto, CA, USA</b>         | <b>1988, 1989</b> |
| <b>2.</b> | <b>Bruno Scrosati, Rome, Italy</b>                  | <b>1990, 1991</b> |
| <b>3.</b> | <b>Gregory C. Farrington, Philadelphia, PA, USA</b> | <b>1992, 1993</b> |
| <b>4.</b> | <b>Osamu Yamamoto, Tsu Mie, Japan</b>               | <b>1994, 1995</b> |
| <b>5.</b> | <b>Werner Weppner, Kiel, Germany</b>                | <b>1996, 1997</b> |
| <b>6.</b> | <b>Wayne L. Worrell, Philadelphia, PA, USA</b>      | <b>1998, 1999</b> |
| <b>7.</b> | <b>Hiroyasu Iwahara, Nagoya, Japan</b>              | <b>2000, 2001</b> |

# **International Society for Solid State Ionics**

## **President**

W.L. Worrell, University of Pennsylvania, USA

## **Vice President**

H. Iwahara, Nagoya University, Japan

## **Secretary/Treasurer**

C.G. Vayenas, University of Patras, Greece

## **Past President**

W. Weppner, University of Kiel, Germany

## **Councillors**

B.E. Liebert, University of Hawaii, USA  
T.-L. Wen, Shanghai Institute of Ceramics, China  
D.M. Schleich, University of Nantes, France  
S.P.S. Badwal, CSIRO, Australia  
T. Gür, Stanford University, USA  
J. Mizusaki, Tohoku University, Japan

## **PROGRAM COMMITTEE**

Prof. W. Worrell,  
Chairman  
Department of Materials  
and Engineering  
University of Pennsylvania  
Philadelphia, PA 19104, USA

Prof. C.G. Vayenas  
Co-Chairman  
Chemical Engineering  
1, Caratheodory St.  
University of Patras  
Patras, 26500, Greece

Prof. M. Stoukides  
Co-Chairman  
Chemical Engineering Science  
Aristotle University  
54006, Thessaloniki  
Greece

Prof. H. Iwahara  
Center for Integrated Research in  
Science and Engineering  
Nagoya University  
Furo-cho, Chikusa-ku  
Nagoya 464-8603, Japan

Prof. S. Bebelis  
Chemical Engineering  
1, Caratheodory St.  
University of Patras  
Patras, 26500  
Greece

## **LOCAL ORGANIZING COMMITTEE**

S. Bebelis (U. Patras)  
S. Brosda (U. Patras)  
E. Hatzikraniotis (AUTH),  
O. Kalogirou (AUTH)  
K. Paraskevopoulos (AUTH),

M. Stoukides (AUTH, co-Chairman)  
R. Thoma (U. Patras),  
P. Tsiakaras (U. Thessaly)  
D. Tsiplakides (U. Patras)  
C.G. Vayenas (U. Patras, Chairman)

## INTERNATIONAL ADVISORY COMMITTEE

J. R. Akridge, Eveready Battery Co., Ohio, USA  
M. Armand, University of Montreal, Montreal, Canada  
S. Badwal, CSIRO, Clayton, Australia  
J. Bates, Oak Ridge National Laboratory, USA  
B. Boukamp, University of Twente, The Netherlands  
S. Bredikhin, Russian Academy of Sciences, Russia  
P. Bruce, University of San Andrews, Scotland, UK  
D. Cahen, The Weizmann Institute of Science, Israel  
S. Chandra, Banaras Hindu University, India  
L. Chen, Chinese Academy of Sciences, Beijing, China  
B.V.R. Chowdari, National Univ. of Singapore, Singapore  
M. Dokiya, Yokohama National University, Japan  
G. Farrington, University of Pennsylvania, USA  
W. Göpel, Universität Tübingen, Tübingen, Germany  
L. Gauckler, ETH, Zürich, Switzerland  
J.B. Goodenough, University of Texas, Austin, USA  
A. Gorenstein, IFGW/UNICAMP, Brazil  
P. Hagemuller, ICMCB-CNRS, France  
L.L. Hegedus, ELF Atochem, Pennsylvania, USA  
A.J. Jacobson, University of Houston, Texas, USA  
T. Kudo, University of Tokyo, Tokyo, Japan  
Q. Lin, Georgia Institute of Technology, Atlanta, USA  
E.M. Logothetis, Ford Research Lab., Michigan, USA  
J. Maier, Max Planck Institute, Stuttgart, Germany  
T.J. Mazanec, BP Chemicals, Cleveland, USA  
M. Mogensen, Riso National Lab., Roskilde, Denmark  
I. Murin, St. Petersburg State University, Russia  
T. Norby, University of Oslo, Oslo, Norway  
A. Nowick, Columbia University, New York, USA  
J. Nowotny, Ansto Materials, Menai, Australia  
T. Ramanarayanan, Exxon Research, Annandale, USA  
I. Riess, Technion-Israel Institute of Technology, Israel  
J. Schoonman, Delft Univ. of Technology, The Netherlands  
B. Scrosati, University of Rome, Rome, Italy  
S. Singhal, Westinghouse, Pittsburgh, USA  
B. Steele, Imperial College, London, UK  
J. Thomas, Uppsala University, Uppsala, Sweden  
H.L. Tuller, MIT, Cambridge, USA  
W. Weppner, Christian Albrechts University, Kiel, Germany  
A. R. West, University of Aberdeen, Aberdeen, UK  
M.S. Whittingham, State University of New York, USA  
O. Yamamoto, Mie University, Japan

## Program Overview

SSI-12, June 6-12, 1999

		ROOM A	ROOM B	ROOM C	ROOM D
<b>Monday (7/6)</b>	AM	A1. Lithium Batteries	C1. Mixed Conducting Oxides	G1. Solid State Devices and Sensors	M1. Nanocrystalline Materials
	PM	A2. Lithium Batteries	C2. Mixed Conducting Oxides	G2. Solid State Devices and Sensors	I1. Electrocatalysis, Electrochemical Promotion
<b>Tuesday (8/6)</b>	AM	A3. Lithium Batteries	B1. Fuel Cells	D1. Anion Conductors	I2. Electrocatalysis, Electrochemical Promotion
	PM	G3. Solid State Devices and Sensors	B2. Fuel Cells	D2. Anion Conductors	K1. Glasses
<b>Wednesday (9/6)</b>	AM	A4. Lithium Batteries	C3. Mixed Conducting Oxides	G4. Solid State Devices and Sensors	N1. Theory
<b>Thursday (10/6)</b>	AM	A5. Lithium Batteries	B3. Fuel Cells	E1. Proton Conductors	L1. Polymers
	PM	A6. Lithium Batteries	C4. Mixed Conducting Oxides	I3. Electrocatalysis, Electrochemical Promotion	L2. Polymers
<b>Friday (11/6)</b>	AM	F1. Cation Conductors	B4. Fuel Cells	E2. Proton Conductors	J1. Structural Aspects and Experimental Techniques
	PM	F2. Cation Conductors	K2. Glasses	E3. Proton Conductors	J2. Structural Aspects and Experimental Techniques

**Monday, Tuesday, Thursday, Friday:** Refreshments: 10:30 – 11:00  
17:00 – 17:30  
Luncheon breaks: 13:00 – 15:30

**Sunday to Saturday:** Dinner served: 19:30 – 21:00

**Sunday 6/6:** **Registration** at Sani Beach Hotel 13:00 – 18:00  
Registration desk open daily 08:30 – 14:00

### Social Program

**Sunday 6/6:** Reception at Sani Beach Hotel 18:00 – 20:00

**Tuesday 8/6:** Slide presentation of Mount Athos 21:00 – 22:00

**Wednesday 9/6:** Mount Athos Cruise  
Buses leave Sani Beach Hotel 10:45  
return to Sani Beach Hotel 20:00

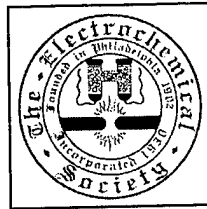
**Thursday 10/6:** Greek night 21:00

**Monday to Friday:** Daily excursions for accompanying persons start at 8:30 (Mo), 8:00 (Tu), 10:30 (W), 9:00 (Th), 9:00 (F)  
Detailed information at Registration desk.

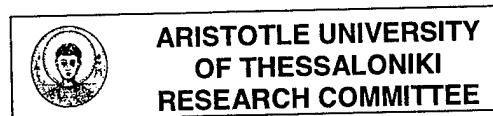
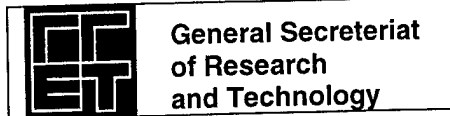
# Sessions, Plenary, Keynote Speakers, (Chairmen and Co-Chairmen)

		ROOM A	ROOM B	ROOM C	ROOM D
<b>MONDAY (7/6)</b> J.M. Tarascon (D. Guyomard)	AM	A1. Lithium Batteries (M. Yoshimura/C. Delmas /D. Guyomard) P.G. Bruce	C1. Mixed Conducting Oxides (S. Singhal/J. Maier) L.J. Gauckler	G1. Solid State Devices and Sensors (E. Logothetis/P. Knauth) W. Goepel	M1. Nanocrystalline Materials (J. Schoonman/M. Kanatzidis) H.L. Tuller - P. Heitjans
	PM	A2. Lithium Batteries (B. Scrosati/T. Kudo) G. Ceder	C2. Mixed Conducting Oxides (H.D. Wiemhöfer/J.A. Kilner) A.J. Jacobson	G2. Solid State Devices and Sensors (W. Göpel/T. Etsell) W. Weppner	I1. Electrocatalysis, Electrochemical Promotion (E. Smotkin/C. Comninellis) R. Lambert
<b>TUESDAY (8/6)</b> S. Gottesfeld (W. Worrell)	AM	A3. Lithium Batteries (P.G. Bruce/B. Chowdari) B. Bates	B1. Fuel Cells (J. Mizusaki/B. Steele) S.C. Singhal	D1. Anion Conductors (T. Ramanarayanan/T. Atake) T. Esaka	I2. Electrocatalysis, Electrochemical Promotion (R. Lambert/H.G. Lintz) Ch. Comninellis
	PM	G3. Solid State Devices and Sensors (R.V. Kumar/H. Naefe)	B2. Fuel Cells (G.-A. Nazri/M. Mogensen) F. Kalhammer	D2. Anion Conductors (T. Esaka/ G. Fafilek) I.V. Murin	K1. Glasses (T. Minami/E. Kamitsos) H. Eckert
<b>WEDNESDAY (9/6)</b>	AM	A4. Lithium Batteries (J. Bates/A. Belanger) B. Scrosati	C3. Mixed Conducting Oxides (I. Riess/K. Yamada) J. Maier	G4. Solid State Devices and Sensors (D.J. Fray/S. Somov) N. Yamazoe	N1. Theory (M. Ishigame/B. Boukamp) A.S. Nowick
	PM	<b>MOUNT ATHOS CRUISE</b>			
<b>THURSDAY (10/6)</b> J. Schoonman (B. Boukamp)	AM	A5. Lithium Batteries (M. Wakihara/A. Magistris) G.-A. Nazri	B3. Fuel Cells (L.J. Gauckler/K. Eguchi) W. Worrell	E1. Proton Conductors (K.-D. Kreuer/B.E. Mellander) H. Iwahara	L1. Polymers (M. Gauthier/M. Armand) I. Riess
	PM	A6. Lithium Batteries (M. Inaba/C. Julien)	C4. Mixed Conducting Oxides (F.W. Poulsen/W. Sitte) T.J. Mazanec	I3. Electrocatalysis, Electrochemical Promotion (G. Haller/R.M. Ormerod)	L2. Polymers (M. Morita/P. Pissis)
<b>FRIDAY (11/6)</b> M. Ishigame (H. Iwahara)	AM	F1. Cation Conductors (A. Lunder/M. Tatsumisago) N. Imanaka	B4. Fuel Cells (S. Haile/A. Khandkar) M. Mogensen	E2. Proton Conductors (N. Bonanos/M. Stoukides/ T. Schober) T. Norby - K.D. Kreuer	J1. Structural Aspects and Experimental Techniques (B. Rambabu, H.-M. Vieth) J.A. Kilner
	PM	F2. Cation Conductors (N. Imanaka/T. Schober)	K2. Glasses (H. Eckert/B. Roling) T. Minami	E3. Proton Conductors (H. Iwahara/T. Norby/ S. Chandra)	J2. Structural Aspects and Experimental Techniques (T. Matsui/J. Irvine) H.-M. Vieth - J. Irvine

## SPONSORS AND SUPPORTERS



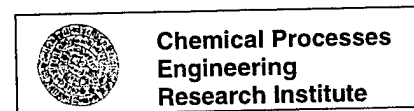
**COMMERCIAL BANK OF GREECE**



**GlaxoWellcome**



**Energizer**



George P. Vasilopoulos, S.A.



**LPC Hellas S.A.**

**G. Karelas  
winery**

**Athenian Brewery S.A.,  
Patras plant**

**Parparousis  
winery**

**Ballas terra gres**

**Healthcon Ltd**

**OINOPHOROS  
winery**

## Research Trends, Advances and Challenges in Lithium Batteries

J-M. Tarascon

*\* Laboratoire de Réactivité et Chimie des Solides*  
Université de Picardie Jules Verne  
33 rue Saint Leu, 80039, Amiens, France

Rechargeable lithium batteries have long been considered as a superior alternative power source for a wide variety of applications. However, it is only since the 90's that rechargeable Li-ion cells have become key components of the portable, entertainment, computing and telecommunications equipment required by an information-rich, mobile society. Consumers are in constant demand for batteries with larger autonomy (e.g., greater capacity).

Capacity improvements within a battery technology can be the result of either 1) an improvement in the chemistry of the system (e.g., better materials) or 2) engineering-type improvements (e.g., electrode forming and packing). Usually, for mature-type technologies such as Ni/Cd, engineering improvements, which are incremental, are those expected while for emerging battery technologies, materials improvements can be drastic. This is especially true for the Li-ion technology that incorporates materials (LiCoO<sub>2</sub>) for which only 50% of the total capacity is tapped. So the hunt is still on for better electrode materials.

Better in terms of electrochemical "jargon" or performance does not always mean new materials but also enlists known ones with enhanced performances obtained through morphology changes and/or chemical substitution or surface modifications. The scope of this paper is to briefly retrace the historical development of the lithium batteries, review the ongoing research activities towards the development of new electrode/electrolyte materials so as to build a comprehensive database to elaborate on future research directions both at the fundamental and applied levels without forgetting the safety issues.

Among the various investigated routes towards the search for better electrodes are 1) the stabilization of the structural layered framework by an electrochemically inert cationic substituant for Ni or Co (Al, Ga) to allow an extended Li removal without the structure collapsing, and 2) the synthesis of the LiFeO<sub>2</sub> or phase with a layered structure to take advantage of the Fe<sup>+4</sup>/Fe<sup>+3</sup> redox couple. A different route presently pursued by Goodenough with Fe-type compounds, and based on the Fe<sup>+3</sup>/Fe<sup>+2</sup> redox couple consists in adjusting the ionic/covalent character of the M-X bond in a Fe-related NASICON-type structure by replacing the anion by a polyanion. Therefore such materials that reversibly intercalate 0.8 Li per 3d-metal at potentials ranging from 3 to 4V are still suffering from poor rate capabilities.

With respect to the negative electrode, besides always addressing the problems of dendrites on Li metal, the research is focused on 1) enhancing the electrochemical characteristics of the carbonaceous negative electrode, and 2) finding alternative materials to substitute for the carbonaceous negative electrode in lithiated intercalation cells. Approaches such as pyrolytic processing of organic materials or mechanical milling of carbons are pursued. Recently, it has been shown that some lithiated vanadium oxide-based electrodes could display large electrochemical capacities vs. Li with, however, a poor capacity retention. Following the metal-oxide

route, FUJI has recently disclosed the fruits of their long-lasting research effort with the discovery of a negative amorphous tin composite oxide (ATCO) material, which has an intercalation voltage of about 0.5V, and a reversible capacity twice that of carbon despite a huge irreversible capacity during the first cycle. This announcement has re-focused research activities towards the "composite negative alloy electrodes" proposed twenty years ago by Huggins et al. For instance, by manufacturing a composite negative electrode with, for example, microscopic grains of electrochemically active alloy phase ( $\text{Sn}_2\text{Fe}$ ) dispersed in a matrix of electrochemically inactive ( $\text{SFe}_3\text{C}$ ) but conducting material, Dahn et al. have shown that they can partially alleviate the irreversible capacity disadvantage of the ATCO's.

Finally dealing with today's fluorinated-based electrolytes, their main drawback is their cost, which to a certain extent, dictates the price of the Li-ion technology. An effort is presently being made in the search for substitutes.

As the portable electronics devices are becoming smaller, thin and flexible batteries are urgently needed. In today's liquid-electrolyte Li technology does not meet the shape flexibility requirements, and is limited to cylindrical or prismatic shapes. Rechargeable polymer Li batteries could provide shape flexibility, but, after years of research and development the rechargeable polymer lithium battery technology still cannot efficiently function at room temperatures favoring its use for elevated temperature applications ( $> 60^\circ\text{C}$ ) such as EV applications for instance. To completely reap the benefits of solid electrolytes, however, better lithium-conducting polymers materials for room temperature must be developed. Midway between the rechargeable lithium batteries using liquid and pure polymer electrolytes are those using the hybrid electrolytes, e.g., polymers swollen in liquid electrolytes. They combine the advantages of both liquid (high power rate) and polymer electrolyte (no electrolyte leakage, easier scalability) batteries. One of the most recent advances which addresses the Li-ion battery as a whole is the introduction of the plastic Li-ion (PLiONTM) battery based on a fluorinated polymer hybrid electrolyte which, while having the performance of the Li-ion liquid technology, adds shape and performance design flexibility, enhances safety and resistance to vibrations. The real advantage of the plastic technology resides in its design flexibility based on a plate-type architecture that can be achieved using an existing industrial lamination process.

It should be realized that the Li-ion technology, while being today the most attractive, is still in its infancy, and drastic breakthroughs in materials have yet to come. It is left to the creativity and innovation of the solid state chemists to design and elaborate new intercalation electrodes to ensure that such an advantage lasts over the next decades. To succeed in this task, further efforts must be placed on a) a better understanding of the role of the crystalline nature (amorphous vs. crystallized) of an electrode material, its state of division, porosity, texture and morphology on its electrochemical performances, and b) a better awareness of the importance and need to control parasite chemical/electrochemical reactions, linked to the surface states of the electrode materials for more performing and safer energy storage systems. While the search for synthesis methods to make known materials of well defined morphology or new materials and new Li-based salts must be pursued as eagerly as before, a more pluridisciplinary research effort should be devoted towards understanding the surface chemistry of electrode materials, and of the electrode/electrolyte interfaces using today's arsenal of ex-situ/in-situ characterization techniques. Finally, the long-lasting burning question related to the safety of these systems must always be on our mind. We should not, as chemists addressing this issue, through the addition of chemical thermal switches, let this issue be only electronically controlled. In short, there are still numerous exciting challenges that remain for all of us to be solved.



## Research Advances, Challenges and Trends in Polymer Electrolyte Fuel Cells and Electrochemical Reactors

Shimshon Gottesfeld

Los Alamos National Laboratory  
Los Alamos, NM 87545  
USA

The polymer electrolyte fuel cell (PEFC) has clearly emerged as a technology of choice for the development of electric vehicle propulsion systems. The level of investment in projects for the development of this technology in the automotive industry worldwide, has increased from tens of millions to billions of dollars within the last 2-3 years. The reason behind this interest is a unique package of merit characteristics. A PEFC power system has the potential for power densities of 0.3-0.5 kW/kg (the stack itself exceeds 1 kW/kg) and energy conversion efficiency, e.g., methanol chemical energy-to-dc electric power, of around 40% under realistic power demands. A PEFC powered vehicle would qualify as a zero-emission or ultra-low emission vehicle and will be comparable to conventional vehicles in range covered between refueling points. The materials and processes which enable such a unique set of features have been developed during the last 30 years, starting with the first introduction in the 1960's of the poly-perfluorosulfonic acid (PFSA) membrane (Nafion<sup>R</sup>, by DuPont). These proton conductors have specific conductivities in fully hydrated form of the order of 0.1 S/cm at 80°C, enabling the high power densities of PEFCs to be achieved at such low temperatures. During the last 10 years, the membrane/electrode assembly (MEA) technology for PEFCs has strongly developed in terms of a dramatic lowering in precious metal catalyst loading (key for achieving affordable cost) while demonstrating excellent performance stability, as well as in terms of introduction of composite membranes (e.g., by W.L. Gore) that exhibit high mechanical strength at thickness as low as 10 - 30 micrometers. Such thin membranes help to resolve the important challenge of effective water management in the PEFC, by providing sufficient "back diffusion" of water from cathode to anode to effectively counteract electro-osmotic drag of water from anode to cathode. Most recently, the challenge in MEA development has been high tolerance to low level impurities, particularly carbon monoxide, in the fuel feed stream. This need for "CO tolerance" arises from the presence of 10-100 ppm CO in hydrogen generated from the processing of liquid fuels, e.g., methanol or gasoline, as required to generate on board the vehicle a hydrogen-rich gaseous feed to the PEFC anode. Binary precious metal anode catalysts can tolerate up to 10 ppm CO at 80°C without significantly losing performance in the complete dynamic range of the PEFC. However, use of low level air bleed into the anode feed stream enables to increase the tolerance by more than an order of magnitude, without a significant penalty in fuel efficiency.

Whereas most of the recent developments devoted to PEFC systems for transportation applications have focused on the option of liquid fuel reforming on board, Direct fuel cells remain an interesting challenge. This is because of a much simpler power system with significantly smaller number of major components. There are such two known

options in the context of low temperature, PEFCs: direct hydrogen and direct methanol fuel cells

(DMFCs). Potential introduction of direct hydrogen fuel cells depends on effective storage of hydrogen on board and on significant infrastructure issues. The DMFC has the important advantage of liquid fuel of high energy density, plus some previous experience with introduction of infrastructure for transportation. Recent developments (see, e.g., related papers in the Proceedings of the ECS Symposium on Proton Conducting Membrane Fuel Cells II, 1998), show that, in terms of stack power density and overall conversion efficiency, DMFCs have reached levels comparable to those of a PEFC system based on methanol reforming on board. Projected stack cost per kW is still significantly higher, however part of this extra gap would be compensated by eliminating fuel processing components.

When examining some fundamental features of PEFCs, it becomes clear that some of these features could be also attractive for potential applications in electrochemical reactors. In fact, the first industrial level introduction of PFSA membranes was in the chlor-alkali industry. Experience gained with fuel cell technology has highlighted further potential applications of such electrochemical reactors, for cases where the reactants are gaseous. The excellent gas separation properties of the ionomeric membrane enable utilization of gaseous reactants of high reactivity (when directly combined) on the opposite sides of a thin MEA, achieving high energy and current efficiencies. Examples will be given of electrochemical cells based on MEAs and utilizing gaseous reactants, that would operate at high energy and current efficiencies in manufacturing of chemicals, or in processes devoted to waste minimization.

## NANO-STRUCTURED MATERIALS IN SOLID STATE IONICS

J. Schoonman  
Delft Interfaculty Research Institute: Renewable Energy  
Laboratory for Inorganic Chemistry  
Delft University of Technology  
Julianalaan 136  
2628 BL Delft  
The Netherlands

## ABSTRACT

Nanophase materials have recently become a very active research field in the areas of solid state physics, solid state chemistry, materials engineering, medical sciences, and nanobiotechnology. Anticipated applications range from organic solar cells, rechargeable batteries, fuel cells, superplastic ceramics, hybrid materials, molecular electronics, single-electron devices, scanning probes, biosensors, food with improved texture, biocompatible implant materials, diagnostic sensor chips, and drug delivery systems. Many of these anticipated applications illustrate the broad spectrum of nanotechnology and are beyond the field of solid state ionics (1).

Atomic diffusion in nanophase materials has been found to be very rapid compared with conventional materials. Here the atomistic structure of interfaces, their structural relaxation, and free volumes play an important role.

The materials research and development for a variety of energy conversion, conservation, and storage devices is covered by the field of solid state ionics. The use of nanostructured materials for these applications requires amongst others insight into enhanced ionic motion along grain boundaries in both pure and multi-phase nanostructured materials, the dependence of defect generation and the degree of non-stoichiometry on the particle size and on the interface-to-volume ratio, the role of quantum confinement effects, grain-boundary structure and composition on electronic carrier concentration and mobility, the influence of nanosize features on the optical blue-shift of insertion electrodes for electrochromic displays, and processing routes for achieving desired tailored structures and compositions (1-8).

Major achievements have been reported in the recent literature and in this lecture the applications which aim at sustainability will be highlighted. In particular, the value of the nanotechnology approach in the development of novel solar cells, improved batteries, fuel cells, and chemical gas sensors will be discussed and some examples of devices will be demonstrated. In addition, attention will be focused on health hazards of nanophase materials.

## References

1. A. ten Wolde (ed): Nanotechnology - Towards a molecular construction kit. Netherlands Study Centre for Technology Trends (STT), 1998, The Hague, The Netherlands. ISBN 90-804496-1-X.
2. J. Schoonman: in ref. 1, in Chapter 3, F.E. Kruis and H. Fissan: in ref. 1, in Chapter 3.
3. H.L. Tuller: *J. Electroceramics* 1 (1997) 211.
4. J. Maier: *Progr. Solid State Chem.* 23 (1995) 171.
5. R. Dagani: *Chem. & Eng. News*, September 21 (1998) 70.
6. I. Kosacki and H.U. Anderson: *Sensors and Actuators B48* (1998) 263.
7. A.S. Edelstein and R.C. Cammarata (eds): *Nanomaterials - Synthesis, Properties, and Applications*, Institute of Physics Publishing, 1998, Bristol and Philadelphia. ISBN 0-7503-

0358-1.

8. C.H. Chen, J. Schoonman, Y. Kamlag and I. Colbeck: High-Temperature Superconductors and Novel Inorganic Materials, 33-38. G. Van Tendeloo et al. (eds.). 1999 Kluwer Academic Publishers.

## ION DYNAMICS IN SOLID

Mareo Ishigame, Takeshi Hattori, and Noriko Sata

Research Institute for Scientific Measurements, Tohoku University  
Sendai, Japan

## 1. Introduction

Ion dynamics of crystal lattice have been investigated by typical traditional experimental technics, Raman Scattering, infrared spectroscopy, neutron scattering, NMR, and etc. Recently, however, new experimental technics-application has been developed to study the ion dynamics in relation to a fast ion motion in superionic conductors.

In this paper, as new applicable technics to superionic conductors, the site-selective spectroscopy by hole burning effect and quasi-elastic light scattering are introduced from a stand point of an application to the ion dynamics studies on superionic conductors.

## 2. Quasi-elastic light scattering.

Generally, it is well known that, a non-periodic fluctuation in polarizability of material gives a low frequency light scattering, called as the quasi-elastic light scattering (QELS). In the superionic conductors, the hopping motion of the mobile ions causes a non-periodic fluctuation in the polarizability and gives the QELS. The importance of this phenomenon was recognized since the middle of the 1970's and several experimental results were reported for silver iodides and cuprous iodide at relatively early stage.

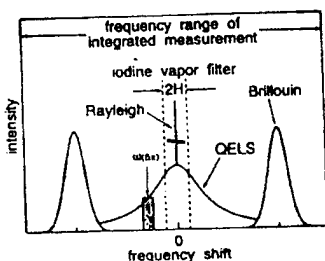


Fig. 1 Schematic low-frequency light-scattering spectrum of superionic conductor.

Theoretically, the QELS spectrum  $I(\omega)$  is treated by several theorists. A model based on the site-depended polarizability for mobile ions was proposed by Klein et al, and a pair diffusion model was proposed by Dietrich and Peschel, following an idea of a collision induced scattering mechanism by Nemanichi et. al.

Following the Klein's theoretical treatment,  $I(\omega)$  is

expressed by a superposition of a Lorentzian of  $|R^2|\Gamma^2 / (\Gamma^2 + \omega^2)$ ; here  $\Gamma$  is a hopping rate of ions and  $R$  is Raman tensor. Fig. 1 shows a schematic low-frequency light scattering spectrum of a superionic conductor. In this figure, a very weak band centered at  $0 \text{ cm}^{-1}$  is a QELS due to ionic hopping of conduction ions. Experimentally, to remove the strong Rayleigh component centered at  $0 \text{ cm}^{-1}$ , an iodine gas filter is used. Then, the observed QELS spectrum is deformed by the absorption of an iodine molecule.

As you can see from this figure, there are several methods possible to study the dynamical properties of hopping ions. First is the usage of QELS spectral shape, because the halfwidth of this spectrum gives a hopping rate of ions. This method is well known

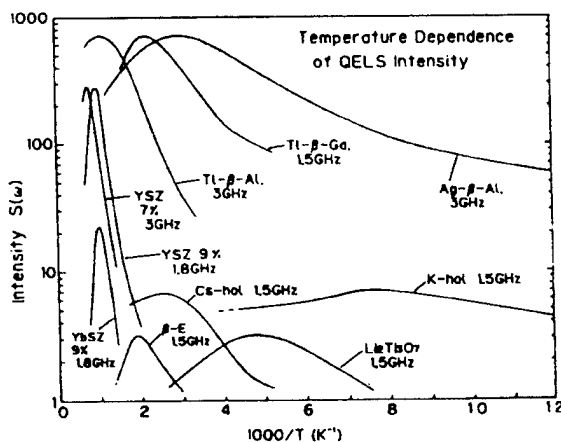


Fig. 2 Temperature dependence of the QELS intensity at fixed-frequency

historically, and has been used to study the dynamical property of  $\alpha$ -AgI, RbAg<sub>4</sub>I<sub>5</sub>, CuI, and others.

The second is the use of the temperature dependence of scattered light intensity measured at a fixed frequency  $\omega_{(fix)}$  as indicated in figure 1. In this case, assuming an activation type temperature dependence for hopping rate  $\Gamma$ ,  $I(\omega, T)$  has a maximum at a temperature where  $\Gamma = \omega_{(fix)}$ , and from  $\omega_{(fix)}$  dependence of  $\Gamma$ , we can obtain the activation energy  $\Delta$  for hopping ions.

This QELS method has been presently applied to many superionic conductors shown in Fig.2 and dynamical properties of ions can be discussed through  $\Gamma$  and  $\Delta$ . Furthermore, some extended application is developed to study more detailed ion dynamics.

### 3. Hole-burning study on ion dynamics in proton conductors.

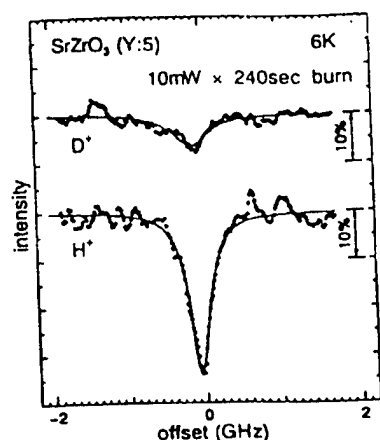


Fig. 3 Hole spectra of SrZrO<sub>3</sub>(Y:5).

We have applied hole burning spectroscopy to the perovskite-type proton conductors. A hole burning effect based on proton motion has been observed, and proton dynamics can be investigated by using temperature cycling experiment.

Figure 3 shows typical hole spectra of protonated and deuterated SrZrO<sub>3</sub>(Y:5) measured at 6K. The shape of spectral holes were well fitted by a Lorentzian, and no anti-holes were observed. Assuming a Gaussian type distribution  $P(V) \propto \exp[-(V - V_0)^2 / 2\sigma_V^2]$  for potential barrier height which is necessary for the relaxation of system to ground state. Where  $V_0$  is the central value of distribution, and  $\sigma_V$  is the width of distribution. Then from an excursion temperature dependence of hole area, a distribution of barrier height is estimated.

The obtained values of  $V_0$  and  $\sigma_V$  are tabulated in Table 1. For composition, we have also measured electric conductivity for protonated samples, and activation energy  $\Delta E$  is obtained from its temperature dependence. The results are also shown in Table 1.

From these results dynamical properties of proton in perovskite type oxide are discussed and the microscopic motion of proton is revealed.

sample	hole burning		electric conductivity
	$V_0$ (eV)	$\sigma_V$ (eV)	$\Delta E$ (eV)
SrZrO <sub>3</sub> (Y:5):H <sup>+</sup>	0.22	0.10	0.56
SrZrO <sub>3</sub> (Y:5):D <sup>+</sup>	0.22	0.09	
SrZrO <sub>3</sub> (Sc:5):H <sup>+</sup>	0.18	0.05	
SrZrO <sub>3</sub> (Sc:5):D <sup>+</sup>	0.17	0.06	

Table. 1 The values of  $V_0$  and  $\sigma_V$  obtained by temperature cycling experiment, and  $\Delta E$  obtained by electric conductivity measurement.

## STRUCTURE AND ELECTROCHEMISTRY OF LITHIUM BATTERY MATERIALS

Peter G. Bruce, School of Chemistry,  
University of St. Andrews, St. Andrews, Scotland

The structure and electrochemistry of two important classes of solid state ionic compounds will be discussed, namely, lithium intercalation electrodes and polymer electrolytes.

The phenomenal success of commercial lithium ion rechargeable batteries has led to a renaissance of interest in the synthesis and characterisation of new lithium intercalation hosts. In particular there is a need to replace the  $\text{LiCoO}_2$  cathodes in the current generation of rechargeable lithium batteries with materials that are of a lower cost and toxicity, are safer in practical cells and can store more charge per unit weight and volume. Several compounds will be discussed in this context including the development of tunnel structures and new layered compounds based on  $\text{LiMnO}_2$  doped with a variety of transition metal ions.

Although there has been a great deal of activity in the area of gel-based polymer electrolytes the goal of developing a true (solvent free) high molecular weight polymer electrolyte which can offer satisfactory performance over a wide temperature range in practical cells still remains. A major barrier to this has been a lack of knowledge concerning the structural chemistry of polymer electrolytes. By developing new state-of-the-art methods for establishing the structures of crystalline polymer electrolytes from powder diffraction data it has been possible to advance the understanding of the structural chemistry of these compounds. By combining this with spectroscopic studies, greater insight into the structures of the amorphous (conducting) materials has been possible. Some developments in this area will be discussed.

## FIRST-PRINCIPLES STUDY OF PHASE STABILITY AND ELECTROCHEMICAL PROPERTIES IN LITHIUM-METAL OXIDES:

G. Ceder

Department of Materials Science and Engineering  
Massachusetts Institute of Technology  
Cambridge, MA 02139-4307

Many of the properties of insertion electrodes can be directly computed with first-principles methods. Such computations are solely based on the basic laws of Physics and therefore require no experimental data. This makes them particularly suitable for predicting the properties of novel or incompletely characterized materials. We have recently demonstrated the applicability of first-principles methods to predict the Li-insertion potential and the phase stability in lithium-metal oxides [1-3]. This has already been used to predict the insertion behavior of previously untested compounds[4].

We present first-principles results for the phase stability in the  $\text{Li}_x\text{CoO}_2$  and  $\text{Li}_x\text{MnO}_2$  systems. In  $\text{Li}_x\text{CoO}_2$  we predict the occurrence of "staging" at low Li concentrations. In  $\text{LiMnO}_2$  we find that anti-ferromagnetism plays an important role in stabilizing the orthorhombic structure. Calculations are also highly effective in studying the electronic changes that occur in the material upon lithiation. While Li insertion in  $\text{Li}_x\text{CoO}_2$  transfer an extra electron to the  $t_{2g}$  band of the material we find that the net-electron increase is largely located around the oxygen ions. This is due to the increased ionicity of the cobalt-oxygen bond upon lithiation. We demonstrate how this effect relates to important cathode properties such as the average lithiation voltage and the variation of lattice constant with Li content.

Kinetic properties of Li transport are studied with a kinetic Monte Carlo model.

### References

1. M. K. Aydinol, A. F. Kohan, G. Ceder, K. Cho, J. Joannopoulos, *Physical Review B* 56, (1997) 1354-1365 .
2. A. Van der Ven, M. K. Aydinol, G. Ceder, *Journal of the Electrochemical Society* 145, (1998) 2149-2155.
3. G. Ceder, A. F. Kohan, M. K. Aydinol, P. D. Tepesch, A. Van der Ven, *Journal of the American Ceramics Society* 81, (1998) 517-525 .
4. G. Ceder, Y.-M. Chiang, D. R. Sadoway, M. K. Aydinol, Y.-I. Jang, B. Huang, *Nature* 392, (1998) 694-696 .



## THIN-FILM LITHIUM AND LITHIUM-ION BATTERIES

J. B. Bates, N. J. Dudney, B. Neudecker, A. Ueda, and C. D. Evans  
Oak Ridge National Laboratory  
Oak Ridge, Tennessee

Research over the last decade at ORNL has led to the development of solid state thin-film lithium and lithium-ion batteries. The batteries are less than 15 micrometers thick, they can be deposited directly onto chips or chip packages in any shape or size, and they can be recharged thousands of times. When fabricated on plastics or thin metal foils, they are quite flexible. The batteries consist of cathodes that are crystalline and nanocrystalline oxide-based lithium intercalation compounds such as  $\text{LiCoO}_2$  and  $\text{LiMn}_2\text{O}_4$ , a glassy lithium phosphorus oxynitride ("Lipon") electrolyte, and anodes of lithium metal, inorganic compounds such as silicon-tin oxynitrides,  $\text{Sn}_3\text{N}_4$  and  $\text{Zn}_3\text{N}_2$ , or metal films such as Cu in which the anode is formed by lithium plating on the initial charge. Except for lithium anodes which are deposited by thermal evaporation, the remaining components are deposited by magnetron sputtering. Presently several companies are exploring the manufacturing of these batteries for application in a variety of consumer and medical products. In addition to their practical applications, thin-film batteries are useful research tools for exploring the properties of lithium intercalation compounds.

Polycrystalline thin films of  $\text{LiCoO}_2$  fabricated by sputtering of  $\text{LiCoO}_2$  followed by annealing at  $700^\circ\text{C}$  in  $\text{O}_2$  exhibit a high degree of preferred orientation in which the majority of the grains have their (101) and (104) planes parallel to the substrate. Because this aligns the planes containing the  $\text{Li}^+$  ions parallel or nearly parallel to the direction of current flow, thin-film cells with these textured cathodes are capable of high discharge rates. Using lithium anodes, for example, cells with capacities of  $0.2 \text{ mAh/cm}^2$  can deliver  $0.1 \text{ mAh/cm}^2$  at rates up to  $6 \text{ mA/cm}^2$ . As a consequence of the layered hexagonal structure of  $\text{LiCoO}_2$ , the preferred orientation is due to the tendency to minimize volume strain energy in the films that arises from differential thermal expansion between the film and substrate during the annealing step.

While Li- $\text{LiCoO}_2$  thin-film cells exhibit good rate capability and extraordinary cycle lives (e.g. less than 5% capacity loss after >10,000 cycles), the low melting point of lithium precludes integration of these batteries into circuits using the solder reflow or surface mount techniques which require exposure to temperatures of  $250\text{--}300^\circ\text{C}$  for a few minutes. Recently, several inorganic thin-film anode materials with high specific capacities including silicon-tin oxynitride ( $\text{SiSn}_{0.87}\text{O}_{1.20}\text{N}_{1.72}$ ),  $\text{Sn}_3\text{N}_4$ , and  $\text{Zn}_3\text{N}_2$  have been synthesized, allowing the fabrication of lithium-ion cells that can be heated to  $250^\circ\text{C}$  for up to 10 min with no degradation in performance. "Lithium free" lithium cells with crystalline  $\text{LiCoO}_2$  cathodes also have been fabricated by depositing a metal current collector such as Cu over the Lipon electrolyte. On the initial charge, lithium metal is plated at the Cu-Lipon interface, and on subsequent cycles, the stripping and plating of lithium occurs with 100% columbic efficiency. In the as-deposited or the fully discharged state, the battery can withstand the same heat treatment as the lithium-ion cells.

Much of our research has focused on investigating the properties of  $\text{LiMn}_2\text{O}_4$  thin films. The films deposited by sputtering of  $\text{LiMn}_2\text{O}_4$  are manganese deficient with  $\text{Li}^+$  ions occupying both the tetrahedral and octahedral sites in the spinel lattice. The as-deposited films are nanocrystalline, exhibiting only weak, broad x-ray diffraction peaks and gradually sloping discharge curves. After thousands of cycles at 25 and  $100^\circ\text{C}$ , the diffraction peaks

sharpen significantly, and the charge-discharge curves resemble those of well-crystallized  $\text{LiMn}_2\text{O}_4$  films indicating that significant grain growth or recrystallization has occurred.

Polycrystalline  $\text{LiMn}_2\text{O}_4$  films with a defect spinel structure are formed by heating as-deposited films in  $\text{O}_2$  at temperatures from 400–800°C. The capacity above 3.8 V of about 1 Li per  $\text{Mn}_2\text{O}_4$  is divided between plateaus at 4 V and 5 V. Depending on the deposition and annealing conditions, a monoclinic  $\text{Li}_2\text{MnO}_3$  phase also is present in the cathode films giving rise to a long two-phase plateau at 4.6 V on the initial charge. The distribution of capacity at 4 V and 5 V in these cathodes can be explained as caused by the fractional occupancy of the tetrahedral sites by  $\text{Mn}^{2+}$  ions, consistent with the results of in-situ x-ray diffraction and x-ray absorption measurements. Charging at 5 V is presumed to result in the oxidation of the  $\text{Mn}^{2+}$  ions followed by their migration from the tetrahedral to the octahedral sites. This migration explains why the capacity at 5 V decreases with continued cycling between 5.3 V and 3.8 V. Doping  $\text{LiMn}_2\text{O}_4$  films with Zn and Ti increases the capacity at 4 V at the expense of the capacity at 5 V, whereas doping with Ni stabilizes the capacity at 5 V. On discharging  $\text{LiMn}_2\text{O}_4$  cells in the  $\text{LiMn}_2\text{O}_4$ - $\text{Li}_2\text{MnO}_3$  two-phase region, the potential makes a sudden step from ~2.8 V, characteristic of the two-phase mixture, to ~2 V indicating the formation of another phase of  $\text{Li}_{2+x}\text{Mn}_2\text{O}_4$  at the cathode-electrolyte interface. The progressively slow relaxation from 2 V to 2.8 V on cessation of the current appears to be caused by a diffusionless process that has the electrochemical signature of nucleation. The layered construction of a thin-film cell affords the opportunity of investigating this behavior in a uniquely simple, one-dimensional geometry in which phase boundary motion proceeds from the cathode-electrolyte interface into the bulk of the cathode film in a linear fashion.

The separation of the charge-discharge curves of thin-film lithium batteries with nanocrystalline  $\text{LiMn}_2\text{O}_4$  or amorphous  $\text{V}_2\text{O}_5$  cathodes is found to be due to a true hysteresis and not to a kinetic hindrance. The appearance of hysteresis means that the thermodynamic activity of lithium in the intercalation compound is not only a function of the composition but also depends on the cycle path followed to reach a particular composition. Classic scanning curves have been obtained by cycling thin-film batteries slowly between different voltage limits. The loops observed represent the energy dissipated due to an irreversible process such as plastic deformation or the motion of grain boundaries. Free energy curves have been calculated to model the intercalation behavior, although the structural basis for the hysteresis is still undetermined.

This research was sponsored by the U.S. Department of Energy Division of Materials Sciences under contract No. DE-AC05-96OR22464 with Lockheed Martin Energy Research Corp.

Abstr1SS-12.doc

# NANOCOMPOSITE POLYMER ELECTROLYTES AND THEIR IMPACT ON THE LITHIUM BATTERY TECHNOLOGY

F. Croce, G.B. Appetecchi, L. Persi & B. Scrosati

Dipartimento di Chimica, Università "La Sapienza", 00185 Rome, Italy

Considerable progress has been achieved in the lithium polymer rechargeable batteries. However, some problems still exist for batteries based on "classical" PEO-LiX electrolytes. They are in essence : i) the cyclability and safety, due to the reactivity of the lithium metal anode and ii) the temperature of operation, due to the temperature dependence of the lithium ion transport in the polymer electrolyte. Therefore, it is of paramount importance to induce electrolyte modifications which may provide: i) a favourable type of lithium passivation layer, such as to assure efficient lithium deposition-stripping processes and ii) an enhancement of the electrolyte conductivity at low temperature.

We have found that an effective approach for reaching both these goals is that of dispersing low-particle size ceramic powders in the polymer electrolyte bulk (1-3). In fact, results obtained in our laboratory have demonstrated that these new types of nanocomposite polymer electrolytes have a very stable lithium electrode interface and an "activated" high low temperature ionic conductivity, combined with good mechanical properties.

The most relevant of these results will be presented in this paper to demonstrate that, due to their important properties, the nanocomposite polymer electrolytes are quite promising for the development of improved, rechargeable lithium batteries.

## ACKNOWLEDGEMENTS.

This work has been carried out with the financial support of ENEA under contracts N. 2814 and N.

1221.

MATERIALS ASPECTS OF LITHIUM-ION BATTERY FOR ELECTRIC BASED  
TRANSPORTATION. Gholam-Abbas Nazri, General Motors Research and Development  
Center, RCEL, Warren, Michigan, 48090-9055, USA

There have been unprecedented research and development activities on electric based transportation systems during the last decade. The main driving force for these activities are environmental issues and there is a clear tendency of moving from polluting and inefficient combustion process to a cleaner and more efficient electrochemical technology. Among various physical and chemical energy conversion devices the electrochemical power sources are the most efficient and practical devices which transform chemical energy to clean electricity.

There has been tremendous progress in the development of electric vehicle, EV, and its components. However, it is apparent that the power source is the key obstacle to the full development of a practical EV. The battery improvement is critical to the development of practical EV. The electric propulsion systems are very advanced and energy efficient, however, improvement in battery area is crucial. Recent progress and breakthroughs in the field of battery concepts and materials have provided a realistic possibility to develop EV system to perform in many respects exceedingly better than conventional combustion engine vehicles. The new battery technology will incorporate many breakthroughs in the field of solid state ionics, and will take advantage of many advancements made in electronic control and power management systems. The development of power source for electric based transportation has provided a unique opportunity for scientists and engineers in the field of solid state ionics to incorporate the latest innovations in materials chemistry and design engineering in to the new battery technology.

During last few years, we have developed a scientific methodology to predict the property of materials and composites at molecular levels. Our challenges have been to design and develop materials with desired properties from abundant and low cost materials, through optimization of chemical bonds within proper geometry and structure. The possibilities are endless. We have utilized advance molecular modeling, combinatorial synthesis, materials characterization, and property screening techniques to accelerate the discovery of new materials and new systems for application in power sources for electric based transportation.

In recognition of future prospects for EV systems, there are coordinated efforts nationally and internationally to develop practical EV. Many organizations are currently contributing to the development of electric based transportation, i.e., the United States Battery Consortium, (USABC), Partnership for New Generation of Vehicles (PNGV), Department of Energy (DOE) through its advanced Automotive Technology AAT), Advanced Technology Development (ATD) and Exploratory programs, and other related government programs under US-DOE and DOD also contributing to the development of electric based transportation. Similar activities exist in Europe and Japan where coordinated efforts are underway among industry R&D, government agencies, and national laboratories to accelerate the development of electric based transportation systems.

The challenges are to design and develop electrode materials to satisfy many contradictory requirements of high-energy and high-power electrodes. The novel electrode materials with the following characteristics have been considered; high available sites for lithium insertion/extraction, (this translates to battery energy or vehicle range), high chemical potential difference between state of lithium in anode and cathode (which provides high cell voltage and modifies power for vehicle acceleration), chemical and electrochemical stability in the operating cell voltage (to provide safety and long cycle life), high rate of lithium diffusion in and out of

electrode material (to provide high cell power and fast charging capability), low cost, inherent safety, and compatibility with environmental issues are also important factors in design of new material.

Considering all requirements mentioned, a composite of graphitic materials is chosen as one the most promising anode for the battery as they provide close theoretical energy 372 Ah/Kg for  $\text{LiC}_6$ , (twice the energy of state-of-the art cathode). The rate capability of the composite has been tailored to meet the desirable high-energy and high-power applications. The graphitic materials are environmentally safe and they are abundant at low cost.

Among various cathodic materials, the transition metal oxide with layer structure are the most promising as they provide high energy, high rate capability and high cell voltage, close to 4 volts vs. fully lithiated graphite anode. The chemical and electrochemical stability of the layered oxide are tailored by elemental substitution within the layer oxide  $\text{MO}_2$ , and further modification of their electronic conductivity by cation doping. The high rate capability of the metal oxides is tailored by adjusting the inner-layer spacing of the metal oxide slabs. The layer oxides have provided a unique opportunity to optimize their composition and crystal structure by optimization of chemical bonds within the oxide slabs to achieve desirable performances.

Electrolytes for the lithium batteries have been developed to satisfy both the low temperature performances and high temperature stability. The most advanced electrolyte for the lithium battery consists of carbonate-based solvent and  $\text{LiPF}_6$  salt. The low temperature performance of the battery has been achieved by the use of mixed carbonate solvents containing symmetric and asymmetric linear and cyclic carbonates. These electrolyte systems can perform from -30 to 70 C at considerable ionic conductivity. Further power capability improvement has been achieved by application of smart thermal management of battery pack. However, future electrolytes may provide considerable conductivity at low temperatures and lower heat generation at peak power to eliminate the use of thermal management system and make the battery pack more energy dense. The electrochemical stability of the electrolyte toward oxidation and reduction are sufficiently high within the operating range of cell voltages. The safety of large batteries is a major concern, and we have considered battery safety improvement in both intrinsic and extrinsic ways. The intrinsic way of making the cell component safe is to tailor their chemical properties to resist decomposition and enhance their stability. The extrinsic methods of making the battery components safe include addition of auxiliary redox couple in the battery chemistry, and application of fire-retarding and smoke scuffling agents in the cell components to provide wide nonflammability envelope. In addition to chemical improvement of cell components, electronic control of each individual cell within the battery pack to monitor their voltages, resistance, pressure, and heat may provide extra safety margin.

## THE ANATOMY OF HIGH-TEMPERATURE CELL FAILURE IN A LITHIUM-ION BATTERY

Josh Thomas

Inorganic Chemistry, Ångström Laboratory,  
Uppsala University, Box 538, SE-751 21 Uppsala, Sweden.

Despite the fact that Li-ion and more recently Li-ion polymer batteries are capturing an ever-increasing fraction of low-power battery markets (typically for cellular 'phone and lap-top applications), their performance and even their *safety* at elevated temperatures still leave very much to be desired; hence the warning text: "Not to be used above 140°F". Many factors, each coupled to the onset of deleterious reactions at elevated temperatures, underlie this challenging problem area, which must be viewed in a whole-cell perspective, since the result of some unwanted reaction at one point in the cell will be readily mediated to and influence performance elsewhere in the cell.

Our attention here has focussed particularly on two familiar problem areas in the general context of a < graphite anode | liq. el. | spinel cathode > cell configuration; namely, SEI-layer formation on the graphite anode [1-3] and corrosion of the spinel cathode [4,5]. Such system variables as: choice of salt and solvent, state of charge, and particle morphology have been addressed through the combined use of thermal analysis, *in situ* XRD, cyclic voltammetry and XPS.

### References:

- [1] E. Peled, D. Golodnitsky, G. Ardel and V. Eshkenazy, *Electrochim. Acta*, 40, 2204 (1995).
- [2] D. Aurbach, Y. Ein-Eli, B. Markovsky, A. Zaban, S. Luski, Y. Carmeli and H. Yamin, *J. Electrochem. Soc.*, 142, 2882 (1995).
- [3] A.M. Andersson, K. Edström and J.O. Thomas, *J. Power Sources*. In press.
- [4] G. Amatucci, A. Blyr, C. Sigala, P. Alfonse and J.-M. Tarascon, *Solid State Ionics*, 104, 13 (1997).
- [5] T. Eriksson, T. Gustafsson and J.O. Thomas, *Symposium Proceedings of the Fall Meeting of the ECS, Boston, 1998*. In press.

*Work supported by the EU(Joule III) Programme and by MISTRA, NUTEK and NFR in Sweden.*

## ELECTRONIC STRUCTURE AND REACTIVITY OF INTERCALATION COMPOUNDS

J. Molenda

*Department of Solid State Chemistry, Stanislaw Staszic University of Mining and Metallurgy,  
Al. Mickiewicza 30, 30-059 Cracow, Poland*

Transition metal compounds with a general formula  $\text{Li}_x\text{M}_a\text{X}_b$  ( $\text{M}$ = transition metal,  $\text{X}$ = O, S, Se) constitute a group of potential electrode materials for a new generation of lithium batteries. This application is related to the fact that these compounds can reversibly intercalate high amounts of alkaline ions (1 or more moles per mole of  $\text{M}_a\text{X}_b$ ) already at room temperature, without significant changes in their crystallographic structure. In the intercalation process the basic structural elements do not undergo any significant changes except some small reversible deformations. Structural stability during the intercalation is related to the existence of strong ionic-covalent bonds between  $\text{M}$  and  $\text{X}$  atoms. The ionic transport in these systems is related to appreciable mobility of lithium ions in two-dimensional interlayer spaces or tunnels whereas the electronic transport is related to  $d$  electrons. The properties of  $d$  electrons in these compounds are variable, starting from insulator properties of  $\text{VO}_2$  and  $\text{TiO}_2$  through semiconducting ones of  $\text{MoS}_2$  and  $\text{WSe}_2$ , small polarons system of  $\text{Li}_x\text{Mn}_2\text{O}_4$  and  $\text{Li}_x\text{CoNiO}_2$  to the metallic ones of  $\text{TiS}_2$ . This complex behavior of  $d$  electrons is enhanced by nonstoichiometry which sometimes exceeds ten atomic percent. From the viewpoint of electronic structure the nonstoichiometry introduces local dopant centres which on ionization produce additional charge carriers in the system. Nonstoichiometry occurring in such systems can lead to insulator-metal transition similarly as in the case of Mott's transition in doped semiconductors.

The investigations of a defect structure and transport properties (deviation from stoichiometry, electrical conductivity, thermoelectric power) carried out under the conditions of thermodynamic equilibrium at elevated temperatures allow to determine the ionic and electronic defect structure, charge transport mechanism and optimum thermodynamic parameters ( $T$ ,  $p\text{X}_2$ ) for the synthesis of electrode materials with the desired transport properties.

The author of this work basing on her own investigations of  $\text{A}_x\text{M}_a\text{X}_b$  ( $\text{A}=\text{Li}, \text{Na}$ ;  $\text{M}=3d, 4d, 5d$ ;  $\text{X}=\text{O}, \text{S}, \text{Se}$ ) has demonstrated that the electronic structure of these materials plays an important role in the intercalation process. The intercalation of alkaline metal into transition metal compounds showing metallic or semiconducting properties can be considered as a reversible topotactic redox reaction in which the transition metal changes its valency.

Variations of emf of the  $\text{Li}/\text{Li}^+/\text{Li}_x\text{M}_a\text{X}_b$  cell, accompanying the intercalation reaction, correspond to those of electrochemical potential of electrons (Fermi level) of the cathode material brought about by alkaline metal doping. High density of states near the Fermi level is associated with wide range of alkaline metal concentration and weak compositional dependence of the cathode potential, whereas the existence of delocalized electronic states ensures rapid relaxation of the cathode material and good properties. The investigations of physico-chemical properties of the intercalated systems as a function of alkaline metal concentration have an important cognitive aspect. Modification of electronic structure of the intercalated material permits to follow the relations between structure, composition, disorder and reactivity of solids which still remains an open question in materials science. Taking as an example the  $\text{Li}_x\text{MO}_2$  ( $\text{M}=\text{V}, \text{Mo}, \text{Co}, \text{Ni}$ ) system it has been shown that chemical diffusion coefficient of lithium in the cathode material is determined by transport properties of electronic carriers.

# ELECTROCHEMICAL LITHIUM INTERCALATION INTO HEXAGONAL WO<sub>3</sub> AND ITS STRUCTURAL CHANGE

Mitsuhiro Hibino, Wonchull Han and Tatsuichi Kudo  
Institute of Industrial Science, The University of Tokyo,  
Roppongi, Minato-ku, Tokyo 106-8558, Japan

Although hexagonal tungsten bronzes M<sub>x</sub>WO<sub>3</sub> (M = K, Rb, etc.) have long been known, their empty framework itself (i.e., the hexagonal form of WO<sub>3</sub>, h-WO<sub>3</sub>) has been synthesized only comparatively recently from a precursor WO<sub>3</sub>(H<sub>2</sub>O)<sub>1/3</sub>. [1] Since then, a variety of synthetic routes [2-5] have been investigated, because this framework, being able to serve as an intercalation host of lithium, are thought to be useful for a cathode material for rechargeable lithium batteries. Very recently, we have found [6] that h-WO<sub>3</sub> is yielded by decomposing the orthorhombic form of ammonium paratungstate decahydrate (NH<sub>4</sub>)<sub>10</sub>[H<sub>2</sub>W<sub>12</sub>O<sub>42</sub>]·10H<sub>2</sub>O at relatively low temperature (340~370°C). This method is advantageous because of simplicity. However, the compound thus obtained contains ammonium species to a little extent depending on the synthetic conditions. We have not succeeded in obtaining a completely pure compound. These ammonium cations are believed to locate at the hexagonal tunnels in the host framework. The purpose of this study is to evaluate a h-WO<sub>3</sub> type host with ammonium cations and counter anions in their hexagonal tunnels and to investigate lithium insertion/desertion properties under influence of existence of these ions.

On electrochemical lithium intercalation, the OCV curves show a very much pronounced hysteresis loop between the discharge (lithium insertion) and charge (extraction) process, as shown in Fig. 1. This irreversible nature of OCV behavior found in the present h-WO<sub>3</sub> is likely to be related to a slower kinetic process associated with the extraction of lithium. The polarization becomes dramatically high at the end stage of charging. Similar polarization behavior has also been reported by Schlasche et al. [3] for their h-WO<sub>3</sub>, synthesized by oxidation of ammonium tungsten bronze, in which, it is thought, a small amount of NH<sub>4</sub><sup>+</sup> is left, for its color and lattice parameters. [7] Such a kinetic effect may be attributed partly to the formation of insulating surface layers (empty WO<sub>3</sub>), as Schlasche et al. have pointed out. In fact, the discharging process also shows higher polarization near  $x = 0$ , though not so pronounced. It is thought that the effect of NH<sub>4</sub><sup>+</sup> or/and their counter anions located in the tunnel of the h-WO<sub>3</sub> is also important.

We propose a model to explain the hysteresis of the OCV in relation to remarkable polarization on lithium extraction process of this compound. Correlation of structural change of h-WO<sub>3</sub> with lithium intercalation is also discussed.

## REFERENCES

- [1] B. Gerand, G. Nowogrocki, J. Guenot and M. Figlarz, *J. Solid State Chem.*, **29**, 429 (1979).
- [2] K.H. Cheng, A. J. Jacobson, and M. S. Whittingham, *Solid State Ionics*, **5**, 355 (1981).
- [3] B. Schlasche and R. Schollhorn, *Rev. Chim. Miner.*, **19**, 534 (1982).
- [4] J. Oi, A. Kishimoto, and T. Kudo, *J. Solid State Chem.*, **96**, 13 (1992).
- [5] Naoki. Kumagai, Nobuko. Kumagai, Y. Umetzu, K. Tanno and J.P. Pereira-Ramos, *Solid State Ionics*, **86-88**, 1443 (1996).
- [6] W. Han, M. Hibino and T. Kudo, *Bull. Chem. Soc. Jpn.*, **71**, 933 (1998).
- [7] M. Figlarz, *Prog. Solid State Chem.*, **19**, 1 (1989).

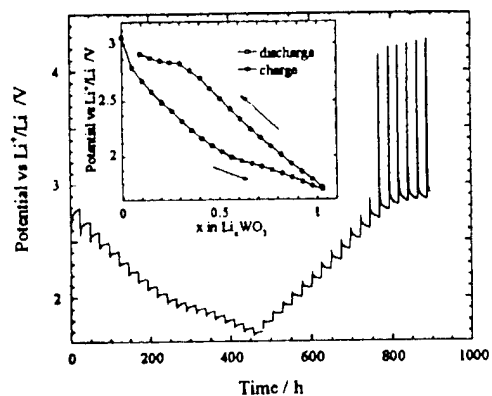


Fig. 1 Intermittent discharge and charge curves of sample at room temperature. (An inserted figure: each potential after 23 hour of rest time.)



## EFFECT OF IRON ON THE ELECTROCHEMICAL BEHAVIOUR OF LITHIUM NICKELATE : FROM $\text{LiNiO}_2$ TO $2\text{D-LiFeO}_2$

C. Delmas, G. Prado, A. Rougier, E. Suard\* and L. Fournès

Institut de Chimie de la Matière Condensée de Bordeaux ICMCB-CNRS and ENSCP de Bordeaux, Av. Dr Schweitzer, 33608 Pessac Cedex (France).

\*Institut Laue Langevin, BP 166X, 38042 Grenoble cedex

Some lithium nickel oxide derivatives are considered to be very promising positive electrode materials for 4V lithium-ion batteries.  $\text{LiNiO}_2$  exhibits two main advantages vs  $\text{LiCoO}_2$  : lower cost and higher reversible capacity. Nevertheless, the greater unstability of the material in the oxidised state and the fading upon cycling necessitate improvement of this material by cationic substitution.

In the frame of our general studies on the  $\text{LiNiO}_2$  system, an investigation of iron substitution has been undertaken. These materials have been characterised by classical structural and electrochemical methods. Moreover, extended fundamental studies can be realised thanks to the presence of iron cations which allows Mössbauer spectroscopy characterisation. This technique provides interesting information on the environment and on the oxidation state of iron.

### Structural characterisation of the $\text{LiNi}_{1-y}\text{Fe}_y\text{O}_2$ phases

As previously reported by Reimers et al. [1] for the  $\text{LiNi}_{1-y}\text{Fe}_y\text{O}_2$  composition, a single phases, isostructural to  $\text{LiNiO}_2$ , can be obtained in the  $0 \leq y \leq 0.3$  range. In this structure, alternate layers of Li and (Ni, Fe) occupy the octahedral sites of a cubic close packing of oxide ions, leading to a rhombohedral structure (R-3m space group). For higher amounts of iron, the layered phase is mixed with a disordered rocksalt one, which is obtained pure for  $y \geq 0.6$ . The layered phases ( $y \leq 0.3$ ) have been characterised by Rietveld profile refinement of the powder X-ray diffraction patterns. In all cases a significant amount (5% to 15%) of 3d cations (Ni or Fe) was found in the lithium site. This amount is very sensitive to the experimental conditions. A Rietveld profile refinement of the neutron diffraction pattern realised on the " $\text{Li}(\text{Ni}_{0.8}\text{Fe}_{0.2})\text{O}_2$ " phase has shown that there are no lithium ions in the Ni(Fe) planes. This result confirms our previous work realised on the  $\text{Li}_{1-z}\text{Ni}_{1+z}\text{O}_2$  system [2] which has shown that materials obtained in a suitable temperature range (700°C-750°C) present only a departure from Li/Ni stoichiometry but no extra-Li/Ni mixing.

In order to understand the role of iron substitution on the cationic distribution, a Mössbauer study was performed at room temperature. The isomer shifts are characteristic of  $\text{Fe}^{3+}$  in high spin state in octahedral oxygen surrounding. The spectra were fitted with a distribution of quadrupolar splittings which reflect the asymmetry of the charge distribution surrounding the iron nucleus. Therefore, this analysis provides information on the ionic distribution around the iron probe. For  $y = 0.1$ , the iron distribution has only one component ; for iron amounts up to thirty per cent a second component appears in the distribution of quadrupolar splittings. Its intensity increases with the number of 3d cations within the lithium site. For the homologous  $\text{Na}(\text{Ni}_{0.7}\text{Fe}_{0.3})\text{O}_2$ , which exhibits a strictly 2D structure, only one component is observed. This behaviour can be related to the presence of iron in the lithium site for the  $y = 0.2$  and  $0.3$  phases.

### Electrochemical behaviour

All these materials have been used as positive electrode of lithium batteries. Although a high irreversibility was observed at the first cycle, satisfactory cycling properties were obtained for the  $y = 0.1$  phase (Fig. 1). For higher amounts of iron the cycling performances decrease rapidly. Comparison with the behaviour of the  $\text{Li}_x\text{NiO}_2$  system leads to the following comments :

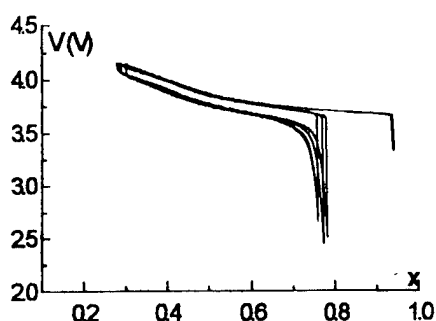


Fig. 1 : Electrochemical cycling of a Li/LiClO<sub>4</sub>-PC/Li(Ni<sub>0.9</sub>Fe<sub>0.1</sub>O<sub>2</sub>) cell (C/10)

- the Ni/Fe disorder, which inhibits the lithium ion ordering during lithium deintercalation, hinders the structural phase transitions and, therefore, the plateaux on the cycling curve have disappeared.
- the observed cell voltage increase indicates that it is more difficult to oxidise the material in presence of iron.
- the increasing amount of 3d ions in the interslab space and the cell voltage increase, which limits the working potential window, lead to a significant decrease in the cell capacity.

### X-ray and Mössbauer characterisation of the Li<sub>x</sub>Ni<sub>0.9</sub>Fe<sub>0.1</sub>O<sub>2</sub> phases

Samples with various lithium compositions were obtained electrochemically (Fig. 2). Their X-ray diffraction patterns show the existence of an Li<sub>x</sub>Ni<sub>0.9</sub>Fe<sub>0.1</sub>O<sub>2</sub> solid solution during lithium deintercalation in good agreement with the electrochemical behaviour. As commonly observed in layered oxides, the *a* parameter decreases while the *c* parameter increases upon lithium deintercalation. This behaviour results from the decrease in the ionic radius of the 3d cation and from the loss of cohesiveness when lithium ions are removed.

The change in the Mössbauer spectra (Fig. 2) of the positive electrode upon cycling was studied. The global shift of the spectra to lower velocity values as the charge proceeds indicates a modification of the iron oxidation state. Indeed, high spin tetravalent iron ions and average valence iron ions, "Fe<sup>3.5+</sup>" (resulting from a fast electron hopping between high spin Fe<sup>3+</sup> et Fe<sup>4+</sup> ions) are observed in the oxidised phases. This result shows that nickel and iron ions are simultaneously oxidised in this material during the cell charge.

This behaviour accounts for the cell voltage increase mentioned previously. A general comparison to the LiNi<sub>1-y</sub>Co<sub>y</sub>O<sub>2</sub> system shows that in these systems the competition between oxidation to the tetravalent state of nickel, cobalt and iron results directly from the difference in size between the cations involved. The effects of the nature of the substituting cation on the cell voltage will be discussed in a general way. These results will be extended to the behaviour of 2D-LiFeO<sub>2</sub> [3].

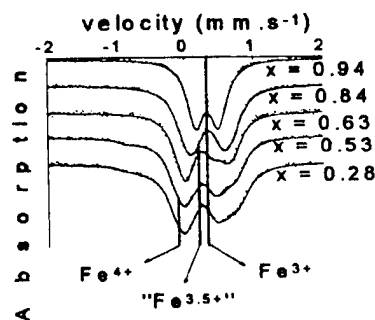
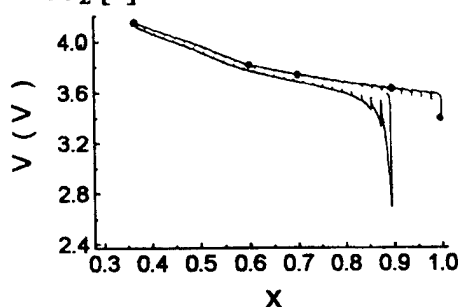


Fig. 2 : First intermittent charge-discharge curve for Li/LiNi<sub>0.9</sub>Fe<sub>0.1</sub>O<sub>2</sub>. The black dots correspond to compositions characterised by Mössbauer spectroscopy .

### **Acknowledgements**

The authors wish to thank CNES and Région Aquitaine for financial support.

### **References**

- [1] J.N. Reimers, E. Rossen, C.D. Jones and J.R. Dahn, Solid State Ionics, **61**, 335 (1993).
- [2] C. Poullierie, J.P. Pérés, G. Prado, E. Suard and C. Delmas, Solid State Ionics, (submitted).
- [3] R. Kanno, T. Shirane, Y. Inaba, Y. Kawamoto, J. Power Sources, **68**, 145 (1997).

ORDER-DISORDER TRANSITION OF  $\text{Li}_x\text{Mn}_2\text{O}_4$  SPINEL AT LOW TEMPERATURE

Tetsuichi Kudo, Hironobu Abiko and Mitsuhiro Hibino  
Institute of Industrial Science, University of Tokyo

Since the  $\text{Li}_x\text{Mn}_2\text{O}_4$  spinel has attracted much attention as an economical positive electrode material for rechargeable lithium batteries, its intercalation electrochemistry has been studied extensively. It is well known that the potential ( $\phi$ )-composition ( $x$ ) curve of  $\text{Li}_x\text{Mn}_2\text{O}_4$  at room temperature ( $\sim 25^\circ\text{C}$ ) shows a steep potential change at  $x=1/2$  with two quasi-plateaus ranging from  $x=0.9$  to  $0.6$  and  $0.4$ - $0.2$ . This  $\phi$ - $x$  profile is often discussed [1] in relation to ordering of Li in the 8a sites of the spinel structure which has a commensurate ZnS arrangement at  $x=1/2$ . However, such a profile can also be reproduced by a chemical potential of the disordered state assuming, for example, Bethe's approximation, if the Li-Li repulsion is relatively strong [2]. In this paper we report a dramatic profile change, which seems to indicate the "true" order-disorder transition in the compound, occurs at low temperature around 278 K.

According to X-ray measurements [3],  $\text{Li}_x\text{Mn}_2\text{O}_4$  is in a single cubic phase (Fd3m) in the range  $x=1$ - $0.4$  at room temperature. For this region of the composition, the  $\phi$ - $x$  relationship may be simulated by a cooperative model assuming the Li-Li interaction ( $J>0$ ) in the diamond-type 8a host lattice in the compound. The potential (for the disordered state) calculated [2] using the configuration entropy equivalent to Bethe's approximation is given by

$$\phi_B = -(kT/e)[E_s/kT + CJ/2kT + (C/2)\ln\{(Cx/2-p)/(C(1-x)/2-p)\} + (C-1)\ln\{(1-x)/x\}] \quad (1)$$

in which  $E_s$  is the site energy,  $C$  the coordination number of the site ( $=4$  for the diamond lattice), and  $p$  the smaller root of the following quadratic equation:

$$(Cx/2-p)(C(1-x)/2-p)/p^2 = \exp(-J/kT) \quad (2)$$

If we adopt the entropy analogous to the exact one for the 1-D lattice,

$$\phi_{1D} = -(kT/e)[E_s/kT + CJ/2kT + \ln\{(Cx/2-p)/(C(1-x)/2-p)\} + \ln\{(1-x)/x\}] \quad (3)$$

where  $p$  is the smaller root of

$$(Cx/2-p)(C(1-x)/2-p)/p^2 = \exp(-CJ/2kT) \quad (4)$$

As shown in Fig. 1, both  $\phi_B$  and  $\phi_{1D}$  give a curve with a steep voltage change at  $x=1/2$  that features the  $\phi$ - $x$  profile of  $\text{Li}_x\text{Mn}_2\text{O}_4$ . It is noted that, as  $J/kT$  is lowered,  $x=1/2$  is changed from the maximum point of  $|d\phi/dx|$  to its minimum at a certain critical value (about 0.6 for  $\phi_{1D}$ ).

Experimental  $\phi$ - $x$  curves recorded at various temperatures during the extraction of Li from the compound at  $x=1$  are shown in Fig. 2. Specimen  $\text{LiMn}_2\text{O}_4$ , prepared by the solid state reaction of  $\text{Li}_2\text{CO}_3$  and  $\text{MnCO}_3$  at  $750^\circ\text{C}$ , was almost a stoichiometric spinel ( $a=0.82430(44)$  nm, average manganese valence  $=3.497(4)$ , and  $T_c$  for the J-T structural transition  $=290$  K). The observed curve at 298K is very well fitted by the calculated  $\phi_{1D}$  at the same temperature in Fig. 1 with  $J=48$  meV and  $E_s=-4.18$  eV. Fitting by  $\phi_B$  (with 67 meV) is less satisfactory. It has been shown that the 1-D approximation is better than the Bethe, if the interaction is as strong as  $J/kT > 1$ . The curve at 283K is almost the same in shape, though the slope at  $x=1/2$  is slightly steeper. However,

profiles at 273 and 263 K are essentially different. This dramatic change took place around 278 K. Low temperature profiles show three perfectly flat stages with two very steep voltage slopes (almost steps) at  $x=1/2$  and about 0.7. Neither  $\phi_{ID}$  nor  $\phi_B$  can reproduce such a feature of the  $\phi$ - $x$  curve at low temperature; the slope of calculated curves at  $x=1/2$  is not so sensitive to temperature, as shown in Fig. 1.

Those curves in Fig. 2 strongly suggest that two new phases are generated at  $x=0.5$  and 0.7 at low temperature (i.e., below 278 K). It is reasonable to consider the former to be a Li-ordered phase; the diamond type intercalation lattice has only one commensurate arrangement at  $x=0.5$ . Note that  $\phi_{ID}$  as well as  $\phi_B$  is derived from the free energy for the disordered lattice, neglecting possible existence of the ordered state. Let us estimate the critical temperature for this order-disorder transition. Although the theoretical critical energy ( $J/kT_c$ ) for the diamond-type lattice is unknown, it has been calculated as 1.762 for the square lattice which takes the same C value as the diamond. Assuming  $J=48$  meV, this leads to  $T_c=316$  K, assuring that the ordering of Li (at  $x=1/2$ ) takes place at temperature not far from room temperature. The origin of another new phase at  $x=0.7$  will be discussed in another our paper.

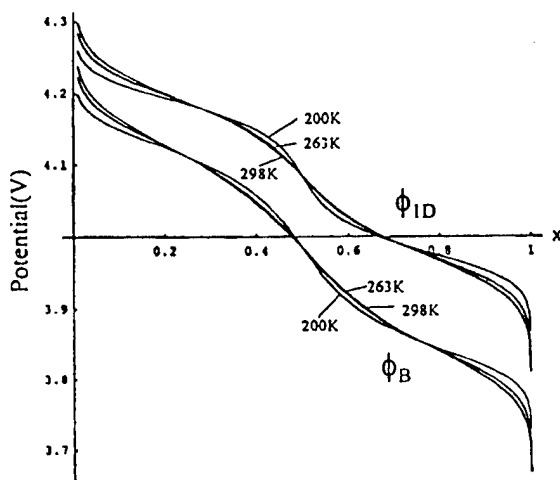


**Figure 1.** Calculated potential-composition curves for some temperatures (200–298 K).  $\phi_{ID}$ : 1-D approximation ( $J=48$  meV),  $\phi_B$ : Bethe's approximation ( $J=67$  meV, the best value for fitting to the observed curve at 298 K).  $\phi_B$  is shifted down by 0.1 V for clarity.

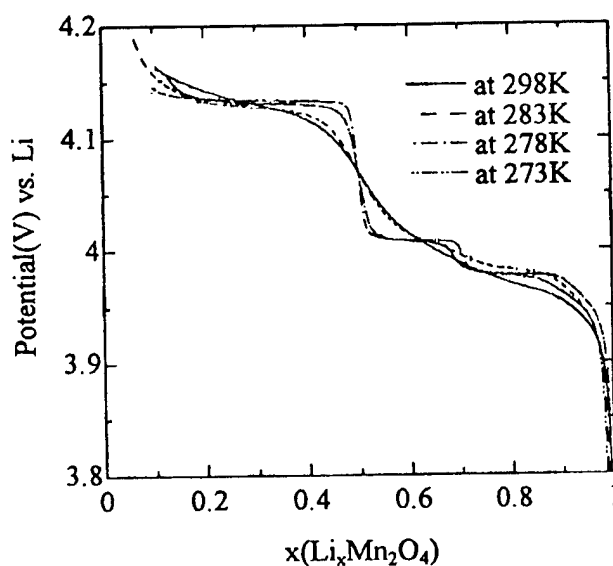


**Figure 2.** Potential-composition curves recorded at various temperatures during the first de-intercalation process.

#### References:

1. Y. Gao, J.N. Reimers and J.R. Dahn, *Physical Rev. B* **54**, 3878 (1996)
2. T. Kudo and M. Hibino, *Electrochim. Acta* **43**, 781 (1998)
3. S. Mukerjee, T.R. Thurston, N.M. Jisrawi, X.Q. Yang and J. McBreen, *J. Electrochem. Soc.* **145**, 466 (1998)

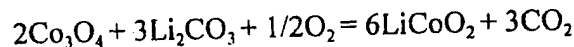
## MECHANISM OF $\text{Li}_{1+x}\text{CoO}_2$ SYNTHESIS AND THE INFLUENCE OF X VALUES ON PERFORMANCE

Renmin Liu, Xinhe Yang, Guoliang Wu, Weihua Jin  
(General Research Institute of Non-Ferrous Metals, Beijing 100088, China)

Qin Lin  
(University of Science and Technology, Beijing, Beijing 100083, China)

The synthesis mechanism of  $\text{Li}_{1+x}\text{CoO}_2$  from  $\text{Co}_3\text{O}_4$  and  $\text{Li}_2\text{CO}_3$  was studied by thermogravimetric analysis, and the influence of x values on the performance was investigated by XRD structure analysis and electrochemical test.

The thermogravimetric curves are shown in Fig.1a and Fig.1b. We can find two endothermal reaction peaks at temperatures of 725°C and 740°C respectively in the DTA curve. According to the shapes of these two peaks and TG we can identify that  $\text{Li}_2\text{CO}_3$  melts at 725°C, and the synthesis reaction occurs around 740°C. It seems that the  $\text{Li}_2\text{CO}_3$  is molten first and coated on the  $\text{Co}_3\text{O}_4$  particles. Therefore the synthesis process carries out throughout and the product is homogeneous. At 900°C the process completes. The reaction equation is following:



The weight loss is 16.5%, which consists with the tested result of 17.0% by TG.

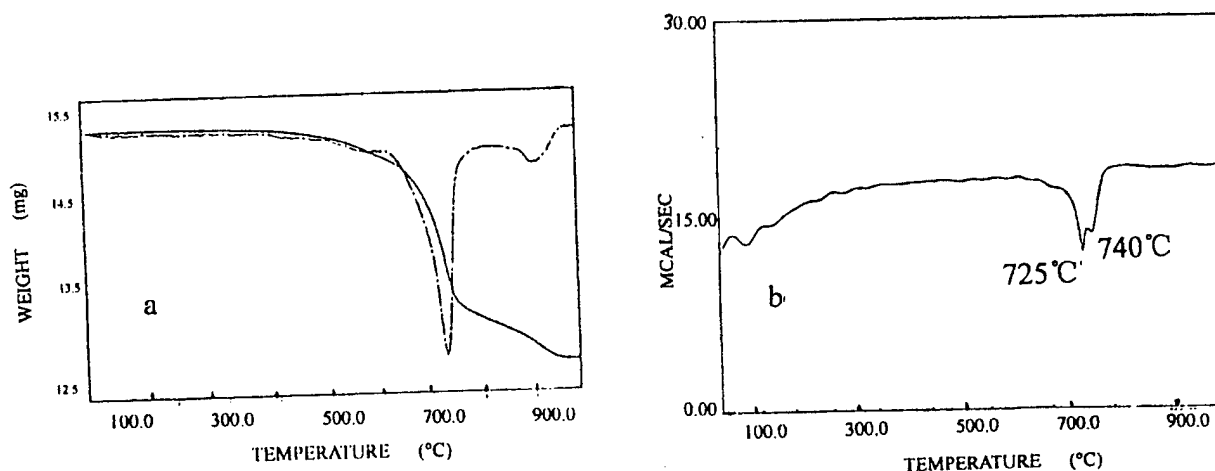


Fig.1 TG and DTA curves of  $\text{LiCoO}_2$  synthesis from  $\text{Co}_3\text{O}_4$  and  $\text{Li}_2\text{CO}_3$   
(a: TG, b: DTA)

$\text{Li}_{1+x}\text{CoO}_2$  ( $x=0, 0.015, 0.03$  and  $0.05$ ) demonstrates the XRD diffraction pattern, the main d and I values are shown in table 1. Plane distances for  $\text{Li}_{1+x}\text{CoO}_2$  almost do not change, but the

strength of  $I_{104}$ ,  $I_{101}$ , and  $I_{012}$  decreases with  $x$  values increasing from 0 to 0.05 obviously. We used  $\text{Li}_{1+x}\text{CoO}_2$  with  $x=0, 0.015, 0.03$  as cathode materials for Li-ion batteries (type 18650), and tested the performance of them. We found that the excess Li in  $\text{Li}_{1+x}\text{CoO}_2$  ( $x>0$ ) effects on the cycle life of Li-ion batteries, as shown in table 2.

Table 1. XRD pattern of  $\text{Li}_{1+x}\text{CoO}_2$  with different  $x$ 

x	0		0.015		0.03		0.05	
hkl	d( × 10nm)	I	d( × 10nm)	I	d( × 10nm)	I	d( × 10nm)	I
003	4.6670	100	4.6671	100	4.6866	100	4.6671	100
101	2.3976	37	2.3976	27	2.4001	21	2.3976	10
006	2.3329	6	2.3376	6	2.3399	8	2.3352	7
012	2.2985	12	2.2985	9	2.3030	7	2.2985	3
104	2.0010	71	1.9994	51	2.0027	47	1.9994	25

Table 2. Performance of Li-ion Batteries with  $\text{Li}_{1+x}\text{CoO}_2$  as cathode

x Values	1st capacity and efficiency (mAh)	(%)	1C/0.2C (%)	50th capacity (mAh)	150th capacity (mAh)	250th capacity (mAh)
0	1419	89	98.5	1308	1226	1185
0.015	1479	89	97.4	1290	1148	998
0.03	1344	88	98.2	1222	1101	993

## Reference

- [1] Mingfeng Guo, Ruimin Yang, Zebo Zhang, Jinying Ye  
Proceeding of 21th National Conference of Chemical and Physical Energy Sources, 1992, China.
- [2] D. Larcher, M. R. Palacin, G. G. Amatucci and J.-M. Tarascon  
Journal of Electrochemical Society, **144** (2), 408, (1997).
- [3] R. Alcantara, P. Lavela, J. L. Tirado, R. Stoyanova and E. Zhecheva  
Journal of Electrochemical Society, **145** (3), 730, (1998).
- [4] C. Wolverton and Alex Zunger  
Journal of Electrochemical Society, **145** (7), 2424, (1998).

## INFLUENCE OF STRUCTURAL DEFECTS OF $\gamma$ -MnO<sub>2</sub> ON THE CATION INSERTION REACTION : COMPARISON OF H<sup>+</sup> AND Li<sup>+</sup>.

D. Guyomard, S. Sarciaux, S. Jouanneau, A. Le Gal La Salle and Y. Piffard.  
Institut des Matériaux de Nantes - 2, rue de la Houssinière  
BP 32229 - 44322 Nantes Cedex 3 - France

$\gamma$ -MnO<sub>2</sub> compounds are positive electrode materials of both rechargeable alkaline and lithium batteries. EMD (Electrolytic Manganese Dioxides), prepared by anodic electrodeposition from boiling MnSO<sub>4</sub> solutions, are used in aqueous systems. EMD and CMD (Chemical Manganese Dioxides) need to be dehydrated by a thermal treatment in the range 250-400°C before their use in rechargeable lithium batteries, leading to so-called HTMD (Heat Treated Manganese Dioxides).

Whatever the synthesis procedure, giving rise to EMD, CMD and HTMD, the structure of these  $\gamma$ -MnO<sub>2</sub> compounds consists of a random intergrowth of blocks of the Pyrolusite structure (De Wolff defects with a P<sub>r</sub> rate) within the Ramsdellite structure, and contains microtwinning defects (with a Mt rate). Consequently, their structural characterization by diffraction techniques is complex and requires simulation of the powder patterns [1].

With the use of unusual preparation conditions (especially by scanning the voltage or the current density and upon moderate thermal treatments), a large variety of  $\gamma$ -MnO<sub>2</sub> compounds was prepared. The compounds were characterized in terms of physico-chemical characteristics, such as average oxidation state of Mn and content of crystallization water. Their structural parameters P<sub>r</sub> and Mt were determined by using an extension of the method previously used [1] for the simulation of X-ray powder patterns in order to take into account the simultaneous influence of De Wolff and microtwinning defects.

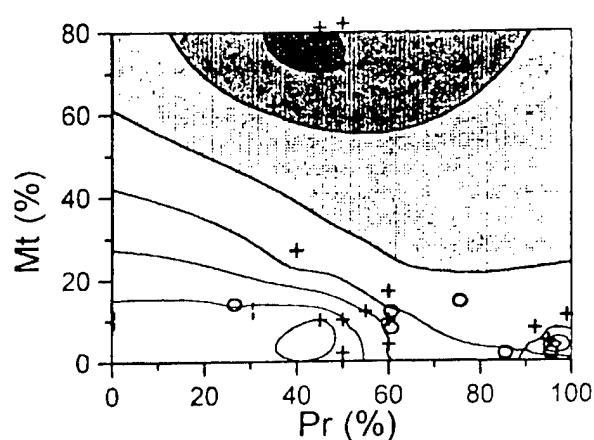
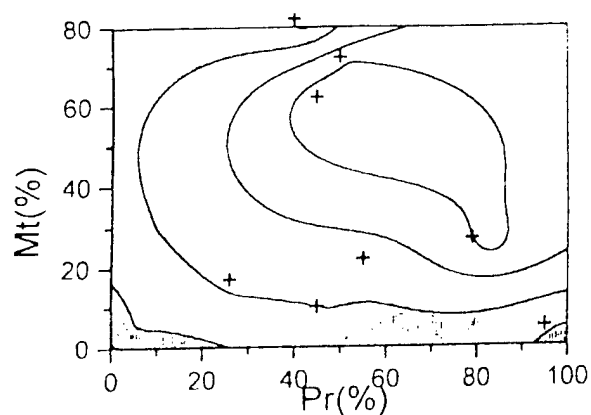
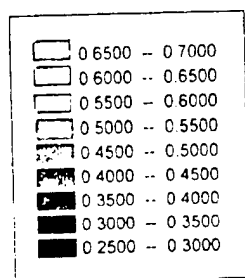
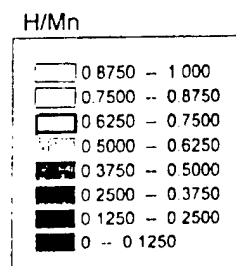
Some of these compounds have been selected for a comparative study of H<sup>+</sup> insertion in aqueous alkaline medium and Li<sup>+</sup> insertion in a non-aqueous organic electrolyte, in order to study which structural parameter controls each cation insertion behavior.

Electrodes were prepared by mixing the active material (85% by mass) with carbon black (Super P, from Chemetals) (10%) and an organic binder (PVDF) (5%). Such electrodes were studied in two-electrodes cells, such as Li/EC + DMC + LiPF<sub>6</sub> / electrode, and in three-electrodes cells (counter electrode : Pt; reference : Hg/HgO) using a 1M KOH solution. Both potentiostatic and galvanostatic modes of a Macpile battery tester were used.

### 1) Li insertion

The first electrochemical insertion of Li into  $\gamma$ -MnO<sub>2</sub> compounds induces an irreversible transformation leading to  $\gamma$ -Li<sub>x</sub>MnO<sub>2</sub> compounds similar to those prepared by solid state reaction in the range 250-400°C, starting from a Li salt and  $\gamma$ -MnO<sub>2</sub>. This transformation corresponds to important structural modifications, especially when the P<sub>r</sub> rate of De Wolff defects is high. Thus it appears that as P<sub>r</sub> becomes larger, the transformation kinetics become slower, although there is also a dependence on the water content. It has been shown that crystallization water slows down the transformation. Furthermore, the Li content x in  $\gamma$ -Li<sub>x</sub>MnO<sub>2</sub> is maximum for the largest values of the average oxidation state of Mn.

In addition, correlations have been established between the material characteristics and the performances in lithium batteries (reversible capacity and cycling behavior). It has been shown that the reversible Li intercalation capacity of  $\gamma$ -Li<sub>x</sub>MnO<sub>2</sub> compounds is maximum when both the P<sub>r</sub> and Mt rates of the starting  $\gamma$ -MnO<sub>2</sub> compounds are small (see Figure 1). An exception to this rule is observed for  $\gamma$ -Li<sub>x</sub>MnO<sub>2</sub> compounds prepared from so-called "faulted" Pyrolusite (i.e. with P<sub>r</sub> > 90%) that have the smallest Mt values (Figure 1). Concerning the cycling behavior, the best materials are those prepared from  $\gamma$ -MnO<sub>2</sub> compounds containing only Mn<sup>4+</sup>.

Figure 1:  $\text{Li} / \text{MnO}_2$ Figure 2:  $\text{H} / \text{MnO}_2$ 

## 2) Proton insertion

As a function of the value of the structural parameters  $P_r$  and  $M_t$ , linear sweep voltammetry curves show 3 different types of current-voltage behavior at first discharge and 2 different types of behavior at first charge. These behaviors are discussed in comparison to the simplified mechanism published in the literature. The  $\text{H}^+$  insertion mechanism involves at least one biphasic phase transformation.

Results show that the reversible insertion capacity depends strongly on the initial structure. Intermediate values of  $P_r$  and  $M_t$ , in a range close to  $P_r=50-80\%$  and  $M_t=30-70\%$ , give the largest reversible capacities. These capacities decrease over the 20 first cycles and stabilize to about 100Ah/kg after 100 cycles.

## 3) Conclusion

Results show that, to get a maximum Li insertion reversible capacity, the optimal structure needs to contain a low amount of disorder. On the contrary, structures with maximum disorder lead to the largest proton insertion reversible capacities. It could be explained by the very small size of the proton compared to  $\text{Li}^+$  ion, leading to different diffusion paths for the two cations in the  $\gamma\text{-MnO}_2$  structure.

## Reference

- [1] - Y. Chabre and J. Pannetier, *Prog. Solid State Chem.*, 23 (1995) 1



## IN SITU FABRICATION OF FUNCTIONAL DOUBLE OXIDE FILMS BY SOFT SOLUTION PROCESSING BELOW 200°C

Masahiro YOSHIMURA, Kyoo-Seung HAN, and Wojciech SUCHANEK  
*Center for Materials Design, Materials and Structures Laboratory  
Tokyo Institute of Technology, 4259 Nagatsuta, Midori, Yokohama 226, Japan*

The films of functional double oxides like  $\text{BaTiO}_3$ ,  $\text{SrTiO}_3$ ,  $\text{CaWO}_4$ ,  $\text{LiNiO}_2$ , etc., have been fabricated mostly by "dry process" like CVD, MOCVD using gaseous precursors, or "vacuum process" like vacuum deposition, sputtering, plasma and/or beam technologies. Moreover, other activation processes like magnetron, microwave, laser, etc., have been added to fabricate high-quality films. Those processings, however, should consume a lot of energies because they are using highly energetic and diluted species as their precursors. In addition to those energetic problems, exhaust gas(es) problems must be considered because exhaust gas(es) particularly after vacuum pumping are almost impossible to cycle/recycle due to their diluted concentrations and huge volumes. Therefore, those "dry process" and "vacuum process" should cause severe environmental loads on the earth.

Considering those problems, we are proposing "soft solution processing (SSP)" to fabricate those double oxide films in aqueous solutions at RT-200°C without post-firing. In SSP, interfacial reactions between a substrate/reactant (mostly of a metal) and speci(es) in a solution have been activated electrochemically, hydrothermally, hydrothermal-electrochemically, etc., to fabricate the films of double oxides. We have already succeeded to fabricate well-crystallized films of  $\text{LiCoO}_2$  and  $\text{LiNiO}_2$  which are electrochemically active, in addition to  $\text{BaTiO}_3$ ,  $\text{SrTiO}_3$ ,  $\text{SrWO}_4$ ,  $\text{BaMoO}_4$ , and etc. Details of preparation and properties of them will be presented. I will talk also about feature and future of SSP.

### [Reference]

- (1) J. Mater. Res., 13 [4] 796-802 (1998)
- (2) J. Mater. Res., 13 [4] 875-879 (1998)
- (3) Chemistry of Materials, 10 [8] 2183-2188 (1998)
- (4) J. Mater. Chem., 8 [9] 2043-2048 (1998)

## NEW MATERIALS FOR POLYMER ELECTROLYTES

Piercarlo Mustarelli, Eliana Quartarone, Corrado Tomasi, Aldo Magistris  
Department of Physical Chemistry of the University of Pavia and CSTE-CNR  
Via Taramelli 16, 27100 Pavia, Italy

The increasing request for high-energy-density, solid-state batteries for portable electronics and electric vehicles constitutes a strong driving force to explore new concepts and related materials. To date, the winning choice for both the applications is the lithium-ion rechargeable battery which employs polymer electrolytes as the separator membrane (1). Nearly all the polymer electrolytes studied to date belong to two families: i) the poly(ethylene oxide) (PEO)-based, and ii) the gel-type ones.

The electrolytes belonging to the former group are obtained by mixing a lithium salt (e.g.  $\text{LiPF}_6$ ,  $\text{LiClO}_4$ ,  $\text{LiN}(\text{CF}_3\text{SO}_2)_2$ ) to high or low-molecular weight PEO (or to a PEO-based copolymer). Organic plasticizers (e.g. propylene carbonate, PC), as well as organic or inorganic fillers (2) may be added in order to improve the thermal, mechanical and transport properties of the films. Conductivity values at room temperature in excess than  $10^{-4} \text{ ohm}^{-1}\text{cm}^{-1}$  have been reported in the literature (3). The mayor drawbacks are related to the poor mechanical properties of the PEO amorphous phases in which the transport takes place, and to the relatively low melting temperature of crystalline PEO ( $\sim 60^\circ\text{C}$ ), or PEO-based complexes. Recently, the use of nanoscale fillers has been proven to determine a relevant improvement in both mechanical and transport properties (4, 5).

The second family embraces heterogeneous systems in which a liquid electrolyte (e.g. EC/PC/lithium salt) is trapped into a polymer (or copolymer) like poly(acrylonitrile) (PAN), poly(methyl methacrylate) (PMMA), or poly(vinylidene fluoride) (PVdF). In this case, conductivity values at room temperature higher than  $10^{-3} \text{ ohm}^{-1}\text{cm}^{-1}$  have been reported (6). While mechanical properties like filmability and processability may be better than for PEO-based systems (in particular if PVdF-based copolymers are employed), a relevant problem may be caused by the loss of solvent due to syneresis, which limits the use of these membranes above room temperature.

In this paper we briefly discuss both the strengths and the defects of the two above mentioned families of electrolytes starting from our experience. The data we have obtained on PEO-based composite electrolytes, as well as on PVdF-HFP (hexafluoropropylene) gels, will be summarized. Thermal analysis (MDSC, TGA) allows to understand the stability limits on heating and also on annealing under normal storage conditions. Impedance spectroscopy and solid-state nuclear magnetic resonance highlight the transport mechanisms, the ion-ion and ion-polymer levels of interaction, and the electrochemical stability towards the electrodes. Finally, pathways are suggested in order to optimize the performances of both the classes of electrolytes we will discuss here.

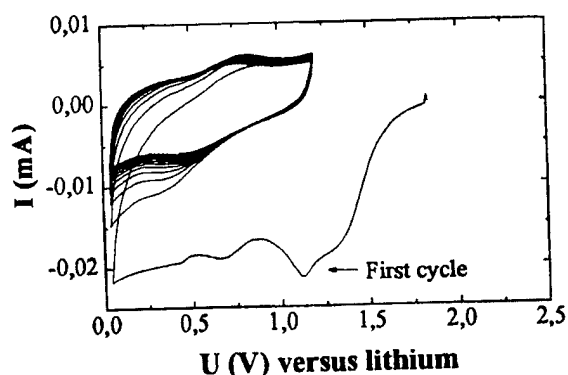
- (1) B. Scrosati, *La Chimica e l'Industria*, **79**, 463 (1997).
- (2) E. Quartarone, P. Mustarelli, A. Magistris, *Solid State Ionics*, **110**, 1 (1998).
- (3) W. Wieczorek, *Composite Polyether Based Electrolytes*, Oficyna Wydawnicza Politechniki Warszawskiej, Warszawa, 1995 (in English).
- (4) F. Croce, G.B. Appetecchi, L. Persi and B. Scrosati, *Nature*, **394**, 456 (1998).
- (5) C. Capiglia, P. Mustarelli, E. Quartarone, C. Tomasi and A. Magistris, *Int. Conf. on Applications of Electrically Conducting Polymers*, Rome, 13-16 April 1997, p. 120
- (6) K.M. Abraham, *Applications of Electroactive Polymers*, B. Scrosati ed., Chapman&Hall, London, 1993, p.75.

## SEARCH FOR SUITABLE MATRIX FOR THE USE OF TIN-BASED ANODES IN LITHIUM ION BATTERIES

*O.Crosnier, T.Brousse, J.Santos-Peña, P.Fragnaud, R.Marchand, P.Paillard and D.M.Schleich*  
*ISITEM, Laboratoire Génie des Matériaux, rue Christian Pauc, BP90604,*  
*F44306, Nantes cedex 3, FRANCE*

**Introduction :** Recently, Sn based compounds ( $\text{SnO}_2$ ,  $\text{SnSiO}_3$ , Sn nanocrystallites) have been investigated as possible anodes for lithium ion batteries [1-3]. Despite the high reversible capacities usually observed for such materials, several drawbacks have been pointed out. A substantial limitation is the fade in capacity observed after a few hundred cycles [4]. This capacity fade can be assigned to both a mechanical disintegration of the electrode during the cycling [3], and the loss of electrical contact due to tin grain growth during the cycling [4]. This drawback is mainly due to the lack of a suitable matrix able to accommodate the impressive volume changes occurring during the charge-discharge cycles. Furthermore, the matrix must assure electronic conductivity throughout the electrode. In order to increase the capacity and the cyclability of tin-based anodes, we have designed a suitable matrix to cancel the drawbacks previously explained. Since we wanted to avoid irreversible capacity on the first cycle, metallic tin has been chosen as the active component instead of tin oxides.

**Results :** Several electrodes have been prepared using tin as the electrochemically active material. In a first approach, we dispersed tin in a carbon matrix. For example,  $\text{SnCl}_2$  was added to polyacrylic acid and the resulting mixture was dried at  $100^\circ\text{C}$  for 12 hours before being heated at  $400^\circ\text{C}$  under a reducing atmosphere. The black powder thus obtained contains only a small amount of metallic tin. Despite the interesting cycling performance of this compound, a huge capacity loss still occurred during the first cycle (figure 1).



In order to solve this problem, we have designed electrodes with nanocrystalline tin powder mixed with different carbonaceous compounds and polymers in order to improve both the electronic conductivity during the cycling and the mechanical properties of the electrodes.

**References :** See for examples :

- [1] I.A.Courtney and J.R.Dahn, *J. Electrochem. Soc.* **144** (1997) 2045.
- [2] T.Brousse, R.Retoux, U.Herterich and D.M.Schleich, *J. Electrochem. Soc.*, **145** (1998) 1.
- [3] J.Yang, M.Winter and J.O.Besenhard, *Solid State Ionics*, **90** (1996) 281.
- [4] R.Retoux, T.Brousse and D.M.Schleich, submitted to *J. Electrochem. Soc.*

# TEM ANALYSIS OF TWO-PHASE REACTION IN ELECTROCHEMICAL LITHIUM INSERTION WITHIN MoO<sub>3</sub>

Yasutoshi Iriyama, Takeshi Abe, Minoru Inaba, and Zempachi Ogumi

*Department of Energy and Hydrocarbon Chemistry,*

*Graduate School of Engineering, Kyoto University, Sakyo-ku, Kyoto 606-8501, Japan*

## Introduction

Lithium insertion materials, e.g. graphite and LiCoO<sub>2</sub>, are now widely used as active materials in lithium-ion batteries and extensive work has been done on their electrochemical properties and crystal structures, etc. It is well-known that most of these materials show two-phase coexistence regions during their electrochemical lithium insertion/extraction reactions. For example, lithium is intercalated within graphite through a series of stage transformation between two different stages. Such two-phase coexistence is easily explained thermodynamically; however, the kinetics of two-phase reactions is complicated and must be fully understood. In this work, we chose electrochemical lithium insertion into layered MoO<sub>3</sub> as a model reaction and studied the mechanism and kinetics of a two-phase reaction involved in the lithium insertion reaction by transmission electron microscopy (TEM).

## Experimental

Electrochemical measurements were carried out using three electrode cells. Counter and reference electrodes were lithium metal. The electrolyte solution was 1M LiClO<sub>4</sub> dissolved in EC : DEC (1:1 by volume, Mitsubishi Chemicals). Two kinds of working electrodes were used in this study. For XRD experiments, powder electrodes made of MoO<sub>3</sub> powder, 10% carbon black, and 15% PTFE were used. For TEM observation, MoO<sub>3</sub> thin films were deposited on Au microgrid by pulsed laser ablation and used as working electrodes. The experimental conditions for thin film preparation are shown in Table 1. The working electrodes were discharged electrochemically to a given lithium content, and their XRD patterns and TEM images were obtained. All electrochemical measurements were performed in an ar-

Table 1 Experimental condition for MoO<sub>3</sub> thin film preparation by pulsed laser ablation

Laser	KrF Excimer Laser (248 nm)
Substrate Temperature	873 K
O <sub>2</sub> pressure	53.2 Pa
Target-substrate distance	50 mm
Energy Fluence	1.6 ~ 1.8 J / cm <sup>2</sup>
Repetition frequency	5 Hz
Target	MoO <sub>3</sub> (sintered at 973K for 12h)
Deposition time	30 ~ 60 min

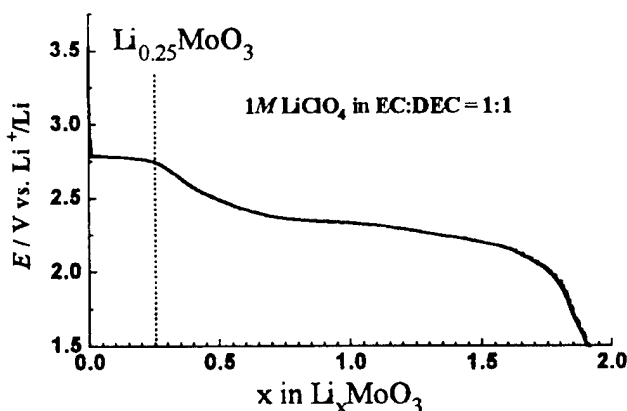


Fig. 1 Galvanostatic reduction of MoO<sub>3</sub> in 1M LiClO<sub>4</sub> / EC+DEC (1:1). I = 28.8  $\mu$  A

gon-filled glove box.

## Results and Discussion

Figure 1 shows the first discharge profile of  $\text{MoO}_3$ . Between 3.5 V and 1.5 V, a clear plateau was observed at about 2.7 V in the range  $0 < x < 0.25$  in  $\text{Li}_x\text{MoO}_3$ . Figure 2 shows XRD patterns of  $\text{Li}_x\text{MoO}_3$  ( $x = 0, 0.05, 0.10, 0.15, 0.20, 0.25$ ). In addition to peaks assigned to the original  $\text{MoO}_3$  (dotted lines), additional peaks of a lithium-inserted phase appeared at  $x = 0.05, 0.10, 0.15, 0.20$  (dashed lines). The interlayer spacing in the newly formed phase was about 0.79 nm.  $\text{Li}_{0.25}\text{MoO}_3$  showed only peaks assigned to the lithium inserted phase (dashed lines). Because the peaks of the inserted phase were very sharp, the inserted phase should have a crystallite size of at least a few tens of nanometers.

In TEM images of  $\text{MoO}_3$  and  $\text{Li}_{0.3}\text{MoO}_3$ ,  $\text{MoO}_3$  layers with interlayer spacings of 0.69 and 0.79 nm, respectively, were observed, which is in agreement with the above XRD results. Figure 3 shows TEM images of  $\text{Li}_x\text{MoO}_3$  in the two-phase region. In this figure, a mixed feature of both phases was observed with 0.69 and 0.79 nm interlayers. The figure shows that lithium insertion in a  $\text{MoO}_3$  layer causes expansion of two interlayers adjacent to the  $\text{MoO}_3$  layer by 0.1 nm. No clear phase boundary between the two phase was observed and expanded interlayers were located randomly in the lattice.

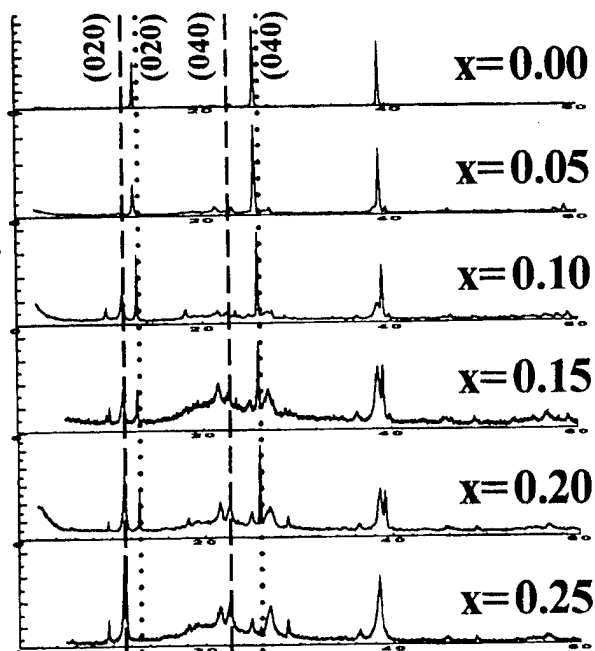


Fig. 2 XRD patterns of  $\text{Li}_x\text{MoO}_3$  ( $x = 0, 0.05, 0.10, 0.15, 0.20$ , and  $0.25$ )

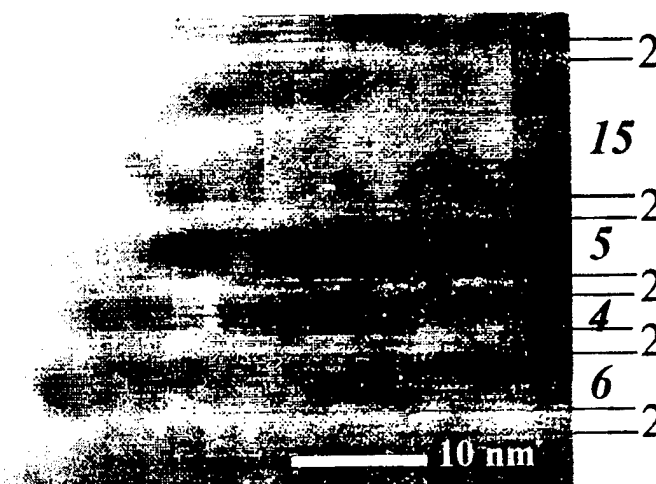


Fig. 3 TEM image of  $\text{Li}_x\text{MoO}_3$  ( $0 < x < 0.25$  : in two-phase region). Numbers of stacked layers are shown (plain: 0.79 nm interlayer; bold: 0.69 nm interlayer).

## Reference

- [1] J. N. Reimers and J. R. Dahn, *J. Electrochem. Soc.*, Vol. 139 (1992) 2091
- [2] J. R. Dahn, R. Fong, and M. J. Spoon, *Phys. Rev. B*, Vol. 42 No. 10 (1990) 6424
- [3] T. Senoh, T. Mukae, T. Miura, and T. Kishi, *Denki Kagaku*, No. 9 (1994) 858
- [4] T. Tsumura and M. Inagaki, *Solid State Ionics*, 104 (1997) 183

## Acknowledgment

This work has been supported by CREST of JST (Japan Science and Technology).

## GRAPHITE INTERCALATION COMPOUNDS AS CATHODES FOR LITHIUM BATTERIES

S. Zhang and D.M. Schleich  
Laboratoire de Génie des Matériaux  
ISITEM  
Rue Christian Pauc, BP90604  
44306 Nantes CEDEX 3  
France

For almost ten years the lithium ion battery has been in commercial use. In this battery one uses an anode (negative electrode) of carbon and a cathode (positive electrode) made from a transition metal oxide containing lithium (i.e.,  $\text{LiCoO}_2$ ,  $\text{LiMn}_2\text{O}_4$ ,  $\text{LiNiO}_2$ ) as well as an electrically conducting carbon and binder. This system has been chosen due to the added stability of a carbon insertion electrode versus a lithium electrode upon cycling. The carbon anode has a theoretical capacity of 372 mAh/g and normally shows an irreversible first cycle of less than 20%. This electrode cycles quite well and although can cointercalate certain solvents when graphite is used as the carbon source it is a very acceptable electrode. On the other hand if one examines the cathodes commonly used there appear to be several obvious problems. The most common commercial electrode is prepared from  $\text{LiCoO}_2$ . This compound shows a theoretical capacity of only about 135 mAh/g. Although the desired layered phase is quite easy to synthesize, the high cost of cobalt limits use to rather small applications (especially if one wishes to use lithium ion batteries for electric vehicles). In addition, overcharging of the electrode can result in compounds with less than 0.5 Li which are not stable. If one examines the other lithiated oxides one finds similar or other problems. In the case of  $\text{LiMn}_2\text{O}_4$  the theoretical capacity is only about 150mAh/g; however, in reality values greater than 125mAh/g are rarely found and decay upon cycling. In addition, discharging to voltages less than 3 Volts results in a Jahn-Teller type distortion that causes a loss in capacity. In the case of  $\text{LiNiO}_2$ , although the theoretical capacity is higher than the isostructural cobalt compound, synthesis is very difficult in order to avoid nickel atoms entering into the lithium plane and disrupting the lithium ionic mobility. In all of these lithiated transition metal oxides, the total capacity is substantially lower than that found in carbon, and the preparation of the electrodes is rather difficult due to the poor electronic conductivity of these inorganic compounds. In addition, the low ionic mobility of lithium (usually in the range of  $10^{-10}$ - $10^{-13}$  cm<sup>2</sup>/sec), ultimately limits the speed at which this type of battery can be charged or discharged.

In order to avoid this long list of problems that exists concerning the cathodes of various lithium ion batteries we have started to explore alternative cathode materials. The cathode of choice is to be composed of a material with a high electronic conductivity, no decomposition problems over the voltage range to be explored, and high rapidity in both charge and discharge. We have used a graphite compound previously intercalated with a species that can undergo an oxidation and a reduction within the carbon matrix. Our initial choice for these studies has been the ferrocene molecule. Although this species may not yield the highest capacity as a function of weight or volume, electrochemically the rapid loss of one electron in passing to the ferrocenium species is well documented. We have studied the use of this material as an active cathodic species in a standard lithium battery, comparing systems where the ferrocene is free to migrate (dissolved in the liquid electrolyte), where migration is limited (use of a viscous polymeric medium), and where migration outside of the graphite framework is very difficult (ferrocene intercalated into graphite). We have been specifically interested in studying the response of this electrode when the graphite is intercalated.

Electrochemically we have observed how the system cycles versus a lithium electrode as a function of the quantity of ferrocene intercalated into the graphite (modification of chemical conditions of intercalation). We have been especially interested in the rate behavior of such an electrode especially since the electrode rate is now limited by the transfer of negative counter ions within the battery rather than the transfer of lithium within the cathode.

## LITHIUM AND PROTON INSERTION IN SPINEL-STRUCTURED LITHIUM MANGANESE OXIDES

**M. Saiful Islam<sup>a</sup>, Brett Ammundsen<sup>b</sup>, Jacques Roziere<sup>b</sup> and Gary R. Burns<sup>c</sup>**

<sup>a</sup> *Department of Chemistry, University of Surrey, Guildford GU2 5XH, UK*

<sup>b</sup> *Laboratoire des Agregats Moleculaires et Materiaux Inorganiques ESA 5072, Universite Montpellier 2, 34095 Montpellier Cedex 5, France*

<sup>c</sup> *School of Chemical and Physical Sciences, Victoria University, Wellington, New Zealand*

Atomistic simulation techniques are used to investigate lithium and proton insertion in spinel lithium manganates which are important materials for both lithium battery and selective ion-sorption applications. Such computational methods are now well established techniques for studying solid state ionic materials at the atomic level.

The energetics of lithium extraction and insertion by redox reactions in the  $\text{LiMn}_2\text{O}_4$ - $\lambda$ - $\text{MnO}_2$  system are evaluated with respect to the formation of lithium vacancies and interstitials. We also investigate the mechanisms and pathways for lithium ion migration through the interstitial space of the spinel lattice. The local structures around Mn (16d) vacancies in spinels of composition  $\text{LiMn}_2\text{O}_{4+\delta}$  and  $\text{Li}_{1+x}\text{Mn}_{2-x}\text{O}_4$  are modelled to determine the effects of these vacancies on lithium and proton sites. Possible orientations of O-H groups formed by inserted protons are examined, and an energetic preference for the hydroxyl groups to coordinate to the Mn (16d) vacancies is found.

We have examined the effects on local structure and lithium migration energies resulting from substitution of Mn in  $\text{LiMn}_2\text{O}_4$  by various cation dopants (e.g., Ti, Cr, Co and Ga); the simulations are compared with the available data from x-ray absorption studies. Recent work includes simulations of the lattice vibrational modes of  $\text{LiMn}_2\text{O}_4$  and  $\lambda$ - $\text{MnO}_2$  allowing their Raman and infrared spectra to be assigned for the first time.

Ammunsen B. et al., *J. Phys. Chem. B* **101**, 8156 (1997); *J. Power Sources* (1999) in press



THE REDOX PROCESS IN LITHIUM INSERTION HOST  $V_6O_{13}$ 

Torbjörn Gustafsson, Helen Björk and Josh Thomas  
Inorganic Chemistry, Ångström Laboratory, Uppsala University, Box 538,  
SE-751 21 Uppsala, Sweden

A suitable cathode material for lithium batteries should have high enough electronic conductivity, diffusion paths for lithium ions and a wide redox range. A number of transition metal oxides show these properties. It seems however, that in most cases the useful redox range is limited to about one unit change in the transition metal oxidation number. This means that the capacity for most lithium insertion hosts is less or equal to one lithium ion / transition metal atom.

The reason for this is the well-known changes in co-ordination chemistry associated with oxidation state changes. The changes in bonding distances and preferred co-ordination number on oxidation / reduction will increase the total energy and eventually the structure collapses.

$V_6O_{13}$  is a well-known cathode material (Fig. 1), which cycles reversibly between zero and one lithium ion per vanadium atom. During the insertion / extraction process six different phases are formed. Four of these have been studied with single crystal diffraction[1,2,3]. Information about unit cell dimensions, co-ordination geometries and deformation electron densities can be extracted from this diffraction data. The insertion / extraction process will be discussed in the light of this information.

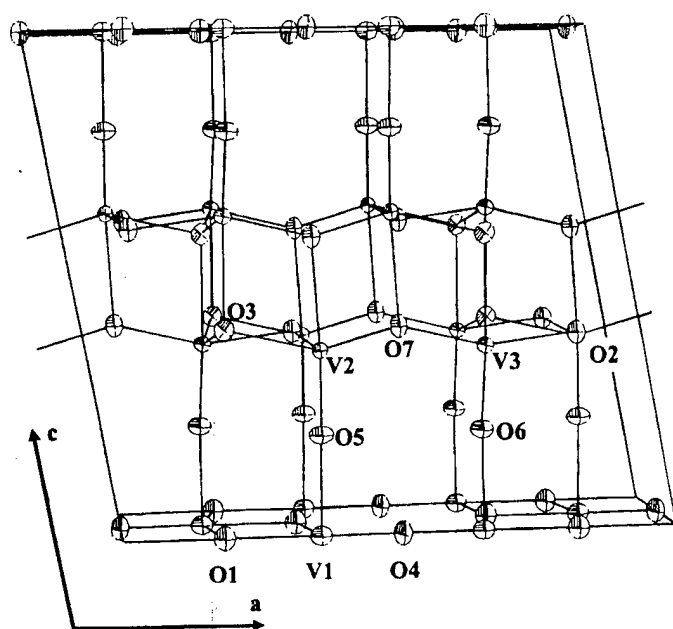


Fig. 1

- [1] K. A. Wilhelmi, K. Waltersson and L. Kihlberg, *Acta Chem Scand.* **25**, 2675 (1971).
- [2] Ö. Bergström, T. Gustafsson and J. Thomas, *Acta Cryst* **C53**, 528 (1997).
- [3] Ö. Bergström, T. Gustafsson and J. Thomas, *Acta Cryst* **C54**, 1204 (1998).

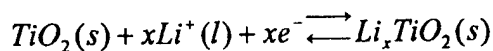
## LITHIUM INSERTION INTO SELF-ORGANIZED MESOSCOPIC TiO<sub>2</sub> (ANATASE) ELECTRODES

Petr Krtíl<sup>1</sup>, Dina Fattakhova<sup>1</sup>, Ladislav Kavan<sup>1</sup>, Shelly Burnside<sup>2</sup>, Michael Grätzel<sup>2</sup>

<sup>1</sup>J. Heyrovský Institute of Physical Chemistry, Academy of Sciences of the Czech Republic,  
Dolejšková 3, CZ 18223, Prague, Czech republic.

<sup>2</sup>Laboratory of Photonics and Interfaces, Ecole Polytechnique Fédérale de Lausanne, CH-1015,  
Lausanne, Switzerland.

Electrochemical lithium insertion into titanium dioxide is practically applicable in many types of devices, including electrochromic devices [1,2] and secondary lithium batteries [3-7]. The anatase crystal form of TiO<sub>2</sub> is one of the prospective electrode materials for 2 volt lithium ion batteries due to its convenient formal potential around 1.85 V (Li/Li<sup>+</sup>) [7,8]. The insertion/extraction of the lithium proceeds according to the following equation:



*x* is usually around 0.5, giving the specific capacity of ca 170 mAh/g for this electrode material. The actual performance of polycrystalline anatase electrodes (the insertion capacity, coulombic efficiency of the insertion process, etc.) is strongly affected by the electrode morphology. In this paper we present the results of electrochemical and electrochemical quartz crystal microbalance (EQCM) study of the electrochemical activity of self-organized mesoscopic anatase layers.

Anatase samples were prepared by sol-gel technique with subsequent hydrothermal treatment of peptized suspension at temperatures ranging between 190 and 230 °C for 4.5 hours [9]. A detailed description of the synthetic procedure may be found elsewhere [9]. Films were made by a doctor-blade technique directly on one of the contacts of an AT-cut 10 MHz quartz crystal and sintered at 450°C in air. Electrochemical and EQCM experiments were carried out in three electrode arrangement in 0.5 M Li(CF<sub>3</sub>SO<sub>2</sub>)<sub>2</sub>N/propylene carbonate solution. Mass change connected with insertion into/extraction from self-organized anatase electrodes was recorded using EQCM.

Typical SEM image of the ordered anatase film is shown in Fig. 1. The effect of the hydrothermal treatment temperature on the electrode morphology is shown Table 1.

Table 1

Autoclaving temperature	Surface area [m <sup>2</sup> /g]	Pore diameter [nm]	Porosity [%]
190°C	66	3.5	26
210°C	61	3.8	27
230°C	50	8.5	29
250°C	39	30	42

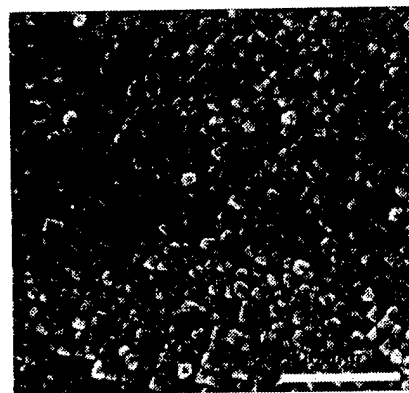


Figure 1 SEM image of the self-organised anatase electrode.

The data in Table 1 show that increasing the temperature of the hydrothermal treatment leads to decreased surface areas. This indicates also a bigger crystal size and a more open morphology of the films made from colloids treated at higher temperatures.

A comparison of cyclic voltammograms of self-organized and non-ordered anatase electrodes with the same surface area is shown in Figure 2. Insertion/extraction processes are in both cases expressed by one cathodic and one anodic peak. There is only negligible difference in peak potentials between ordered and non-ordered electrodes. There is, however, a difference in the insertion coefficient  $\alpha$  characterizing the attainable level of lithium insertion. Ordered electrodes showed higher insertion coefficients by ca. 15% comparing with those of non-ordered electrodes with the same specific surface area. This effect may be related to closer packing and more regular pore distribution, which leads to increase in number of "surface states". The attainable insertion levels of the ordered electrodes accordingly increase with increased specific surface area (see Fig. 3). Insertion coefficients exceeding 0.5 were observed for self-organized films with specific surface area higher than 60 m<sup>2</sup>/g.

Lithium insertion into self-organized anatase electrodes was reversible in terms of the coulombic and mass efficiencies are concerned. The total observed mass change was, however, lower than that predicted by Faraday's law. This discrepancy may be explained by electrochemical side-reactions proceeding simultaneously with lithium insertion. An alternative explanation may be a convection solvent transfer triggered by density gradients in the electrode vicinity.

#### Acknowledgement

P.K., D.F. and L.K. have been supported by the Grant Agency of the Czech Republic under contract 96/203/1088. M.G. and S.B. have been supported by a European Union Joule Project JOR3-CT97-0147. We thank Valery Shklover of the ETH-Zurich for the SEM analysis.

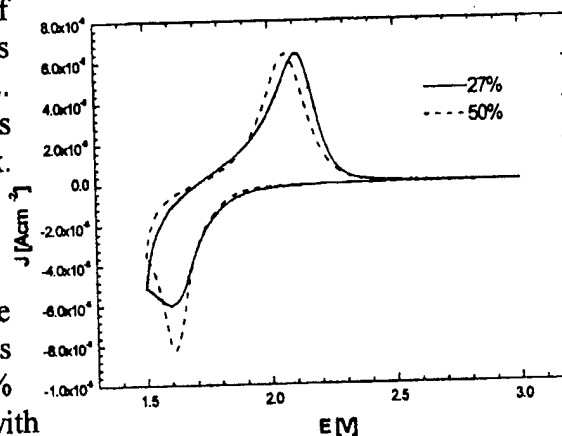


Figure 2 Cyclic voltammograms of organised (solid line) and non-ordered (dashed line) anatase electrodes with the same specific surface area.

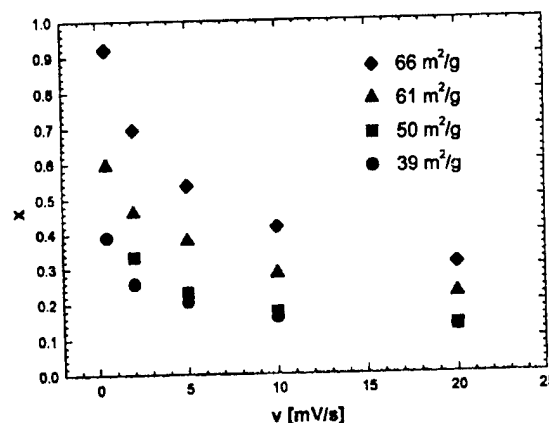


Figure 3 Insertion coefficients for different self-organised anatase electrodes as a function of applied scan rate.

#### Reference List

- [1.] T. Ohzuku and T. Hirai, *Electrochim. Acta.*, **27**, 1263 (1982).
- [2.] M. Ottaviani, S. Panero, S. Morsilli and B. Scrosati, *Solid State Ionics.*, **20**, 197 (1986).
- [3.] T. Ohzuku, Z. Takehara and S. Yoshizawa, *Electrochim. Acta.*, **24**, 219 (1979).
- [4.] W.J. Macklin and R.J. Neat, *Solid State Ionics.*, **53-56**, 694 (1992).
- [5.] K. Kanamura, K. Yuasa and Z. Takehara, *J. Power Sources.*, **20**, 127 (1987).
- [6.] T. Ohzuku, T. Kodama and T. Hirai, *J. Power Sources.*, **14**, 153 (1985).
- [7.] S.Y. Huang, L. Kavan, M. Grätzel and I. Exnar, *J. Electrochem. Soc.*, **142**, 142 (1995).
- [8.] S.Y. Huang, L. Kavan, A. Kay, M. Grätzel and I. Exnar, *Act. Pass. Electronic Comp.*, **18**, 23 (1995).
- [9.] S.D. Burnside, V. Shklover, C. Barbe, P. Comte, F. Arendse, K. Brooks, et al., *Chem. Mater.*, **10**, 2419 (1998).

SYNTHESIS, STRUCTURE AND ELECTROCHEMICAL PROPERTIES OF  $\text{Li}_{1-x}\text{Ni}_{1+x}\text{O}_2$ Atsushi Hirano<sup>1</sup>, Ryoji Kanno<sup>1</sup>, Yoji Kawamoto<sup>1</sup>, Syuji Kawasaki<sup>2</sup> and Mikio Takano<sup>2</sup><sup>1</sup>Department of Chemistry, Faculty of Science, Kobe University, Kobe, Hyogo 657-8501, Japan<sup>2</sup>Institute for Chemical Research, Kyoto University, Uji, Kyoto-fu 611, Japan

## 1. Introduction

Lithium nickel oxides,  $\text{LiNiO}_2$ , has been studied for possible use as cathode candidate of rechargeable lithium batteries. The stoichiometry of  $\text{LiNiO}_2$  affects the charge and discharge characteristics and the magnetic properties [1, 2]. However, stoichiometric  $\text{LiNiO}_2$  is difficult to obtain, because the high-temperature treatment of  $\text{LiNiO}_2$  leads to a decomposition from  $\text{LiNiO}_2$  to  $\text{Li}_{1-x}\text{Ni}_{1+x}\text{O}_2$  which has a partially disordered cation distribution at the Li site. In the present study, the  $\text{Li}_{1-x}\text{Ni}_{1+x}\text{O}_2$  with various compositions were synthesized using various synthesis conditions and their compositions and structures were clarified using neutron diffraction, X-ray diffraction, and magnetic measurements. The relationship between the compositions and the charge-discharge characteristics was also studied.

## 2. Experimental

Non-stoichiometric  $\text{Ni}_{1/3}\text{O}$  and  $\text{Li}_2\text{O}_2$  were used as starting materials. The starting materials were mixed with various molar ratio and heated at 650-700°C. The electrochemical intercalation and de-intercalation were carried out using lithium cells. Neutron diffraction data were taken on a time-of-flight (TOF) neutron powder diffractometer, VEGA, at the KENS pulsed spallation neutron source at the High Energy Accelerator Research Organization (KEK). Temperature dependence and magnetic field dependence of the magnetization was measured by a SQUID magnetometer between 5 and 300 K.

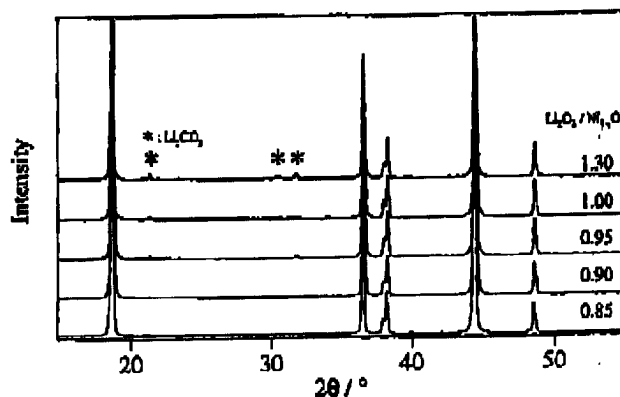


Fig. 1 X-ray diffraction patterns for the samples synthesized at 690 °C with various  $\text{Li}_2\text{O}_2 / \text{Ni}_{1/3}\text{O}$  ratio.

## 3. Result and discussion

Figure 1 shows the X-ray diffraction patterns for the samples synthesized at 690 °C with various mixing ratios of starting materials,  $\text{Li}_2\text{O}_2$  and  $\text{Ni}_{1/3}\text{O}$ . The samples with the starting

compositions of  $\text{Li}_2\text{O}_2 / \text{Ni}_{1.5}\text{O} \leq 0.90$  showed the mono-phasic properties. However, the samples with the ratio  $\text{Li}_2\text{O}_2 / \text{Ni}_{1.5}\text{O} > 0.90$  showed  $\text{Li}_2\text{CO}_3$  as an impurity. The compositions,  $x$ , determined by X-ray Rietveld method were consistent with the ratio  $\text{Li}_2\text{O}_2 / \text{Ni}_{1.5}\text{O}$  of the starting materials. The sample with the stoichiometric composition was obtained at the synthesis temperature of 690 °C with the ratio of 1.30. Figure 2 shows the charge-discharge characteristics of the lithium cell using  $\text{Li}_{1-x}\text{Ni}_{1+x}\text{O}_2$  cathodes. The capacities decreased with increasing number of cycles for the sample synthesized with the ratio of 0.85. The samples synthesized with the ratio of 1.00 and 1.30 showed good reversibility. Figure 3 shows the temperature dependences of the magnetic susceptibilities. The samples synthesized with the ratio  $\text{Li}_2\text{O}_2 / \text{Ni}_{1.5}\text{O} = 1.30$  showed typical spin glass behavior around 8K. The relationships between the compositions and the structures determined using neutron diffraction measurements, and the magnetic properties will be discussed.

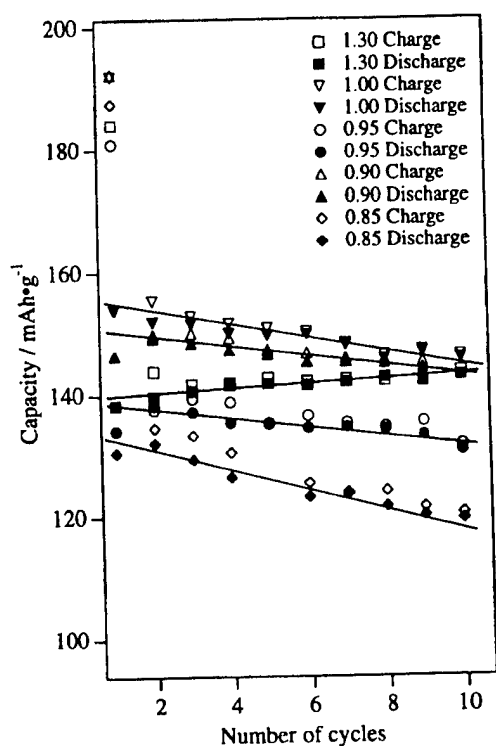


Fig. 2 Relationship between the capacity and the number of cycles.

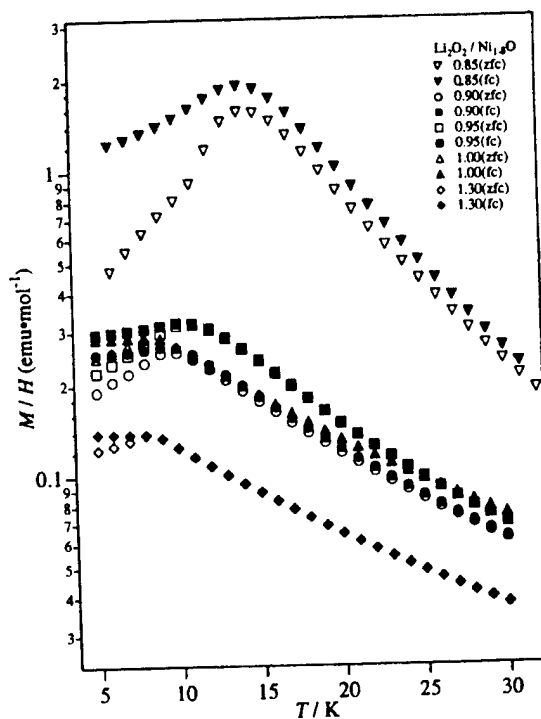


Fig. 3 Temperature dependences of the magnetic susceptibilities for the samples synthesized with various  $\text{Li}_2\text{O}_2 / \text{Ni}_{1.5}\text{O}$  ratio.

#### Reference

- [1] A. Hirano, R. Kanno, Y. Kawamoto, Y. Takeda, K. Yamaura, M. Takano, K. Ohyama, M. Ohashi and Y. Yamaguchi, *Solid State Ionics*, **78**, 123 (1995).
- [2] K. Yamaura, M. Takano, A. Hirano and R. Kanno, *J. Solid State Chem.*, **127**, 109 (1996).

**TRANSPORT AND ELECTROCHEMICAL PROPERTIES OF  $\text{LiMn}_2\text{O}_4$** 

J. Molenda, K. Świerczek, W. Kucza, J. Marzec

*Department of Solid State Chemistry, Stanisław Staszic University of Mining and Metallurgy,  
Al. Mickiewicza 30, 30-059 Cracow, Poland*

Possible application of a manganese spinel  $\text{LiMn}_2\text{O}_4$  as a cathode material in lithium ions batteries (rocking chair) has brought about intensification of its electrochemical and crystallographic studies. Good electrochemical properties of this material are generally ascribed to its spinel structure but systematic studies on its ionic and electronic defects are still lacking.

This paper presents the high temperature measurements of electrical conductivity and thermoelectric power of  $\text{LiMn}_2\text{O}_4$  as a function of temperature (870-1070K) and oxygen pressure ( $10^{-3}$ -1 atm) in thermodynamic equilibrium condition in order to assess the structure of point defects in this material. The electrical properties have been analysed with reference to those concerning deviation from stoichiometry. The observed reverse character of the pressure dependencies of the deviation from stoichiometry (negative slope) and electrical conductivity (positive) is extremely rare and indicates a complex defect structure of  $\text{LiMn}_2\text{O}_4$ . Thermoelectric power data are in agreement with those of deviation from stoichiometry. The negative sign of thermoelectric power indicates that electrons are effective charge carriers.

The low temperature measurements of electrical conductivity and thermoelectric power suggest the contribution of hopping mechanism in spinel  $\text{LiMn}_2\text{O}_4$ .

**Mechanochemical synthesis of  $\text{LiMn}_2\text{O}_4$  cathode material for lithium batteries**

N. V. Kosova, N. F. Uvarov, E. T. Devyatkina, E. G. Avvakumov

*Institute of Solid State Chemistry, Siberian Branch of Russian Academy of Science  
Kutateladze 18, Novosibirsk-128, 630128, Russia*

Lithium – manganese oxides with spinel – type structure possess a number of unique properties and are the most promising materials as insertion electrodes for rechargeable lithium batteries. Synthesis of  $\text{Li}_x\text{Mn}_y\text{O}_z$  by conventional thermal treatment procedure results, as a rule, in formation of poor dispersed product with insufficient electrochemical activity. Therefore it is of importance to find new ways for the preparation of the high-quality materials. A mechanochemical technique [1] is the efficient method which permits to obtain compounds with homogeneous composition in the form of high dispersed particles with narrow particle size distribution. Morphology of materials can be controlled by variation of both mechanical activation parameters and conditions of consequent thermal treatment.

In this work the results are reported of mechanochemical synthesis of  $\text{LiMn}_2\text{O}_4$  from various starting reagents: manganese oxides ( $\text{MnO}_2$ ,  $\text{Mn}_2\text{O}_3$ ,  $\text{MnO}$ ) and different lithium compounds ( $\text{LiOH}$ ,  $\text{LiOH}\cdot\text{H}_2\text{O}$ ,  $\text{Li}_2\text{CO}_3$ , et al.). Mechanical activation (MA) was carried out using an EI-2/150 activator with steel jars and balls (8 mm, 660 rp/min). Composition and properties of the products was studied by X-ray powder diffraction analysis, IR, X-ray photoelectron and  $^1\text{H}$ ,  $^7\text{Li}$  NMR spectroscopy and complex impedance technique.

Two different mechanisms of mechanochemical action was observed. In mixtures with  $\text{LiOH}$ , having relatively soft lattice,  $\text{LiOH}$  easily spreads on the manganese oxide surface forming an amorphous layer. On contrary, in mixtures containing more rigid salts, like  $\text{Li}_2\text{CO}_3$ , fragile grinding is observed. It is established that at the first stages of MA intermediate states form which determine surface and electrochemical properties [2]. As a result of mechanochemical synthesis, lithium-manganese oxide  $\text{LiMn}_2\text{O}_4$  with spinel structure was obtained. The material is characterized by high specific surface values  $15\text{-}25\text{ m}^2/\text{g}$ , which do not change appreciably on heating up to temperatures  $450^\circ\text{C}$ .

The spinels were investigated by complex impedance technique. For all the samples under study experimental impedance  $Z'' - Z'$  diagram comprises single semicircle. The data may be satisfactorily described in terms of the equivalent circuit consisting of a parallel array of conductivity, capacity and constant phase element. No contribution of ac- or dc-electrode polarization was detected, therefore conductivity is electronic. Conductivity of non-sintered pellets measured with carbon or copper electrodes is relatively low,  $10^{-5}\text{-}10^{-6}\text{ S/cm}$ , strongly depends on the synthesis conditions, especially on kind of starting reagents, and increases after the heat treatment. Pellets sintered at  $T > 600^\circ\text{C}$  have conductivity of about  $1\cdot 10^{-4}\text{ S/cm}$  irrespectively on starting materials used. The most probably, the conductivity values relate to intergrains resistivity. Test experiments in the electrochemical cell  $\text{Li} / \text{LiPF}_6/\text{EC} / \text{LiMn}_2\text{O}_4/\text{C}$  showed that lithium-manganese oxide obtained by the mechanochemical method is promising cathode material for 4V lithium batteries.

- [1]. E. G. Avvakumov. Mechanical methods for activation of chemical processes. Novosibirsk. Nauka, 1986. 305 p. (in Russian).
- [2]. N.V.Kosova, S.G.Kozlova, S.P.Gabuda and E.G.Avvakumov, Doklady Akad. Nauk **362**, (1998).

## RELATIONSHIP BETWEEN ELECTROCHEMICAL PROPERTIES AND STRUCTURE OF LITHIUM MOLYBDENUM OXIDES

Hironori Kobayashi, Mitsuharu Tabuchi, Masahiro Shikano, A. Mary Sukeshini, Hiroyuki

Kageyama, Tadashi Ishida, Hideo Nakamura\*, Yutaka Kurioka\*, Ryoji Kanno\*\*

Osaka National Research Institute, 1-8-31 Midorigaoka, Ikeda, Osaka, 563-8577 Japan

\*Department of Electrical Engineering, Faculty of Science and Technology, Kinki University,

Kowakae, Higashi-Osaka, Osaka, 577-8502 Japan

\*\* Department of Chemistry, Faculty of Science, Kobe University, Nada, Kobe, Hyogo, 657-8501 Japan

The layered oxides  $\text{Li}_2\text{MO}_3$  ( $M$  = transition metals) have a cubic close-packed oxide-ion lattice with basal planes of octahedral interstices filled alternately by  $\text{Li}^+$  only and by  $1/3\text{Li}^+$ ,  $2/3M^{4+}$  [1].  $\text{Li}_2\text{MoO}_3$  has rhombohedral symmetry where Li sites are nearly similar to  $\alpha\text{-NaFeO}_2$ . The ternary Li-Mo-O system contains many types of layered and spinel compounds, which are suitable for Li diffusion in the structure, and has a wide variety of the valence states from  $\text{Mo}^{3+}$  to  $\text{Mo}^{6+}$ . We have already reported that  $\text{Li}_2\text{MoO}_3$  allowed reversible electrochemical extraction/insertion [2]. In this study, the relationship between electrochemical property and structure of  $\text{Li}_2\text{MoO}_3$  was investigated.

$\text{Li}_2\text{MoO}_3$  was synthesized from  $\text{Li}_2\text{MoO}_4$  at 923-1073 K for 36-48 h under hydrogen gas flow. The ratios of Li/Mo and valence states of samples obtained were investigated by ICP spectroscopy and Mo K-edge XANES spectra, respectively, and the composition was confirmed to be  $\text{Li}_2\text{MoO}_3$ . X-ray Rietveld analysis clarified that all samples have layered structure with rhombohedral symmetry. Results of EXAFS analysis indicated the increase of long-range ordered arrangements of  $\text{MoO}_6$  in  $\text{Mo}_{2/3}\text{Li}_{1/3}\text{O}_6$  layers with increasing synthesis temperature.  $\text{Li}_{2-x}\text{MoO}_3$  was synthesized electrochemically using coin-type cells with Li/1M  $\text{LiClO}_4$  in EC:DMC(1:1)/ $\text{Li}_2\text{MoO}_3$  couple. Lithium deintercalation from samples synthesized at 1073 K proceeded from  $x=0$  to 1.2 with a current density of  $0.2 \text{ mA/cm}^2$ . The difference between 1st and 2nd charge curves indicates the change in the crystal structure at the 1st charge process. All Li/ $\text{Li}_2\text{MoO}_3$  (923-1073 K) cells showed the discharge capacity of about 190 mAh/g in the voltage ranges of 1.5-4.3 V in 1st cycle and the discharge capacity gradually decreased with cycling. The cycling reversibility of  $\text{Li}_2\text{MoO}_3$  was improved with increasing synthesis temperature. The relationship between the electrochemical properties and the structure will be discussed in detail.

### References

- [1] A. C. W. P. James *et al.*, J. Solid. State. Chem., **76**, 87 (1988)
- [2] H. Kobayashi *et al.*, J. Power Sources, in press.



# STRUCTURE AND LITHIUM ION DIFFUSION PROPERTIES IN $\text{Li}_x\text{CoO}_2$ AND $\text{Li}_x\text{NiO}_2$ AS INVESTIGATED BY MOLECULAR DYNAMICS.

Ken Suzuki, Yasuto Yokoi, Takayuki Onozu, Yasunori Oumi, Seiichi Takami,  
Momoji Kubo and Akira Miyamoto  
Department of Materials Chemistry, Graduate School of Engineering, Tohoku University  
Aoba 07, Sendai 980-8579, Japan.

Masahiro Kikuchi, Nobuyuki Yamazaki, and Muneo Mita  
Nippon Chemical Industrial. Co., Ltd, Koto-ku, Tokyo 136-0071, Japan.

Lithium secondary batteries have numerous applications in portable electric devices because of their high energy density, long cycle life, low self-discharge rates and high operating voltage. Lithium secondary batteries use lithium transitional-metal oxides such as  $\text{LiCoO}_2$ ,  $\text{LiNiO}_2$  and  $\text{LiMn}_2\text{O}_4$  as the positive electrode cathode. In commercially available lithium secondary batteries,  $\text{LiCoO}_2$  is now used because it can be easily prepared and it gives higher voltage in comparison to other probable cathode material candidates. However, there are some limitations of  $\text{LiCoO}_2$ , for example, in spite of the theoretical capacity of  $\text{LiCoO}_2$ , which is 274 mAh/g, the rechargeable capacity is limited to 140 mAh/g. Furthermore,  $\text{LiNiO}_2$ ,  $\text{LiMn}_2\text{O}_4$  and other cathode materials also have some limitations respectively in terms of capacity, rechargeability and so on. This shows that presently available cathode materials can by no means be regarded as the best. Under these circumstances, it is necessary to develop new materials in order to improve the cell performance, therefore possible candidate cathode materials have been well investigated. In addition to experimental studies, theoretical studies are also required to design better materials for lithium secondary batteries. In the present study, we applied molecular dynamics (MD) and computer graphics (CG) methodologies to investigate the behavior of lithium ion diffusion in  $\text{Li}_x\text{CoO}_2$  and  $\text{Li}_x\text{NiO}_2$  as lithium is deintercalated from  $\text{LiCo(Ni)O}_2$  and also to rationalize its structural features.

MD simulations were carried out using the MXDORTO program developed by Kawamura [1] with a simulation box comprising 360 ions in the case of  $\text{LiCoO}_2$ . We performed MD calculations on  $\text{Li}_x\text{CoO}_2$  and  $\text{Li}_x\text{NiO}_2$  ( $x < 1.0$ ) at 300K. The structure of  $\text{Li}_x\text{CoO}_2$  and  $\text{Li}_x\text{NiO}_2$  used in MD calculations were modeled in such a way that charge-compensating counterions get oxidized from  $\text{Co}^{3+}$  ( $\text{Ni}^{3+}$ ) to  $\text{Co}^{4+}$  ( $\text{Ni}^{4+}$ ) agree with the number of lithium ions. For example, in case of  $\text{Li}_{0.6}\text{CoO}_2$  structure, we modeled this system by eliminating 36 lithium ions from  $\text{LiCoO}_2$  unit cell ( $90 \text{ Li} + 90 \text{ Co} + 180 \text{ O}$ ) and replace 36  $\text{Co}^{3+}$  by 36  $\text{Co}^{4+}$  in order to keep the system electrically neutral.

Figure 1 shows the final structure of  $\text{Li}_{0.6}\text{CoO}_2$  (a) and  $\text{Li}_{0.3}\text{CoO}_2$  (b) in MD simulation. It is found from this figure that both the structures retain the layered type structure with the existence of  $\text{CoO}_2$  sheets. In the case of  $\text{Li}_{0.3}\text{CoO}_2$ , the layered structure is still retained but it

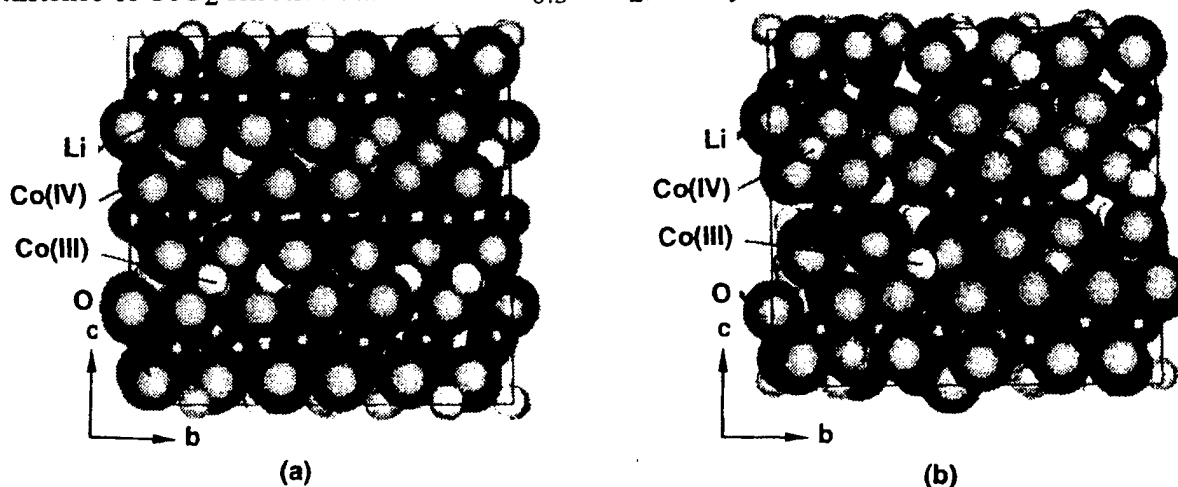


Figure 1 Structures of  $\text{Li}_x\text{CoO}_2$  at final step from MD method. (a)  $\text{Li}_{0.6}\text{CoO}_2$ , (b)  $\text{Li}_{0.3}\text{CoO}_2$ .

undergoes distortion where Co moves into the lithium layer. This behavior was observed for the structures where the lithium concentration is lower than  $x = 0.4$ . In the case of  $\text{Li}_x\text{NiO}_2$ , Ni moved into the lithium layer more easily than Co. Figure 2 shows the distribution of O ions to  $c$ -axis direction in (a)  $\text{Li}_{0.4}\text{CoO}_2$  and (b)  $\text{Li}_{0.4}\text{NiO}_2$ . Since both  $\text{LiCoO}_2$  and  $\text{LiNiO}_2$  have layered rock-salt structure with lithium atomic layers sandwiched between the  $\text{CoO}_2$  ( $\text{NiO}_2$ ) octahedral layers, the distribution of O ions might be orderly in case where the layered structure was kept. It is found from this figure that the peaks which correspond to the average number of O ions per calculation step at the  $c$  distance are broadened in the case of  $\text{Li}_{0.4}\text{CoO}_2$ . Broadened peaks indicate that the layered structure undergoes disorder. This results suggest that the layered structure of  $\text{Li}_x\text{NiO}_2$  at lower lithium concentration could be retained very well than that of Co system.

The interlayer lithium ions can be reversibly deintercalated-intercalated during the charge-discharge processes. In this study, we estimated the lithium self-diffusion coefficient ( $D$ ) in  $\text{Li}_x\text{CoO}_2$  and  $\text{Li}_x\text{NiO}_2$  by MD simulations. The self-diffusion coefficients of lithium ions obtained from the gradient of the plot of mean-square displacements (MSD) against time are given in Table 1. It is known through experiments that the lithium chemical diffusion coefficient is  $10^{-8}$ - $10^{-9}$   $\text{cm}^2/\text{s}$ . The calculated average value of the lithium self-diffusion coefficient is  $10^{-9}$   $\text{cm}^2/\text{s}$ , which in qualitative terms, seems reasonable. The MD technique is useful for understanding the mechanistic details at the atomic level which is otherwise difficult from experimental studies. Analysis of the ion trajectories confirms the lithium ion motion in  $\text{Li}_x\text{CoO}_2$ . The trajectory plots of constituting atoms in  $\text{Li}_{0.5}\text{CoO}_2$  are shown in Figure 3. These plots are viewed from (001) plane. The circle in Figure 3 is the initial site of lithium in this calculation. The lithium ion diffusion process is as follows. First, the lithium ion present in an octahedral site migrates into the adjacent tetrahedral site. Next, it hops into a vacant octahedral site. The hopping of lithium ion directly into the neighboring vacant octahedral site has not been observed. Lithium undergoes diffusion by passing through the network of octahedral-tetrahedral, which corresponds to the migration pathway of lithium. We found the same trend for lithium ions self diffusion in  $\text{Li}_x\text{NiO}_2$ .

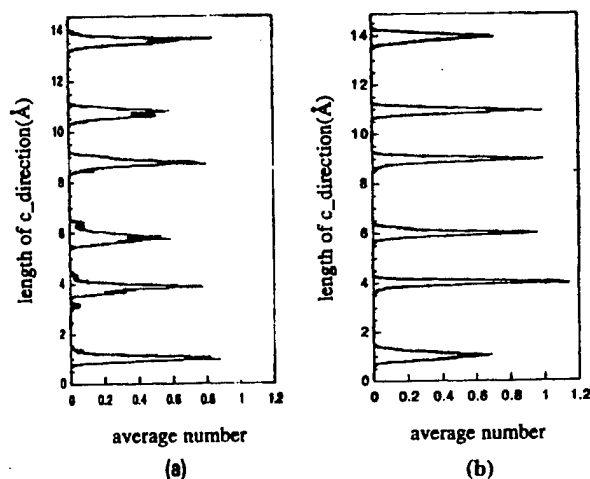


Figure 2 Distribution of O ions in (a)  $\text{Li}_{0.4}\text{CoO}_2$ , (b)  $\text{Li}_{0.4}\text{NiO}_2$

Table 1 Calculated self-diffusion coefficients ( $D$ ) of lithium ion in  $\text{Li}_x\text{CoO}_2$  and  $\text{Li}_x\text{NiO}_2$  at 300K.

	$D (\times 10^{-8} \text{cm}^2/\text{s})$	
	Co	Ni
$\text{Li}_{0.7}$	0.292	—
$\text{Li}_{0.6}$	0.597	0.934
$\text{Li}_{0.5}$	1.141	1.878
$\text{Li}_{0.4}$	0.928	0.989

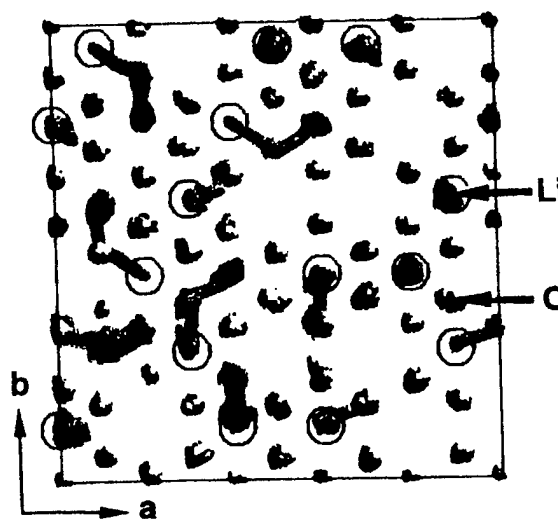


Figure 3 Trajectory plots in  $\text{Li}_{0.5}\text{CoO}_2$

# ANOMALY IN THE POTENTIAL-COMPOSITION PROFILE OF $\text{LiMn}_2\text{O}_4$ SPINEL AT LOW TEMPERATURE

Hironobu Abiko, Mitsuhiro Hibino and Tetsuichi Kudo  
Institute of Industrial Science, University of Tokyo

The spinel type  $\text{LiMn}_2\text{O}_4$  shows reversible intercalation of lithium, and it has attracted attention as a candidate for positive-electrode material for rechargeable lithium-ion batteries. The compound shows a characteristic potential-composition ( $\phi$ - $x$ ) profile having a steep voltage change at  $x=1/2$ . As we have reported [1], such a profile can be explained by a cooperative model based on the configuration entropy equivalent to Bethe's approximation or that analogous to the exact entropy of the one-dimensional lattice assuming the repulsion  $J$  between the nearest Li neighbors. Especially, the  $\phi$ - $x$  curve (for the disorder state) calculated on the latter entropy with  $J=48$  meV fits well the experimental curve at 298K in the single-phase region of the compound ( $0.4 < x < 1$ ). Recently, however, we found that a dramatic profile change, unexplainable with the model, took place near 278 K, when the initial composition of samples was close to stoichiometry [2]. Profiles at low temperature, showing a three plateau feature with two voltage steps in between at  $x=0.5$  and  $0.7$ , suggest that new phases are generated at the respective compositions. One of them at  $x=0.5$  may be attributed to the Li-ordered phase. However, assignment of the other is not so simple, because this manganese spinel undergoes a Jahn-Teller structural distortion in the same temperature region [3]. The purpose of the present study is to investigate the origin of a new phase at  $x=0.7$  in relation to the J-T structural transition.

Powder specimens of stoichiometric  $\text{LiMn}_2\text{O}_4$  were prepared by the solid state reaction. A mixture of  $\text{Li}_2\text{CO}_3$  and  $\text{MnCO}_3$  was sintered at  $750^\circ\text{C}$  in air for 72h after pre-sintering for 48 h at  $550^\circ\text{C}$ . Then it was quenched into liquid nitrogen. Non-stoichiometric samples (i.e., Li-excess  $\text{Li}_{1+y}\text{Mn}_2\text{O}_4$  ( $y=0-0.05$ ) and Li-deficient  $\text{Li}_{1-y}\text{Mn}_2\text{O}_4$  ( $0 < y' \leq 0.05$ ) were prepared in the same way. Powder X-ray diffraction confirmed that all specimens used were in a single cubic (Fd3m) phase. The lattice parameter of the stoichiometric sample was 0.8243 nm. As excess Li was increased, the parameter was decreased;  $a=0.8234$  for  $y=0.05$ . On the other hand, it was increased, as deficiency of Li was increased;  $a=0.8277$  for  $y'=0.05$ . This suggests an atomic arrangement such as  $\text{LiMn}_8\text{Mn}_2\text{O}_4$  ( $\delta=2y/(1-y')$ ) for Li-deficient samples.

The phase transition due to the J-T effect was monitored by the DSC technique. Measurements were performed at a rate of 5K/min for both heating and cooling process in the range between 203K and 343K. The results for some typical samples are shown in Figure 1. The curves for stoichiometric  $\text{LiMn}_2\text{O}_4$  (Figure 1a) show a clear peak both in the heating process and in cooling process. This suggests the existence of a first-order Jahn-Teller phase transition around 300K. In contrast, there is no peak in the curves for non-stoichiometric samples, as shown in Figure.1b for  $\text{Li}_{0.95}\text{Mn}_2\text{O}_4$  and Figure.1c for  $\text{Li}_{1.05}\text{Mn}_{1.95}\text{O}_4$ . Therefore these two samples are free from such a transition in the range 203-343 K. The limits for the samples to show the transition were  $y < 0.01$  (Li-excess side) and  $y' \leq 0.03$  (Li-deficient side).

The  $\phi$ - $x$  curves were recorded under a constant-current condition for the first charging (deintercalating) process, using a gas-tight three electrode cell. Specimen electrodes were prepared as follows; A powder mixture (7:3:0.5 in weight) of  $\text{LiMn}_2\text{O}_4$  (typically 70mg), acetylene black and Teflon was pressed into a disk (13mm diameter and 1mm thick) under light pressure (about 10kg/cm<sup>2</sup>). A 1M  $\text{LiClO}_4$ /propylene carbonate solution was used as electrolyte. To suppress polarization overpotential, we selected a small value of the current density of 0.43mA/g of  $\text{LiMn}_2\text{O}_4$ . The cell temperature was controlled within  $\pm 0.1^\circ\text{C}$  using a Peltier thermostatic bath.

The  $\phi$ - $x$  curves recorded for stoichiometric  $\text{LiMn}_2\text{O}_4$  at 298 and 273 K are shown in Figure 2a. The profile at 298 K is familiar for this compound, but that at 273 K is essentially different. The profile at 273K strongly suggests that four phases exist at low temperature; phase I ( $0.9 < x < 1$ ), phase II ( $x \approx 0.7$ ), phase III ( $x=0.5$ ) and phase IV ( $x < 0.2$ ). Each flat stage may be due to the two-phase coexistence of I - II,

II-III and III-IV. Phase IV may be accounted for as one of the cubic spinel phases coexisting continuously from room temperature. Phase III can be taken as the Li-ordered phase, because the host diamond-type 8a lattice has a commensurate ZnS-type arrangement at  $x=1/2$ . As for phase I and II, the situation is not so simple. If phase I is taken as a J-T distorted phase, it would be possible to take phase II as a cubic phase caused by the dilution effect of Li. However, this idea is not feasible, because a Li-deficient sample, remaining in a cubic phase in the relevant temperature region, shows the same anomaly as the stoichiometric one at low temperature, as shown in Figure 2b. This indicates that the origin of the anomalous  $\phi$ - $x$  profile of  $\text{LiMn}_2\text{O}_4$  at low temperature is not directly related to the Jahn-Teller structural transition. Presumably, a kind of ordering in the manganese lattice is responsible. Further study to make the origin of phase II clear is strongly needed.

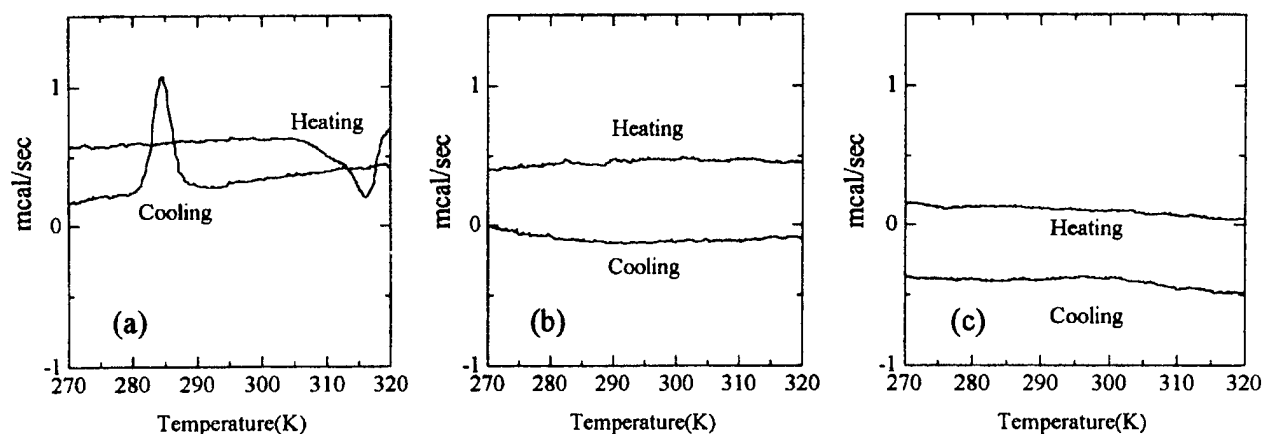


Figure 1. DSC curves for (a)  $\text{LiMn}_2\text{O}_4$  (b)  $\text{Li}_{0.95}\text{Mn}_2\text{O}_4$  (c)  $\text{Li}_{1.05}\text{Mn}_{1.95}\text{O}_4$

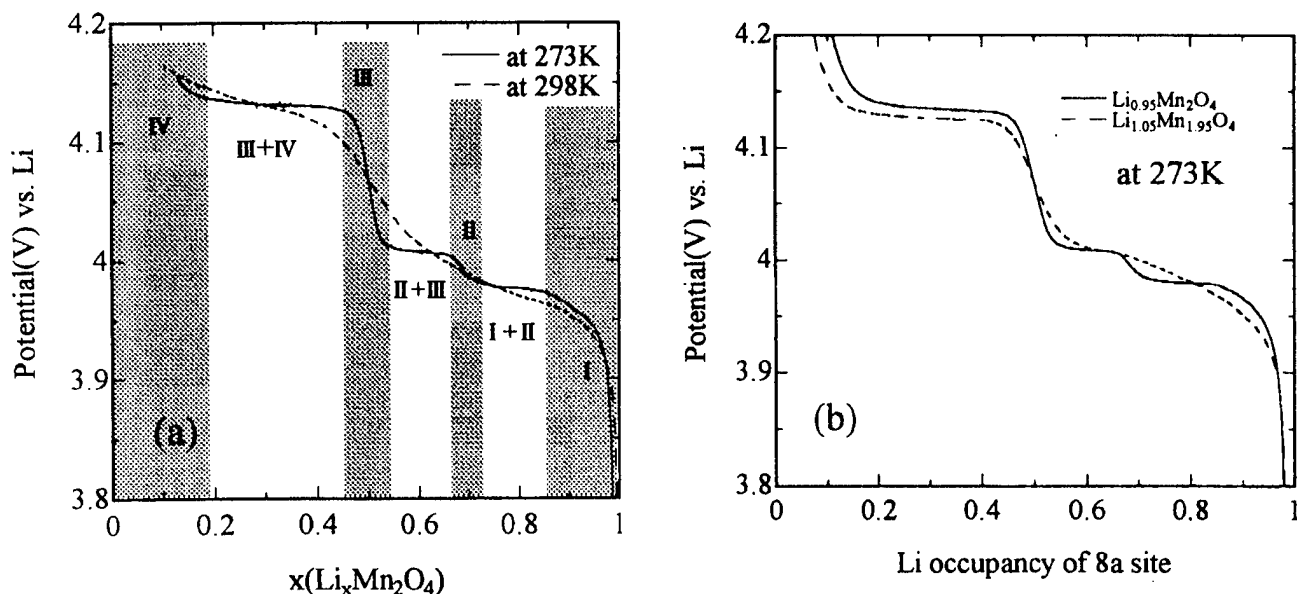


Figure 2. Potential-Composition curves of (a) stoichiometric  $\text{LiMn}_2\text{O}_4$  (b)  $\text{Li}_{0.95}\text{Mn}_2\text{O}_4$  and  $\text{Li}_{1.05}\text{Mn}_{1.95}\text{O}_4$

#### References

- [1] T.Kudo and M.Hibino, *Electrochimica Acta*, **43**, 781-789 (1998)
- [2] H.Abiko, M.Hibino and T.Kudo, *Electrochemical and Solid-State Letters*, **1**, (3), 114-116 (1998)
- [3] A.Yamada and M.Tanaka, *Materials Research Bulletin*, **30**, 715-721 (1996)

PERIODIC DENSITY FUNCTIONAL STUDY ON  $\text{LiCoO}_2$  AND  $\text{LiNiO}_2$ 

Ken Suzuki, Yasuto Yokoi, Takayuki Onozu, Yasunori Oumi, Seiichi Takami,  
Momoji Kubo and Akira Miyamoto

Department of Materials Chemistry, Graduate School of Engineering, Tohoku University  
Aoba 07, Sendai 980-8579, Japan.

Masahiro Kikuchi, Nobuyuki Yamazaki, and Muneo Mita  
Nippon Chemical Industrial. Co., Ltd, Koto-ku, Tokyo 136-0071, Japan.

Lithium secondary batteries have numerous applications in portable electric devices because of their high energy density, long cycle life, low self-discharge rates and high operating voltage. Lithium secondary batteries use lithium transitional-metal oxides such as  $\text{LiCoO}_2$ ,  $\text{LiNiO}_2$  and  $\text{LiMn}_2\text{O}_4$  as the positive electrode cathode. In commercially available lithium secondary batteries,  $\text{LiCoO}_2$  is now used because it is easier to prepare and it gives higher voltage in comparison to other probable cathode material candidates. However, there are some limitations of  $\text{LiCoO}_2$ , for example, in spite of the theoretical capacity of  $\text{LiCoO}_2$ , which is 274 mAh/g, the rechargeable capacity is limited to 140 mAh/g. Furthermore,  $\text{LiNiO}_2$ ,  $\text{LiMn}_2\text{O}_4$  and other cathode materials also have some limitations respectively in terms of capacity, rechargeability and so on. This shows that presently available cathode materials can by no means be regarded as the best. Under these circumstances, it is necessary to develop new materials in order to improve the cell performance, therefore possible candidate cathode materials have been well investigated. In addition to experimental studies, theoretical studies are also required to design better materials for lithium secondary batteries. Since first principles quantum chemistry can predict physical and chemical properties of solids, we should make attempts to use this tool for designing favorable new electrode materials, and also can avoid needless experimentation. In this study, we have performed periodic density functional calculations to investigate the atomic and electronic structural features of  $\text{LiCoO}_2$  and  $\text{LiNiO}_2$ .

Quantum chemical calculations based on the periodic density functional method were performed with the CASTEP program package (from MSI) which uses a conjugated gradient technique in a direct minimization of the Kohn-Sham energy functional and pseudopotentials to represent core electrons. By using this program, we can calculate the three-dimensional bulk structure, by locating its replicas around a unit cell. Basis sets are plane-wave functions. These calculations were performed at two levels of the approximations for the exchange-correlation potentials within density functional theory. For the single self-consistent field (SCF) energy calculations and geometry optimizations we applied local spin density approximation (LSDA). In order to calculate more accurate energy difference values we employed the generalized gradient approximation functional for the optimized geometries obtained from local level calculations. We

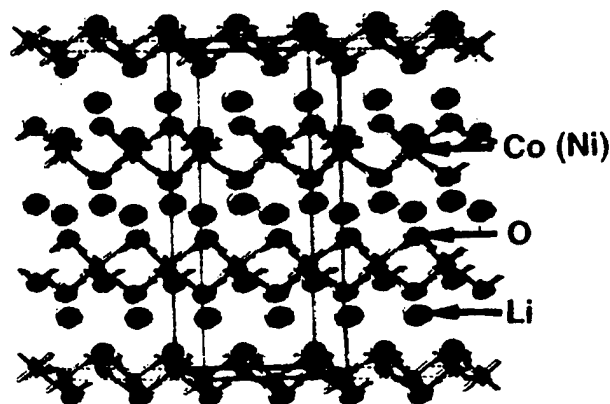


Figure 1  $\text{LiCoO}_2$  ( $\text{LiNiO}_2$ ) unit cell for DF calculations

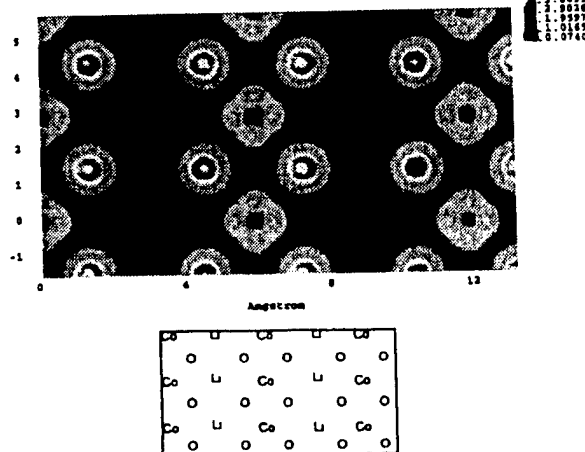


Figure 2 Charge Density of  $\text{LiCoO}_2$

used plane-wave cutoff energy of 900 eV. The unit cell contains 24 atoms, six Li, six Co (Ni) and 12 oxygen atoms (Figure 1).

Figure 2 shows the charge density of  $\text{LiCoO}_2$ . These plots reveal that lithium has no charge in contrast to oxygen and cobalt. As the pseudopotential concept allows only valence electrons to be considered in the calculations, no charge density in lithium means that the lithium remains in +1 ionic state. We found the same trend for lithium ionic state in  $\text{LiNiO}_2$ .

It is known that the local distortion of the  $\text{NiO}_6$  octahedron with four short Ni-O distances and two long ones results from the Jahn-Teller effect of the trivalent nickel ion in the low spin state  $t_2^6 e^1$ . The calculated Ni-O bond lengths show two values, short distances are 1.93 Å on average and long ones are 2.12 Å which are in good agreement with experimental values[1]. In contrast to  $\text{LiNiO}_2$ , the calculated Co-O bond lengths in  $\text{LiCoO}_2$  has only one value (1.97 Å) as the trivalent cobalt ion is in the low spin state  $t_2^6$ .

Since the interlayer lithium ions can be reversibly deintercalated-intercalated during the charge-discharge processes and trivalent Co and Ni are oxidized to tetravalent one when lithium is removed from  $\text{LiCoO}_2$  and  $\text{LiNiO}_2$  respectively, it is important to investigate the atomic and electronic structural features of  $\text{Li}_x\text{CoO}_2$  and  $\text{Li}_x\text{NiO}_2$  ( $x < 1$ ). In  $\text{LiCoO}_2$  and  $\text{LiNiO}_2$ , the oxygen atoms reside in sites with three lithium neighbors, but the number of lithium neighbored oxygen in  $\text{Li}_x\text{CoO}_2$  and  $\text{Li}_x\text{NiO}_2$  is less than three. In both  $\text{Li}_x\text{CoO}_2$  and  $\text{Li}_x\text{NiO}_2$ , we found that between Co(Ni) and O with no lithium neighbors, the distances were shorter than that of  $\text{LiCo(Ni)O}_2$  regardless of the state of Co and Ni as trivalent or tetravalent. Moreover, it was found that  $\text{Li}_x\text{NiO}_2$  has the difference between trivalent Ni-O distances and tetravalent Ni-O ones were shorter than trivalent Ni-O length. On the other hand, we could not observe the clear difference between trivalent and tetravalent Co-O distances in  $\text{Li}_x\text{CoO}_2$ . The density of state (DOS) on  $\text{LiCoO}_2$ ,  $\text{Li}_{0.67}\text{CoO}_2$  and  $\text{CoO}_2$  are presented in Figure 3 (a), (b) and (c) respectively, and highest occupied molecular orbital (HOMO) in  $\text{LiCoO}_2$  is shown in figure 4. When the  $\text{Li}^+$  ion is removed from the host material, an electron is also removed from the topmost occupied state (Co 3d) of the host. Thus, as lithium is deintercalated, the Fermi level moves down. We also want to try to characterize the surface of  $\text{LiCoO}_2$  and  $\text{LiNiO}_2$ .

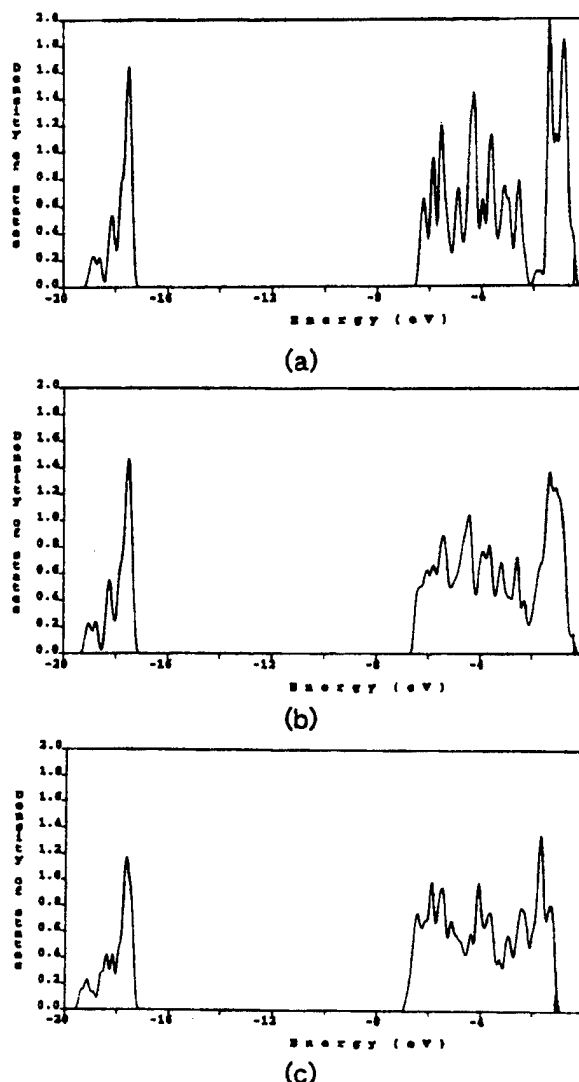


Figure 3 DOS (Density of State) Of  
(a)  $\text{LiCoO}_2$ , (b)  $\text{Li}_{0.67}\text{CoO}_2$ , (c)  $\text{CoO}_2$

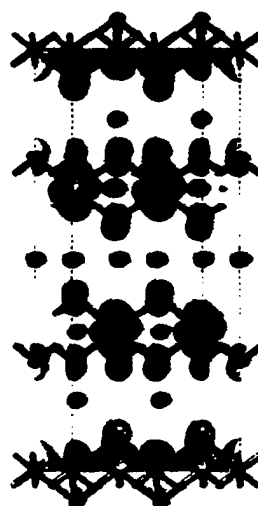


Figure 4 HOMO of  $\text{LiCoO}_2$

[1] A. Rougier, C. Delmas, A. V. Chadwick. Solid State Commun. 94, 123 (1995).

## ELECTROCHEMICAL PERFORMANCES OF LAYERED $\text{LiM}_{1-y}\text{M}'_y\text{O}_2$ ( $\text{M}=\text{Ni, Co}$ ; $\text{M}'=\text{Mg, Al, B}$ ) OXIDES IN LITHIUM BATTERIES

G.A. Nazri<sup>1)</sup>, A. Rougier<sup>2)</sup> and C. Julien<sup>3)</sup>

<sup>1)</sup>General Motors R & D Center, Physics and Physical-Chemistry Department  
30500 Mound Road, Warren, Michigan 48090, USA

<sup>2)</sup>Laboratoire de Reactivite et Chimie des Solides, Université Jules Verne  
33 rue Saint-Leu, 80033 Amiens cedex, France

<sup>3)</sup>Laboratoire des Milieux Désordonnés et Hétérogènes, UMR 7603, Case 86,  
Université Pierre et Marie Curie, 4 place Jussieu, 75252 Paris cedex 05, France

Advanced rechargeable lithium batteries are currently using an intercalation compound as the positive electrode, which consists in an oxide of a first-row transition metal. Because their good electrochemical performances, layered oxides  $\text{LiMO}_2$  ( $\text{M}=\text{Ni, Co}$ ) are considered as the prototype materials in the first commercial lithium-ion products. Recently, alternative materials have been proposed due to several advantages in comparison with  $\text{LiCoO}_2$  and  $\text{LiNiO}_2$  [1]. Structural and electrochemical properties of  $\text{LiNi}_{1-y}\text{Co}_y\text{O}_2$  solid solution and sp-element doped  $\text{LiMO}_2$  materials have been studied [2-3]. Exhibiting a lower potential, the  $\text{LiNi}_{1-y}\text{Co}_y\text{O}_2$  oxides are less active for an organic electrolyte oxidation and prevent the nickel dioxide formation which occurs with an associated exothermic reaction.

In the present paper, we report on the study of substituted layered oxides  $\text{LiM}_{1-y}\text{M}'_y\text{O}_2$  ( $\text{M}'=\text{Mg, Al, B}$ ) as cathode materials in lithium batteries. These materials have been made through solid state reaction of precursors in an oxygen rich atmosphere. The structure and morphology of  $\text{LiM}_{1-y}\text{M}'_y\text{O}_2$  powders were investigated using x-ray diffraction and scanning electron microscopy. X-ray analysis was performed by Rietveld refinement. Local structure and cationic environment have been investigated using Fourier transform infrared spectroscopy.

X-ray data and Rietveld refinement of  $\text{LiM}_{1-y}\text{M}'_y\text{O}_2$  oxides have shown that single phase impurity free can be made through careful selection of precursors. The layered structure of these materials is preserved upon considerable substitution, except for the boron-substituted compounds, for which residual impurity phases were observed due to a more glassy nature of the products.

FTIR measurements of  $\text{LiM}_{1-y}\text{M}'_y\text{O}_2$  oxides confirm their x-ray patterns. The IR spectra indicate formation of compressed  $\text{CoO}_6$  and  $\text{NiO}_6$ , and  $\text{LiO}_6$  elongated octahedra. Upon sp element substitution, the vibrational mode of  $\text{LiO}_6$  units observed in the far-infrared region remains quite stable. This result shows that the local environment of lithium ions surrounded by oxygen anions is not affected by doping.

Electrochemical measurements were carried out in cells using a 1M  $\text{LiPF}_6$  in EC-DMC (65/35 mole ratio) electrolyte at ambient temperature. The voltage profiles of the layered oxides and substituted oxides were monitored against lithium electrode. Substitution of Al and B in the

layered oxide, raised the voltage plateau by about 200 mV. The open circuit voltages of the cathode materials clearly indicate higher voltages for the Al and B substituted oxides. The higher voltage plateaus can be attributed to the bond competition between the transition metal and sp metals for oxygen.

The overall capacity of the oxides have been reduced due to the sp metal substitution, however, a more stable charge-discharge cycling performances have been observed when electrodes are charged to 4.3 volts as compared to the performances of the native oxides. In most cases, less than 20% capacity fading was observed at the end of 300 deep charge-discharge cycles performed between 2.8 and 4.3 volts. The capacity of the Li//LiNi<sub>1-y</sub>Al<sub>y</sub>O<sub>2</sub> system changes almost linearly with respect to the Al content up to 25 atom%. This result indicates a solubility limit in the formation of solid solution between LiAlO<sub>2</sub> and LiNiO<sub>2</sub>. Boron doped LiCoO<sub>2</sub> also provide very low polarization during charge-discharge cycling, with capacity over 130 mAh/g when charged up to 4.3 V vs. Li/Li<sup>+</sup>. Specific capacities of the cathode materials were between 120 and 160 mAh/g depending on the amount of substitution.

#### References

- [1] T. Ohzuku, A. Ueda and M. Kouguchi, J. Electrochem. Soc. **142**, 4033 (1995).
- [2] I. Saadoune and C. Delmas, J. Mater. Chem. **6**, 193 (1996).
- [3] G.A. Nazri, A. Rougier and N. Kia, Mat. Res. Soc. Symp. Proc. **453**, 635 (1997)



## CRYSTAL STRUCTURE OF THE ORTHORHOMBIC FORM OF THE SPINEL $\text{LiMn}_2\text{O}_4$

G. Rousse<sup>†</sup>, C. Masquelier<sup>†</sup>, J. Rodríguez-Carvajal<sup>\*</sup> and M. Hervieu<sup>‡</sup>

<sup>†</sup> *Laboratoire de Chimie des Solides, Université Paris-Sud, 91405 Orsay Cedex, FRANCE*

<sup>\*</sup> *Laboratoire Léon Brillouin (CEA-CNRS), CEA/Saclay, 91191 Gif sur Yvette Cedex, FRANCE.*

<sup>‡</sup> *CRISMAT, ISMRA, 6 Bld du Maréchal Juin, 14050 Caen Cedex, FRANCE.*

Much attention is being paid to Li-Mn-O spinels for their potential use as positive electrodes in lithium rechargeable battery systems. As in the perovskite systems, the great ability of Mn to change its valence easily in  $\text{Li}_{1+x}\text{Mn}_{2-x}\text{O}_{4+x}$  is at the origin of most of the interesting physical properties of these materials.

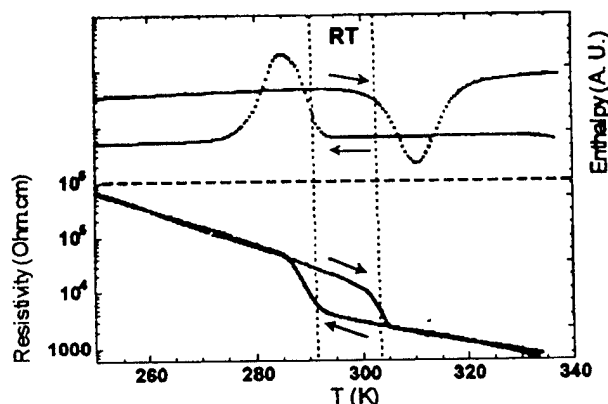


Figure 1 : DSC and resistivity data of stoichiometric  $\text{LiMn}_2\text{O}_4$ , recorded between 250K and 335K

Stoichiometric  $\text{LiMn}_2\text{O}_4$  (space group  $\text{Fd}\bar{3}\text{m}$ ,  $a=8.248(1)$  Å), prepared by solid-state reaction at 1073K from  $\text{Li}_2\text{CO}_3$  and  $\text{MnO}_2$ , undergoes a phase transition from cubic to orthorhombic symmetry when cooled below 290K. DSC, conductivity and specific heat measurements demonstrate that this is originated by a first-order transition with an hysteresis of 10K (figure 1) [1,2,3]. This was, up to now, attributed to a Jahn-Teller effect on  $\text{Mn}^{3+}$  ions resulting in the coexistence of a cubic and a tetragonal phase [1].

We performed electron, X-ray and neutron diffraction at many temperatures, below and above the transition. Electron diffraction clearly shows that the transition is associated with the appearance of a unique phase of orthorhombic symmetry [4,5,6] and with extra reflections characteristic of a superstructure with a tripled periodicity on [100] and [010] (figure 2). All the X-ray and neutron diffraction reflections can be indexed using a  $a=24.7435(5)$ ,  $b=24.8402(5)$  and  $c=8.1989(1)$  Å unit cell in the space group  $\text{Fddd}$  (Figure 3) [7,8]. The crystal structure was entirely determined by Rietveld refinements from the neutron diffraction pattern recorded at 230K ( $\lambda=1.2253$  Å).

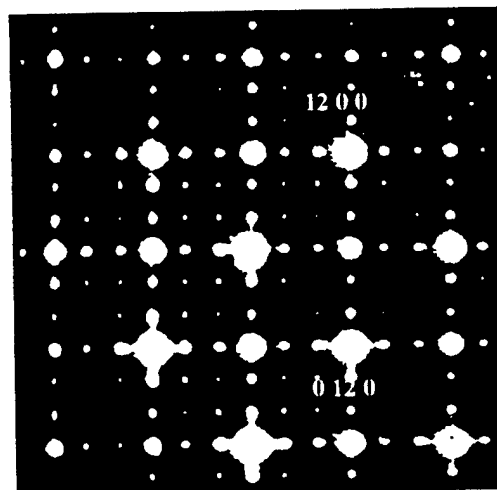


Figure 2 : Electron diffraction pattern along [001] of the low temperature phase of  $\text{LiMn}_2\text{O}_4$ .

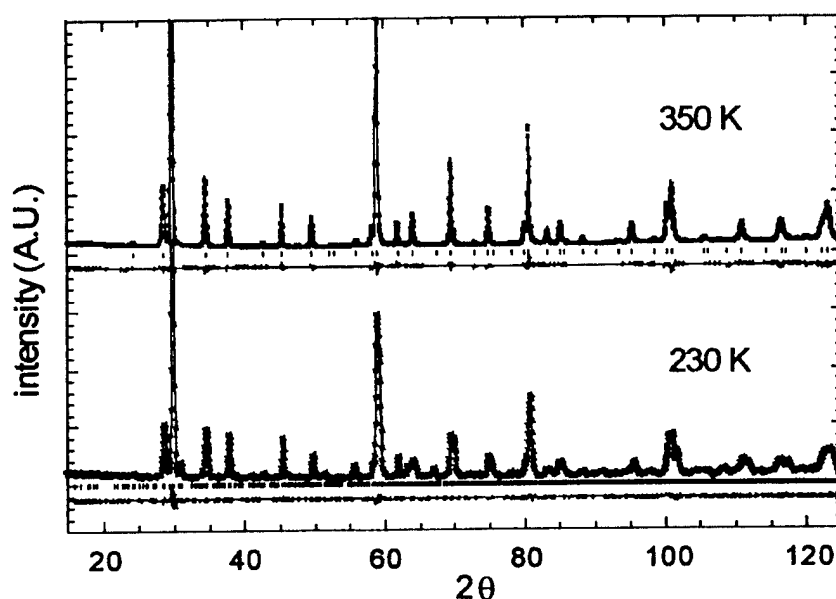


Figure 3 : Details of the observed and calculated neutron diffraction patterns ( $\lambda=1.2253 \text{ \AA}$ ) of the high temperature form (350K), and of the low temperature form (230K) of  $\text{LiMn}_2\text{O}_4$ .

Bond-Strength analysis indicates that this transition is associated with a charge ordering on the manganese sites. Two of the five sites of manganese are close to  $\text{Mn}^{4+}$  ions, the three others

are close to  $\text{Mn}^{3+}$  ions. The low-valence manganese ions are distributed along two types of columns running along  $[001]$ , which are surrounded by  $\text{Mn}^{4+}$  (figure 4).

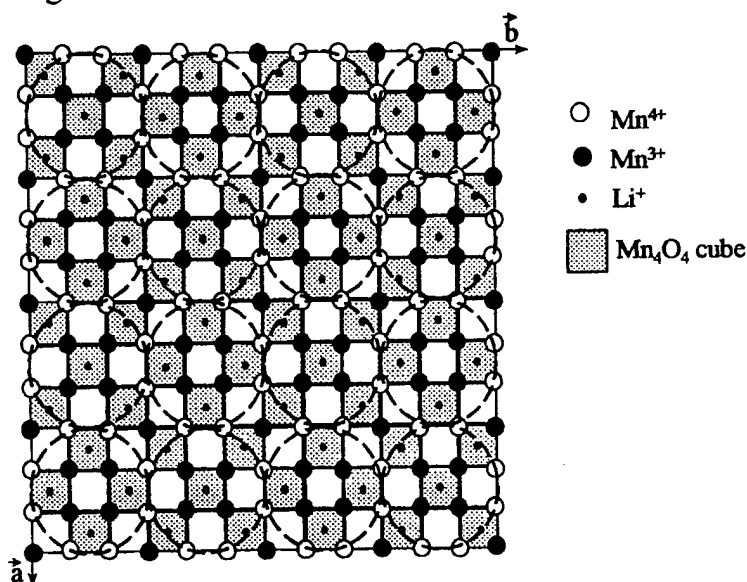


Figure 4 : Schematic projection of the superstructure of  $\text{LiMn}_2\text{O}_4$  along  $[001]$ . Only the lithium (x) and the  $\text{Mn}^{3+}$ -type sites are represented.

The charge ordering is not complete, and electron hopping persists in the LT phase, as demonstrated by only a minor change in the activation energies for electronic conduction below and above the transition [8].

- [1] A. Yamada, K. Miura, K. Hinokuma, and M. Tanaka, *J. Electrochem. Soc.*, **142**, 2149 (1995).
- [2] V. Massarotti, D. Capsoni, M. Bini, G. Chiodelli, C. B. Azzoni, M. C. Mozzati, and A. Paleari, *J. Solid State Chem.* **131**, 94 (1997).
- [3] Y. Shimakawa, T. Numata, and J. Tabuchi, *J. Solid State Chem.* **131**, 138 (1997).
- [4] J. Tabuchi, T. Numata, Y. Shimakawa, and M. Shirakata, *Mat. Res. Soc. Symp. Proc.* **496**, 287, (1997).
- [5] H. Hayakawa, T. Takada, H. Enoki, E. Akiba, *J. Mater. Sc. Letters* **17**, 811 (1998).
- [6] K. Oikawa, T. Kamiyama, F. Izumi, B. Chakoumakos, H. Ituka, M. Wakihara, J. Li, and Y. Matsui, *Solid State Ionics* **109**, Issue 1-2, 35 (1998).
- [7] G. Rousse, J. Rodriguez-Carvajal., C. Masquelier, and M. Hervieu., *Electrochem. and Solid State Letters*, **2**, 1,6 (1999).
- [8] J. Rodriguez Carvajal., G. Rousse, C. Masquelier, and M. Hervieu, *Phys. Rev. Letters*, **81**, 4660 (1998).

## STRUCTURAL CHANGE OF $\text{LiMn}_2\text{O}_4$ ELECTRODE SYNTHESIZED BY THE EMULSION DRYING METHOD

Seung-Taek Myung and Hoon-Taek Chung  
Dept. of Ceramic Eng., Dongshin Univ., 252, Daeho-dong, Naju, Chonnam, 520-714,  
South Korea

### Introduction

In recent, as portable communication is developing, demands for the lithium ion battery as portable energy source increase drastically.  $\text{LiMn}_2\text{O}_4$  is one of the most promising cathode materials for use in lithium ion batteries because of low cost and environmental problems. Unfortunately, it exhibits significant capacity fading with cycling[1].

Synthesizing  $\text{LiMn}_2\text{O}_4$  powder using solution method, because lithium and manganese mixed in nanoscale and nucleation reaction initiated at room temperature, exhibited more homogeneous distribution, larger specific area and smaller particle size than using the solid state reaction method[2]. In the present work, we have adapted the emulsion drying method and its various modified forms. Using this method, it is possible to obtain high purity crystalline spinel phase  $\text{LiMn}_2\text{O}_4$  after burning out at temperature as low as 300°C for 15 minutes. Electrochemical study was also performed to show that the material prepared by the emulsion drying method appear to offer high quality performance and to understand for the structural stability with intercalation of  $\text{Li}^+$  and cycles.

### Experimental

Aqueous solution was prepared by dissolving  $\text{LiNO}_3$ (Kanto, 95%) and  $\text{Mn}(\text{NO}_3)_2 \cdot 6\text{H}_2\text{O}$ (Kanto, 98%) in distilled water with the mole ratio of  $\text{Li}:\text{Mn} = 1 : 2$ . Emulsifying agent named Tween #85(Polyoxyethylene Sorbitan Trioleate) was also mixed with kerosene. The aqueous solution fell into the oil mixture 4 or 5 droplets per second, and stirred over 1,000 rpm by the impeller to synthesize emulsion. As soon as the emulsion drops into the hot kerosene, water and kerosene contained in the emulsion distilled through the spiral type condenser, finally resultant powder precursor sank on the bottom of the glass bottle. The obtained powder precursor was heated in a steel tray to burn out the residual oil phase approximately 300°C for 15 minutes.

The electrochemical cell consisted of a  $\text{LiMn}_2\text{O}_4$ -based composite as the working electrode, Li metal as the counter electrode, and an electrolyte of 1M  $\text{LiPF}_6$  in EC(ethylene carbonate)-DEC(diethylene carbonate) solution. The cathode was a mixture of 93wt% of active material, 5wt% of carbon black(Vulcan XC-72) and 2wt% of PVDF(Polyvinylidene fluoride, Aldrich). XRD and SEM experiment with discharge were also performed to know the structural change at various cut-off voltage as a function of lithium content(SOC) and cycle. The electrochemical impedance measurements were carried out by applying AC-amplitude of 10mV<sub>rms</sub> on an equilibrium electrode potential of 2.9V to 4.4V<sub>Li/Li<sup>+</sup></sub>.

### Results and discussion

Fig.1 shows the XRD patterns for the sample calcined at various temperatures. All diffraction peaks were indexed by a cubic spinel structure and refined with a space group  $\text{Fd}3\text{m}$ . Cubic spinel phase was formed at low temperature as low as 300°C. Sample calcined at 850°C for 24 hours showed the highest intensity.

Fig. 2 depicts the initial charge and discharge curve of the half-cells of which base materials were calcined at 650°C, 750°C and 850°C for 24 hours. Initial discharge capacity was 109mAh/g, 108mAh/g and 118mAh/g, respectively. Their efficiency between charge and discharge was approximately 97%, implicating reversible electrode reaction.

To know the structural change of cathode in discharge, XRD experiment was also carried out as a function of lithium content(SOC) and cycle. It was illustrated in Fig. 3. When  $\delta$  is 0.3,

(400) peak split into two peaks irrespective of calcination temperature. As intercalation content of lithium increased, lattice parameter increased with increasing lithium content due to reduction of  $Mn^{4+}$  to  $Mn^{3+}$ . Notably, in the case of using  $LiMn_2O_4$  powders prepared by the emulsion drying method, spinel structure was continuously maintained after 20th cycling in the all samples.

Through SEM experiment, it was also found that particles were disrupted, and the degree of disruption was severe with cycles (Fig. 4). This reaction might cause the dissolution of  $Mn^{3+}$  into  $Mn^{2+}$  and  $Mn^{4+}$  into the electrolyte so that capacity loss might be occurred. Impedance study shows that  $R_{ab}$  increased with lithium content and cycle (Fig. 5). From these facts, it could be strongly suggested that the emulsion drying method is suitable to synthesize the  $LiMn_2O_4$  powder for lithium ion battery cathode material.

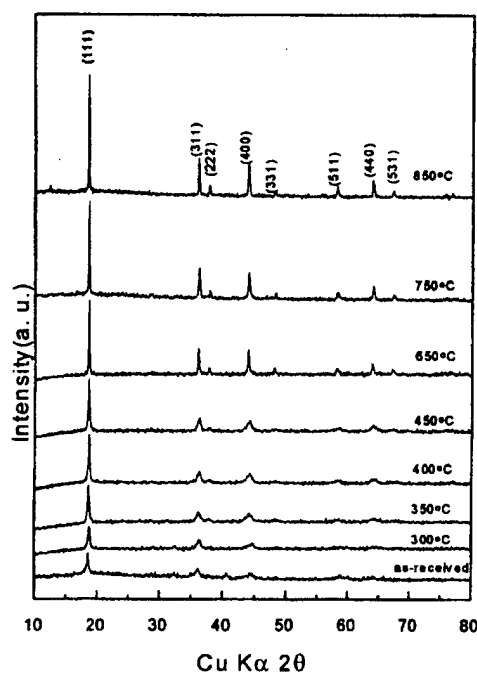


Fig. 1. XRD patterns for the samples calcined at various temperatures.

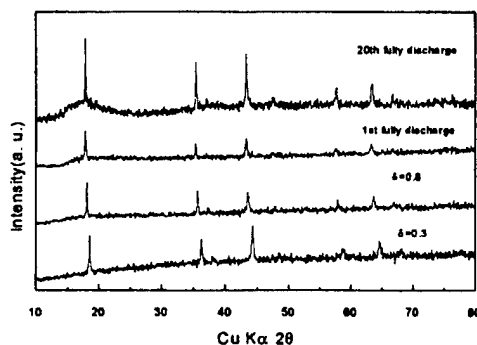


Fig. 3. XRD patterns of  $Li_{\delta}Mn_2O_4$  electrode.  $\delta$  is the amount of intercalated  $Li^+$  in state of charge. The base material was calcined at 850°C for 24 hours.

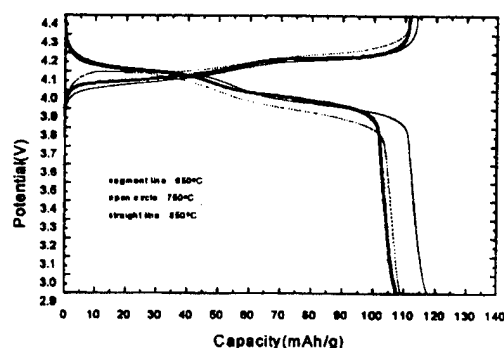


Fig. 2. Initial charge and discharge curves for the calcined samples.

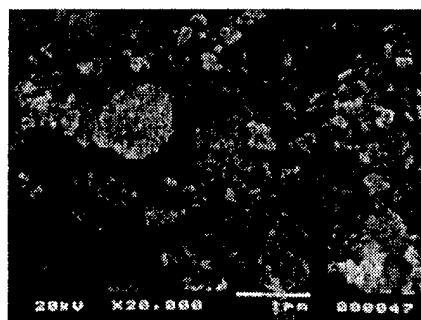


Fig. 4. SEM micrograph of the  $LiMn_2O_4$  calcined at 650°C after 20th discharge

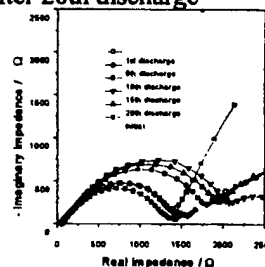


Fig. 5. Nyquist impedance plots of the half cell  $Li/1M LiPF_6$  EC-DEC solution/ $LiMn_2O_4$  electrode with cycle. Used powder calcined at 850°C.

- [1] J. M. Tarascon, E. Wang, F. K. Shokoohi, W. R. Mckinnon and S. Colson, J. Electrochem. Soc., Vol. 138, No. 10, pp. 2859-2864, 1991  
 [2] Z. Jiang and K. M. Abraham, J. Electrochem. Soc., Vol. 143, No. 5, pp. 1591-1598, 1996

## THE NOVEL SYNTHETIC ROUTE TO $\text{LiCo}_y\text{Ni}_{1-y}\text{O}_2$ AS A CATHODE MATERIAL IN LITHIUM SECONDARY BATTERIES

S.G. Kang, H. Rim, K.S. Ryu, and S.H. Chang

Electronics and Telecommunication Research Institute, Taejeon, 305-350, KOREA

$\text{LiCoO}_2$ ,  $\text{LiNiO}_2$ , and  $\text{LiCo}_y\text{Ni}_{1-y}\text{O}_2$  have been intensively studied as cathode active materials in lithium secondary batteries [1-5]. According to previous studies,  $\text{LiNiO}_2$  has been nonstoichiometric compound with the formula of  $[\text{Li}_{1-z}\text{Ni}^{2+}_z][\text{Ni}^{3+}\text{Ni}^{2+}_z]\text{O}_2$  ( $0 \leq z \leq 0.2$ ) depending on preparation conditions[3,6]. A small amount of structural disorder due to the displacement of nickel and lithium ions in  $\text{LiNiO}_2$  strongly affects the electrochemical properties such as the working voltage and rechargeable capacity. As the deintercalation reaction proceeds below  $x=0.5$  in  $\text{Li}_x\text{NiO}_2$ , some structural irreversible rearrangements occur, leading to irreversible electrochemical reactions[7].  $\text{LiCoO}_2$  is easily prepared and gives a high voltage and a good reversibility in  $\text{Li/LiMO}_2$  cells. Although the  $\text{LiCoO}_2$  does not have a structural disorder,  $\text{LiCoO}_2$  is expensive compare with others and has higher voltage(4 V) than  $\text{LiNiO}_2$  (3.5 ~4.0V) so that the oxidation of the nonaqueous electrolyte during prolonged cycling is occurred.

These considerations have led to the electrochemical studies of  $\text{LiCo}_y\text{Ni}_{1-y}\text{O}_2$  series. In this study, the structure and electrochemical properties of the  $\text{Li}_x\text{Co}_y\text{Ni}_{1-y}\text{O}_2$  ( $y=0.1, 0.3, 0.5, 0.7, 1.0$ ) system synthesized by solid state reaction with various starting materials have been investigated in order to optimize the characteristics and synthetic conditions of the  $\text{Li}_x\text{Co}_y\text{Ni}_{1-y}\text{O}_2$ .

The  $\text{Li}_x\text{Co}_y\text{Ni}_{1-y}\text{O}_2$  compounds were prepared by conventional solid state reactions. The starting materials are  $\text{LiOH}$ ,  $\text{Li}_2\text{CO}_3$ ,  $\text{NiO}$ ,  $\text{NiCO}_3$ ,  $\text{Co}_3\text{O}_4$ ,  $\text{CoCO}_3$ . The  $\text{Li}_x\text{Co}_y\text{Ni}_{1-y}\text{O}_2$  compounds consist of heating a mixture of starting materials (ex.  $\text{LiOH}$ ,  $\text{NiO}$ , and  $\text{Co}_3\text{O}_4$ ) in appropriate ratio, at 700 ~ 900°C for 40hrs with intermittent grinding in air after preheating 600°C for 20hrs, in air.

The X-ray diffraction patterns for the  $\text{Li}_x\text{Co}_y\text{Ni}_{1-y}\text{O}_2$  have been indexed hexagonal symmetry ( $R\bar{3}m$ ). The cell parameters have been calculated by indexing the peaks with a hexagonal cell. The  $a$  and  $c$  parameters, related to the intralayer metal-metal distance and interslab distance respectively, decreases with increasing cobalt content ( $y$ ) due to the difference in size between the trivalent cobalt ( $r(\text{Co}^{3+}) = 0.53 \text{ \AA}$ , low spin ( $t_{2g}^6 e_g^0$ )) and nickel ( $r(\text{Ni}^{3+}) = 0.56 \text{ \AA}$ , low spin ( $t_{2g}^6 e_g^1$ )) ions. The  $c/a$  ratio, indicating the structural anisotropy of the compounds, increase when  $\text{Co}^{3+}$  is substituted for nickel ( $c/a = 2\sqrt{6}$  for a cubic lattice). This variation indicates that the 2D character is increased with substituting cobalt for nickel ions. The results of structural analysis for the  $\text{Li}_x\text{Co}_y\text{Ni}_{1-y}\text{O}_2$  are similar regardless of synthetic conditions.

According to the scanning electron microscopy of the  $\text{Li}_x\text{Co}_y\text{Ni}_{1-y}\text{O}_2$ , particle sizes of  $\text{Li}_x\text{Co}_y\text{Ni}_{1-y}\text{O}_2$  compounds were less than 5 $\mu\text{m}$ . The SEM image shows the particle size of  $\text{Li}_x\text{Co}_y\text{Ni}_{1-y}\text{O}_2$  decreases with increasing the cobalt concentration ( $y$ ). However, the particle size increases with increasing the synthetic temperature.

The electrochemical cell was fabricated as follows. A cathode was made 89% (wt. %)  $\text{Li}_x\text{Co}_y\text{Ni}_{1-y}\text{O}_2$ , 10% acetylene black, and 1% PTFE binder. The electrolyte used was 1M  $\text{LiPF}_6$  in ethylene carbonate (EC): diethyl carbonate (DEC) (1:1) solution. A lithium metal anode was used in this study. Test cells were assembled in a glove box filled with argon. The cells were cycled in the voltage range 3.2 ~ 4.3V with current density of 200 $\mu\text{A}/\text{cm}^2$  using galvanostatic charge/discharge cycle tester. The first discharge capacities of  $\text{Li}_x\text{Co}_y\text{Ni}_{1-y}\text{O}_2$  are 60mAh/g ~ 180 mAh/g with synthetic conditions. The differences in intercalation rate of the  $\text{Li}_x\text{Co}_y\text{Ni}_{1-y}\text{O}_2$

in first charge/discharge cycle increase with cobalt content (y). The first discharge capacity of  $\text{Li}_x\text{Co}_y\text{Ni}_{1-y}\text{O}_2$  increase with increasing the cobalt concentration. On the contrary, the drastic decrease of capacities was observed during prolonged cycle when the cobalt ion was substituted for nickel ion. The charge/discharge behavior of the  $\text{Li}_x\text{Co}_y\text{Ni}_{1-y}\text{O}_2$  compounds show that the best cycling properties were observed in the  $\text{Li}/\text{Li}_x\text{Co}_{0.3}\text{Ni}_{0.7}\text{O}_2$  cells. This behavior means that any structural disorder due to the displacement of nickel (and/or cobalt) and lithium ions in the  $\text{Li}_x\text{Co}_{0.3}\text{Ni}_{0.7}\text{O}_2$  are not appeared.

The structure and the electrochemical properties of the  $\text{Li}_x\text{Co}_y\text{Ni}_{1-y}\text{O}_2$  are prepared by various synthetic conditions were investigated. Among them,  $\text{Li}_x\text{Co}_{0.3}\text{Ni}_{0.7}\text{O}_2$ , which is prepared with  $\text{LiOH}$ ,  $\text{NiO}$ , and  $\text{Co}_3\text{CO}_4$  at  $850^\circ\text{C}$ , has the best electrochemical properties. The first discharge capacity of the compound is 180 mAh/g. In this study, we will be discussed about the correlation of the electrochemical properties and the synthetic condition for the  $\text{Li}_x\text{Co}_y\text{Ni}_{1-y}\text{O}_2$  compounds.

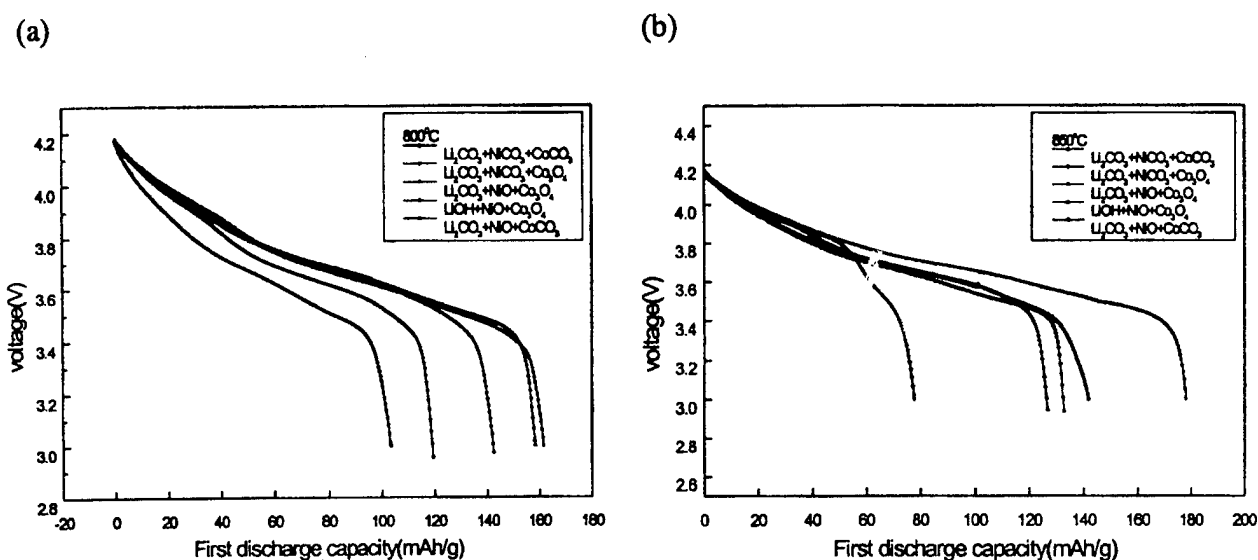


Fig. 1. First discharge capacities of  $\text{Li}/\text{Li}_x\text{Co}_{0.3}\text{Ni}_{0.7}\text{O}_2$  with synthetic conditions (a)  $800^\circ\text{C}$ , (b)  $850^\circ\text{C}$ .

## REFERENCES

- [1] K. Mizushima, P.C. Jones, P.J. Wiseman, J.B. Goodenough, *Mat. Res. Bull.*, 15, (1980), 783.
- [2] J.R. Dahn, J.N. Reimers, U. von Sacken, *J. Electrochem Soc.*, 140, (1992), 2752.
- [3] A. Rougier, C. Delmas, and A.V. Chadwick, *Solid State Comm.*, 94, (1995), 123.
- [4] S.H. Chang, S.G. Kang and K.H. Jang, *Bull. Kor. Chem. Soc.*, 18, (1997), 61.
- [5] S.G. Kang, S.Y. Kang, K.S. Ryu, and S.H. Chang, 11<sup>th</sup> Int'l Conf. on Solid State Ionics, Honolulu, 1997, p3.
- [6] E. Zhecheva, and R. Stoyanova, *Solid State Ionics* 66, (1993), 143.
- [7] J. Morales, C. Perez-Vicente, J.L. Tirado, *Mat. Res. Bull.* 25,(1990), 623.

# THE STANDARD GIBBS FREE ENERGY OF FORMATION OF LiCoO<sub>2</sub>

Kenichi Kawamura, Shirou Nagano, Yutaka Nigara, Atsushi Kaimai,  
Tatsuya Kawada and Junichiro Mizusaki  
Research Institute for Scientific Measurement, Tohoku University, 2-1-1 Katahira,  
Aoba-ku, Sendai 980-8577, JAPAN.

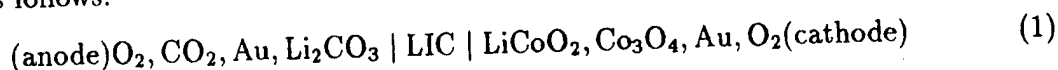
## 1 INTRODUCTION

Many researchers investigate cathode materials, such as LiCoO<sub>2</sub> and LiMn<sub>2</sub>O<sub>4</sub>, for a lithium second battery. To keep a constant output voltage, the cathode material should be stable thermodynamically. When we have thermodynamic data, we can estimate the phase stability. However, there is few thermodynamic data in thermodynamic data tables [1, 2, 3, 4].

Moreover, double oxide composed by lithium and transition metal is considered as candidate of reference material for CO<sub>2</sub> gas sensor with lithium ion conductor as a electrolyte [5]. In the present study, to determine standard Gibbs free energy of formation of LiCoO<sub>2</sub>, the lithium activity equilibrated between LiCoO<sub>2</sub> and Co<sub>3</sub>O<sub>4</sub> is measured by using a solid-state electrochemical cell at high temperature.

## 2 EXPERIMENTAL

The lithium concentration cells with Li ion conductor (LIC) as electrolyte was constructed as follows:



where LIC was Li glass composed of Li<sub>2</sub>O, TiO<sub>2</sub>, P<sub>2</sub>O<sub>5</sub> and Al<sub>2</sub>O<sub>3</sub> [7]. Separation between anode and cathode atmospheres was obtained by Ag seal. Premixed gas, N<sub>2</sub>-21%O<sub>2</sub>-1%CO<sub>2</sub>, was flowed on anode at which lithium activity was determined by the equilibrium between Li<sub>2</sub>CO<sub>3</sub>-O<sub>2</sub>-CO<sub>2</sub>. The anode was worked as a reference electrode. The oxygen partial pressure at cathode was controlled by gas mixture of N<sub>2</sub>-21 ~ 0.1%O<sub>2</sub>.

The electromotive force (emf) were measured using an electrometer with an input impedance of 10<sup>12</sup> Ω at 723 ~ 823 K.

## 3 RESULTS AND DISCUSSION

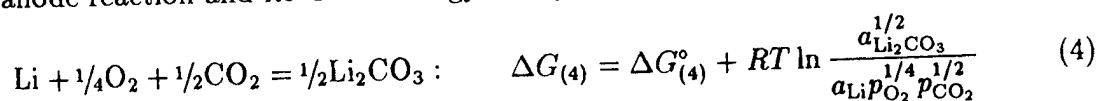
Figure 1 shows the emf as a function of temperature. The least squares fits give the emf,  $E$ , in the following expression.

$$E/\text{mV} = 288 \pm 2 - 0.672T \quad (723 \sim 823 \text{ K}) \quad (2)$$

The emf is related to the lithium activities,  $a_{\text{Li}}$ , as follows.

$$E = \frac{RT}{F} \ln \frac{a_{\text{Li}}^{\text{cathode}}}{a_{\text{Li}}^{\text{anode}}} \quad (3)$$

The anode reaction and its Gibbs energy change are represented by



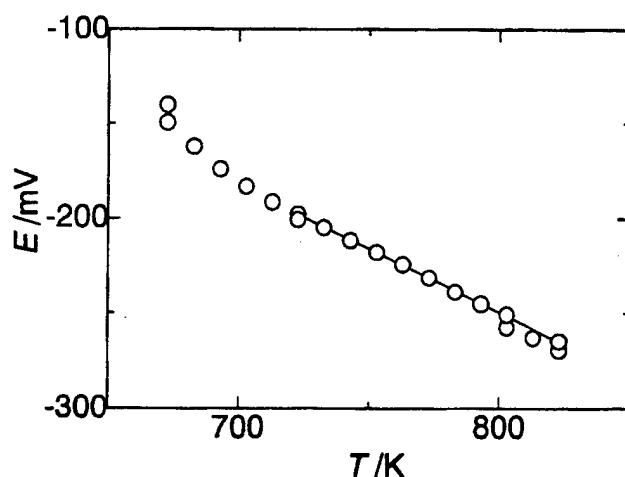
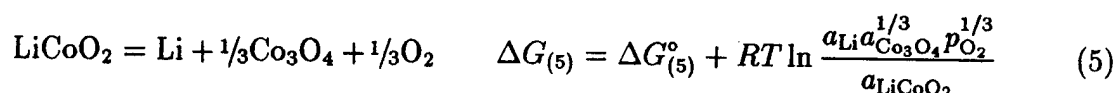


Figure 1: Emf of the cell as a function of temperature.

where  $\Delta G_{(4)}^\circ$  is the standard Gibbs free energy change of the reaction (4) and can be calculated by using values in thermodynamic table [4]. When the anode was at equilibrium,  $\Delta G_{(4)}$  was equal to zero. Since  $p_{O_2}$  and  $p_{CO_2}$  was fixed by gas supply and  $a_{Li_2CO_3}$  was equal to unity, we can calculate  $a_{Li}$  at anode. Using calculated  $a_{Li}^{anode}$ , obtained  $E$  and eq. 3,  $a_{Li}^{cathode}$  can be determined.

The cathode reaction of the cell and its Gibbs energy change are represented by



Using the condition,  $\Delta G_{(5)} = 0$ ,  $a_{Co_3O_4} = 1$ ,  $p_{O_2} = 0.21$  and determined  $a_{Li}^{cathode}$ , we can calculate  $\Delta G_{(5)}^\circ$ . From  $\Delta G_{(5)}^\circ$  and the standard Gibbs energy of formation of  $Co_3O_4$ , the standard Gibbs energy of formation of  $LiCoO_2$  [4] is obtained as

$$\Delta_f G^\circ(LiCoO_2)/kJmol^{-1} = (-674.4 \pm 2.5) + (0.221 \pm 0.003)T \quad (T = 723 \sim 823K) \quad (6)$$

At the meeting, the phase stability of Li-Co-O system will be added and discussed.

## REFERENCES

- [1] JANAF Thermochemical Tables Third Edition, ed. by M. W. Chase *et al.*, (American Chemical Society and the American Institute of Physics for the National Bureau of Standards, Michigan U.S.A., 1985)
- [2] I. Barin, *Thermochemical Data of Pure Substances*, (VCH Publishers, Weinheim, 1989)
- [3] *Thermochemical Properties of Inorganic Substances 2nd Edition*, ed. by O. Knacke *et al.*, (Verlag Stahleisen, Düsseldorf, 1991)
- [4] MALT2 Materials-oriented Little Thermodynamic Database, The Japan Society of Calorimetry and Thermal Analysis, (Kagaku Gijutsu Sha, Japan, 1992)
- [5] H. Narita, Y. C. Zhang, J. Mizusaki and H. Tagawa, *Solid State Ionics*, **79**, 349 (1995)
- [6] Y. C. Zhang, H. Narita, J. Mizusaki and H. Tagawa, *Electrochemical Society Proceedings*, **27**, 107 (1996)
- [7] J. Hu, *Solid State Ionics*, **96**, 195 (1997)



## HYDROTHERMAL PREPARATION, ELECTROCHEMICAL AND MAGNETIC PROPERTIES OF Fe DOPED LiCoO<sub>2</sub>

Mitsuharu Tabuchi, Hironori Kobayashi, Hikari Shigemura, Kazuaki Ado, Hiroyuki Kageyama, Hikari Sakaebe, Atsushi Hirano\*, Ryoji Kanno\*, Masayuki Wakita\*\*, and Saburo Nasu\*\*, (Osaka National Research Inst., 1-8-31 Midorigaoka, Ikeda, Osaka 563-8577, Japan, Kobe Univ.\*, Osaka Univ.\*\*)

### 1. Introduction

LiCoO<sub>2</sub> with a layered rock-salt ( $\alpha$ -NaFeO<sub>2</sub> type) structure is mainly used for the cathode materials for rechargeable lithium-ion battery. To improve its electrochemical property and decrease the cost of the cathode, Ni and other metals have been doped into LiCoO<sub>2</sub>. Fe doping is effective for above purposes and some groups have tried to prepare Fe doped LiCoO<sub>2</sub> by solid-state reaction above 500°C [1,2]. However LiFeO<sub>2</sub> with cubic NaCl type structure was easily formed at high temperature and could prevent the formation of homogeneous solid solution. In this work, hydrothermal method is used for preparation, because relatively higher solubility limit could be expected due to the low preparation temperature below 250°C.

### 2. Experimental

Fe doped LiCoO<sub>2</sub> was prepared by hydrothermal reaction from Co<sup>3+</sup>-Fe<sup>3+</sup> co-precipitates with different Fe content and LiOH·H<sub>2</sub>O at 220 or 300°C for 5-48h [3] (co-precipitation method). The co-precipitate was prepared by bubbling air through Co<sup>2+</sup>-Fe<sup>3+</sup> mixed hydroxides obtained by adding NaOH aq. solution to cobalt and iron nitrate one. LiCoO<sub>2</sub> was also obtained hydrothermally from Co(NO<sub>3</sub>)<sub>2</sub> aq. solution with the LiOH·H<sub>2</sub>O-NaOH-NaClO<sub>3</sub> or LiOH·H<sub>2</sub>O-KOH-KClO<sub>3</sub> mixture [3] (oxidation method). In these systems, NaClO<sub>3</sub> and KClO<sub>3</sub> act as oxidants. Residual salts and alkaline in the hydrothermally-obtained products were removed by washing with distilled water, filtration and drying processes.

The samples obtained were characterized by X-ray diffraction (XRD), chemical analysis, and Co-K XANES spectroscopy. Charge-discharge tests were performed using Li/1M LiClO<sub>4</sub> in EC+DMC/sample cells between 3.0 and 4.3V with a constant current density (0.5mA/cm<sup>2</sup>). Magnetic susceptibility was measured using SQUID and Faraday balance below 300K and <sup>57</sup>Fe Mössbauer spectra was measured at 300K.

### 3. Results and Discussion

All XRD patterns of Fe doped/undoped LiCoO<sub>2</sub> samples in Fig. 1 could be fitted by a single-phase model of rhombohedral unit-cell ( $R\bar{3}m$ ) with ideal cation

ordering. Both  $a$  and  $c$  axis parameters increased linearly with Fe content toward to those of  $\text{LiFeO}_2$  with layered rock-salt structure [4]. However, highly Fe doped sample ( $x=0.4$  in  $\text{LiFe}_x\text{Co}_{1-x}\text{O}_2$ ) is a mixture of rhombohedral and cubic rock-salt phases, indicating that Fe could be incorporated up to 0.25 into  $\text{LiCoO}_2$ . Cation content analysis indicates the formation of  $\text{LiFe}_x\text{Co}_{1-x}\text{O}_2$  solid solution. The value of solubility limit is higher than previous data (0.15, [2]). Large difference in XRD peak sharpness between two  $\text{LiCoO}_2$  samples reflects the degree of crystal growth, because  $\text{LiCoO}_2$  obtained by oxidation method has higher particle size ( $\approx 10\mu\text{m}$ ) than that obtained by co-precipitation one ( $< 1\mu\text{m}$ ).

Co K-XANES and  $^{57}\text{Fe}$  Mössbauer spectra for Fe doped samples indicate no detectable valence change of Co and Fe, compared to both end members, meaning that both cations could be regarded as trivalent state ( $S=0$  for Co,  $S=5/2$  for Fe).

Electrochemical test for  $\text{Li}/\text{LiFe}_x\text{Co}_{1-x}\text{O}_2$  cells reveals that initial charge and discharge capacities decrease with Fe content (discharge capacity; 107mAh/g for  $x=0.05$ , 83mAh/g for  $x=0.25$ ). The small spontaneous magnetization ( $0.2\mu_B$  per transition metal ion for  $x=0.16$  sample at 5K) was detected for all Fe doped samples below 40K.  $^{57}\text{Fe}$  Mössbauer spectra at 5K confirm the presence of magnetic ordering for these samples.

#### References

- [1] R. Alkántara et al., *Extended Abstracts of IMLB-9*, II-Thur52 (1998).
- [2] H.Sakaebe et al., *Extended Abstracts of IMLB-9*, II-Thur106 (1998).
- [3] M.Tabuchi et al., *J. Material Chemistry*, in press.
- [4] K.Ado et al., *J. Electrochem. Soc.*, **144** (1997) L177.

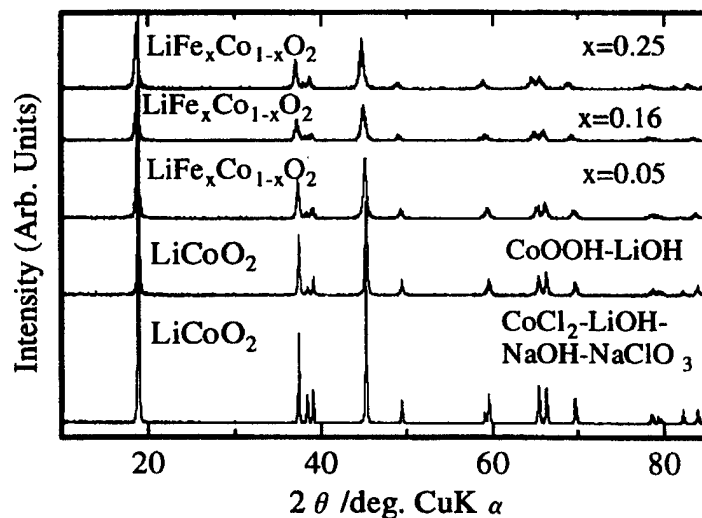


Fig. 1 XRD patterns of Fe doped/undoped  $\text{LiCoO}_2$  prepared by hydrothermal reaction at  $220^\circ\text{C}$ .

## SYNTHESIS AND STUDY OF $\text{LiMg}_x\text{Ga}_y\text{Ni}_{1-x-y}\text{O}_2$ AS CATHODE MATERIAL FOR LITHIUM ION BATTERIES

Aishui Yu<sup>1</sup>, G. V. Subba Rao<sup>1</sup> and B.V.R.Chowdari<sup>1,2</sup>

<sup>1</sup>Institute of Materials Research and Engineering, <sup>2</sup>Department of Physics,  
National University of Singapore, Singapore 119260.

$\text{LiNiO}_2$  has been studied extensively as cathode material for lithium ion batteries due to its low cost and relatively larger capacity compared with the first commercial material  $\text{LiCoO}_2$ . Substitution of a portion of Ni with other cations has been pursued to suppress the phase transformations (on charging) and, if possible, improve its safety characteristics. Recent work has shown that dopants like gallium or magnesium ( $\leq 5$  atom %) can suppress the phase transformations, and the 2 at. % doped Ga-compound exhibited capacity of 190 mAh/gm and no fading up to 100 cycles. In this work, we report on the synthesis, X-ray characterization and cathodic behaviour of co-doped  $\text{LiGa}_x\text{Mg}_y\text{Ni}_{1-x-y}\text{O}_2$ .

Compounds with  $x=0.02$  and  $y=0.03$  &  $0.05$  were prepared by the solution technique: Stoichiometric amounts of Li, Ga, Mg, Ni salts were dissolved in distilled water and then evaporated using a rotary evaporator. As the evaporation of water proceeded, the sol turned into a viscous gel. The gel precursors obtained were calcined at  $750^\circ\text{C}$  for 20h in a flowing oxygen atmosphere to obtain black, polycrystalline powders.

The XRD patterns of compounds showed the layered structure of the parent compound,  $\text{LiNiO}_2$ . No other peaks were observed, indicating the formation of pure phases. However, the (003) peak shifts to a larger  $2\theta$  value, indicating that the  $c$  lattice parameter decreases with an increase of the Mg content. Furthermore, the (108) and (110) peaks could be well resolved meaning that the compounds are well ordered. The electrochemical tests on the  $\text{LiGa}_x\text{Mg}_y\text{Ni}_{1-x-y}\text{O}_2$  compounds showed improved behaviour relative to the pristine oxide. The discharge capacity (140-150 mAh/gm) remained stable up to 20 cycles, which indicates the good reversibility of the modified  $\text{LiNiO}_2$  compounds.

ENHANCEMENT OF DISCHARGE CAPACITY OF  $\text{Li}_3\text{V}_2(\text{PO}_4)_3$  BY STABILIZING ORTHORHOMBIC PHASE AT ROOM TEMPERATURE

Mineo Sato, Koichi Ohkawa, Kenji Yoshida, Mai Saito, Kazuyoshi Uematsu and Kenji Toda

Department of Chemistry and Chemical Engineering, Faculty of Engineering, Niigata University, Ikarashi 2 no-cho 8050, Niigata, Niigata 950-2181, Japan

## ABSTRACT

$\text{Li}_3\text{V}_2(\text{PO}_4)_3$  and solid solutions of  $\text{Li}_{3-2x}(\text{V}_{1-x}\text{M}_x)_2(\text{PO}_4)_3$  ( $\text{M}=\text{Ti}, \text{Zr}$ ) were prepared by a solid state reaction. A high temperature orthorhombic phase of  $\text{Li}_3\text{V}_2(\text{PO}_4)_3$  with a  $\beta\text{-Fe}_2(\text{SO}_4)_3$ -type was successfully stabilized at room temperature by substituting Ti or Zr for V with substitution ratios beyond  $x=0.50$ . The pure material of  $\text{Li}_3\text{V}_2(\text{PO}_4)_3$  exhibited a cathode performance with two well defined regions of plateau at around 3.7 and 4.1 V vs.  $\text{Li}/\text{Li}^+$  upon charging and 3.6 and 4.0 V vs.  $\text{Li}/\text{Li}^+$  upon discharging, respectively, suggesting two types of phase produced upon the charge/discharge process. On the other hand, the cathode performance of the orthorhombic stabilized materials showed almost the same charge/discharge voltages as those of the pure material, but, with two plateaus slightly sloping, and also showed a considerably improved charge/discharge cycle performance compared to that of the pure material. Such improvement on the charge/discharge cycle performance is suggested to come from the disordered lithium ion arrangement in the orthorhombic phase.

## 1. INTRODUCTION

Framework oxides such as NASICON materials have been known to undergo topotactic insertion/extraction of a mobile atom and therefore are candidates as electrode materials for rechargeable lithium batteries. This may be supported by their open structure within the  $\text{M}_2(\text{XO}_4)_3$  frameworks built up of  $\text{XO}_4$  tetrahedra sharing corners with  $\text{MO}_6$  octahedra and vice versa.

$\text{Li}_3\text{V}_2(\text{PO}_4)_3$  crystallizes two modifications of NASICON-type and  $\beta\text{-Fe}_2(\text{SO}_4)_3$ -type, among of which only  $\beta\text{-Fe}_2(\text{SO}_4)_3$ -type modification can be obtained by a conventional solid state reaction. The  $\beta\text{-Fe}_2(\text{SO}_4)_3$ -type structure is a NASICON related structure, where  $\text{V}_2(\text{PO}_4)_3$  frameworks are also built up of  $\text{PO}_4$  tetrahedra sharing corners with  $\text{VO}_6$  octahedra. Okada et al. [1] reported that monoclinic  $\text{Li}_3\text{V}_2(\text{PO}_4)_3$  with  $\beta\text{-Fe}_2(\text{SO}_4)_3$ -type showed a cathode performance with two plateaus at 3.8 and 1.75 V vs.  $\text{Li}/\text{Li}^+$  associated with  $\text{V}^{4+}/\text{V}^{3+}$  and  $\text{V}^{3+}/\text{V}^{2+}$  redox couples, respectively. They also could remove reversibly two moles of lithium ions from  $\text{Li}_3\text{V}_2(\text{PO}_4)_3$  on charging to 4.3 V vs.  $\text{Li}/\text{Li}^+$ . It should be noted that the theoretical energy density of  $\text{Li}_3\text{V}_2(\text{PO}_4)_3$  is  $499.7 \text{ mWh} \cdot \text{g}^{-1}$  while that of  $\text{V}_2\text{O}_5$  is  $471.5 \text{ mWh} \cdot \text{g}^{-1}$ .

$\text{Li}_3\text{Sc}_2(\text{PO}_4)_3$ , known as a lithium ionic conductor with  $\beta\text{-Fe}_2(\text{SO}_4)_3$ -type, has three structural modifications: low temperature monoclinic  $\alpha$ -phase, middle temperature monoclinic  $\beta$ -phase and high temperature orthorhombic  $\gamma$ -phase. The phase transitions are all reversible. The  $\gamma$ -phase exhibits what is called superionic conductivity. In the previous study [2], we reported that the  $\gamma$ -phase was successfully stabilized at room temperature by substituting aliovalent ions such as Ti, Zr, Nb, Ta and Mg for Sc sites. In our preliminary experiment, it was found that  $\text{Li}_3\text{V}_2(\text{PO}_4)_3$  also has the same reversible phase transitions as  $\text{Li}_3\text{Sc}_2(\text{PO}_4)_3$  does. This fact indicates that the structure of the  $\gamma$ -phase of  $\text{Li}_3\text{V}_2(\text{PO}_4)_3$  gives good environment for lithium ion diffusion. The  $\gamma$ -phase stabilized  $\text{Li}_3\text{V}_2(\text{PO}_4)_3$ , if possible, thus can provide a considerable enhancement of the cathode performance of  $\text{Li}_3\text{V}_2(\text{PO}_4)_3$ .

In this study the stabilization of  $\gamma$ -phase of  $\text{Li}_3\text{V}_2(\text{PO}_4)_3$  at room temperature was succeeded by substituting Zr and Ti for V sites. The cathode performance was discussed on the basis of the  $\gamma$ -phase stabilized  $\text{Li}_3\text{V}_2(\text{PO}_4)_3$  structure, which was refined by X-ray diffraction and neutron diffraction methods.

## 2. EXPERIMENT

$\text{Li}_3\text{V}_2(\text{PO}_4)_3$  and  $\text{Li}_{3-2x}(\text{V}_{1-x}\text{M}_x)_2(\text{PO}_4)_3$  ( $\text{M}=\text{Ti}, \text{Zr}$ ) were prepared by a conventional solid-state reaction. The starting materials were high purity  $\text{Li}_3\text{CO}_4$ ,  $\text{V}_2\text{O}_5$ ,  $\text{NH}_4\text{H}_2\text{PO}_4$ ,  $\text{TiO}_2$ . The mixtures with stoichiometric amounts of these materials were ground in an agate mortar, preheated at  $300^\circ\text{C}$  for 6h in Ar atmosphere. The samples was grounded and pressed into a pellet, and then heated at  $1100^\circ\text{C}$  for 12h in Ar. The

completion of the reaction and the phase purity of the products were confirmed by powder X-ray diffraction. Thermogravimetric analysis (TG) and differential thermal analysis (DTA) were conducted between 20°C and 500°C with a heating rate of 5°C min<sup>-1</sup>.

The cathode performance was obtained by using a galvanic cell, which was assembled on a glove box filled with an argon atmosphere. The electrode was composed of the sample, acetylene black and PTFE in a weight ratios of 7:2.5:0.5. Lithium plates cut from lithium metal ingots were used for both negative and reference electrodes. The electrolyte was LiClO<sub>4</sub> (1 mol·dm<sup>-3</sup>) dissolved in a 1:1 weight ratio mixture of propylene carbonate and dimethoxyethane. Charge/discharge performance was evaluated at a constant current of 0.5 mA·cm<sup>-2</sup> in the range between 3.0 and 4.5 V vs. Li/Li<sup>+</sup>.

The X-ray diffraction pattern was collected by a step-scanning mode in the range of 10-100° with a step width of 0.02° and a step time of 4 s. The neutron diffraction data were collected by a multi-scanning mode in the 2θ range from 5° to 155° with a step width of 0.05° and a monitoring time of 16 min.

Powder neutron diffraction patterns for the refinement were recorded. The structure refinement was carried out by the Rietveld method for both X-ray and neutron diffraction.

### 3. RESULTS AND DISCUSSION

The powder X-ray diffraction patterns of Li<sub>3-2x</sub>(V<sub>1-x</sub>M<sub>x</sub>)<sub>2</sub>(PO<sub>4</sub>)<sub>3</sub> (M=Ti, Zr) indicated that the samples had a single phase with a monoclinic or an orthorhombic symmetry in the substitution within x=0.2. DTA analysis of Li<sub>3</sub>V<sub>2</sub>(PO<sub>4</sub>)<sub>3</sub> showed two reversible phase transition points at about 120°C associated with α to β transition and at about 180°C associated with β to γ transition, while Li<sub>3-2x</sub>(V<sub>1-x</sub>M<sub>x</sub>)<sub>2</sub>(PO<sub>4</sub>)<sub>3</sub> (M=Ti, Zr) with substitution ratios over x=0.5 did not exhibit any endo- or exo-thermic heat in the whole temperature range measured. The Rietveld refinement results based on both X-ray and neutron diffraction patterns gave the γ-phase modification as the most reliable structure for the samples without phase transition, implying the high temperature phase to be stabilized at room temperature.

Figure 1 shows typical charge/discharge curves for pure and Zr-substituted sample where the γ-phase is stabilized at room temperature. The pure sample shows two well defined regions of plateau at around 3.7 and 4.1 V vs. Li/Li<sup>+</sup> upon charging and 3.6 and 4.0 V vs. Li/Li<sup>+</sup> upon discharging, respectively, suggesting two types of phase produced upon the charge/discharge process. On the other hand, the stabilized samples show a similar charge/discharge performance to those of the pure material, but, with two plateaus slightly sloping, and also showed a considerably improved discharge performance compared to that of the pure material. Such improvement observed for the substituted samples is suggested to come from a disordered lithium ion arrangement shown in the orthorhombic structure refined by Rietveld method.

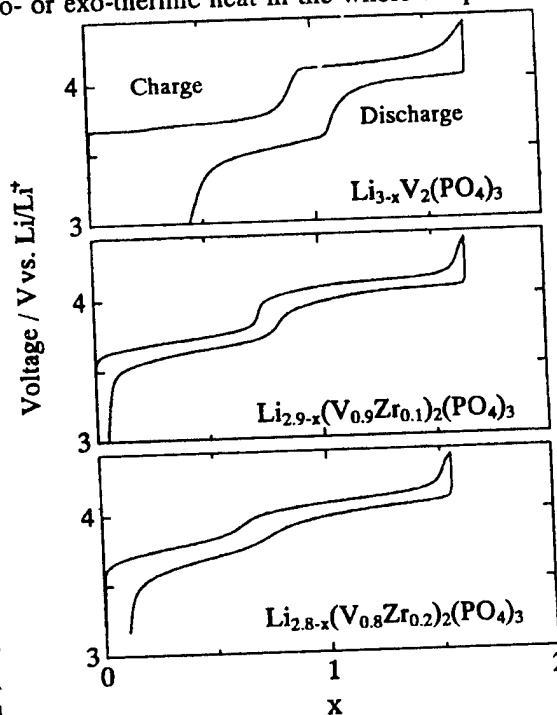


Fig.1 Charge/discharge curves of pure and Zr-substituted samples at 0.5 mA·cm<sup>-2</sup>.

#### Acknowledgments

This work was supported by the "Research for the Future, Preparation and Application of Newly Designed Solid Electrolytes (JSPS RFTF96P00102)" program from the Japan Society for the Promotion of Science (JSPS).

#### REFERENCES

- [1] S. Okada, et al., *International Symposium on Lithium Batteries*, September, 1996, Tokyo, Abs. P.19.
- [2] T. Suzuki, et al., *Solid State Ionics*, **104**, 27(1997).

## NEUTRON DIFFRACTION STUDIES OF $\text{Li}_3\text{Fe}_2(\text{XO}_4)_3$ ( $\text{X} = \text{P}, \text{As}$ ) : POLYANION STRUCTURES HOSTS FOR THE REVERSIBLE INSERTION OF $\text{Li}^+$

Christian Masquelier and Juan Rodriguez-Carvajal\*

*Laboratoire de Chimie des Solides, Université Paris-XI Orsay, Bat. 414, 91405 Orsay Cedex, France*

*\* Laboratoire Léon Brillouin (CEA-CNRS), CEA/Saclay, 91191 Gif sur Yvette Cedex, FRANCE.*

Intensive research on transition-metal oxides suitable as hosts for a rapid insertion / extraction of alkali ions has led to the recent development of  $\text{LiCoO}_2$  (layered rock salt) or  $\text{Li}[\text{Mn}_2]\text{O}_4$  (spinel) as cathode materials in rechargeable lithium batteries. Cost, environment and shelf-life considerations have also prompted a search for alternative cathode systems, among which are the NASICON-related framework structures ( $\text{A}_x\text{M}_1\text{M}_2(\text{XO}_4)_3$ ) were proposed [1-7]. Besides the identification of new cathode materials operating on the  $\text{Ti}^{4+}/\text{Ti}^{3+}$ ,  $\text{Fe}^{3+}/\text{Fe}^{2+}$ ,  $\text{V}^{4+}/\text{V}^{3+}$  or  $\text{V}^{3+}/\text{V}^{2+}$  redox couples, these studies allowed a systematic tuning of transition-metal redox energies through the inductive effect, *i.e.* the effect of the nature of the polyanion  $(\text{XO}_4)^n$ ;  $\text{X} = \text{Mo}, \text{W}, \text{S}, \text{P}, \text{As}$ ) and of the crystal structure on the energy level of the  $\text{M}^{n+}/\text{M}^{(n-1)+}$  redox couples.

Depending on the preparation route and on the nature of the  $(\text{XO}_4)^{3-}$  polyanion group,  $\text{Li}_3\text{Fe}_2(\text{XO}_4)_3$  ( $\text{X} = \text{P}, \text{As}$ ) may adopt three different crystal structures, denoted "A", "B" or "C" ("A"-LFX, "B"-LFP, "C"-LFA) [8-9]. It was shown recently that approximately 2 lithium per formula unit, associated with the electrochemical reduction of  $\text{Fe}^{3+}$  to  $\text{Fe}^{2+}$ , may be reversibly intercalated into the three structures [6]. The position of the  $\text{Fe}^{3+} / \text{Fe}^{2+}$  redox couple below the lithium-anode Fermi energy is nearly independent of the structure and of whether  $\text{X} = \text{P}$  or  $\text{As}$ . There is, however, a clear dependence of : i) the shape of the  $\text{V}_{\text{oc}}$  vs  $x$  curves for  $\text{Li}_{3+x}\text{Fe}_2(\text{XO}_4)_3$  and ii) the charge-discharge rate capabilities, on the crystal structure of the cathode material.

A series of systematic studies of the structural modifications induced by the insertion of lithium into the  $\text{Li}_3\text{Fe}_2(\text{XO}_4)_3$  frameworks was recently undertaken. Among them, ex-situ XRD experiments showed that the integrity of the NASICON framework could be maintained with 5 alkali cations per formula unit, *i.e.* in B- $\text{Li}_3\text{Fe}_2(\text{PO}_4)_3$  [10]. Here, we present the crystal structures, obtained from the Rietveld refinements of neutron diffraction data from powder samples, of "A"-LFP (monoclinic), "B"-LFP (rhombohedral) and "C"-LFA (rhombohedral). The "B" and "C" structures will be compared with their sodium analogs "B"-NFP and "C"-NFA from which they were prepared by ionic exchange at 300°C in molten  $\text{LiNO}_3$ .

The two structural forms "A" and "B" are built of  $\text{FeO}_6$  octahedra and  $\text{PO}_4$  tetrahedra connected to each other through all their vertices. They form the well-known  $\text{Fe}_2[\text{PO}_4]_3$  lanterns whose relative orientations lead either to the "A" or "B" form. The main difference lies into the six or eight-membered oxygen "rings" that constitute bottlenecks between neighbouring alkali positions (Fig. 1).

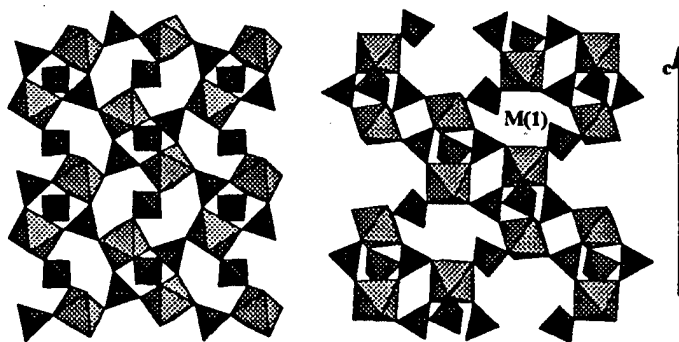


Fig. 1 : The "A" (left) and "B" (right) forms of  $\text{Li}_3\text{Fe}_2(\text{PO}_4)_3$

In the "A" form, lithium ion ordering at RT leads to a monoclinic distortion ( $P2_1/n$ ) with 3 and 2 independent Li and Fe crystallographic sites, respectively. The structure is isotypic with  $\text{Li}_3\text{In}_2(\text{PO}_4)_3$  [11] and could be refined satisfactorily with lattice parameters :  $a = 8.5709(2) \text{ \AA}$ ,  $b = 8.6162(2) \text{ \AA}$ ,  $c = 12.0171(3) \text{ \AA}$  and  $\beta = 90.524(2)^\circ$ .

The framework in the "B" form of  $\text{Li}_3\text{Fe}_2(\text{PO}_4)_3$  is of NASICON-type. The stable form of LFP is "A", but "B"-LFP may be prepared by ionic exchange from the sodium analog  $\text{Na}_3\text{Fe}_2(\text{PO}_4)_3$  [8]. "B"-NFP itself undergoes at RT ( $\alpha$ -form) a monoclinic distortion of the rhombohedral NASICON framework as a result of sodium ordering. The ordering leads to a superstructure whose bragg reflections are clearly visible on both powder X-ray and Neutron diffraction patterns. At  $T > 150^\circ\text{C}$ , "B"-NFP adopts a rhombohedral symmetry ( $R\text{-}3c$ ,  $a=8.731 \text{ \AA}$ ,  $c=21.569 \text{ \AA}$ ) with  $1/3$  of  $\text{Na}^+$  on the M(1) position and  $2/3$  of  $\text{Na}^+$  on the M(2) position [12].

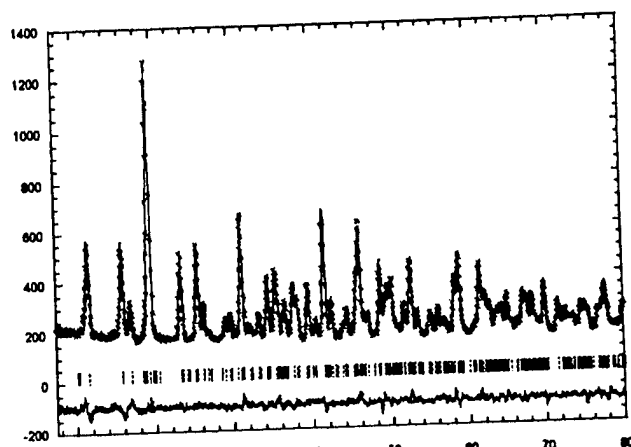


Fig. 2 : Observed and calculated neutron diffraction patterns ( $\lambda=1.2251 \text{ \AA}$ ) for B-LFP

Table 1 : Atomic positions in "B"-LFP

Atom	x	y	z	$B_{iso}$
Fe1	0	0	.1462(2)	0.22(5)
Fe2	0	0	.6528(2)	0.26(5)
P	.2924(4)	.0012(5)	.2512(2)	0.25(4)
O1	.1920(6)	-.0103(6)	.1923(2)	2.43(9)
O2	.7657(5)	.9134(5)	.6991(1)	1.35(6)
O3	.2423(5)	-.1996(5)	.2659(2)	1.31(7)
O4	.5004(4)	.8792(5)	.7557(1)	0.91(6)
Li	.346(2)	.029(2)	.3810(7)	2.7(2)

The monoclinic distortion, i.e. the alkali cation ordering on the M(1) and M(2) sites of the NASICON structure, is suppressed when  $\text{Li}^+$  is substituted for  $\text{Na}^+$ , leading to a rhombohedral unit-cell :  $a=8.3167(4) \text{ \AA}$ ,  $c=22.4741(5) \text{ \AA}$ . The interesting point is that this rhombohedral unit-cell cannot be indexed in the space group  $R\text{-}3c$ . The space group is  $R\text{-}3$  and the M(1) site is emptied when  $\text{Na}^+$  is replaced by  $\text{Li}^+$ . This results, interestingly, in an important increase of the  $c$  parameter and a parallel may be drawn with the rhombohedral metastable form of  $\text{Li}_3\text{Ti}_2(\text{PO}_4)_3$  prepared by electrochemical insertion of lithium into  $\text{LiTi}_2(\text{PO}_4)_3$  [1]. The absence of alkali cation on the M(1) site of the NASICON framework, located halfway between two  $\text{FeO}_6$  octahedra along [001], results in stronger O-O repulsions between adjacent octahedral faces. Lithium is surrounded by 4 oxygen at distances ranging from 1.87 to 2.25  $\text{\AA}$ , in a similar fashion to what reported for the rhombohedral form of  $\text{Li}_3\text{In}_2(\text{PO}_4)_3$  [13].

1. C. Delmas, A. Nadiri and J. L. Soubeyroux, *Solid State Ionics* **28-30**, 419 (1988).
2. A. Manthiram and J. B. Goodenough, *Journal of Power Sources* **26**, 403 (1989).
3. O. Tillement, J.C. Couturier, J. Angenault and M. Quarton, *Solid State Ionics* **48**, 249 (1991).
4. A. K. Padhi, K. S. Nanjundaswamy, C. Masquelier and J. B. Goodenough, *J. Elec. Soc.*, **144**, 2581 (1997).
5. A. K. Padhi, K. S. Nanjundaswamy, C. Masquelier, S. Okada and J. B. Goodenough, *J. Elec. Soc.*, **144**, 1609 (1997).
6. C. Masquelier, A. K. Padhi, K. S. Nanjundaswamy and J. B. Goodenough, *J. Solid State Chem.*, **135**, 228 (1998).
7. J. Gaubicher, Ph.D. doctoral thesis, Paris (1998).
8. F. d'Yvoire, M. Pintard-Scrépel, E. Bretey, and M. de la Rochère, *Solid State Ionics* **9 & 10**, 851 (1983).
9. F. d'Yvoire, M. Pintard-Scrépel, and E. Bretey, *Solid State Ionics* **18 & 19**, 502 (1986).
10. C. Masquelier and J. Gaubicher, in preparation.
11. D. Tran Qui and S. Hamdoun, *Acta Cryst.* **C43**, 397 (1987).
12. M. de la Rochère, Ph.D. doctoral thesis, Paris (1984).
13. E.A. Genkina, L.A. Muradyan, B.A. Maksimov, B.V. Merinov and S.E. Sigarev, *Sov. Phys. Cryst.*, **32**, 40 (1987).

# INFLUENCE OF THE DEPOSITION PARAMETERS ON THE ELECTROCHEMICAL BEHAVIOR OF $\text{LiCoO}_x$ THIN FILMS DEPOSITED BY R.F. SPUTTERING

C. N. Polo da Fonseca, J. Davalos, A. Gorenstein<sup>(1)</sup>, M.A.E. Sanchez and M.C.A. Fantini<sup>(2)</sup>

<sup>1</sup>Universidade Estadual de Campinas, Instituto de Física "Gleb Wataghin", CP 6165, CEP 13081-970, Campinas, SP, Brasil - [cpolo@ifi.unicamp.br](mailto:cpolo@ifi.unicamp.br)

<sup>2</sup>IFUSP, CP 66318, 05315-970, SP, Brasil - [mfantini@if.usp.br](mailto:mfantini@if.usp.br)

The charge/discharge process of a lithium battery is strongly dependent on the composition and microstructure of the cathode material. In thin film form, these properties can be controlled by the synthesis method. In the present study, we report on the variation of the deposition parameters for the obtention of r.f. sputtered  $\text{LiCoO}_x$  thin film. The deposition atmosphere was  $\text{Ar} + \text{O}_2$ , and the total pressure was  $7.0 \times 10^{-6}$  mbar. The target was fabricated by cold-pressing  $\text{LiCoO}_2$  powder, and the deposition parameters were varied as follows:

- Power  $P = 50$  and  $100$  W
  - Oxygen flow  $\phi = 0.9$  and  $9.0$  sccm
  - Target/substrate distance  $H = 7.5$  and  $12$  cm
- All samples had the same thickness ( $\sim 0.2 \mu\text{m}$ ).

A three-electrode electrochemical cell was employed in the electrochemical measurements. Two distinct lithium foils were used as counter and reference electrodes. The electrolyte was  $1 \text{ M LiClO}_4/\text{PC-EC } 1:1$ .

The cyclic voltammograms were measured with a scan rate of  $0.5 \text{ mV s}^{-1}$  in the potential range  $2.5\text{--}4.3 \text{ V vs Li}$ , using a potentiostat /galvanostat EG&G - PAR Model 273A. The electrochemical impedance spectroscopy experiments were performed in the frequency range of  $10^{-2}$  to  $10^5 \text{ Hz}$  with a perturbation signal of  $10 \text{ mV}$ . A Schlumberger Model 1255 Frequency Analyzer was used. All the electrochemical experiments were performed in a dry box with purified argon gas.

X-Ray diffraction was used to characterize the phase and crystallinity of the different films. The results indicated that the films deposited at the highest target substrate-distance ( $H=12 \text{ cm}$ ) were amorphous. Films deposited at low  $H$  were polycrystalline, and the identified phases were  $\text{Li}_{1.47}\text{Co}_3\text{O}_4$  and  $\text{LiCoO}_2$ . The grain size  $D$  was small ( $\sim 30 \text{ \AA}$ ).

Figure 1 presents the cyclic voltammograms. The form and position of the anodic and the cathodic peaks, related to the lithium extraction and insertion process, respectively, is strongly dependent on the deposition conditions. On cycling, these peaks become more defined, and are displaced to more positive potentials, for all films. This behavior can be attributed to the formation/destruction of the original phases, and a general increase of the electronic resistance of the material. The cyclic voltammetric experiments indicated that amorphous samples presented superior electrochemical behavior, since they are capable of withstanding a larger number of cycles.

The results obtained by impedance measurements indicated that, with the increase of  $\phi$ , the films presented an increase of the charge transfer resistance, which is more important for samples deposited at low  $P$  (Figure 2). The increase of  $H$  also decreases the charge transfer resistance.

The best sample, in what concerns charge capacity and cycling, was deposited at the highest target/substrate distance ( $H=12 \text{ cm}$ ), low  $\phi$  ( $0.9 \text{ sccm}$ ) and low power ( $P=50 \text{ W}$ ). Figure 3 presents the behavior of the diffusion coefficient as a function of the applied potential, for this sample. The maximum value ( $D \sim 2 \times 10^{-9} \text{ cm}^2 \text{ s}^{-1}$ ) was obtained for potentials in the deintercalation region; the obtained value is comparable to the one obtained by other authors, for films deposited by another technique. [1].



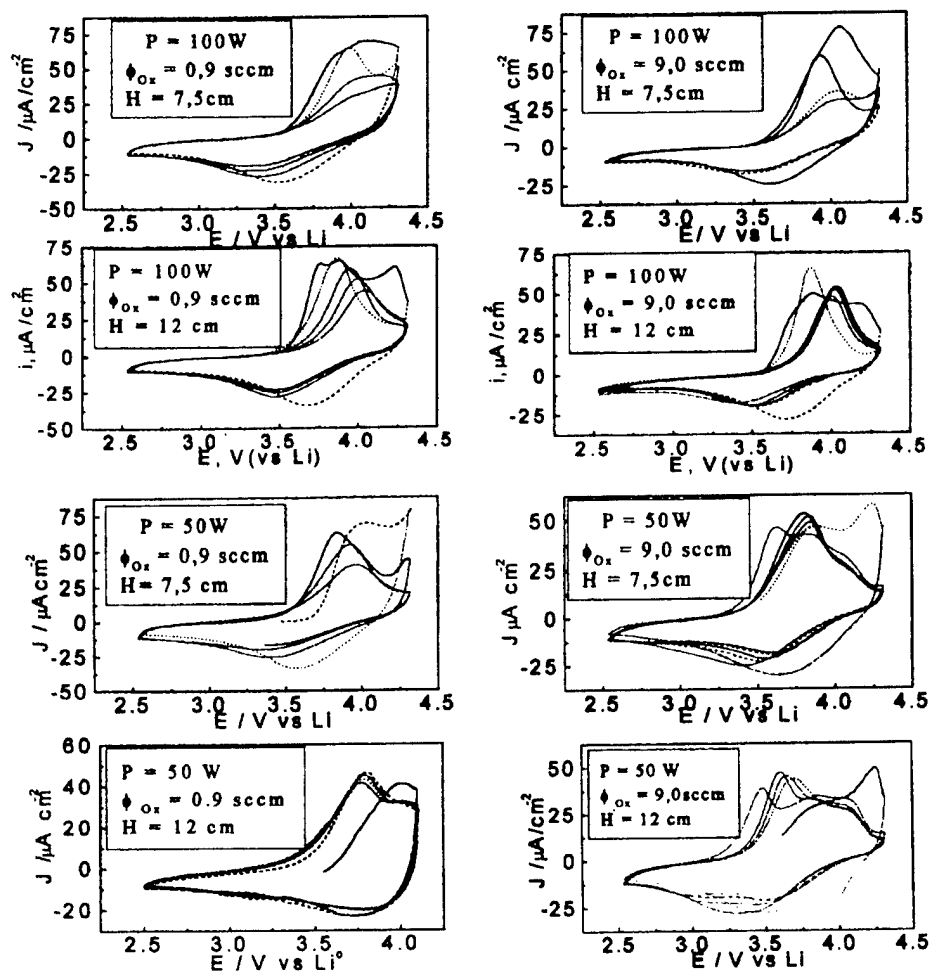


Figure 1: Cyclic voltammograms of  $\text{LiCoO}_x$  films deposited at distinct conditions.

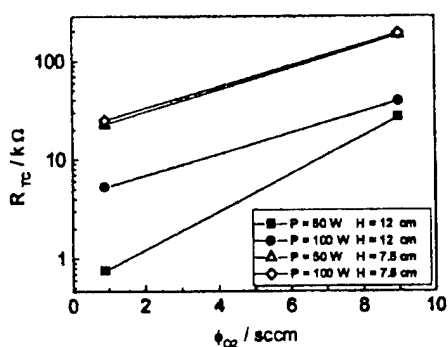


Figure 2: Charge transfer resistance vs oxygen flow.

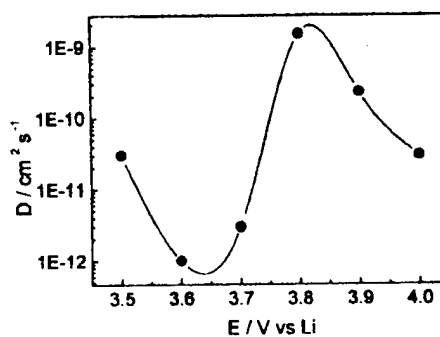


Figure 3: Diffusion coefficient as a function of potential for the best film.

## REFERENCES

- [1] H. Sato, D. Takahashi, T. Nishina e I. Uchida, J. Power Sources **68**, 540 (1997).

**Acknowledgements:** C.N. Polo da Fonseca and J. Davalos acknowledges FAPESP for a post-doctoral scholarship (Process 97/10988-9 and 97/06780-3 ).

ON THE DIFFUSION OF Li<sup>+</sup> DEFECTS IN LiCoO<sub>2</sub> AND LiNiO<sub>2</sub>

Koichi Nakamura, Hideki Ohno, Kazuhiro Okamura<sup>2</sup>,  
Yoshitaka Michihiro, Ichiro Nakabayashi<sup>1</sup>, Tatsuo Kanashiro

Department of Physics, <sup>1</sup>Department of Chemical Science and Technology,  
Faculty of Engineering, Tokushima University,  
Minami-Josanjima-Cho, Tokushima 770-8506, Japan

<sup>2</sup>Matsushita Battery Industrial Co., Ltd., Matsushita-Cho, Moriguchi 570-8511, Japan

NMR measurements were performed to elucidate the diffusion of Li<sup>+</sup> defects in LiCoO<sub>2</sub> and LiNiO<sub>2</sub>, which have attracted much interest in the practical use for lithium ion rechargeable battery electrode. [1–3]

Fourier-transformed NMR spectra of <sup>7</sup>Li have been measured in LiCoO<sub>2</sub> and LiNiO<sub>2</sub> above 77K to 630K. NMR spectra of LiCoO<sub>2</sub> and LiNiO<sub>2</sub> markedly change above 380K and 480K with increasing temperature, respectively as shown in Fig.1. This means so-called motional narrowing originated from the motion of Li<sup>+</sup> defects. In contrast to this, the temperature independent full width at half maxima (FWHM) of both samples below room temperature is consistent with the results from second moment,  $\langle \Delta\omega^2 \rangle$  based on the nuclear dipole interaction of <sup>7</sup>Li on the rigid lattice in both samples.

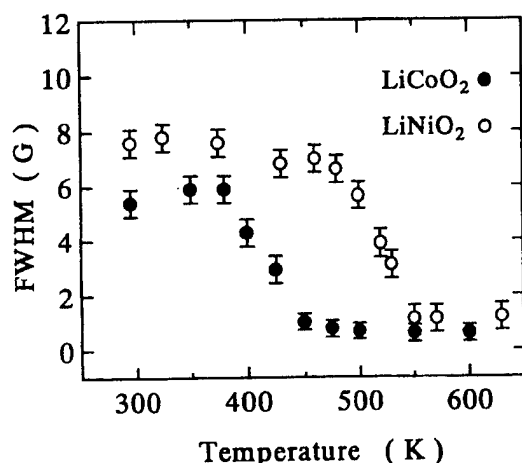


Figure 1: T-dependence of FWHM.  
Data were taken at 10.08MHz.

Assuming the temperature dependence of FWHM with thermally activated type, we evaluated the activation energy of diffusing Li<sup>+</sup> defects in LiCoO<sub>2</sub> and LiNiO<sub>2</sub> to be about 0.35 and 0.45eV, respectively. The lower onset temperature of FWHM in LiCoO<sub>2</sub> suggests that the diffusing of Li<sup>+</sup> defects at low temperature is active in LiCoO<sub>2</sub> more than in LiNiO<sub>2</sub>. This would be related to the degradation of charge/discharge characteristics of LiNiO<sub>2</sub> at low temperatures.

On the other hand, the characteristic behavior with the diffusion of Li defects appear also in the relaxation of both samples. Figure 2 show the temperature dependence of spin-lattice relaxation rate,  $1/T_1$  of LiCoO<sub>2</sub> and LiNiO<sub>2</sub> in the Arrhenius plot.

The data of  $1/T_1$  of LiNiO<sub>2</sub> is larger by one order than that of LiCoO<sub>2</sub>. No typical Bloembergen-Purcell-Pound(BPP) like behavior based on the motion of Li defects were observed. Above room temperature, however,  $1/T_1$  of both samples indicate the significant decrease with increasing temperature and the linear relation. Such behaviors remind of BPP-like behavior at  $\omega\tau \ll 1$  in the high temperature region. We applied the BPP model to the data in the high temperature region.

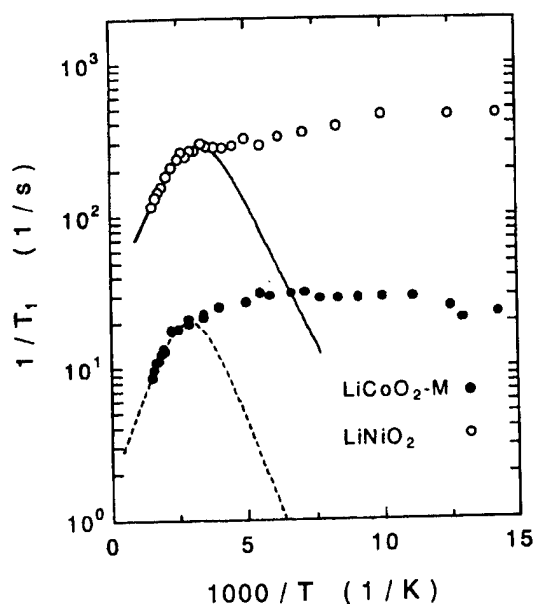


Figure 2:  $T$ -dependence of  $1/T_1$ . Data were taken at 10.08MHz with a conventional pulse NMR technique.

The results are represented by dashed and solid line for  $\text{LiCoO}_2$  and  $\text{LiNiO}_2$ , respectively in Fig.2. This results in the small activation energy  $\sim 0.08\text{eV}$  in both samples. This is not consistent with the evaluation from line width. The reason is not clear at present.

Thus, these results strongly indicate that the aspect of motion of  $\text{Li}^+$  defects would change from the rigid lattice model in the low temperature region into the diffusing model at high temperatures with increasing temperature.

#### References

- [1] R. Kanno, H. Kubo, and Y. Kawamoto, T. Kamiyama, F. Izumi, Y. Takeda, and M. Takano, *J. Solid State Chem.* **110**, 216 (1994).
- [2] A. Hirano, R. Kanno, Y. Kawamoto, K. Oikawa, T. Kamiyama, F. Izumi, *Solid State Ionics* **86-88**, 791 (1995).
- [3] K. Yamaura, M. Takano, A. Hirano, R. Kanno, *J. Solid State Chem.* **127**, 109 (1996).

## ALL-SOLID-STATE Li-ION BATTERIES FOR A BATTERY-BASED SOCIETY

M.J.G. Jak, E.M. Kelder, and J. Schoonman

Delft Interfaculty Research Center; Renewable Energy  
Laboratory for Inorganic Chemistry  
Delft University of Technology  
Julianalaan 136, 2628 BL, Delft  
The Netherlands

This paper deals with a possible solution for the existing problems related to Li-ion batteries containing liquid and/or polymer-based electrolytes. The current state-of-the-art commercial Li-ion batteries all have a liquid or polymer-based electrolyte which, inherently, causes stability failures due to low decomposition potentials, leakage, and low decomposition temperatures [1-6]. A stable ceramic electrolyte may solve these problems [7,8], but also results in new problems concerning the ionic conductivity and interfaces. From literature it is known that the Li<sup>+</sup>-ion conductivity of ceramic electrolytes is 2 to 4 orders of magnitude lower compared with liquid or polymer-based electrolytes [6]. Furthermore, the interfacial resistances between the solid electrolyte and solid electrodes are substantial compared with the liquid/solid interfaces present in the current Li-ion batteries.

At this moment no stable ceramic electrolyte with an ionic conductivity comparable with the commercial electrolytes is available. In the past years we have developed a cheap ceramic electrolyte, Li-doped BPO<sub>4</sub>, with an acceptable Li<sup>+</sup>-ion conductivity. The ionic conductivity of nano-structured Li-doped BPO<sub>4</sub> ranges between 10<sup>-7</sup> and 10<sup>-4</sup> S/cm at room temperature, depending on the doping level, particle size, and compaction method [9-13]. This value of the ionic conductivity is still lower than the polymer-based electrolytes. Therefore, the high resistance of the electrolyte should be decreased by adjusting the cell design. One of the advantages of using a solid, composite electrolyte is the flexibility in the cell design. When using thin foils of the ceramic electrolyte with a polymer binder and foils or coatings of the electrodes on the metallic current collectors, a spirally wound battery can be made, resulting in large interface areas. The improved aspect ratio of the electrolyte foils could be sufficient with respect to improving the total resistance of the electrolyte.

The interface problems can be solved by using dynamic compaction of the green, wound battery (Fig. 1). In previous papers [14-17] we demonstrated the improvement of the solid-solid interfaces by dynamic compaction. With dynamic compaction a high-energetic pressure pulse is applied on the sample for a short period of time. Dynamic compaction results in densification of the separate battery components without altering the particle size of the starting material and "forging" the components together, leading to an increased interface contact area (Fig. 2). Especially, magnetic pulse compaction (MPC) is a very

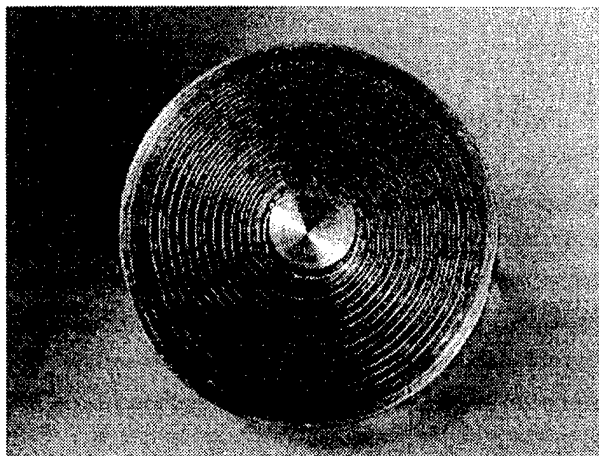


Fig. 1: Cross-section of a magnetic pulse compacted wound Li-ion battery (outer diameter 16 mm, foil length 100 cm).

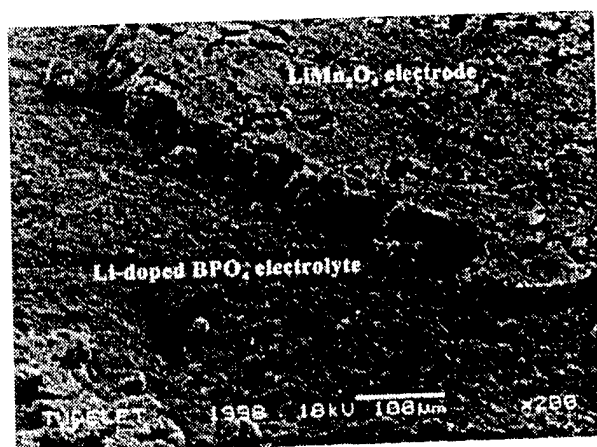


Fig. 2: Side view cross-section interface Li-doped BPO<sub>4</sub> (composite foil) and LiMn<sub>2</sub>O<sub>4</sub> (coating) magnetic pulse compacted Li-ion battery.

suitable technique for compaction all-solid-state Li-ion batteries. MPC generates pressure pulses up to 5 GPa with a pulse duration less than 200  $\mu$ s. Furthermore, a compaction rate of one compaction per second can be achieved.

We will present the Li<sup>+</sup>-ion conductivity mechanism of the Li-doped BPO<sub>4</sub> electrolyte in terms of defect chemistry and conduction pathways. Furthermore, the improvement of the interface contact area with dynamic compaction will be demonstrated. Finally, the latest results and specifications of dynamically compacted all-solid-state Li-ion prototype batteries will be presented.

#### References:

- [1] P. Arora, R.E. White, and M. Doyle, *J. Electrochem. Soc.*, **145**, 3647 (1998).
- [2] L.A. Dominey, in *Lithium Batteries (Industrial Chemistry Library, Volume 5)*, G. Pistoia, Editor, p. 278, Elsevier Science, Amsterdam (1994).
- [3] Z.X. Shu, R.S. McMillan, and J.J. Murray, *J. Electrochem. Soc.*, **140**, L101 (1993).
- [4] Z. Jiang, M. Alamgir, and K.M. Abraham, *J. Electrochem. Soc.*, **142**, 333 (1995).
- [5] H. Moa, J.N. Reimers, Q. Zhong, and U. von Sacken, *Electrochem. Soc. Proceedings* **9-28**, 245 (1995).
- [6] S. Hossain, in *Handbook of Batteries*, Chapter 36, 2<sup>nd</sup> edition, ed. D. Linden, MacGraw-Hill, New York, 1995.
- [7] Y. Harada, T. Ishigaki, H. Kawai, and J. Kuwano, *Solid State Ionics*, **108**, 407 (1998).
- [8] Panel discussions IMLB-8, Nagoya, Japan, June 21, 1996.
- [9] M.J.G. Jak, E.M. Kelder, N.M. van der Pers, A. Weisenburger, and J. Schoonman, *J. Electroceramics*, **2**, 127 (1998).
- [10] E.M. Kelder, M.J.G. Jak, F. de Lange, and J. Schoonman, *Solid State Ionics*, **85**, 285 (1996).
- [11] M.J.G. Jak, E.M. Kelder, and J. Schoonman, *J. Solid State Chem.* (1998) (in press).
- [12] M.J.G. Jak, E.M. Kelder, Z.A. Kaszkur, J. Pielaszek, and J. Schoonman, *Solid State Ionics* (1998) (in press).
- [13] M.J.G. Jak, E.M. Kelder, S.J. Everstein, and J. Schoonman, *J. Power Sources* (1998) (submitted).
- [14] M.J.G. Jak, E.M. Kelder, M. Stuiyinga, and J. Schoonman, *Solid State Ionics*, **86-88**, 897 (1996).
- [15] M.J.G. Jak, E.M. Kelder, A.A. van Zomeren, and J. Schoonman, 8<sup>th</sup> International Meeting on Lithium Batteries, Extended Abstracts, p. 322, June 1996, Nagoya, Japan (1996).
- [16] M.J.G. Jak, E.M. Kelder, A.A. van Zomeren, and J. Schoonman, in W.A. Adams, B. Scrosati, and A.R. Landgrebe, (ed.), *Exploratory Research and Development of Batteries for Electric and Hybrid Vehicles*, PV96-14, *The Electrochemical Society Proceedings Series*, Pennington, NJ, 1996, p. 58.
- [17] M.J.G. Jak, E.M. Kelder, Z.A. Kaszkur, J. Pielaszek, V.W.J. Verhoeven, and J. Schoonman, *The Electrochemical Society Proceedings Series*, Pennington, NJ, 1998 (submitted).

## THE EFFECT OF GRAFTED PEO-CHAINS ON THE STATE OF ELECTROLYTE AND THE PROPERTIES OF ION CONDUCTING GELS

D. Ostrovskii<sup>1</sup>, J. Adebahr<sup>1</sup>, P. Gavelin<sup>2</sup>, P. Jannasch<sup>2</sup>, B. Wesslen<sup>2</sup>, P. Jacobsson<sup>1</sup>

<sup>1</sup> Department of Physics, Chalmers University of Technology, SE-412 96 Göteborg, Sweden

<sup>2</sup> Polymer Science & Engineering, Lund University, SE-221 00 Lund, Sweden

Gel electrolyte materials consisting of a polymeric matrix, a non-aqueous solvent and a lithium salt, which combine the high ionic conductivity of liquid electrolytes with good mechanical properties, have been developed recently [1]. To improve the general performance of the materials, such as ionic conductivity, behavior vis-à-vis the electrodes, chemical and mechanical stability, it is very important to understand the role of each of the components of the gel electrolyte. Therefore, the knowledge about the different intermolecular and ionic interactions occurring in such complicated systems is of a great importance. In particular, it has been found that specific behavior of the salt anions may result in a deterioration of the mechanical properties of the material [2], and that the composition of the polymer matrix yields the distinct properties of the whole gel regarding Li-metal electrode compatibility [3].

It is well-established that the choice of "polymer host - solvent" pair may determine in a large extent the performances of the final material. Up until now, a number of polymer hosts (PAN, PMMA, PVdF, PVdF-HFP *etc.*) as well as numerous solvent compositions have been tested, and the behavior of different polymers were reported to be everything from completely "inert" (PMMA) to quite "active" (PAN).

In the present paper we report on the results of an FTIR and Raman study of some novel ionic conducting gel electrolytes prepared using PEO-grafted copolymers. A number of systems with varying compositions (amounts and characteristics of the graft copolymer, solvent types *etc.*) are investigated. It is found that the presence of grafted PEO-chains substantially changes the Li<sup>+</sup>-solvent coordination and a clear correlation between the matrix composition/structure and the state of the electrolyte is observed. Spectroscopic studies suggest that Li<sup>+</sup>-PEO coordination is strongly favored, in competition with the solvent molecules, and that the amount of coordinated solvent molecules to lithium decreases with increasing salt concentration.

A comparison of the ion conductivity data and the results of the spectroscopic investigation is also reported.

*This work was financially supported by the MISTRA program (Sweden).*

### References:

- [1] B. Scrosati, *Nature* **373**, 557 (1995).
- [2] J. Adebahr, P. Gavelin, D. Ostrovskii, L.M. Torell and B. Wesslen. *J. Molecular Structure*, in print
- [3] D. Ostrovskii, A. Brodin, L.M. Torell, G.B. Appetecchi and B. Scrosati, *J. Chem. Phys.* **109**, 7618 (1998).

**CHARGE TRANSPORT IN  $\text{LiI-P(EO)}_n$  POLYMER ELECTROLYTES.****D. Golodnitsky<sup>1</sup>, E. Peled<sup>1</sup>, S.H. Chung<sup>2</sup>, and S. Greenbaum<sup>2</sup>**<sup>1</sup>*School of Chemistry, Tel Aviv University, Tel Aviv 69978, Israel*<sup>2</sup>*Physics Department, Hunter College of CUNY, New York, NY10021, USA*

The vast majority of studies on lithium batteries for the last 20 years have been directed toward the development of highly conductive solid polymer electrolytes. This is due to their promising applications in all-solid-state rechargeable lithium or lithium-ion batteries. A central aspect of research on these electrolytes is the mechanism of ion transport. Theoretical models for the conductivity mechanism have been proposed [1-4]. Despite this activity the exact conduction mechanism in polymer electrolytes is still a matter of some controversy, but it is commonly agreed that above the melting point of the eutectic ( $T_m$ ) the effective ionic conduction occurs mainly in the molten phase, and that both ionic species are mobile.

Semi-crystalline solid poly(ethylene oxide) (PEO) is the most intensively studied polymer for polymer electrolytes. PEO has an extended helical structure with repeat units. Using IR, XRD and Raman spectroscopy it was found that the length of each repeat unit, consisting of seven  $-\text{O}-\text{CH}_2-\text{CH}_2-$  groups in two turns of the helix, is 19.3 Å [4, 5]. Bruce et al [5, 6] were the first to show, that in the polymer-salt complex, PEO chains are wrapped around the cation with each  $\text{Li}^+$  coordinated by three ether oxygens from the polymer chain. They predicted preferred ion conductivity inside the PEO helix.

Thus it was of prime interest to determine the effect on ion conductivity of an extending load applied to the polymer electrolyte film [7]. We recently found that under a stretching load of 520 kg/cm<sup>2</sup> the  $\text{LiI-P(EO)}_{20}$  polymer electrolyte film began to flow [8]. Flowing of the polymer electrolyte accompanied by the reorganization of polymer chains resulted in about a five-fold increase in the ionic conductivity. While the pristine sample is characterized by clear-grain crystalline structure, the stretched sample shows fibrous structure in the direction of force. DSC thermograms of stretched polymer electrolyte show two endothermic transitions. The first one at about 60 °C is sharp and is similar to that of the pristine sample and an additional broad endotherm appears (which is absent in the pristine film), indicating the formation of the second crystalline phase. An increase in the axial

polymer electrolyte conductivity and reorganization of its structure on stretching provide a convincing demonstration of predicted preferred movement of cations along channels within the PEO helices. A decrease in the transverse ion conductivity is expected to accompany the polymer electrolyte stretching. A series of experimental measurements including conductivity, XRD and solid NMR is being carried out in order to test this prediction.

Of crucial importance, in any discussion of ion-transport mechanisms, is the number of charge carriers, in other words, the electrolyte concentration. Moreover it was found that the addition of nano-size inorganic fillers improves the ionic conductivity of polymer electrolytes [9,10]. The conduction processes for composite solid electrolytes (CSE,  $n \leq 3$ ) at  $T < 60^\circ\text{C}$  were found to be entirely different from those of the composite polymer electrolytes (CPEs,  $n > 3$ ). [8] We have demonstrated that in  $\text{LiI-P(EO)}_n\text{-Al}_2\text{O}_3$  CSEs with  $n < 3$  the conductivity jump in the Arrhenius plots and low activation energy ( $E_a$ ) values reflect an interfacial conduction between the solid  $\text{LiI P(EO)}_3$  complex and the ceramic particles [9]. The effect of the stretching of the CPEs and CSEs on ionic conductivity will be discussed.

Understanding of transport processes offers a fertile field for research and development in the synthesis of new rigid polymers with ordered channels and composition appropriate for enhanced ion transport.

## References

1. M.A. Ratner, Polymer Electrolyte Reviews – 1, Eds. J. R. MacCallum and C.A. Vincent, Elsevier Applied Science Publishers, London, (1987)
2. M.A. Ratner and A. Nitzan, Farad. Discuss. Chem. Soc., **88**, 19, (1989)
3. S. Arumugam, J. Shi, D. P. Tunstall and C.A. Vincent, J. Phys. (C), **5**, 153, (1993)
4. F.M.Gray. Solid Polymer Electrolytes. VHC, New York (1991).
5. J.B. Thomson, P. Lightfoot, P.G. Bruce, Solid State Ionics, **85**, 203, (1996)
6. Solid State Electrochemistry, Ed: P.G. Bruce, Cambridge University Press, (1995)
7. A. Nitzan, Private communication
8. D.Golodnitsky, E. Peled, Electrochimica Acta, submitted, (1998)
9. D. Golodnitsky, G.Ardel, E.Strauss, E.Peled, Y. Lareah and Yu. Rosenberg J. Electrochem.Soc, **144**, 10, 3484, (1997)
10. F. Croce, G. B. Appetecchi, L. Persi and B. Scrosati, Nature,**394**, (1998), 456



## ELECTROCHEMICAL AND TRANSPORT PROPERTIES OF NANOCOMPOSITE POLYMER ELECTROLYTES

F. Croce, L. Persi and B. Scrosati

Dipartimento di Chimica, Università 'La Sapienza', P.le A. Moro, 5 – 00185 Roma, Italy

P. Mustarelli, D. Marchesini, E. Quartarone, A. Magistris

Dipartimento di Chimica Fisica and CSTE-CNR, Via Taramelli, 16 – 27100 Pavia, Italy

The usefulness of nanocomposite polymer electrolytes in solid-state electrochemical devices operating above room temperature has been recently proposed to the scientific community attention [1]. The addition of nanoscale ceramic powders to PEO-LiX systems allows a substantial increases of the conductivity, better mechanical properties and good compatibility towards the lithium anode. In addition, the feasibility of true solvent-free films (for example by hot pressing) is of strict interest for technological applications.

We have recently shown that the addition of nanoscale SiO<sub>2</sub> to PEO-LiClO<sub>4</sub> and PEO-LiN(CF<sub>3</sub>SO<sub>2</sub>)<sub>2</sub> leads to room-temperature conductivities better than 10<sup>-4</sup> ohm<sup>-1</sup>cm<sup>-1</sup> [2,3]. While relevant effects on the recrystallization kinetics of the polymer [1], and on the cation transport number [1, 3] have been observed, the exact role played by the nanoscale filler is still under investigation. We recently showed by solid-state <sup>7</sup>Li NMR that SiO<sub>2</sub> particles act as scattering centres for the cations motion [4].

In this paper we compare the electrochemical and transport properties of nanocomposites PEO<sub>30</sub>-LiX (X = ClO<sub>4</sub><sup>-</sup>, PF<sub>6</sub><sup>-</sup>) - 10 wt% SiO<sub>2</sub> that were prepared in our two laboratories. The use of the highly reactive LiPF<sub>6</sub> salt is justified by the presence of dried silica that acts as trapping centre for the moisture [3], and by the relatively low salt content ( $n = [O]/[Li] = 30$ ). As far as concerns the electrochemistry, we devote attention to the electrolytes stability towards lithium metal and to their cyclability performances of standard lithium cells. Determination of cations transport numbers and conductivity up to 80 °C, finally, defines the transport characteristics of the composite electrolytes.

- [1] F. Croce, G.B. Appetecchi, L. Persi and B. Scrosati, *Nature* **394**, 456 (1998).
- [2] C. Capiglia, P. Mustarelli, E. Quartarone, C. Tomasi and A. Magistris, *Int. Conf. on Applications of electrically conducting polymers: batteries, electrochromics and supercapacitors*, Rome, 13-16 April 1997, p. 120.
- [3] C. Capiglia, P. Mustarelli, E. Quartarone, C. Tomasi and A. Magistris, *Solid State Ionics*, in press.
- [4] P. Mustarelli, E. Quartarone, C. Capiglia, C. Tomasi, A. Magistris, L. Linati, *Phys. Rev. B*, submitted.

## ELECTRICAL CONDUCTIVITY AND NMR STUDIES OF PEG AND PPG CONTAINING LITHIUM SALTS\*

J. J. Fontanella, M. C. Wintersgill, C. A. Edmondson, P. E. Stallworth, S. A. Newman  
Physics Department, U.S. Naval Academy, Annapolis, MD 21402-5026, USA

S.H. Chung, Y. Wang, S. G. Greenbaum  
Hunter College of CUNY, New York, NY 10021, USA

Electrical conductivity studies have been carried out on 20:1 poly(propylene glycol) (PPG) and poly(ethylene glycol mono-methyl ether) (PEG) containing  $\text{LiCF}_3\text{SO}_3$  in the ratio of 1:20 (lithium ions:repeat unit). Complex impedance measurements were performed at frequencies from 10 Hz to 100 MHz at pressures up to 0.3 GPa (3 kbar) over the temperatures from about 150 to about 350K. In addition, differential scanning calorimetry studies and  $^7\text{Li}$  spin-lattice relaxation and pulsed field gradient diffusion studies were carried out on all materials.

The usual non-Arrhenius behavior is observed for the temperature variation of the electrical conductivity when the materials are non-crystalline. Those data are analyzed in terms of Vogel-Tamann-Fulcher (VTF), Williams-Landel-Ferry (WLF) and Bendler-Shlesinger (BENSH) formalisms. In addition, literature data for viscosity and relaxation times for relevant systems are analyzed using the same formalisms. The data make it possible to evaluate the relationship between the macroscopic viscosity and electrical conductivity. Finally, the results are compared with VTF/WLF fitting parameters for other polymer electrolytes and various propylene carbonate (PC)-based systems including a PVdF-HFP composite electrolyte. In all cases, large variations are found in both the VTF and WLF fitting parameters with temperature interval. The non-constancy of the parameters with temperature is due to the failure of both formalisms and shows that care must be taken when utilizing the VTF/WLF parameters to draw conclusions concerning the behavior of systems. The quality of the fit of the BENSH equation is compared for that for the other theories.

Next, in general, the effect of pressure is to decrease the electrical conductivity. The magnitude of the decrease is on the order of that reported for other ion-conducting polymers. Further, the change in conductivity with pressure decreases as temperature increases. This result is used to discuss recent calculations concerning the activation volume. In addition, the conductivity shows curvature in a plot of  $\log(\text{Conductivity})$  vs. pressure. In fact, the preliminary results are that ion-conducting PPG and PEG show opposite curvature. Comparisons are made with the  $^7\text{Li}$  NMR results gathered at 116 MHz in providing further evidence of the differences between materials. These results are discussed in terms of various theories of solvent-free ion conducting polymers.

\*Work supported in part by the U. S. Office of Naval Research. S. A. Newman was supported by the SEAP program.

# NOVEL TIN OXIDE BASED ANODES FOR LI-ION BATTERIES

Paul A. Connor, Frédérique Belliard, Mårten Behm, John T. S. Irvine

School of Chemistry, University of St Andrews, St Andrews, Fife KY16 9ST, Scotland

At present the main focus of Li-ion battery research is on improving the capacity and cyclability of cathode materials, as the existing carbon based anodes have significantly higher capacity than the cathodes. This does not however preclude further research into anode materials. Any improvements in anode capacity still will lead to lighter, more compact, batteries.

Tin oxides are one group of materials that show promise as Li-ion battery anodes [1,2]. These oxide materials have high reversible capacities, e.g. theoretical reversible capacity of  $\text{SnO}_2 \sim 800 \text{ mAh g}^{-1}$ , significantly larger than those of carbon, whilst having insertion voltages about 1 V vs.  $\text{Li/Li}^+$ , which is very similar to those of carbon anodes. The method of insertion of  $\text{Li}^+$  into these oxides is thought to proceed by an initial reduction to metallic tin, followed by the reversible alloying of lithium into the dispersed metal [1,2]. The insertion and removal of lithium into bulk tin metal creates large volumetric changes, thus rendering it unsuitable as an electrode material. The improved stability on cycling of the tin oxide anodes, compared with the bulk metal, is attributed to the presence of the remaining oxide framework surrounding very small metallic particles.

To investigate the influence of the oxide matrix on electrode performance, various tin based oxides, such as mixed metal oxides and tin glasses, have been prepared, characterised, and studied as possible anode materials. Conventional voltammetric studies have been used to investigate both capacity (Fig 1) and cycle life of the various materials. They have also been studied using various spectroscopic techniques (e.g. *in situ* XRD and EXAFS (Fig 2)) to test the existing model and to compare the mode of lithium insertion into the various materials. Results from these studies will be presented, and the data from the various techniques correlated to identify the material with the best reversible capacity.

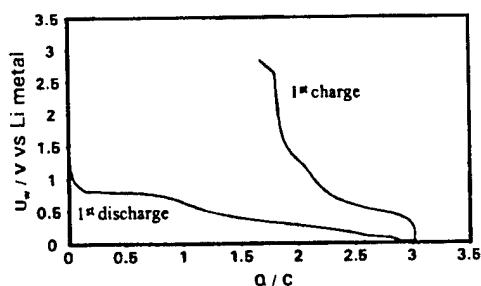


Fig 1 First charge-discharge cycle for  
Li- $\text{SnO}_2$  battery

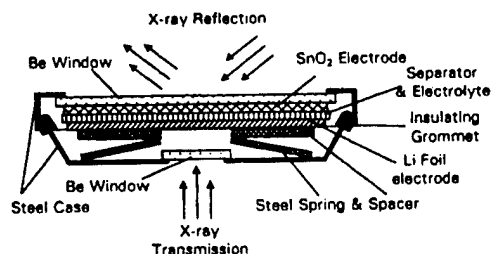


Fig 2 In situ EXAFS / XRD Button Cell

- [1] I. A. Courtney and J. R. Dahn, *J. Electrochem. Soc.* **144**, 2045 (1997).
- [2] W. F. Liu, X. J. Huang, Z. X. Wang, H. Li, and L. Q. Chen, *J. Electrochem. Soc.* **145**, 59 (1998).

## VITREOUS TIN OXIDE-BASED THIN FILM ELECTRODES FOR LI-ION BATTERIES

C. Branci, J. Sarradin and M. Ribes

Laboratoire de Physicochimie de la Matière Condensée  
UMR 5617, Université Montpellier II, CC 03  
F 34095 Montpellier Cedex 5, FRANCE

Research concerning the development of miniaturized systems for energy storage has gained considerable attention during the last decade. All solid state lithium-ion batteries elaborated by stacking thin layers of anodic, electrolyte and cathodic materials are attractive because of their high energy density. The practical significance of the thin film concept is that high performance electrodes can be elaborated without conductivity enhancing additive. Moreover, the very low thickness of the thin films may allow an easier diffusion of the lithium ion throughout the electrode.

Glasses and / or amorphous materials are well suited to the production of thin film-based host electrode allowing insertion-deinsertion of lithium ion without major change in volume. Indeed, the "open" structure of the vitreous state gives rise to a large number of available insertion sites. As a consequence, a better cycleability may be expected, the capacity losses often being the result of a partial destruction of the core structure of the electrode.

Carbon-based electrodes are widely used as the anode in lithium-ion batteries, but – among alternatives to the carbon based electrode – promising results were recently obtained with tin-based amorphous oxide[1]. A mechanism was suggested in order to explain the high specific capacity of that new material : the tin oxide would react to form  $\text{Li}_2\text{O}$  and subsequently Li-Sn alloys[2].  $\text{SnO}_2$ -based thin films [3] as well as amorphous thin films of silicon tin oxynitride [4] are presently under study. In this way, we focused the research on vitreous sputter deposited thin films elaborated from a  $\text{Sn} / \text{SnB}_{0.6}\text{P}_{0.4}\text{O}_{2.9}$  composite target. The vitreous nature of the thin films was checked out by X-ray diffraction while their thickness was measured by SEM.

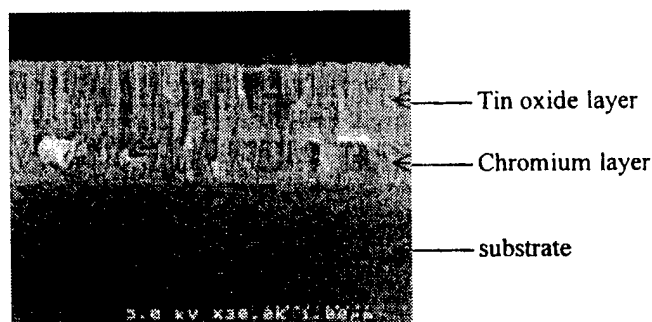


Figure 1 : Cross-sectional view of a  $\text{Sn} / \text{SnB}_{0.6}\text{P}_{0.4}\text{O}_{2.9}$ -based thin film

Figure 1 shows a cross-sectional view of a sputter deposited thin film under argon plasma. The sub-layer corresponds to a previously sputtered chromium film acting as the current collector of the electrode. In both cases, a columnar structure is observed. The thicknesses of the upper layer (tin oxide film) and sub-layer (chromium film) correspond to  $0.8 \mu\text{m}$  and  $0.4 \mu\text{m}$  respectively.

Mössbauer spectroscopy and XPS measurements were used to study the local environment of tin in the thin films while their chemical composition was determined by Energy Dispersive X-ray (EDX) analysis.

Electrical conductivity of the glassy thin film is close to  $10^{-5}$  S/cm, which is a high value compared to that measured on the bulk materials (approximately  $10^{-7}$  S/cm).

Regarding the electrochemical behavior, the first galvanostatic tests were carried out on  $1\text{cm}^2$  electrode in a (1M)  $\text{LiPF}_6$  / PC-EC-3DMC electrolyte using a three-electrode cell. The potential of the charge process corresponding to the uptake of Li ions into the tin oxide film and the potential of the discharge process (release of Li ions) occurred at ca. 1.1 V/Li and 1.5 V/Li respectively. These values are higher compared to the potentials already observed on bulk materials [1, 2]. Experiments are currently in progress in order to determine the coulombic capacity and cycleability of these thin films-based electrodes.

### References:

- [1] Y. Idota, T. Kubota, A. Matsuji, Y. Maekawa, T. Miyasaka, *Science*, **276**, 1397 (1997).
- [2] I.A. Courtney, J.R. Dahn, *J. Electrochem. Soc.*, **144**, 2943 (1997).
- [3] T. Brousse, R. Retoux, U. Herterich, D.M. Schleich, *J. Electrochem. Soc.*, **145**, 1 (1998).
- [4] B.J. Meudecker, J.B. Bates, *Proceedings of the 9<sup>th</sup> International Meeting on Lithium Batteries*. Edinburg. July 1998

## SnSb<sub>x</sub>-BASED COMPOSITE ELECTRODE FOR LITHIUM ION CELL

J. Yang, Y. Takeda, N. Imanishi, T. Ichikawa, and O. Yamamoto  
Department of Chemistry, Faculty of Engineering, Mie University  
Kamihamacho, Tsu 514, Japan

Cycling stability of Li-alloy anodes in lithium ion cell is often limited by the fast mechanical disintegration due to drastic volume changes of metallic host matrices. In order to decrease mechanical stress in the electrodes and thus to improve the cycling performance, several highly dispersed multiphase host matrices for Li-insertion have been proposed on the basis of "the mixed-conductor matrix concept" [1]. Some of them demonstrated improved or even excellent cycling performance [2-3]. It was found that electrodeposited SnSb<sub>x</sub> alloy film as host matrix had much better morphological and cycling stability than Sn film [4]. However, the cycling tests were confined to very thin thickness of the films (< 4  $\mu\text{m}$ ) and limited charge input. The limitation of the thickness and charging depth of the bulk host matrix can be effectively overcome by the use of Li-alloy composite electrodes with highly dispersed SnSb<sub>x</sub> ( $x = 0.14\text{-}0.19$ ) host powders (particle size < 1  $\mu\text{m}$  or 0.3  $\mu\text{m}$ ).

The electrodes with a composition of 10% Ni, 10% polyethylene and 80% SnSb<sub>x</sub> were fabricated by pressing a mixture containing the respective powders on a stainless steel grid. Thickness of the electrodes was 50-60  $\mu\text{m}$ . X-ray diffraction analysis showed SnSb<sub>x</sub> intermetallic alloy consisted of Sn phase and SnSb phase. Electrochemical Li-insertion into this alloy was involved in 4 potential plateaus in the charging curve with a current density of 0.4  $\text{mAcm}^{-2}$ . The first plateau (ca. 0.81 V vs. Li/Li<sup>+</sup>) was related with Li-insertion into SnSb phase, which caused a phase split to form Li<sub>3</sub>Sb phase and Sn phase [4]. After that Li-insertion into Sn phase occurred (below 0.66 V vs. Li/Li<sup>+</sup>). With a decrease of the particle size, distinguish of the plateaus became more difficult. This is because the proportion of the interphase layer in the whole host material rises owing to great surface area of ultra-fine powder. The full Li-insertion capacity at the first cycle was ca. 1000  $\text{mAhg}^{-1}$  with the finest SnSb<sub>x</sub> powder (< 0.3  $\mu\text{m}$ ).

The cycling performance of SnSb<sub>x</sub>-based composite electrodes was strongly dependent on potential range for cycling and polymer binder. As potential upper-limit was controlled under 0.8 V vs. Li/Li<sup>+</sup>, i.e. before Li-extraction from Li<sub>3</sub>Sb phase, the capacity retention can be apparently improved (Fig. 1). In this case, mixed-conducting Li<sub>3</sub>Sb phase was still inert and highly dispersed in active tin phase. It could contribute to a better mechanical and conducting properties of the electrode.

Even for increased particle size of  $\text{SnSb}_x$  powder ( $< 1 \mu\text{m}$ ), the superiority of low potential range to high potential range was also apparent. Moreover, in comparison with  $\text{SnSb}_x$ -based composite electrode, Sn-based composite electrode had poor cycling performance at the same condition. On the other hand, it was noted that the physical and chemical stability of polymer binder in the organic electrolyte had great influence on the electrode performance. Unpolar polyethylene with ultra-high molecular weight (m.p.  $144^\circ\text{C}$ ) was superior to weak-polar PVDF and middle density polyethylene (m.p.  $110^\circ\text{C}$ ).

The difference in cycling stability between two  $\text{SnSb}_x$  powders whose particle size was respectively smaller than  $1 \mu\text{m}$  and  $0.3 \mu\text{m}$  was not remarkable under potential cut-off of  $0/0.8 \text{ V}$  vs.  $\text{Li/Li}^+$ . But the electrode with larger particle size corresponded to a higher coulombic efficiency at the first cycle due to decreased surface area and surface filming which consumed lithium. As the discharging potential arrived at  $0.8 \text{ V}$  vs.  $\text{Li/Li}^+$ , 57%-60% of inserted lithium could be extracted for the electrode with larger  $\text{SnSb}_x$  particle size.

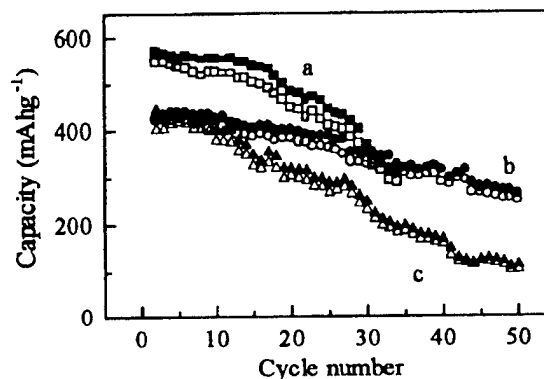


Fig.1 Cycling stability of  $\text{SnSb}_x$  ( $< 0.3 \mu\text{m}$ ) composite electrode in  $1 \text{ M LiClO}_4/\text{EC} + \text{DEC}$  (1:1) under different cut-off, (a)  $0.1/1.2 \text{ V}$ , (b)  $0.0/0.77 \text{ V}$ , (c)  $0.26/1.4 \text{ V}$  vs.  $\text{Li/Li}^+$ ,  $i_c = i_d = 0.4 \text{ mAcm}^{-2}$ , solid dot: Li-insertion, hollow dot: Li-extraction.

## References

- [1] R. A. Huggins, J. Power Sources, 26, 109 (1989).
- [2] O. Mao and J. R. Dahn, 9<sup>th</sup> International Meeting on Lithium Batteries, Edinburgh, July 12-17, 1998, Book of Abstracts, Tues 34.
- [3] Y. Idota, T. Kubota, A. Matsufuji and Y. Maekawa, T. Miyasaka, Science, 276, 1395 (1997).
- [4] J. O. Besenhard, J. Yang and M. Winter, J. Power Sources, 68, 87 (1997).

## THE CRYSTAL STRUCTURAL EVOLUTION OF NANO-SI ANODE DURING LITHIUM INSERTION AND DE-INSERTION

Hong Li, Xuejie Huang and Liquan Chen

Lab. for Solid State Ionics, Institute of Physics, Chinese Academy of Sciences  
Beijing 100080, China

It is indicated that nanosize Si may be used as a novel anode active material for lithium rechargeable batteries at room temperature <sup>[1, 2]</sup>. Nano-Si can alloy with lithium at nonaqueous electrolyte and shows an extremely high reversible capacity more than 2000mAh/g <sup>[2]</sup>. It means that large amount of lithium ions can insert into Si lattice and de-insert from it in discharge/charge processes.

In this paper, the structure of nano-Si at original, discharge and charge states was investigated by SEM, HRTEM and SAED.

It was found from SAED figures that the spotty ring diffraction pattern of nano-Si disappeared at deep discharged state. This means that the insertion of lithium ions destroys the crystal structure of nano-Si and forms an amorphous structure. An order Li-Si alloy structure was not observed as expected. However, a few of diffraction rings appeared again at charged state indicating the existence of short-distance order structure. Therefore, the destroyed crystal structure of nano-Si was recovered to a certain extent after de-insertion of lithium ions. It means that the neighbor Si atoms present a strong interaction. It is believed that the destruction of the crystal structure may induce the irreversible capacity loss.

The microstructure variation of nano-Si was also investigated by HRTEM. It also occurred a large variation during lithium ions insertion and de-insertion. Many nano-Si particles were found to be connected together at deep discharged state and formed a larger continuous network at charged state. This network was a dense layer structure confirmed by SEM.

In order to clarify the structure evolution of Si caused by Li ions doping, a Si powder anode with large particle size at shallow discharged state has also been investigated. Deformation of Si crystal lattice was observed by SAED. The observed spotty ring pattern was transformed into more complicated electron diffraction pattern even during the focusing of electron beam on the sample. The detail analysis will be reported at the meeting.

### References:

- 1: A. M. Wilson, B. M. Way and J. R. Dahn, J. Appl. Phys. 77, 2363(1995)
- 2: Hong Li, Xuejie Huang and Liquan Chen, (submitted)

### Acknowledgements:

This work was supported by Ford-NSFC Foundation (contact No. 9712304), NSFC (contact No.59672027) and National 863 Key Program (contact No. 715-004-0280)



## SILICIDE ANODE WITH HIGH ENERGY DENSITY FOR LITHIUM ION BATTERY

M. Wakihara, T. Morita, A. Modeki and H. Ikuta

Department of Chemical Engineering, Tokyo Institute of Technology  
2-12-1 Ookayama, Meguro-ku, Tokyo, 152-8552, Japan

In rechargeable lithium ion batteries, carbon materials are usually used as anode active materials. Although the carbon materials show good reversibility for many cycles, their storage capacity are limited to 300-400mAh·g<sup>-1</sup>. Recently, amorphous tin-based oxides [1] have been proposed as candidate for lithium ion batteries to overcome some faults of carbon materials such as relatively low capacity density and low discharge rate. Our research group have proposed SnSO<sub>4</sub> as a new anode material with relatively high capacity of 500mAh·g<sup>-1</sup> and high rate capability [2]. Also, we proposed the possibility of silicides as an anode material in lithium ion battery [3]. In this study, we will present more concrete data for the silicide anode.

Silicon composite anode which contained silicon powder (100mesh) : acetylene black : PTFE=55:40:5 by weight showed very large capacity about 4000 mAh·g<sup>-1</sup> at first charge, which corresponds to the incorporation of four mole of lithium per one mole of silicon. On the contrary, the capacity was about 3000 mAh·g<sup>-1</sup> at the first discharge (Fig.1). The capacity of the silicon anode gradually decreased with cycle numbers. The durability was improved by the addition of acetylene black and PTFE.

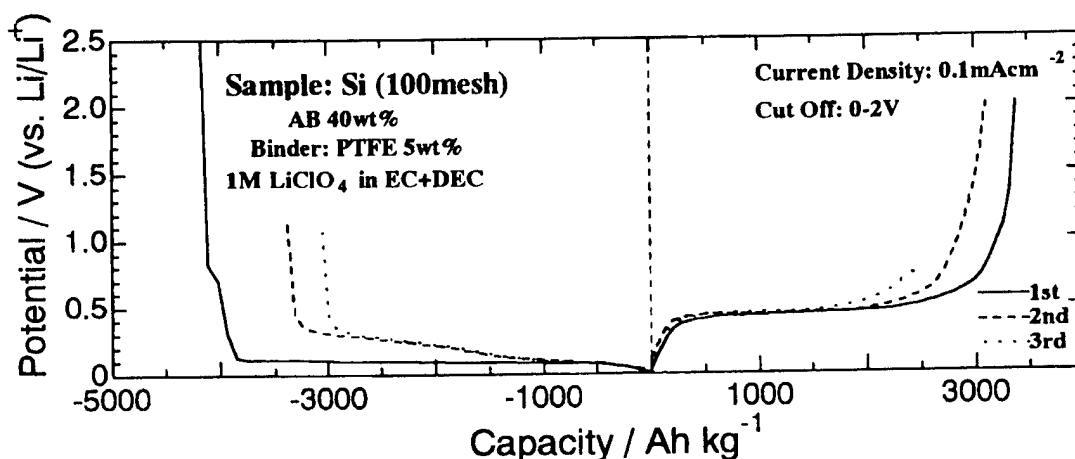


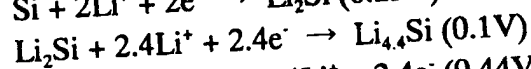
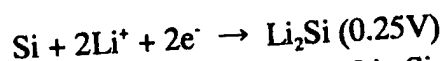
Fig. 1 Charge-discharge curves for Li | 1M LiClO<sub>4</sub> in EC+DEC | Si cell.

Fig.2 shows cyclic voltammogram of silicide anode at a low scan rate of 0.05mA·s<sup>-1</sup>. From the cyclic voltammetry (CV) and electrochemical voltage spectroscopy (EVS) analysis, two peaks were observed on each insertion and extraction process. The XRD profiles for the several stages on charge and discharge processes revealed the coexistence of silicon and lithium silicide (Fig.3). The intensity of the newly formed lithium silicide gradually increased with increasing the amount of lithium, and finally the lithium silicide was only observed on deeply charged to 0V vs. Li/Li<sup>+</sup>. There are no impurity peaks except for silicon and lithium silicide even after 100 cycles. Only silicon peaks were observed at 107th cycle after lithium was completely removed.

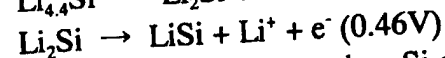
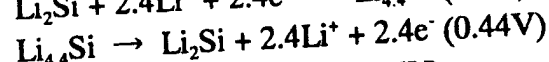
From the results of CV, EVS, OCV and XRD measurements, charge-discharge process of silicon anode occurs following processes with two steps through the formation of lithium

silicides,

Lithium insertion



Lithium extraction



The cell volume of the  $\text{Li}_{4.4}\text{Si}$  is four times larger than Si estimated from ICDD card. During lithium insertion, silicon undergoes large volumetric change. It is considered that the expansion and contraction of lithium silicide during the charge-discharge cycling led to pulverizing of the parent silicon and/or formed silicides powder. It would bring to the breakdown of the electrode, which results in losing of the capacity during several cycles. Some new technology developments are necessary to overcome this problem for actual use.

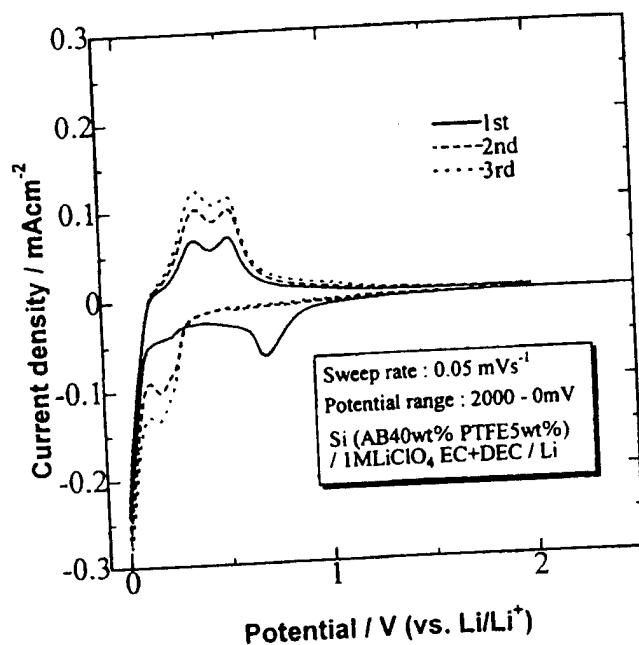


Fig.2 Cyclic voltammogram for Si anode.

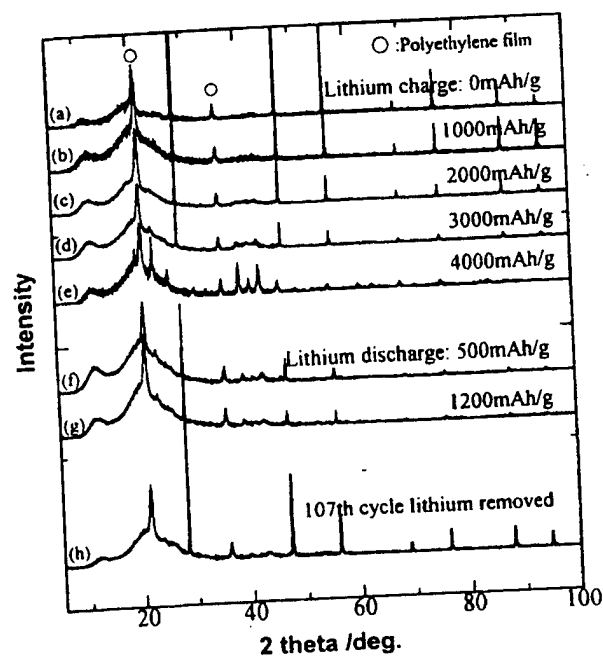


Fig.3 XRD patterns for Si anode at various charged and discharged state.

#### References

- [1] Y. Idota, T. Kubota, A. Matsufuji, Y. Maekawa and T. Miyasaka, *Science*, **276**, 1395 (1997)
- [2] M. Nagayama, T. Morita, H. Ikuta, M. Wakihara, M. Takano and S. Kawasaki, *Solid State Ionics*, **106**, 33 (1998)
- [3] H. Ikuta, T. Morita, A. Modeki and M. Wakihara, IMLB9, Extended Abstract, P1, 58 (1998)

## IMPROVEMENT OF LI CHARGE/DISCHARGE CYCLEABILITY OF LESS GRAPHITIZED CARBONS BY MAKING A C/C COMPOSITE WITH THERMOSETTING RESINS

Tsutomu Takamura

Petoca, Ltd., Kioicho, Chiyodaku, Tokyo 102-0094, Japan,

Morihiro Saito and Kyoichi Sekine

Department of Chemistry, Rikkyo University, Nishiikebukuro, Toshimaku  
Tokyo 171-0021, Japan

### Abstract

In an attempt to improve the Li charge/discharge performance of low temperature prepared mesophase carbon fiber felts, C/C composites have been prepared with an epoxy- or a phenolic-resins. The cycleability was found to be much improved by making the felt into C/C composite. The cycleability was dependent on how each individual fiber is bound together by the binder carbon, and how the electrical conductivity of the consisting material is increased as well. Epoxy resin was difficult to form a smooth binding but still gave an improved cycleability. Phenolic resin of resol type showed a very smooth binding, giving rise to a much stabilized cycleability. The importance of the binding of individual active material particle with an electro-conductive material has been shown for obtaining a long cycle life.

### Introduction

Li-ion secondary batteries are believed to be one of the most promising secondary batteries. Due to the user's demand, increase of the capacity is still required also for the anode. Low temperature mesophase carbons have been focused attention because of their extraordinary high charge capacity up to 900 mAh/g which is far over two times larger than that of graphite. In spite of this attractive property the material has a great issue of the short cycleability. The cause of the short cycleability has been ascribed to the irreversible storing of Li at the less oriented vacant site where once inserted lithium is considered to be difficult to be removed again completely [1].

In our preliminary experiment, however, we have found that the poor cycleability of some low temperature carbons could be improved by modifying the surface of the carbon [2-3]. One of the resulting effect of the surface modification was found to improve the electrical contact of the fabricated test electrode. We, therefore, initiated a study to explore an effective way to obtain a good electrical contact in the test electrode. To make a C/C composite by binding the active material with a conductive carbonaceous material appears to be an attractive way. In the present paper we would like to show how to prepare the effective C/C composite and how the proposed method is effective to improve the cycleability.

### Experimental

#### Materials:

Carbon fiber felt samples prepared at several temperatures from mesophase pitch were made of Petoca (Melblon) with a mean fiber diameter of about 10  $\mu\text{m}$ .

#### Preparation of C/C composite:

The pristine carbon felt was cut into a 3 mm thick and 1x1 cm square piece, and heated at 250 °C for 2 hrs in vacuo as a preliminary treatment. The sample piece was then dipped into a methyl-ethyl ketone solution of the precursor epoxy- or resol resin and dried in air and cured at about 150-200 °C, then, heated in vacuo to a desired temperature up to 850 °C for carbonization.

#### Electrochemical evaluation:

The test electrode was fabricated by sandwiching the sample piece between two sheets of Ni expanded metal and the rims were spot-welded for tight holding. The test electrode was set in a three electrode glass cell filled with propylene carbonate (PC) or a mixture of ethylene carbonate (EC) and dimethyl carbonate (DMC) (1:1 in v/v) containing 1 M  $\text{LiClO}_4$  and offered to obtain cyclic voltammograms (CV's) or constant current cycle test figures in an argon stream glove box.

### Results and Discussion

In Fig. 1 CV's are compared for the 950°C carbon fiber with and without the epoxy resin

carbon bound. As seen in the figure the cycleability is far better for the C/C sample than that of the single component fiber sample. An example of a constant current cycle test performed with a 1.5 C heavy duty charge and discharge is shown in Fig. 2, where we see the cycleability is well improved for the C/C composite. A more improved cycle performance could be obtained with a resol carbon bound C/C (see Fig. 3). The reason why the better performance could be obtained is due to a better binding action for the resol carbon as seen in Fig. 4, where the different binding appearance can be recognized for the C/C's obtained with two different resins. The cycleability was confirmed to be much more improved for the more conductive carbon and more tight binding.

The authors acknowledge the financial support of the National PEC Fund(MITI).

## References

- [1] N. Takami, A. Satoh, T. Ohsaki and M. Kanda, *J. Electrochem. Soc.*, **145**, 478(1998).
- [2] M. Kikuchi, Y. Ikezawa and T. Takamura, *J. Electroanal. Chem.*, **39**, 451(1995).
- [3] T. Takamura, H. Awano, T. Ura and K. Sumiya, *J. Power Sources*, **68**, 114(1997).

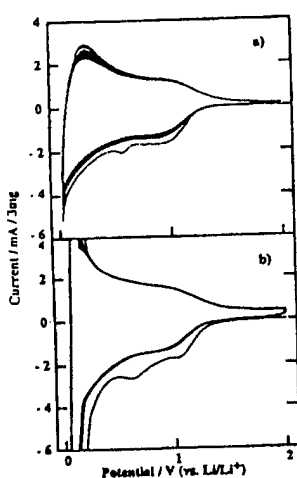


Fig.1 CV's of carbon fiber of pristine(a) and C/C composite(b) composed of carbon fiber and carbonized epoxy. Potential sweep rate: 1 mV/s.

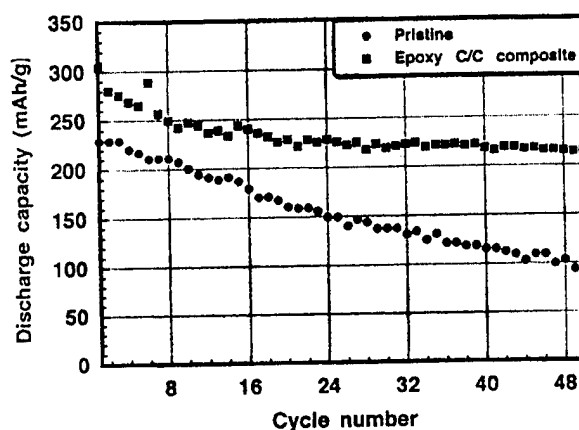


Fig.2 Constant current cycle performance of carbon fiber of pristine (lower curve) and epoxy based C/C composite. Charge/discharge rate: 1.5 C.

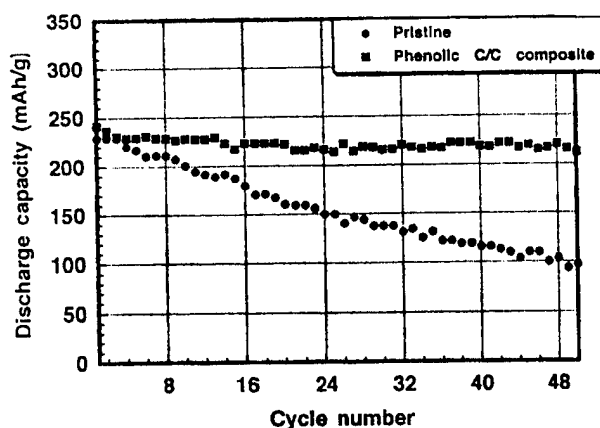


Fig.3 Constant current cycle performance of carbon fiber of pristine (lower curve) and resol based C/C composite. Charge/discharge rate: 1.5 C.



Fig.4 SEM photographs of C/C composites made with epoxy(top) and resol(bottom).

## SURFACE MODIFICATION OF CARBON MATERIALS FOR LITHIUM ION BATTERIES

T. Tsumura<sup>1</sup>, A. Katanosaka<sup>1</sup>, I. Souma<sup>1</sup>, T. Ono<sup>2</sup>, Y. Aihara<sup>2</sup>, and J. Kuratomi<sup>2</sup>

1) NARD Institute, Ltd., 6-1-2, Nishinagasu-cho Amagasaki 660-0805, Japan

2) Yuasa Corporation, 6-6, Josai-cho Takatsuki 569-5065, Japan

Carbon anode for lithium ion batteries is expanded by lithium insertion and is shrunk by lithium extraction. In polymer battery system, the volume change during the charge-discharge cycle causes a cleavage of interface between carbon anode and polymer electrolyte and is thought to decrease the capacity with the increase of the cycle number.

In the present paper, poly(ethylene oxide) (PEO) was grafted on the graphite powder in order to improve wettability of carbon surface to polymer electrolyte (PEO) [1]. There is little acidic group, which is the site for grafting of polymer, on the graphite particles. Therefore, graphite particles were coated with low-crystalline carbon by a mechanical mixing with poly(vinyl chloride) (PVC) powders and heating at a temperature 500 °C in nitrogen gas flow [2-3], and then the carbon-coated particles obtained were oxidized at 400 °C in the air to acidic group on the carbon surface. To evaluate wettability of carbon surface, dispersibility of particles in water was investigated.

PEO-grafted graphite particles were prepared as follows: natural graphite particles and PVC powders (50/50 in weight %) were mixed in a bottle by shaking. The mixtures were heated at 500 °C for 1 h under nitrogen gas flow. After heating, graphite particles were covered with carbonized PVC homogeneously and the weight of residue carbon was about 13 wt.% of PVC mixed. The carbon-coated particles obtained were heated at 400 °C for 4 h in the air to make carboxyl group on the surface. The amount of carboxyl group on carbon surface was determined by titration, and was  $3.1 \times 10^{-5} \text{ mol g}^{-1}$ . The grafting of PEO onto the carbon particles was achieved by esterification of carboxyl group on the carbon with terminal hydroxyl group of PEO. The carboxyl group on the carbon was converted into acid chloride group with  $\text{SOCl}_2$  in benzene at 80 °C for 2 h. After the reaction benzene and unreacted  $\text{SOCl}_2$  were distilled away under reduced pressure. Then acid chloride group on the carbon was reacted with PEO (MW 4,000) in benzene at 80 °C for 24 h. The product was washed with successive, benzene, acetone, and water, and was dried at 100 °C under reduced pressure. The gain of product was 1.8 wt.%, that is, 15 % of carboxyl group on the carbon surface were reacted with PEO.

The dispersibility of the PEO-grafted particles in water was improved compared to that of pristine graphite particles.

### Acknowledgement

This research has been supported by New Energy and Industrial Technology Development Organization (NEDO).

### References

- [1] N. Tsubokawa, Prog. Polym. Sci. 17, (1992) 417.
- [2] M. Inagaki, H. Miura, and H. Konno, J. Euro. Ceram. Soc., in press.
- [3] M. Inagaki, Y. Okada, H. Miura, and H. Konno, Carbon, in press.

## IMPEDANCE STUDY OF THE LITHIUM/ELECTROLYTE INTERFACE UPON CYCLING

François Orsini, Mickaël Dollé, Jean-Marie Tarascon

Laboratoire de Réactivité et de Chimie des Solides, 33 rue Saint Leu 80039 Amiens Cédex France

The plating/stripping process of lithium anode was studied by means of in-situ impedancemetry on a so-called  $\text{Li}^0$ -battery (fig. 1) that consists of a lithium anode coupled with a  $\text{LiMn}_2\text{O}_4$  plastic cathode, both separated by a polymer matrix (PVdF) containing an EC/DMC electrolyte ( $\text{LiPF}_6$  1M). The impedance spectra were acquired during the cycling by means of an Autolab system, and equivalent circuits were used to model the experimental data. From these results a description of the plating/stripping mechanism is proposed, and correlated with the SEM images obtained with a Philips SEM XL30 FEG equipped with a movable airlock [1].

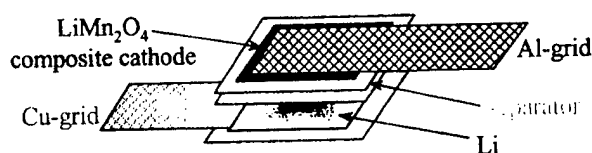


Fig. 1: Configuration of a  $\text{Li}^0$ -battery

The Nyquist plots for different states of charge are shown in fig. 2. During the charge the resistance continuously decreases, whereas it increases during the following discharge.

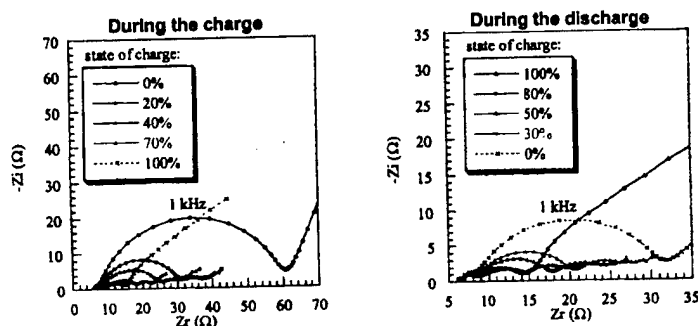


Fig. 2: Nyquist plots recorded during the first cycle

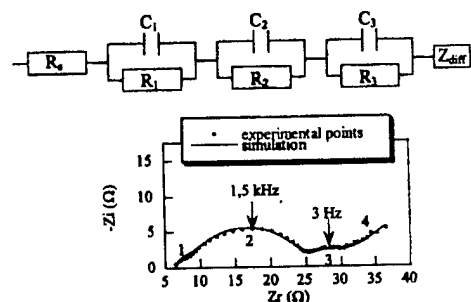
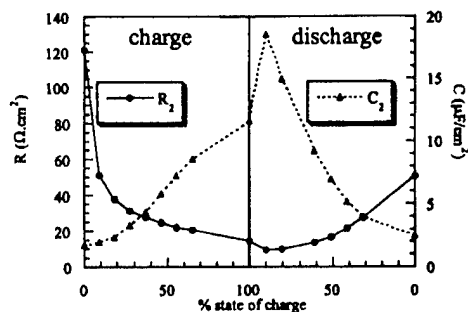
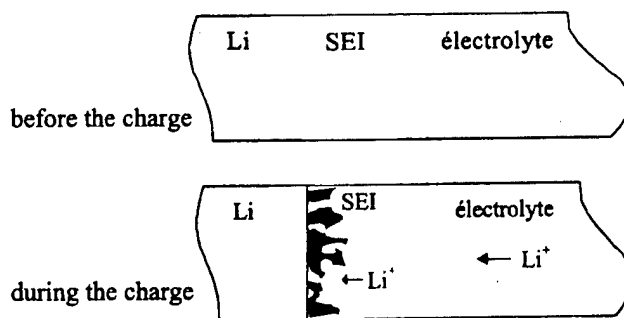


Fig. 3: Example of a fitted diagram

Except for the completely charged/discharged state, each diagram was composed of 4 regions: a high frequency semi-circle (1), a medium frequency semi-circle (2), a low frequency semi-circle (3) and a diffusion tail (4). Then the equivalent circuit of fig. 3 was used to fit the Nyquist plots. On the base of symmetrical cells [2], the high and low frequency semi-circles were attributed to the cathode, while the medium frequency semi-circle (2) mainly represents the  $\text{Li}^0$ /electrolyte interface. Hence the variations of  $R_2$  and  $C_2$  could be determined, with namely an increase and a decrease in  $C_2$  with charge and discharge, respectively, while  $R_2$  decreased and increased over the same sequence (fig. 4).

Fig. 4: Evolution of  $R_2$  et  $C_2$ Fig. 5: Plating mechanism of a  $\text{Li}^0$ -battery

As the charge corresponds to lithium deposition at the anode, the increase in  $C_2$  during the first charge could be ascribed to an increase in the active surface area, due to the morphology of the Li-deposit, as shown by the image fig. 6 that displays the mossy morphology of the deposited lithium, whose texture presents a high surface area. How this Li-deposition occurs is

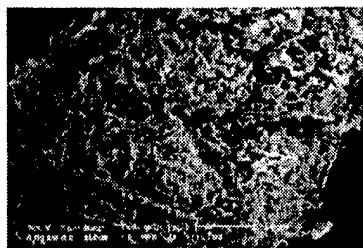


Fig. 6: Mossy Li-deposit

schematized in fig. 5. Another possibility to account for the variations of the  $R_2$  and  $C_2$  values resides in the change in the SEI layer. The contribution of this latter in the semi-circle (2) could be characterized by its resistance and geometric capacitance:  $R = \rho \ell / S$  and  $C = \epsilon S / \ell$ . Besides the increase in the surface value  $S$ , it is known that the thickness  $\ell$  decreases during the plating process [3], which implies an increase in  $C_2$  and a decrease in  $R_2$ .

During the discharge the opposite process reversibly occurs: the specific surface area of the lithium anode decreases, and the film layer tends to grow. Therefore the  $R_2$  values increase and the  $C_2$  values decrease.

In short we showed a clear reversible evolution of the impedance spectra of a lithium battery, which was galvanostatically cycled. These experimental data were modeled in order to separate the different contributions of the cell parts to the Nyquist plot. The interpretation of these results led, among others, to a plating/stripping mechanism mediated by the SEI layer, which was confirmed by in situ SEM observations.

## References:

- [1] F. Orsini, A du Pasquier, J-M Tarascon, M. Trentin, N. Langenhuizen, P. Notten, J. Power Sources, **76**, 19-29 (1998).
- [2] F. Orsini, Thesis, University of Amiens, France.
- [3] E. Peled, in "Lithium Batteries", J.P. Gabano, Editor, Academic Press, London (1983).

## EFFECTS OF PHASE CHANGE ON LITHIUM INSERTION IN GRAPHITE

Melanie Gray, Adam Whitehead and John OwenDepartment of Chemistry  
University of Southampton  
Southampton SO17 1BJ, UK.

The Potentiostatic Intermittent Transient Technique (PITT)[1] is now a standard technique for the study of insertion electrodes and under ideal circumstances this is a good method to determine the diffusion coefficient of the electroactive ion as a function of composition. However, in cases where the insertion causes phase change the interpretation of the results can be difficult due to a change in the conditions of the diffusion and, in particular, the boundary conditions for solving the diffusion equation.

Graphite is studied here as a model system in which most of the insertion capacity occurs across phase boundaries rather than within single phase regions. In this case, the normal PITT equations are inapplicable over most of the charge-discharge cycle. Thermodynamic equilibrium is often not achieved in a slow-scan cyclic voltammogram, and a differential capacity plot formed by pulsed galvanostatic titration shows singularities in the value of  $(dx/dV)$  at the potentials of phase change.

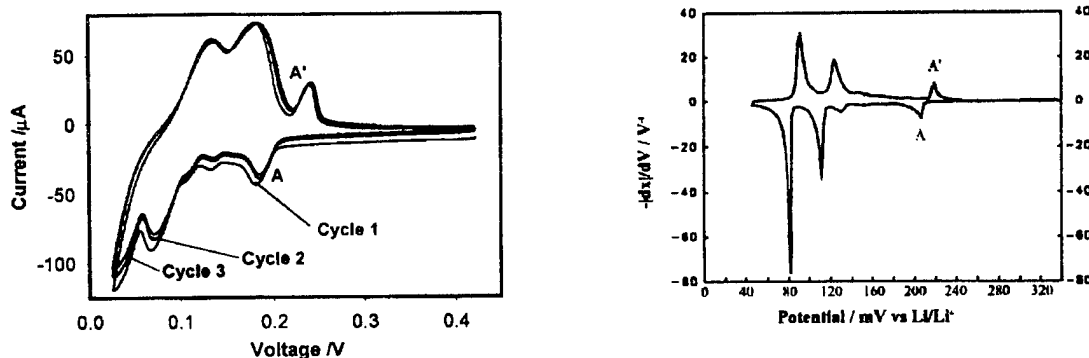


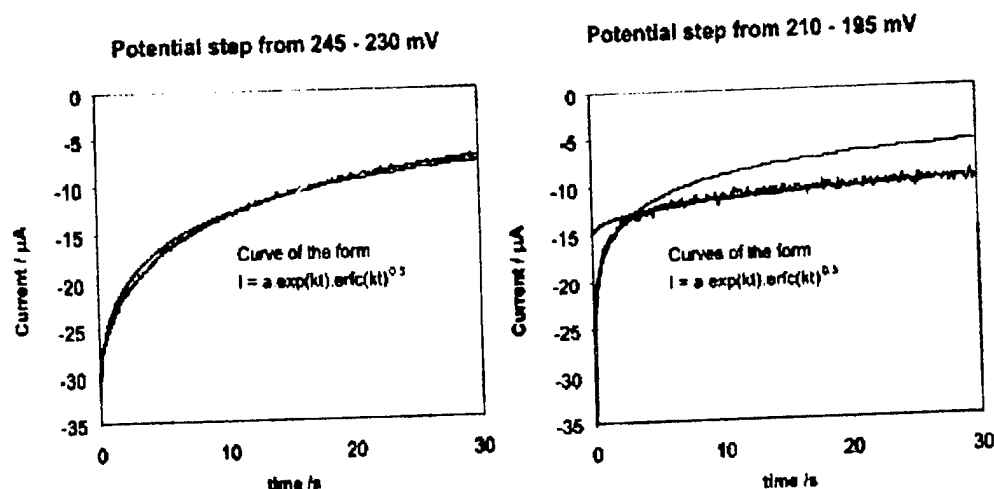
Fig.1 slow scan CV and differentiated composition/voltage plots.

The current response to a potential step across the 1'-4 phase boundary, labelled A in the above diagrams is compared in Fig. 2 with the response in the single phase region. Both have an initial behaviour given by

$$i = a \cdot \exp(kt) \cdot \operatorname{erfc}(kt)^{0.5}$$

as predicted by semi-infinite diffusion boundary conditions and the effect of a series resistance due to the electrolyte and electronic contacts.





In the second case, however, the best fit is obtained by the lowest trace through the superimposition two such curves as in Fig.2. This result is interpreted as the appearance of the new phase at the point where the curves cross. Before the phase change the constant values "a" and "k" are related to diffusion through phase 1'. After the phase change the new values of the constants in the function are related to the diffusion coefficient of phase 4'. Apart from the differences in diffusion coefficient we have a change in boundary conditions, with a moving boundary in the second case, which also leads to the same basic expression in a treatment similar to that of the derivation of the parabolic tarnishing law.

These results will be discussed among some additional results for the voltage response to current pulses across phase boundaries, in an aim to prescribe methods for investigating the charge-discharge kinetics of insertion reactions with phase change.

[1] C.J. Wen, B.A. Boukamp, W.A. Huggins and W. Weppner, J. Electrochem.Soc. (79)126 2258

# LITHIUM INSERTION BEHAVIOUR OF $\text{Li}_{2+2x}\text{V}^{+5}_{6-2x}\text{V}^{+4}_{2x}\text{O}_{16\pm y}$ SYNTHESIZED BY SOL-GEL METHOD.

Ivanov-Schitz A.K.<sup>a</sup>, Pushko S.V.<sup>b</sup>, Chaban N.G.<sup>b</sup>

<sup>a</sup>Institute of Crystallography, Russian Academy of Science, Leninsky pr., 59, Moscow, Russia

<sup>b</sup>Moscow Academy of Fine Chemical Technology, Vernadsky pr., 86, Moscow, Russia

Lithium Vanadium Oxide Bronze  $\text{Li}_{2+2x}\text{V}^{+5}_{6-2x}\text{V}^{+4}_{2x}\text{O}_{16\pm y}$  was synthesized as single phase material from lithium and vanadium alcoholates by hydrolysis of their mixture followed by vacuum firing of xerogels obtained. The phase was identified by X-ray powder diffraction data and chemical analysis. The polycrystalline samples were strongly textured. This fact was discovered by X-ray analysis and electron scanning microscopy data.

Lithium insertion into/from oxide structure was investigated by three electrode method at the galvanostatic mode. 1M  $\text{LiClO}_4$  solution in PC (70% mass.) & DME (30% mass.) was used as electrolyte. Discharge curves at different current densities are shown on Fig.1. The material demonstrates an excellent insertion behaviour in range  $x=0\ldots 0.7$ . The plateau is appeared on the discharge curves in this range at different rates of electrochemical reaction. The X-ray data show that the cell parameter  $a$  is increased during lithium extraction. This fact may be explained by O-O interaction between V-O polyhedrons in adjacent layers.

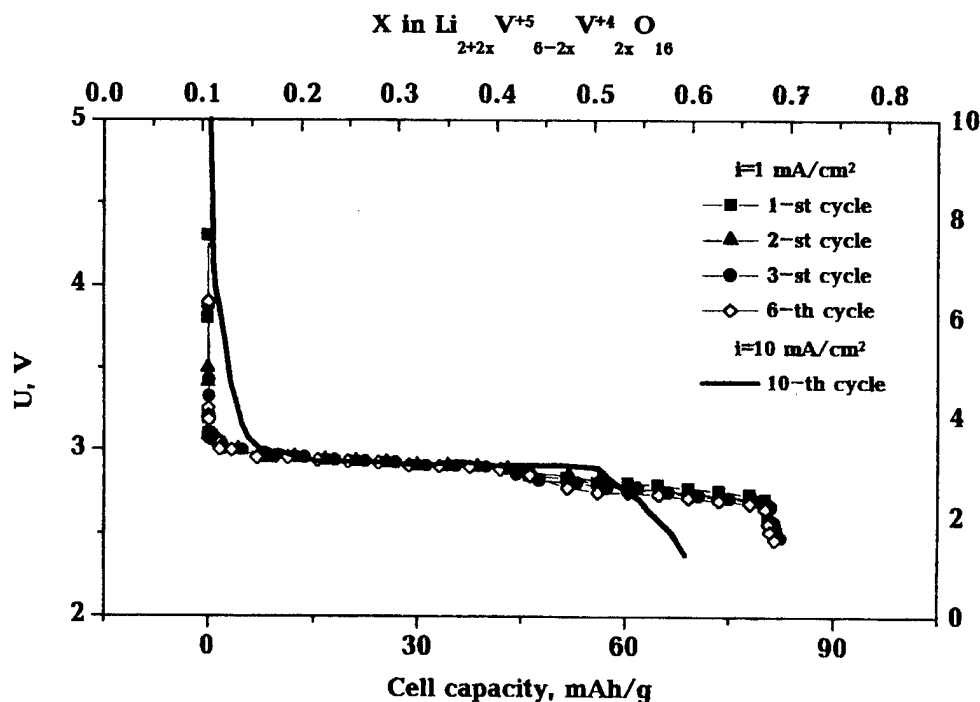


Fig.1 Discharge curves of  $\text{Li}_{2+2x}\text{V}^{+5}_{6-2x}\text{V}^{+4}_{2x}\text{O}_{16\pm y}$  at 10  $\text{mA}/\text{cm}^2$  and 1  $\text{mA}/\text{cm}^2$ .

# EFFECT OF THE LACTATE PRECURSORS ON THE MICROSTRUCTURE OF $\text{Li}_{1+x}\text{Mn}_{2-x}\text{O}_4$ WITH $0 \leq x \leq 0.33$

M. Gorova and E. Zhecheva

Institute of General and Inorganic Chemistry, Bulgarian Academy of Sciences,  
1113 Sofia, Bulgaria, e-mail: banchem@bas.bg

Extensive studies have been devoted to the synthesis, the composition and the electrochemical properties of  $\text{Li}_{1+x}\text{Mn}_{2-x}\text{O}_4$  spinels, but little work has been done on their microstructure [1-2].

In this study we propose a lactate method for the preparation of  $\text{Li}_{1+x}\text{Mn}_{2-x}\text{O}_4$  spinels in a large concentration range:  $0 \leq x \leq 0.33$ . This method consists in the thermal decomposition of Li-Mn-lactate precursors obtained by freeze-drying. EPR of  $\text{Mn}^{4+}$  was used as an experimental tool to monitor the effect of the lactate precursors on the microstructure of the spinels.

In order to apply successfully the low-temperature synthesis techniques, there is a need to mix the initial components on an atomic level [3]. In this sense, the use of the lactic acid,  $\text{CH}_3\text{CH}(\text{OH})\text{COOH}$ , as a chelating ligand via the hydroxyl and carboxylate groups permits a chemical design of the precursors. The complex formation in Li-Mn-organic acid solutions was explored by EPR of  $\text{Mn}^{2+}$ . It is found that  $\text{Mn}^{2+}$  forms both isolated and polymeric complexes with the lactic acid. During the freeze-drying of the solutions, the polymeric  $\text{Mn}^{2+}$ -organic acid complexes are developed at the expense of the disappearance of  $\text{Mn}^{2+}$ -aqua and isolated  $\text{Mn}^{2+}$ -lactate complexes. Finally, amorphous whitish powders with compositions  $\text{LiMn}_2\text{Lac}_6 \cdot x\text{H}_2\text{O}$ , where  $x=2-4$ , are formed. The coordination of the organic acids to  $\text{Mn}^{2+}$  through carboxylate groups are manifested in the IR spectra of the precursors, where the asymmetric and symmetric stretching modes of carboxylate groups,  $\text{COO}^-$ , grow in intensity as compared with the protonated carboxyl groups,  $\text{COOH}$ .

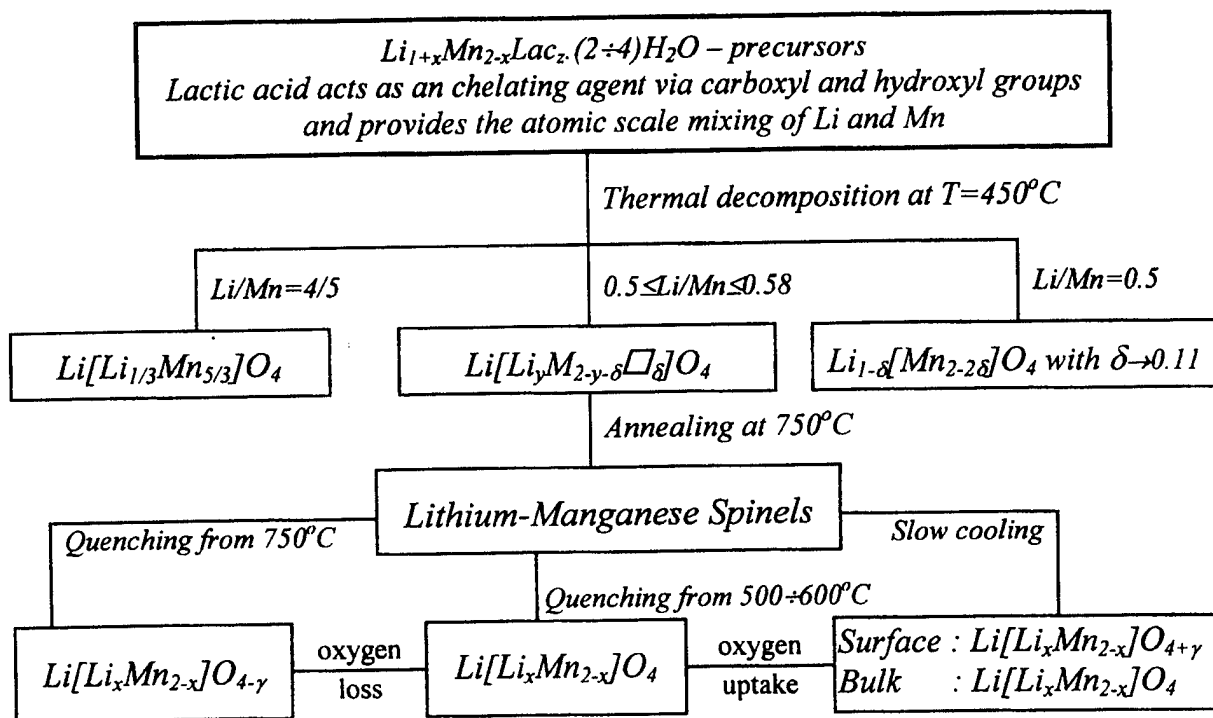
Above  $400^\circ\text{C}$ , Li-Mn-lactate precursors decompose to lithium-manganese spinels, their compositions being dependent on the decomposition rate and the atmosphere used. In oxygen atmosphere, it is possible to prepare at  $450^\circ\text{C}$  and at short heating time (5 hours) well-crystallized lithium-rich and vacancies-rich spinels:  $\text{Li}[\text{Li}_{1/3}\text{Mn}_{5/3}]\text{O}_4$  with  $x=0.33$  and  $\text{Li}_{1-\delta}[\text{Mn}_{2-\delta}]\text{O}_4$  with  $\delta \rightarrow 0.11$ , respectively. It must be pointed out that the lactate method permits to reproduce both compositions, which is hard available by the solid state reactions [4].

For  $\text{Li}_{1+x}\text{Mn}_{2-x}\text{O}_4$  with  $0 \leq x \leq 0.1$  obtained from lactate precursors, the main EPR signal is interpreted within the framework of the bottleneck relaxation mechanism. Depending on the preparation conditions, additional low-intensity EPR signals are resolved. On the basis of the relationship between EPR and structural parameters, cation distribution in the  $\text{Li}_{1+x}\text{Mn}_{2-x}\text{O}_4$  spinels obtained from lactate precursors can be deduced.

At  $0 \leq x < 0.1$ , thermal decomposition of Li-Mn-lactate precursors at  $450^\circ\text{C}$  in air yields  $\text{Li}[\text{Li}_y\text{Mn}_{2-y-\delta}\square_\delta]\text{O}_4$  spinels, in which the excess  $\text{Mn}^{4+}$  and the corresponding vacancies are randomly distributed. Additional annealing of the spinels at  $750^\circ\text{C}$  leads the excess  $\text{Mn}^{4+}$  ions (and the corresponding metal vacancies) leaving the spinel bulk, as a result of which the spinel bulk is close to the stoichiometric:  $\text{Li}[\text{Li}_x\text{Mn}_{2-x}]\text{O}_4$ . In the same time, at these temperatures there is an oxygen release that leads to the formation of complex associates of defects consisting of several  $\text{Mn}^{3+}$  and oxygen vacancies:  $\text{Li}[\text{Li}_x\text{Mn}_{2-x}]\text{O}_{4-\gamma}$ . During the slow cooling from  $750^\circ\text{C}$  in air, the oxygen vacancies annihilate. Thus, the stoichiometric  $\text{Li}[\text{Li}_{0.05}\text{Mn}_{1.95}]\text{O}_4$  spinel is approached by quenching from  $500^\circ\text{C}$ . Below  $500^\circ\text{C}$ , the spinel surface is able to uptake the oxygen in the course of cooling, thus accommodating the non-stoichiometric  $\text{Mn}^{4+}$  ions. The formation of a  $\text{Mn}^{4+}$ -rich surface layer depends not only on the cooling rate, but also on the

sample morphology, which is controlled by sample biography. It is important that, in comparison with spinels obtained by solid state reaction, the spinel compositions obtained from lactate precursors display a stronger sensitivity on the cooling rate.

The data obtained can be summarized schematically as follow:



In conclusion, the results on the microstructural aspects of lithium-manganese spinels can be used for a better comprehension of the well-known effect of the synthesis procedure on the electrochemical properties of  $Li_{1+x}Mn_{2-x}O_4$ .

#### Acknowledgment

Financial support from National Research Foundation of Bulgaria (Contract Ch810/98) is gratefully acknowledged.

#### References

- [1] R. Koksang, J. Barker, H. Shi and M.Y. Saïdi, Solid State Ionics 84, 1 (1996).
- [2] P.G. Bruce, Chem. Commun., 1817 (1997).
- [3] W. Liu, G.C. Farrington, F. Chaput, B. Dunn, J. Electrochem. Soc. 143, 879 (1996).
- [4] F. le Cras, P. Strobel, M. Anne, D. Bloch, J.-B. Soupart and J.-C. Rousche, Eur. J. Solid State Inorg. Chem. 33, 67 (1996).

EPR STUDY OF  $\text{Li}_{1+x}\text{Mn}_{2-x}\text{O}_4$  SPINELS WITH  $0 \leq x \leq 0.33$ 

R. Stoyanova, E. Zhecheva and M. Gorova

Institute of General and Inorganic Chemistry, Bulgarian Academy of Sciences,  
1113 Sofia, Bulgaria, e-mail: banchem@bas.bg

Lithium-manganese spinels,  $\text{Li}_{1+x}\text{Mn}_{2-x}\text{O}_4$ , are able to intercalate/deintercalate lithium reversibly in a large concentration range [1]. This capability provides the opportunity to use  $\text{Li}_{1+x}\text{Mn}_{2-x}\text{O}_4$  as cathode materials in lithium-ion batteries [2]. The interest in  $\text{Li}_{1+x}\text{Mn}_{2-x}\text{O}_4$  is not only practical, but also theoretical, aimed at understanding the electronic and magnetic structure of oxo-bridged mixed-valence  $\text{Mn}^{3+}$ - $\text{Mn}^{4+}$  pairs with a  $90^\circ$  configuration.

The present EPR study of lithium-manganese spinels provides an experimental evidence on Li/Mn distribution in octahedral spinel sites in  $\text{Li}_{1+x}\text{Mn}_{2-x}\text{O}_4$  with  $0 \leq x \leq 0.33$ . We report data on the electron-phonon interaction in  $\text{Li}_{1+x}\text{Mn}_{2-x}\text{O}_4$  with  $0 \leq x \leq 0.1$  in terms of bottleneck relaxation mechanism. EPR of  $\text{Mn}^{4+}$  is used to monitor the cation distribution in  $\text{Li}_{1+x}\text{Mn}_{2-x}\text{O}_4$  with one and the same Li/Mn ratio in respect of cooling rate.

EPR spectrum of  $\text{Li}[\text{Li}_{1/3}\text{Mn}_{5/3}]\text{O}_4$ , which contains only  $\text{Mn}^{4+}$ , displays two overlapping signals with Lorentzian line shape and with  $g = 2.0089$  and  $g = 1.9975$  (Fig. 1). The intensities of the two signals vary with registration temperature, the Curie-Weiss law being obeyed:  $\Theta = 19$  K and  $\Theta = 36$  K for broader and narrower signals, respectively. The intensity of the broader signal is about 10 times higher than that of the narrower signal. These EPR parameters allow assigning both signals to ferromagnetically coupled  $\text{Mn}^{4+}$  ions. Analysis of the EPR line width in terms of magnetic dipole-dipole and exchange interactions points to two kinds of  $\text{Mn}^{4+}$  in octahedral spinel sites: one of them has as first neighbours 5 paramagnetic  $\text{Mn}^{4+}$  and 1 diamagnetic  $\text{Li}^+$ , whereas the second type of  $\text{Mn}^{4+}$  is in  $4\text{Mn}^{4+}$  and  $2\text{Li}^+$  surrounding. In the case of random  $\text{Li}^+/\text{Mn}^{4+}$  distribution in 16d octahedral sites, the mean metal coordination number of  $\text{Mn}^{4+}$  in respect to the number of paramagnetic  $\text{Mn}^{4+}$  neighbours is 5. This shows that only 90% of the  $\text{Mn}^{4+}$  ions registered by EPR exhibit the mean metal coordination number ( $z = 5$ ), while the remaining 10% of the  $\text{Mn}^{4+}$  ions are in Li-rich surrounding ( $z = 4$ ). Although the 16d spinel sites are crystallographically equivalent, EPR data reveal a non-random Li/Mn distribution on 16d octahedral sites: there are regions where Li/Mn are statistically distributed and regions richer in  $\text{Li}^+$ .

With respect to the magnetic properties, the second spinel compositions,  $\text{Li}_{1-\delta}[\text{Mn}_{2-2\delta}]\text{O}_4$  with  $\delta=0.08$ , which contains predominantly  $\text{Mn}^{4+}$ , should be close to  $\text{Li}[\text{Li}_{1/3}\text{Mn}_{5/3}]\text{O}_4$  because the vacancies in octahedral sites would dilute the  $\text{Mn}^{4+}$  magnetic sublattice as was the case for diamagnetic  $\text{Li}^+$  ions. The EPR spectrum of this composition contains a Lorentzian line with  $g = 2.004$  and line width of 240 mT (Fig. 1). The significant broadening of the EPR line of  $\text{Mn}^{4+}$  in  $\text{Li}_{1-\delta}[\text{Mn}_{2-2\delta}]\text{O}_4$  as compared to that of  $\text{Mn}^{4+}$  in  $\text{Li}[\text{Li}_{1/3}\text{Mn}_{5/3}]\text{O}_4$  reflects the contribution of the impurity  $\text{Mn}^{3+}$  ions to the  $\text{Mn}^{4+}$  EPR line width. The presence of small amount of  $\text{Mn}^{3+}$  also suppresses the ferromagnetic interactions and favours the antiferromagnetic interactions in the manganese sublattice: the Curie-Weiss constant determined from the temperature dependence of the EPR signal intensity is  $\Theta = -65$  K.

Taking into account the broadening effect of  $\text{Mn}^{3+}$  on the  $\text{Mn}^{4+}$  line width, one may expect that the  $\text{LiMn}_2\text{O}_4$  spinel in which  $\text{Mn}^{3+}$  and  $\text{Mn}^{4+}$  are present in equal amounts,  $\text{Li}[\text{Mn}^{3+}\text{Mn}^{4+}]\text{O}_4$ , would be EPR-silent. Nevertheless, already at 400 K the EPR spectrum of  $\text{LiMn}_2\text{O}_4$  exhibits a Lorentzian line with a  $g$  factor whose value is equal to that of the  $g$  factor of  $\text{Mn}^{4+}$  (Fig. 1). These peculiarities of the EPR spectrum of  $\text{Mn}^{4+}$  in  $\text{LiMn}_2\text{O}_4$  spinels resemble the main features of the relaxation mechanism called "bottleneck effect" [3]. According to this

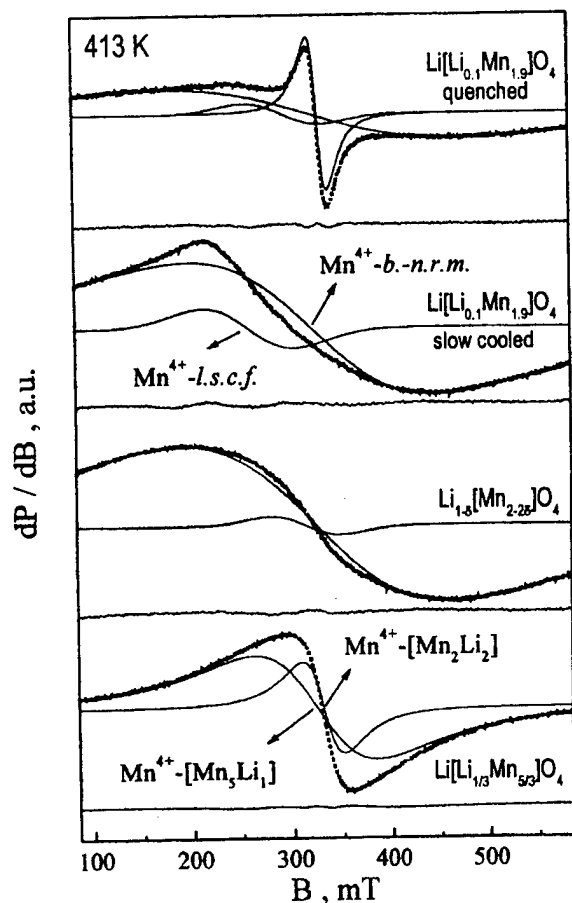


Fig. 1 EPR spectra of lithium-manganese spinels. The dotted and solid lines correspond to the experimental and simulated spectra, respectively.

during slow cooling, a random Li/Mn distribution is achieved.

Summarizing, EPR of  $\text{Mn}^{4+}$  provides new insights into Li-Mn distribution in octahedral sites of  $\text{Li}[\text{Li}_{1/3}\text{Mn}_{5/3}]\text{O}_4$  and  $\text{Li}[\text{Li}_x\text{Mn}_{2-x}]\text{O}_4$  with  $0 \leq x \leq 0.1$ . Besides to the statistical distribution of Li and Mn in 16d spinel sites, EPR of  $\text{Mn}^{4+}$  in  $\text{Li}[\text{Li}_{1/3}\text{Mn}_{5/3}]\text{O}_4$  enables to separate regions rich in lithium. For  $\text{Li}[\text{Li}_x\text{Mn}_{2-x}]\text{O}_4$  with  $0 \leq x \leq 0.1$ , the EPR spectra of  $\text{Mn}^{4+}$  in 16d spinel sites were interpreted in terms of the bottleneck relaxation mechanism. One additional low intensity signal is observed that is attributed to  $\text{Mn}^{4+}$  ions located near oxygen vacancies. It has been demonstrated that EPR of  $\text{Mn}^{4+}$  allows selecting more precisely (as compared to XRD method)  $\text{Li}_{1+x}\text{Mn}_{2-x}\text{O}_4$  spinels on the basis of Li/Mn distribution. This information can be used to develop an EPR method for the control of the cation distribution in  $\text{Li}_{1+x}\text{Mn}_{2-x}\text{O}_4$  spinels, which is of significant meaning for the understanding and, correspondingly, for the improvement of their electrochemical properties.

#### Acknowledgment

Financial support from National Research Foundation of Bulgaria (Contract Ch810/98) is gratefully acknowledged.

#### References

- [1] M.M. Thackeray, W.I.F. David, P.G. Bruce and J.B. Goodenough, Mater. Res. Bull. 18, 461 (1983).
- [2] J.M. Tarascon, A.S. Gozdz, C. Schmutz, F. Shokoohi and P.C. Warren, Solid State Ionics 86, 49 (1996).
- [3] S.E. Barns, Adv. Phys. 30, 801 (1981).

mechanism, the EPR signal observed in  $\text{Li}_{1+x}\text{Mn}_{2-x}\text{O}_4$ ,  $0 \leq x \leq 0.1$ , corresponds to the collective motion of the total magnetic moment of a  $\text{Mn}^{3+}$  and  $\text{Mn}^{4+}$  spin system.

In addition to the main signal, the EPR spectra of  $\text{Li}_{1+x}\text{Mn}_{2-x}\text{O}_4$ ,  $0 \leq x \leq 0.1$ , exhibit a weak signal, whose resonance frequency and line width depend strongly on the temperature of registration. Most probably, this signal might be attributed to  $\text{Mn}^{4+}$  ions in a low-symmetry crystal field ( $\text{Mn}^{4+}$ -l.s.c.f., Fig. 1). The relatively large line width ( $\Delta H_{pp} \approx 90$  mT) is a clear indication that these  $\text{Mn}^{4+}$  ions are localized close one to another, but are isolated from the main  $\text{Mn}^{3+}$  -  $\text{Mn}^{4+}$  spin system. Taking into account the thermal stability of lithium-manganese spinels, one may assume to localize the  $\text{Mn}^{4+}$  ions in low-symmetry crystal fields near oxygen defects.

The EPR parameters of the  $\text{Mn}^{4+}$  ions in lithium-manganese spinels allow distinguishing between spinel compositions with the same Li/Mn content depending on the cooling rate. It is found for quenched samples with enhanced Li/Mn ratio ( $x = 0.1$ , Fig. 1) that part of  $\text{Li}^+$  ions tend to segregate while

## **ELECTRIC PROPERTY AND CHARACTERIZATION OF POLYANILINE DOPED WITH LI IONIC SALT AS POLYMER ELECTRODE IN LI SECONDARY BATTERY**

KwangSun Ryu, Gyejoong Lee\*, Seong-Gu Kang, and SoonHo Chang

Electronics and Telecommunication Research Institute  
161 Kajong-Dong, Yusong-Gu, Taejeon, 305-350, KOREA

\* Department of Chemistry, Sunmoon University, Chungnam 336-840, KOREA

Among the conducting polymers, polyaniline and polypyrrole are expected to be good materials for secondary batteries as polymer electrode since they are stable and have good electrochemical properties. Especially, polyaniline has been described as the most stable conducting polymer and can be used as the positive electrode material of lithium secondary batteries [1,2]. However, the theoretical energy density as well as the specific capacities of the positive electrodes in Li secondary battery depend on the concentration and doping method of the dopant in the electrolyte solution.

Since the Li secondary batteries using the polyaniline doped with acid as the positive electrode have an some problem, the electrical property and characteristics of polyaniline films which are doped with Li ionic salt were investigated in this research. We have tried to fabricate Li ionic salt doping polyaniline and find out the factor that affects electrochemical properties of the polyaniline as positive electrode. Finally, we suggest the mechanism of charge and discharge reaction.

The synthesis of polyaniline powder and film fabrication procedure was already reported by MacDiarmid et al.[3].  $\text{LiPF}_6$  or  $\text{LiBF}_4$  (1M, 0.1M, 0.01M, 0.001M) in EC:DMC(1:1wt%) (EC=ethylene carbonate, DMC=dimethyl carbonate) solution was used as the Li ionic salt doping solution for polyaniline films. The polyaniline films were soaked in the Li ionic salt solution that is also used as electrolyte here, and dried films for using positive electrode.

After the polyaniline film was doped with Li ionic salt, the D.C. conductivity and ESR were measured at the room temperature to prove the doping process of polyaniline with Li ionic salt. If Li salt doping is possible, the poralons are made in polymer chain and the electrical conductivity and ESR signals are detected.

The electrical conductivity of polyaniline film doped with 1M  $\text{LiPF}_6$  is  $\sim 3\text{S/cm}$ , which is similar with electrical conductivity( $\sim 5\text{S/cm}$ ) of one doped with protonic acid(HCl). Moreover, it is dramatically decreased as the concentration of Li salt decreased. The electrical conductivity of polyaniline film doped with 1M  $\text{LiBF}_4$  is  $\sim 1 \times 10^{-2}\text{S/cm}$  and is decreased upon the decresing concentration of Li salt, too. The ESR signals are detected and the g values are  $\sim 2.00265$  in all samples. Therefore, Li salt doping is completely successful.

We measured the cycle voltammometric curves of the Li/polyaniline cell with a scanning rate 1mV/s. There are two broad peak of redox at  $\sim 3.75$  and  $\sim 2.75\text{V}$ (vs  $\text{Li/Li}^+$ ), corresponding to the reduction( $\text{Li}^+$  and  $\text{PF}_6^-$  or  $\text{BF}_4^-$  dedoping) and oxidation( $\text{Li}^+$  and  $\text{PF}_6^-$  or  $\text{BF}_4^-$  doping) processes of polyaniline. This indicates that the doping and dedoping processes of  $\text{Li}^+$  and  $\text{PF}_6^-$  ions are fairly reversible.

The electrochemical cell, which a positive and negative electrodes were made with doped polyaniline films and Li metal was fabricated, respectively. In addition, EC:DMC: $\text{LiPF}_6$  or  $\text{LiBF}_4$  was used as electrolyte and the glass filter as separator. The lithium, separator and doped polyaniline film were accumulated like sandwich in a test cell holder. The cells were tested in the voltage range 2.0~3.9V with constant current density ( $0.2\text{mA/cm}^2$ ) using galvanostatic charge/discharge cycler[4].

Figure 1. is discharge curves of the 1, 5, 10 cycles for Li/polyaniline cell that used the 1M  $\text{LiPF}_6$ .

It is clear that the discharge capacity is nearly not changed with cycling. After one or two cycles, the capacity becomes stable and constant. Nevertheless, discharge curves of the 1, 5, 10 cycles for Li/polyaniline cell that used the 1M LiBF<sub>4</sub> is not stable. The discharge capacity of it is gradually increased until ~12cycle. We obtained the stable discharge capacity about ~40mAh/g and ~35mAh/g, respectively. The theoretical capacity of polyaniline salt is 142.6mAh/g (polyaniline unit doped Li salt). Therefore, the efficiencies of these batteries are ~28% and ~25%.

It is well known that the energy density and the specific capacities of polymer electrode depends on the concentration and doping method of the dopant in the electrolyte solution. In here, we have tried to find out the factor that affect electrochemical properties of the polyaniline as electrodes and suggest the mechanism of charge and discharge reaction.

First, all polyaniline film was doped with 1M LiPF<sub>6</sub> and LiBF<sub>4</sub>, and the electrolyte solutions with different Li salt concentrations were used. Figure 2. is the discharge curve of Li/polyaniline (doped with 1M LiPF<sub>6</sub>) which used the electrolyte solution that is composed with 1M, 0.1M, 0.01M, 0.001M LiPF<sub>6</sub> Li salt concentration. It shows that the electrolyte solution with high concentration is good for discharge capacity. It was also same in case of LiBF<sub>4</sub>. Therefore, Li salt concentration in electrolyte solution is very important in battery ability.

However, if intercalation (Li ion doping) and deintercalation (Li ion dedoping) ion in polymer chain is occurred, Li salt concentration in electrolyte solution does not affect the charge and discharge processes. Then, we compared the polyaniline electrodes that is doped with different Li salt concentration, using the same electrolyte solution. This result shows that the battery composed with polyaniline electrode which is doped with high Li salt concentration has a larger discharge capacity than battery composed with one of low Li salt concentration. Therefore, Li salt concentration used in doping is very important, too.

Finally, we measured the D.C. conductivity and ESR signal of the polyaniline films which is used as a positive electrode after charge and discharge processes in order to identify whether intercalation and deintercalation of Li ion in polymer chain is occurred or not. From these results, the mechanism of charge and discharge reaction will be discussed in detail.

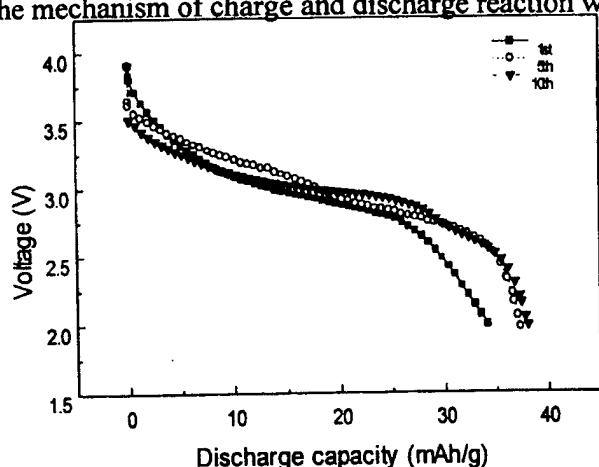


Fig. 1. Discharge curves of the 1, 5, 10 cycles for Li/polyaniline cell that used the 1M LiPF<sub>6</sub>.

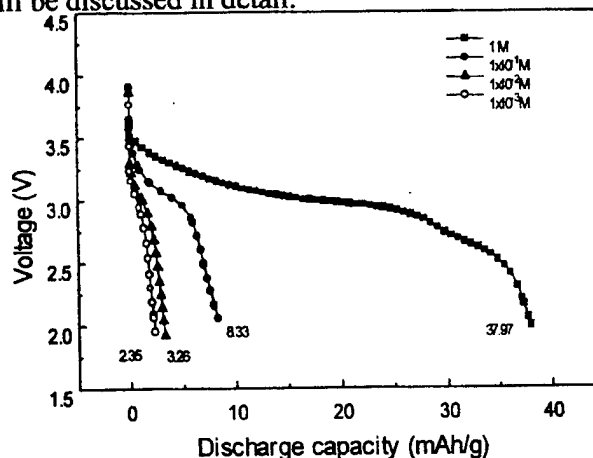


Fig. 2. Discharge curves of Li/polyaniline (doped with 1M LiPF<sub>6</sub>) which used different the electrolyte solution

#### [REFERENCE]

- [1] Goto, F.; Abe, K.; Okabayashi, K.; Yoshida, T.; Morimoto, H. *J. Power Source*, **1987**, 20, 243.
- [2] Yang, L. S.; Shan, Z. Q.; Liu, Y. D. *J. Power Source*, **1991**, 34, 141.
- [3] MacDiarmid, A. G.; Chiang, J. C.; Richter, A. F.; Somasiri, N. L. D.; Epstein, A. J. In, *Conducting Polymers*; L. Alcacer, Eds.; Reidel: Dordrecht, Netherlands, 1987; p 105.
- [4] Chang, S. H.; Kang, S. G.; Jang, K. H.; Ryu, K. S. *Bull. Kor. Chem. Soc.*, **1998**, 19(2), 261.



## TRANSPORT AND ELECTROCHEMICAL PROPERTIES OF $\text{Bi}_2\text{Sr}_2\text{CaCu}_2\text{O}_{8+\delta}$ SUPERCONDUCTOR

J. Molenda, I. Nowak

*Department of Solid State Chemistry, Stanisław Staszic University of Mining and Metallurgy,  
Al. Mickiewicza 30, 30-059 Cracow, Poland*

Investigations of ionic and electron defect structure in ceramic superconductors is of vital importance. It allows to determine optimum conditions for obtaining such superconductors and also to study the influence of point defect structure on superconducting properties. The conditions of technological process, that means annealing of a material at a given temperature and defined oxygen pressure as well as a cooling rate are the factors responsible for the differentiated properties of a final material, in particular different temperature of transition into a superconducting state and different content of superconducting phase.

The role of oxygen non-stoichiometry is complex. Non-stoichiometry affects the relation  $\text{Cu(III)}:\text{Cu(II)}$ ,  $\text{Bi(V)}:\text{Bi(III)}$ , the value of the lattice parameters and it is responsible for the disordered state of the system. The dependence of electrical conductivity and thermoelectric power on oxygen pressure at constant temperature under thermodynamic equilibrium conditions has been investigated for  $\text{Bi}_2\text{Sr}_2\text{CaCu}_2\text{O}_{8+\delta}$ . The investigations were carried out in the range of 600-1100 K and oxygen pressure of  $1-10^{-4}$  atm.

The layered structure of the bismuth superconductor studied in this work and its high electrical conductivity allows introducing foreign ions, particles or atoms into its structure in a reversible mode. The study presents the results of electrochemical introduction of lithium into the bismuth superconductor, up to the content of 1 mole of lithium per 1 mole of  $\text{Bi}_2\text{Sr}_2\text{CaCu}_2\text{O}_{8+\delta}$ . It has been found that the reaction takes place preserving the host crystalline structure, without formation of a new phase. The analysis of electrical and electrochemical properties of this material has shown their close correlation. Investigations of the electrical properties of the  $\text{Li}_x\text{Bi}_2\text{Sr}_2\text{CaCu}_2\text{O}_{8+\delta}$  system have revealed a modification of electronic properties during intercalation. It has been observed that this system displays the best transport properties for lithium content of 0.4 mol/1mol  $\text{Bi}_2\text{Sr}_2\text{CaCu}_2\text{O}_{8+\delta}$ . For this concentration of lithium also the maximum of lithium chemical diffusion coefficient is observed. This indicates that the effectiveness of intercalation process ( $D_{\text{Li}}$ ) is related to transport properties of electron carries. The measurements carried out in this work indicate that the bismuth superconductor may be considered as a cathode material in reversible lithium cells.

## **ELECTRONIC STRUCTURE AND ELECTROCHEMICAL PROPERTIES OF $\text{Li}_x\text{Ni}_y\text{Co}_{1-y}\text{O}_2$**

J. Molenda, P. Wilk

*Department of Solid State Chemistry, Stanislaw Staszic University of Mining and Metallurgy,  
Al. Mickiewicza 30, 30-059 Cracow, Poland*

The  $\text{Li}_x\text{Ni}_y\text{Co}_{1-y}\text{O}_2$  system has evoked great interest within the past few years because of its high potential in relation to lithium and possible application in a Li-ion battery. In spite of keen interest in  $\text{Li}_x\text{Ni}_y\text{Co}_{1-y}\text{O}_2$  system, its properties are not sufficiently known. There is no data on its transport properties, electrical properties and nonstoichiometry. It has been reported that the potential, capacity and current-voltage characteristics of  $\text{Li}_x\text{Ni}_y\text{Co}_{1-y}\text{O}_2$  cathode are strongly dependent on the temperature  $\text{Li}_x\text{Ni}_y\text{Co}_{1-y}\text{O}_2$  synthesis and on the cooling rate. This behaviour can be related to nonstoichiometry which depends on heat treatment conditions, i.e. temperature, oxygen pressure and cooling rate.

This work was aimed at extensive studies of structural, transport and electrochemical properties of  $\text{Li}_x\text{Ni}_y\text{Co}_{1-y}\text{O}_2$  system in order to find a correlation between the effectiveness of lithium intercalation and transport properties of the electrode material. The physico-chemical properties (structure, electrical conductivity, thermoelectric power, chemical diffusion coefficient of lithium) of  $\text{Li}_x\text{Ni}_y\text{Co}_{1-y}\text{O}_2$  were studied as function of lithium concentration. These investigations are very important because they enable the determination of the relation between electronic and reactivity of the cathode material.

## SYNTHESIS AND ELECTROCHEMICAL PROPERTIES OF LITHIUM NICKELATE SYSTEM BY EMULSION DRYING METHOD

Jin Gyun Kim<sup>1</sup>, Yong Joon Park<sup>1</sup>, Moon Kyu Kim<sup>1</sup>, Hoon Taek Chung<sup>2</sup>,  
Seung Taek Myung<sup>2</sup> and Ho Gi Kim<sup>1</sup>

<sup>1</sup>Department of Materials Science and Engineering, Korea Advanced Institute of Science and Technology (KAIST), 373-1 Kusong-dong, Yusong-gu, Taejeon, 305-701 Korea

<sup>2</sup>Department of Ceramic Engineering, Dong-shin Univeristy, 252 Naju, Chonnam  
520-714, Korea

### Introduction

The preparation problems of  $\text{LiNiO}_2$ , which have inhibited for years the development of the lithium-carbon battery with this materials as the positive electrode. From the fundamental point of view, numerous studies related to the material synthesis[1] and characterizasion, to the unit cell modifications induced by the lithium deintercalation[2-3], and to the effect of various substituting cations have been reported[4-9].

### Experimetal

Emulsion powder of  $\text{LiNiO}_2$  system was prepared at various temperature, heating time by using  $\text{LiNO}_3$  and  $\text{Ni}(\text{NO}_3)_2 \cdot 6\text{H}_2\text{O}$  as the starting materials. The test electrode was prepared by forming a paste made of the active material, carbon black, poly(vinylidenedifluoride) (PVDF) solution and NMP solvent. The paste was then coated on an stainless steel exmet. The electrochemical performances of  $\text{LiNiO}_2$  system were evaluated in a glass cell containing a lithium foil anode, a lithium reference electrode and an electrolyte consisting of 1M  $\text{LiClO}_4$  dissolved in PC or 1M  $\text{LiPF}_6$  dissolved in EC+DMC (1:1). The cells were cycled between the voltage limits of 4.3 to 2.5V at C/7 rate during both charge and discharge.

### Results and Discussion

The materials prepared under a flow of oxygen show a large intergrated intensity ratio  $I_{(003)}/I_{(104)}$  and a clear split of the (006) and (012) as well as (108) and (110) peaks which are indicative of less disorder in the structure. The reaction mechanisms of materials prepared by emulsion drying method( $\text{LiNO}_3$  and  $\text{Ni}(\text{NO}_3)_2 \cdot 6\text{H}_2\text{O}$ ) were investigated by differential thermal (DTA) and thermogravimetric (TG) analysis in air atomosphere. TG and DTA result indicates that several step reactions take place during the preparation process. Three peaks observed at lower than 100°C, 400°C and upper than 700°C. The endothermic observed at a temperature lower than 100°C, associated with a limited weight loss, corresponds to the elemination of the water molecule absorbed by  $\text{LiNO}_3$ . The second exothermic peak is probably the result of burning kerosine and organics. The remaining other prak is the result of reaction of the precursors. Fig 1. Shows the charge and discharge characteristics of the several cycle of  $\text{LiNiO}_2$  prepared by emulsion drying method.

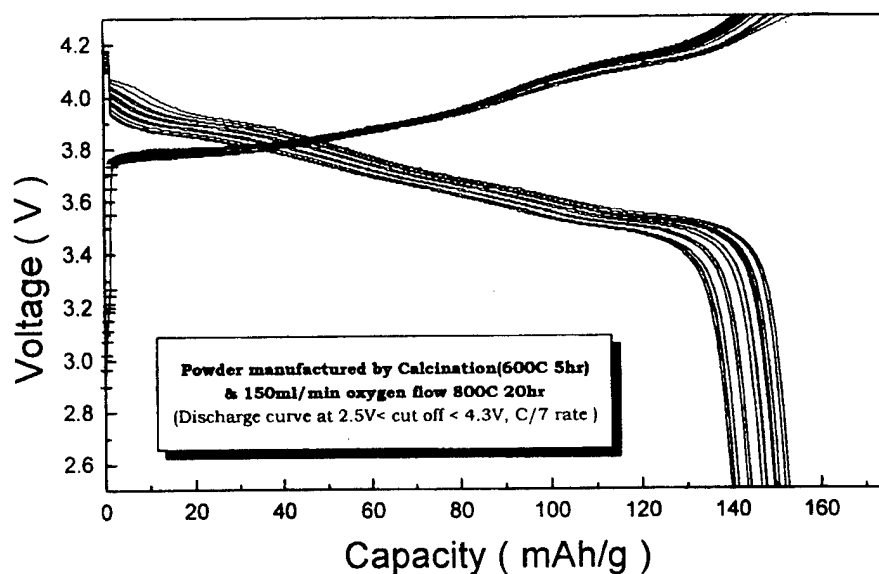


Fig.1. Charge and discharge capacity with several cycle of  $\text{LiNiO}_2$  prepared by emulsion drying method in  $\text{Li}/1\text{M LiClO}_4\text{-PC}$  or  $1\text{M LiPF}_6\text{-EC+DMC}(1:1)/\text{LiNiO}_2$  (at 2.5-4.3V, C/7 rate)

### References

- [1] A. Rougier, P. Gravereau, C. Delmas, J. Electrochem. Soc. 143, 1168(1996)
- [2] T. Ohzuku, A. Ueda, M. Nagayama, J. Electrochem. Soc. 140, 1862(1993)
- [3] W. Li, J. N. Reimers, J. R. Dahn, Solid State Ionics 67, 123(1993)
- [4] C. Demas, I. Saadoune, A. Rougier, J. Power Sources 43/44, 595(1993)
- [5] C. Demas, I. Saadoune, Solid State Ionics 53/56, 370(1992)
- [6] A. Ueda, T. Ohzuku, J. Electrochem. Soc. 141, 2013(1994)
- [7] T. Ohzuku, A. Ueda, M. Kouguchi, J. Electrochem. Soc. 142, 4033(1995)
- [8] J. N. Reimers, E. Rossen, C. D. Johns, J. R. Dahn, Solid State Ionics 61, 335(1993)
- [9] E. Rossen, C. D. Johns, J. R. Dahn, Solid State Ionics 57, 311(1992)

## STUDY ON ALL SOLID-STATE LITHIUM-ION CELLS CONTAINING $\text{LiMn}_2\text{O}_4$ THIN FILM

Y. J. Park<sup>1</sup>, J. G. Kim<sup>1</sup>, M. K. Kim<sup>1</sup>, H. T. Chung<sup>2</sup> and H. G. Kim<sup>1</sup>

<sup>1</sup>Department of Materials Science and Engineering, Korea Advanced Institute of Science and Technology(KAIST), 373-1 Kusong-dong, Yusong-gu, Taejeon, Korea

<sup>2</sup>Department of Ceramic Engineering, Dong-shin Univeristy, 252 Naju, Chonnam 520-714, Korea

Currently, Advances in the microelectronics industry have reduced the current and power requirement of electronic devices. Therefore, all solid-state microbattery have attracted more attention for various application field such as micromechanics and memory devices[1-2]. The film-electrode for microbattery have usually been fabricated by using sputtering, E-beam evaporation, pulse-laser deposition, and CVD. These methods, however, have several disadvantages such as difficulty in controlling the stoichiometry, long period of deposition, and high cost fabrication. We have been interested in preparing thin films for electrode of microbattery by sol-gel method to overcome these problems. The sol-gel method offers the several advantages such as excellent control of stoichiometry, easy control of crystallinity, density, and microstructure. Moreover, cost for fabrication is relatively low and deposition rate is high.

In our previous work[3], the films of  $\text{LiMn}_2\text{O}_4$  is fabricated by sol-gel method successfully. The films had the smooth and dense surface, small and uniform grains, and good rechargeability. Fig.1 shows the good rechargeability of  $\text{LiMn}_2\text{O}_4$  thin-film electrode.

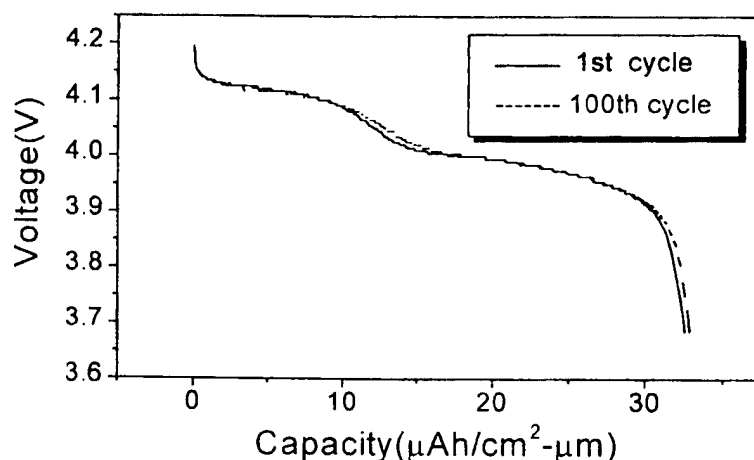


Fig. 1 Comparison of discharge curves between first cycle and 100th cycle for the cell of Li/1M  $\text{LiClO}_4$ -PC solution/ $\text{LiMn}_2\text{O}_4$  thin film (current density is  $100\mu\text{A}/\text{cm}^2$ ).

In the present work, we fabricated all solid-state lithium ion cells containing  $\text{LiMn}_2\text{O}_4$  thin-film by using solid electrolyte. The electrochemical properties of these cells were extensively investigated. We specially focused the comparison of rechargeability between the cell using the solid electrolyte and the cell using the liquid electrolyte.

### References

- [1] S. D. Jones, J. R. Akridge, F. K. Shokoohi, Solid State Ionics, 69 (1994) 357 -368
- [2] J. B. Bates, G. R. Gruzalski, N. J. Dudney, C. F. Luck, X. Yu, Solid State Ionics 70/71 (1994) 619-623
- [3] Y.-J. Park, J.-G. Kim, M.-K. Kim, H.-T. Chung, W.-S. Um, M.-H. Kim and H.-G. Kim, J. Power Sources, 76/1, (1998) 41-47

# DETERMINATION OF THE $\text{Li}^+$ CHEMICAL DIFFUSION COEFFICIENT IN AN ELECTROLYTIC $\text{V}_2\text{O}_5$ BY DIFFERENT ELECTROCHEMICAL TECHNIQUES

E. Potiron, D. Guyomard, V. Legagneur, A. Le Gal La Salle and Y. Piffard.

Institut des Matériaux de Nantes - 2, rue de la Houssinière

BP 32229 - 44322 Nantes Cedex 3 - France

Many electrochemical techniques can be found in the literature in order to evaluate the chemical diffusion  $D_{\text{Li}}$  of  $\text{Li}^+$  ion in a host structure. We have used 4 complementary techniques to determine  $D_{\text{Li}}$  in an electrolytic- $\text{V}_2\text{O}_5$  compound, called e- $\text{V}_2\text{O}_5$ . Results are compared and discussed in relation to literature data on e- $\text{V}_2\text{O}_5$  and other  $\text{V}_2\text{O}_5$  polymorphs.

e- $\text{V}_2\text{O}_5$  is a promising positive electrode material for lithium batteries, prepared by oxidative electrodeposition from an aqueous vanadyl sulfate solution [1]. This poorly crystallized material exhibits a layered structure. On account of its chemical formula, it can be considered as either a polyvanadic acid  $\text{H}_x\text{V}_2\text{O}_5 \cdot n\text{H}_2\text{O}$  or a hydrated vanadium oxide  $\text{V}_2\text{O}_{5.82} \cdot n'\text{H}_2\text{O}$ . It is stable up to 200°C in air. At higher temperature, the loss of structural water induces a phase transition leading to  $\alpha$ - $\text{V}_2\text{O}_5$ .

The Li intercalation behavior of dehydrated e- $\text{V}_2\text{O}_5$  was investigated in Li batteries ( $\text{Li}/\text{LiPF}_6$  (1M) in EC+DMC (2:1)/e- $\text{V}_2\text{O}_5$ ). It is intermediate between those of crystallized and amorphous  $\text{V}_2\text{O}_5$ , with two main intercalation processes at 3.15 and 2.55 V vs Li, as shown in Figure 1. Intercalation of more than 1.5 Li per  $\text{V}_2\text{O}_5$  leads to an apparent voltage plateau at 1.7V under current, with an equilibrium potential in the continuity of the equilibrium potential of the 2.55V process. Chrono-amperometry experiments have shown that these processes correspond to single phase intercalation reactions involving  $\text{Li}^+$  ion diffusion.

The following 4 techniques have been used to determine  $D_{\text{Li}}$  :

- galvanostatic intermittent titration techniques (GITT), with three different variations :
  - the long current pulse technique,
    - with fitting the voltage variation upon current flow [2] or
    - with fitting the voltage variation under relaxation (after the current interruption) [3],
  - the short current pulse technique, with fitting the voltage variation under relaxation [4].
- the potentiostatic technique of the voltage step, with fitting the variation of current vs. time [2].

These different techniques lead to the experimental determination of the product  $D_{\text{Li}} A^2$  or the ratio  $D_{\text{Li}}/L^2$  ( $A$  is the electrochemically active surface and  $L$  is the characteristic diffusion distance). The true BET surface area and the average particule size were used to extract the  $D_{\text{Li}}$  value from these product or ratio.

Results show that all techniques are not suitable in the whole Li composition range. The different techniques give very similar relative variations of  $D_{\text{Li}}$  with the Li composition. However, differences in  $D_{\text{Li}}$  values of more than one order of magnitude have been obtained with the different methods. The possible origin of these discrepancies will be discussed.

Results obtained with the first technique [2] are shown in Figure 2. With increasing Li composition,  $D_{\text{Li}}$  increases first, then stabilizes and finally decreases up to  $x=1.5$ .  $D_{\text{Li}}$  decreases abruptly by two orders of magnitude when moving to the 1.7V voltage plateau, indicating that the observed increase in polarization comes mainly from a slower diffusion kinetics.

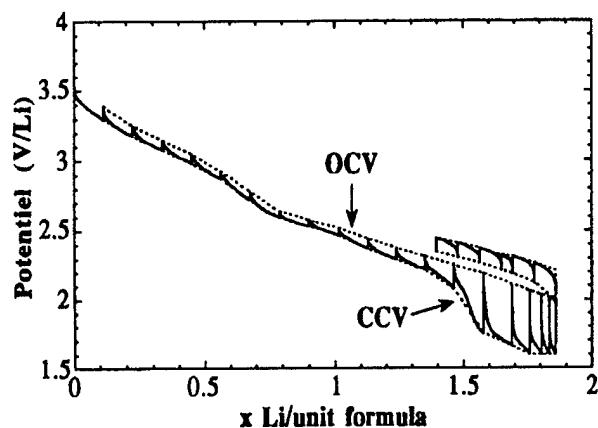


Figure 1: First discharge of an  $e\text{-V}_2\text{O}_5$  using GITT.

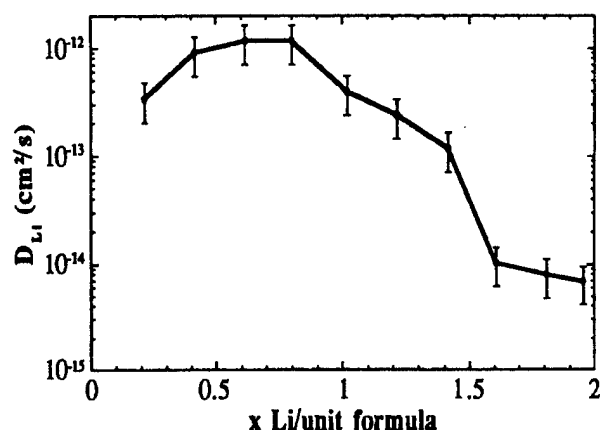


Figure 2: Variations of the lithium chemical diffusion coefficient of an  $e\text{-V}_2\text{O}_5$  versus the intercalation rate during the first discharge - Determination by the short current pulse technique (Basu and Worrell).

### References

- [1] - Y. Sato, T. Nomura, H. Tanaka and K. Kobayakawa, *J. Electrochem. Soc.*, 138(9), L37, 1991.
- [2] - W. Weppner and R.A. Huggins, *J. Electrochem. Soc.*, 124, 1977, 1569  
- C.J. Wen, B.A. Boukamp, R.A. Huggins and W. Weppner, *J. Electrochem. Soc.*, 126, 1979, 2258
- [3] - A. Honders, E.W.A Young, A.H. van Heeren, J.H.W; de Wit and G.H.J. Broers, *Solid State Ionics*, 9-10, 1983, 375-382  
- A. Honders, J.M. der Kinderen, A.H. van Heeren, J.H.W. de Wit and G.H.J. Broers, *Solid State Ionics*, 15, 1985, 265
- [4] - S. Basu and W.L. Worrell, in: Fast ion transport in solids, eds. P. Vashista, J.N. Mundy and E.K. Shenoy, 1979, 149-152



# $\text{Li}_2\text{Mn}(\text{VO}_3)_4 \cdot 2\text{H}_2\text{O}$ : PREPARATION, STRUCTURE AND LITHIUM INSERTION - DEINSERTION BEHAVIOR.

V. Legagneur, A. Le Gal La Salle, Y. Piffard and D. Guyomard.  
 Institut des Matériaux de Nantes - 2, rue de la Houssinière  
 BP 32229 - 44322 Nantes Cedex 3 - France

In the course of ongoing investigations for the design of new materials that could be used as electrode materials for lithium batteries, syntheses have been done in the Li-Mn-V-O system under hydrothermal conditions. Our interest in mixed manganese / vanadium compounds stems from the possibility that both Mn and V can display mixed valency, and as such these compounds may exhibit valuable insertion / deinsertion properties. This presentation will report the preparation under hydrothermal conditions of the new compound  $\text{Li}_2\text{Mn}(\text{VO}_3)_4 \cdot 2\text{H}_2\text{O}$ , its crystal structure, and its lithium insertion/deinsertion behavior.

Crystals of  $\text{Li}_2\text{Mn}(\text{VO}_3)_4 \cdot 2\text{H}_2\text{O}$  were prepared in water at 110°C from a mixture of LiOH,  $\text{MnSO}_4 \cdot \text{H}_2\text{O}$  and  $\text{LiVO}_3$  in a molar ratio of 2:1:4. The title compound crystallizes in space group C2/m of the monoclinic system with  $a=19.286(5)\text{\AA}$ ,  $b=3.523(1)\text{\AA}$ ,  $c=8.164(2)\text{\AA}$  and  $\beta=105.38(3)^\circ$ . Its structure, displayed in figure 1, was determined from single crystal data. It is built up from  $\text{MnO}_6$  octahedra and  $\text{VO}_5$  square pyramids. The  $\text{VO}_5$  polyhedra share edges with each other to form  $(\text{VO}_3)_n^-$  chains that run along the b axis. These chains are linked together via corner sharing by parallel rutile-type chains of edge-sharing  $\text{MnO}_6$  octahedra, leading to a two-dimensional arrangement. Water molecules and lithium atoms are located within the interlayer space.

On account of the main features of its structure (interlayer space for lithium,  $\text{MnO}_6$  octahedra which can accommodate  $\text{Mn}^{n+}$  cations with  $2 \leq n \leq 4$ , and  $\text{VO}_5$  square pyramids which can be occupied by both  $\text{V}^{5+}$  and  $\text{V}^{4+}$  cations) one may anticipate for  $\text{Li}_2\text{Mn}(\text{VO}_3)_4 \cdot 2\text{H}_2\text{O}$  both a  $\text{Mn}^{2+}/\text{Mn}^{4+}$  oxidation upon Li deintercalation, and a  $\text{V}^{5+}/\text{V}^{4+}$  reduction upon Li intercalation.

A thermal analysis shows that the dehydration process occurs in one step at 150°C. It is irreversible and leads to a mixture of  $\text{LiVO}_3$  and  $\text{MnV}_2\text{O}_6$ . Consequently, electrochemical experiments were undertaken on the hydrated compound.

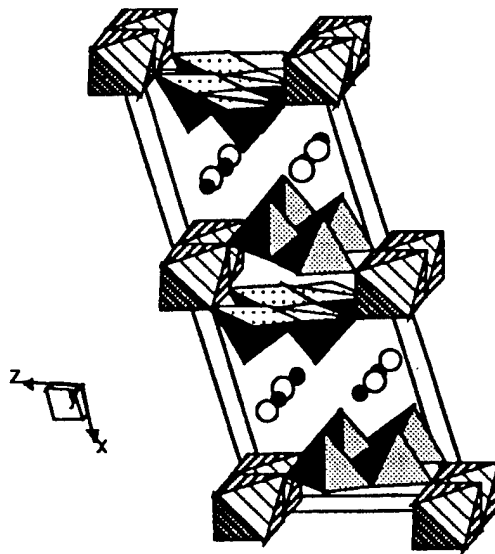


Figure 1:  $\text{Li}_2\text{Mn}(\text{VO}_3)_4 \cdot 2\text{H}_2\text{O}$  - Perspective view of the structure along the b axis

Lithium insertion at constant current into  $\text{Li}_2\text{Mn}(\text{VO}_3)_4 \cdot 2\text{H}_2\text{O}$  shows a reduction phenomenon occurring at low voltage (1.6V vs. Li), while lithium deinsertion gives an oxidation phenomenon at high voltage (4.5V vs. Li).

In order to better understand this behavior, a GITT study has been undertaken, coupled with ex-situ XRD at different steps of the insertion/deinsertion behavior, in order to check possible structural modifications. Low currents have been chosen, corresponding to the insertion (or deinsertion) of 1 Li per formula unit in 50hrs, and different relaxation conditions have been tried (from 5mV/h to 0.1mV/h).

Preliminary GITT studies indicate that, during discharge down to 1.5V vs. Li, some lithium is inserted until a composition close to  $\text{Li}_{10}\text{Mn}(\text{VO}_3)_4 \cdot 2\text{H}_2\text{O}$ . During subsequent recharge, the voltage increases rapidly to about 4.5V/Li, which seems to correspond to a very poor reversibility of the insertion reaction. After starting directly in charge, the next discharge presents the same V-x shape as when starting directly in discharge, showing that the compound has not been modified by oxidation. This behavior seems to indicate that the oxidation process is not a lithium deinsertion reaction.

## COMBUSTION SYNTHESIS AND PROPERTIES OF SUBSTITUTED LITHIUM COBALT OXIDES IN LITHIUM BATTERIES

C. Julien<sup>a</sup>, M. Camacho-Lopez<sup>a</sup>, M. Lemal<sup>a</sup>, T. Mohan<sup>b</sup>, S. Chitra<sup>b</sup>, P. Kalyani<sup>b</sup> and S. Gopukumar<sup>b</sup>

<sup>a</sup>Laboratoire des Milieux Désordonnés et Hétérogènes, UMR 7603, Case 86, Université Pierre et Marie Curie, 4 place Jussieu, 75252 Paris cedex 05, France

<sup>b</sup>Lithium Batteries Group, CECRI, Karaikudi 630006, India

$\text{LiCo}_{1-y}\text{Ni}_y\text{O}_2$  compounds which are isostructural with the layered oxide end-members exhibit interesting electrochemical features as cathode materials in lithium batteries [1]. With a lower insertion potential, they are expected to be oxidatively less demanding on the electrolyte phase. In recent years, there has been a great deal of interest in the preparation of these materials, using low-temperature (LT) techniques such as sol-gel, combustion, and precipitation methods using complexing agents like succinic, oxalic, malic or tartaric acids [2]. Solution preparative techniques allow a better mixing of the elements and thus a better reactivity of the mixture to obtain purer reaction products. Lower reaction temperature and shorter reaction time are then possible to yield a compound of high homogeneity and high specific area. Moreover, these LT methods make use of lower calcination temperatures resulting in particles of smaller size and a highly strained lattice.

In this work, we are studying the physical and electrochemical properties of  $\text{LiCo}_{1-y}\text{Ni}_y\text{O}_2$  materials prepared by fuel-nitrate combustion method. The synthesis procedure was using aqueous solutions containing the respective metal nitrates i.e.,  $\text{Ni}(\text{NO}_3)_2$ ,  $\text{Co}(\text{NO}_3)_2$ , and  $\text{LiNO}_3$ , and a fuel substance in stoichiometric amounts. Fuels such as urea and glycine were used. The mixtures, when dried and heated in the temperature range 300-600°C, ignite and yield submicron-sized powders. Physical properties of the synthesized products were investigated in the light of structural (XRD, SEM), spectroscopic (FTIR and Raman), and thermal (DTA/TG) analyses.

DTA results display that the material formation occurred below 400°C. A strong exothermic peak appears in the range 230-250°C after the departure of the remaining water molecule at ca. 120°C. The formation temperature of the oxide prepared from the combustion-method is dependent on the nickel content in the Li-Ni-Co oxide precursor. The exothermic effect corresponds to the combustion of either glycine-nitrates or urea-nitrates.

X-ray analysis was carried out on the synthesized products at various preparation stages of  $\text{LiNi}_{1-y}\text{Co}_y\text{O}_2$  powders to monitor the phase purity and structure, phase concentrations and the amorphous content. X-ray diffraction patterns show that single-phase impurity free with a well-defined  $\alpha\text{-NaFeO}_2$ -type structure can be made through careful selection of precursors. Fig. 1 shows the XRD diagrams of  $\text{LiNi}_{1-y}\text{Co}_y\text{O}_2$  powders grown by the glycine-assisted method. When a material was precalcined at 400°C, a significant amount of the  $\text{LiNi}_{1-y}\text{Co}_y\text{O}_2$  phase peaks and a small amount of the impurity peaks are detected. This is quite consistent with the DTA data which show the crystallization peak at 380-398°C.

Fourier transform far-infrared measurements probed the cationic environment in layered

structure in order to investigate the cation distribution, the cationic mixing effect and local distortion in the lithiated lattice [3]. FTIR measurements confirm XRD data showing the formation of pure phases. However, we got additional information on the lattice structure, especially on the distribution of the transition metal in the (Ni, Co)O<sub>2</sub> slabs. The shape of the FTIR spectra of the cobalt-rich products shows the predominance of the stretching modes. The frequency shift of both the IR bending and stretching modes are due to the change in the volume of the unit cell and, of course, to the modification of the covalency of the (Ni<sub>1-y</sub>Co<sub>y</sub>)O<sub>2</sub> layers upon Co substitution. The frequency shift of the LiO<sub>6</sub> mode has two origins: (i) the slight expansion of the interslab distance (*c*<sub>hex</sub> cell parameter) in LiNi<sub>1-y</sub>Co<sub>y</sub>O<sub>2</sub> samples and (ii) the small mixing of Li-O stretching and O-M-O bending motion present in the low-wavenumber peak.

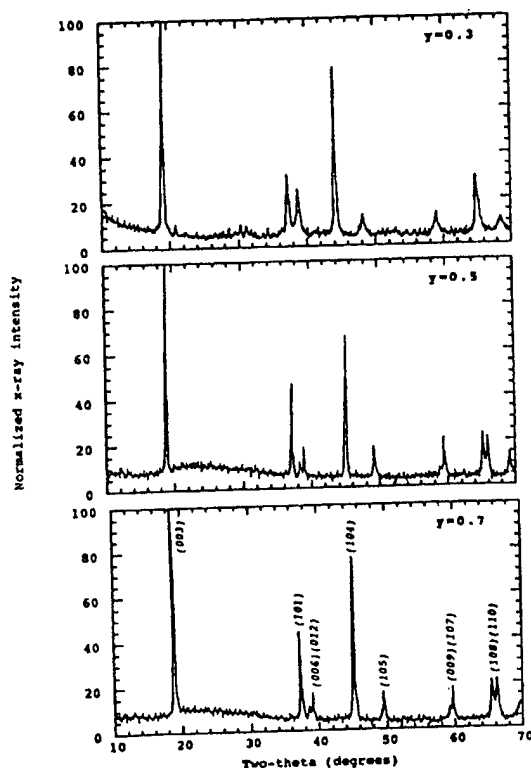


Fig. 1 X-ray diffraction diagrams of LiNi<sub>1-y</sub>Co<sub>y</sub>O<sub>2</sub> (0.3 ≤ *y* ≤ 0.7) powders grown by a wet chemistry technique using the glycine-assisted combustion method. XRD peaks were indexed in the hexagonal system assuming the R $\bar{3}$ m symmetry.

Performances of layered oxides as cathode materials in lithium batteries have been investigated. Cells Li//LiCo<sub>1-y</sub>Ni<sub>y</sub>O<sub>2</sub> were fabricated using 1M LiClO<sub>4</sub> in PC and the voltage profiles were monitored against lithium electrode. The substitutive effects of Ni for Co on structural and electrochemical properties of LiCo<sub>1-y</sub>Ni<sub>y</sub>O<sub>2</sub> oxides are discussed. Stable charge-discharge features have been observed for Li//LiCo<sub>1-y</sub>Ni<sub>y</sub>O<sub>2</sub> cells cycled in the potential range from 2.5 to 4.2 volts.

#### References

- [1] C. Delmas and I. Saadoune, *Solid State Ionics* **53-56**, 370 (1992).
- [2] J.P. Pereira-Ramos, *J. Power Sources* **54**, 120 (1995).
- [3] C. Julien, M. Massot, C. Perez-Vicente, E. Haro-Poniatowski, G.A. Nazri and A. Rougier, *Mater. Res. Soc. Symp. Proc.* **496**, 415 (1998).

LANTHANUM LITHIUM TITANATE :  
THE GRAIN SIZE EFFECT STUDIED BY  $^7\text{Li}$  NMR

O.Bohnké<sup>\*</sup>, J.Emery, N.Randrianantoandro, J.L.Fourquet<sup>\*</sup>, J.Y.Buzaré

<sup>\*</sup> Laboratoire des Fluorures (UPRESA 6010 CNRS)

Laboratoire de Physique de l'Etat Condensé (UPRESA 6087 CNRS)

Université du Maine, Avenue O.Messiaen, 72085 Le Mans Cedex 9, France

$^7\text{Li}$  nuclear magnetic resonance spin - lattice relaxation time  $T_1$  versus temperature is reported in the 150K - 400K temperature range on lithium lanthanum titanate fast ionic conductors. These compounds which belong to the solid solution  $(\text{La}_{2/3-x}\text{Li}_{3x/3-2x})\text{TiO}_3$  present a perovskite type structure  $\text{ABO}_3$  with cation deficiency at the A-sites. The presence of these A-sites vacancies is favourable for high mobility of lithium ions ( $\sigma = 8 \times 10^{-4} \text{ S cm}^{-1}$  at room temperature [1-4]).

$^7\text{Li}$  NMR techniques has been used to study the influence of the grain size on the short-range dynamics of  $\text{Li}^+$  ions. The titanates have been mechanically grinded in ethanol to decrease the grain size. X-Ray diffraction has been used to detect any change in the structure of the material after treatment and the particule size has been determined by laser granulometry. Fig.1 shows the variation of the spin-lattice relaxation time  $T_1$  as a function of temperature and Fig.2 the variation of the particule diameter as a function of grinding time.

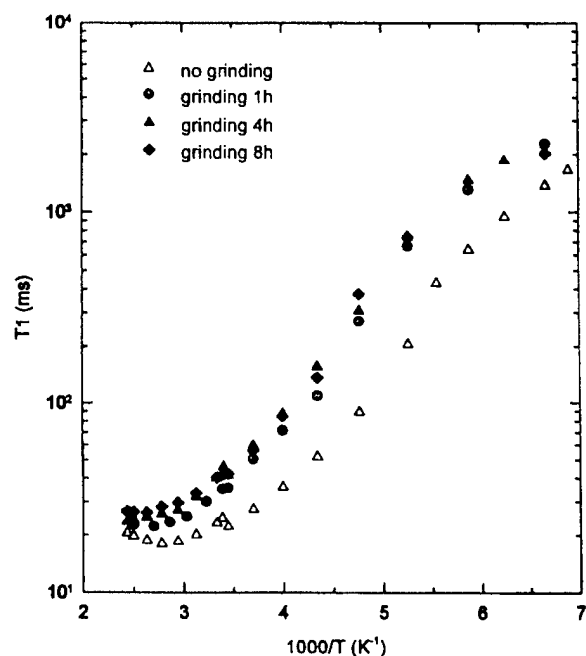


Fig1 -Spin - lattice relaxation time as a function of reciprocal temperature before and after grinding of the oxide.

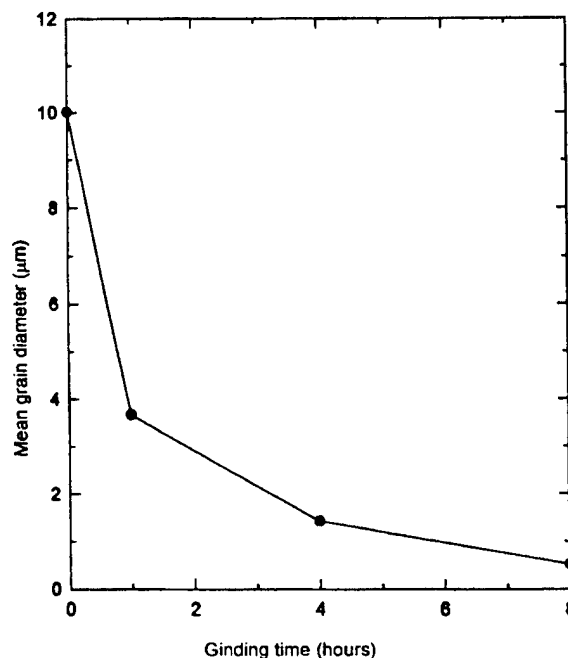


Fig.2 - Variation of the particule diameter as a function of grinding time.

The relaxation time increases as the grain size decreases and the minimum of the curve is slightly displaced towards the high temperatures. These results suggest that the correlation time is not greatly influenced by the particule size but rather by the modifications of the interactions of the  $\text{Li}^+$  nuclei with the environment (expressed by the constant C) in the well-

known relationship between the spin lattice relaxation time  $T_1$  and the characteristic correlation time of the  $\text{Li}^+$  motion  $\tau_c$  :

$$\frac{1}{T_1} = C \left[ \frac{\tau_c}{1 + (\omega_0 \tau_c)^2} + \frac{4\tau_c}{1 + (2\omega_0 \tau_c)^2} \right]$$

Moreover the spin lattice relaxation time  $T_1$  (Fig.1) can be related to the particule diameter (Fig.2). The most important decrease of the grain size occurs during the first hour of grinding. It is accompanied by an important increase of  $T_1$ . Similar results have been obtained by one of us on pyrolyzed graphite. The analysis of these results as well as the variation of the spin-spin relaxation time  $1/T_2$  with temperature will be presented at the conference.

#### References

- [1] J.L.Fourquet, H.Duroy, M.P.Crosnier-Lopez, J. Solid State Chem. 127 (1996) 283.
- [2] O.Bohnké, C.Bohnké, J.L.Fourquet, Solid State Ionics 91 (1996) 21.
- [3] J.Emery, J.Y.Buzaré, O.Bohnké, J.L.Fourquet, Solid State Ionics 99 (1997) 41.
- [4] O.Bohnké, J.Emery, A.Veron, J.L.Fourquet, J.Y.Buzaré, P.Florian, D.Massiot, Solid State Ionics 109 (1998) 25.

# INTERCALATION OF LITHIUM INTO LANTHANUM LITHIUM TITANATE : <sup>7</sup>Li NMR AND CONDUCTIVITY MEASUREMENTS

O.Bohnké, J.Emery\*, J.L.Fourquet, J.Y.Buzaré\*, P.Florian\*\*, D.Massiot\*\*

Laboratoire des Fluorures (UPRESA 6010 CNRS)

\* Laboratoire de Physique de l'Etat Condensé (UPRESA 6087 CNRS)

Université du Maine, Avenue O.Messiaen, 72085 Le Mans Cedex 9, France

\*\* Centre de Recherche sur la Physique des Hautes Températures CNRS, 45071 Orléans  
 Cedex 2, France

The compounds belonging to the solid solution  $(\text{La}_{2/3-x}\text{Li}_{1/3-2x})\text{TiO}_3$  present a perovskite-type structure  $\text{ABO}_3$  with cation deficiency at the A-sites. Previous studies have shown that a pure phase solid solution exists only in the domain  $0.04 < x < 0.14$  [1]. The presence of these A-sites vacancies is favourable for high mobility of lithium ions. A maximum ionic conductivity of  $8 \times 10^{-4} \text{ S cm}^{-1}$  has been found at room temperature for the composition  $x = 0.08$  after sintering [2]. Previous studies have also shown that lithium ions can be reversibly inserted into this oxide and that its diffusion coefficient is very high and of the order of  $10^{-8} \text{ cm}^2 \text{ s}^{-1}$  [3,4]. As far as we know, this is one of the highest diffusion coefficient observed in a lithium inserted oxide. Variable temperature <sup>7</sup>Li NMR techniques and impedance spectroscopy have been used to study the short-range and long-range dynamic in intercalated  $(\text{La}_{0.56}\text{Li}_{3x+dx0.13-dx})(\text{Ti}_{dx}^{3+}\text{Ti}_{1-dx}^{4+}\text{O}_3)$  compounds. Comparison will be made with the non inserted material that we previously studied [5].

Intercalation of lithium has been carried out galvanostatically in an electrochemical cell with a sintered pellet of the oxide as the working electrode. No mixture of the active material with graphite and binder but only the monolithic pellet was used to exclude any side electrochemical reactions during intercalation and any side interactions in <sup>7</sup>Li NMR. The intercalation was accompanied by a color change from pale yellow to dark blue in the whole pellet.

Intercalation has been carried out on three pellets leading to  $(\text{La}_{0.56}\text{Li}_{3x+dx0.13-dx})(\text{Ti}_{dx}^{3+}\text{Ti}_{1-dx}^{4+}\text{O}_3)$  with  $dx = 0.01, 0.03$  and  $0.11$  respectively. Fig1 presents the dc conductivity obtained as a function of the inverse of temperature. The conductivity of the oxide before intercalation is also reported for comparison. These materials change from purely ionic to mixed (ionic and electronic) conductors by intercalation. The conductivity changes by 6 orders of magnitude at low temperatures (from  $10^{-8} \text{ S cm}^{-1}$  at 150K) when  $\text{Li}^+$  ions are intercalated into the oxide. Moreover, the total conductivity increases as intercalation increases meaning that the injected electrons are delocalized as it is generally observed in intercalated transition metal oxides. At low temperatures, the total conductivity is mainly dominated by the electronic one. On the other hand at high temperatures the ionic conductivity becomes more important and dominates as revealed by the impedance spectroscopy diagrams.

NMR experiments were performed on a Bruker MSL 300 spectrometer equipped with a variable temperature system from 150K to 400K and on a Bruker ADX 300 spectrometer for higher temperatures. The <sup>7</sup>Li spectra were recorded at 116 MHz with non selective irradiation. The line positions, line widths of the resonance peak and spin-lattice relaxation times  $T_1$  were studied versus temperature.

The intercalation process leads to a sudden decrease of the resonance peak width (Fig.2) and to an increase of the spin-lattice relaxation time  $T_1$  (Fig.3). The increase of the time  $T_1$  was not expected because of the increase of the free electron density as intercalation occurs. As shown in Fig.3 the maximum of the  $T_1$  vs  $1000/T$  curve does not considerably change meaning that the increase of  $T_1$  is mainly due to a change of the interaction between the  $\text{Li}^+$  nuclei and their environment. As intercalation proceeds, the time  $T_1$  increases as well as the linewidth of the resonance peak. Moreover the  $T_1$  vs temperature measurements seem to indicate the existence of two motions that separate in the 200K to 300K temperature range and which is very pronounced for high  $dx$  value ( $dx = 0.011$ ).

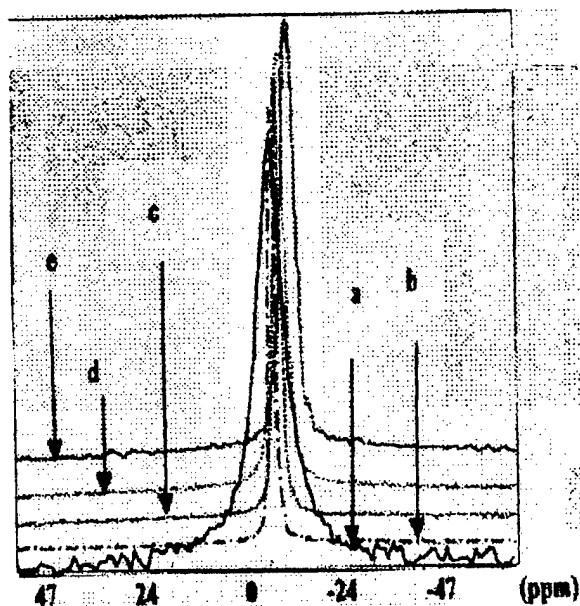


Fig.2 -  $^7\text{Li}$  static NMR spectra of (a) non intercalated oxide, (b to e) intercalated oxides : (b)  $dx=0.01$ , (c)  $dx=0.03$ , (d)  $dx=0.06$ , (e)  $dx=0.11$

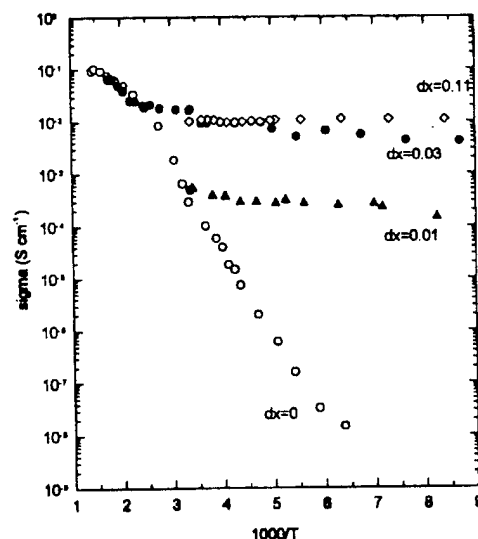


Fig.1 - dc conductivity as a function of temperature for intercalated and non intercalated materials.

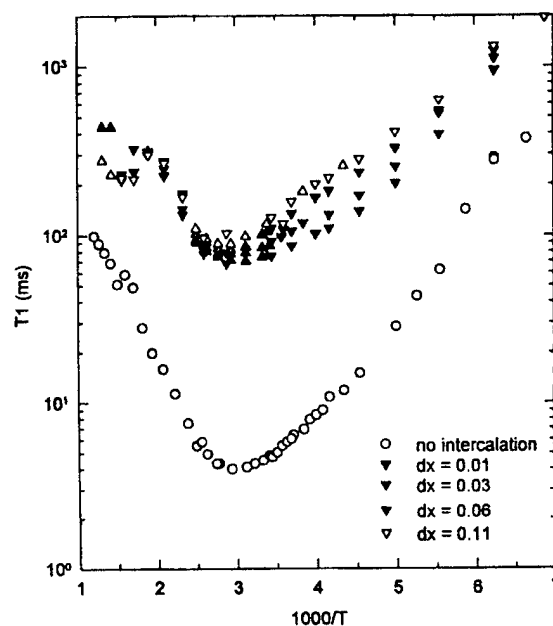


Fig.3 - Spin lattice relaxation time  $T_1$  as a function of the reciprocal of temperature for intercalated and non intercalated materials

#### References

- [1] J.L.Fourquet, H.Duroy, M.P.Crosnier-Lopez, J. Solid State Chem. 127 (1996) 283.
- [2] J.Emery, J.Y.Buzaré, O.Bohniké, J.L.Fourquet, Solid State Ionics 99 (1997) 41.
- [3] O.Bohniké, C.Bohniké, J.L.Fourquet, Solid State Ionics 91 (1996) 21.
- [4] P.Birke, S.Scharner, R.A.Huggins, W.Weppner, J. Electrochem. Soc. 144 (1997) L167.(1997).
- [5] O.Bohniké, J.Emery, A.Veron, J.L.Fourquet, J.Y.Buzaré, P.Florian, D.Massiot, Solid State Ionics 109 (1998) 25.



## SYNTHESIS OF COPPER-IRON OXIDE AND ION-EXCHANGE WITH LITHIUM SALT

A.Mary Sukeshini, Hironori Kobayashi, Mitsuharu Tabuchi  
and Hiroyuki Kageyama  
Osaka National Research Institute, AIST  
1-8-31 Midorigaoka, Ikeda-shi  
Osaka 563-8577, Japan

Materials research on lithium batteries focuses on new and improved versions of extraction/insertion compounds that can serve as electrodes. The structures of spinel and layered compounds offer extensive scope for physicochemical studies due to their ability to intercalate/deintercalate lithium[1,2]. The present work involves a systematic study of copper-iron oxide spinel,  $\text{CuFe}_2\text{O}_4$  and delafossite,  $\text{CuFeO}_2$  in order to assess their structural and magnetic properties and to explore the possibility of using them as cathode/anode material in lithium batteries.

$\text{CuFe}_2\text{O}_4$  and  $\text{CuFeO}_2$  were prepared from  $\text{Fe}_2\text{O}_3$  and  $\text{CuO/Cu}_2\text{O}$ . The cubic form of spinel  $\text{CuFe}_2\text{O}_4$  was obtained by firing the pellets between 920 to 950°C for 24 hours in air and quenching in liquid nitrogen. The tetragonal of  $\text{CuFe}_2\text{O}_4$  phase was obtained by heating to 900°C in air and then slowly cooling the sample over 80 hours to room temperature.  $\text{CuFeO}_2$  was synthesized by firing at temperatures between 850°C and 1050°C for 12-48 hours under argon/vacuum atmosphere. Ion exchange was carried out by a solid state reaction. A mixture of copper-iron oxide and  $\text{LiCl/KCl}$  in the ration of 1:25 was heated for 2 hours at different temperatures from 500°C to 900°C. The melt was allowed to cool for a few minutes and then washed with distilled water several times. It was then washed with acetone and dried.

From Rietveld analysis, it could be concluded that the optimum synthesis condition for ideal spinel and delafossite structures was 950°C and 1000°C/48 hours under argon atmosphere respectively. Fig.1 shows the XRD patterns of cubic  $\text{CuFe}_2\text{O}_4$  ion exchanged with  $\text{LiCl/KCl}$  at different temperatures 600°C - 900°C. The lattice parameter of  $\text{CuFe}_2\text{O}_4$  is  $a=8.3906(12)\text{\AA}$  which is consistent with the reported value[3]. The XRD pattern is seen to go from tetragonal to cubic as the temperature of ion-exchange rises from 600 to 900°C. The XRD patterns for 800°C and 900°C show cubic phase similar to the host and their lattice parameters are  $a=8.3456(10)\text{\AA}$  and  $a=8.3343(10)\text{\AA}$  respectively. It can also be seen that the 111 reflection of the host  $\text{CuFe}_2\text{O}_4$  has almost disappeared for the ion-exchanged sample prepared at 900°C. The disappearance of 111 reflection and reduced lattice parameters for samples obtained after ion-exchange reaction suggest that some ion exchange has occurred at 800/900°C with rearrangement of ions. In the case of delafossite, samples ion-exchanged below 500°C showed the presence of  $\text{LiFeO}_2$  and original  $\text{CuFeO}_2$ . At 550 and 600°C, a

mixture of  $\text{LiFeO}_2$  and  $\text{LiFe}_3\text{O}_8$  was seen. However, more investigations regarding the valence state of Fe and Cu will be required to understand the mechanism and extent of ion exchange. Mössbauer spectroscopy, magnetic susceptibility measurements, electrochemical measurements are in progress.

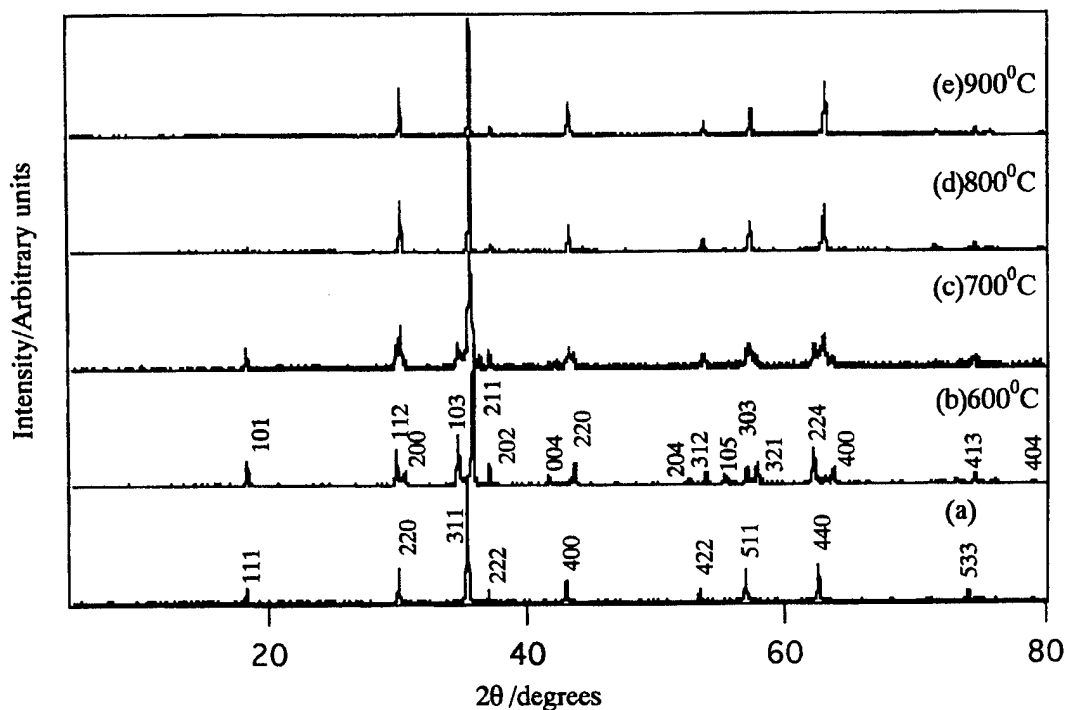


Fig.1  $\text{CuFe}_2\text{O}_4$ (a) and  $\text{CuFe}_2\text{O}_4$  ion exchanged with  $\text{LiCl/KCl}$  at different temperatures(b-e).

### References

- [1] M.M.Thackeray, W.I.F.David and J.B.Goodenough, *Mat. Res. Bull.*, 17(1982)785.
- [2] J.B. Goodenough, M.M.Thackeray, W.I.F.David and P.G.Bruce, *Rev. Chim. Min.*, 21(1984) 435 .
- [3] JCPDS Powder Diffraction File, PDF no. 25-0283.

## PLASTIC PVDF-HFP ELECTROLYTE LAMINATES PREPARED BY A PHASE-INVERSION PROCESS

A. Du Pasquier<sup>^</sup>, I. Plitz\*, G.G. Amatucci, T. Zheng\*, A. S. Gozdz\*, and J.-M. Tarascon<sup>^\*</sup>

<sup>^</sup>Universite de Picardie Jules Verne, 33 rue Saint-Leu, 8000 Amiens, France

\*Bellcore, 331 Newman Springs Road, Red Bank, NJ 07701, USA

A method of preparing microporous separator and electrode films suitable for the fabrication of bonded, plastic Li-ion cells without a plasticizer is described. The process utilizes phase inversion of a PVdF-HFP copolymer solution in a mixture of a solvent and non-solvent, in which the evaporation rate of the non-solvent is lower. As its concentration in the cast layer increases, the non-solvent brings about a gradual precipitation of the polymer in the form of a continuous microporous matrix in which solid components are occluded. After the volatile components are completely removed by evaporation, the resulting electrode and separator films exhibit high porosity and good mechanical strength.

The morphology of such porous films differs significantly from that of the previously reported films obtained by the liquid-liquid extraction of the plasticizer (the PLiON<sup>TM</sup> process)<sup>1</sup>. Field-emission scanning electron micrographs exhibit a connected, asymmetric, and coarser structure than that seen in the latter (Figure 1). This porous, connected structure of such films is preserved even after thermal processing (lamination) which is necessary to bond these films into multi-layer plastic rechargeable cells (Figure 2). Due to the high uptake of a liquid electrolyte by such laminated films, Li-ion rechargeable cells with satisfactory discharge rate capabilities were constructed.

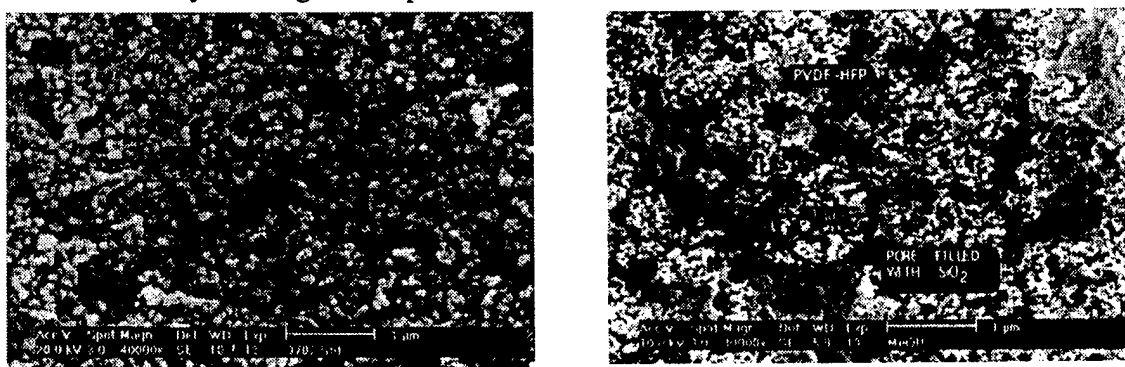


Figure 1: SEM micrographs of PVDF-HFP:SiO<sub>2</sub> separators made from DBP extraction (left) or phase inversion (right).

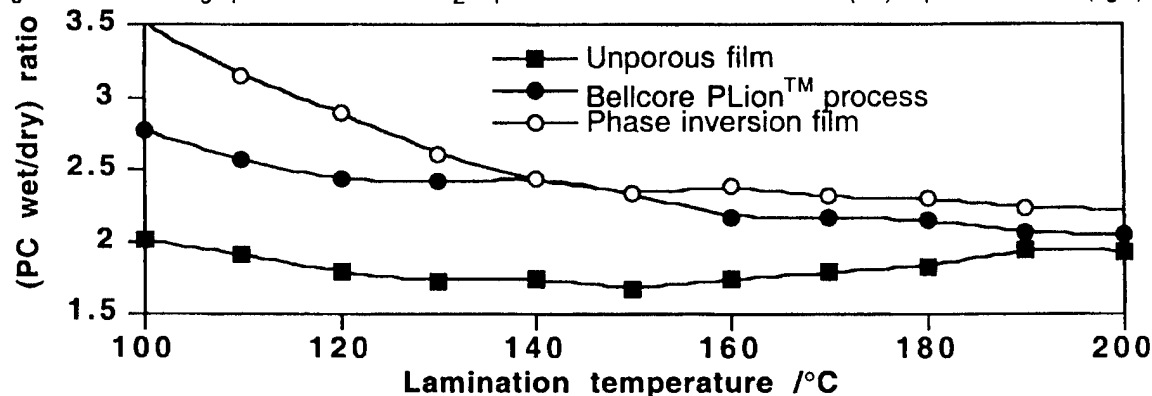


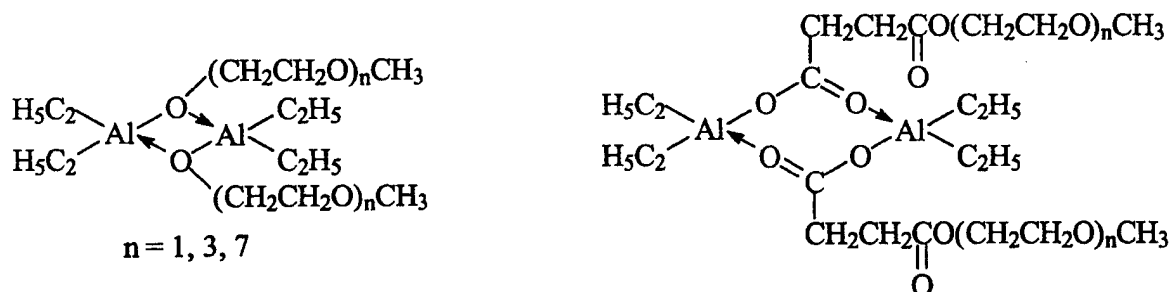
Figure 2: Uptake of propylene carbonate by PVdF-HFP-based plastic separators prepared by various methods as a function of the lamination temperature.

<sup>1</sup> Tarascon, J.-M.; Gozdz, A. S.; Schmutz, C.; Shokoohi, F.; Warren, P. C., Solid State Ionics (1996), 86-88(Pt. 1), 49-54.

## GEL POLYELECTROLYTES COMPRISING ORGANIC DERIVATIVES OF ALUMINUM

Z. Florjańczyk, E. Zygadło-Monikowska, E. Rogalska  
Warsaw University of Technology, Faculty of Chemistry,  
ul. Noakowskiego 3, 00-664 Warsaw, Poland

Ternary gels comprising polymers, organic solvents and alkali metal salts have been recently intensively studied in respect to their potential application as electrolytes in lithium batteries and other electrochemical devices. One of the approaches has involved the application of organoaluminum compounds capable of forming a stable physical network with PEO. Diethylaluminum alkoxides and diethylaluminum carboxylates containing poly(oxyethylene) units in their structure were used as organometallic compounds.



The gel electrolytes obtained were characterized by high ionic conductivity of the order of  $10^{-4} \text{ S}\cdot\text{cm}^{-1}$  at room temperature and  $10^{-3} \text{ S}\cdot\text{cm}^{-1}$  at  $70^\circ\text{C}$ . Gel electrolytes comprising carboxylic derivatives of aluminum are characterized by very good mechanical properties (up to 70 wt. % content of plasticizer) and these properties do not change within time.

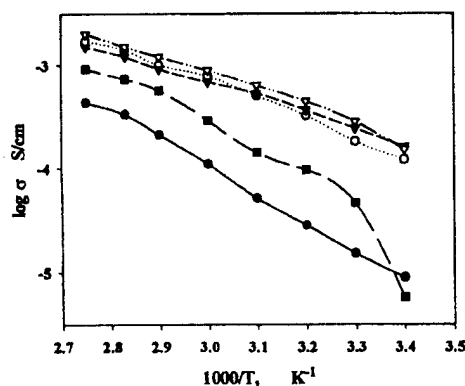


Figure: Ionic conductivity as a function of inverse temperature for gel electrolytes containing:  $\text{P(EO)}_{10}\text{LiCF}_3\text{SO}_3$ , 33 wt. %  $\text{CH}_3(\text{OCH}_2\text{CH}_2)_3\text{OOCCH}_2\text{CH}_2\text{COOAl}(\text{C}_2\text{H}_5)_2$  and (V) - 70 wt. %; (○) - 60 wt. %; (▼) - 50 wt. %; (■) - 0 wt. %; (●) - 10 wt. % ethylene carbonate.

Gradual degradation of the polymer was observed in the case of systems comprising aluminum alkoxides. This degradation is initiated probably by the products of the reaction of aluminum alkoxides with the ethylene carbonate or propylene carbonate added.

Initial stability studies of gels comprising aluminum carboxylates in a system of lithium electrodes has been carried out.

STRUCTURAL CHARACTERISATION OF NEW METASTABLE NiO<sub>2</sub> PHASES

L. CROGUENNEC, C. POULLERIE and C. DELMAS

Institut de Chimie de la Matière Condensée de Bordeaux-ICMCB-CNRS  
 Ecole Nationale Supérieure de Chimie et Physique de Bordeaux  
 Av. du Dr A. Schweitzer, 33608 Pessac cedex (France)

An investigation of highly deintercalated Li<sub>x</sub>Ni<sub>1.02</sub>O<sub>2</sub> phases obtained at very high oxidising potential has been undertaken; two phases with slightly different interslab distances were obtained (Fig. 1). One of them (called R3,  $d_{\text{interslab}} = 4.45 \text{ \AA}$ ) was previously reported by other authors, it crystallises in a rhombohedral system (R-3m space group; O3 structural type) [1-4]. Since the second one (called H4,  $d_{\text{interslab}} = 4.35 \text{ \AA}$ ) was never reported before, a more systematic study of the deintercalation process in various conditions has been undertaken.

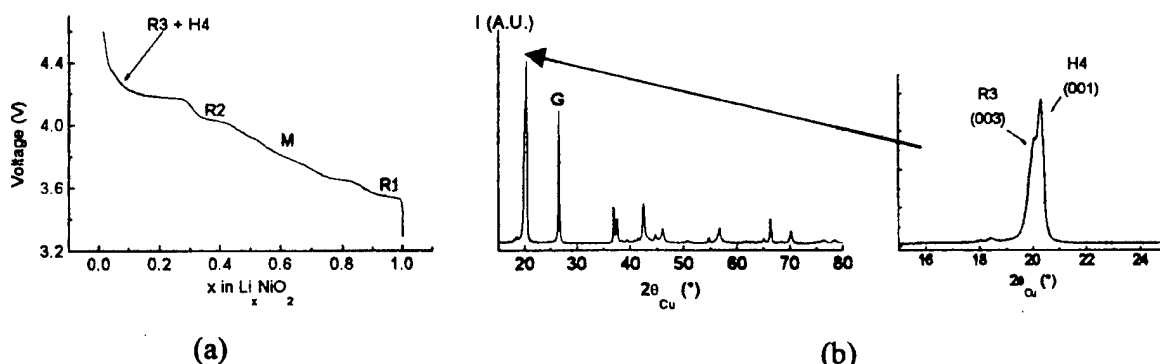


Fig. 1: First galvanostatic charge curve for Li/Li<sub>x</sub>Ni<sub>1.02</sub>O<sub>2</sub> (a) and X-ray diffraction diagram obtained at the end of this charge (b).

During the potentiostatic charge of the Li/Li<sub>x</sub>Ni<sub>1.02</sub>O<sub>2</sub> cells, at 4.2 V the R3 rhombohedral phase is formed in a first step. The relative amount of the H4 phase increases with time and then decreases to the benefit of a phase close to R3, called R3' (with a smaller interlayer distance of 4.41 Å). At higher potential (4.45 V), the same evolution is observed but the H4 phase predominates for short duration. The H4 phase appears, therefore, to be metastable.

The H4 phase exhibits a single-layered AB oxygen stacking, isostructural with CoO<sub>2</sub> [4]. Its cell parameters are  $a = 2.8145(6) \text{ \AA}$  and  $c = 4.346(2) \text{ \AA}$ . The X-ray diffraction pattern in best agreement with the experimental one has been calculated with nickel and oxygen ions in the 1a (0,0,0) and the 2d ( $1/3, 1/3, z \approx 0.22$ ) sites respectively (P-3m1: space group). An abnormal broadening of the (10l) diffraction lines was observed, it results from ABC type stacking faults (Fig. 2).

During the oxidation of Li<sub>x</sub>Ni<sub>1.02</sub>O<sub>2</sub>, the initial expansion of the interlayer distance results from an increase of the electrostatic repulsion between the [NiO<sub>2</sub>] slabs due to the removal of the Li ions from the structure. The later decrease of the interlayer distance is mainly due to the shrinkage of the interslab space resulting from the removal of pillaring lithium ions. Indeed, as oxidation of the compound proceeds, the covalence of the nickel-oxygen bonds increases so that there is a smaller net charge on the oxygen anions and a decrease in the electrostatic repulsion between the [NiO<sub>2</sub>] slabs. This stacking with shorter interslab oxygen-oxygen distances could be also stabilised by the formation of holes in the anionic band and therefore of short contacts through the interslab space.

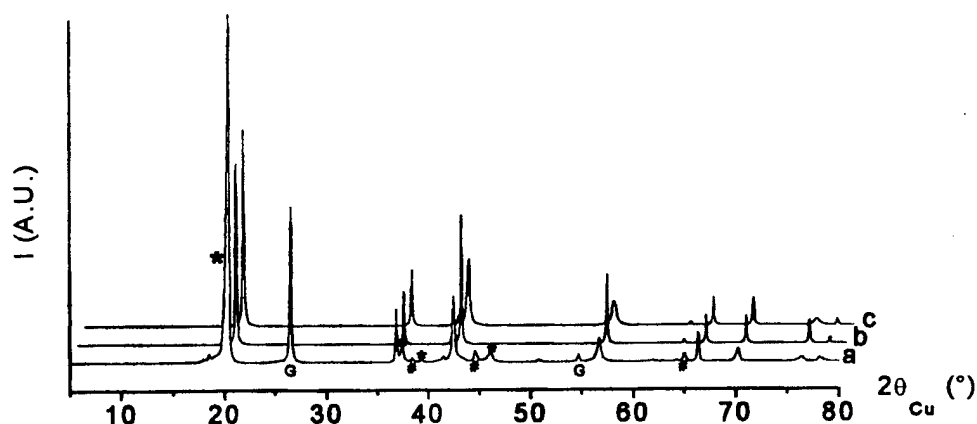


Fig. 2: The H4 experimental X-ray diffraction pattern (a), the calculated patterns for an ideal *AB* stacking (b) and for 3 % *ABC* faults in an *AB* stacking (c). G, \* and # respectively indicate the lines of graphite, the R3 phase and the sample-holder.

The R3 (*ABC*) and the H4 (*AB*) structures are so intimately related that the [NiO<sub>2</sub>] slabs of R3 need only to glide with respect to each other to form the *AB* stacking for H4. The *AB* type packing is stabilised versus the *ABC* one for the fully delithiated transition metal oxide because it enables a minimisation of the interactions between either the p oxygen orbitals, or to a smaller extent, the t<sub>2g</sub> orbitals (d<sub>xy</sub>, d<sub>xz</sub> and d<sub>yz</sub>) from two adjacent slabs. The Li/Li<sub>x</sub>NiO<sub>2</sub> system is highly reversible; as soon as lithium is reintercalated in the host structure, the *AB* stacking becomes unstable and is converted back to the *ABC* one. The lithium ions prefer the octahedral sites of the *cfc* structure because of the octahedra face sharing in the *hc* structure.

As discussed above, the H4 hexagonal phase has surprisingly not been previously reported for the Li/Li<sub>x</sub>NiO<sub>2</sub> system [1-4]. NiO<sub>2</sub> was always claimed to maintain the R-3m structure. The study of the Li<sub>x</sub>Ni<sub>1.07</sub>O<sub>2</sub> showed that no H4 phase was present. The presence of a significant amount of nickel ions in the interslab space prevents the slab glidings and the formation of the *AB* type stacking. The cell parameters calculated for Ni<sub>1.07</sub>O<sub>2</sub> are a = 2.812 Å and c = 13.472 Å and are in good agreement with the results obtained by other authors [1-4].

The H4 phase was shown to be unstable at high potential and to convert to the R3' rhombohedral phase, which seems to exhibit the (Ni<sub>1-x</sub>)<sub>3b</sub>(Ni<sub>1-x</sub>)<sub>3a</sub> cationic distribution. As discussed by Goodenough *et al.*, migration of nickel to the interslab is very difficult. Therefore, only a very small amount of nickel moves to the interslab space, leading to the *ABC* oxygen packing. As only a few nickel ions are concerned, there is no formation of the spinel type phase.

#### Acknowledgements

The authors wish to thank SAFT, CNES and Région Aquitaine for financial support.

#### References

- [1] T. Ohzuku, A. Ueda and M. Nagayama, *J. Electrochem. Soc.*, **140**, 1862 (1993).
- [2] W. Li, J.N. Reimers and J.R. Dahn, *Solid State Ionics*, **67**, 123 (1993).
- [3] H. Arai, S. Okada, H. Ohtsuka, M. Ichimura and J. Yamaki, *Solid State Ionics*, **80**, 261 (1995).
- [4] G.G. Amatucci, J.M. Tarascon and L.C. Klein, *J. Electrochem. Soc.*, **143**, 1114 (1996).
- [5] M.G.S.R. Thomas, W.I.F. David, J.B. Goodenough and P. Groves, *Mat. Res. Bull.*, **20**, 1137 (1985).

## LITHIUM FAST ION CONDUCTORS BASED ON KAOLINITE AND THEIR APPLICATIONS IN BATTERIES( II ) \*

Wenji WANG   Yurong ZHANG  
Department of Chemistry, Fuzhou University  
Fuzhou Fujian 350002, CHINA

### ABSTRACT

Refined natural layered aluminosilicate kaolinite ( $\text{Al}_2[\text{Si}_4\text{O}_{10}](\text{OH})_2$ ) has been used as a starting material for preparing a new lithium fast ion conductors  $\text{Li}_{1+2x+y}\text{Al}_x\text{Yb}_y\text{Ti}_{2-x-y}\text{Si}_x\text{P}_{3-x}\text{O}_{12}$  (hereafter referred to as Al-Yb-Lisicon) by high temperature (950 – 1150°C) solid phase reaction for about 20 hours. The synthesis temperature lowers with increasing the value of  $x$  for the Al-Yb-Lisicon.

X-ray powder diffraction shows that a Lisicon phase with a  $R\bar{3}c$  space group exists in the composition range of  $y < 0.5$ ,  $x < 0.4$ . The volume of unit-cell changes regularly with the change of the values of  $x$  and  $y$ . The composition with  $y = 0.3$ ,  $x = 0.1$  possesses maximum ionic conductivity which reaches up to  $1.63 \times 10^{-2} \text{ S/cm}$  at 623K with an activation energy of 38.3 KJ/mol and its electronic conductivity (about  $10^{-8} \text{ S/cm}$ ) is negligible as compare with its ionic conductivity. So it is a good candidate electrolyte using in  $\text{Li}^+$ -ion secondary batteries.

The test cell is constructed as following:

C/Al-Yb-Lisicon/composite electrode \* \*

\*  $\text{V}_2\text{O}_5$  or  $\text{MnO}_2$  and other materials.

The carbon is employed to replace the metal lithium as negative electrode in order to overcome the high reactivity of lithium. The I-V characteristics, discharge characteristics and some other parameters of test cells have been measured and will be reported.

## IMPEDANCE AND X-RAY ABSORPTION INVESTIGATIONS AND AB-INITIO CALCULATIONS ON LITHIUM MANGANESE OXIDES

Th. Buhrmester, M. Martin

Institute of Physical Chemistry, Darmstadt University of Technology  
Petersenstraße 20, 64287 Darmstadt, Germany

The recent interest in the development of high performance, second generation lithium batteries such as rocking-chair or lithium-ion cells stimulated the research in this field [1]. The development of anode materials went from lithium metal to the most promising carbon components with layered structure, which improved the cycle stability and safety of the cells drastically [2,3].

Investigations on positive electrodes lead from  $\text{LiMO}_2$  ( $M \equiv \text{Co, Ni}$ ) to a class of spinel structured, 4 V intercalation materials such as  $\text{Li}_{1+x}\text{Mn}_{2-x}\text{O}_{4-\delta}$ . Since it was found that the electrochemical characteristics of this environmentally friendly and low cost material strongly depend on the crystallite size, shape and the lithium content [4], various preparation techniques were developed to increase the specific capacity [5].

The spinel materials used in our experiments were prepared by a modified Pechini [6] method with two subsequent sintering steps. Within the region which is most important for technical use (that is:  $\text{Li}_{1+x}\text{Mn}_{2-x}\text{O}_{4-\delta}$  ( $0.01 \leq x \leq 1.33$ )) samples with different lithium content were prepared. For comparison we also produced samples with other lithium contents.

To obtain dense pellets, the samples were first pressed uniaxially and in a second step hydrostatically. These samples have been investigated with impedance spectroscopy and exhibit a strong temperature dependent conductivity. The influence of the lithium content will be discussed as well as the influence of temperature and the oxygen partial pressure.

X-ray absorption experiments were carried out at the manganese K- and L-2,3- edges as well as on the O-K edge [7,8]. First results from the spectra show a consistent change of the absorption at both energies. The XANES of the K-edge spectra exhibit a change with lithium content.

Ab initio calculations based on the ASW (augmented spherical wave) model [9] have been performed. Unfortunately the energy of the exchange and the crystal field splitting are of the same order of magnitude. Differences in the model calculations for the ferro- and anti-ferromagnetic states are discussed.

### Literature:

- [1] J. Owen Chem. Soc. Rev. **26**, 259 (1997)
- [2] Besenhard J. O., Schöllhorn R., J. Power Sources **1**, 267 (1977)
- [3] Chen L., Huang X., Kelder E., Schoonmann J., Solid State Ionics **76**, 91-96 (1995)
- [4] P. Endres, B. Fuchs, S. Kemmler-Sack, K. Brandt, G. Faust-Becker, H. W. Praas  
Solid State Ionics **89** 221 (1996)
- [5] C. Tsang, A. Manthiram Solid State Ionics **89** 305 (1996)
- [6] M. P. Pechini, U.S. Patent Nummer 3 330 697, 11. July (1967).
- [7] HASYLAB annual report I 855 (1997)
- [8] Dr. Z. Hu FU-Berlin, private communication (1997)
- [9] H. Anton, V. Eyert, P.C. Schmidt TU-Darmstadt, unpublished (1998)



## SINGLE STEP FABRICATION AND PROPERTIES OF $\text{Li}_{1-x}\text{Ni}_{1+x}\text{O}_2$ and $\text{LiCoO}_2$ FILMS BY SOFT SOLUTION PROCESSING AT 20-200°C

Kyoo-Seung HAN, Seung-Wan SONG, Hirofumi FUJITA, and Masahiro YOSHIMURA,  
*Center for Materials Design, Materials and Structures Laboratory,  
Tokyo Institute of Technology, 4259 Nagatsuta, Midori, Yokohama 226, Japan*

Well crystallized and electrochemically active  $\text{Li}_{1-x}\text{Ni}_{1+x}\text{O}_2$  and  $\text{LiCoO}_2$  thin-film electrodes for lithium rechargeable microbatteries have been fabricated in a single synthetic step using an economical, energy and material efficient, and environmentally friendly "Soft Solution Processing" in a concentrated LiOH solution at fixed temperatures between room temperature and 200°C without any post-synthesis heat treatments. The used LiOH solution containing dissolved nickel or cobalt species can be recycled by filtering it and replenishing the LiOH, which is environmentally and economically beneficial.

While the purely hydrothermal treatment of cobalt metal substrates directly leads to the formation of  $\text{LiCoO}_2$  films, by the use of the electrochemical- hydrothermal approach under supplementary galvanostatic charge with the same hydrothermal conditions,  $\text{Li}_{1-x}\text{Ni}_{1+x}\text{O}_2$  films can only effectively be fabricated in a single synthetic step out of nickel metal substrates. Such difference in designed combination of activation methods can be ascribed to the different metal cation valency between dissolved nickel species (that contain divalent nickel ions) and dissolved cobalt species (that should possess trivalent cobalt ions). That is confirmed by the film formation mechanism study. In addition, the investigation of morphology evolution during Soft Solution Processing proposes that the transformation mechanism for  $\text{LiCoO}_2$  film formation fully follows dissolution-precipitation model. In the case of Ni system, the transformation mechanism for  $\text{Li}_{1-x}\text{Ni}_{1+x}\text{O}_2$  film formation does not follow only dissolution-precipitation model, but also in-situ transformation model. According to the film formation mechanism study, the reaction pathway of  $\text{LiCoO}_2$  film formation can be described by the oxidative dissolution of Co metal to produce  $\text{CoO}_2^-$  ions and precipitation of  $\text{CoO}_2^-$  ions with  $\text{Li}^+$  ions. Otherwise, the reaction pathway of  $\text{Li}_{1-x}\text{Ni}_{1+x}\text{O}_2$  film formation consists of oxidative dissolution of Ni metal to produce  $\text{HNiO}_2^-$  ions, precipitation of  $\text{HNiO}_2^-$  ions with  $\text{H}^+$  ions to produce  $\text{Ni(OH)}_2$  film, oxidation of  $\text{Ni(OH)}_2$  film to  $\text{NiOOH}$  film and cationic exchange reaction between  $\text{H}^+$  and  $\text{Li}^+$  ions. Here, the oxidation of  $\text{Ni(OH)}_2$  film to  $\text{NiOOH}$  film and cationic exchange reaction between  $\text{H}^+$  and  $\text{Li}^+$  ions seem to follow the in-situ transformation model.

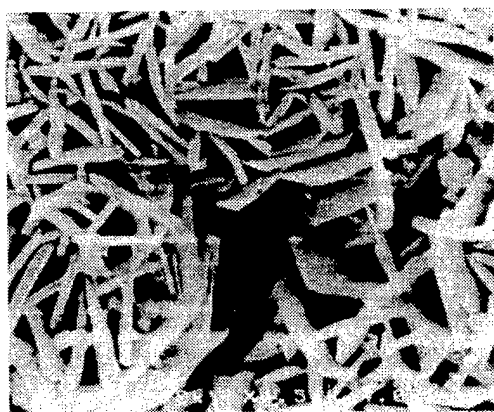
The prepared films exhibit a prospective electrochemical activity, however, the film property is dependent on the synthetic conditions. In the fabrication of  $\text{LiCoO}_2$  films in particular, while spinel (space group Fd3m) lithium cobalt oxide films were prepared below 100°C, layered (space group R-3m) lithium cobalt oxide films were prepared over 100°C. The film formation mechanism study also shows that Soft Solution Processing is capable of preparing advanced inorganic materials with planned properties through the active control of reaction conditions.

## SIMULTANEOUS AND DIRECT FABRICATION AND PROPERTIES OF LiCoO<sub>2</sub> FILM AND POWDER IN LiOH SOLUTION AT 100 °C

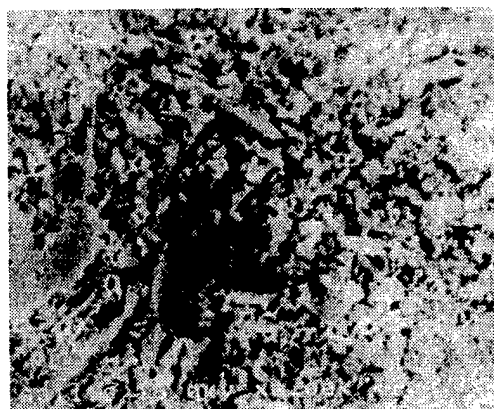
Seung-Wan Song, Kyoo-Seung Han, Itsuro Sasagawa, Tomoaki Watanabe and  
Masahiro Yoshimura\*

*Center for Materials Design, Materials and Structures Laboratory,  
Tokyo Institute of Technology, Yokohama 226, Japan*

LiCoO<sub>2</sub> powders and film have been directly prepared at the same time by hydrothermal treatment of cobalt metal substrate in concentrated LiOH solution at 100 °C. X-ray diffraction, scanning electron microscopic, X-ray photoelectron, Raman and Co K-edge X-ray absorption spectroscopic analyses, and cyclic voltammetry have been carried out for both powder and film samples to characterize their structure, morphology and electrochemical activity. From the comparative experiments, it becomes clear that powders are crystallized in a hexagonal layer structure (*R-3m*) as a precipitates by hydrothermal processing, whereas film the mixture of hexagonal and cubic spinel (*Fd3m*) phases. Such difference in the structure of LiCoO<sub>2</sub> is clearly revealed in SEM micrographs as represented in Figure 1; well crystallized hexagonal platelet with an average grain size of 2.5 μm is shown in the powder sample, however, poor crystalline spherical shape with the grain size of 0.35 μm in the surface of film with film thickness of 16 μm. On the basis of present experimental findings, it is suggested that homogeneous and heterogeneous nucleation followed by crystal growth lead to the formation of powders and film, respectively. Well crystallized LiCoO<sub>2</sub> powders as well as film have been simultaneously prepared at ≥ 100 °C, whereas only film could be obtained below 100 °C. For this reason, it is assumed that supersaturation step followed by homogeneous nucleation for the formation of LiCoO<sub>2</sub> powders is highly dependent upon the synthetic temperature.



(a)



(b)

Figure 1. SEM micrographs for (a) LiCoO<sub>2</sub> powders and (b) the surface of film obtained from hydrothermal processing.

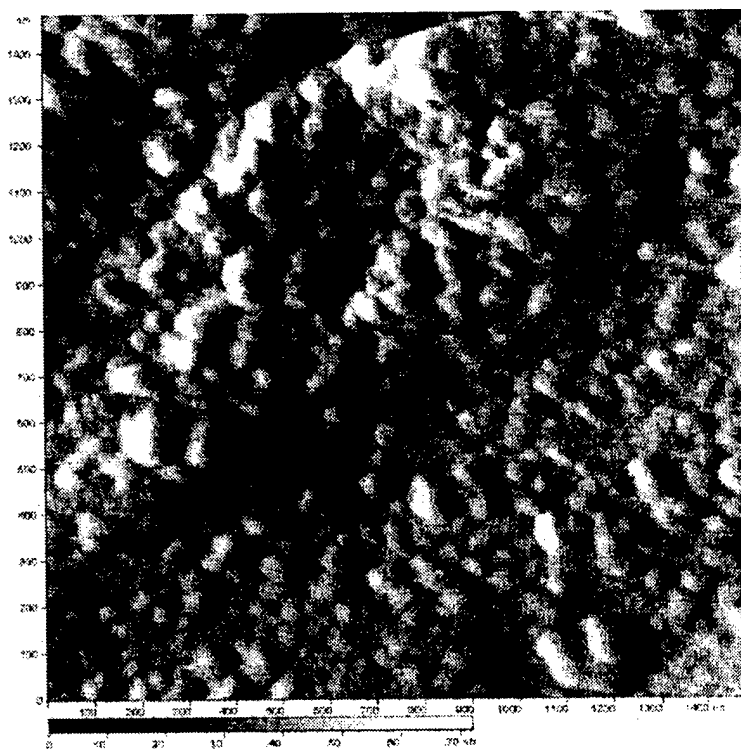
CHARACTERIZATION OF THE PASSIVATION LAYER AT THE POLYMER  
ELECTROLYTE/LITHIUM ELECTRODE INTERFACEMaryline Le Granvalet-Mancini<sup>a</sup> and Dale Teeters<sup>b</sup><sup>a</sup>Institut des Matériaux de Nantes, Laboratoire de Chimie des Solides

UMR CNRS N° 110 - Université de Nantes

B.P. 32229, 44322 Nantes cedex 3, France

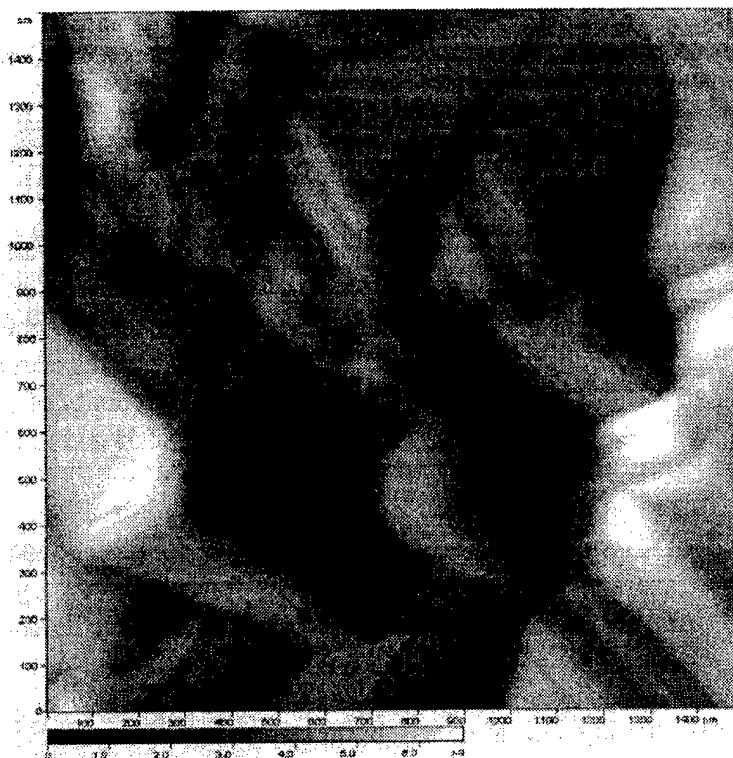
<sup>b</sup>Department of Chemistry, The University of Tulsa, 600 S. College Ave.,  
Tulsa, OK 74104-3189, U.S.A.

The characterization of the passivation layer at the lithium electrode/polymer electrolyte interface and understanding how it is formed is of major importance for the development of lithium polymer batteries. This work investigates the formation of a passivation layer at this interface. PEO-lithium triflate electrolyte films were used in cells having lithium as both electrodes (lithium symmetric cells). The time-dependent formation of the passivation layer was observed with A.C. impedance spectroscopy as the growth of a second semicircle in Nyquist plots. The cells were disassembled under an argon atmosphere and characterized by atomic force microscopy (AFM) once again in an argon environment. Lithium surfaces from the lithium symmetric cells and from lithium metal before it had been exposed to the PEO electrolyte were studied. As shown in the figure at the right, the lithium surface before exposure to the PEO electrolyte has elliptical grains that on the average have a size of 100 nm.



This looks similar to previous AFM images obtained by Morigaki and Ohta [1] of pristine lithium surfaces in dry atmospheres. After exposure to the PEO electrolyte for 3 days, these grains appear to have enlarged to an average size of 250 nm. In addition, some regions of the surface as shown in the figure on the next page appear to have developed crystal-like structures. *In situ* FT-IR spectra of the lithium-PEO electrolyte interface were collected by using attenuated total reflection (ATR) spectroscopy. These data indicated that at least part of the passivation layer was composed of Li-O-R type compounds.

Previous work in our laboratory [2] has shown that self-assembled molecular layers adsorbed on the PEO electrolyte surface can help to prevent a passivation layer from forming on the lithium surface. A.C. impedance, AFM, and ATR FT-IR data will be presented for PEO electrolytes with the adsorbed molecular layers and compared to the data for the unprotected lithium-PEO electrolyte interfaces discussed above.



[1] K. Morigaki and A. Ohta, *J. Power Sources*, **76**, 159 (1998)

[2] R. N. Mason, M. Smith, T. Andrews and D. Teeters, *Solid State Ionics*, in press

## SOL-GEL CHROMIUM-VANADIUM MIXED OXIDES AS LITHIUM INSERTION COMPOUNDS

P. Soudan <sup>a</sup>, J.P. Pereira-Ramos <sup>a</sup>, J. Farcy <sup>a</sup>, G. Grégoire <sup>b</sup> and N. Baffier <sup>b</sup>

a. Laboratoire d'Electrochimie, Catalyse et Synthèse Organique, C.N.R.S. UMR 7582

2, rue Henri-Dunant 94320 Thiais, France

b. Laboratoire de Chimie Appliquée de l'Etat Solide, C.N.R.S. UMR 7574

11, rue Pierre et Marie Curie 75231 Paris, France

Among the cathodic materials for lithium batteries, the vanadium pentoxide  $V_2O_5$  is still the subject of many works, owing to its layered structure which allows the insertion of a large amount of lithium ions. The insertion of more than one lithium per  $V_2O_5$  involves important and irreversible structural deformations which govern the electrochemical behaviour of the cathode material for cycling [1]. The sol-gel process is used here to incorporate chromium ions in the  $V_2O_5$  lattice in order to obtain new compounds with improved performances. Indeed, previous works have demonstrated the interest of the sol-gel method for preparing cathodic materials [2,3]. Recently we have shown that the sol-gel compound  $Fe_{0.11}V_2O_{5.16}$  obtained by incorporating  $Fe^{3+}$  ions presents a structure that better adapts oneself to high Li uptake than  $V_2O_5$  [4-6]. We present here the results concerning new mixed oxides :  $Cr_{0.11}V_2O_{5.16}$ ,  $Cr_{0.06}VO_{2.09}$  and  $Cr_{0.33}V_6O_{13.5}$ . Their electrochemical properties are investigated for Li insertion. In the case of  $Cr_{0.11}V_2O_{5.16}$ , detailed thermodynamic, kinetic and structural data are obtained and discussed.

The basic material is a vanadium pentoxide gel prepared by passing a metavanadate solution ( $C > 0.1$  M) through a cation exchange resin. The resulting decavanadic acid solution gives rise to the gel by spontaneous polycondensation [7]. The red viscous gel deposited on a glass plate loses most of its water readily at room temperature, leading to a thin film of  $V_2O_5$ , 1.6  $H_2O$  xerogel (VXG). The 0.33  $H_3O^+$  ions per  $V_2O_5$  contained in the VXG are exchanged by soaking the film in a 0.1 M  $Cr(NO_3)_3$  aqueous solution. A further heat treatment of the exchanged VXG at 520 °C for two hours in air gives rise to the formation of a thin film of the mixed oxide  $Cr_{0.11}V_2O_{5.16}$ . When the exchanged xerogel is heat-treated in a hydrogenated atmosphere ( $Ar-10\%H_2$ ), the oxides  $Cr_{0.06}VO_{2.09}$  or  $Cr_{0.33}V_6O_{13.5}$  are obtained depending on the temperature, 500°C and 450°C respectively. The chromium content was determined from atomic absorption experiments. The vanadium content and its oxidation number were determined from redox titrations after acid dissolution.

For  $Cr_{0.11}V_2O_{5.16}$  we show that the compound exhibits an orthorhombic symmetry (Pmmn space group) with cell parameters very close to that of the parent oxide :  $a = 11.4849(7)$  Å,  $b = 3.5648(2)$  Å and  $c = 4.3817(3)$  Å as compared with the  $V_2O_5$  ones :  $a = 11.5125(5)$  Å,  $b = 3.5640(1)$  Å and  $c = 4.3713(2)$  Å. A Rietveld refinement allows to localize  $Cr^{3+}$  ions in an octahedral oxygen environment within the  $V_2O_5$  layers and additional  $O^{2-}$  ions between the layers [8]. These additional ions could limit the structural rearrangements of  $V_2O_5$  layers occurring when large amounts of lithium enter the  $V_2O_5$  host lattice.

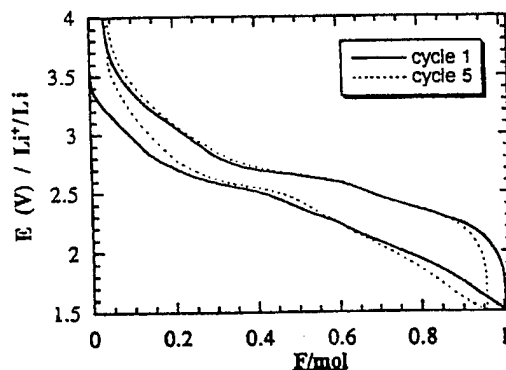
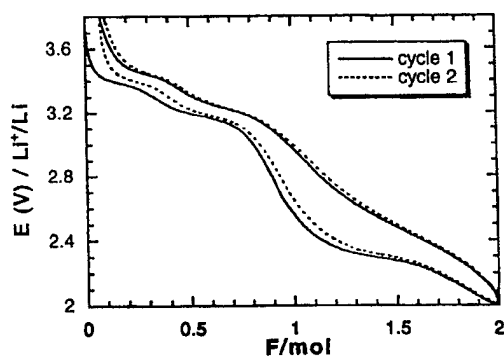
The discharge-charge experiments performed on composite electrodes have allowed to emphasize the high faradaic yield available at 2V cutoff voltage and illustrate the good rechargeability of the compound. Indeed the total faradaic yield of 2F per mole of oxide corresponds to a specific capacity of 280 Ah/kg at C/10 rate. In contrast to  $V_2O_5$  the potential change between the two composition ranges  $x < 1$  and  $x > 1$  gradually takes place. The efficiency

of the first oxidation process is 95% with a shape of the working discharge profile which suggests limited structural changes. For instance, the additional oxidation step observed at 3.65V for  $V_2O_5$  and corresponding to Li extraction from the  $\gamma$  phase [1] does not appear for the mixed oxide. Investigation of XRD patterns of  $Li_xCr_{0.11}V_2O_{5.16}$  electrodes vs  $x$  shows that only the  $\alpha$  and  $\epsilon$  phases are involved in the redox process for  $0 < x < 2$  while the  $\alpha$ ,  $\epsilon$ ,  $\delta$  and  $\gamma$  phases successively appear in  $Li_xV_2O_5$  [1]. The interlayer parameter  $c$  increases from 4.38 Å to 4.76 Å for  $x = 2$  while the  $a$  parameter slightly contracts from 11.48 Å to 11.35 Å. The presence of the puckered  $\gamma$  phase is never detected. The chromium ions act as stabilizing agents of the host lattice as Li accommodation proceeds and hinder the formation of the  $\gamma$  phase.

A.c. impedance spectroscopy, PITT and pulse relaxation measurements have been used to determine the evolution of the chemical diffusion coefficient  $D_{Li}$  vs  $x$ . This evolution ( $10^{-9}/10^{-11} \text{ cm}^2\text{s}^{-1}$ ) is discussed in relation with structure changes. Structural data obtained on cycled electrodes confirm that limited structural rearrangements occur. The  $\epsilon$  phase is maintained during cycling which explains the high specific capacity of 260 Ah/kg achieved after 20 cycles.

The exchanged  $Cr^{3+}$ -xerogel heat-treated under hydrogen atmosphere at 500°C leads to the formation of  $Cr_{0.06}VO_{2.09}$ . XRD patterns exhibit the typical lines of the monoclinic structure of  $VO_2$  (B) with close lattice parameters. Preliminary investigations indicate a single step for Li insertion-extraction in the voltage range 3.5V-1.5V with a high specific capacity near 300Ah/kg corresponding to the intercalation of 1 Li ion per mole of oxide. This capacity declines with cycles to stabilize around 240 Ah/kg after 10 cycles at C/10 rate in the potential window 4V-1.5V. The main electrochemical features of  $Cr_{0.06}VO_{2.09}$  and  $Cr_{0.33}V_6O_{13.5}$  are investigated.

- [1] C. Delmas, H. Cognac-Auradou, J. M. Cocciantelli, M. Ménétrier and J.P. Doumerc, *Solid State Ionics*, **69**, 257 (1994)
- [2] J.P. Pereira-Ramos, N. Baffier, G. Pistoia in : G. Pistoia (Ed.), *Lithium Batteries : New Materials, Developments and Perspectives*, Elsevier, p.281, (1994).
- [3] J. P. Pereira-Ramos, *J. Power Sources*, **54**, 120 (1995).
- [4] S. Maingot, Ph. Deniard, N. Baffier, J. P. Pereira-Ramos, A. Kahn-Harari, R. Brec, P. Willmann, *J. Power Sources*, **54**, 342 (1995).
- [5] S. Maingot, R. Baddour, J. P. Pereira-Ramos, N. Baffier, P. Willmann, *J. Electrochem. Soc.*, **140**, L158 (1993).
- [6] J. Farcy, S. Maingot, P. Soudan, J.P. Pereira-Ramos, N. Baffier, *Solid State Ionics*, **99**, 61(1997).
- [7] P. Aldebert, N. Baffier, N. Gharbi, J. Livage, *Mat. Res. Bull.*, **16**, 669 (1981).
- [8] G. Grégoire, N. Baffier, A. Kahn-Harari, and J.C.Badot, *J. Mat. Chem.*, **8**, 2103 (1998)



Discharge-charge curves of  $Cr_{0.11}V_2O_{5.16}$  and  $Cr_{0.06}VO_{2.09}$  (C/10)

## ADVANCES IN SOLID OXIDE FUEL CELL TECHNOLOGY

S.C. Singhal  
Science & Technology Center  
Siemens Westinghouse Power Corporation  
1310 Beulah Road  
Pittsburgh, PA 15235, U.S.A.

### Introduction

Solid oxide fuel cells (SOFCs) based on oxygen ion conducting zirconia electrolyte offer a clean, pollution-free technology to electrochemically generate electricity at high efficiencies. The current technology tubular SOFCs are fabricated using a doped lanthanum manganite tube that is extruded and sintered to about 30 to 35 percent porosity. This tube serves as the air electrode onto which other cell components are fabricated in thin layer form. The materials and fabrication processes for different components in these cells are summarized in Table 1. The electrochemical vapor deposition (EVD) process deposits high quality, uniformly thick, gas-tight yttria-stabilized zirconia (YSZ) electrolyte film over porous air electrode.

Table 1. Materials and Fabrication Processes

Component	Material	Thickness	Fabrication Process
Air Electrode Tube	Doped LaMnO <sub>3</sub>	2.2 mm	Extrusion-sintering
Electrolyte	ZrO <sub>2</sub> (Y <sub>2</sub> O <sub>3</sub> )	40 μm	EVD
Interconnection	Doped LaCrO <sub>3</sub>	85 μm	Plasma spraying
Fuel Electrode	Ni-ZrO <sub>2</sub> (Y <sub>2</sub> O <sub>3</sub> )	100 μm	Slurry coat-EVD

### Cell Performance

Over two thousand tubular cells have been electrically tested for up to about 20,000 h, either as single cells, in cell bundles, or in 25 and 100 kW SOFC power generation systems. These cells have performed well under a variety of operating conditions with less than 0.1% per 1000 h performance degradation. These cells have also been found to tolerate small levels of air-side (moisture, SO<sub>2</sub>, seawater mist) and fuel side (NH<sub>3</sub>, HCl, H<sub>2</sub>S) impurities without any significant long-term performance problems. In addition, these cells have shown the ability to be thermally cycled to ambient temperature from 1000°C without any mechanical damage or performance loss.

The tubular SOFCs have also been tested at pressures up to 15 atmospheres on both hydrogen and natural gas fuels. Operation at elevated pressures yields a higher cell voltage at any current density due to increased Nernst potential and reduced cathode polarization, and thereby permits higher stack efficiency and greater power output. With pressurized operation, SOFCs can be successfully used as replacements for combustors in gas turbines; such integrated SOFC-gas turbine power systems are expected to reach efficiencies approaching 70%.

### Investigations to Further Reduce Cell Cost

Over 90% of the weight of a tubular SOFC is that of the doped lanthanum manganite air electrode tube. Presently, the air electrode material is synthesized using high purity raw materials such as La<sub>2</sub>(CO<sub>3</sub>)<sub>3</sub> and MnO<sub>2</sub>. Significant reduction in the cost of air electrode material is possible by the use of lower purity raw materials instead of pure lanthanum compounds to synthesize the air electrode powder. Air electrode material cost can also be reduced by utilizing compositions that have lower rare

earth content. Use of such lower cost materials in fabricating SOFC air electrode tube has been successfully demonstrated by fabricating and electrically testing cells with these materials.

Deposition of a Ni-YSZ slurry over the YSZ electrolyte followed by sintering has also yielded fuel electrodes that are equivalent in electrical conductivity to those fabricated by the EVD process. Cells with sintered fuel electrodes have shown electrical performance equivalent to those with the EVD fuel electrodes. In fact, the sintered fuel electrode polarization is even lower than the already very low (7-15 mV) polarization for the EVD fuel electrodes. This is believed to be due to a larger contact area and a greater number of electrochemically active sites at the electrolyte/sintered fuel electrode interface.

The EVD process deposits uniformly thick (20 to 40  $\mu\text{m}$ ) gas-tight electrolyte film over the porous air electrode, reliably, uniformly, and in acceptable cycle time. Nonetheless, deposition of the electrolyte film by a more cost-effective sintering process utilizing nanosize YSZ powders for slurry making and colloidal/electrophoretic technique for slurry deposition over porous air electrode is also being investigated.

Alternate geometry, higher power density SOFCs are also being investigated to reduce the physical size and cost of SOFC generators. The electrical current path in tubular cells is circumferentially around the air electrode and fuel electrode, and through the thickness of the electrolyte and interconnection. The power output of these cells can be increased by shortening the current conduction path. As shown in Figure 1, ribs can be built into flattened air electrode that act as bridges for the current to reduce the average current path length. These shorter current pathways reduce cell internal resistance and improve power output. Such cells retain all the advantages of the tubular SOFCs, e.g. not requiring any high temperature seals, yet provide higher power per unit length and higher volumetric power density; the stacks assembled with these alternate geometry cells pack more efficiently, requiring about 33% less volume for a given kW rating generator. Development of such alternate geometry cells is currently underway.

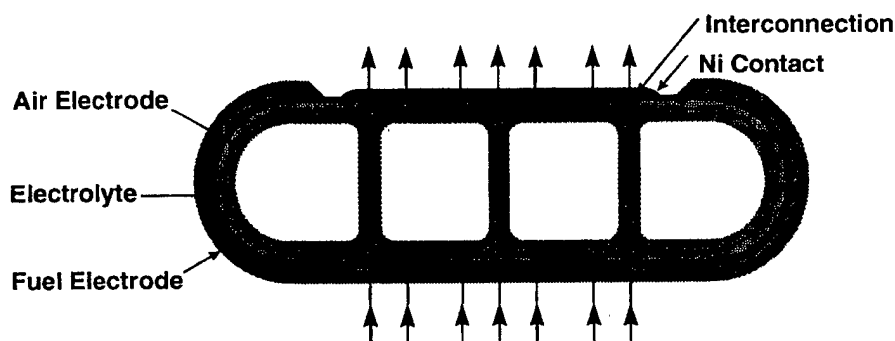


Figure 1. Current Path in a Flattened, Ribbed Cell.

### SOFC Power Generation Systems

Since 1984, successively larger size SOFC power generation systems have been designed, built, and successfully operated. Recently, a 100 kW atmospheric SOFC power generation system, consisting of 1152 commercially prototypic cells of 2.2 cm diameter and 150 cm active length, began operation in The Netherlands. This system provides over 100 kW ac to the Dutch grid and approximately 85 kW of hot water for the local district heating system. Presently, a 250 kW hybrid pressurized SOFC-gas turbine power generation system is being fabricated. This system will integrate a 200 kW SOFC stack (1152 cells) operating at about 3.5 atm pressure with a 50 kW microturbine generator, and is expected to achieve an electrical efficiency of about 57%.



## POLYMER ELECTROLYTES AND THE ELECTRIC VEHICLE

Fritz R. Kalhammer  
Menlo Park, California, U.S.A.

Over the past thirty years, substantial efforts and resources have been devoted in the industrialized countries to develop and introduce electric vehicles, as a fundamental solution to the serious urban emission and pollution problems caused by rapidly growing populations of automobiles and other oil-based transportation modes. Two other important motivations for a shift to electric vehicles and electric transportation in general have emerged over the past two decades: the awareness that petroleum is a finite resource and exclusive dependency on it for mobility is strategically and economically undesirable, and the growing concern about the climate-changing potential of continuing increases in the atmospheric concentration of carbon dioxide.

Despite these efforts and motivations, electric vehicles have failed to capture even a modest share of the market for personal automobiles, and the record is similarly disappointing for road-based public transportation. While there is more than one cause for these failures, one reason stands out: the only power sources presently available for autonomous electric vehicles, electrochemical batteries, have been unable to deliver the energy and power needed to compete with the internal combustion engine. Limited life and rather high costs of batteries have been other major barriers, especially for applications such as buses and on-road work vehicles for which the performance of existing batteries appears marginally acceptable.

Over the last five years, this situation has begun to change. Large investments are now being made worldwide in the development of electrochemical power sources -- both batteries and fuel cells -- for automotive propulsion. Advanced batteries are emerging which promise practical performance and driving ranges for a new generation of capable electric vehicles. Fuel cell "engines" for automobiles have become the target of large development programs in Europe, Japan and North America. Although a number of formidable technical and cost challenges remain, the progress made in these programs has raised expectations that fuel cell electric vehicles could become commercially available as early as 5-7 years from now.

Polymer electrolytes are playing very important roles in overcoming some of the most difficult barriers to the development of batteries and fuel cells into practical automotive power sources. To understand the technology-enabling roles of polymer electrolytes, performance and other critical requirements for electric vehicle batteries and fuel cells are discussed with the help of criteria developed in two major industry-government programs, the U.S. Advanced Battery Consortium (USABC) and the Partnership for a New Generation of Vehicles (PNGV).

Batteries with lithium negative electrodes have the best potential to meet the criterion for high specific energy, thus promising practical ranges for battery-powered electric vehicles. The development of polymer electrolytes based on polyethylene oxide is now permitting the use of metallic lithium in secondary batteries that exhibit promising specific energy and cycle life and that are safe to operate when charging and discharge are controlled on the single cell level. With further development of high-capacity positive electrodes, these "lithium-polymer" batteries might eventually achieve specific energies approaching or even exceeding 200 Wh/kg, sufficient to give future electric vehicles a range of 300 km or more on a single charge.

Polymer electrolytes also might offer a fundamental solution to the safety issue posed by the flammable organic electrolytes used in so-called lithium-ion batteries which use negative electrodes of lithium electrochemically intercalated into various types of carbon. If low-impedance versions of lithium-ion batteries with polymer electrolytes can be developed, the resulting combination of high specific power capability, good specific energy and operating safety could be particularly attractive for hybrid power sources. Last not least, polymer electrolytes with adequate mechanical strength would lend themselves well to the development of low-cost processes for battery manufacturing in which continuous sheets of polymer would be used as the base to which lithium foil and the positive active material are attached (on opposite sides) by suitable continuous processes such as lamination, printing, etc.

The successful use of proton-conducting polymers as fuel cell electrolytes was a major breakthrough that dates back to the 1950s when General Electric developed the sulfonated polystyrene electrolyte used in their fuel cell technology for the Gemini spacecraft. A subsequent materials breakthrough -- the shift to perfluorinated polymers as carriers of sulfonic acid anions -- gave polymer electrolytes the chemical stability needed for practical electrochemical applications the most important of which so far is as a separator membrane in industrial electrolytic cells. A third breakthrough -- the deposition of highly active supported platinum metal catalysts in very small amounts directly on these fluorinated polymer electrolytes -- established the technical base for development of a proton exchange membrane ("PEM") fuel cell technology with the performance and prospective costs that promise to meet the criteria for automotive applications. Importantly, PEM-type electrolytes offer a low-cost manufacturing route to the so-called MEA (membrane-electrode assembly), a composite of the polymer electrolyte sandwiched between the catalyzed fuel cell anode and cathode, respectively.

While polymer electrolytes thus are playing key roles in the development of competitive electric vehicle power source technologies, much remains to be done and major opportunities beckon for polymer electrolytes to become enablers of increased capabilities and entirely new possibilities in this dynamic field. The technical challenges fall into two broad areas: achievement of higher conductivity and other important bulk properties; and better understanding of the interfaces of polymer electrolytes with adjacent functional phases, with the objective to optimize key factors controlling battery and fuel cell performance, life and cost. Several important challenges and opportunities are discussed, and research directions to address them are identified.

## **Current Trends in Planar Solid-Oxide-Fuel-Cell Research**

Wayne L. Worrell and Conghua Wang

Department of Materials Science and Engineering

University of Pennsylvania

Philadelphia, PA U. S. A.

### **Introduction**

Solid-oxide fuel cells (SOFCs) are being developed for a variety of power-generation applications, but the major barrier for timely commercialization of SOFCs is their high capital cost. Planar SOFC programs are not as near commercialization as the tubular programs due to the significant challenges with seals and interconnects. However planar SOFCs are capable of higher current and power densities and potentially lower costs than those of the tubular design. Thus materials and processes that could reduce capital costs are generating the current trends in planar SOFC research. This paper is focused on the current trends in three areas: planar cell design, thin-film YSZ (yttria-stabilized zirconia) electrolyte fabrication, and electrode design and materials.

### **Trends in Planar Cell Design**

Probably the major trend in planar-cell research is the development of reduced temperature (650 to 800°C) cells. This is an attractive approach because metallic seals and interconnects can be used which would lower materials and fabrication costs. However lower operating temperatures would increase significantly the resistance loss associated with the YSZ electrolyte. One solution is the use of an oxide electrolyte that has higher oxygen-ion conductivity than that of YSZ at temperatures below 900 °C. However this approach has not been successful to date due to either higher costs or the poor chemical/electrochemical stabilities of faster oxygen-ion conductors in the typical fuel cell environments. Thus at this time the better solution appears to be the use of a very thin-film (5 to 30  $\mu\text{m}$ ) YSZ electrolyte to reduce the YSZ resistance loss to acceptable levels. However this requires low-cost fabrication of the thin-film YSZ electrolytes on a porous electrode substrate.

### **Trends in Thin-Film YSZ Electrolyte Fabrication**

A number of approaches are being used to develop a cost-effective fabrication process. For example a tape calendar method (Allied Signal Aerospace) and a dip coating process (Lawrence Berkeley Lab, Univ. of Utah) are being used to fabricate YSZ thin-films on a NiO-YSZ composite. After annealing in air at elevated temperatures to form a dense YSZ thin film, the NiO in the composite is then reduced to nickel in the anodic environment to form a Ni-YSZ anode. At the University of Pennsylvania we are also using a low-cost fabrication method to fabricate pore-free YSZ thin-film (3 to 10  $\mu\text{m}$ ) YSZ electrolytes on electrode substrates.

### **Trends in Electrode Design and Materials**

There are numerous efforts to optimize electrode design and electrode materials to reduce electrode-polarization losses in reduced temperature SOFCs. For example, polarization losses in Ni/YSZ anode-supported thin-film YSZ cells and stacks are

being minimized at the University of Utah. This has been accomplished with a novel design to maximize the three-phase gas-anode-electrolyte interface. The reported maximum single-cell power densities are  $\sim 1.9 \text{ W/cm}^2$  at  $800^\circ\text{C}$  and  $\sim 0.8 \text{ W/cm}^2$  at  $650^\circ\text{C}$  for an anode thickness of typically 0.75 to 1.0 mm. The thickness of the YSZ electrolyte and the LSM/YSZ cathode is  $10 \mu\text{m}$  and  $50 \mu\text{m}$ , respectively. Although the initially measured power density for a 4-cell stack is  $\sim 0.5 \text{ W/cm}^2$  at  $800^\circ\text{C}$ , their maximum estimated in-stack power density is  $\sim 1 \text{ W/cm}^2$  at  $800^\circ\text{C}$ .

Another approach to minimize electrode-polarization losses is being used at the University of Pennsylvania, where we are doping YSZ with multivalent cations to introduce significant electronic conductivity. An advantage of these YSZ-based mixed-conductors is that they can reduce significantly the overpotential losses of the currently used porous electrode structures. Indeed selected compositions of our YSZ-based mixed conductors have lower electrode-polarization losses than those of the currently used LSM cathode and the Ni-YSZ anode under similar conditions. Other advantages of doped-YSZ electrodes include their chemical compatibility with a YSZ electrolyte, and a thermal-expansion coefficient which should be quite close to that of YSZ. A YSZ based mixed-conducting anode should also have superior sulfur tolerance over that of the nickel/YSZ cermet anodes.

#### **Acknowledgements**

The financial support of the Gas Research Institute and the previous research contributions of Dr. Ping Han, Dr. Karen Swider and Professor Yoshiharu Uchimoto are gratefully acknowledged.

## CHARACTERISATION AND PERFORMANCE OF SOFC ELECTRODES: A CRITICAL ANALYSIS

Mogens Mogensen, Søren Primdahl, Mette Juhl Jørgensen  
Materials Research Department, Risø National Laboratory  
P.O. Box 49, DK-4000 Roskilde, Denmark  
mogens.mogensen@risoe.dk

During recent years a large number of papers concerning solid oxide fuel cell (SOFC) electrodes have been published. In spite of this the general tendency has been towards increasing disagreement about mechanisms and the factors which control the performance of the electrodes. It appears that not all published experimental results can have the meaning assigned to them by the authors. In this paper an analysis of selected results from the literature is given. The analysis shows that more care is needed in controlling the experimental conditions. Based on this observation and experience gained in this area during the last decade, recommendations are given about practice and methods. Procedures of how to avoid some of the problems, e.g. mass transport limitations, are suggested.

Some of the important aspects are:

- Geometry of the three-electrode set-up: The positioning of the working electrode relative to the counter and reference electrode [1,2,3].
- Arrangement of the working electrode compartment: Hindrances for gas flow and diffusion, gas flow rate compared to volume of the working electrode compartment, gas residence time [4,5].
- Current collection arrangement: Contact quality and in-plane resistance of the material transporting the electrical charge from the reaction sites to the working electrode lead. It is especially important to assure that the in-plane resistance is much smaller than the electrolyte cross-plane resistance in order to obtain an evenly distributed current density.
- Stability of the reference electrode potential: The potential of the popular reference electrode, Pt/air/YSZ, varies with temperature, and the potential of the reference electrode in a one-atmosphere set-up will naturally vary with the variation of the gas composition.
- Stability of the working electrode: Occasionally it is observed that the electrode under investigation changes with time. The electrode stability in time should in principle always be demonstrated. This may be troublesome as time constants are some times of the order of days.
- Stability of the temperature: When high current densities are flowing in solid electrolytes with a relative low conductivity, ohmic heating occurs [6]. This will of course affect the electrode processes.
- Reproducibility: It has been found that it may be necessary to characterise a large number of nominally identical electrodes in order to get a statistically meaningful value for the electrode performance [7]. In principle, this is trivial, but it will be shown that the assessment of the exact uncertainties of the measured polarisation resistances is far from trivial.

The analysis reveals that apparent high performance electrode results reported in the open literature may in reality be due to inadequate measurement set-ups and interpretations of the measurements. Ways of alleviating the problems will be given in the paper.

An example of how to avoid mass transport limitations in the surroundings of the electrode is given below. It may be difficult to avoid gas diffusion limitations through a volume of stagnant gas outside an electrode, because the necessary current collection arrangements will often prevent a free flow or convection of gas resulting in diffusion limitations [5]. A set-up where the mass transport problems are minimised is shown in Fig. 1. An auxiliary cell equal to the test cell is positioned so that the working electrodes are face to face. The current is forced through both cells. In case of reversible electrochemical processes, the reactants used on the working electrode will be produced with exactly the same rate in the electrode of the auxiliary cell, and also the products from the working electrode will be consumed with the same rate. Thus, no mass transport from outside is needed.

### References

- [1] M. Nagata, Y. Ito and H. Iwahara, *Solid State Ionics*, **67**, 215 (1994)
- [2] J. Winkler, P. V. Hendriksen, N. Bonanos and M. Mogensen, *J. Electrochem. Soc.*, **145**, 1184 (1998)
- [3] G. Reinhardt and W. Göpel, in: *Proc. Third Int. Symp. on Ionic and Mixed Conducting Ceramics*, Proc. vol. 97-24, pp 610 - 630, The electrochemical Society, (1997)
- [4] S. Primdahl and M. Mogensen, *J. Electrochem. Soc.* **145**, 2431 (1998)
- [5] S. Primdahl and M. Mogensen, submitted to *J. Electrochem. Soc.*
- [6] S. Primdahl and P. V. Hendriksen, in : *Proc. 17th Risø International Symposium on Materials Science*, pp 403 - 410 (1996)
- [7] M. Juhl Jørgensen, S. Primdahl and M. Mogensen, accepted for publication in *Electrochim. Acta* (1999)

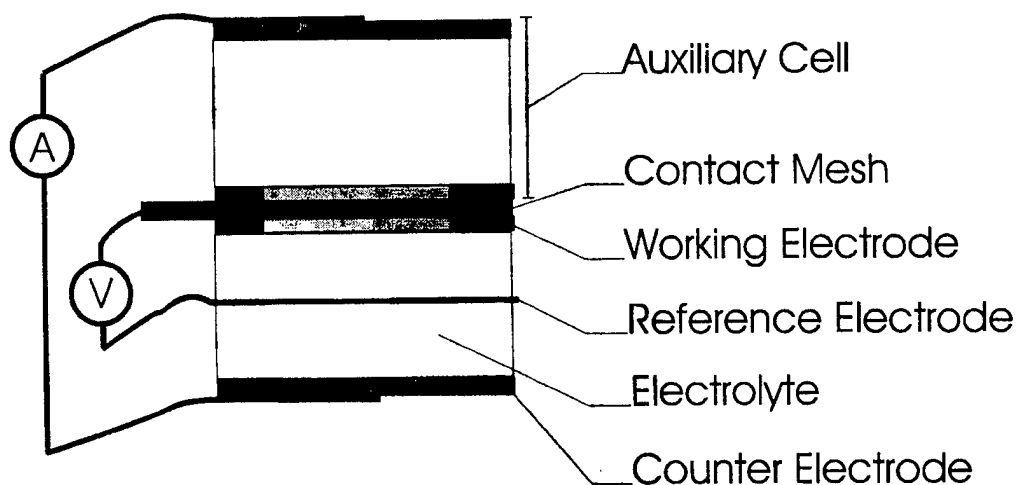


Fig. 1 Illustration of a simple electrode characterisation set-up where no mass transport from the surroundings is needed in case of reversible electrode reactions. The reactants consumed in the working electrode will be produced with the same rate by the auxiliary cell and vice versa with products evolved in the working electrode.

## **A TECHNO-ECONOMIC MODEL FOR SOFC POWER SYSTEMS**

**A. Khandkar, J. Hartvigsen and S. Elangovan**

**SOFCo**

**2425 South 900 West**

**Salt Lake City, Utah 84119, USA**

### **Abstract**

The combination of specified operating and performance parameters for a SOFC system, such as fuel flow rates, operating voltage and power density, are factors affecting capital and operating costs. Additional components of the cost of electricity are attributable to finance costs and system maintenance costs. While computing the cost of electricity from a given set of conditions is fairly straightforward, minimization of the cost of electricity generated from a solid oxide fuel cell power system requires development of functional relationships between the various design and operating parameters. Such a set of relationships is developed for a simple cycle natural gas fueled SOFC power system. This work extends to analysis of SOFC operation on natural gas, a method previously shown by the authors. Relationships between fuel flow rates, stack resistance and operating voltage were defined in a closed form parametric model to predict power density, fuel utilization and efficiency at a specified operating point. The stack performance model was coupled via mass and energy balances with design equations to size system components such as heat exchangers and insulation. Estimated component costs, based on the required size of each component, are used to obtain an estimate of total system capital cost. The cost of electricity for some typical operating conditions is then calculated. The cost framework provides a useful tool for determining opportunities for cost minimization. The overall strategy employed in developing such a model is described and illustrated with various examples. This cost framework can be extended to SOFC power systems involving gas turbine combined cycles as well.

## Operating protocols and activation processes at SOFC electrode interfaces

A. J. McEvoy,

Laboratory for Photonics and Interfaces,  
Ecole Polytechnique Fédérale de Lausanne,  
CH-1015 Lausanne, Switzerland

The voltage obtainable from a solid oxide fuel cell operating at a given current density is reduced relative to the Nernst potential essentially due to two loss mechanisms, the ohmic resistance of the materials used for electrolyte and electrodes, and the polarisation effects at the interfaces. It has been recognised that for most SOFC configurations these polarisation losses dominate, so much of the evolution in performance of these devices achieved over the past ten years has followed on an understanding of the mechanisms involved, followed by the implementation of appropriate counter measures. As systems designers now demand cells with high power density but operating at lower temperatures in order to confront the materials selection and compatibility problems, alternative electrolyte materials of higher ionic conductivity have been sought. Unfortunately those candidate materials to replace the conventional yttria-stabilised zirconia (YSZ) have all, to date, been associated with technical inadequacies such as levels of electronic conductivity leading to low transport numbers. Consequently the most promising route to lower materials resistance has been through the use much thinner, electrode-supported zirconia. Control of interface behaviour therefore assumes even greater importance in this context.

There is a long history of interface engineering in order to optimise behaviour. Attention was first given to the cathodic interface on the understanding that the greater part of the losses occurred there. Based on the three-phase boundary model of charge exchange, for example, interlayers with mixed conduction properties were inserted to delocalise the charge exchange process. However, only relatively recently was it perceived that the appropriate electrode microstructure, to avoid diffusion polarisation in the gas phase and to provide the adsorption area necessary to associate the diatomic oxygen with the solid phase and make it available for ionisation and insertion into the electrolyte, is a necessary but not sufficient condition for a low-polarisation interface. A critical attention to the interface nanostructure has also proved essential. Nanoscale imaging and analysis has established that, particularly as a result of high temperature fabrication processes, topotactic processes between electrode and electrolyte materials can lead to formation of insulating interphases such as lanthanum zirconates as the lanthanum strontium manganate (LSM) perovskite electrode reacted with the YSZ. In fact it is now recognised that the electrode/electrolyte interface is not a passive contact between two stable materials, but is rather a dynamic system, the steady state of which is determined both by the mutual chemical activity of those materials in the particular operating environment, and also by the operating history of the device. The potential difference represented by the polarisation at the interface translated into a lower oxygen chemical activity, injecting oxygen ions into the electrolyte but also migrating cations in the opposite direction. As long as the zirconate has not been allowed to grow to a thickness which inhibits all ion exchange, it is then possible to reverse its growth and thereby "activate" the interface.

Additionally, close attention to the distribution of chemical species on and within the electrolyte surface has given rise to electrocatalytic effects. One approach has been the "domain" cell. In this case, rather than introduce a mixed conducting layer as was done in the 1960's, with resistance due to its material properties as well as an extra interface, small amounts of transition metal ions were introduced into the electrolyte lattice by pyrolysis and diffusion. Electrocatalysis was indicated by impedance spectroscopy, and by the spectacular reduction of polarisation losses. Where manganese was used, it was also shown to have inhibiting effects on the growth of interphase zirconates. It was then demonstrated the with attention to the defect chemistry of the LSM, particularly the use of a A-site (lanthanum)-



deficient material, the same desirable results could be achieved without a separate high temperature treatment for domain fabrication. Additionally, the oxygen transport properties of the cathode materials are enhanced.

To quantify these effects, recent studies have been carried out with ion-implanted electrolytes, the process being capable of precisely determining the amount and the distribution profile of an electrocatalytic element. Cerium and manganese have been studied. Unexpectedly, the evidence is that the electrocatalytic effect cannot be attributed to a single general mechanism, whether the introduction of some degree of mixed conductivity for delocalisation of the charge exchange process, or a redox process facilitating oxygen ion injection into the electrolyte. Each implanted material seems to have its own function, for example the enhancement of the kinetics of oxygen transfer to sites neighbouring cerium. On concentration, the local presence of the implanted species for effective electrocatalysis is of the order of 1%.

These observations clear a path to further progress with the development of solid solution electrolytes doped to concentrations which do not effect bulk transport properties but which do exhibit superior interface behaviour. These materials can also be used in composite anodes and cathodes. The ultimate YSZ SOFC device, with composite electrodes associated with a supported-film solid solution electrolyte, will reduce the high-power operating temperature to a level compatible with standard ferritic steels as bipolar structures, a prerequisite for commercial success.

## REACTION MECHANISMS AT SOLID OXIDE FUEL CELL ANODES

A. Bieberle, L. J. Gauckler

ETH Zürich, Department of Materials, Chair of Nonmetallic Materials,  
 Swiss Federal Institute of Technology  
 CH-8092, Zürich, Switzerland  
 Tel: +41-1-632 7156 Fax: +41-1-6321132  
 email: bieberle@nonmet.mat.ethz.ch

## Introduction

Further development and better performance of solid oxide fuel cell (SOFC) anodes at intermediate temperatures (500-800°C) demand a thorough understanding of the reaction mechanisms. So far, the reaction mechanisms at SOFC anodes are not exactly known.

The reaction steps proposed in the literature [1, 2, 3] are in most cases based on the interpretation of experimental impedance measurements of Ni-YSZ cermet anodes. The electrochemical impedance spectra (EIS) are usually discussed in terms of equivalent circuits [4] which give no information about the electrochemical system and the reaction steps. In addition, Ni-YSZ cermet anodes are very complicated due to the two interpenetrating networks with unspecified triple phase boundary (tpb) length.

In order to overcome these problems, we focus on the simplified anodic system Ni, H<sub>2</sub>-H<sub>2</sub>O | YSZ and combine experimental work with simulations.

## Approach

From the relevant surface science literature, we extract as much information as possible about the system. A first electrochemical model for the reaction mechanisms is then established. The model is described in state-space form and implemented into the computer, so that EIS can be calculated. The experimentally obtained impedance spectra are reduced to the Faraday impedance and are then compared with the simulated impedance spectra. Kinetic constants can be estimated. Repeating experiments and simulations give step by step information about the kinetics of the system (Figure 1).

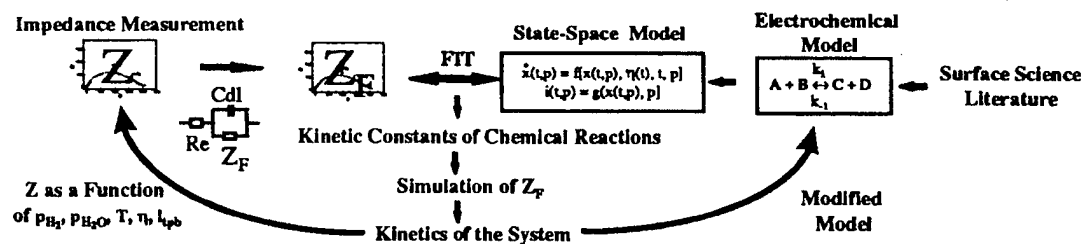


Figure 1: Approach for the investigation of the reaction mechanism at SOFC anodes.

## Electrochemical Model

In our work, we used the simplified anodic system Ni, H<sub>2</sub>-H<sub>2</sub>O | YSZ. Most of the surface science literature is dealing with this system at low temperatures (about 300 K) [5, 6, 7]. At higher temperatures (500-800°C), the proposed reaction steps and reaction rate constants as well as sticking, adsorption, desorption, and surface diffusion coefficients, can only be taken as a first hint. Some information can be obtained from studies on Pt catalysts [8, 9]. A first model with the following main reaction steps is derived:

- (1) Dissociative adsorption of hydrogen:  $\text{H}_2(\text{g}) + 2\text{ad} \leftrightarrow 2\text{H}_{\text{ad}}$   
 (2) Removal of oxygen from the electrolyte:  $\text{O}_x^\circ + \text{ad} \leftrightarrow \text{O}_{\text{ad}}^- + \text{V}_\circ^{\cdot\cdot} + \text{e}^-$   
 (3) Formation of hydroxyl:  $\text{O}_{\text{ad}}^- + \text{H}_{\text{ad}} \leftrightarrow \text{OH}_{\text{ad}}^- + \text{ad}$   
 (4) Dissociative adsorption of water/recombination of hydroxyl:  
 (4a)  $\text{H}_2\text{O}(\text{g}) + \text{O}_{\text{ad}}^- + \text{ad} + \text{e}^- \leftrightarrow 2\text{OH}_{\text{ad}}^-$   
 (4b)  $\text{H}_2\text{O}(\text{g}) + 2\text{ad} + \text{e}^- \leftrightarrow \text{OH}_{\text{ad}}^- + \text{H}_{\text{ad}}$

where ad signifies free adsorption sites.

In addition to the discussed chemical and electrochemical reactions, the model is based on the following assumptions: a) hydrogen, oxygen, and hydroxyl are considered as time depending surface species in the dynamic system; b) all surface species can diffuse on the surface of Ni and YSZ; c) water is assumed to adsorb and to desorb from the Ni surface without any time-dependence; d) the removal of oxygen from the YSZ electrolyte is the only charge transfer reaction; e) gas phase diffusion is not included into the model.

### Simulations

The transformation of the electrochemical model into state-space form as well as the linearization, the transfer function calculation, and the impedance calculation are done similarly as for the Pt,  $\text{O}_2|\text{YSZ}$  system [10, 11]. Electrochemical impedance spectra based directly on the chemical and electrochemical equations are calculated for a set of kinetic parameters. The spectra are simulated as a function of temperature, gas composition, overpotential, and tpb length.

### Experiments

Electrochemical impedance spectra are obtained from sputtered Ni patterned anodes (1  $\mu\text{m}$  thick) on single crystalline YSZ. The Ni electrodes are structured by photolithography and chemical etching. Electrochemical impedance measurements are carried out in a sealed SOFC measurement set-up at various temperatures, gas compositions, overpotentials, and tpb lengths.

### Conclusions

Combining literature data, simulations, and experiments, more insight into the kinetics of the Ni,  $\text{H}_2\text{-H}_2\text{O}|\text{YSZ}$  system is obtained. Experimental impedance spectra can be interpreted in terms of the electrochemical reaction steps.

### References

- [1] S. Primdahl, M. Mogensen, *J. Electrochem. Soc.* **144**, 3409 (1997).
- [2] S. P. Jiang, S. P. S. Badwal, *J. Electrochem. Soc.* **144**, 3777 (1997).
- [3] J. Mizusaki, Tagawa, H., Saito, T., Yamamura, T., Kamitani, K., Hirano, K., Ehara, S., Takagi, T., Hikita, T., Ippomatsu, M., Nakagawa, S., Hashimoto, K., *Solid State Ionics* **70/71**, 52 (1994).
- [4] B. de Boer, PhD Thesis, University of Twente, Twente (1998).
- [5] T. N. Troung, G. Hancock, D. G. Truhlar, *Surf. Sci.* **214**, 523 (1989).
- [6] R. H. Stulen, P. A. Thiel, *Surf. Sci.* **157**, 99 (1985).
- [7] H. Yang, J. L. Whitten, *Surf. Sci.* **223**, 131 (1989).
- [8] B. Hellsing, B. Kasemo, V. P. Zhdanov, *J. Catalysis* **132**, 210 (1991).
- [9] E. Fridell, A. Rosen, *Langmuir* **10**, 699 (1994).
- [10] A. Mitterdorfer, L. J. Gauckler, *Solid State Ionics* in press (1998).
- [11] A. Mitterdorfer, L. J. Gauckler, *Solid State Ionics* in press (1998).

**MIXED CONDUCTING OXIDE ANODES FOR SOLID OXIDE FUEL CELL**

Shizhong Wang, Yi Jiang<sup>1</sup>, Yahong Zhang, Wenzhao Li, Jingwang Yan, Zigui Lu  
Dalian Institute of Chemical Physics, Chinese Academy of Sciences, Dalian 116023, P.R.China

**Introduction**

Solid oxide fuel cell (SOFC) is one of the most advanced fuel cell systems for generating electricity in an efficient and environmentally friendly way. The principal advantages of SOFC over other types of fuel cells are fuel adaptability and long term stability. A variety of perovskite oxides have been used as cathode materials [1,2], while the anode material selection is only limited to a few materials such as Ni-YSZ etc. Mixed Ionic-Electronic Conductor (MIEC) oxides exhibit the peculiar characteristic of both high ionic and electronic conductivities at elevated temperatures. Some of them appear sufficiently stable under reducing atmosphere [3]. They are attractive candidate materials for several important applications, including SOFC electrodes, oxygen separation membranes etc [3,4]. In this paper, the electrochemical performances of MIEC oxide anodes and their Ni-YSZ interlayered anodes were investigated.

**Experimental**

$\text{La}_{0.6}\text{Sr}_{0.4}\text{Fe}_{0.8}\text{Co}_{0.2}\text{O}_{3-\delta}$ ,  $\text{SrFeCo}_{0.5}\text{O}_x$  and  $\text{SrCo}_{0.8}\text{Fe}_{0.2}\text{O}_{3-\delta}$ , below referred as to LSFC, SFC<sub>0.5</sub> and SF<sub>0.2</sub>C<sub>0.8</sub> respectively, were all prepared by a solid state reaction from  $\text{La}_2\text{O}_3$ ,  $\text{SrCO}_3$ ,  $\text{Co}(\text{NO}_3)_2 \cdot 6\text{H}_2\text{O}$  and  $\text{Fe}_2\text{O}_3$ , which were mixed stoichiometrically and ground thoroughly in ethanol. Oxide powders were obtained by firing the mixtures in air at 900°C for 16 h. The both electronic and ionic conductivities of the oxides were measured by AC impedance and a blocking electrode technique. LSFC, SF<sub>0.2</sub>C<sub>0.8</sub> and SFC<sub>0.5</sub> anodes were prepared by screen printing oxide pastes on the YSZ plate and calcined in air for 2 h. The paste was prepared from mixing the respective MIEC oxide powders with an appropriate amount of binder and solvent. The interlayered Ni-YSZ anode was prepared by depositing an outer layer of an Ni-YSZ paste on the oxide layer and fired *in situ* in air at 980°C for 2 h. Cathodes and reference electrodes were  $\text{La}_{0.8}\text{Sr}_{0.2}\text{MnO}_3 + 20 \text{ wt\% YSZ}$  composite electrodes and Pt reference electrodes described in detail elsewhere [5]. The YSZ plate was sealed with a glass sealing material to a two open ends YSZ tube (16 cm in length, 2 cm in diameter). The anode sealed inside the tube was exposed to the fuel, either  $\text{H}_2$  or  $\text{CH}_4$  and the cathode to ambient air.

**Results**

The total and ionic conductivities of three oxides at 950 °C decreased with decreasing  $P_{\text{O}_2}$ . In air, the total and ionic conductivities for LSFC, SFC<sub>0.5</sub> and SF<sub>0.2</sub>C<sub>0.8</sub> were 110, 10, 61.7  $\text{S}\cdot\text{cm}^{-1}$  and 0.3, 5.3, 6.4  $\text{S}\cdot\text{cm}^{-1}$ . Under  $\text{CH}_4$  reducing gas, SFC<sub>0.5</sub> and SF<sub>0.2</sub>C<sub>0.8</sub> were more or less stable and the total conductivity decreased to 3.0 and 2.0  $\text{S}\cdot\text{cm}^{-1}$  with still high ionic transference numbers. Results indicated that SFC<sub>0.5</sub> and SF<sub>0.2</sub>C<sub>0.8</sub> are indeed MIEC oxide in the wide range of  $P_{\text{O}_2}$ . The electrochemical performances of the oxide anodes on  $\text{H}_2$  at 950 °C are remarkably different among three anodes (Fig. 1). SF<sub>0.2</sub>C<sub>0.8</sub> gives the best performance with a maximum power density of about 0.08  $\text{W}/\text{cm}^2$ . The maximum power outputs of LSFC and SFC<sub>0.5</sub> are around 0.05  $\text{W}/\text{cm}^2$  and 0.03  $\text{W}/\text{cm}^2$ . The performance order on  $\text{CH}_4$  is LSFC > SFC<sub>0.5</sub> > SF<sub>0.2</sub>C<sub>0.8</sub>, which is different from the cell performance order running on  $\text{H}_2$ . The maximum

<sup>1</sup> Corresponding author, Dalian Institute of Chemical Physics, Dalian 116023, P.R.China,

Fax: +86-411-4691570, Email: jiangyi@ms.dicp.ac.cn.

power output of the LSFC anode was  $0.09 \text{ W/cm}^2$ . Polarization and AC Impedance experiments showed that the performance of the MIEC anode is determined by the activation overpotential and the ohmic resistance, which are conspicuously different among the MIEC oxide anodes under study. For all three anodes, activation overpotentials were very large, suggesting insufficient activities to  $\text{CH}_4$ . With depositing a thin layer of Ni-YSZ to form an interlayered anode, the performance of the interlayered anode was improved significantly, in particular, for  $\text{SFC}_{0.5}$  oxide. In the case of  $\text{SFC}_{0.5}$ , the maximum power density reached  $0.25 \text{ W/cm}^2$  and exceeded those of both  $\text{SFC}_{0.5}$  and the Ni-YSZ as anodes alone, showing a synergetic effect (Fig. 2). In the other two cases, although there were improvements in power output for the MIEC oxide anodes, the power outputs were lower or close to that of the Ni-YSZ. Further studies revealed that the activation overpotential and the ohmic resistance of the interlayered anode were substantially reduced due to the Ni-YSZ which is good catalyst for  $\text{CH}_4$  activation and a much better conductor. In the meanwhile, the existence of  $\text{SFC}_{0.5}$  effectively enlarges the electrochemically active area. The reason for the good performance of  $\text{SrFeC}_{0.5}$  over the other two oxides is most likely associated with its superior mixed conductivity and structure stability even at very reduced oxygen environment.

The main products evolving from the electrochemical oxidation over three oxide anodes when  $\text{CH}_4$  is fed at a flow rate of  $60 \text{ ml/min}$  are generally same,  $\text{CO}$  and  $\text{H}_2$ . The results show that these oxides are not only active but also selective as anodes for SOFCs for producing syngas with the spontaneous generation of electrical energy.

## References

- [1] W. Drenckhahn, H. Greiner, E. Ivers-Tiffée, *Power Journal*, 4, 36-38(1994)
- [2] N. Q. Minh, *J. Am. Ceramics Soc.*, 76(3): 563(1993)
- [3] B. Ma, U. Balachandran, and J-H. Park, *J. Electrochem. Soc.*, 143(5), 1736(1996)
- [4] Y. Teraoka, H. Zhang, K. Okamoto, and N. Yamazeo, *Mat. Res. Bull.*, 51(1998)
- [5] Y. Jiang, S. Z. Wang, Y.H. Zhang, J. W. Yan, W. Z. Li, *J. Electrochem. Soc.*, 145(2), 373(1998)

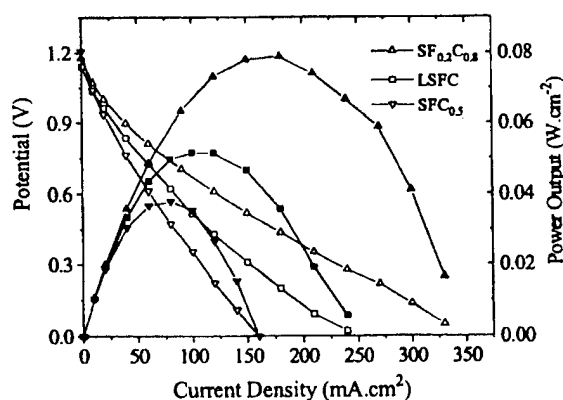


Fig. 1 Cell performances of three SOFCs with  $\text{SFC}_{0.5}$ ,  $\text{SF}_{0.2}\text{C}_{0.8}$  and LSFC oxides as anodes at  $950^\circ\text{C}$  on  $\text{H}_2$ .

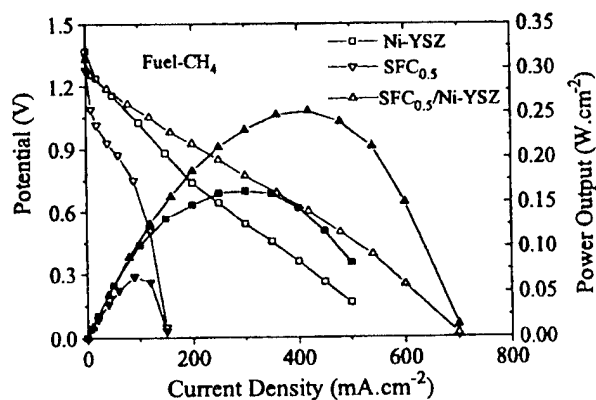


Fig. 2 Comparison of cell performances of SOFCs with the Ni-YSZ,  $\text{SFC}_{0.5}$  and  $\text{SFC}_{0.5}$  interlayered Ni-YSZ anodes at  $950^\circ\text{C}$  on  $\text{CH}_4$ .

## HIGH PERFORMANCE ELECTRODES FOR MEDIUM-TEMPERATURE SOLID OXIDE FUEL CELLS - ACTIVATION OF $\text{La}(\text{Sr})\text{CoO}_3$ CATHODE WITH HIGHLY DISPERSED Pt METAL ELECTROCATALYSTS

Hiroyuki Uchida, Shin-ichi Arisaka, and Masahiro Watanabe

Faculty of Engineering, Yamanashi University, Takeda 4-3, Kofu 400-8511, Japan

It is desirable to operate solid oxide fuel cells (SOFCs) at a medium temperature around 800°C, since a high-temperature operation causes many serious problems: degradation of the components, a limited choice of materials, etc. Besides a reduction of ohmic loss in solid electrolytes, it is essential to develop high performance electrodes because the electrode reaction rates must be slow down at such temperatures.

We have developed a porous catalyzed-reaction layer for medium-temperature SOFCs [1]. Mixed conducting oxide particles, samaria-doped ceria  $[(\text{CeO}_2)_{0.8}(\text{SmO}_{1.5})_{0.2}]$ , denoted as SDC for the anode and  $\text{La}_{0.85}\text{Sr}_{0.15}\text{MnO}_3$  (LSM) for the cathode, were employed in combination with highly dispersed (nanometer-sized) metal electrocatalysts on their surfaces. Ru-dispersed SDC and Pt-dispersed LSM exhibited fairly high performances at medium temperatures [1-3]. Both the overpotential and the ohmic resistance of SDC anodes and LSM cathodes were appreciably lowered by controlling their microstructures [4-6]. The performances of both SDC anode and LSM cathode with their optimized microstructures were enhanced further with highly dispersed Ru and Pt. It is possible to apply our design concept on the catalyzed-reaction layer to other mixed-conducting materials with higher activity. It has been known that  $\text{La}(\text{Sr})\text{CoO}_3$  (denoted as LSC) exhibited higher cathodic performance than LSM but LSC reacted with zirconia electrolytes to form  $\text{La}_2\text{Zr}_2\text{O}_7$  or  $\text{SrZrO}_3$  with high ohmic resistance at high temperatures.

In this paper, we report on the effect of controlling microstructure of LSC cathode layers on an enhancement of the electrocatalytic activity and that of the nm-sized Pt metal catalysts.

An 8 mol% yttria-stabilized zirconia disk (YSZ, diameter: 13 mm, thickness: 1 mm) was used as the solid electrolyte.  $\text{La}_{0.6}\text{Sr}_{0.4}\text{CoO}_3$  (LSC, mean diameter,  $d = 0.7 \mu\text{m}$ ) with and without Pt particle loading were used as the cathode material. In order to avoid unfavorable solid-state reactions between the LSC cathode and YSZ electrolyte, a thin film of SDC was attached on one side of YSZ surface before coating the LSC cathode layer. Under an atmosphere of SOFC cathode, SDC is expected to act as a pure oxide ionic conductor with higher conductivity than that of YSZ. The SDC thin film was prepared by screen-printing a mixed solution of cerium and samarium nitrates ( $\text{Ce} : \text{Sm} = 8 : 2$ ), followed by heat treatment at 400°C for 0.5 h [4, 5]. Then, the same solution was screen-printed again, followed by the second heat treatment at 400°C or 1150°C for 4 h. These SDC thin films thus prepared on YSZ surface are denoted as SDC400 and SDC1150, respectively. Porous LSC cathodes were prepared by screen-printing a paste of LSC particles dispersed in n-pentanol, followed by firing at 1050°C or 1150°C for 1 h (LSC1050 and LSC1150, projected area = 0.26 cm<sup>2</sup>). The construction of a test fuel cell was the same as in our previous work [1]. The IR-free polarization characteristics ( $I - E$  curves) of various LSC cathodes in oxygen or air were measured by a current-interruption method in a three-electrode configuration (with Pt anode and Pt/air reference electrode) at 800 to 1000°C.

First, we examined the effect of sintering temperatures of SDC interlayer and LSC cathode on their properties. Observations of SDC400 and SDC1150 films on YSZ surface by using SEM with EDX indicated that SDC1150 was uniform and dense film with

a thickness of *ca.* 1  $\mu\text{m}$  whereas SDC400 was one with fine cracks exposing YSZ partly. Figure 1 shows the polarization curves of various LSC cathodes prepared on SDC interlayers. The LSC1050 cathode prepared on SDC400 interlayer (LSC1050/SDC400) exhibited relatively large IR-free polarization loss ( $\eta$ ) and large ohmic resistance ( $R_{\text{LSC}}$ ). In this case, a formation of  $\text{SrZrO}_3$  was observed by X-ray diffraction; LSC reacted with YSZ uncovered by SDC. In contrast, fairly small  $\eta$  and very low  $R_{\text{LSC}}$  were seen for LSC1050/SDC1150 over the entire temperature range between 1000 and 800°C. This result together with its XRD indicated that YSZ electrolyte coated with SDC1150 interlayer was protected against the unfavorable solid-state reaction. However, when LSC was sintered at 1150°C on the SDC1150 interlayer (LSC1150/SDC1150), the values of  $\eta$  and  $R_{\text{LSC}}$  increased due to the formation of  $\text{SrZrO}_3$ .

Although LSC1050/SDC1150 showed fairly high current density of 0.3  $\text{A cm}^{-2}$  at  $\eta = -0.05$  V in  $\text{O}_2$  at 800°C, there is still room for an improvement of the performance with respect to gas-diffusion rates. Then, fine polymer beads ( $d = 1.2$   $\mu\text{m}$ ) were added to the LSC paste. The pore-size distribution in the electrodes was measured by a mercury porosimeter. Two different types of micropores were found in all LSC layers, *i.e.*, primary-pore ( $0.2 < d < 1$   $\mu\text{m}$ ) and secondary-pore ( $d > 10$   $\mu\text{m}$ ). The addition of polymer beads (0.5 to 1 wt%), followed by sintering, preferentially increased a volume of the secondary-pore. As shown in Fig. 2, the overpotential of LSC1050/SDC1150 measured in air was appreciably lowered by controlling the microstructure. The value of  $R_{\text{LSC}}$  was not increased by the polymer addition. In order to activate a LSC cathode with optimized microstructure (LSC1050/SDC1150 with 1 wt% polymer), nanometer-sized Pt catalysts were highly dispersed on its surface (0.1  $\text{mg/cm}^2$ ). Pt loading significantly enhances the performance of the optimized cathode especially at 800°C. At  $\eta = -0.05$  V operated at 800°C with air, the current density on the Pt-LSC was 0.7  $\text{A cm}^{-2}$ , which is 3 times higher than that of the original one.

- [1] M. Watanabe, H. Uchida, M. Shibata, M. Mochizuki, and K. Amikura, *J. Electrochem. Soc.*, **141**, 342 (1994).
- [2] H. Uchida, N. Mochizuki, and M. Watanabe, *ibid.*, **143**, 1700 (1996).
- [3] H. Uchida, A. Tsuno, and M. Watanabe, *Denki Kagaku*(Eng. Eds.), **64**, 686 (1996).
- [4] H. Uchida, H. Suzuki, and M. Watanabe, *J. Electrochem. Soc.*, **145**, 615 (1998).
- [5] H. Uchida, T. Osuga, and M. Watanabe, *J. Electrochem. Soc.*, in contribution.
- [6] H. Uchida, T. Osuga, M. Watanabe, *65th Meeting of Electrochem. Soc. Jpn., Extended Abstract*, p. 148 (1998).

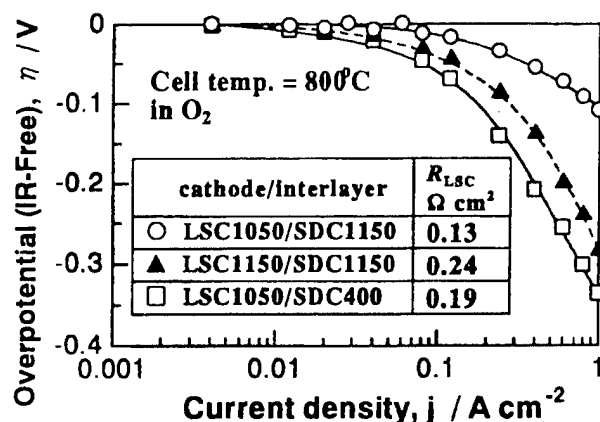


Fig. 1. Polarization curves (IR-free) of various LSC cathodes prepared on SDC interlayers. The area-specific ohmic resistance of LSC ( $R_{\text{LSC}}$ ) determined in the similar manner as in Ref. [4,5] is shown in table.

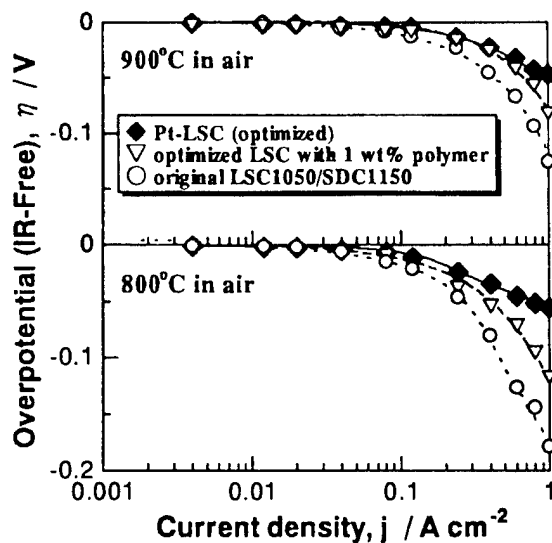


Fig. 2. Polarization curves (IR-free) of various LSC cathodes measured in air.

## CATHODIC REACTION MECHANISM OF DENSE $\text{La}_{0.8}\text{Sr}_{0.2}\text{CoO}_3$ AND $\text{La}_{0.8}\text{Sr}_{0.1}\text{MnO}_3$ ELECTRODES FOR SOFC

A. Endo, H. Fukunaga, C. Wen and K. Yamada

Dept. of Chemical System Engineering, School of Engineering, the University of Tokyo, 7-3-1 Hongo, Bunkyo-Ku, Tokyo 113-8656, Japan

### 1. Introduction

To decrease the operation temperature of SOFC from 1000°C to lower than keeping 800°C high efficiency, and high reaction rate is a key factor to realize a SOFC system on a large scale. Main issues are to lower the solid electrolyte resistance and the overpotential at electrode/electrolyte interface especially for cathode at a low temperature. The ceria based oxides would be an effective electrolyte to solve the problem. On the other hand, a high performance cathode is still unknown. It is known that there are two major pathways for the cathodic reaction. One is the reaction pathway through the three phase boundary (TPB) of gas/electrode/electrolyte. In the case of using metal or low ionic conducting oxides like  $\text{La}_{1-x}\text{Sr}_x\text{MnO}_3$  (LSM), this pathway is considered to be dominant and the length of TPB is important for electrode properties. [1-2]. The other is the reaction pathway through the bulk electrode. In the case of using the high oxide ionic conductive materials, such as  $\text{La}_x\text{Sr}_x\text{CoO}_3$  (LSC), this pathway becomes effective and reaction site is not limited at/around TPB. If the oxide ionic conductivity of electrode is large enough, the rate determining step of the electrode reaction is the absorption of oxygen onto the electrode surface or gas phase diffusion of oxygen molecules[3].

Aiming to clarify how the ionic conductivity of electrode and catalytic activity of oxygen reduction at electrode surface influence the electrode performance, we used the dense electrode for which the structure could be well defined and simple as the first step. In this paper, we investigated two kinds of electrode material, LSM as a low ionic conductive material and LSC as a high ionic conductive material. Electrochemical properties of the dense electrodes were measured. The reaction model for dense electrode were constructed. The relationship between the ionic conductivity and catalytic activity of electrode materials, and electrode performance was discussed.

### 2. Experimental

Dense electrodes of LSM and LSC were prepared by a laser ablation method. The light source was KrF excimer laser which wavelength is 248nm and the energy density was 900-980mJ/pulse. The temperature of substrate was 800°C, oxygen partial pressure was  $10^{-3}$  atm and laser repetition rate was 10Hz. The deposition rate was less than 1µm/hr. By changing the deposition time, different thickness of the dense electrodes were obtained.

All samples were annealed at 1000°C for 5 hours in air. The XRD measurement was revealed that the formed LSM and LSC films had the same crystalline structure as the targets. No cracks or micropores was observed in the SEM observation and the denseness was kept after the annealing treatment. As electrolytes, single crystalline disks of YSZ (9.6m/o, supplied from earth jewel co. ltd.) for LSM electrode and sintered  $\text{Sm}_{0.2}\text{Ce}_{0.8}\text{O}_2$  (SDC) disks (20m/o, supplied from Token sangyo Co. ltd.) for LSC electrode were used.

The AC impedance was measured measurements and the electrode interfacial conductivity ( $\sigma_E$ ) was calculated ( $\sigma_E = 1 / AR_E$ ) where A is the surface area of the electrode and  $R_E$  is the electrode resistance (excluding the ohmic resistance). If there were some semi-arcs in cole-cole plot, the fitting analysis using Equivalent Circuit was conducted and  $R_E$  for each process was calculated.

### 3. Results and Discussion

#### 3.1 Electrochemical properties of dense LSM and LSC electrode

As reported in our previous paper, the interfacial conductivity for dense LSM electrodes was proportional to the film thickness [11]. By this result and the dependence of the interfacial conductivity on oxygen partial pressure, it is concluded that the diffusion of oxide ion in the bulk of LSM is the rate determining step in the cathodic reaction of the dense LSM electrode. This result agrees well with the fact that the three boundary phase interface is an important place to determine the overpotential of the porous LSM electrode. It means that the oxide ion tends to diffuse through over the surface of the LSM instead of the bulk of LSM.



On the other hand, for the dense LSC/SDC systems, the interfacial conductivity was independent of the film thickness of LSC. The dependence of the interfacial conductivity on the oxygen pressure is shown in Fig. 1. It can be seen that the interfacial conductivity is almost proportional to the square root of the oxygen partial pressure. This results is quite different from that of the LSM/YSZ system.

### 3.2 Reaction model of dense perovskite electrodes

The reaction at the dense perovskite electrodes is classified into the in following processes 1)diffusion of oxygen in gas phase. 2)absorption and adsorption of oxygen on the electrode surface. 3)ionization of absorbed oxygen. 4)diffusion of oxygen ion in dense electrode.

These elementary processes are connected in serial and 1), 3) is not considered to be the rate determining step as reported[4].

Constructing the reaction model, the oxygen occupancy was defined as  $\Theta$  which is the ratio of the sites occupied by the oxygen atom to the total sites for oxygen atom adsorption on the electrode. Under the equilibrium conditions at the oxygen partial pressure of  $P_{O_2}$ , the occupancy was defined as  $\Theta^*$ . Then the rate equation of oxygen absorption can be expressed as the following equation, where  $r$  is the net rate of oxygen absorption and  $k, k'$  is the rate constant.

$$r = kP_{O_2}(1-\Theta)^2 - k'\Theta^2 \quad (1)$$

The diffusion of oxygen ion in dense electrode can be expressed by using the oxygen ionic conductivity  $\sigma_{ion}$ , the oxygen ion density  $c_o(x)$  and the Faraday constant  $F$  as equation(2), where  $R$  is the gas constant,  $T$  is the temperature and  $x$  is the distance from the electrode/electrolyte interface. The electrode polarization  $\eta$  at electrode/electrolyte interface can be expressed by equation(3)

$$j/2F = (\sigma_{ion} RT / 4F^2) \times (\partial \ln c_o(x) / \partial x) \quad (2)$$

$$2F\eta = RT \ln c_o^* / c_o(0) \quad (3)$$

In dense electrode, the flux of oxygen is equal everywhere, so the following equation can be established.

$$j/2F = \sigma_{ion} RT / 4F^2 \times (\partial \ln c_o(x) / \partial x) = kP_{O_2}(1-\Theta)^2 - k'\Theta^2 \quad (4)$$

From equation(4), consequently, the relationship between the overpotential and the current density becomes as follows.

$$\eta = (RT/2F) \{ \ln KP_{O_2}^{1/2} - \ln [K^2 P_{O_2} - (K^2 P_{O_2} + j/2k'F(K^2 P_{O_2} - 1)^{1/2})] \} + j\ell / \sigma_{ion} \quad (5)$$

The electrode interfacial conductivity is the inverse of the gradient of current density vs. overpotential curve at  $j = 0$ . Here differentiating the equation (5), we obtain the next formula. So, the electrode interfacial conductivity can be expressed as follows.

$$\sigma_E = 1 / [ (8k'F^2/RT) B^2 / (B+1) + \ell / \sigma_{ion} ] \quad (6)$$

, where  $B = (k/k')^{1/2} P_{O_2}^{1/2}$ . The first term of the denominator of the right side represents the resistance caused by the surface reaction and the second represents the resistance caused by the diffusion of the ion in the bulk electrode. In the case of an electrode having low ionic conductivity, such as LSM, the electrode interfacial conductivity is determined only by the ionic conductivity and film thickness. On the other hand, in the case of an electrode having high ionic conductivity, such as LSC, the first term of the right side of equation . (6). dominates. If  $B \gg 1$ , then the  $P_{O_2}$  dependence of  $\sigma_E$  agrees well with the experimental result as shown in Fig.1(  $\sigma_E \propto P_{O_2}^{1/2}$  ).

The detail of the model and the experimental results will be discussed in the presentation

<Reference>

- [1] M.Suzuki et.al., in Proceedings of the 4th international symposium on Solid Oxide Fuel Cells, 187(1995).
- [2] A.Endo, S.Wada, C.Wen, H.Komiyama and K.Yamada, J.Electrochem.Soc., 145, L35(1998).
- [3] A.Endo, M.Ihara, H.Komiyama and K.Yamada, Solid State Ionics, 86-88,1191(1996).
- [4] K.Tsuncyoshi, K.Mori, A.Sawata, J.Mizusaki and H.Tagawa, Solid State Ionics, 35,63(1989)

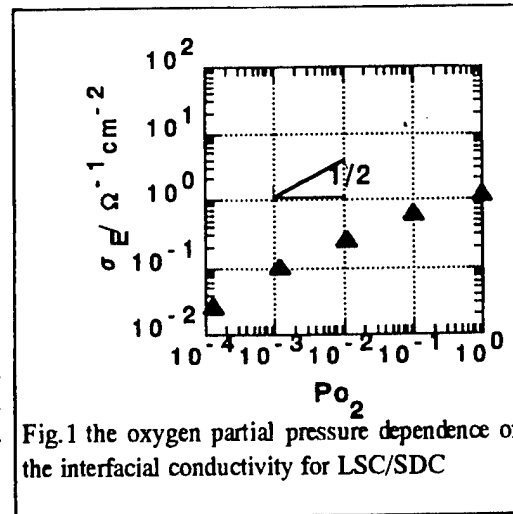


Fig.1 the oxygen partial pressure dependence of the interfacial conductivity for LSC/SDC

## SYNTHESIS OF (La,Sr)MeO<sub>3</sub> (Me=Cr, Mn, Fe, Co) SOLID SOLUTIONS FROM AQUEOUS SOLUTIONS

Takeshi YAO, Yoshiharu UCHIMOTO, Takuya SUGIYAMA and Yusuke NAGAI  
Department of Fundamental Energy Science, Graduate School of Energy Science,  
Kyoto University

Yoshida, Sakyo-ku, Kyoto, 606-8501, JAPAN

(La,Sr)MeO<sub>3</sub> (Me=Cr, Mn, Fe, Co) solid solutions, which are partly substituted by Sr for La, have interesting properties and now are paid a great attention as a candidate for cathode, anode or interconnecting materials for solid oxide fuel cells and high-temperature steam electrolyzer. Thin films, either dense or porous, are desirable because of the high surface area, the reduction of both the ion-diffusion path length and electrical resistance, light and compact system construction and so on. Chemical vapor deposition, sputtering and sol-gel methods are used for preparing thin films, however, these methods have some disadvantages in actual use. For chemical vapor deposition and sputtering, expensive vacuum equipment is required and the film area is restricted. For sol-gel method, the film geometry is limited, and moreover, heat-treatment, which is injurious because of the possibility of a change in the shape and/or size of the film and crack formation, is inevitable to form crystalline states. A method for forming films from an aqueous solution is expected to be advantageous because no vacuum, no high temperature and no expensive apparatus will be required and substrates even with wide areas and/or complicated shapes are available. Previously, we have presented the methods for synthesizing ZrO<sub>2</sub>[1,3], or LaMeO<sub>3</sub> (Me=Cr, Mn, Fe, Co) perovskite oxides[2,3] from aqueous solutions. In this study we will present a method for synthesizing (La,Sr)MeO<sub>3</sub> solid solutions from aqueous solutions at ordinary temperature and ordinary pressure.

We have considered that the chemical equilibrium between (La,Sr)MeO<sub>3</sub> solid solution and La-,Sr- and Me-fluorocomplexes will hold analogous to that presented for LaMeO<sub>3</sub> perovskite synthesis[2,3]. When boric acid is added, boron reacts with fluoride ion to form BF<sub>4</sub><sup>-</sup> complex, fluoride ion is consumed, then the equilibrium between (La,Sr)MeO<sub>3</sub> solid solution and La-, Sr- and Me-fluorocomplexes is shifted to the direction of (La,Sr)MeO<sub>3</sub> solid solution formation in order to increase fluoride ion. In this process, the valence state control of the transition metal ions is very important, and we have contrived a sophisticated technique as follows. (La,Sr)MeO<sub>3</sub> solid solution was produced by the usual solid state reaction, then the product was dissolved in hydrofluoric acid solution, which is expected to neither oxidize nor reduce the transition metal ions. Consequently, the fluorocomplex solution, having the same valence state as those in the solid solution, was obtained.

Lanthanum oxide, strontium carbonate and chromium oxide or iron(III) oxide or manganese carbonate or cobalt carbonate were mixed with a molar ratio of La:Sr:Me=1-x:x:1, pressed into a disk, and heat-treated at 1400 °C for 5 h in an electric furnace. Then the products were milled to fine powders by an electric mortar. We refer to powders thus obtained as the raw powder hereafter. The raw powders were analyzed by X-ray diffraction, and the formation of La<sub>1-x</sub>Sr<sub>x</sub>MeO<sub>3</sub> solid solution were confirmed respectively. For each solid solution, the raw powder was dissolved into 25 wt.% hydrofluoric acid solution by stirring for 24 h. The undissolved raw powder was removed by the filtration. Then boric acid was added to the filtrate. The sample solutions were prepared by taking the filtrate. We soaked a poly-ethylterephthalate (PET) substrate, abraded with 1000# SiC pad on one side, in each sample solution. After the soaking, the substrates were washed moderately with distilled water and dried at room temperature with no heat treatment.

The surface of the substrate after the soaking was analyzed by a thin-film X-ray diffraction [TF-XRD]. Scanning electron microscope images were obtained with a scanning electron microscope [SEM] and the elemental analyses of La, Sr and Me were performed by an energy-dispersive electron probe X-ray microanalyzer [EPMA] attached to the microscope.

For the soaked substrates, the TF-XRD peaks attributed to (La,Sr)MeO<sub>3</sub> solid solution were observed. The peaks were sharp and strong enough to confirm the high crystallinity. Fig.1 gives SEM micrograph of the substrate surface soaked in the sample solution for (La,Sr)CoO<sub>3</sub> synthesis. The particle size was measured about 7 μm from the image. It was confirmed by EPMA analysis that the La-containing region, Sr-containing region and Co-containing region agreed with one another and they all agreed exactly with the particle locations. Taking the result of the TF-XRD

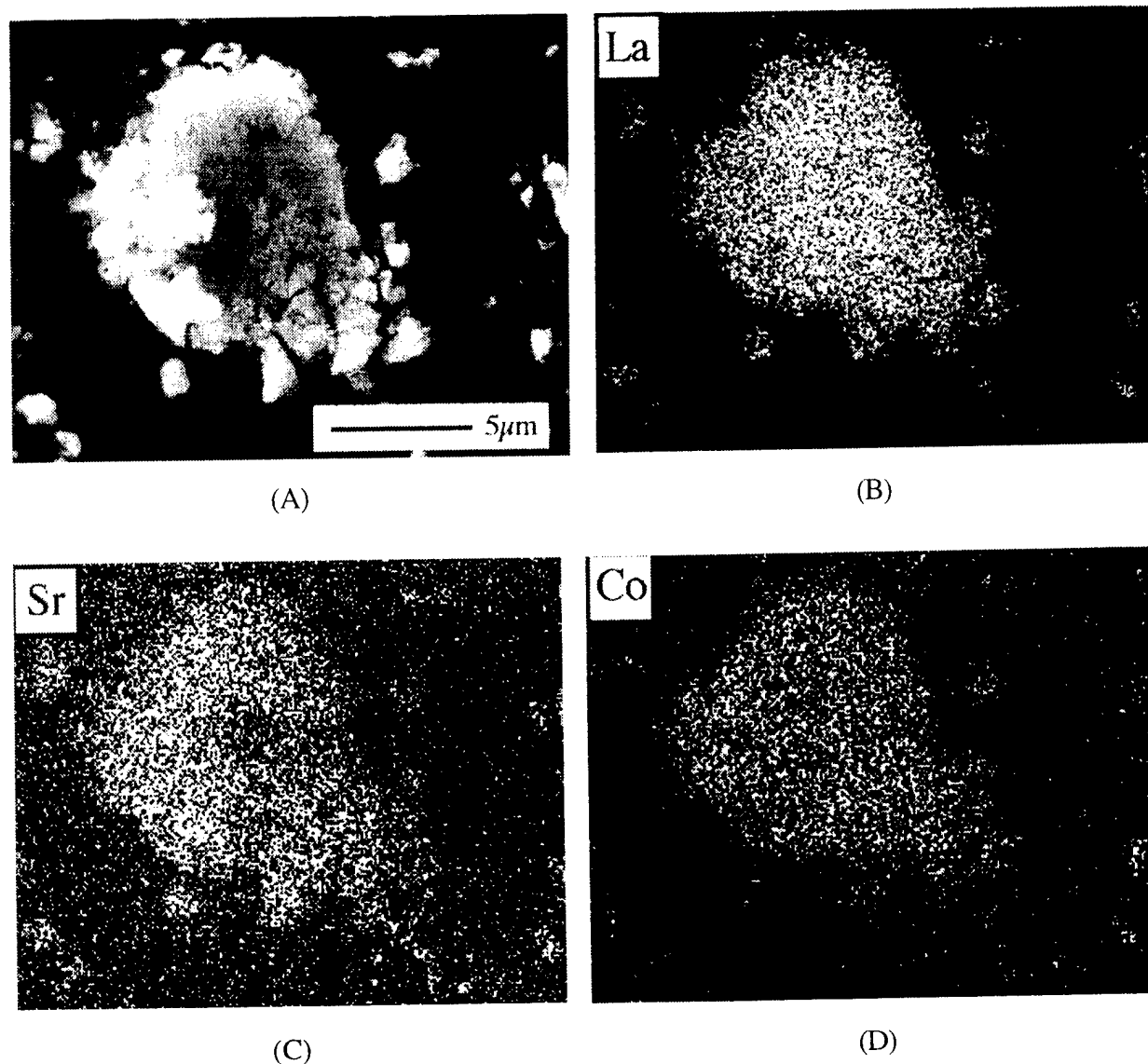


Fig. 1. (A) SEM micrograph of the substrate surface soaked in the aqueous solution for  $(\text{La,Sr})\text{CoO}_3$  synthesis and EPMA elemental analysis maps (B) for La, (C) for Sr and (D) for Co. La-containing region, Sr-containing region and Co-containing region agreed with one another and they all agreed exactly with the particle locations.

measurements into account, it is sure that the particles observed in the SEM micrograph are  $(\text{La,Sr})\text{CoO}_3$  solid solution.

In summary,  $(\text{La,Sr})\text{MeO}_3$  solid solutions were synthesized from aqueous solution at ordinary temperature and pressure by the hydrolysis reaction of La-, Sr- and Me-fluorocomplexes. This method is promising for preparing films of  $(\text{La,Sr})\text{MeO}_3$  solid solutions for a number of functional uses.

#### Reference

- [1] T.YAO, T.INUI and A.ARIYOSHI, *J. Am. Ceram. Soc.*, **79**, 3329 (1996).
- [2] T.YAO, A.ARIYOSHI and T.INUI, *J. Am. Ceram. Soc.*, **80**, 2441 (1997).
- [3] T.YAO, *J. Mater. Res.*, **13**, 1091 (1998)

## CERAMIC CONDUCTORS FOR ELECTROCHEMICAL CELL APPLICATIONS : NEW PERSPECTIVES IN MATERIALS AND SYNTHESIS

JR Jurado

*Instituto de Cerámica y Vidrio, CSIC. , Arganda del Rey, 28500 Madrid, Spain.*

Nowadays an important effort is being done world wide to find new materials and new synthesis and processing routes for electrochemical devices, catalysis, electrodes, gas separator membranes etc. The current work is focussed on looking for materials with high electrocatalytic activity, mainly attempting to reduce the cost noble metal materials imply, using cheaper ceramic compounds instead of precious metals is an acceptable alternative. In MCFC and SOFC electrochemical devices, ceramic materials, with perovskite, spinel and transition metal mixed oxides have already replaced noble metals. However, in PAFC, PEMFC and DMFC devices, Pt is still used.

Other activities are focussed on seeking new synthesis methods, being the main objective to obtain very reactive powders with high electrocatalytic activity, achieving a very low particle size with nanocrystalline structure. That objective could allow developing electrocatalysts with high specific surface area, which is one of the key parameter for improving the efficiency in electrochemical devices. A great deal of compounds with interesting conducting electronic properties, such as ceramic metallic conduction, metal-semiconductor transition and ionic-electronic mixed conduction, with perovskite oxide structure can be prepared, by combining properly Ln and M in the general formula  $\text{Ln MO}_3$ , being Ln= La, Sm, Y, Sr and M= Ni, Co, Mn, Fe.

Some examples are described in this work, being the main cases:  $\text{SmCoO}_3$  compound, which shows metal-semiconductor transition, or is also considered a Mott Insulators, this material can be used as electrocatalyst in direct methanol oxidation.  $\text{LaNiO}_3$  is a ceramic with metallic conduction, and at low temperatures (100-300°C) is a good electrode in oxygen reduction process.  $\text{Sr (Ti,Fe)O}_3$  is a semiconductor at 800-900°C, exhibits an excellent electronic-oxygen vacancy mixed conduction, at 800-900°C, therefore it can be used as cathode in SOFC. Concerning to  $\text{RuO}_2\text{-TiO}_2$ , they are materials with high electrocatalytic activity and it is used in chloride industry as dimensionally stable anodes, and also in CO and  $\text{CO}_2$  hydrogenation, they can be used in Fuel Cell at temperatures lower than 800°C. The system  $\text{ZrO}_2\text{-Y}_2\text{O}_3\text{-RuO}_2$ , where  $\text{RuO}_2$  can be or not in solid solution into zirconia matrix, could be employed as mixed conductor/matrix anode in SOFC, as well as catalyst in the Fischer-Tropsch mechanism.

Finally materials with 5 to 10 mol % of  $\text{TiO}_2$  in the system  $\text{ZrO}_2\text{-Y}_2\text{O}_3\text{-TiO}_2$ , are mixed conductors and they can be applied as air electrolyzers and also as matrix anode for SOFC. Further, all these materials are prepared by new synthesis methods either Sol-Gel Polymeric, Colloidal and also Combustion Synthesis, the features of these techniques for each materials are also detailed. Finally, the powders were characterize and the material electrochemical studies were discussed.

TOPIC B. CONFERENCE

## PREPARATION OF THIN FILM SOFCs WORKING AT REDUCED TEMPERATURE

P. Charpentier, P. Fragnaud, D.M. Schleich, Y. Denos\* and E. Gehain\*

Laboratoire Génie des Matériaux, ISITEM,

La Chantrerie, Rue Christian Pauc, BP 90604, F-44306 Nantes cedex 3, France

\* GAZ DE FRANCE, Direction de la Recherche,

361, Avenue du Président Wilson, BP 33, 93211 St Denis La Plaine, Cedex, France

Energy conversion using solid oxide fuel cells (SOFCs) is a highly efficient and an environmentally friendly technology. Pollutants such as NO<sub>x</sub>, carbon monoxide and hydrocarbons are reduced over power sources that rely on combustion. Recently, there has been substantial interest in the polymer electrolyte fuel cell (PEMFCs), especially as a power source for electric vehicles. This interest is directly related to the low operating temperature of such a cell. The Solid Oxide Fuel Cell (SOFC) has received less attention for electric vehicles, but has promise in the domain of cogeneration (heat and electricity).

In the conventional SOFC, the electrolyte is a ceramic oxide, normally Yttria Stabilized Zirconia (YSZ), with a thickness of about 200  $\mu\text{m}$ . This electrolyte is the mechanical support of the cell and is then contacted with an anode, often Ni-YSZ and a cathode, often La<sub>1-x</sub>Sr<sub>x</sub>MnO<sub>3</sub>. The classical SOFC functions at high temperature typically 1000°C, this high temperature allows for a good efficiency and high power density. However, one of the main problems to be overcome in such devices are the complex materials problems at these high temperatures. These problems are difficult to solve in a cost effective manner and have so far limited commercial development. Therefore it is desirable to drop the operating temperature of the cell from 1000°C to less than 800°C.

Nevertheless, with decreasing operating temperature, resistive losses across the electrolyte increase, overpotentials at electrodes are magnified and therefore the performance of the cell decreases. To overcome this problem, one can imagine two materials approaches: either preparing new improved materials or preparing conventional SOFC materials but reducing the component thickness, optimize electrodes and improve interfaces where the transfer of electrons and ions occurs. For the fabrication of the components of a SOFC working at intermediate temperature, there has been in recent years an enormous increase in the application of thin film technologies. The advantages of synthesizing the cell components by thin film processes are that in general lower temperatures are required than with sintering, that ohmic losses can be reduced, and that interfaces can be easily controlled. We will therefore approach the problem of a SOFC operating at reduced temperature by preparing a thin film electrolyte as well as a thin film cathode onto an anode substrate which supports the cell.

Ni/YSZ cermet anodes have been prepared by a conventional ceramic method, Thin Yttria Stabilized Zirconia electrolytes (YSZ) have been deposited by three methods: RF sputtering, DC sputtering and powder spraying onto the Ni/YSZ anode substrate. The La<sub>0.7</sub>Sr<sub>0.3</sub>MnO<sub>3</sub> (LSM) thin cathodes have been deposited onto the electrolytes by a spray-pyrolysis method. We have shown the feasibility of such thin SOFC cells and we present here the preparation, the characterization of each component and electrochemical performance at 850°C.

Not  
GivenTHE STRUCTURE OF  $(\text{La},\text{Sr})\text{CrO}_{3-\delta}$  AND  $(\text{La},\text{Ca})\text{CrO}_{3-\delta}$  FUEL CELL INTERCONNECT MATERIALS UNDER REDUCING CONDITIONS

*Geoff Staneff, Rob Woodman, Kwang Hyun Ryu, Ersan Üstündag and Sossina M. Haile*  
Materials Science 138-78, California Institute of Technology, Pasadena, CA, 91125

The "interconnect" in a stacked solid oxide fuel cell serves to isolate oxidizing and reducing atmospheres, and to transport electrical current. The materials of choice for this application are doped lanthanum chromites. While these oxides have a great many attractive features, such as chemical stability under the conditions of operation and high electronic conductivity, the oxygen partial pressure gradient to which they are exposed during fuel cell operation can induce mechanical failure. The oxygen partial pressure gradient induces an internal gradient in the concentration of oxygen vacancies, which in turn, leads to a gradient in internal strain and thus generates internal stress. It is these stresses which are, in part, responsible for the observed mechanical failures. In the present work, we have examined the structural changes that take place in Sr and Ca doped lanthanum chromites under reducing conditions as a first step towards understanding the mechanism of stress generation, which will ultimately enable the design of mechanically robust fuel cells.

Samples of composition  $\text{La}_{1-x}\text{Sr}_x\text{CrO}_{3-\delta}$ , where  $x = 0.10, 0.15$  and  $0.20$ , and  $\text{La}_{1-x}\text{Ca}_x\text{CrO}_{3-\delta}$ , where  $x = 0.10, 0.20$  and  $0.30$ , were prepared by solid state reaction. Powders were partially sintered to yield porous samples of 55-65% theoretical density. Reduction was carried at an oxygen partial pressure of  $10^{-16}$  atm ( $\text{CO}:\text{CO}_2 = 10:1$ ) and a temperature of  $1000^\circ\text{C}$ . The sample dimensions were monitored *in situ* using a controlled-atmosphere dilatometer during the course of the reduction to establish the time necessary to reach equilibration ( $\sim 12$  days). After the completion of the reduction step, samples were quenched to room temperature.

Structural characterization of these doped lanthanum chromite materials was carried out by time-of-flight (TOF) neutron diffraction. Data were collected with the general purpose powder diffractometer (GPPD) at the Intense Pulsed Spallation Source (IPNS), Argonne. Samples were examined both at room temperature, in the as-quenched state, and at  $1000^\circ\text{C}$  in a reducing atmosphere ( $\text{PO}_2 = 10^{-16}$  atm). The results of the room temperature data collection are shown in Figure 1. It is evident that there are subtle changes in symmetry with dopant type and concentration. The peak at  $d = 1.25 \text{ \AA}$ , for example, has a very different shape for the Sr and Cr doped samples, whereas a small peak at  $d = 2.25 \text{ \AA}$  is present for low dopant concentration samples and absent for those of higher concentration. Crystallographic parameters, based on Rietveld refinements utilizing these data, are presented and discussed.

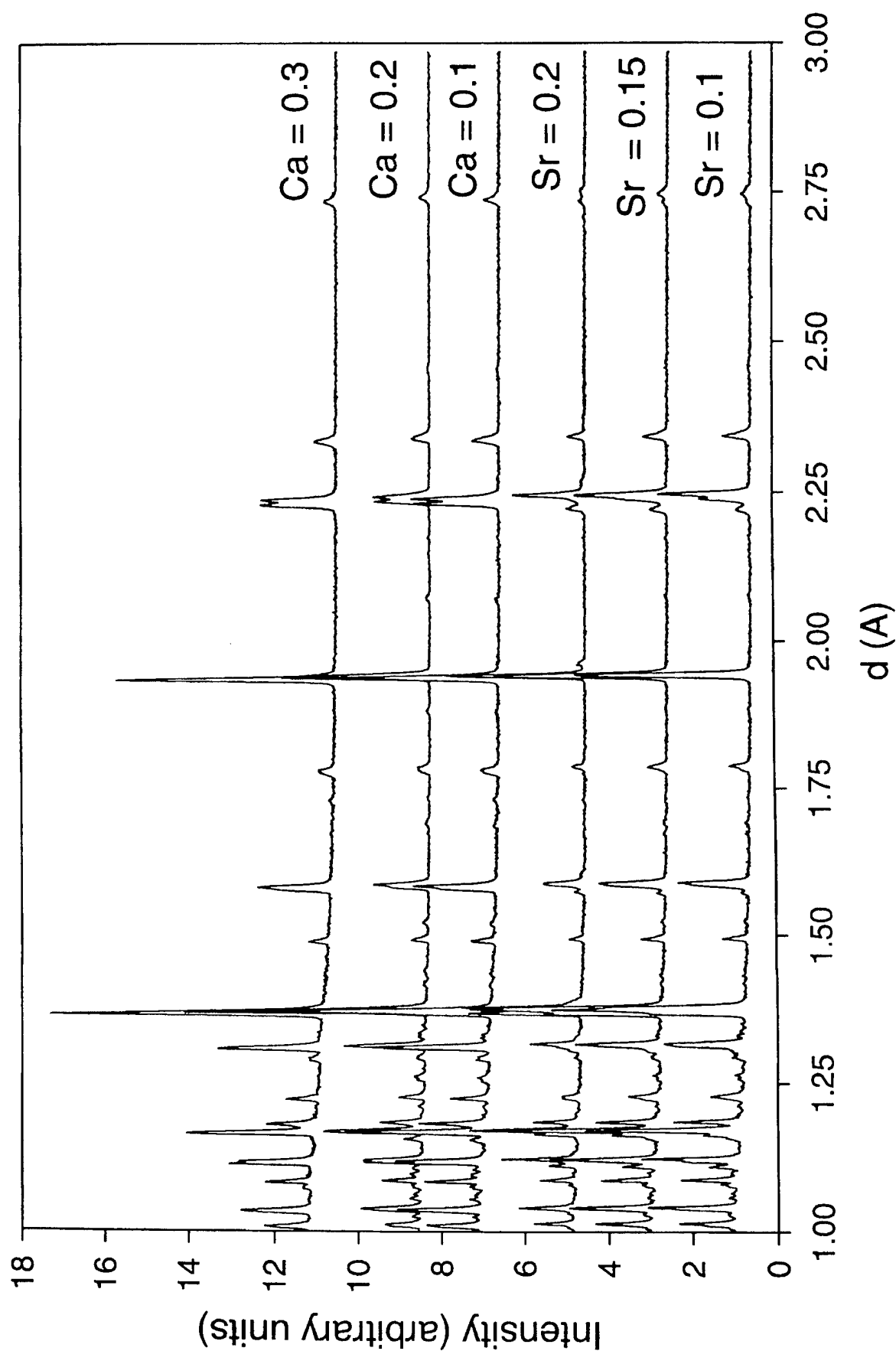


Figure 1. Neutron time-of-flight diffraction patterns of  $\text{La}_{1-x}\text{M}_x\text{CrO}_{3.6}$  obtained from as-quenched samples.

## ELECTRICAL CONDUCTIVITY AND MECHANICAL PROPERTIES OF ALUMINA-DISPERSED DOPED LANTHANUM GALLATES

Isamu Yasuda<sup>1</sup>, Yoshio Matsuzaki<sup>1</sup>, Takahiro Yamakawa<sup>2</sup> and Toshiyuki Koyama<sup>2</sup>

<sup>1</sup> Fundamental Technology Research Laboratory, Tokyo Gas Co., Ltd.

Shibaura, Minato-ku, Tokyo 105-0023, Japan

<sup>2</sup> Research and Development Center, Kiyosumi Laboratory, Taiheiyo Cement Corp.

Kiyosumi, Koutou-ku, Tokyo 135-8410, Japan

### INTRODUCTION

Doped lanthanum gallates (LaGaO<sub>3</sub>) showing oxide ion conductivity higher than the conventional stabilized zirconias have been considered as potential electrolyte materials of solid oxide fuel cells (SOFCs) for reduced temperature operation. The applicability of LaGaO<sub>3</sub>-based electrolytes has recently been discussed from various aspects including chemical stability and minor electronic conductivity. Mechanical properties, however, have only scarcely been reported, in spite of their high importance in view of practical applications as ceramic components. This study is aimed at increasing the mechanical strength of doped LaGaO<sub>3</sub> materials. The effects of alumina dispersion on microstructure, electrical conductivity, thermal expansion and bending strength are reported.

### EXPERIMENTAL

Combustion-synthesized powder of La<sub>0.9</sub>Sr<sub>0.1</sub>Ga<sub>0.8</sub>Mg<sub>0.2</sub>O<sub>2.85</sub> (Praxair Specialty Ceramics, Inc.; hereafter denoted as LSGM) was intimately mixed with commercial alumina powder, pressed, and sintered at 1400°C in air for 6 hours to obtain rectangular bar samples. The alumina addition was changed at 9 levels of weight ratio between 0 and 10 vs. 100 of LSGM. The thermal expansion coefficient was measured in air and 4% H<sub>2</sub>-N<sub>2</sub> with a differential thermal dilatometer using an alumina standard. The bending strength was measured by the standard 3-point bending tests at room temperature and 800°C in air. The electrical conductivity was measured by the *d.c.* 4-point technique at 600 to 1000°C in a stream of O<sub>2</sub>, O<sub>2</sub>/Ar or CO/CO<sub>2</sub>.

### RESULTS AND DISCUSSION

The list of the measured properties is given in Table I. At alumina additions of ≥ 2 wt%, the relative density of the sample was high enough (≥ 99%) to be used as solid electrolytes. There can be seen a trend for the thermal expansion coefficient (TEC) to decrease with increase of the alumina content. But, the change of TEC with alumina addition is small, which is favorable from the view point of TEC matching among the cell components. It is also found that the TECs in oxidizing and reducing atmospheres showed no distinct differences. This leads to the conclusion that doped LaGaO<sub>3</sub> with and without alumina addition are dimensionally stable against changes of oxygen partial pressure (*P*O<sub>2</sub>) in the atmosphere and can be used with no fears of deformations and internal stresses under a *P*O<sub>2</sub> gradient like the electrolyte of SOFC. The bending strength of the samples greatly increased with alumina additions, and it is to be noted that the degree of improvement of bending strength is greater at 800°C than at room temperature. The microstructure observations revealed that the average grain size greatly decreased by the alumina addition. The uniform dispersion of the added alumina preferably along grain boundaries was found to be effective



for retarding the grain growth of the perovskite phase and thereby increasing the bending strength.

The electrical conductivity measured in  $O_2$  at  $800^\circ C$  was found to decrease with the alumina content. With alumina additions of  $\geq 5$  wt%, the dispersed grains block the transport of oxide ions between the perovskite grains and lowered the electrical conductivity to unacceptable levels. There is no systematic trend for the variation of the activation energy with the alumina addition. In this way, the optimum alumina addition for increasing the bending strength without deleteriously affecting the thermal expansion coefficient and electrical conductivity has been determined as 2 wt%. Then, the  $PO_2$  dependence of electrical conductivity of the optimized composition (2 wt% of alumina addition) was measured at  $800^\circ C$  and compared with that of LSGM (without alumina addition). The results showed no  $PO_2$  dependence of electrical conductivity over a wide range of  $PO_2$  (from  $\log(PO_2/atm) = -22$  to 0) for the samples with and without alumina additions. This suggests that ionic conduction dominates in LSGM with and without alumina additions.

To confirm the possibility of using the optimized composite material (LSGM +2wt%  $Al_2O_3$ ) as the solid electrolyte, a single-cell was manufactured and tested at  $800^\circ C$ . (Pr,Sr) $MnO_3$  and Ni/YSZ both modified by (Ce,Sm) $O_2$  were used as the cathode and anode, respectively. The thickness of the tape-casted and sintered electrolyte was 0.2 mm, and the active electrode area was  $4\text{ cm}^2$ . The electrolyte sheet made of LSGM alone easily cracked during the electrode fabrication process due to its poor mechanical strength, while the composite electrolyte was strong enough to be fabricated into complete cells with high reproducibility. The single-cell thus fabricated showed an open circuit voltage of 1.05 V using 20%  $H_2O-H_2$  as the fuel and air as the oxidizer. This is very close to the theoretical Nernst potential, which also suggests that oxide-ionic conduction prevails over the wide  $PO_2$  range. The cell stably worked, giving a power density of  $0.177\text{ W/cm}^2$  at 0.7 V and the maximum power density of  $0.245\text{ W/cm}^2 (= 0.446\text{ V} \times 0.55\text{ A/cm}^2)$ . The cell performance is expected to improve by optimizing the composition and microstructure of the electrodes.

Table I. Tabulated summary of measured thermal expansion coefficient, bending strength and electrical conductivity of lanthanum gallates with 9 levels of alumina addition.

alumina addition [wt%]	relative density [%]	thermal expansion coefficient <sup>a)</sup> [ $10^{-6}K^{-1}$ ]		bending strength <sup>b)</sup> [MPa]		electrical conductivity ( $800^\circ C$ , in $O_2$ ) [ $Sm^{-1}$ ]	activation energy <sup>c)</sup> [kJ/mol]
		in air	in 4% $H_2-N_2$	at r.t.	at $800^\circ C$ (in air)		
0	96	10.4	10.4	120	80	10.2	73 (109)
0.5	88	10.1	10.0	130	90	6.11	87 (117)
1	89	10.3	10.0	170	110	7.96	78 (132)
2	99	10.6	10.5	255	190	8.80	66 (-)
3	99	10.2	10.1	210	185	4.28	81 (181)
4	100	10.4	10.2	220	174	3.44	69 (132)
5	100	9.9	9.8	270	240	0.15	81 (153)
7.5	100	11.4	11.1	300	200	0.08	89 (119)
10	99	9.9	9.7	210	240	0.05	94 (-)

a) Average linear thermal expansion coefficient between  $30$  and  $800^\circ C$

c) 3-point bending strength.

d) Values in the parentheses are for temperatures of lower than  $750^\circ C$ .

## VAPORIZATION PROCESS OF Ga FROM DOPED LaGaO<sub>3</sub> ELECTROLYTES UNDER REDUCING ATMOSPHERES

K. Yamaji, H. Negishi, T. Horita, N. Sakai and H. Yokokawa

National Institute of Materials and Chemical Research, Tsukuba, Ibaraki, Japan

As an electrolyte for Solid Oxide Fuel Cells, doped LaGaO<sub>3</sub> must be chemically stable under reducing atmosphere. At high temperatures, significant deficits of Ga have been measured on the surface of the samples. This result is originated from the high partial pressure of Ga oxides such as Ga<sub>2</sub>O. In this investigation, the effects of dopants are studied on the vaporization process of Ga in the doped-LaGaO<sub>3</sub> under a reducing atmosphere.

Several kinds of doped LaGaO<sub>3</sub> were polished, put onto the Al<sub>2</sub>O<sub>3</sub> plate and set in the tubular furnace. Annealing was made in Ar-H<sub>2</sub> gas with a flowing rate of 30 cc/min and humidified by bubbling in water at 283K. During cooling(5 K/min) after the annealing, dry Ar was flown. The amount of the Ga deficit from the surface was measured by SIMS(CAMECA, ims5f), and secondary phases formed on the annealed samples were identified by XRD.

Figure 1 shows the Ga depletion curves from the samples with different compositions which were annealed at 1173 K for 10 h in H<sub>2</sub>-1.2%H<sub>2</sub>O gas. In the figure,  $C_{Ga}/C_{Ga\_bulk}$  means that the concentration of Ga at each point was divided by the concentration of Ga at no deficient area. The addition of Sr to A-site accelerated the Ga depletion, but the addition of Mg to B-site did not. Figure 2 shows the diffusion coefficient of Ga ions which was calculated from the Ga depletion curves of LSGM9182 annealed at various temperature for 10 h in H<sub>2</sub>-1.2%H<sub>2</sub>O gas. The data at low temperatures were fitted well with the calculated curves, but the data at high temperatures are not fitted with the curves because of the formation of secondary phases on the surfaces. This result suggests that the rate of the Ga depletion in the primary stage is determined by the diffusion of Ga and the vaporization of Ga<sub>2</sub>O from the surface. With increasing the deficit of Ga, during annealing at high temperatures, secondary phases were formed on the surface of the samples so that it is difficult to clarify the rate-determining factor of the Ga depletion.

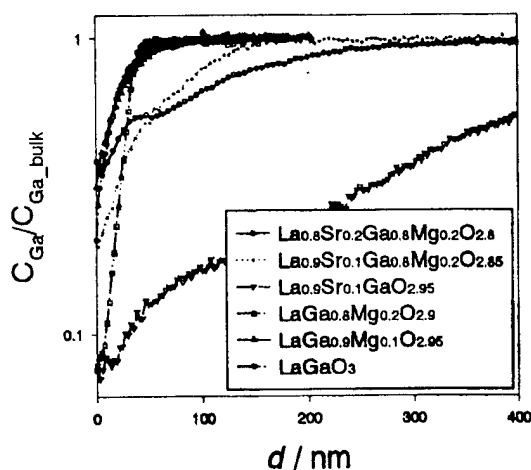


Fig. 1 Ga depletion curves of doped LaGaO<sub>3</sub>.

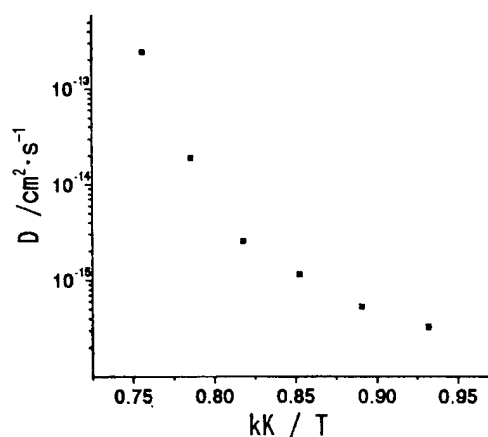


Fig. 2 Diffusion coefficient of Ga in LSGM9182.

## FABRICATION OF THIN FILMS OF $\text{La}_{1-x}\text{Sr}_x\text{Ga}_{1-y}\text{Mg}_y\text{O}_{3-(x+y)/2}$ BY PULSED LASER ABLATION.

Tom Mathews\*, P. Manoravi\*\*, M. P. Antony\*\*\*, J. R. Sellar\* and B. C. Muddle\*.

\*Department of Materials Engineering,  
Monash University, Clayton 3168, Victoria, Australia.  
Fax (+61) 3 9905 4940, E-mail: thomas.mathews@eng.monash.edu.au

\*\*Physicalisch-Chemisches Institut,  
University of Zurich, Irchel, Winterthurer Strasse, 190,  
Zurich, CH -8057, Switzerland.

\*\*\*Department of Materials,  
University of Leeds, Leeds, LS2 9JT, U. K.

Solid oxide fuel cells (SOFC) offer a clean pollution-free technology for the electrochemical generation of electricity at high efficiencies [1]. A typical SOFC utilises thin membranes of yttria stabilized zirconia (YSZ) as the solid electrolyte and operates near 1000° C. There is a need to reduce the operating temperature to ~600° C in order to widen the choice of materials, (such as the interconnect), for cell stacking, to increase the life time of the cells and to decrease the material, fabrication and operation costs. This can be achieved by using dense, pore-free thin films of materials having superior oxide ion conductivity to that of YSZ as the solid electrolyte. The most promising traditional materials are alkaline earth oxides, MO, doped  $\text{CeO}_2$  and  $\text{Y}_2\text{O}_3$  stabilized  $\text{Bi}_2\text{O}_3$ . But at the high temperatures and reducing atmospheres prevailing at the anode these materials undergo large departures from stoichiometry due to reduction, giving rise to electronic conduction [2 - 4]. However, a new oxide ion conductor with superior properties,  $\text{La}_{1-x}\text{Sr}_x\text{Ga}_{1-y}\text{Mg}_y\text{O}_{3-(x+y)/2}$  (LSGM), has been identified recently [5, 6]. It has a high ionic conductivity of ~0.1 S/cm, at 800° C (comparable to that of YSZ at 1000° C) and negligible electronic conduction at temperatures  $T < 1000^\circ \text{C}$  over a wide range of oxygen partial pressures ( $P_{\text{O}_2} = 1 \text{ atm. to } P_{\text{O}_2} \sim 10^{-22} \text{ atm}$ ) [5-9]. Thus in principle an SOFC based on LSGM can be operated at 800° C. Operation at a still lower temperature (~600° C) can be achieved by using thin films of LSGM. In this paper we report studies on the fabrication of LSGM thin films of various compositions using pulsed laser ablation technique.  $\text{La}_{1-x}\text{Sr}_x\text{Ga}_{1-y}\text{Mg}_y\text{O}_{3-(x+y)/2}$  corresponding to the various dopant concentrations ( $0.1 \leq x \leq 0.2$ ,  $0.1 \leq y \leq 0.2$ ) were prepared by urea/metal nitrate solution combustion synthesis. X-ray diffraction patterns indicate a primitive cubic phase for each composition prepared. High density pellets (97%) were obtained by sintering at 1500° C for 5 h. LSGM thin films of the various compositions were fabricated using pulsed laser ablation technique. A Q-switched Nd:YAG laser (M/s Continuum Model NY/61, USA) operating at 532 nm, having a pulse width of 8 nsec (FWHM) with a typical pulse energy of 80 mJ was used as the laser source. Thin films were grown on quartz substrates under high vacuum ( $10^{-7}$  torr) and 200 mtorr of background oxygen pressure. The as-deposited films upon x-ray diffraction (XRD) analysis were found to be amorphous in nature. The films deposited under high vacuum on annealing in air at 700° C for 4 h gave cubic single phase material whereas the films grown under 200 mtorr of oxygen pressure up on annealing under same conditions gave multi-phase structure. The surface morphology of the films were examined using scanning electron microscopy. Particulate deposition was observed on the film surface. The in-situ laser ablation plume composition was analyzed using a laser induced vaporization quadrupole mass spectrometry facility. The major species found in the laser vaporized plume are  $\text{O}^+$ ,  $\text{O}$ ,  $\text{Ga}^+$ ,  $\text{Ga}$  and  $\text{La}^+$ . The velocity of the various ionic species were of the order of  $3 \times 10^5 \text{ cm/sec}$  and the neutral species have velocity in the range  $2.5 \times 10^4$  to  $5 \times 10^4 \text{ cm/sec}$ . The thermal expansion coefficient (TEC) of

the LSGM material was determined using high temperature XRD analysis. The TEC value obtained is higher than that of YSZ.

### References

- [1] N. Q. Minh, J. Am. Ceram. Soc., **76**, 245 (1987)
- [2] H. L. Tuller and A. W. Nowick, J. Electrochem. Soc., **122**, 255 (1975).
- [3] M. Godickemeier, K. Sasaki, L. I. Gauckler and I. Riess, J. Electrochem. Soc., **144**, 1635 (1997).
- [4] P. Shuk, H.-D. Wiemhofer, U. Guth, W. Gopel and M. Greenblatt, Solid State Ionics, **89**, 179 (1996)
- [5] M. Feng and J. B. Goodenough, Eur. J. Solid State Inorg. Chem., **T31**, 663 (1994).
- [6] T. Ishihara, H. Matsuda and Y. Takida, J. Am. Chem. Soc., **116**, 3801 (1994).
- [7] K. Huang, M. Feng and J. B. Goodenough, J. Am. Ceram. Soc., **79**, 1100 (1996).
- [8] P. Huang and A. Petric, J. Electrochem. Soc., **143**, 1644 (1996).
- [9] K. Huang, M. Feng, J. B. Goodenough and M. Schmerling, J. Electrochem. Soc., **143**, 3630 (1996).

## CONDUCTIVITY AND DEFECT STRUCTURE OF $\text{ZrO}_2\text{-CeO}_2\text{-Y}_2\text{O}_3\text{-Gd}_2\text{O}_3$ SOLID SOLUTIONS

A. Tsoga\*, A. Naoumidis, D. Stöver

Institute for Materials and Processing in Energy Systems, IWV1, Research Center Jülich

\*TMR Grant Holder

### ABSTRACT

Lowering the operating temperature of SOFCs below 1000°C is of great interest for allowing the use of lower cost materials, reducing stack thermal insulation requirements and increasing cell long term stability as a result of reduced thermal degradation and thermal cycling stress. In order intermediate temperature operating SOFCs to be technically feasible two significant parameters should be addressed. The minimization of the resistance of the electrolyte and the increase of the catalytic activity of the electrodes. These require a  $\approx 10\mu\text{m}$  thick state-of-the-art yttria-stabilized-zirconia-electrolyte (YSZ) and Co-containing perovskites for the cathodic side, which however have shown to exhibit chemical compatibility problems towards YSZ [1]. Since ceria based materials have proven to be the only compatible materials towards Co-containing perovskites [2], the possibility of using a gadolinia-doped-ceria (CGO) protective layer between electrolyte and cathode electrode was suggested and studied in a previous work [3].

As was found however the chemical compatibility of YSZ with CGO is not without problems, since the two materials diffuse to each other during sintering process, already at temperatures of 1200°C. The formed YSZ-CGO solid solutions exhibit lower ion conductivity by about two orders of magnitude than YSZ itself. Additionally, defects in microstructure, observed in the Ce-rich region, resulting from the differences in diffusivity of the counter diffusing cations (Kirkendahl effect), negatively influence the performance of the electrolyte. In order to avoid extended interdiffusion at the YSZ/CGO interface the incorporation of a  $\text{CGO}_{0.5}\text{YSZ}_{0.5}$  solid solution interlayer was tested, to act as a diffusion barrier. Although it was found to succeed in reducing the diffusion rates of the counter-diffusing cations, its application is still problematic, due to the lower conductivity, by one order of magnitude, than that of YSZ.

With objective to optimize the composition of the interlayer to be used towards obtaining a material with better conductivity and keeping the cation diffusion rates between YSZ and CGO low, a study was carried out in order to clarify the influence of the composition to the conductivity of the material. As a first step of the approach different compositions of the system  $\text{CGO}_x\text{YSZ}_{1-x}$  were selected, prepared and characterized with objective to correlate their crystal and defect structure to their transport properties. Total conductivity measurements performed in air showed that with progressive substitution of CGO for YSZ the ionic conductivity decreases, reaching a minimum at about the composition of  $\text{CGO}_{0.5}\text{YSZ}_{0.5}$  and then increasing again to reach the ionic conductivity of CGO for complete substitution of CGO for YSZ. Under measurement conditions the contribution of the electrical conductivity is negligible, and therefore the conduction results by the migration of oxygen ions through the channels formed by the neighboring cations under the influence of an applied field. Considering this, the variation of the conductivity is discussed relating to the concentration of the oxygen vacancies presenting as well as with the change in the free channel radius through which an oxygen anion can move as a result of the change in lattice parameter and in average cation radius. Both of the above mentioned parameters fail however to explain the experimentally observed variation of the conductivity suggesting that mobility and scattering of the oxygen vacancies should be affected to a significantly greater extend so as to offset the effect of the increase in oxygen vacancy concentration and free channel radius. Based on the compositions studied as well as on literature data concerning different compositions of the system  $\text{ZrO}_2\text{-CeO}_2\text{-Y}_2\text{O}_3\text{-Gd}_2\text{O}_3$  it was confirmed

that the extend of the oxygen vacancy scattering reaches a maximum when Zr and Ce are present in equimolar quantities, due to a significant distortion of the lattice. In order to clarify the influence of the presenting trivalent cations on the transport properties of the material further experiments were performed, keeping constant the Ce/Zr atomic ratio and varying the concentration and the nature of the trivalent cations. The results obtained are discussed on the basis of what type of an interlayer between YSZ and CGO can be used and under what conditions, so that a double layer YSZ-CGO electrolyte to be technically feasible.

#### REFERENCES

1. E.Syskakis, G.Stochniol, A.Naoumidis and H.Nickel, in Proc. of the 2<sup>nd</sup> Intern. Conf. on "Ceramics in Energy Applications", ed. by The Institute of Energy, Pergamon Elsevier Science, London U.K. (1996), pp.91.
2. B.C.H.Steele, K.Zheng, R.A.Rudkin, N.Kiriazis and M.Christie, in Proc. of the "Fourth International Symposium on Solid Oxide Fuel Cells", ed. by M.Dokiya, O.Yamamoto, H.Tagawa and S.C.Singhal, The Electrochemical Soc., Yokohama-Japan (1995), pp.1028.
3. A.Tsoga, A.Gupta, A.Naoumidis, D.Skarmoutsos and P.Nikolopoulos, Ionics 1999 (to be published).

Proposed Scientific Session: B. Solid State Fuel Cells

AN IMPEDANCE STUDY OF HYDROGEN OXIDATION ON A  
GADOLINIA-DOPED CERIA ANODE

Olga A. Marina, Søren Primdahl and Mogens Mogensen

Risø National Laboratory, Materials Research Department,  
P.O. Box 49, 4000 Roskilde, Denmark

The ceria-based anode is an appealing alternative to the conventional Ni-YSZ cermet anode in a high-temperature solid oxide fuel cell (SOFC) [1-3]. First of all, the doped ceria anode has been demonstrated to survive oxidation-reduction cycles at 1000°C [3], where nickel-based anodes fail [4]. Secondly, to obtain controlled internal reforming of methane or natural gas, an anode with little or no catalytic activity towards methane conversion can be applied in combination with an adjusted amount of reforming catalyst. In the case of Ni-YSZ cermet anodes, total conversion of methane may occur over the first few millimetres of the anode length resulting in thermal stress capable of damaging stack components [5].

40 mole % gadolinia-doped ceria,  $\text{Ce}_{0.6}\text{Gd}_{0.4}\text{O}_{1.8}$  (CG4), has been considered as a promising anode material for the SOFC [1-3]. Preliminary results revealed an excellent electrochemical activity of the CG4 anode for hydrogen oxidation. An area specific polarisation resistance of  $0.4 \Omega\text{cm}^2$  was measured at 1000°C in moist hydrogen atmosphere ( $P_{\text{H}_2}=97 \text{ kPa}$ ,  $P_{\text{H}_2\text{O}}=3 \text{ kPa}$ ) [2]. This value has later been realised to include mass transport restrictions outside the anode [6]. Single SOFCs comprising the CG4 anode, a composite  $\text{La}_{0.85}\text{Sr}_{0.15}\text{Mn}_{1.1}\text{O}_3$  cathode and an yttria-stabilised zirconia (YSZ) electrolyte generated a power density of  $700 \text{ mW/cm}^2$  at 1000°C in  $45\%\text{H}_2+1.2\%\text{H}_2\text{O}$  vs. air [3]. An area specific internal cell resistance of  $0.39 \Omega\text{cm}^2$  was obtained.

In the present work hydrogen oxidation on the  $\text{Ce}_{0.6}\text{Gd}_{0.4}\text{O}_{1.8}$  electrode deposited on a YSZ electrolyte is reported. The thickness of the porous ceria layer was 15-18  $\mu\text{m}$ , the geometric area was  $0.44 \text{ cm}^2$ . Experiments were performed at atmospheric pressure in the temperature range 700-1015°C. The partial pressure of hydrogen was varied in the range 1-97 kPa. The partial pressure of water was varied from 3 to 25 kPa.

Complex impedance spectra were obtained in  $\text{H}_2/\text{H}_2\text{O}$  atmospheres while altering the temperature, hydrogen and water partial pressures, the gas flow rate and applied potential. All impedance spectra obtained contained three arcs and were fitted using the equivalent circuit  $\text{LR}_s(\text{RQ})_1(\text{RQ})_2(\text{RC})_3$ , where annotations 1, 2 and 3 are assigned to the respective processes by increasing time constant. The low frequency semicircle with a summit close to 1 Hz was described by two parameters, a resistor R and a capacitance C in parallel, and attributed to the gas conversion above the electrode according to ref. [6]. Medium frequency and high frequency semicircles were described by a resistor and a constant-phase element Q with a frequency power of 0.75 and 0.5, respectively. The summits and radius of both arcs were dependent on temperature and applied potential. Decreasing temperature from 1000°C or increasing applied potential shifted summits of medium frequency and high frequency semicircles from 20 Hz and

10 kHz, respectively, to the lower frequency range. The medium frequency part of the spectrum was ascribed to gas diffusion in a stagnant gas layer of finite thickness over the anode [7]. The high frequency semicircle was attributed to chemical or physical limitations in the anode.

After correction for gas conversion, an actual polarisation resistance of the CG4 electrode of  $0.085 \Omega\text{cm}^2$  was measured at  $1000^\circ\text{C}$  at  $P_{\text{H}_2} = 97 \text{ kPa}$ . The polarisation resistance was stable while decreasing  $P_{\text{H}_2}$  from 97 to 5 kPa under the open-circuit conditions and increased with increasing the partial pressure of water. At very low partial pressure of hydrogen in the fuel gas ( $P_{\text{H}_2} < 5 \text{ kPa}$ ) the polarisation resistance increased linearly with decreasing hydrogen partial pressure. This was suggested to be due to a partial loss of the electronic conductivity in CG4 at higher oxygen partial pressures. The effect of the applied potential on the polarisation resistance is discussed as well.

## References

- [1] M. Mogensen, B. Kindl and B. Malmgren-Hansen, in: Program and Abstracts of Fuel Cell Seminar/1990, p.195, Phoenix, AZ (1990).
- [2] O.A. Marina, S. Primdahl, C. Bagger and M. Mogensen, in Proc. of the 5<sup>th</sup> Int. SOFC Symp. (U. Stimming et al, Eds.), PV 97-40, p. 540. The Electrochemical Society, (1997).
- [3] O.A. Marina, C. Bagger, S. Primdahl and M. Mogensen, in Proc. of the 3<sup>rd</sup> Europ. SOFC Forum, 1998 (P. Stevenson, Ed.), p. 427. Nantes, France (1998).
- [4] M. Mori, T. Yamamoto, H. Itoh, H. Inaba and H. Tagawa, J. Electrochem. Soc., **145**, 1374 (1998).
- [5] P.V. Hendriksen, in Proc. of the 5<sup>th</sup> Int. SOFC Symp. (U. Stimming et al, Eds.), PV 97-40, p. 1319. The Electrochemical Society, (1997).
- [6] S. Primdahl and M. Mogensen, J. Electrochem. Soc., **145**, 2431 (1998).
- [7] S. Primdahl and M. Mogensen, submitted to J. Electrochem. Soc., (1998).



## OBSERVATION OF DIFFUSE ELECTRON SCATTERING IN Sr- AND Mg- DOPED LaGaO<sub>3</sub>

Tom Mathews and J. R. Sellar.

Department of Materials Engineering,  
Monash University, Clayton 3168, Victoria, Australia.  
Fax (+61) 3 9905 4940, E-mail: thomas.mathews@eng.monash.edu.au

The recent appearance of the perovskite-based oxygen ion conducting alloy system La<sub>1-x</sub>Sr<sub>x</sub>Ga<sub>1-y</sub>Mg<sub>y</sub>O<sub>3-(x+y)/2</sub> (LSGM) signals the possibility of an SOFC solid electrolyte with conductivity higher than yttria stabilized zirconia (YSZ), allowing the operation of fuel cells at temperatures perhaps 200° C lower than those currently envisaged. Such a temperature reduction would relax considerably the materials requirements for SOFC construction, especially those for the interconnect [1].

Although the properties of LSGM resemble those of a mechanically softer stabilised zirconia [2,3], a great deal less is known about the correlations between its structure and performance. There are various reports of LSGM possessing several phases in the range ( $x \leq 0.2$ ,  $y \leq 0.2$ ) and these appear to depend upon the preparation pathway. Large-scale twinning and wide intensity variation in symmetry-related x-ray reflections have been reported [4]. Similarly, superlattices attributable to oxygen lattice ordering have been observed[5].

La<sub>1-x</sub>Sr<sub>x</sub>Ga<sub>1-y</sub>Mg<sub>y</sub>O<sub>3-(x+y)/2</sub> samples of various compositions were prepared using the "nitrate-urea" solution combustion synthesis technique. In this technique appropriate amounts of metal nitrates of constituent cations were dissolved in distilled water. To this solution urea was added (as complexant and fuel). The amount of urea added was that required to completely consume the excess oxygen in the nitrate precursors and is called the stoichiometric amount. The nitrate-urea solution was saturated by slow evaporation on a hot plate. The saturated solution was then introduced into an open muffle furnace maintained at 500° C. At this temperature water is removed from the solution resulting in gel formation and its instantaneous combustion. The resulting fine powder was calcined at 1000° C for 2 h to burn off residual organic materials. The calcined powder was then pelletised and sintered at 1500° C for 5 h in air. The sintered pellets were pulverized to fine powder and characterized using x-ray diffraction.

To the best of our knowledge there have been no studies yet reported explicitly describing diffuse scatter from LSGM alloys. In the present paper, we report the observation of several different kinds of diffuse electron scatter from alloys in the composition range ( $x, y \leq 0.2$ ) prepared by the "nitrate-urea" solution combustion method described above, which should permit excellent cation mixing. Since the YSZ ionic conductors display strong diffuse scatter, it is not surprising that alloys in the ion-conducting range of the LSGM system should display diffuse scatter as well.

### References

- [1] M. Feng and J. B. Goodenough, *Eur. J. Solid State Inorg. Chem.*, **T31**, 663 (1994).
- [2] J. Drennan, V. Zelizko, D. Hay, F. T. Ciacchi, S. Rajendran and S. P. S. Badwal, *J. Mater. Chem.*, **7**, 79 (1997).
- [3] N. Sammes, F. M. Keppeler, H. Nafe, K. Aldinger and G. A. Tompsett, *J. Aust. Ceram. Soc.*, **34**, 99 (1998).
- [4] M. Sundberg, P. E. Werner, M. Westdahl and K. Mazur, *Mat. Sci. Forum*, **166-169**, 795 (1994).
- [5] K. Huang, R. S. Tichy and J. B. Goodenough, *J. Am. Ceram. Soc.*, **81**, 2565 (1998).

ELECTRODE POLARISATION OF  $\text{Sr}_{1-x}\text{Ti}_{1-y}\text{Nb}_y\text{O}_3$  MATERIALS ON YTTRIA STABILISED ZIRCONIA BASED SOFC CELLSA.A.L. Ferreira<sup>(1)</sup>, J.C.C. Abrantes<sup>(1)</sup>, J.A. Labrincha<sup>(2)</sup>, J.R. Frade<sup>(2)</sup><sup>1</sup>ESTG, Polytechnic Institute of Viana do Castelo, Apt. 574, 4900 Viana do Castelo, Portugal<sup>2</sup>Dept. of Ceramics and Glass Engineering, UIMC, University of Aveiro, 3810 Aveiro, Portugal

The continuous research on solid oxide fuel cells (SOFCs) field was recently concentrated in two main topics concerning the decrease of working temperature (600-800°C) and the use of natural gas as fuel. By this reason, the search of new components was found again necessary, in order to keep or increase the overall cell performance at lower temperatures. As electrolyte, ceria-based materials (e.g., gadolinia-doped ceria - GCO) were suggested, due to their higher electrical conductivity when compared with the standard yttria stabilised zirconia (YSZ). However, the electrolytic domain of the ceria-based compositions is narrow and its chemical stability is poorer. The search of new anode materials for direct methane conversion is also required.

The study of  $\text{SrTiO}_3$ -based compositions for high temperature applications revealed some interesting characteristics [1,2] that suggested their use as potential candidate as electrode materials for SOFCs: (i) easy change of transport properties by choosing the appropriated dopant for A (e.g., La) or B (e.g., Nb or Fe) sites of the perovskite structure; (ii) thermal expansion compatibility with YSZ and GCO; (iii) reasonable high electrical conductivity values in reducing or oxidising conditions depending on suitable donor/acceptor additions.

Nb for Ti substitution promotes an increasing n-type conductivity (-1/4 power dependence of oxygen partial pressure on Figure 1), and suggests the use of these materials in reducing atmospheres (as anodes). However, the response time of Nb-doped materials was found very high (several hours) when using well densified samples, but is less than 1 minute for porous samples as found in the case of electrodes.

In the present work, screen-printing was used to deposit  $\text{Sr}_{1-x}\text{Ti}_{1-y}\text{Nb}_y\text{O}_{3\pm\delta}$  ( $x \leq 0.05$ ,  $y \leq 0.1$ ) films onto YSZ pellets. The slight A-deficiency (samples D) was used to increase the chemical stability, and as an attempt to improve the ionic conductivity of the samples. The reactivity between the anode and electrolyte materials was evaluated by XRD, by preparing powder mixtures (1:1 %wt) which were pressed and then fired at high temperatures. The electrode behaviour was evaluated in reducing atmospheres to ensure that the electrical conductivity remains relatively high and to simulate real anodic operation conditions. Impedance spectroscopy was used to study the effects of different electrode deposition/firing conditions. Variable dc bias was applied to simulate the effects of increasing current densities, and to revert from anodic to cathodic polarisation.

The reactivity was found irrelevant, without signs of products formation at 1500°C. However, a slight change on lattice parameters suggests some ionic diffusion to and from the electrolyte. The anodic performance is very poor, when compared with Pt (Figure 2). This behaviour might be due to the relatively low electrical conductivity values and/or to the expected slow ionic mobility of the material.

Changes on similar compositional electrodes fired at different temperatures suggest a relevant effect of the preparation/working conditions on the final performance of the material, due to the preponderant role of the grain boundaries. This points out for the need of a careful control of the processing/operation conditions.

[1] J.C.C. Abrantes, J.A. Labrincha, J.R. Frade, *Ionics*, 3, 16-22, (1997).[2] J.C.C. Abrantes, J.A. Labrincha, J.R. Frade, *Sensors and Actuators B*, (accepted).

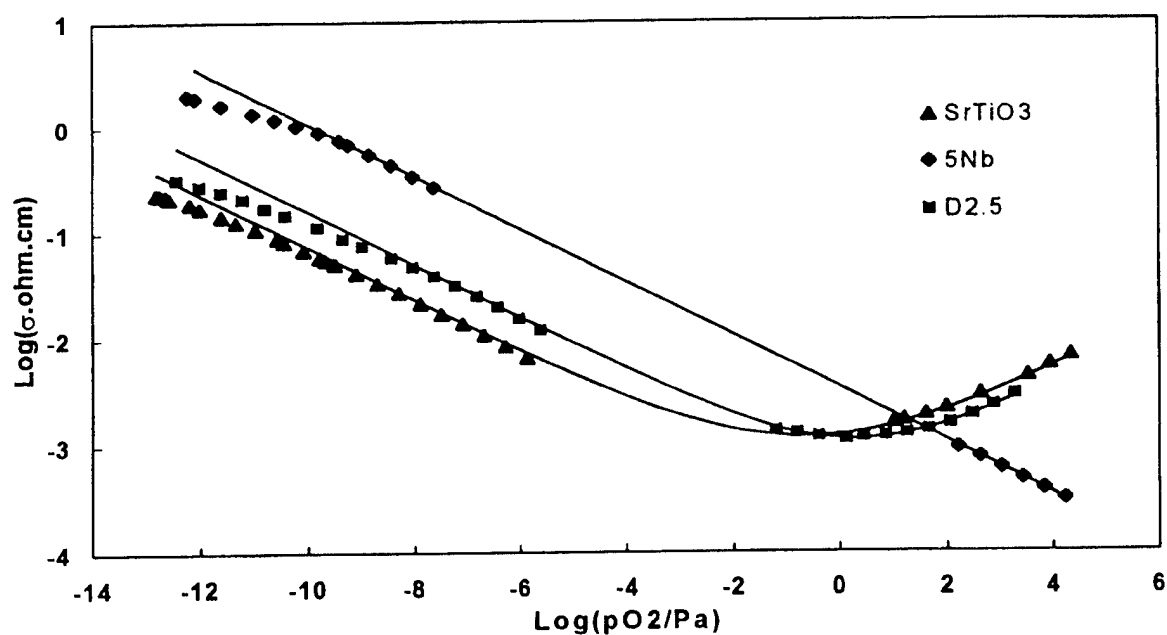


Figure 1 – Dependence of the electrical conductivity on the oxygen partial pressure, measured at 1000°C, for 5%Nb-doped (porous), stoichiometric, and Sr-deficient ( $x=0.025$ ) samples.

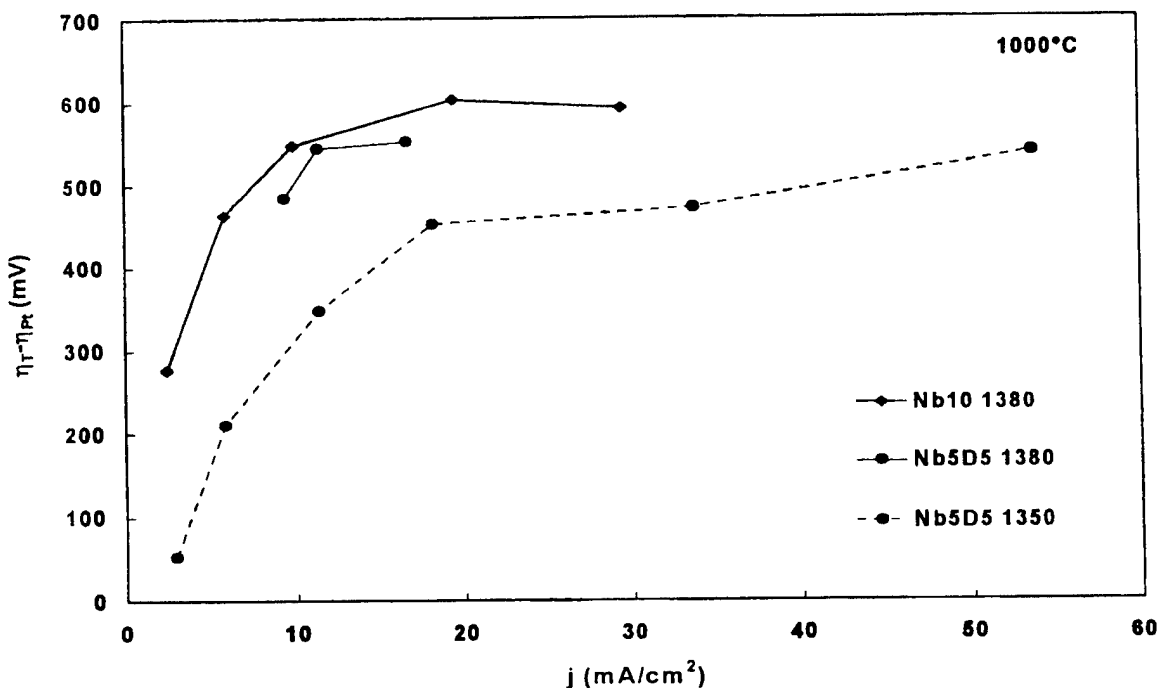


Figure 2 – Total overpotential (corrected from Pt measured values) as a function of the current density measured at 1000°C for  $\text{Sr}_{1-x}\text{Ti}_{1-y}\text{Nb}_y\text{O}_{3\pm\delta}$  electrodes fired at different temperatures.

## WATER UPTAKE IN H<sup>+</sup>-Na<sup>+</sup> MIXED CONDUCTING NAFION<sup>®</sup> 117 MEMBRANES

Shizhong Wang, Atsushi Kaimai, Ken-ichi Kawamura, Yutaka Nigara, Tatsuya Kawada,  
and Junichiro Mizusaki

Research Institute for Scientific Measurements, Tohoku University, 2-1-1 Katahira,  
Sendai 980-8577, Japan

### Introduction

Polymer electrolyte membrane fuel cells have attracted more attention during the last ten years due to their merits of high efficiency, low pollution and low cost for maintenance. They are being considered as a candidate for stationery as well as transportation application. [1-3]

Water uptake in Nafion membranes has been researched extensively for its close relationship with cell performance. At least two kinds of water have been identified. One is proton-bonded water, and another is the free water for wetting Nafion matrix. Yet there were no further reports on the two kinds of water, i.e., their amounts, their adsorption mechanism, and their function. Up to present time, the dependency of water uptake on relative humidity is still described with an experimental third order polynomial equation. [3]

In this paper, we prepared five H<sup>+</sup>-Na<sup>+</sup> mixed conducting Nafion membranes through ion exchange method, and measured the water uptake from water vapor and liquid water, through which we try to obtain further view on water uptake in Nafion membranes.

### Experimental:

The commercial Nafion<sup>®</sup> 117 membrane from Du Pont Nemours and Company was pretreated in the method described by Hinatsu [3], after which the counter ions in membrane were protons. The pretreated membranes were then immersed in some NaCl solutions at room temperature for 24 hours, and followed by rinsing in boiling deionized water repeatedly. The amount of protons in various membranes was measured by titration [3], and the relative concentration of protons was defined as:

$$C_H = [H^+] / ([H^+] + [Na^+]) \quad (1)$$

where  $C_H$  represents the relative concentration of protons,  $[H^+]$  stands for the amount of protons and  $[Na^+]$  for the amount of sodium ions.

Water uptakes from water vapor were measured at 326 K within the relative humidity range of 0.22-1.0. Relative humidity was adjusted through controlling the temperature of the bubbling bottle embedded in a thermostatic bath. High purity nitrogen was used as the bubbling gas. The samples were weighed in a weighing bottle immediately after removing it from the feeding system. Water uptake from liquid water was measured within the temperature range of 318 – 338 K. Samples were weighed immediately after the surface water was blotted with a filter paper.

Dry weights of Nafion membranes were determined by drying the samples in a vacuum oven at room temperature for 24 hours followed by 105 °C for 2 h.

### Results and discussion

The dependency of water uptake on the relative concentration of protons under various relative humidity is shown in Fig.1, from which an almost linear increase of water uptake with increasing proton concentration is observed. The lines in Fig.1 can be fitted with a first order polynomial equation (Eq.(2)), where  $V_0$  and  $P$  are constants.

$$\text{Water uptake} = V_0 + P * C_H \quad (2)$$

Equation (2) demonstrates that there are at least two kinds of water in Nafion membranes, one

of which is determined by proton concentration, while the other kind is less sensitive to proton concentration than the first one.

Parameter P in Eq.(2) corresponds to the difference between the amount of water adsorbed on per proton and sodium ion. Since this kind of water showed strong dependency on counter ions, it should be the proton-bonded water as defined by other authors. [4] It can be estimated from Fig.1, that the proton-bonded water is about 2-3 mol H<sub>2</sub>O/mol SO<sub>3</sub>.

V<sub>0</sub> represents the water that is not sensitive to the species of counter ions. It corresponds to the free water for wetting membranes, which is assumed to stay around the membrane matrix.

The different dependency of free water and proton-bonded water on relative humidity is due to their adsorption mechanisms.

Water can adsorb on protons strongly through H-bond. The maximum number of H-bonded water for each proton is about four, two presenting their negative ends and two presenting their positive ends to the proton. [6] The equilibrium constant for the adsorption of each water molecule decreases dramatically with increasing adsorbed water due to the steric as well as electrostatic effect, which determines that the proton-bonded water can only be adsorbed step by step. Applying this assumption, it is easy to understand the result that the first two to three water molecules can adsorb on protons easily, while the further increase of proton-bonded water is very slow.

Free water in Nafion locates on Nafion matrix, and water can be further adsorbed on vacant sites as well as water-covered sites. The adsorption of water on water covered sites is easier than that on vacant sites due to the hydrophobic character of Nafion matrix. Assuming that water adsorbed on water-covered sites can easily transfer to the vacant sites, and water exists only in the state of single layer [2], the dependency of free water on relative humidity can be expressed with equation (3), which agrees well with our experimental results.

$$W = P_1 \times \alpha_{H_2O} / (1 - P_2 \times \alpha_{H_2O}) \quad (3)$$

Here, W denotes the amount of free water, P<sub>1</sub> and P<sub>2</sub> are constants related to the adsorption and desorption rate constants,  $\alpha_{H_2O}$  represents the activity of water vapor, i.e., relative humidity.

Free water adsorbed from liquid water increases with increasing temperatures, while the proton-bonded water decreases instead (Fig.2), which agrees with the results of Rieke. [4]

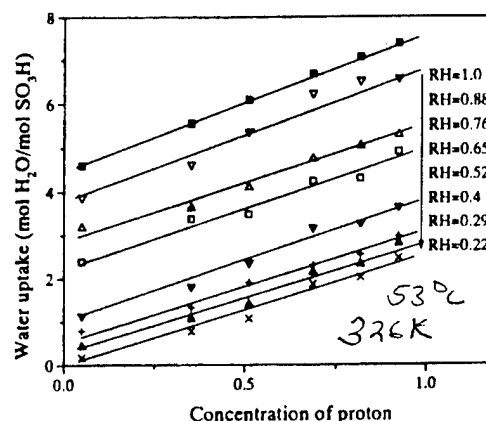


Fig.1. Dependency of water uptake on the relative concentration of protons in various H<sup>+</sup>-Na<sup>+</sup> membranes.

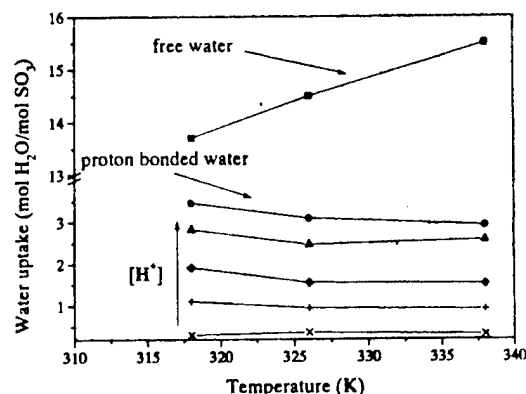


Fig.2. Dependency of free water and proton bonded water on temperature for samples immersed in liquid water

## References

1. T. R. Ralph, Platinum Metals Rev., 41(3), 102 (1997)
2. T. D. Gierke, G. E. Munn, F. C. Wilson, J. Polymer Science, 19, 1687 (1981)
3. J. T. Hinatsu, M. Mizuhata, H. Takenaka, J. Electrochem. Soc., 141, 1493 (1994)
4. M. Falk, Can. J. Chem., 58, 1495 (1980)
5. P. C. Rieke, N. E. Vanderborgh, J. Membrane Science, 32, 313 (1987)
6. C. W. Davies, Electrochemistry, Philosophical Library Inc., 1967, P48

## CONDUCTIVITY OF H<sup>+</sup>-Na<sup>+</sup> MIXED CONDUCTING NAFION<sup>®</sup> 117 MEMBRANES

Shizhong Wang, Atsushi Kaimai, Ken-ichi Kawamura, Yutaka Nigara, Tatsuya Kawada,  
and Junichiro Mizusaki

Research Institute for Scientific Measurements, Tohoku University, 2-1-1 Katahira,  
Sendai 980-8577, Japan

### Introduction

Polymer electrolyte membrane fuel cells (PEMFC) are efficient and environmental clean electrical generators, which are being developed for transportation as well as stationary applications. [1]

PEMFC employed perfluoro-sulfonate ionomers such as Nafion as electrolyte, the property of which depended strongly on water uptake and temperature. [2-4] Proper hydration of ionomers was critical for cell performance. Though some general characteristics of the conductivity of Nafion membrane have been unveiled recently, there is still not much knowledge on the special property of the migration of protons in Nafion, which might afford guidelines for the further design of new membranes.

We have reported our results on the water uptake in H<sup>+</sup>-Na<sup>+</sup> mixed conducting Nafion membranes. [5] In this paper, we investigated the conductivity of above membranes in water vapor as well as liquid water, through which we try to obtain some further view on the properties of Nafion membranes.

### Experimental

The commercial Nafion<sup>®</sup> 117 membrane from Du Pont Nemours and Company was pretreated in the conventional method described by Hinatsu, after which the counter ions in membranes were protons. [4] H<sup>+</sup>-Na<sup>+</sup> mixed conducting membranes were prepared with the method of ion exchange. [5] The amount of protons in various membranes was measured by titration [4], and the relative concentration of protons was defined as:

$$C_H = [H^+] / ([H^+] + [Na^+]) \quad (1)$$

where  $C_H$  represents the relative concentration of protons,  $[H^+]$  stands for the amount of protons and  $[Na^+]$  for the amount of sodium ions.

The conductivity of various samples was investigated in water vapor at 326 K within the relative humidity range of 0.22-1.0, and in liquid water within the temperature range of 318-338 K. The conductivity was measured with a four - electrode AC impedance method in the longitudinal direction of samples. The overall spectrum was collected for determining the high frequency resistance.

The conductivity was investigated with a frequency response analyzer (NF Electronic Instruments 5080) and potentiostat (Toho Technical Research Potentiostat/Galvanostat 2000) within the frequency range of 1 K to 2 M Hz. The magnitude of input signal was less than 10 mV.

### Results and discussion

The dependency of conductivity on water uptake of various samples is shown in Fig.1, from which it can be found that under low water uptake (2-3 mol H<sub>2</sub>O/mol SO<sub>3</sub>), the conductivity of various samples is very sensitive to the amount of water uptake in the membrane. This phenomenon has also been reported by other authors, and usually explained with percolation theory. [2, 3] The samples we investigated showed a sharp increase of conductivity within the

similar water uptake region, which conformed to the percolation theory that the percolation threshold is determined mainly by the microstructure of membranes.

The dependency of conductivity on the relative concentration of protons under various amounts of water uptake can be abstracted from Fig.1 as shown in Fig.2. It can be observed from Fig.2 that the conductivity increases rapidly with the increase of proton concentration within the water uptake range of 4-14.5 mol H<sub>2</sub>O/ mol SO<sub>3</sub>. The dependency of conductivity on proton concentration can be best described with equation (2),

$$\sigma = \sigma_{H^+} * x^{1.8} + \sigma_{Na^+} * (1-x) \quad (2)$$

where  $\sigma$  stands for overall specific conductivity,  $\sigma_{H^+}$  for the conductivity of proton-form Nafion,  $\sigma_{Na^+}$  for the conductivity of sodium-form Nafion. The results calculated with equation (2) are shown in Fig.2.

Equation (2) demonstrates that the conductivity originated from sodium ions is proportional to the concentration of sodium ions, while the conductivity from protons has a ~1.8 power dependency on its concentration.

Take the definition of specific conductivity into consideration, we can draw the conclusion that the mobility of proton increases with the increase of its relative concentration in membranes, while the mobility of sodium ions is not sensitive to the change of its relative concentration. The different dependency of mobility on species concentration between sodium ions and protons is due to the different migration mechanism.

Sodium ions migrate in Nafion through a bulk migration mechanism, and the mobility is affected mainly by electrostatic repulsion among ions, which was not changed dramatically after replacing sodium ions with protons.

Protons migrate through a quantum-mechanical tunneling in parallel with the bulk migration of H<sub>3</sub>O<sup>+</sup>. They are accompanied by the field-assisted rotation of water dipoles, which is sensitive to the structure of water. [6] The difference between the structure of water near proton and that of water near sodium leads to the change of proton migration mobility [7], which changes proton conductivity accordingly.

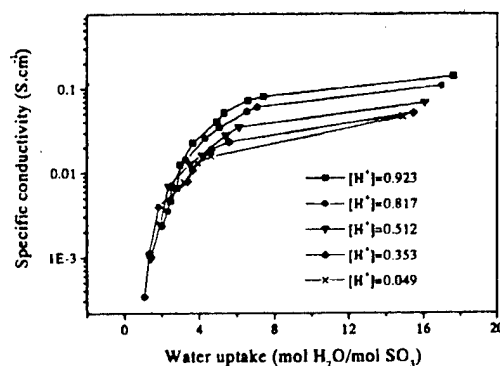


Fig.1. Dependency of specific conductivity on the relative concentration of protons under various humidity

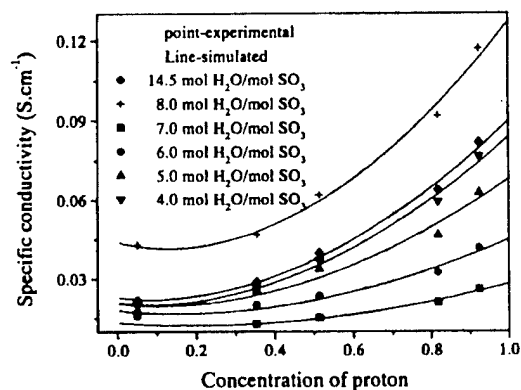


Fig.2 The specific conductivity of various H<sup>+</sup>-Na<sup>+</sup> mixed conductors under various amounts of water uptake

## References

1. T. R. Ralph, *Platinum Metals Rev.*, 41(3), 102 (1997)
2. Y. Sone, P. Ekdunge, and D. Simonsson, *J. Electrochem. Soc.*, 143, 1254 (1996)
3. T. A. Zawodzinski Jr., T. E. Springer, F. Uribe, S. Gottesfeld, *Solid State Ionics* 60, 199 (1993)
4. J. T. Hinatsu, M. Mizuhata, H. Takenaka, *J. Electrochem. Soc.*, 141, 1493 (1994)
5. S. Wang, A. Kaimai, K. Kawamura, Y. Nigara, T. Kawada, J. Mizusaki, *Solid State Ionics*, submitted (1998)
6. B. E. Conway, *Physical Chemistry – An Advanced Treatise*, ed. by H. Eyring, Volume 14 / *Electrochemistry*, Academic Press, New York / London, 1970, P120.
7. C. W. Davies, *Electrochemistry*, Philosophical Library Inc., 1967, P48.

## ELECTRODEPOSITION OF PLATINUM CATALYSTS FOR POLYMER ELECTROLYTE MEMBRANE FUEL CELLS

**Scott D. Thompson, Larry R. Jordan, Maria Forsyth**

Department of Materials Engineering, Monash University, Wellington Road, Clayton, Victoria 3168, Australia

Conventionally, catalysts for polymer electrolyte membrane fuel cells (PEMFCs) are prepared by the chemical reduction of platinum onto suspended carbon-black particles. The resulting Pt/C agglomerates are then mixed into a paste with the polymer electrolyte (Nafion ionomer), and painted onto a porous carbon support. However, the platinum utilisation with this approach may be as low as 10%, since not all of the platinum is contacted by the electrolyte. This suggests that platinum loadings (and hence the overall electrode cost) may be reduced substantially, if this catalyst layer is optimised.

Platinum electroreduction is thought to proceed selectively at carbon/Nafion interfaces when a suitable potential is applied. The resulting platinum catalyst will have contact with both the electrically conducting carbon as well as the ionically conducting Nafion, forming the three-phase reaction zones where the electrocatalysis of gases is known to occur. This electrochemical deposition method should therefore result in high platinum utilisations, even at relatively low catalyst loadings.

In this work two novel electrodeposition procedures were investigated. The first method involved the potentiodynamic reduction of Pt<sup>IV</sup> from a platinum solution contained above the preformed carbon-black/recast Nafion support. The applied potential regime allowed time for diffusion of the platinum salt into the catalyst support layer, before being reduced at a lower potential. In the second procedure, diffusion limitations were avoided by mixing the platinum salt directly into the carbon/Nafion support, and subsequently reducing the salt *in situ* in the fuel cell test station. Surface areas and catalyst utilisations were characterised by cyclic voltammetry, and compared with conventional electrodes made from E-TEK Pt/C catalysts. Scanning Electron Microscopy was used to characterise the electrode morphology.



## COMPLEX IMPEDANCE AND NMR STUDIES OF PROTON-CONDUCTING DOW MEMBRANES\*

C. A. Edmondson, P. E. Stallworth, J.J. Fontanella, M.C. Wintersgill  
Physics Department, U.S. Naval Academy, Annapolis, MD 21402-5026, USA

S.H. Chung, Y. Wang, S.G. Greenbaum  
Hunter College of CUNY, New York, NY 10021, USA

Electrical conductivity studies have been carried out on DOW 800 and DOW 1000 membranes. Complex impedance studies were made at frequencies from 10 Hz to 100 MHz at various relative humidities and consequently, water contents. The measurements were also made at pressures up to 0.3 GPa (3 kbar) and various temperatures over the range from about 200 to 350K.

New results for the atmospheric pressure electrical conductivity measurements extended to low water contents were obtained. A gradual decrease in electrical conductivity with decreasing water content is observed. Consequently, no clear percolation threshold is observed.

For very low water content materials the variation of the proton conductivity with temperature is non-Arrhenius exhibiting approximately Vogel-Tamann-Fulcher (VTF) or Williams-Landel-Ferry (WLF) behavior. The ability of the VTF/WLF formalisms to account for the data is described. The results are similar to those for Nafion materials but are different than is observed for the sulfonated hydrocarbon materials manufactured by Dais Corporation which exhibits Arrhenius behavior. For the low water content materials the variation with pressure is very large giving rise to apparent activation volumes larger than 30 cm<sup>3</sup>/mol. Both the temperature and pressure variation confirm that segmental motions control the proton conductivity at low water contents. The behavior is very similar to that observed for typical solvent-free polymer electrolytes. Of most interest is the detailed comparison of the pressure results with those for both Nafion and the Dais sulfonated hydrocarbon materials. The sulfonated polymer side chains which are thought to move and thus control proton conductivity, are different in each of these materials. The DOW side chains are similar to but shorter than those found in Nafion samples. The Dais sulfonated hydrocarbon side chains have a significantly different type of linkage for the sulfonate group.

Results for the temperature and pressure dependence of the electrical conductivity for both medium and high water content materials are also reported. Again the results are compared with those for other materials and for water. For example, for Nafion, while the proton conductivity decreases as pressure increases for low water content materials, it increases for high water contents. This behavior approaches that of water which, according to the literature, shows a larger increase in the electrical conductivity as pressure increases. The results are also discussed in terms of the activation volume. For Nafion, the activation volume is zero or slightly negative while for water the activation volume is negative. Additionally, ambient-pressure, variable-temperature <sup>1</sup>H and <sup>2</sup>H broadline and <sup>1</sup>H pulsed field gradient NMR measurements for saturated DOW membranes are presented. Typically, the nuclear spin-lattice relaxation behavior between 175 to 200K is Arrhenius yielding activations energies around 0.3 eV. The electrical conductivity and NMR results for the DOW membranes are compared both with these results and with those for the sulfonated hydrocarbon materials.

\*Work supported in part by the U. S. Office of Naval Research.

## CATHODE SUPPORTED THIN-FILM ELECTROLYTES FOR INTERMEDIATE TEMPERATURE SOLID OXIDE FUEL CELLS

C. Kleinlogel, M. Gödickemeier, K. Honegger\*  
and L.J. Gauckler

*ETH-Zürich, Swiss Federal Institute of Technology  
Dept. of Materials, Nonmetallic Materials  
CH-8092 Zürich*

*\*Surface Engineering, Sulzer Innotec Ltd  
CH-8404 Winterthur*

### Introduction

Solid oxide fuel cells (SOFCs) based on yttria-stabilized zirconia (YSZ) have to be operated at high temperatures (800-1000°C) to insure sufficient ionic conductivity. These operating temperatures result in high material costs for interconnector materials and insulation. They also accelerate degradation due to reactions at the interfaces between cell components [1][2]. These problems can be overcome by lowering the operating temperature to intermediate temperatures (IT) of 700°C. On possibility to achieve low resistance and high efficiency is to use thin YSZ layer electrolyte layers [3].

The objective of this study is to set up an IT-SOFC based on a cathode support structure. A several micrometer thin electrolyte bi-layer as well as a micrometer thin active anode layer has been deposited on top of this substrate by reactive magnetron sputtering. We will present microstructural results as well as electrochemical performance data.

### Experimental

Cathode substrates have been prepared on the base of a ceramic foam and an active cathode layer (Fig. 1). The ceramic foam acts as mechanical supporting element as well as an air distributor and current collector. The active cathode layer has been prepared by tape casting and subsequent sintering at temperatures between 1100 and 1200°C to obtain the desired microstructure (pore size and surface roughness). Thin layers of  $\text{Ce(Y)O}_{2-x}$ ,  $\text{Zr(Y)O}_{2-x}$  and  $\text{Ni-Zr(Y)O}_{2-x}$  were deposited on these substrates by DC reactive magnetron sputtering in  $\text{O}_2$ -Ar plasmas using metallic targets. Dense, micro-columnar film structures were already obtained at substrate temperatures as low as 250°C during deposition. The specific function and thickness of the different elements are listed in Table 1.

SOFC element	material	preparation method	thickness [μm]	microstructure	function
foam support	$\text{LaSrCoFeO}_3$ / $\text{CeGdO}_{2-x}$	slurry infiltration	5 mm	open structure	mechanical support, air distributor, current collector
active cathode	$\text{LaSrCoFeO}_3$ / $\text{CeGdO}_{2-x}$	tape-casting	100-150	microporous	substrate for thin-film deposition, active cathode, current collector
buffer-layer	$\text{Ce(Y)O}_{2-x}$	sputtering	1	dense	chemical compatible layer
electrolyte	$\text{Zr(Y)O}_{2-x}$	sputtering	4	dense	electrolyte
active anode	$\text{Ni-Zr(Y)O}_{2-x}$	sputtering	2	microporous (after reduction)	active anode, current collector

Table 1: Characteristics of the different functional elements.

## Results

Fig. 2 shows the cross-sectional view of the perovskite composite cathode substrate with the electrolyte layers on top. The porosity of the cathode substrates is of about 25% with a maximum pore size of less than 1  $\mu\text{m}$ . The electrolyte layers are uniform and crack free. Electrochemical measurements will be presented at temperatures between 600 and 900°C in air/ $\text{H}_2$ (+3%  $\text{H}_2\text{O}$ ). As electrolyte a double layer of CYO (5  $\mu\text{m}$ ) and YSZ (1  $\mu\text{m}$ ) has been used.

The open circuit voltage of 0.97 V corresponds to more than 90% of the theoretical value of the Nernst voltage which indicates that the electrolyte layers are dense, and crack free. The maximum power density achieved at 700°C was 325  $\text{mW}/\text{cm}^2$  at 0.7 V (Fig. 3) and even 340  $\text{mW}/\text{cm}^2$  at 600°C. The measurement of the different losses reveal that the ohmic drop at maximum power output of the cell (700°C) is  $\delta V_{\text{el}} \sim 45 \text{ mV}$ , the anodic overpotential  $\eta_{\text{A}} \sim 25 \text{ mV}$  and the cathodic overpotential  $\eta_{\text{C}} \sim 170 \text{ mV}$  (Fig. 4)

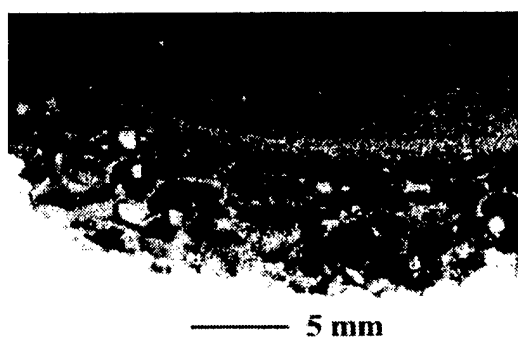


Fig. 1: Picture of a foam support structure with active cathode layer on top.

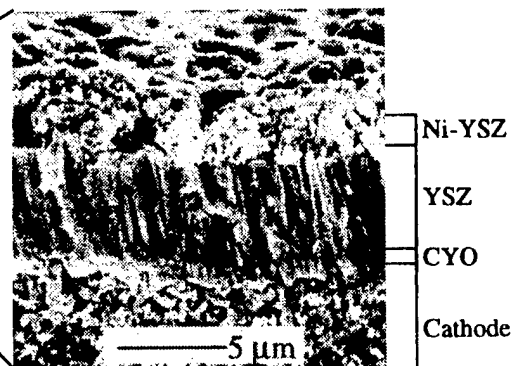


Fig. 2: Cross-sectional view of a cathode support (C) with a ceria-yttria (CYO), an yttria-zirconia (YSZ), and a Ni-YSZ layer on top. The layers have been deposited by reactive magnetron sputtering.

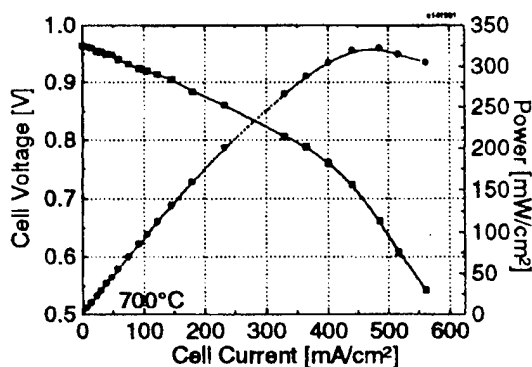


Fig. 3: I-V characteristics of a cathode supported thin-film electrolyte SOFC with a sputtered CYO/YSZ bi-layer and a sputtered Ni-YSZ anode.

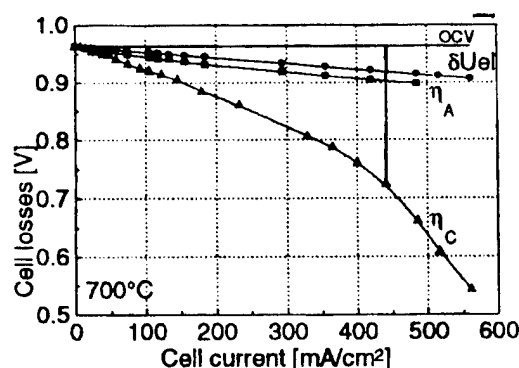


Fig. 4: Potential drop of the electrolyte ( $\delta U_{\text{el}}$ ) and at the cathode ( $\eta_{\text{C}}$ ) and anode ( $\eta_{\text{A}}$ ) interface of a cathode supported thin-film electrolyte SOFC.

## References

1. N.Q. Minh, J. Am. Ceram. Soc., **76**, 563 (1993)
2. A. Mitterdorfer, L.J. Gauckler, Solid State Ionics, **111**, 185-218 (1998)
3. S.A. Barnett, Solid State Ionics, **15**, 1-9 (1990)

## ALTERNATIVE ANODE MATERIAL FOR INTERNAL METHANE STEAM REFORMING IN SOLID OXIDE FUEL CELLS

P. Vernoux, M. Guillo, S. Linderth\*, J. Guindet and A. Hammou

Laboratoire d'Electrochimie et de Physico-chimie des Matériaux et des Interfaces (LEPMI)  
(INPG, CNRS and UJF), 1130, rue de la piscine, B.P. 75,  
F-38402 Saint Martin d'Hères Cedex - France

\* Materials Research Department, Risø National Laboratory, DK-4000, Denmark

The main Solid Oxide Fuel Cell (SOFC) application should be cogeneration with simultaneous production of electricity and heat from natural gas. We have recently [1] proposed a new concept : the gradual internal methane reforming based on local coupling between steam reforming of the fuel which occurs on a catalyst and hydrogen electrochemical oxidation which occurs at the electrode triple-phase perimeter. In order to implement this process, we have developed [2,3] doped lanthanum chromites as alternative anode materials.

In this study, catalytic and electrochemical properties of  $\text{La}_{0.8}\text{Sr}_{0.2}\text{Cr}_{0.97}\text{V}_{0.03}\text{O}_3$  (LSCV) were investigated. This perovskite was synthesised at Risø National Laboratory by glycine method [4]. Tests of the catalytic activity for methane steam reforming were performed at 800°C and 850°C. LSCV exhibits low conversion of methane. The most important fact is that no carbon deposit was detected after 30 hours operation.

Composite LSCV/YSZ (75%wt of LSCV) was deposited on YSZ pellet by spray-painting. Electrochemical characteristics of this electrode were investigated by impedance spectroscopy at 800°C in  $\text{H}_2/\text{H}_2\text{O}$  and  $\text{CH}_4/\text{H}_2\text{O}$  atmospheres.

In  $\text{H}_2/\text{H}_2\text{O}$ , impedance diagrams are composed of two semicircles at high-frequency (HF) and medium frequency (MF). Electrochemical performances were compared to those of an optimised Ni/YSZ cermet, with a three-layer graded structure. In both cases, the MF resistance is predominant. It is higher for LSCV/YSZ by only a factor 3. For a first approach, these results are encouraging. In fact, the large difference comes from the HF resistance which is lower for the Ni/YSZ cermet by a factor 20.

In  $\text{CH}_4/\text{H}_2\text{O}$ , an additional semicircle at low frequency (LF) has been observed. It might be associated with the slow rate of the methane steam reforming reaction. At 800°C, the polarisation resistance was higher than that observed in  $\text{H}_2/\text{H}_2\text{O}$  by about a factor 4.

Ruthenium, as a steam reforming catalyst, was added to the electrode material because of its beneficial effect. At 800°C, in pure methane mixed with 5% of steam, this anode material shows similar results than those observed in  $\text{H}_2/\text{H}_2\text{O}$  atmosphere without ruthenium. Moreover, electrochemical behaviours are stable with time and no carbon deposit was detected after 100 hours operation. These results demonstrate that the gradual internal reforming of methane can be implemented.

This work has been supported by Gaz de France and BRITE-EURAM III LOCO-SOFC (Contract No. BRPR-CT97-0413).

## References

- [1] P. Vernoux, J. Guindet and M. Kleitz, J. Electrochem. Soc., **145**, 3487 (1998).
- [2] P. Vernoux, J. Guindet and E. Gehain, in Proceedings of the third European SOFC forum, P. Stevens Ed., Oberrohrdorf, 237 (1998).
- [3] P. Vernoux, Ionics, **3**, 270 (1997).
- [4] N. Christiansen and P. Gordes, in Proceedings of the 2<sup>nd</sup> Int. Symposium on SOFC, F. Grosz, P. Zegers, S.C. Singhal and O. Yamamoto Eds., Brussels, 495 (1991).

## PEROVSKITE MATERIALS FOR DIRECT METHANE OXIDATION IN SOLID OXIDE FUEL CELLS

G. Pudmich <sup>a,\*</sup>, B. A. Boukamp <sup>b</sup>, M. Gonzalez <sup>b</sup>, W. Jungen <sup>a</sup>, and F. Tietz <sup>a</sup>

<sup>a</sup> Institute for Materials and Processes in Energy Systems (IWV-1),  
Forschungszentrum Jülich, D-52425 Jülich, Germany

<sup>b</sup> Faculty of Chemical Technology (CT 1733), University of Twente,  
7500 AE Enschede, The Netherlands

The currently used material for anodes in solid oxide fuel cells (SOFCs) is a Ni/ZrO<sub>2</sub> cermet, which is optimized for the oxidation of hydrogen. The nickel metal in the cermet tends to agglomerate after prolonged operation time leading to reduced contact area and increasing resistances. The use of humidified natural gas causes carbon deposition on the anode, poisoning by sulphur and finally a breakdown of cell performance. The reforming and cleaning of methane to obtain pure hydrogen requires additional components in the power plant and increases the investment costs.

Therefore, a search for new anode materials is being carried out with the aim of identifying ceramic materials with stable catalytic activity in fuel gases with a high amount of hydrocarbons. Ceramic oxides show several advantages over metals. They tend to be less likely to promote coking and to suffer from sulphur poisoning. Some work has already been performed in this field by various groups before [1-5].

A new material has to fulfil several requirements:

- good stability under reducing conditions
- appropriate catalytic activity
- high electrical conductivity
- compatibility with the thermal expansion coefficients (TEC) of other cell components
- no chemical reaction with the electrolyte or the interconnect, even at high temperatures and after long operation time

Some perovskite materials, mostly based on lanthanum chromite La<sub>1-x</sub>A<sub>x</sub>Cr<sub>1-y</sub>B<sub>y</sub>O<sub>3</sub> (with A = Ca, Sr; B = Ti, Fe, V, Nb), were synthesized using the Pechini method [5] and investigated by X-ray diffraction (XRD), differential thermal analysis (DTA) and thermogravimetry (TG). Sintered pellets (10 h at 1400 °C) were examined by conductivity measurements both in oxidizing (air) and reducing atmosphere (argon with 4% H<sub>2</sub>) and dilatometric measurements for materials selection. Selected samples were investigated by impedance spectroscopy and electron microscopy after screen-printing onto YSZ substrates and sintering.

The average particle sizes of the powders were 0.3 to 3 µm. Most ceramics were stable up to 1400°C with no melting. After calcination at 900 °C XRD often indicated more than one phase, after sintering at 1400 °C mostly a single phase or only insignificant impurities (usually of binary oxides).

Some materials (fig.1) showed a conductivity of up to 100 S/cm in reducing atmosphere. Usually, the conductivity dropped considerably in air (about 1 to 5 orders of magnitude, depending on the composition). For chromium-rich samples the conductivity in air was higher than in hydrogen.

In dilatometric measurements the thermal expansion coefficient (TEC) was determined between room temperature and 1000 °C. The TEC of the anode has to be of the order of 11·10<sup>-6</sup> K<sup>-1</sup> to fit the TECs of cathode and electrolyte. Figure 2 shows the thermal expansion of La<sub>0.7</sub>Ca<sub>0.3</sub>Cr<sub>0.5</sub>Ti<sub>0.5</sub>O<sub>3</sub> in different atmospheres. The pellet was first heated up to 1200 and 1100 °C, then cooled down to 1000 and 800 °C, respectively, and kept at constant temperature over several hours in air. The atmosphere was then switched to argon/4%H<sub>2</sub> for about 2 hours

and then back to argon/20%O<sub>2</sub>. Only a very small alteration due to the atmosphere can be seen. Some other materials (e.g. La<sub>0.7</sub>Ca<sub>0.3</sub>Cr<sub>0.8</sub>Fe<sub>0.2</sub>O<sub>3</sub> and La<sub>0.7</sub>Sr<sub>0.3</sub>Cr<sub>0.8</sub>Ti<sub>0.2</sub>O<sub>3</sub>) showed a much larger alteration, which makes the material insufficient for use in a SOFC stack due to mechanical failure.

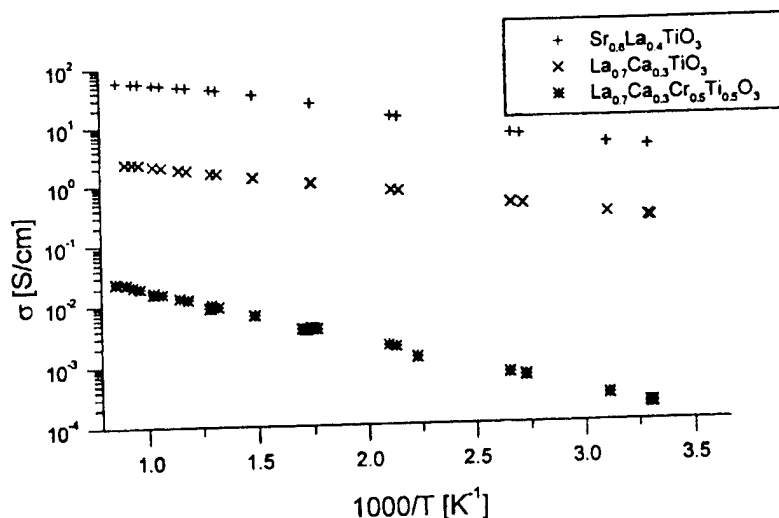


Fig.1: Conductivity of some titanate materials in Ar/4%H<sub>2</sub>

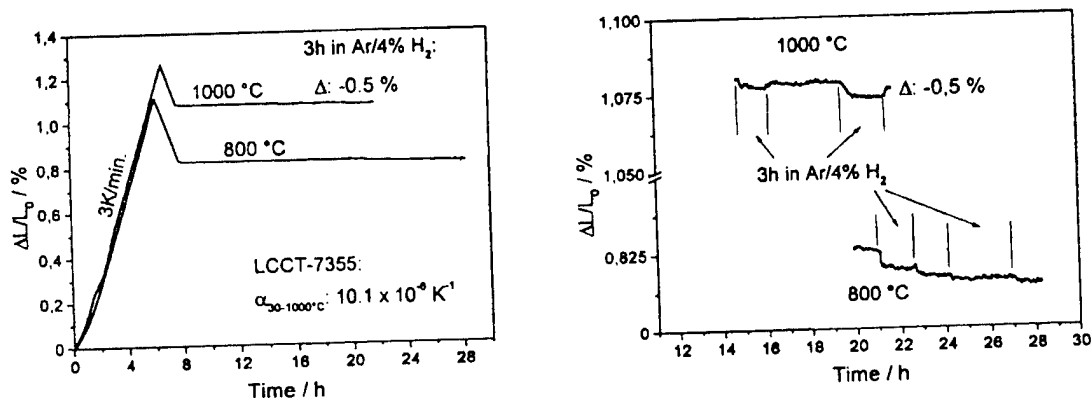


Fig.2: Thermal expansion of La<sub>0.7</sub>Ca<sub>0.3</sub>Cr<sub>0.5</sub>Ti<sub>0.5</sub>O<sub>3</sub>. On the left an overview, right an enlarged picture of the small changes due to the alternation of oxidizing and reducing atmospheres.

- [1] D.P.Fagg, S.M.Fray and J.T.S.Irvine, Solid State Ionics 72, 235 (1994)
- [2] R.Moos and K.H.Härdtl, J.Appl.Phys. 80 [1], 393 (1995)
- [3] J.T.S.Irvine, D.P.Fagg, J.Labrincha and F.M.B.Marques, Catalysis Today 38, 467 (1997)
- [4] P.R.Slater and J.T.S.Irvine, in Proc. 3rd Europ. SOFC Forum, Nantes, 1998, pp.417
- [5] P.Vernoux, J.Guindet, E.Gehain and M.Kleitz, Proc. SOFC V, eds. U.Stimming, S.C.Singhal, H.Tagawa and W.Lehnert, Electrochem. Soc. (1997) 219
- [6] M.P.Pechini, US Patent 3,330,697 (1967)

\* Corresponding author, Tel. +49 2461 61 4594, Fax +49 2461 61 5700,  
e-mail G.Pudmich@FZ-Juelich.de

5mol% TiO<sub>2</sub>-DOPED YSZ/Ni ANODE CERMETS FOR SOLID OXIDE FUEL CELLS

D. Skarmoutsos, A. Tsoga<sup>\*,\*\*</sup>, A. Naoumidis<sup>\*</sup> and P. Nikolopoulos  
Chemical Engineering Dpt., University of Patras, GR 265 00 Patras, Greece

<sup>\*</sup>Institute for Materials and Processing in Energy Systems, IWV1,  
Research Center Juelich, D-52425 Juelich

<sup>\*\*</sup>TMR Grant Holder

## ABSTRACT

YSZ/Ni cermet is the state-of-the-art anode material used for SOFCs with hydrogen fuel, due to its low cost and the high catalytic activity of Ni for hydrogen oxidation [1]. When using methane as a fuel for SOFCs this anode electrode presents the disadvantage of rapid carbon deposition, due to the fact that Ni promotes the catalytic cracking of hydrocarbon reactions. This phenomenon becomes even more pronounced with higher hydrocarbons present in natural gas. In order then to utilise methane as fuel in SOFCs, it has to be reformed either externally or internally. In the former case the major costs of the plant increases significantly, rendering this approach unattractive. In the later case problems do exist due to temperature gradients resulting from the endothermic reforming reaction and the exothermic oxidation reaction. Other disadvantages of the YSZ/Ni cermet anode are its sulphur intolerance, when natural gas is used as a fuel, and the agglomeration of Ni under long term operation.

An attractive possible candidate as alternative to the YSZ/Ni cermet is the use of mixed conducting oxides. Their utilization offers the advantage of promoting the charge-transfer reactions over the whole area of the electrode/gas interface. Consequently polarization and efficiency losses are significantly less than with electrodes exhibiting only electrical conductivity. Additionally they are potentially less likely to promote coking and they are less likely to suffer from sulfur poisoning. A novel anode, however, must fulfil also the remaining requirements of an anode electrode i.e. high electronic conductivity, chemical compatibility with the electrolyte, mechanical stability, low cost and simple fabrication process.

The system ZrO<sub>2</sub>-Y<sub>2</sub>O<sub>3</sub>-TiO<sub>2</sub> has been extensively studied with respect to its electrical properties [2-5] and has been shown that for TiO<sub>2</sub>-contents close to the solubility limits of TiO<sub>2</sub> ( $\approx 10\text{mol}\%$ ) into YSZ [2], the incorporation of TiO<sub>2</sub> into YSZ lattice results in decreasing of the ionic conductivity due to the block of oxygen ions by titanium ions, while the electronic conductivity of the system becomes significant at low enough oxygen partial pressures, i.e. lower than  $10^{-17}$  atm at 1000°C for a content of 10 mol % TiO<sub>2</sub> and increases in general with increasing titania concentration and temperature and decreasing oxygen partial pressure [4]. In every case, however, the electronic conductivity is not high enough to be used as an electrode and therefore a promising alternative is to form a cermet with Ni. The advantage of the doped cermet against YSZ/Ni cermet anode is the possibility of reducing the Ni-content in the doped cermet, due to the expected contribution of the electronic conductivity of the ceramic and thus the suppression of the coking effect. Additionally, it has been shown that the TiO<sub>2</sub> doping of YSZ improves the interfacial adhesion between the ceramic and Ni suppressing in this way the agglomeration of the Ni-particles and thus improving the long term stability of the electrode [6,7].

The current paper reports on the influence of doping YSZ with TiO<sub>2</sub> on the microstructure, the thermal expansion coefficient and the conductivity of the cermet containing different contents of Ni, before and after long term annealing at 1000°C. The properties of these cermets are compared to the YSZ/Ni cermet with 45vol% Ni, whose preparation followed the same chemical route and the same processing.

Both YSZ and TiO<sub>2</sub>-doped YSZ ceramics were prepared by the spray drying technique using the corresponding metallic nitrate precursors. As a first step of the approach a ceramic solid solution with a TiO<sub>2</sub>-content of 5mol% into YSZ was used. For the prepared cermets the content



of Ni after reduction varied in the range 30-45 vol%. Examination of the microstructure of the so prepared cermets showed that titania doping improves the dispersion of Ni particles permitting a better distribution compared to the undoped cermet. Thermal expansion coefficient (TEC) measurements showed that the contribution of  $\text{TiO}_2$  is negligible giving comparable TEC values for both the doped and undoped ceramic matrix and their corresponding cermets. The temperature dependence of the total electrical conductivity was measured by standard four-probe dc technique. The ionic conduction activation energy for the ceramic specimens containing titania was found to be 13% higher than YSZ itself, while under reducing conditions ( $\text{Ar}+4\text{vol}\%\text{H}_2$  atmosphere) no difference to the activation energy was measured. Comparable activation energy values were found for both YSZ/Ni and  $\text{TiO}_2$ -doped YSZ/Ni cermets, were the titania doped cermet showed better conductivity.

Technical feasibility of the titania doped cermets is further discussed means of time variation of their properties after annealing at  $1000^\circ\text{C}$ .

#### References

1. T. Setoguchi, K.Okamoto, K.Eguchi and H.Arai, J. Electrochem. Soc. 139 (1992) 2875
2. L.S.M. Traqueira, T.Pagnier and F.M.B. Marques, J. Eur. Ceram. Soc. 17 (1997) 1019
3. S.S.Liou and W.L. Worrell, Appl. Phys. A49 (1989) 25
4. H.Naito and A. Arashi, Solid State Ionics 53-56 (1992) 436
5. K. Kobayashi, Y.Kai, S.Yamaguchi, N.Fukatsu, T.Kawashima and Y.Iguchi, Solid State Ionics 93 (1997) 193.
6. A.Tsoga, A. Naoumidis and P.Nikolopoulos, Acta mater. 44 (1996) 3679
7. A. Tsoga P.Nikolopoulos and A. Naoumidis, Ionics 2 (1996) 427

-0.44 W/cm<sup>2</sup>  
- at 550 °C

## ELECTRICAL CONDUCTIVITY And CATALYTIC BEHAVIOUR Of CeO<sub>2</sub>-Y<sub>2</sub>O<sub>3</sub>-Nb<sub>2</sub>O<sub>5</sub> SOLID SOLUTIONS

K.M.Liddicott and B.C.H.Steele

Ceramic Ion Conducting Membranes Group

Imperial College, London, SW7 2BP, UK

[b.steele@ic.ac.uk](mailto:b.steele@ic.ac.uk)

Doped CeO<sub>2</sub> solid solutions (DCS) have many of the attributes specified for selection of anode materials [1] in solid oxide fuel cells (SOFC). Due to the predominant anion lattice disorder and associated high values for oxygen self-diffusion and surface exchange useful kinetics for the complete oxidation of dry methane have been noted without the complications of carbon deposition. However simple binary DCS materials incorporating trivalent dopants have only moderate electronic conductivity values ( $\sim 1 \text{ Scm}^{-1}$  at 900C for  $P_{\text{O}_2}$  values around  $10^{-18}$  bar. Moreover oxidation-reduction cycles at fluctuating anode potentials induce large changes in stoichiometry, which are accompanied by significant changes in lattice parameters. The associated expansion-contraction of the anode material can eventually cause structural failure, and loss of adhesion to the electrolyte.

In an effort to overcome these disadvantages investigations were undertaken on the ternary CeO<sub>2</sub>-Y<sub>2</sub>O<sub>3</sub>-Nb<sub>2</sub>O<sub>5</sub> system. Selected compositions have been characterised by electronic and ionic conductivity measurements, together with thermogravimetry, electron microscopy, X-ray diffraction, and in-situ catalytic examinations. Some preliminary results were reported earlier [2] which indicated that the introduction of Nb<sup>5+</sup> decreased the oxygen self-diffusion values as the concentration of anion vacancies was reduced, but increased the electronic conductivity at high oxygen partial pressures. More recent data has confirmed that double doping can increase the solubility of Nb from 1 to 5 atomic % for compositions incorporating 3.7/3.8%Y, and the enhanced solubility was accompanied by a reduction in the lattice parameter. However it did not prove possible to reduce the lattice expansion at low  $P_{\text{O}_2}$  values, as the expansion was dominated by the thermodynamics of the Ce<sup>4+</sup>/Ce<sup>3+</sup> redox equilibria. This behaviour has been interpreted in terms of available data on the relevant defect chemistry.

Double doped ceria was also shown to be a good catalyst for the oxidation of CH<sub>4</sub> at temperatures above 450C and could be an effective anode material for low temperature operation if combined with a good electronic conductor in a composite anode structure. This suggestion appears to have been recently confirmed at 600C by Murray et al [3].

1. B.C.H.Steele, P.H.Middleton, and R.A.Rudkin: Solid State Ionics, **40/41**, 388, 1990
2. S.Carter, R.J.Chater, J.Kajda, K.M.Liddicott, J.A.Kilner, and B.C.H.Steele, p.84 in Proc. 1<sup>st</sup> Intl. Symp. on Ionic and Mixed Conducting Ceramics, Eds. T.A. Ramanarayanan et al., Proc.Vol. 91-12 (Electrochem.Soc., New Jersey, USA, 1991)
3. E.Murray, T.Tsai, and S.Barnett, Abstract #120, p.418 in US Fuel Cell Seminar, November 16-19, 1998, (Courtesy Associates Inc. Washington, DC, USA)

## ZIRCONIA-BASED SOFC WITH NON-NOBLE ELECTRODES FED BY AIR-METHANE MIXTURE

Anatoly K. Demin and Fyodor Ya. Gulbis

Institute of High Temperature Electrochemistry, Ural Division RAS  
620219 Ekaterinburg, S.Kovalevskoy Str., 20

*- Carbon  
deposition on Ni  
- will power  
in AMM?*

It was demonstrated in many experiments that an electrochemical cell with two different electrodes, which are in contact with non-equilibrium air-methane mixture (AMM), could produce an electrical energy (see, for instance [1] and references in it). This effect was discovered for electrolytes based on zirconia, ceria and cerates. Gold electrodes were used as anodes in all experiments. Gold is inactive to the methane partial oxidation reaction (MPOR) and active to electrochemical reactions. Platinum electrodes were used as cathodes practically in all experiments. Platinum is active both to the MPOR and to electrochemical reactions. It is obvious that the noble metals are not acceptable for practical application and search of suitable non-noble electrodes is highly actual.

Replacement of platinum by nickel-cermet as an anode material seems to be quite logical. As to cathode materials, it is obvious that they must be stable in oxidising atmosphere and have acceptable conductivity. The most promising materials possessing these properties seem to be perovskites, for instance, manganites. However, at high temperatures (800-1000°C) which were characteristic for the experiments with these cells, perovskites are quite active to the MPOR. So it is senseless to use manganites as the anodes in the cells fed by the AMM at high temperatures. Nevertheless it was interesting to prove possibility to use manganites at moderate temperatures.

As we demonstrated, the AMM fed SOFC based on zirconia electrolyte has an advantage in comparison with the cerate-based AMM fed SOFC [3]. So we focused on studying of zirconia-based SOFCs.

In our experiment, we used a 10YSZ disc (about 0.7 mm thick) covered with an anode of ceria-doped Ni-YSZ-cermet (0.07 mm thick) from one side and with a cathode of lanthanum-strontium manganite (0.17 mm thick) from another side. A ratio oxygen/methane in the AMM was equal to 0.5. The cell was tested at temperatures 550 - 700°C. An EMF decreased practically uniformly from about 900 mV at 550°C to about 700 mV at 670°C. At higher temperature, an EMF oscillation was observed. At 700°C, an oscillation amplitude reached 100 mV. A reason of this effect is not clear.

Volt-ampere dependences were measured. It was stated that polarisation losses were negligible comparing to ohmic losses at 550 and 600°C. At 650°C polarisation losses were higher than ones at 600°C and became comparable with ohmic losses. Very likely, at 650°C manganite began to catalyse the MPOR and presence of reduced components caused manganite partial decomposition and subsequent increase in polarisation losses. At 500 mV, current densities were 14, 22 and 15 mA/cm<sup>2</sup> for the temperatures 550, 600 and 650°C, respectively. Replacement of supporting electrolyte by thin film one can lead to significant increase in current densities.

### References

- [1] K. Asano and H. Iwahara, J. Electrochem. Soc., **144**, 3125 (1997).
- [2] A. K. Demin and F. Ya. Gulbis, Abstracts of CIMTEC'98 - 9<sup>th</sup> Int. Conf. on Modern Materials and Technologies, Florence, Italy, 14-19 June, p. 208.

## POLARIZED ELECTROCHEMICAL VAPOUR DEPOSITION FOR CERMET ANODES IN SOLID OXIDE FUEL CELLS

J. L. Young and T. H. Etsell

Department of Chemical and Materials Engineering

University of Alberta

Edmonton, Alberta, Canada T6G 2G6

A new process originally developed for sensors[1] shows promise in the deposition of Me-YSZ (metal - yttria stabilized zirconia) cermet anodes for SOFC (solid oxide fuel cells). Several anode preparation techniques are commonly in use today, including sputtering[2], tape casting [3,4], screen printing[5], gel precipitation[6] and slurry coating[7]. However, there is a concern which arises from these "traditional" preparation techniques which have implications for the final product. A metal precursor of some sort (usually an oxide, which is reduced in the fuel environment) is commonly used, resulting in a randomly interspersed Me-YSZ matrix of particles. Maintaining Me to Me contact in the cermet anode is the most important aspect in the processing of Me-YSZ anodes; yet when the metal precursor is reduced, the metal particles tend to sinter and become separated from one another[8]. Accordingly, the randomly interspersed matrix can be highly discontinuous. As a result, the anode must be made thicker to prevent the conductivity from being severely impeded.

With the new polarized electrochemical vapour deposition technique (PEVD), a thin layer of YSZ is deposited over the entire surface of the metal, which has previously been sintered to a continuous layer on the fuel cell electrolyte. Complete coverage can be realized irrespective of the electrode microstructure. This process is similar to electrochemical vapour deposition, in that it takes advantage of the electronic and ionic conductivity of YSZ for film fabrication. In the PEVD process, a negative potential bias is applied to the electrolyte, as illustrated in Figure 1, providing electrons for the reduction of oxygen molecules. The oxygen ions transport through the electrolyte to the anode, where they react with zirconium and yttrium chlorides, releasing electrons back through the external electrical circuit.

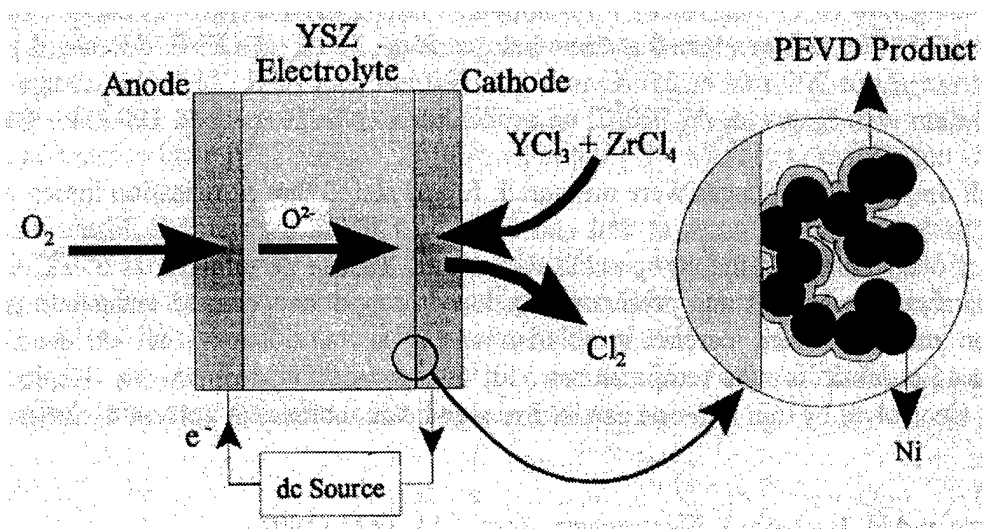


Figure 1 - Schematic of PEVD process.

Film growth behaviour is entirely dependent on the electronic and ionic conductivity of the film. Because the ionic conductivity of the YSZ film being deposited is much greater than its electronic conductivity, film growth is favoured along the metal electrode, or the X direction in Figure 2, which has a high electronic conductivity. The relationship involving ionic and electronic conductivity is presented in Equation 1 [9]:

$$\frac{X}{Y} \approx \frac{1.265 \sqrt{\sigma_{O^{2-}}}}{\sqrt{\sigma_{e^{-}}}} \quad (1)$$

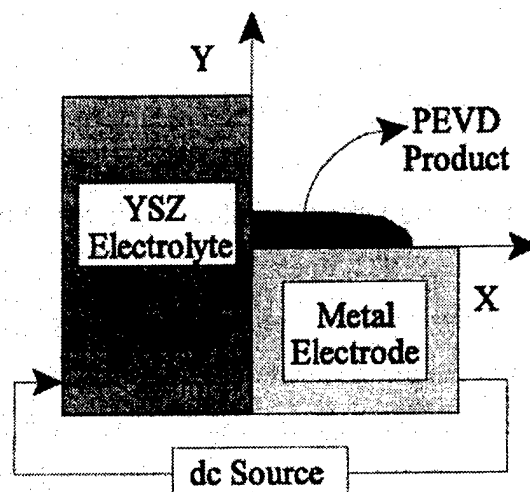


Figure 2 - Preferred growth direction of an ionic conducting layer on an electronic conducting substrate.

A thin coating of YSZ has been successfully coated onto the surface of a metal anode, producing a cermet. It is expected that the conductivity and triple phase boundary length in the anode will be improved, while electrode degradation due to sintering, poisoning (by impurities, such as  $H_2S$ ), and evaporation (due to the high vapour pressure of some metals) should be reduced. This process shows promise not only for anode deposition, but also for cathodes, interconnects, and for dual and multilayered electrolytes. More testing is required to determine if the thermal expansion coefficient will be compatible and to evaluate the expected improvement in fuel cell performance.

- [1] E. Z. Tang and T. H. Etsell, *Solid State Ionics* 91, 213 (1996).
- [2] L. S. Wang and S. A. Barnett, *Solid State Ionics* 61, 273 (1993).
- [3] A. L. Lee, R. F. Zabransky and W. T. Huber, *Ind. Eng. Chem. Res.* 29, 766 (1990).
- [4] T. Kawada, N. Sakai, H. Yokokawa, M. Dokiya and I. Anzai, *J. Ceram. Soc. Japan, Int. Ed.* 100, 838 (1992).
- [5] J. Mizusaki, H. Tagawa, T. Saito, K. Kamitani, T. Yamamura, K. Hirano, S. Ehara, T. Takagi, T. Higita, M. Ippommatsu, S. Nakagawa and K. Hashimoto, *J. Electrochem. Soc.* 141, 2129 (1994).
- [6] M. Marinsek and J. Macek, *Key Engineering Materials* 132-136, 948 (1997).
- [7] S. Sridhar and U. B. Pal, *Powder Technology* 88, 173 (1996).
- [8] T. Kawada and H. Yokokawa, *Key Engineering Materials* 125-126, 187 (1997).
- [9] R. A. Rapp and D. A. Shores, *Techniques of Metals Research* 4 [2], 123 (1970).

## OPTIMISATION OF COMPOSITE CATHODES FOR INTERMEDIATE TEMPERATURE SOFC

V. Dusastre and J. A. Kilner

*Centre for Ion Conducting Membranes, Dept. of Materials,  
Imperial College of Science, Technology and Medicine,  
London SW7 2BP, UK.*

### Abstract

Ceramic composite cathodes offer the possibility of yielding high performance electrodes [1,2] for intermediate temperature SOFC operation. To this end we have investigated the electrochemical properties of symmetrical cells based on a  $\text{Ce}_{0.9}\text{Gd}_{0.1}\text{O}_{1.95}$  electrolyte with electrodes consisting of porous composites of the ceramic materials  $\text{La}_{0.6}\text{Sr}_{0.4}\text{Co}_{0.2}\text{Fe}_{0.8}\text{O}_{3-x}$  and  $\text{Ce}_{0.9}\text{Gd}_{0.1}\text{O}_{1.95}$ . The cells have been characterised and investigated at intermediate temperatures (500-700°C) using AC impedance spectroscopy. Results indicate that the electrochemical properties of these composite electrodes are quite sensitive to the composition and the microstructure. Optimum  $\text{Ce}_{0.9}\text{Gd}_{0.1}\text{O}_{1.95}$  addition (30% by weight) to  $\text{La}_{0.6}\text{Sr}_{0.4}\text{Co}_{0.2}\text{Fe}_{0.8}\text{O}_{3-x}$  resulted in a 4 times lower area specific resistivity indicating that this composite is a promising cathode material for solid oxide fuels based on  $\text{Ce}_{0.9}\text{Gd}_{0.1}\text{O}_{1.95}$ .

The observed composition dependence of the composite electrodes (Figure 1.) is consistent with the prediction of the effective medium percolation theory [3,4], which gives the ambipolar transport behaviour of composite mixed ionic-electronic conductors as a function of the volume fraction of each randomly-distributed constituent phase. Quantitatively, a slight discrepancy between measurements and theory was observed. This is believed to be due to the fact that the overall performance of a porous electrode is not only determined by the mixed conducting transport properties in the solid phase of the electrode, but also by the inherent catalytic property of the triple phase boundary, and by the gas transport to or away from the triple phase boundary. These factors are not taken into account by the current theory.

The results obtained for the composite cathodes will be discussed in the light of isotope exchange experiments [5] on the composite materials.

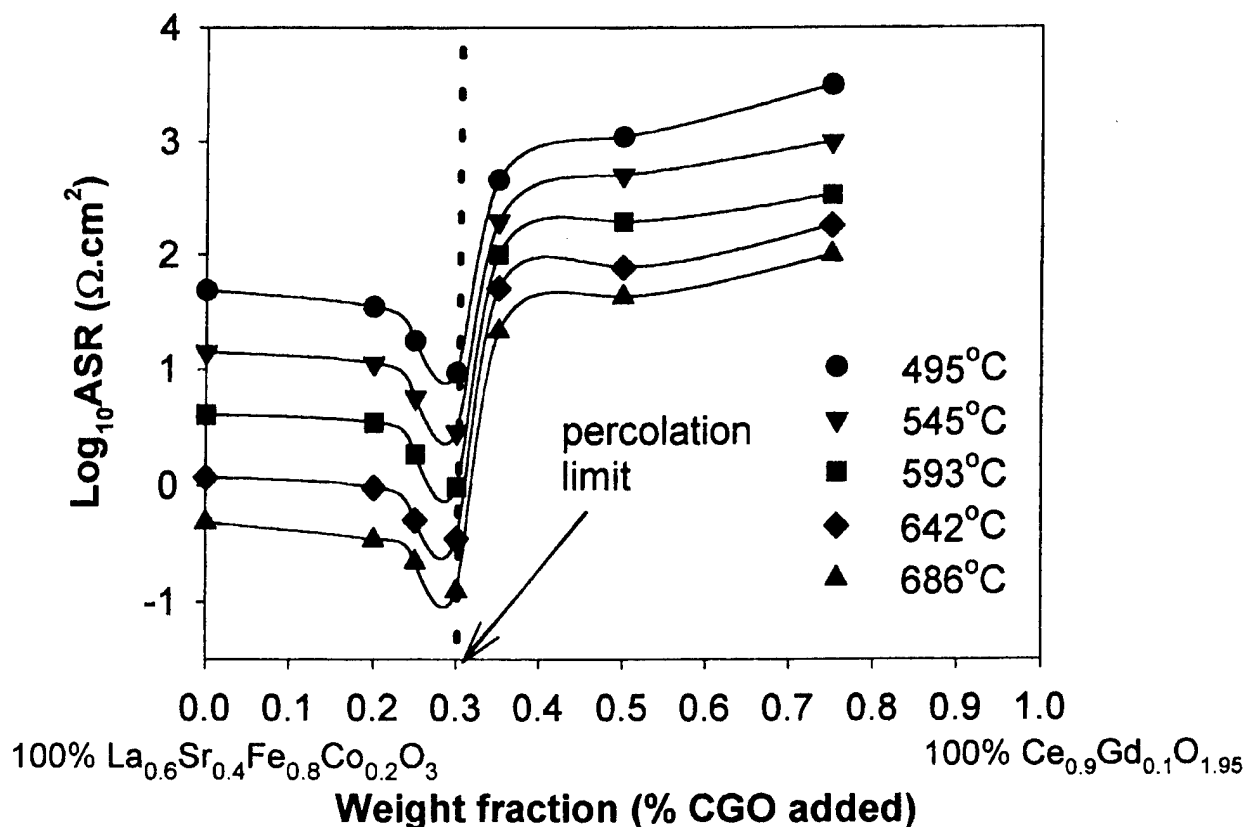


Fig 1. The Area Specific Resistance (ASR) of a composite system vs. weight fraction of CGO added

### References

- [1] C. W. Tanner, K-Z. Fung and A. V. Virkar, 1997, *J. Electrochem. Soc.*, **144**, 21.
- [2] Z. L. Wu and M. L. Liu, *J. Am. Ceram. Soc.*, 1998, **81**(5), 1215.
- [3] D. S. McLachlan, M. Blaszkiewicz and R. E. Newham, *J. Am. Ceram. Soc.*, 1990, **73**(8), 2187.
- [4] Z. Wu and M. Liu, *Solid State Ionics*, 1997, **93**, 65.
- [5] J. A. Kilner and R. A. Souza, 1996, *Proceeding of the 17<sup>th</sup> Riso International Symposium on Materials Science: High Temperature Electrochemistry: Ceramics and Metals*, eds F. W. Poulsen, N. Bonanos, S. Linderroth, M. Mogensen and B. Zachau-Christiansen, 41.

## SOFC ELECTRODE PROPERTIES OF RUTHENIUM-CONTAINING PYROCHLORE OXIDES

T. Takeda, R. Kanno, Y. Kawamoto, Y. Takeda\*, O. Yamamoto\*

Faculty of Science, Kobe University, Kobe 657-8501, Japan

\*Faculty of Engineering, Mie University, Tsu 514-8507, Japan

### 1. Introduction

Cobalt and Manganese based perovskites have been studied as a cathode material for solid oxide fuel cells (SOFC). However, the Co-based perovskite that shows high catalytic activity reacted with the yttria stabilized zirconia (YSZ) to form the low-conductivity products. The Mn-based perovskites have good stability at high temperature; however, during long annealing time, the pyrochlores formed at the boundary between the perovskites and YSZ. Better electrode materials that are less reactive with YSZ are required. In this study, the ruthenium pyrochlores,  $\text{Pb}_2\text{Ru}_2\text{O}_{6.5}$  and  $\text{Bi}_2\text{Ru}_2\text{O}_7$  were found to have good cathodic properties for the SOFC electrode of low operating temperature. The cathodic properties, electrical conductivity, thermal expansion and reactivity with YSZ were studied. The cathodic properties of the ruthenium-based perovskites ( $\text{CaRuO}_3$  and  $\text{SrRuO}_3$ ) were also clarified.

### 2. Experimental

Starting materials ( $\text{RuO}_2$ ,  $\text{PbO}$ , and  $\text{Bi}_2\text{O}_3$ ) were weighed, mixed, pelletized and heated for 24-48h at a fixed temperature, 900-950°C. The samples obtained were characterized by X-ray diffraction (XRD). Electrical resistivity was measured by the dc four-probe method with Pt-paste contacts. The oxygen reduction polarization on the pyrochlore electrode was studied on a three-electrode cell by the current interruption technique to remove IR-drop contribution. Pyrochlore thin films, used as the working electrodes, were prepared on one side of the YSZ tablet by RF-sputtering technique and fired at 900°C for 2h. The reactivity test of the pyrochlores with YSZ was carried out using mixtures of the oxides and YSZ (1:1 weight ratio) at 900°C for 96h. Thermal expansion measurements were carried out from room temperature to 900°C using quartz as a reference.

### 3. Results and Discussion

The X-ray diffraction patterns of the pyrochlores sputtered on YSZ were characteristic of amorphous materials. After the sample were treated at 900°C,



crystalline phases appeared. Figure 1 shows the cathodic polarization curves for  $\text{Pb}_2\text{Ru}_2\text{O}_{6.5}$  and  $\text{Bi}_2\text{Ru}_2\text{O}_7$ . The lead pyrochlore showed excellent cathodic properties even at low temperature at  $800^\circ\text{C}$ , and the overpotentials are comparable to the cobaltite perovskite. The bismuth pyrochlore showed slightly higher overpotentials than  $\text{Pb}_2\text{Ru}_2\text{O}_{6.5}$ . However, the perovskites,  $\text{CaRuO}_3$  and  $\text{SrRuO}_3$ , showed much higher overpotentials even at  $1000^\circ\text{C}$  than the pyrochlores.

The electrical resistivity measurements showed the metallic behavior and the conductivity values of the pyrochlores are comparable to those of the Mn based perovskites and are acceptable as cathodes in SOFC.

The reactivity tests showed no reaction between the  $\text{Pb}_2\text{Ru}_2\text{O}_{6.5}$  and YSZ. For  $\text{Bi}_2\text{Ru}_2\text{O}_7$ , when the sample contained an impurity phase, the monoclinic zirconia phase appeared after the reaction. However, the reaction study using the monophasic pyrochlore of  $\text{Bi}_2\text{Ru}_2\text{O}_7$  showed no changes in the diffraction patterns. The reaction might be caused between the impurity phase and the yttria in the YSZ, and the cubic zirconia transformed to the monoclinic phase.

The thermal expansion coefficient of  $\text{Bi}_2\text{Ru}_2\text{O}_7$  is  $0.99\text{--}1.00 \times 10^{-5}\text{K}^{-1}$ , which is almost comparable to that of YSZ. On the other hand,  $\text{Pb}_2\text{Ru}_2\text{O}_{6.5}$  showed a slightly higher expansion rate of  $1.10\text{--}1.21 \times 10^{-5}\text{K}^{-1}$  than the bismuth pyrochlore.

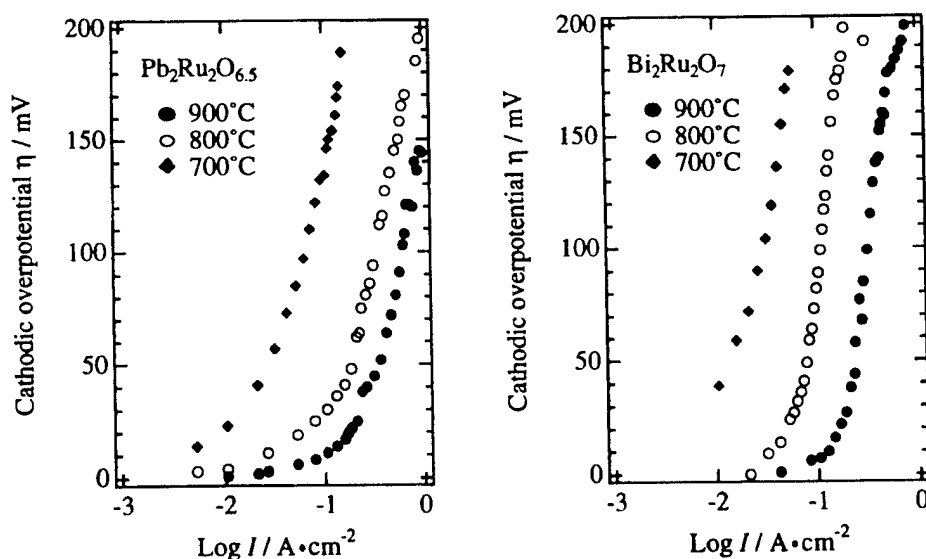


Fig.1 Cathodic overpotential curves for  $\text{Pb}_2\text{Ru}_2\text{O}_{6.5}$  and  $\text{Bi}_2\text{Ru}_2\text{O}_7$ . The polarization curves are measured at  $900^\circ\text{C}$  (●),  $800^\circ\text{C}$  (○), and  $700^\circ\text{C}$  (◆).

ELECTRODE PERFORMANCE OF COMPOSITE  $\text{LaCoO}_3/\text{La}_2\text{Zr}_2\text{O}_7$  CATHODE

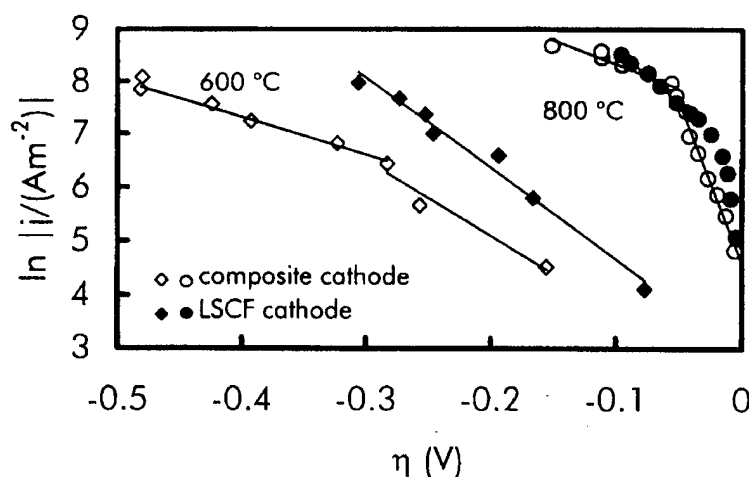
F.M.Figueiredo, F.M.B.Marques, J.R.Frade

Ceramics and Glass Eng. Dep., UIMC, University of Aveiro, 3810 Aveiro, Portugal

High temperature reaction of YSZ with excess of  $\text{LaCoO}_3$  yields three phase  $\text{LaCoO}_3/\text{La}_2(\text{Zr},\text{Y})_2\text{O}_7/\text{CoO}_{1+\delta}$  materials which match the thermal expansion of ceria-gadolinia (GCO) electrolytes[1]. Those composite materials were screen printed onto GCO disks, fired at temperatures from 1200 to 1400°C, and characterised as potential cathodes. Changes in the solid to liquid ratio of the slurries, and double layer depositions were used to change the thickness and other microstructural features of the cathodes. Excessively high temperatures cause densification, and possibly even segregation of components of the composite cathode, thus spoiling the fine microstructures.

Steady state cathodic polarisation curves were obtained at temperatures in the range 600-800°C, and demonstrate that the electrode behaviour is very dependent on the microstructures, the best results being attained for electrodes with open porosity and fine pore size.

Tafel plots of the actual composite cathodes usually suggest different mechanisms for the ranges  $|\eta_c| < |\eta_{tr}|$ , and  $|\eta_c| > |\eta_{tr}|$ , where  $\eta_{tr}$  is a transition overpotential revealed by Tafel plots. A similar change in mechanism was reported for  $\text{La}_{1-x}\text{Sr}_x\text{MnO}_{1-\delta}$  electrodes [2]. This change may be interpreted on assuming formation of ionic defects ( $\text{V}_{\text{O}}^{\bullet\bullet}$ ) for sufficiently high values of  $|\eta_c|$ , thus extending the electrode reactions to the overall electrode. Note that Tafel plots of the actual composite cathodes in the range  $|\eta_c| > |\eta_{tr}|$  resemble the behaviour of an alternative cathode ( $\text{La}_{1-x}\text{Sr}_x\text{Co}_{1-y}\text{Fe}_y\text{O}_{3-\delta}$ ) with high concentration of ionic charge carriers. At low overpotentials the electrode reaction is expected to take place mainly at electrolyte-electrode-atmosphere contacts.



[1]. F.M.Figueiredo, J.R.Frade, F.M.B.Marques, Solid State Ionics (in press)

[2]. B.Gharbage, T.Pagnier, A.Hammou, Solid State Ionics 72 (1994) 248

## CHROMIUM DIFFUSION IN LANTHANUM CHROMITES

N. Sakai, K. Yamaji, T. Horita, H. Negishi, and H. Yokokawa  
National Institute of Materials and Chemical Research (NIMC)

Interconnect material is one of the most important targets to be developed in Solid Oxide Fuel Cell (SOFC). There are two candidate materials, one is doped lanthanum chromite (LC) with high chemical stability, and the other is heat-resisting alloys with high electronic conductivity and mechanical strength. The most serious problem in utilizing Cr-containing alloy as interconnect is the oxidation on both air and fuel sides forming  $\text{Cr}_2\text{O}_3$  as an insulation layer. Taniguchi *et al.* have reported that the  $\text{CrO}_3(\text{g})$  vaporized from  $\text{Cr}_2\text{O}_3$  reacts with  $\text{La}_{0.8}\text{Sr}_{0.2}\text{MnO}_3$  and increases the cathode overpotential[1]. The coating of doped LC on alloy has been tested to prevent this undesirable chromium transport[2]. In the present study, the tracer diffusion coefficient of chromium was determined by using a stable isotope ( $^{50}\text{Cr}$ ) and SIMS analyses in order to estimate the extent of chromium transport in LC coating layer on alloy interconnect. If the chromium diffusion coefficient is larger than those of other cations (lanthanum or calcium),  $\text{Cr}_2\text{O}_3$  will precipitated at the cathode/interconnect interface and gaseous transport of  $\text{CrO}_3$  will be enhanced. On the other hand, if the chromium diffusion coefficient is much smaller than other cations, it would result in the precipitation of  $\text{Cr}_2\text{O}_3$  at LC/alloy interface.

The samples used as matrices were  $\text{La}_{0.75}\text{Ca}_{0.25}\text{CrO}_3$  (LCC, prepared by liquid mixing method) and  $\text{La}_{0.95}\text{Sr}_{0.05}\text{CrO}_3$  (LSC, provided by Nikkato Co., Japan). The densities of the samples were 97% ~ 99 %. The both surface of the samples were polished by using diamond paste. The aqueous solution of  $\text{M}^{50}\text{CrO}_4$  ( $\text{M} = \text{Ca}$  or  $\text{Sr}$ ) was painted and dried on the LCC or LSC surface several times, and the samples were annealed for several hundreds hours at  $T = 1173 \sim 1373$  K in air. After the annealing, the remaining  $\text{M}^{50}\text{CrO}_4$  on the surface was removed in dilute  $\text{HNO}_3(\text{aq.})$ . The depth profiles of  $^{50}\text{Cr}^+$  concentration were obtained by using secondary ion mass spectrometry (SIMS, CAMECA ims 5f, France) with  $\text{O}_2^+$  as a primary ion. The depth of analyzed area was measured by using surface profiler (Dektak<sup>3</sup>, USA).

A depth profile of relative concentration of  $^{50}\text{Cr}$  is shown in Fig. 2. The shallow part of the profile can be well fitted to the following

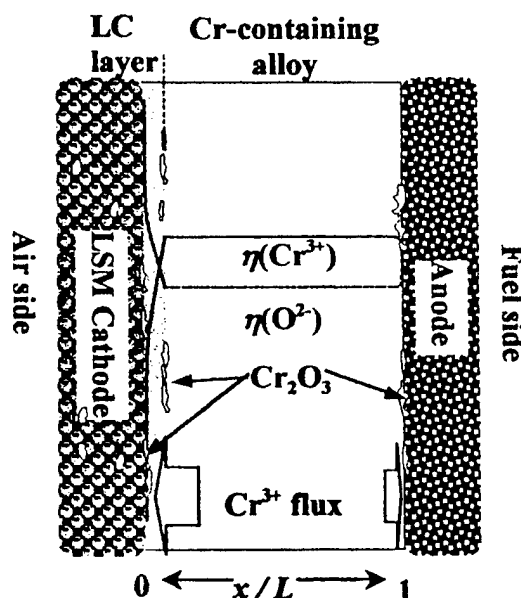


Fig. 1 Schematic view of chromium transport in LC-alloy interconnect.

equation[3]:

$$C(x, t) - C_0 = (C_s - C_0) \left[ 1 - \operatorname{erf} \left( \frac{x}{2\sqrt{Dt}} \right) \right]$$

However, the relative concentration of  $^{50}\text{Cr}$  did not reach to the natural abundance (4.35%), which indicates the contribution of grain boundary diffusion. The grain boundary diffusion coefficient was determined from the slope of  $\ln C(x, t)$  vs.  $x^{6/5}$  plot and the equation which was proposed by Le Claire [4]. The width of grain boundary was assumed to be ca. 1 nm which was evaluated from TEM images of LCC.

The temperature dependence of chromium tracer diffusion coefficients were shown in Fig. 3 with literature data of diffusion coefficients of  $\text{La}^{3+}$  in  $\text{LaCrO}_3$ [5], or Sr-Ca interdiffusion coefficients in LCC[6]. The absolute values of chromium tracer diffusion coefficients in LCC are ca.  $1/10 \sim 1/100$  of Ca-Sr interdiffusion coefficient, and the activation energy was  $158 \text{ kJ mol}^{-1}$  for LCC and  $18 \text{ kJ mol}^{-1}$  for LSC. For LSC case, the diffusion depth was ca. 100 nm, in which the effect of atom-mixing by primary ion beam is not negligible in SIMS. This effect causes the apparent small activation energy, so that the real diffusion coefficient of LSC will be much smaller than obtaining values at  $T < 1273 \text{ K}$ .

## References

- [1] S. Taniguchi, *et al.*, *Denki Kagaku*, **64**(6), 568 (1996).
- [2] K. Barthel *et al.*, in the Proceedings of the IEA Workshop "Materials and Processes", Annex VII: held on January 28 -31 1997 in Les Diablerets, Switzerland, pp.168 (1997)
- [3] J. Crank *The Mathematics of Diffusion*, Oxford Science Publications, (1975)
- [4] A. D. Le Claire, *J. Appl. Phys.* **14**, 151 (1963)
- [5] T. Akashi, *et al.*, *J. Electrochem. Soc.*, **145**(6), 2090 (1998).
- [6] T. Horita, *et al.*, *Solid State Ionics*, **108**, 383 (1998).

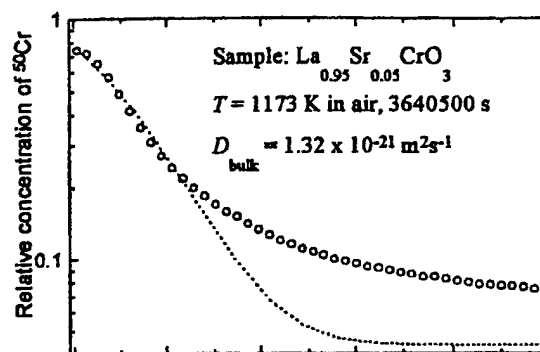


Fig. 2 Depth profile of  $^{50}\text{Cr}$  diffusion in LSC

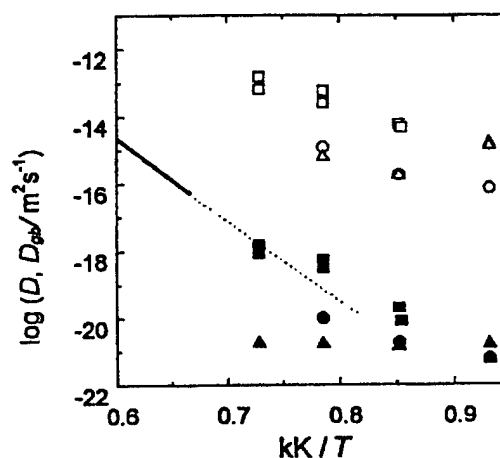


Fig. 3 Temperature dependence of diffusion coefficients of bulk (closed symbols) and grain boundary (open symbols):  $\bullet, \circ$ ;  $^{50}\text{Cr}$  in LCC,  $\blacktriangle, \triangle$ ;  $^{50}\text{Cr}$  in LSC,  $\blacksquare, \square$ ; Sr-Ca in LCC [6], solid line;  $\text{La}^{3+}$  in  $\text{LaCrO}_3$  [5].

## CHARACTERISTICS OF LANTHANUM STRONTIUM CHROMATE PREPARED BY GLACINE NITRATE PROCESS

Yong-Ji Yang, Ting-Lian Wen, Hengyong Tu, Da-Qian Wang and Jianhua Yang,  
Shanghai Institute of Ceramics, Chinese Academy of Sciences,  
200050 Shanghai China, tlwen@sunm.shcnc.ac.cn

### INTRODUCTION

Due to the fact that lanthanum chromate based materials exhibit at high temperatures good mechanical property and electrical conductivity as well as chemical stability in both oxidizing and reduction atmospheres, therefore the materials have been increasingly used in various purposes, such as the interconnector in solid oxide fuel cell, the heating element in high temperature furnaces and the current collecting electrode in MHD and so on[1]. However, Cr in the materials is easily oxidized in air at high temperatures to form vaporizing compounds such as  $\text{CrO}_x$ ,  $\text{CrO}_x(\text{OH})_y$  and  $\text{Cr}(\text{OH})_3$ [2]. Because of Cr vaporization the materials are difficultly sintered to high density and their intrinsic properties are affected. In order to diminish Cr vaporization in lanthanum chromate based materials several ways have been tried. One of them is to prepare high active powder with high specific surface so as to lower the sintering temperature.

In the present work glycine-nitrate-process(GNP) was used for synthesizing lanthanum strontium chromate in order to acquire high active powder, because GNP can in very short time prepare high specific surface powder with single phase composition. It is especially appropriate for the multicomponent system such as doped perovskite compounds[3, 4].

### EMPERIMENTAL

The super fine powder with composition of  $\text{La}_{1-x}\text{Sr}_x\text{CrO}_3$  ( $x=0., 0.1, 0.15, 0.2$  and  $0.3$ ) were synthesized by GNP. The starting materials are glycine(as the fuel), La, Sr, and Cr nitrates(as the oxidant). The glycine was added into the mixed nitrate solution in a molar ratio of 2:1 for fuel/oxidant. After drying, the mixture was heated up to around  $200^\circ\text{C}$ . Then the combustion reaction took place within a few minutes to form the primary powder. The as-synthesized powder was calcined at  $500^\circ\text{C}$  for 30 minutes and was determined by DTA/TG and TEM.

The calcined powder was isostatically pressed into pellets and sintered at  $1550^\circ\text{C}$  for 4 hours. Measurements of the density and the electrical conductivity as well as the phase composition were made on the sintered samples.

The powder of composition of  $\text{La}_{0.8}\text{Sr}_{0.2}\text{CrO}_3$  was sprayed by plasma flame on the Cr substrate to form a coated interconnector for SOFC. The futures of the composite interconnector were examined.

### RESULTS AND DISCUSSIONS

DTA/TG determination showed that the as-synthesized powder contained small amount of residue amorphous carbon, which can be removed by calculation at  $500^\circ\text{C}$ . XRD measurements demonstrate that the as-synthesized and calcined powders belong to the orthorhombic structure without detected single oxide impurity phase. However network-like powder agglomeration of the powder was observed by TEM. The agglomerates could be eliminated by ultrasonic treatment or moderately ball milling. The mean size of the primary

particle is around 30nm.

The sintering study showed that the shrinkage fraction and the relative density of the powder increase as increasing  $x$  in  $\text{La}_{1-x}\text{Sr}_x\text{CrO}_3$  (Fig. 1). It may be attributed to  $\text{CrO}_3$  volatilization in a form of  $\text{CrO}_3$  during sintering so that the local  $\text{Cr}$  vacancy at grain boundaries and then  $\text{Sr}$  precipitation took place, and, as a result,  $\text{SrCrO}_4$  intermediate transient liquid phase with low melting point ( $<1300^\circ\text{C}$ ) was formed, which promoted the sintering of  $\text{La}_{1-x}\text{Sr}_x\text{CrO}_3$  [5, 6].

The electrical conductivity  $\sigma$  of  $\text{La}_{1-x}\text{Sr}_x\text{CrO}_3$  enhances with increase in  $x$  when  $x < 0.2$ . The  $\sigma$  of  $\text{La}_{0.8}\text{Sr}_{0.2}\text{CrO}_3$  amounts to  $14.7\text{S/cm}$  at  $1000^\circ\text{C}$ . However, when  $x > 0.2$  the conductivity shows a little decreasing (Fig. 2). Due to  $\text{Sr}$  doping,  $\text{Cr}$  valence increases in order to maintain the electrical neutrality so that electronic hole concentration was increased resulting in an enhancement in conductivity. However when  $x$  further increasing, oxygen vacancies with positive charge would be formed for balancing the electrical valence, thus resulting in decrease in conductivity because of hindering the motion of electrical holes.

$\text{La}_{0.8}\text{Sr}_{0.2}\text{CrO}_3$  powder was coated on  $\text{Cr}$  plate by plasma flame spraying technique. The coating layer is of  $50\text{--}100\mu$  thickness and after treating in air or hydrogen atmosphere at  $1000^\circ\text{C}$ , exhibited good adherence to  $\text{Cr}$  substrate and retained the electrical conductivity of the as-sintered  $\text{La}_{0.8}\text{Sr}_{0.2}\text{CrO}_3$ . Therefore the  $\text{La}_{0.8}\text{Sr}_{0.2}\text{CrO}_3$ -coated  $\text{Cr}$  composite is suitable for application for an interconnector in SOFC. It could prevent  $\text{Cr}$  from oxidation and volatilization at high temperature in oxygen atmosphere during SOFC operation condition.

## REFERENCES

- [1] K. Flandemeyer, M. M. Nasrallah, A. K. Agarwal and H. U. Anderson, *J. Am. Ceram. Soc.* **67**, 195 (1984).
- [2] D. H. Peck, M. Müller, H. Nickel, and Proceedings of 4<sup>th</sup> Internl. Symp. on SOFC, eds. M. Dokiya, H. Tagawa and O. Yamamoto, (Yokohama, 1995) 858-868.
- [3] L. A. Chick, L. R. Pederson, G. D. Maupin, and J. L. Bates, *Material Letters*, **10**, 6 (1990).
- [4] Yan Y.-J. And T.-L. Wen, Proceedings of 5<sup>th</sup> Internl. Symp. on SOFC, eds. U. Stimming, S. C. Singhal, H. Tagawa, W. Lehnert (Aachen Germany, 1997) 956-964.
- [5] L. Chick, J. Liu, J. W. Stevenson, and T. R. Armstrong, *J. Am Ceram. Soc.* **80**, 2109 (1997).
- [6] N. Sakai, T. Kawada, H. Yokohama, M. Dokiya, *J. Am Ceram. Soc.* **76**, 609 (1993).

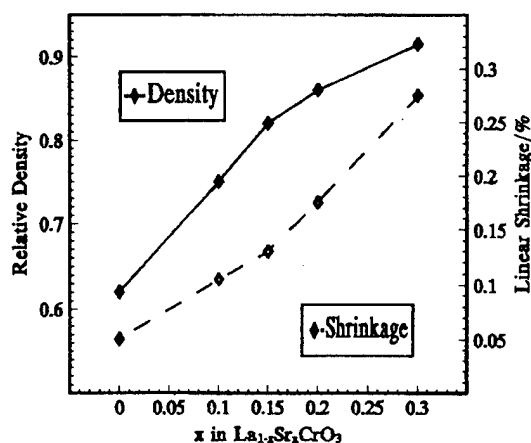


Fig. 1. Effect of Sr doping concentration on Density and shrinkage of  $\text{La}_{1-x}\text{Sr}_x\text{CrO}_3$  sintered samples.

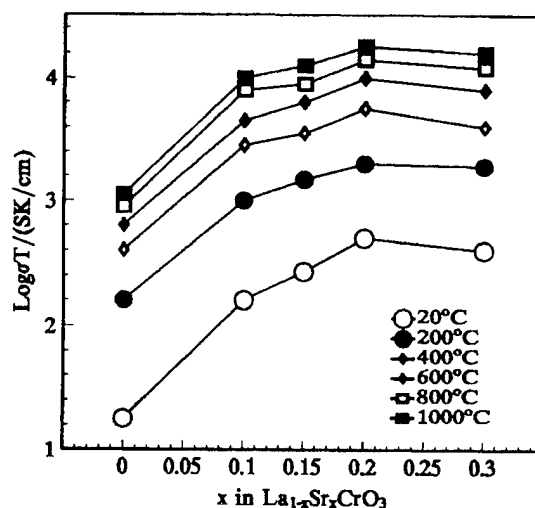


Fig. 2. Plot of  $\text{Log}\sigma T$  as function of  $x$  in  $\text{La}_{1-x}\text{Sr}_x\text{CrO}_3$  sintered at  $1550^\circ\text{C}$  4hrs.

## OXYGEN CHEMICAL POTENTIAL VARIATION IN CERIA-BASED SOLID OXIDE FUEL CELLS DETERMINED BY RAMAN SPECTROSCOPY

A. Mineshige<sup>1</sup>, T. Taji<sup>1</sup>, Y. Muroi<sup>1</sup>, M. Kobune<sup>1</sup>, S. Fujii<sup>1</sup>, N. Nishi<sup>2</sup>, M. Inaba<sup>2</sup> and Z. Ogumi<sup>2</sup>

<sup>1</sup>Department of Applied Chemistry, Himeji Institute of Technology,  
Himeji, Hyogo 671-2201, Japan

<sup>2</sup>Department of Energy and Hydrocarbon Chemistry, Graduate School of Engineering,  
Kyoto University, Kyoto 606-8501, Japan

Doped-CeO<sub>2</sub> is one of the successful candidate for electrolyte materials of solid oxide fuel cells (SOFCs) because it exhibits pure and high oxide ionic conductivity under high  $P(\text{O}_2)$  atmosphere (e.g. in air). However, it becomes a mixed ionic and  $n$ -type electronic conductor at low  $P(\text{O}_2)$  as is encountered in the fuel side of SOFCs. The appearance of the electronic conduction at low  $P(\text{O}_2)$  is due to partial reduction of Ce<sup>4+</sup> into Ce<sup>3+</sup> in doped-CeO<sub>2</sub>. Under operating conditions of SOFCs, a  $P(\text{O}_2)$  gradient exists across the electrolyte and this determines the degree of mixed conduction at a given position along the thickness. To evaluate the mixed conduction accurately in the doped-CeO<sub>2</sub> under operating conditions, it is necessary to know oxygen chemical potential, or  $P(\text{O}_2)$ , variation across the electrolyte. In the present work, the oxygen chemical potential variation in doped-CeO<sub>2</sub> was determined using Raman spectroscopy.

It has been reported that a band assigned to oxygen vacancies is observed in Raman spectra of CeO<sub>2</sub>-based materials [1]. In the previous work [2], it was proved that the concentration of oxygen vacancy,  $\delta$  in Ce<sub>1-x</sub>Sm<sub>x</sub>O<sub>2-δ</sub>, can be determined using a relative peak area of this band and the main band, which is an allowed lattice mode of fluorite structure metal dioxides. The value of  $\delta$  depends only on  $P(\text{O}_2)$  if Sm-content,  $x$ , and temperature are fixed. Hence, the oxygen chemical potential variation in the sample was determined by evaluating the oxygen nonstoichiometry variation in quenched Ce<sub>1-x</sub>Sm<sub>x</sub>O<sub>2-δ</sub> sample along the  $P(\text{O}_2)$  gradient, and the relationship between  $P(\text{O}_2)$  and  $\delta$ .

Raman spectra of quenched Ce<sub>0.8</sub>Sm<sub>0.2</sub>O<sub>2-δ</sub> ( $x = 0.2$ ) samples after annealed under various  $P(\text{O}_2)$  showed that the relative intensity of the band assigned to oxygen vacancies increases with decreasing  $P(\text{O}_2)$  at  $P(\text{O}_2) \leq 10^{-8}$  atm. Calculated peak area ratio of  $S_{\text{Vo}}/(S_0 + S_{\text{Vo}})$ , where  $S_0$  and  $S_{\text{Vo}}$  are the areas of the main and vacancy bands, respectively, shows an approximately linear relationship with  $\delta$  [2]. Using this relationship,  $P(\text{O}_2)$  dependency of the oxygen nonstoichiometry [ $P(\text{O}_2)$ - $\delta$  diagram] of Ce<sub>0.8</sub>Sm<sub>0.2</sub>O<sub>2-δ</sub> sample at 1273 K was obtained. In the range  $P(\text{O}_2) \leq 10^{-8}$  atm, a linear relationship existed between  $\log P(\text{O}_2)$  and  $\log \delta$ .

Using the  $P(\text{O}_2)$ - $\delta$  diagram, the oxygen chemical potential variation in a Ce<sub>0.8</sub>Sm<sub>0.2</sub>O<sub>1.9</sub> ( $x = 0.2$ ) sample annealed under an influence of  $P(\text{O}_2)$  gradient was evaluated. It was proved that the low  $P(\text{O}_2)$  mixed conducting region occupies the entire region of the sample except for the region near the solid/air interface, as predicted theoretically [3].

### References

- [1] J. R. McBride, K. C. Hass, B. D. Poindexter and W. H. Weber, *J. Appl. Phys.* **76**, 2435 (1994).
- [2] A. Mineshige, M. Takata, M. Kobune, S. Fujii, S. Nakanishi, M. Inaba and Z. Ogumi, Extended Abstracts of 11th International Conference on Solid State Ionics (1997) p. 350.
- [3] P. Soral, U. Pal and W. L. Worrell, *J. Electrochem. Soc.* **145**, 99 (1998).

## ELECTROTRANSPORT-INDUCED DEMIXING IN MULTI-COMPONENT OXIDES

Jeong-Oh Hong and Han-Il Yoo

Solid State Ionics Research Lab., School of Materials Science and Engineering  
Seoul National University, Seoul 151-742, Korea

A solid oxide fuel cell (SOFC) employs different kinds of multi-component oxides, e.g., a cathode  $\text{La}_{1-x}\text{Sr}_x\text{MnO}_3$  and an interconnector  $\text{La}_{1-x}\text{Ca}_x\text{CrO}_3$ . These oxides should serve in an electric field at the elevated temperatures for an extended period of time. When a ternary or higher oxide is brought under a generalized thermodynamic force, e.g., a gradient of component chemical potential, redistribution of the composition so called kinetic demixing may occur in the initially homogeneous oxide due to the difference in mobility of constituent cations. During the operation of an SOFC, thus, kinetic demixing is inevitably induced in those oxides, eventually leading to the degradation of the oxides.

In the present work, we examined theoretically and experimentally the demixing behavior in a semiconducting ternary oxide under a constant current condition. A ferrite spinel ( $\text{Mn}_x\text{Fe}_{1-x}$ ) $_3\text{O}_4$  was chosen as a model system, for which the diffusivity of cations are comparatively well documented in literatures.

It is known [1,2] for the ferrite spinel,  $\text{MnFe}_2\text{O}_4$  that the majority type of defects is Frenkel disorder and the diffusivity ratio of cations,  $D_{\text{Mn}}^*/D_{\text{Fe}}^* = 1.3$  in the vacancy prevailing region and  $= 2$  in the interstitial prevailing region at  $1200^\circ\text{C}$ . Demixing experiments were, therefore, performed under the oxygen partial pressures of  $10^{-1.5}$  (vacancy regime) and  $10^{-6.0}$  atm (interstitial regime) at  $1200^\circ\text{C}$  by passing a constant current of  $24 \sim 30 \text{ A/cm}^2$  for the period of time necessary for the steady state to be reached. Figure 1 shows the typical microstructure of the sectioned surfaces along the current direction after a demixing run. Demixing profiles were established at different positions from the cathode to the anode. The results are as shown in Fig. 2 where  $x$  in  $(\text{Mn}_x\text{Fe}_{1-x})_3\text{O}_4$  is plotted against the relative distance  $\xi/\Delta\xi$ . Mn with higher diffusivity was always enriched at cathode, but the extents of demixing were smaller than the expected (solid line in Fig. 2) from the ratio of component diffusivities and the average valence ( $=8/3$ ) of cations. It is found that, in demixing under an electric field, the degree of demixing is determined not only by the difference in diffusivity of the cations but also by their effective charges. From the demixing profiles, we extract the effective charge of cations, which are 1.4 and 1.6 for Mn and Fe ions, respectively.

Time evolution of demixing profiles under a constant current condition are calculated by numerically solving the continuity equations with the appropriate initial and boundary conditions, and compared with the experimental results.

### References

- [1] P. Franke and R. Dieckmann, *Solid State Ionics* **32-33**, 817 (1989)
- [2] F. H. Lu and R. Dieckmann, *Solid State Ionics* **53-56**, 290 (1992)



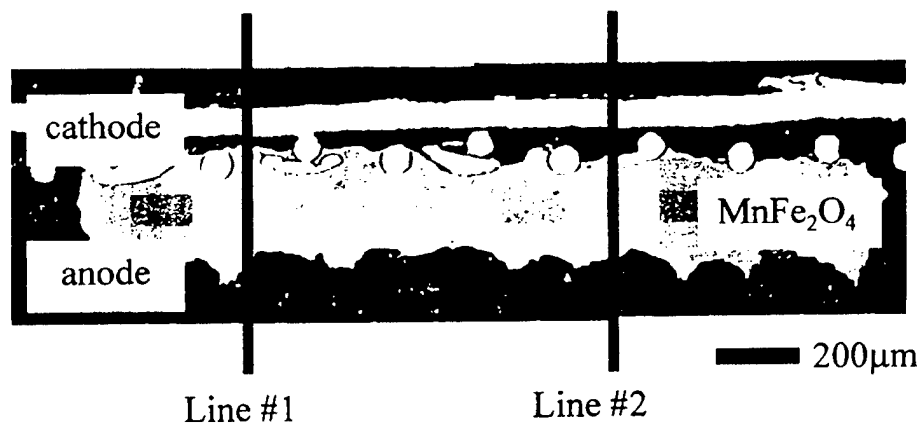


Fig. 1. Photomicrograph of the sectioned surfaces after a demixing run ( $i = 28.3 \text{ A/cm}^2$ ) at  $P_{O_2} = 10^{-6.0} \text{ atm}$  and  $1200^\circ\text{C}$  for 218h. Line #1 and #2 denote the microprobe-scanning lines.

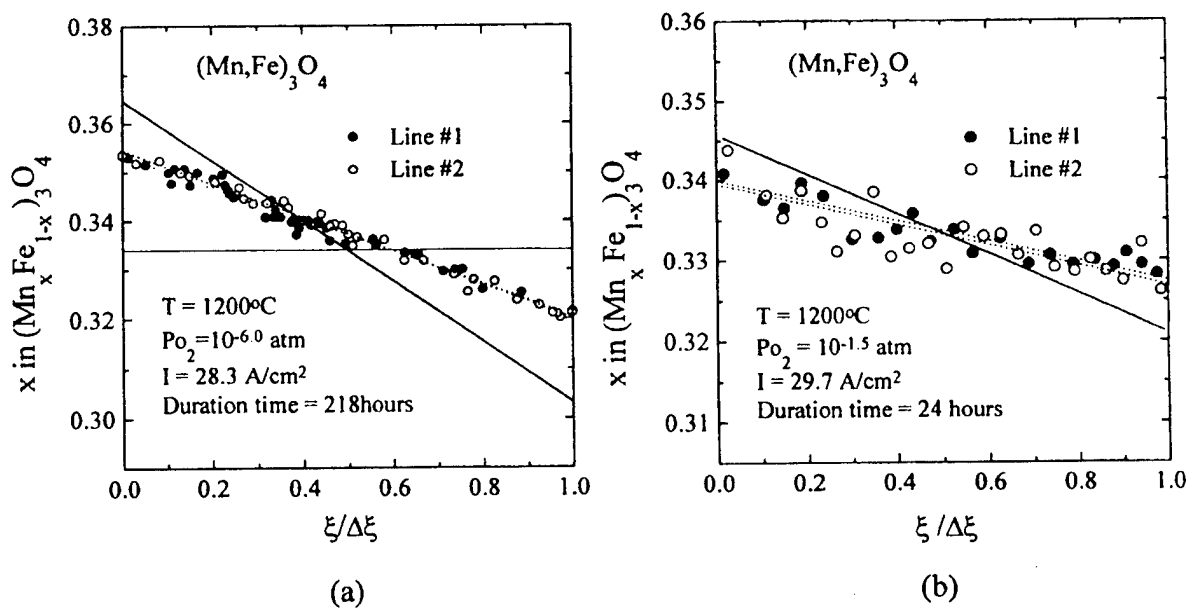


Fig. 2. Composition distributions after demixing at  $1200^\circ\text{C}$ .  $\xi/\Delta\xi$  designates the relative distance from the cathode ( $\xi/\Delta\xi=0$ ) to the anode ( $\xi/\Delta\xi=1$ ). The experimental conditions are (a)  $P_{O_2}=10^{-6.0} \text{ atm}$ ,  $i=28.3 \text{ A/cm}^2$ ,  $t=218 \text{ h}$  and (b)  $P_{O_2}=10^{-1.5} \text{ atm}$ ,  $i=29.7 \text{ A/cm}^2$ ,  $t=24 \text{ h}$ . The solid lines are the expected from the ratio of component diffusivities and the average valence ( $=8/3$ ) of the cations.

## MICRO-SOFC SYSTEM USING BUTANE AND PROPANE FUELS

N.M.Sammes and R.Boersma  
The Department of Technology  
Private Bag 3105, Hamilton,  
New Zealand

Solid oxide fuel cells (SOFC) are efficient all-ceramic electrochemical reactors that convert a fuel, such as hydrogen, directly into electricity without the limitations of the Carnot cycle inherent in traditional thermal-reactor based technologies. The tubular SOFC is the most technologically advanced system and probably the closest to full commercialisation. This is primarily due to the system not requiring a sealant to separate the fuel-gas from the air-gas, as required in the planar design, for example. Recently, a novel tubular SOFC system has been fabricated using an extrusion technique that allowed for a relatively cheap and easy manufacturing route, rather than the very expensive method usually used for the tubular design [1-2]. The other advantage observed in this novel tubular SOFC design, was that of rapid start-up. The electrolyte could be heated to working temperature in a matter of seconds, as compared to several hours usually required for all types of SOFC systems.

This paper describes the use of these novel tubular SOFC systems using alternative fuels such as propane and butane. Single fully stabilised zirconia (FSZ) based cells (2.5mm o.d. and 150 $\mu$ m thickness) were extruded and sintered (1400 °C) using the technique described by Hatchwell *et al.* [3].  $\text{La}_{0.82}\text{Sr}_{0.18}\text{MnO}_3$  (LSM) was used as the cathode outside the tube (with a LSM/FSZ contacting layer), while a conventional Ni/FSZ anode was used inside the tube. 0.25mm silver wire was used as a cathode current collector, and 0.5mm Ni wires were used as an anode current collector.

The open-ended cell was connected to a gas supply at one end, while the other end vented the spent fuel into the atmosphere; the spent fuel was burnt, with a consideration for recycling the heat back into the cell environs.

The single SOFC cells were tested using humidified propane and butane fuels, via an insulated water bubbler. All lines to the SOFC were heated to reduce the loss of water to the SOFC. Results from the humidified gases were compared to those from operation on dry and humidified hydrogen. This paper will describe the results obtained using the gas systems described above (at 900 °C, and a flow rate between 5 – 20 cm<sup>3</sup>/min.), in relation to the steam/carbon ratios examined, and compared to the thermodynamic limits for soot formation. The effect of odourant addition in the gas will also be described, and whether it is necessary to remove these odourants prior to use in the SOFC.

### References

1. I.P. Kilbride, J. Power Sources, **61**, 167 (1996).
2. K. Kendall, and M. Prica, in the First European SOFC Forum, Lucern, Switzerland, U. Bossel (Ed), pps 163-170 (1994).
3. C.E. Hatchwell, N.M. Sammes, and K. Kendall, J. Power Sources, **70**, 85 (1998).

## LOSSES RESULTING FROM IN-PLANE ELECTRICITY CONDUCTION IN A TUBULAR SOLID OXIDE FUEL CELL

R.J.Boersma, N.M.Sammes, and C.J.Fee

Department of Technology, The University of Waikato, Private Bag 3105,  
Hamilton, New Zealand

Solid oxide fuel cells (SOFC) are efficient all-ceramic electrochemical reactors that convert a fuel, such as hydrogen, directly into electricity without the limitations of the Carnot cycle inherent in traditional thermal-reactor based technologies. Recently, a novel tubular SOFC system has been fabricated using an extrusion technique that allows for a relatively cheap and easy manufacturing route, rather than the very expensive vapour deposition technique usually used for the tubular design [1,2]. The other advantage observed in this design was that of rapid start-up. The electrolyte could be heated to working temperature in a matter of seconds, as compared to several hours required for other types of SOFC systems [2].

As opposed to the planar fuel cell, in the tubular system electricity has to be transported over a relatively long distance before connecting to the next cell (figure 1). Consequently, the potential difference between anode and cathode near the gas outlet will have to be greater than near the inlet. This is required to create sufficient electrical potential to drive electrons towards the gas inlet. The paper examines the magnitude of the resulting losses by means of modelling calculations, which are compared with experimental data.

The model is based on an electrical network representation of the fuel cell and consists of resistors parallel to the axis of the cell and perpendicular to the axis of the cell (figure 2). The latter result from electrode polarisation and ionic resistance, while the former result from losses in the current-collecting materials that contact the electrodes. The network equations are substituted in a difference form of the Nernst equation. A differential equation results, which is solved by using the mathematical tool Mathcad<sup>TM</sup>. The results are compared with test results of an experimental tubular fuel cell system (figure 3).

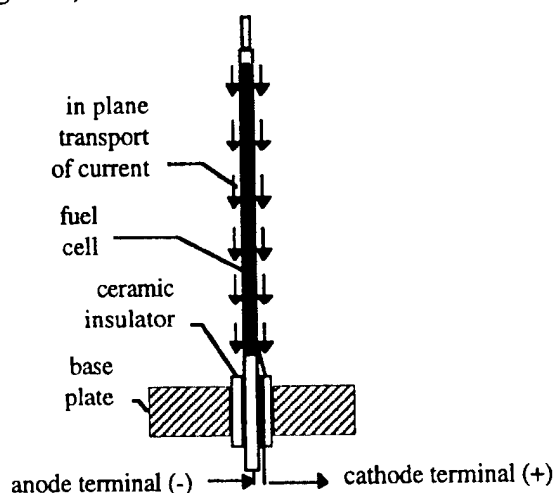


Figure 1. Schematic representation of the fuel cell system. The fuel cell consists of an yttria stabilized zirconia (YSZ) tube, with on the inside with a Ni-YSZ anode, and on the outside a  $\text{La}_{0.82}\text{Sr}_{0.18}\text{MnO}_3$  cathode. The electrical current enters the fuel cell through the anode terminal, which is a wire, that is in contact with the anode. The electrical potential of the current is increased by the fuel cell and current passes along the outside of the tube through a suitable conductor, such as silver [3].

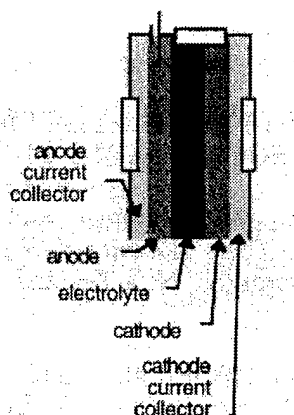


Figure 2. Cross section of the cell and electrical equivalent circuit used to calculate the losses.

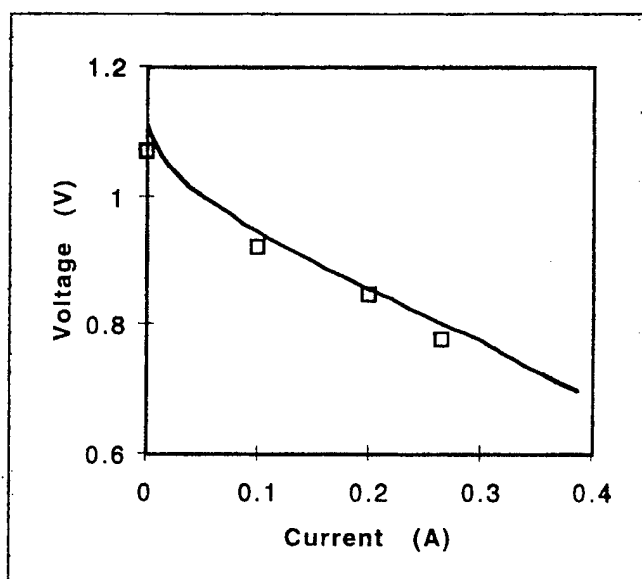


Figure 3. Measured ( $\square$ ) and calculated (—) current-voltage characteristic of a tube of 88 mm length at a hydrogen flow rate of 3.3 ml/min. At 0.7 V the hydrogen utilization is 82%.

## References

- [1] Kendall K., Prica M., First European Solid Oxide Fuel Cell Forum, ed. U.Bossel, Lucerne, Switzerland, 163, (1994).
- [2] Singhal S.C., Proceedings of the 2nd International Symposium On Solid Oxide Fuel Cells, ed. Singhal S.C., Athens, Greece, 25, (1991).
- [3] Boersma R.J., Sammes, N.M., Zhang Y, J.Australasian Cer. Soc., Ed. Sellar J.R., Melbourne, 34, no1, 242, (1998).

## INTERMEDIATE TEMPERATURE FUEL CELLS USING ALKALINE EARTH FLUORIDE-BASED ELECTROLYTES

Bin Zhu<sup>a</sup>, Guangyao Meng<sup>b</sup>, Bengt-Erik Mellander<sup>c</sup><sup>a</sup>Department of Chemical Engineering & Technology, Royal Institute of Technology (KTH), S-100 44 Stockholm, Sweden<sup>b</sup>Department of Materials Science and Engineering, University of Science and Technology of China, 230026 Hefei, Anhui, China<sup>c</sup>Physics and Engineering Physics, Chalmers University of Technology, S-412 96 Göteborg, Sweden

For stationary fuel cell plants, solid oxide fuel cells (SOFC) may in some respects be seen as an ideal source to generate electricity due to its high efficiency, flexibility regarding choice of fuel, and low emissions of greenhouse gases. Therefore, SOFCs are one of the cleanest and most efficient green power sources for the 21st century. However, the high operating temperature (~1000°C) puts very high demands on the materials and technology, this still poses a major challenge for the commercialisation of the current SOFC technology. Therefore, alternative electrolytes that have sufficient ionic conductivity to enable fuel cell (FC) operation at reduced or intermediate temperatures, say 400-800°C need to be developed. Intermediate temperature FCs using proton conducting salts and relevant composites as electrolytes have been studied for nearly a decade [1-3]. Very recently it has been discovered that the fluoride-based electrolytes may be a good candidate to meet the requirement for developing new advanced ceramic FC technology for the intermediate temperature range [4]. Among many fluorides, the alkaline earth fluorides, MF<sub>2</sub> (M = Ca, Ba, Sr) are the more promising. In this paper we report new progress on these fluoride-based materials used as FC electrolytes and related FC applications.

Fuel cells were constructed using alkaline earth fluoride-based materials as electrolytes. Oxides with a layered rock salt structure, e.g., LiNiO<sub>2</sub> and LiCoO<sub>2</sub> were used as anode and cathode for the electrode-supported cells, while Pt (Leitplatin 308A, Hanau, Germany) paste was used for the electrolyte-supported cells. The electrode-supported cells were made by directly pressing anode, electrolyte and cathode as a sandwich in one step, and the cell was then heat-treated at 600°C for 1 hour. The electrolyte-supported cells were made by using a sintered electrolyte disk, about 1.0 mm thick, with Pt paste anode and cathode. In this case the heat-treatment of the complete cell was performed at 600°C for 0.5 hour. Both electrode and electrolyte supported FCs have the following configuration: (H<sub>2</sub> chamber) anode / MF<sub>2</sub>-based electrolyte / cathode (air chamber), the cell size was normally:  $\phi 13 \times 1.0$  to 2.0 mm.

Usually, the electrode supported fuel cells, especially with LiNiO<sub>2</sub> anode, show much better performance than the electrolyte supported cells with Pt paste electrodes. Fig. 1 shows typical I-V characteristics for the anode supported alkaline earth fluoride fuel cells. It can be seen that a current density of 200 mA/cm<sup>2</sup> has been achieved at near 0.4 and 0.6 V respectively for BaF<sub>2</sub>-Al<sub>2</sub>O<sub>3</sub> and NaF-CaF<sub>2</sub>-Al<sub>2</sub>O<sub>3</sub> FCs at 750°C; the CaF<sub>2</sub>-NaF-Al<sub>2</sub>O<sub>3</sub> FC has reached a peak power density of 0.11 W/cm<sup>2</sup> at 250 mAcm<sup>-2</sup>. A fuel cell with the same electrolyte but using Pt electrodes only reached about half of the current densities at the same voltages. The FC polarisation studies showed that the power loss was mainly caused by the electrolyte/electrode interfaces. The interfacial structure between the electrolyte/electrode plays an important role for the performance. These results have only been shown for bulk materials without any technical efforts for obtaining practical devices, e.g., using porous and dense ceramic membrane

technologies to prepare electrode cements and electrolytes; soft-chemistry, e.g., sol-gel and precipitation techniques and nano-technology to prepare bulk materials. Further studies are thus being carried out using these techniques to prepare the cell components and scale up the planar type FCs to large area for practical FC stack devices.

Fluorides have many similarities to oxides, e.g., high melting point (1633K for  $\text{CaF}_2$ ), good mechanical properties, water resistance, relatively good chemical stability, sufficient conductivity, and have also shown a good compatibility among cell components for the studied materials. Therefore, the development of these new systems may directly benefit from the well-developed SOFC technology, and provide opportunities for new advanced ceramic FC technology based on the fluoride systems. Present status, problems, possible solutions and future opportunities for further development will also be discussed.

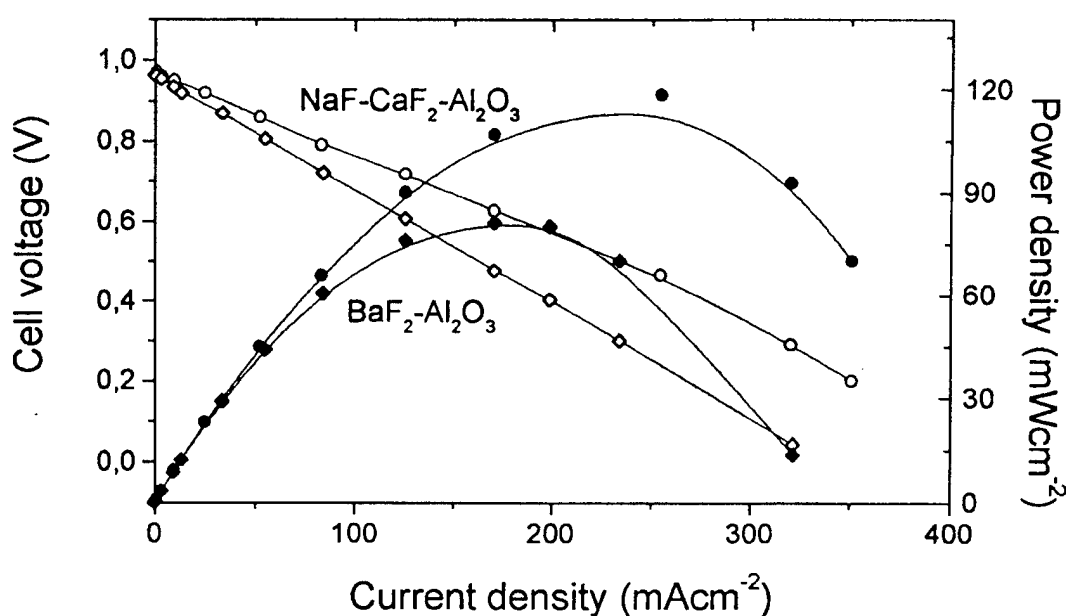


Fig. 1. Typical I-V characteristics for alkaline earth-fluoride based electrolyte FCs at 750°C

## REFERENCES

- [1] B. Heed, B. Zhu, B.-E. Mellander and A. Lundén, *Solid State Ionics*, 46, 121 (1991).
- [2] B. Zhu and B.-E. Mellander, *J. Power Sources*, 52, 289 (1994).
- [3] B. Zhu, *Ionics*, 2, 386 (1996).
- [4] B. Zhu, I. Albinsson, B.-E. Mellander and G.-Y. Meng, "Intermediate temperature proton conducting fuel cells – present experience and future opportunities", presented at "9th International Conference on Solid State Protonic Conductors", August 17-21, 1998, Bled, Slovenia.

---

Corresponding author: Bin Zhu, Department of Chemical Engineering & Technology, Royal Institute of Technology (KTH), S-100 44 Stockholm, Sweden, Tel.: 46-8-7908419, Fax.: 46-8-108579, e-mail: [binzhu@ket.kth.se](mailto:binzhu@ket.kth.se)

## CATHODIC LOSSES IN SOLID OXIDE FUEL CELLS INVESTIGATED BY GEOMETRICALLY DEFINED MICROELECTRODES

V. Brichzin, J. Fleig, K. Sasaki, H.-U. Habermeier and J. Maier

Max-Planck-Institut für Festkörperforschung, Heisenbergstr. 1, 70569 Stuttgart, Germany

$\text{La}_{1-x}\text{Sr}_x\text{MnO}_3$  (LSM) has been receiving much attention for its application as the air-electrode in solid oxide fuel cells (SOFC) using yttria-stabilized zirconia (YSZ) as the electrolyte. Since the electrode performance of an SOFC is often determined by the oxygen reduction reaction that takes place at the cathode side, much research has been focused on the oxygen reduction mechanism at the LSM electrode. It has been concluded that the oxygen reduction occurs at the triple-phase boundary (TPB) of the interface LSM/YSZ/ $\text{O}_2$  and that the reduction mechanism is comprised of a number of serial and/or parallel mechanisms, such as the adsorption and reaction of  $\text{O}_2$  at the LSM surface, surface diffusion of an oxygen species on the LSM surface towards the TPB, bulk diffusion of oxygen through the LSM towards the LSM/YSZ interface and incorporation of oxygen into the YSZ at the TPB.

Despite progress in explaining the oxygen reduction mechanism and its kinetics, many studies suffer from a poor knowledge of the LSM/YSZ interface, especially the contact morphology. Thus, several researchers have tried to gain better control over the properties of the LSM/YSZ interface by either varying the sintering conditions to control the electrode contact area [1, 2] or by using cone-shaped LSM electrodes that are pressed on the YSZ electrolyte [3-5]. However, measurements with such microelectrodes are again subject to uncertainties since the morphology of the LSM/YSZ interface is still unclear.

In this contribution we present measurements on LSM electrodes exhibiting a well-defined structure, geometry and contact area with the YSZ. By using photo-lithographic techniques on a thin laser-ablated film (2000 Å) of LSM deposited on YSZ we were able to create well-defined circular microelectrodes. Figure 1 shows a picture of the LSM electrodes on the YSZ electrolyte. The diameter of the electrodes was varied from 20 µm to 200 µm. These electrodes were investigated employing the set-up shown in Figure 2. By the means of standard electrochemical methods (AC impedance spectroscopy, I-U characteristics) we examined the relationship between polarization impedance and electrode geometries for various temperatures and bias voltages. The experiments and in particular the different dependencies of parts of the spectra on the microelectrode diameter will be discussed in terms of the processes occurring at the LSM electrode for the oxygen reduction mechanism as well as with regard to the role and size of the TPB.

- [1] H. Kamata, A. Hosaka, J. Mizusaki and H. Tagawa, *Solid State Ionics* **106**, 237 (1998)
- [2] F. van Heuveln, H. J. M. Bouwmeester and F. P. F. Berkel, *J. Electrochem. Soc.* **144**, 126 (1997)
- [3] E. Siebert, A. Hammouche and M. Kleitz, *Electrochimica Acta* **40**, 1741 (1995)
- [4] M. Odgaard and E. Skou, *Solid State Ionics* **86-88**, 1217 (1996)
- [5] G. Reinhardt, V. Baitinger and W. Göpel, *Ionics* **1(5 & 6)**, 504 (1995)

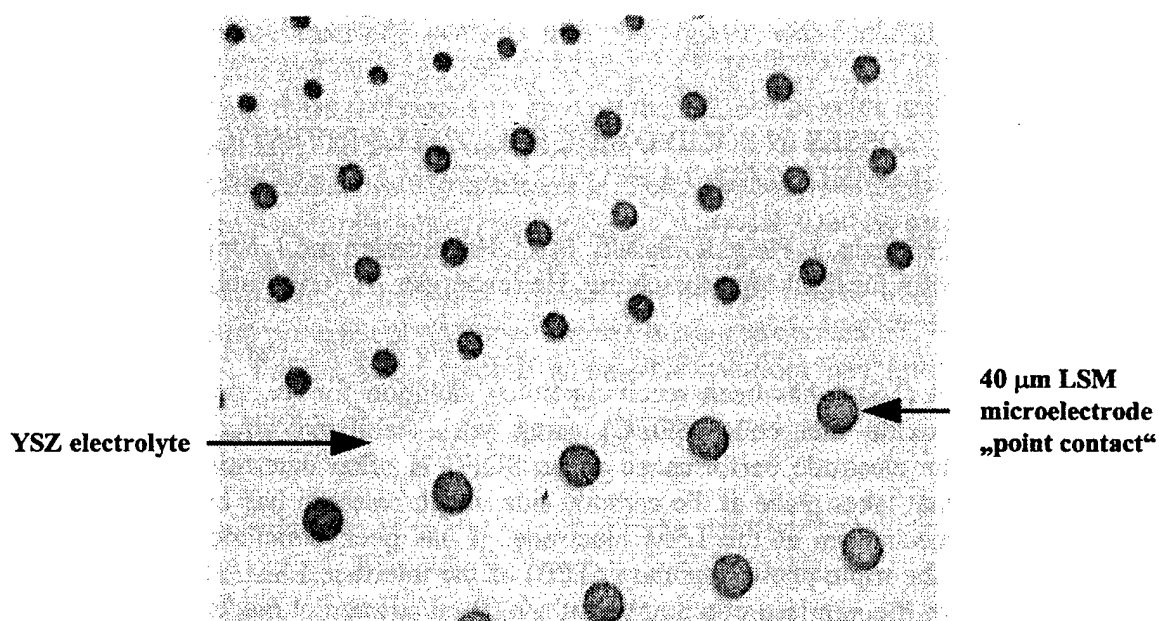


Figure 1: CCD-camera picture of circular LSM „point-contact“ microelectrodes on the YSZ electrolyte

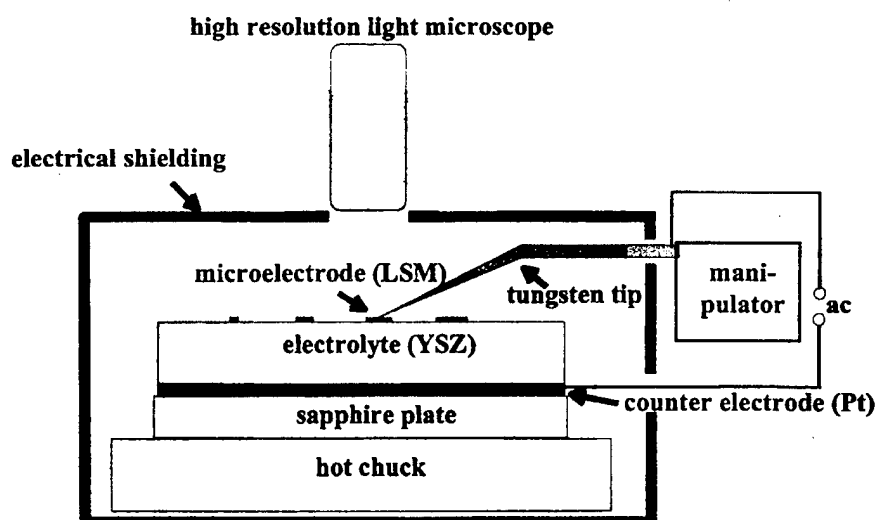


Figure 2: Schematic overview of the instrumental set-up for the microelectrode measurements



DOPED  $\text{Mg}_2\text{TiO}_4$  SPINELS AS POTENTIAL SOFC ANODE MATERIALSD.M. Flot and J.T.S. Irvine

School of Chemistry, University of St-Andrews, St-Andrews, Fife KY16 9ST Scotland

Solid oxide fuel cells are currently at the forefront of research into new generations of energy conversion, owing to their high efficiency and environmentally friendly nature. A major objective is the development of Solid Oxide Fuel Cell (SOFC) anodes capable of operating in natural gas, without suffering from carbon build up due to catalytic cracking and sulfur poisoning like the currently used Ni/ZrO<sub>2</sub> cermet. Alternative anode materials must exhibit a good mixed electronic and oxide conductivity, catalytic activity for the decomposition from natural gas to H<sub>2</sub> and CO<sub>2</sub>, compatibility with solid electrolyte substrate (thermal expansion and interdiffusion value), stability in anode environment including gaseous species (H<sub>2</sub>, H<sub>2</sub>O, CO, CO<sub>2</sub>...); oxides are probably the more promising materials for these applications.

Mixed valence state (Ti<sup>3+</sup>/Ti<sup>4+</sup>) titanates such  $\text{Mg}_2\text{TiO}_4$ - $\text{MgTi}_2\text{O}_4$  spinel [1,2,3,4,],  $\text{Ti}_2\text{O}_3$ - $\text{MgTiO}_3$  geikielite [5] and  $\text{Ti}_3\text{O}_5$ - $\text{MgTi}_2\text{O}_5$  [6,7] pseudobrookite-type are proposed as possible candidate oxides for SOFC anodes. They exhibit high electronic conductivities at low pO<sub>2</sub> but they are synthesized under reducing conditions and only stable at low pO<sub>2</sub> (less than 10<sup>-17</sup> atm for  $\text{Mg}_2\text{Ti}_{0.9}\text{Nb}_{0.1}\text{O}_4$  [2]) and, so, hardly useable as SOFC anodes. So, the present studies are concerned with the effect of doping by Mn, Fe and Co on the electrical conductivity of the magnesium titanate spinel  $\text{Mg}_2\text{TiO}_4$  compounds synthesized in air and their applicability as SOFC anode materials.

Three different series of compounds have been studied with substitution of only one cation ( $\text{Mg}_{2-x}\text{M}_x\text{TiO}_4$ ,  $\text{Mg}_2\text{Ti}_{1-x}\text{M}_x\text{O}_4$ ) or both cations ( $\text{Mg}_{2-x}\text{Ti}_{1-y}\text{M}_{x+y}\text{O}_4$ ) with different transition elements (Mn, Fe, Co) and compositions ( $0.1 \leq x \leq 0.6$ ) and their electrical properties have been studied. High DC conductivities, using the four points technique, have been measured in reducing atmosphere (5% H<sub>2</sub>/95 %Ar). AC conductivities have been measured in air or different atmospheres and at different temperatures. Phase stability has been studied

under reducing atmospheres. A low content of substitution does not significantly improve the conductivity in air ( $\sigma_{930^\circ\text{C}} = 2.9 \cdot 10^{-5} \text{ S.cm}^{-1}$  for  $\text{Mg}_{1.9}\text{Mn}_{0.1}\text{TiO}_4$ ,  $7.4 \cdot 10^{-6} \text{ S.cm}^{-1}$  for  $\text{Mg}_{1.9}\text{Fe}_{0.1}\text{TiO}_4$  and  $8.4 \cdot 10^{-6} \text{ S.cm}^{-1}$  for  $\text{Mg}_{1.9}\text{Co}_{0.1}\text{TiO}_4$ ) but the increase of the dopant can increase the air conductivity as for the  $\text{Mg}_{2-x}\text{Mn}_x\text{TiO}_4$  series ( $\sigma_{930^\circ\text{C}} \cong 2.6 \cdot 10^{-3} \text{ S.cm}^{-1}$  for the initial composition  $\text{Mg}_{1.6}\text{Mn}_{0.4}\text{TiO}_4$ ).

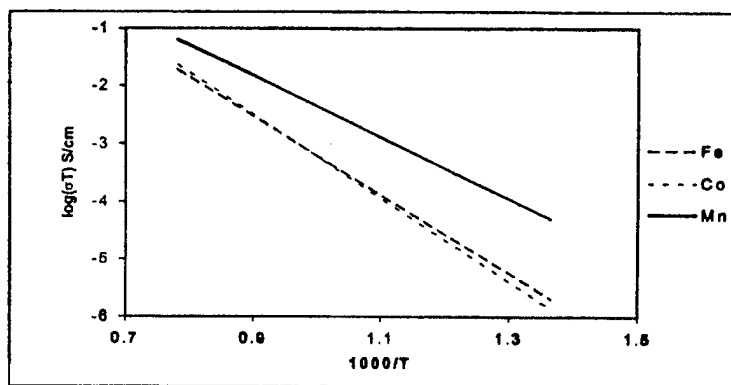


Fig 1:  $\log(\sigma T) = f(1000/T)$  plot for  $\text{Mg}_{1.9}\text{M}_{0.1}\text{TiO}_4$  ( $M = \text{Mn, Fe, Co}$ )

DC measurements shown that the different compounds exhibit a n-type conductivity in very low oxygen partial pressures. Typically, values of  $10^{-2} \text{ S.cm}^{-1}$  were reached at oxygen partial pressure  $p(\text{O}_2)$  at the order of  $10^{-19} \text{ atm}$  for  $\text{Mg}_{1.9}\text{M}_{0.1}\text{TiO}_4$  ( $M = \text{Mn, Fe, Co}$ ) as well for  $\text{Mg}_2\text{Ti}_{0.9}\text{M}_{0.1}\text{O}_4$  ( $M = \text{Mn, Fe, Co}$ ) and for the  $\text{Mg}_{2-x}\text{Mn}_x\text{TiO}_4$  series.

- [1] T.J. Cogle, C.A.S. Mateus, J.H. Binks and J.T.S. Irvine, *J. Mater. Chem*, **1**, 289 (1991).
- [2] H.-J. Steiner, P.H. Middleton and B.C.H. Steele, *J. Alloys Comp.*, **190**, 279-285 (1993).
- [3] A. Feltz and M. Steinbrück, *J. less-Common Met.*, **167**, 233 (1991).
- [4] D.P. Fagg, S.M. Fray and J.T.S. Irvine, *Solid State Ionics*, **72**, 235-239 (1994).
- [5] M. Steinbrück and A. Feltz, *Z. anorg. allg. Chem.*, **590**, 137 (1990).
- [6] M. Steinbrück and A. Feltz, *Z. anorg. allg. Chem.*, **594**, 157 (1990).
- [7] H.-J. Steiner, X. Turillas and B.C.H. Steele, *J. Mater. Chem*, **2**(12), 1249 (1992).

## DEFECT PROPERTIES AND ION MIGRATION IN THE $\text{LaGaO}_3$ - BASED OXYGEN ION CONDUCTOR

**M. Saiful Islam and M. Sakib Khan**

*Department of Chemistry, University of Surrey, Guildford, GU2 5XH, UK*

*E-mail: m.islam@surrey.ac.uk*

Computer modelling techniques are now well established tools for probing structural properties and transport mechanisms in solid state ionic materials. This presentation will highlight recent modelling work on the defect and transport properties of the  $\text{LaGaO}_3$  perovskite, which is attracting much attention as an oxygen-ion conductor competitive with yttria-stabilised zirconia. We first consider a range of cation dopant substitutions with oxygen vacancy compensation. Favourable acceptor-dopants (on energetic grounds) are predicted to be Sr at La and Mg at Ga, in accord with experimental work that finds the highest ionic conductivity in the  $(\text{La}, \text{Sr})(\text{Ga}, \text{Mg})\text{O}_{3-\delta}$  system.

Oxygen vacancy migration is along the  $\text{GaO}_6$  octahedron edge with a curved trajectory and a calculated migration energy of 0.73eV. The formation of dopant-vacancy clusters is examined and may be related to the higher activation energies at higher dopant concentrations. We have also examined cation vacancy transport which reveals high migration energies ( $> 4\text{eV}$ ) and confirms the much slower diffusion rates in comparison to oxygen. Consideration of water incorporation suggests that proton conduction will not be significant in this material. We have recently examined dopant substitution of transition metal ions (e.g. Cr, Fe, Co, Cu) which may be effective in promoting mixed (ionic/electronic) conduction.

M.S. Khan et al., *J. Phys. Chem. B* **102**, 3099 (1998)

## AN INVESTIGATION INTO THE USE OF Sr/Fe DOPED LaCoO<sub>3</sub> AS ANODES IN SOFC'S

M. Weston and I.S. Metcalfe\*

School of Chemical Engineering, University of Edinburgh,  
Mayfield Road, Edinburgh, EH9 3JL, UK

\* tel: +44 131 6508553, fax: +44 131 6506551, email: i.metcalfe@ed.ac.uk

### Summary

A chosen sample of perovskites from the La<sub>(1-x)</sub>Sr<sub>x</sub>Co<sub>(1-y)</sub>Fe<sub>y</sub>O<sub>3</sub> family were examined using TP (temperature programmed) and electrochemical techniques for use as alternative anodes in SOFCs using direct methane oxidation. Activity for methane oxidation, redox behaviour and the susceptibility towards deactivation by carbon deposits were primarily investigated. Over the temperature range 600-800°C the perovskites exhibited comparable catalytic activity with the standard Ni/YSZ cermet but showed significant reduction in deactivation through the formation of carbon.

### Introduction

There is much continuing interest in developing anode materials for use in SOFCs (solid oxide fuel cells) that can operate effectively on methane feeds without the necessity for an expensive endothermic steam reforming stage to produce hydrogen fuel. The Ni based cermets that are currently used are highly susceptible to deactivation by the formation of carbonaceous species on the surface of the catalyst. Previous research has shown that certain oxide materials may be more suitable for use as anodes under these conditions [1].

Traditional catalysts for methane combustion are supported noble metal catalysts that activate both the methane C-H and the oxygen O-O bonds and exhibit high activity at temperatures as low as 350°C. However their use in this situation is hampered by the relatively high volatility of the oxides, the ease of sintering at elevated temperatures and their cost. It is for these reasons that much effort has been directed to the substitution of the noble metal catalysts with mixtures of selected metal oxides. Perovskite-like mixed oxides (ABO<sub>3</sub>) have been repeatedly shown to be excellent catalysts for oxidation of light hydrocarbons and, in particular, of methane [2,3]. These materials can be modified by changing either the A-site or the B-site metal ion to give a wide range of catalytic activity. A further degree of catalytic fine-tuning is available through partial substitution at either site with another metal cation to produce a large family of similarly catalytic materials. This fine-tuning can strongly effect catalytic activity due to stabilisation of unusual oxidation states of the B site ion and by creation of a number of catalytically active structural defects.

This paper details the results of experiments carried out to determine the suitability of the perovskite material LaSrCoFeO<sub>3</sub> (LSCF) for use as an anode material in direct methane SOFC's.

### *Experimental*

In these experiments different  $\text{La}_{(1-x)}\text{Sr}_x\text{Co}_{(1-y)}\text{Fe}_y\text{O}_3$  perovskites were obtained ( $x/y = 0.4/0.8, 0.2/0.8, 0.8/0.2$ ), via either a commercial pyrolysis route or from solid state reaction of the precursors. These samples were tested under anodic conditions as detailed below.

Experiments were undertaken to generate kinetic data enabling easy comparison between the perovskites and the literature. The experiments mainly used temperature programmed techniques where the temperature of a catalytic reactor is slowly changed and its contents continually analysed by mass spectrometry. The studies followed the format prescribed below -

- 1) Pre-treatment – the sample was exposed to either an oxidising ( $\text{O}_2$ ), reducing ( $\text{H}_2$ ) or neutral (He) atmosphere, at a given temperature, to clean the catalyst of any possible contamination and provide a uniform starting condition for each material.
- 2) Reaction (TPRx) – the sample was exposed to the reaction gas which contained a mixture of  $\text{CH}_4$ ,  $\text{O}_2$  and  $\text{H}_2\text{O}$ . In some cases the temperature was held steady for some time to examine the long-term effects of exposure.
- 3) Oxidation (TPO) – the formation of any carbon species was indicated by the oxidation of the surface to produce  $\text{CO}_2$

Varying the gas mixture in these experiments was used to elucidate the effect of  $\text{H}_2\text{O}$  concentration on the kinetics of the reforming reaction and in general allowed the quantification of the selectivities and overall reactivity as a function of conditions. Information on the adsorption/desorption properties of the perovskites was obtained by TPD experiments

The performance of the perovskites was analysed to determine the best candidate for anodic studies, with major emphasis placed on catalytic activity, resistance to carbon deposition, and material stability. The best performer was incorporated into a test fuel cell and its electrochemical characteristics examined.

The results from these experiments and their comparison with the standard Ni/YSZ material will be discussed.

- [1] R.T. Baker, I. Metcalfe, Ind. Eng. Chem. Res., 34 [5] (1995) 1558
- [2] U. Balachandran, J.T. Dusck, R.L. Mieville, R.B. Poeppel, M.S. Kleefisch, S. Pei, T.P. Kobylinski, C.A. Udovich, A.C. Bose, Applied Catalysis A, 133 (1995) 19-29
- [3] L. Marchetti, L. Forni, Applied Catalysis B, 15 (1998) 179-187

## BORATE DOPED YTTRIA STABILISED ZIRCONIA AS A POTENTIAL SOFC ELECTROLYTE

Jeremy Dobson and John Irvine

University of St. Andrews, School of Chemistry  
St. Andrews, Fife, KY16 9ST, U.K.

Yttria-stabilised zirconia (YSZ) has been extensively investigated as a component for solid oxide fuels cells (SOFCs). First generation SOFC electrolytes are likely to be 8 mole percent YSZ, although 8.5 % may be more suitable, due to its improved resistance to ageing.

Doping YSZ on the metal site has been extensively investigated, however relatively little work has been done on other methods of doping. Replacement of the oxygen with a molecular ion such as borate ( $\text{BO}_3^{3-}$ ) is an interesting possibility. In this study, phase formation in the  $\text{Y}_2\text{O}_3\text{-ZrO}_2\text{-B}_2\text{O}_3$  system has been investigated as a possible alternative electrolyte material.

Synthesis of these compounds has been difficult due to the loss of borate at the high (1350-1500°C) temperatures required for solid state synthesis, however these have been worked round through the use of sol-gel routes and the use of sacrificial powders.

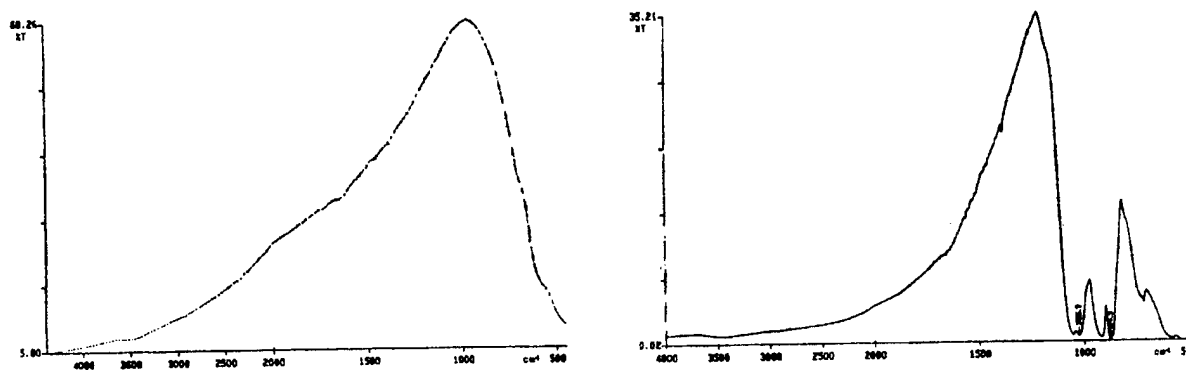


Figure 1

Comparison of the Infra Red patterns of standard YSZ (left) and YSZ doped with borate (right), showing the large peaks attributable to the borate.

In figures 1 and 2 we compare the Infra-Red spectrum and the XRD powder patterns for  $\text{Y}_{0.25}\text{Zr}_{0.75}\text{O}_{1.875}$  and  $\text{Y}_{0.25}\text{Zr}_{0.75}\text{B}_{0.1}\text{O}_{1.725}$ . The Infra-Red spectrum for the system clearly show the presence of B-O stretches in the  $800\text{-}1000\text{ cm}^{-1}$  region whilst the XRD patterns for both samples are clearly single phase fluorite.

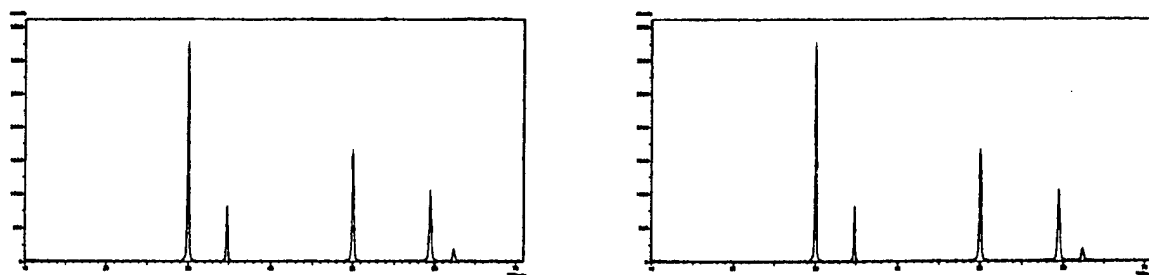


Figure 2

Comparison of the XRD patterns of standard YSZ (left) and YSZ doped with borate (right).

Results will be presented to show the extent of borate solubility in the yttria-zirconia system and data on various  $\text{Y}_2\text{O}_3\text{-ZrO}_2\text{-B}_2\text{O}_3$  systems will be presented and discussed, with reference to their electrical properties and potential SOFC applications. This will include data from a variety of techniques including XRF,  $^{11}\text{B}$  NMR, EXAFS, differential weight analysis and AC Impedance.

TETRAGONAL TUNGSTEN BRONZE TYPE PHASES (COMPOSITION):  
MATERIAL CHARACTERISATION AND PERFORMANCE AS SOFC ANODES

\*A. Kaiser, \*J. Bradley, \*\*P.R. Slater, \*J.T.S Irvine

\* University of St. Andrews, School of Chemistry, St. Andrews, Fife KY16 9AJ, UK

\*\* University of Surrey, Department of Chemistry, Guildford, Surrey. GU2 5XH

**Abstract**

Solid oxide fuel cells (SOFC) are energy converters, which can directly transform the chemically stored energy of combustible gases with very high efficiency into electrochemical energy by oxidation. Currently the favored anode is based on a Ni/YSZ cermet. This is the most investigated SOFC anode system at the moment, but it has several disadvantages. Ni/YSZ anodes require the use of H<sub>2</sub> or H<sub>2</sub>-CO mixtures. The Cermet itself has a relative high thermal expansion coefficient (TEC) compared to the currently used electrolytes, based on yttria stabilized zirconia. During long-term operation at 900-1000°C the cermet performance can be negatively effected by a change of the electronic conducting nickel pathways in the microstructure. Hydrocarbons like methane (CH<sub>4</sub>), which are highly available for example in natural gas and which are less expensive, can only be used after conversion to H<sub>2</sub> and CO by an external reforming process. The external reforming step is currently necessary, because in internal reforming the Ni-YSZ cermet suffers from carbon build up and sulfur poisoning. On the other hand external reforming causes additional expenses and a reduction of the overall efficiency of the system.

We focussed our work on the investigation of new oxide materials, specifically mixed conducting materials. These oxides are promising candidates for the direct oxidation of hydrocarbons, because they are less likely to promote coking or to suffer from sulfur poisoning. Slater et al. [1,2] showed in previous work that tetragonal tungsten bronze type phases with the general structures A<sub>0.6</sub>BO<sub>3</sub> are interesting materials for the use as anode materials.

In this paper, we report some further important material properties for an SOFC anode based on the system (Sr<sub>1-x</sub>Ba<sub>x</sub>)<sub>0.6</sub>Ti<sub>0.2</sub>Nb<sub>0.8</sub>O<sub>3</sub>, including thermal expansion coefficients and ionic conductivity. Additionally the electrochemical performances of these materials were tested in half-cell configurations.

The total conductivity of dense pellet samples were measured in different oxygen partial pressure atmosphere using the four probe dc technique at a temperature of 930°C. The pellets were reduced in situ under flowing H<sub>2</sub>-Ar and subsequently re-oxidised by leaking oxygen into the ceramic tube. The conductivity  $\sigma T$  was followed as a function of oxygen partial pressure (measured by an oxygen sensor). The system (Sr<sub>1-x</sub>Ba<sub>x</sub>)<sub>0.6</sub>Ti<sub>0.2</sub>Nb<sub>0.8</sub>O<sub>3</sub> showed a good conductivity of more than 5 S cm<sup>-1</sup> in low oxygen partial pressures ( $p(O_2)=10^{-20}$  atm).

The anode reactions were investigated from voltage-current density (V-I) and impedance measurements on single cells with the structure tungsten bronze based anode (H<sub>2</sub>-Ar)/YSZ/Pt (air) electrode. Additionally impedance measurements were performed on symmetrical single cells (anode/YSZ/anode) in H<sub>2</sub>/Ar. For the preparation of the cells 0.3 mm electrolytes (CeramTec AG) were used. The anodes with an area of 2 cm<sup>2</sup> were screen printed onto the electrolytes after the ceramic powders based on the tungsten bronzes were mixed with a binder by a short ball milling step.

The I-V curves show a steep drop of the cell voltage at low current densities between 0.01 A cm<sup>-2</sup> and 0.1 A cm<sup>-2</sup>. A diffusion limited process is indicated by a Warburg-type spike in the AC impedance spectra. The reason for this behavior is believed to be a low oxygen ion conductivity of the tungsten bronze anode, which limits the diffusion of oxygen ions from the



electrolyte into the anode (or into the three phase boundary, TBP). Additionally an increasing overpotential of the cells with increasing current density is due to an intrinsic decrease of the electronic part of the conductivity of the tungsten bronze anode material at lower cell voltages (more oxidising conditions).

#### Literature

- [1] P.R. Slater and J.T.S. Irvine, "Niobium based Tetragonal Tungsten bronzes as potential anodes for solid oxide fuel cells: Synthesis and Electrical Characterisation", Solid State Ionics, in press.
- [2] P.R. Slater and J.T.S. Irvine, "Synthesis and electrical characterisation of the tetragonal tungsten bronze type phases,  $(\text{Ba/Sr/Ca/La})_{0.6}\text{M}_x\text{Nb}_{x-1}\text{O}_{3-\delta}$  (M=Mg, Ni, Mn, Cr, Fe, In, Sn): evaluation as potential anode materials for solid oxide fuel cells, submitted to Solid State Ionics.

## INFLUENCE OF ISOSTATIC PRESSING ON DENSIFICATION AND MICROSTRUCTURE OF TAPE CASTING YSZ MEMBRANES

Ming Chen, Ting-Lian Wen and Zhi-Yi Lu

Shanghai Institute of Ceramics, Chinese Academy of Sciences,  
200050 Shanghai, China, tlwen@sum.shcnc.ac.cn

Tape casting is a low-cost process for making large-area, thin flat ceramic parts. It has been largely used to fabricate ceramic capacitors and zirconia electrolyte membranes for planar SOFC. However, the density of sintered tape is not very high because of the pressureless sintering and low green density. Normally the relative density of YSZ sintered tape can reach about 90% and it is difficult to get higher than 95%. And the sintering dynamics of the tape are needed to be further studied.

We investigated the effects of each component of the casting slurry such as solvents, binders and plasticizers on the density of green and sintered tape as well as their microstructures. It was found that the fewer the solvents was added into the slurry, the higher was the density of sintered tape and the less the diameter of pore. Nevertheless there is an appropriate content of binder and plasticizers in the slurry to get the highest sintering density. The weight of porous  $\text{ZrO}_2$  plate which was loaded on the tape during sintering was important for getting a flat YSZ tape.

A novel technique that combined tape casting and isostatic pressing was used to fabricate YSZ membranes. In the present work, the density measurement results showed that the isostatic pressing can raise the density of green tape by 8~11% and the relative density of as-sintered tape by 5~10%. The pore diameter and distribution in green tape also become more homogeneous. The SEM photographs (Fig. 1) have shown that after being isostatically pressed, the sintered tape becomes much denser and the diameter of pores contracts much smaller. The combined forming technique was not complicated and could be used for a scale fabrication of large-area ceramic tape.

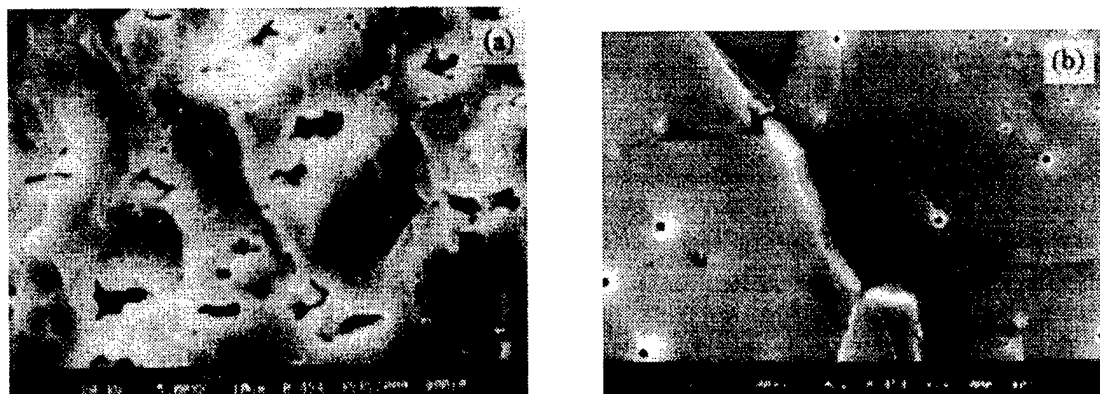


Fig. 1. SEM photographs of fracture section of as-sintered tape (sintered at 1550°C)  
(a) without isostatic pressing, (b) with isostatic pressing at 200MPa

## STUDY OF TAPE-CASTING YSZ MEMBRANES REINFORCED BY ALUMINA FIBER

Ming Chen, Ting-Lian Wen and Zhi-Yi Lu

Shanghai Institute of Ceramics, Chinese Academy of Sciences,  
200050 Shanghai, China, tlwen@sum.shcnc.ac.cn

Tape casting is known as an inexpensive technique for making thin flat and large area ceramic membranes. It has commonly been used to fabricate zirconia electrolyte membranes for planar SOFC. But when the thickness of sintered tape is below 200  $\mu\text{m}$ , the tape is very fragile. In this work, two kinds of alumina fibers were added into the tape in order to improve the strength of tape. The density and electrical conductivity as well as strength of sintered tape were studied.

The preparation procedures of YSZ green tape reinforced by  $\text{Al}_2\text{O}_3$  fiber consisted of the following steps. Firstly, YSZ powder, solvents and dispersant were put together to mix for 24 hours to form a slurry. Then, binder and plasticizers were added into the slurry to mix for 24 hours. Finally, the alumina fiber was added into the slurry and milling for another 12-hour. Thus the slurry was ready for tape casting. The green tape was obtained after the evaporation of solvent. The sintering was carried in air at 1550°C for 5 hours.

The density of sintered tape was assessed by Archimedes method. The microstructure of green and sintered tape were observed by Scanning Electronic Microscope (SEM). The conductivity of sintered tape was measured by using complex impedance technique. The strengths of green and sintered tape were also tested.

The results showed that the suitable milling time and appropriate viscosity of the casting slurry were important for achieving a uniform dispersion of the  $\text{Al}_2\text{O}_3$  fiber in the YSZ matrix. The bunch-like fiber was much easier to disperse in the slurry than the cotton-like fiber. The strengths of green and sintered tape were improved. As shown in Fig. 1, there is an obvious fiber pulling-out at the fracture section of green and sintered tape indicating that  $\text{Al}_2\text{O}_3$  fiber reinforces the tape. The complex impedance plots showed that the conductivity of sintered tape reinforced by alumina fiber was slightly lower than that without alumina fiber. The addition of alumina fiber had a tiny effect on the density of sintered tape.

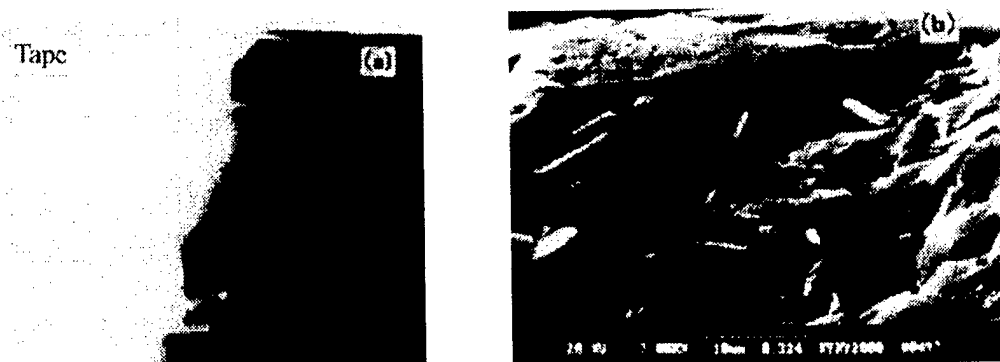


Fig.1. SEM photographs of fracture section of YSZ tape.  
(a) green tape, (b) sintered tape

LOW FREQUENCY IMPEDANCE BEHAVIOR  
OF STRONTIUM DOPED LANTHANUM COBALTITE

A. Ringuedé, J. Guindet, J. Fouletier

Laboratoire d'Electrochimie et de Physico-chimie des Matériaux et des Interfaces  
(INPG,UJF and CNRS)Domaine Universitaire - 1130 rue de la piscine, B.P. 75  
38402 Saint Martin d'Hères cédex (France)

Due to of its high chemical reactivity with Ytria Stabilized Zirconia (YSZ) at high temperature [1], doped lanthanum cobaltite could not be used as cathode material in Solid Oxide Fuel Cells (SOFC). However, due to its very good electrocatalytic activity [2], it can be considered as an alternative cathode material in intermediate temperature fuel cells. Recent works have demonstrated the interest of using electrodes whose reactions are limited by the oxygen diffusion through the oxide layer [3]. High current density could be obtained with duplex layer structure, i.e., a thin and dense layer deposited onto the electrolyte surface, covered by a thick and porous layer.

This work presents results obtained with a thin (0.35  $\mu\text{m}$ ) and dense (100 %) layer of  $\text{La}_{0.7}\text{Sr}_{0.3}\text{CoO}_{3-\delta}$  deposited by RF sputtering on YSZ. The investigations were carried out as a function of temperature (300 - 530°C) and oxygen partial pressure ( $0.21 - 2 \times 10^{-5}$  bar) by impedance spectroscopy at equilibrium using an Autolab Ecochimie Frequency Response Analyzer (10 kHz - 1 mHz). Impedance diagrams were deconvoluted into two loops characterizing of the electrode polarization. The high frequency component has been previously attributed to the electrode morphology. The low frequency component is the subject of this study.

Depending on the oxygen partial pressure, the low frequency loop can be described either as a finite Warburg element or as a semi-circle.

Figure 1 shows the variation of the low frequency resistance as a function of the oxygen partial pressure.

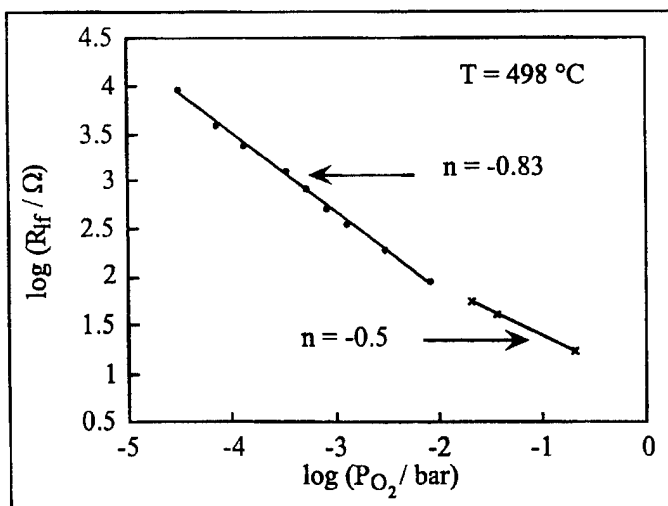


Figure 1 : Variation of low frequency resistance at  $T = 498^\circ\text{C}$  as a function of oxygen partial pressure.

Two oxygen pressure domains observed:

- for oxygen partial pressure lower than  $6 \times 10^{-3}$  bar, the low frequency component can be described by a semi-circle. The resistance, referred to as  $R_{lf}$ , varies according to a  $P_{O_2}^{-0.83}$  law,
- for oxygen partial pressure higher than  $6 \times 10^{-3}$  bar, the low frequency phenomenon is described by a finite diffusion element. The associated resistance varies as  $P_{O_2}^{-0.5}$ .

As shown in fig. 2, two temperature domains can be observed from the Arrhenius plot of the low frequency:

- at temperature higher than 480 °C the activation energy is 1.42 eV,
- at temperature lower than 480 °C, the activation energy is 0.71 eV.

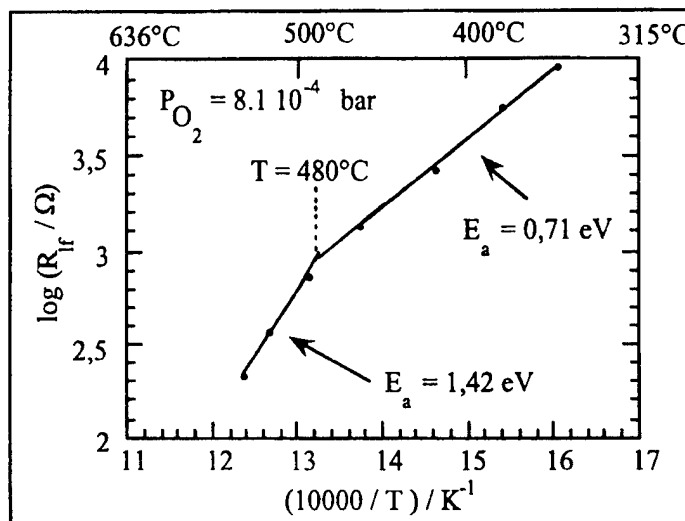


Figure 2 :Arrhenius plot of the low frequency resistance versus temperature at  $P_{O_2} = 8.1 \times 10^{-4}$  bar .

It should be pointed out that the low frequency loop was always deconvoluted into one semi-circle.

The results are interpreted according to the reaction paths described as below (see fig. 3): a finite diffusion element in serie with two different adsorption mechanisms in parallel, i.e., a molecular adsorption or a dissociative adsorption.

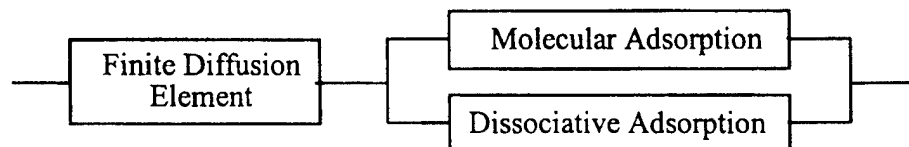


Figure 3: Schematic reaction scheme

#### References.

- [1] F.M. Figueiredo, J.A. Labrincha, J.R. Frade and F.M.B. Marques, Solid State Ionics, **101**, 343 (1997).
- [2] Y. Takeda, R. Kanno, M. Noda and O. Yamamoto, J. Electrochem. Soc., **11**, 2656 (1987)
- [3] M. Kleitz and F. Petibon, Solid State Ionics, **92**, 65 (1996).

## **ELECTROCHEMICAL CHARACTERIZATION OF CERAMIC METALLIC CONDUCTORS FOR FUEL CELL APPLICATIONS: DMFC AND PEMFC**

A. Martínez, L. Sánchez, P. Recio, C. Pascual, J.R. Jurado.

*Instituto de Cerámica y Vidrio, CSIC., Arganda del Rey, 28500 Madrid, Spain.*

The constant evolution that DMFCs and PEMFCs electrochemical devices suffer nowadays imply several demands, attending to economic and operative reasons. Concerning to the electrodes, a drastic Pt load reduction up to  $0.3 \text{ mg/cm}^2$ , even less, is currently the common objective, alternatives like the partial or total Pt replacement, by other electrocatalysts are considered a challenge.

Performance of polymer electrolyte fuel cells using ceramic compounds as electrodes with or without Pt load is studied in this work. Most of the transition metal perovskite oxides  $\text{LaNiO}_3$ ,  $(\text{La}, \text{Sm})\text{CoO}_3$ , and  $\text{Sr}(\text{Pt}, \text{Ru}, \text{Pd})\text{O}_3$ , which have been selected as suitable materials for this experience, are metallic conductors and some present metallic-semiconductor transitions.

Although there are many incentives to develop fuel cells which directly oxidise methanol as the fuel, but they show short term performance efficiency due to poisoning effects in precious metal anode electrocatalysts by methanol oxidation intermediates.

Development of direct methanol fuel cells (DMFC) makes necessary partial or total substitution of Pt in the electrodes. High specific surface area perovskite electrocatalysts, which can incorporate very small metallic particle ( $\text{Pt}, \text{Pd}, \text{Ru}$ ) in their structure, seems to be a good alternative because of their high catalytic activity towards promoting direct fuel oxidation avoiding poisoning effects. The electrical properties of these materials also play an important role in the cell performance. Their study, in connection with both Band Theory (correlation between electronic structure and their electroactive characteristics), and material microstructure will allow to design compositions with optimum properties for this kind of application.

Two different synthesis methods: Sol-gel and Combustion Synthesis are involved to prepare the corresponding inks and build up the membrane electrode assembly (MEAS). A 3 nm average particle size was achieved, then crystalline and amorphous phases were detected. In this work is described the preparation and electrical characterization of MEAS incorporating these electrocatalysts. The study of the behaviour of this cell is carried out by the Complex Impedance Spectroscopy method in addition with the characterisation of the Nafion type polymer electrolyte membrane conductivity by the four probe technique, and the different interface contributions to the properties of the cell using I-V characteristic and polarisation curves.

### **TOPIC B. POSTER**

## CHEMICAL REACTIVITY OF PEROVSKITE OXIDE SOFC CATHODES AND YTTRIA STABILIZED ZIRCONIA

G. Ch. Kostogloudis, G. Tsiniarakis and Ch. Ftikos

*Lab. of Inorganic Materials Technology, Department of Chemical Engineering, National  
Technical University of Athens, 9 Heroon Polytechniou Str., Zografou Campus, GR-157 80,  
Athens, Greece*

A requirement of crucial importance for the successful operation of solid oxide fuel cell (SOFC) is the thermodynamic stability of the cathode with respect to the electrolyte [1]. In the present study results are reported on the reactivity of various perovskite oxide cathodes and yttria stabilized zirconia (YSZ) solid electrolyte. The cathode materials that were examined belong to the systems  $\text{La}_{1-x}\text{Sr}_x\text{Co}_{0.2}\text{Mn}_{0.8}\text{O}_{3-\delta}$ ,  $\text{La}_{1-x}\text{Sr}_x\text{Co}_{0.2}\text{Fe}_{0.8}\text{O}_{3-\delta}$ ,  $\text{La}_{1-x}\text{Ca}_x\text{Co}_{0.2}\text{Fe}_{0.8}\text{O}_{3-\delta}$  ( $0 \leq x \leq 0.5$ ), and also to the A-site deficient systems  $\text{La}_{0.6-z}\text{Sr}_{0.4}\text{Co}_{0.2}\text{Fe}_{0.8}\text{O}_{3-\delta}$ ,  $\text{La}_{0.6}\text{Sr}_{0.4-z}\text{Co}_{0.2}\text{Fe}_{0.8}\text{O}_{3-\delta}$  and  $(\text{La}_{0.6}\text{Sr}_{0.4})_{1-z}\text{Co}_{0.2}\text{Fe}_{0.8}\text{O}_{3-\delta}$  ( $z=0, 0.05, 0.1, 0.2$ ).

The perovskite oxide powders were prepared by the amorphous citrate process. After calcination at 1100°C, all samples were single phase, according to their X-ray diffraction (XRD) patterns. The powders were ball-milled in acetone to obtain sub micron grain size. Equimolar amounts of perovskite and commercial YSZ (Alfa) powders were thoroughly mixed in an agate mortar using acetone. The mixtures were pressed into pellets and heated at 1100°C for 120 h in air. The sintered samples were crushed in a mortar, mixed with Si-powder, and examined by (XRD) to identify the formation of any reaction products. Si served as an internal standard for d-value calibration during the determination of the lattice parameter of cubic YSZ. It was expected that a shift in the lattice parameter of YSZ would occur, due to diffusion of cations from the perovskite into the YSZ lattice.

The main products formed were  $\text{La}_2\text{Zr}_2\text{O}_7$  for the undoped compounds or for low dopant concentration, and  $\text{SrZrO}_3$  or  $\text{CaZrO}_3$  at higher concentrations of Sr- or Ca-dopant cations, respectively. The Sr-doped compounds react at a higher rate than the Ca-doped ones. Moreover, higher concentration of reaction products was found in the case of perovskites containing Fe than those containing Mn at the B-site. The A-site deficiency of the Fe-containing perovskites did not seem to reduce the amount of  $\text{SrZrO}_3$  formed, except in the case of  $\text{La}_{0.6}\text{Sr}_{0.4-z}\text{Co}_{0.2}\text{Fe}_{0.8}\text{O}_{3-\delta}$ . For  $\text{La}_{0.6-z}\text{Sr}_{0.4}\text{Co}_{0.2}\text{Fe}_{0.8}\text{O}_{3-\delta}$  and  $(\text{La}_{0.6}\text{Sr}_{0.4})_{1-z}\text{Co}_{0.2}\text{Fe}_{0.8}\text{O}_{3-\delta}$ , increase of deficiency generally led to increased rate of  $\text{SrZrO}_3$  formation. On the other hand, preliminary results on A-site deficient perovskites containing Mn instead of Fe, showed the opposite effect: the deficient compound was more stable than the stoichiometric one.

A shift in the lattice parameter of cubic YSZ ( $a_{\text{YSZ}}$ ), corresponding to a lattice contraction, was identified after the heat treatment for all samples. The contraction is due to diffusion of cations from the perovskite lattice into the YSZ phase. It is expected that the larger  $\text{La}^{3+}$ ,  $\text{Sr}^{2+}$  and  $\text{Ca}^{2+}$  cations compared to  $\text{Zr}^{4+}$ , would cause a lattice expansion in YSZ. On the other hand the smaller size of the transition metal cations would have the opposite result. The observed contraction of  $a_{\text{YSZ}}$  indicates that the diffusion of the transition metal cations dominates over the diffusion of  $\text{La}^{3+}$ ,  $\text{Sr}^{2+}$  and  $\text{Ca}^{2+}$ . Lower values of  $a_{\text{YSZ}}$  in the case of the Fe-containing compositions are probably caused by the higher rate of diffusion of  $\text{Fe}^{3+}$  compared to  $\text{Mn}^{3+}$ . The decrease of  $a_{\text{YSZ}}$  with increasing x in  $\text{La}_{1-x}\text{A}_x\text{Co}_{0.2}\text{Fe}_{0.8}\text{O}_{3-\delta}$  (A=Sr, Ca) suggests that the concentration of Fe and/or Co in YSZ is increasing while A is consumed by formation of  $\text{AZrO}_3$ .

### References

- [1] J.A.M. van Roosmalen and E.H.P. Cordfunke, *Solid State Ionics* 52, 303 (1992).

# CRYSTAL STRUCTURE, THERMAL EXPANSION AND ELECTRICAL CONDUCTIVITY OF $\text{Pr}_{1-x}\text{Sr}_x\text{Co}_{0.2}\text{Fe}_{0.8}\text{O}_{3-\delta}$ ( $0 \leq x \leq 0.5$ )

G. Ch. Kostoglou and Ch. Ftikos

*Lab. of Inorganic Materials Technology, Department of Chemical Engineering, National Technical University of Athens, 9 Heroon Polytechniou Str., Zografou Campus, GR-157 80, Athens, Greece*

Solid oxide fuel cells (SOFCs) operating at intermediate temperatures (700°C) provide advantages over those operating at high temperatures (900-1000°C). An issue of significant importance for the development of intermediate temperature SOFCs is the selection of an appropriate material, which will serve as cathode. Selected low Co-containing perovskite oxide compositions are considered more promising [1]. In this study, oxides in the system  $\text{Pr}_{1-x}\text{Sr}_x\text{Co}_{0.2}\text{Fe}_{0.8}\text{O}_{3-\delta}$  ( $0 \leq x \leq 0.5$ ) were prepared and characterized.

The powders were synthesized by the amorphous citrate process. Then, they were calcined at 1100°C, milled, compacted, and sintered at 1300°C. The crystal structure, thermal expansion and electrical conductivity of all compositions were studied by XRD, dilatometry and 4-point DC, respectively.

The structure of the compounds with  $0 \leq x \leq 0.4$  is orthorhombic, and becomes cubic for  $x=0.5$ . The lattice parameters were calculated using the LSUCR computer program and they are illustrated in Fig. 1. As can be seen, the deviation among the parameters, which is quantitatively expressed by the orthorhombic deformation (D), is high in the case of the undoped compound, and it is gradually reduced as x increases.

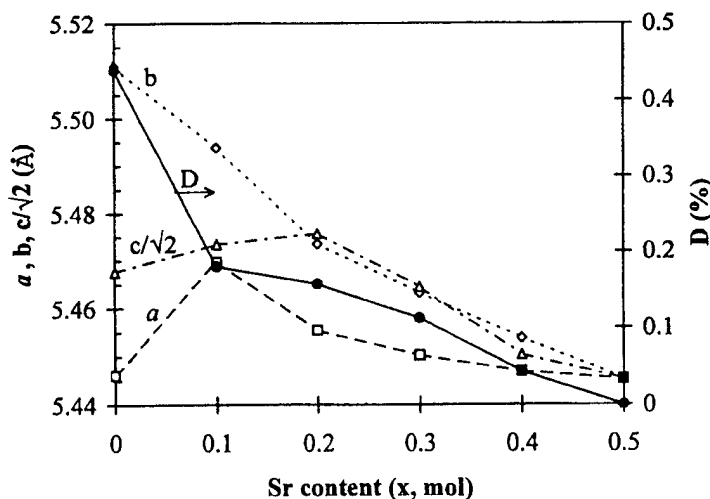


Fig. 1. Lattice parameters and orthorhombic deformation (D) of  $\text{Pr}_{1-x}\text{Sr}_x\text{Co}_{0.2}\text{Fe}_{0.8}\text{O}_{3-\delta}$  as function of Sr content.

The thermal expansion curves, shown in Fig. 2, are linear, but they become steeper at elevated temperatures. The increase of the slope of the curves is greater as x increases. This is caused by the loss of lattice oxygen and the formation of oxygen vacancies, a process which is enhanced as the Sr-doping level is increased. The thermal expansion coefficient (TEC) decreases for  $x=0.1$ , and then constantly increases.

The logarithm of electrical conductivity versus reciprocal temperature in air is shown in Fig. 3. For the compositions with  $x=0, 0.1$ , the conductivity increases with temperature in the whole examined temperature range. For higher x values the conductivity increases up to a



maximum value and then it decreases. As  $x$  increases in the range  $0.2 \leq x \leq 0.5$ , the fall of conductivity becomes steeper, and in addition, the onset temperature for the conductivity decrease becomes lower. The observed behavior is a result of the formation of oxygen vacancies at high temperatures, and it is consistent with the results of the thermal expansion measurements.

The conductivity increases as the Sr-doping level is increased. When bivalent  $\text{Sr}^{2+}$  cations are substituted for trivalent  $\text{Pr}^{3+}$  cations, the transition metal cations that occupy the B-site of the perovskite are oxidized:  $\text{B}^{3+} \rightarrow \text{B}^{4+}$  ( $\text{B}=\text{Co}$  or  $\text{Fe}$ ). The conductivity proceeds via hopping of  $\text{B}^{4+}$  small polarons. As  $x$  increases the concentration of  $\text{B}^{4+}$  charge carriers also increases, and so does the conductivity. Moreover, the activation energy for hopping decreases with increasing  $x$ .

The composition  $\text{Pr}_{0.8}\text{Sr}_{0.2}\text{Co}_{0.2}\text{Fe}_{0.8}\text{O}_{3.5}$  showed the best performance, since its TEC and conductivity values at  $700^\circ\text{C}$  ( $14 \times 10^{-6} \text{ cm}(\text{cm}^\circ\text{C})^{-1}$  and  $159 \text{ Scm}^{-1}$ , respectively), meet the requirements for application in SOFC cathodes.

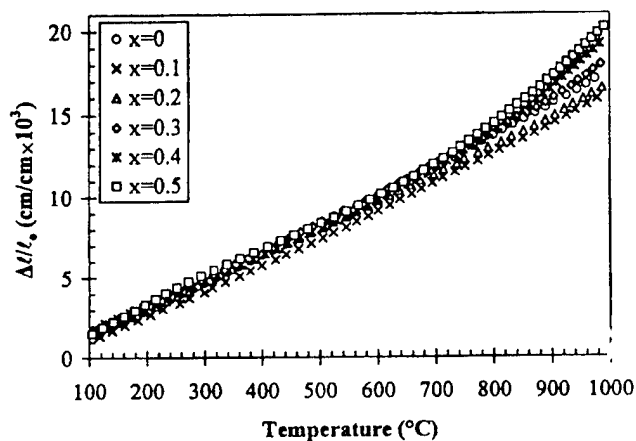


Fig. 2. Thermal expansion curves for  $\text{Pr}_{1-x}\text{Sr}_x\text{Co}_{0.2}\text{Fe}_{0.8}\text{O}_{3.5}$  in air.

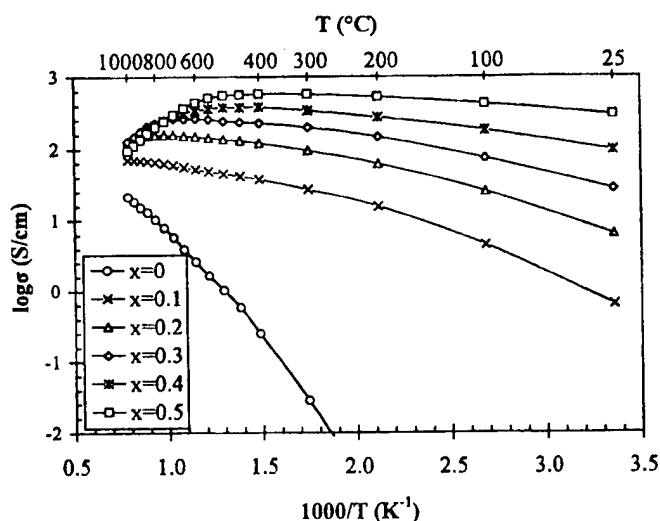


Fig. 3.  $\log \sigma$  versus  $1000/T$  for  $\text{Pr}_{1-x}\text{Sr}_x\text{Co}_{0.2}\text{Fe}_{0.8}\text{O}_{3.5}$  in air.

## References

- [1] B.C.H. Steele, *J. Power Sources* **49**, 1 (1994).

# MATERIAL PROPERTIES OF $\text{La}_{0.8}\text{Sr}_{0.2}\text{Ga}_{0.9\pm x}\text{Mg}_{0.1}\text{O}_{3-\delta}$ AS A FUNCTION OF Ga CONTENT

A. Ahmad-Khanlou, F. Tietz, D. Stöver

Research Centre Jülich, Institute for Materials and Processes in Energy Systems IWV1, Germany

The possible use of substituted lanthanum gallates as membrane materials in solid oxide fuel cells (SOFCs) is being studied as an alternative to the currently used solid electrolyte consisting of yttria-stabilized zirconia (YSZ). A decrease of the operating temperature from 1000 °C to 800 °C aimed at for reasons of long-term stability would be conceivable with such electrolytes since they exhibit higher ionic conductivities in comparison to YSZ [1]. In various studies published to date, different substitutions were made on the basis of  $\text{LaGaO}_3$ . Thus, for example, lanthanum was partially replaced by Sr, Ca, Ba [2] or other rare earth elements such as Nd or Sm [3]. Similarly, gallium was replaced by other elements such as Mg, In, Al or Zn [2,4]. It was shown that  $\text{La}_{1-x}\text{Sr}_x\text{Ga}_{1-y}\text{Mg}_y\text{O}_{3-\delta}$  with  $0.1 < x < 0.2$  and  $0.1 < y < 0.2$  exhibits comparatively high ionic conductivities in reducing and oxidizing atmosphere [5] in addition to suitable thermal expansion coefficients [6]. The perovskite based on  $\text{LaGaO}_3$ , however, reacts very sensitively to small changes in stoichiometry by the formation of impurity phases. For instance, Ishihara et al. [2] discovered that the solubility limit of Sr in the  $\text{La}_{1-x}\text{Sr}_x\text{GaO}_3$  system is at  $x=0.1$ , since higher Sr contents led to the formation of  $\text{SrGaO}_3$  and  $\text{La}_4\text{SrO}_7$ . Further investigations of the compound  $\text{La}_{0.9}\text{Sr}_x\text{Ga}_{0.8}\text{Mg}_{0.2}\text{O}_3$  with  $x=0.09, 0.1, 0.11$  have shown that only a slight Sr hyperstoichiometry leads to single-phase material [7]. Slight changes of the Sr or Mg content influence the phases identified in such a way that in addition to the perovskite phase  $\text{Sr}_3\text{Ga}_2\text{O}_6$ ,  $\text{LaSrGa}_3\text{O}_7$  and  $\text{LaSrGaO}_4$  compounds are formed in the temperature range from 1300 °C to 1500 °C [8,9]. Specific Sr/Mg ratios must be given (see Fig. 1) in order to obtain single-phase material. The conductivity of the single-phase materials is higher than that of materials containing impurity phases. The highest conductivity of  $\sigma=0.17$  S/cm was measured for  $\text{La}_{0.8}\text{Sr}_{0.2}\text{Ga}_{0.83}\text{Mg}_{0.17}\text{O}_{3-\delta}$  at 800 °C [9].

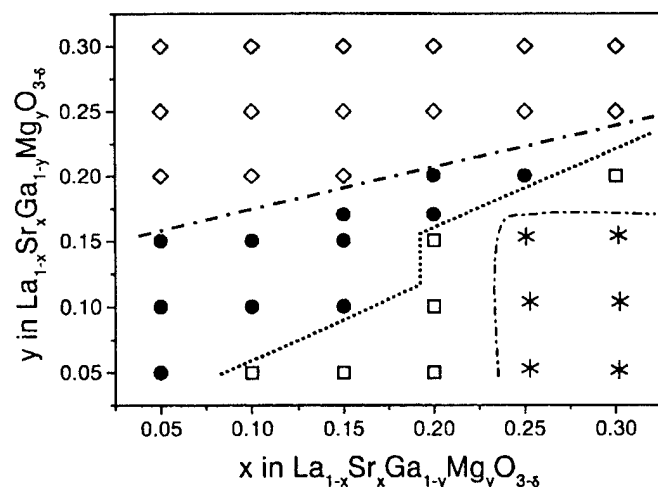


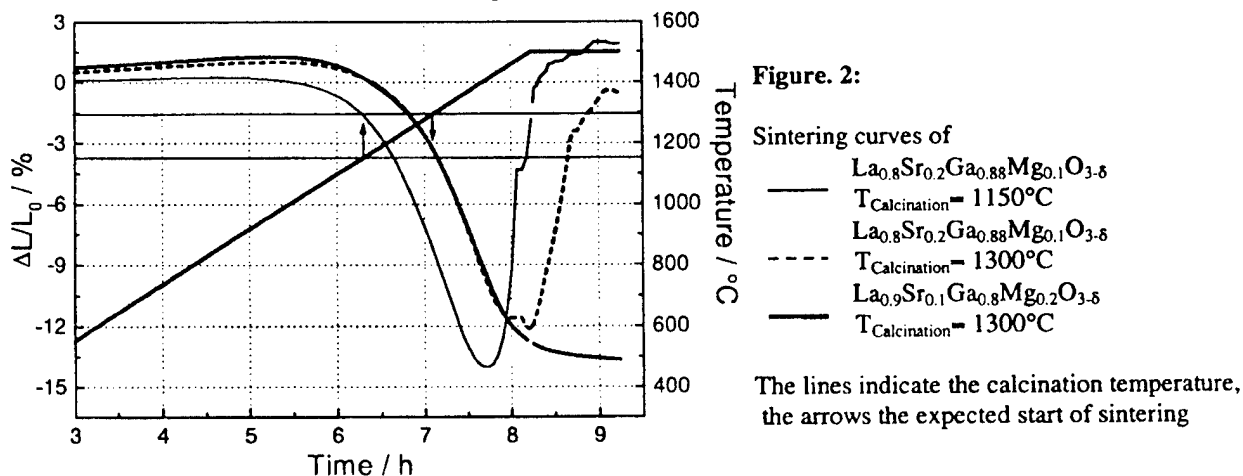
**Figure. 1:**  
Phasefield diagram for  $\text{La}_{1-x}\text{Sr}_x\text{Ga}_{1-y}\text{Mg}_y\text{O}_{3-\delta}$  at 1470°C after [9]. The dashed and dotted lines are a guide to the eye for the different stability regions.

## Phases:

- perovskite single phase (p)
- ◇ (p) +  $\text{LaSrGaO}_4$
- (p) +  $\text{LaSrGa}_3\text{O}_7$
- \* (p) +  $\text{LaSrGaO}_4$  +  $\text{LaSrGa}_3\text{O}_7$

Based on previous investigations [6,9], the  $\text{La}_{0.8}\text{Sr}_{0.2}\text{Ga}_{0.9\pm x}\text{Mg}_{0.1}\text{O}_{3-\delta}$  compound is characterized in this study examining the influence of the gallium content. The characterization of the impurity phases, their influence on the material properties and a possible prevention of the formation of these phases is addressed. The phases formed and the resultant sintering behaviour, the microstructure and the electrical conductivity are studied by varying the Ga content in the range  $-0.2 < x < 0.04$ . Initial observations on substoichiometric material ( $\text{La}_{0.8}\text{Sr}_{0.2}\text{Ga}_{0.88}\text{Mg}_{0.1}\text{O}_{3-\delta}$ )

have shown that an increase of the calcination temperature (900 °C, 1150 °C and 1300 °C) reduces the formation of impurity phases during sintering (1270 °C to 1370 °C) and, consequently, coarsening of the microstructure. This composition showed unusual behaviour in sintering experiments in the dilatometer in the temperature range from 1300 °C to 1500 °C. A volume increase was observed which had not been reported in previous studies on lanthanum gallates. In order to elucidate this phenomenon, sintering curves of the substoichiometric material calcined at 1150 °C and 1300 °C were recorded. Fig. 2 shows these sintering curves in comparison with  $\text{La}_{0.9}\text{Sr}_{0.1}\text{Ga}_{0.8}\text{Mg}_{0.2}\text{O}_{3.8}$  calcined at 1300 °C. The horizontal lines correspond to the calcination temperatures, the arrows indicate the expected start of sintering. While the sintering process starts in the temperature range approximately expected for  $\text{La}_{0.8}\text{Sr}_{0.2}\text{Ga}_{0.88}\text{Mg}_{0.1}\text{O}_{3.8}$  calcined at 1150 °C, sintering of the materials calcined at 1300 °C also sets in at approx. 1100 °C. This observation might be explained by the additional gallate phases which influence the sintering process due to their softening. This assumption is supported by XRD measurements which show that the substoichiometric material contains  $\text{LaSrGa}_3\text{O}_7$  and  $\text{LaSrGaO}_4$  after corresponding calcination. The  $\text{La}_{0.9}\text{Sr}_{0.1}\text{Ga}_{0.8}\text{Mg}_{0.2}\text{O}_{3.8}$  compound showed a very small content of  $\text{LaSrGa}_3\text{O}_7$  after calcination at 1300 °C. Actual shrinkage can be attributed to the sintering of the matrix since the temperature range of the maximum sintering rates is shifted by the temperature difference of the calcination temperatures. Apart from expansion during the heating phase, the  $\text{La}_{0.8}\text{Sr}_{0.2}\text{Ga}_{0.88}\text{Mg}_{0.1}\text{O}_{3.8}$  material also showed a volume increase at constant temperature ( $T=1500$  °C). It may be assumed that the impurity phases exert a significant influence on the material's sintering behaviour. However, their different lattice parameters and densities alone cannot cause this strong volume increase.



### References:

- (1) Ishihara, T., Matsuda, H., Takita, Y.: J. Am. Ceram. Soc, **75**, 1012 (1994)
- (2) Ishihara, T., Matsuda, H., Takita, Y.: J. Am. Chem. Soc, **116**, 3801 (1994)
- (3) Ishihara, T., Matsuda, H., Takita, Y.: Solid State Ionics, **79**, 147 (1995)
- (4) Petric, A., Huang, P., Skowron, A.: Proc. of the 2<sup>nd</sup> Europ. SOFC Forum, Oslo, Norway, Ed.: B. Thorstensen, p. 151 (1996)
- (5) Huang, P. and Petric, A.: J. Electrochem. Soc., **143**, 1644 (1996)
- (6) Tietz, F.: Proc. 9<sup>th</sup> Int. Conf. Modern Mater. Techn. (CIMTEC'98), Florence-Italy, Ed.: P. Vincenzini, Abstr.-No. S VII-1:L07, (1998) (in press)
- (7) Bai, W., Choy, K., Steele, B. C.: Proc. (Poster) of the 3<sup>rd</sup> Europ. SOFC Forum, Nantes, France, Ed.: P. Stevens, p. 1 (1998)
- (8) Djurado, E. and Labeau, M.: J. Europ. Ceram. Soc, **18**, 1397 (1998)
- (9) Huang, K., Tichy, R. S., Goodenough, J. B.: J. Am. Ceram. Soc., **81**, 2565 (1998)

## NEW MEMBRANES FOR LOW-TEMPERATURE FUEL CELLS

Calum R.I. Chisholm<sup>1</sup>, Dane Boysen<sup>1</sup>, Sekharipuram Narayanan<sup>2</sup> and Sossina M. Haile<sup>1</sup>

<sup>1</sup>Materials Science 138-78, California Institute of Technology, Pasadena, CA, 91125

<sup>2</sup>Jet Propulsion Laboratory, California Institute of Technology, Pasadena, CA, 91109

Direct methanol fuel cells (DMFCs) have high potential for use in transportation applications because the fuel, unlike hydrogen, is relatively simple to generate, transport and store. To date, most DMFCs have been demonstrated using sulfonated polymer membranes, e.g., Nafion, as the electrolyte. While such polymers are generally adequate for H<sub>2</sub>/O<sub>2</sub> fuel cells, they have serious drawbacks when applied to MeOH/O<sub>2</sub> cells. In particular, the polymeric membrane allows a large fraction of the methanol to diffuse directly from the anode to the cathode, where it is consumed in a parasitic combustion reaction. Moreover, the temperature range over which Nafion can be utilized is limited to less than ~ 90°C. At these rather low temperatures anode reaction kinetics are slow, resulting in high anode polarization losses and requiring the use of large quantities of precious metal catalysts. Thus, if the potential of DMFCs are to be realized, alternative membranes, ones which are impermeable to methanol and able to withstand slightly elevated temperatures, are required.

In the present work composite polymer/solid electrolyte materials have been evaluated for DMFC applications. Unlike other alternative membranes which have been recently proposed, the present materials contain no liquid phase. The polymer serves to provide mechanical stability and flexibility, whereas the solid electrolyte provides a pathway for proton transport. The conductivity of the composites at 130°C as a function of weight fraction polymer is shown in Figure 1. These samples were prepared by hot-pressing, and the conductivity measured under air by a.c. impedance spectroscopy. In addition we report the results of permeability measurements and the performance of prototype fuel cells. Optimization of the composite microstructure is expected to ultimately yield high conductivity membranes with the desired mechanical, chemical and thermal properties for DMFC applications.

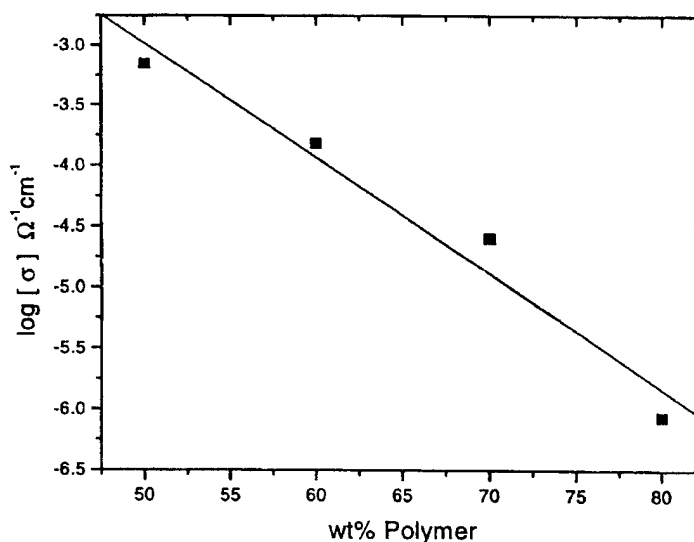


Fig. 1. Conductivity of the polymer/solid electrolyte composite at 130°C as a function of composition.

# PREPARATION AND CHARACTERISATION OF PEROVSKITE-TYPE SOLID OXIDE FUEL CELL-MATERIALS

O. Schulz, M. Martin

Institute of Physical Chemistry, Darmstadt University of Technology,  
Petersenstraße 20, 64287 Darmstadt, Germany

For the investigation of diffusion and degradation processes in polycrystalline SOFC-components it is essential to prepare very dense and homogeneous samples with a defined distribution of grain sizes. Experiments have shown that a modified Pechini-method [1] is extraordinary suitable for this purpose. As a precursor based method it starts from an aqueous solution of ethyleneglycole, citric acid and nitrates of the cations to be part of the desired oxide [2]. Heating up those mixtures results in fine powders, which have to be sintered under defined conditions.

Those conditions can be investigated by the use of a high-temperature in situ x-ray diffraction system. It gives

the opportunity to observe the different phases appearing during the annealing process and further on to decide which is the right sintering temperature for a special system.

On the other side it is possible to adjust different grain sizes by varying the length of sintering time which is important for future grain boundary and bulk-diffusion experiments.

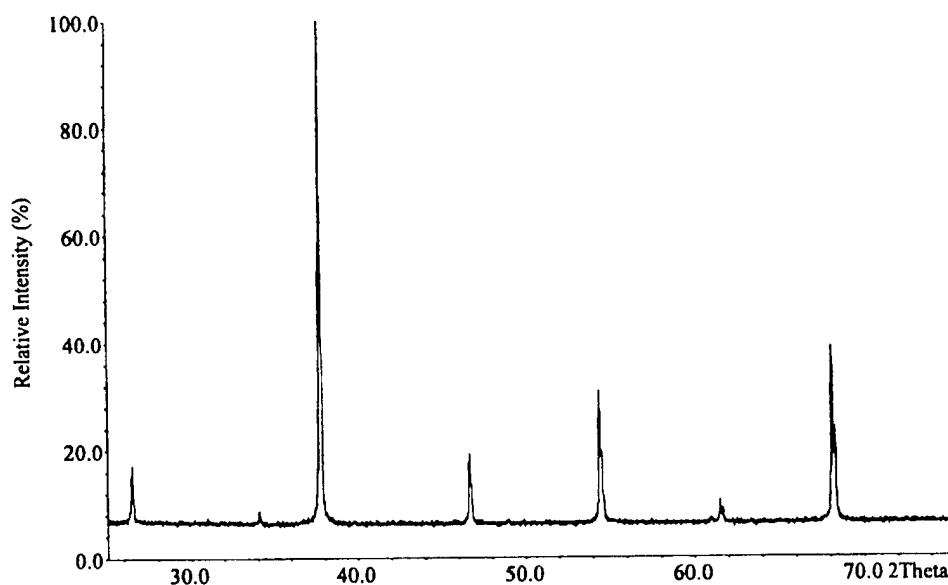


Fig. 1: Ex situ diffraction pattern of the  $\text{La}_{0.9}\text{Sr}_{0.1}\text{Ga}_{0.9}\text{Mg}_{0.1}\text{O}_{3-\delta}$  powder, sintered for 120 h at 1450°C

In the case of the perovskite-type SOFC-electrolytes LSGM (strontium and magnesium doped lanthanumgallates) this investigation lead to a sintering temperature of 1450°C and sintering time of 120 hours to achieve polycrystalline, single-phase materials (Fig. 1) with grain sizes around 40  $\mu\text{m}$ . The samples are investigated by powder-diffraction and electron probe micro analysis (EPMA). The uniaxially pressed samples have densities of more than 95% of the theoretical density. The first results of cation diffusion experiments will be discussed.

[1] M. P. Pechini, U.S. Patent Number 3 330 697, 11. July 1967

[2] Lone-Wen Tai, Paul A. Lessing, J. Mater. Res., Vol. 7, No. 2, Feb 1992

## APPLICATION OF MANOMETRIC METHOD TO DETERMINE THE CHEMICAL DIFFUSION COEFFICIENT OF (La,Sr)MnO<sub>3</sub>

S.P.S. BADWAL<sup>1,2</sup>, S.P. JIANG<sup>1</sup>, J. LOVE<sup>2</sup>, J. NOWOTNY<sup>3</sup> and M. REKAS<sup>3</sup>

1. CSIRO, Manufacturing Science and Technology, Private Bag 33, Clayton, Victoria 3169, Australia
2. Ceramic Fuel Cell Limited, 170 Browns Road, Noble Park, Victoria 3174, Australia
3. School of Materials Science and Engineering, The University of New South Wales, Sydney, NSW 2052, Australia

### ABSTRACT

This paper describes application a manometric method for the determination of the chemical diffusion coefficient for the electrode material (La<sub>0.8</sub>Sr<sub>0.2</sub>)MnO<sub>3</sub> in the temperature range 500-850°C. In the manometric method the progress of chemical reaction, such as oxygen incorporation into an oxide specimen, can be monitored by the determination of changes in oxygen partial pressure. It was observed that the diffusion data obtained for oxidation and reduction differ essentially in both absolute values and their temperature dependence.

### INTRODUCTION

There is a need to develop an oxide electrode material for solid oxide fuel cells that exhibits (i) high oxygen conductivity, (ii) low over-potential losses for oxygen transfer across the electrolyte/electrode interface, and (iii) low reactivity at this interface. This paper describes a manometric method that allows monitoring of the gas/solid reaction at the oxygen/electrode interface. This method was used to determine chemical diffusion coefficient for the electrode material (La,Sr)MnO<sub>3</sub>, (LSM).

### EXPERIMENTAL

The equilibration kinetics in the system O<sub>2</sub>/(La,Sr)MnO<sub>3</sub> was monitored using the measurements of the p(O<sub>2</sub>) changes during a reaction between oxygen and the electrode material involving both oxidation and reduction experiments. Assuming that these changes are negligibly small the equilibration process can be considered as quasi-isobaric. The equilibration experiments were performed isothermally within both oxidation and reduction runs. The oxidation experiments involved successive sudden imposition of an increased p(O<sub>2</sub>) over an initially equilibrated specimen. This sudden increase in p(O<sub>2</sub>) was followed by a decrease in p(O<sub>2</sub>) due to oxygen consumption by the oxide specimen. The rate of this decrease was monitored by the measurement of the p(O<sub>2</sub>) changes as a function of time. The reaction volume was adjusted in such a way that overall p(O<sub>2</sub>) changes during oxygen consumption remained within several % of the initial p(O<sub>2</sub>) value. Consequently, the experimental conditions can be considered as quasi-isobaric.

### CHEMICAL DIFFUSION COEFFICIENT

The chemical diffusion coefficient was determined from approximate solutions of Fick's second law derived by Price and Wagner [1]. For long equilibration time, corresponding to large

$$\log(1-\gamma) = \log\left(\frac{8}{\pi}\right) - \frac{2.303\pi^2 Dt}{4r^2}$$

values of the equilibration degree,  $\gamma$ , the logarithmic equation is applicable:

where  $D$  is the chemical diffusion coefficient,  $t$  is time,  $r$  is the radius of a sphere-shape grain. The

$$\gamma = \frac{\Delta p_t}{\Delta p_\infty}$$

degree of equilibration is defined as:

where  $\Delta p_t$  and  $\Delta p_\infty$  denote changes of  $p(\text{O}_2)$  after time  $t$  and the time after new equilibrium is reached, respectively. For small values of the equilibration degree the parabolic equation is

$$\gamma^2 = \frac{Dt}{\pi} \left( \frac{q}{v} \right)^2$$

applicable:

where  $q$  and  $v$  denote surface area and volume of the grain or specimen, whatever is applicable.

## RESULTS

The diffusion data obtained in this work exhibit the activation energy that for reduction and oxidation remains in the range 116-118 kJ/mol and 155-196 kJ/mol, respectively. This differences indicates that the equilibration process for the LSM material is faster for reduction than that for oxidation. This effect can be considered in terms of either (i) a surface reaction which is rate controlling the oxidation process, or (ii) the effect of non-stoichiometry on transport.

The first scenario assumes that a surface reaction, such as oxygen incorporation into the boundary layer or its transport across this layer, may be rate controlling the oxidation kinetics while the reduction is bulk diffusion controlled. Concordantly, one could expect that the transport during oxidation is retarded by a segregation-induced diffusive resistance formed by a potential barrier in the boundary layer.

The dissimilar oxidation and reduction kinetics may also be considered in terms of essentially different defect structure accompanying oxidation and reduction. The predominant defects participating in the transport during the reduction experiments, taking place at low  $p(\text{O}_2)$ , are oxygen vacancies, while at higher oxygen partial pressure (oxidation runs) the transport mainly occurs via cation vacancies [2]. This difference in defect chemistry of the LSM materials during reduction and oxidation runs may be responsible for the difference in the observed equilibration kinetics.

## CONCLUSIONS

This paper describes the manometric method that was used to determine the chemical diffusion coefficient for LSM. This diffusion coefficient is a certain measure of oxygen transport kinetics. It has been shown that the manometric method applied in this study is a very convenient way of evaluation of the oxygen transport in non-stoichiometric oxide materials, such as LSM.

It appears that the chemical diffusion coefficient is strongly dependent on oxygen non-stoichiometry. Accordingly, the chemical diffusion data differ for oxidation and reduction experiments. The chemical diffusion coefficient determined for oxidation exhibits larger activation energy than that determined during reduction.

## REFERENCES

1. JB Price and J.B. Wagner, Jr., *Z. Physik.Chem., Neue Folge*, 49 (1966) 257.
2. J. Nowotny and M. Rekas, *J.Am.Ceram.Soc.*, 81 (1998) 67

# SURFACE ELECTRICAL PROPERTIES OF (La,Sr)(Co,Fe,Mn)O<sub>3</sub>

S.P.S. BADWAL<sup>1,2</sup>, T. BAK<sup>3</sup>, S.P. JIANG<sup>1</sup>, J. LOVE<sup>2</sup>, J. NOWOTNY<sup>3</sup>, M. REKAS<sup>3</sup>  
and C.C. SORELL<sup>3</sup>

1. CSIRO, Manufacturing Science and Technology, Private Bag 33, Clayton, Victoria 3169, Australia
2. Ceramic Fuel Cell Limited, 170 Browns Road, Noble Park, Victoria 3174, Australia
3. School of Materials Science and Engineering, The University of New South Wales, Sydney, NSW 2052, Australia

## ABSTRACT

Surface electrical properties of electrode material (La,Sr)(Co,Fe,Mn)O<sub>3</sub> at 1073 K are reported. The electrical effects are considered in terms of two effects, such as (i) the surface charge produced by oxygen chemisorption, and (ii) changes of oxygen non-stoichiometry and related Fermi energy due to oxygen incorporation.

## INTRODUCTION

The transfer of mass through the electrode has been generally considered as rate controlled by bulk oxygen conduction while surface reactions, such as adsorption, dissociation and ionization, have been assumed as very fast. However, it has been an accumulation of experimental data indicating that the mass transfer at the gas/solid interface can be determined by a surface reaction [1].

This paper reports the electrical effect at the oxygen/electrode interface and related electrical effects using work function (WF) measurements for the electrode material of different compositions. This study aims at understanding the reactivity between oxygen and the electrode materials (La,Sr)(Co,Fe,Mn)O<sub>3</sub>.

## WORK FUNCTION

WF can be defined as work required to remove the electron from the Fermi energy level,  $E_F$ ,

$$\phi = E_F - E_0$$

to a reference level:

where the  $E_0$  level either corresponds to a zero level, at which  $E=0$ , or to a reference level of which energy is known. WF of compounds has a very complex physical meaning. However, the measurements of WF changes may be used to monitor surface reactions, such as chemisorption and the changes in defects concentration at the surface.

$$\Delta\phi = E_F^2 - E_F^1$$

WF changes in equilibrium can be directly related to the shift in Fermi energy:

Then WF changes can be considered in terms of defect chemistry of the boundary layer.

The most convenient method of WF measurements at elevated temperatures and under controlled gas phase composition is the Kelvin method [1]. In this method the WF of a surface is

$$CPD = \frac{1}{e}(\phi_x - \phi_R)$$

measured against a reference surface forming a contact potential difference, CPD:

where subscripts x and R correspond to the studied specimen and a reference level, respectively. Then:



$$\Delta\phi_x = \Delta\phi_R + e(\Delta CPD)$$

Concordantly, the WF change may be determined only if the reference level,  $\Delta\phi_R$ , is known.

In thermodynamic equilibrium the concentration of defects in metal oxides are determined by temperature and  $p(O_2)$ . Assuming a simple Boltzmann statistics, application of the mass action law to defect equilibria results in the following relationship between the WF

$$\frac{I}{n_\phi} = \frac{I}{kT} \frac{\Delta\phi}{\Delta \ln p(O_2)}$$

change and  $p(O_2)$ :

where  $n_\phi$  is the parameter determined by defect equilibria.

## RESULTS

Effect of  $p(O_2)$  on WF of  $(La_{0.8}Sr_{0.2})(Co,Fe,Mn)O_3$  at 1073 K is shown in Table in terms of the parameter  $n_\phi$ .

SPECIMEN	$n_\phi$
$La_{0.8}Sr_{0.2}MnO_3$ (LSM)	1.7
$La_{0.72}Sr_{0.18}Co_{0.1}Mn_{0.9}O_3$	3.6
$La_{0.72}Sr_{0.18}Co_{0.25}Mn_{0.75}O_3$	5.6
$La_{0.72}Sr_{0.18}Co_{0.5}Mn_{0.5}O_3$	5.9
$La_{0.72}Sr_{0.18}Co_{0.75}Mn_{0.25}O_3$	2.6
$La_{0.8}Sr_{0.2}CoO_3$ (LSC)	2.0
$La_{0.72}Sr_{0.18}Fe_{0.25}Mn_{0.75}O_3$	3.6
$La_{0.72}Sr_{0.18}Fe_{0.5}Mn_{0.5}O_3$	4.8
$La_{0.72}Sr_{0.18}Fe_{0.75}Mn_{0.25}O_3$	5.9
$La_{0.72}Sr_{0.18}FeO_3$ (LSF)	5.6

As seen, in the range 25-50 mol% of Co, the parameter  $n_\phi$  remains within the bulk defect chemistry regime while at lower and higher Co content there is a marked contribution corresponding to the surface charge produced by chemisorption. Though there is no obvious relationship between the surface charge produced by chemisorption and the effect of Co on chemical diffusion, the CPD kinetic data suggests that the mechanism of oxygen incorporation is entirely different for undoped LSM and LSC on one side and that for their solid solutions on the other side.

## CONCLUSIONS

Maximum of the measured surface electrical effect is observed for both LSM and LSC while LSM-LSC-LSF solid solutions as well as undoped LSF exhibit substantially smaller values. The reported values of the parameter  $n_\phi$  will be considered in terms of oxygen reactivity with the surface of the electrode material [2].

## REFERENCES

1. J. Nowotny, J.Chim.Phys., 75, 689 (1978)
2. S.P.S. Badwal, T. Bak, S.P. Jiang, J. Love, J. Nowotny, M. Rekas and C.C. Sorrell Solid State Ionics (full paper).

## PREPARATION AND PROPERTIES OF NANOSIZED CERIA SOLID SOLUTIONS FOR SOLID OXIDE FUEL CELLS

L.J. Gauckler and C. Kleinlogel

*ETH-Zürich, Swiss Federal Institute of Technology  
Dept. of Materials, Nonmetallic Materials  
CH-8092 Zürich*

### Introduction

Some mixed ionic electronic conductors (MIEC) like  $\text{CeO}_2$  solid solutions exhibit an ionic conductivity which is 3 to 5 times higher than YSZ or ScSZ [1][2]. These materials are slightly reduced at low oxygen partial pressures and develop increasingly electronic conductivity. For a system with reversible electrodes it has been shown theoretically, that high efficiency and power output can be obtained [3]. We then have demonstrated the advantages of  $\text{CeO}_2$  based electrolytes for larger systems [4] in which we combined the  $\text{CeO}_2(\text{ss})$  with La-Sr-cobaltite (LSC) cathode.

Conventional sintering of  $\text{CeO}_2(\text{ss})$  to full density needs temperatures around  $1300^\circ\text{C}$  [5][6] resulting in microstructures with grain sizes of several microns to  $\sim 50\text{ }\mu\text{m}$  in diameter. These electrolytes have low mechanical stability. This hinders the use of  $\text{CeO}_2$  in SOFC application despite its superior electrochemical performance.

The aim of the present paper is to give a short description of the performance and efficiency of SOFC systems with mixed conducting electrolytes. As a good example for such a material serves  $\text{CeO}_2$  doped with  $\text{Gd}_2\text{O}_3$ . As electrolyte we used submicron ( $< 160\text{ nm}$ ) grain sized, fully dense  $\text{CeO}_2(\text{ss})$  materials that were obtained after sintering powder components at temperatures as low as  $900^\circ\text{C}$  using a new class of dopants ( $< 2\text{mol}\%$ ).

### Results

$\text{CeO}_2$  powders with a crystallite size of  $\sim 40\text{ nm}$  can be sintered to full density with dopants of  $\text{CoO}$ ,  $\text{CuO}$ ,  $\text{NiO}$ ,  $\text{MnO}$  and  $\text{Fe}_2\text{O}_3$  added in concentrations of  $< 1\text{mol}\%$  to the  $\text{Ce}_{0.8}\text{Gd}_{0.2}\text{O}_{2-x}$ .

The sintering of  $\text{Ce}_{0.8}\text{Gd}_{0.2}\text{O}_{2-x}$  with the dopant  $\text{CoO}$ , as an example, is depicted in Fig. 1. It shows the linear shrinkage rate ( $d(\Delta L/L_0)/dT$ ) of  $\text{Ce}_{0.8}\text{Gd}_{0.2}\text{O}_{2-x}$  as a function of temperature for different Co concentrations at a constant heating rate of  $10\text{ K/min}$ . With increasing dopant concentration the temperature of the maximum shrinkage rate decreases below  $840^\circ\text{C}$ . Sintering of a  $1\text{mol}\%$   $\text{CoO}$  doped  $\text{Ce}_{0.8}\text{Gd}_{0.2}\text{O}_{2-x}$  at  $900^\circ\text{C}$  for 2 h leads to 99% dense samples with an average grain size of  $160\text{ nm}$  as shown in Fig. 2, whereas undoped  $\text{Ce}_{0.8}\text{Gd}_{0.2}\text{O}_{2-x}$  had to be sintered at  $1400^\circ\text{C}$  for 2 h to reach 95% density. This material exhibits an average grain size of about  $2\text{ }\mu\text{m}$ .

In Fig. 3 the total conductivity of  $1\text{mol}\%$  Co doped  $\text{Ce}_{0.8}\text{Gd}_{0.2}\text{O}_{2-x}$  is plotted as a function of  $p(\text{O}_2)$  for  $600$ ,  $700$  and  $800^\circ\text{C}$ . At high  $p(\text{O}_2)$  the conductivity is predominantly ionic and at lower  $p(\text{O}_2)$  the material becomes a mixed ionic/electronic conductor. This behaviour is identical to that of pure  $\text{Ce}_{0.8}\text{Gd}_{0.2}\text{O}_{2-x}$  [7] (straight lines in Fig. 3 from [8]). This shows, that the  $\text{CoO}$  sintering aid neither decreases the stability of  $\text{Ce}_{0.8}\text{Gd}_{0.2}\text{O}_{2-x}$  nor it influences its electrolytic domain boundary.

The sintering kinetics and the resulting submicron microstructures of the  $\text{Ce}_{0.8}\text{Gd}_{0.2}\text{O}_{2-x}$  sintered with dopants are discussed on the basis of enhanced diffusion and liquid phase sintering.

These  $\text{CeO}_2(\text{ss})$  are well suited as electrolytes in SOFC's at intermediate operating temperatures giving high power output.

## Conclusion

Dense submicron  $\text{CeO}_2(\text{ss})$  can be obtained by sintering nanoscaled powders. The densification kinetics during sintering is strongly enhanced by the addition of small amounts of some metal oxides and the sintering temperature is lowered well below  $900^\circ\text{C}$  for  $>99\%$  dense samples. The electrochemical performance in terms of oxygen ion conductivity and electrolytic domain boundary remains unchanged compared to pure  $\text{Ce}_{0.8}\text{Gd}_{0.2}\text{O}_{2-x}$ . Due to the small grain size of  $<200\text{ nm}$  we can expect high mechanical stable electrolytes.

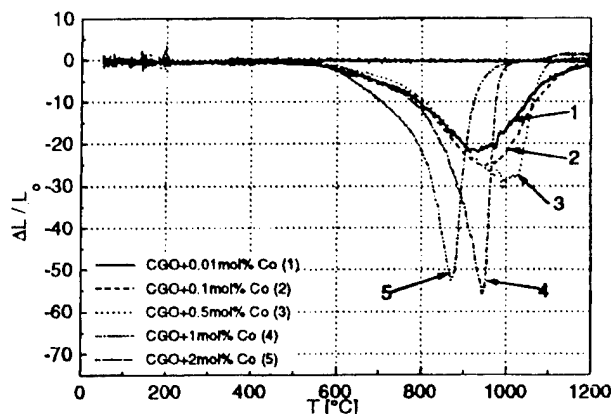


Fig. 1: Linear shrinkage rate as a function of temperature for the  $\text{Ce}_{0.8}\text{Gd}_{0.2}\text{O}_{2-x}\text{-Co}$  system.1

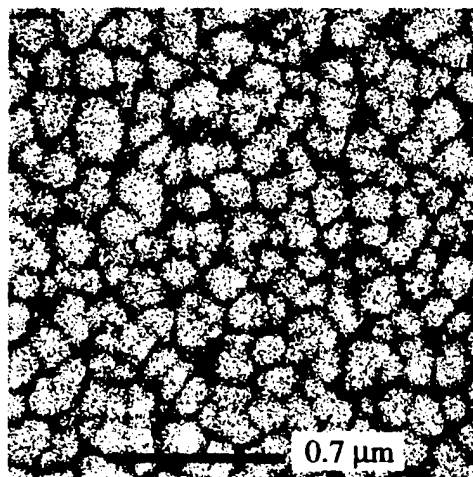
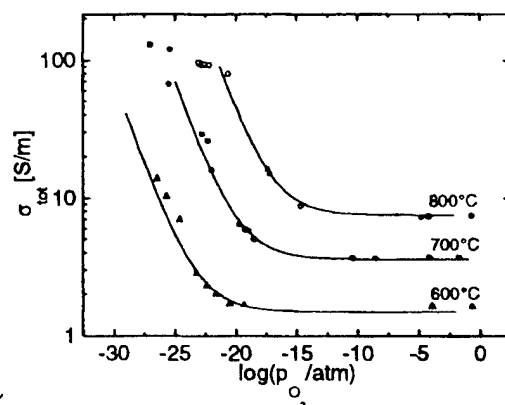


Fig. 2: Microstructure of 1mol% doped  $\text{Ce}_{0.8}\text{Gd}_{0.2}\text{O}_{2-x}$  sintered at  $900^\circ\text{C}$  for 2 h.



✓ Fig. 3: Total conductivity of  $\text{Ce}_{0.8}\text{Gd}_{0.2}\text{O}_{2-x}$  doped with 1mol% Co at different temperatures (• ○ Δ). Solid lines are undoped  $\text{Ce}_{0.8}\text{Gd}_{0.2}\text{O}_{2-x}$  (ref.)

## References

- [1] T.H. Etsell and S.N. Flengas, *Chem. Rev.*, **70** (1970) 339
- [2] N. Q. Minh, *J. Am. Ceram. Soc.*, **76** (1993) 563
- [3] I. Riess, *Solid State Ionics*, **52** (1992) 127.
- [4] I. Riess, M. Gödickemeier and L.J. Gauckler, *Solid State Ionics*, **90** (1-4), (1996) 91-104.
- [5] P.-L. Chen and I.-W. Chen, *J. Am. Ceram. Soc.*, **76** [6], (1993) 1577-83
- [6] Y.C. Zhou and M.N. Rahaman, *J. Am. Ceram. Soc.*, **78** [4], (1995) 981-85
- [7] T. Kudo and H. Obayashi, *J. Electrochem. Soc.*, **133** [3], (1976) 415-19
- [8] D. Schneider, M. Gödickemeier and L.J. Gauckler, *J. Electroceramics*, **1:2**, (1997) 165-72

OXYGEN TRANSPORT KINETICS IN THE MIXED CONDUCTOR  $\text{La}_{0.5}\text{Sr}_{0.5}\text{Fe}_{0.8}\text{Ga}_{0.2}\text{O}_{3-x}$ 

Allan J. Jacobson, S. Kim, S. Wang, Y. L. Yang, and B. Abeles, Materials Research Science and Engineering Center, University of Houston, Houston, Texas 77204-5500, USA.

Over the past decade ceramic membranes of mixed conducting oxides have attracted much interest for use in a cost-effective alternative to conventional methane conversion processes. Such membranes separate pure oxygen from air by selective diffusion and allow the integration of oxygen separation and partial oxidation of methane to synthesis gas ( $\text{CO} + \text{H}_2$ ) into a single step. The membranes must maintain their structural and chemical integrity as well as high oxygen permeability under the very reducing conditions under which reactors operate. It is a challenge therefore to find materials that meet these requirements. The perovskite oxide  $(\text{La}, \text{Sr})\text{FeO}_3$  has been intensively studied as one of the potential candidate materials [1]. Recently,  $(\text{La}, \text{Sr})(\text{Ga}, \text{Mg})\text{O}_3$  compositions have been found to have high oxygen ionic conductivity and also show high chemical stability [2]. Together, these facts suggest that partial substitution of Ga for iron in  $(\text{La}, \text{Sr})\text{FeO}_3$  might be a promising approach to synthesize new candidate materials for the membrane application. Consequently, we have synthesized and investigated the properties of a new perovskite composition,  $\text{La}_{0.5}\text{Sr}_{0.5}\text{Fe}_{0.8}\text{Ga}_{0.2}\text{O}_{3-x}$  (LSFGO), which might be expected to have benefits of both  $\text{LaFeO}_3$  and  $\text{LaGaO}_3$ -based materials. We have used both membrane permeation and electrical conductivity relaxation to characterize LSFGO with respect to the surface exchange kinetics relative to the bulk diffusion rate.

We have previously reported that the transport kinetics can be determined from the pressure dependence of oxygen flux through the membrane [3]. However, the kinetics under large oxygen partial pressure gradients, corresponding to those encountered under actual operating conditions in oxygen separation membranes, are not yet well understood [4]. In the present study, we have investigated the transport kinetics in the LSFGO membrane under large oxygen partial pressure gradients, that result from the CO oxidation reaction at the permeate side of the membrane, as well as under small gradient conditions. By modeling the pressure dependence of the oxygen flow rate under small pressure gradient membrane an ambipolar diffusion coefficient  $D_a$  and a surface exchange coefficient  $k_{10}$  were determined. In air/ $\text{CO}$ ,  $\text{CO}_2$  on the permeate side, the permeability increases linearly with the partial pressure of CO.

Electrical conductivity relaxation (ECR) has also been used to determine the chemical diffusion coefficient  $D_{\text{chem}}$  and oxygen surface exchange rate  $K$  in mixed ionic electronic conductors [5,6]. To determine the transport coefficients, the time dependence of the electrical conductivity after a switch in the oxygen partial pressure was fitted by the solution to the linear diffusion equation with boundary conditions appropriate to the sample geometry and to the applied gas pressure swings. The interpretation of the ECR is based on the assumption that surface exchange kinetics is first order and that the change in conductivity is linearly proportional to the change in oxygen ion concentration.

We have made ECR measurements on LSFGO as a function of temperature and over a wide range of initial and final pressures in order to investigate the oxygen kinetics. Fig. 1 shows the normalized conductivity  $g(t)$  measured on a sample rod of dimensions 1.3mm x 1.5mm x 5.5mm with the oxygen partial pressure ( $p_{\text{O}_2}$ ) switched from 10% to 40% and back from 40% to 10%. Fig. 2 shows  $g(t)$  measured at three different temperatures with  $p_{\text{O}_2}$  switched from 10% to 40%. All of the observed conductivity relaxation curves could be well fitted by the exponential function  $1 - \exp(-t/\tau)$ . The full curves in the figures were calculated using this relation with the values of the time constants ( $\tau$ ) used as the fitting parameter indicated. As can be seen in Fig. 1 the transient is appreciably faster when the switch is from low to high oxygen partial pressure than in the reverse switch. These results together with the permeation measurements and data on

stability will be used to assess the possible use of LSFGO as membrane material for partial oxidation of methane.

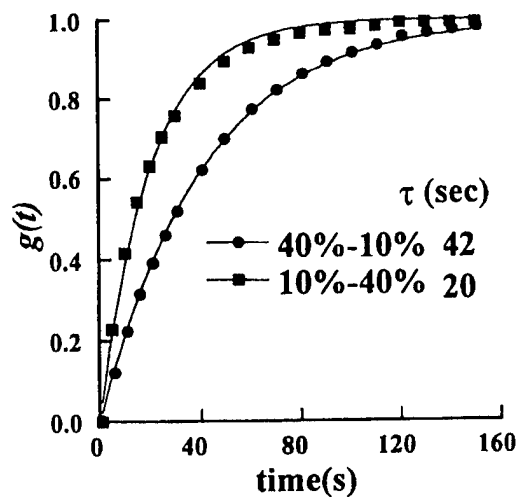


Fig. 1 Normalized conductivity relaxation on a rod at 927°C with  $p(\text{O}_2)$  switched from 10% to 40% and back from 40% to 10%.

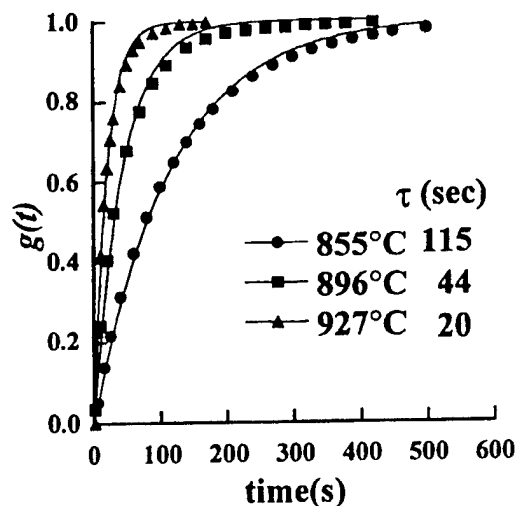


Fig. 2 Normalized conductivity relaxation on a rod measured at the temperatures indicated,  $p(\text{O}_2)$  switched from 10% to 40%.

#### References

- [1] J.E. ten Elshof, H.J.M. Bouwmeester and H. Verweij, *Solid State Ionics*, **81**, 97, (1995).
- [2] T. Ishihara, H. Matsuda and Y. Takita, *J. Am. Chem. Soc.*, **116**, 3801 (1994).
- [3] S. Kim, Y.L. Yang, A.J. Jacobson and B. Abeles, *Solid State Ionics*, **106**, 189 (1998).
- [4] J.E. ten Elshof, H.J.M. Bouwmeester and H. Verweij, *Solid State Ionics*, **89**, 81, (1996).
- [5] J.E. ten Elshof, M. H. R. Lankhorst and H.J.M. Bowmeester, *J. Electrochem. Soc.*, **144**, 1060 (1997), *Solid State Ionics*, **99**, 15 (1997) and references therein.
- [6] I. Yasuda and M. Hishinuma, *Solid State Ionics*, **80**, 141 (1995).

## INTERACTION OF OXYGEN WITH OXIDES: THE ROLE OF EFFECTIVE RATE CONSTANTS

J. Maier

Max-Planck-Institut für Festkörperforschung  
Heisenbergstraße 1, 70569 Stuttgart, Germany

The oxygen interaction with oxides plays an important double role. On one hand it is a prototype process for the understanding of solid state kinetics and on the other hand it represents a fundamental interaction of devices such as fuel cells and sensors.

Different steps of the interaction of oxygen with oxides are considered. These are essentially adsorption, ionisation, charge transfer, transfer through surface space charge regions, bulk transport through and along internal boundaries.

Three experimental situations are referred to: electrical experiment (Q), tracer incorporation (\*) and chemical incorporation ( $\delta$ ).

By using chemical kinetics and the concepts of the rate determining step of quasi-stationarity, it is shown how defined analytical expressions can be derived for the respective interfacial rate constants ( $\bar{k}^Q, \bar{k}^*, \bar{k}^\delta$ ) as a function of microscopic rate constants and defect concentrations.

The chemical kinetic treatment [1] using the concepts of the rate determining step and quasi-stationarity of the elementary steps (reactions steps, hopping steps) yield defined expressions of effective interfacial rate constants ( $\bar{k}^Q, \bar{k}^*, \bar{k}^\delta$ ) as a function of microscopic rate constants and defect concentrations. In this way the dependencies on the control parameters  $P_{O_2}$ , temperature and doping content are obtained. There are far-reaching similarities but also differences compared to the analogous well-known situation for the respective diffusion coefficients ( $D^Q, D^*, D^\delta$ ). For electron-rich materials (e.g. fuel cell electrodes) conceptional differences are most important, while for electron-poor examples (solid electrolytes) the possibility of different rate determining steps is emphasised referring to the different role of electrons in all three experiments. While for the electrical experiment the electron take-up is not a problem, they are explicitly needed in the chemical experiment. In the tracer experiment there is the possibility that the rate determining step may be a direct exchange in which electrons do not appear explicitly.

Detailed experimental work on effective rate constants in  $SrTiO_3$  is presented (determination of the  $\bar{k}$ 's as a function of crystallography, surface treatment,  $P_{O_2}$ , temperature, doping content, coating) and evaluated in the light of the before-mentioned treatment. Other examples (SOFC materials) are also included in the discussion.

### References

- [1] J. Maier, Solid State Ionics **112**, 197 (1998).

Solid State Ionics 12

June 1999

Thessaloniki, Greece

## ***DENSE CERAMIC MEMBRANES FOR OXIDATION REACTIONS***

*T. J. Mazanec*

*BP Chemicals*

*Warrensville Research Center*

*Cleveland, Ohio 44128*

*USA*

Dense ceramic membranes transport oxygen as lattice ions at elevated temperatures. Since only oxygen can readily substitute into the crystal lattice, these membranes are capable of infinite selectivity ratios in oxygen separation. The development of chemical processes exploiting the dense ceramic membranes has accelerated recently due to rapid strides in materials, processing and element fabrication. What were once mere laboratory curiosities are beginning to be seen as promising new vehicles capable of re-inventing mature technologies. Oxygen production and partial oxidation are the two major emerging applications of the dense ceramic membranes due to the possibility of generating inexpensive oxygen and of introducing oxygen into organic molecules and reaction mixtures in novel ways. In this paper the status of the dense ceramic membrane technology and prospects for its commercialization will be presented.

## Process of Solid State Reaction between Doped ceria and Zirconia

K. Eguchi, N. Akasaka, H. Mitsuyasu, Y. Nonaka

Department of Molecular and Materials Sciences,  
Graduate School of Engineering Sciences, Kyushu University,  
Kasugakoen, Kasuga, Fukuoka 816-8580, Japan  
TEL:+81-92-583-7526, FAX:+81-92-573-0342

Cation-doped ceria has been investigated as an ionic conductor of oxygen which may be operative at lower temperatures than Y-stabilized zirconia, though its reduction in hydrogen atmosphere is one problem for the practical application. We have previously proposed to overcome this difficulty using an electrolyte consisting of cation-doped ceria and stabilized zirconia, in which high chemical stability of zirconia and high ionic conductivity of ceria were simultaneously achieved. These two fluorite phases of zirconia and ceria undergo solid state reaction at elevated temperatures. The interfacial reaction between these two phases is particularly important for the electrochemical applications. Our previous work has revealed that the Ce component preferentially migrates in to the zirconia lattice at the ceria /zirconia interface as was observed by TEM and XRD. The purpose of the present investigation was to reveal the effect of the preparation procedure of ceria and zirconia, the dopant level, and the kind of dopant on the process of the solid state reaction between two phases. The influence of the solid state reaction on the electrical conductivity was also discussed.

The source powder of rare earth doped ceria was prepared by three methods, i.e., (1) Thermal decomposition of the corresponding nitrate salts, (2) Precursor method using citric acid or malic acid, and (3) coprecipitation method using oxalic acid. The resultant precursor heated at 1200°C to produce single doped-ceria phase. Yttria-doped zirconia was prepared by the similar method described above. Commercially available powders from TOSOH were also used for the reaction. The composition of the sample was expressed hereafter as dopant, its atomic fraction, and host material, e.g.,  $\text{Sm}_{0.2}\text{Ce}$  or  $\text{Y}_{0.15}\text{Zr}$  which corresponds to  $(\text{SmO}_{1.5})_{0.2}(\text{CeO}_2)_{0.8}$  or  $(\text{YO}_{1.5})_{0.15}(\text{ZrO}_2)_{0.85}$ . Powder X-ray diffraction was carried out after the solid state reaction between doped ceria and Y-doped zirconia

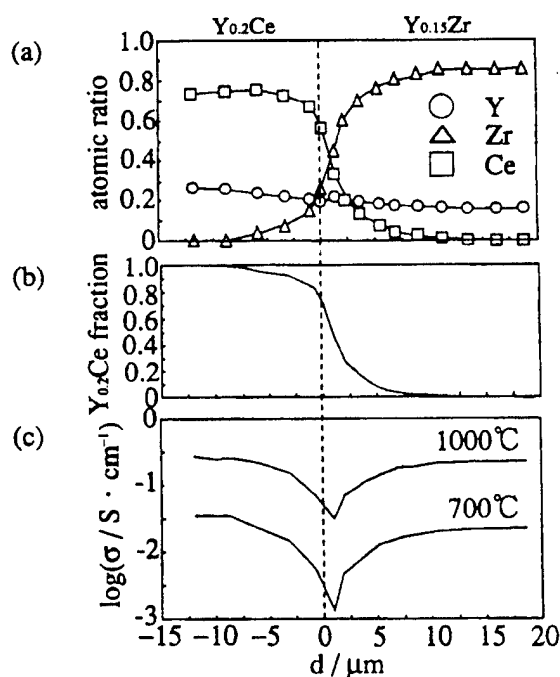
The mirror-polish faces of the  $\text{Y}_{0.2}\text{Ce}$  and  $\text{Y}_{0.15}\text{Zr}$  pellets were attached each other and heated at 1700°C for the reaction. The composition across the interface was measured by EPMA. The original interface was determined by position of a Pt marker which was inserted prior to the reaction. The compositional gradient in Fig. 1 was observed for both Zr and Ce, but the steep changes of them were mostly occurred in the zirconia part of the sample. This means that the solid state reaction proceeded as a preferential migration of the Ce component in the zirconia lattice. The electrical conductivity was measured for the samples after complete reaction



between  $Y_{0.2}Ce$  and  $Y_{0.15}Zr$ . The compositional dependence of the electrical conductivity was then expressed as a function of Ce fraction,  $Ce / (Ce + Zr)$ . The experimentally obtained Ce fraction for the diffusion couple of the Fig. 1a was shown in Fig. 1b. Then, the electrical conductivity was estimated from the compositional dependence of the conductivity was shown in Fig 1c. Significant drop of the ionic conductivity was expected at the interface region because of the solid state reaction.

The reaction of  $Y_{0.2}Ce$  and  $Y_{0.15}Zr$  was investigated by heating the powder mixture at 1100-1500°C and subsequent XRD analysis. The XRD pattern of the mixture before the reaction consisted of two fluorite phases from ceria and zirconia. The solid state reaction at 1300°C gave rise to the systematic shift of the zirconia lines to lower angles and the weakening of the ceria lines. This behavior of the XRD pattern also reflects the preferential migration of the Ce component to the zirconia phase. Although the size and reactivity of the particles were dependent on the preparation method, the reaction process was common to every combination of the  $Y_{0.2}Ce / Y_{0.15}Zr$  sample. The powder from malic acid precursor method was so reactive that the solid state reaction to produce a single

fluorite phase completed even at 1300°C. The ceria and zirconia samples with different dopant concentration were also subjected to the solid state reaction. ( $Y_{0.1}Ce$ ,  $Y_{0.2}Ce$ ,  $Y_{0.3}Ce$ ,  $Y_{0.08}Zr$ ,  $Y_{0.15}Zr$ , and  $Y_{0.2}Zr$ ) Again, the reaction was proceeded by the preferential dissolution of Ce component to the zirconia phase in every case as was observed by XRD. Three rare earth dopants were employed for ceria powder, i.e.,  $Sm_{0.2}Ce$ ,  $Y_{0.2}Ce$ , and  $Gd_{0.2}Ce$ . The reactivity with  $Y_{0.15}Zr$  was quite faster for  $Y_{0.2}Ce$  than for the other two samples. The preferential migration of ceria was not observed for  $Sm_{0.2}Ce$  and  $Gd_{0.2}Ce$ . Therefore the reaction process was strongly affected by the kind of dopant for ceria.



✓ Fig.1 Solid state reaction at interface between  $Y_{0.2}Ce/Y_{0.15}Zr$   
( $d=0$ , original interface marked by Pt)  
(a) compositional analysis by EPMA  
(b) Ce fraction :  $Ce/(Ce+Zr)$   
(c) conductivity,  $\sigma$ , expected from Ce fraction

# STRUCTURE, RAMAN SPECTRA AND DEFECT CHEMISTRY MODELING OF CONDUCTIVE PYROCHLORE OXIDES

F.W. Poulsen, M. Glerup and P. Holtappels

Materials Research Department

Risø National Laboratory

DK-4000 Roskilde Denmark

**Abstract.** Oxides with the pyrochlore structure,  $A_2B_2O_7$ , can serve as host lattice for interstitial oxygens, protons [1] and electronic defects. The properties can to large extent be tailored by suitable doping on the A- and B-site [2]. The defect chemistry can be described by 4 chemical equilibria + the linear equations originating from site-, mass- and electroneutrality restrictions. In this paper n-type, p-type, electrolyte- and MIEC-behaviour of pyrochlores is modelled with an new algorithm [3], which differs markedly from previous numerical solution methods [2,6]. The experimentally observed Raman spectra, the variation of lattice parameter and the variation of electrical properties with type and concentration of dopant are discussed on basis of the defect model. The synthesis and measurements of electrical properties of the studied pyrochlores are described in a separate paper at this conference [4]. Below is shown a selection of the experimental data and a model calculation of the concentration distributions as function of  $pO_2$  for  $Gd_2Ti_{2-x}Mn_xO_{7\pm\delta}$ .

**Structure and phase purity**  $Gd_2MoTiO_7$ ,  $Gd_2Mo_{1.4}Ti_{0.6}O_7$ ,  $Pr_2Sn_{2-x}In_xO_7$ ,  $Pr_2Zr_{2-x}Mn_xO_7$  ( $x = 0, 0.1$ ) and  $La_2Zr_2O_7$  were investigated with x-ray powder diffraction: the cubic lattice constants are in the range 10.270-10.709 Å;  $Z = 8$ , space group:  $Fd3m$ . The Mn and In solubility limit was found to be below  $x = 0.2$ ,  $PrMnO_3$  and  $PrInO_3$  were among the identified impurity phases.

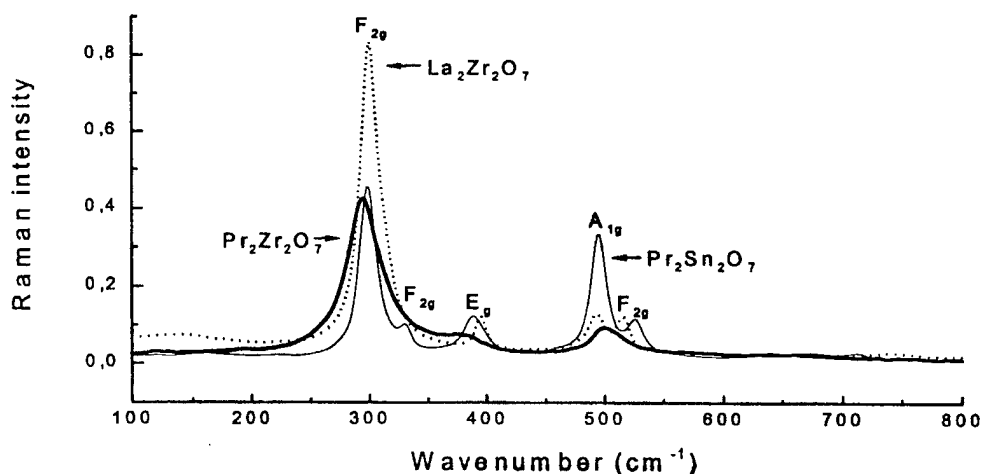


Figure 1. Room temperature Fourier Transform-Raman spectra of three undoped pyrochlores. Excitation with 1064 nm NIR radiation from a Nd-YAG laser, 15-75 mW.

**Raman spectra** were obtained at room temperature from 3 undoped and 7 doped pyrochlores, including  $La_2Zr_2O_7$  as a reference compound [5], cf. Figure 1. The vibrational normal modes were predicted by factor group analysis ( $O_h^7$ ,  $Z'=2$ ) with the result: Raman

active modes:  $1A_g + 1E_g + 4F_{2g}$ ; IR-active modes:  $7F_{1u}$ ; inactive modes:  $2F_{1g} + 3A_{2u} + 3E_u + 4F_{2u}$ ; acoustic modes:  $1F_{1u}$ . Comparison with the vibrational spectra of solids with the same elements in 6, 7- and 8-fold coordination will be discussed.

**Defect modelling** The mathematical trial and error method for calculating defect concentrations is described in details in ref.[3]. The model for  $Gd_2Ti_{2-x}Mn_xO_{7 \pm \delta}$  contains the following species: a trivalent Gd ion on the A-site;  $Ti_B^*$  (Ti+4),  $Mn_B'$  (Mn+3),  $Mn_B^*$  (Mn+4) on the B-site,  $O_O^*$  and  $V_O^{**}$  on the O site; interstitial oxygens  $O_i''$ ; and finally delocalised electrons and electron holes  $n = [e']$ ,  $p = [h^*]$ . The defect concentrations and oxygen stoichiometry of the material are determined by the magnitude of four equilibrium constants:

$$K_A = [Mn_B'] / (n \cdot [Mn_B^*]); \quad K_i = n \cdot p;$$

$$K_{AF} = [V_O^{**}] \cdot [O_i''] / [O_O^*]; \quad pO_2^{1/2} K_{ox} = [O_O^*] [h^*]^2 / [V_O^{**}].$$

Some of these equilibrium constants are known from the work of Porat et al [6]. The remaining constants have been ascribed plausible values in the model calculation shown below.

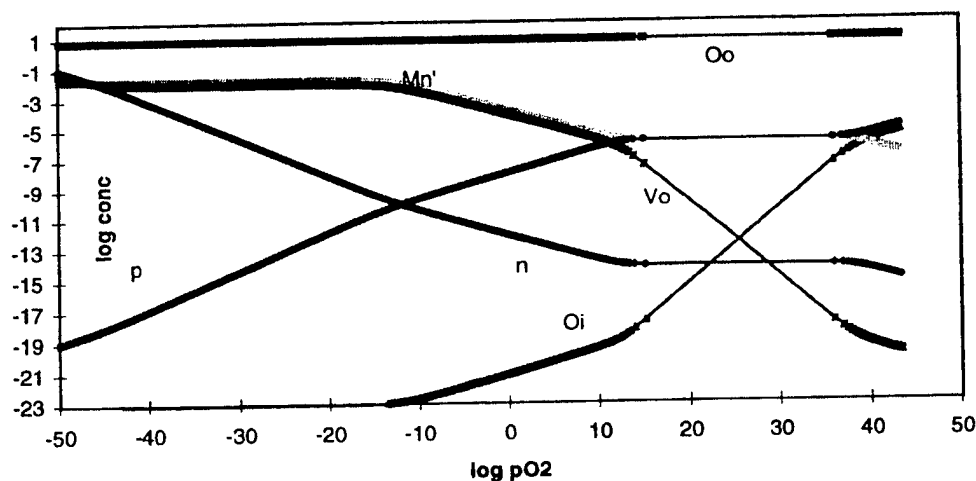


Figure 2. Brouwer diagram referring to  $Gd_2Ti_{2-x}Mn_xO_{7 \pm \delta}$ , 820°C. Doping level and equilibrium constants:  $x = 0.02$ ;  $K_A = 10^{12}$ ;  $K_i = 10^{-23}$ ;  $K_{AF} = 10^{-25}$ ;  $K_{ox} = 10^{-15}$ .

**Acknowledgements** The financial support of the DK-SOFC-programme(FWP), Forskerakademiet (MG), and an EU-TMR-grant (PH) is greatly acknowledged.

#### References:

- [1]. J.A. Labrincha, J.R.Frade, F.M.B. Marques, *Protonic conduction in  $La_2Zr_2O_7$ -based pyrochlore materials*, Solid State Ionics (1997) **99**, 33.
- [2]. H.L. Tuller, *Semiconduction and mixed ionic-electronic conduction in nonstoichiometric oxides: impact and control*, Solid State Ionics (1997) **94**, 63.
- [3]. F.W. Poulsen, *Method for calculating ionic and electronic defect concentrations in proton containing perovskites*, accepted for publ. in J. Solid State Chem. 1999.
- [4]. P.Holtappels, F.W. Poulsen and M. Mogensen, *Preparation of mixed conducting pyrochlores as SOFC anodes*, these proceedings, SSI-12.
- [5]. F.W. Poulsen and N. van der Puil, *Phase relations and conductivity of Sr- and La-zirconates*, Solid State Ionics (1992) **53-56**, 777.
- [6]. O. Porat, M.A. Spears, C. Heremans, I. Kosacki and H.L. Tuller, *Modelling and characterisation of mixed ionic-electronic conduction in  $Gd_2Ti_{2-x}Mn_xO_{7 \pm \delta}$* , Solid State Ionics **86-88** (1996) 285, and *ibid* **94**, (1997) 63.

## TRANSPORT PROPERTIES OF MIXED CONDUCTORS WITH COMPARABLE IONIC AND ELECTRONIC CONDUCTIVITIES

W. Sitte

Institute of Physical and Theoretical Chemistry  
Graz University of Technology, A-8010 Graz, Austria

Mixed conductors with comparable ionic and electronic conductivities (like e.g. yttria-stabilized zirconia-terbia or various pyrochlores) are promising candidates for SOFC-electrodes, as such materials can minimize polarization losses due to an enlargement of the reaction area for the electrochemical transfer reaction.

For conductivity measurements we use the van der Pauw-technique as with this technique only the thickness of the sample and not the exact positions of the four contacts on one surface of the sample need to be known. With blocking electrodes electronic and ionic conductivities of mixed conductors can be obtained even if the ionic conductivity is in the same order of magnitude as the electronic one. Nevertheless, with electronic conductivity measurements on mixed conductors the activity gradient created during the conductivity measurements has to be taken into account in order to increase the stoichiometric resolution of the results [1,2].

Chemical diffusion coefficients of mixed conductors can be obtained by galvanostatic or potentiostatic polarization techniques as well as impedance spectroscopy in symmetric or asymmetric electrochemical cells. If these techniques are combined with coulometric titration, the composition dependence of the chemical diffusion coefficient is available with high stoichiometric resolution. Recently, the theory of mixed ionic-electronic conductors with arbitrary electronic transport numbers has been investigated by us [3]. For an asymmetric cell, when the mixed ionic-electronic conductor (MIEC) is located between an electronically and an ionically blocking electrode, Fick's second law of diffusion has been solved under adequate boundary conditions by the help of the Laplace transform method and we calculated concentration profile plots for various electronic transport numbers for galvanostatic and potentiostatic polarization processes. We could show that if the electronic transport number  $t_e$  deviates from unity, chemical diffusion processes are stimulated at the electronically and the ionically blocking electrode and concentration gradients build up at both types of electrodes. Only for  $t_e=1$  the concentration gradient at the ionic electrode vanishes. All relevant parameters for polarization/depolarization processes of mixed conductors with arbitrary electronic transport numbers compared with those from literature for  $t_e=1$  will be reported. Approximations for the short and long time behavior of the polarization/depolarization voltages allow the determination of the chemical diffusion coefficients of materials even with comparable ionic and electronic conductivities. Experimental results will be given for model materials with predominately electronic conductivity (e.g.  $\alpha$ -Ag<sub>2</sub>Te) as well as comparable electronic and ionic conductivities (e.g. Ag<sub>1.92</sub>Te with  $t_e=0.8-0.9$ ). The values of the chemical diffusion coefficient as obtained from galvanostatic and potentiostatic polarization experiments are in good agreement with the results from impedance spectroscopy.

- [1] D. Grientschnig and W. Sitte, J. Phys. Chem. Solids **52**, 805 (1991).
- [2] W. Preis and W. Sitte, Solid State Ionics **76**, 5 (1995).
- [3] W. Preis and W. Sitte, J. Chem. Soc. Faraday Trans. **92**, 1197 (1996).

## LIMITATIONS OF CHARGE-TRANSFER MODELS FOR MIXED-CONDUCTING OXYGEN ELECTRODES

S. B. Adler

Chemical Engineering Department, Case Western Reserve University  
10900 Euclid Avenue, Cleveland, OH 44106, USA

Debate surrounds the mechanism of oxygen-reduction on a porous mixed-conducting electrode. In analogy to a porous metal catalyst (e.g. Pt on zirconia), many workers apply a traditional paradigm in which O<sub>2</sub> reduction is limited by a charge-transfer process occurring locally at the one-dimensional "three-phase boundary" interface between electrode, electrolyte, and gas. With many materials, however, oxygen absorption and transport in the bulk of the mixed conductor play a significant (if not dominant) role in determining the electrode polarization. Charge transfer models (such as equivalent circuits) cannot account properly for oxygen absorption and solid-state/gaseous diffusion, and leave the electrode reaction mechanism only vaguely or empirically defined.

In order to establish a connection between performance and properties of mixed-conductors, several workers have developed continuum models to treat explicitly the non-charge-transfer processes occurring in a membrane<sup>1</sup> or electrode<sup>2,3</sup>. One model that uses this approach (the ALS model),<sup>2,4,5</sup> has shown strong evidence that for mixed conductors with fast ionic transport (such as La<sub>1-x</sub>Sr<sub>x</sub>Co<sub>1-y</sub>Fe<sub>y</sub>O<sub>3-δ</sub>), the impedance is dominated by surface chemical exchange of O<sub>2</sub> and solid-state oxygen diffusion. As shown schematically in Fig. 1, this model treats the overall electrode reaction,  $\frac{1}{2}\text{O}_2 + 2\text{e}^- \rightarrow \text{O}^{2-}$ , as a homogeneous chemical reaction occurring over the internal surface area of the electrode material. The absorption of neutral oxygen by the mixed-conductor serves to convert electronic to ionic current over a finite region of the electrode thickness. The impedance, as well as the size of the active region ( $\delta$ ), are related to the exchange and diffusion properties of the mixed conductor.

The linear polarization behavior of La<sub>1-x</sub>Sr<sub>x</sub>CoO<sub>3-δ</sub> (LSCO) electrodes on ceria has been measured as a function of  $x$ ,  $T$ , and  $P_{\text{O}_2}$  using a.c. impedance<sup>5</sup>. These measurements appear to agree well with the ALS model, and provide a database on a clean, well-characterized electrode system with little or no interfacial impedance (Fig. 2). Analysis of the electrode kinetics using the model yields values for the oxygen vacancy diffusion coefficient ( $D_v$ ) and surface-exchange rate constant ( $r_0(\alpha_f + \alpha_b)$ ) as a function of  $x$ ,  $T$ , and  $P_{\text{O}_2}$ . These values agree well with those calculated from published measurements of oxygen chemical diffusion and isotope surface exchange ( $\tilde{D}$  and  $k$ ). The distance ( $\delta$ ) that the reaction extends beyond the electrode/electrolyte interface depends on  $D_v$  and  $r_0$ , varying between 0.3 and 10 microns for a typical electrode surface area.

<sup>1</sup> H. Deng, M. Zhou, and B. Abeles, *Solid State Ionics* **74**, 75 (1994).

<sup>2</sup> S. B. Adler, J. A. Lane, and B. C. H. Steele, *J. Electrochem. Soc.*, **143**(11), 3554 (1996).

<sup>3</sup> A. M. Svensson, S. Sunde, and K. Nisanciuglu, *J. Electrochem. Soc.* **145**, 1390 (1998).

<sup>4</sup> S. B. Adler, J. A. Lane, and B. C. H. Steele, *J. Electrochem. Soc.*, **144**(5), 1884 (1997).

<sup>5</sup> S. B. Adler, *Solid State Ionics* **111**(1-2), 125 (1998).

Fig. 1

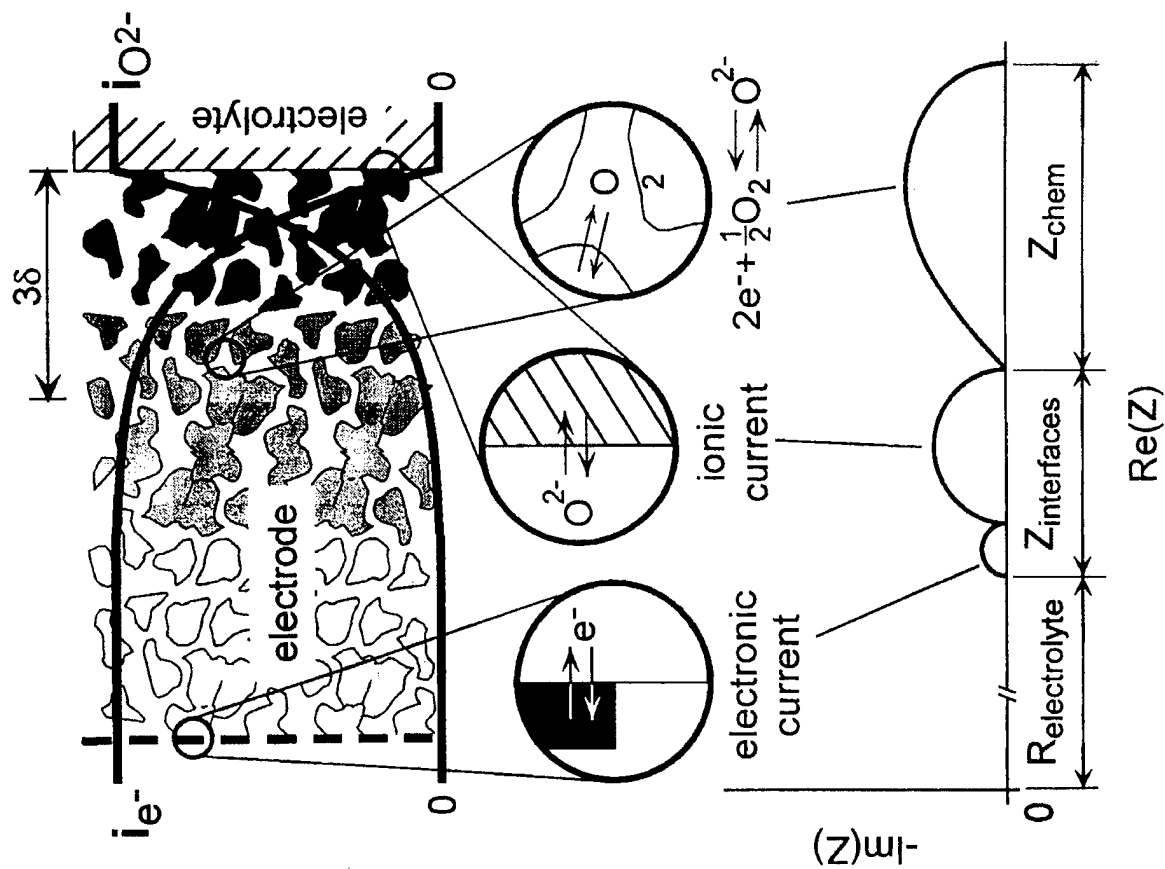
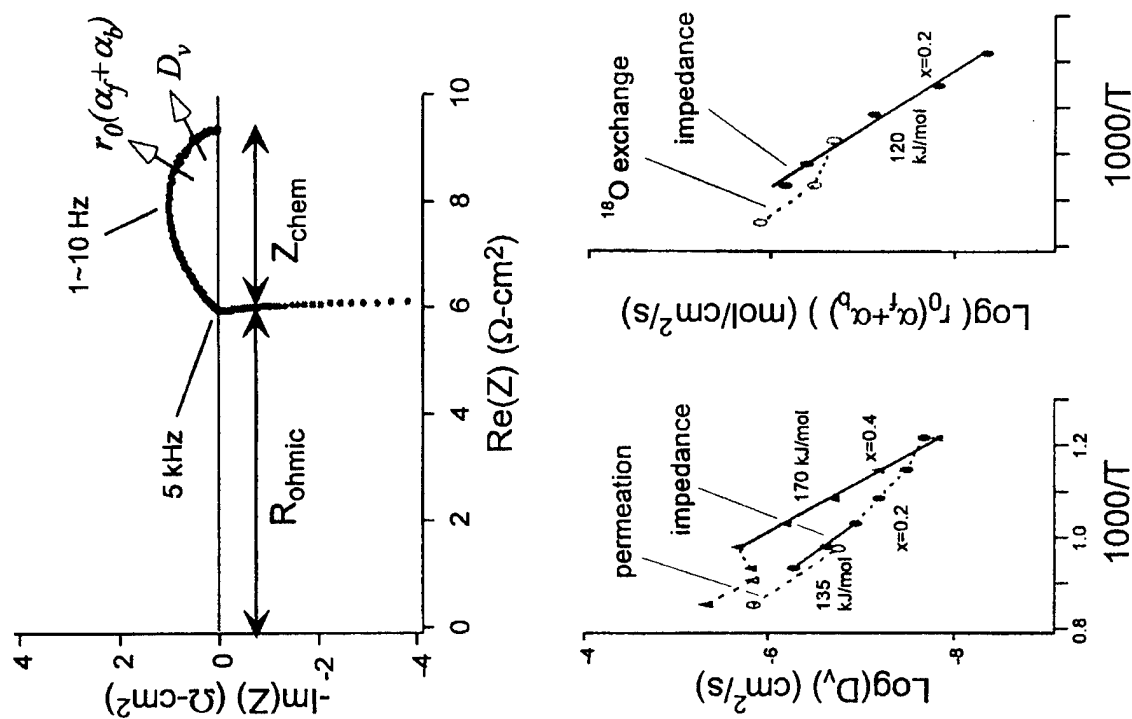


Fig. 2



# STUDY OF OXYGEN EXCHANGE AND TRANSPORT IN MIXED CONDUCTING COBALTATES BY ELECTROCHEMICAL IMPEDANCE SPECTROSCOPY

Alexandre Closset, Stefan Diethelm, Jan Van herle, and A. J. McEvoy

Laboratoire de Photonique et Interfaces  
École Polytechnique Fédérale de Lausanne  
CH 1015 Lausanne, Switzerland

Kemal Nisancioglu

Department of Materials Technology and Electrochemistry  
Norwegian University of Science and Technology  
N-7034 Trondheim, Norway

Mixed conducting oxides have been proposed as air electrodes for solid oxide fuel cells, oxidation catalysts, and gas separation membranes for oxygen recovery or purification. For the purpose of characterizing oxygen transport, electrochemical techniques have been developed, in particular for the measurement of the chemical diffusion coefficient of oxygen [1,2]. Despite accurate measurement, data analysis was not straightforward in cases where the surface exchange reaction was irreversible. For this purpose, oxygen exchange at the specimen/electrolyte interface was assigned first order reaction kinetics to solve Fick's second law for oxygen transport in a disk shaped pellet. The modification of data analysis suggested by this approach for the potential-step technique [1,2] in obtaining both the chemical diffusion and surface exchange coefficients from the same set of relaxation data was previously discussed [3]. In this work, we investigate the applicability of a similar approach to the analysis of analogous data obtained by electrochemical impedance spectroscopy (EIS).

An electrochemical *blocked cell* design similar to that of Gür *et al.* [1,2], shown in Fig. 1, was used for the theoretical analysis and experimental work. A mathematical analysis of this system, with results expressed in the frequency domain, suggested the validity of the equivalent circuit depicted in Fig. 2. Here, the resistance  $R_{YSZ}$  in serial connection with an  $RC$  circuit simulates the platinum electrode interfacing the sample, as well as the ohmic drop within the electrolyte. The second part represents the oxygen transport in and out of the sample pellet, where  $R_k$  is the surface exchange resistance,  $Z_d$  is the finite length diffusion element, and  $CPE_g$  is the distributed capacitance to account for gaseous and adsorbed oxygen at the sample's surface.

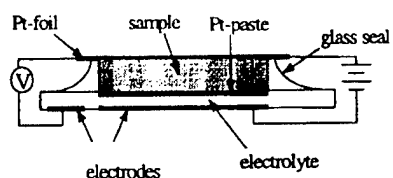


**Figure 1.** Electrochemical blocked cell design.

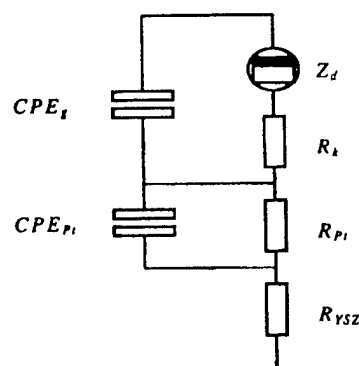


**Figure 2.** Equivalent circuit for the cell.

The solution of Fick's second law for the specimen in the Laplace plane leads to the derivation of a complex impedance in the form [4]

$$Z_T(j\omega) = \frac{\Delta \tilde{E}}{\tilde{I}} = \frac{V_M \left( \frac{dE}{d\delta} \right)_s}{zFSk} + \frac{V_M \left( \frac{dE}{d\delta} \right)_s}{zFS\sqrt{j\omega\tilde{D}}} \coth \sqrt{\frac{j\omega L^2}{\tilde{D}}} \quad (1)$$

The first term in Eq. (1), independent of frequency, is the surface exchange resistance  $R_k$ . The second term of Eq. (1), named  $Z_d$ , is a well known expression describing finite-length bulk diffusion [5]. A similar result has recently been reported by ten Elshof *et al.* [6].

To test this model by EIS, a sample pellet of the compound  $\text{SrCo}_{0.5}\text{Fe}_{0.5}\text{O}_{3-\delta}$ , a highly nonstoichiometric material, was selected for the present study. Measurement at 880°C on this *blocked cell* is plotted in the complex plane in Fig. 3. The equivalent circuit model in Fig. 2 was used to perform a nonlinear least square fit on these data, and the result is also shown in Fig. 3. The chemical diffusion coefficient calculated from the fit results was  $1.2 \times 10^{-5} \text{ cm}^2/\text{s}$ . Similar value for the chemical diffusion coefficient was extracted from the impedance data with asymptotic equations derived directly from the solution of Fick's second law, thus justifying the choice of the equivalent circuit model. This is, furthermore, in excellent agreement with the result obtained previously for the same material by use of the potential-step technique [3].

From the  $R_k$  value obtained and Eq. (1), the surface exchange coefficient was estimated as  $3.0 \times 10^{-4} \text{ cm/s}$ . While this result is affected by the formation of a zirconate phase at the specimen-electrolyte interface, the measured chemical diffusion coefficient for bulk diffusion of oxygen is clearly not influenced by interfacial phenomena. This was separately confirmed by measurements in a cell where the sample was separated from the electrolyte by use of a gold-ring spacer.

Finally, the fit in Fig. 3 gave values for  $R_{Pt}$  and  $CPE_{Pt}$  well in accordance with the characteristics of platinum electrodes on YSZ reported by Van herle *et al.* [7].

### Acknowledgments

This work was supported by the Federal Office for Energy (CH), the Priority Program for Materials (CH), Norsk Hydro a.s. (N) and Statoil a.s. (N).

### References

- [1] T. M. Gür, A. Belzner and R. A. Huggins, *J. Membrane Sci.*, **75**, 151 (1992).
- [2] K. Nisancioglu and T.M. Gür, *Solid State Ionics*, **72**, 199 (1994).
- [3] S. Diethelm, A. Closset, K. Nisancioglu, J. Van herle, A. J. McEvoy and T. M. Gür, submitted to *J. Electrochem. Soc.*
- [4] A. Closset, *Dipl. Thesis*, EPFL, Lausanne (1997).
- [5] I.D. Raistrick and R. A. Huggins, *Solid State Ionics*, **7**, 213 (1982).
- [6] J. E. ten Elshof, M. H. R. Lankhorst, and H. J. M. Bouwmeester, *J. Electrochem. Soc.*, **144**, 1060 (1997).
- [7] J. Van herle and A. J. McEvoy, *Ber. Bunsenges. Phys. Chem.*, **97**, 470 (1993).

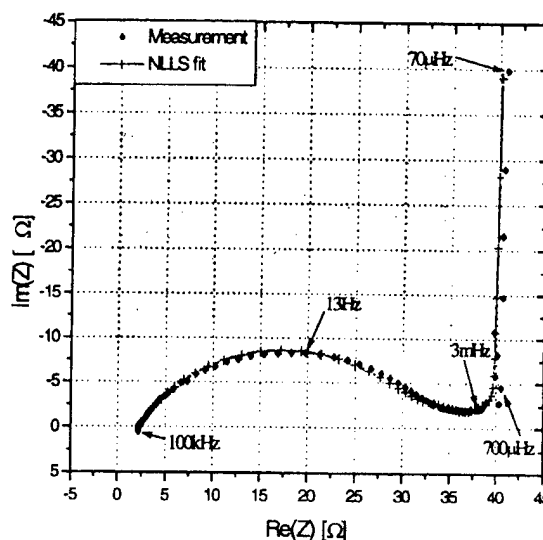


**Figure 3.** Measured impedance of the electrochemical cell shown in Fig. 1 at 880°C plotted in the complex plane.



**CHEMICAL DIFFUSIVITY AND DEFECT STRUCTURE OF BaTiO<sub>3-δ</sub>****Han-Il Yoo and Chang-Rock Song**Solid State Ionics Research Lab, School of Materials Science and Engineering  
Seoul National University, Seoul, 151-742, Korea

BaTiO<sub>3-δ</sub> enjoys a wide application as a main ingredient material in modern, electronic technology, e.g., positive temperature coefficient resistors (PTCR), multilayer ceramic capacitors (MLCC), dynamic random access memory (DRAM), and ferroelectric random access memory (FRAM), just to name a few examples. The oxide has thus been a subject of numerous studies since nearly half a century before. It is actually one of the most studied perovskite oxides particularly for the understanding of their defect structure and electrical transport properties. Notwithstanding its practical importance in processing the structure-sensitive properties of BaTiO<sub>3-δ</sub>, however, the chemical diffusivity as a measure of nonstoichiometry ( $\delta$ ) equilibration kinetics of the oxide has little been known. Up to date, only 11 data sets, including tracer diffusivities, have been reported, which are limited to an oxygen partial pressure range of  $p(\text{O}_2)/\text{atm} \geq 0.001$  at best and given only as a function of temperature.

We have recently measured, by a conductivity relaxation technique, the chemical diffusion coefficient of "undoped" polycrystalline and Al-doped single-crystal BaTiO<sub>3</sub>, respectively, against oxygen partial pressure in the widest ever range of  $10^{-18} \leq p(\text{O}_2)/\text{atm} \leq 1$ , at elevated temperatures in the range of  $800 \leq T/^\circ\text{C} \leq 1100$ . [1] The result,  $\tilde{D}$  vs.  $\log p(\text{O}_2)$ , together with the corresponding electrical conductivity are shown in Fig. 1 for the undoped and in Fig. 2 for the Al-doped.

It has been found that the chemical diffusivity varies convex-upwardly over the n-type to p-type transition region of  $p(\text{O}_2)$  across the conductivity minimum in each case, leaving a maximum approximately at the oxygen partial pressure where the conductivity minimum falls. This sort of behavior of chemical diffusivity is observed for the first time in oxide systems.

In this presentation, we will report on the methodology to extract the chemical diffusivity from conductivity relaxation in an n/p mixed regime, and analyze the chemical diffusivity isotherms in the light of Wagner's classic theory of chemical diffusion [2] and the defect structure of BaTiO<sub>3</sub>. This analysis will consequently enable one to evaluate the concentration product of electrons and holes (i.e.,  $np = K_i$ ), without having recourse to any assumption at all, and their mobilities ( $\mu_n$ ,  $\mu_p$ ) separately. These parameters evaluated will lead to a further insight into the defect structure of BaTiO<sub>3</sub>.

**References**

- [1] C.-R. Song and H.-I. Yoo, submitted to Solid State Ionics.
- [2] C. Wagner, Z. Phys. Chem. B **21**, 25 (1933).

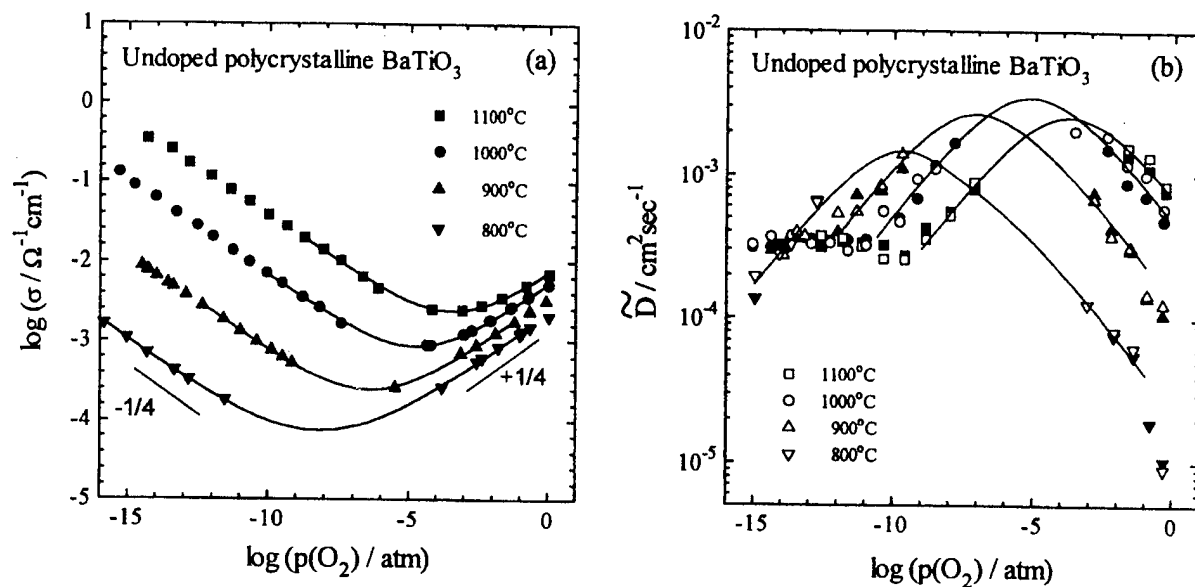


Fig. 1. (a) Electrical conductivity and (b) chemical diffusivity of “undoped” BaTiO<sub>3</sub> against oxygen partial pressure at different temperatures. The solid lines are the best-fitted to the theory.

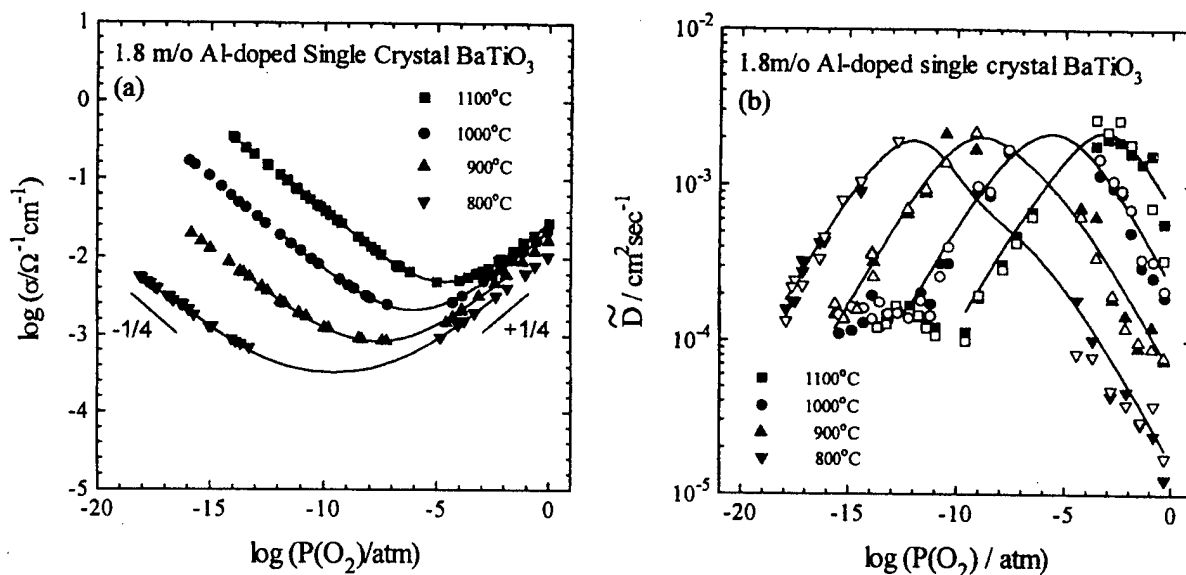


Fig. 2. (a) Electrical conductivity and (b) chemical diffusivity of 1.8m/o Al-doped BaTiO<sub>3</sub> against oxygen partial pressure at different temperatures. The solid lines are the best-fitted to the theory.

## SPECTROSCOPY OF ELECTRONIC DEFECTS IN COMPLEX OXIDES

K. Ullrich, D. Mack, S. Wissmann and K.D. Becker  
 Institute of Physical and Theoretical Chemistry  
 Braunschweig University of Technology, Braunschweig, Germany

Results on the electronic defect structure of olivines, spinels and perowskites will be reported that have been obtained from high-temperature *in situ* studies using optical spectroscopy and Mössbauer spectroscopy. The examples span the range from diluted point defects to constitutional electronic disorder.

In numerous oxides [1-3], we have observed defect-related optical absorption indicating the formation of electronic defects due to redox reactions. In the case of MnO for example, oxygen is incorporated according to



Using an electroneutrality  $2[\text{V}_{\text{Mn}}''] = [\text{h}^{\bullet}]$ , a power-law of the form  $[\text{h}^{\bullet}] \propto p_{\text{O}_2}^{-m}$  is deduced for the dependence of hole concentration on oxygen partial pressure,  $p_{\text{O}_2}$ , with  $m = 1/6$ . Indeed, the optical defect absorption followed this dependence, allowing the identification of the type of defect that gave rise to the defect-related absorption. The shape of the defect-induced absorption gave evidence of a small-polaron hopping process [1].

Recent studies on single crystals of the simple silicate fayalite,  $\text{Fe}_2\text{SiO}_4$ , have revealed similar  $p_{\text{O}_2}$ -dependent effects. However, the observed partial pressure dependence does not conform to the behaviour expected for free holes with  $m = 1/5$ . Instead, a much stronger dependence was found with an  $m$ -parameter around 0.5. Such a high value points to the existence of associates between holes and vacancies, yielding either singly charged cation vacancies or neutral ones. We have studied the kinetics of this defect species by means of oxygen partial pressure jump experiments. The orientation dependent diffusion coefficients of the defects derived from these isothermal relaxation experiments are discussed in the framework of the existing data on the electrical conductivity and cation tracer diffusion of fayalite [4,5].

Formally, the mixed-valence spinel magnetite,  $\text{Fe}_{3-x}\text{O}_4$ , can be considered as composed of ferrous and ferric cations. However, above the so-called Verwey transition at about 120 K, the huge increase in electrical conductivity observed at this transition is attributed to rapid electron hopping. Electrons can be considered as being distributed over the ferric ion cores:  $(3 \text{Fe}^{3+}, \text{e}^-)\text{O}_4$ . The distribution of electrons over the cation sites is a function of temperature and leads to a temperature-dependent average charge state of the iron ions. Mössbauer spectroscopy reflects averaged charge states in the position of the spectra. This so-called Mössbauer shift  $\delta$  is given by a chemical, valency-dependent contribution and by a second order Doppler effect:

$$\delta = \delta_{\text{C}} + \delta_{\text{SOD}}$$

For a harmonic solid the Doppler contribution can be eliminated yielding the chemical contribution as a function of temperature. Results for the thermodynamic data of the

temperature dependent electron distribution in magnetite are given and discussed [6].

An example of intermediate electronic disorder is represented by the perovskite  $\text{SrFeO}_{3-\delta}$ . Results of our *in situ* Mössbauer study on the average charge state of iron will be reported [7].

- [1] T. He, K.D. Becker, Ber. Bunsenges. Phys. Chem. **96**, 1886 (1992)
- [2] K.D. Becker, Phil. Mag. A **68**, 767 (1993)
- [3] T. He, K.D. Becker, Solid State Ionics **101-103**, 337 (1997)
- [4] T.-L. Tsai, R. Dieckmann, Mater. Sci. Forum **239-241**, 399 (1997)
- [5] S. Aggarwal, J. Töpfer, T.-L. Tsai, R. Dieckmann,  
Solid State Ionics **101-103**, 321 (1997)
- [6] S. Wissmann, V. v. Wurmb, F.J. Litterst, R. Dieckmann, K.D. Becker  
Phys. Chem. Solids **59**, 321 (1998)
- [7] D.E. Mack, D. Stüber, S. Wissmann, K.D. Becker, Ionic and Mixed Conducting  
Ceramics III, Electrochemical Society, 1998, 188

## C. Mixed Conducting Oxides and Applications in Oxygen Membranes

MIXED OXIDE ION CONDUCTIVITY AND OXYGEN PERMEATING PROPERTY OF Fe, Co, or Ni DOPED  $\text{LaGaO}_3$  PEROVSKITE OXIDE

Tatsumi Ishihara, Takashi Yamada, Hiroshi Arikawa, Hiroyasu Nishiguchi and Yusaku Takita

Department of Applied Chemistry, Faculty of Engineering, Oita University, Dannoharu 700, Oita 870-1192, Japan

Separation of oxygen from air is of highly importance in various process. In particular, oxygen permeable ceramic membrane is essential for developing  $\text{CH}_4$  oxidative reforming process. For the separation of air, electron or hole and oxide ion mixed conductor is preferable comparing the pure oxide ion conductor, since no outside circuit is required. In the conventional study, perovskite oxide of  $\text{LaCoO}_3$  [1] or  $\text{LaFeO}_3$  based oxide have been investigated [2], however, development of further higher oxygen permeation property is required. In addition, stability against reduction and oxidation is also required for the application of  $\text{CH}_4$  oxidative reforming process. This is because oxygen separating membrane is exposed to both air and  $\text{CH}_4$ . In our previous study, it was found that oxide ion conductivity of  $\text{LaGaO}_3$  perovskite was increased with doping Co, however hole conduction was also appeared. In the present study, the authors investigated electric hole and oxide ion mixed conductivity of Fe, Co, or Ni doped  $\text{La}_{0.8}\text{Sr}_{0.2}\text{GaO}_3$  perovskite oxide. Furthermore, the application of the  $\text{LaGaO}_3$  based oxide for  $\text{CH}_4$  oxidative reforming process was studied.

The specimens studied in this study were always prepared by the conventional powder mixing method. Ceramic samples of composition  $\text{La}_{0.8}\text{Sr}_{0.2}\text{Ga}_{0.7}\text{M}_{0.3}\text{O}_3$  (M=Fe, Co, Ni) were prepared by mixing commercial powders of  $\text{La}_2\text{O}_3$  (Kishida, 99.99% in pure),  $\text{SrCO}_3$  (Wako, 99.9%),  $\text{MgO}$  (Wako, 99.9%), and  $\text{Fe}_2\text{O}_3$ ,  $\text{CoO}$ , or  $\text{NiO}$  (Rare metal, 99.9%) and  $\text{Ga}_2\text{O}_3$  (Kishida, 99.99% in pure) in stoichiometric proportions. The starting powders were mixed in  $\text{Al}_2\text{O}_3$  pestle and mortar and then precalcined at 1273 K for 6 h. The mixture was pulverized again with pestle and mortar and pressed into disks of 20 mm in diameter and 1.5 mm in thickness. After isostatic pressing at 275 MPa, the disks were sintered at 1773 K for 6 h in air. Conductivity was measured with dc four probe method. The oxygen permeation property was measured by measurement of permeated oxygen into  $\text{N}_2$  from air with gas chromatograph.  $\text{La}_{0.6}\text{Sr}_{0.4}\text{CoO}_3$  was coated on membrane.

Figure 1 shows the Arrhenius plots of electrical conductivity of  $\text{La}_{0.8}\text{Sr}_{0.2}\text{Ga}_{0.7}\text{M}_{0.3}\text{O}_3$  (M=Fe, Co, Ni). It is obvious that high electrical conductivity was exhibited on all specimens. However, electrical conductivity did not increase monotonously with increasing temperature suggesting that semiconduction was dominant. In particular, all specimens exhibited the metallic like dependence of conductivity at high temperature, namely, decreases in conductivity with increasing temperature was observed at temperatures higher than 973 K. On the other hand, conductivity of all specimens decreased with decreasing oxygen partial pressure. Therefore, it is evident that electronic charge carrier is electronic hole. However, dependence of electrical conductivity on oxygen partial pressure was far smaller than 1/6 or 1/4. This suggests that contribution of oxide ion conductivity on total conductivity was still high on all specimens. Therefore,

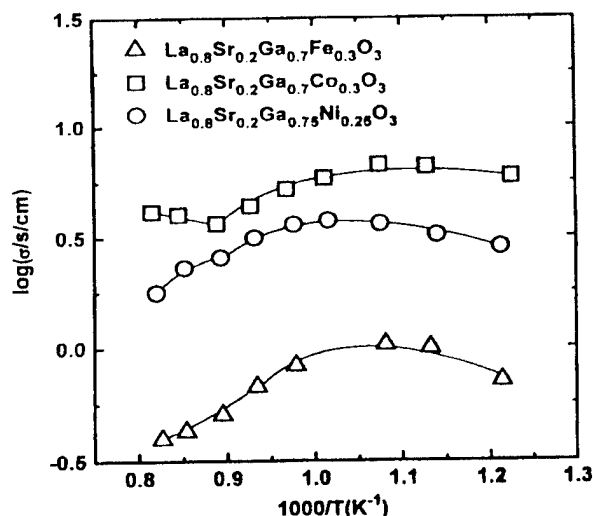


Fig. 1 shows Arrhenius plots of electrical conductivity of  $\text{La}_{0.8}\text{Sr}_{0.2}\text{Ga}_{0.7}\text{M}_{0.3}\text{O}_3$  (M=Fe, Co, Ni).

electrical conductivity of Fe, Co, or Ni doped LaGaO<sub>3</sub> is consisted of electronic hole and oxide ion conductivity, however, transport number of oxide ion is far larger than that of the conventional mixed ion conductor such as LaCoO<sub>3</sub>. Among the examined transition metal dopant, the highest electrical conductivity was obtained on Co doped ones.

Figure 2 shows the temperature dependence of oxygen permeation rate from air to N<sub>2</sub>. In this figure, oxygen permeation property of La<sub>0.8</sub>Sr<sub>0.2</sub>Fe<sub>0.8</sub>Co<sub>0.2</sub>O<sub>3</sub> which is generally considered as oxygen separation membrane was also shown for the comparison. It is clear that Fe, Co, and Ni doped LaGaO<sub>3</sub> based oxide exhibited the higher oxygen permeation rate at temperature higher than 1173 K. In particular, La<sub>0.8</sub>Sr<sub>0.2</sub>Ga<sub>0.7</sub>Ni<sub>0.3</sub>O<sub>3</sub> exhibited the higher oxygen permeation rate at all temperature. Oxygen permeation rate in Ni doped sample was further studied in details and it was found that La<sub>0.8</sub>Sr<sub>0.2</sub>Ga<sub>0.75</sub>Ni<sub>0.25</sub>O<sub>3</sub> exhibited the maximum oxygen permeation rate of 87.7 and 46.1 μmol/min.cm<sup>2</sup> at 1273 K and 873 K, respectively, among Ni doped LaGaO<sub>3</sub>. Therefore, Ni doped LaGaO<sub>3</sub> based oxide is attractive as an oxygen permeation film at low temperature. On the other hand, Fe doped one is highly stable in reducing atmosphere, while the conductivity and oxygen permeation rate was the smallest among three specimens. Therefore, combination of Fe doped LaGaO<sub>3</sub> based oxide membrane with CH<sub>4</sub> oxidative reforming was further studied.

Figure 3 shows temperature dependence of CH<sub>4</sub> conversion when La<sub>0.8</sub>Sr<sub>0.2</sub>Ga<sub>0.6</sub>Fe<sub>0.4</sub>O<sub>3</sub> (LSGF) and La<sub>0.8</sub>Sr<sub>0.2</sub>Fe<sub>0.8</sub>Co<sub>0.2</sub>O<sub>3</sub> (LSFC) plate were used for the separation of air. It is clear that CH<sub>4</sub> conversion was always higher on LSGF than that on LSFC as air separation membrane. This suggests that amount of oxygen supplying through LSGF is higher than that of LSFC membrane. In addition, there is no significant changes on crystal phase observed by XRD measurement. It is reported that crack was formed on LaFeO<sub>3</sub> based oxide membrane by an expansion caused by reduction [2], however, no significant crack was also observed on both face of the membrane by SEM observation. Therefore, it can be said that stability of LSGF membrane is enough for the application of oxygen separation membrane in CH<sub>4</sub> oxidative reforming. This study reveals that oxide ion conductivity was improved by doping Fe, Co, or Ni for Ga site of LaGaO<sub>3</sub> based oxide. Also, LaGaO<sub>3</sub> based oxide doped with Fe, Co, or Ni for Ga site is promising electronic hole and oxide ion mixed conductor, which can be applied for the air separation membrane for CH<sub>4</sub> oxidative reforming process.

## References

- 1) Y. Teraoka, H.M. Zhang, K. Okamoto, and N. Yamazoe, Mater. Res. Bull. 23, 51 (1988).
- 2) C.Y. Tsai, A.G. Dixon, Y.H. Ma, W.R. Moser, and M.R. Pascucci, J. Am. Ceram. Soc., 81, 1437 (1998).

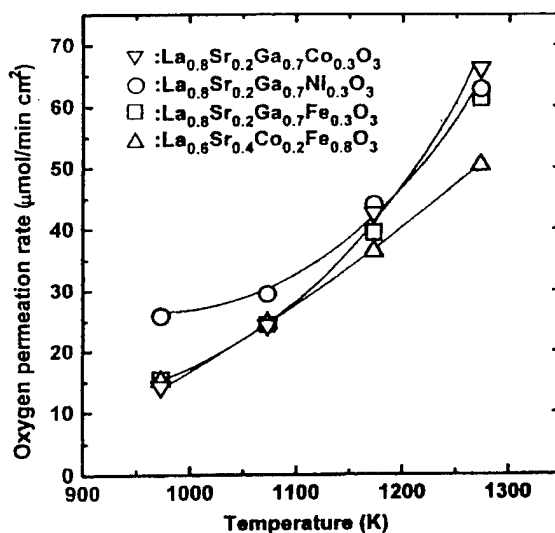


Fig. 2 Temperature dependence of oxygen permeation rate from air to N<sub>2</sub>.

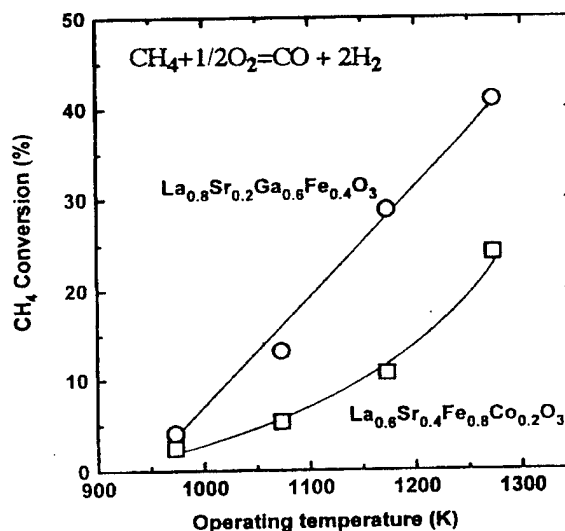


Fig. 3 Temperature dependence of CH<sub>4</sub> conversion by using LSGF and LSFC plate were used for the separation of air.

PREPARATION OF LaSrCoFeO<sub>3-x</sub> MEMBRANES

J. Luyten, A. Buekenhoudt, W. Adriansens, J. Coymans, H. Weyten, R. Leysen  
Process Technology, VITO, Boeretang 200, B-2400 Mol, Belgium

Perovskite mixed electron-oxygen conducting membranes are bulk membranes with a thickness of the order of 1 mm, showing oxygen fluxes of the order of 0.1 - 0.8 Nm<sup>3</sup>/m<sup>2</sup>/h at a temperature of 850°C (feed oxygen partial pressure 0.2 bar, permeate oxygen partial pressure 0.033 bar). To reach commercially more interesting fluxes, membranes with a much higher surface/volume ratio or multilayer membranes with a thin dense skin need to be developed.

In our lab, dense hollow fibers and porous multilayer substrates were synthesised. The hollow fibers were synthesised using a polymeric spinning technique based on phase inversion. The multilayer porous substrates were manufactured following conventional ceramic processing routes.

## The powder preparation

La<sub>2</sub>O<sub>3</sub>, SrCO<sub>3</sub>, Co<sub>3</sub>O<sub>4</sub> and Fe<sub>2</sub>O<sub>3</sub> powders in the right combination were milled and calcined at 900°C for 10 hours. The LaSrCoFeO<sub>3-δ</sub> powders obtained by solid state reaction were reactivated by intensively milling before shaping. Sintering to obtain dense materials was performed at 1225°C for 24 hours.

## The multilayer membrane

To increase the flux through a membrane, the conventional approach is constructing a multilayer membrane composed of different layers with a gradual decrease in layer thickness and pore size. Because of the high expansion coefficient of LaSrCoFeO<sub>3-δ</sub> ( $20 \times 10^{-6}/^{\circ}\text{C}$ ) compared to more conventional ceramics, it was decided to choose the same material for the porous substrate. For the substrate layers with relatively big pores, MgO was added to keep the pores of that layer open during the densification thermal treatment of the next layer.

Two-layer substrates in a disc shape, were successfully produced by using cold isostatic pressing for the macroporous under layer (pores of 0.5 to 0.8 μm) and by using a tape casting technique for the second layer.

Efforts will be done in the near future to increase the pore size of the macroporous support and to make the step from two-layer discs to two-layer tubes. Tubes are a more practical and conventional shape for constructing membrane modules. Thereby we will try to develop a sol gel technique to get a final dense top layer.

## Hollow fibers

Hollow fibers were produced by a spinning technique based on phase inversion. The flow sheet of the manufacturing route is given in Figure 1.

This technique is conventionally used for polymeric membranes and involves the conversion of a polymer solution of two or more components into a two-phase system by precipitation in a non-solvent for the polymer. The difference here is that the starting suspension is also loaded with a certain volume of ceramic powder and that the polymeric part is burned out later on.

To construct a membrane module with these hollow fibers it is not only necessary to look a brazing material for this special perovskite material, but in a first instance the fibers themselves must be strong enough to withstand the stresses generated due to the joining.

Till now the maximum strength obtained in 4-point bending tests was 75 Mpa. Because this strength value is strongly depending on the microstructure produced by the spinning technique, the details of the manufacturing route will have to be fixed to optimise the fiber strength.

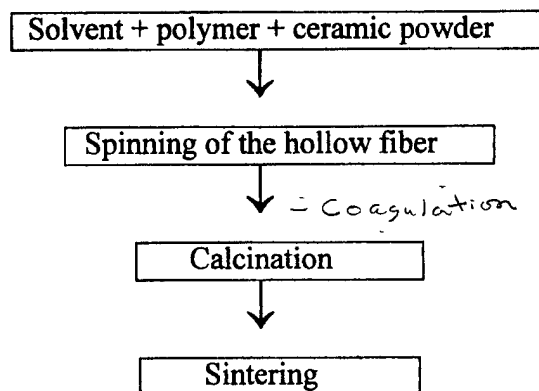


Figure 1. Manufacturing route for ceramic hollow fibers,  
Based on the phase inversion technique

#### References

- [1] J. Luyten, W. Adriansens, I. Genné, J. Coymans and R. Leysen, Accepted for publication in Ceramic Processing Science.
- [2] J. Luyten, A. Buekenhoudt, H. Weyten, W. Adriansens, J. Coymans, R. Leysen, Proceedings of the Fifth International Conference on Inorganic Membranes, Nagoya, Japan, (ICIM'98), A-211, 96-99 (1998).



**Modification of Electrical Conduction by Ion Implantation in  $Y_2O_3$  doped  $ZrO_2$** 

S. Raz\*, N. Stelzer<sup>#</sup>, J. Maier<sup>+</sup>, R. Kalish\* and I. Riess\*

\*Physics Department, Technion Israel Institute of Technology, Haifa 32000, Israel

<sup>+</sup>Max Planck Institute FKF, Heisenberg str. 1, D - 70569 Stuttgart, Germany

<sup>#</sup>Austrian Research Centers, Materials Technology Functional Materials

2444 Seibersdorf, Austria

**Abstract**

This paper presents the characterization of electronic conductivity in  $Y_2O_3$  doped  $ZrO_2$  (YSZ) implanted with different ions as measured at low temperature  $T \leq 200^\circ C$ . The ions used for doping the YSZ were: Mn, Bi, Se, Fe, Cu and Te. The effect of temperature, oxygen partial pressure and the concentration of dopant on the conductivity were measured. The activation energy for conduction ranged between 0.64 eV for Mn implanted YSZ to 0.92 eV for Te implanted YSZ at the low temperature regime ( $T \leq 200^\circ C$ ). We found that for most of the samples at low concentration of dopant ( $\sim 0.1$  mol%) the conductivity mechanism could be interpreted as variable range hopping.

## MODIFICATION OF SOLID OXIDE ELECTROLYTES FOR FUEL CELLS

F. Berckemeyer and W. Weppner

Chair for Sensors and Solid State Ionics  
Technical Faculty, Christian-Albrechts University zu Kiel  
Kaiserstr. 2, D-24143 Kiel, Germany

In a search for an improvement of ionic conductivity and electrode processes of zirconia solid electrolytes, various alternative materials were investigated and optimized with regard to the ionic and electronic properties for the application in high-temperature fuel cells.

Cerium-gadolinium oxide shows high ionic conductivity but the conductivity of excess electrons under reducing conditions needs to be decreased by about a factor of 3. The investigation considered the doping by compounds with 2

p-type conduction which might in this way decrease the n-type conductivity. Among these materials the oxides of iron, cobalt, magnesium, chromium and terbium were chosen. It was found that the partial conductivities of both types of electronic charge carriers may be controlled separately by doping, i.e. the mass action equilibrium constant varies with the dopant type and concentration.

Strontium and magnesium doped lanthanum gallates show a continuous drift and decrease in the total conductivity in the temperature range between 700 and 800 °C which may be related to the uptake of oxygen and ordering phenomena in the oxygen lattice. The whole conduction could be increased by a factor of 5 and 6 by doping with 5 % iron and chromium, respectively. The properties of the doping cations may be not generally derived from the properties of the binary oxides since in the case of iron the stable oxide is an n-type conductor. The perovskite structure results in an oxidation of the cations compared to the binary oxides. Chemical degradation occurs at voltages as low as 1.2V versus air at 800 °C. The doping by cerium and titanium has no influence on the n-type conductivity.

ELECTRONIC TRANSPORT PROPERTIES AND ELECTRONIC  
STRUCTURE OF TiO<sub>2</sub> DOPED YSZKiyoshi KOBAYASHI<sup>b</sup>, Shu YAMAGUCHI<sup>a</sup>, Toru HIGUCHI<sup>c</sup>, Shik SHIN<sup>d</sup>, and Yoshiaki  
IGUCHI<sup>a</sup><sup>a</sup>Department of Materials Science and Engineering, Nagoya Institute of Technology, Gokiso-  
cho, Showa-ku, Nagoya 466-8555, Japan<sup>b</sup>National Institute of Materials and Chemical Research, Higashi 1-1, Tsukuba 305-8565, Japan<sup>c</sup>Faculty of Science, Science University of Tokyo, 1-3, Kagurasaka, Shinjuku, Tokyo 162-  
0825, Japan<sup>d</sup>Institute of Solid State Physics, University of Tokyo, Tanashi 188-8501, Japan

## Introduction

Mixed electronic and oxide ion conductors have attracted attention for applications as anode materials in solid oxide fuel cell, oxygen gas separators, and other electrochemical devices for various energy conversion systems. Especially, titania-doped yttria stabilized zirconia (YSZ) has been focused since the report on the mixed conductivity by Liou and Worrell [1]. The present authors have reported about the electronic conductivity in YSZ doped with 5 and 10 mol% of TiO<sub>2</sub> measured by the dc-polarization technique using the Hebb-Wagner's asymmetric cell [2-3]. However, the origin of the change in the electronic structure and electronic transport properties by the TiO<sub>2</sub> doping have not been clarified yet. In the present study, the electronic conductivity of yttria stabilized zirconia doped with 2 mol% of TiO<sub>2</sub> was measured using dc-polarization method, and the change in the electronic structure is discussed based on the X-ray absorption spectra for 2, 5, and 10 mol% of TiO<sub>2</sub>-doped YSZ samples.

## Experimental

Dc-polarization measurements were made using the disk shaped sample synthesized by the conventional solid-state reaction method with the composition of  $\text{Zr}_{0.835}\text{Y}_{0.145}\text{Ti}_{0.02}\text{O}_{1.927}$ . The blocking electrode was fabricated using the gold plate, alumina disk, and Pyrex glass gasket as described in the previous report [2]. The measurements were made at 1273, 1223, 1173, 1123, and 1073 K. Oxygen partial pressures at the reversible electrode were fixed at 1.0 atm by flowing pure oxygen gas. Details of experimental procedures of the dc-polarization measurements and the analysis methods have been reported in the previous paper [2].

The X-ray absorption spectroscopy (XAS) was carried out at undulator beamline BL-19B in the Photon Factory at High Energy Accelerator Research Organization (Tsukuba, Japan). Synchrotron radiation from the undulator was monochromatized using a grating monochromator VLM19. The resolution of the beamline was about 50 meV at  $h\nu = 500$  eV. The XAS spectra were measured by the XUV silicon photodiode.

Samples of yttria stabilized zirconia doped with 2, 5, and 10 mol% of TiO<sub>2</sub> are denoted as 2TD-YSZ, 5TD-YSZ, and 10TD-YSZ, respectively.

## Results and Discussions

Arrhenius plots of the partial conductivities of holes and electrons at unit oxygen partial pressure ( $p_{\text{O}_2}$ ),  $\sigma_p$  and  $\sigma_n$  is shown in Fig. 1. Previous results of non-doped YSZ are also plotted for comparison.  $\sigma_n$  values increase with increasing TiO<sub>2</sub> concentration, while those of  $\sigma_p$  are almost independent of TiO<sub>2</sub> content. Values of the activation energy, calculated from the slope of the Arrhenius plots for  $\sigma_n$  ( $E_{\text{an}}$ ), decreased with increasing TiO<sub>2</sub> concentration. The  $E_{\text{an}}$  values for 5TD-YSZ (2.7 eV) and 10TD-YSZ (2.8 eV) tend to the  $E_{\text{an}}$  value of TiO<sub>2</sub>

(2.0 eV). Contrary, the values of activation energy of  $\sigma_p$  ( $E_{ap}$ ) for 2TD-YSZ (1.9 eV), 5TD-YSZ (1.8 eV), and 10TD-YSZ (1.9 eV) are almost the same with those in non-doped YSZs (1.5-1.9 eV). From the defect model of  $\text{TiO}_2$  doped YSZ [2], the forbidden gap ( $E_g$ ) is given by  $E_{an} + E_{ap}$  with the assumption that values of the activation energy for mobility of electrons and holes are negligibly small. The  $E_{an} + E_{ap}$  values are found to decrease by the  $\text{TiO}_2$  doping, and this experimental results are qualitatively in good agreement with the  $E_g$  dependence on  $\text{TiO}_2$  content, estimated by the EELS measurements [4].

O1s XAS spectra of 2TD-YSZ, 5TD-YSZ, and 10TD-YSZ are shown in Fig. 2. In the light 3d and 4d transition metal compounds, the dipole selection rules indicate that the O1s XAS spectra correspond to transitions into O2p character hybridized with unoccupied metal d-states. The peak at  $\sim 531.5$  eV is the t2g subband of the unoccupied Ti3d states. The peak at  $\sim 533.5$  eV is the t2g subband of the unoccupied Zr4d states. The eg subbands of Zr4d and Ti3d states are not shown in this figure, because electronic transport properties are not affected by the eg subbands. From this spectra, the decrease in  $E_g$  value by the  $\text{TiO}_2$  doping may be due to the propagation of the Ti3d orbital. The relationship between  $E_g$  and mol fraction of  $\text{TiO}_2$  will be further discussed using the percolation model.

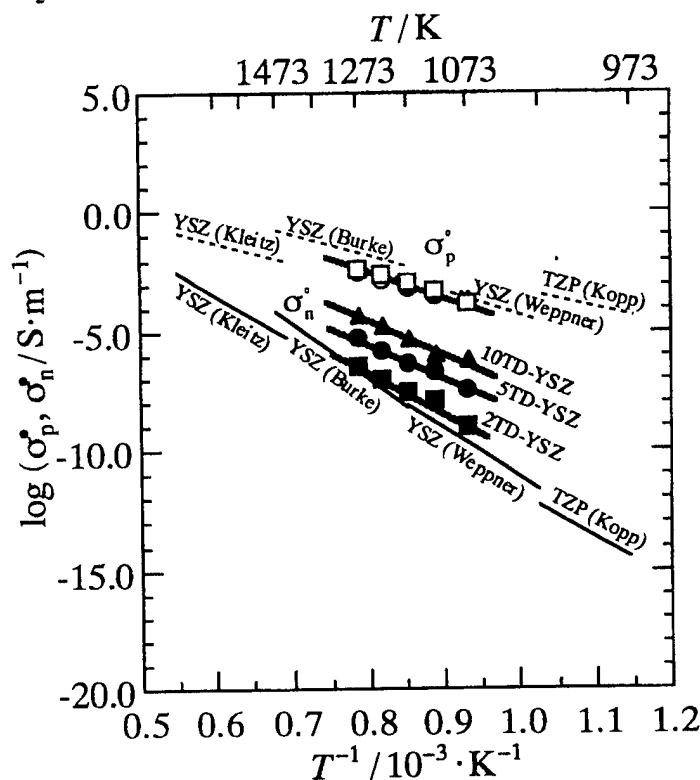


Fig. 1. Arrhenius plot of the partial conductivities for holes and electrons at unit oxygen partial pressure.

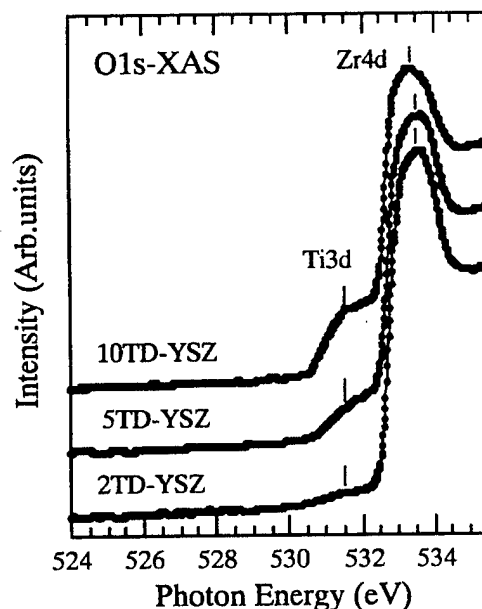


Fig. 2. O1s X-ray absorption spectra of 2TD-YSZ, 5TD-YSZ, and 10TD-YSZ.

## References

- [1] S. S. Liou and W. L. Worrell, Appl. Phys. A **49**, 25 (1989)
- [2] K. Kobayashi et al., Solid State Ionics, **93**, 193 (1997)
- [3] K. Kobayashi et al., The Korean Journal of Ceramics, **4**, 114 (1998)
- [4] U. Vohrer et al., Sensors and Actuators B, **4**, 411 (1991)

ELECTRICAL CONDUCTIVITY of CeO<sub>2</sub>-DOPED YSZ

Chang Ho Lee and Gyeong Man Choi

Department of Materials Science and Engineering, Pohang University of Science and Technology, Pohang 790-784, Korea

## Introduction

Mixed conducting materials which show both electronic and ionic conductivity are promising electrode materials for solid oxide fuel cell or gas separating membrane. CeO<sub>2</sub>-doped YSZ solid solutions are formed at the interface of stabilized zirconia and ceria when they are in use as a composite membrane. Cales and Baumann[1,2] have previously investigated the electrical properties of these materials at temperatures above 1000°C for their use as a possible gas separating membrane. In this study, we have measured the Po<sub>2</sub>-dependence of electrical conductivities of CeO<sub>2</sub>-doped YSZ between 850°C and 1000°C for use as an electrode of solid oxide fuel cell. The conductivity was measured as a function of temperature and oxygen partial pressure, and were fitted by using an equation derived from a defect model. The electronic transference numbers were also calculated by the fitting.

## Experimental Method

The solid solutions, [(ZrO<sub>2</sub>)<sub>1-x</sub>(CeO<sub>2</sub>)<sub>x</sub>](Y<sub>2</sub>O<sub>3</sub>)<sub>0.08</sub> (x=0, 0.1, 0.2, and 0.3), were prepared by the solid-state reaction of respective oxide powders: calcined ceria from cerium nitrate (99.9%, Kojundo Chemical Laboratory Co., Japan) at 800°C in air, 8 mol% yttria-stabilized zirconia (TZ8Y, TOSHO, Japan), and yttria (99.99%, AC&T Co.). Appropriate proportions of CeO<sub>2</sub>, TZ8Y, and Y<sub>2</sub>O<sub>3</sub> powders were ball milled in ethanol (99.9%) and dried in air. After pressing, the specimens were sintered in air for 10 h at 1600°C. The specimens with the relative sintered densities of 96-97% were cut into 2×3×15mm bar. 4-probe d.c. conductivity, using platinum-pasted (Engelhard No.6926) electrode, was measured with varying temperatures (between 850 and 1000°C) and oxygen partial pressures (1~10<sup>-16</sup> atm).

## Results and Discussion

Fig.1 shows the measured electrical conductivity for the samples with a)x=0 and 0.1 and b)x=0.2 and 0.3. For the x=0.1, the ionic conductivity at high Po<sub>2</sub> is clearly reduced from that of

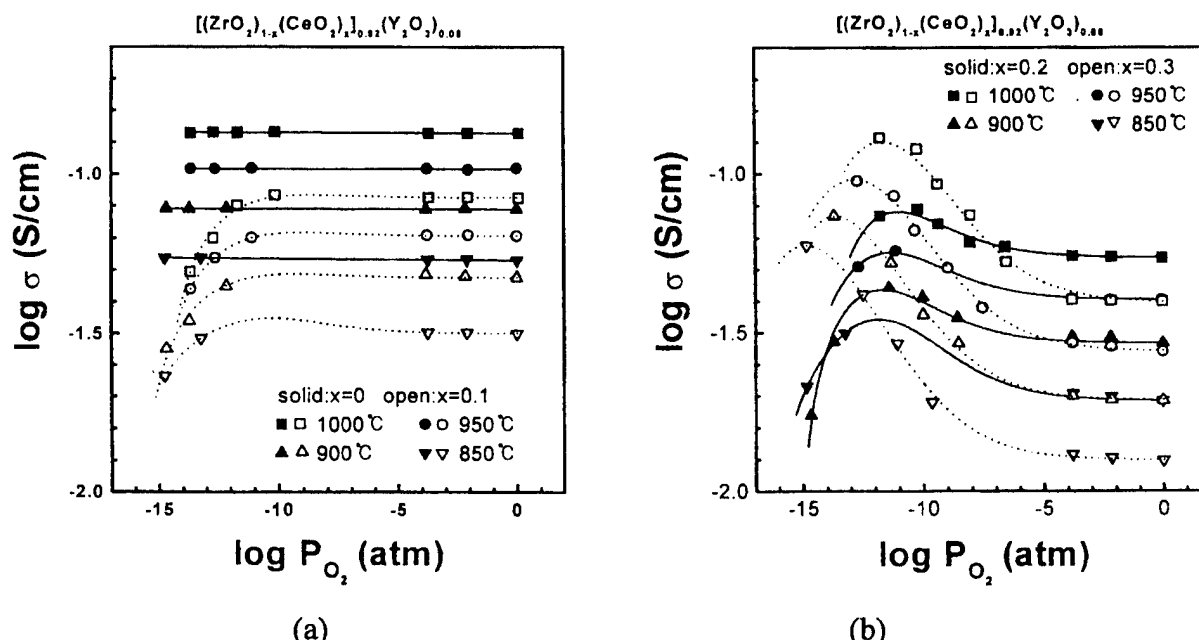


Fig.1. Electrical conductivity of [(ZrO<sub>2</sub>)<sub>1-x</sub>(CeO<sub>2</sub>)<sub>x</sub>](Y<sub>2</sub>O<sub>3</sub>)<sub>0.08</sub> at 850-1000°C versus oxygen partial pressure for the samples (a)x=0 and x=0.1 and (b)x=0.2 and x=0.3. The lines are the fitted curves using Eq.1.

undoped YSZ and as the Po<sub>2</sub> further decreases the conductivity drops below the value at the plateau.(Fig.1a) However for the specimens with higher Ce content, the conductivity increases with decreasing Po<sub>2</sub> and finally decreases after showing maximum of conductivity.(Fig.1b) The appearance of the conductivity maximum is explained by the reduction of Ce ion with Po<sub>2</sub> decrease, resulting in the increased n-type electronic conductivity from that of YSZ. Since the observed ionic ( $\sigma_{ion}$ ) and the electronic( $\sigma_{elec}$ ) or hopping( $\sigma_h$ ) conductivity may be summed, the total conductivity is given by;

$$\begin{aligned}\sigma_{total} &= \sigma_{ion} + \sigma_{elec} = \sigma_{ion} + \sigma_h \\ &= (\sigma_{ion,o} - AP_{O_2}^{-1/4}) + \left[ \frac{BP_{O_2}^{-1/4}}{(CP_{O_2}^{-1/4} + 1)^2} \right]\end{aligned}\quad (1)$$

where  $\sigma_{ion,o}$  is the oxygen ionic conductivity at  $P_{O_2}=1$  atm and A, B, and C are constants which determine the  $P_{O_2}$  dependence of the decreasing oxygen ion conductivity, the magnitude of electronic conductivity, and the  $P_{O_2}$  at which maximum conductivity appears, respectively.

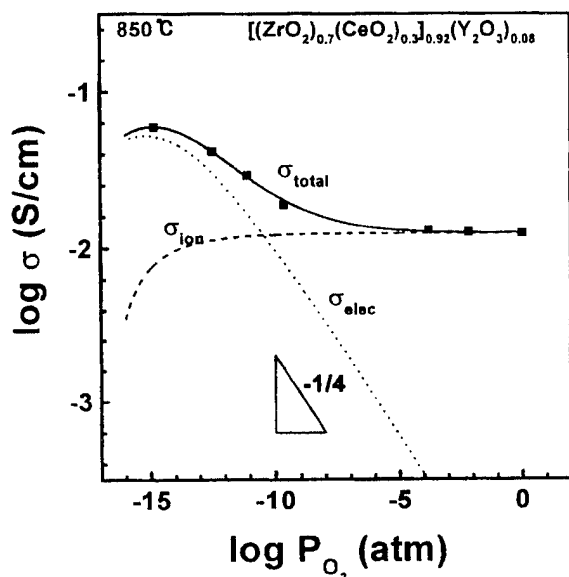


Fig.2. The total, the ionic, and the electronic conductivity of  $[(ZrO_2)_{0.7}(CeO_2)_{0.3}](Y_2O_3)_{0.08}$  at 850°C obtained by fitting the measured conductivity using Eq.1.

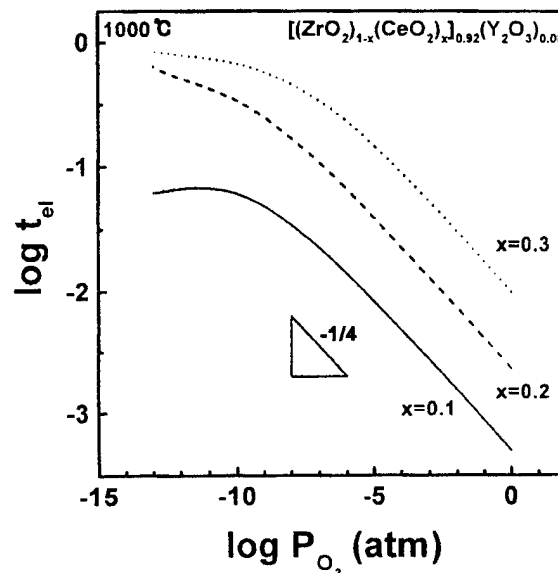


Fig.3. Electronic transference numbers of  $[(ZrO_2)_{0.7}(CeO_2)_{0.3}](Y_2O_3)_{0.08}$  at 1000°C.

Both dotted and solid lines in Fig.1 are fitted curves using Eq. (1). Fig.2 shows an example of the separated ionic and electronic conductivity, showing the effect of the increasing electron and the decreasing oxygen-ion conductivity with decreasing  $P_{O_2}$ . The electronic transference numbers ( $t_{el}$ ) were also calculated by the fitting and were shown in Fig.3. The  $t_{el}$  value increases with decreasing  $P_{O_2}$  and increasing Ce content. At 1000°C in oxygen atmosphere, the  $t_{el}$  value increases to as high as 0.01.

### Conclusions

The electrical conductivity of  $[(ZrO_2)_{1-x}(CeO_2)_x](Y_2O_3)_{0.08}$  ( $x=0, 0.1, 0.2$ , and  $0.3$ ) was measured below 1000°C in a wide  $P_{O_2}$  range and fitted by an equation following the assumed defect model. The electronic transference number ( $t_{el}$ ) was calculated from the curve fitting of data and was shown to increase with increasing  $CeO_2$  content and decreasing  $P_{O_2}$ .

### References

1. B.Cales and J.F. Baumard, Rev. int. hautes Temper. Refract. **17**, 137-147(1980)
2. B.Cales and J.F.Baumard, J.Electrochem.Soc., **131**, 2407(1984)

INFLUENCE OF DOPANT VALENCE ON ELECTRICAL PROPERTIES OF DOPED LaInO<sub>3</sub>Hongpeng He, Xuejie Huang and Liquan ChenLaboratory for Solid State Ionics, Institute of Physics, Chinese Academy of Sciences,  
P.O. Box 603-29, Beijing, 100080, China

Doped ZrO<sub>2</sub>, CeO<sub>2</sub> based oxides are the most extensively studied solid oxide electrolytes for using in solid oxide fuel cell (SOFC). It is well known that these kinds of materials have some problems in practice. For last few years, large attentions are paid to the perovskite oxides (ABO<sub>3</sub>), e.g. LaGaO<sub>3</sub>, NdGaO<sub>3</sub>, and NdAlO<sub>3</sub><sup>[1-3]</sup> etc. Low valence oxides are doped in these materials to increase the oxygen ion vacancies. In perovskite type oxide, both A and B sites could be doped.

In this paper, we report our studies on the electrical properties of doped LaInO<sub>3</sub>. The dopants include metal ions with valence different from +3. If the valence of dopant is lower than +3, i.e., Sr<sup>2+</sup> was doped at La<sup>3+</sup> site, according to the chemical reaction:  $(\text{SrO}) \rightarrow \text{Sr}'_{\text{La}} + \frac{1}{2} V_{\text{O}}^{\bullet\bullet}$

+  $\frac{1}{2} \text{La}_2\text{O}_3$ , oxygen ion vacancy can be created and its electrical conductivity will increase. If two high valence ions, i.e., Zr<sup>4+</sup>, were doped, from electrical neutrality rule, one interstitial oxygen will be produced. If both lower and higher valence ions were doped at the same time, the interstitial oxygen ions introduced by Zr<sup>4+</sup> doping will compensate the oxygen vacancies created by Sr<sup>2+</sup> doping. When equal amounts of Sr<sup>2+</sup> and Zr<sup>4+</sup> are doped at La<sup>3+</sup> and In<sup>3+</sup> sites respectively, there will be no more extra oxygen vacancy or interstitial oxygen theoretically. The experimental results show that the electrical conductivity of La<sub>0.9</sub>Sr<sub>0.1</sub>In<sub>0.9</sub>Zr<sub>0.1</sub>O<sub>3</sub> (LSIZ) is smaller than that of La<sub>0.9</sub>Sr<sub>0.1</sub>InO<sub>3</sub> (LSI), but higher than that of LaInO<sub>3</sub>. When the amount of Sr<sup>2+</sup> increases to 20%, that is La<sub>0.8</sub>Sr<sub>0.2</sub>In<sub>0.9</sub>Zr<sub>0.1</sub>O<sub>3</sub> (LS2IZ), the electrical conductivity is close to that of LSI.

The electrical conductivity as a function of oxygen partial pressure has also been measured. The results show that doped LaInO<sub>3</sub> is a good mixed-conductor. As oxygen partial pressure decreases, the electrical conductivity drops firstly, and then keeps as constant, finally increases slightly. It means that in high and low oxygen partial pressure ranges, p- and n-type conductivity becomes obvious, while in intermediate oxygen partial pressure range, the main charge carrier is oxygen ion.

**Acknowledgment**

This work was financially supported by NSFC (No.29601006)

**References**

- [1] Tatsumi Ishihara et al., J. Am. Chem. Soc. 116, 3801 (1994).
- [2] Anthony Petric, Pengnian Huang, Solid State Ionics, 92, 113 (1996).
- [3] Tatsumi Ishihara et al., J. Electrochem. Soc., 141, 3444 (1994).

# CHEMICAL DIFFUSION PROPERTY IN $\text{ZrO}_2\text{-CeO}_2\text{-CaO}$ SYSTEM STUDIED BY ELECTRONIC RAMAN SCATTERING

Takanori OTAKE<sup>A</sup>, Hiroo YUGAMI<sup>A</sup>, Hitoshi NAITO<sup>A\*</sup>,

Kenichi KAWAMURA<sup>B</sup>, Tatsuya KAWADA<sup>B</sup>, Junichiro MIZUSAKI<sup>B</sup>

<sup>A</sup>Graduate School of Engineering, Tohoku University, Sendai 980-8579, Japan

<sup>B</sup>Research Institute for Scientific Measurements, Tohoku University, Sendai 980-8577, Japan

Ceria doped calcia stabilized zirconia ( $\text{ZrO}_2\text{-CeO}_2\text{-CaO}$  system) shows electron-ion mixed conduction at high temperature under reduced atmosphere. In this system, the electronic conductivity is caused by electrons, which may diffuse by hopping conduction between  $\text{Ce}^{4+}$  and  $\text{Ce}^{3+}$ . We have measured the depth profile of  $\text{Ce}^{3+}$  concentration in quenched samples by electronic Raman scattering and evaluated the chemical diffusion coefficient of the system. The chemical diffusion coefficient increases with increasing the amount of ceria dopant. However it is found that the electronic Raman intensity decreases with increasing the Ce-content.

## 1. Introduction

Ceria doped calcia stabilized zirconia ( $\text{ZrO}_2\text{-CeO}_2\text{-CaO}$  system: Ce-CSZ) is a mixed conducting material at high temperature under reduced atmosphere. In this system, it is considered that the electronic conductivity is caused by electrons, which result from reduction of cerium ions from  $\text{Ce}^{4+}$  to  $\text{Ce}^{3+}$ .

In this study, the valence change of cerium ion in Ce-CSZ mixed conductor was measured by electronic Raman scattering from  $\text{Ce}^{3+}$  centers and the chemical diffusion coefficient was evaluated from the depth profile of electronic Raman intensity.

## 2. Experimental

Solid solutions of  $[(\text{ZrO}_2)_{1-x}(\text{CeO}_2)_x]_{0.9}(\text{CaO})_{0.1}$  covering  $x=0.2, 0.4, 0.8$  were prepared by solid state reaction. Appropriate proportions of  $\text{ZrO}_2$ ,  $\text{CeO}_2$ , and  $\text{CaCO}_3$  powders were mechanically mixed and preannealed, isostatically pressed and fired at 1953K for 5h in air. The samples were cut to  $5 \times 5 \times 2\text{mm}$ .

The samples were situated in a silica tube and heated by an infrared light heating apparatus

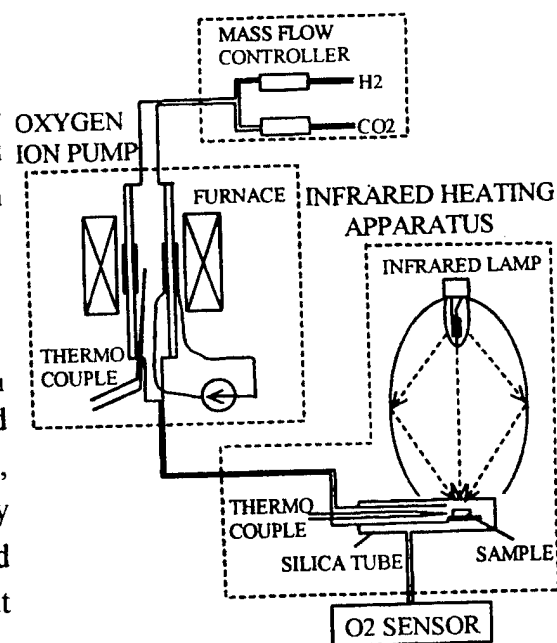


Fig.1 Schematic diagram of the experimental apparatus

\*Present Address; National Aerospace Laboratory, Chofu, Tokyo 182-8522, Japan



(Fig.1). The H<sub>2</sub>-CO<sub>2</sub> mixture gas was used in this study. The oxygen partial pressure was controlled by mass flow controllers and the oxygen ion pump. The experimental procedure is that (1) the samples were annealed at 973K in high p(O<sub>2</sub>) for a certain time to reach equilibrium, (2) the oxygen partial pressure was rapidly changed to low p(O<sub>2</sub>) by the oxygen ion pump and the samples were quenched down to room temperature after 600s keeping time at 973K, and (3) the samples were cut and Raman spectra of the cross section were measured.

### 3. Result

Raman spectra of Ce-CSZ (X=0.2) at d=0, 400, and 800μm (d: depth from surface of the samples) are shown in Fig.2. The Raman peak at about 2100cm<sup>-1</sup> is attributed to the <sup>2</sup>F<sub>7/2</sub> ↔ <sup>2</sup>F<sub>5/2</sub> electronic transition of Ce<sup>3+</sup> ion. It is considered that the electrons introduced in reduced condition will be trapped at Ce ion. Thus the spatial distribution of Ce<sup>3+</sup> concentration can be related to the chemical diffusion of oxygen in this system. The depth profile of the electronic Raman intensities that are normalized by the phonon peaks at about 600cm<sup>-1</sup> is shown in Fig.3. The data points were fitted to the diffusion equation for one-dimensional diffusion into a semi-infinite medium given by J.Crank [1].

$$\frac{C(d,t)}{C_0} = \operatorname{erfc} \frac{d}{2\sqrt{\tilde{D}_0 t}} - \exp(hd + h^2 \tilde{D}_0 t) \times \operatorname{erfc} \left\{ \frac{d}{2\sqrt{\tilde{D}_0 t}} + h\sqrt{\tilde{D}_0 t} \right\} \quad (1)$$

Where C(d,t) is the electronic Raman intensity, C<sub>0</sub> is the electronic Raman intensity of the surface,  $\tilde{D}_0$  (cm<sup>2</sup>/s) is the chemical diffusion coefficient,  $h = K_0 / \tilde{D}_0$ , K<sub>0</sub> is the surface exchange coefficient.  $\tilde{D}_0$  obtained from the fitted curve is  $1.44 \times 10^{-5}$  (X=0.2),  $2.36 \times 10^{-5}$  (X=0.4), and  $6.36 \times 10^{-5}$  cm<sup>2</sup>/s (X=0.8). The chemical diffusion coefficient increases with increasing the concentration of ceria. But the electronic Raman intensity decreases with increasing Ce-content. This would be related to the nonstoichiometry of this material [2,3].

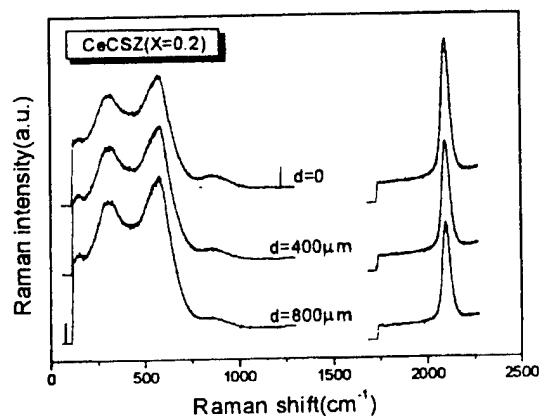


Fig.2 Raman spectra of Ce-CSZ (X=0.2)

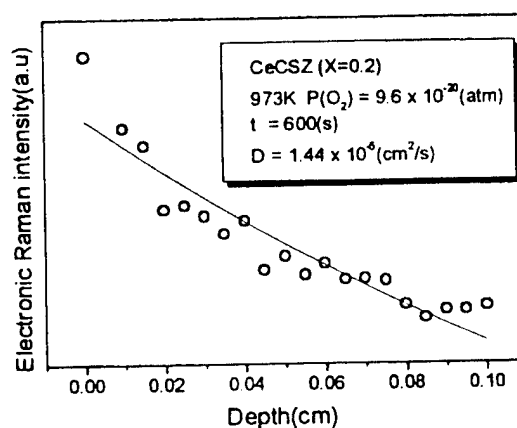


Fig.3 Depth profile of electronic Raman intensities of Ce-CSZ (X=0.2)

[1] J.Crank, "The Mathematics of Diffusion, 2nded." Oxford Univ. Press. 36 (1975).

[2] K.Kawamura et al., J.Electrochem.Soc., **145**, 2552 (1998).

[3] K.Kawamura et al., Proc. US-JAPAN Workshop Electrically Active Ceram. Interfaces, 189 (1998).

OXYGEN TRANSPORT PROPERTIES IN  $\text{ZrO}_2\text{-CeO}_2\text{-Y}_2\text{O}_3$  BY SIMS ANALYSESHitoshi NAITO<sup>A</sup>, Natsuko SAKAI<sup>B</sup>, Takanori Otake<sup>C</sup>, Hiroo YUGAMI<sup>C</sup>, Harumi YOKOKAWA<sup>B</sup><sup>A</sup>National Aerospace Laboratory, Chofu, Tokyo 182-8522, JAPAN<sup>B</sup>National Institute of Materials and Chemical Research (NIMC), Tsukuba 305-8565, JAPAN<sup>C</sup>Graduate School of Engineering, Tohoku University, Sendai 980-8579, JAPAN

Zirconia based mixed conductors have many applications such as electrodes, and membranes for gas separation.  $\text{ZrO}_2\text{-CeO}_2\text{-Y}_2\text{O}_3$  (Ce-YSZ) is a mixed conductor at high temperature and low oxygen partial pressure. It shows anomalous behaviors of electrical conductivity depending on oxygen partial pressure and  $\text{CeO}_2$  concentration [1, 2]. These behaviors are considered to correlate oxygen ion diffusion in sample and surface exchange reaction. These properties can be monitored by the use of oxygen isotope. We measured surface exchange coefficients and oxygen tracer diffusion coefficients of YSZ with various  $\text{CeO}_2$  concentration by secondary ion mass spectrometer (SIMS; CAMECA, ims-5f) installed in National Institute for Materials and Chemical Research (NIMC), Japan.

Samples were synthesized by means of a solid state reaction. The prepared samples were formulated as  $\{(\text{ZrO}_2)_{1-x}(\text{CeO}_2)_x\}_{0.9}(\text{Y}_2\text{O}_3)_{0.1}$ . The concentration ratio  $x$  of  $\text{CeO}_2$  was varied from 0 (YSZ) to 1 (YDC). The cubic fluorite structure was confirmed by X-ray diffraction analyses and the relative density of 95% was derived for all specimens. Sintered specimens were cut into  $4 \times 3 \times 2 \text{ mm}^3$  parallelepipeds and surfaces were polished.  $^{18}\text{O}/^{16}\text{O}$  isotope exchange have been performed in a oxygen partial pressure ( $P_{\text{O}_2}$ ) of  $2.1 \times 10^4$  (air condition) and  $1 \times 10^{-15} \text{ Pa}$  at 973 K.  $^{18}\text{O}_2$  gas or  $\text{Ar}(1\%\text{H}_2)+\text{C}^{18}\text{O}_2$  mixture gas was used to control  $P_{\text{O}_2}$ . A sample was heated rapidly to 973 K using an infrared furnace and the isotope exchange reaction was taken in 300 sec and then quenched. The sample was cut and cross section was polished to monitor isotope diffusion profile. The oxygen isotope distribution in the sample was measured using SIMS.

Fig. 1 shows a depth profile of oxygen isotope diffusion in the sample (Ce-YSZ,  $x=0.8$ , treated in  $P_{\text{O}_2}=2.1 \times 10^4 \text{ Pa}$  at 973 K).  $^{18}\text{O}$  concentration ratio was derived from the intensity of SIMS signals. The oxygen isotope diffusion coefficient,  $D^*$ , and the surface reaction coefficient,  $k$  were obtained by fitting a following eqn. (1) [3].

$$\frac{C - C_2}{C_0 - C_2} = \text{erfc} \frac{x}{2\sqrt{D^*t}} - \exp(hx + h^2 D^*t) \text{erfc} \left\{ \frac{x}{2\sqrt{D^*t}} + h\sqrt{D^*t} \right\}, \quad (1)$$

$$h = k / D^*$$

where  $C$  is a concentration at a distance  $x$  from the surface,  $C_2$  is a concentration at initial state in a semi-infinite medium and  $C_0$  is concentration (pressure) in gas phase. The fitted line was also plotted in the figure. Fig. 2 shows the  $\text{CeO}_2$  concentration dependence of  $k$ ,  $D^*$  and total electrical conductivity,  $\sigma$ , at 973 K in  $P_{\text{O}_2}=2.1 \times 10^4$  and  $1 \times 10^{-15} \text{ Pa}$ . In air atmosphere (Fig. 2), the Ce concentration dependence of oxygen tracer diffusion coefficient corresponds with that of the total electrical conductivity, in which ionic conductivity is dominant. The surface reaction rate, however, had a higher value in the region of 20~60 mol% $\text{CeO}_2$  containing YSZ. This region of  $\text{CeO}_2$  concentration exhibits high electronic transference number at reduced atmosphere. Therefore, electronic conductivity in air condition is considered to show relatively high compared to other region of Ce concentration. The oxygen tracer diffusion coefficient and the

surface reaction rate are considered to affect ionic and electronic conductivity, respectively. The ionic conductivity is considered to slightly increase as observed in high temperature [2] in reduced condition.  $D^*$ 's especially in the Ce concentration range of 0.2 to 0.4 show higher value compared to those in air. The measurements of ionic and electronic conductivity of these samples and evaluations of transference number have been in progress to reveal the relationship between conductivity and  $D^*$  and  $k$ .

- [1] B. Cares, and J.F. Baumard, Rev. int. hautes Temper. Refract., 17, 137 (1980).  
 [2] H. Arashi, M. Nakata, and H. Naito, Solid State Ionics, 76, 315 (1995).  
 [3] J. Crank, "The Mathematics of Diffusion, 2nd ed.", Oxford Univ. Press, 36 (1975).

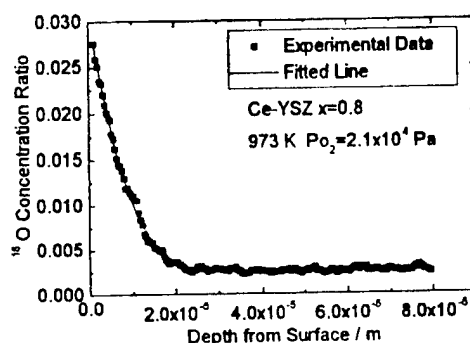


Fig. 1 Depth profile of oxygen isotope diffusion in Ce-YSZ( $x=0.8$ ) at 973 K in  $P_{O_2}=2.1 \times 10^4$  Pa.

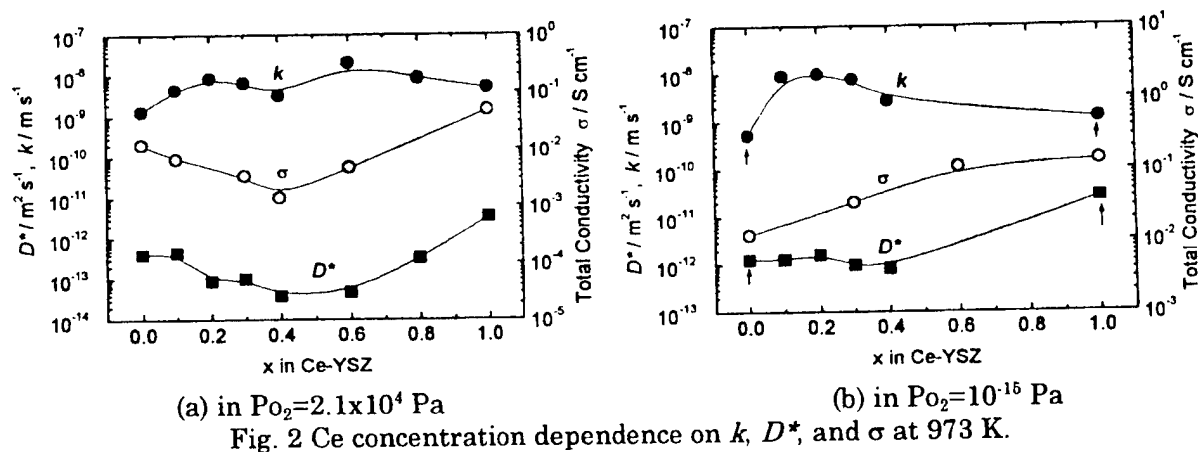


Fig. 2 Ce concentration dependence on  $k$ ,  $D^*$ , and  $\sigma$  at 973 K.

## PREPARATION OF MIXED CONDUCTING PYROCHLORES AS SOFC ANODES

P. Holtappels, F.W. Poulsen and M. Mogensen  
 Materials Research Department, Risø National Laboratory  
 P.O. Box 49, DK-4000 Roskilde, Denmark  
 peter.holtappels@risoe.dk

Mixed conducting pyrochlores may be used as anode materials in methane fuelled SOFC because of two main reasons: a) mixed conductivity of electrons and oxygen ions might help to overcome the limitation of the three phase boundary line as the electrochemically active reaction zone and b) lower carbon sensitivity and reforming activity can be expected compared to the state-of-the-art material which is a Ni-YSZ cermet. High electronic conductivity at low  $p(\text{O}_2)$ , as required for an electrode material, are reported for the pyrochlore solid solution  $\text{Gd}_2(\text{Ti}_{1-x}\text{Mo}_x)_2\text{O}_7$  by Porat, Heremans and Tuller [1]. Ionic conductivity can be assumed in dizirconates of Gd, Nd and Y, which show electrical conductivities independent of  $p(\text{O}_2)$  [2, 3]. In the Pr-zirconate  $\text{Pr}_2\text{Zr}_2\text{O}_7$ , the total conductivity in air and slightly reduced  $p(\text{O}_2)$  is assumed to be 90% electronic most likely resulting from the multivalent A cation  $\text{Pr}^{+3/+4}$ . Besides a sufficient electronic and –at least aimed– ionic conductivity, other requirements, e.g. phase and dimensional stability in a reasonable wide range of  $p(\text{O}_2)$ , chemical compatibility with the electrolyte, and matching thermal expansion coefficients, must also be fulfilled.

We prepared the pyrochlore solid solution  $\text{Gd}_2\text{TiMoO}_7$  and the pyrochlores  $\text{Pr}_2\text{Zr}_2\text{O}_7$  and  $\text{Pr}_2\text{Sn}_2\text{O}_7$  according to the mixed oxide method. Pellets containing stoichiometric mixtures of  $\text{Gd}_2\text{O}_3$ ,  $\text{TiO}_2$ ,  $\text{MoO}_3$  were sintered 13 h at 1300 °C in a mixture of 1%  $\text{H}_2$ /3%  $\text{H}_2\text{O}$  in  $\text{N}_2$ . Mixtures of  $\text{Pr}_6\text{O}_{11}$  with either  $\text{SnO}$  or  $\text{ZrO}_2$  have been sintered at 1400 °C in air for 16 h or  $2 \times 16$  h, respectively. The phase purity was verified by XRD at room temperature.

The phase stability of  $\text{Pr}_2\text{Sn}_2\text{O}_7$  at reduced  $p(\text{O}_2)$  was tested in 9%  $\text{H}_2$ /3%  $\text{H}_2\text{O}$  in  $\text{N}_2$  at 1000°C for 50 h. The reactivity with zirconia containing 8mol% yttria (8YSZ, Tosoh Corp.) was tested for  $\text{Pr}_2\text{Sn}_2\text{O}_7$  and  $\text{Gd}_2\text{TiMoO}_7$  for 1000 h in 1% $\text{H}_2$ /3% $\text{H}_2\text{O}$  at 1000 °C.

The D.C. conductivity was measured in the temperature range of 25 °C to 1000°C and at different  $p(\text{O}_2)$  at 1000°C by using A.C. impedance (Solartron 1260 FRA) or D.C. polarisation measurements (HP multiplexer).

The D.C. conductivity of the pyrochlore solid solution  $\text{Gd}_2\text{TiMoO}_7$  at 1000°C in 1% $\text{H}_2$ /3% $\text{H}_2\text{O}$ /96%  $\text{N}_2$  was 5 S/cm (see Fig. 1). The value of 0.16 eV for the apparent activation energy at a constant  $p(\text{H}_2)$  and  $p(\text{H}_2\text{O})$ , note that  $p(\text{O}_2)$  changes also with T, might indicate a high electronic contribution to the total conductivity in this material.

The XRD pattern after the reaction studies of  $\text{Gd}_2\text{TiMoO}_7$  with YSZ show only peaks that can be assigned to  $\text{Gd}_2\text{TiMoO}_7$  and YSZ. The lattice parameter obtained for the pyrochlore phase is  $10.272 \pm 0.004$  Å before and after the reaction studies. No indications for a reaction between  $\text{Gd}_2\text{TiMoO}_7$  and YSZ are given by XRD.

Mixed conductivity was observed for  $\text{Pr}_2\text{Zr}_2\text{O}_7$  (Fig. 2). This pyrochlore material shows a p-type like conductivity at  $p(\text{O}_2) > 0.002$  bar. Ionic conductivity is indicated in the low  $p(\text{O}_2)$  regime. The activation enthalpy in the ionic regime is of 1 eV. However, the total conductivity is too low for using this material in SOFCs.

The D.C. conductivity of  $\text{Pr}_2\text{Sn}_2\text{O}_7$  at  $p\text{O}_2 > 0.002$  bar is also included in Fig 2. First simulations (lines in Fig. 2) indicate that the p-type conductivity is lower for the stannate than for the zirconate. Measurements at lower  $p(\text{O}_2)$  were not performed because  $\text{Pr}_2\text{Sn}_2\text{O}_7$  decomposes, most likely due to a reduction and loss of Sn. This was indicated in the XRD diffractograms after both stability and reaction studies at reduced  $p(\text{O}_2)$ .

From the results we conclude that the pyrochlore solid solution  $\text{Gd}_2\text{TiMoO}_7$  may be a possible candidate as an anode material in an SOFC based on the electrolyte YSZ. Attempts to extend the  $p(\text{O}_2)$  range, where the pyrochlore structure is stable, are in progress. Although  $\text{Pr}_2\text{Zr}_2\text{O}_7$  is a mixed conductor at high  $p(\text{O}_2)$  the material shows almost pure ionic conductivity at the operating conditions of an anode. Significantly higher electronic conductivity is required in order to use this material in SOFC's. An enhancement of the electronic conductivity might be achieved by the addition of Mn.  $\text{Pr}_2\text{Sn}_2\text{O}_7$  can be excluded as an anode candidate material because the material is not stable in  $\text{H}_2/\text{H}_2\text{O}$  atmospheres.

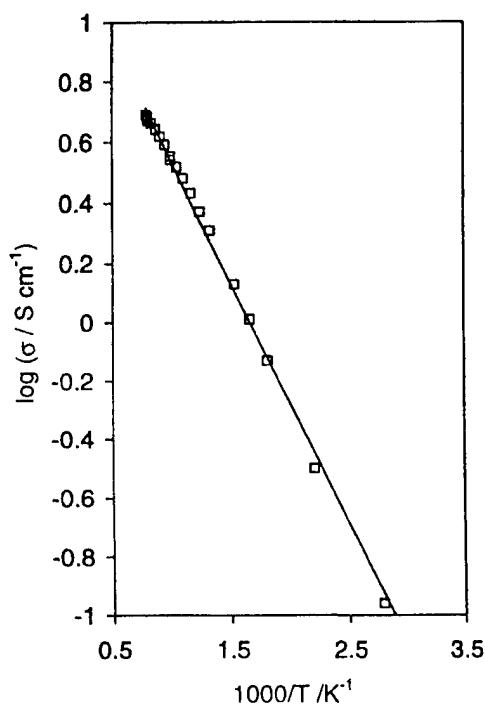


Fig. 1: temperature dependence of the D.C. conductivity of  $\text{Gd}_2\text{TiMoO}_7$  in 1% $\text{H}_2$ /3% $\text{H}_2\text{O}$  in  $\text{N}_2$

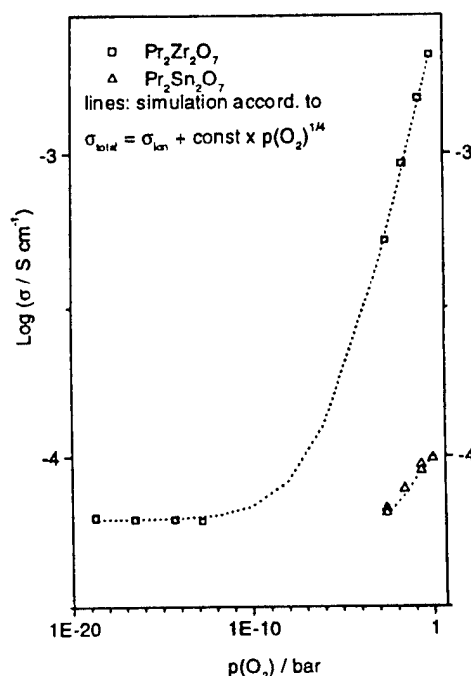


Fig. 2:  $p(\text{O}_2)$ -dependence of the D.C. conductivity at 1000°C;  $\square$ :  $\text{Pr}_2\text{Zr}_2\text{O}_7$ ;  $\triangle$ :  $\text{Pr}_2\text{Sn}_2\text{O}_7$

### References

- [1] O. Porat, C. Heremans, H.L. Tuller, J. Am. Ceram. Soc. **80**(9), 2278 (1997).
- [2] H.L. Tuller, Solid State Ionics **94**, 63 (1997).
- [3] R.A. Chapman, D.B. Meadowcroft, A.J. Walkden, J. Phys. D: Applied Phys. **3**, 307 (1970).

## Diffusion and surface exchange of $\text{La}_{1-x}\text{Sr}_x\text{CoO}_{3-\delta}$ studied with electrical conductivity relaxation

L.M. van der Haar, M.W. den Otter, H.J.M. Bouwmeester

Cobalt based perovskite-type oxides are of interest as potential oxygen separation membranes [1]. Under operating conditions, usually above 700°C, oxygen ions are transported through the membrane, charge compensated by a simultaneous flow of electronic charge carriers. The driving force for transport is a difference in the oxygen partial pressure applied across the membrane. For  $\text{La}_{1-x}\text{Sr}_x\text{CoO}_{3-\delta}$  perovskites high oxygen fluxes have been reported, increasing with Sr content, which A-site substituent serves the creation of oxygen vacancies in the  $\text{ABO}_3$  perovskite lattice. In the selection of suitable materials for application as thin supported dense membranes, a useful criterion is the value of the characteristic membrane thickness  $L_c$  [1]. The value of this parameter indicates at which thickness the transition occurs from predominant permeation rate control by diffusion to that by surface exchange. The value of  $L_c$  in a chemical relaxation type of experiment is determined by the ratio of the chemical diffusion coefficient of oxygen and the apparent surface exchange coefficient:  $L_c = \tilde{D}/K_{ex}$ .

In the present study electrical conductivity relaxation experiments were employed. The essence of this technique is that the response of the electrical conductivity of the material is monitored after a stepwise change in ambient oxygen partial pressure. The observed transient is fitted with a model using  $\tilde{D}$  and  $K_{ex}$  as fitting parameters.

Perovskite powders were prepared by thermal decomposition of the appropriate amount of metal-EDTA complexes. After calcination, pressing and sintering, thin rectangular samples were cut from the sintered bodies. Gold electrodes were attached to the samples for the conductivity measurements, which were carried out using an AC technique. Experiments were conducted on  $\text{La}_{1-x}\text{Sr}_x\text{CoO}_{3-\delta}$  ( $x = 0.2, 0.5$  and  $0.7$ ) in the temperature range of 400 to 800 °C and the  $p\text{O}_2$  range of 1 to  $1 \cdot 10^{-6}$  bar. The results were compared to isotope exchange and permeation data. In addition, the effect on the surface exchange kinetics achieved by doping with small amounts of Ni and Cu was investigated. A typical example of the relative change in apparent electrical conductivity of  $\text{La}_{0.3}\text{Sr}_{0.7}\text{CoO}_{3-\delta}$  is given in figure 1.

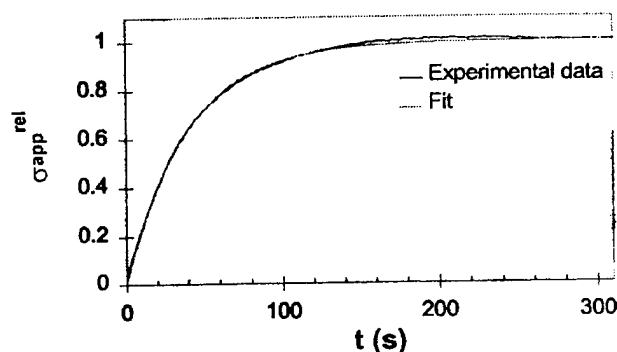


**Figure 1:** Experimental and fitted data for  $\text{La}_{0.3}\text{Sr}_{0.7}\text{CoO}_{3-\delta}$  at 700 °C. The  $p\text{O}_2$  was changed from 0.9 to 0.3 bar. Fit parameters are:  $\tilde{D} = 2.5 \cdot 10^{-5} \text{ cm}^2 \text{ s}^{-1}$ ,  $K_{ex} = 7.7 \cdot 10^{-4} \text{ cm s}^{-1}$

1. H.J.M. Bouwmeester, A.J. Burggraaf, Dense ceramic membranes for oxygen separation, In The CRC Handbook of Solid State Electrochemistry, Eds. P.J. Gellings, H.J.M. Bouwmeester, chapter 14, CRC Press Inc., Boca Raton (1997)

# OXYGEN TANSPT THROUGH $\text{Sr}_4\text{Fe}_4\text{Co}_2\text{O}_y$ COUPLED WITH OXIDATION OF CARBON MONOXIDE

C.S. Chen\*, S. Ran, W. Liu, D. Wang, M. Jiang, D.K. Peng

Department of Materials Science and Engineering,

University of Science and Technology of China

Hefei, Anhui 230026, P.R. China

The  $\text{Sr}_4\text{Fe}_4\text{Co}_2\text{O}_y$  oxide is reported to have great oxygen semi-permeability and acceptable mechanical and chemical stability at elevated temperatures. The most exciting application envisioned is to use the oxide to make high temperature chemical reactors for converting methane into syngas ( $\text{CO}/\text{H}_2$ ). The characteristics of the reactor is the integration of the two processes of oxygen separation from air via the oxide membrane and the partial oxidation of methane [1]. This paper is present the results of the study on the oxygen transport through the oxide coupled with the oxidation of CO at the permeate side.

$\text{Sr}_4\text{Fe}_4\text{Co}_2\text{O}_y$  ceramics were prepared by sintering the compact of the oxide powders at  $1200^\circ\text{C}$  for 5 hrs in air. The sintered disk-shaped specimen of 1.48 mm in thickness and 12 mm in diameter was sealed to an alumina tube to form a permeation cell using a glass sealant by heating to  $920^\circ\text{C}$ . Air was supplied to one side of the cell; at the other side CO (1.2 ml/min) was introduced by high purity helium (11.6 ml/min) to react with the oxygen that permeated from the air side. The composition of the effluent helium stream was analyzed with a Varion 3400 gas chromatograph. The oxygen permeation flux  $J_{\text{O}_2}$  through the specimen was calculated from

$$J_{\text{O}_2} = \frac{R}{A} * [C_{\text{CO}_2}^{\text{out}} + \frac{1}{2}C_{\text{CO}}^{\text{out}} - \frac{1}{2}C_{\text{CO}}^{\text{in}}]$$

where  $R$  is the flow rate at the outlet,  $C_i^{\text{in}}$  and  $C_i^{\text{out}}$  are the inlet and outlet concentration of the species  $i$ ,  $A$  the surface area of the specimen at the CO side. For the specimen measured, the surface area was 7 mm in diameter. Note that the glass sealing method makes the accessible surface area at the CO side smaller than that at the air side.

Fig.1 shows the oxygen flux as functions of temperature. It can be seen that with reducing temperature from 900 to  $850^\circ\text{C}$  the oxygen flux decreases slightly as marked by a small activation energy (36 kJ/mol). With further decreasing temperature oxygen flux decreases significantly as characterized by the large activation energy (135 kJ/mol). The inflection of the oxygen flux at  $850^\circ\text{C}$  may be caused by phase transformation. The drastic changes in electrical conductivity, oxygen chemical diffusion and nonstoichiometry of the oxide also indicate the occurrence of phase transformation [2]. The formation of  $\text{SrCO}_3$  at temperatures below  $850^\circ\text{C}$  may also contribute to the decrease of the oxygen flux. As  $\text{SrCO}_3$  should

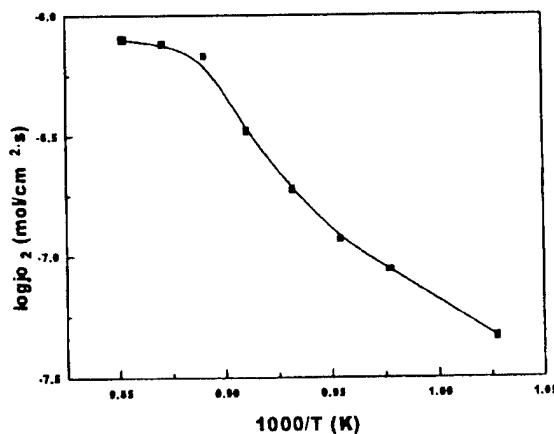


Fig.1 Oxygen permeation flux as functions of temperature

decompose into SrO and CO<sub>2</sub> at higher temperature, the specimen was re-heated to 900°C and second round permeation measurements were performed. The oxygen flux was recovered and became even higher than the value measured in the first round, as shown in Table 1. This may arise from the increased surface reaction area as the consequence of the decomposition of the SrCO<sub>3</sub>.

**Table.1 Oxygen permeation through Sr<sub>4</sub>Fe<sub>4</sub>Co<sub>2</sub>O<sub>y</sub> coupled with oxidation of CO**

Temperature (C°)	J <sub>O<sub>2</sub></sub> measured in the 1 <sup>st</sup> round (μmol/cm <sup>2</sup> ·s)	J <sub>O<sub>2</sub></sub> measured in the 2 <sup>nd</sup> round (μmol/cm <sup>2</sup> ·s)
900	0.79	0.85
875	0.76	0.81

The effect of CO partial pressure on the oxygen permeation process was investigated by varying the flow rate of CO stream at 875°C, and the results are given in Fig. 2. The oxygen flux reached as high as  $1.8 \times 10^{-6}$  mol cm<sup>-2</sup> s<sup>-1</sup> at P<sub>CO</sub> of 0.05 atm. It can be seen that oxygen permeation flux is proportional to P<sub>CO</sub>. Based on this observation, one may assume that the rate-limiting step for oxygen permeation is the adsorption of CO on the membrane surface and the subsequent reaction with oxygen ions that diffuse from the air side to the CO side.

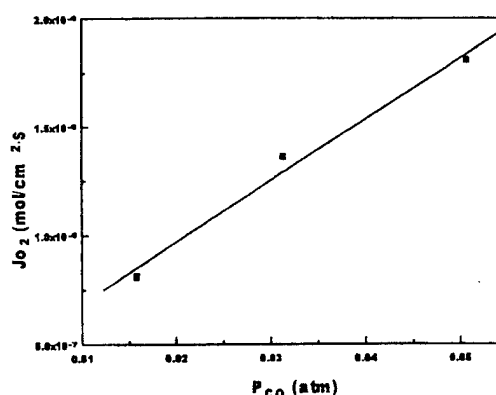


Fig.2 Oxygen permeation flux vs CO partial pressure

In summary, the oxide shows excellent oxygen permeability and good stability under reducing atmosphere (e.g. CO), and the oxygen separation membrane made of the oxide has a great potential for promoting oxygen-involved chemical reaction at elevated temperatures.

## References

- [1] U. Balachandran, T.J. Dusek, S. M. Sweeney, R.B. Poepel, R.L. Mieville, P.S. Maiya, M.S. Kleefisch, S. Pei, T.P. Kobylinski, and C.A. Udivich, *Amer. Ceram. Soc. Bull.* **74**, 71(1995).
- [2] W. Liu, G.G. Zhang, J.Q. Xie, S. Xie, C.F. Zhu, C.S. Chen, "Preparation, electrical conductivity and oxygen chemical diffusion coefficient of Sr<sub>4</sub>(Fe,Co)<sub>6</sub>O<sub>y</sub>" (to be published).



→ Co based  $\text{Sr}_4\text{Fe}_6\text{O}_{13}$  has lower oxygen transport than the  $\text{Sr}_4\text{Fe}_6\text{O}_{13}$  at low  $P_{\text{O}_2}$   
 INVESTIGATION OF SURFACE RATE KINETICS, CHEMICAL DIFFUSION AND  $\text{Sr}_4\text{Fe}_6\text{O}_{12}$   
 ELECTRICAL CONDUCTIVITY IN PURE AND DOPED  $\text{Sr}_4\text{Fe}_6\text{O}_{13}$  MIXED CONDUCTOR - may  
 MATERIALS decrease  
 at  $P_{\text{O}_2} \sim 10^{-8}$  atm

Rune Bredeesen<sup>a</sup>, Truls Norby<sup>b</sup>, Asgeir Bardal<sup>c</sup>

<sup>a</sup>SINTEF Materials Technology, P.O.Box 124 Blindern, 0314 Oslo, Norway

E-mail: Rune.Bredeesen@matek.sintef.no

<sup>b</sup>Centre for Materials Science, University of Oslo, Gaustadalleén 21, 0371 Oslo, Norway

E-mail: truls.norby@fys.uio.no

<sup>c</sup>SINTEF Materials Technology, Sem Sælandsvei 7, 7034 Trondheim, Norway

E-mail: Asgeir.Bardal@matek.sintef.no

## Introduction

Mixed oxygen anion and electron conducting materials are potential materials for oxygen selective membranes. These membranes can be used for production of pure oxygen and as a means to supply oxygen in integrated (partial) oxidation processes. In normal membrane operations an oxygen rich gas such as air will serve as the oxygen source and will be fed on one side of the membrane. The oxygen flux,  $J_{\text{O}_2}$ , through the membrane bulk is given by

$$J_{\text{O}_2} = \frac{RT}{16F^2L} \int_{\ln P_{\text{O}_2}^{\text{I},b}}^{\ln P_{\text{O}_2}^{\text{II},b}} \frac{\sigma_{\text{el}} \sigma_{\text{ion}}}{\sigma_{\text{el}} + \sigma_{\text{ion}}} d \ln P_{\text{O}_2} \quad (1)$$

where  $F$  is the Faraday number,  $L$  is the membrane thickness,  $P_{\text{O}_2}$  oxygen partial pressure, and  $\sigma$  electrical conductivity. From Eq. 1 it can be seen that the oxygen flux increases with decreasing membrane thickness, increasing oxygen partial pressure difference between the two sides (denoted I and II) of the membrane, and the electronic and oxygen anion conductivity, respectively. However, at a certain flux level, the rate of the surface reactions may become limiting for the overall oxygen transport. In terms of the chemical potential of oxygen,  $\mu_{\text{O}_2}$  across the membrane, this would mean that a significant drop in potential occurs at one or both gas-membrane interfaces, see Fig. 1.

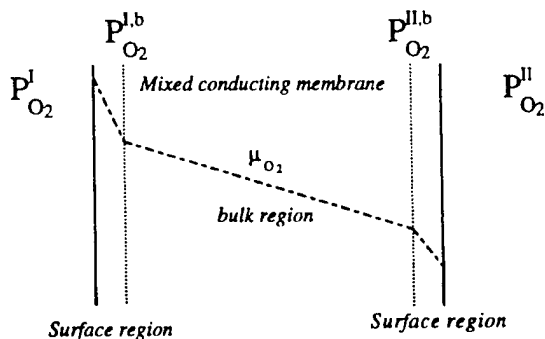


Figure 1. Schematic illustration of variation in oxygen chemical potential across a membrane having ambient oxygen partial pressures  $P_{\text{O}_2}^{\text{I}}$  and  $P_{\text{O}_2}^{\text{II}}$  on the two sides, and potential drops corresponding to  $P_{\text{O}_2}^{\text{I}} - P_{\text{O}_2}^{\text{I},b}$  and  $P_{\text{O}_2}^{\text{II},b} - P_{\text{O}_2}^{\text{II}}$  due to the surface reactions.

### Experimental

Thin membrane materials (thickness < 200  $\mu\text{m}$ ) of  $\text{Sr}_{4-x}\text{La}_x\text{Fe}_{6-y}\text{Ti}_y\text{O}_{13+(x+y)/2}$  ( $x = 0, 0.4, y = 0, 0.4$ ) were made by tape casting of powders prepared by solid state reaction of various precursors ( $\text{SrCO}_3$ ,  $\text{Fe}_2\text{O}_3$ ,  $\text{La}_2\text{O}_3$ ,  $\text{TiO}_2$ ). The surface exchange rate constant and the defect chemical diffusion coefficient in the membranes were studied by so-called transient thermogravimetric measurements. In these measurements the membranes were first equilibrated in air before the atmosphere rapidly was changed to pure oxygen. After a few seconds, the weight change of the membrane was recorded as a function of time. The recorded weight change data were fitted to a model involving both bulk diffusion and surface exchange kinetics given by [1]

$$\frac{M_t}{M_\infty} = 1 - \sum_{n=1}^{\infty} \frac{2L^2 \exp\left(-\frac{b_n^2 D t}{l^2}\right)}{b_n^2 (b_n^2 + L^2 + L)} \quad (2)$$

where  $M_t$  denotes the weight change from start at time  $t$ , and  $M_\infty$  the total weight change observed through the experiment.  $L = lk/D$ , where  $k$  is the surface exchange rate constant,  $D$  the defect chemical diffusion coefficient and  $l$  is half the thickness of the membrane.  $b_n$  are positive roots of the equation  $b \tan b = L$  [2].

The electrical conductivity of the different membrane materials was measured by the van Pauw method. The microstructure and phase composition of the tape cast membranes were studied by electron microscopy, EDS, and X-ray diffraction methods.

### Results

The results show that the estimated surface exchange rate constant is in the range of  $2\text{-}20 \cdot 10^{-4}$   $\text{cm/s}$  between  $700\text{-}1000^\circ\text{C}$ . The values of the defect chemical diffusion coefficient vary between  $1\text{-}30 \cdot 10^{-6}$   $\text{cm}^2/\text{s}$  in the same temperature range. No significant effects of the dopants could be observed on the kinetic parameters. However, the relative weight change of the membrane was highest for the samples with La-doping. Furthermore, doping with Ti gave also larger weight changes compared to pure  $\text{Sr}_4\text{Fe}_6\text{O}_{13}$ . This suggests that the effect of doping on the oxygen point defect concentration is higher when doping occurs on A-sites (Sr) compared to B-sites (Fe).

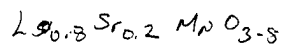
The electrical conductivity measurements show p-type conductivity approaching  $\log \sigma \propto 1/4 \log P_{\text{O}_2}$  at high oxygen partial pressures. By decreasing the partial pressure of oxygen the conductivity goes through a minimum indicative of n-type conduction at low pressures. Compared to undoped material, the p-type electrical conductivity increases with both La and Ti addition.

Detailed microstructural analysis shows that the La-doped membrane contains a fine-scale intergrowth of different phases. The microstructure of the membrane appears to undergo changes during the thermogravimetric measurement. Further details will be reported in the full-length paper.

### References

1. J. Crank. "The Mathematics of Diffusion", Oxford Science Publications, 1975 p 61-62.
2. Carslaw and Jaeger. "Conduction of heat in solids", Oxford Science Publications, 1959, p 491.

# PREPARATION AND CHARACTERISATION OF NEW LSGM/LSM MIXED-CONDUCTIVE COMPOSITE MATERIALS



H.Ahn and J.A.Kilner

LSGM composite

Centre for Ion Conducting Ceramics (CICM)  
Department of Materials  
Imperial College of Science, Technology and Medicine  
London SW7 2BP  
U.K.

LSGM : 175 S/cm at 500°C  
LSGM → { 0.1 S/cm " "  
12.1 × 10<sup>-6</sup> S/F

In recent studies, LaGaO<sub>3</sub>-based perovskite materials have received much attention for application as solid electrolytes for intermediate temperature SOFCs (Solid Oxide Fuel Cells) [1-3]. Many investigators have concluded that the high oxygen ion conductivity can be attained by the incorporation of cation dopants, particularly Sr and Mg (La<sub>1-x</sub>Sr<sub>x</sub>Ga<sub>1-y</sub>Mg<sub>y</sub>O<sub>3-δ</sub> where, 0.1 ≤ x ≤ 0.2, 0.1 ≤ y ≤ 0.2) [4-6]. Mixed and electronically conducting perovskite, such as LaMnO<sub>3</sub>-based materials, have been used as electrode materials for SOFCs due to their high electronic conductivity. In this study, we move the attention to the composite materials LSGM(La<sub>1-x</sub>Sr<sub>x</sub>Ga<sub>1-y</sub>Mg<sub>y</sub>O<sub>3-δ</sub>, where x=0.1, 0.2, y=0.1, 0.2)/LSM (La<sub>0.8</sub>Sr<sub>0.2</sub>MnO<sub>3-δ</sub>). This mixed-conductor can be applied as a fuel cell cathode, oxygen separator membrane or in sensors.

In this paper we present results on LSGM/LSM composite materials which were prepared by mixing the two components in the ratio of LSGM(6):LSM(4), LSGM(5):LSM(5) and LSGM(4):LSM(6). These composites were sintered at different temperatures and atmospheres (in Ar, O<sub>2</sub> and air) to investigate the best sintering conditions. The materials were also characterised by X-ray diffraction(XRD), scanning electron microscopy (SEM) and d.c.conductivity measurements. The sintered materials appear to have the perovskite structure and all pellets have densities greater than 93% theoretical density. The sample which was sintered in O<sub>2</sub> showed the highest density (about 95%) and the Ar sintered sample showed degradation, characteristic of reaction between the two compounds. Microscopic analysis of the reaction zone revealed the presence of a glassy phase.

## References

- [1] T.Ishihara, H.Matsuda and Y.Takita, J.Am.Chem.Soc. **116**, 3801 (1994).
- [2] P.Hung and A.Petric, J.Electrochem. Soc. **143**, 1644 (1996).
- [3] J.Drennan, V.Zelizko, D.Hay, F.T.Ciacchi, S.Rajendran and S.P.S.Badwal, J.Mater. Chem. **7**, 79 (1997).
- [4] T.Ishihara, H.Matsuda, H.Nishiguchi and Y.Takita, Solid State Ionics **79**, 147 (1995).
- [5] T.Ishihara, J.A.Kilner, M.Honda and T.Takia, J.Am.Chem.Soc. **119**, 2747 (1997).
- [6] K.Huang, R.S.Tichy and J.B. Goodenough, J.Am.Ceram.Soc. **81**, 2579 (1998).

## HYDROTHERMAL SYNTHESIS AND PROPERTIES OF MIXED CONDUCTING MATERIALS BASED ON CeO<sub>2</sub>

M. Greenblatt, P. Shuk and M. Croft\*

Department of Chemistry, Department of Physics and Astronomy\*, Rutgers, the State University of New Jersey, 610 Taylor Rd, Piscataway, NJ 08854-8087

The solid electrolyte is a key component of solid-state electrochemical devices, which are increasingly important for applications in energy conversion, chemical processing, sensing and combustion control [1]. In the past, many investigations have been carried out on various aspects of ceria solid solutions, the most promising material for the application as a solid electrolyte in solid oxide fuel cells (SOFC), mostly prepared by conventional ceramic methods [2]. However, the preparation temperature or time needed to obtain a homogeneous solid solution depends significantly on the particle size of starting materials. Recently we have shown that solid solutions of Ce<sub>1-x</sub>Sm<sub>x</sub>O<sub>2-x/2</sub> and Ce<sub>x</sub>Ca<sub>1-x</sub>O<sub>2-x</sub> can be hydrothermally prepared in a wide substitution range of Sm or Ca. [3]. While past efforts focused on expanding the electrolytic domain of oxide-ion conducting solid electrolytes for application in SOFC, more recently efforts begun to introduce enhanced electronic conduction in high ion conductive matrices to develop mixed conductors for oxygen membrane application [4]. For this application equally high electronic and ionic conductivities are required to achieve maximum of oxygen flux through the membrane needed for oxygen separation. The structural and chemical integrity as well as very high thermal expansion coefficients ( $> 20 \times 10^{-6} \text{ K}^{-1}$ ) are limiting factors for the application of the acceptor-doped perovskite oxides Ln<sub>1-x</sub>A<sub>x</sub>Co<sub>1-y</sub>B<sub>y</sub>O<sub>3-δ</sub> (A= Ca, Sr, Ba; B= Fe, Cu, Ni, Mn) as oxygen membranes [4]. More reliable oxygen membranes may be developed based on fluorite-type oxide ion conducting solid electrolytes, which are more stable and have considerably smaller thermal expansion coefficients ( $\sim 10^{-5} \text{ K}^{-1}$ ), if equally high electronic conductivity can be introduced into the fluorite matrix. Two rare earth elements Tb and Pr are known to have mixed valency at atmospheric pressure and contribution to electronic conductivity in oxide ion conducting solid electrolytes based on Bi<sub>2</sub>O<sub>3</sub>.

In this paper we present a systematic study of the structure, ionic and electronic conductivities and thermophysical properties of terbium or praseodymium substituted mixed conducting ceria solid solutions.

Solid solutions of Ce<sub>1-x</sub>(Tb/Pr)<sub>x</sub>O<sub>2-x</sub> (x=0-0.30) were synthesized by the hydrothermal method. The appropriate quantities of nitrates were dissolved separately in water, mixed and coprecipitated with ammonium hydroxide at pH= 10. The precipitated gels were sealed into teflon-lined steel autoclaves and hydrothermally treated at 260°C and ~ 10MPa for 10 hrs. The room/high temperature powder X-ray diffraction patterns (PXD) of the ultrafine powders were obtained with a SCINTAG PAD V diffractometer. The reflection from the (422) plane was used for the determination of average crystallite size. The average crystallite size, D, of the hydrothermally prepared powders was calculated from the Scherrer formula. Differential thermal analysis (DTA) and thermogravimetric analysis (TGA) measurements were carried out in the temperature range 25-750°C with a TA Instruments DSC 2910 and TGA 2050. The powder samples were pelletized and sintered at 1300-1400°C for 4 h with a programmed heating and cooling rate of 5°C/min. The sintered samples were over 95-97 % of the theoretical density in all cases. The microstructure of sintered samples was studied with an Atomic Force Microscope (AFM, QScope Model 250, Quesant Instrument Corporation, CA). The ionic conductivity measurements were performed by the complex impedance method on isothermal plateaus one hour long, in air on heating and cooling. The oxide ion transfer numbers were determined using concentration electrochemical cell. The oxygen permeability, J(O<sub>2</sub>), was calculated from electronic and ionic contributions to the total conductivity,  $\sigma_{\text{total}}$ , using Wagner equation.

The PXD data show that  $\text{Ce}_{1-x}\text{Tb}(\text{Pr})_x\text{O}_{2.8}$ , prepared by hydrothermal synthesis for the first time, forms solid solutions with the fluorite structure in a wide substitution range  $x=0-0.30$ . Ultrafine

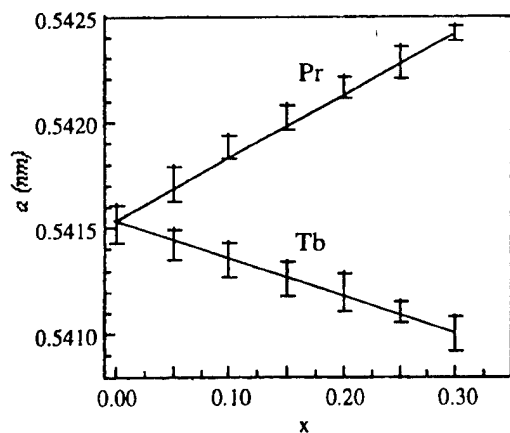


Fig. 1. Lattice constants of  $\text{Ce}_{1-x}(\text{Tb/Pr})_x\text{O}_{2.8}$  solid solutions as a function of  $x$ .

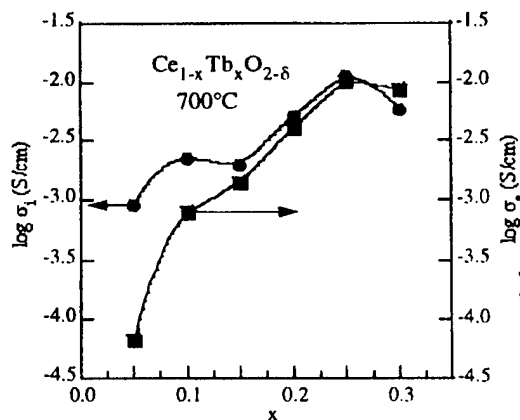


Fig. 2. Concentration dependence of the ionic and electronic conductivities of  $\text{Ce}_{1-x}\text{Tb}_x\text{O}_{2.8}$  solid solutions.

particles of uniform crystallite dimension, ~ 20 nm can be formed in 30 min. under hydrothermal conditions (260°C, 10 MPa). Further heat treatment slowly increases the crystallinity of the powder to ~ 25-50 nm in 12 hrs. The small particle size (25-50 nm) of the hydrothermally prepared materials allows sintering of the samples into highly dense ceramics at 1300-1350°C, ~300°C lower temperatures than required for samples prepared by solid state techniques. The unit cell parameter  $a$  slowly decreases with increasing Tb- and increasing with Pr-content (Fig. 1) in good agreement with effective ionic radii considerations.

X-ray absorption near edge spectroscopy (XANES) shows that at lower Tb substitution in  $\text{Ce}_{1-x}\text{Tb}_x\text{O}_{2.8}$   $\text{Tb}^{3+}$  is dominant. The formal valence of 3.0 and 3.26 for Tb was found in  $\text{Ce}_{1-x}\text{Tb}_x\text{O}_{2.8}$  for  $x=0.05$  and  $x=0.30$  respectively.

The total conductivity of  $\text{Ce}_{1-x}(\text{Tb/Pr})_x\text{O}_{2.8}$  solid solutions increases systematically with increasing the Pr or Tb substitution till  $x=0.30$ . With increasing Tb/Pr concentration the electronic contribution to the total conductivity increases due to the hopping of small polarons between  $\text{Tb}^{3+}/\text{Pr}^{3+}$  and  $\text{Tb}^{4+}/\text{Pr}^{4+}$ . The electronic conductivity exceeds the oxide ion conductivity at  $x > 0.25$  (Fig. 2). The oxide ion conductivity reaches a maximum at 25 % substitution (Fig. 2). The highest total conductivity was found for the Tb substitution at  $x=0.25$  ( $\sigma_{\text{TOT}} = 2.1 \times 10^{-2}$  S/cm,  $E_a = 0.49$  eV), and for the Pr at  $x=0.30$  ( $\sigma_{\text{TOT}} = 1.4 \times 10^{-2}$  S/cm,  $E_a = 0.47$  eV) with electronic

contribution to the total conductivity around 40-50 %. The thermal expansion coefficients, determined from high-temperature X-ray data, are  $11.8 \times 10^{-6} \text{ K}^{-1}$  for  $\text{CeO}_2$  and slowly increase with increasing Pr substitution ( $12.4 \times 10^{-6} \text{ K}^{-1}$  at  $x=0.30$ ) and decrease with Tb substitution ( $10.8 \times 10^{-6} \text{ K}^{-1}$  at  $x=0.30$ ).

The oxygen permeability,  $J(\text{O}_2)$ , calculated from ionic and electronic conductivities, systematically increases with increasing Tb/Pr substitution and temperature and is close to the oxygen permeability of the mixed conductors based on the best conductive bismuth oxide solid electrolytes [ $J(\text{O}_2) = 2.9 \times 10^{-10} \text{ mol/s} \cdot \text{cm}$  at 700°C for  $\text{Ce}_{0.75}\text{Tb}_{0.25}\text{O}_{1.875 \pm 0.08}$ ].

- [1] T. Takahashi, ed. High Conductivity Solid Ionic Conductors (World Scientific, Singapore, 1989).
- [2] H. Inaba and H. Tagawa, Solid State Ionics **83**, 1 (1996).
- [3] W. Huang, P. Shuk and M. Greenblatt, Chem. Mater. **9**, 2240 (1997).
- [4] H. J.-M. Bouwmeester and A.J. Burggraaf, in Solid State Electrochemistry, eds. P.J. Gellings and H. J.-M. Bouwmeester (CRC Press, New York, 1997).

# MEASUREMENT OF THE IONIC CONDUCTIVITY OF MIXED CONDUCTING PEROVSKITES USING MICROELECTRODES

Wolfgang Zipprich<sup>1</sup>, H.-D. Wiemhöfer<sup>2</sup>

<sup>1</sup> Laboratory of Inorganic Materials Science, Department of Chemical Technology, University of Twente, PO Box 217, 7500 Enschede, the Netherlands

<sup>2</sup> Institute of Inorganic Chemistry, Wilhelm Klemmstr. 8, 48161 Muenster, Germany

## Introduction

Substituted  $A^{III}B^{III}O_3$  oxides with perovskite structure with  $B = Co, Fe, \text{ or } Cu$  and a three-valent rare earth ion on A-sites, most often La, are currently under investigation in many groups due to the mixed ion and electron conductivity which makes these materials good candidates for oxygen electrodes in gas sensors and fuel cells at lowered temperatures as well as for gas separation membranes. In this study two series of mixed conducting perovskites  $La_{1-x}(Sr, Ca)_xCoO_{3-\delta}$  ( $0.1 \leq x \leq 0.5$ ),  $La_{0.8}Sr_{0.2}CuO_{3-\delta}$  and  $La_{0.8}Sr_{0.2}Co_{1-y}Fe_yO_{3-\delta}$  ( $0 \leq y \leq 1$ ), were prepared and their oxygen ion conductivity determined as a function of the oxygen partial pressure. For this purpose the inset of ion conducting microelectrodes (radius 40-100  $\mu m$ ) was chosen. The primary advantages of microelectrodes are due to their small area of contact: the interface capacitance is small, the transport processes are concentrated to a region near the interface resulting in small diffusion lengths which enables an easier and faster measurement of slow diffusion processes [1].

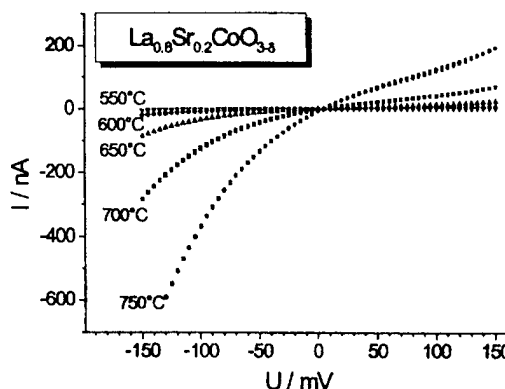
## Sample preparation and measurement set-up

Powders of the investigated perovskites were prepared by different method as complexation, a sol-gel process and a spray-freezing/freeze drying process. Best results concerning density and lowered sintering temperatures are obtained by applying the last two methods. Ceramics with a relative density of  $>95\%$  were thus prepared by firing the pressed pellets at  $950^\circ C$  and a subsequent sintering step at  $1150^\circ C$  for 12 hours. This method yielded a homogeneous powder with very small particle sizes in the range of 200 - 500 nm. Decomposition and calcination yielded the crystalline perovskite oxide at  $950^\circ C$ . For the conductivity measurements compact pellets were obtained by uniaxial pressing and subsequent sintering ( $T = 1140-1160^\circ C$ ;  $t = 8-12$  h). Measurements were performed in a two-electrode set-up in a vertical set-up with an ion-conducting microelectrode (YSZ) on top of the perovskite pellet [2].

## Results and discussion

The oxygen partial pressure at the micro-electrode is determined by the applied voltage corresponding to the Nernst equation. Oxygen ion conductivity of the sample can be calculated from the slope of the current voltage curve.

Fig. 1 a) Current voltage curves of  $La_{0.8}Sr_{0.2}CoO_{3-\delta}$  at  $700^\circ C$



The second derivation of the current voltage curve gives indication about the reaction mechanism, a positive curvature for a transport via vacancies, a negative one for an interstitial transport [3]. For a hemispherically shaped tip with a radius  $a$  as used in this study the oxygen ion conductivity can be calculated from the slope of the current voltage curve. This is shown for the example of the  $\text{La}_{0.8}\text{Sr}_{0.2}\text{CoO}_{3.5}$  in Fig. 1. The values of the oxygen ion conductivity for  $\text{La}_{1-x}\text{Sr}_x\text{CoO}_{3.5}$  are increasing with increasing Sr content, i.e. decreasing rhomboedric distortion, until the cubic structure is reached ( $x(\text{Sr}) = 0.5$ ).

For the  $\text{La}_{0.8}\text{Sr}_{0.2}\text{Co}_{1-y}\text{Fe}_y\text{O}_{3.5}$  an interesting trend of the ionic conductivity was found with increasing iron content (see Fig. 2): it increases for lower iron contents and decreases for larger iron contents. This corresponds to the structure that shows at higher temperatures a decreasing rhomboedric distortion for lower iron content and an increasing rhomboedric distortion for larger iron content.

For both the  $\text{La}_{0.8}\text{Sr}_{0.2}\text{CoO}_{3.5}$  and the  $\text{La}_{0.8}\text{Sr}_{0.2}\text{Co}_{1-y}\text{Fe}_y\text{O}_{3.5}$  a transport via vacancies was found. With the  $\text{La}_{0.8}\text{Sr}_{0.2}\text{CuO}_{3.5}$  a material as an example of an oxide perovskite with an interstitial transport mechanism was detected.

### Acknowledgement

S. Waschilewski is thanked for preparing some of the materials investigated in this study.

### References

- [1] H.-D. Wiemhöfer, Ber. Bunsenges. Phys. Chem., **97** (3), 461-469 (1993).
- [2] W. Zipprich, S. Waschilewski, F. Rocholl, H.-D. Wiemhöfer, Solid State Ionics, **101-103**, 1015-1023 (1997).
- [3] H.-D. Wiemhöfer, F. Rocholl, W. Zipprich, T. Hauber and G. Reinhardt, Defects and Diffusion Forum **143-147** 1701-1706 (1997).

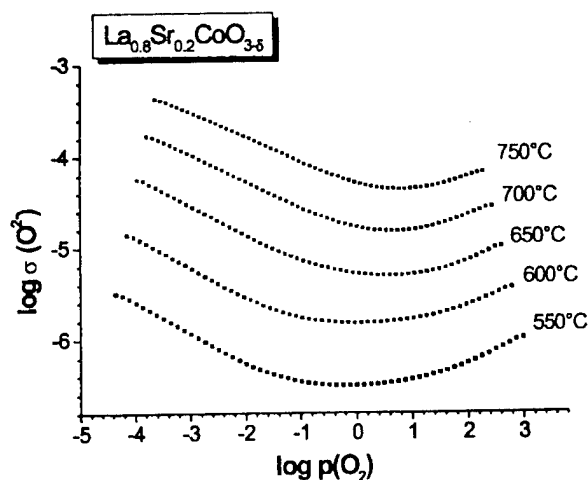


Fig 1 b) Oxygen ion conductivity of  $\text{La}_{0.8}\text{Sr}_{0.2}\text{CoO}_{3.5}$  as a function of the oxygen partial pressure at 700°C.

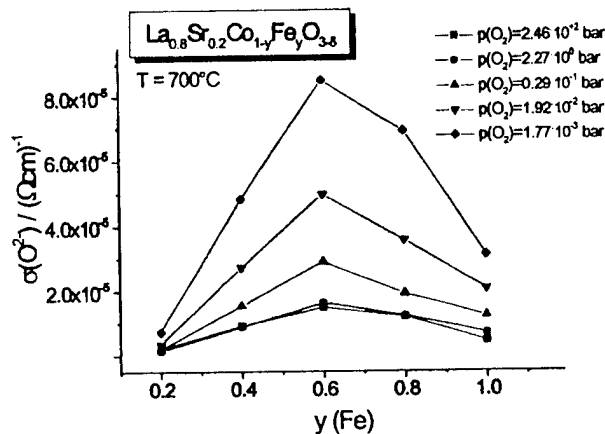


Fig. 2 Oxygen ion conductivity of the  $\text{La}_{0.8}\text{Sr}_{0.2}\text{Co}_{1-y}\text{Fe}_y\text{O}_{3.5}$  as a function of the iron content.

## OXYGEN NONSTOICHIOMETRY IN (La,Sr)CoO<sub>3-δ</sub> THIN FILMS

T. Kawada<sup>1</sup>, J. Suzuki<sup>1</sup>, S. Haga<sup>1</sup>, A. Kaimai<sup>1</sup>, K. Kawamura<sup>1</sup>, Y. Nigara<sup>1</sup>, J. Mizusaki<sup>1</sup>,  
and H. Yugami<sup>2</sup>

<sup>1</sup>Research Institute for Scientific Measurements, Tohoku University,  
2-1-1 Katahira, Aoba-ku, Sendai 980-77, JAPAN

<sup>2</sup>Faculty of Engineering, Tohoku University, Aramaki, Aoba-ku, Sendai 980-77, JAPAN

### INTRODUCTION

Lanthanum cobaltite based perovskites show high ionic and electronic conductivities and are expected to be used as the cathode for a reduced temperature SOFC. In our previous works [1,2], we have investigated the electrochemical properties of a dense La<sub>0.6</sub>Sr<sub>0.4</sub>CoO<sub>3-δ</sub> film deposited on a Ce<sub>0.9</sub>Gd<sub>0.1</sub>O<sub>1.95</sub> electrolyte. The electrochemical reaction was found to be controlled by the chemical reaction at the electrode surface. The interface capacitance was attributed to the formation of oxygen vacancies in the electrode. In this paper, the oxygen nonstoichiometry in the thin film is calculated from the capacitance and compared with the bulk values.

### EXPERIMENTAL

The thin dense films of (La,Sr)CoO<sub>3-δ</sub> were deposited on Ce<sub>0.9</sub>Gd<sub>0.1</sub>O<sub>1.95</sub> by a laser ablation method. The chemical composition and its distribution in the film was investigated by inductively coupled plasma atomic emission spectrometry and secondary ion mass spectrometry. The surface morphology was observed by scanning electron microscope. A porous (La,Sr)CoO<sub>3-δ</sub> counter electrode was deposited on the opposite side of the pellet, and a platinum counter electrode on the periphery. The sample was heated to 873 K ~ 1073 K in a mixed O<sub>2</sub>-Ar gas of a controlled oxygen partial pressure. The ac impedance measurements were performed with and without dc bias. The interface capacitance was determined by complex impedance analysis.

### RESULTS AND DISCUSSION

Figure 1 shows a typical impedance plot obtained for the La<sub>0.6</sub>Sr<sub>0.4</sub>CoO<sub>3-δ</sub> film of 1.5 μm thick. The small arc observed in the higher frequency range was attributed to the grain boundary impedance of the Ce<sub>0.9</sub>Gd<sub>0.1</sub>O<sub>1.95</sub> electrolyte. The lower frequency arc came from the electrode polarization and was fitted well with a simple equivalent circuit of a parallel resistor and a capacitor. From our previous studies [1,2], the resistance was found to come from the surface chemical reaction. The magnitude of the capacitance was almost proportional to the electrode thickness. The physical meaning of the capacitance was attributed to the oxygen vacancy formation in the film as explained by the following equation,

$$C = \frac{\partial Q}{\partial \eta} = \frac{\partial}{\partial \eta} \int_0^L \left( \frac{-2F}{V_m} \delta \right) dx \quad (1)$$

where  $\eta$  is the overvoltage,  $L$  is the sample thickness and  $V_m$  is the molar volume of the perovskite. Since oxygen potential gradient inside the film is negligibly small compared with the oxygen potential drop at the surface, it is expected that the oxygen potential in the electrode film is determined by the applied voltage, i.e. the effective oxygen potential in the film is represented by the following equation.

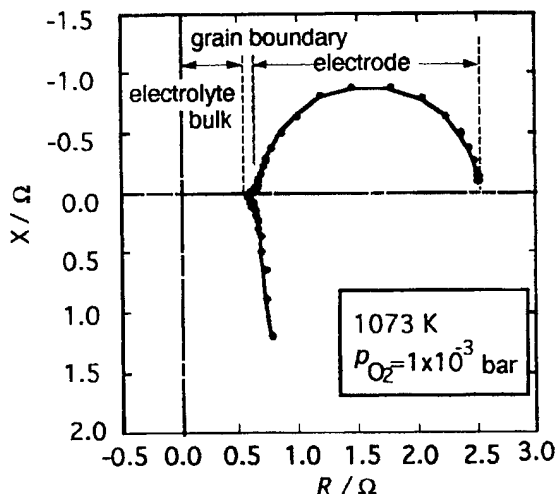


Fig.1 Typical impedance plot of La<sub>0.6</sub>Sr<sub>0.4</sub>CoO<sub>3-δ</sub> film of 1.5 μm thick.



$$p_{O_2}^{eff} = p_{O_2} \exp(4FE/RT) \quad (2),$$

where  $p_{O_2}$  is the equilibrium oxygen partial pressure in the gas phase. From Eqs.(1) and (2), the capacitance can be related to the effective oxygen potential in the film as

$$C = \frac{8F^2L}{V_m RT} \frac{\partial \delta}{\partial p_{O_2}^{eff}} \quad (3).$$

In figure 2, the observed capacitances are plotted against the effective oxygen partial pressure determined by Eq.(2). The open symbols represent the data taken when the film is equilibrated with the gas phase, i.e. overpotential is zero. The other data were obtained under the positive or negative dc bias. Those two kinds of data were on a single curve for each temperature, which proves the assumption that the surface reaction impedance is the main reason of the overvoltage. The oxygen nonstoichiometry in the bulk (La,Sr)CoO<sub>3</sub> was reported by Mizusaki et al [3]. According to them, the oxygen partial pressure dependence can be explained by a regular solution model. The partial molar free energy change of oxygen for the vacancy formation reaction is represented by the following equation

$$\Delta\mu_O = (\Delta h_O^\circ - a\delta) - T\{\Delta s_O^\circ + R\ln(\delta/3-\delta)\} \quad (4)$$

Their data were fitted well when  $-85-289\delta$  /kJ mol<sup>-1</sup>, was used for the enthalpy term and  $-69.5$  /J mol<sup>-1</sup> for  $\Delta s_O^\circ$ . The observed capacitance, however, was somehow smaller than expected. The best fit curves shown in Fig.2 were obtained with the larger enthalpy value,  $-124-332\delta$  /kJ mol<sup>-1</sup>, whereas the entropy term remained same. It means that the oxygen vacancy formation energy increased by making a film. Since the film is not so thin, the quantum effects are not expected to appear. One of the possible explanations is the effect of the mechanical stress in the film. Since the crystal structure of the film was highly oriented, strong interaction can be expected between the film and the substrate. Mismatches in the lattice constant, thermal expansion constant, and the volume expansion due to the vacancy formation can be the reason of the mechanical stress. Further systematic studies with various perovskite films are necessary to clarify this phenomenon.

## REFERENCES

- [1] K. Masuda et al., Proc. 5th Intrn. Symp. SOFC, 1-5 June 1997, Aachen, edt. by U. Stimming et al., pp.473-482 (1997)
- [2] T. Kawada et al., submitted to Solid State Ionics (Proc. SSI 11).
- [3] J. Mizusaki et al., J. Solid State Chem. **80**, 102 (1969)

## ACKNOWLEDGEMENT

This work has been carried out as a research project of "Core research of evolutionary science and technology" supported by science and technology agency.

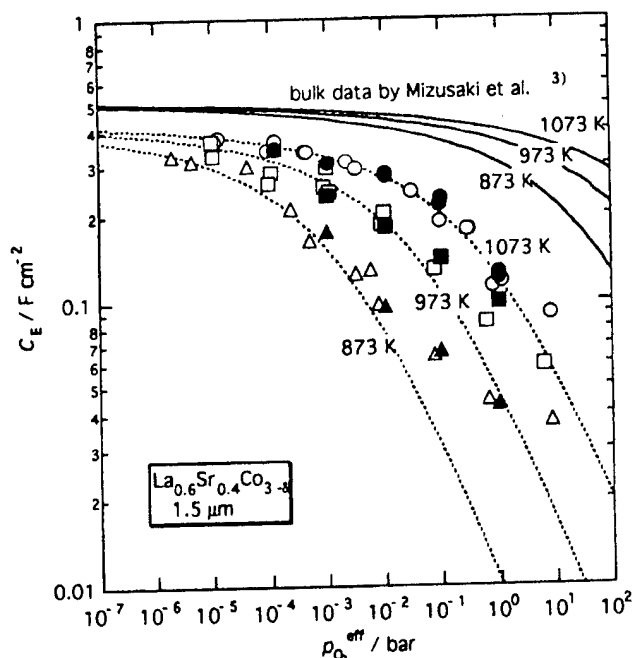


Fig.2 The capacitance of the La<sub>0.6</sub>Sr<sub>0.4</sub>CoO<sub>3-δ</sub> film of 1.5 μm thick as a function of the effective oxygen potential observed in equilibrium with the gas phase (open symbols) and under dc bias (closed symbols). The real lines were calculated from the bulk data of oxygen nonstoichiometry reported by Mizusaki et al. [3]. The dashed lines are the best fit curves with the regular solution model.

OXYGEN DIFFUSION AND SURFACE EXCHANGE IN  $\text{La}_{2-x}\text{Sr}_x\text{NiO}_{4+\delta}$ 

J.A.Kilner and S.J.Skinner

Centre for Ion Conducting Membranes, Department of Materials, Imperial College, Prince Consort Road, London, SW7 2BP, U.K.

## Abstract

Perovskite type oxides,  $\text{ABO}_3$ , have been extensively studied as candidates for use as membranes for ceramic oxygen generators (COG's) and as cathodes in solid oxide fuel cells (SOFC). Much of this interest has stemmed from the fact that materials such as  $\text{La}_{1-x}\text{Sr}_x\text{Co}_{1-y}\text{Fe}_y\text{O}_{3-\delta}$  (LSCF) and  $\text{La}_{1-x}\text{Sr}_x\text{Co}_{1-y}\text{Ni}_y\text{O}_{3-\delta}$  (LSCN) form with oxygen deficiencies which provide a mechanism for oxygen transport via anion vacancies. To date there has been little interest in related structure types such as  $\text{K}_2\text{NiF}_4$  which can accommodate a wide variety of oxygen stoichiometries.

In this work the compounds  $\text{La}_{2-x}\text{Sr}_x\text{NiO}_{4+\delta}$  have been prepared with an oxygen excess of  $\delta = 0.19$  and the oxygen tracer diffusion coefficient and surface exchange coefficient of the materials have been determined by the Isotope Exchange Depth Profile method (IEDP).  $^{18}\text{O}$  anneals were performed at temperatures up to  $\sim 1100\text{K}$  and the resultant diffusion profiles were determined by secondary ion mass spectrometry (SIMS).  $\text{La}_2\text{NiO}_{4+\delta}$  was found to have oxygen diffusivity considerably higher than that of LSCF and one order of magnitude lower than the best LSC. Predictions of the oxygen flux for various membrane thicknesses indicate that  $\text{La}_2\text{NiO}_{4+\delta}$  will have an oxygen permeability comparable with the perovskite materials, and in combination with the thermal stability of  $\text{La}_2\text{NiO}_{4+\delta}$ , this material seems to be a good candidate for use in COGs and SOFCs. Furthermore, optimisation by a combination of donor and/or acceptor doping should improve the properties here reported.

OXYGEN PERMEATION OF  $\text{SrFe}_{0.67}\text{Co}_{0.33}\text{O}_{3-d}$ I. L. Tangen<sup>1,2</sup>, S. Aasland<sup>1</sup>, K. Wiik<sup>2</sup> and R. Ødegård<sup>1</sup><sup>1</sup>Statoil Research Centre, Trondheim, Norway<sup>2</sup>Institute of Inorganic Chemistry, The Norwegian University of Science and Technology, Trondheim, Norway

During the last couple of years, the interest in oxides with mixed ionic and electronic conductivity has increased due to their potential application as oxygen transferable membranes for separation of oxygen from air [1] and the supply of oxygen in partial oxidation reactions [2]. The research activity has largely been focused on oxides with an  $\text{ABO}_3$  perovskite type structure and with a large number of oxygen vacancies. The oxygen content of the perovskites varies with temperature and degree of substitution on A and B-site. In this work we have studied the oxygen permeation of  $\text{SrFe}_{0.67}\text{Co}_{0.33}\text{O}_{3-d}$ . The oxygen content of this composition at 1000 °C is close to 2.5 [3].

$\text{SrFe}_{0.67}\text{Co}_{0.33}\text{O}_{3-d}$  powder was synthesised using a spray pyrolysis technique with nitrate solutions of the metal ions, followed by ball milling and calcination at 900 °C for 10 hours. Uniaxially pressed discs of the powder sample were sintered at 1050-1100 °C for 15-30 hours and slowly cooled in air.  $\text{SrFe}_{0.67}\text{Co}_{0.33}\text{O}_{3-d}$  was shown by x-ray powder diffraction to be a single phase material with a cubic perovskite structure,  $a=3.866$  Å. A bulk density of the sintered discs of 5.25 g/cm<sup>3</sup>, corresponding to a closed porosity around 3 %, and with an open porosity around 0.5 vol% were measured by the Archimedean method. Microstructural observations by scanning electron microscope showed grain sizes of 1-15 µm, with a mean grain size of 6-7 µm.

Oxygen fluxes were measured for sintered discs of varying thickness (1.0, 1.5 and 2.0 mm) with air on the primary side and mixtures of He and air on the secondary side to vary the oxygen partial pressure difference across the membrane. Polished discs were sealed with gold rings to alumina tubes on both sides and very low leakage rates were obtained. The oxygen flux was calculated from gas chromatography analysis of the gas flow in and out of the secondary side of the disc.

The temperature in the experiment was varied between 900 °C and 1000 °C, and an apparent activation energy of  $105 \pm 4$  kJ/mol was obtained for  $\text{SrFe}_{0.67}\text{Co}_{0.33}\text{O}_{3-d}$ . A maximum oxygen flux of 2.8 ml/min cm<sup>2</sup> was obtained at 1000 °C with pure He on the secondary side. Good reproducibility of the results was obtained for two different discs of 2 mm thickness as shown in Figure 1. A decrease in the difference in oxygen partial pressure across the disc gave an almost linear decrease in the oxygen flux for a 2 mm thick disc, as expected from the Wagner equation for bulk diffusion [4]. The variation in the oxygen flux with the thickness of the disc was however lower than would be expected from the Wagner equation, indicating that both bulk diffusion and surface reactions are important.

Transient oxygen flux measurements were carried out by monitoring the oxygen flux variations during relatively rapid changes in either temperature or oxygen

partial pressure at the secondary side. A change in  $pO_2$  or temperature is followed by a relatively long (some hours) transient period due to slow processes involved with the redistribution of oxygen within the sample as well as establishing stable surface layers.

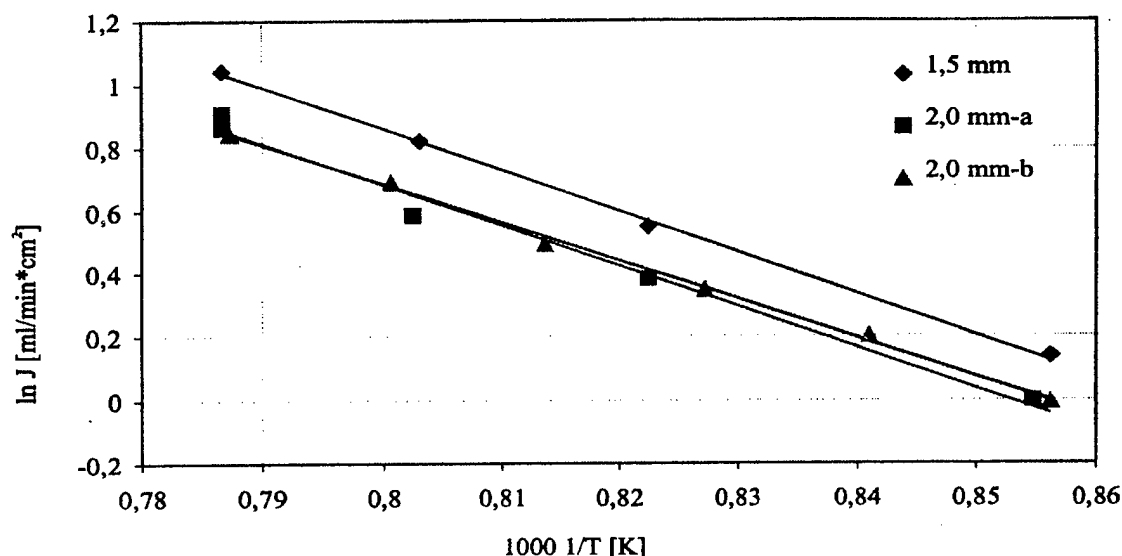


Figure 1. Oxygen flux vs. temperature.

The  $SrFe_{0,67}Co_{0,33}O_{3-d}$  samples were investigated after the permeation measurements by x-ray diffraction and scanning electron microscope. Both the microstructure and the crystal structure on the secondary side of the discs were mainly unchanged. On the primary side small ( $< 1 \mu m$ ) regions of a new phase was observed on the grain boundaries and also some very weak peaks, not assigned to the cubic perovskite, could be observed in the x-ray diffractogram. Unfortunately, the amount of the new phase was too small for identification. Formation of new phases at the grain boundaries at the primary side may be explained by cation migrations in the opposite direction of the oxygen ions.

The authors want to acknowledge Rita Glenne, Norsk Hydro, for preparation of sintered discs. Financial support from the Norwegian Research Council is gratefully acknowledged.

- [1] Y. Teraoka, H.-M. Zhang, K. Okamoto and N. Yamazoe, *Mat. Res. Bull.* **23**, 51 (1988).
- [2] T. J. Mazanec, T. L. Cable and J. G. Frye Jr., *Solid State Ionics* **53-56**, 111 (1992).
- [3] A. Holt and T. Norby, Institute of Chemistry, University of Oslo, Norway, to be published.
- [4] C. Wagner, *Z. Phys. Chem.* **B21**, 25 (1933).

## ION CONDUCTING COMPLEX PEROVSKITES

H. Runge, U. Guth

Institute of Physical Chemistry, University of Greifswald,  
Soldmannstr. 23, D-17489 Greifswald, Germany

Perovskites and perovskite-like solid electrolytes offer an interesting alternative to well known fluorite systems based on zirconia or bismuth oxide. The perovskite  $\text{La}_{0.9}\text{Sr}_{0.1}\text{Ga}_{0.8}\text{Mg}_{0.1}\text{O}_{3-\delta}$  exhibits a higher ionic conductivity than YSZ at comparable temperatures [1-3]. Thereby, lower operating temperatures for SOFC's around 800°C are possible. In addition, these perovskite based solid electrolytes have similar structures and chemical composition to cathode materials based on e.g. manganites. This advantage should result in thermal and chemical compatibility and better interconnection between electrode material and solid electrolyte.

Perovskites are very versatile regarding to accommodate a wide range of A- and B-cations [4-5]. By doping with lower valence cations it is possible to create oxygen vacancies like in the material  $\text{La}_{0.9}\text{Sr}_{0.1}\text{Ga}_{0.8}\text{Mg}_{0.1}\text{O}_{3-\delta}$  or in complex (mixed) perovskite proton conductors. The general formulas of complex proton conducting perovskites are  $\text{A}_2(\text{B}'_{1-x}\text{B}''_{1-x})\text{O}_{6-\delta}$  and  $\text{A}_3(\text{B}'_{1+x}\text{B}''_{2-x})\text{O}_{9-\delta}$  [6]. The A-ion is always charged +2. In the first case the B' and B'' are charged +3 and +5 respectively, while in the second case the B' and B'' are di- and pentavalent cations. The charge compensation results by a creation of oxygen vacancies, an important requirement for oxygen conductors as well as for proton conductors.

The appearance of the oxygen ion conductivity apparently depends on crystallographic-related parameters like free volume, critical radius and metal oxygen bond energy of perovskite lattice [7]. We investigated complex  $\text{A}^{2+}_{1-x}\text{A}^{3+}_{1-x}\text{B}^{4+}_{1-y}\text{B}^{3+}_{1+y}\text{O}_{6-\delta}$  systems concerning these empirical relationships. Through different combination of  $\text{A}^{2+}\text{B}^{4+}\text{O}_3$  and  $\text{A}^{3+}\text{B}^{3+}\text{O}_3$  - perovskites it should be possible to create oxygen vacancies and to influence the crystallographic parameters. In our work only the  $\text{A}^{2+}$  ( $\text{Sr}^{2+}$ ;  $\text{Ba}^{2+}$ ) and the  $\text{B}^{3+}$  ( $\text{Ga}^{3+}$ ;  $\text{In}^{3+}$ ) - ions were changed, while in all combinations the  $\text{La}^{3+}$  is used as  $\text{A}^{3+}$ -ion and the  $\text{Zr}^{4+}$  as  $\text{B}^{4+}$ -ion.

Samples were prepared by conventional solid state reaction. X-ray investigations were carried out in order to detect the structure of the combinations and to calculate lattice parameters. The electrical conductivity was measured as function of temperature and oxygen partial pressure by impedance spectroscopy. To detect a proton conduction, the water vapour dependence of the conductivity was investigated too.

- [1] T. Ishihara, H. Matsuda, Y. Takita, J. Am. Chem. Soc. **116**, 3801-3803 (1994)
- [2] T. Ishihara, H. Matsuda, Y. Takita, Solid State Ionics **79**, 147-151 (1995)
- [3] P.-N. Huang, A. Petric, J. Electrochem. Soc. **143**, 1644-1648 (1996)
- [4] H. Runge, U. Guth, P. Shuk, Dechema-Monographien **12**, 232-240 (1998)
- [5] K.-P. Sandow, S. Jakobs, D. Westphal, S. Thiemann, R. Hartung, U. Schöner, U. Guth, Ionics, **2**, 435-441 (1996)
- [6] A.S. Nowick, Y. Du, Solid State Ionics **77**, 137 (1995)
- [7] R.L. Cook, A.F. Sammels, Solid State Ionics **45**, 311 (1991)

# OXYGEN PERMEATION THROUGH $\text{Gd}_{0.7}\text{Ca}_{0.3}\text{CoO}_{3-\delta}$ , $\text{Gd}_{0.7}\text{Sr}_{0.3}\text{CoO}_{3-\delta}$ AND $\text{La}_{0.7}\text{Sr}_{0.3}\text{CoO}_{3-\delta}$ MEMBRANES

E.W.J. Römer, H.J.M. Bouwmeester, H. Verweij

Laboratory of Inorganic Materials Science, Department of Chemical Technology, University of Twente, PO Box 217, 7500 AE Enschede, the Netherlands

Mixed conducting perovskite-type oxides show great potential for use as dense ceramic membrane, providing a low cost source of oxygen for a variety of applications [1]. At operating conditions, typically above 700°C, oxygen ions travel through the membrane, compensated by a simultaneous flow of electronic charge carriers, which process is driven by a oxygen pressure differential imposed across the membrane. Teraoka et al. [2] reported very high oxygen fluxes especially through perovskites with composition  $\text{Ln}_{1-x}\text{A}_x\text{CoO}_{3-\delta}$ , in which the partial substitution of the lanthanide ion with alkaline earth ions ( $\text{A} = \text{Sr}, \text{Ca}$ ) serves to create oxygen vacancies in the  $\text{ABO}_3$  perovskite lattice. In this study we present detailed oxygen permeation measurements on perovskites  $\text{La}_{0.7}\text{Sr}_{0.3}\text{CoO}_{3-\delta}$ ,  $\text{Gd}_{0.7}\text{Sr}_{0.3}\text{CoO}_{3-\delta}$  and  $\text{Gd}_{0.7}\text{Ca}_{0.3}\text{CoO}_{3-\delta}$ . Preliminary investigations in our laboratory revealed high oxygen fluxes through the compositions with strontium as the A-site substituent, but significantly reduced values when calcium was used instead. This observation prompted us to study the oxygen permeation characteristics of the aforementioned perovskites into more detail.

Perovskite oxides were prepared by the thermal decomposition of precursor complexes derived from nitrate solutions using ethylenediaminetetraacetic acid (EDTA) as a complexing agent. Isothermal oxygen permeation measurements between 700 - 1100 °C were performed as a function of membrane thickness (0.5 - 2mm) using different gradients of oxygen partial pressure across the membrane. Glass rings were used to seal the disc membrane into a quartz permeation reactor. A gas chromatograph connected to the exit of the helium sweep line at the permeate side of the membrane was used to measure both oxygen and nitrogen concentrations. Any small leakage could be detected by measuring nitrogen in the helium gas, typically found to be below 1%. The permeation apparatus has been described in detail elsewhere [3].

Figure 1 shows data of oxygen permeation through 1.5 mm thick membranes of  $\text{La}_{0.7}\text{Sr}_{0.3}\text{CoO}_{3-\delta}$ ,  $\text{Gd}_{0.7}\text{Sr}_{0.3}\text{CoO}_{3-\delta}$  and  $\text{Gd}_{0.7}\text{Ca}_{0.3}\text{CoO}_{3-\delta}$ . Ambient air (100 ml (STP)  $\text{min}^{-1}$ ) was used as feed gas. As can be seen the flux  $\text{Gd}_{0.7}\text{Ca}_{0.3}\text{CoO}_{3-\delta}$  is 2-3 orders of magnitude below that of the other two compositions. A tentative explanation for this behaviour is the apparent ordering of oxygen vacancies in  $\text{Gd}_{0.7}\text{Ca}_{0.3}\text{CoO}_{3-\delta}$ , which renders the oxygen vacancies immobile. Some credence for this hypothesis was obtained from thermogravimetric measurements. Beside oxygen permeation measurements we wish to present at the conference results from analysis of data from electron microscopy and diffraction.

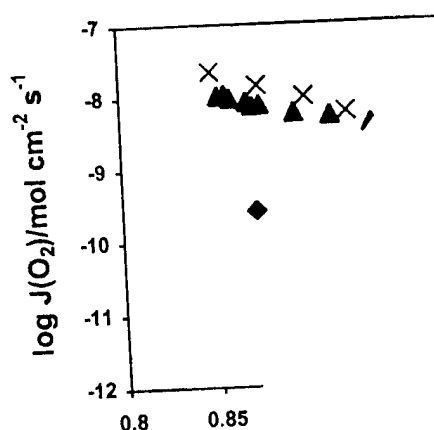


Figure 1: Arrheni  
Gd<sub>0.7</sub>S  
(X). 1.

**References**

- [1] H.J.M. Bouwmeester, A.J. Burggraaf, Dense ceramic membranes for oxygen separation, in *The CRC Handbook of Solid State Electrochemistry*, Eds. P.J. Gellings, H.J.M. Bouwmeester, pp. 481-553, CRC Press, Inc., Boca Raton (1997).
- [2] Y. Teraoka, T. Nobunaga and N. Yamazoe, *Chem. Lett.* 503 (1998).
- [3] J.E. ten Elshof, H.J.M. Bouwmeester and H. Verweij, *Solid State Ionics* **81**, 97 (1995).

# EVALUATION OF La-Sr-Co-Fe-O PEROVSKITES FOR SOLID OXIDE FUEL CELLS AND GAS SEPARATION MEMBRANES

A. Petric<sup>1</sup>, P. Huang<sup>2</sup>, F. Tietz<sup>3</sup>

<sup>1</sup>McMaster University, Hamilton, Canada; <sup>2</sup>Global Thermoelectric, Calgary, Canada;

<sup>3</sup>Forschungszentrum Jülich, Germany

Among the different applications of solid oxide fuel cells (SOFC), a near-term need exists for small-scale electrical generation in remote areas or for domestic use of combined heat and power. Reduced operating temperatures (700-800 °C) are preferred for improving the lifetime of the device. Under such conditions highly electrochemically active electrodes are needed to minimize overpotentials. Cobalt-rich perovskites have been proposed as cathode materials [1 – 4] due to their high electronic and ionic conductivity. However, increasing conductivity is combined with rising thermal expansion for compositions with the general formula  $\text{La}_{1-x}\text{Sr}_x\text{Co}_{1-y}\text{Fe}_y\text{O}_{3-\delta}$  [1, 4, 5] having high cobalt and strontium content.

To identify the relevant composition regime, three series of samples were prepared: a)  $x = 0.2, 0.3$  and  $0.4$  with fixed  $y = 0.8$ , b) fixed  $x = 0.7$  and  $y$  varying in steps of  $0.1$  from  $0 - 1.0$ , and c)  $x = 0.2 - 0.9$  varying in steps of  $0.1$  and fixed  $y = 0$ . All samples were investigated by electrical conductivity measurements and dilatometry. Together with detailed investigations which have been performed previously [4, 6] a broad compositional overview can be gained to define relevant stoichiometry regimes for SOFC cathode development.

The results of the  $\text{La}_{0.3}\text{Sr}_{0.7}\text{Co}_{1-y}\text{Fe}_y\text{O}_{3-\delta}$  series are shown in Fig. 1 in the form of isothermal conductivity data at 800 °C and linear thermal expansion coefficients (TEC) between 30 and 1000 °C. For these compositions a rather irregular dependence of TEC with decreasing Co content was obtained. This is due to a varying slope change at 400 °C of the thermal expansion in combination with fluctuations in the high temperature part of the curves, presumably related to oxygen losses [4, 6]. However, a clear trend of decreasing TEC with increasing Fe content can be

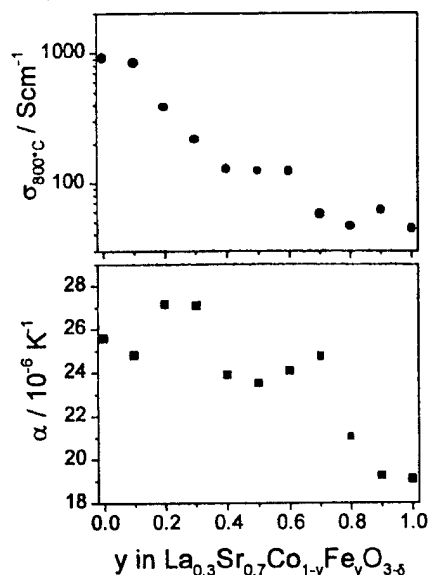


Fig. 1: Isothermal conductivity data at 800 °C (top) and linear TEC from 30 to 1000 °C (bottom) for the system  $\text{La}_{0.3}\text{Sr}_{0.7}\text{Co}_{1-y}\text{Fe}_y\text{O}_{3-\delta}$

found. Furthermore, the TEC values are extraordinarily high, up to twice the thermal expansion of most perovskites. The electrical conductivities of this series decrease rapidly to less than 200 S/cm for  $y \geq 0.2$ .

In the second series,  $\text{La}_{1-x}\text{Sr}_x\text{CoO}_{3-\delta}$ , a minimum of TEC with  $\alpha = 18.5 \times 10^{-6} \text{ K}^{-1}$  was obtained at  $x \approx 0.2$  [7] in agreement with [1]. A more detailed description of the expansion curves and the related phenomena occurring with increasing Sr content is given in [7]. The electrical conductivity measurements revealed high performance for  $0.1 < x < 0.5$  with conductivities  $> 1000 \text{ S cm}^{-1}$  at 800 °C and a rapid fall off at  $x = 0.7$ . By comparing the conductivity data with literature values and from own experience during sample preparation, a rather large scatter in results were found especially for the highly conductive specimens. This observation is explained by a strong sensitivity of these materials to preparation and sintering conditions thus leading to changing influences of grain



boundaries [8]. Also these compositions have disadvantageously high TEC and cannot be recommended for SOFC development, because they are not compatible with other cell components.

The TEC values between 30 and 1000 °C and the electrical conductivity data at 800 °C are shown in Fig. 2 and 3, respectively, for the entire La-Sr-Co-Fe-O system. In both figures, the light grey regions indicate the preferred compositions for SOFC cathodes. As can be seen, the compositions with acceptable thermal expansions do not coincide with stoichiometries having advantageous electronic and ionic conductivities [2, 3]. In case of gas separation membranes the thermomechanical properties are less important, because a homogeneous membrane, no laminate, is used. However, the mechanical properties become worse with increasing Sr and Co content, i.e. the samples investigated here have shown an increasing brittleness and were very sensitive to cracking during thermal cycling. Therefore the materials selection for membrane technology has to be a compromise between mechanical and electrical properties.

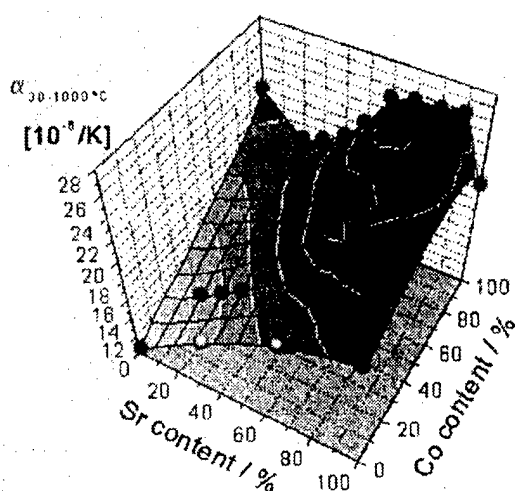


Fig. 2: TEC between 30 and 1000 °C for the system  $\text{La}_{1-x}\text{Sr}_x\text{Co}_{1-y}\text{Fe}_y\text{O}_{3-\delta}$ . The black dots indicate investigated compositions, white dots refer to literature data [5].

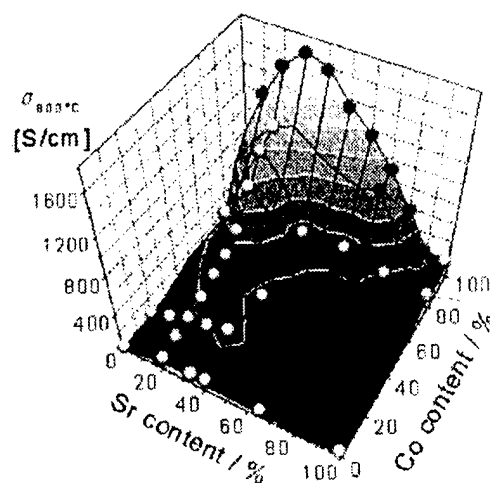


Fig. 3: Electrical conductivities at 800 °C for the system  $\text{La}_{1-x}\text{Sr}_x\text{Co}_{1-y}\text{Fe}_y\text{O}_{3-\delta}$ . The black dots indicate investigated compositions, the white dots refer to various literature data.

#### References:

- [1] Y. Ohno, S. Nagata, H. Sato, *Solid State Ionics* **9&10** 1001 (1983)
- [2] I. C. Fullarton, J. A. Kilner, B. C. H. Steele, P. H. Middleton, *Proc. 1st Symp. Ionic and Mixed Conducting Ceramics*, eds. T. A. Ramanarayanan, W. L. Worrell, H. L. Tuller, The Electrochem. Soc., Pennington, NJ, 1994, p. 9
- [3] Y. Teraoka, T. Nobunaga, K. Okamoto, N. Miura, N. Yamazoe, *Solid State Ionics* **48** 207 (1991)
- [4] L.-W. Tai, M. M. Nasrallah, H. U. Anderson, D. M. Sparlin, S. R. Sehlin, *Solid State Ionics* **76** 259 (1995)
- [5] H. Nagamoto, I. Mochida, K. Kagotani, H. Inoue, A. Negishi, *J. Mater. Res.* **8** 3158 (1993)
- [6] L.-W. Tai, M. M. Nasrallah, H. U. Anderson, D. M. Sparlin, S. R. Sehlin, *Solid State Ionics* **76** 273 (1995)
- [7] F. Tietz, *Proc. 9th Int. Conf. Modern Materials & Technologies (CIMTEC '98)*, June 1998, Florence/Italy, ed. P. Vincenzini, in press
- [8] G. Garcia-Belmonte, J. Bisquert, F. Fabregat, V. Kozhukharov, J. B. Carda, *Solid State Ionics* **107** 203 (1998)

# OXYGEN PERMEATION THROUGH $\text{Sr}_4\text{Fe}_4\text{Co}_2\text{O}_y$ OXIDE

W. Liu, S. Xie, G.G. Zhang, C.S. Chen, G.Y. Meng, D.K. Peng\*

Department of Materials Science and Engineering,

University of Science and Technology of China

Hefei, Anhui 230026, P.R. China

Dense ceramic membranes possessing high oxygen ionic and electronic conductivities hold promise for applications in high-temperature electrochemical devices and in catalysis. U. Balachandran et al. [1] have reported that Sr-Fe-Co oxides exhibit structural stability as well as high electronic and oxygen ionic conductivities. The membrane reactors made of the oxide designed to convert methane to syngas have been operated for more than 1000hr; the methane conversion coefficients larger than 98% were attained at 850°C in the presence of a reforming catalyst, [2]. In this paper, results obtained from the study of oxygen transport through  $\text{Sr}_4\text{Fe}_4\text{Co}_2\text{O}_y$  oxide is presented.

Samples were prepared via a solid state reaction route. Appropriate amounts of  $\text{SrCO}_3$  (AR),  $\text{Fe}_2\text{O}_3$  (AR) and  $2\text{CoCO}_3 \cdot 3\text{Co}(\text{OH})_2 \cdot x\text{H}_2\text{O}$  (CP) were weighted and grounded in a mortar followed by calcination. Two batches of powders were prepared under different calcination conditions. For batch A, the mixed powder was only calcined at 850°C in air; for batch B, the mixed powders were calcined in air at 850°C, 1000°C, 1100°C with intermittent grinding. The calcined powders were then uniaxially pressed at 350Mpa, followed by sintering in air at 1200°C for 5hr. Oxygen permeation measurements were performed on three sintered disk-shaped samples all with thickness of 1.5 mm and diameter of 12 mm. Details of the measurements can be found elsewhere [3]. The results obtained from the measurements are shown in Fig.1.

Sample A, which was made from batch A powder and had a relative density of 83%, shows considerable oxygen permeability. The oxygen permeation flux corrected for the leakage through the gas-through pores is in the order of  $10^{-9}$  to  $10^{-10}$  mol  $\text{cm}^{-2}$   $\text{s}^{-1}$  in the temperature range of 1100-900°C. It is somewhat surprising that with such a porous specimen, the resulting oxygen enrichment factor still can be as large as about 4 at 1100°C.

Sample B made from Batch B powder, had a sufficiently high relative density of 93% and thus did not contain gas-through pore. As can be seen from Fig.1, the oxygen permeability of Sample B is almost twice as high as that of Sample A. The larger oxygen permeability for sample B can not be totally attributed to the smaller porosity. The difference in phase composition may be partly responsible for it. SEM observation revealed that Sample A consisted of many needle-shaped grains, while Sample B did not.

Sample C, which was prepared in the same condition as Sample B and subjected to

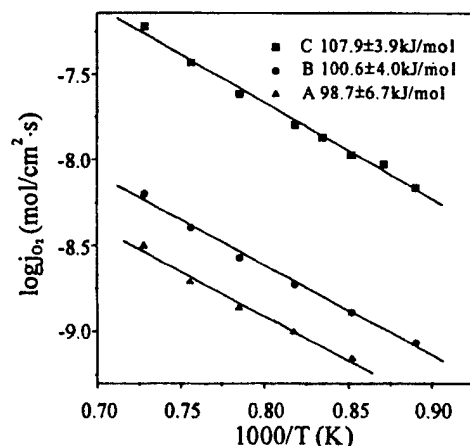


Fig. 1 Temperature dependence of the oxygen permeation rate of different  $\text{Sr}_4\text{Fe}_4\text{Co}_2\text{O}_y$  samples

treatment with 2 M nitric acid for 10 min, shows much improved oxygen permeability. At 950°C, the oxygen permeation flux through Sample C is about  $1.59 \times 10^{-8} \text{ mol/cm}^2 \cdot \text{s}$ . For the membrane with the same nominal composition, S. Kim et al observed a flux of about  $2 \times 10^{-8} \text{ mol/cm}^2 \cdot \text{s}$  at 942°C [4]. The positive effect of the nitric acid treatment on the oxygen permeability has also been observed by Mirua et al who attributed it to the removal of surface impurities like SrO [5]

In summary, oxygen permeation through  $\text{Sr}_4\text{Fe}_4\text{Co}_2\text{O}_y$  oxide is affected by the microstructure, phase composition and surface composition, and further research are needed to clarify these effects.

### References

- [1] U. Balachandran, M. S. Kleefisch, T. P. Kobylinski, S. L. Morissette and S. Pei, U. S. Patent 5580497, Dec. 1996
- [2] U. Balachandran, J. T. Dusek, S. M. Sweeney, R. B. Poeppel, R. L. Mieville, P. S. Maiya, M. S. Kleefisch, C. A. Udcvich and A. C. Bose, *Am. Ceram. Soc. Bull.*, **74**, 71(1995).
- [3] S. Xie, W. Liu, K. Wu, P.H. Yang, G.Y. Meng, C.S. Chen, "Mixed oxygen ionic and electronic conduction in  $\text{CaFe}_{0.2}\text{Ti}_{0.8}\text{O}_{3.6}$ : a combined oxygen permeation and electrical conductivity study", *Solid State Ionics* (accepted)
- [4] S. Kim, Y. L. Yang, R. Christoffersen and A. J. Jacobson, *Solid State Ionics*, **109**, 187 (1998).
- [5] N. Muira, Y. Okamoto, J. Taamaki, K. Morinag and N. Yamazoe, *Solid State Ionics*, **79**, 195(1995).

## CONDUCTIVITY RELAXATION EXPERIMENTS ON $\text{Ni}_{1-\delta}\text{O}$ AT HIGH TEMPERATURES

I. Rom, W. Jantscher, M. Holzinger and W. Sitte  
Institute of Physical and Theoretical Chemistry  
Graz University of Technology, A-8010 Graz, Austria

$\text{NiO}$  is thermodynamically stable in a wide temperature and oxygen activity range. It is a metal-deficit p-type semiconductor with a small phase width. Regarding its defect structure metal vacancies with a temperature dependent degree of ionization and electronic holes are the primary defects. As the electronic conductivity varies significantly with oxygen activity,  $\text{NiO}$  is well suited for the application of the conductivity relaxation method to study the chemical diffusion coefficient as a function of oxygen activity and temperature.

With conductivity relaxation experiments the oxygen content of the ambient atmosphere surrounding the sample is changed stepwise using appropriate gas mixtures or oxygen pumps (made from yttria-stabilized zirconia) and the re-equilibration of the sample is followed by monitoring the electronic conductivity. This relaxation process is accompanied with oxygen exchange at the surface and chemical diffusion in the bulk of the oxide. Conductivity relaxation can be used without further precautions when chemical diffusion within the sample and not the surface exchange process is rate limiting. Additionally, defect chemistry must allow to assume a linear relationship between the change of the oxygen content of the specimen and the charge carrier concentration.

The electronic conductivity was measured using the van der Pauw-method. This method is experimentally preferable because only the thickness of the disk-shaped sample and not the exact spacings between the four electronic contacts on the surface of the sample needs to be known. For all measurements polycrystalline samples have been used, which had been sintered in air. The chemical diffusion coefficient as a function of oxygen activity and temperature between 700 and 1000°C as well as experimental details will be given and the results of the present study will be compared with the few available data from literature.

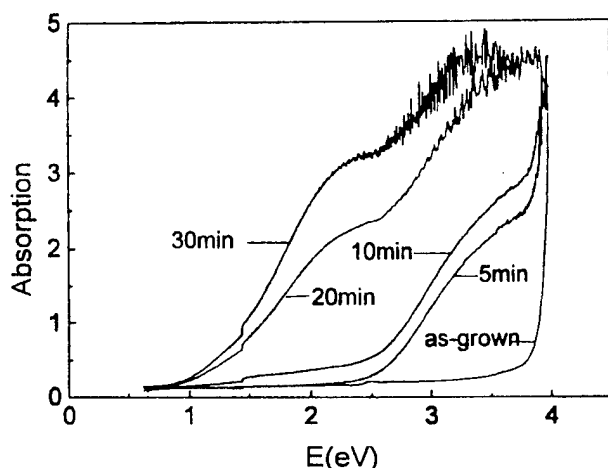
# PECULIARITY OF O<sup>-2</sup> AND Li<sup>+</sup> ELECTRODIFFUSION INTO LITHIUM NIOBATE SINGLE CRYSTALS

S. Bredikhin<sup>1</sup>, S.Scharner<sup>2</sup>, M.Klinger<sup>2</sup>, V.Kveder<sup>1</sup>, B.Red'kin<sup>1</sup>, W.Weppner<sup>2</sup>

<sup>1)</sup> Institute of Solid State Physics, Russian Academy of Science,  
142432 Chernogolovka, Moscow Region, Russia

<sup>2)</sup> Chair for Sensors and Solid State Ionics, Christian Albrechts-University,  
Kaiserstr. 2, D-24143 Kiel, Germany

The high oxygen and lithium ionic conductivity in LiNbO<sub>3</sub> is investigated and interpreted in terms of a major amount of lithium and oxygen vacancies already present in congruently grown single crystals. It is found that the stoichiometry of lithium niobate crystals can be changed with respect to lithium or oxygen. We have recorded the optical absorption spectra of a sample with a thickness of 400 μm (Ø=10 mm) as a function of the annealing time at 1100 °C in an argon atmosphere. The results are shown in Fig. 1. As one can see from Fig. 1, the first stage of the reduction process is associated with only one absorption band at E<sub>1</sub>=3.55 eV and corresponds to F<sup>+</sup>-centers (V<sub>O</sub><sup>•</sup>). A further increase of the annealing time shifts the Fermi level higher than E<sub>1</sub> and results in the occupation of the second energy level E<sub>2</sub>. Therefore F-centers (V<sub>O</sub><sup>••</sup>) are created. At this stage the second optical absorption band with a maximum at E<sub>2</sub>=2.32 eV appears.



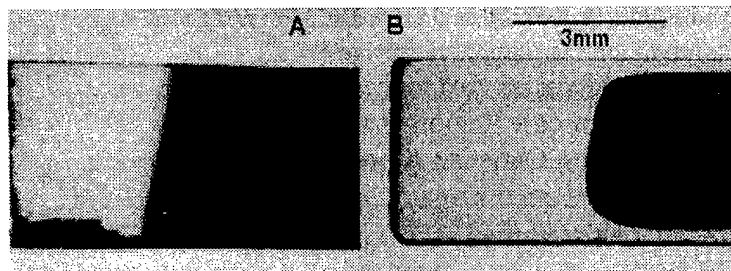
From this consideration we conclude that a certain amount of positively charged oxygen vacancies is already present in congruently as-grown LiNbO<sub>3</sub> single crystals and their positive charge is compensated by the negative charge of lithium vacancies.

The optical and electrical properties of electrocolored LiNbO<sub>3</sub> crystals are studied. We changed the stoichiometry of the oxygen in lithium niobate single crystals by using an experimental cell arrangement which is schematically represented as follows:



An external voltage was applied to a cell with a positive side at the oxygen conducting electrode. The ZrO<sub>2</sub>/LiNbO<sub>3</sub> junction is absolutely reversible with respect to the transfer of oxygen ions. A double charge injection should be possible in this experimental cell: removal of oxygen ions through the heterojunction LiNbO<sub>3</sub>/ZrO<sub>2</sub> and injection of electrons through the heterojunction Pt/LiNbO<sub>3</sub>. Passing a current through this geometry (1) should decrease the concentration of oxygen ions in the LiNbO<sub>3</sub> crystal and increase the concentration of oxygen vacancies. We have found that after passing a current at 600 - 700 °C the sample becomes black in the visible light. The optical absorption spectrum taken from such a black crystal is similar to that of a thermally reduced one. The subsequent increase of the electric charge passed through the cell (1) leads to an increase of the concentration of the F- and F<sup>+</sup>-centers, which become almost homogeneously distributed in the whole LiNbO<sub>3</sub> crystal. It is shown that the absorption spectra of thermally reduced and electrocolored samples are identical.

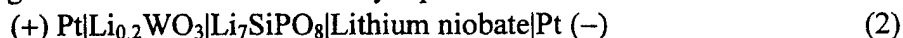
The creation of stoichiometric domains (regions with different stoichiometry) due to the injection of additional lithium or oxygen into the  $\text{LiNbO}_3$  crystals is observed and investigated. The change of polarity of the external voltage applied to the cell (1) allows us to inject oxygen ions into  $\text{LiNbO}_3$  through the reversible heterojunction  $\text{ZrO}_2|\text{LiNbO}_3$  at the one side of the cell and the extraction of electrons on the other side by the use of the ion blocking Pt-electrode. This process can be made visible if thermally reduced  $\text{LiNbO}_3$  crystals are used. The injection of additional



oxygen should decrease the concentration of  $\text{F}^+$ - and F-centers and therefore decolor a thermally reduced  $\text{LiNbO}_3$  crystal. The two images of Fig. 2 show two thermally reduced  $\text{LiNbO}_3$  crystals using white light. Crystal (A) is shown after the injection of oxygen into the sample

through the reversible heterojunction  $\text{ZrO}_2|\text{LiNbO}_3$  in pure Ar gas and crystal (B) in the case of air. At crystal (A), a voltage of 10V was applied at 750 °C and at crystal (B) a voltage of 50 V at 600 °C. In both cases the voltages were applied for 175 min.

The presence of lithium vacancies and the lithium ionic conductivity of  $\text{LiNbO}_3$  allows us to inject additional  $\text{Li}^+$  ions into this material. As the  $\text{Li}^+$  ions must be charge compensated by electrons the lithium stoichiometry of the crystal can so be changed. We have done this by using an experimental cell arrangement which is schematically represented as follows:



The heterojunction  $\text{Li}_7\text{SiPO}_8|\text{LiNbO}_3$  is reversible with respect to the  $\text{Li}^+$  ions but blocks the electrons. At the same time the heterojunction  $\text{LiNbO}_3|\text{Pt}$  is reversible with respect to the electrons while blocking the ionic component of the current. An external voltage was applied to the cell with the positive side at the lithium supplying electrode. Therefore  $\text{Li}^+$  ions are injected through the heterojunction  $\text{Li}_7\text{SiPO}_8|\text{LiNbO}_3$  and electrons through the heterojunction  $\text{LiNbO}_3|\text{Pt}$ .

The change of the polarity of cell (2) decreases the concentration of the lithium ions and electrons inside the lithium niobate crystal and causes it to decolor. A decrease in the lithium concentration leads to the movement of a concentration "domain" inside a initially homogeneous sample similar as if additional oxygen is injected into a thermally reduced  $\text{LiNbO}_3$  crystal. Therefore the origin of the absorption processes must be the same in both cases. The creation of stoichiometric domains (regions with different stoichiometry) due to the injection of additional lithium or oxygen into the  $\text{LiNbO}_3$  crystals is observed and investigated. The motion of stoichiometric domains through a  $\text{LiNbO}_3$  crystal from one electrode to the other is studied and described in terms of electrodiffusion of the ions and electrons. A model is proposed where the creation of concentration profiles in the originally homogeneous material considers the injection of oxygen ions or lithium vacancies. The numerical calculation of the concentration profiles shows that the calculated concentration profiles are very close to those which are experimentally observed.

# DIFFERENT TYPES OF SURFACE EXCHANGE AND DIFFUSION OF OXYGEN IN $\text{YBa}_2\text{Cu}_3\text{O}_{6+x}$

V.I. Tsidilkovski, A.N. Ezin, E.Kh. Kurumchin, G.K. Vdovin

Institute of High-Temperature Electrochemistry, RAS, Ekaterinburg, Russia

The experimental data for  $\text{YBa}_2\text{Cu}_3\text{O}_{6+x}$ , obtained by the method of isotopic exchange with gas phase analysis [1], have been treated using our theoretical approach [2]. This approach allows the simultaneous determination from the experiment of not only the tracer diffusivity  $D^*$  and total heteroexchange rate  $R$  but also of the rates of different types of the surface exchange. It is known that the various mechanisms of the oxygen isotopic exchange boil down to the three kinetically distinguishable types - without direct participation of the oxide oxygen (type 1), with the replacement of one atom in a gas oxygen molecule by an oxygen atom from the solid (type 2) and with the replacement of both molecule atoms for oxide oxygen (type 3) [2].

The rates of all types of exchange have been calculated from the time variations of  $^{16}\text{O}^{16}\text{O}$ ,  $^{18}\text{O}^{16}\text{O}$  and  $^{18}\text{O}^{18}\text{O}$  molecules concentrations in the gas in the course of isotopic exchange. The experimental data have been obtained under adsorption-desorption oxide-gas equilibrium conditions at the temperatures 870 to 950 K and oxygen pressures 350 to 1250 Pa. The calculated rates are  $K_1 \approx 8.6 \times 10^{32} \exp[-2.9\text{eV}/(kT)]$ ,  $K_2 \approx 8.6 \times 10^{26} \exp[-1.86\text{eV}/(kT)]$  and  $K_3 \approx 4.4 \times 10^{21} \exp[-1.05\text{eV}/(kT)]$  molecule  $\text{O}_2/(\text{cm}^2\text{s})$  at  $P_{\text{O}_2} = 665$  Pa. The  $P_{\text{O}_2}$  dependences of  $K_i$  can be approximated by the power functions:  $K_1 \propto (P_{\text{O}_2})^{1.4}$ ,  $K_2 \propto (P_{\text{O}_2})^{0.65}$  and  $K_3 \propto (P_{\text{O}_2})^{0.8}$ . The obtained oxygen heteroexchange rate  $R = (0.5K_2 + K_3)$  is approximately the same as in [1]:  $R \approx 4.0 \times 10^{25} \exp[-1.65\text{eV}/(kT)]$  molecule  $\text{O}_2/(\text{cm}^2\text{s})$ . The main contribution to  $R$  at temperatures under study is made by the exchange processes of the second type and at lower temperatures, as the extrapolation shows, of the third one.

The present analysis confirms our previous conclusion that diffusion of oxygen in the dense  $\text{YBaCuO}$  ceramics follows a two-stage course [1,2]. At the first stage the diffusivity is at least an order higher than in the bulk. This stage may be caused by the grain boundary diffusion or diffusion in subsurface regions different from the bulk in the oxygen transfer rate [1,2]. The bulk diffusivity determined  $D^* \approx 10^{-3} \times \exp[-1.15\text{eV}/(kT)] \text{ cm}^2/\text{s}$  exhibits a slight dependence on  $P_{\text{O}_2}$ :  $D^* \approx 10^{8.9} \times (P_{\text{O}_2}/\text{Pa})^{-0.3 \pm 0.15} \text{ cm}^2/\text{s}$  ( $T = 870$  K). The corresponding weak decrease of  $D^*$  with oxygen content in  $\text{YBa}_2\text{Cu}_3\text{O}_{6+x}$  agrees well with new theoretical results for the oxygen transport coefficients obtained by the dynamical cluster method taking into account essential oxygen-oxygen interactions [3].

[1] E.Kh. Kurumchin, V.I. Tsidilkovski, A.N. Ezin, G.K. Vdovin and I.A. Leonidov, *Sverhprovodimost': Fizika, Khimiya, Tekhnika* 7, 1065 (1994).

[2] A.N. Ezin, V.I. Tsidilkovski and E.Kh. Kurumchin, *Solid State Ionics* 84, 105 (1996).

[3] V.I. Tsidilkovski, In *Proc. of 5th Euroconf. on Solid State Ionics*, Spain, 1998 (to be published in *Ionics*).

## SINTERING BEHAVIOUR IN AIR FOR Ca OR Sr DOPED $\text{LaCrO}_3$ PEROVSKITES INCLUDING SECOND PHASE OF $\text{Cr}^{6+}$

Masashi MORI, Yoshiko HIEI,  
Chemical Energy Engineering Department,  
Central Research Institute of Electric Power Industry  
2-6-1 Nagasaka, Yokosuka, Kanagawa, 240-0196  
Nigel SAMMES  
Centre for Technology, The University of Waikato  
Private Bag 3105, Hamilton, New Zealand

Lanthanum chromite,  $\text{LaCrO}_3$ , and its solid solutions with Ca or Sr, are well known as high electronic conductors and have been widely applied as separator or interconnector materials for high-temperature solid oxide fuel cells using  $\text{Y}_2\text{O}_3$ -stabilized  $\text{ZrO}_2$  electrolyte. The perovskites with stoichiometric compositions are known to be chemically stable under oxidizing or reducing atmospheres, as well as having poorly sinterable in air [1]. The reason for the poor sintering is that the chromium-vapor component starts to evaporate as gaseous  $\text{CrO}_3$  at temperatures over 1273 K. This disturbs the densification of the  $\text{LaCrO}_3$  particles by the evaporation, which reduces the ability of producing a dense sintered body [2].

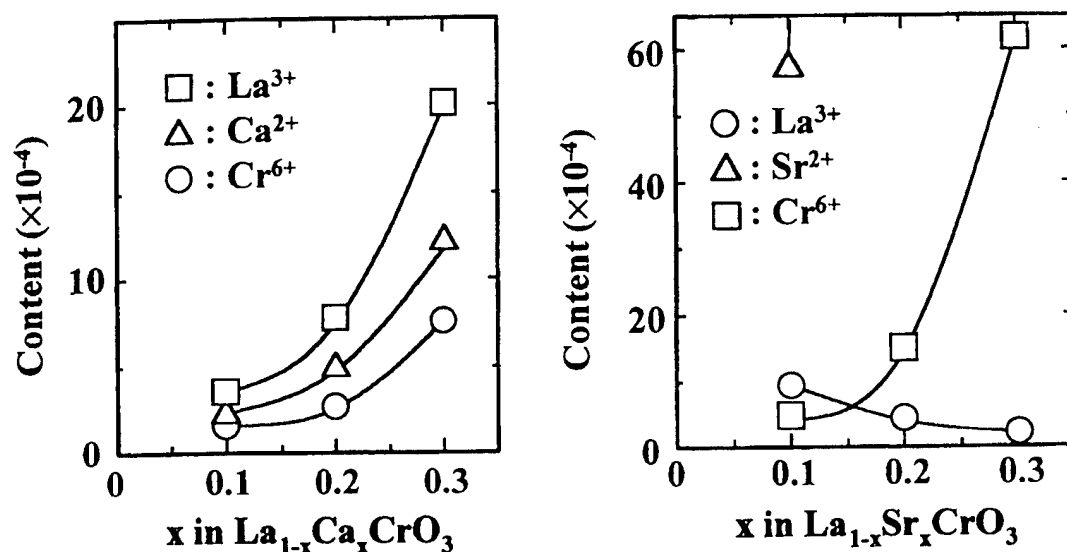
In recent years, the relationship between sintering and second phase has been focused upon the alkaline earth metal (AE)-doped lanthanum chromites with non-stoichiometric composition, which have the low-temperature sintering characteristics in air [5]. An understanding of the sintering mechanism of lanthanum chromites with AE-dopant in air is quite important, and an appropriated way of fabricating a dense plate with relative densities over 94 % must be found for gas tightness to be assured [6].

The purpose of the work was to experimentally determine a relationship between sintering, second phases and non-stoichiometric composition for Ca- or Sr-doped  $\text{LaCrO}_3$  perovskite powders fabricated by the solid-state reaction method in air. Sintering properties of AE-doped lanthanum manganites,  $(\text{La}_{1-x}\text{AE}_x)_{1+y}\text{CrO}_3$  (AE=Ca and Sr,  $0 \leq x \leq 0.3$ ,  $0 \leq y \leq 0.02$ ), have been discussed in air at 1873 K. For the case of stoichiometric  $\text{La}_{1-x}\text{AE}_x\text{CrO}_3$  perovskites, their results are shown as follows:

Figs. 1 show the amounts of  $\text{La}^{3+}$ ,  $\text{Ca}^{2+}$ ,  $\text{Sr}^{2+}$  and  $\text{Cr}^{6+}$  in the  $\text{La}_{1-x}\text{AE}_x\text{CrO}_3$  powders after heating at 1473 K for 10 h and milling twice for 15 min. In the case of Ca-doped lanthanum chromites, the contents of  $\text{La}^{3+}$ ,  $\text{Ca}^{2+}$  and  $\text{Cr}^{6+}$  in the samples increased with Ca content, and the atomic ratio of  $(\text{La}^{3+} + \text{Ca}^{2+})/\text{Cr}^{6+}$  was constantly 1 for all the Ca-doped perovskites. For the Sr-doped sample, the amounts of  $\text{Sr}^{2+}$  and  $\text{Cr}^{6+}$  increased with Sr-content, whereas the amount of  $\text{La}^{3+}$  decreased. The Sr contents were  $387.4 \times 10^{-4}$  mol for  $x = 0.2$  and  $870.5 \times 10^{-4}$  mol for  $x = 0.3$ . The atomic ratio of  $(\text{La}^{3+} + \text{Sr}^{2+})/\text{Cr}^{6+}$  in these perovskite samples was not however 1. This explained that the powders might contain a small amount of  $\text{Cr}_2\text{O}_3$  as non-reacted starting powder. Although the  $\text{La}_{0.7}\text{Sr}_{0.3}\text{CrO}_3$  powder had a  $\text{SrCrO}_4$  phase with low-melting point around 1373 K in air, it did not show the excellent sintering property.

After firing the  $\text{La}_{1-x}\text{AE}_x\text{CrO}_3$  perovskites at 1873 K for 20 h in air, the relative density of the doped  $\text{LaCrO}_3$  increased with AE-content. The sintering properties of the  $\text{La}_{1-x}\text{Ca}_x\text{CrO}_3$  are lower than those of the  $\text{La}_{1-x}\text{Sr}_x\text{CrO}_3$ , when  $x \leq 0.2$ . However, the reverse results were observed at  $x = 0.3$ . The second phase of  $\text{SrCrO}_4$  did not cause the remarkable sintering property for the  $\text{La}_{1-x}\text{Sr}_x\text{CrO}_3$  with stoichiometric composition.





**Figs. 1**  $\text{La}^{3+}$ ,  $\text{Ca}^{2+}$ ,  $\text{Sr}^{2+}$  and  $\text{Cr}^{6+}$  in the  $\text{La}_{1-x}\text{AE}_x\text{CrO}_3$  after heating at 1473 K for 10 h and milling twice for 15 min (AE=Ca and Sr).

## REFERENCES

1. B. F. Flandemeyer, M. M. Nasrallah, D. M. Sparlin, and H. U. Anderson, High Tem. Sci., **20**[259], 265(1985).
2. H. Yokokawa, N. Sakai, T. Kawada, and M. Dokiya, J. Electrochem. Soc., **138**[4], 1018(1991).
3. D. P. Karim and A. T. Aldred, Physical Review B, **20** [6], 2255(1979).
4. M. Mori, T. Yamamoto, H. Itoh, and T. Watanabe, **32** [9], 2233(1997).
5. for example, N. Sakai, T. Kawada, H. Yokokawa, M. Dokiya, and T. Iwata, J. Mater. Sci., **25**, 4531(1990).
6. B. K. Flandermeyer, J. T. Dusek, P. E. Balckburn, D. W. Dees, C. C. McPheeters, and R. B. Poeppel, Abstract of National Fuel Cell Seminar, Tucson, Arizona, 86(1986).

## CHARACTERISATION OF Co-DOPED LANTHANUM GALLATE

F.M. Keppeler<sup>\*1</sup>, N.M. Sammes<sup>2</sup>, H. Naefe<sup>1</sup> and F. Aldinger<sup>1</sup>

<sup>1</sup> Max-Planck-Institut fuer Metallforschung, Department Aldinger, Heisenbergstrasse 5,  
D-70569 Stuttgart, Germany, e-mail: keppeler@aldix.mpi-stuttgart.mpg.de

<sup>2</sup> The University of Waikato, Department of Technology, Private Bag 3105, Hamilton

In recent years a big effort has been made to find a new material for use as an electrolyte in medium temperature solid oxide fuel cell (SOFC) applications. The aim was hereby to replace the common-used yttria doped zirconia for the sake of reducing the operation temperature of the fuel cell stacks. Therefore, perovskite structured materials ( $\text{ABO}_3$ ) have been examined by various research groups [1-3]. Ishihara et al. [4], and Feng and Goodenough [5] have been the first to report on the promising properties of A- and B-site doped lanthanum gallate, using strontium on the A-site and magnesium on the B-site. These materials showed high oxygen ion conductivities while revealing oxygen ion transference numbers close to unity even under very reducing conditions

[4-8]. Baker et al. [9] showed that additions of Fe or Cr in  $\text{La}_{0.9}\text{Sr}_{0.1}\text{Ga}_{1-x}\text{M}_x\text{O}_{3\pm\delta}$  ( $\text{M} = \text{Fe}$  or  $\text{Cr}$ , from 0 to 0.2) increased the p-type conductivity, while the ionic contribution was reduced. They assumed the formation of  $\text{Fe}^{4+}$  and  $\text{Cr}^{4+}$  to lower the oxygen vacancy concentration in the material. Ishihara et al. [10] investigated the effect of doping cobalt in  $\text{La}_{0.8}\text{Sr}_{0.2}\text{Ga}_{0.8}(\text{Mg},\text{Co})_{0.2}\text{O}_{3\pm\delta}$  and showed that the electrical conductivity of the material increased with increasing Co content. The authors [10] also observed that the ionic transport number of  $\text{La}_{0.8}\text{Sr}_{0.2}\text{Ga}_{0.8}\text{Mg}_{0.15}\text{Co}_{0.05}\text{O}_{3\pm\delta}$  remained relatively constant between oxygen partial pressures of 1 and  $10^{-22}$  bar, with negligible p-type conduction, and thus concluded that the material is a promising electrolyte in SOFC applications.

The presented work was aimed to reveal the mixed conducting properties of materials of the composition  $\text{La}_{0.8}\text{Sr}_{0.2}\text{Ga}_{0.85-x}\text{Co}_x\text{Mg}_{0.15}\text{O}_{3-\delta}$  ( $x=0.01-0.25$ ) to find out if they are suitable as mixed conductors, and to reveal the effect of interdiffusion of Ga and Co observed by Huang et al. [11]. The samples were produced using a solid state technique. Therefore, high purity precursor powders were mixed and calcined at proper calcining temperatures revealed by DTA/TGA-measurements. The obtained materials revealed high relative densities of about 97% and showed no secondary phases present, so it was not necessary to carry out additional calcining steps reducing the problem of material losses due to evaporation during heat treatment.

Various techniques were applied to the samples to examine the properties of the obtained materials. To show the influence of temperature and oxygen partial pressure on the conduction properties of the materials, four-probe technique measurements were carried showing a transition in conduction behaviour from ionic-like to mixed ionic/electronic with rising cobalt content. Figure 1 shows the effect of variation of oxygen partial pressure on various samples at 900 °C. To clear up the sample behaviour of decreasing ionic conductivity at cobalt contents  $x \geq 0.05$ , rutherford backscattering spectroscopy (RBS) and NMR-measurements have been carried out.

\* on leave at the University of Waikato, New Zealand

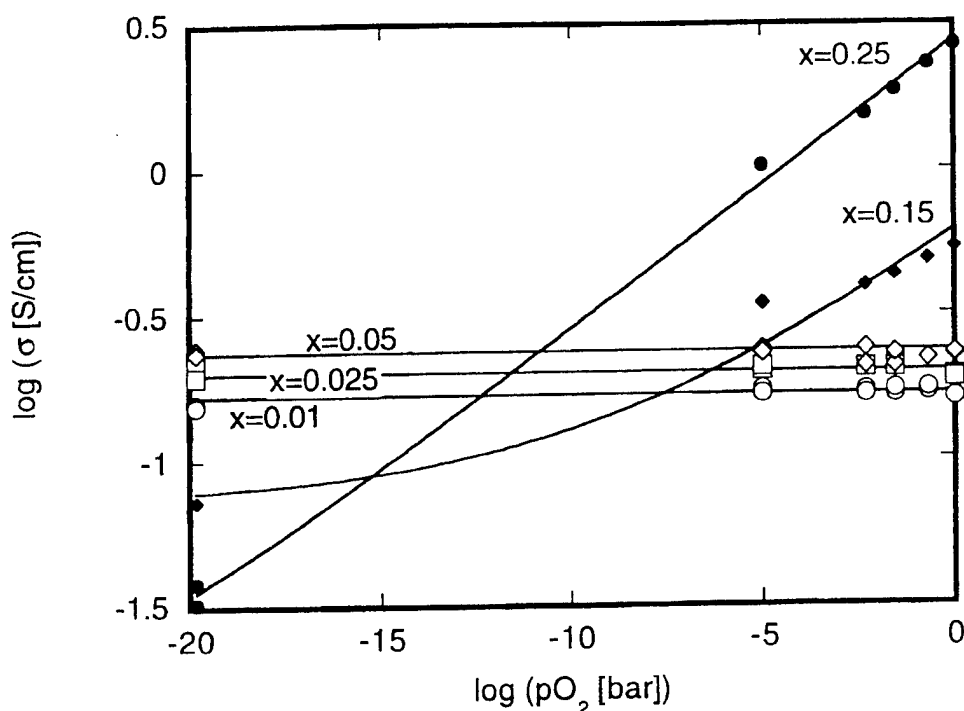


Figure 1: Partial pressure dependance of the total conductivity of  $\text{La}_{0.8}\text{Sr}_{0.2}\text{Ga}_{0.85-x}\text{Co}_x\text{Mg}_{0.15}\text{O}_{3-\delta}$  ( $x=0.01-0.25$ ) at 900 °C.

### References

- [1] K.R. Kendall, C. Navas, J.K. Thomas, and H-C zur Loye, *Solid State Ionics* **82**, 215 (1995).
- [2] Y. Takeda, N. Imanishi, R. Kanno, T. Mizuno, H. Higuchi, O. Yamamoto, and M. Takano, *Solid State Ionics*, **53-56**, 748 (1992).
- [3] T. Ishihara, H. Matsuda, Y. Mizuhara, and Y. Takita, *Solid State Ionics*, **70/71**, 234 (1994).
- [4] T. Ishihara, H. Matsuda, and Y. Takita, *J. Am. Chem. Soc.*, **116**, 3801 (1994).
- [5] M. Feng and J.B. Goodenough, *Eur. J. Solid State Inorg. Chem.*, **131**, 663 (1994).
- [6] A. Petric, P. Huang, and A. Skowron, in *Proc. of the 2<sup>nd</sup> European SOFC Forum*, ed. B. Thorstensen (Morgenacher, Oberrohrdorf, Switzerland, 1996) 751.
- [7] P. Huang and A. Petric, *J. Electrochem. Soc.*, **143** [5], 1644 (1996).
- [8] T. Ishihara, H. Matsuda, and Y. Takita, *Solid State Ionics*, **79**, 147 (1995).
- [9] R.T. Baker, B. Gharbage, and F.M.B. Marques, *J. Electrochem. Soc.*, **144** [9], 3130 (1997).
- [10] T. Ishihara, T. Akbay, H. Furutani, and Y. Takita, in *11<sup>th</sup> International Conference on Solid State Ionics, Extended Abstracts*, (Honolulu, Hawaii, USA, 1997) 362.
- [11] K.Q. Huang, M. Feng, J.B. Goodenough and M. Schmerling, *J. Electrochem. Soc.*, **143** [11], 3630 (1996).

## TRANSFER PHENOMENA IN ELECTROCHEMICAL REACTOR BASED ON MIXED OXIDE CONDUCTOR

Anatoly K. Demin and Lilya A. Dunyushkina  
Institute of High Temperature Electrochemistry, Ural Division RAS  
620219 Ekaterinburg, S.Kovalevskoy Str., 20

It is known that oxides with mixed ionic and electronic conductivity can be used in the devices for gas separation and gas mixtures reforming without electrical energy consumption. In particular, a mixed conducting membrane (MCM) can be used for hydrogen production in so-called electrochemical reformer (ECR). In the ECR, an anode compartment is supplied with gas containing fuel components whereas a cathode compartment is fed by steam. Due to a difference in oxygen activities in the compartments, oxygen permeates through a mixed conductor from the cathode compartment into the anode one. So, in the cathode compartment, steam transforms into hydrogen.

The main requirements to the MCM are acceptable oxygen permeability and stability at working conditions (high temperature and reduced atmosphere). For some reasons, the MCM can be stable only within relatively narrow interval of low oxygen partial pressure ( $P_{O_2}$ ). Nevertheless, it might be successfully used in the ECR if it works at proper conditions. The MCM ionic conductivity does not depend on  $P_{O_2}$ , whereas its electronic conductivity is a function of  $P_{O_2}$ . In the case when ionic and electronic conductivities are comparable the oxygen permeability is a complex function of  $P_{O_2}$  at both sides of the MCM. It was interesting to determine ECR operating parameters in dependence on input gases parameters and MCM properties.

The ECR-system consisted of an electrochemical section, a pre-reformer, a burner, a vaporiser and a condenser was considered. As a first assumption, it was accepted that heat produced by the burner and the electrochemical section is completely absorbed by the pre-reformer and the vaporiser, whereas heat produced by the condenser can not be utilised. It was shown from the heat balance equation that a hydrogen output expressed as a ratio  $H_2/CH_4$  depends only on hydrogen concentration in the outlet cathode gas and the ratio can theoretically reach value of 2.7.

In the electrochemical section, the gas mixtures in the corresponding compartments are non-homogeneous along the flows: fuel components concentrations decrease in the anode gas and hydrogen concentration increases in the cathode gas. It is quite obvious that the only flow geometry in the electrochemical section to provide the positive EMF within all MCM area is the counter-flow mode. Due to non-homogeneity of oxygen activities in the gases which are in the contact with both sides of the MCM its resistance is also non-homogeneous. This leads, together with the EMF non-homogeneity, to the non-homogeneity in the current density and as a consequence in the heat fluxes produced by MCM.

There are some limitations for the inlet gases parameters. The fuel components concentrations in the inlet anode gas must not be too high to avoid carbonisation. The hydrogen concentration in the inlet cathode gas must not be too low to avoid MCM decomposition. The mentioned concentrations and the hydrogen concentration in the outlet cathode gas as well as the MCM electrical properties and size were varied in the numerical simulation. The distributions of the resistance, EMF, current density and heat flux in the MCM were found. It was shown that the current density increases with the increase in the fuel components concentrations in the inlet anode gas, with the decrease in the hydrogen concentration both in the inlet and outlet cathode gas. In the latter case, however, the hydrogen output decreases.

## DEFECT CHEMISTRY AND TRANSPORT PROPERTIES OF SINGLY CRYSTALLINE Y<sub>2</sub>O<sub>3</sub>-DOPED ZrO<sub>2</sub> INCLUDING THE INFLUENCE OF REDOX-ACTIVE IMPURITY IONS

K. Sasaki and J. Maier

Max-Planck-Institut für Festkörperforschung

D-70569 Stuttgart, Germany

(Fax) +49-711-689-1722

(e-mail) sasaki@chemix.mpi-stuttgart.mpg.de

The impurities such as transition metal ions are always present in *real* ionic and mixed conductors. Several effects of such ions on transport and electrochemical properties have been reported in literature [1-6]. The influence of such ions is thus of technological as well as scientific relevance.

Defect chemistry and transport properties of Y<sub>2</sub>O<sub>3</sub>-doped ZrO<sub>2</sub> are discussed, including the influence of redox-active impurity ions as well as ionic and electronic charge carriers. The equilibrium defect chemistry at a temperature, *T*, may be described by the oxygen exchange equilibrium (with the constant *K<sub>O</sub>*), the impurity ionization equilibrium (with *K<sub>M</sub>*), the electronic equilibrium (with *K<sub>B</sub>*), and the mass conservation conditions [1]. It is well established that the electron and hole concentrations are fixed by *K<sub>O</sub>*, *pO<sub>2</sub>*, and [*Y'*], and their conductivities are not affected by the redox-active impurities, as long as the simplification of the overall electroneutrality condition is valid. At lower temperatures in partially frozen-in states, the oxygen exchange equilibrium is no longer reversible, but the trapping reaction is still reversible. By taking into account the conservation condition of free and trapped holes in oxidizing atmosphere (or electrons in reducing atmosphere), it can be analytically shown [1,4,5] how the electron (hole) concentration and their conductivities are affected directly by the internal ionization with these deep dopants.

In order to study the influence of such redox-active ions in this solid electrolyte material, single crystalline ZrO<sub>2</sub>(Y<sub>2</sub>O<sub>3</sub>) selectively doped with 3d transition metal (Ti, V, Cr, Mn, Fe, Co, Ni, Cu) or selected rare earth (Ce, Pr, Gd) ions is used as a model material. EPR and optical absorption spectroscopy are applied to identify the valence state/change as well as to quantify the concentration of ions with a specific valence state. Redox-active ions specified in YSZ (10<sup>-20</sup> ≤ *pO<sub>2</sub>* ≤ 1 bar) are: Mn<sup>3+</sup> ↔ Mn<sup>2+</sup>, V<sup>4+</sup> ↔ V<sup>3+</sup>, Fe<sup>3+</sup> ↔ Fe<sup>2+</sup>, Ce<sup>4+</sup> ↔ Ce<sup>3+</sup>, and Ti<sup>4+</sup> ↔ Ti<sup>3+</sup> [1].

The chemical diffusion coefficient, determined as the ambipolar diffusion of oxygen ions and electrons, is usually described as  $\tilde{D} = t_{V_o^{\bullet\bullet}} \cdot D_{eon} \cdot w_{eon} + t_{eon} \cdot D_{V_o^{\bullet\bullet}} \cdot w_{V_o^{\bullet\bullet}}$  where *w* is thermodynamic factor, *t* is transference number, and *D* is particle diffusion coefficient. If ions of variable charges are involved, acting as sink or source of electrons or holes, the above equation has to be generalized by introducing the trapping factor [3], indicating the importance of redox-active ions for the chemical diffusion. Since the amount of oxygen exchanged is appropriately correlated with the change in the defect concentrations, the time-dependent relaxation of defect concentrations yields the chemical diffusion coefficient  $\tilde{D}$  and/or the surface exchange coefficient  $\tilde{k}$ .  $\tilde{D}$  and  $\tilde{k}$  describe the kinetics of the reequilibration.

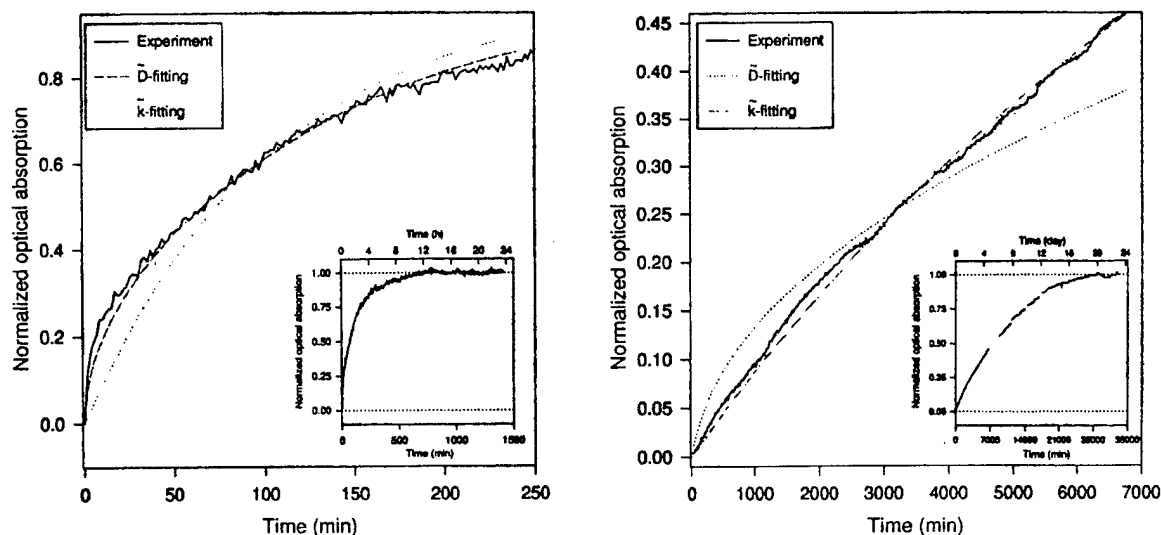


**Figure 1:** Chemical relaxation of the optical absorption of  $\text{Mn}^{3+}$  in YSZ, measured *in-situ* at (a) 875 and (b) 700°C by the  $p_{\text{O}_2}$  change from air to pure  $\text{O}_2$ .

*In-situ* optical absorption has been applied to quantify the chemical diffusion and surface exchange coefficients. Figure 1 shows the relaxation of the optical absorption of  $\text{Mn}^{3+}$  by the  $p_{\text{O}_2}$  change from air to pure  $\text{O}_2$  at (a) 875°C and (b) 700°C. The relaxation curve measured at 875°C indicates the chemical diffusion rate-limited reequilibration with  $\tilde{D}=2.5 \times 10^{-8} \text{ cm}^2/\text{s}$ . The chemical diffusion coefficient of YSZ doped with Mn oxide obtained in the oxidizing atmosphere was one of the lowest chemical diffusion coefficients of oxygen reported in the YSZ literature, confirming the trapping effect of Mn through the valence change between  $\text{Mn}^{2+}$  and  $\text{Mn}^{3+}$ . This is well in agreement with the band scheme of YSZ. On the other hand, the relaxation curve measured at 700°C indicates a surface exchange rate-limited reequilibration with  $\tilde{k}=4.4 \times 10^{-8} \text{ cm/s}$ , leading to considerable reequilibration time ( $\approx 3$  weeks even at 700°C) [2]. The surface exchange mechanism of oxygen is discussed using  $T$ ,  $p_{\text{O}_2}$ , and dopant concentration dependencies of chemical rate constants and comparison with literature tracer data [7].

## References

- [1] K. Sasaki, P. Murugaraj, M. Haseidl, and J. Maier, p. 1190, in *Proc. 5th Intl. Symp. Solid Oxide Fuel Cells*, The Electrochem. Soc. Proc. Series, PV 97-40, (1997).
- [2] K. Sasaki, M. Haseidl, and J. Maier, p. 123, *Proc. Eurosolid 4*, (1997).
- [3] J. Maier, *J. Am. Ceram. Soc.*, **76**, 1223 (1993).
- [4] K. Sasaki and J. Maier, *J. Europ. Ceram. Soc.*, in press.
- [5] K. Sasaki, J. Claus, and J. Maier, *Solid State Ionics*, to be published.
- [6] E.J.L. Schouler and M. Kleitz, *J. Electrochem. Soc.*, **134**, 1045 (1987).
- [7] J. Maier, *Solid State Ionics*, **112**, 197 (1998).

## EQUIVALENT CIRCUIT MODELS FOR IMPEDANCE SPECTROSCOPY AND CHEMICAL DIFFUSION

J. Jamnik, M. Leonhardt and J. Maier  
Max-Planck-Institut für Festkörperforschung  
Heisenbergstr. 1, 70569 Stuttgart, Germany

Owing to their lucidity equivalent circuit models are an indispensable tool in impedance spectroscopy of mixed conductors. Equivalent circuits are usually derived intuitively or empirically. In this contribution we follow the approach proposed by Franceschetti [1] and derive the equivalent circuit directly from Nernst-Planck-Poisson set of equations. For a sample with laterally homogeneous electrodes and two charge carriers which can not be generated or recombined within the sample - a situation typical for mixed conductors - the resulting equivalent circuit is shown in Fig. 1. Besides usual elements (resistors  $R_{j,i}$  and electrostatic capacitors  $C_e$ ) chemical capacitors  $C_{j,i}$  defined as the inverse of the derivative of the chemical potential over the corresponding carrier concentration are introduced.

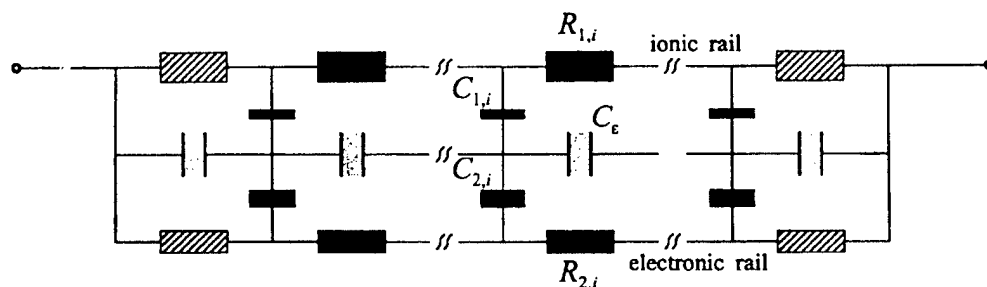


Fig. 1: Master equivalent circuit

The master equivalent circuit shown in Fig. 1 can be tailored and thus simplified for a specific class of materials and for a particular type of experiments. Here we give two examples.

### 1) Impedance spectroscopy of mixed conductors using selectively blocking electrodes

In this technique, which is important for determination of ionic and electronic conductivities, the electrodes are either blocking for ions and reversible for electrons or vice versa. There have been an ongoing debate whether mixed conductors with dominant ionic or electronic conductivity necessarily exhibit Warburg diffusion (45° line) in the impedance spectra. There are many measurements in the literature (see for example Ref. [2]) demonstrating that the low frequency part of the spectra exhibit a 90° rise referring to the electrode capacitance rather than 45° line reflecting diffusion. The 90° rise, has however, to turn into a semicircle at lower frequencies and eventually to reach the real axis referring to the DC conductivity of the unblocked carrier.

For samples much thicker than the Debye length the master equivalent circuit simplifies yielding a closed form expression for the impedance. In addition, a simple criterion to predict the type of the response, is obtained: if the chemical capacitance of the sample is much higher than the electrode capacitance the low frequency part of the spectra is of Warburg type while in the opposite case a semicircle appears in the low frequency part of the spectra. If, for example, the electrode capacitance is on the order of  $10\mu\text{F}/\text{cm}^2$  and the sample thickness is 1mm, then a minority carrier concentration greater than  $10^{14}/\text{cm}^3$  leads to a Warburg type of impedance and a

minority carrier concentration smaller than  $10^{14}/\text{cm}^3$  to a perfect semicircle. Experimental examples from the literature are discussed.

## 2) Chemical diffusion of oxygen through $\text{SrTiO}_3$ bicrystal

The master equivalent circuit does not only apply to impedance spectroscopy but to effectively one-dimensional chemical diffusion problems as well. In this case the driving force is the component chemical potential (see the right hand side of the circuit depicted in Fig. 2a). We applied the equivalent circuit shown in Fig. 2a to model the diffusion of oxygen into iron doped  $\text{SrTiO}_2$  bicrystals[3] (Fig. 2b). The only unknown parameters which had to be determined were the rate constant of the oxygen incorporation reaction and the chemical resistance of the grain boundary. As shown in Fig. 2c the agreement of measured and fitted curves is very good. The chemical resistance of the grain boundary was in this case explained by the Schottky barriers. The height of the Schottky barrier calculated from the chemical resistance was in good agreement with the values derived from the impedance spectroscopy data[3].

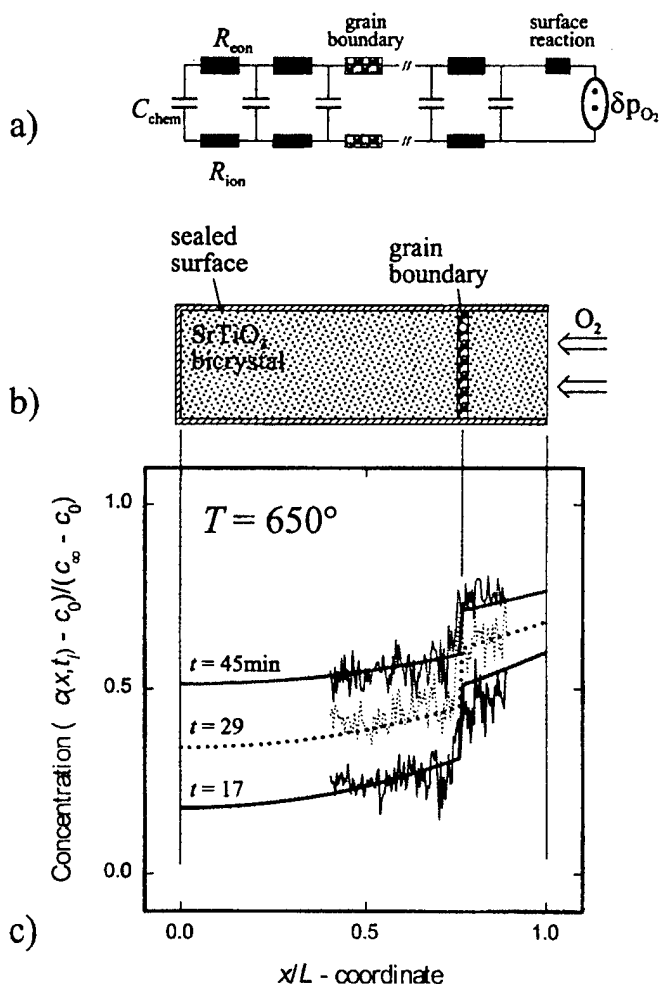


Fig. 2: a) Equivalent circuit for the chemical diffusion experiment sketched in Fig. 2b. c) Measured and modelled concentration profiles of the in-diffusing oxygen. A steep change of the concentration at  $x/L=0.76$  reflects the „blocking“ character of the grain boundary. Symbols  $c_0$ , and  $c_\infty$  denote the initial and end state concentrations, respectively. Symbol  $L$  denotes the thickness of the sample.

### References:

- [1] D.R. Franceschetti, Solid State Ionics 70/71, 542 (1994).
- [2] W.I. Archer and R.D. Armstrong, "Specialist Periodical Report", p. 157, The Chemical Society, London (1980).
- [3] M. Leonhardt, Ph D thesis, Stuttgart, in preparation.



## CHARGE TRANSFER IN TWO- AND THREE-CATION OXIDE CRYSTALS

A. E. NOSENKO and V. N. SHEVCHUK

Department of Physics, L'viv State University,  
50 Dragomanov str., L'viv 290005 Ukraine

In this paper the single crystals undoped and doped with *d*- and *f*- ion impurities of  $Re_3Ga_5O_{12}$  (*Re* – rare-earth ions) and  $Ca_3Ga_2Ge_3O_{12}$  (garnet structure), and  $Ca_3Ga_2Ge_4O_{14}$  (*Ca*-gallogermanate acentric structure) are investigated. Crystals were grown by Chochralsky method.

The total electrical conductivity  $\sigma$  at direct and alternating external electric field in interconnection with polarization effects, nature of the electrical active defects, electrical transfer features at linear temperature variation are considered. The electrical charge transfer in temperature range  $T = 100-1200$  K in vacuum (I) and air (II) atmosphere are studied. The measurements realized on a samples with dimensions about  $0.5 \times 10 \times 10$  mm<sup>3</sup>. External electric field were applied to samples along of the growth axis and perpendicular direction to the latter in *Ca*-gallogermanate case. The previous data of electrical characteristics measurements in these crystals are proposed in [1,2].

The under investigation crystals have the mixed ion-electronic conductivity with *p* – type of the electronic conductivity component. The latter is connected with  $O^-$ -type centres. Transfer of the hole is realized chiefly by hops from site to site at low temperatures and described by small-polarons theory. Cationic component of ionic conductivity is determined by cation in octahedral environment by oxygen that is *Ga*. The crystals are characterized by nonequilibrium relaxational processes which are accompanied by conductivity variation or by anomalies in the dependence of conductivity versus high-temperature in the case of the structural rebuilding what observed, e.g., in  $Ca_3Ga_2Ge_3O_{12}$  crystal at  $\sim 1300$  K [3]. In this phenomena main role ascribe to cationic sublattices of crystals.

The dependence  $\sigma(T)$  in corresponding temperature ranges (see table) is approximated by law  $\sigma \sim \exp(-E_a/kT)$ , here  $E_a$  is energies of activation,  $k$  is Boltzman's constant. The parameters of the electrical transfer are determined. The some data of dc and ac conductivity given in the table. Nature of the charge carriers, mechanisms of conductivity and other electrical phenomena in different temperature regions are discussed. The structural-response region of conductivity is dependet on: concentration and sharge state of impurity, substitution of oxygen position by activator and corresponding of electrical active point defects formation in crystalline matrix. Dependence of the conductivity from the latters circumstance, stoichiometry, method monocrystal growth and distribution of point defects in grovn crystals are investigated. The probable ways of cation migration through crystalline structure are analysed. The results for isotropic and anisotropic crystals are compared.

Results of conductivity investigations were analysed with polarizational phenomena: thermally stimulated polarization and depolarization currents. The correlation of equilibrium and thermally stimulated currents are considered. Nature of dipolar centers what caused, in particular, the polarization peaks in temperature range 280-360 K with dipolons [1] are connected. The parameters of thermally stimulated current peaks what conditioned by charge carriers and dipolar relaxation are calculated.

**Table.** Some data of conductivity measuring of the complex oxide crystals.

Crystal	$\sigma$ ( $\Omega\text{hm}^{-1} \times \text{cm}^{-1}$ )			$E_a$ (eV)			
	$T$ (K)	I	II	$T$ (K)	I	II	
$\text{Nd}_3\text{Ga}_5\text{O}_{12}$	300	$6.2 \cdot 10^{-17}$		430 – 500	1.77		
$\text{Sm}_3\text{Ga}_5\text{O}_{12}$	300	$6.1 \cdot 10^{-17}$		430 – 500	1.92		
$\text{Gd}_3\text{Ga}_5\text{O}_{12}$	300	$4.4 \cdot 10^{-17}$	$1.2 \cdot 10^{-16}$	435 – 500	1.80	1.57	
	470	$9.1 \cdot 10^{-14}$	$5.5 \cdot 10^{-13}$	500 – 600	1.38		
$\text{Ca}_3\text{Ga}_2\text{Ge}_3\text{O}_{12}(\text{G})$	300	$1.0 \cdot 10^{-16}$	$4.0 \cdot 10^{-14}$	300 – 350	1.23	1.09*	
	450	$4.7 \cdot 10^{-13}$	$5.5 \cdot 10^{-12}$	350 – 500	1.68		
	1200		$2.0 \cdot 10^{-5*}$	870 – 1200			
G : Cr, G : Co	300	$4.6 \cdot 10^{-15}$	$2.0 \cdot 10^{-12}$	300 – 350		0.12	
	450	$6.6 \cdot 10^{-14}$	$8.4 \cdot 10^{-12}$	390 – 445		0.25	
				445 – 500		0.53	
				500 – 570		1.18	
G : Mn	300		$3.1 \cdot 10^{-12}$	300 – 350		0.06	
	450		$1.3 \cdot 10^{-11}$	440 – 490		0.35	
				490 – 570		1.08	
G : Er	300		$6.2 \cdot 10^{-12}$	450 – 490		0.49	
	450		$1.8 \cdot 10^{-11}$	490 – 570		1.09	
G : Nd	1000		$8.1 \cdot 10^{-7*}$	870 – 1100		1.09*	
$\text{Ca}_3\text{Ga}_2\text{Ge}_4\text{O}_{14}$	300		$\sim 10^{-16}$	300 – 450		z	x, y
				450 – 500			
				500 – 530			
				530 – 560			
				560 – 650			
					0.03	0.07	
					2.09	0.21	
					1.12	0.85	
						2.51	
						1.48	

Value of the residual gas pressure at vacuum measuring is 0.03 Pa.

\*) Frequency of electrical field of measuring is 1 kHz. In other cases the data in reference to dc conductivity are given.

Values of impurity concentration are 0.02 at %.

For anisotropic case  $E_a$  values along crystalline axes  $z$  and  $x, y$  are given.

## REFERENCES

1. A.E.Nosenko, V.N.Shevchuk, *Rad. Eff. and Def. in Solids* **134** (1995) 251.
2. A.E.Nosenko, V.N.Shevchuk, *Fizika tverdogo tela* **39** (1997) 871 (in russ.).
3. A.E.Nosenko, V.N.Shevchuk, *Neorganicheskie materialy* **27** (1991) 2213 (in russ.).

## OXYGEN-DEFICIENT PEROVSKITE COMPOUNDS WITH OXIDE ION CONDUCTION

Y. Arachi<sup>1</sup>, T. Asai<sup>1</sup>, O. Yamamoto<sup>2</sup>, Y. Takeda<sup>2</sup> and N. Imanishi<sup>2</sup>

<sup>1</sup>Chemical Branch, Faculty of Engineering, Kansai University,

Yamate-cho 3-3-35, Suita-city, Osaka 564-8680, JAPAN

<sup>2</sup>Department of Chemistry, Faculty of Engineering, Mie University,

Kamihama 1515, Tsu-city, Mie 514-8507, JAPAN

In the course of search for new types of oxide ion conductors, a perovskite oxide has been synthesized by use of the conventional solid state reaction. The basic composition is  $\text{Sr}_4\text{In}_2\text{Zr}_2\text{O}_{11}$ , and the phase obtained shows a cubic perovskite structure indicating that the oxygen vacancies are disordered in this phase. The system substituted of  $\text{Ga}^{3+}$  for  $\text{In}^{3+}$  or  $\text{Y}^{3+}$  for  $\text{Zr}^{4+}$  was tried to investigate the relationship between oxide ion conduction and the crystal structure. It was found that these materials have relatively high oxide ion conduction and  $\text{Sr}_4\text{In}_2\text{Zr}_2\text{O}_{11}$  has the conductivity of 0.02 S/cm at 1273K.

All samples were prepared by conventional solid state reaction of powder mixture of  $\text{SrCO}_3$ ,  $\text{In}_2\text{O}_3$ ,  $\text{ZrO}_2$ ,  $\text{Ga}_2\text{O}_3$  and  $\text{Y}_2\text{O}_3$ . The mixture was calcinated at 1273K for 24h and the obtained powders were pressed isostatically into a disk under pressure of 170MPa followed sintered at 1773K for 24h in air. The electrical conductivity measurements were carried out for samples with platinum electrodes. The ac conductivity was measured using a frequency response over frequency  $10^{-1}$  to  $10^6$  Hz with applied potential 0.2V.

$\text{Sr}_4\text{In}_2\text{Zr}_2\text{O}_{11}$  obtained shows a cubic perovskite structure with  $a = 4.1107(2)\text{\AA}$ . This implies that the oxygen vacancies are disordered in this phase, and  $\text{In}^{3+}$  and  $\text{Zr}^{4+}$  are arrayed in B site of perovskite at random. The cubic perovskite structure was retained in the solid solution range,  $0.0 < x < 1.2$ , in  $\text{Sr}_4\text{In}_{2-x}\text{Ga}_x\text{Zr}_2\text{O}_{11}$  and the lattice parameter decreased in accordance with ionic radius. One semicircle was observed in the complex impedance plane that was related to ion diffusion in the bulk including grain boundary. The same behaviors were almost observed for other samples. The electrical conductivity increased linearly with a rise in temperature as shown in fig.1 and of the system substituted  $\text{Ga}^{3+}$  for  $\text{In}^{3+}$  decreased, and the activation energy increased with increasing the content of Ga. These results suggest that the oxide ion conductivity depends on the crystal size as well as the concentration of the oxygen vacancy.

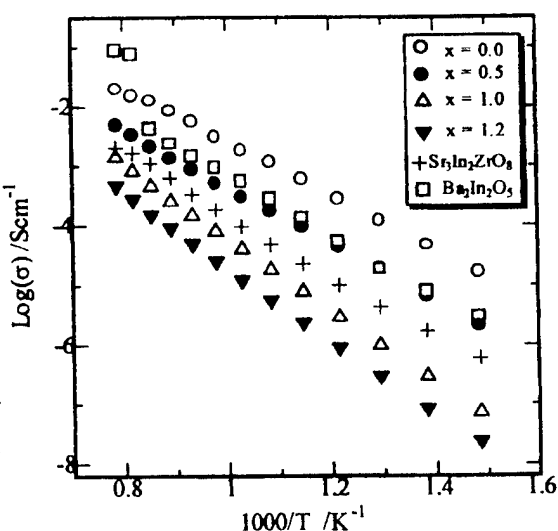


Fig.1 Arrhenius plots of electrical conductivity for  $\text{Sr}_4\text{In}_{2-x}\text{Ga}_x\text{Zr}_2\text{O}_{11}$ .

[1] J.B. Goodenough, J.E. Ruinzi-Dianz and Y.S. Zhen, Solid State Ionics **44**, 21(1990)

[2] Y. Takeda, N. Imanishi, R. Kanno, T. Mizuno, H. Higuchi and O. Yamamoto, Solid State Ionics **53**, 748(1992)

OXYGEN STOICHIOMETRY OF  $\text{Sr}_{1-x}(\text{Ti,Fe})\text{O}_{3-\delta}$  MATERIALSA.A.L.Ferreira<sup>1</sup>, J.C.C.Abrantes<sup>1</sup>, J.R.Jurado<sup>2</sup>, J.R.Frade<sup>3</sup><sup>1</sup>Instituto Politécnico, E.S.T.G., Ap. 574, 4901 Viana do Castelo, Portugal<sup>2</sup>Instituto de Ceramica y Vidrio, CSIC, Arganda del Rey, Madrid, Spain<sup>3</sup>Ceramics and Glass Eng. Dep., University of Aveiro, 3810 Aveiro, Portugal

A correct evaluation of changes in oxygen stoichiometry may contribute to understand the defect chemistry and transport properties of  $\text{Sr}_{1-x}(\text{Ti,Fe})\text{O}_{3-\delta}$  materials. Thermogravimetric analysis (TGA) and a coulometric titration (CT) technique were thus used to measure the relative changes in oxygen stoichiometry with temperature and oxygen partial pressure, and these results were used to re-examine the defect chemistry.

The samples undergo significant weight gain on cooling which were attributed to changes in valence of Fe ions, as previously reported for Fe-doped strontium titanate [1]. However, the oxygen gain attained by  $\text{Sr}_{1-x}\text{Ti}_{1-y}\text{Fe}_y\text{O}_{3-\delta}$  (with  $0.1 \leq y \leq 0.5$ ) at room temperature is lower than expected on assuming a complete conversion of  $\text{Fe}^{3+}$  to  $\text{Fe}^{4+}$ . The effects of oxygen partial pressure were evaluated by comparing TGA results obtained in air and in  $\text{N}_2$ , and also from coulometric titration results, using a closed cell with a small potentiometric sensor, and an electrochemical pump.

Changes in oxygen stoichiometry were used to re-examine the defect chemistry of the actual materials. The dependence of the electrical conductivity on the oxygen partial pressure, and electrochemical permeability measurements [2] were also used to revise the transport properties. These materials are promising mixed conductors which are mainly p-type in oxidising conditions, n-type in reducing conditions. The ionic conductivity results are comparable to those of yttria stabilised zirconia electrolytes.

[1] T.Bieger, J.Maier, R.Waser, Solid State Ionics, 53-6, 578, (1992)

[2] J.R.Jurado et alia, Solid State Ionics, (in press).

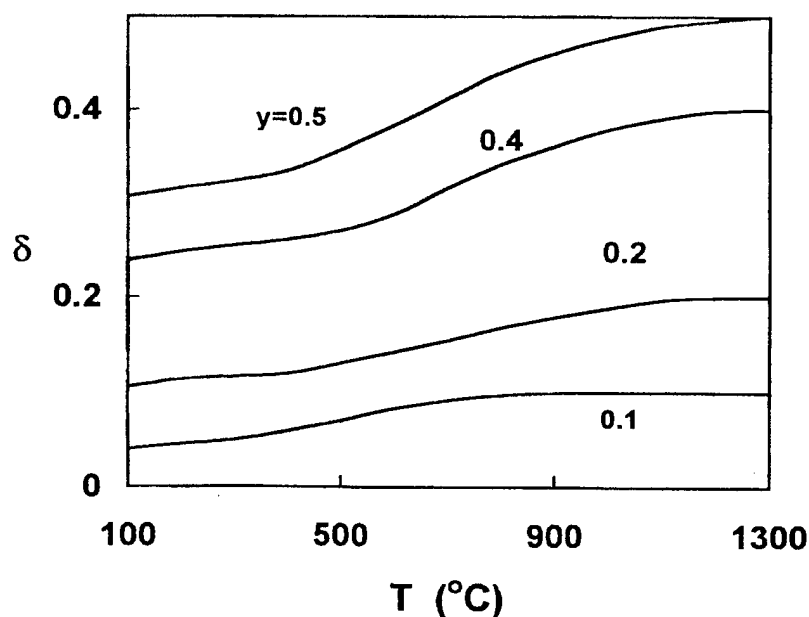


Figure 1: Changes in oxygen stoichiometry of  $\text{Sr}_{1-x}\text{Ti}_{1-y}\text{Fe}_y\text{O}_{3-\delta}$  obtained by TGA.

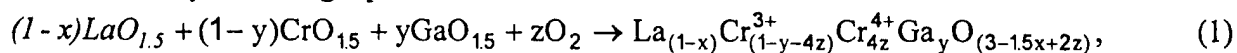
## STRUCTURAL AND ELECTRICAL INVESTIGATIONS OF

D. Westphal<sup>1</sup>, S. Jakobs<sup>2</sup>, O. Schäf<sup>1,2</sup>, H. Wulff<sup>2</sup>, U. Guth<sup>1,2</sup><sup>1</sup> Sensor Research Center Greifswald, Germany<sup>2</sup> Institute for Chemistry and Biochemistry, University of Greifswald, Germany

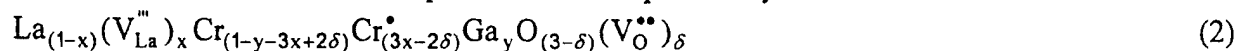
Perovskite type oxides of the  $\text{ABO}_3$  composition allow to modify the electrochemical and catalytical properties by partial doping of A- and B-site-cations without changing structure [1]. Chromites are very promising materials for studying because of their low catalytic activity of chromium ions as compared to manganites or cobaltites. It could be shown that the low catalytic activity for the combustion of hydrocarbons can be further diminished by partial replacing of chromium ions with Gallium [2]. Furthermore it could be shown that the perovskite structure permits a small value of A-site-deficiency without forming a second phase [3]. Beside doping a deficiency of A-site-cation seems to be responsible for the electrochemical properties of those electrode materials too.

In order to develop material which can be used as sensitive electrode materials in zirconia based sensors gallium doped  $\text{LaCrO}_3$  with the formula  $\text{La}_{1-x}\text{Cr}_{0.8}\text{Ga}_{0.2}\text{O}_{3-\delta}$  ( $x = 0$  to  $0.3$ ) prepared by the conventional oxide method were investigated regarding to the influence of lanthanum deficiency on structure and conductivity. Conventional XRD investigations showed a single phase ( $\text{GdFeO}_3$ -type orthorhombic structure) up to a lanthanum deficiency of  $x = 0.3$ . Our assumption was that the formation of a second phase starts already at a lower A-site-deficiency ( $x < 0.3$ ). Therefore we used SEM and TEM to find very small amounts of other phases like starting oxides.

The conductivity mechanism in  $\text{LaCrO}_3$  is well understood by thermically hopping of defect electrons. According to the charge neutrality in a chromite with lanthanum deficiency the formation of defect electrons by both the change of  $\text{Cr}^{3+}$  to  $\text{Cr}^{4+}$  and the generation of oxygen vacancies has to be considered. The formation of the perovskite-type  $\text{La}_{1-x}\text{Cr}_{1-y}\text{Ga}_y\text{O}_{3-\delta}$  phase can be described by following equation:



while the defect order of the compounds can be expressed by this formula:



The conductivity of the mixed oxide depends on the lanthanum deficiency. We found that the total conductivity of  $\text{La}_{1-x}\text{Cr}_{0.8}\text{Ga}_{0.2}\text{O}_{3-\delta}$  goes through a maximum in dependence on  $x$ . The highest conductivity was found at  $x = 0.2$ . Theoretically the highest conductivity was expected to be at  $x = 0.133$  for the ratio  $[\text{Cr}^{3+}]/[\text{Cr}^{4+}] = 1$  under the assumption that oxygen vacancies are not generated. These difference conforms our hypothesis that with increasing  $x$  the generation of oxygen vacancies is in competition with the change of  $\text{Cr}^{3+}$  to  $\text{Cr}^{4+}$ .

- [1] S. Jakobs, R. Hartung, U. Lawrenz, P. Sandow, U. Schönaier, U. Guth; Ionics 2; (1996) 451
- [2] K.-P. Sandow, S. Jakobs, D. Westphal, S. Thiemann, R. Hartung, U. Schönaier, U. Guth; Ionics 2; (1996) 435
- [3] H. Runge, U. Guth; Int. Conf. on Solid State Ionics; SSI 11; Honolulu;(1997); proceeding in press

MIXED COBALT AND NICKEL CONTAINING PEROVSKITE AND PEROVSKITE  
RELATED OXIDES FOR HIGH TEMPERATURE ELECTROCHEMICAL APPLICATIONS

C.K.M. Shaw, J.A. Kilner and S.J. Skinner

Centre for Ionic Conducting Ceramics (CICM)  
Department of Materials  
Imperial College of Science, Technology and Medicine  
London, SW7 2BP  
U.K.

Perovskites based on doped  $\text{La}_{1-x}\text{Sr}_x\text{Co}_{1-y}\text{Tm}_y\text{O}_{3-\delta}$  (where Tm is a transition metal element) have been shown to be suitable for use as cathodes in Solid Oxide Fuel Cells (SOFCs) and as membranes for Ceramic Oxygen Generators (COGs). The effect of Ni substitution on the transition metal site has been well studied. The work by Inoue *et al.* [1] found that the composition  $\text{La}_{0.6}\text{Sr}_{0.4}\text{Co}_{0.98}\text{Ni}_{0.02}\text{O}_{3-\delta}$  (LSCN) was the most effective for use in oxygen sensors even at the low temperature of 473K. Visco *et al.* [2] achieved a peak power density of  $650\text{mW/cm}^2$  at  $750^\circ\text{C}$  using a thin film ceria electrolyte with a composite cathode of LSCN and CGO.

What has not been well characterised is the effect of the small Ni addition on the basic oxygen transport parameters such as the oxygen self-diffusivity and surface exchange coefficient, and how they differ from the parent LSC composition ( $\text{La}_{0.6}\text{Sr}_{0.4}\text{CoO}_{3-\delta}$ ). These materials are oxygen deficient and the transport properties are expected to be dominated by oxygen vacancies. In this work, we have measured the transport kinetics of LSCN using Isotope Exchange Depth Profile (IEDP) technique coupled with Secondary Ion Mass Spectroscopy (SIMS) over the temperature range  $500\text{--}800^\circ\text{C}$  at an oxygen partial pressure of 1atm. At  $500^\circ\text{C}$  for example, the values for  $D^*$  and  $k$  are  $2 \times 10^{-10}\text{cm}^2\text{s}^{-1}$  and  $7 \times 10^{-8}\text{cm s}^{-1}$ .

In addition to the work on oxygen deficient perovskites, we have started a series of investigations into oxygen excess oxides based on the  $\text{K}_2\text{NiF}_4$  structure. These oxides represent members of the Ruddlesden-Popper series of compounds  $\text{La}_{(n+2)}\text{Ni}_{(n+1)}\text{O}_{(3n+4)+\delta}$ . The first member of the series ( $n=0$ ) is  $\text{La}_2\text{NiO}_{4+\delta}$ . This material can be doped on the Ni site to give  $\text{La}_2\text{Ni}_{1-y}\text{Co}_y\text{O}_{4+\delta}$  (LNC) analogous to the LSCN's mentioned above, except that oxygen interstitials are thought to be the mobile species. The transport properties of the LSCN's and LNC's will be compared and contrasted with reference to the mobile species.

[1] T. Inoue, N. Seki, D. Eguchi, and H. Arai, *J. Electrochem. Soc.*, 137, 2523 (1990)

[2] S.J. Visco, C. Jacobsen, and L.C. De Jonghe, *Proceedings of the 5<sup>th</sup> International Symposium on Solid Oxide Fuel Cells*, The Electrochem. Soc., 710 (1997)

# INVESTIGATION OF HYDROPHILIC SITES IN POLYCRYSTALLINE SILICEOUS SANDSTONE BY THERMAL DEPOLARIZATION SPECTROSCOPY

A.N.Papathanassiou and J.Grammatikakis

University of Athens, Department of Physics, Section of Solid State Physics,  
Panepistimiopolis, GR 157 84 Zografos, Athens, Greece

Dielectric relaxation spectroscopy techniques have been employed recently, so as to understand the dipole relaxation processes [1-4], the interfacial polarization [5] and the transport phenomena [6] in natural minerals and rocks of the calcite family. In this task, the Thermal Depolarization Spectroscopy (Thermally Stimulated Depolarization Current, TSDC) scheme proved to be a powerful high resolution tool.

In the present work, we investigate the dielectric relaxation in sandstone, which is a silicate multi-phase compound. We traced and characterized the dielectric relaxation mechanisms in virgin samples of sandstone by means of the TSDC technique. The dielectric spectrum is complicated in general and is dominated by a strong relaxation maximizing around 225 K (Figure 1). The variation of the electrode material and the proper selection of the polarizing conditions yield to dielectric characteristic of each mechanism. We sampled some components of the thermogram by applying the thermal sampling scheme. The data were analyzed by full-curve fitting of a modified TSDC equation to the experimental data. The temperature distribution of the activation energy was obtained by the partial heating technique.

The pore network was outgassed at  $10^{-4}$  mbars by annealing the samples at elevated temperatures. The variation of the dielectric spectrum, in relation to that the virgin (as received) samples, permits the identification of certain relaxation mechanisms to hydrophilic sites.

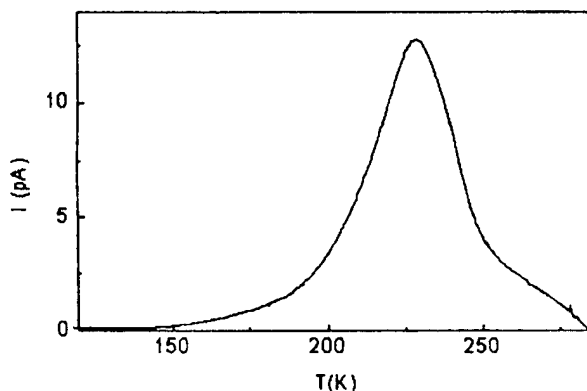


**Figure 1** Thermal depolarization spectrum of natural sandstone. The sample was polarized at  $T_p=270$  K by an electric field of intensity  $E_p=1$  kV/mm for the time interval  $t_p=1$  min. The heating rate was 0.04 K/s.

## References

- [1] A.N.Papathanassiou, J.Grammatikakis, V.Katsika and A.B.Vassilikou- Dova Rad.Effects and Defects in Solids 134, 247 (1995)
- [2] A.N.Papathanassiou and J. Grammatikakis, Phys.Rev.B 53, 16253 (1996)
- [3] A.N.Papathanassiou and J.Grammatikakis, Phys. Rev. B 56, 8590 (1997)
- [4] A.N.Papathanassiou and J. Grammatikakis, Phys. Rev. B 56, 8590 (1997)
- [5] N. Bogris, J. Grammatikakis and A.N. Papathanassiou, Phys. Rev. B, *in print*
- [6] A.N.Papathanassiou and J. Grammatikakis, J.Phys.Chem.Solids 58, 1063 (1997)

# IONIC CONDUCTION IN THE SUBSTITUTED SCHEELITE-TYPE OXIDES

Takao ESAKA

Department of Materials Science, Faculty of Engineering, Tottori University  
Minami 4-101, Koyamacho, Tottori 680-0945, JAPAN

## § 1. Introduction

In order to design super ionic conductors, different kinds of ionic conductors have to be synthesized and their conduction behavior must be investigated. For these objectives, this study was carried out focusing on the syntheses and characterization of new high temperature-type ionic conductors. As a result, several new ionic conductors were able to be found in the substituted Scheelite-type oxides. In this paper, the typical results will be mentioned.

## § 2. Oxide ion conductivity

The typical examples of Scheelite-type oxides are  $\text{CaWO}_4$  and/or  $\text{PbWO}_4$ . Both of these are generally classified into the oxysalts. It is reasonable to consider the former as an oxysalt. Taking account of the electronegativity of each atom, however, the latter should be seen as a deformed fluorite-type oxide, where lead and tungsten atoms are assumed to be equivalent in the crystal. As a result, the former would be a based compound of oxide ion conductor [1,4,5].

Substituted samples shown by  $\text{Pb}_{1-x}\text{Ln}_x\text{WO}_{4+x/2}$  ( $\text{Ln} = \text{La}, \text{Nd}, \text{Sm}, \text{Pr}$  and  $\text{Tb}$ ) have been synthesized and the conduction properties at higher temperatures were investigated. The typical Arrhenius plots of conductivity are shown in Fig. 1. By substitution of Sm, a large enhancement in conductivity from the pure  $\text{PbWO}_4$  was observed and the transport number of oxide ion was found to be almost unity. Similar behaviors were observed in all the cases; that is, irrespective of the changeable valence of lanthanide ions such as Pr and Tb to be substituted, conduction properties in these system were the similar to those of the other lanthanide ion-substituted  $\text{PbWO}_4$ 's.

By X-ray diffraction, the composition to form the single phase was determined in each system. In Fig. 2, the conductivity isotherm at 800 °C is indicated; open and closed symbols show the compositions with single and mixed phases. It was found that the solubility range depends on the ionic radius of dopant; the larger, the wider. In  $\text{Pb}_{1-x}\text{La}_x\text{WO}_{4+x/2}$ , the solubility range extends to  $x = 0.4$  at least and the highest conductivity at 800 °C was obtained as  $\sigma = 6 \times 10^{-2} \text{ Scm}^{-1}$  for  $x = 0.2$ . Surprisingly the present Ln-substituted  $\text{PbWO}_4$  with the Scheelite-type structure are supposed to exhibit good oxide ion conduction

by interstitial oxide ions in the solid solution region.

## § 3. Lithium ion conductivity

As mentioned above,  $\text{CaWO}_4$  belongs to an oxysalt. Therefore, it can be seen as a based material of lithium ion conductor, if some calcium sites could be substituted by lithium [2,3].

X-ray diffraction patterns of samples of  $x < 0.10$  in  $\text{Ca}_{1-x}\text{Li}_x\text{WO}_4$  showed the single tetragonal phase. Representative Arrhenis plots of conductivity measured in air are shown in Fig. 3. For pure  $\text{CaWO}_4$  the conductivity is lower than  $10^{-5} \text{ Scm}^{-1}$  at 900 °C. Enhanced conductivities are observed in the substituted samples. An abrupt

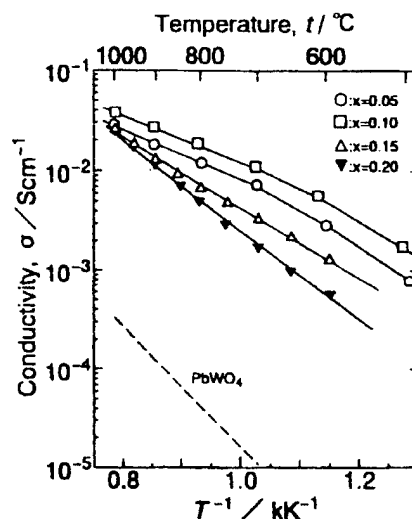


Fig. 1 Arrhenius plots of conductivity of the samples in the system  $\text{Pb}_{1-x}\text{Sm}_x\text{WO}_{4+x/2}$ .

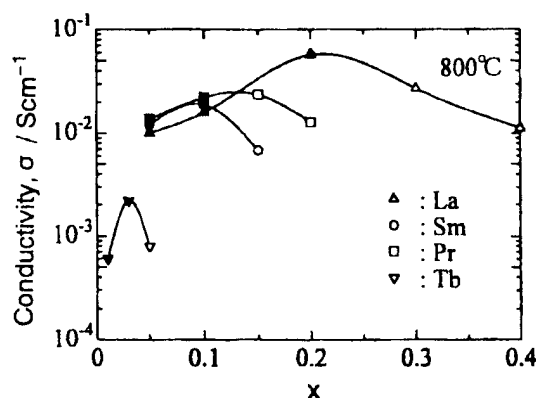


Fig. 2 Conductivity isotherms of  $\text{Pb}_{1-x}\text{Ln}_x\text{WO}_{4+x/2}$ .



conductivity change is observed at  $x = 0.10$ , which was found to be ascribed by the phase change (solid-solid two phases  $\leftrightarrow$  solid-liquid two phases). According to the oxygen gas concentration cell measurements and the electrolysis, it was found that the main charge carriers are neither electrons nor oxide ions for the substituted samples but would be lithium ions.

Next, the movement of conductive ions was tried to be visualized using neutron radiography (NR). In this case, two disc samples for electrolysis were prepared. Both samples have the same chemical compositions. But the catholyte sample was synthesized using  $^7\text{Li}$  and the anolyte sample using  $^6\text{Li}$ . Thus the former transmits neutron much more easily than the latter. These two samples were piled, electrolyzed at  $900^\circ\text{C}$  and irradiated by neutron to obtain images on films.

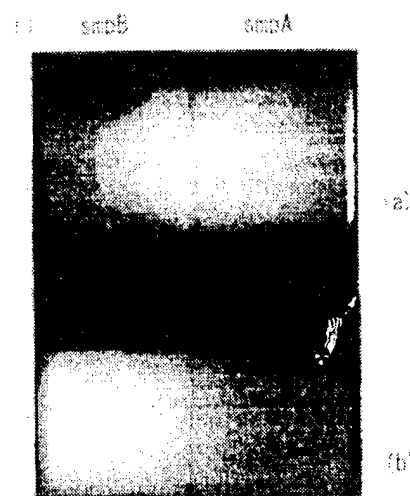


Fig. 4 NR images to show the lithium ion movement. (A) After electrolysis and (B) after only standing at  $900^\circ\text{C}$  for 16 min in air.

#### § 4. Conclusion

New types of ionic conductors were found; oxide ion conductor in the Scheelite-type solid solutions based on  $\text{PbWO}_4$ , and lithium ion conductor in  $\text{AE}_{1-x}\text{Li}_x\text{WO}_4$  ( $\text{AE} = \text{Ca}, \text{Sr}$  and  $\text{Ba}$ ). Neutron radiography (NR) is confirmed to be effective to visualize the lithium ion conduction and to calculate the lithium ion transport number.

#### References

- [1] T. Esaka, T. Mina-ai, H. Iwahara, *Solid State Ionics*, **57**, 319, 1992. [2] T. Esaka, M. Kamata, H. Saito, *Solid State Ionics*, **86-88**, 73, 1996. [3] M. Kamata, T. Esaka *et al.*, *Solid State Ionics*, **91**, 303, 1996.
- [4] T. Esaka, R. Tachibana, S. Takai, *Solid State Ionics*, **92**, 129, 1996. [5] S. Takai, K. Sugiura, T. Esaka, *Mat. Res. Bull.*, in press.

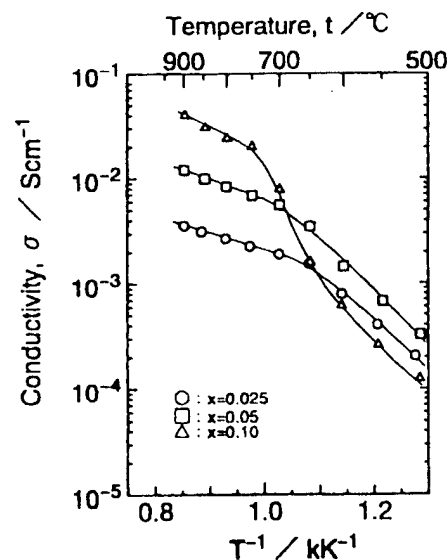


Fig. 3 Arrhenius plots of conductivity of  $\text{Ca}_{1-x}\text{Li}_x\text{WO}_4$ .

NR images of  $\text{Ca}_{0.95}\text{Li}_{0.10}\text{WO}_4$  are presented in Fig. 4, to which is added the NR image of samples kept without electrolysis. In Fig. 4(b), some thermal diffusion is observed. From Fig. 4(a), it can be obviously seen that  $^6\text{Li}$  in the sample moved into another. Using the blackness of standard samples containing defined amounts of  $^7\text{Li}$ , the profile of  $^7\text{Li}$  content could be obtained from the NR image. This is shown in Fig. 5, from which it can be known that the lithium ion transport number of the oxide is 0.99 and that the lithium ion conduction was preferably ascribed to lithium ions in the interstitial sites. The similar lithium ion conduction was observed in the Scheelite-type phase of  $\text{Sr}_{1-x}\text{Li}_x\text{WO}_4$  and  $\text{Ba}_{1-x}\text{Li}_x\text{WO}_4$ .

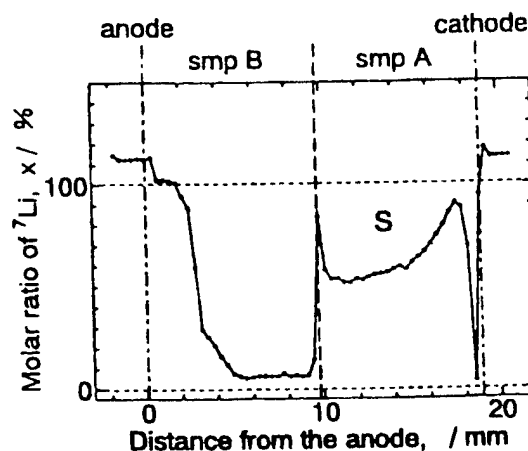


Fig. 5  $^7\text{Li}$  profile of the electrolyzed samples of  $\text{Ca}_{0.95}\text{Li}_{0.10}\text{WO}_4$  along the axial direction.

## SYNTHESIS AND TRANSPORT PROPERTIES OF SUPERIONIC CONDUCTORS WITH PREDOMINANT CHLORINE CONDUCTIVITY.

I.V.Murin, O.V.Glumov, N.A.Melnikova

Department of Chemistry, St. Petersburg University,  
Universitetskij pr.2, 198904 St. Petersburg, Russia

There is an increasing interest to elucidate the transport phenomena in chlorine-conducting solid electrolytes with cottunnite structure ( $\text{PbCl}_2$ ), mainly because of their practical importance (e.g. solid state electrochemical devices). These materials conform to the criteria for good superionic conductors as small coordination number for  $\text{Cl}^-$  ions, large coordination number and strong electronic polarizability for antagonist ions, low entropies of melting, existence of phase transition and similarity of entropies of melting and phase transition.

New solid electrolytes based on  $\text{PbCl}_2$  and  $\text{SnCl}_2$  were synthesised and it was shown the important role of preparation technique on electrophysical properties of  $\text{PbCl}_2$  and  $\text{SnCl}_2$  -type materials. The peculiarities of ionic transport and phase transition in single crystals  $\text{PbCl}_2$  and  $\text{PbCl}_2$  doped with  $\text{KCl}$  (0,45 m/o) and in some ceramic materials  $\text{KPb}_2\text{Cl}_5$ ,  $\text{KPbSn}_2\text{Cl}_7$ ,  $\text{Pb}_3\text{O}_2\text{Cl}_6$ ,  $\text{SnCl}_2$  and  $\text{SnCl}_2$  doped  $\text{KCl}$  (0,5 m/o),  $\text{CsSnCl}_3$ . For single crystals  $\text{PbCl}_2$  and  $\text{PbCl}_2$  - 0,45 m/o  $\text{KCl}$  high anisotropy of electroconductivity and self-diffusion coefficients measured with the microtome sectioning technique was investigated. It was found that ionic conductivity and self-diffusion coefficients are much higher in the direction  $\perp c$  than  $\parallel c$  ( $D_{\perp c} \gg D_{\parallel c}$ ,  $\sigma_{\perp c} \gg \sigma_{\parallel c}$ ) in the temperature range 300-600 K. For all individual compounds analysis of electroconductivity as function of temperature allowed us to find thermodynamical and kinetical parameters which characterize the defect formation and defect migration.

The interesting electrophysical properties are shown for  $\text{CsSnCl}_3$ . Monoclinic modification of  $\text{CsSnCl}_3$  existing below 400 K has low values of electroconductivity. The «white - yellow» phase transition of  $\text{CsSnCl}_3$  to the cubic phase with perovskite structure brings to the drastic changes in the electrolytic characteristics. This phase after cooling may being kept in the metastable state in vacuum or under dry nitrogen atmosphere. The high values of conductivity ( $10^{-4}$ - $10^{-3}$  S/cm) were observed for this phase in the temperature range 290 - 473 K.

Studies of ionic conductivity as function of high hydrostatic pressure (up to  $10^9$  Pa over the temperature range 300-600 K) in cottunnite crystal give direct information on the elastic volume relaxation associated with diffusive motion of ionic defects. The strain energy Zener model in Gruneisen approximation was used for the theoretical estimation of activation volume. The additional conformation that  $\text{PbCl}_2$ ,  $\text{SnCl}_2$  and related compounds belong to the good superionic conductors is the small value ( $\Delta V_m = 1.4$ - $7 \text{ cm}^3/\text{mol}$ ) of activation volumes of defect migration. For all investigated solid electrolytes electronic and hole conductivity was estimated ( $\sigma_{e,h} \leq 10^{-3} \sigma_i$ ).

Analysis of the obtained result allows us to establish relation between transport properties and crystallochemical peculiarities of  $\text{PbCl}_2$  and  $\text{SnCl}_2$  - type materials.

This work was supported by Russian Foundation for Basic Research (Project 96-03-33134).

## FAST IONIC CONDUCTION OF INORGANIC FLUORIDE AND OXIDE EUTECTIC COMPOSITES PREPARED FROM THE MELT

V. Trnovcová<sup>1</sup>, P.P. Fedorov<sup>2</sup>, V. Labaš<sup>1</sup>, M.Yu. Starostin<sup>3</sup>, R. Čička<sup>1</sup> and B.P. Sobolev<sup>2</sup>

<sup>1</sup>Faculty of Materials Science and Technology, Slovak University of Technology,  
SK-91724 Trnava, Slovakia

<sup>2</sup>Shubnikov's Institute of Crystallography, Russian Academy of Sciences, Moscow, Russia

<sup>3</sup>Institute of Solid State Physics, Russian Academy of Sciences, Chernogolovka, Russia

Composites are important multiphase engineering materials noted for their enhanced mechanical strength, thermal-shock resistance and fracture-toughness. In dispersed composite solid electrolytes, which contain insulating nanosized second-phase particles, a conductivity enhancement often takes place. Space charge effects, adsorption effects, percolation effects and a formation of new phases are supposed to be responsible for this conductivity enhancement.

Eutectic composites prepared from the melt are noted for their relatively low melting temperature, large area of phase-to-phase boundaries, fine-graded and highly ordered microstructure, coherent phase boundaries, orientational relation of both phases and good thermal stability of eutectical structure. When the volume fractions of both coexisting phases are comparable, a lamellar microstructure appears. When the volume fraction of one of the phases is lower than 0.29, a fibrous or rod-like microstructure appears. The interphase spacing decreases with increasing growth rate and/or with increasing temperature gradient at the crystallization front. In some eutectic composites, also a type of the microstructure depends on the growth characteristics.

When the melting temperature of the eutectic composite is lower than those of phase transition temperatures of both phases, the superionic phase, with a destructive high-temperature phase transition, can be prepared in eutectic composites in a form of single-crystalline fibers, lamellae or matrix.

Due to enhanced fracture toughness, fluoride eutectic composites represent a technologically prospective combination of good superionic and mechanical properties at low and moderate temperatures. Alumina-zirconia eutectic composites are characterized both by a good ionic conductivity at high temperatures and by excellent mechanical properties and corrosion resistance.

The aim of this paper is to show the relations between 1/ the physical properties of fluoride and oxide eutectic composites prepared from melt and those of both corresponding single phases, 2/ the physical properties and the microstructure of composites, 3/ the composition, preparation technique and microstructure of composites, in superionic fluoride and oxide systems. Eutectic composites of  $\text{CaF}_2$ - $\text{MgF}_2$ ,  $\text{PbF}_2$ - $\text{PbCl}_2$ ,  $\text{LiF}$ - $\text{LiBaF}_3$ ,  $\text{MgF}_2$ - $\text{GdF}_3$ ,  $\text{PbF}_2$ - $\text{AF}$  ( $\text{A} = \text{Li}, \text{Na}$ ),  $\text{PbF}_2$ - $\text{RF}_3$  ( $\text{R} = \text{Ho}, \text{Yb}, \text{Sc}$ ),  $\text{PbF}_2$ - $\text{MgF}_2$ ,  $\text{LiF}$ - $\text{RF}_3$  ( $\text{R} = \text{La} - \text{Lu}$ ),  $\text{Al}_2\text{O}_3$ - $\text{Y-FSZ}$  and  $\text{Al}_2\text{O}_3$ - $\text{Y-PSZ}$  systems are investigated.

Fluoride eutectic composites are prepared from the melt in a fluorizing atmosphere by using: 1/ a simple solidification of the melt, 2/ the Bridgman method, 3/ a horizontal directional solidification (Bagdasarov method). The  $\text{Al}_2\text{O}_3$ - $\text{ZrO}_2$  eutectic composites are prepared by using the Stepanov (EFG) method in Ar. The zirconia phase of the composites is either fully stabilized (5.5 Y-FSZ) or partially stabilized (2.5 Y-PSZ).

Phase diagrams of all systems are examined. Phase composition and micromorphology of eutectic and near-eutectic composites are determined. A special emphasis is placed on the fast anionic conduction, dielectric response, microhardness, fracture toughness and cracking process of the composites. Anisotropy of physical properties is studied and discussed. Bulk ionic

conductivity and relative static permittivity are determined by using the impedance or modular analyses. Painted silver electrodes and a dry Ar atmosphere are used for these measurements. The microhardness and crack paths are investigated using Vickers indentation method. By using the finite elements method (FEM) and the SYSTUS general purpose program, the field of residual stresses in "as-prepared" composites and the stress field near the crack tip are simulated. The influence of this field on cracking process and plausible mechanisms of fracture toughness enhancement are discussed.

The most important conclusions are as follows:

1/ In directionally solidified eutectic composites, a high degree of crystallographic ordering and a fine, regular microstructure takes place.

2/ Due to a much faster cooling rate during the simple solidification, the microstructure of polycrystalline composites is much finer than that of the directionally solidified ones. Interlamellar and/or interfibrillar distances are equal to 100 - 500 nm in polycrystalline composites, and to 1 - 5  $\mu\text{m}$  in directionally solidified ones. However, electrical and dielectric properties of both types of composites are similar.

3/ In eutectic composites prepared from the melt, the conductivity enhancement can be observed only at low conductivities (up to  $10^{-6} \text{ S cm}^{-1}$ ). In composites containing a superionic phase, the conductivity is always lower than that of the single superionic phase.

4/ In eutectic composites prepared by unidirectional crystallization, the fastest ionic conductivity is usually found in the direction of the crystal growth. The anisotropy of physical properties is pronounced in eutectic composites prepared at high growth rates by using horizontal solidification, and is influenced mainly by the convection flows in the melt.

5/ In  $\text{LiF-LiYF}_4$  and  $\text{CaF}_2\text{-MgF}_2$  eutectic composites, the type of the microstructure changes by changing the growth characteristics. The ionic conductivity reaches maximum in the composites with fine long fibers.

6/ In  $\text{Al}_2\text{O}_3\text{-ZrO}_2$  eutectic composites, alumina is the leading phase which determines the eutectic solidification. A preferred [2221] orientation of  $\alpha\text{-YrO}_2$  along the growth direction is obtained. Fine zirconia fibers are aligned along the growth direction, and form well defined colonies in the alumina matrix. For cubic and tetragonal zirconia, the preferential orientations are [110], [100] or [110], [001]. Two types of colonies are observed: typical colonies and faceted ones. The colonies occupy 48-58 vol-% of the composite. Most densely packed colonies are found in composites with a hypereutectic composition of the melt. In these composites, zirconia dendrites in alumina matrix are formed. In composites containing Y-FSZ, the faceted colonies develop at higher growth rates. In composites containing Y-PSZ, they appear at arbitrary growth rates.

7/ The ionic conductivity of composites is determined by the conductivity of the zirconia phase but it is always slightly lower than that of the corresponding zirconia ceramics. The highest conductivity is found in hypereutectic composites containing the Y-FSZ phase.

8/ The relative static permittivity of eutectic composites is determined by the relative static permittivities and volume fractions of both phases.

9/ Simulation of the residual stress field shows that the matrix is stressed at maximum near the phase boundaries and that the stress field tries to deflect the main crack. The microcracking near the phase boundaries and the crack deflection seem to be the main mechanisms for the enhancement of fracture toughness.

10/ The relatively low melting temperature, fast ionic conductivity and enhanced fracture toughness of some eutectic composites make them very suitable for applications in solid state ionics. The fastest anionic conductivity is found in  $\text{PbF}_2\text{-ScF}_3$  and  $\text{PbF}_2\text{-NaF}$  eutectic composites. The highest fracture toughness at room temperature is found in the  $\text{Al}_2\text{O}_3\text{-Y-PSZ}$  eutectic composite.

## IONIC AND ELECTRONIC CONDUCTION IN STOICHIOMETRIC AND SUB-STOICHIOMETRIC PEROVSKYTES

D. Westphal<sup>1</sup>, G. Matter<sup>2</sup>, F.M.B. Marques<sup>2</sup>, S. Jakobs<sup>1</sup>, U. Guth<sup>1</sup>

<sup>1</sup> Institut of Physical Chemistry, University of Greifswald, 17489 Greifswald, Germany

<sup>2</sup> Ceramics and Glass Engineering Dept., University of Aveiro, 3810 Aveiro, Portugal

### Abstract

Yttria stabilised zirconia (YSZ) is still the state of the art electrolyte for high temperature technological applications of oxygen ion conductors like Solid Oxide Fuel Cells or Steam Electrolysers. However, the relatively poor ionic conductivity of YSZ requires high operating temperatures or relatively expensive technologies to produce dense films with small thickness to avoid excessive ohmic losses in the system. Alternative electrolytes (e.g., ceria or bismuth based electrolytes) show better conductivities than YSZ, but also a narrow  $\text{Po}_2$  stability domain and/or degradation of electrolytic properties at high temperature under reducing conditions.

$\text{LaGaO}_3$  based oxygen ion conductors, recently discovered, possess a perovskite ( $\text{ABO}_3$ ) type structure. Different dopants were already tested to improve the ionic conductivity of these materials, to suppress the p-type conductivity or to enhance mixed conduction. Sr doping in the A-site and Mg doping in the B-site were found effective in promoting the oxygen ion conductivity of these materials, while Nd doping in the A-site decreased the p-type conductivity of these materials. Doping with transition metals (e.g., Fe and Cr) was also found effective in designing mixed conduction [1-5].

Although a number of compositions were already studied, the versatile characteristics of the perovskite structure in accommodating different dopants leaves an open field to the exploitation of new compositions. Considering the well-established stability domain, defect structure and electrical properties of  $\text{LaCrO}_3$ -based perovskites [6-8], the aim of this work was the evaluation of the impact of a progressive replacement of Ga by Cr on the electrical transport properties of Sr-doped  $\text{LaGaO}_{3,\delta}$ .

This work also reports on the role of A-site sub-stoichiometry in these Sr-doped  $\text{La}(\text{Ga,Cr})\text{O}_3$  materials. The formation of metal vacancies in the A-site of a perovskite is usually compensated by the formation of oxygen vacancies or electron holes. In the first case improved ionic conductors might be obtained. In the second case enhanced electronic conductivity or mixed conduction are the expected results. All these categories of materials might prove interesting for a variety of functions concerned with technological applications of oxygen ion conductors. This was the major reason to study a number of A-site sub-stoichiometric materials.

$\text{La}_{0.95}\text{Sr}_{0.05}\text{Ga}_{1-x}\text{Cr}_x\text{O}_{3,\delta}$ , and  $\text{La}_{0.90}\text{Sr}_{0.05}\text{Ga}_{1-x}\text{Cr}_x\text{O}_{3,\delta}$ , with  $x = 0, 0.2, 0.4, 0.6, 0.8$  and  $1$ , were prepared by solid state reaction starting from oxides and carbonates. After wet-milling in ethanol, the different precursors were calcined at  $1100^\circ\text{C}$  for 12 hours, ball-milled again, dried and screened to select a powder fraction with small particle size. These powders were pressed into disks and sintered for 4 hours at  $1500^\circ\text{C}$ . All compositions were characterised by XRD and SEM. Screen-printing was also used for the deposition of perovskite films onto alumina substrates for electrical characterisation, as a function of temperature and  $\text{Po}_2$ .

Four probe van der Pauw conductivity measurements performed in air (in the range  $25$ - $1000^\circ\text{C}$ ) with pellets of all compositions showed a clear increase in conductivity with increasing Cr dopant level, as expected. The heavily Cr-doped samples showed roughly the same behaviour, irrespective of the A-site sub-stoichiometry. However, for the Cr-free samples, the stoichiometric materials showed better conductivity than the sub-stoichiometric. A reversal in relative magnitude of conductivities was observed already for the 20% Cr-doped samples, with the sub-stoichiometric materials showing higher conductivity than the stoichiometric materials. In the case of 20% Cr-doped samples, this might be partly explained by the apparently poorer phase purity of the stoichiometric sample with respect to the sub-stoichiometric one. Insulating secondary phases along

doped samples, this might be partly explained by the apparently poorer phase purity of the stoichiometric sample with respect to the sub-stoichiometric one. Insulating secondary phases along grain boundaries are known to block the electrical transport. The same comments also hold for the 40% Cr-doped sample. The existence of two phases was suggested from the XRD patterns but attempts to identify the secondary phase were inconclusive.

Cr-free samples showed high activation energies while the Cr-heavily doped samples showed low activation energies, only slightly composition dependent. The change of the electrical conductivity and activation energy with increasing Cr-content suggests a shift from dominant oxygen ion conductivity to electronic conductivity.

Cr-free samples (with either 5 or 10% Sr in the A-site, but no sub-stoichiometry) were already studied in the past and almost pure electrolytic behaviour could be demonstrated because of the independence of the conductivity on  $P_{O_2}$  [5,9]. Because of the similarity in behaviour (dc conductivity and activation energy) between the stoichiometric and sub-stoichiometric Cr-free samples, dominant ionic conductivity can be assumed for both materials.

Moving to the Cr-doped compositions, materials with 20% Cr showed increasing conductivity with increasing oxygen partial pressure in the temperature range 800-1000°C, a feature typical of p-type conduction. However, the relatively small  $P_{O_2}$  dependence of the electrical conductivity within a large  $P_{O_2}$  range (from about  $10^{-20}$  atm to air) suggests an important ionic contribution.

As expected, doping of  $(La,Sr)GaO_{3.8}$  with Cr is quite effective to promote electronic conductivity in the base material, while preserving the redox stability. Cr-doped A-site substoichiometric materials show the same trend as for stoichiometric materials, but the conductivity enhancement with increasing doping level is more pronounced. Structural (higher phase purity) and microstructural (negligible formation of insulating secondary phases) effects might explain this apparent role of sub-stoichiometry on the electrical transport properties.

## References

1. T. Ishihara, H. Matsuda, Y. Takita, J. Am. Chem. Soc. 116, 3801 (1994).
2. T. Ishihara, H. Matsuda, Y. Takita, Solid State Ionics, 79, 147 (1995).
3. T. Ishihara, Y. Hiei, Y. Takita, Solid State Ionics, 79, 371 (1995).
4. Peng-nian Huang, A. Petric, J. Electrochem. Soc. 143, 5, 1644 (1996).
5. R.T. Baker, B. Gharbage, F.M.B. Marques, J. Electrochem. Soc., 144, 9, 3130 (1997).
6. T. Nakamura, G. Petzow, L.J. Gauckler, Mat. Res. Bull. 14, 649 (1979).
7. G.V. Subba Rao, B.M. Wanklyn, C.N.R. Rao, J. Phys. Chem. Solids 32, 345 (1971).
8. J. Mizusaki, T. Sasamoto, W.R. Cannon, H.K. Bowen, J. Am. Ceram. Soc. 66, 4, 247 (1983).
9. P.S. Anderson, F.M.B. Marques, D.C. Sinclair, A.R. West, "Ionic and Electronic Conduction in  $La_{0.95}Sr_{0.05}GaO_{3.8}$ ,  $La_{0.95}Sr_{0.05}AlO_{3.8}$ , and  $Y_{0.95}Sr_{0.05}AlO_{3.8}$ ", Solid State Ionics (in press)

OXYGEN DEFECT OF NON-STOICHIOMETRIC RARE EARTH ORTHONIOBATE,  
 $\text{Ln}_x\text{NbO}_{4-1.5(1-x)}$

Kenji Toda, Yoko Ishimoto, Zuo-Guang YE and Mineo Sato  
Department of Chemistry and Chemical Engineering, Faculty of Engineering, Niigata University,  
8050 Ikarashi 2-nocho, Niigata 950-2181, Japan.

ABSTRACT

Crystal chemistry of non-stoichiometric rare earth orthoniobate,  $\text{Ln}_x\text{NbO}_{4-1.5(1-x)}$ , prepared in  $\text{Rb}_2\text{CO}_3$  flux was studied. The lattice parameters vary clearly with the rare earth content of the orthoniobate specimens. In  $\text{Ln}_2\text{O}_3$  -  $\text{Nb}_2\text{O}_5$  system without a flux, the non-stoichiometric compound could not be synthesized as a single phase. In  $\text{Ln}_2\text{O}_3$  -  $\text{Nb}_2\text{O}_5$  system with a flux, a rare earth deficient nonstoichiometric solid-solution is suggested to be formed by the generation of oxygen vacancy. These nonstoichiometric compounds have a potential to act as new "Oxide ion conductor".

## 1. INTRODUCTION

The phase relation of  $\text{Ln}_2\text{O}_3$  -  $\text{Nb}_2\text{O}_5$  system including a stoichiometric  $\text{LnNbO}_4$  compound has been reported by many investigators [1]. However there is no direct evidence on the non-stoichiometry in rare earth orthoniobate crystal. Moreover, the existence of the solid-solution region in most orthoniobate crystal has not been reported experimentally. In this study, the existence of non-stoichiometric phase in orthoniobate has been examined by the compositional variations in the lattice parameters.

## 2. EXPERIMENTAL

The stoichiometric rare earth orthoniobate,  $\text{LnNbO}_4$ , was prepared by a conventional solid state reaction [2]. On the other hand, the rare earth and oxygen-deficient orthoniobates,  $\text{Ln}_x\text{NbO}_{4-1.5(1-x)}$ , were prepared in  $\text{Rb}_2\text{CO}_3$  flux. Component oxides,  $\text{Ln}_2\text{O}_3$  and  $\text{Nb}_2\text{O}_5$  for starting composition  $\text{Ln}_x\text{NbO}_{4-1.5(1-x)}$  ( $0.2 \leq x \leq 1$ ) were mixed with  $\text{Rb}_2\text{CO}_3$  in mole ratio 1 : 1.3. The mixture were pressed into disk-shape pellets of 10 mm in diameter and about 1 mm thick under a pressure of 40 MPa for 10 min. The pellets were heated at 1273 K for 4 h in air. The product was cooled to room temperature and residual flux was washed out with distilled water. White powder was filtered and dried at 383 K. Final composition of these compounds was obtained from the Electron Probe Micro-Analysis (EPMA) using a Shimadzu EPMA-8705. Powder X-ray diffraction patterns were recorded at room temperature using the Rigaku RAD-rA diffractometer. The data were collected at a step-scanning mode with a step width  $0.02^\circ$  and a step time 4 s. The powder XRD patterns obtained were indexed with the aid of the computer program CELL [3]. The structure refinement was carried out by the Rietveld method, using the RIETAN94 profile refinement program [4].

## 3. RESULTS AND DISCUSSION

Two kinds of rare earth orthoniobate samples were prepared with and without  $\text{Rb}_2\text{CO}_3$  as a flux. In  $\text{Ln}_2\text{O}_3$  -  $\text{Nb}_2\text{O}_5$  system without a flux, the non-stoichiometric compound could not be synthesized as a single phase; instead the composition consists of a mixture of stoichiometric  $\text{LnNbO}_4$  and  $\text{Nb}_2\text{O}_5$ . This result is in good agreement with that reported in literature. For example, the solubility limits of  $\text{YNbO}_4$  monoclinic phase are 0.2 ( $\pm 0.4$ ) mol%  $\text{Y}_2\text{O}_3$  at 1923 K [1]. The

synthesis of the non-stoichiometric rare earth orthoniobates could only be achieved by the reaction in  $\text{Rb}_2\text{CO}_3$  flux. Powder X-ray diffraction pattern of typical non-stoichiometric compound is shown in Fig.1. For the starting composition of  $\text{Eu}_x\text{NbO}_{4-1.5(1-x)}$  ( $0.2 \leq x \leq 1$ ) in  $\text{Eu}_2\text{O}_3 - \text{Nb}_2\text{O}_5$  system, compounds crystallized in the monoclinic fergusonite-related structure. Powder diffraction data reveal that all compositions can be successfully indexed in monoclinic space group without any impurities. A increase in lattice parameters as the decrease of rare earth content  $y$  has been observed, which can be correlated with the enhancement of electrostatic repulsion by the loss of oxygen ions.

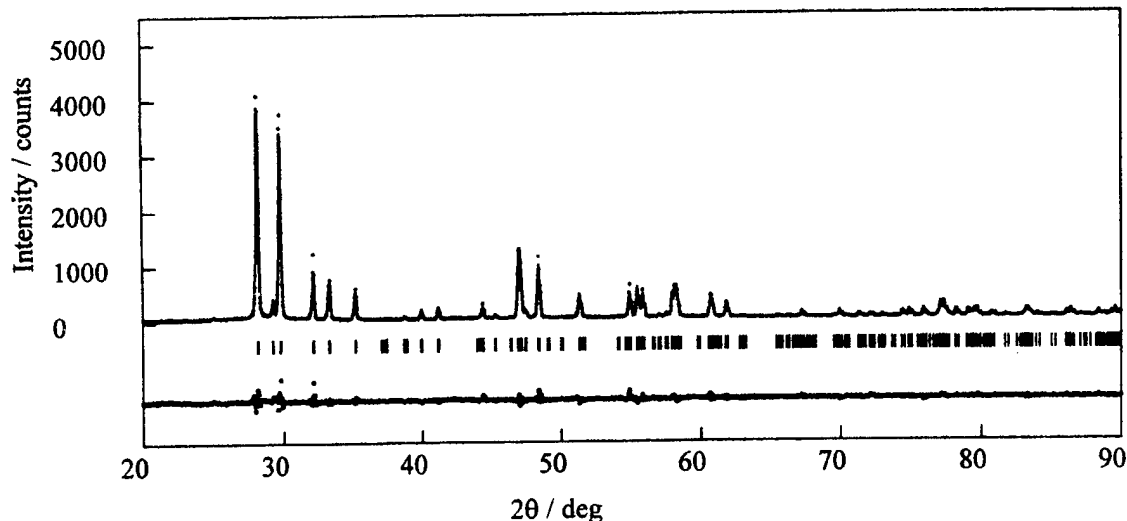


Fig.1. Powder XRD patterns of nonstoichiometric europium orthoniobate,  $\text{Eu}_{0.5}\text{NbO}_{3.25}$ .

#### Acknowledgments

This work was supported by the "Research for the Future, Preparation and Application of Newly Designed Solid Electrolytes (JSPS RFTF96P00102)" program from the Japan Society for the Promotion of Science (JSPS).

#### REFERENCES

- [1] J-H. Lee, M. Yashima, M. Kakihana and M. Yoshimura, *J. Am. Ceram. Soc.*, **81**, 894 (1998).
- [2] A. T. ALDRED, *Acta Cryst. B.*, **40**, 569 (1984).
- [3] Y. Takaki, T. Taniguchi, H. Yamaguchi and K. Nakada, *J. Ceram. Soc. Jpn., Inter. Ed.*, **96**, 56 (1987).
- [4] Y. -I. Kim and F. Izumi, *J. Ceram. Soc. Jpn.* **102**, 401 (1994).



## D. Anion Conductor

OXIDE ION CONDUCTIVITY IN Sr DOPED  $\text{La}_{10}\text{Ge}_6\text{O}_{27}$  APATITE OXIDE

Hiroshi Arikawa, Hiroyasu Nishiguchi, Tatsumi Ishihara  
and Yusaku Takita

Department of Applied Chemistry, Faculty of Engineering, Oita University,  
DannoHaru 700, Oita 870-1192, Japan

Oxide ion conductor is important functional material which can be used as electrolytes of fuel cells, oxygen sensors, and films separating oxygen from air. At present, tetravalent oxides with fluorite structure such as  $\text{ZrO}_2$  or  $\text{CeO}_2$  are extensively investigated as the oxide ion conductors. However, there are some reports on the novel oxide ion conductor. In particular, the authors group found that  $\text{LaGaO}_3$  based oxide exhibits notably high oxide ion conductivity. On the other hand, large part of fast oxide ion conductor have a cubic or pseudo cubic crystal structure and the report on the non-cubic structured oxide showing the fast oxide ion conduction have been limited in number. Recently, Nakayama et al reported that apatite structured  $\text{La}_{10}\text{Si}_6\text{O}_{27}$  exhibits the oxide ion conductivity [1]. Advantage of this oxide is low activation energy for oxide ion conduction. However, the oxide ion conductivity in the related oxide is not studied thoroughly. In the present study, the oxide ion conductivity of  $\text{La}_{10}\text{Ge}_6\text{O}_{27}$  was investigated. Furthermore, doping effects of Sr for La site of  $\text{La}_{10}\text{Ge}_6\text{O}_{27}$  on oxide ion conductivity was studied.

The specimens studied in this study were always prepared by the conventional powder mixing method. Ceramic samples of composition  $\text{La}_{10}\text{Ge}_6\text{O}_{27}$  or  $\text{La}_{10}\text{Si}_6\text{O}_{27}$  were prepared by mixing commercial powders of  $\text{La}_2\text{O}_3$  (Kishida, 99.99% in pure),  $\text{SrCO}_3$  (Wako, 99.9%),  $\text{GeO}_2$  (Kishida, 99.99%) and  $\text{SiO}_2$  (Idemitsu, 99.99 %) in stoichiometric proportions. The starting powders were mixed in  $\text{Al}_2\text{O}_3$  pestle and mortar and then precalcined at 1273 K for 6 h. The mixture was pulverized again with pestle and mortar and pressed into disks of 20 mm in diameter and 1.5 mm in thickness. After isostatic pressing at 275 MPa, the disks were sintered at 1873-1923 K for 6 h in air. Conductivity was measured with dc four probe method. Pt paste (Tanaka TR7902) is applied and fired at 1223 K for 30 min to prepare electrode.

Figure 1 shows the XRD patterns of the prepared  $\text{La}_{10}\text{Ge}_6\text{O}_{27}$  and  $\text{La}_{10}\text{Si}_6\text{O}_{27}$  mixed oxide. Although the crystallinity of  $\text{La}_{10}\text{Ge}_6\text{O}_{27}$  was slightly lower than that of  $\text{La}_{10}\text{Si}_6\text{O}_{27}$  mixed oxide, the similar diffraction patterns was observed on both oxides. Therefore, it seems more likely that crystal structure of  $\text{La}_{10}\text{Ge}_6\text{O}_{27}$  is close to hexagonal apatite structure, although powder dif-

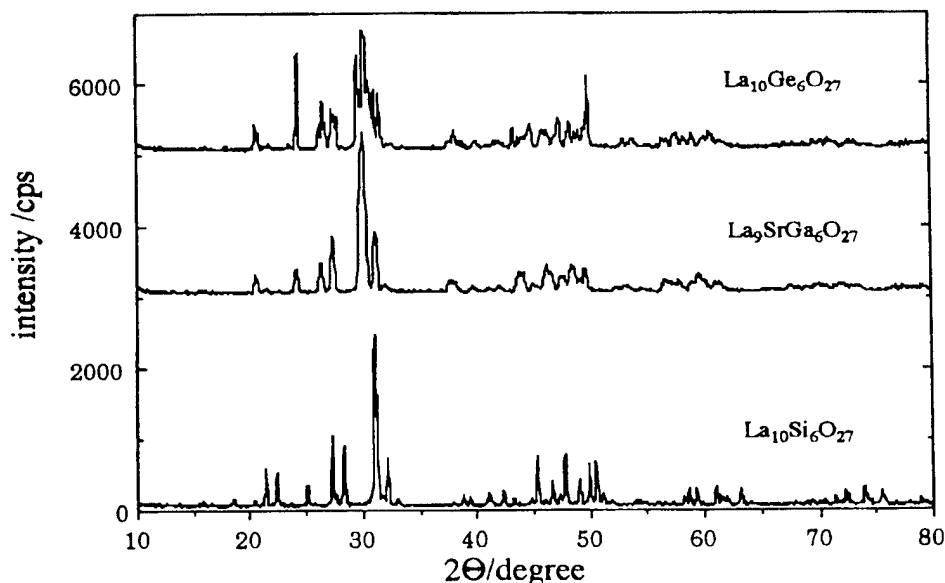


Fig.1 XRD pattern of  $\text{La}_{10}\text{Si}_6\text{O}_{27}$ ,  $\text{La}_9\text{SrGe}_6\text{O}_{26.5}$ , and  $\text{La}_{10}\text{Ge}_6\text{O}_{27}$

fraction pattern is not contained in JCPDS files. In Fig.1, XRD pattern of Sr doped  $\text{La}_{10}\text{Ge}_6\text{O}_{27}$  was also shown. It is obvious that the crystallinity was greatly improved by doping Sr but more similar diffraction pattern with  $\text{La}_{10}\text{Si}_6\text{O}_{27}$  was shown. Therefore, it is expected that substitutional solid solution of Sr into  $\text{La}_{10}\text{Ge}_6\text{O}_{27}$  was occurred. Since the ionic radius of  $\text{Ge}^{4+}$  is larger than that of

Si<sup>4+</sup>, all diffraction peaks were shifted to a lower angle suggesting that unit lattice size of La<sub>10</sub>Ge<sub>6</sub>O<sub>27</sub> is enlarged by changing Si to Ge.

Figure 2 shows the Arrhenius plots of the electrical conductivity of La<sub>10</sub>Si<sub>6</sub>O<sub>27</sub> and La<sub>10</sub>Ge<sub>6</sub>O<sub>27</sub>. In agreement with the report by Nakayama et al. [1], electrical conductivity of La<sub>10</sub>Si<sub>6</sub>O<sub>27</sub> was high but slightly lower than that of 8mol% Y<sub>2</sub>O<sub>3</sub> stabilized ZrO<sub>2</sub> (YSZ). However, La<sub>10</sub>Si<sub>6</sub>O<sub>27</sub> oxide exhibits the higher electrical conductivity than that of YSZ at low temperature due to a small activation energy for electrical conductivity. On the other hand, electrical conductivity of La<sub>10</sub>Ge<sub>6</sub>O<sub>27</sub> was higher than that of YSZ and La<sub>10</sub>Si<sub>6</sub>O<sub>27</sub> at the examine temperature range. However, it was evident that a large change in slope of Arrhenius plot of electrical conductivity was observed on La<sub>10</sub>Ge<sub>6</sub>O<sub>27</sub>. Since the activation energy at high temperature is almost the same as that of La<sub>10</sub>Si<sub>6</sub>O<sub>27</sub>, this may suggest that crystal phase was transferred from a disordered lattice to hexagonal apatite at high temperature. On the other hand, doping small amount of Sr is effective to improve the electrical conductivity in low temperature range and change in activation energy was disappeared. Considering the XRD pattern in Fig.1, doping small amount of Sr for La site of La<sub>10</sub>Ge<sub>6</sub>O<sub>27</sub> seem to stabilize the apatite structure to low temperature. Therefore, it became clear that La<sub>10</sub>Ge<sub>6</sub>O<sub>27</sub> doped with Sr exhibits the higher electrical conductivity than that of YSZ in the examined temperature. The electrical conductivity of La<sub>10</sub>Ge<sub>6</sub>O<sub>27</sub> and Sr doped ones hardly dependent on the oxygen partial pressure from 1 to 10<sup>-21</sup> atm. Therefore, it is expected that La<sub>10</sub>Ge<sub>6</sub>O<sub>27</sub> exhibits an oxide ion conductivity over wide oxygen partial pressure range.

Transport number of oxide ion in La<sub>10</sub>Ge<sub>6</sub>O<sub>27</sub> was estimated with H<sub>2</sub>-O<sub>2</sub> and N<sub>2</sub>-O<sub>2</sub> gas concentration cell. Figure 3 shows the temperature dependence of estimated transport number of oxide ion in La<sub>10</sub>Ge<sub>6</sub>O<sub>27</sub>. Electromotive forces in H<sub>2</sub>-O<sub>2</sub> and N<sub>2</sub>-O<sub>2</sub> cell were almost corresponded to those estimated with Nernst equation based on the difference in oxygen partial pressure. Consequently, it can be concluded that electrical conductivity of La<sub>10</sub>Ge<sub>6</sub>O<sub>27</sub> is wholly ionic. Therefore, this study reveals that the apatite oxide of La<sub>10</sub>Ge<sub>6</sub>O<sub>27</sub> doped with Sr exhibited almost pure oxide ion conduction which is higher than YSZ. The oxide ion conductivity of this oxide attained to log( $\sigma$ /S $\cdot$ cm<sup>-1</sup>) = 0.84 at 1223 K. Consequently, it can be concluded that La<sub>10</sub>Ge<sub>6</sub>O<sub>27</sub> is a new family of fast oxide ion conductor.

## References

- 1) S. Nakayama and M. Sakamoto, J. European Ceramic Society, 18, 1413 (1998).

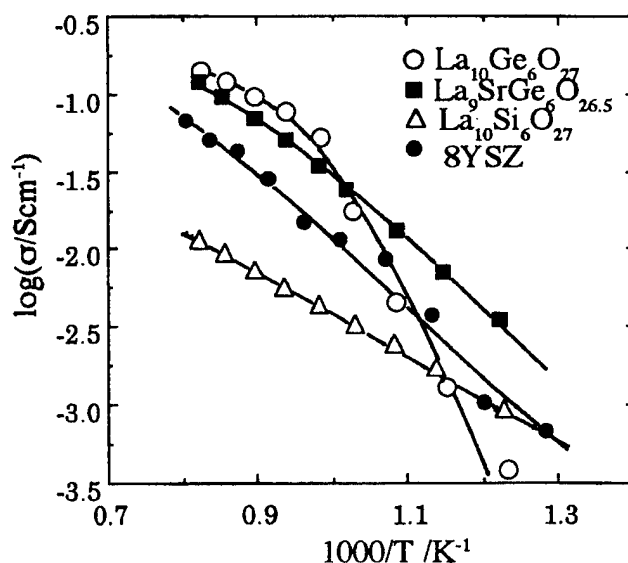


Fig.2 Arrhenius plots of the electrical conductivity of La<sub>10</sub>Ge<sub>6</sub>O<sub>27</sub>, La<sub>9</sub>SrGe<sub>6</sub>O<sub>26.5</sub>, La<sub>10</sub>Si<sub>6</sub>O<sub>27</sub>, and 8mol%Y<sub>2</sub>O<sub>3</sub>-ZrO<sub>2</sub>

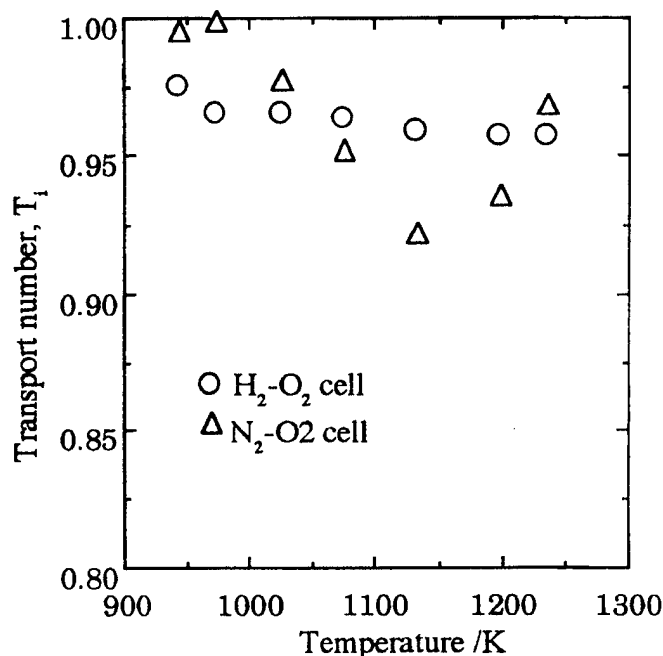


Fig.3 Temperature dependence of transport number of oxide ion in La<sub>10</sub>Ge<sub>6</sub>O<sub>27</sub>

## LOW TEMPERATURE THERMODYNAMIC PROPERTIES AND THE IONIC CONDUCTIVITY OF YTTRIA STABILIZED ZIRCONIA

Tooru ATAKE,<sup>a)</sup> Takeo TOJO,<sup>a)</sup> Toshiyuki MORI,<sup>b)</sup> Hiroshi YAMAMURA<sup>c)</sup>  
and Osamu YAMAMOTO<sup>d)</sup>

<sup>a)</sup>Materials and Structures Laboratory, Tokyo Institute of Technology,  
Yokohama, 226-8503 JAPAN

<sup>b)</sup>National Institute for Research in Inorganic Materials, Tsukuba,  
305-0044 JAPAN

<sup>c)</sup>Department of Applied Chemistry, Faculty of Engineering, Kanagawa University,  
Yokohama, 221-8686 JAPAN

<sup>d)</sup>Department of Chemistry, Faculty of Engineering, Mie University,  
Tsu, 514-8507 JAPAN

The heat capacity of yttria-stabilized and scandia-stabilized zirconia (YSZ, ScSZ) has been measured precisely between 13 and 300 K by adiabatic calorimetry and it has been found that the heat capacity is strongly affected by the dopant concentration in stabilized zirconia. It is well known that the doping of a lower valent oxide (CaO, Y<sub>2</sub>O<sub>3</sub>, Sc<sub>2</sub>O<sub>3</sub>, etc.) into zirconia leads to formation of oxygen vacancies and results in high ionic conductivity at high temperatures. The conductivity, however, shows a maximum at about 8 mol% of yttria doping and it decreases by further doping. The mechanism of this phenomenon is not clarified yet. Figure 1 shows the heat capacity of pure zirconia and 4, 8, 10 and 11 mol% yttria stabilized zirconia in the low temperature region, where  $C_p^*$  is normalized heat capacity:

$$C_p^* = C_p \cdot 3 / (3 + 2x); (x = 0, 0.04, 0.08, 0.10, 0.11). \quad (1)$$

Evidently, the heat capacity increases by yttria doping and becomes a maximum at 8 mol% YSZ. Such behaviour should correspond to the ionic conductivity at elevated temperatures. The excess heat capacity of YSZ compared with pure zirconia is attributed to so-called low-lying modes, which should be a characteristics of superionic conductors. The number of the low-lying modes should be strongly correlated to the mobility of the oxygens. The vibrational motion of ions in the crystal is very sensitive to their local

environment, and thus the formation of the defect structures in YSZ and ScSZ results in the excess heat capacity. Molecular dynamics simulations have been performed to elucidate the relationships between the defect structure and the vibrational density of states (VDOS). The calculation of the VDOS and defect structure gives an reasonable explanation for the observed heat capacity. The details of the analysis of the heat capacity data and the results of the molecular dynamics simulations will be reported.

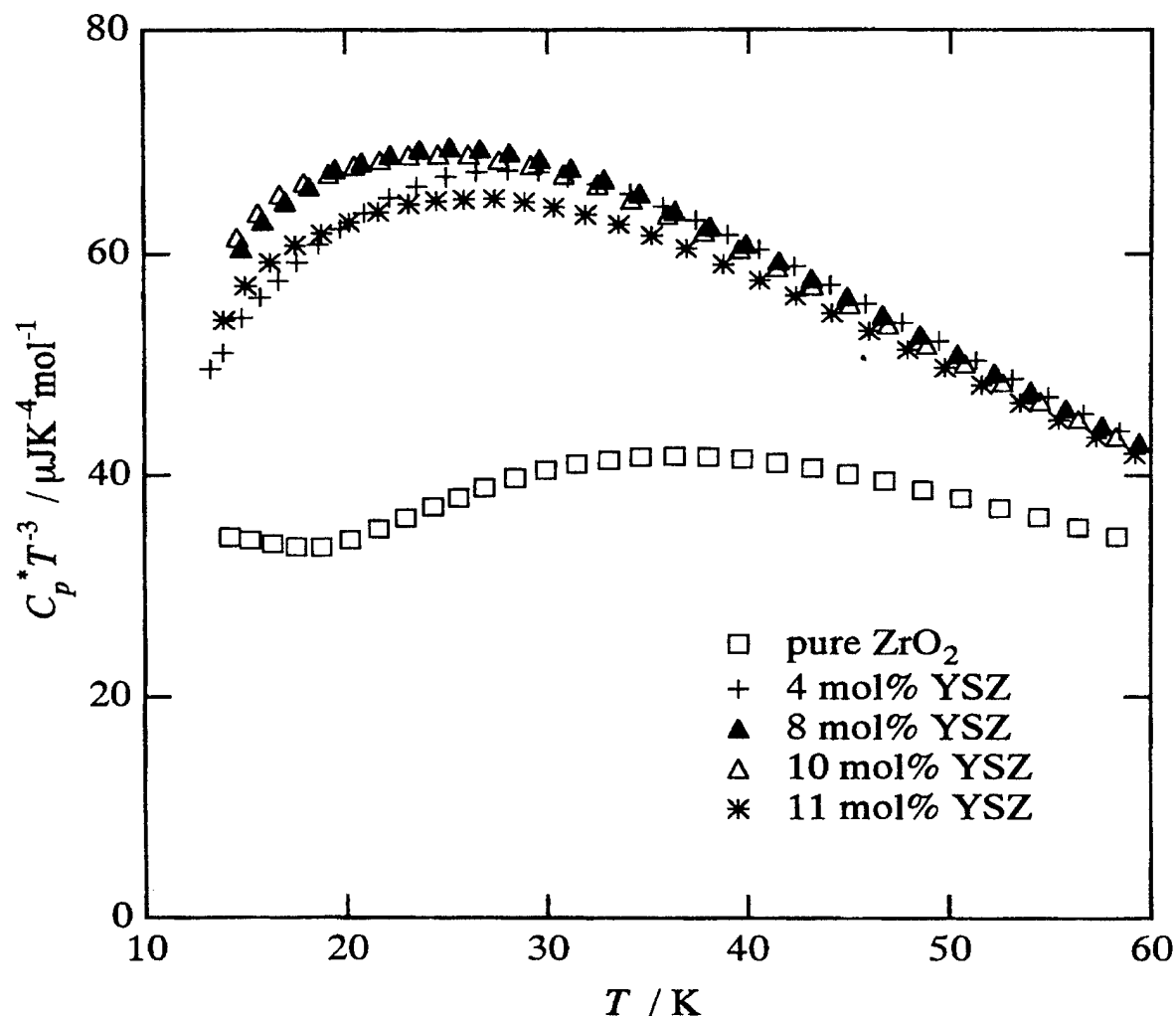


Fig. 1. Low temperature heat capacity of pure zirconia and yttria stabilized zirconia (YSZ) at low temperatures.

#### References

- [1] T. TOJO, T. ATAKE, T. MORI and H. YAMAMURA, *J. Chem. Thermodyn.* (in press).
- [2] T. TOJO, T. ATAKE, T. MORI and H. YAMAMURA, submitted to *J. Thermal Analysis & Calorimetry*.

## ELECTRICAL CHARACTERISTICS OF THE NITROGEN-STABILIZED ZIRCONIA

Jong-Sook Lee, Tai-Joo Chung, Doh-Yeon Kim

Creative Research Initiative Center for Microstructure Science of Materials,  
Seoul National University, Seoul 151-742, Korea

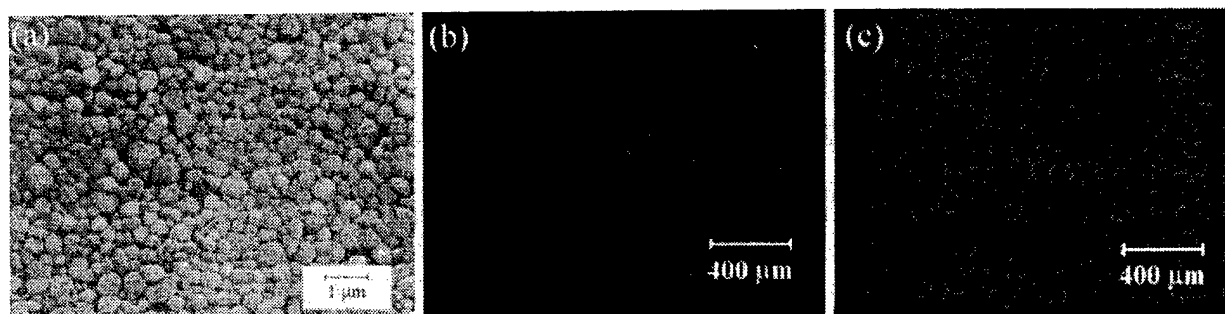
It has been reported that, when nitrogen is incorporated into yttria-doped tetragonal zirconia polycrystals (Y-TZP), the cubic phase of zirconia is stabilized with formation of additional oxygen vacancies [1]. Chung et al. proposed that the low temperature degradation of Y-TZP can be therefore prevented by surface nitrification of the sintered Y-TZP specimens [2]. The nitrogen source can be either atmospheric nitrogen or a solid nitride like ZrN. When Y-TZP specimen is embedded in ZrN powder and heat-treated at high temperatures, the nitrified surface layer was found to grow according to a parabolic rate law. The nitrogen diffusion through the transformed layer was supposed to control the transformation process [3]. Columnar grains with large aspect ratios of 10 to 20 were developed along the nitrogen flux lines and their growth was limited to a critical thickness at a given treatment temperature such as 400  $\mu\text{m}$  at 1500°C and 800  $\mu\text{m}$  at 1600°C [3]. In this work, the nitrogen-stabilized zirconia specimen consisting entirely of columnar grains were prepared and the transport properties of the nitrogen-stabilized cubic zirconia are investigated.

Figure 1(a) shows the microstructure of the as-sintered 2Y-TZP (TZ-2Y, Tosoh) at 1450°C for 3 h in air with an average grain size of 0.4  $\mu\text{m}$ . Figure 1(b) and (c) show the microstructures of nitrified specimens. The sintered specimens embedded in ZrN powder were heat-treated at 1700°C for 4 h. The columnar grains grown from each surface impinge against each other in the middle of the specimen (Fig. 1(b)). Fig. 1(c) is the section perpendicular to the length direction of columnar grains. It consists of grains of uniform size of around 50  $\mu\text{m}$ . Figures 2 show the impedance spectra obtained from the specimens: Y-TZP specimen (a) and the nitrogen-stabilized zirconia as measured *perpendicular* to the columnar direction (b) exhibit the well-distinguished three arcs of bulk, grain boundary and electrode response. As measured *along* the columnar direction, on the other hand, no appreciable grain boundary impedance was detected. Consistent specific bulk resistance can be obtained in both directions (see Fig. 2(b) and (c)) as confirmed with two sets of specimens in different geometry. The grain boundary impedance can be thus unambiguously attributed to the parallel boundaries of the columnar grains. Figure 3 displays the temperature dependence of the respective conductivities. The activation energy of bulk conductivity in nitrogen-stabilized cubic zirconia (1.05 eV) is higher than that of Y-TZP (0.83 eV) and the grain boundary contribution is more highly activated (1.60 eV) than that of Y-TZP (1.04 eV). The defect structure of nitrogen-stabilized cubic zirconia and the grain boundary characteristics will be discussed in more detail.

[1] Y.-B. Cheng, D. P. Thompson, J. Am. Ceram. Soc. **76** 683 (1993).

[2] T.-J. Chung, H. Song, G.-H. Kim and D.-Y. Kim, J. Am. Ceram. Soc., **80** 2607 (1997).

[3] T.-J. Chung, J.-S. Lee, D.-Y. Kim and H. Song, J. Am. Ceram. Soc., submitted.



**Fig. 1** Microstructure of 2Y-TZP (a) and nitrified TZP (b,c): (b) Section exhibiting symmetrically grown columnar grains and (c) section perpendicular to the length direction of columnar grains showing almost uniform two-dimensional microstructure

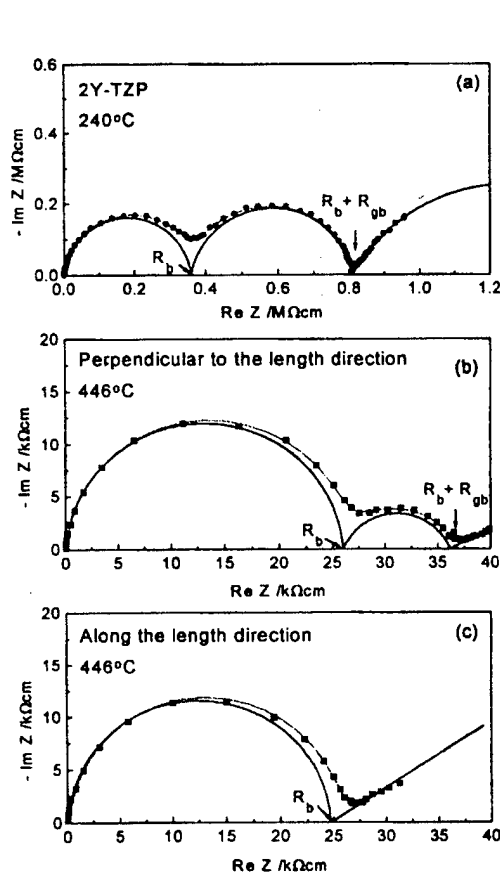


**Fig. 2** Typical impedance spectra for 2Y-TZP (a) and for nitrified cubic zirconia (b,c).

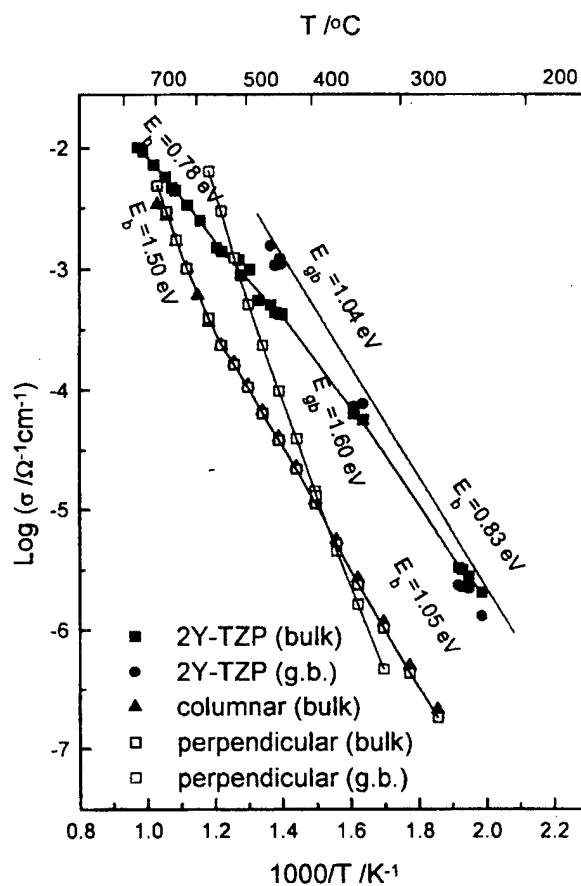


**Fig. 3** Ionic conductivity of 2Y-TZP and nitrified cubic zirconia along and perpendicular to the columnar direction, respectively.

ELECTRICAL DOUBLE LAYER CAPACITANCE OF THE M, O<sub>2</sub> / YSZ INTERFACES  
(M=Pt, Au, Pd, In<sub>2</sub>O<sub>3</sub>)

B. L. Kuzin, D. I. Bronin

Institute of High-Temperature Electrochemistry, Ural Division of Russian Academy of Sciences, Ekaterinburg

The behaviour of the electrode systems M, O<sub>2</sub>/YSZ, where M= porous Pd, Pt, Au, and dense In<sub>2</sub>O<sub>3</sub> ; YSZ - single-crystal solid electrolyte 0.90 ZrO<sub>2</sub>-0.10 Y<sub>2</sub>O<sub>3</sub>, was studied by means of impedance measurements.

The porous palladium electrode was studied in the air atmosphere. At the temperatures below 814 °C the electrode is oxidised and consists of PdO. At higher temperatures PdO is decomposed to the metallic palladium.

The behaviour of the porous platinum electrode was investigated in a closed electrochemical cell made of solid electrolyte based on ZrO<sub>2</sub> and supplied with oxygen pump and oxygen sensor. The range of oxygen pressure in the cell was varied between 10<sup>-7</sup> and 35 atm. Changing oxygen pressure in the cell oxidation of platinum and reduction of platinum oxide were easily controlled. As was shown in [1] not all platinum could be oxidised in the electrode but only 10 % of the whole mass of platinum at the most.

The porous gold electrode also was studied in the closed electrochemical cell at different temperatures and oxygen pressures.

The dense indium oxide electrode was tested in the air and it was studied in two different states: as an ion blocking electrode and as reversible electrode.

The high-frequency part of the impedance spectra was described, using the Boucamp notation, by an equivalent electrical circuit of the type

$$R_{el}(Z_{CPE}^h R_{\eta}^h), \quad (1)$$

where  $R_{el}$  is the electrolyte resistance of the measuring cell;  $Z_{CPE}^h$  - the impedance of the constant phase element (CPE) of the high-frequency relaxation process;  $R_{\eta}^h$  - the polarisation resistance of the high-frequency relaxation process. The impedance of the CPE is expressed in the form of the following formula:

$$Z_{CPE} = (j\omega)^{-n} / B, \quad (2)$$

with  $B$  and  $n$  being the CPE parameters ( $0 < n < 1$ ),  $j = (-1)^{1/2}$ , and  $\omega$  - the angular frequency. The complete impedance spectra can include low frequency electrode relaxation processes and be more complicated.

Detailed investigations of the electrode system Pt, O<sub>2</sub> / YSZ showed that the dimension of the symmetrical electrochemical cell influence significantly the value of the parameter  $n$ . It was concluded that the nature of the CPE can be attributed to a nonuniform distribution of current on the electrode surface. In such case the CPE parameters  $n$  and  $B$  may be related to each other by [2]:

$$B = (C_{dl})^n (R_{el})^{n-1}, \quad (3)$$

where  $C_{dl}$  is the double layer capacitance and  $R_{el}$  the resistance of the electrolyte in a cell. Then  $C_d$  of the interface electrode - electrolyte can be determined. The validity of the expression (3) was verified by comparing the experimental values of  $R_{el}$  with those calculated from the linear  $\ln B - n$  dependencies which corresponded to each other.

It was found that  $C_{dl}$  of Pd, Pt and Au porous electrodes in a metallic state has value of several micro-Farad per square centimetre of the electrode.  $C_{dl}$  of Pd and Pt oxidised electrodes is about one order of value lower. The electrochemical activity was far less for the oxidised electrodes than for the metallic electrodes.

Cooling of the cell with Au electrode down to the room temperature at oxygen pressure in the cell of 18 atm and following heating of the cell led to decrease of  $C_{dl}$  and its value became as low as in case of oxidised Pt and Pd electrodes. Electrochemical activity of the gold electrode also fell down considerably. The properties of the gold electrode were restored to its original values only after a long cathodic polarisation of the electrode: -380 mV at 763 °C. This fact can indicate oxidation of the surface of the Au electrode although no thermodynamic data confirm a possibility for gold to be oxidised at such conditions.

$C_{dl}$  of the of india electrode is about 3  $\mu\text{F}/\text{cm}^2$  and does not depends on whether it is in a blocking or in a reversible state.

Transition of the metallic electrodes to a "passive state" with lower rates of the electrochemical processes and  $C_{dl}$  was observed for all the noble metal electrodes. In case of Pd electrode this transition is due to formation of the bulk phase of PdO. "Passive state" of the Pt electrode is connected with Pt oxidation to the depth of many atomic layers but the bulk of the electrode is not oxidised. The change in properties of the Au electrode can be explained by formation of some surface oxide.

If to take into account that real contact of porous metallic electrodes with electrolyte is approximately 10-30 times lower than visible electrode area [3] then the specific  $C_{dl}$  of the real interface electrode-electrolyte is between 30 and 150  $\mu\text{F}/\text{cm}^2$  for the electrodes in a metallic state and between 1 and 10  $\mu\text{F}/\text{cm}^2$  in an oxidised state.

The india electrode was very dense and had ultimate contact with the electrolyte. So, one may suppose that 3  $\mu\text{F}/\text{cm}^2$  is the real specific  $C_{dl}$  of the oxide electrode which is of the same order of value as  $C_{dl}$  for metallic oxidised electrodes.

The temperature and oxygen pressure dependencies of  $C_{dl}$  for all the electrodes tested are very weak or absent (experiments with variation of oxygen pressure were carried out only with Pt and Au electrodes).

This circumstance and the values of  $C_{dl}$  of the oxidised and india electrodes point to the application of the Helmholtz model of the electrical double layer structure to the studied interfaces when the main potential drop across the interface electrode-electrolyte is realised in the dense part of the electrical double layer. The Helmholtz model predicts  $C_{dl}$  capacity of about 10  $\mu\text{F}/\text{cm}^2$  if to assume the dielectric constant of the gap between two plates of the double layer capacitor of unity and the distance between the plates as 1 Å.

If to believe that the structure of the ionic part of the electrical double layer is the same both in case of metallic electrodes and oxidised electrodes then the reason for higher  $C_{dl}$  in case of metallic electrodes could be less effective distance between the double layer plates due to the "tail" of quasi free electrons which goes outside the ionic skeleton of the metal (see, for example, [4]).

#### References

- [1] B. L. Kuzin, M. A. Komarov, *Elektrokhimija* (Russian) **29**, 1374 (1993)
- [2] G. J. Brug, A. L. G. van den Eeden, M. Sluyters-Rehbach, J. H. Sluyters, *J. Electroanal. Chem.* **176**, 275 (1984)
- [3] T. Kenjo, Y. Yamakoshi, K. Wada, *J. Electrochem. Soc.* **140**, 2151 (1993)
- [4] A. A. Kornyshev, *Electrochim. Acta* **34**, 1829 (1989)



## AN INVESTIGATION OF THE MICROSTRUCTURE/IONIC CONDUCTIVITY RELATIONSHIP IN INDIUM DOPED LSGM

J. Kimpton<sup>1</sup>, T. H. Randle<sup>1</sup>, J. Drennan<sup>2</sup>, and G. J. Auchterlonie<sup>2</sup>

<sup>1</sup> Swinburne University of Technology, Melbourne, Victoria, 3122, Australia

<sup>2</sup> Centre for Microscopy and Microanalysis, University of Queensland, Brisbane, Queensland, 4072, Australia

Considerable interest has developed in the perovskite-related ceramic  $\text{La}_{0.9}\text{Sr}_{0.1}\text{Ga}_{0.8}\text{Mg}_{0.2}\text{O}_{2.85}$ , (LSGM) since Ishihara et al [1] first reported high oxygen-ion conductivity for this system. The material represents a significant departure from the well-known doped fluorite systems such as the stabilised zirconia ceramics and opens new avenues in the search for novel oxygen-ion conductors. As a consequence, a detailed knowledge of the effect on the conductivity of LSGM, with changes in crystal chemistry is essential in understanding the conduction processes taking place in this system.

A number of workers have shown that the composition suggested by Ishihara is optimised for this particular elemental suite. As a consequence, if any improvements are to be made on the ionic conductivity of this material, alternative strategies must be used. One such approach is to substitute alternative cations with larger ionic radii on the existing sites with a view to further "opening" the structure. In line with these ideas,  $\text{In}^{3+}$  was chosen as the substituting dopant cation, replacing the smaller  $\text{Ga}^{3+}$ . A series of substitutions were made in which the vacancy concentrations remained constant whilst  $\text{Ga}^{3+}$  was gradually replaced by  $\text{In}^{3+}$ . This approach would also provide marker cations to determine the location and influence that the various site substitutions will have on electrical properties.

Although the conductivity results proved to be inconclusive, the use of analytical transmission electron microscopy in combination with the conductivity results proved to be very instructive in determining the location and distribution of the substituting cation in the ceramic composite. Continuous substitution of  $\text{In}^{3+}$  for  $\text{Ga}^{3+}$  in the LSGM was confirmed, with the  $\text{In}^{3+}$  clearly going to the  $\text{Ga}^{3+}$  sites. The substitution was observed both by x-ray diffraction and analytical electron microscopy to be uniform for each of the samples produced, up to a level of 8mol% substitution. However, accompanying the substitution of In into the LSGM was the occurrence of an Indium rich secondary phase. The level of this phase increased systematically in line with the increasing Indium content and was consistently formed irrespective of processing conditions. The phase was identified by electron diffraction as  $\text{LaInO}_3$ . The occurrence of this secondary phase complicates the interpretation of the conductivity results and possibly masks any actual improvements, which may have occurred in the host LSGM material. The formation of  $\text{LaInO}_3$  is believed to be simply a function of the kinetics of reaction in that the formation of this phase proceeds the formation of the more complex LSGM.

[1] T. Ishihara, H. Matsuda, and Y. Takita, J. Am. Chem. Soc., 116, 3801, (1994)

# A NEW CLASS OF MONODIMENSIONAL BISMUTH-BASED OXIDE ANION CONDUCTORS WITH A STRUCTURE BASED ON $[\text{Bi}_{12}\text{O}_{14}]_{\infty}$ COLUMNS

Rose-Noëlle VANNIER, Francis ABRAHAM, Guy NOWOGROCKI and Gaëtan MAIRESSE

Laboratoire de Cristallographie et Physicochimie du Solide, ENSCL, UPRESA CNRS 8012,  
BP 108, 59652 Villeneuve d'Ascq Cedex, France

We recently evidenced a new family of oxide anion conductors with a structure based on  $[\text{Bi}_{12}\text{O}_{14}]_{\infty}$  columns [1]. The parent compound of this series can be formulated  $\text{Bi}_{26}\text{Mo}_{10}\text{O}_{69}$  and its structural characteristics extend within a continuous solid solution in the ternary  $\text{Bi}_2\text{O}_3$ - $\text{MoO}_3$ - $\text{V}_2\text{O}_5$  system. Its symmetry is triclinic at room temperature ; it reversibly transforms to a monoclinic form at about 310°C. The increase of bismuth content, or the introduction of at least 10% of vanadium in bismuth site leads to the stabilization of the high temperature monoclinic form at room temperature. The structure of these materials has been solved in the P2/c space group combining both X-ray and neutron diffraction data. It consists of covalent  $[\text{Bi}_{12}\text{O}_{14}]_{\infty}$  columns connected with Mo, O species, in which the mean-square displacements of the oxygen atoms display unusual high values, likely correlated with some softness of this part of the structure which favors the oxide anion mobility.

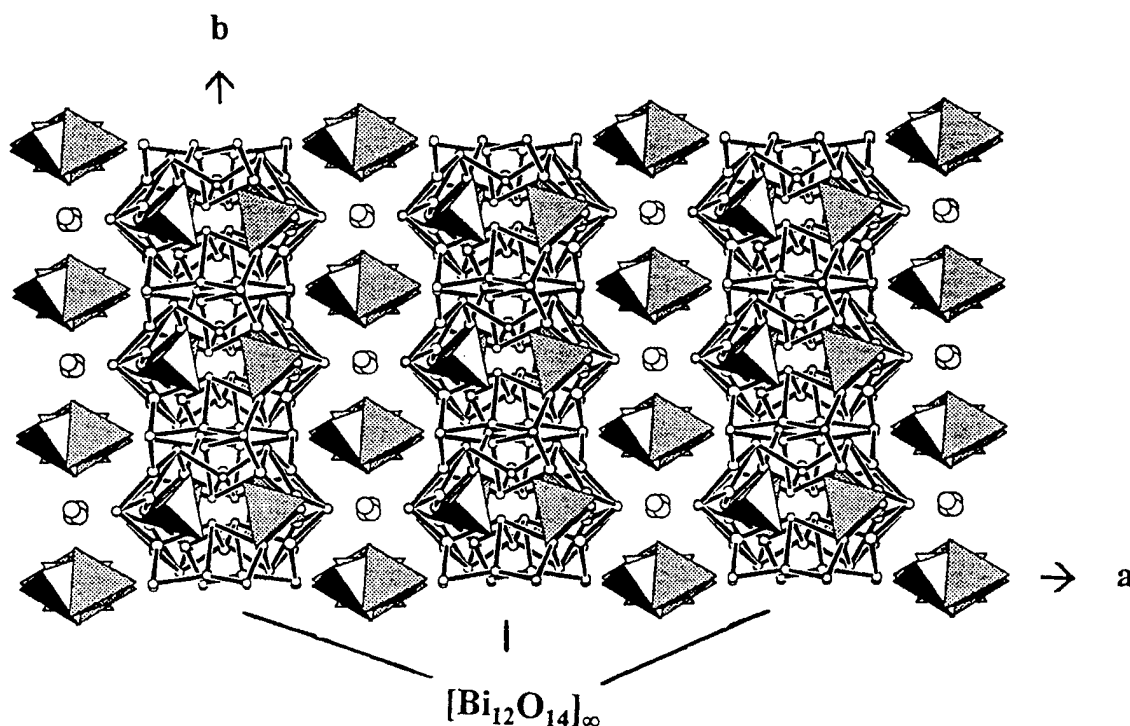
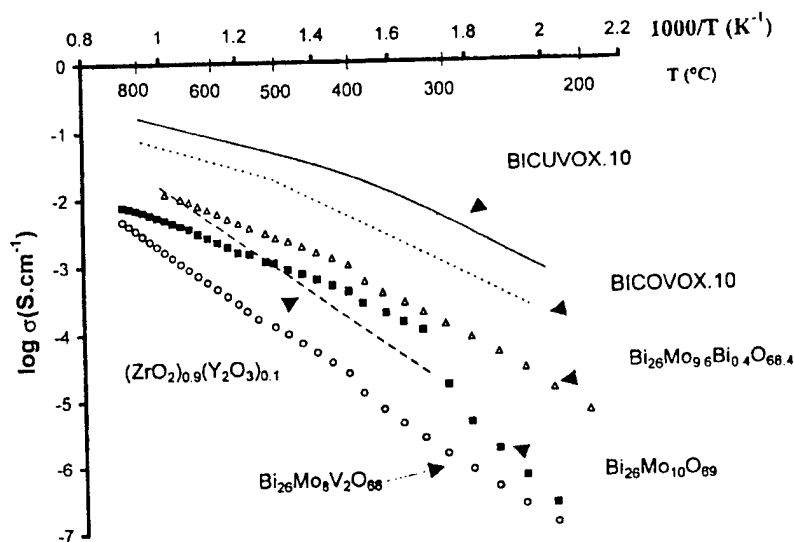


Figure 1 : (a, b) projection of  $\text{Bi}_{26}\text{Mo}_{10}\text{O}_{69}$  structure with  $[\text{Bi}_{12}\text{O}_{14}]_{\infty}$  columns extending along the twofold axis

These materials are pure oxide anion conductors. The conduction process likely takes place along the direction of the  $[\text{Bi}_{12}\text{O}_{14}]_{\infty}$  columns and they can therefore be considered as monodimensional oxide anion conductors. Their electrical properties are reported in figure 2. They are compared to those of the well known BIMEVOX and YSZ. If they are in the range of YSZ ones, they remain one order of magnitude under those of the BIMEVOX that derive from  $\text{Bi}_4\text{V}_2\text{O}_{11}$  by partial substitution of vanadium by numerous elements.



**Figure 2 :** Conductivity versus temperature of  $\text{Bi}_{26}\text{Mo}_{10}\text{O}_{69}$  and its derivatives compared to YSZ, BICUVOX.10 and BICOVOX.10

In the aim of enhancing its electrical properties, partial substitutions have been performed in  $\text{Bi}_{26}\text{Mo}_{10}\text{O}_{69}$ . Several dopants have been checked i)  $\text{Pb}^{\text{II}}$ ,  $\text{Ca}^{\text{II}}$ ,  $\text{Sr}^{\text{II}}$ ,  $\text{Ba}^{\text{II}}$  for bismuth site ii)  $\text{P}^{\text{V}}$ ,  $\text{V}^{\text{V}}$ ,  $\text{W}^{\text{VI}}$  for molybdenum site. Seven solid solutions have been evidenced. In a general way, increasing oxygen vacancies led to a small decrease of the performances, but partial substitution for molybdenum with the isovalent tungsten cation gave rise to very attractive properties.

[1] R.N.Vannier, G.Mairesse, F.Abraham and G.Nowogrocki, J. Solid State Chem. 122, 394 (1996)

**BICUVOF: A COPPER FLUORIDE DOPED BIMEVOX**I. Abrahams,<sup>1</sup> J.A.G. Nelstrop<sup>1</sup> and F.Krok<sup>2</sup><sup>1</sup>Structural Chemistry Group, Dept. of Chemistry, Queen Mary and Westfield College, University of London, Mile End Road, London E1 4NS, United Kingdom<sup>2</sup>Institute of Physics, Warsaw University of Technology,  
ul. Koszykowa 75, 00-662, Warsaw, Poland.

The search to improve the conductivity in the BIMEVOX family has mainly focused on the substitution of the cation sublattice i.e. Bi and V. The principle charge carriers in BIMEVOX compounds are the oxide ions of the vanadate layer. The introduction of other possible charge carriers into the BIMEVOX system has generally not been investigated. The substitution of O<sup>2-</sup> ions for F<sup>-</sup> must lead to changes in the vacancy concentration in the vanadate layer and might lead to mixed F<sup>-</sup> and O<sup>2-</sup> ion conductivity. Incorporation of fluoride ions may also aid in the understanding of the conductivity mechanism within the vanadate layer. In this study we examine the relationship between conductivity and structure of a new fluoride containing BIMEVOX compound, BICUVOF.

Ceramic samples of chemical composition Bi<sub>2</sub>V<sub>1-x</sub>Cu<sub>x</sub>O<sub>5.5-(5x/2)</sub>F<sub>2x</sub> (0.10 ≤ x ≤ 0.20) were prepared by conventional solid state techniques using appropriate molar quantities of Bi<sub>2</sub>O<sub>3</sub>, CuF<sub>2</sub> and V<sub>2</sub>O<sub>5</sub>. Structure and electrical properties were examined using X-ray powder diffraction and a.c. impedance spectroscopy.

All the X-ray diffraction patterns showed a tetragonal γ phase pattern. A general increase in the cell dimensions with increasing x value was observed over the composition range studied. This increase in the cell dimensions can be rationalised by the gradual substitution of V<sup>5+</sup> by larger Cu<sup>2+</sup> ions, which would more than compensate for the loss of oxygen through the solid solution mechanism. However oxygen is also being partially replaced by fluorine. O<sup>2-</sup> and F<sup>-</sup> ions have similar ionic radii and can easily substitute for one another in an ionic lattice. In BICUVOF for every oxide ion substituted, two fluoride ions are required to maintain electroneutrality. This causes a portion of the otherwise vacant sites to be filled; one of the fluoride ions can substitute directly into the empty oxygen site with the other occupying a normally vacant site. Thus the addition of fluoride ions into the structure reduces the number of vacancies.

A dramatic decrease in conductivity over several orders of magnitude upon doping was observed; as x increases the conductivity decreases about one order of magnitude per 0.02 increase in x. The activation energy generally increases with x. These phenomena cannot solely be due to the reduction in the number of vacancies present in the structure. A possible explanation may be a mixed anion effect analogous to the mixed cation effect seen in many systems.

**VOLTAMMETRY ON BIMEVOX (ME=Cu, Ni, Zn, Mg) MICROSAMPLES**

G.Fafilek\*, P.Kurek\*\*

\*Institute of Technical Electrochemistry, Vienna University of Technology  
Getreidemarkt 9, A-1060 Vienna, Austria\*\*Institute of Physics, Warsaw University of Technology,  
ul. Koszykowa 75, 00-662 Warsaw, Poland**Abstract:**

High temperature cyclic voltammetry on microsamples has turned out to be a suitable technique for the observation of reduction and oxidation processes in oxides [1,2]. This technique was applied successfully to the determination of the electrochemical stability range of BICUVOX.10 which is known to be a very good oxygen ion conductor [3]. The same technique was used now for a systematic search if other members of the BIMEVOX family exhibit differences in the stability with respect to reduction.

The electrochemical measurements were performed on a 3-electrode cell of the type:  $N_2, Pt|microsample|YSZ|Pt, N_2$  with the interface  $N_2, Pt|YSZ$  as a pseudo reference electrode. The cell consisted of a disc of yttria stabilized zirconia (YSZ) with directly applied platinum paste electrodes for the counter and the reference electrode. The working electrode was a small platinum plate which contacts the microsample. The sample was pressed onto the surface of the YSZ disc. The YSZ served as a kind of inert supporting electrolyte. The experiments were performed in nitrogen or argon as an inert atmosphere. The residual oxygen in the inert gas is necessary to protect the sample against chemical reduction and for a stable reference potential. It should not be too high to avoid an overlapping current from the reduction of the oxygen.

In general, the stability of the BIMEVOX is determined by the stability of the main compound  $Bi_2O_3$ . None of the samples showed a higher stability against complete reduction than BICUVOX. Nevertheless some differences in the reduction processes at less negative potentials than the standard potential of  $Bi_2O_3$  have been observed. A redox process in this potential region could be related to valence changes of vanadium from  $V^{5+}$  to  $V^{4+}$  and, at more negative potentials, from  $V^{4+}$  to  $V^{3+}$ . This may indicate differences in the strength of bonding of the oxygen to the vanadium in the different BIMEVOX compounds.

**References:**

- [1] G.Fafilek, Solid State Ionics 113/115, 673 (1998)
- [2] G.Fafilek, S.Harasek, Solid State Ionics, submitted
- [3] F.Abraham, J.C.Boivin, G.Mairesse and G.Novogrocki, Solid State Ionics, 40/41, 934 (1990)

## SMALL SIGNAL RESPONSE OF THE BICUVOX/NOBLE METAL/OXYGEN ELECTRODE SYSTEM.

Bernard A. Boukamp

Laboratory of Inorganic Materials Science, Department of Chemical Technology,  
University of Twente, PO Box 217, 7500 AE Enschede, the Netherlands

### Introduction

The family of BiMeVOx materials ( $\text{Bi}_2\text{Me}_x\text{V}_{1-x}\text{O}_{5.5-\delta}$ , Me = Co, Cu, etc.) show very high oxygen ion conductivity at moderate temperatures. This makes these materials very attractive for application in medium temperature oxygen pumps. But besides high oxygen ion conductivity also very active electrodes are needed. In this study the electrochemical properties of  $\text{Bi}_2\text{Cu}_{0.1}\text{V}_{0.9}\text{O}_{5.35}$ /noble metal/ $\text{O}_2$  electrodes have been studied by impedance spectroscopy and polarisation measurements in a three-electrode cell. It is well known that the choice of electrode metal has a significant influence on the electrode properties of yttria stabilized zirconia, with Ag as the best, although geometrically very unstable noble metal and Au as the poorest [1]. Hence the electrode resistances can be ranked by:  $R_{\text{Ag}} < R_{\text{Pt}} \ll R_{\text{Au}}$ . On the other hand it has been observed for the stabilized  $\delta$ -bismuth sesqui-oxides, in particular  $\text{Bi}_{1.5}\text{Er}_{0.5}\text{O}_3$  (abbreviated BiEr25) [2,3], that for these materials there is very little difference in performance between Pt and Au electrodes with similar electrode morphology. This has been explained qualitatively by assuming that the electrolyte surface, exposed to the ambient, is more catalytically active with respect to the oxygen dissociation and charge transfer than the noble metal electrodes are. Oxygen isotope exchange measurements [4,5] have presented corroborating evidence for this model.

### Sample and electrode preparation and measurement

Ceramic disks of BiCuVOx (10% Cu) were kindly provided by B.Dunn at UCLA. Annularly shaped noble metal electrodes were sputtered onto both sides of the disk. The silver electrodes were also vacuum deposited for improved layer thickness. The same type metal was applied to both sides. For Au and Pt typical open structures were obtained upon annealing. The Ag electrodes were annealed in situ. The impedance of the electrode was measured in a three-electrodes setup (with a central point reference electrode) as function of temperature, polarisation and partial pressure of oxygen. Data analysis was performed with the software package 'Equivalent Circuit' [6]. Also a few polarisation experiments were performed.

### Results and discussion

For both the Au and the Pt electrode a similar semi-infinite diffusion type impedance (Warburg) was observed in the intermediate temperature range (250-500°C). Polarisation measurements indicated that the predominant process in this temperature range is a reduction/oxidation of the bulk material at the electrode under influence of the applied potential and virtually without actual oxygen transport through the electrode. This is indicated by the subsequent positions of the 'zero current' polarisations in Fig. 1, and is explained by a small but significant electronic conductivity.

Only at higher temperatures ( $T > 650^\circ\text{C}$ ) a dc-electrode resistance can be extrapolated from the impedance measurements. The electrode dispersion is dominated by the

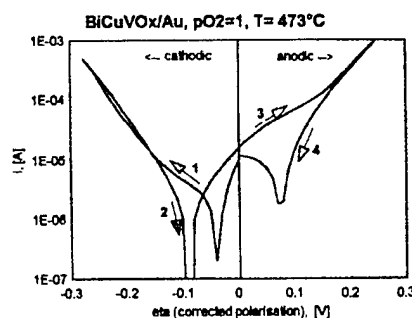


Fig.1 Polarisation curve for an Au electrode on BiCuVOx at 473 °C and  $p\text{O}_2 = 1$  atm. Direction of measurement is indicated.

parallel combination of a Warburg (diffusion) and a resistance in the mid-frequency range (0.1 to 100 Hz). The Warburg, which in the admittance is represented by  $Y(\omega) = Y_0 [j\omega]^{1/2}$ , shows a strong  $PO_2$  dependence with  $Y_0 \sim (PO_2)^{1/2}$ , see Fig. 2. This implies faster diffusion at lower partial pressures of oxygen. At the same time the parallel resistance decreases with increasing  $PO_2$ .

Similar behaviour is observed for  $Y_0$  under polarisation, a decreasing  $Y_0$  value with increasing (cathodic to anodic) polarisation level. The parallel resistance, however, has the characteristics of a charge transfer resistance, see Fig. 3. In this respect the behaviour is dissimilar to the observed electrode behaviour of BiEr25 [2,3], although in principle the same general model seems to apply. This tentative model is based on a continuous exchange of oxygen at the electrolyte/ambient interface. At zero bias the anodic and cathodic oxygen fluxes are equal, hence no electrode current flows. Essential for this model is some degree of electronic conductivity, which is present in BiCuVOx and also at high temperatures in BiEr25 [2,3]. Due to electron injection at the metal electrode under cathodic polarisation the oxygen reduction reaction is enhanced while the anodic reaction is diminished, leading to a net flow of oxygen into the sample. As the path of the electrons is perpendicular to the oxygen flux, concentration profiles of absorbed, charged species and of charge carrying defects in the surface region will develop. These profiles extend outward from the electrode perimeter and will result in the observed diffusion behaviour in the impedance spectra. Consequently, as the metal electrode only functions as current source/sink, the electrode properties are independent of the choice of noble metal, but strongly related to microscopic electrode morphology.

### Acknowledgement

The author wishes to express his gratitude towards the 'European Office of Aerospace Research and Development' (EOARD) for sponsoring this research under contract F61708-97-W0049. The author is indebted to Prof. B. Dunn (UCLA) and his research group for providing the BiCuVOx ceramic disks. Also Ms. Silvie Ladet is thanked for her assistance in the experimental work.

### References

- [1] S.P.S. Badwal, M.J. Bannister and M.J. Murray, *J. Electroanal. Chem.* **168**, 363 (1984).
- [2] I.C. Vinke, B.A. Boukamp, K.J. de Vries and A.J. Burggraaf, *Solid State Ionics* **58**, 33 (1992).
- [3] B.A. Boukamp, B.A. van Hassel, I.C. Vinke, K.J. de Vries and A.J. Burggraaf, *Electrochimica Acta* **38**, 1817 (1993).
- [4] B.A. Boukamp, I.C. Vinke, K.J. de Vries and A.J. Burggraaf, eds B. Scrosati, A. Magistris, C.M. Mari and G. Mariotto, *NATO ASI Series, Series E: Appl. Sci.* Vol. **250** (Kluwer Academic, Dordrecht, 1993) pp 167-180.
- [5] I.C. Vinke, B.A. Boukamp, K.J. de Vries and A.J. Burggraaf, *Solid State Ionics* **51**, 249 (1992).
- [6] B.A. Boukamp, *Solid State Ionics* **18-19**, 136 (1986) & **20**, 31 (1986).

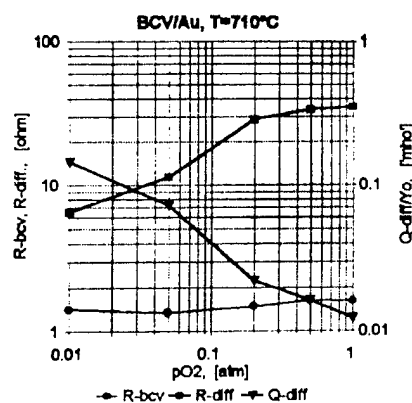


Fig. 2  $pO_2$  dependence of the major diffusion element parameters. The electrolyte resistance is presented for comparison.

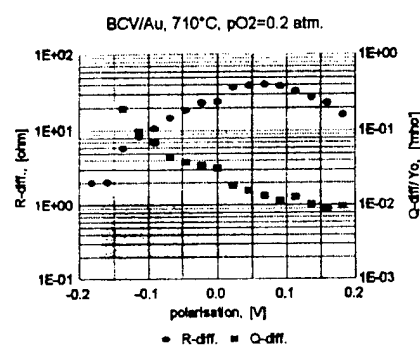


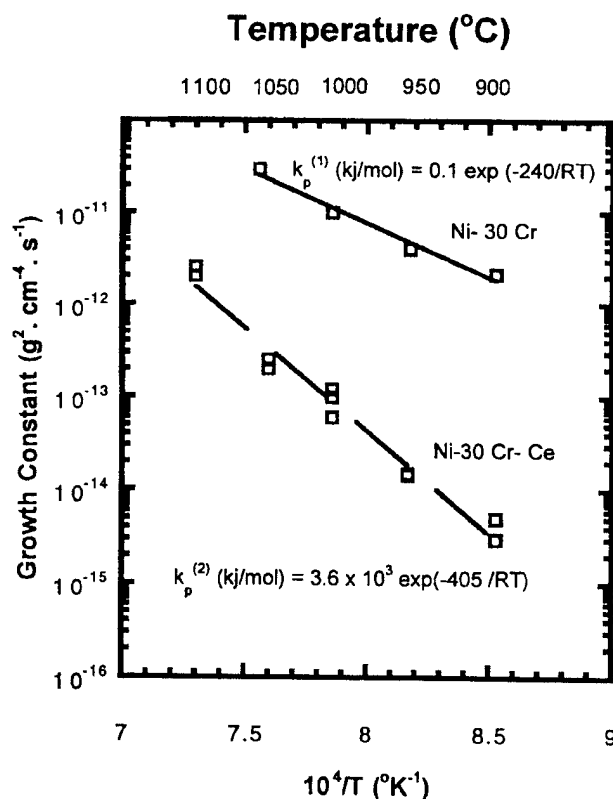
Fig. 3 Polarisation dependence of the major dispersion elements,  $R_{diff}$  and  $Q_{diff}$  for the Au-electrode.

# IONIC TRANSPORT THROUGH Cr<sub>2</sub>O<sub>3</sub> FILMS

T.A. Ramanarayanan, R.A. Petkovic and J.D. Mumford  
Exxon Research and Engineering Company  
Route 22 East, Annandale, NJ 08801, USA

In designing corrosion resistant alloys for high temperature service, protection against corrosion is generally achieved through the formation of a ceramic oxide film on the alloy surface. Three properties are critical for such oxide films to carry out their function; excellent adherence to the substrate alloy, slow transport rates of ionic species and finally high thermodynamic stability over a range of temperatures and chemical compositions of corrosive environments.

Cr<sub>2</sub>O<sub>3</sub> films provide the basis for corrosion protection in a number of Fe-based and Ni-based high temperature alloys. In the present paper, results of research carried out in the author's laboratory on the transport properties of chromium oxide are presented. The model systems used in the investigation consisted of pure Ni - Cr alloys as well as Ni - Cr - Ce and Ni - Cr - Y alloys containing very small concentrations of Ce or Y. Cr<sub>2</sub>O<sub>3</sub> films were grown on the alloy surface in CO/CO<sub>2</sub> mixtures of well defined oxygen partial pressure at temperatures ranging from 900 - 1125°C. The growth kinetics of the films was determined thermogravimetrically. Inert markers were used to infer the mode of growth of the oxide film formed on the different model alloys. In agreement with previous investigations [1-3], the oxide film formed on the Ni-30 Cr alloy grew by the outward migration of chromium. On the other hand, in the alloys containing Y or Ce, the oxide film grows by the inward migration of oxygen.





As shown in the figure, the presence of Ce in the alloy decreases the growth rate of  $\text{Cr}_2\text{O}_3$  by one to two orders of magnitude depending on the temperature[4]. Similar effects have been observed in the yttrium containing alloy[5].

Investigations of the chromium oxide film by transmission electron microscopy have revealed that Ce as well as yttrium dope into the film during oxide growth. A point defect analysis of the growth kinetics indicates that in undoped chromium oxide chromium interstitials are the predominant defects in agreement with previous studies by Kofstad and Lillerud[6]. Our analysis further shows that in the case of  $\text{Cr}_2\text{O}_3$  films doped by Y or Ce, oxygen vacancies are the main migrating species.

### References

1. C.S. Giggins and F.S. Pettit, *Met. Trans.* **2**, 1071 (1971)
2. J. Stringer, B.A. Wilcox and R.I. Jaffee, *Oxid. Metals*, **5**, 11 (1972)
3. D.P. Whittle and J. Stringer, *Phil. Trans. R. Soc. London, Ser. A*, **295**, 309 (1980)
4. N. Patibandla, T.A. Ramanarayanan and F. Cosandey, *J. Electrochem. Soc.*, **138**, 2176 (1991)
5. T.A. Ramanarayanan and R. Petkovic-Luton, *Ber. Bunsen-Ges. Physik. Chem.*, **89**, 402 (1985)
6. P. Kofstad and K.P. Lillerud, *J. Electrochem. Soc.*, **127**, 2410 (1980)

## SCANDIA – ZIRCONIA ELECTROLYTES FOR INTERMEDIATE TEMPERATURE SOLID OXIDE FUEL CELL OPERATION

S.P.S. Badwal and F.T. Ciacchi  
Ceramic Fuel Cells Limited

170 Browns Road, Noble Park, Vic 3174 Australia

A shift in the operating temperature of solid oxide fuel cells (from 1000°C down to around 800°C) would result in an increase in the cell stability (low degradation of component performance) and allow the use of cheaper materials such as stainless steel for interconnects. However, better electrolyte and electrode materials are required to maintain the high temperature performance. Thus, scandia - zirconia materials are a candidate electrolyte for use in intermediate temperature (700-850°C) solid oxide fuel cells because of their high ionic conductivity compared with yttria - zirconia electrolyte materials.

In this study conductivity of several compositions in the scandia – zirconia system ( $\text{Sc}_2\text{O}_3$  content between 7 and 11 mol%) have been investigated as a function of temperature and time at the nominal fuel cell operating temperature of 850°C. For comparison, stability of electrolyte compositions was also studied at 1000°C by monitoring conductivity degradation as a function of time (four-probe DC technique). The contribution of grain boundary impedance was determined in as-sintered and annealed specimens (850 and 1000°C) with electrochemical impedance spectroscopy. The phase assemblage was determined with X-ray diffraction.

All compositions showed conductivity degradation as a function of time both at 850 and 1000°C, however, it was much lower in compositions containing 10 and 11 mol%  $\text{Sc}_2\text{O}_3$  especially at 1000°C. The maximum conductivity was observed for the 9 mol%  $\text{Sc}_2\text{O}_3$  –  $\text{ZrO}_2$  composition both at 850 and 1000°C. The 10 and 11 mol%  $\text{Sc}_2\text{O}_3$  –  $\text{ZrO}_2$  compositions showed the presence of an ordered phase ( $\text{Sc}_2\text{Zr}_7\text{O}_{17}$  also known as the beta-phase) at room temperature. Clearly hysteresis loops were observed in the conductivity – temperature plots around 500-600°C due to the transformation of the low conducting beta-phase to high conductivity cubic-phase on heating and the reverse on cooling.

The contribution from the grain boundary resistivity was relatively small for all specimens studied. Annealing at both 850 and 1000°C, in general, led to an increase in both grain boundary and volume or lattice resistivities.

# FLUORIDE ION CONDUCTOR $\text{ASn}_2\text{F}_5$ STUDIED BY $^{119}\text{Sn}$ , $^{19}\text{F}$ NMR AND X-RAY DIFFRACTION

Koji Yamada, Keiji Saisho, Hiroshi Ohki and Tsutomu Okuda  
Department of Chemistry, Faculty of Science, Hiroshima University,  
Kagamiyama 1-3, Higashi-Hiroshima 739-8526, Japan

Halogeno-complexes containing lower oxidation states of Ge, Sn, Sb and Bi provide us many interesting phenomena, such as characteristic phase transition, electronic conductivity and ionic conductivity.[1, 2] This is mainly due to the bonding property of these hypervalent compounds, i.e., each X-M-X bond in the octahedral environment is orbital deficient and hence shows a characteristic *trans* effect. In this study we have synthesized a series of  $\text{ASn}_2\text{F}_5$  (A= $\text{NH}_4$ , Na, K, Rb and Cs) crystalline samples and investigated the mechanism for the anionic diffusion on the basis of the hypervalent property of these samples. High anion conductivities for  $\text{ASn}_2\text{F}_5$  have been already reported by measuring  $^{19}\text{F}$  NMR.[3] Figure plots  $^{119}\text{Sn}$  NMR  $T_1$  for  $\text{KSn}_2\text{F}_5$ ,  $\text{RbSn}_2\text{F}_5$  and  $\text{CsSn}_2\text{F}_5$  against  $1/T$ . K and Rb salts, which were reported to be excellent anionic conductors having layer structures, showed asymmetric minima.  $^{119}\text{Sn}$  NMR spectrum for K or Rb salt changed to a sharp singlet with no chemical shift anisotropy above 400K.  $^{19}\text{F}$  NMR also changed from an asymmetric broad spectrum over 80kHz to a sharp singlet above 300K at 6.4T. These findings suggest that the all fluoride ions in the crystal contribute to the conductivity and their motions average out both the dipole-dipole and the chemical shift anisotropy.

[1] K. Yamada et al, *Z. Naturforsch.*, **51a**, 739 (1996).

[2] K. Yamada et al, *Solid State Ionics*, **79**, 152 (1995).

[3] J. P. Battut et al, *Solid State Ionics*, **22**, 247 (1987).

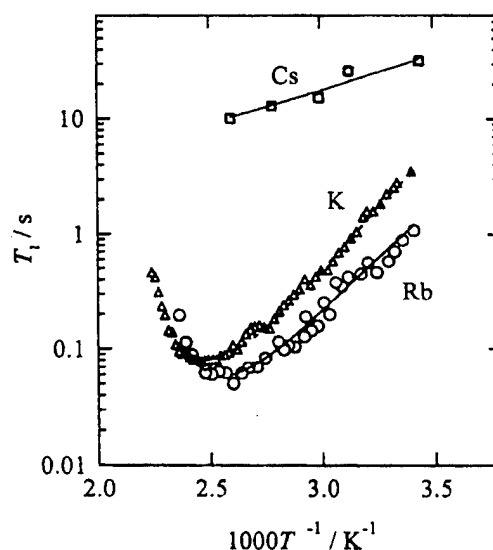


Fig. 1  $^{119}\text{Sn}$  NMR  $T_1$  for  $\text{ASn}_2\text{F}_5$ .

## PROCESSES AT THE INTERFACE BETWEEN FLUORIDE SOLID ELECTROLYTE AND METALS

M. S. Turaeva, I. A. Pegova,

*Research Institute of Agrophysics, Grazhdanskij pr. 14, 195220 St. Petersburg, , Russia*

S. A. Kot, O. V. Glumov, I. V. Murin,

*St. Petersburg State University, Universitetskij pr. 2, 198904 St. Petersburg, Russia*

Reactions at the interface between fluoride solid electrolyte and metals Ag, Sn and Bi are studied by voltammetry. Tysonite-type single crystals  $\text{LaF}_3$  and  $\text{CeF}_3$  doped with  $\text{Sr}^{2+}$  (5 mol.%) was used as solid electrolyte. It is revealed, that in the two-electrode clamp cell  $\text{Sn, SnF}_2 | \text{LaF}_3 | \text{Me}$  (where Me - the working electrode,  $\text{Sn, SnF}_2$  - the reference electrode) at anodic polarization of the  $\text{LaF}_3 | \text{Me}(+)$  contact developed solid-phase processes with formation compounds, which one at cathode potential sweep were characterized by single-peak curves (Fig. 1.). Influencing technology of preparation  $\text{Sn, SnF}_2$  electrode on response of the cell is revealed, and the voltammetric control of the properties of electrode is offered. Influencing generation potential on nature of the curves of cathodic decomposition is established. At the optimal generation potential the cathodic peak current (obtained at potential sweep rate  $0.01 \text{ Vs}^{-1} \div 0.05 \text{ Vs}^{-1}$  from stationary potential) had linear dependence from  $V^{1/2}$  (Fig. 2., the correlation coefficient  $R$  - 0.992 for Ag, 0.998 for Sn, 0.996 for Bi) and the quantity of charge  $Q_a$  consumed on generation of compounds. The peak potential corrected for the ohmic polarization of the contact was independent of the potential sweep rate. In this case, the standard potentials of the anodic generated electrodes determined from emfs of the cells (with Ag  $E_{\text{st}} = 1.3 \text{ V}$ , with Sn  $E_{\text{st}} = 0.054 \text{ V}$ , with Bi  $E_{\text{st}} = 0.39 \text{ V}$ ) are close to the standard potentials calculated from  $\Delta G_{298}^\circ (\text{MeF}_n)$ .

At the  $\text{CeF}_3 | \text{Me}$  interface (where Me - Ag and Bi) solid-phase reactions during experiment were replaced by reactions of  $\text{O}_2$  reduction (at the oxygen partial pressure  $p_{\text{O}_2} = 0.21 \text{ atm}$ ), and the stationary potential shifted toward at the more negative values ( $\Delta E \cong 1 \text{ V}$ ). Reactions of  $\text{O}_2$  reduction were inhibited at the presence  $\text{N}_2$ . The precipitation of oxygen reactions at the presence of oxides at the surface of metal electrodes and the decrease of the hysteresis in the moist air are revealed.

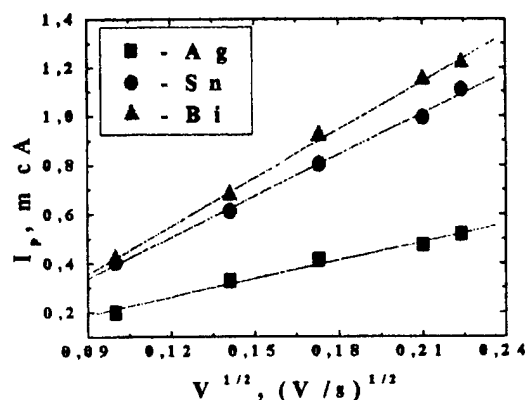
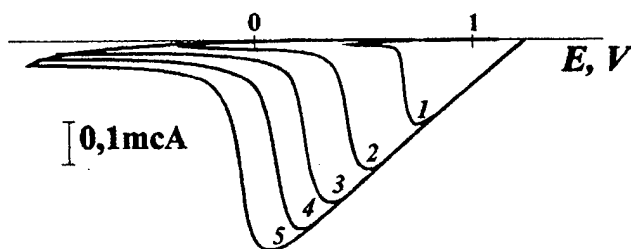


Fig. 1. Potentiodynamic cathodic current-potential curves of decomposition  $\text{AgF}$ . Potential sweep rate  $V \text{ (Vs}^{-1}\text{)}$ : (1) 0.01, (2) 0.02, (3) 0.03, (4) 0.04, and (5) 0.05.

Fig. 2. Dependence of cathodic peak current vs. potential sweep rate.

## STUDY ON THE MANUFACTURE OF ZIRCONIA TUBES III. THE SLIP CASTING PROCESS

Suntai Qiu, Jiayin Xu and Changgui Shao  
China Institute of Atomic Energy, P. O. Box 275(29)  
Beijing 102413, China

Zirconia tubes used for oxygen sensors should have characteristics of high electric conductance, high mechanic strength, high thermal shock resistance, etc. The green casts made by slip casting have smaller grain size and more homogeneous microstructure compared to those made by isostatic pressing. The stability of the suspension slip is the key factor to determine the microstructure of the product. In this paper,  $\text{ZrO}_2\cdot\text{Y}_2\text{O}_3\cdot\text{Gd}_2\text{O}_3$  slip with average grain size of  $1\mu\text{m}$  was studied. The pH value of suspension slip, the concentration of dispersing agent (Poly acrylic acid, PAA) and gum Arabic influence on the stability and mobility of the slip. High solid volume loading in the suspension fluid ( $\sim 70\text{vol}\%$ ) was obtained by adjusting the prominent factors, e.g. concentration, viscosity and Zeta potential of the slip, which results in high green density ( $3.80\text{ g/cm}^3$ ). Optimizing  $\text{ZrO}_2\cdot\text{Y}_2\text{O}_3\cdot\text{Gd}_2\text{O}_3$  suspension fluid to have good properties of distribution, sedimentation volume and a low viscosity enhances the particulate diffusion in the process of sintering. The microstructure of the sintering products can also be much improved. In addition, a reinforced plaster mold with serve life of 40~50 times designed for this optimized slip and the slip casting/sintering process were described. The zirconia tubes produced by this method have high thermal shock resistance, low electrical resistance, and high density.

## STUDY OF THE IMPACT OF CALCINATION TEMPERATURE ON GRAIN SIZE OF CO-PRECIPITATED YSZ POWDER

Jeremy Rutman and Ilan Riess  
Physics Department  
Technion-Israel Institute of Technology  
Haifa 32000, Israel

Co-precipitation followed by thermal decomposition is a simple route to well-mixed fine-grained oxide mixtures<sup>1</sup>. This method was used to synthesize fine-grained powders of Yttrium-stabilized Zirconium, and grain size vs. calcination temperature was studied using X-ray crystallography.

Yttrium-stabilized Zirconium ( $Y_2O_3$ )<sub>1</sub>( $ZrO_2$ )<sub>9</sub> was coprecipitated from an aqueous solution (.1 molar) of corresponding nitrates. Upon addition to a basic (~150 ml  $NH_3OH$  in 700 ml water) solution of .4 molar ammonium oxalate, insoluble Zr- and Y-oxalates precipitated immediately, forming a white suspension. After drying, portions of the resulting gel were calcined at a variety of temperatures, and crystallographic X-ray measurements were subsequently made. From these the dependence of grain-size upon calcination temperature was determined, by comparing peak-width broadening. Minimum grainsize was found at 620 degrees C. (See figure below.)

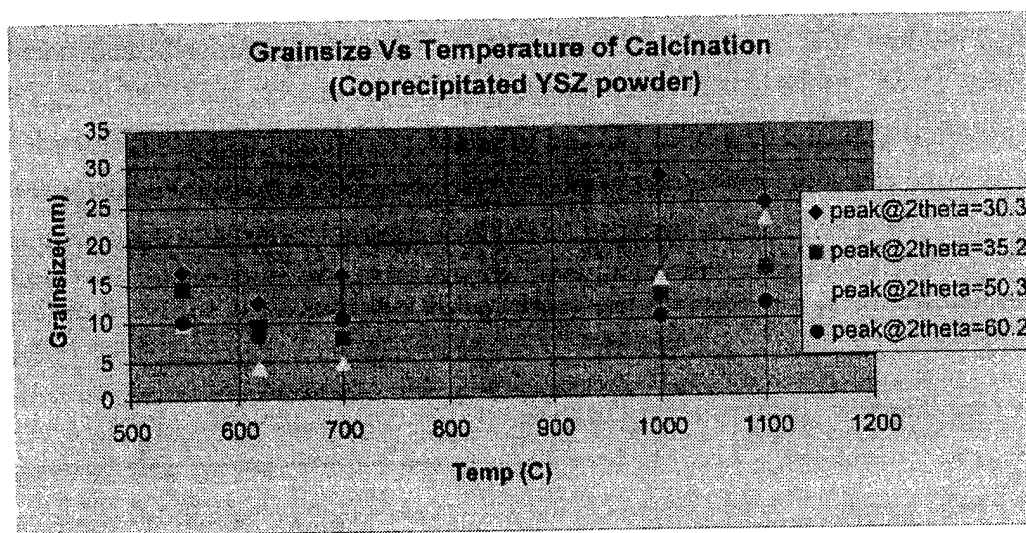
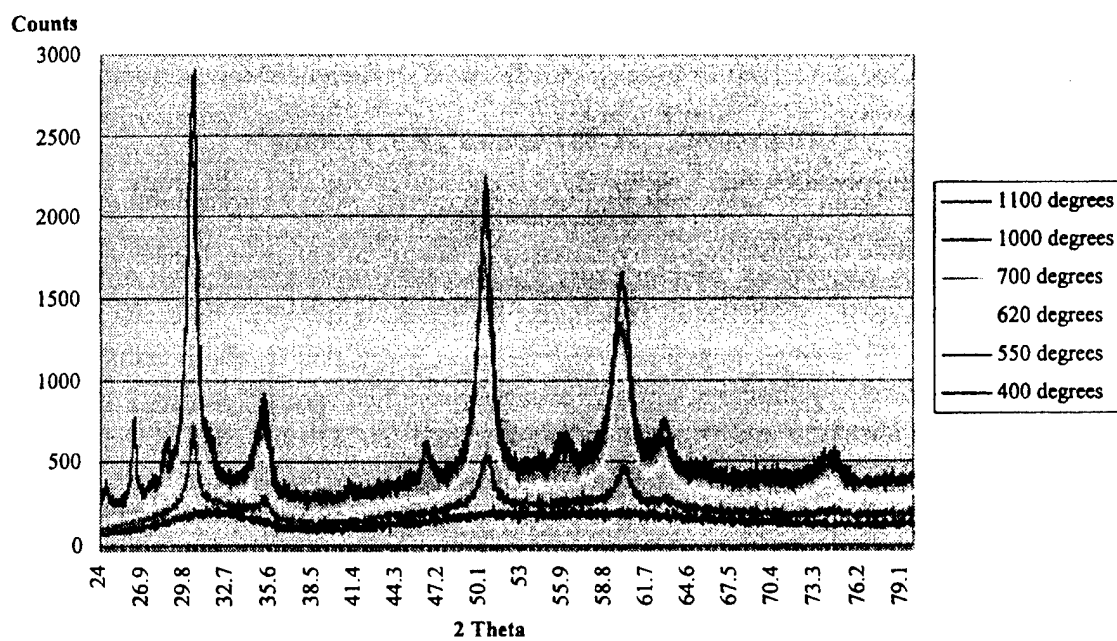


Figure 1: Grainsize vs. temperature of calcination

A white gas (presumably the evaporating oxalate components) escaped the samples from about 350 to 400 degrees, and a color change was also observed ranging from dark brown below 400 to white at 620 and above. The spectrum of the sample calcined at 400 degrees was very broad indicating either extremely small grain sizes, incomplete oxalate decomposition, or both. Further study of grain size dependence upon time of calcination and reagent concentrations are intended.

<sup>1</sup>A.. Overs, I. Riess, Journal of the American Ceramic Society 65, (12) 1982

## X-Ray Crystallographic Data

Figure 2: X-Ray Spectra (Cu K- $\alpha$ )

## FAST IONIC CONDUCTIVITY OF RARE EARTH TRIFLUORIDES WITH ORTHORHOMBIC AND TYSONITE STRUCTURES.

V. Tmrovcová<sup>1</sup>, E.A. Krivandina<sup>2</sup>, P.P. Fedorov<sup>2</sup><sup>1</sup>Faculty of Materials Science and Technology, Slovak University of Technology, SK-91724 Trnava, Slovakia<sup>2</sup>Shubnikov's Institute of Crystallography, Russian Academy of Sciences, Moscow, 117333, Russia

Rare earth trifluorides crystallize in three structural types: the trigonal tysonite  $\text{LaF}_3$  structure, orthorhombic  $\beta\text{-YF}_3$  structure and trigonal  $\alpha\text{-YF}_3$  structure (stable only at high temperatures). The tysonite structure is typical for rare earth trifluorides with large cations ( $\text{La}^{3+}\text{-Nd}^{3+}$ ). The rare earth trifluorides with smaller cations ( $\text{Sm}^{3+}\text{-Lu}^{3+}, \text{Y}^{3+}$ ) adopt orthorhombic structural type at low temperatures. However, only in some of them ( $\text{TbF}_3, \text{DyF}_3, \text{HoF}_3$ ), this structural type is stable up to melting temperature. At high temperatures, the  $\text{SmF}_3, \text{EuF}_3, \text{GdF}_3$  transform to the tysonite structure, and the  $\text{ErF}_3, \text{TmF}_3, \text{YbF}_3, \text{LuF}_3, \text{YF}_3$  transform to the trigonal  $\alpha\text{-YF}_3$  structure. As to grow the  $\beta\text{-YF}_3, \beta\text{-GdF}_3$  and  $\beta\text{-ErF}_3$  single crystals, it is necessary to undercool the melt to the temperature of metastable melting of the  $\beta$ -modification. As to obtain dimorphous rare earth trifluorides in the orthorhombic form, a preparation temperature lower than that of the  $\alpha \rightarrow \beta$  phase transition is required. Therefore, a directional solidification of eutectic composites and ceramic technology enable to prepare dimorphous rare earth trifluorides in their orthorhombic form. The choice of orthorhombic rare earth trifluorides is enlarged by using the  $\text{RF}_3\text{-R}'\text{F}_3$  ( $\text{R}, \text{R}' = \text{rare earth elements}$ ) isomorphous substitution with the mean cationic radius close to that of the  $\text{Tb}^{3+}$  ion. However, because heterovalent doping destabilizes the orthorhombic structure, it is impossible to enhance the concentration of defects and the ionic conductivity of orthorhombic rare earth trifluorides by heterovalent doping.

The fast fluoride ion conductivity of the tysonite-structured trifluorides is well known. The high ionic conductivity is observed also in the high-temperature  $\alpha\text{-YF}_3$  modification of rare earth trifluorides. The structural similarity of the tysonite-structured and  $\beta\text{-YF}_3$  structured crystals leads to an assumption that a fast fluoride ion mobility takes place in the orthorhombic  $\beta\text{-YF}_3$  structured crystals as well. The  $^{19}\text{F}$  NMR spectra indicate the closeness of the fluoride ion motion characteristics in the tysonite ( $\alpha\text{-SmF}_3$ ) and orthorhombic ( $\beta\text{-SmF}_3$ ) modifications because the  $\beta \rightarrow \alpha$  phase transition in  $\beta\text{-SmF}_3$  crystals does not affect the width of spectral lines.

In the  $\text{RF}_3\text{-MF}_2$  systems ( $\text{M} = \text{alkali earth element}$ ), broad regions of fluorite-structured solid solutions (up to 50 m/o  $\text{RF}_3$ ) and of tysonite structured solid solutions (up to 20 m/o  $\text{MF}_2$ ) are observed. The high concentration of charge compensating defects in both concentrated nonstoichiometric solid solutions results in their enhanced ionic conductivity.

The aim of this work is 1/ to examine the fluoride ion conductivity and dielectric response, 2/ to study the anisotropy of the properties, and 3/ to elucidate the mechanism of the fluoride ion transport in orthorhombic (stoichiometric) and tysonite-structured (both stoichiometric and nonstoichiometric) rare earth trifluorides, which are prepared as single crystals, eutectic composites and ceramics.

The transparent orthorhombic  $\text{ErF}_3, \text{TbF}_3, \text{HoF}_3$  and  $\text{YF}_3$  are prepared by the Bridgman method in fluorinating atmosphere. The oxygen content in samples does not exceed 0.01-0.005 w/o. The  $\text{ErF}_3$  and  $\text{YF}_3$  single crystals are prepared in a "needle-like" form because their growth requires a strong undercooling of the melt. For growing of the  $\text{Gd}_{0.5}\text{Y}_{0.5}\text{F}_3$  and  $\text{Gd}_{0.3}\text{Er}_{0.7}\text{F}_3$



single crystals, the Czochralski method is used. The  $\text{MgF}_2$  -  $\text{GdF}_3$  eutectic composite, which contains 52 m/o  $\beta$ - $\text{GdF}_3$ , are prepared using the Bridgman method of directional solidification. The  $\text{LiF-SmF}_3$  eutectic composite (25 m/o  $\beta$ - $\text{SmF}_3$ ) is prepared using the Bagdasarov method of horizontal directional solidification in a "sheet-like form". The ceramic  $\text{ErF}_3$  sample was prepared in the fluorinating atmosphere.

The tysonite-structured  $\text{LaF}_3$ ,  $\text{NdF}_3$ ,  $\text{PrF}_3$  and  $\text{LaF}_3\text{:SrF}_2$  (0 - 15 m/o  $\text{SrF}_2$ ) single crystals are prepared by using the Stockbarger method in He, growth rate of 3 mm/h. All fluoride reagents are purified in fluorizing atmosphere at high temperatures. An oxygen scavenger, 5 m/o  $\text{PbF}_2$ , is added to the melt. The  $\text{SrF}_2$  content in samples is checked by measurements of the lattice parameters of samples.

Electrical and dielectric properties are measured on samples with painted silver contacts, in dry Ar up to 650 °C, at 1 Hz - 1 MHz. The bulk ionic conductivity and static permittivity are determined by using the impedance or modular analyses, respectively. From the frequency dependence of the conductivity, the hopping rate of fluoride ions is calculated. Modeling of the conduction paths is made by using the POWCELL program. The anisotropy of the properties is studied on  $\text{Gd}_{0.5}\text{Y}_{0.5}\text{F}_3$  and  $\text{PrF}_3$  single crystals (in both cases the anisotropy of the conductivity is negligible but the anisotropy of the permittivity is significant). The other crystals are measured in an arbitrary direction and/or perpendicularly to the cleavage plane.

The temperature dependences of the bulk ionic conductivities of various orthorhombic rare earth trifluorides are very close one to another. The conductivity at 500 K and the conduction activation enthalpy are equal to  $1.1(4) \times 10^{-5}$  S/cm and 0.70(3) eV, respectively. The conductivities of the "needle-like" crystals, composites and ceramics are slightly lower. The  $\beta \rightarrow \alpha$   $\text{SmF}_3$  phase transition is found at 496(6) °C. The conductivity of the orthorhombic rare earth trifluorides lags far behind the conductivity of nominally pure tysonite-structured ones. Moreover, in tysonite-structured  $\text{LaF}_3\text{:SrF}_2$  solid solutions, the maximum conductivity and minimum activation energy is observed at 7 m/o  $\text{SrF}_2$ .

The Schottky defects are supposed to form the dominant intrinsic disorder in both structures. An enhanced amount of these defects is created by heterovalent doping in tysonite-structured crystals and it is frozen-in during preparation of the orthorhombic crystals. A vacancy mechanism of fluoride ion migration is supposed in both structures. As to understand the cause of the great difference between the conductivities of the orthorhombic  $\beta$ - $\text{YF}_3$  structured rare earth trifluorides and those of the tysonite structured ones, a careful analysis of the  $\beta$ - $\text{YF}_3$  structure is performed.

The  $\beta$ - $\text{YF}_3$  structure consists of plane layers, which are perpendicular to the b axis and contain both cations and anions. In these planar mixed layers, the cations form a distorted hexagonal network and all the fluoride ions are in equivalent positions ( $\text{F}_1$ ). The other type of fluoride ions ( $\text{F}_2$ ) forms puckered layers in-between the plane mixed layers. The shortest interionic distances occur between the  $\text{F}_2$  ions and the most probable jumps of the mobile  $\text{F}_2$  ions are towards a neighbouring vacant  $\text{F}_2$  position. Within the  $\text{F}_1$  network, the shortest hopping distance of fluoride ions is perpendicular to the mixed planar layer but the hopping distance is very large (3.56 Å in  $\beta$ - $\text{YF}_3$ ). Therefore, this type of fluoride ion motion, which contributes substantially to the conductivity in the tysonite structured fluorides, is improbable in the  $\beta$ - $\text{YF}_3$  structured rare earth trifluorides.

CONDUCTIVITY RELAXATION PHENOMENA OF THE OXIDE ION  
CONDUCTOR  $\text{Zn}_{2-2x}\text{Ti}_{1+x}\text{O}_4$

Shigeomi Takai, Yasushi Asahi and Takao Esaka

Faculty of Engineering, Tottori University, Koyama, Tottori 680-0945, Japan

The oxide ion conductivity of  $\text{Zn}_2\text{TiO}_4$  at high temperatures was enhanced by substituting tantalum as  $\text{Zn}_{2-2x}\text{Ti}_{1-x}\text{Ta}_x\text{O}_4$  or changing the cation ratio Zn / Ti as  $\text{Zn}_{2-2x}\text{Ti}_{1+x}\text{O}_4$  to make cation vacancies<sup>1)</sup>. We have already measured the complex impedance for tantalum-substituted  $\text{Zn}_2\text{TiO}_4$ . The frequency dependence of the imaginary part of the electric modulus  $M''$  for cubic phase in the lower tantalum concentration region was observed as a single peak, while that for tetragonal phase in the higher concentration region represents the double maxima. We therefore assumed that the tetragonal phase had two types of relaxation of the conduction oxide ions, suggesting that another conduction path and/or the intermediate site were formed in the tetragonal phase in comparison with that of cubic phase. In the present study, to clarify the relationship among these phases and the relaxation phenomena, the frequency dependence of the impedance for another type of the cation deficient compounds,  $\text{Zn}_{2-2x}\text{Ti}_{1+x}\text{O}_4$ , have been measured and the conductivity relaxation property was considered.

$\text{Zn}_{2-2x}\text{Ti}_{1+x}\text{O}_4$  samples were prepared by the solid state reaction method from the stoichiometric mixtures of ZnO (3N) and  $\text{TiO}_2$  (anatase-form, 3N). From the powder X-ray diffraction patterns, those obtained samples of  $\text{Zn}_{2-2x}\text{Ti}_{1+x}\text{O}_4$  with the compositions  $x \leq 0.15$  were found to form the cubic phase. The typical size of the sample disc was 10 mm in diameter and 1 mm in thickness. Platinum paste was applied for the electrode and the precision LCR meter (HP4284A) was employed for the impedance measurements in the frequency range from 20 Hz to  $10^6$  Hz. Measurements were carried out up to 600 °C with the heating and cooling rate of 0.6 °C min<sup>-1</sup>. The obtained impedance data were analyzed by the electric modulus formula,  $M^* = 1 / \epsilon^* = M' + i M''$ .

The measured frequency dependence of the modulus for the  $\text{Zn}_{2-2x}\text{Ti}_{1+x}\text{O}_4$  ( $x = 0.10$ ) was plotted in Fig. 1. The  $M''$  profile represented the double peak shape, which resembled that of the tetragonal phase of tantalum-substituted compounds, while the present sample showed the cubic symmetry. As both of the peak frequencies varied systematically with increasing  $x$  in the formula, this double peak profile was supposed to be intrinsic one. Assuming that the conductivity relaxation phenomena are essentially related to the hopping of oxide ions, the local structure around these ions is supposed to be similar to the tetragonal phase of highly tantalum-

substituted compounds, whereas the long range nature is the cubic one as observed by X-ray diffraction.

Fig. 2 shows the both types of the activation energies obtained from Arrhenius plots of the relaxation frequencies, where the open and closed circles denote those for lower and higher frequency peaks, respectively. Comparing with that of higher temperature conductivity, plotted as triangles, the activation energy of the lower frequency peak is close to that of conductivity. This suggests that the lower frequency peak is mainly related to the long range ionic motion.

#### Reference

- 1) T. Esaka, T. Ikebe and M. Kamata, *Solid State Ionics*, **76** (1995) 237.

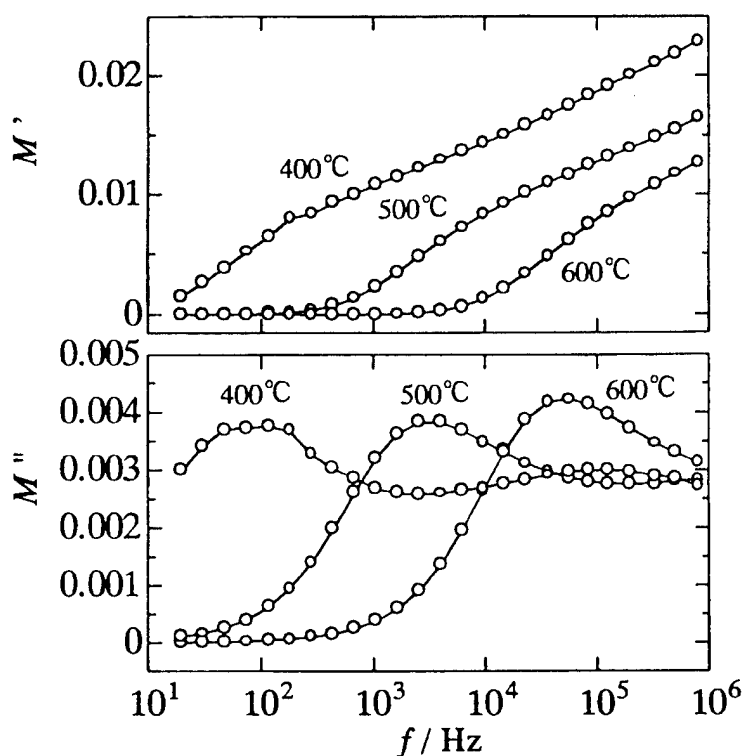


Fig. 1 Frequency dependence of electric modulus for  $\text{Zn}_{1.8}\text{Ti}_{1.1}\text{O}_4$  ( $x = 0.10$ ) at various temperatures.

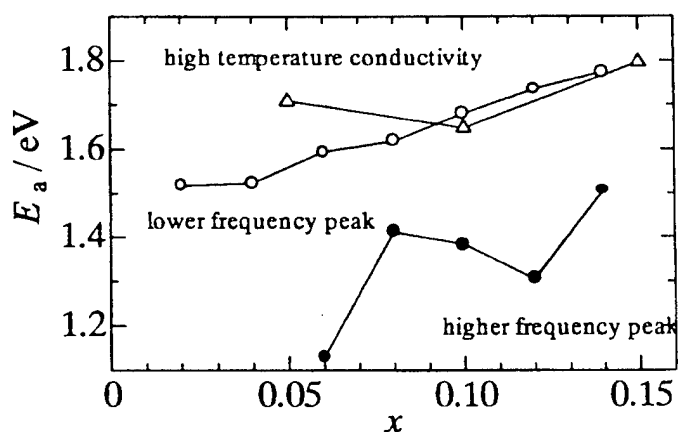


Fig.2 Activation energies of conductivity and relaxation for  $\text{Zn}_{2-2x}\text{Ti}_{1+x}\text{O}_4$ .

## BISMUTH URANATE OXIDE ANION CONDUCTORS

Rose-Noëlle Vannier<sup>a</sup>, Odile Théry<sup>a</sup>, Christophe Kinowski<sup>a</sup>, Marielle Huvé<sup>a</sup>, Gustaaf Van Tendeloo<sup>b</sup>, Emmanuelle Suard<sup>c</sup> and Francis Abraham<sup>a</sup>

<sup>a</sup> Laboratoire de Cristallographie et Physicochimie du Solide, UPRESA CNRS 8012, ENSCL-USTL, B.P. 108, 59652 Villeneuve d'Ascq Cedex, France

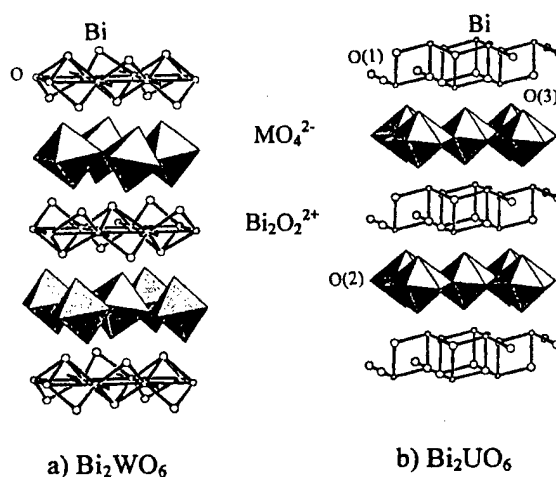
<sup>b</sup> EMAT, University of Antwerp (RUCA), Groenenborgerlaan 171, B-2020 Antwerp, Belgium

<sup>c</sup> Institut Laue Langevin, Avenue des Martyrs, BP 156, 38042 Grenoble Cedex 9, France

Among the bidimensional oxide anion conductors, the BIMEVOX family compounds led to an increasing interest during the last ten years [1]. They derive from  $\text{Bi}_2\text{VO}_{5.5}$  by partial substitution for vanadium with numerous metals. Their average structure is related to that of the first member of the Aurivillius family i.e.  $\text{Bi}_2\text{WO}_6$ . It consists of  $\text{Bi}_2\text{O}_2^{2+}$  sheets alternating with  $(\text{VO}_{3.5}\square_{0.5})^{2-}$  oxygen deficient perovskite slabs. The layer structure and the presence of oxygen vacancies in the perovskite layers lead to high oxide anion conduction.

In contrast,  $\text{Bi}_2\text{WO}_6$  that contains no oxygen vacancy, is a very bad conductor ; its conduction properties are however widely enhanced by partial substitution for  $\text{W}^{\text{VI}}$  with  $\text{Ta}^{\text{V}}$  or  $\text{Nb}^{\text{V}}$  [2].

The bismuth uranate  $\text{Bi}_2\text{UO}_6$ , is another layer compound which presents very interesting conduction properties [3]. A.S. Koster *et al* described its structure as a stacking of slabs of edge-sharing  $\text{UO}_8$  polyhedra sandwiched between  $\text{Bi}_2\text{O}_2^{2+}$  sheets [4]. It is compared to that of  $\text{Bi}_2\text{WO}_6$  in the following figure. Although the formulation of the  $\text{Bi}_2\text{O}_2^{2+}$  layers is the same in both compounds, they are structurally very different. The first, found in Aurivillius family, are built up from a plane of oxygen with bismuth atoms alternately up and down, whereas the second can be viewed as double  $\text{BiO}$  sheets.



N. Bonanos suggested this material to be a two dimensional oxide anion conductor but did not manage to demonstrate it [3].

Owing to the similarities in the structures and properties of  $\text{Bi}_2\text{VO}_{5.5}$  or  $\text{Bi}_2\text{WO}_6$  on one hand and  $\text{Bi}_2\text{UO}_6$  on the other, the  $\text{Bi}_2\text{VO}_{5.5}\text{-Bi}_2\text{UO}_6$  and  $\text{Bi}_2\text{WO}_6\text{-Bi}_2\text{UO}_6$  systems have been investigated. Two solid solutions with BIMEVOX and  $\text{Bi}_2\text{WO}_6$  structural types have been evidenced respectively. However  $\text{V}^{\text{V}}$  and  $\text{W}^{\text{VI}}$  did not substitute for uranium in the bismuth uranate [5].

Consequently, several other attempts for doping this uranate were carried out. Zirconium led us to the stabilization of a  $\text{Bi}_2\text{U}_{1-x}\text{Zr}_x\text{O}_{6-x}$  solid solution which has been characterized by X-ray diffraction and electrical measurements. Powder neutron diffraction combined with electron microscopy enabled us to confirm the bidimensional electrical character of these materials and to suggest preferential migration pathways.

- [1] F.Abraham, J.C.Boivin, G.Mairesse and G.Nowogrocki, Solid State Ionics **40-41**, 934 (1990)
- [2] N.Baux, R.N.Vannier, G.Mairesse, G.Nowogrocki, Solid State Ionics **91**, 243-248 (1996)
- [3] N.Bonanos, Mat. Res. Bull, Vol **24**, 1531-1540 (1989)
- [4] A.S.Koster, J.P.P.Renaud and G.D.Rieck, Acta Cryst **B31**, 127 (1975)
- [5] O.Théry, R.N.Vannier, C.Dion, F.Abraham, Solid State Ionics **90**, 105 (1996)

# BISMUTH-BASED OXIDE ION CONDUCTORS RELATIONSHIP BETWEEN DIMENSIONALITY, THERMAL STABILITY AND IONIC CONDUCTIVITY

Rose-Noëlle VANNIER, Jean-Claude BOIVIN, Guy NOWOGROCKI and Gaëtan MAIRESSE  
Laboratoire de Cristallochimie et Physicochimie du Solide, UPRESA CNRS 8012,  
ENSCL-USTL, BP 108, 59652 Villeneuve d'Ascq Cedex, France

$\text{Bi}_2\text{O}_3$  based solid electrolytes are well known for their high oxide ion conduction properties. Among these materials, the BIMEVOX family particularly generated an increasing interest during the last ten years, following the initial paper of Abraham *et al.* on BICUVOX [1].

Bismuth based oxide anion conductors are very exciting materials. Their exceptionally high conductivity is due to specific structural features related to the presence of  $\text{Bi}^{3+}$  cations. The stereochemically active non bonding electronic pairs of these cations are responsible for the very loose and dynamically deformable structures which are particularly suitable for anion migration.

Depending on their structural dimensionality, these materials can be classified in three groups.

*Three-dimensional oxide ion conductors* were, for a long time, the most extensively investigated bismuth-based oxides. They belong to the fluorite  $\delta$   $\text{Bi}_2\text{O}_3$  type structure and can be "stabilized" at low temperature ( $T < 730^\circ\text{C}$ ) by numerous dopants from divalent to hexavalent cations. Another example of 3D conductors is the so-called  $\beta$ -type phase in the bismuth-oxide - lead oxide system which exhibits an anti  $\alpha$ -AgI crystal structure. This structural type has also been evidenced in  $\text{Bi}_2\text{O}_3$ -CdO,  $\text{Bi}_2\text{O}_3$ -CdO-PbO,  $\text{Bi}_2\text{O}_3$ -Sb $_2\text{O}_3$ -PbO and  $\text{Bi}_2\text{O}_3$ -Ln $_2\text{O}_3$ -PbO (Ln=Gd, Dy, Tm) systems. All the chemical bonds in these materials are mainly ionic, leading to very high oxide ion conduction, but poor stability as a function of the temperature is the counterpart [2].

Three types of materials belong to the *two-dimensional oxide ion conductors group*. The first one is the rhombohedral solid solution, first obtained by partly substituting alkaline earth cations for bismuth [3]. The second is the Aurivillius-type family formulated  $(\text{Bi}_2\text{O}_2)(\text{A}_{n-1}\text{B}_n\text{O}_x)$  where  $n$  indicates the number of perovskite layers sandwiched between bismuth-oxygen sheets. It encompasses extrinsic oxide ion conductors such as  $n=1$   $\text{Bi}_2\text{WO}_6$  substituted with Nb or Ta [4],  $n=2$   $(\text{Bi}_2\text{O}_2)_2[\text{Ca}_{1-x}\text{Na}_x(\text{Nb})_2\text{O}_{7-x/2}]$  with  $x$  in the range  $0 \leq x \leq 1$  [5],  $n=3$   $(\text{Bi}_2\text{O}_2)_2[\text{Sr}_2(\text{M}_2^{\text{V}}\text{M}^{\text{III}})\text{O}_{9.5}]$  with  $\text{M}^{\text{V}}=\text{Nb}$ , Ta and  $\text{M}^{\text{III}}=\text{Al}$ , Ga [6]... and the  $\gamma\text{Bi}_4\text{V}_2\text{O}_{11}$  and related BIMEVOX phases that are intrinsic oxide anion conductors. In both rhombohedral and Aurivillius type materials, covalent two-dimensional blocks containing short Bi-O bonds alternate with predominantly ionic sheets. In both cases the nonbonding electronic  $6s^2$  lone pairs of the  $\text{Bi}^{\text{III}}$  cations are oriented toward the ionic conduction layer and strongly favor the oxide ion mobility. The third two-dimensional type derives from  $\text{Bi}_2\text{UO}_6$ . These phases are clearly bidimensional oxide ion conductors but the role of the non bonding  $6s^2$  lone pair in the conduction process is not so obvious.

The recently reported  $\text{Bi}_{26}\text{Mo}_{10}\text{O}_{69}$  compound and its derivatives constitute the first example of *monodimensional bismuth based oxide ion conductors* [7]. The structure consists of covalent  $[\text{Bi}_{12}\text{O}_{14}]_\infty$  columns characterized by short Bi-O bonds and small atomic thermal parameters connected with Mo-O species in which oxygen atoms exhibit unusual high thermal vibration. These materials are pure oxide ion conductors, their conductivity remains lower than that of the BIMEVOX materials but can be significantly increased by partial substitution for molybdenum with tungsten.

Structure dimensionality, thermal stability and ionic conductivity of the various bismuth

based oxide conductors are strongly correlated. The purpose of this paper is to underline and discuss the relationship between these criteria and to attempt to provide some useful guidelines for the synthesis of new fast oxide ion conductors.

- [1] F.Abraham, J.C.Boivin, G.Mairesse and G.Nowogrocki, Solid State Ionics **40-41**, 934 (1990)
- [2] J.C.Boivin, G.Mairesse, Chem. Mater. **10**, 2870-2888 (1998)
- [3] P.Conflant, J.C.Boivin, G.Nowogrocki, D.Thomas, Solid State Ionics **3-4**, 457 (1981)
- [4] N.Baux, R.N.Vannier, G.Mairesse and G.Nowogrocki, Solid State Ionics **91**, 243-248 (1996)
- [5] A.Q.Pham, M.Puri, J.F.Dicarlo and A.J.Jacobson, Solid State Ionics **72**, 309 (1994)
- [6] K.R.Kendall, J.K.Thomas and H.C.Zur Loye, Solid State Ionics **70/71**, 221 (1994)
- [7] R.N.Vannier, G.Maresse, F.Abraham and G.Nowogrocki, J. Solid State Chem. **122**, 394 (1996)

# MODEL OF STRUCTURAL LATTICE DISORDERING IN SUPERIONIC CRYSTALS LIKE $\text{LaF}_3$ BY THE QUASIELASTIC LIGHT SCATTERING STUDY

Aliev A. E., Krivorotov V. F., Kholmanov I. N.

Heat Physics Department, Academy of Sciences, Katartal str. 28,  
Tashkent 700135, Uzbekistan

In this paper the results of study of structural disordering kinetics in crystalline  $\text{LaF}_3$  and  $\text{CeF}_3$  by the spectrum of quasielastic light scattering have been considered. The low frequency scattering spectra ( $\nu=2\div 100\text{ cm}^{-1}$ ) have been obtained near the elastic peak excited by laser line in the temperature range  $80\div 600\text{ K}$ .

The relaxation wing of scattering line, which significantly increases at low frequencies, in many authors opinion, directly caused by the disordering processes of crystalline lattice. This case allows us to assume, that the significantly increase of scattering intensity in superionic phase transition (above  $T=280\text{ K}$ ) is defined by mass ionic transportation in sublattice F(1), F(2) and F(3). It has been shown, that experimental wing of quasielastic scattering line in the temperature range  $80\div 600\text{ K}$  is well approximated by three Lorentz counters:

$$I = I_0 [ \delta^2 / (\nu^2 + \delta^2) ] \quad (1)$$

Here  $I_0$  is the intensity in a maximum of Lorentz counter (at  $\nu=0$ ),  $\delta$  is its half-width and  $\nu$  is the moving frequency corresponding to intensity  $I$ .

It has been established, that most "narrow" Lorentz counter with  $\delta=(0.4\div 2.1)\text{ cm}^{-1}$  half-width is defined by the characteristic times  $\tau=(0.25\div 1.2)\cdot 10^{-11}\text{ sec}$ . and caused by the low frequency jumps of ions F(1) and F(2) near their regular lattice sites in a distance  $2\cdot 0.042\text{ nm}$  and  $2\cdot 0.046\text{ nm}$ , respectively (for  $\text{LaF}_3$ ). These low frequency microjumps, which are activated at about  $T=180\text{ K}$  determine the beginning of "melting" of crystalline lattice and make possible the longwavelength ion jumps at high temperature. The average Lorentz counter with half-width  $\delta=(4.2\div 2.7)\text{ cm}^{-1}$  has a maximum of integral intensity at about  $T=280\text{ K}$ . The widest Lorentz counter has half-width  $\delta$  in range  $(42\div 96)\text{ cm}^{-1}$ . The characteristic times  $\tau=(10^{-12} - 10^{-13})\text{ sec}$ . defined by these Lorentzians, are caused by the longwavelength jumps of fluoride ions and describe the time of stay of mobile ions in lattice sites in superionic phase.

By the maximum intensity  $I_0$  of Lorentzians and their half-width  $\delta$  the integral intensities have been estimated. It has been shown, the temperature behavior of these intensities are very dynamically. Moreover, their maximums correspond to the highest disordering process of sublattice F(1), F(2), F(3).

It is well known, the temperature change of relaxation peak parameters describes not only intracell jump kinetics, but also energetic characteristics of disordering process, since specific times of such transitions are directly determined by the potential barriers  $E_m$  which restrict the motion of ions. In addition, the frequencies of such jumps depend on the temperature by the Boltzmann factor  $\exp(-E_m/kT)$ .

It has been established that, in some temperature range the behaviors of half-width  $\delta$  of Lorentzians obey the Arrhenius dependence.

Thus in this paper has been determined the dynamics of potential barriers  $E_m$  in superionic phase transition. In first phase transition at  $T>T_{c1}\cong 270\text{ K}$  the potential barriers are decreased from  $0.26\text{ eV}$  to  $0.05\text{ eV}$ , and in the second phase transition ( $T>T_{c2}\cong 360\text{ K}$ ) the barriers are decreased from  $0.32\text{ eV}$  to  $0.06\text{ eV}$ . It is shown, that precisely significantly decrease of value of



barriers  $E_m$  describes mass disordering process of anion sublattice in crystals  $\text{LaF}_3$  and  $\text{CeF}_3$  at superionic phase transition.

The model of structural sequential disordering of crystalline lattice in super-ionic materials like  $\text{LaF}_3$  has been considered.

## CORRELATION BETWEEN MICROSCOPIC AND MACROSCOPIC PROPERTIES OF YTTRIA STABILIZED ZIRCONIA

M. Hartmanová<sup>1</sup>, F. Kundracik<sup>2</sup>, V. Navrátil<sup>3</sup>, H. Schulz<sup>4</sup>, and E.E. Lomonova<sup>5</sup>

<sup>1</sup>Institute of Physics, Slovak Acad.Sci., 84228 Bratislava, Slovakia

<sup>2</sup>Department of Physics, Faculty of Mathematics and Physics, Comenius University, 84215 Bratislava, Slovakia

<sup>3</sup>Department of Physics, Faculty of Education, Masaryk University, 60300 Brno, Czech Republic

<sup>4</sup>Institute of Crystallography and Mineralogy of LMU, 80333 Munich, Germany

<sup>5</sup>General Physics Institute of Russian Acad.Sci., 117942 Moscow, Russia

Zirconia ( $\text{ZrO}_2$ ) is one of the best examples in materials science where structure, microstructure, defects and phase compositions / transformations are intimately connected with macroscopic properties such as thermal and electrical conductivity, mechanical strength and optical absorption. It is well-known that zirconia has three polymorphs - monoclinic, tetragonal and cubic phases. Addition of certain amounts of other divalent or trivalent oxides such as  $\text{CaO}$ ,  $\text{MgO}$ ,  $\text{Y}_2\text{O}_3$  and other rare earth oxides stabilizes metastable non stoichiometric structures.

The aim of studying in detail zirconia polymorphism is based on the interest in a better understanding of the correlation between microscopic structure and macroscopic properties on both electrical and mechanical properties. This is obviously needed for the improvement of practical device design.

The investigated crystalline samples of 1 - 34 mol%  $\text{Y}_2\text{O}_3$  were grown by one of the authors (E.E.L.) by skull-melting. The crystals obtained are milky (more or less), clear-colourless and clear-light brown coloured in dependence on the amount of dopant (stabilizer)  $\text{Y}_2\text{O}_3$ .

The experiments have been made on the phase composition (structure), electrical conductivity as well as on the microhardness.

The X-ray powder diffraction method was used to determine the phase composition and the lattice parameters. The diffraction patterns indicated the presence of cubic (c), tetragonal (t) and monoclinic (m) phase. The (t) and (m) phases exist in the composition range of  $c < 9$  mol%  $\text{Y}_2\text{O}_3$  and the cubic fluorite structure is possible to find when the amount of  $\text{Y}_2\text{O}_3$  in the sample is  $c \geq 9$  mol %  $\text{Y}_2\text{O}_3$ . Both cubic and tetragonal  $\text{ZrO}_2$  stabilized with  $\text{Y}_2\text{O}_3$  exhibit appreciable ionic conductivity  $\sigma$ .

The electrical conductivity was investigated using impedance spectroscopy and the results obtained were analysed by electrical equivalent circuit method. The present data show a maximum in  $\sigma$  vs  $c$  followed by a drop of  $\sigma$  accompanied by an increase in activation energy  $E_a$ . For a better understanding of the characteristic pattern of behaviour of the isothermal electrical conductivity, especially within the maximum, it seems to be significant to take into account the difference between conductivities of tetragonal and cubic phases as well as the association phenomena at higher  $\text{Y}_2\text{O}_3$  amounts ( $> 9$  mol%). The secondary phase formations are important at the highest used  $\text{Y}_2\text{O}_3$  concentration (34 mol%).

A partially stabilized zirconia (PSZ), i.e. a matrix of cubic and tetragonal ( or monoclinic) zirconia, at a concentration of dopant less than that needed for the cubic phase (FSZ), i.e.  $< 9$  mol %  $\text{Y}_2\text{O}_3$  in our case, presents a good mechanical properties as it is evident from the investigation of microhardness performed by indentation method.

In the present stage of knowledge, a rather vague compromise between doping, processing, structure and properties has to be chosen for the practical device design.

**Acknowledgements.** The work was partially supported by the research grants No.2 / 5081 / 98, 1 / 4253 / 97 of the Slovak Grant Agency and No.106 / 96 / 0322 of the Grant Agency of Czech Academy of Sciences. One of the authors (M.H.) thanks the Deutscher Akademischer Austauschdienst for a fellowship, during which period, the XRD measurements were performed.

THERMAL BEHAVIOR OF  $\text{Bi}_5\text{Pb}_3\text{O}_{10.5}$ 

Akiteru Watanabe

National Institute for Research in Inorganic Materials  
1-1 Namiki, Tsukuba, Ibaraki 305-0044 Japan

Phase equilibrium studies in the system  $\text{Bi}_2\text{O}_3$ - $\text{PbO}$  [1,2] identified a compound  $\text{Bi}_8\text{Pb}_5\text{O}_{17}$  (55.55 mol% $\text{PbO}$ ) which has three polymorphs. Since the high oxide-ion conduction was found [3] in the unquenchable high-temperature stable modification (labelled  $\beta$ ) having an anti- $\alpha$ - $\text{AgI}$ -type bcc structure ( $a=4.40\text{\AA}$  at  $600^\circ\text{C}$ ) with the space group  $\text{Im}\bar{3}\text{m}$ , polymorphism of this compound was more intensively investigated [4-7] to date. However reported results are largely contradictory and very little is known about structures of modifications except the  $\beta$  phase.

Recently Watanabe et al. [8] re-examined the phase equilibrium of this compound. As a result, the composition of  $\text{Bi}_8\text{Pb}_5\text{O}_{17}$  turned out to be a mixture of  $\text{Bi}_5\text{Pb}_3\text{O}_{10.5}$  (54.54 mol% $\text{PbO}$ ) and  $\text{Pb}_3\text{O}_4$ ; in other words, a true composition of the present compound was  $\text{Bi}_5\text{Pb}_3\text{O}_{10.5}$ . The low-temperature stable modification named  $\beta_L$  crystallizes in the triclinic system with  $a=14.903(1)\text{\AA}$ ,  $b=14.184(1)\text{\AA}$ ,  $c=7.2115(7)\text{\AA}$ ,  $\alpha=97.216(8)^\circ$ ,  $\beta=118.434(6)^\circ$ ,  $\gamma=80.647(8)^\circ$  and  $Z=4$ , and has a superstructure based on a pseudo-bcc  $\beta$ -type subcell by the transformation matrix  $-2, 2, 2 / 1, -1, 3 / 3/2, 1/2, -1/2$ . The topotactic relations between the triclinic axes and the subcell ( $a'\approx 4.3\text{\AA}$ ) are  $a\approx 2\sqrt{3}a'$ ,  $b\approx \sqrt{11}a'$ , and  $c\approx (\sqrt{11}/2)a'$  as shown in Fig.1. The metastable modification termed  $\beta_2$  crystallizes in the tetragonal system with the possible space group  $\text{P}4_2/\text{n}$  with  $a=12.132(1)\text{\AA}$ ,  $c=20.059(2)\text{\AA}$ , and  $Z=9$ . The structure of the  $\beta_2$  phase is connected to that of red tetragonal  $\text{PbO}$ -type structure according to  $3, 0, 0 / 0, 3, 0 / 0, 0, 4$ . The  $\beta_L$  phase transforms to the  $\beta$  phase at about  $585^\circ\text{C}$ ; on subsequent cooling, however, at about  $560^\circ\text{C}$  the  $\beta$  phase changes inevitably to the  $\beta_2$  phase which is kept to room temperature. The  $\beta_2$  phase reverts to the  $\beta_L$  phase by annealing at low temperatures, e.g., at  $500^\circ\text{C}$ . In the present study, we have checked the phase transformations more precisely using thermal analysis technique, i.e., TG-DTA.

The samples were synthesized by solid-state reaction of  $\text{Bi}_2\text{O}_3$  and  $\text{PbO}$  in air with covered gold crucibles. The product was air-quenched to room temperature at the end of the reaction, ground well in an agate mortar, and checked by X-ray powder diffraction (XRPD) method using  $\text{CuK}\alpha$  radiation and a diffracted-beam monochromator. The  $\beta_L$  phase was prepared by heating a stoichiometric mixture between  $500^\circ$  and  $550^\circ\text{C}$  for 60 h or more; the same heat treatment was repeated several times after intermediate grindings to complete the reaction. The  $\beta_2$  phase was easily obtained by heat treatment at  $600^\circ\text{C}$  for 10 h or more.

The thermal behavior was examined by differential thermal analysis (Rigaku TG 8120). About 50 mg of powder sample put in a platinum or gold sample holder underwent heating-cooling cycles at a rate of  $2^\circ$ ,  $3^\circ$ ,  $5^\circ$ , or  $10^\circ\text{C min}^{-1}$  in air to the maximum temperature of  $685^\circ\text{C}$ . The reference material was  $\alpha$ - $\text{Al}_2\text{O}_3$ . Transition temperatures were determined from onsets of peaks on DTA curves during the heating cycle. The dc conductivity measurement was carried out on a sintered circular pellet (14 mm in diameter and about 3 mm thick) in the same way as described previously [9].

Figure 2 shows DTA results of the starting phase of  $\beta_L$ - $\text{Bi}_5\text{Pb}_3\text{O}_{10.5}$ . The  $\beta_L$ -phase transforms to the  $\beta$ -phase at  $587^\circ\text{C}$  and melts at  $650^\circ\text{C}$  as indicated in Fig.2(a). It is noted that the heat of transformation from  $\beta_L$  to  $\beta$  is larger than the heat of fusion. We have observed the same phenomenon in  $\text{Bi}_2\text{O}_3$  [10]. That is, oxide-ions can move more easily in the solid rather than the melt; in other words, the  $\beta$ -phase as well as  $\delta$ - $\text{Bi}_2\text{O}_3$  is an excellent

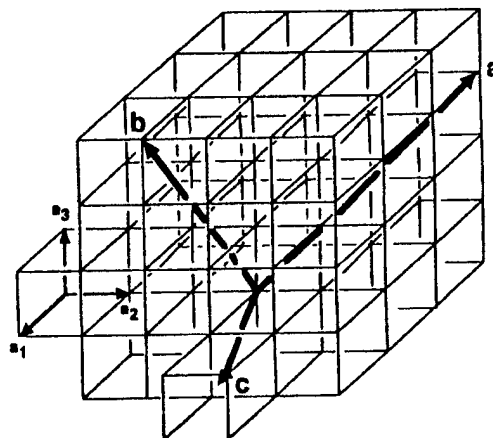


Fig. 1. Schematic representation of the unit-cell axis relations between the triclinic cell ( $a$ ,  $b$ ,  $c$ ) of  $\beta_L$ - $\text{Bi}_5\text{Pb}_3\text{O}_{10.5}$  and the pseudo-bcc subcell ( $a_1$ ,  $a_2$ ,  $a_3$ ;  $a'\approx 4.3\text{\AA}$ ) related to the  $\beta$ -phase.

oxide-ion conductor [3]. In the cooling direction, the melt solidifies to the  $\beta$ -phase at a lower temperature than 650°C due to supercooling, and the  $\beta$ -phase transforms to the  $\beta_2$ -phase as mentioned above. Thus, in the subsequent second cycle in Fig.2(b), the  $\beta_2$ -phase is the starting one; upon heating, we can observe two endothermic peaks, one at 569°C and the other at 588°C, prior to fusion in contrast to the first cycle. The former peak corresponds to the  $\beta_2$ -to- $\beta$  transition and the latter peak implies the  $\beta_L$ -to- $\beta$  transition. Namely, part of  $\beta_2$ -phase transforms gradually to the  $\beta_L$ -phase during heating process below 569°C, and the quantity of the  $\beta_L$ -phase thus generated depends on a heating rate; the slower, the more. In addition, when a very slow heating rate of 20°C h<sup>-1</sup> was employed in high-temperature X-ray powder diffraction method using a Guinier-Lénne camera, the  $\beta_2$ -phase transforms completely to the  $\beta_L$ -phase at 450°C and subsequently the  $\beta_L$ -to- $\beta$  transition occurred at 590°C [3]. The dependence of the  $\beta_2$ -to- $\beta_L$  transformation upon heating rate also indicates that the  $\beta_2$ -phase is metastable.

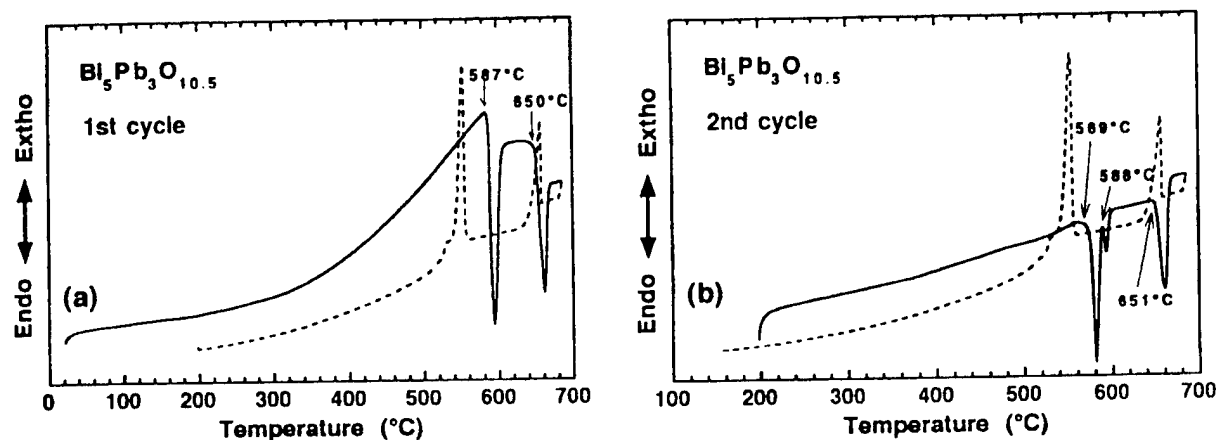


Fig. 2. DTA curves in the heating (solid line) and cooling (broken line) cycle for  $\text{Bi}_5\text{Pb}_3\text{O}_{10.5}$ , (a) the first cycle and (b) the subsequent second cycle.

#### References

- [1] J.C. Boivin and G. Tridot, C. R. Acad. Sci., Paris, Ser. C, **278**, 865 (1974).
- [2] R.M. Biefeld and S.S. White, J. Am. Ceram. Soc. **64**, 182 (1981).
- [3] F. Honnart, J.C. Boivin, D. Thomas and K.J. De Vries, Solid State Ionics **9/10**, 921 (1983).
- [4] G.A. Bordovskii and A.B. Zarkoi, Phys. Stat. Sol., **A87**, K7 (1985).
- [5] N.M. Sammes, R.J. Phillips and M.G. Fee, Solid State Ionics **69**, 121 (1994).
- [6] N.M. Sammes, G. Tompsett and A.M. Cartner, Solid State Commun. **96**, 545 (1995).
- [7] M.G. Fee, N.M. Sammes, G. Tompsett, T. Stoto and A.M. Cartner, Solid State Ionics **95**, 183 (1997).
- [8] A. Watanabe, Y. Kitami, S. Takenouchi, J.C. Boivin and N. Sammes, submitted for publication in J. Solid State Chem.
- [9] A. Watanabe and T. Kikuchi, Solid State Ionics **21**, 287 (1986).
- [10] H.A. Harwig and A.G. Gerards, Thermochim. Acta **28**, 121 (1979).

# CHARACTERISATION OF $\text{La}_{1-x}\text{Sr}_x\text{Ga}_{1-y}\text{Mg}_y\text{O}_{3-\delta}$ , ( $x = 0 - 0.20$ , $y = 0 - 0.20$ ) BY X-RAY DIFFRACTION AND RAMAN SPECTROSCOPY

G. A. Tompsett<sup>a\*</sup>, M. Mori<sup>b</sup> and N. M. Sammes<sup>a</sup>

<sup>a</sup>Department of Technology, University of Waikato, Private Bag 3105, Hamilton, New Zealand.

FAX: 64-7-8384865, Email: g.tompsett@waikato.ac.nz

<sup>b</sup>On leave from Chemical Energy Engineering Department, Chemical Power Generation Group, Central Research Institute of Electric Power Industry, 2-6-1 Nagasaka, Yokosaka, Kanagawa 240-01, Japan.

Doped  $\text{LaGaO}_3$  is a promising electrolyte material for application as intermediate temperature (650-800°C) electrolytes in solid oxide fuel cells (SOFC's). For example, Huang and Petric [1] showed that the optimum conductivity of  $\text{La}_{0.8}\text{Sr}_{0.2}\text{Ga}_{0.85}\text{Mg}_{0.15}\text{O}_{2.825}$  (LSGM) was found to be 0.14 S/cm at 800°C.

$\text{LaGaO}_3$  has an orthorhombic structure based on the  $\text{ABO}_3$  perovskite. Singly doped  $\text{LaGaO}_3$  with Mg on the B-site ie  $\text{LaGa}_{1-y}\text{Mg}_y\text{O}_3$  was studied by Phillips et al. [2] and these workers, using x-ray diffraction and Raman spectroscopy, observed the presence of a  $\text{La}_4\text{Ga}_2\text{O}_9$  secondary phase in all the samples prepared.

Sammes et al. [3] prepared  $\text{La}_{0.8}\text{Sr}_{0.2}\text{Ga}_{1-y}\text{Mg}_y\text{O}_{3-\delta}$ , ( $y = 0.02 - 0.20$ ), and showed that at Mg dopant levels of less than  $y = 0.1$ , a single phase could not be formed after repeated firing at 1520°C. Secondary phases of  $\text{La}_2\text{O}_3$ ,  $\text{Ga}_2\text{O}_3$  and  $\text{Sr}_3\text{Ga}_2\text{O}_6$  were identified using x-ray diffraction, and Raman spectroscopy similarly indicated the presence of a secondary phase at dopant levels of <10 mol% Mg. Above 10 mol% Mg dopant level in LSGM, single orthorhombic perovskite phase could be formed.

In this paper, we investigate the interdependence of both Sr doping on the A-site and Mg doping on the B-site of  $\text{LaGaO}_3$ . The phase composition of the materials formed is determined using dual techniques of x-ray diffraction and Raman spectroscopy.

Ceramic compacts of  $\text{La}_{1-x}\text{Sr}_x\text{Ga}_{1-y}\text{Mg}_y\text{O}_{3-\delta}$ , ( $x = 0 - 0.20$ ,  $y = 0 - 0.20$ ) were prepared using the standard solid state technique with sintering at twice at 1520°C for 12 h. The phase composition was determined using powder x-ray diffraction (XRD) and Raman spectroscopy of the powders at room temperature. Fig. 1 shows the XRD patterns of  $\text{La}_{0.95}\text{Sr}_{0.05}\text{Ga}_{1-y}\text{Mg}_y\text{O}_{3-\delta}$ , ( $y = 0 - 0.20$ ). It can be seen that secondary phases are present at all compositions. At low Sr dopant concentrations a single perovskite phase can not be formed. Fig. 2 shows the XRD patterns of  $\text{La}_{1-x}\text{Sr}_x\text{Ga}_{0.8}\text{Mg}_{0.2}\text{O}_{3-\delta}$ , ( $x = 0 - 0.20$ ). In comparison to Fig. 1, the presence of high Sr dopant levels ( $\geq 10$  mol%) simultaneously with high Mg dopant levels produces a single perovskite phase. Therefore, it can be concluded that the presence of both the Sr doping on the A-site and Mg doping on the B-site is required at greater than 10 mol% level to form a single perovskite phase.

\*Corresponding Author

[1] P. Huang and A. Petric, *J. Electrochem. Soc.*, **143** [5], 1644 (1996).

[2] N.M. Sammes, G.A. Tompsett, R.J. Phillips and A.M. Cartner, *Solid State Ionics*, **111** [1-2], 1 (1998)

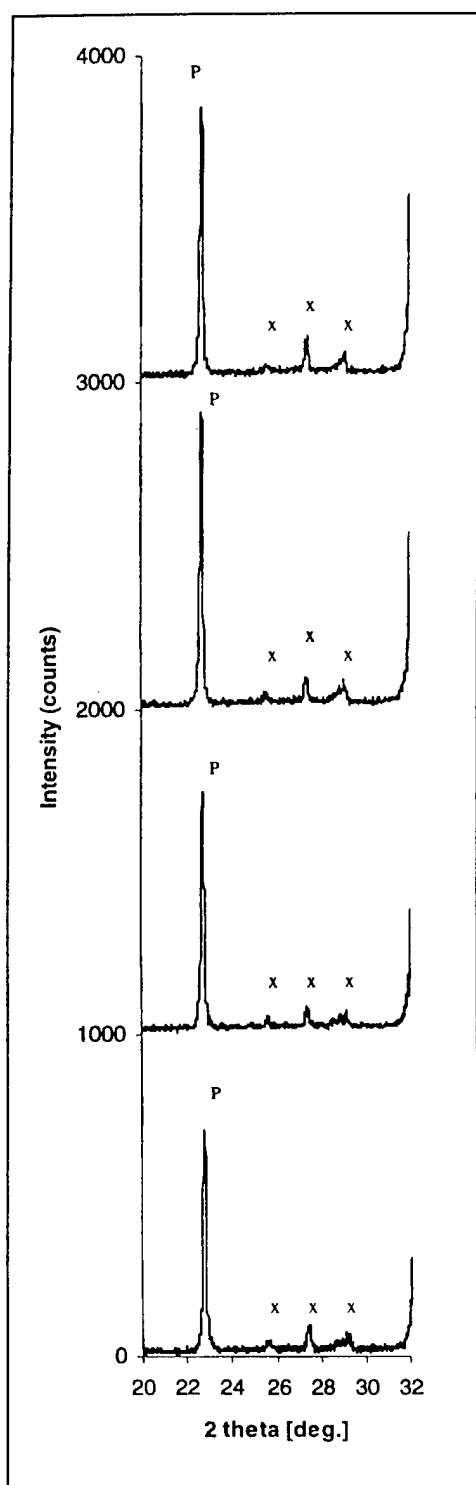


Fig. 1 XRD patterns of  $\text{La}_{0.95}\text{Sr}_{0.05}\text{Ga}_{1-y}\text{Mg}_y\text{O}_{3-\delta}$ , where  $y = 0.05$  (a),  $0.10$  (b),  $0.15$  (c) and  $0.20$  (d).  
P = perovskite, x = secondary phase

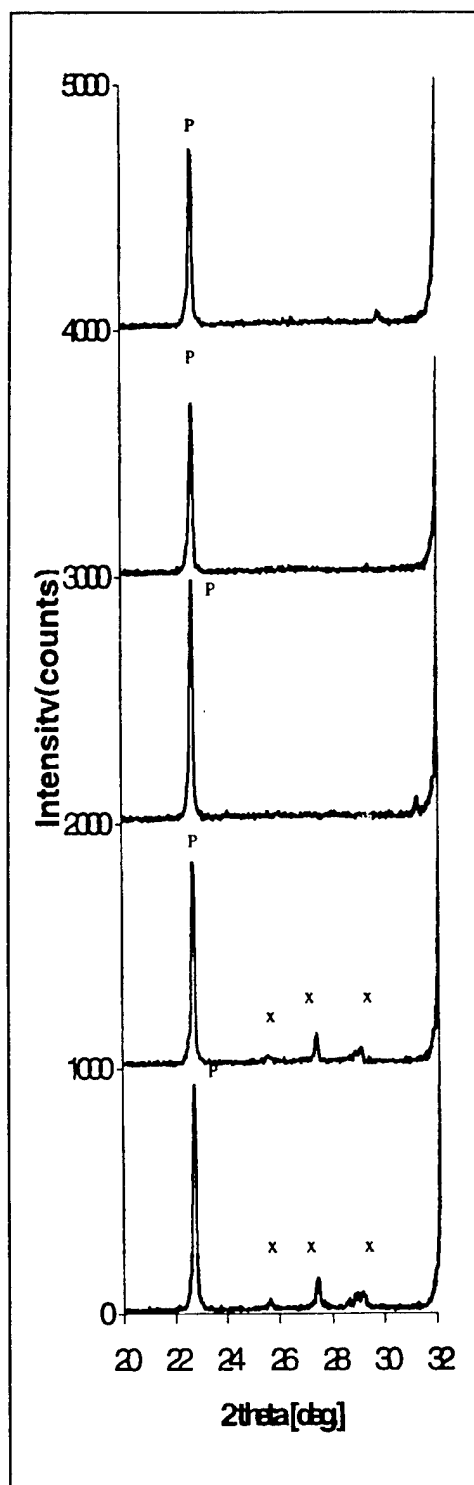


Fig. 2 XRD patterns of  $\text{La}_{1-x}\text{Sr}_x\text{Ga}_{0.80}\text{Mg}_{0.20}\text{O}_{3-\delta}$ , where  $x = 0$  (a),  $0.05$  (b),  $0.10$  (c),  $0.15$  (d) and  $0.20$ .  
P = perovskite, x = secondary phase.

## STRUCTURAL AND ELECTRICAL CONSEQUENCES OF HIGH DOPANT LEVELS IN THE BIMGVOX SYSTEM

F. Krok,<sup>1</sup> I. Abrahams,<sup>2</sup> M. Malys,<sup>1</sup> W. Bogusz<sup>1</sup>, J.R. Dygas<sup>1</sup> J.A.G. Nelstrop<sup>2</sup> and A.J. Bush<sup>2</sup>

<sup>1</sup>Institute of Physics, Warsaw University of Technology,  
ul. Koszykowa 75, 00-662, Warsaw, Poland.

<sup>2</sup>Structural Chemistry Group, Dept. of Chemistry, Queen Mary and Westfield College,  
University of London, Mile End Road, London E1 4NS, United Kingdom

The fast oxide ion conducting BIMEVOXes have been the subject of a great deal of research in recent years. These compounds are solid solutions based on substitutions in the parent material  $\text{Bi}_4\text{V}_2\text{O}_{11}$ . Particular interest has focused on divalent substitutions i.e.  $\text{Bi}_2\text{V}_{1-x}\text{Me}_x\text{O}_{5.5-3x/2}$  (where Me is a divalent metal). In the present work the Mg doped system  $\text{Bi}_2\text{V}_{1-x}\text{Mg}_x\text{O}_{5.5-3x/2}$  (BIMGVOX) has been studied with particular interest in the heavily doped compositions.

Polycrystalline samples of BIMGVOX ( $0.05 \leq x \leq 0.40$ ) were prepared from  $\text{Bi}_2\text{O}_3$ ,  $\text{MgO}$  and  $\text{V}_2\text{O}_5$  by conventional solid state techniques. Slow cooling of samples to room temperature was employed to enable relaxation of the structure. Crystal structure parameters and electrical conductivity were investigated using X-ray powder diffraction and a.c. impedance spectroscopy.

A compositional dependence is observed for both structural and electrical parameters. Four compositionally dependent structural ranges are seen in the X-ray data for the BIMGVOX system, between  $0.05 \leq x \leq 0.40$ . Below  $x = 0.10$ , the orthorhombic  $\alpha$ -phase structure is observed while, in the composition range  $0.10 \leq x \leq 0.25$  the tetragonal  $\gamma$ -phase is predominant at room temperature. At high dopings,  $x > 0.25$ , a loss of tetragonal symmetry occurs with a return to an orthorhombic  $\alpha$ -type phase. At  $x = 0.40$  the limit of the solid solution has been exceeded and the emergence of a  $\text{Bi}_2\text{O}_3$  related phase is seen in the X-ray diffraction pattern. The appearance of an  $\alpha$ -type phase at high dopant levels has been observed before in the trivalent doped system BIFEVOX [1] but we believe this to be the first example in a divalent doped system.

Generally the Arrhenius plots of conductivity show two linear regions one at low temperatures and one at high temperatures. The exact limits of these regions are composition dependent as is the way in which these two regions are linked. At low values of  $x$  ( $< 0.10$ ) the lower temperature region corresponds to a  $\beta$ -phase while the higher temperature region (above c.a.  $500^\circ\text{C}$ ) is related to the highly conducting  $\gamma$ -phase. In the region  $0.10 \leq x \leq 0.25$  the low temperature region corresponds to the modulated  $\gamma'$ -phase as confirmed in the X-ray data, with a transformation to the fully disordered  $\gamma$ -phase above c.a.  $550^\circ\text{C}$ . A small difference is seen in the conductivity behaviour for the highly doped BIMGVOX compositions ( $x > 0.25$ ), which reflects the more complex structural changes which involve transformation of the room temperature  $\alpha$ -type phase.

### Reference

- [1] O. Joubert, M. Ganne, R.N. Vannier, G. Mairesse, Solid State Ionics 83, 199 (1996).



## **AN INTEGRATED APPROACH FOR DETERMINING OXYGEN STOICHIOMETRIES IN OXIDES**

A. Hartley, D. Mantzavinos, M. Sahibzada, I.S. Metcalfe\*

School of Chemical Engineering, The University of Edinburgh,  
Mayfield Road, Edinburgh EH9 3JL, United Kingdom

\*corresponding author: tel: +44 131 6508553, fax: +44 131 6506551, e-mail: i.metcalfe@ed.ac.uk

### **Summary**

The degree of non-stoichiometry of a wide range of doped lanthanum cobaltite perovskites has been determined as a function of both oxygen partial pressure and temperature, using electrochemical (Oxylt) and inertial microbalance (TEOM) methods. The two techniques may be used independently (thus extending the accessible range of experimental conditions) or in conjunction, by using the microbalance system as the reactor. Mutual validation of the techniques is demonstrated via an oxygen material balance.

### **Introduction**

In Solid Oxide Fuel Cells (SOFCs) operating at intermediate temperatures it has been found that oxygen transport kinetics at the cathode can limit cell performance<sup>1</sup>. It is important, therefore, in mixed conducting oxide cathodes, to maximise both catalytic reduction of oxygen at the cathode surface, and transport of oxide ions through the cathode lattice to the electrode/electrolyte interface. The oxygen vacancy concentration of the material is one factor which strongly affects this behaviour.

The purpose of this study was to determine the degree of oxygen hypostoichiometry as a function of temperature and oxygen partial pressure for a wide range of potential cathode materials based mainly on lanthanum strontium cobaltite ferrite perovskites (LSCFs). Low oxygen partial pressures (in the range  $0.21 \cdot 10^{-5}$  atmospheres) were of primary interest since in a real fuel cell under cathodic bias, the material near the electrode/electrolyte interface is expected to be in a reduced state.

Oxygen stoichiometry has been determined by two complementary methods. Each method has a somewhat different range of application thus extending the total range of conditions which can be investigated. However, sufficient overlap is present to provide mutual validation of the two techniques.

### Experimental

A system of two solid state electrochemical cells is used in conjunction with an intervening reactor. A carrier gas stream is dosed with a well-defined oxygen concentration by the first cell, thus fixing the ambient oxygen pressure at the sample. Changes in sample temperature then lead to changes in the gas stream oxygen partial pressure downstream of the sample, through the release (or uptake) of oxygen by the powder sample. These changes are continuously and sensitively monitored by the second electrochemical cell, by holding its cell voltage constant and following the changes in induced cell current. Thus the total quantity of oxygen absorbed or released by the sample over a given temperature range may be calculated. This system is capable of operating at low, or very low, oxygen partial pressures (below about  $3 \cdot 10^{-3}$  atmospheres) and temperatures up to 1200°C. The reactor itself may be a simple quartz tube furnace, or may consist of a novel inertial microbalance system (TEOM) which is used to measure real-time mass changes in a catalyst bed. Originally developed for detecting particulates in the effluent of combustion systems, the TEOM microbalance has also been used to study in situ gas adsorption as well as catalyst deactivation. Its main advantage over classical gravimetric methods (i.e. TGA) is that it provides a packed bed of catalyst through which all the feed gases flow, and hence a very well-controlled flow regime which is appropriate for the acquisition of kinetic data. The operation of the TEOM microbalance is based on the relationship between the natural frequency of an oscillating quartz element that contains the catalyst sample, and its mass. A mechanical drive causes the tapered element to oscillate at its natural frequency, while optics (transmitter and receiver) located at opposite sides of the element perform the required frequency counting which is then related to mass changes. Sample mass changes due to oxygen partial pressure and/or temperature changes can be measured and then related to oxygen uptake or release. The TEOM is designed to accurately detect mass changes as low as a few  $\mu\text{g}$  at time resolutions as low as 0.1s with a catalyst bed mass up to 50 mg. This system is limited to temperatures up to 600°C, but is capable of operating at relatively high oxygen partial pressures, e.g. in air.

This novel apparatus has been used to study LSCF-type perovskites with a variety of La/Sr and Co/Fe ratios, and also alternative B-site dopants, over a temperature range up to 900°C, at oxygen partial pressures from that of air to  $10^{-5}$  atmospheres. Detailed results will be discussed.

### References

1. M.Sahibzada, B.C.H. Steele, K.Zheng, R.A. Rudkin, I.S. Metcalfe, *Catalysis Today*, **38** (1997) 459-466.

( Keynote Lecture )

**ELECTROCHEMICAL DEHUMIDIFICATION  
USING PROTON CONDUCTING CERAMICS****H. Iwahara, H. Matsumoto and K. Takeuchi**Center for Integrated Research in Science and Engineering, Nagoya University  
Furo-cho, Chikusa-ku, Nagoya 464-8603, Japan

In general, mobile ionic species in a solid electrolyte is limited to one kind of ions which compose the electrolyte material. This means that a solid electrolyte has a function of preferential permeation of specified ions and that this function can be utilized effectively in principle.

Regarding proton conducting solid electrolytes, one can selectively transport hydrogen by sending direct current to them. This is a kind of electrochemical hydrogen pump. This pump may be applied to the devices for the separation, the removal or the supply of hydrogen. In addition, the hydrogen pump has a possibility of modifying into other devices such as a steam electrolyzer and a steam pump for dehumidification that can be equipped to the small scientific instruments.

The principle of the electrochemical dehumidifier is as follows:

Water vapor can be electrolyzed at the anode on the proton conducting ceramic electrolyte to form protons. The protons thus formed migrate across the electrolyte membrane to the cathode where they discharge to form hydrogen molecules in the inert gas or react with oxygen in air to form water vapor. Hence, water vapor in the anode compartment decreases, whereas that in the cathode compartment increases. Outwardly, this can be regarded as an electrochemical dehumidifier although the real pumped species are not water molecule but hydrogen.

In our laboratory, such electrochemical dehumidifiers were made by way of experiment using perovskite-type oxide proton conducting ceramics and their performances have been investigated at elevated temperatures. In these experiments,  $\text{SrCe}_{0.95}\text{Yb}_{0.05}\text{O}_{3-\alpha}$  was used as a proton conductor and porous platinum as electrode material. We could confirm that this type of device worked well at 500 ~ 900°C. Air in the anode compartment was desiccated as the electrolytic current increased, whereas in the cathode compartment it was humidified. This method has a potential application to control the humidity in the closed system at elevated temperatures. Clear isotope effect in the evolution rate could be observed between  $\text{H}_2\text{O}$  and  $\text{D}_2\text{O}$  rate at the cathode. This may also be applied to an isotope concentrator under strongly radioactive conditions.

Using this device, pre-dried argon gas with frost point of about -25 ~ -30°C could be further desiccated down to the dew point of -45°C at the operating temperature of 800°C. This method might be applied to dehumidifier equipped to the small vessel of scientific instruments such as bell jar for vacuum.

## MIXED PROTONIC-ELECTRONIC CONDUCTORS FOR HYDROGEN PERMEABLE MEMBRANES

Truls Norby

Department of Chemistry, University of Oslo,  
Centre for Materials Science, Gaustadalleen 21, N-0371 Oslo, Norway.

### Introduction

Following the recent quest for oxygen permeable membranes for production of oxygen from air or syngas ( $\text{CO} + \text{H}_2$ ) from methane, there is emerging interest in the possibility of developing ceramic mixed protonic-electronic conductors for hydrogen separation. Potential applications comprise extraction of pure hydrogen from the syngas stream or from other oxidation or dehydrogenation steps, as well as hydrogen purification systems in general.

Oxygen permeable membranes operate in a large chemical potential gradient (e.g. syngas production) or in a merely hydrostatic pressure difference under oxidising conditions (oxygen production). Hydrogen permeable membranes, on the other hand, may only be foreseen to work in a hydrostatic pressure difference of hydrogen, and thus only under reducing conditions. This has important consequences for the strategies of materials development.

Alternatives to the mixed conductor are the use of a palladium membrane or of a two-phase system of one proton conductor and one electronically conducting (e.g. metallic) phase. Hydrogen is also well suited for relatively efficient filtering through (nano)porous materials. However, here the topic is that of hydrogen permeability based on mixed protonic-electronic conduction. Focus will be on oxide and hydroxide systems, although other systems can be of interest also.

### General constraints

The material in question must exhibit protonic conduction. It must thus contain a proton sublattice with defects or contain non-structural protonic interstitial defects. The protonic defect concentration may be increased by doping or non-stoichiometry. The material must also be a good electronic conductor, considered achievable only in materials with mixed-valency elements. The smallest out of the protonic and electronic conductivities must usually be at least 0.1 S/cm, depending on membrane thickness and other factors. Most important, perhaps, when we look at the individual classes of materials and their conduction behaviour, is that we consider their stability and validity under reducing conditions. We may have to consider unusually low oxidation states, and n-type conduction will be relatively more important than the p-type conduction often encountered in the oxygen permeable membranes.

### Materials strategies

The development of materials with mixed protonic-electronic conduction may follow different, often overlapping, strategies:

Acceptor doping of oxides or other nominally proton-free compounds increases the concentration of protons, and also of electron holes, yielding p-type conduction. As the latter often vanishes under reducing conditions, one either has to use cations in low oxidation states such that they may be p-type conductors even under reducing conditions (e.g.  $\text{Cr}^{3+}$ ) or one has to utilise n-type conduction, which may be considerable under reducing conditions even in an acceptor-doped oxide. The latter is achievable with a reducible cation present, as illustrated by the relatively high n-type conduction of acceptor-doped  $\text{SrCeO}_3$  and  $\text{BaCeO}_3$  under reducing

conditions. It is noteworthy, however, that acceptor-doping of oxides giving high protonic conductivity typically results also in a high concentration of oxygen vacancies.

Proton incorporation by reduction with hydrogen may take place via the reaction  $\text{H}_2(\text{g}) + 2\text{O}_{\text{O}}^{\times} = 2\text{OH}_{\text{O}}^{\cdot} + 2\text{e}'$  which creates protonic and electronic defects directly. A somewhat reducible cation is desirable. Also in this class of materials competition from oxygen vacancies (or metal interstitials) may be expected.

Metallic or intrinsically electronic compounds are of potential interest given that the mixed valency giving rise to the half-filled bands or small band gaps exist and prevale under reducing conditions. However, proton concentration and mobility is then most often unknown, and need to be determined by methods different from conductivity studies, e.g. isotope exchange/SIMS.

Intercalation compounds. Many oxides take up large quantities of protons and/or hydrogen by intercalation, often at moderate temperatures. Examples include  $\text{MnO}_2$  and  $\text{WO}_3$  which may be reduced by hydrogen forming oxyhydroxides and so-called bronzes. These may possess high concentrations and transport rates of protons or hydrogen at relatively low temperatures.

Materials with structural protons: hydroxides, oxyhydroxides, acids, hydrates. The best low-temperature proton conductors contain structural protons, in which case it is necessary to promote proton transport by creating proton vacancies or interstitials thermally or by doping. Examples comprise  $\text{CsHSO}_4$  with its thermally disordered protons. However, most of the established proton conductors in the class exhibit no electronic transport. Mixed conduction may, however, be foreseen in systems with mixed valency cations. For instance, the system  $\text{NiOOH}/\text{Ni}(\text{OH})_2$  is in operation in rechargeable electrodes in accumulators and expectedly transports both protons and electrons with relative ease.

### **A strategy for reducing oxygen permeability**

As mentioned, a general problem for many of the materials candidates will be the parasitic transport of oxygen. Oxide classes with high oxygen transport comprise fluorite- or perovskite-derived systems, having relatively ionic oxygen bonds and/or corner-sharing oxygen polyhedra. In comparison, systems with separated and largely covalent oxygen tetrahedra do not exhibit considerable oxygen mobility, while in some cases protons still transfer easily, aided by the dynamics of the tetrahedra. The  $\text{CsHSO}_4$  mentioned before provides one example, and phosphates such as  $\text{LaPO}_4$  are shown to exhibit ionic conduction solely by interstitial protons dissolved from water. It appears advisable to pursue this in order to develop electrolytes and mixed conductors with minimum oxygen transport. Candidate systems comprise sulfates and phosphates, as mentioned, and furthermore vanadates, niobates, tungstates, and others. Some of these contain already the mixed valency that may give electronic conduction.

### **Concluding remarks**

At present, only a handful of groups internationally have started a systematic search of mixed protonic-electronic conductors. The few materials investigated, mainly perovskite-related oxides with reducible cations, have shown modest qualities with respect to use as hydrogen separation membranes. A number of strategies for further search have been pointed out. Nevertheless, one should bear in mind that while ceramic oxygen separation membranes have little direct competition, a ceramic mixed conducting hydrogen separation membrane is but one of a number of possibilities for hydrogen separation. Probably, the ceramic option will have its strength in high temperature applications, in which one wants to maintain and utilise the heat contained in the in-stream.

## ABOUT THE COMPLEXITY OF PROTON CONDUCTION PHENOMENA

K. D. Kreuer

Max-Planck-Institut für Festkörperforschung  
 Heisenbergstr. 1, D-70569 Stuttgart  
 kreuer@chemix.mpi-stuttgart.mpg.de

In contrast to metals in which hydrogen (proton) transfer reactions usually take place between octahedral or tetrahedral sites, already result in long-range hydrogen (proton) transport, i.e. diffusion, proton mobility in non-metallic environments requires not only proton transfer reactions within hydrogen bonds but also structural reorganisations as schematically illustrated in fig. 1.

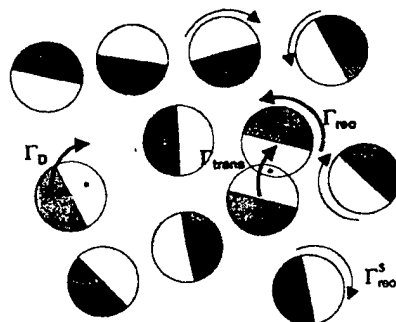


Fig. 1

Schematic illustration of different modes involved in long range proton transport (see text)

The role of hydrogen bonds in such processes is somewhat ambivalent [1]: Rapid proton transfer is favoured in short, strong hydrogen bonds, while structural reorganisation requiring breaking of hydrogen bonds is supposed to be suppressed by strong hydrogen bonding. This is demonstrated in fig.2 for a simple proton / acceptor system ( $\text{H}_5\text{O}_2^+$ ): For a donor / acceptor separation  $Q \approx 290$  pm, where the proton transfer barrier  $E_{\text{trans}}$  equals the energy to break the central hydrogen bond  $E_{\text{bond}}$ , the energies are well above 0.5 eV, which is significantly higher than the activation enthalpy of proton mobility in bulk water ( $\approx 0.1$  eV). It is obviously the mutual interaction of many particles which is essential for the appearance of high rates of proton transfer and structural reorganisation.

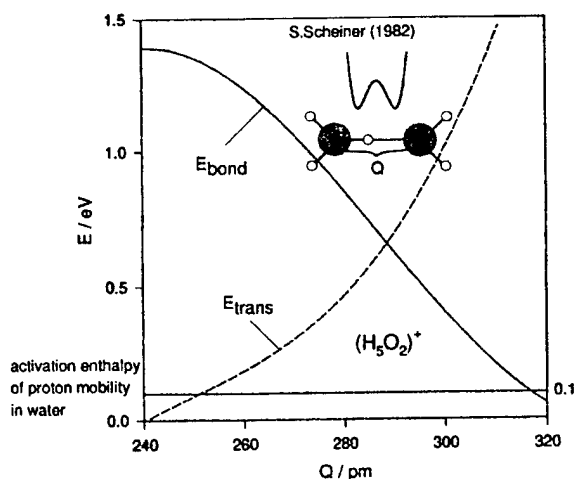


Fig.2

Proton transfer barrier  $E_{\text{trans}}$  and hydrogen bond energy as a function of proton donor / acceptor separation in the dimer  $\text{H}_5\text{O}_2^+$  as obtained from a Hartree Fock calculation [2].

This makes long range proton transport in non-metallic compounds a complex process. Some common but also specific features of proton transport mechanisms for different families of compounds (water containing systems, oxo-acids and their salts, hydroxides, oxides) will be presented.

One essential feature of all good proton conductors is an effective balancing of chemical interactions over a wide increment in phase space, i.e. a variety of configurations and momentum distributions are accessible by thermal excitation at moderately high temperatures. As an example, this is demonstrated for a proton in a perovskite-type oxide ( $\text{BaCeO}_3$ ). Fig. 3 (top) shows the  $\text{CeO}_6$  octahedron of the perovskite lattice from the top one proton forming a covalent bond with one oxygen. Quantum-MD simulations [3-5] of a box of  $3 \times 3 \times 3$  unit cells of  $\text{BaCeO}_3$  using periodic boundary conditions revealed the free energy curves as a function of the separation of two regular lattice oxygens and as a function of the separation of the protonic defect and the next nearest oxygen, which actually rapidly changes in the simulation as a results of the rapid rotational diffusion of the defect ( fig. 3 bottom). This indicates a significant softening of the oxygen separation coordinate in the presence of the proton. Obviously, the hydrogen bond energy just compensates for the energy required to deform the  $\text{CeO}_6$  octahedron over a wide range of OH / O separations. This corresponds to strong, high energy hydrogen bonding, which is also indicated by IR-spectroscopy. Even for low thermal excitations, this leads to tremendous fluctuations of the oxygen separations, which supports proton transfer as well as structural reorganisation.

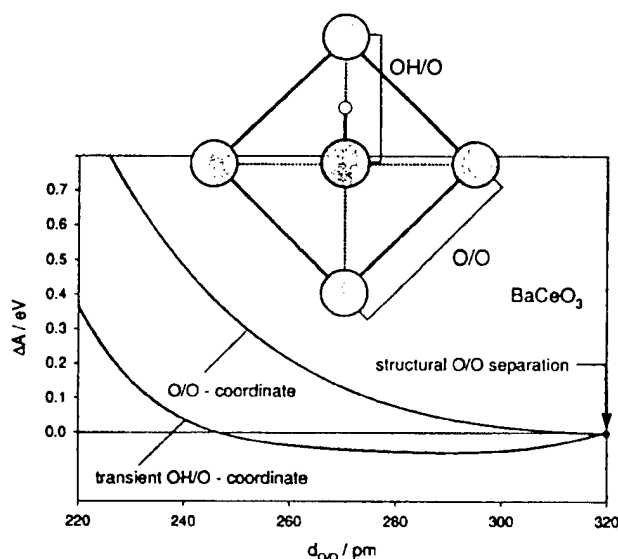


Fig. 3

Free energy of  $\text{BaCeO}_3$  as a function of the OH / O and O / O separation demonstrating the lattice softening around protonic defects (see text).

This effect is even more pronounced in  $\text{BaZrO}_3$  based materials. This stable compound, which is rather hard as a result of significant covalent bonding, also shows the above described softening effect around protonic defects due to very negative hydrogen bond energies. The compound is indeed one of the very few compounds combining very high proton mobility and thermodynamic phase stability.

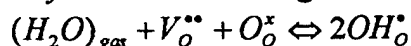
- [1] K. D. Kreuer, Chemistry of Materials **8**, 610 (1996)
- [2] St. Scheiner, J. Am. Chem. Soc. **103**, 315 (1981)
- [3] K. D. Kreuer, W. Münch, U. Traub, J. Maier, Ber. Bunsenges. Phys. Chem. **102**, 552 (1998)
- [4] K. D. Kreuer, Solid State Ionics (Proc. SSPC-9), in press
- [5] W. Münch, K. D. Kreuer, G. Seifert, J. Maier, Solid State Ionics (Proc. SSPC-9), in press

# THE PROTON CONDUCTOR Ba<sub>3</sub>Ca<sub>1.18</sub>Nb<sub>1.82</sub>O<sub>9.8</sub> (BCN18): THE EFFECT OF REDUCING ENVIRONMENTS

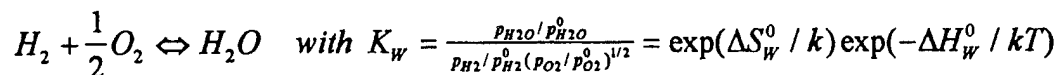
T. Schober and J. Friedrich

Institut für Festkörperforschung, Forschungszentrum Jülich  
52425 Jülich, Germany

The high-temperature proton conductor Ba<sub>3</sub>Ca<sub>1.18</sub>Nb<sub>1.82</sub>O<sub>9.8</sub> belonging to the class of mixed perovskites of type BaCa<sub>(1+x)/3</sub>Nb<sub>(2-x)/3</sub>O<sub>3-x/2</sub> with x=0.18 has served in the last years as a model substance [1-8]. It has an abundance of oxygen vacancies in the dry state which may be filled according to:

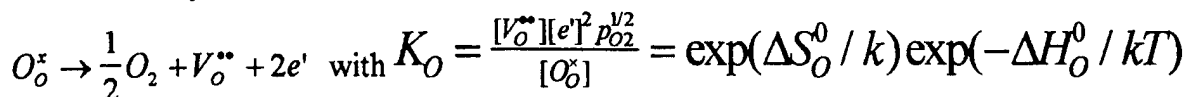


The solution enthalpy is about -0.8 eV [6]. There is good proton conductivity in the interior of the grains whereas the grain boundaries constitute obstacles to proton conduction [7]. The DC conductivity is dominated at high p<sub>O2</sub> values by hole conduction which leads to small proton transport numbers. An application of BCN18 in a SOFC would require operation on the anode side at a p<sub>O2</sub> of about 10<sup>-24</sup> bar. Annealing of BCN18 in highly reducing hydrogen atmospheres, however, was found to lead to a degradation of the mechanical strength caused by grain boundary cavities [8]. Proton uptake was found to be accompanied by a considerable lattice expansion [5,9] which may lead to cracking of bulk samples if the stresses become too high. In the present work, thermogravimetry (TG) data on the weight loss of BCN18 in very reducing dry and moist hydrogen atmospheres with known partial pressures of water is presented. The oxygen partial pressure was calculated using the equilibrium constant of the reaction :



where  $\Delta S_w^0$  and  $\Delta H_w^0$  are the standard entropy and enthalpy change. Two types of TG experiments were performed: (a) starting with a totally dry sample annealed in carefully dried synthetic air the sample was isothermally (900 °C ≥ T ≥ 600 °C) exposed first to nominally dry Ar-4%H<sub>2</sub> and then to a sequence of Ar-4%H<sub>2</sub> atmospheres with *increasing* humidities; (b) starting with a totally dry sample annealed in dry synthetic air the sample was exposed at 900 °C to an Ar-4%H<sub>2</sub> atmosphere with a known, low humidity. After reaching an equilibrium, the temperature was successively lowered to 600 °C in steps of 100 °C. The weight losses of BCN18 in dry gas were attributed to a change in oxygen stoichiometry.

Fig. 1 provides an example of the first kind of experiments. Starting from the left upper corner, the dried sample is first exposed to P<sub>2</sub>O<sub>5</sub>-dried synthetic air (the reference state A), then to P<sub>2</sub>O<sub>5</sub>-dried argon (level B), to P<sub>2</sub>O<sub>5</sub>-dried Ar-4%H<sub>2</sub> (unknown but very low humidity-level C) and then to Ar-4%H<sub>2</sub> with increasing levels of water vapor (levels D, E, F and G). To exclude the possibility of irreversible processes (such as sample decomposition) we again switched to dry Ar-4%H<sub>2</sub> (level H), dry Ar and dry synthetic air. The present experiments were evaluated using the following reactions: (a) loss of oxygen in very reducing atmospheres as described by:



(b) water uptake of BCN18 :



$$K_3 = \frac{[OH^*]^2}{p_{H_2O}[V_O^{\bullet\bullet}][O_O^x]} = \exp(\Delta S_3^0 / k) \exp(-\Delta H_3^0 / kT)$$

Adding the above reactions yields:  $H_2 + 2O_O^x \Rightarrow 2[OH^*] + 2e'$

which describes uptake and desorption of *hydrogen* gas with the mass action law:

$$K_H = K_3 K_O K_W = \frac{[OH^*]^2 [e']^2}{p_{H_2} [O_O^x]} = \exp(\Delta S_H^0 / k) \exp(-\Delta H_H^0 / kT)$$

(c) we also consider valence changes of Nb:  $2Nb_{Nb}^x + 2e' \Leftrightarrow 2Nb_{Nb}^{\bullet}$

Using the above equations and some approximations we deduce from the present data for the *oxygen* loss:  $\Delta H_O^0 = 2.59$  eV and  $\Delta S_O^0 \approx 0.00106$  eV/K. For the first time, enthalpy and entropy of the *hydrogen* absorption reaction were indirectly determined. The numerical values are:

$$\Delta H_H^0 = -0.8 \text{ eV and } \Delta S_H^0 = -6.6 \times 10^{-4} \text{ eV/K.}$$

#### References

- [1] K.C. Liang, Yang Du, A.S. Nowick, Solid State Ionics **69** 117 (1994)
- [2] A.S. Nowick, Yang Du, Solid State Ionics **77** 137 (1995)
- [3] Yang Du, A.S. Nowick, Mat.Res. Soc.Symp. **369** 289 (1995)
- [4] Yang Du, A. S. Nowick, Solid State Ionics **91** 85 (1996)
- [5] T. Schober, J. Friedrich, D. Triefenbach, F. Tietz, Solid State Ionics **100** 173 (1997)
- [6] F. Krug, T. Schober, Solid State Ionics **92** 297 (1996)
- [7] H.G. Bohn, T. Schober, T. Mono, W. Schilling, Solid State Ionics, in press
- [8] T. Schober, H. G. Bohn, T. Mono, W. Schilling, Solid State Ionics, in press
- [9] T. Mono, T. Schober, Solid State Ionics **91** 155 (1996)

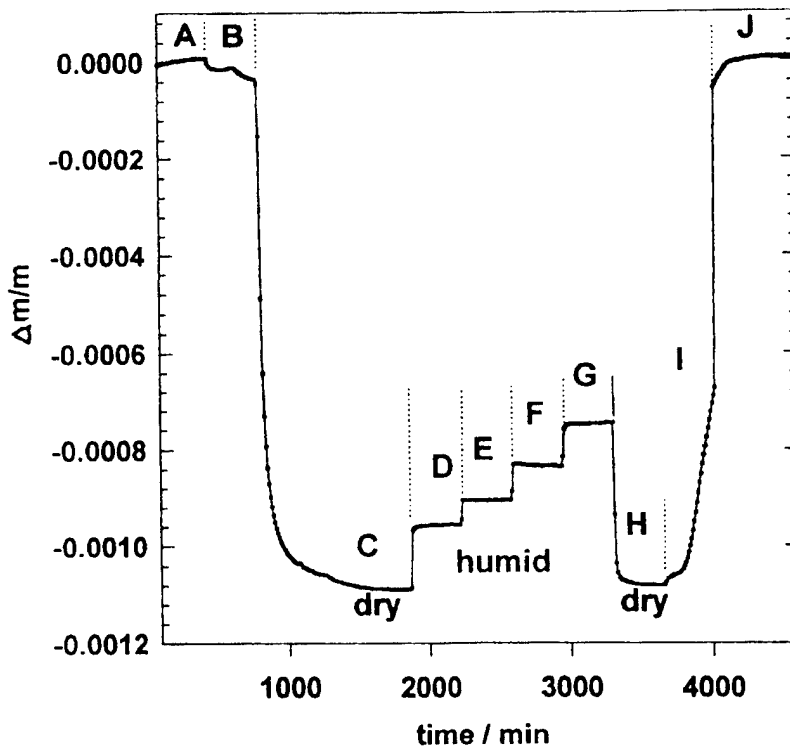


Fig. 1. Relative mass change of a BCN18 powder sample in various atmospheres at 700 °C: level A:  $p_{O_2}=0.21$  bar,  $p_{Ar}=0.79$  bar, level B: 100% Ar,  $p_{O_2} \approx 10^{-5}$  bar, level C:  $P_2O_5$  -dried Ar-4% $H_2$ , level D: Ar-4% $H_2$ ,  $p_{H_2O}=5$  mbar, level E: Ar-4% $H_2$ ,  $p_{H_2O}=10$  mbar, level F: Ar-4% $H_2$ ,  $p_{H_2O}=20$  mbar, level G: Ar-4% $H_2$ ,  $p_{H_2O}=40$  mbar, level H:  $P_2O_5$  -dried Ar-4% $H_2$ , level I: 100% Ar,  $p_{O_2} \approx 10^{-5}$  bar, level J:  $p_{O_2}=0.21$  bar,  $p_{Ar}=0.79$  bar

## PRESSURE EFFECT ON SUPERPROTONIC PHASE TRANSITIONS IN MIXED $[(\text{NH}_4)_x\text{Rb}_{1-x}]_3\text{H}(\text{SO}_4)_2$ CRYSTALS.

V.V.Sinitsyn<sup>1</sup>, A.I.Baranov<sup>2</sup> and E.G.Ponyatovsky<sup>1</sup>

<sup>1</sup>*Institute of Solid State Physics RAS, 142432 Chernogolovka, Moscow distr., Russia.*

<sup>2</sup>*Institute of Crystallography RAS, 117333 Leninskii pr. 59, Moscow, Russia.*

The pressure effect on phase transitions in the mixed  $[(\text{NH}_4)_x\text{Rb}_{1-x}]_3\text{H}(\text{SO}_4)_2$  crystals was studied at high hydrostatic pressure up to 2.0 GPa. At room temperature and atmospheric pressure these mixed compounds belong to the same structure type as other solid acid sulfates and selenates of  $\text{Me}_3\text{H}(\text{AO}_4)_2$  family. As it is known, in the number of the crystals of the group are realized the superprotonic phase transitions accompanied by the changing of the crystal symmetry  $A2/a \Leftrightarrow R\bar{3}m$ . The similar structure relation during superprotonic phase transition for

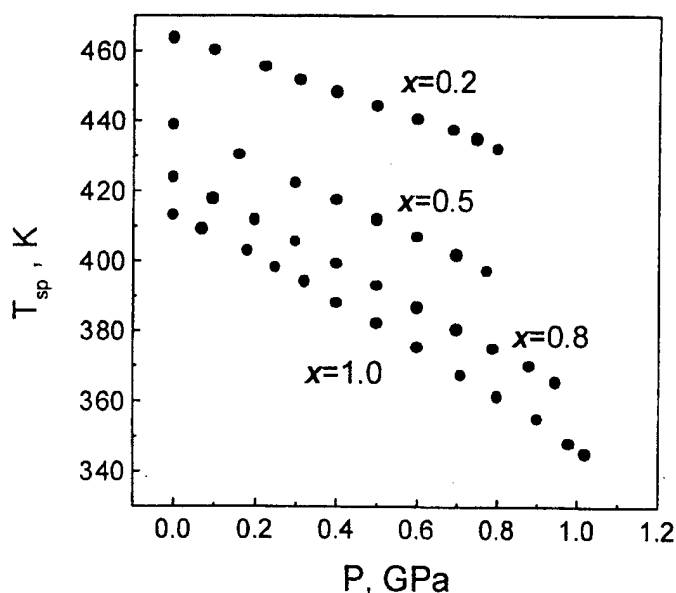


Fig.1 Pressure dependencies of  $T_{sp}$  for some  $[(\text{NH}_4)_x\text{Rb}_{1-x}]_3\text{H}(\text{SO}_4)_2$  crystals.

mixed  $[(\text{NH}_4)_x\text{Rb}_{1-x}]_3\text{H}(\text{SO}_4)_2$  crystals is observed only at the concentration  $x \geq 0.1$ . The pressure dependencies of superprotonic phase transition temperature  $T_{sp}$  for this concentration range are shown on the Fig.1. As it can be seen from the Figure, the temperature  $T_{sp}$  is decreased with pressure. The total drop of  $T_{sp}$  values are very essential and achieve  $30 \div 70$  degree in depending on concentration  $x$ .

The symmetry changing at the superprotonic phase transition becomes another type at  $x < 0.1$ . The high conductivity state has cubic symmetry in this case, according to our preliminary data. To understand the peculiarities of pressure effect on  $T_{sp}$  for compounds

with  $x \leq 0.2$ , the  $P$ - $T$  phase diagram of  $\text{Rb}_3\text{H}(\text{SO}_4)_2$  was studied more detail. Unlike to above considered mixed crystals, the  $T_{sp}$  value increase with pressure at  $P \leq 0.2$  GPa in  $\text{Rb}_3\text{H}(\text{SO}_4)_2$ . The pressure  $P > 0.2$  GPa introduces new high conductivity phase on the  $T$ - $P$  plane. The activation enthalpy value of protonic conductivity in the new high pressure phase is typical for rhombohedral (sp. gr.  $R\bar{3}m$ ) superprotonic phases of  $\text{Me}_3\text{H}(\text{AO}_4)_2$  crystals.

## HYDROGEN ISOTOPE CELL AND ITS APPLICATION TO HYDROGEN ISOTOPE SENSING

H. Matsumoto and H. Iwahara

Center for Integrated Research in Science and Engineering, Nagoya University,  
Furo-cho, Chikusa-ku, Nagoya 464-8603, Japan

Several doped perovskite type oxides, such as In-doped  $\text{CaZrO}_3$ , Yb-doped  $\text{SrCeO}_3$  and Y-doped  $\text{BaCeO}_3$ , exhibit proton conduction at high temperature. A hydrogen concentration cell using these materials as a solid electrolyte gives a definite EMF based on the Nernst's equation, and thus it has been applied to a hydrogen sensor.

We have reported that besides the difference in hydrogen concentration, the difference in mass number of the two hydrogen isotopes,  $\text{H}_2$  and  $\text{D}_2$ , gave rise to a certain EMF. We termed this cell "hydrogen isotope cell". This experimental fact that such hydrogen isotope cell results in a generation of EMF will not be explained by the Nernst's equation and is based on a different mechanism. On the other hand, this hydrogen isotope cell will serve as hydrogen isotope sensor, since hydrogen isotopes may be electrochemically distinguishable on measuring EMF of the cell. In this work, the EMF of the hydrogen isotope cell is discussed from the experimental data with the In-doped  $\text{CaZrO}_3$  electrolyte and the theoretical estimation from the Wagner's type electrochemical calculation. Hydrogen isotope sensing has also been investigated.

An electrochemical cell with an electrolyte disk of  $\text{CaZr}_{0.90}\text{In}_{0.10}\text{O}_{3-\alpha}$  adhered with porous platinum electrodes were constructed. When  $\text{H}_2$  and  $\text{D}_2$  gases were introduced to respective electrode compartments of the cell, open circuit voltages of about 14 ~ 19 mV were observed at 500 ~ 900°C with the  $\text{D}_2$ -side electrode being positive. The EMF increased with increasing temperature. It has already been reported that hydrogen concentration cell shows EMF based strictly on the Nernst's equation for the electrolyte used in this work. Thus the electronic contribution to the EMF could be neglected.

Assuming two charge carriers,  $\text{H}^+$  and  $\text{D}^+$ , with different mobilities in the electrolyte, EMF of the  $\text{H}_2/\text{D}_2$  cell could be estimated from electrochemical calculation, which consisted of two terms. One was of the redox reactions of  $\text{H}_2$  and  $\text{D}_2$  at the electrode-electrolyte interfaces and the other was based on the potential gradient generated internally in the electrolyte due to the difference in mobilities of  $\text{H}^+$  and  $\text{D}^+$ . The latter term could be calculated to be 35 ~ 40 mV on assuming the ratio of mobility of  $\text{H}^+$  to  $\text{D}^+$  as square root of two, which was in the same polarity as experimentally observed. Thus the observed EMF for the  $\text{H}_2/\text{D}_2$  cell would result from the internal potential gradient due to the difference in mobilities of  $\text{H}^+$  and  $\text{D}^+$  in the electrolyte with a negative contribution from the electrode reactions of  $\text{H}_2$  and  $\text{D}_2$ .

In order to investigate the hydrogen isotope sensing, test gases prepared by mixing  $\text{H}_2$  and  $\text{D}_2$  gases were introduced to the cell. Pure  $\text{H}_2$  or  $\text{D}_2$  gases were supplied to the counter compartment as the standard gas. Observed EMF was almost a linear function of hydrogen isotope composition of the test gases. Such dependence of EMF of hydrogen isotope cell for hydrogen isotope mixture was consistent with the mechanism mentioned above, and would serve as an electrochemical hydrogen isotope sensor.

## ELECTRICAL CONDUCTION IN $\text{SrCeO}_3$ DOPED WITH $\text{Eu}_2\text{O}_3$

Toshihide TSUJI and Takuji NAGANO\*

The Center for New Materials, Japan Advanced Institute of Science and Technology, Hokuriku  
1-1 Asahidai, Tatsunokuchi, Ishikawa, 923-1292 Japan

\*Toyota Motor Corporation, Higashifuji Technical Center, Future Project Division,  
1200 Misyuku, Susono, Shizuoka, 410-1193 Japan

### 1. Introduction

High-temperature proton-conducting solids are useful materials for high-temperature fuel cells, hydrogen sensors, hydrogen gas separators, etc.[1]. Attractive candidates for protonic conductors at high temperatures are the perovskite-type oxides such as  $\text{SrCeO}_3$ ,  $\text{BaThO}_3$  and  $\text{CaZrO}_3$  where some trivalent cations are partially substituted for B site cations[2, 3]. Doped  $\text{SrCeO}_3$  and  $\text{BaThO}_3$  are also known to exhibit hole, protonic and/or oxide ionic conduction depending on the temperature, the oxygen partial pressure and the water vapor pressure[1-3]. However, no fundamental studies on the electrical conduction have been carried out for  $\text{SrCe}_{1-y}\text{Eu}_y\text{O}_{3-x}$  sample. In this study, the electrical conductivity of  $\text{SrCeO}_3$  doped with  $\text{Eu}_2\text{O}_3$  which are one of Moessbauer species has been measured by four inserted wires method as a function of temperature, the oxygen partial pressure and water vapor pressure in order to know electrical conduction mechanism.

### 2. Experimental

The powders of analytical reagent-grade strontium carbonate, cerium dioxide and europium sesquioxide in the required proportion were mixed in an agate mortar and calcined in a platinum crucible at 1523 K for 10h in air. The calcined powders were mixed again and pressed into a cylindrical pellet (10 mm in diameter and 2.5 mm in thickness) at a pressure of 400 kg/cm<sup>2</sup>. Four holes of 0.3 mm in diameter were drilled in a line on the surface of the pellet and a platinum wire of 0.3 mm in diameter was inserted into each hole. The pellet was then sintered at 1823 K for 10 h in air. The experimental density of the sample was 96.5% of the theoretical density.

The electrical conductivity measurement of the sample was carried out by means of the conventional four inserted wires method. The oxygen partial pressure was controlled by mixing argon and oxygen gases. The water vapor pressure was controlled by flowing the ambient gas which was saturated with water kept at a constant temperature.

### 3. Results and discussion

Analysis of X-ray powder diffraction patterns for  $\text{SrCe}_{0.9}\text{Eu}_{0.1}\text{O}_{3-x}$  sample showed the existence of a single phase with orthorhombic structure ( $a=858.0$ ,  $b=601.7$  and  $c=615.6$  pm). The isomer shift for  $\text{SrCe}_{0.9}\text{Eu}_{0.1}\text{O}_{3-x}$  sample ( $\delta = 1.01$  mm/s relative to  $\text{EuF}_3$ ) annealed in air at 1273 K which

was determined by room temperature Moessbauer spectroscopy was close to that of a reference  $\text{Eu}^{3+}$  sample ( $\delta = 1.02$  mm/s for  $\text{Eu}_2\text{O}_3$ ) rather than that of a reference  $\text{Eu}^{2+}$  sample ( $\delta = 13.8$  mm/s for  $\text{EuSO}_4$ ), indicating that the europium ions are existed as the  $\text{Eu(III)}$  state and occupied the B-sites in perovskite-type oxides. The isomer shift ( $\delta = 1.01$  mm/s) of  $\text{SrCe}_{0.9}\text{Eu}_{0.1}\text{O}_{3-x}$  sample annealed at 1273 K in air was a slightly smaller than that ( $\delta = 1.42$  mm/s) annealed in hydrogen gas flow at 1273K.

Total electrical conductivity ( $\sigma_t$ ) of  $\text{SrCe}_{0.9}\text{Eu}_{0.1}\text{O}_{3-x}$  sample is shown as a function of the temperature (T) under various dry hydrogen partial pressures in Fig. 1, where total electrical conductivity is increased with increasing hydrogen partial pressure, indicating a proton conductor. As seen in the figure, the activation energy for proton conduction in the sample varies at 1023K from 1.2 eV in the high temperature range to 0.8 eV in the low temperature range. In TG-DTA measurement for  $\text{SrCe}_{0.9}\text{Eu}_{0.1}\text{O}_{3-x}$  sample in air, the weight loss of the sample in TG and endothermic peak in DTA were observed around 1023 K, reflecting oxygen evolution from the sample. In order to know the origin of this phase transition, high temperature X-ray diffractometry was carried out. High temperature X-ray diffractometry showed crystal structure phase transition from high symmetry phase at high temperature to low symmetry phase at low temperature.

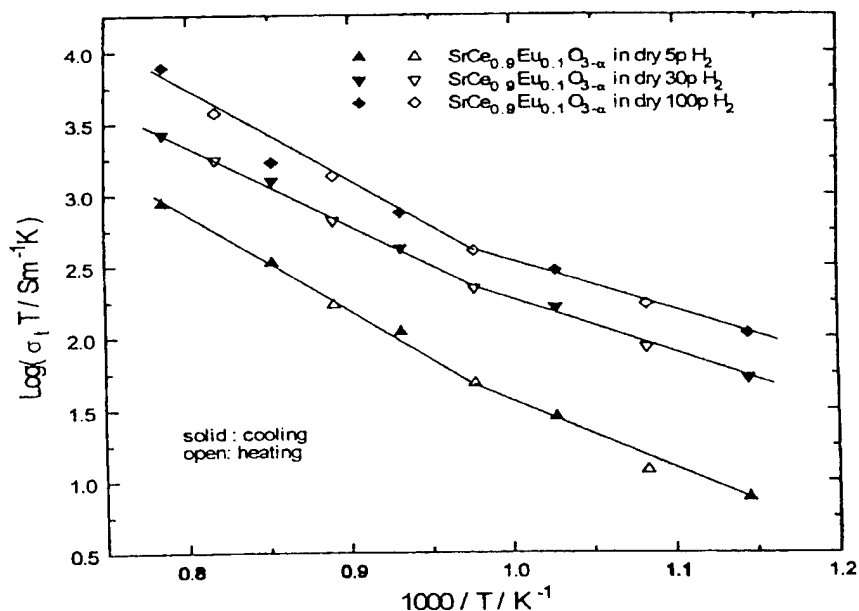


Fig. 1 Temperature dependence of electrical conductivity of  $\text{SrCe}_{0.9}\text{Eu}_{0.1}\text{O}_{3-x}$  sample under various dry hydrogen partial pressure.

#### 4. References

- [1] H.Iwahara, in Proton Conductors, ed. Ph. Colomban(Cambridge Univ. Press, Cambridge, 1992) p.122.
- [2] H.Iwahara, T.Esaka, H.Uchida and N.Maeda, Solid State Ionics **3/4**, 359 (1981).
- [3] T.Tsuji, T.Suzuki and H.Iwahara, Solid State Ionics **70/71**, 291 (1994).

# PROTON DIFFUSION IN PEROVSKITES: COMPARISON BETWEEN CERATES, ZIRCONATES AND TITANTES USING QUANTUM MOLECULAR DYNAMICS

W. Münch, K.-D. Kreuer, G. Seifert<sup>‡</sup>, J. Maier

Max-Planck-Institut für Festkörperforschung

Heisenbergstr. 1, 70569 Stuttgart, Germany

<sup>‡</sup>Technische Universität Dresden, Institut für Theoretische Physik

Mommsenstr.13, 01069 Dresden, Germany

Atomistic numerical calculations have been carried out to simulate proton diffusion for a number of cubic perovskite-type oxides, e.g. [1 - 7]. The numerical estimates of the activation energies and of the time constants for the proton diffusion process can be reproduced in reasonable agreement with experimental results in the quantum molecular-dynamics models. The differing compositions and lattice constants result in distinct proton diffusion processes: for e.g. BaCeO<sub>3</sub> at T = 1000 K proton transfer is rate limiting [3] with only inter-tetrahedra diffusion paths whereas for CaTiO<sub>3</sub> proton transfer and reorientation are found to occur on similar time scales with both intra- and inter-tetrahedra diffusion paths [8]. In this contribution we want to discuss in detail the physical and chemical arguments which may explain the differences in the diffusion processes for cerates, zirconates and titanates.

- [1] M. Cherry, M. S. Islam, J. D. Gale, C. R. A. Catlow; Solid State Ionics **77**, 207 (1995)
- [2] M. Cherry, M. S. Islam, J. D. Gale, C. R. A. Catlow; J. Phys. Chem. **99**, 14614 (1995)
- [3] W. Münch, G. Seifert, K. D. Kreuer, J. Maier; Solid State Ionics **86-88**, 647 (1996)
- [4] W. Münch, G. Seifert, K. D. Kreuer, J. Maier; Solid State Ionics **97**, 39 (1996)
- [5] F. Shimojo, K. Hoshino, H. Okazaki; J. Phys. Soc. Japan **65**, 1143 (1996)
- [6] F. Shimojo, K. Hoshino, H. Okazaki; J. Phys. Soc. Japan **66**, 8 (1997)
- [7] K.-D. Kreuer, W. Münch, U. Traub, J. Maier; Ber. Bunsenges. Phys. Chem. **102**, 552 (1998)
- [8] W. Münch, K. D. Kreuer, G. Seifert, J. Maier; submitted to Solid State Ionics (1998)

## BASICITY AND HYDROXYL CAPACITY OF PROTON CONDUCTING PEROVSKITES

Shu YAMAGUCHI<sup>a</sup>, Kenji NAKAMURA<sup>a</sup>, Toru HIGUCHI<sup>b</sup>, Shik SHIN<sup>b</sup>, and Yoshiaki IGUCHI<sup>c</sup>

<sup>a</sup>Department of Materials Science and Engineering, Nagoya Institute of Technology  
Gokiso-Cho, Showa-Ku, Nagoya 466-8555, Japan

<sup>b</sup>Faculty of Science, Science University of Tokyo, Kagurasaka 1-3, Shinjuku, Tokyo 162-0825,  
Japan

<sup>c</sup>Institute of Solid State Physics, University of Tokyo, Tanashi 188-8501, Japan

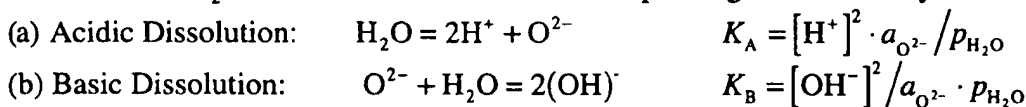
### 1. INTRODUCTION

One of the most important characteristics of proton conducting oxides is the large extent of solubility of protons. The dissolution reaction of protons has been well described by the defect chemical treatment. No discussion, however, has been given on the relation between the basicity and the solubility of protons, since the basicity of complex oxides has never been taken into account in the defect chemical consideration. In the present study, the hydroxyl capacity, proposed by Wagner[1] is applied to the defect chemistry in order to discuss the solubility of protons in perovskites.

### 2. THEORETICAL BACKGROUND

The basicity of complex oxide system is defined as the thermochemical activity of oxide ion ( $a_{O^{2-}}$ ), since  $O^{2-}$  is the common anion in the system. However, it is not measurable without approximation because complex oxide is a concentrated ionic solution. There have been proposed many kinds of measurable measure of the basicity by thermochemical or physical method. Among them, the thermochemical activity of basic oxide and the capacity of gaseous components have been widely accepted as an relative measure of the basicity in liquid oxides.

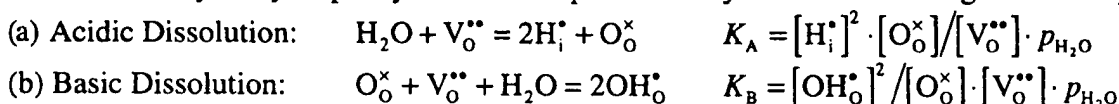
In liquid oxides, there have been proposed two types of dissolution mechanism of water, which indicate that  $H_2O$  works as both acid and base depending on the basicity of solution.



The hydroxyl capacity ( $C_{OH}$ ) is defined as,

$$C_{OH} = [\%HO_{0.5}] \cdot p_{H_2O}^{-1/2} \quad (= [H^+, OH^-] \cdot p_{H_2O}^{-1/2}) = (K_B \cdot a_{O^{2-}})^{1/2}, \text{ or } (K_A \cdot a_{O^{2-}})^{1/2} \quad (1)$$

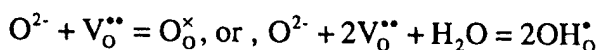
Application of the hydroxyl capacity to solid complex oxides yields the following relationships.



$H_2O$  has been believed to dissolve by the basic dissolution mechanism in  $ABO_3$  perovskite. The apparent hydroxyl capacity of a solid complex oxide can be written, when the basic dissolution takes place, by the following equation.

$$C_{OH} \equiv [OH_O^{\bullet}] \cdot [V_O^{\bullet\bullet}]^{-1/2} \cdot p_{H_2O}^{-1/2} = (K_B \cdot a_{O^{2-}})^{1/2} \quad (2)$$

The activity of  $O_O^{\times}$  ( $a_{O^{2-}}$ ) is further related to  $a_{O^{2-}}$  in equilibrium with crystal through the following relation.



Therefore, the hydroxyl capacity for solid oxides can be defined by the equation below.

$$C'_{OH} \equiv [OH_O^{\bullet}] \cdot [V_O^{\bullet\bullet}]^{-1} \cdot p_{H_2O}^{-1/2} = (K_B \cdot a_{O^{2-}})^{1/2} \quad (3)$$

Finally,  $a_{O^{2-}}$  is related to the activity of a basic oxide,  $AO$ , ( $a_{AO}$ ) by the following equilibrium,

$$AO = A^{2+} + O^{2-}, \text{ where } A^{2+} + V_A'' = A_A^{\times}.$$

The discussion above suggests that the difference between solid and liquid system is a free volume ( $V_O^{\bullet\bullet}$ ) for the dissolution of  $OH^-$  is necessary in solid systems. Since  $a_{AO}$  changes markedly across  $ABO_3$  perovskite phase from AO-rich side to  $BO_2$ -rich side, the change in the  $C'_{OH}$  across  $ABO_3$  is anticipated.

### 3. EXPERIMENTAL

The solubility of water at 900 °C as a function of BaO activity ( $a_{BaO}$ ) in  $BaCeO_3$  doped with 5 mol%  $YbO_{1.5}$  has been examined by a thermogravimetry in order to estimate  $C'_{OH}$  value.  $a_{BaO}$  was controlled by equilibrating with  $CO_2$  in the atmosphere. Prior to the solubility measurements, the activity measurement of BaO in  $BaO-CeO_2-YbO_{1.5}$  system has been made using the formation reaction of  $BaCO_3$  by a thermogravimetry method, in addition to the determination of the isothermal phase relation in  $BaO-CeO_2-YbO_{1.5}$  system.

### 4. RESULTS AND DISCUSSION

The phase relation examined was almost identical to the one reported for  $BaO-CeO_2-NdO_{1.5}$  [2], where three-phase regions of  $BaCeO_3+CeO_2+YbO_{1.5}$  and  $BaCeO_3+Ba_3Yb_4O_9+YbO_{1.5}$  was observed. In addition, the presence of  $BaCeO_3+Ba_3Yb_4O_9+BaO$  was estimated as being present.

Figure 1 shows the homogeneous domain of  $BaCeO_3$  as functions of  $\log a_{BaO}$  and dopant concentration. The thin solid curve indicates the variation of  $\log a_{BaO}$  under a fixed [A-site]/[B-site] ratio ([Ba]/[Ce+Yb] ratio in this case), estimated from the iso-activity lines of BaO. The present results suggest that the Yb substitution increase both  $a_{BaO}$  and the vacancy concentration. This may be a possible reason for the strong dopant-concentration dependency of the equilibrium constant of  $H_2O$  dissolution reaction.

Figure 2 shows the variation of  $\log a_{BaO}$ ,  $2\log C'_{OH}$ , and  $\log a_{Ba^{2+}}$ . The large variation of  $\log a_{Ba^{2+}}$ , which may be caused by the large extent of A-site deficiency, dominantly contributes to the change in  $\log a_{BaO}$  across  $BaCeO_3$  homogeneous domain.

By the dissolution of  $H_2O$ , the increase in the fraction of hybridization of O2p band was observed by the resonating photoelectron spectroscopy measurements, suggesting the ionicity (or the fraction of non-bonding O2p orbital) determined by the spectroscopy is a measure of the basicity in view of the electronic structure.

### REFERENCES

- [1] C. Wagner, Metall. Trans., **6B**, 405 (1975).
- [2] D. Makovec, Z. Samardzija, and D. Kolar, J. Am. Ceram. Soc., **80**, 3145 (1997).

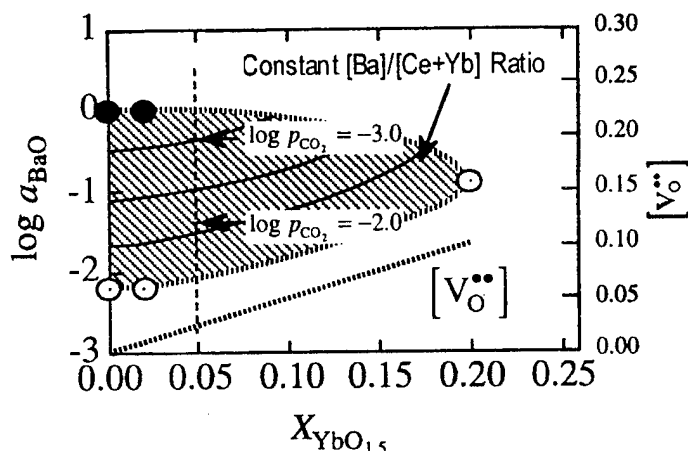


Fig. 1 Variation of activity of BaO with dopant concentration in homogeneous domain of  $BaCeO_3$ .

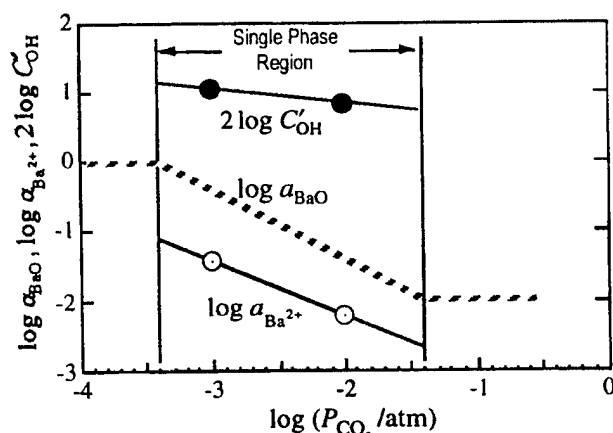


Fig. 2 Variation of activity of  $C'_{OH}$ , BaO, and  $Ba^{2+}$  with  $\log P_{CO_2}$ .



## O-H STRETCHING VIBRATION IN PEROVSKITE-TYPE PROTON CONDUCTORS

N.Sata, H.Sone, N.Kitamura, T.Hattori, M.Ishigame

Research Institute for Scientific Measurements, Tohoku University, Sendai 980-8577, Japan

High temperature type proton conductors, like trivalent cation doped  $\text{SrCeO}_3$  and  $\text{SrZrO}_3$  are now well-known and promising materials with high proton transport number. By using single crystals, it was clearly observed in ir-region that proton is bound by oxygen ion with relatively low binding energy<sup>1)</sup>, which should be come from hydrogen bond character, and that the O-H bond strength is widely spread due to the inhomogenous distribution of proton sites. It is suggested that the local lattice distortion plays an important role for proton dynamics in these perovskite-type oxides. Proton conducting superlattices with different lattice strain were synthesized by pulsed laser ablation method<sup>2)</sup> to study the interaction between proton dynamics and lattice distortion.

By using FTIR-ATR method, O-H stretching vibration was observed in  $\text{SrCe}_{0.95}\text{Yb}_{0.05}\text{O}_3$ - $\text{SrZr}_{0.95}\text{Yb}_{0.05}\text{O}_3$  superlattice as shown in Fig. 1. As indicated by an arrow in the figure, only one broad band was observed in contrast with two broad bands in  $\text{SrCe}_{0.95}\text{Yb}_{0.05}\text{O}_3$  and  $\text{SrZr}_{0.95}\text{Yb}_{0.05}\text{O}_3$  single crystals. The peak wavenumber ratio of O-H and O-D stretching vibration was 1.37. The similar absorption was also observed in another superlattice of  $\text{SrCe}_{0.95}\text{Yb}_{0.05}\text{O}_3$ - $\text{SrZr}_{0.95}\text{Yb}_{0.05}\text{O}_3$ . The peaks of O-D stretching vibration were  $2380\text{cm}^{-1}$  and  $2450\text{cm}^{-1}$ , respectively, as shown in Fig. 2. It is supposed that this wavenumber shift between two different superlattices is due to the difference of lattice strain.

1) S.Shin, H.H.Huang, M.Ishigame and H.Iwahara, Solid State Ionics, 40/41 (1990) 910

2) N.Sata, H.Yugami, Y.Akiyama, T.Hattori, S.Yamaguchi, M.Ishigame, Solid State Ionics, unpublished

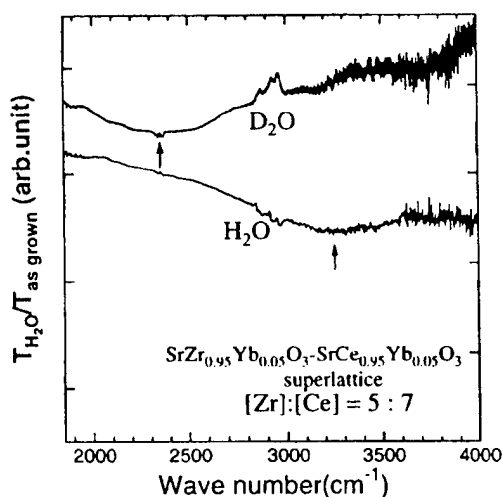


Figure 1: FTIR-ATR spectra of superlattices annealed in  $\text{H}_2\text{O}$  and  $\text{D}_2\text{O}$  atmosphere.

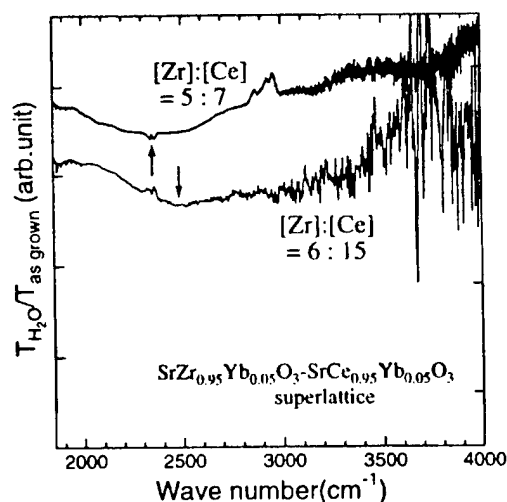


Figure 2: FTIR-ATR spectra of superlattices with different ratio of  $\text{SrCeO}_3/\text{SrZrO}_3$ .

# STRUCTURAL PROPERTIES OF $\text{SrCeO}_3/\text{SrZrO}_3$ PROTON CONDUCTING SUPERLATTICES

Hiroo YUGAMI<sup>A</sup>, Fumitada IGUCHI<sup>A</sup>, and Hitoshi NAITO<sup>B</sup>

<sup>A</sup>Graduate School of Engineering, Tohoku University, Sendai 980-8579, JAPAN

<sup>B</sup>National Aerospace Laboratory, Chofu, Tokyo 182-8522, JAPAN

The structures of  $\text{SrCeO}_3$  and  $\text{SrZrO}_3$  are strongly distorted from the ideal perovskite structure. A unique property of these oxides is a large amount of protons can be introduced and can diffuse at high temperature. This is taken place by high temperature annealing under hydrogen or  $\text{H}_2\text{O}$  containing atmosphere. Many workers have studied the proton dynamics in these materials, and it is found that the oxygen-oxygen distance and structural distortion from the ideal perovskite structure is closely related to the protonic diffusion in the materials. In order to induce the stress between the material interfaces and to change the structural properties, we have been fabricated strained  $\text{SrCeO}_3/\text{SrZrO}_3$  superlattices of these materials[1,2]. In this paper, the structural properties of epitaxial films of  $\text{SrCeO}_3/\text{SrZrO}_3$  superlattices as well as the perovskite-type oxides  $\text{SrMO}_3$  ( $\text{M}=\text{Ce}$  and  $\text{Zr}$ ) thin films have been studied by 4-axis and conventional 2-axis x-ray diffraction (XRD) and Raman scattering spectroscopy on these thin films.

$\text{SrMO}_3$  ( $\text{M}=\text{Ce}$  and  $\text{Zr}$ ) thin films and their superlattices have been made by laser ablation method. Thin films with smooth surface can be grown on  $\text{MgO}$  (110) surface. Epitaxial growth of these films has been confirmed by 4-axis x-ray diffraction analysis. The pole-figure of XRD pattern revealed that the [001] axis of  $\text{SrCeO}_3$  is epitaxially grown on the [001] direction of  $\text{MgO}$  substrate as shown in Fig. 1

Clear satellite peaks in XRD patterns indicate that the superlattice structure is obtained on this film even in  $(\text{SrZrO}_3)_1/(\text{SrCeO}_3)_1$  superlattice. The XRD patterns can be simulated by the simple step model as shown in Fig. 2. This means the superlattice wavelength is controlled by the deposition condition in this study.

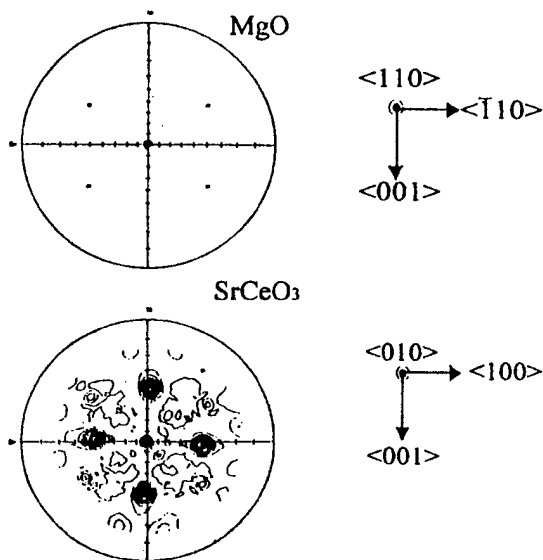


Fig.1 Pole-figures for  $\text{MgO}$  substrate(upper), and  $\text{SrCeO}_3$  thin film(lower).

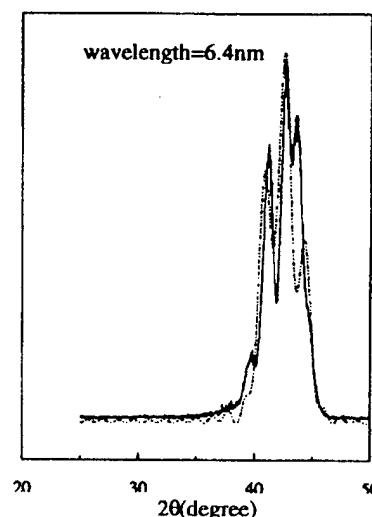


Fig.2 XRD patterns simulated by the simple step model.

Figure 3 shows the superlattice wavelength dependence of lattice constant  $a$ , which is perpendicular to MgO [001] direction, is estimated by 4-axis XRD measurement. Superlattices having shorter period of periodicity shows the same lattice constant in each component, and the value is very close to the lattice constant of MgO substrate. The stress induced at the interface is estimated to be +2.7% (tensile) for SrCeO<sub>3</sub> and -2.6% (compression) for SrZrO<sub>3</sub>.

In contrast to the short periodicity region, the lattice constant is different from each other for the superlattice having long periodicity. This indicates that the strain between the interface is released within the each layer.

The frequency of Raman band for superlattices having various periodicities is shown in Fig.4. The frequency of the strongest bands for SrCeO<sub>3</sub> and SrZrO<sub>3</sub> changes in the short periodicity region. This tendency is well correlate with the results of lattice parameter measurement. It is found from the polarized Raman measurement on SrCeO<sub>3</sub> single crystal that the band is attributed to the B<sub>2g</sub> mode. Since this mode is related the vibration of oxygen octahedron, the high frequency shift of Raman band for SrCeO<sub>3</sub> suggests that the oxygen-oxygen distance in short period superlattice may be shorter than the SrCeO<sub>3</sub> thin films. The electrical properties of this superlattice will be presented in the conference.

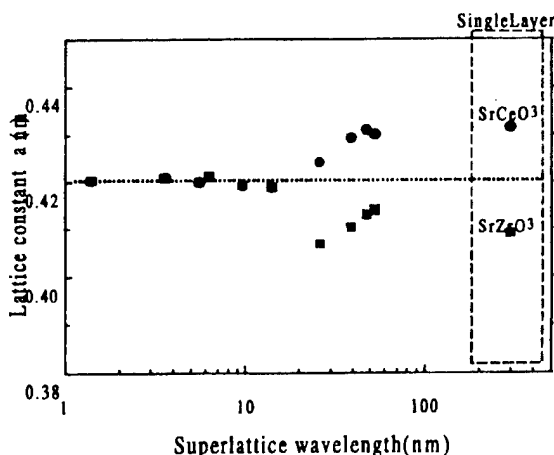


Fig. 3 Lattice constant  $a$  vs superlattice wavelength measured by 4-axis XRD.

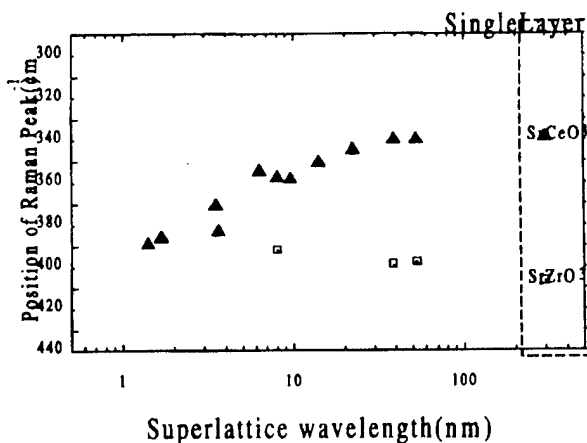


Fig. 4 Raman frequency vs superlattice wavelength.

[1] H. Yugami et al., Applied Surface Science, 113/114 (1997), 222.

[2] H. Yugami et al., Integ. Ferroelectrics, 20 (1998), 241.

## PREPARATION AND CHARACTERIZATION OF BARIUM CERATE BASED THICK FILMS USING A SCREEN - PRINTING PROCESS

Guangyao Meng, Ping Wang and Dingkun Peng

USTC Lab. For Solid State Chemistry and Inorganic Membranes  
University of Science and Technology of China  
Hefei, Anhui 230026 China

M (Ba or Sr)CeO<sub>3</sub> based materials have been paid much attention recent years as electrolytes for high temperature solid state ionic devices, such as hydrogen gas sensors, hydrogen purifier, steam electrolyzer and solid state fuel cells as well as membrane reactors for chemical processes, because of their proton conduction at high temperatures [1,2]. It is no doubt that it is of great significance for all of these potential applications if the materials can be made in a thinner layer or membrane in order to reduce electrical resistance as well as to extend their operation temperature onto lower ones. Unfortunately, however, it has been rare report on this subject, though there were many papers dealing with their bulk sintered materials [3].

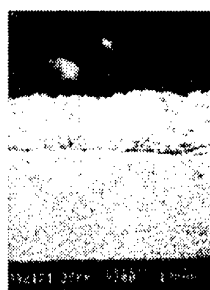
In this work, BaCe<sub>0.9</sub>Nd<sub>0.1</sub>O<sub>3-δ</sub> thick films or membranes on various composite ceramic supports have been prepared by a silk screen-printing process and characterized by XRD, SEM, N<sub>2</sub> permeation measurement and ac impedance spectroscopy technique. As usual for this well known technique to fabricate thick films an uniform and stable printing-paste was first prepared by ball-milling a mixture of the fine BaCe<sub>0.9</sub>Nd<sub>0.1</sub>O<sub>3-δ</sub> powder and organic additives (e.g. ethyl-cellulose dissolved into terpeneol). A homogeneous oxalate co-precipitation method was employed to make BaCe<sub>0.9</sub>Nd<sub>0.1</sub>O<sub>3-δ</sub> ceramic powders, which exhibited a particle size less than 2 μm. Both porous and dense NiO-BaCe<sub>0.9</sub>Nd<sub>0.1</sub>O<sub>3-δ</sub> two phase ceramic composites were used as ceramic substrates. They were prepared by ball-mill mixing the powders of NiO and BaCe<sub>0.9</sub>Nd<sub>0.1</sub>O<sub>3-δ</sub> in a weight ratio of 40 % to 60% and pressing it into pellets, and then sintering at 800°C/10hr for porous substrate and 1300 °C/3hrs for dense ones. BaCe<sub>0.9</sub>Nd<sub>0.1</sub>O<sub>3-δ</sub> paste was printed on the substrates by a silk screen-printing technique. The coated substrates were then dried under infrared lamp and fired in air at temperature ranging from 1360 °C to 1500 °C for 3 hrs to 5 hrs. Thermal analysis including TG and DTA on the dried green membrane samples showed a continuous weight loss from about 150 °C to 390 °C. This indicated that the oxidation of the organic in the paste was completed below 390 °C. Accordingly, the temperature profile for the heat treatment was specifically designed to allow a uniform removal of the organic component in order to avoid cracks of the final membranes. After preparation of the thick films a heat treatment in hydrogen is done on the specimen to reduce NiO component into metal nickel and result in a porous and conductive composite support to facilitate the electric characterization for the membrane.

XRD illustrated that the powder and the final membranes of BaCe<sub>0.9</sub>Nd<sub>0.1</sub>O<sub>3-δ</sub> exhibited an orthorhombic structure with lattice parameters a little bit different from that for pure BaCeO<sub>3</sub>, indicating the solid solution formation with Ce atom sites partly substituted by Nd atoms. No other extra phase rather than NiO and BaCe<sub>0.9</sub>Nd<sub>0.1</sub>O<sub>3-δ</sub> were detected in the resulted NiO-BaCe<sub>0.9</sub>Nd<sub>0.1</sub>O<sub>3-δ</sub> composite. This indicates no reaction taking place between these two components up to 1500 °C. And, this composite can function as a good electrode materials for

$\text{BaCe}_{0.9}\text{Nd}_{0.1}\text{O}_{3.8}$  like the YSZ + Ni composite does for YSZ electrolyte.

The preparation results indicate the substrate situation and the heat treatment procedure are the most important factors in obtaining desired layers. SEM photos in Fig.1 show that the dried green membrane does not have a good adherence to the  $\text{NiO-BaCe}_{0.9}\text{Nd}_{0.1}\text{O}_{3.8}$  substrate (Fig.1a), but after being fired at 1400 °C for 3 hrs and reduced in  $\text{H}_2$ , both substrate and the membrane become porous and adhere each other very well (Fig.1b). An increase of the firing temperature to 1500 °C and firing time to 5 hrs resulted in a dense membrane on the porous substrate. As shown in Fig.2 the derived membrane is a well-sintered layer. The thickness of the membrane is around 10  $\mu\text{m}$  and it is crack free with grain sizes in the range of 2 to 8  $\mu\text{m}$ . Nitrogen permeation test also demonstrated the gas-tight of the membrane. The cross-section view (Fig.2b) indicates the layer looks like compacted fish scale and adhering well with the  $\text{NiO-BaCe}_{0.9}\text{Nd}_{0.1}\text{O}_{3.8}$  substrate which has not been reduced in hydrogen. In contrast to the above specimen; the membrane prepared on dense substrate and reduced in  $\text{H}_2$  under the same conditions is porous as shown in Fig.3. These results imply the different sintering behavior for the membranes on the different substrates.

Fig.4 shows the conductivity curves for the different specimens in the temperature range of 250 - 750°C. It can be seen that the conductivity behaviors of all membranes consist of three regions but with different slopes for dense and porous membranes, indicating various conduction activation energy. It will be discussed in the terms of the membrane microstructure and transport mechanisms. The much lower activation energies for membranes compared with that for bulk pure  $\text{BaCe}_{0.9}\text{Nd}_{0.1}\text{O}_{3.8}$  sample (Fig.4. line-a) is attributed to the nickel diffusion into the membrane from the substrate.



(a)



(b)



(a)



(b)

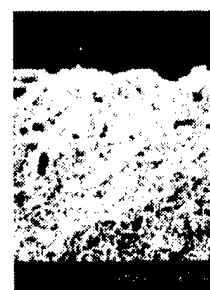


Fig. 3

Fig. 1

Fig. 2

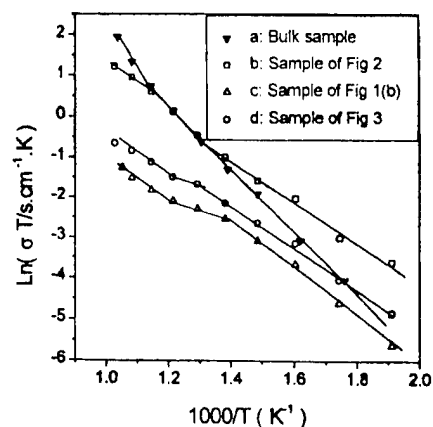


Fig. 4

#### Acknowledgement:

The financial support from Chinese Natural Science Foundation for this work is much acknowledged.

#### References:

- [1] N. Bananos, B. Ellis and M. N. Mahmood, *Solid State Ionics* **44**, 305 (1991).
- [2] Robert C. T. Slade and Narendra Singh, *Solid State Ionics* **46**, 111 (1991).
- [3] S. Hamakawa, T. Hibino, and H. Iwahara, *J. Electrochem. Soc.* **141**, 1720 (1994).

HYDROGEN PERMEATION IN SINTERED  $\text{Ce}_{0.8}\text{Yb}_{0.2}\text{O}_{1.9}$  AT HIGH TEMPERATURES

Y. Nigara, K. Kawamura, T. Kawada and J. Mizusaki

Research Institute for Scientific Measurements, Tohoku University,  
2-1-1 Katahira, Aoba-ku, Sendai 980-8577 Japan

It was found that the sintered  $\text{Ce}_{0.8}\text{Yb}_{0.2}\text{O}_{1.9}$ , which was not perovskite-type but fluorite-type, permeated hydrogen at 1000 - 1800 K. The tube shaped two specimens, the lengths of which were 2.4<sub>0</sub>, 0.5<sub>0</sub> cm, were prepared. The measurement system is shown in Fig.1(a), (b). The hydrogen source gas,  $\text{H}_2(8.0\%) + \text{N}_2 + \text{H}_2\text{O}(2.5\%)$ , was supplied to the outside of specimens ( $200\text{ cm}^3\text{ min}^{-1}$ ). Ar gas was let flow to the inside of specimens. The flow rate to the long specimen was  $21.4\text{ cm}^3\text{ min}^{-1}$  and to the short it was controlled so that the hydrogen concentrations were same value. The measurements of them were carried out independently. The  $\text{H}_2$  concentration in the outlet Ar was analyzed by a gas chromatograph. In the determination of hydrogen permeation, the concentrations of  $\text{H}_2$ ,  $\text{H}_2\text{O}$  and  $\text{O}_2$  at the inside and outside of specimens were calculated by the equilibrium state equation at respective temperatures. The transferred hydrogen could be obtained from the calculated hydrogen concentration inside of specimen and Ar flow rate. It consisted of the permeated hydrogen through the specimen ( $J$ ), Pt O-rings (used to fix the specimen and alumina tube and alumina disk) and the alumina supporting materials ( $J_{\text{PA}}$ ) and of the mechanically leaked one ( $M$ ). The atomic hydrogen permeation ( $J_{\text{H}}$ ) was determined from  $J$  by the dimensional normalization of the specimen.  $\log(J_{\text{H}}\text{ mol h}^{-1}\text{ cm}^{-1})$  increased with the increasing temperature ( $T$ ) and at 1250 K it had a discontinuity (Fig. 2).

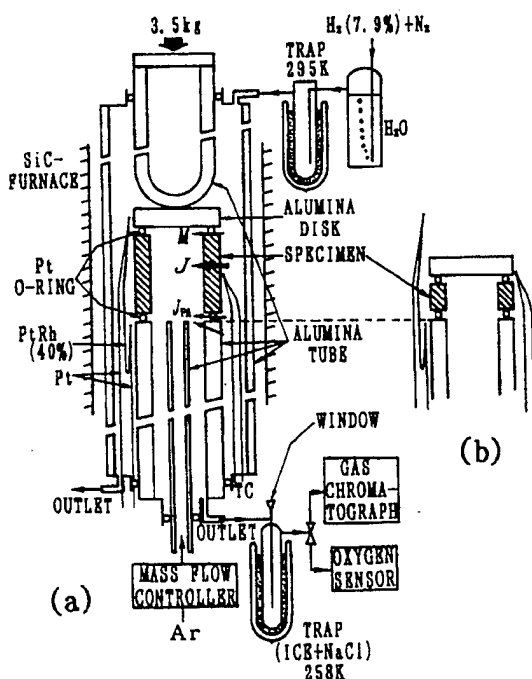


Fig. 1

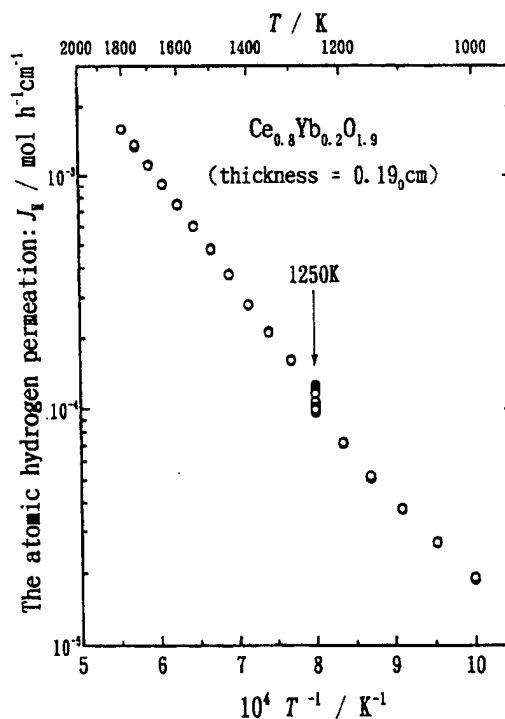


Fig. 2

PROTON AND OXYGEN ION TRANSPORT IN  
FLUORIDE-BASED ELECTROLYTESBin Zhu<sup>a</sup> and Bengt-Erik Mellander<sup>b</sup><sup>a</sup>Department of Chemical Engineering & Technology, Royal Institute of Technology (KTH), S-100 44 Stockholm, Sweden<sup>b</sup>Physics and Engineering Physics, Chalmers University of Technology, S-412 96 Göteborg, Sweden

This work focuses on the behaviour and role of protons and oxygen ions for the electrical properties of fluoride based materials, e.g.,  $\text{MF}_x$  ( $\text{M} = \text{Na}, \text{K}, \text{Ca}, \text{Ba}, \text{Sr}, \text{Pb}, \text{Ce}, \text{Bi}, \text{La}, x = 1-3$ ) with various dopants and composites of these materials with an oxide. The electrical properties were studied using D.C. measurements, employing either gas concentration cell or fuel cell techniques.

Fluoride solid electrolytes have attracted a lot of attention, especially during the period 1970-1985, due to their high anionic  $\text{F}^-$  conductivity. However, studies of the intrinsic conductivity for  $\text{F}^-$  ions is not the purpose for this study. A number of ionic species may be mobile in these materials but our interest is focused on  $\text{H}^+$  or  $\text{O}^{2-}$ . As a comparison it may be mentioned that in the  $\alpha$ -phase of  $\text{Li}_2\text{SO}_4$  which has an anti-fluorite structure a number of "foreign" cations as well as  $\text{H}^+$  are mobile [1,2]. In fact, oxygen ionic conduction has been discovered in a number of fluorides but it has been found to be negligible compared with the  $\text{F}^-$  conductivity [3]. Proton conduction was not studied in the early investigations.

Both oxygen and hydrogen concentration cell measurements as well as defect chemistry studies indicate that the fluoride-based materials may be oxygen ion and proton conduction depending on the composition, type and concentration of dopant, and the gas atmosphere. Stable open circuit voltages (OCVs) in the region of 1.0 to 1.2 V were always obtained from the fuel cells with Pt electrodes, that is close to the theoretical value. During fuel cell operation, water was observed from both sides of the cell in some cases, while in most cases, water was formed much more at the air electrode than at the hydrogen electrode. This demonstrates that in the fluoride-based electrolytes proton conductivity may dominate during fuel cell operation. Some initial results regarding proton and oxygen ion conduction in chlorides and fluorides have been reported elsewhere [4]. A typical proton conductivity value is  $10^{-2}$  S/cm at temperatures larger than 700°C for most nominally pure fluorides. Doping and forming composites with an oxide phase, such as alumina and ceria etc., can lower this temperature effectively and thus enhances the conductivity significantly at low temperatures. Fig. 1 shows some typical results obtained from fuel cell measurements for nominally pure alkaline earth fluorides and their solid solutions formed by doping with NaF and composites with alumina, lanthanum fluoride is used for comparison. It can be seen clearly in Fig. 1 that doping and forming composites with alumina are very efficient means to enhance the conductivity. This is generally true for most fluorides.  $\text{LaF}_3$  is, however, an exception.  $\text{LaF}_3$  has been reported having high conductivity for  $\text{F}^-$  anions even at room temperature [5]. It is believed that the structure of  $\text{LaF}_3$  has high defect concentrations and that  $\text{F}^-$  vacancies rather than  $\text{F}^-$  interstitials cause the very high conductivities at low temperatures. It was discovered that doping and forming composites often made the  $\text{LaF}_3$  conductivity decrease since this fluoride has already high defect concentrations. So far, the proton or oxygen ion conductivity has been found to be higher in pure  $\text{LaF}_3$  than in doped  $\text{LaF}_3$  or in composites with  $\text{LaF}_3$ .

Fluorides can be easily prepared as solid solutions with high concentrations either for F<sup>-</sup> ion interstitials or F<sup>-</sup> ion vacancies in the crystals, which basically cause the high F<sup>-</sup> ionic conductivities. By forming various associates and defect pairs/dipoles with the F<sup>-</sup> interstitials or F<sup>-</sup> ion vacancies, high mobilities and conductivities for oxygen ions and protons in the fluoride-based materials are possible, which have been demonstrated by gas concentration cell and fuel cell devices. Therefore, fluorides with high defect structure are suitable for supporting oxygen ion and proton transport for fuel cell applications.

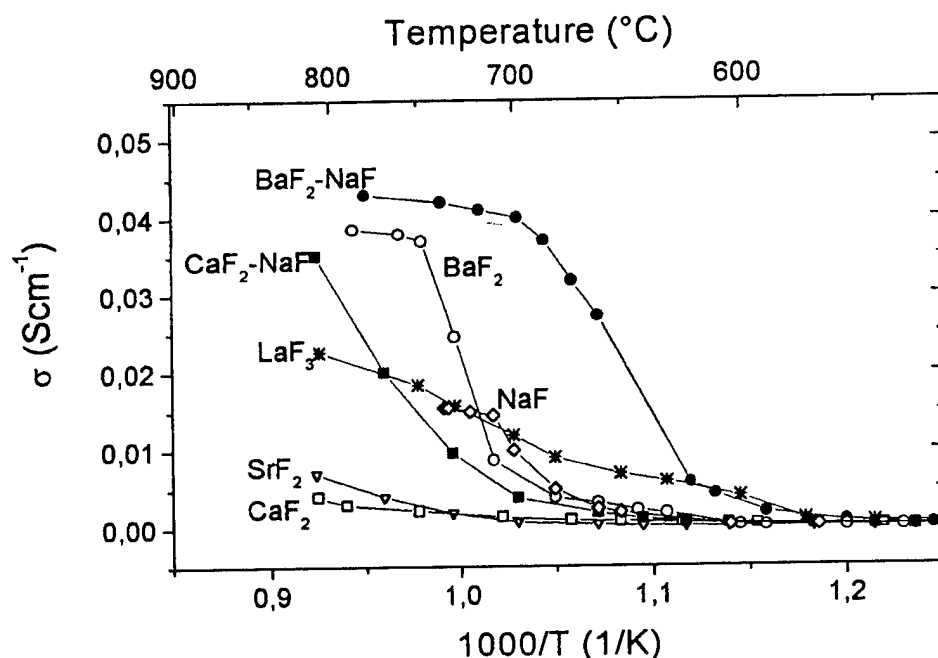


Fig. 1. Temperature dependence of the conductivity for fluoride based electrolytes.

## REFERENCES

- [1] B. Heed, B. Zhu, B.-E. Mellander and A. Lundén, *Solid State Ionics*, 46, 121 (1991).
- [2] R. Tärneberg and A. Lundén, *Solid State Ionics*, 90, 209 (1996).
- [3] see e. g., D. R. Franceschetti, J. Schoonman and J. R. Macdonald, *Solid State Ionics*, 5, 617 (1981).
- [4] B. Zhu, I. Albinsson, B.-E. Mellander and G.-Y. Meng, "Intermediate temperature proton conducting fuel cells – present experience and future opportunities", presented at "9th Inter. Conf. on Solid State Protonic Conductors", Aug. 17-21, 98, Bled, Slovenia.
- [5] see e.g., A. Sher et al, *Phys. Rev. B*, 144 (1966) 593.

Corresponding author: Bin Zhu, Department of Chemical Engineering & Technology, Royal Institute of Technology (KTH), S-100 44 Stockholm, Sweden, *Tel.*: 46-8-7908419, *Fax.*: 46-8-108579, *e-mail*: binzhu@ket.kth.se



## ATOMIC LEVEL MECHANISM OF PROTON TRANSPORT IN ALKALI METAL HYDROGEN SULFATE AND SELENATE SUPERIONIC CONDUCTORS

B.V. Merinov<sup>1</sup> and U. Bismayer<sup>2</sup><sup>1</sup> *Institute of Crystallography of the Russian Academy of Sciences, Leninskii pr. 59, 117333 Moscow Russia, e-mail: merinov@hotmail.com*<sup>2</sup> *Mineralogisch-Petrographisches Institut, Universität Hamburg, Grindelallee 48, D-20146 Hamburg, Germany, e-mail: ubis@mineralogie.uni-hamburg.de*

The observation of superionic conductivity in CsHSO<sub>4</sub> and CsHSeO<sub>4</sub> [1] led to an intensive study of similar anhydrous compounds as potential solid state proton conductors. It turned out, that most of the MXAO<sub>4</sub>, M<sub>3</sub>X(AO<sub>4</sub>)<sub>2</sub> and M<sub>5</sub>X<sub>3</sub>(AO<sub>4</sub>)<sub>4</sub> crystals, where M = NH<sub>4</sub>, K, Rb, Cs; X = H, D; A = S, Se, undergo superionic phase transitions which are ferroelastic simultaneously. Transport properties of these alkali metal hydrogen sulfates and selenates are due to the presence of particularly labile protons and particular structural characteristics incorporating a dynamically disordered hydrogen bond network [2]. Two basic steps, proton motion within a double-well hydrogen bond and HAO<sub>4</sub> rotation, are observed in the superprotonic phases [3]. However, this is a quite simplified representation of the proton diffusion mechanism in the above-mentioned compounds. More detailed investigations of these materials allow the mechanism of proton transport to be modelled. However, many facts of this process are still unknown.

Recent X-ray diffraction single crystal studies of MXAO<sub>4</sub>, M<sub>3</sub>X(AO<sub>4</sub>)<sub>2</sub> and M<sub>5</sub>X<sub>3</sub>(AO<sub>4</sub>)<sub>4</sub> revealed some unusual phenomenon which could be characterised as "the effect of anomalous manifestation of dynamically disordered hydrogen atoms on electron-density maps" [4], which we are able to explain now. An analysis of the electron-density distributions showed the presence of contrast electron density peaks which correspond to dynamically disordered hydrogen atoms with position occupancies 1/6, 1/12 and even less. One would not expect an observation of a visible electron density which is related to hydrogen atoms disordered over their crystallographic positions with such low occupancies. Nevertheless, in the structure determinations of the superionic phases of some MXAO<sub>4</sub>, M<sub>3</sub>X(AO<sub>4</sub>)<sub>2</sub> and M<sub>5</sub>X<sub>3</sub>(AO<sub>4</sub>)<sub>4</sub> crystals we could localise and even refine the positions of the disordered hydrogen atoms. As an example, a hydrogen electron density map of the superprotonic phase of [Rb<sub>0.57</sub>(NH<sub>4</sub>)<sub>0.43</sub>]<sub>3</sub>H(SeO<sub>4</sub>)<sub>2</sub> is shown in Fig. 1. This allows the atomic level mechanism of the superprotonic transport in alkali metal hydrogen sulfates and selenates to be elucidated in details. It can be briefly described as following. During thermal vibrations of the oxygen atoms which participate in hydrogen bonding, and thermal librations of the HAO<sub>4</sub> groups as a whole the hydrogen bonds are deformed and the corresponding potential curves are changed in time as well. In certain conditions, when one of the neighbouring AO<sub>4</sub> tetrahedra occurs in a suitable position and the hydrogen bond becomes quite long, the old hydrogen bond is broken and a new one is formed - *interbond motion*. On the other hand, due to the same thermal processes there occur situations when the hydrogen bond becomes relatively short and the proton can overcome the potential barrier within the hydrogen bond and moves from one potential minimum to the other - *intrabond motion*. It should be noted, that our calculations of potential barriers for the interbond and intrabond motions from the X-ray data result in quite similar values which are in good agreement with Raman spectroscopic data [5]. Our last results seem to indicate that the proton transport in the alkali metal hydrogen sulfates and selenates is a highly-correlated process.

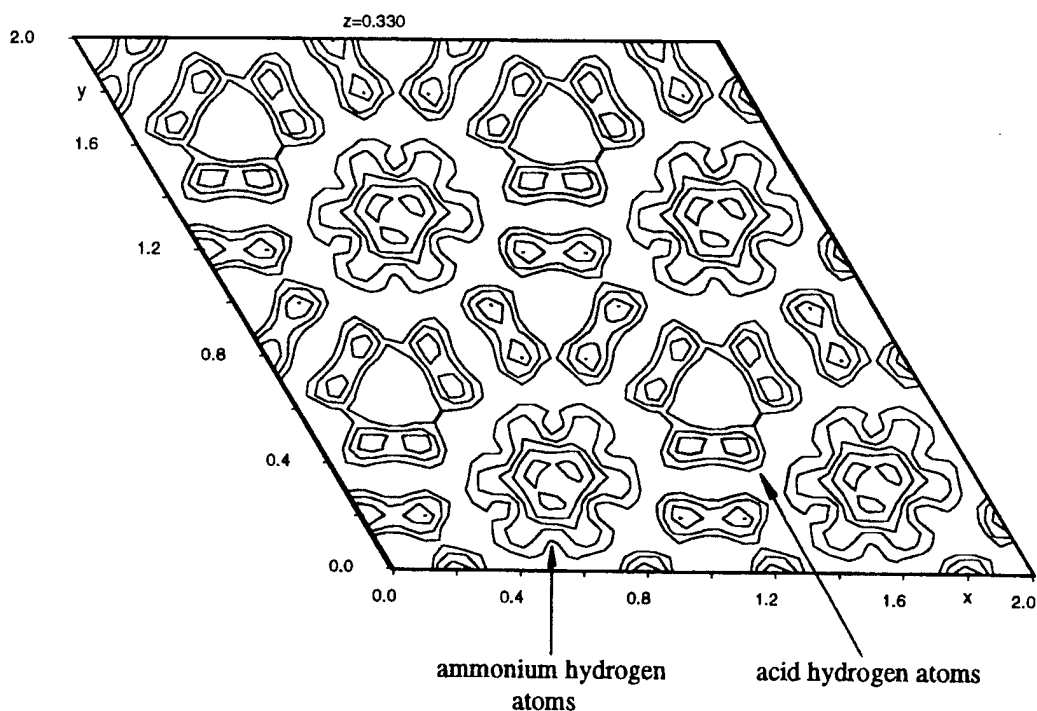


Fig. 1. Difference electron density section which shows the electron density distribution of the dynamically disordered hydrogen atoms in the superprotonic phase of  $[\text{Rb}_{0.57}(\text{NH}_4)_{0.43}]_3\text{H}(\text{SeO}_4)_2$ . Isolines are drawn at a step of  $0.05 \text{ e}\text{\AA}^3$ .

Some peculiarities which are inherent to the  $(\text{NH}_4)_3\text{H}(\text{AO}_4)_2$  compounds due to the presence of the sterical  $\text{NH}_4$  ion, are also analysed.

Financial support from the Alexander von Humboldt Foundation is gratefully acknowledged.

- [1] A.I. Baranov, L.A. Shuvalov and N.M. Schagina, JETP Lett. **36**, 459 (1982).
- [2] B.V. Merinov, Solid State Ionics **84**, 89 (1996).
- [3] R. Blinc, J. Dolinšek, G. Zupancic, L.A. Shuvalov and A.I. Baranov, Phys. Status Solidi (a) **123**, K83 (1984).
- [4] B.V. Merinov, Crystallography Reports **42**, 906 (1997).
- [5] V.P. Dmitriev, V.V. Loshkarev, L.M. Rabkin, S.B. Roshal' and L.A. Shuvalov, Sov. Phys. Crystallogr. **31**, 1138 (1986).

# PROTON TRANSPORT AND STRUCTURAL PHASE TRANSITIONS IN THE NEW SUPERIONIC CONDUCTOR $\text{Cs}_2(\text{HSO}_4)(\text{H}_2\text{PO}_4)$

Calum R.I. Chisholm and Sossina M. Haile

Materials Science 138-78, California Institute of Technology, Pasadena, CA, 91125

Many solid acid sulfates and selenates undergo structural phase transitions that lead to high proton conductivity at elevated temperatures. Recent investigations of the  $\text{CsHSO}_4$ - $\text{CsH}_2\text{PO}_4$  system have shown that mixed sulfate-phosphate compounds, such as  $\beta\text{-Cs}_3(\text{HSO}_4)_2(\text{H}_{2-x}(\text{S}_x\text{P}_{1-x})\text{O}_4)$  [1],  $\alpha\text{-Cs}_3(\text{HSO}_4)_2(\text{H}_2\text{PO}_4)$  [2] and possibly  $\text{Cs}_5(\text{HSO}_4)_3(\text{H}_2\text{PO}_4)_2$  [3], can also undergo such transitions. These studies have been undertaken with the aim of clarifying the role of hydrogen bonding and  $\text{XO}_4$  group chemistry in superprotonic behavior. In the present work, we describe the synthesis and conductivity of a fourth mixed sulfate phosphate,  $\text{Cs}_2(\text{HSO}_4)(\text{H}_2\text{PO}_4)$ . While this new compound has a hydrogen bonding scheme that differs from that of the other phases discovered in this rich system, it, like the others, undergoes a superprotonic transition upon heating.

Single crystals of  $\text{Cs}_2(\text{HSO}_4)(\text{H}_2\text{PO}_4)$  were obtained from aqueous solutions of cesium carbonate, sulfuric acid and phosphoric acid. The mole ratio of  $\text{Cs}:\text{SO}_4:\text{PO}_4$  was 10:5:5 starting with 10g  $\text{CsCO}_3$ . After 7-10 days the solution crystallized to give a mixture of  $\text{Cs}_2(\text{HSO}_4)(\text{H}_2\text{PO}_4)$ ,  $\beta\text{-Cs}_3(\text{HSO}_4)_2(\text{H}_{2-x}(\text{S}_x\text{P}_{1-x})\text{O}_4)$ ,  $\alpha\text{-Cs}_3(\text{HSO}_4)_2(\text{H}_2\text{PO}_4)$  in a ratio of approximately 70:15:15. Crystals so grown were examined by single crystal X-ray diffraction. The new phase is monoclinic, and preliminary investigations indicate it has an arrangement of  $\text{XO}_4$  groups ( $\text{X} = \text{P}, \text{S}$ ) and  $\text{Cs}$  atoms that is rather similar to that of  $\text{CsHSO}_4\text{-II}$ , but that the  $\text{XO}_4$  are connected by hydrogen bonds so as to form layers. Attempts to produce large quantities of  $\text{Cs}_2(\text{HSO}_4)(\text{H}_2\text{PO}_4)$  by rapid precipitation from solution (induced by the introduction of acetone or ethanol) yielded multi-phase products, and hence all experiments were carried out with single crystal samples.

The conductivity of  $\text{Cs}_2(\text{HSO}_4)(\text{H}_2\text{PO}_4)$  was measured by a.c. impedance spectroscopy (20Hz to 1M Hz) in ambient atmosphere. Silver paint served as the electrode material. Thermal analysis was carried out by both differential scanning calorimetry (DSC) to identify phase transitions, and differential gravimetric analysis (TGA) to determine thermal stability. DSC and TGA data were collected under flowing nitrogen at a heating rates of 10 and 5°C/min., respectively.

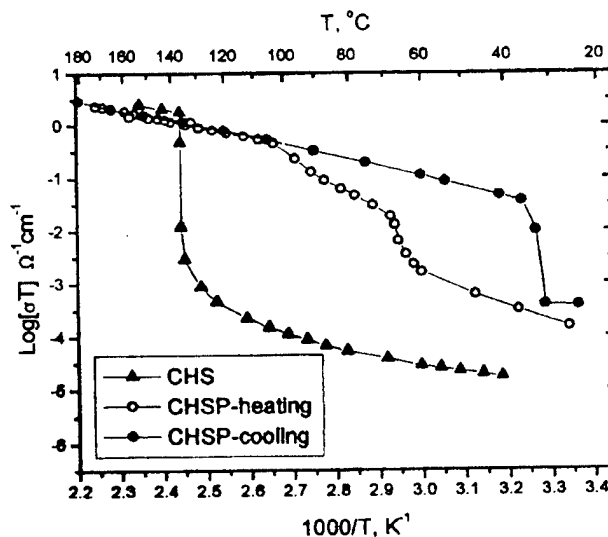


Fig. 1 Conductivity of  $\text{Cs}_2(\text{HSO}_4)(\text{H}_2\text{PO}_4)$  upon heating and cooling

The conductivity of  $\text{Cs}_2(\text{HSO}_4)(\text{H}_2\text{PO}_4)$  is shown in an Arrhenius plot in Figure 1. The open circles represent the data obtained on heating and the filled circles those obtained on cooling. It is evident that, upon heating, the material undergoes a two-step transition to a superprotonic phase. The DSC curve obtained from  $\text{Cs}_2(\text{HSO}_4)(\text{H}_2\text{PO}_4)$  on

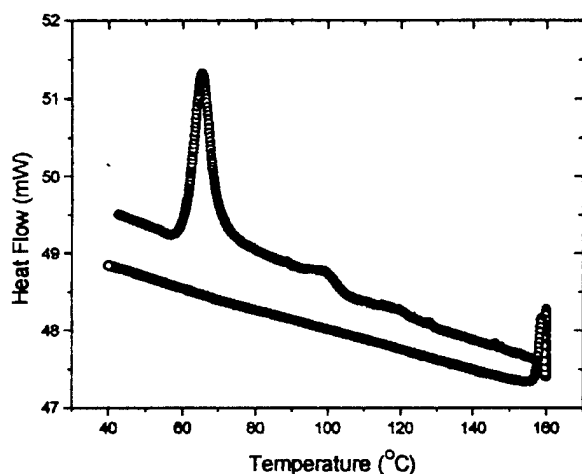


Fig. 2 DSC curve for  $\text{Cs}_2(\text{HSO}_4)(\text{H}_2\text{PO}_4)$  showing superprotonic phase transition

both heating and cooling is shown in Figure 2. Combined, these two sets of data indicate that the onset of the superprotonic transition is at 61°C, the first step of the transition is complete by 75°C, and the second, more gradual step occurs over the temperature range 75 to ~105°C. The activation energy for proton transport in the superprotonic phase is 0.36 eV. This activation energy, and the magnitude of the conductivity in the high temperature phase of  $\text{Cs}_2(\text{HSO}_4)(\text{H}_2\text{PO}_4)$  are comparable to that observed for  $\text{CsHSO}_4$  ( $E_a = 0.33$  eV in the superprotonic phase [4]). The significant hysteresis and the large heat

of transition,  $\Delta H = 46$  J/g, are reminiscent of the properties of the other mixed sulfate-phosphates, and suggests that disorder over P and S sites takes place at the transition. A change from an ordered to a disordered arrangement would lead to a high heat of transition, without increasing the conductivity beyond that observed for  $\text{CsHSO}_4$ .

The TGA results confirmed that  $\text{Cs}_2(\text{HSO}_4)(\text{H}_2\text{PO}_4)$  is thermally stable to temperatures of ~190°C. Decomposition occurs in multiple stages, with the first step (190-290°C) corresponding to the loss of approximately 1.5 water molecules per formula unit, or complete dehydration.

These results demonstrating the electrical behavior of  $\text{Cs}_2(\text{HSO}_4)(\text{H}_2\text{PO}_4)$  are important for several reasons. First, they confirm, together with our earlier investigations, that the chemistry of phosphorous, and presumably that of arsenic also, does not preclude the existence of superprotonic phase transitions, despite the observation that the vast majority of reported superprotonic solid acids are either sulfates or selenates. Second, the hydrogen bond network in  $\text{Cs}_2(\text{HSO}_4)(\text{H}_2\text{PO}_4)$  differs from that observed in any of the known superprotonic conductors, indicating that superprotonic transitions are not the property of specific structure types, but rather, a quite general phenomenon. Moreover, with the exception of  $(\text{NH}_4)_3\text{H}(\text{SeO}_4)$  [5], the superprotonic transition temperature of 105°C is the lowest reported, and raises the likelihood that room temperature superprotonic compounds will soon be identified.

- [1] S. M. Haile, P. M. Calkins, D. Boysen, *Solid State Ionics* **97** (1997) 145-151
- [2] S. M. Haile, G. Lentz, K.-D. Kreuer, J. Maier, *Solid State Ionics* **77** (1995) 128-134.
- [3] S. M. Haile and P. M. Calkins, *J. Solid State Chem.* **140** (1998) in the press.
- [4] A. I. Baranov, L. A. Shuvalov and N. M. Shchagina, *JETP Lett.* **36** (1982) 459-462.
- [5] A. Pawlowski, C. Pawlaczyk and B Hilczer, *Solid State Ionics* **44** (1990) 17-19.

PHASE TRANSITIONS OF KHSO<sub>4</sub> ABOVE ROOM TEMPERATURE

J. E. Diosa, R. A. Vargas, E. Mina, E. Torijano and B.-E. Mellander\*

Departamento de Física, Universidad del Valle, AA 25360 Cali-Colombia.

\*Department of Physics, Chalmers University of Technology, S-412 96 Gothenburg, Sweden.

The hydrogen sulphate family MHSO<sub>4</sub> (M=Na, K, Rb, Cs and/or NH<sub>4</sub>) form an interesting group of materials characterized by the presence of hydrogen bonding pattern between the HSO<sub>4</sub><sup>-</sup> tetrahedral ion [1]. These bonds are also responsible for the ferroelectric phase transition found in ammonium and rubidium hydrogen sulphates [2,3]. The corresponding potassium salt is however non-ferroelectric [4,5]. The structure of KHSO<sub>4</sub> is orthorhombic, space group Pbca, *a*=8.412 (2), *b*=9.800 (3), *c*=18.957 Å [1,6] and there are two HSO<sub>4</sub><sup>-</sup> ions in the asymmetric unit. One type of ion is linked into a polymeric chain by hydrogen bonding along a glide plane, the other forms a dimer across a center of symmetry [1].

On the other hand the growth parameters used for this material could favour of some SO<sub>4</sub><sup>2-</sup> species concentration, as well as some degree of replacement of HSO<sub>4</sub><sup>-</sup> by (SO<sub>4</sub><sup>2-</sup>, H<sup>+</sup>) groups within the polymeric chains [4], which appear to be in agreement with previously reported conductivity data [7]

P. W. Bridgman found three phase transitions at 164, 180, and 205 °C [8] respectively. However, Payan et al, reported only one transition point at 175 °C by X-ray measurements [4] and Abdel-Kader reported two (non-ferroelectric) structural phase transition around 100 and 175 °C respectively by electrical and thermal measurements [5].

In this work we report results on differential scanning calorimetry (DSC), thermogravimetric analysis (TG) and X-ray diffraction, to study the phase behaviour of KHSO<sub>4</sub> (KHS) above room temperature.

The DSC measurements have shown three anomalies, on heating a freshly single-crystal sample, one at around 120 °C (exothermic, Δ*H*=0.61 J/gr and metastable), another one at around 178 °C (endothermic, Δ*H*=15.28 J/gr) and the third one around 212 °C (endothermic, Δ*H*=124.1 J/gr and reversible). However on the subsequent cooling run only one endothermic peak is shown at around 181 °C (Δ*H*=116.228 J/g), see Fig. 1. If a fresh sample is heated only up to a temperature between 178 °C and 212 °C, then the endothermic peak at 178 °C is also observed on the subsequent cooling and heating runs, but the transition temperature is shifted down-ward some degrees.

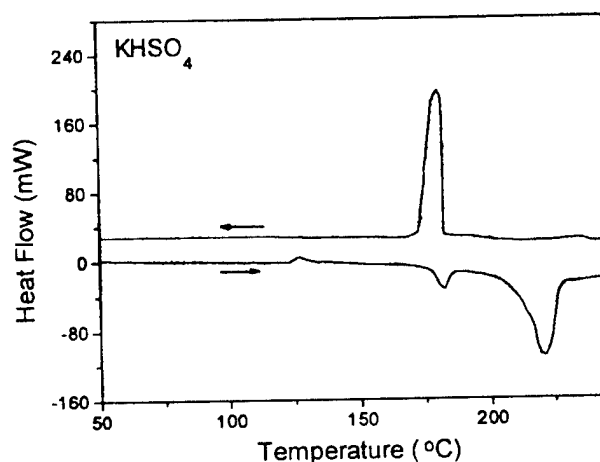


Fig.1 DSC thermogram of a freshly grown single-crystal KHS under a dry nitrogen flux of 80 ml min<sup>-1</sup> in the temperature range 50 - 250 °C. Heating and cooling rate 5 °C min<sup>-1</sup>.

The thermogravimetric measurements have shown weight loss at around the same temperatures as the DSC peaks, at 120 °C and 212 °C, but no TGA anomaly was resolved at 175 °C, see Fig. 2.

The x-ray diffraction patterns have shown some differences between the crystalline phases above and below the phase transitions, see Fig. 3.

The first transition (120 °C) have been interpreted in terms of a metastable phase induced at room temperature by the presence of water traces such that on heating the sample above 120 °C it is restore completely to a stable phase I. We discuss the second phase transition in terms of a further weakening of H bonds and an increasing disorder, fast reorientation of  $\text{HSO}_4^-$  ions and translational disorder of  $\text{K}^+$  ions, that might cause the observed structural change as revealed by the X-ray measurements, see Fig 3.

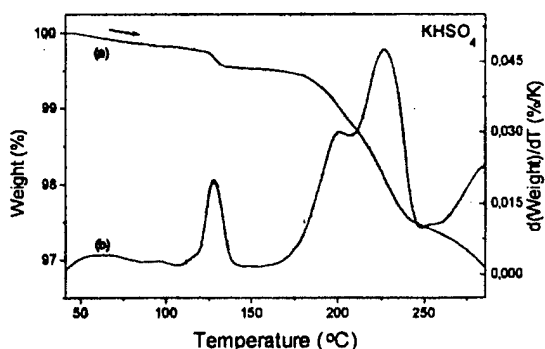


Fig. 2 Thermogravimetric analysis (TGA) of a freshly single crystal KHS under a dry nitrogen flux of 10 ml min<sup>-1</sup>: (a) first heating cycle in the temperature range 45 - 300 °C. Heating rate 5 °C min<sup>-1</sup>; (b) TGA derivative of curve (a)

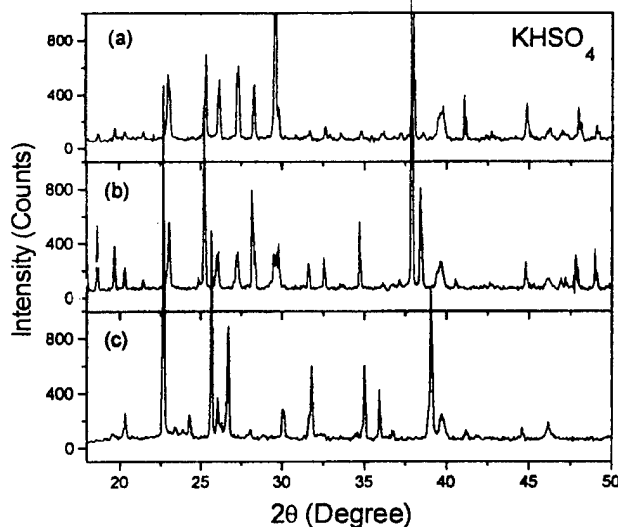


Fig.3 X ray diffraction patterns at 20 °C under a helium atmosphere, for: (a) fresh KHS sample; (b) KHS sample treated at 140 °C for 1 hour; (c) KHS sample treated at 190 °C for 1 hour.

The third transition correspond to the melting point and the big weight loss observed corresponds to the sample descomposition,  $2\text{KHSO}_4 \rightarrow \text{K}_2\text{S}_2\text{O}_7 + \text{H}_2\text{O}$  similar to that proposed for  $\text{CsHSO}_4$  [9].

**Acknowledgements.** The authors would like to acknowledge the support of the Colombian Research Agency, COLCIENCIAS and the International Programs in the Physical Sciences, IPPS, of Uppsala University, Sweden.

#### References

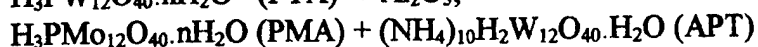
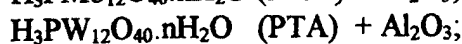
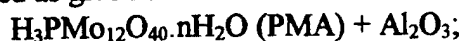
- [1] F. A. Cotton, B. A. Frenz and D. L Hunter, *Acta Cryst.* **B31**, 302 (1975).
- [2] R. Pepinsky, K. Vedam, Y. Okaya and S. Hoshino, *Phys. Rev.* **111**, 1508 (1958).
- [3] R. Pepinsky and K. Vedam, *Phys. Rev.* **117**, 1502 (1960).
- [4] F. Payan and R. Haser, *Acta Cryst* **B32**, 1875 (1976).
- [5] M. M. Abdel-Kader, A. El-Shawarby, W.M. Housny, Z. H. El-Tanahy and F. El-Kabbany, *Materials Research Bulletin*, **29** N° 3, 317 (1994).
- [6] L. H. Loopstra and C. H. MacGillavry, *Acta Cryst.* **11**, 349 (1958).
- [7] S. E. Rogers and A. R. Ubbelohde, *Trans. Faraday Soc.* **46**, 1051 (1950).
- [8] P. W. Bridgman, *Proc. Amer. Acad. Arts Sci.* **52**, 91 (1916/1917)
- [9] Ph. Colomban, M. Phan-Thi and A. Novak, *Solid State Ionics* **24**, 193 (1987).

# THERMAL, THERMO-VOLTAMMETRIC AND ELECTRICAL CONDUCTIVITY STUDIES ON PROTON CONDUCTING COMPOSITES

Lakshmi. N. , Kamlesh Pandey and S. Chandra

Department of Physics, Banaras Hindu University, Varanasi-221 005 (India)

Proton conducting composites consisting of (a reasonable proton conductor + insulating powder) or (a reasonable proton conductor + low conducting proton conductor) have been prepared as given below:



The composites showed unusual thermal behaviour (DTA). For PTA (or PMA +  $\text{Al}_2\text{O}_3$  cases, the DTA endothermic peak at  $\sim 80^\circ\text{C}$  corresponding to the dopant PTA (or PMA) convert to exothermic peak for higher concentrations of  $\text{Al}_2\text{O}_3$ . This could be interpreted as the bond formation of PMA groups to the  $\text{Al}_2\text{O}_3$ . The XRD confirmed also this. The addition of substantial  $\text{Al}_2\text{O}_3$  partly amorphised the composite and PMA (or PTA) related peaks either disappeared or intensity was drastically reduced. It appears that some waters of crystallisation are forming bonds with  $\text{Al}_2\text{O}_3$  (like Al-OH). In PMA + APT composite, trends of a similar bond formation were seen but the effect was much less than that for PTA+ $\text{Al}_2\text{O}_3$  or PMA +  $\text{Al}_2\text{O}_3$ .

The TGA studies also show that all the water of crystallisation does not go out in PTA +  $\text{Al}_2\text{O}_3$  composite while it happens so in pure PTA on heating. The mechanism for this phenomena of possible bonding of water of crystallization with  $\text{Al}_2\text{O}_3$  resulting in a new compound at the interface appears to have the same origin as that which resulted in the endo - exothermic peak reversal in DTA.

The  $\sigma$  Vs  $1/T$  studies also showed the presence of some unusual behaviour related with water bonding with host matrix. The  $\sigma$  Vs  $1/T$  curve showed a sudden decrease in conductivity as a result of dehydration for PTA and PMA. But with  $\text{Al}_2\text{O}_3$ , dehydration does not seem to be as easy as for pure PTA or (PMA) and the temperature dependence shows a slower decrease with temperature (or sometimes even an increase in  $\sigma$  at higher temperature results).

A thermo voltammetry technique was also used to obtain results similar to  $\sigma$  Vs  $1/T$ . In this technique, a voltaic cell of the configuration Zn/electrolyte/Cu is set up and its voltage is monitored with temperature. The e.m.f. developed will be related with the permeability of the mobile ion (or conductivity) in the electrolyte. The e.m.f. decreased suddenly on dehydration in pure PTA or PMA but was not so for the composites in which the possible bonding of water of crystallization with the host matrix has been hypothesised above to explain the thermal and electrical conductivity behaviour.

In conclusion, evidence of formation of new interfacial phase has been formed in proton conducting composites with salt hydrates on the basis of DTA/TGA, XRD, temperature dependence of conductivity and thermovoltammetric studies.

# NMR AND CONDUCTIVITY STUDY OF THE PROTONIC CONDUCTOR $\text{HPb}_2\text{Nb}_3\text{O}_{10} \cdot n\text{H}_2\text{O}$

C.E. Tambelli<sup>1</sup>, J.P. Donoso<sup>1</sup>, C.J. Magon<sup>1</sup>, M.J. Saeki<sup>2</sup>, and A. Florentino<sup>3</sup>

<sup>1</sup>Inst. de Física de São Carlos, Universidade de São Paulo, C.P. 369, 13560-970 SP Brasil

<sup>2</sup>Dept. de Química, UNESP, C.P. 473, 17033-360 Bauru, SP, Brasil

<sup>3</sup>Dept. de Química e Bioquímica, UNESP, C.P. 510, 18618-000 Botucatu, SP, Brasil

The family of the niobate type layered perovskite,  $\text{A}(\text{M}_{n-1}\text{Nb}_n\text{O}_{3n+1})$ , where  $\text{A} = \text{H}, \text{K}, \text{Rb}, \text{Cs}$ ;  $\text{M} = \text{Pb}, \text{La}$  or  $\text{Ca}$ , are interesting materials, not only because of the noticeable photocatalytic activity<sup>[1]</sup> but also due to their ion exchange ability and high ionic conductivity of interlayer ions<sup>[2,3]</sup>. In this work we present results of a NMR and conductivity study of the protonic conductor  $\text{HPb}_2\text{Nb}_3\text{O}_{10} \cdot n\text{H}_2\text{O}$ , for  $n = 1.2, 0.3$  and  $< 0.3$ , including line shape and relaxation times measurements for  $^1\text{H}$ .

The  $\text{HPb}_2\text{Nb}_3\text{O}_{10}$  perovskite was initially synthesized in alkali form by a sol-gel method that consisted of dissolving stoichiometric quantities of  $\text{NaOC}(\text{CH}_3)_3$  and  $\text{Nb}(\text{OC}_4\text{H}_9)_5$  in butanol. The lead sub-acetate,  $\text{Pb}(\text{C}_2\text{H}_3\text{O}_2)_2 \cdot 2\text{Pb}(\text{OH})_2$  was previously dissolved in glacial acetic acid and then added to the solution. The mixture was hydrolyzed at atmospheric humidity followed by calcination at  $650^\circ\text{C}$ . Proton exchange reaction of  $\text{Na}^+/\text{H}^+$  was carried out at room temperature in  $0.3 \text{ M HNO}_3$  for two days. The resulting material was characterized by TGA, XRD and SEM. The protonic conductivity was measured by complex impedance technique between  $1 \text{ Hz}$  and  $1 \text{ MHz}$  in cold pressed pellets. Proton NMR line shapes and spin-lattice relaxation times ( $T_1$ ) were measured in powder samples, with a pulsed NMR spectrometer operating at  $36 \text{ MHz}$ , in the temperature range  $90 - 350 \text{ K}$ . The amount of water absorbed by the powder was obtained by weighting the sample in a analytical balance.

Figure 1 shows the temperature dependence of the conductivity for samples exposed to

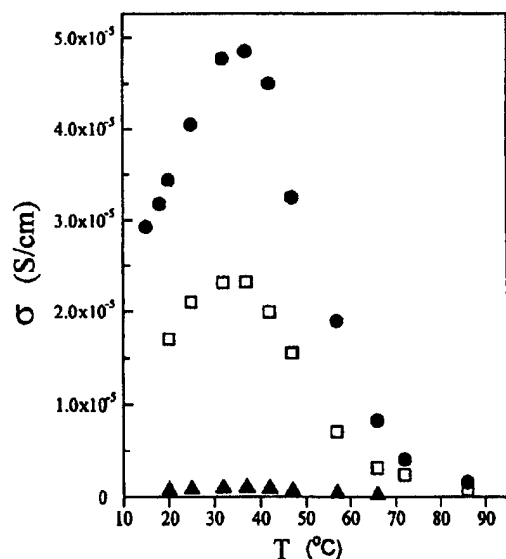


Fig. 1. Temperature dependence of the conductivity of  $\text{HPb}_2\text{Nb}_3\text{O}_{10} \cdot n\text{H}_2\text{O}$  calcinated at  $650^\circ\text{C}$ , for sample exposed to 26% ( $\blacktriangle$ ), 53% ( $\square$ ) and 79% ( $\bullet$ ) relative humidity.

known water vapor pressure in a saturated container. It is clear that the hydration state of the compound is an important factor for its conductivity. Above  $280 \text{ K}$  the conductivity increases with increasing temperature, until a maximum value is attained at approximately  $310 \text{ K}$  in the compounds exposed to 53% and 79% r.h. Assuming that the conductivity result from a thermally activated process expressed by an Arrhenius law, an activation energy of  $0.22 \text{ eV}$  can be extracted from the data of the latest compound. Above  $300 \text{ K}$ , the conductivity decrease with increasing  $T$  up to the highest temperature investigated.

Figure 2 shows the temperature dependence of the linewidth of the central component of the  $^1\text{H}$  NMR spectrum (insert). The experimental lineshape at  $120 \text{ K}$  was simulated with a narrow line of lorentzian shape flanked by a pair of peaks of gaussian shape separated by  $11 \text{ Gauss}$ . This spectral structure is due to



intramolecular dipolar interactions between protons belonging to the same ion or molecule. The side peaks can be attributed to paired protons in H<sub>2</sub>O (Pake doublet) with a proton-proton separation of  $1.55 \pm 0.05 \text{ \AA}$ <sup>[4]</sup>. The central line has been attributed to the superposition of the <sup>1</sup>H signals belonging to the OH<sup>-</sup> and the central component of the oxonium ion (H<sub>3</sub>O<sup>+</sup>) spectrum<sup>[5,6]</sup>.

Bellow 125 K the "rigid lattice" nuclear dipole-dipole interaction is the main source of line broadening. Above 140 K, the mobility of the protons increases enough to cause the averaging of the proton dipolar interactions, which result in a line narrowing (Fig. 2). From the analysis of the line narrowing data we obtain activation energies between  $0.18 \pm 0.05 \text{ eV}$  for  $n = 1.2$  and  $0.40 \pm 0.05 \text{ eV}$  for  $n < 0.3$ <sup>[4]</sup>.

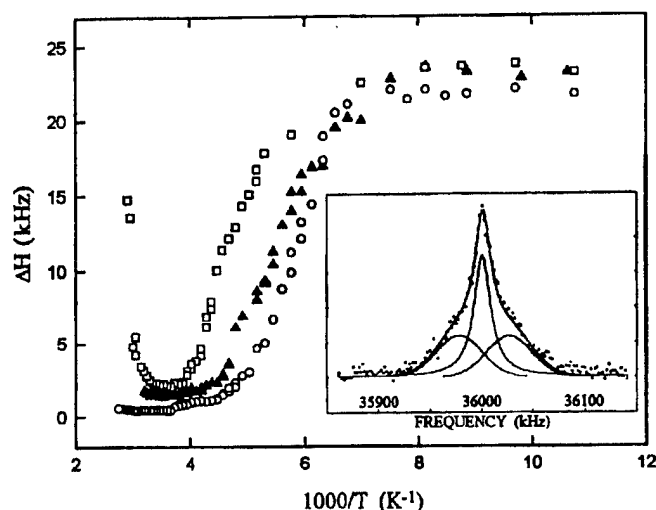


Fig. 2. Temperature dependence of the linewidth of the central line in HPb<sub>2</sub>Nb<sub>3</sub>O<sub>10</sub> · nH<sub>2</sub>O for  $n = 1.2$  (○),  $0.3$  (▲) and  $< 0.3$  (□). In the insert is shown the spectrum of HPb<sub>2</sub>Nb<sub>3</sub>O<sub>10</sub> · 1.2H<sub>2</sub>O at 123 K (•) and the best fit (—).

The temperature dependence of the proton relaxation rates ( $T_1^{-1}$ ) exhibit a maximum at 250 - 273 K in the three samples investigated, which reflects the fast protonic motion. Measurements, in the sample with  $n = 0.3$ , carried out at different Larmor frequencies shows that the relaxation rate has a logarithmic frequency dependence in the extreme narrowing limit ( $\omega\tau \ll 1$ , where  $\tau$  is the correlation time) which is the expected behavior for a two-dimensional motion<sup>[7]</sup>. The activation energies obtained from the relaxation data are between  $0.14 \pm 0.03 \text{ eV}$  for  $n = 1.2$  and  $0.27 \pm 0.03 \text{ eV}$  for  $n < 0.3$ . These values are in good

agreement with those reported for other protonic conductors<sup>[3,5,7]</sup>. Our results are consistent with a Grotthuss-type mechanism for proton diffusion<sup>[6]</sup>.

Partially supported by CNPq, FAPESP and FINEP (Brazil).

- [1] J. Yoshimura, Y. Ebina, J. Kondo, K. Domen and A. Tanaka, *J. Phys. Chem.*, **97**, 1970 (1993).
- [2] M. A. Subramanian, J. Golapalakrishnan and A. W. Sleight, *Mat. Res. Bull.*, **23**, 837 (1988).
- [3] P. Colomban, *Proton Conductors (Solids, membranes and gels - materials and devices)*, Cambridge University Press (1992).
- [4] C. E. Tambelli, M.Sc. Thesis, *Estudo por Ressonância Magnética Nuclear do Condutor Protônico HPb<sub>2</sub>Nb<sub>3</sub>O<sub>10</sub> · nH<sub>2</sub>O*, IFSC, Universidade de São Paulo (1998).
- [5] A.M. Fajdiga-Bulat et al, *Solid State Ionics*, **77**, 101 (1995).
- [6] H. Arribart, and Y. Piffard, *Solid State Communications*, **45**, 571 (1983)
- [7] G. Mangamma et al, *Solid State Ionics*, **58**, 303 (1992)

## INORGANIC-ORGANIC COMPOSITE PROTONIC CONDUCTORS COMPRISING OF SILICOPHOSPHATE GLASS AND ION-EXCHANGE RESIN

M. Nagai, F. Sawada, K. Kobayashi and Y. Nakajima

Department of Energy Science and Engineering, Musashi Institute of Technology

Tamazutsumi, Setagaya-ku, Tokyo, 158-8557, JAPAN Tel:+81-3-3703-3111 Ext.2406

Fax:+81-3-5707-2203 E-mail:nagai@fc.ese.musashi-tech.ac.jp

The demand for fuel cells operating near room temperature is currently accelerated. There is increasing interest in polymer electrolyte fuel cells because of their high energy conversion efficiency and environmental friendliness. However, there is still great room for improving the conductivity, hydration affinity within electrolytes and mechanical strength. One of the solutions for this issue is the formation of composites comprising of inorganic and organic substances. The fabrication and characterization of this type of composites were studied with special emphasis on the conductivity and durability under the operation conditions.

In the first stage,  $\text{POH}(\text{OC}_3\text{H}_7)_2$  was dissolved in  $i\text{-C}_3\text{H}_7\text{OH}$ , followed by adding  $\text{HNONH}_2$ .  $\text{Si}(\text{OC}_3\text{H}_7)_4$  was hydrolyzed with equimolecular amount of  $\text{H}_2\text{O}$  and stirred for 1 hour. The two solutions were mixed keeping the Si/P ratio at 9 and stirred for 1 hour. Subsequently, various amounts of Nafion solution containing both  $\text{H}_2\text{O}$  and  $\text{CH}_3\text{OH}$  was added to the mixture solution and kept for 2 or 3 weeks in order to promote the gelation.

The samples at various stages were examined by IR spectroscopy and X-ray diffraction. Thermal analysis was conducted for the samples having various Si/P ratios. The electrical conductivity was determined by the complex impedance method.

The Si/P mixture solutions became opaque when Nafion was added to them and became transparent as the gelation proceeded. Weight loss below  $150^\circ\text{C}$  was rather decreased by adding Nafion probably due to the affinity with  $\text{H}_2\text{O}$ . However, thermal stability above  $300^\circ\text{C}$  decreased because Nafion underwent decomposition. The composition dependence of thermal stability for the samples with various Si/P ratios was investigated on the basis of the IR spectroscopic results. Preliminary measurement of electrical conductivity suggested that thus-obtained composites would be a good protonic conductor near room temperature.

## A VIBRATIONAL SPECTROSCOPIC STUDY OF PROTON CONDUCTING POLYMER GEL ELECTROLYTES.

**H. Ericson<sup>†</sup>, A. Brodin<sup>†</sup>, A.M. Grillone<sup>‡</sup>, S. Panero<sup>‡</sup>, B. Scrosati<sup>‡</sup>, P. Jacobsson<sup>†</sup>**

<sup>†</sup>*Chalmers University of Technology SE-412 96 Göteborg, Sweden*

<sup>‡</sup>*University of Rome "La Sapienza", Piazzale Aldo Moro 5 BOX 34 Roma 62 00195 Rome Italy*

Despite the success in recent years in the development of polymer-based proton conductors, there is a growing interest in new types of low temperature proton conducting materials with optimised properties [1]. Classical commercially available proton-conducting materials such as Nafion<sup>®</sup>, represent a class of hydrated systems containing sulphonic acid as proton donor. These materials exhibit high protonic conductivity ( $10^{-2}$  S/cm) with sufficient amounts of water in the system [1]. There are, however, a number of applications where a modest conductivity is sufficient, while the presence of water in combination with acid is detrimental. In WO<sub>3</sub>-based electrochromic devices for instance, a compromise is sought between WO<sub>3</sub> stability and polymer electrolyte conductivity by reducing the water content [2]. Anhydrous proton-conducting polymer electrolytes have been formed by complexing a strong acid e.g. H<sub>3</sub>PO<sub>4</sub> or H<sub>2</sub>SO<sub>4</sub> with a polymer such as poly(ethylene oxide) or poly(ethylene imine) [3,4]. Non-aqueous proton conducting gels with H<sub>3</sub>PO<sub>4</sub> and organic solvents in a polymer matrix have also been reported [5].

Gel electrolytes combine the high conductivity inherent to the low-molecular-weight part with the mechanical stability of the polymer matrix. In the present study a new type of water-free proton-conducting polymer gel was prepared following a well-known concept for gel-type Li<sup>+</sup> electrolytes for battery applications. These gels typically consists of a high-molecular-weight polymer, a mixture of organic solvents and a Li<sup>+</sup>-salt [6]. The proton conducting gels presented here consist of a high-molecular-weight poly (methyl methacrylate) (PMMA) matrix, a mixture of organic solvents, for instance ethylenecarbonate (EC) / propylenecarbonate (PC) or EC / PC / dimethylformamide (DMF) but the ionic species is an organic acid. The use of organic acids, such as benzoic or salicylic acid, as the ionic species in this type of gel, is a new approach for proton-conducting materials [7]. The recently developed protonic electrolytes of the present study possess a number of attractive properties, such as optical transparency, ease of altering the electrochemical properties by varying electrolyte composition, and the possibility to produce the electrolyte in almost any shape.

Our first vibrational spectroscopic study [8] showed that the number of charge carriers could be deduced from the intensity ratio of the two components of the symmetric ring vibration of the acids. The acid dissolution was shown to depend on the properties of the solvents. All factors concerning the dissolution of the acids and the interactions with the other gel components are not fully understood and we have therefore undertaken the present Raman and FTIR spectroscopic investigation. In this work we aim to clarify the acid dissociation, the acid-solvent interactions and the effect of the polymer matrix on solvent properties. A number of organic solvent mixtures have been examined and comparisons are made with the conductivity data for these systems.

1. K.D. Kreuer, *Solid State Ionics*, **97**, 1, (1997)
2. O. Bhonke, in: *Chemistry of Solid State Materials, Proton conductors* (edited by P Colombari) p. 551, Cambridge University Press, Cambridge (1992).

3. P. Donoso, W. Gorecki, C. Berthier, F. Defendini, C. Poinsignon, and M.B. Armand, *Solid State Ionics*, **28-30**, 969 (1988).
4. M.F. Daniel, B. Desbat, F. Cruege, O. Trinquet, and J.C. Lassegues, *Solid State Ionics* **28-30**, 637 (1988).
5. J.R. Stevens, W. Wieczorek, D. Raducha, K.R. Jeffrey, *Solid State Ionics*, **97**, 347 (1997).
6. G.B. Appetecchi, F. Croce, B. Scrosati, *Electrochimica Acta*, **40**(8), 991 (1995).
7. A.M. Grillone, S. Panero, B. Retamal, B. Scrosati, *J. Electrochem. Soc.* ~~In press~~ <sup>146 (1), 1999</sup>.
8. H. Ericson, A. Brodin, A.M. Grillone, S. Panero, B. Scrosati, P. Jacobsson. "Poly(methyl methacrylate)-based protonic gel electrolytes: A spectroscopic study", submitted to *Electrochimica Acta*

Not Given

## PROTON POLYMER GEL ELECTROLYTE MEMBRANES

A.M.Grillone, S.Panero &amp; B.Scrosati

Dipartimento di Chimica, Università "La Sapienza", 00185 Rome, Italy

Research in proton-conducting polymer electrolytes has consistently increased in recent years due to their relevance in various important electrochemical applications, such as sensors and, particularly, fuel cells. Nafion<sup>TM</sup> is presently the most used proton conductor since it acts as a good, chemically inert polymer electrolyte membrane. As is well known, the hydrophobic part of this polymer provides relatively good mechanical stability even in the presence of water, while the hydrated hydrophilic domains provides high proton conductivity at water content exceeding 30% wt., via transport through the sulfonic groups attached to the polymer backbone. Because of this vehicular-type of transport mechanism, the conductivity of Nafion strongly depends upon relative humidity.

We have investigated different types of polymeric protonic conductors by developing gel membranes obtained by incorporating organic acids in a highly-plasticized poly(methyl methacrylate) PMMA matrix. We have prepared this new type of gel membranes by using selective solvents mainly consisting of propylene carbonate(PC) - ethylene carbonate(EC) - formamide(F) mixtures. The conductivity of the membranes prepared from these three-solvent mixtures is higher than that of the parent liquid PC/EC solutions. Furthermore, the membranes are stable up to moderately high temperatures and their conductivity is only slightly dependent on the relative humidity conditions. In this paper we describe the chemical and electrochemical properties of these PMMA-based gel proton electrolytes.

## REFERENCES

1)A.M.Grillone, S.Panero, B.A. Retamal and B.Scrosati " Proton polymeric gel electrolyte membranes based on polymethylmethacrylate"

*J.Electrochem.Soc.*, 1999 in press.

## REFERENCES

- 1) G.B.Appetecchi, F.Croce, G.Dautzenberg, M.Mastragostino, F.Ronci, B.Scrosati, F.Soavi, F.Zanelli, F.Alessandrini and P.P.Prosini; "Composite polymer electrolytes with improved metal electrode cyclability. I. Electrochemical properties of dry PEO-LiX systems. *J.Electrochem.Soc.*, **145**, 4126 (1998).
- 2) G.B.Appetecchi, F.Croce, M.Mastragostino, B.Scrosati, F.Soavi and F.Zanelli; "Composite polymer electrolytes with improved metal electrode cyclability. II. Application in rechargeable batteries. *J.Electrochem.Soc.*, **145**, 4133 (1998).
- 3) F.Croce, G.B.Appetecchi, L.Persi, B.Scrosati; "Nanocomposite polymer electrolytes", *Nature*, **394**, 456 (1998)

## STRUCTURE - PROPERTY RELATIONSHIPS IN PROTON CONDUCTORS BASED ON POLYURETHANES

P. Pissis<sup>1</sup>, A. Kyritsis<sup>1</sup>, G. Georgoussis<sup>1</sup>, V. V. Shilov<sup>2</sup> and V. V. Shevchenko<sup>2</sup>*1. National Technical University, Department of Physics, Zografou Campus, 15780 Athens, Greece.**2. National Academy of Science of Ukraine, Institute of Macromolecular Chemistry, 253160 Kiev, Ukraine.*

Novel proton - conducting polyurethanes based on either polytetramethylene oxide (PTMO) or polyethylene oxide (PEO), with the protons being incorporated in the flexible soft segments, were prepared and their properties were investigated. The main interest is focused on the influence of structure and morphology on the mechanisms of molecular mobility and proton conductivity.

The preparation of polyurethane that contain acid (COOH) groups bound to the PTMO chains and hard segments of various length has recently been reported [1]. Similar procedures were followed to prepare samples where PTMO has been replaced by PEO. Samples of different amount of hard segments were prepared and denoted as Bn with n increasing in the order of increasing hard segments content [1].

The structure and the morphology of the polyurethanes were studied by means of differential scanning calorimetry (DSC), wide- and small angle X-ray scattering (WAXS and SAXS) and dynamic mechanical thermal analysis (DMTA). Molecular mobility and proton conductivity were measured by means of broadband dielectric relaxation spectroscopy (DRS,  $10^{-2}$  -  $10^9$  Hz) and of thermally stimulated depolarisation currents techniques (TSDC, 77 - 300 K).

WAXS data show that the systems studied are amorphous. DSC shows that the polyurethanes under investigation are microphase - separated materials, consisting of soft chain matrix and hardchain microdomains. The glass transition temperature,  $T_g$ , of the polyether-rich phase was determined by DCS. A model proposed by Koberstein and coworkers [2] is used to calculate the microphase composition on the basis of DSC data. SAXS data confirm the microphase - separated structure and allow to quantitatively characterise the morphology.

TSDC measurements allow for a quick characterisation of the dielectric behaviour as a function of temperature at low frequencies  $10^{-2}$  -  $10^{-4}$  Hz [3]. The thermograms show two secondary ( $\gamma$  and  $\beta$ ) local relaxations, the  $\alpha$  relaxation associated to the glass transition of the amorphous polyether - rich phase and the interfacial relaxation associated to the microphase - separated structure [4]. Glass transition temperatures determined by TSDC as peak temperatures of the  $\alpha$  relaxation agree well with the values determined by DSC.

The relaxation and conductivity mechanisms were studied in detail by DRS. As examples Figs. 1 and 2 show the frequency dependence of  $\sigma_{ac}$  for the  $B1H^+$  -  $B5H^+$  samples based on PTMO at 298 K and for the  $B1H^+$  sample based on PTMO at several temperatures, respectively.

Dc conductivity values,  $\sigma_{dc}$ , were determined as plateau values in ac conductivity plots (Figs. 1 and 2), as well as from complex impedance (Z) plots, in good agreement with each other.  $\sigma_{dc}$  in Fig. 1 decreases with increasing hard segments content, confirming that conductivity occurs through the soft segments phase. The results have been rationalised in terms of effective medium theories.

$\sigma_{dc}$  in Fig. 2 increases with increasing temperature. The corresponding Arrhenius plot shows that the temperature dependence of  $\sigma_{dc}$  is described by Vogel - Tammann - Fulcher -

Hesse (VTFH), suggesting that the conductivity mechanism is governed by the motion of the chains.

The absolute values of  $\sigma_{dc}$  in Fig. 2 are relatively low. Higher values of  $\sigma_{dc}$  by two orders of magnitude were obtained with polyurethanes based on PEO. This is assigned to the better solvation possibilities of PEO as compared to PTMO.

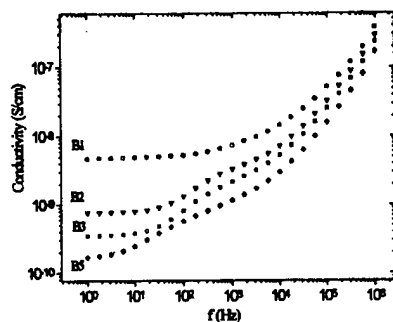


**FIGURE 1.**  $\sigma_{ac}(f)$  plots in B1H<sup>+</sup> - B5H<sup>+</sup> samples based on PTMO at 298 K

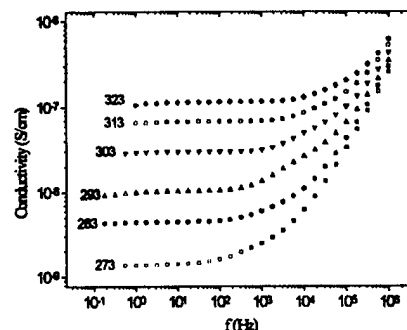


**FIGURE 2.**  $\sigma_{ac}(f)$  plots in B1H<sup>+</sup> samples based on PTMO at selected temperatures indicated in the plot

### References.

- [1] V. V. Shilov, V. V. Shevchenko, P. Pissis, A. Kyritsis, You. P. Gomza, S.D. Nesin and N. S. Klimenko. Solid State Ionics, submitted.
- [2] T. J. Koberstein and M. L. Leung, Macromolecules **25**, 6205 (1992)
- [3] P. Pissis, A. Anagnostopoulou - Konsta, L. Apekis, D. Daoukaki - Diamanti and C. Christodoulides, J. Non-Cryst. Solids, **131-133**, 1174 (1991)
- [4] P. Pissis, A. Kanapitsas, Y. V. Savelyev, E. R. Akranovic, E. G. Privalko and V. P. Privalko, Polymer **39**, 3431 (1998).



## IMIDAZOLIUM-BASED POLYMERIC PROTON CONDUCTORS

Yaser Abu-Lebdeh and John R. Owen

Department of Chemistry  
University of Southampton  
Southampton SO17 1BJ, UK.

Proton conductors based on nitrogen as the electron pair donor are attractive alternatives to water-based proton conductors as they can avoid some of the undesirable chemical activity of water as well as retaining constant properties over a wide range of humidity. Applications include batteries, displays and sensors based on proton transport.

Previous work in this field investigated imidazolium as a *counterion* to a sulphonated polyether ketone [1]. This work concerns the properties of room-temperature eutectic mixtures of imidazole with selected imidazolium salts when introduced as *plasticisers* into suitable support polymers such as poly(vinylidene difluoride), pVdF.

Sample films have been prepared by dissolving the imidazole/imidazolium salt mixtures and the polymer in a co-solvent, usually acetone. Polymers consisted of highly crystalline pVdF (Aldrich) as well poly(vinylidene fluoride-co-hexafluoropropylene) (Aldrich) which is only about 20% crystalline.

Impedance measurements were made by the traditional method of contacting disc-shaped polymer between cylindrical stainless steel electrodes as well as the gap electrode method described recently. The conductivity values obtained were compared with the conductivities of the plasticising liquids as measured by miniature conductivity cells with platinum electrodes.

Room temperature conductivities approaching  $10^{-4}$  S/cm have been obtained, showing that these materials are of interest in the above-mentioned applications. The paper will discuss systematic variations of the conductivity with temperature and the relative amounts of imidazole base, salt and propylene carbonate as an additional plasticiser.

[1] K.Kreuer et al Electrochimica Acta

[2] Y. Abu-Lebdeh and J.R. Owen, Extended Abstracts, SSPC-9, Slovenia, 1998.

## Hole-State and Defect Structure of Protonic Conductor SrTiO<sub>3</sub> Observed by High-Resolution X-ray Absorption Spectroscopy

Tohru HIGUCHI<sup>a,\*</sup>, Takeyo TSUKAMOTO<sup>a</sup>, Noriko SATA<sup>b</sup>, Mareo ISHIGAME<sup>b</sup>, Kiyoshi KOBAYASHI<sup>c</sup>, Shu YAMAGUCHI<sup>d</sup>, Masami FUJISAWA<sup>e</sup>, and Shik SHIN<sup>e</sup>

<sup>a</sup> Faculty of Science, Science University of Tokyo, 1-3 Kagurazaka, Shinjuku, Tokyo 162-0825, Japan

<sup>b</sup> Research Institute of Scientific Measurement, Tohoku University,

<sup>c</sup> National Institute of Materials and Chemical Research, Higashi 1-1, Tsukuba, 305-8565, Japan

<sup>d</sup> Department of Materials Science and Engineering, Nagoya Institute of Technology, Gokiso-cho, Showa-ku, Nagoya 466-8555, Japan

<sup>e</sup> Institute for Solid State Physics, University of Tokyo, 3-2-1 Midori, Tanashi, Tokyo 188-8501, Japan

### 1. Introduction

Recently, it is found that the proton is strongly absorbed in heavily Sc-doped SrTiO<sub>3</sub> [2]. Protonic conduction was observed in Sc-doped SrTiO<sub>3</sub> by ac-conductivity measurements in wet air, while the hole conductivity was observed in dry air. It is supposed that the protonic conductivity increases when the strength of O-H bond becomes weak due to the property of the hydrogen-bond effect.

The electronic structure of *p*-type SrTiO<sub>3</sub> has been studied by the absorption spectra of vacuum ultraviolet region [1]. The energy shift of the absorption edge due to acceptor doping was observed in *p*-type and the band gap was found to increase with increasing the dopant concentration. It is suggested that holes are formed at the top of the valence band of *p*-type SrTiO<sub>3</sub> due to acceptor doping. Furthermore, the Fermi Level shifts to the valence band side with the increasing of Sc ions [2]. These results indicate that the band structure of *p*-type SrTiO<sub>3</sub> obeys the rigid-band model.

In this study, hole state and defect structure of protonic conductor SrTiO<sub>3</sub> has been studied by High-resolution X-ray absorption spectroscopy.

### 2. Experimental

The X-ray absorption spectroscopy (XAS) was carried out at undulator beamline BL-19B in the Photon Factory at High Energy Accelerator Research Organization, Tsukuba in Japan.

Synchrotron radiation from the undulator was monochromatized using a grating monochrometer VLM19. The resolution of the beamline was smaller than about 50 meV at  $h\nu=500$  eV. The XAS spectra were measured by the XUV silicon photodiode.

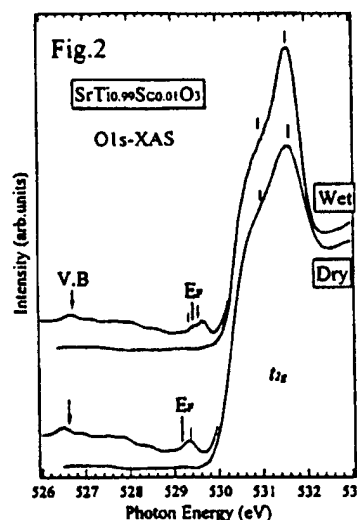
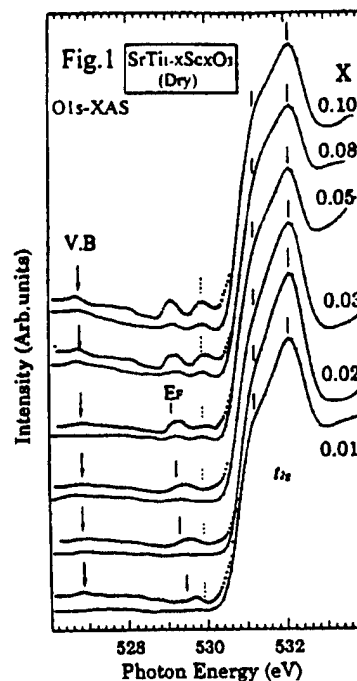
### 3. Results and Discussion

Figure 1 shows the O 1s XAS spectra of Sc-doped  $\text{SrTiO}_3$ . In the Ti 2p XAS study of Ti compounds, the dipole selection rule indicate that the O 1s XAS spectra corresponds to transitions into O 2p state hybridized into the unoccupied Ti 3d states. The Fermi level ( $E_F$ ) is determined by the O 1s photoemission peak. The peak around is the  $t_{2g}$  subband of the Ti 3d states. The V.B shown in arrow is the top of the valence band. The small structure near the V.B is hole state created in the top of the valence band, indicating the doping dependence. This indicates that the doped hole ( $\text{Sc}^{3+}$ ) is introduced into O 2p band. The structure near the  $E_F$  may be impurity (acceptor) level. However, the position is different from the concept of *p*-type semiconductor. The origin does not know at now.

Figure 2 shows the annealing dependence of the O 1s XAS spectra of Sc-doped  $\text{SrTiO}_3$ . The thermal management is Dry and  $\text{H}_2\text{O}$ . Comparing the structure near the V.B, the intensity of  $\text{H}_2\text{O}$  is smaller than that of Dry. This indicates that the doped proton is introduced into the top of the O2p valence band.

### References

- [1] N. Sata, M. Ishigame, and S. Shin, Solid State Ionics
- [2] T. Higuchi et al., Phys. Rev. B 57, 6978 (1998):



## STRONTIUM TANTALATES WITH PEROVSKITE-RELATED STRUCTURE

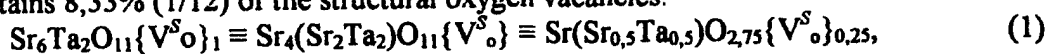
Irina Animitsa, Arkady Neiman, Denis Dildin, Emma Vovkotroob\*.

Inorganic Chemistry Department, Ural State University, 620083, Ekaterinburg, Russia

Institute of High Temperature Electrochemistry, Ural Branch of RAS, Ekaterinburg, Russia \*

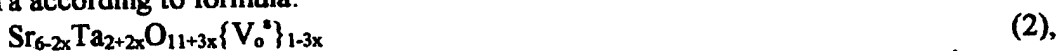
The  $\text{Me}_6\text{M}_2\text{O}_{11}$  (Me - Sr, Ba; M - Nb, Ta) phases with cryolite structure are known as high temperature oxygen ion conductors [1]. Recently it was shown that conductivity of phases belonged to concentration range  $\text{Sr}_6\text{Nb}_2\text{O}_{11}$ - $\text{Sr}_4\text{Nb}_2\text{O}_9$  was very sensitive to water vapour partial pressure at temperatures below 900°C [2]. This work concerns the complex investigation of related system  $\text{Sr}_6\text{Ta}_2\text{O}_{11}$ -  $\text{Sr}_4\text{Ta}_2\text{O}_9$ .

According to structure and phase equilibrium data phases from  $\text{Sr}_6\text{Ta}_2\text{O}_{11}$ -  $\text{Sr}_4\text{Ta}_2\text{O}_9$  system are solid solutions formed on the base of cryolite-type structure. The  $\text{O}^{2-}$ -sublattice of  $\text{Sr}_6\text{Ta}_2\text{O}_{11}$  contains 8,33% (1/12) of the structural oxygen vacancies.



where symbol  $\text{V}_\text{o}^{\bullet}$  indicates the structural nature of oxygen vacancies.

This homogeneity range S6T - S4T is formed via the octahedral-coordinated Sr replacement by Ta according to formula:



This substitution is accompanied by decreasing of structural oxygen vacancies concentration. Complete oxygen sublattice corresponds to perovskite-related phase  $\text{Sr}_4\text{Ta}_2\text{O}_9$ . From this viewpoint phases with highest content of MeO are the most interesting. In general case the substitution of Me by other metals may lead to obtaining of new related materials in the ternary MeO-Me'O-M<sub>2</sub>O<sub>5</sub> systems. Well-known protonic conductor  $\text{Ba}_3(\text{Ca}_{1.18}\text{Nb}_{1.82})\text{O}_9$  (BCN-18) is among them and to be of special interest.

The following experimental techniques were used: TG, conductivity measurements (both in reversible and transient mode), EMF and Tubandt transport numbers determination, tracer diffusion (at temperature up to 1300°C,  $a_{\text{H}_2\text{O}} \cdot 10^{-5} \dots 10^{-2}$ ) IR- and Raman spectroscopy. The water chemical diffusion coefficient was calculated from the data of transient TG

### Conductivity data

There were two linear parts on all  $\lg \sigma_{\text{tot}}(T^{-1})$  dependencies. The largest activation energy was in the high temperature region. The point of transition depended upon the  $a_{\text{H}_2\text{O}}$  value, it moved to high temperatures with  $a_{\text{H}_2\text{O}}$  rise. It was shown that the total conductivity decreased within the homogeneity range from  $\text{Sr}_6\text{Ta}_2\text{O}_{11}$  to  $\text{Sr}_4\text{Ta}_2\text{O}_9$ , while the conductivity activation energy increased. Thus the conductivity changes from  $3 \cdot 10^{-3}$  up to  $1 \cdot 10^{-4} \text{ Sm} \cdot \text{cm}^{-1}$  at 1000°C (where the conductivity is predominantly oxygen-ionic). There is a change in conductivity nature from oxygen to hydrogen with decreasing of temperature and increasing of  $a_{\text{H}_2\text{O}}$ . The following dependence was observed for  $\text{Sr}_6\text{Ta}_2\text{O}_{11}$  at 400°C -  $\sigma_{\text{tot}} \sim a_{\text{H}_2\text{O}}^{1/2}$ , pointed to the predominantly hydrogen conductivity. The activation energy decreased from 1,25 to 0,65 eV in dry ( $a_{\text{H}_2\text{O}} = 10^{-5}$ ) and wet atmosphere ( $a_{\text{H}_2\text{O}} = 10^{-2}$ ), respectively. Similar trends were observed earlier for the  $\text{Sr}_6\text{Nb}_2\text{O}_{11}$ - $\text{Sr}_4\text{Nb}_2\text{O}_9$  system [2,3].

Thermogravimetry measurements

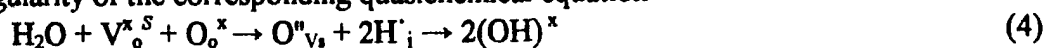
It was observed that at elevated temperatures water might be reversibly incorporated and removed from all  $\text{Sr}_6\text{Ta}_2\text{O}_{11}$ -ss phases. The weight loss for  $\text{Sr}_6\text{Ta}_2\text{O}_{11}$ , preliminary equilibrated with atmosphere air at 150°C corresponded to one mole of  $\text{H}_2\text{O}$ . It coincided with value of the maximal water uptake (absorbed water removes below 100°C) expected from (1) and (2). This result formally corresponds to the full filling of structural oxygen vacancies by  $\text{H}_2\text{O}$ . The total  $\text{H}_2\text{O}$  uptake diminished with increasing of  $\text{Ta}_2\text{O}_5$  content sharper than it followed from (2). It may mean that more complicate processes occur for compositions with  $x > 0$ . During heating the water loss proceeded via two stages (500 and 800-900°C, respectively) for phases with  $x \leq 0,2$ . The DTA-curves confirmed these results by two endothermic effects at the same temperatures. The resolution of stages became worse with gradual increasing of  $x$ . For  $x \geq 0,2$  TG demonstrated the blurred and smooth mass decreasing at 500 - 900°C. The similar behaviour was observed earlier for the  $\text{Sr}_6\text{Nb}_2\text{O}_{11}$ - $\text{Sr}_4\text{Nb}_2\text{O}_9$  system [2].

On the base of described data we came to conclusion that two forms of water insertion are inherent for the system investigated. One of them seems to be the chemical interaction between the complex oxide and water with formation of any oxyhydrate or intercalation phase intergrown with the base matrix or distributed over its surface. The dehydration of this phase proceeds during the low temperature stage. The second form can be considered as randomly distributed  $(\text{OH})^-$ -groups formed by water dissolution in oxide matrix. The total water uptake can be conventionally illustrated by the next hypothetical formula of hydrated  $\text{Sr}_6\text{Ta}_2\text{O}_{11}$  composition as an example



where the  $2y$ -coefficient corresponds to the chemically fixed water.

It seems reasonable to underline the specific features of the formal quasichemical approach application to the phases of type (1). The structure vacancy has a neutral effective charge (similar to unoccupied interstitial positions). Then inserting of oxygen from water into the structure vacancy is a process similar to interstitial oxygen formation  $\{\text{O}^{\text{v}}_i\}$ . This leads to the obvious singularity of the corresponding quasichemical equation



where the  $(\text{OH})$  groups formed have the unusual effective charge.

Thus the water incorporation into the phases with constitutional disordering requires a thorough investigation with a special reference to the nature of processes and localisation of the phases formed. The results of research of structurally disordered perovskites with vacancies in metal and oxygen sublattices are presented in [4].

- [1] A. Neiman, A. Podcorytov, V. Zhukovsky. *Physica Status Solidi(a)*. 1987, v.101, 1, p.371-380
- [2] A. Neiman, I. Animitsa, T. Norby and R. Glockner, 11-th Int. Conf. Solid State Ionics, Honolulu, Hawaii, USA, November 16-21, 1997, Extended Abstracts, p.96-97.
- [3] R. Glöckner, A. Neiman, T. Norby, Y. Larring. 9-th Int. Conf. on Solid State Protonic Conductors, Bled, Slovenia, August 17-21, 1998, Extended Abstracts, p. 13-14
- [4] A. Neiman, I. Animitsa, D. Dildin and A. Sharafutdinov, Abstracts of this Conference.

## PREPARATION AND CONDUCTIBILITY OF VANADOTUNGSTOGERMANIC HETEROPOLY ACID

Q.Y.Wu<sup>1,2</sup> and G.Y.Meng<sup>1,\*</sup>

<sup>1</sup>Department of Materials Science & Engineering, University of Science and Technology of China, Hefei 230026 P.R.China

<sup>2</sup>Institute of Chemical Science & Engineering, Liaoning University, Shenyang 110036 P.R.China

Heteropolyacids(HPA) are of special interest as new materials because of their high-proton conductivities. Due to their exceptionally high-proton conductivity, they belong to the group of the few protonic conductors that are superionic at room temperature[1]. In recent years, the research of HPA in this field became very active. The conductivity results have been reproduced frequently and the material has been suggested for applications in hydrogen-oxygen fuel cells, electrochromic devices, sensors etc.[2]. In the present paper, we report the preparation and characterization as well as conductivity of vanadotungstogermanic heteropoly acid.

The vanadotungstogermanic acid  $H_5GeW_{11}VO_{40} \cdot 22H_2O$  has been prepared for the first time by the stepwise acidification and the stepwise addition of solutions of the component elements. The suitable condition of the synthesis reaction is given. The potentiometric titration shows that five protons are dissociated in one-step. Six characteristic absorption peaks in IR spectrum and two intense charge-transfer bands in UV spectrum are as follows: IR: 979, 888, 825, 775, 535, 463 $cm^{-1}$ ; UV: 264, 204nm. The  $^{51}V$  NMR spectrum showed a peak at -548.3ppm and indicates that there is only one vanadium atom in the heteropolyanion. X-ray powder diffraction is used widely to study the structure of HPA[3]. It can be seen that the characteristic diffraction peaks appear at the following four ranges above  $2\theta$  angles: 7-10°, 16-22°, 25-30°, 33-38°, which is similar to those compounds with Keggin structure. Combined with IR and UV spectra, we confirm that its structure is Keggin structure. Thermal stability is an important consideration. In general, we take the temperature of the exothermic peak of DTA curves as the sign of their thermostability[4]. The TG curve shows that the weight loss of the compound is a three step process. In the DTA curve, there is an exothermic peak at 496.1°C. The thermostability of the HPA had higher than that  $H_4GeMo_{12}O_{40}$  and  $H_4GeW_{12}O_{40}$ .

The AC proton conductivity was measured as follows. The compound was pressed at 20MPa into a compact pellet 15mm in diameter and 3.86mm thickness. Copper slices and copper wires were used as electrodes and lines respectively. The conductivity was determined by complex impedance spectroscopy using a M378 electrochemical impedance analyzer. Measurements were made in frequency ranges from 0.01Hz to  $9.99 \times 10^4$ Hz at room temperature. The result of AC impedance measurement shows that vanadotungstogermanic acid is a new solid high-proton conductor, its proton conductivity is  $2.43 \times 10^{-3} s \cdot cm^{-1}$  at 18°C.

### Acknowledgements

The financial support from the National Natural Science Foundation of China and Natural Science Foundation of Liaoning Province for this work is greatly appreciated.

### References

- [1] O.Nakamura, Kikan Kagaku Sosetsu **20**, 177 (1993).
- [2] S.J.Babinec, Proc. Electrochem. Soc. **94**, 30 (1994).
- [3] Q.Y.Wu, E.B.Wang and J.F.Liu, Polyhedron **12**, 2563 (1993).
- [4] Q.Y.Wu and Y.C.Zhai, Rare Metals **15**, 257 (1996).

## PROTONIC CONDUCTION IN NEW COMPOSITE SUPERIONIC CONDUCTORS.

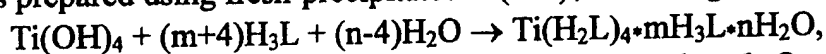
N.G.Bukun\*, V.V.Rodionov\*\*, A.M.Mikhailova\*\*

\*Institute of New Chemical Problems, Russian Academy of Sciences,  
Chernogolovka, Moscow district, Russia

\*\*Saratov State Technical University, Saratov, Russia

It was shown previously [1] that sulphosalicylic acid and its composite with iron(III) sulphosalicylate have purely protonic conduction ( $t_{H^+} \approx 1$ ). The values of their conductivity are as follows:  $\sigma(25^\circ\text{C}) = 4.1 \cdot 10^{-4}$  and  $3.0 \cdot 10^{-4}$  S/cm, respectively.

The objective of this work was to synthesize a new composite of sulphosalicylic acid with Ti(IV) sulphosalicylate and to investigate its transport properties. This Ti-composite was prepared using fresh-precipitated  $\text{Ti}(\text{OH})_4$  according to the reaction:



where  $\text{H}_3\text{L} = \text{C}_7\text{H}_6\text{O}_6\text{S} \cdot 2\text{H}_2\text{O}$  is sulphosalicylic acid,  $m=10$  and  $n=6$ . Orange crystals of Ti-composite were ground and pressed in to the electrochemical cells for a.c. (impedance spectroscopy) and d.c. (Hebb-Wagner's method) measurements. Titanium foil annealed in hydrogen at  $460^\circ\text{C}$  ( $\text{TiH}_x$ ) was used as reversible electrode but glassy carbon as inert one. The total conductivity of Ti-composite is fitted to linear dependence at the temperature interval  $+0.8 - +72^\circ\text{C}$  according to Arrhenius equation

$$\sigma T = (1.1 \pm 0.4) \cdot 10^6 \exp[(0.31 \pm 0.03)/kT].$$

At  $20^\circ\text{C}$  the total conductivity of Ti-composite amounts to  $3.43 \cdot 10^{-5}$  S/cm that is higher by three orders magnitude than its electronic conductivity ( $\sim 10^{-8}$  S/cm), estimated by Hebb-Wagner's methods.

It was observed dependence of conductivity on humidity of air. Therefore all a.c. and d.c. measurements were carried out in air atmosphere with constant relative humidity ( $\sim 52\%$ ).

Thus, new composite of sulphosalicylic acid with Ti(IV) sulphosalicylate of the general formula  $\text{Ti}(\text{H}_2\text{L})_4 \cdot 10\text{H}_3\text{L} \cdot 6\text{H}_2\text{O}$  has a purely protonic conduction with transfer number  $t_{H^+} \approx 1$ .

## Acknowledgments

This work was supported by the Russian Foundation for Basic Research (Projects NN 96-03-33648a and 98-03-32580a).

## References

- [1] N.Bukun, V.Rodionov, A.Mikhailova, Yu.Dobrovolsky, Solid State Ionics 97 (1997) 257.

## PROTONIC CONDUCTIVITY OF NEUTRAL AND ACIDIC SILICOTUNGSTATES

A. Vakulenko, Yu. Dobrovolsky, L. Leonova, A. Karelin, A. Kolesnikova  
Institute for New Chemical Problem RAS, Chernogolovka

Many of heteropolycompounds are known to have significant proton conductivity. The salts of phosphotungstic acid manifested high stability and the highest conductivity. Not only the salts containing bound proton but also crystal hydrates of the neutral salts possess high proton conductivity[1].

The salts of composition  $\text{Me}_4\text{SiW}_{12}\text{O}_{40} \cdot n\text{H}_2\text{O}$  and  $\text{MeHSiW}_{12}\text{O}_{40} \cdot n\text{H}_2\text{O}$  (where  $\text{Me} = \text{Na}^+, \text{K}^+, \text{Rb}^+, \text{Cs}^+, \text{NH}_4^+$ ) are synthesized in the present work and their IR spectra and proton conductivity in broad range of temperature and environmental humidity are studied. The proton conductivity was determined by the method of impedance spectroscopy by means of analysis of impedance hodograph of the symmetrical cells  $\text{Pt}/\text{compound under study}/\text{Pt}$  in the air with controlled humidity.

It is shown that proton conductivity of synthesized samples grows with the increasing content of crystal water in the salts up to  $n = 8$ . When  $n > 8$ , the further increase in the content of crystal water does not result in any significant change in the parameters of the ion transfer.

IR spectroscopy of the samples with high content of crystal water revealed a narrow

absorption band of medium intensity at  $1620\text{--}1640\text{ cm}^{-1}$  and broad band at  $3440\text{--}3480\text{ cm}^{-1}$  assigned to  $\delta(\text{H}_2\text{O})$  and  $\nu(\text{H}_2\text{O})$  respectively. These bands are typical of liquid disordered water and not of regular crystal water. The bands corresponding to vibrations of hydrated proton are not resolved on this background.

The samples with small (less than 3 mol/mol of salt) content of crystal water in the neutral salts

showed absorption bands at  $1720$  and  $3160\text{ cm}^{-1}$ . These bands are assigned to main vibrations of hydrated proton (presumably, in the form of dioxonium ion) ( $\delta_{\text{as}}(\text{HOH}_2)$  and  $\nu_{\text{s,as}}(\text{OH}_2)$

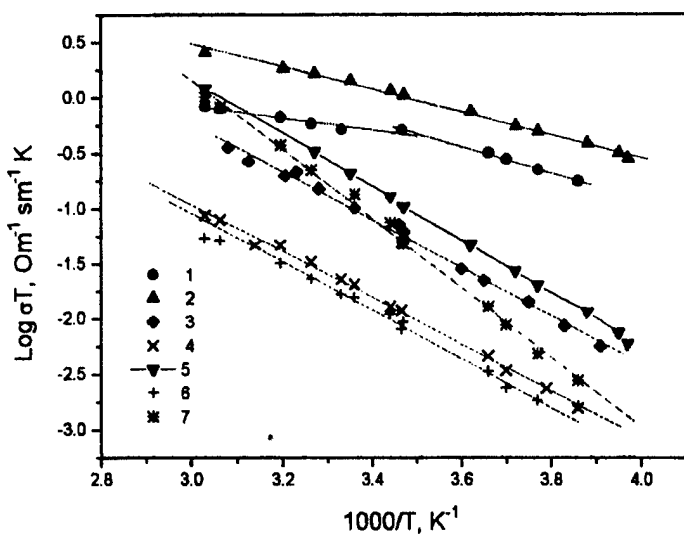


Fig. 1. The temperature dependences of protonic conductivity of silicotungstates with high content of crystal water. Salts: 1-  $\text{Cs}_3\text{HSiW}_{12}\text{O}_{40} \cdot 10\text{H}_2\text{O}$ ; 2-  $\text{Cs}_4\text{SiW}_{12}\text{O}_{40} \cdot 11\text{H}_2\text{O}$ ; 3-  $\text{Na}_3\text{HSiW}_{12}\text{O}_{40} \cdot 8\text{H}_2\text{O}$ ; 4-  $\text{Na}_4\text{SiW}_{12}\text{O}_{40} \cdot 10\text{H}_2\text{O}$ ; 5-  $(\text{NH}_4)_4\text{SiW}_{12}\text{O}_{40} \cdot 17\text{H}_2\text{O}$ ; 6-  $\text{K}_4\text{SiW}_{12}\text{O}_{40} \cdot 10\text{H}_2\text{O}$ ; 7-  $\text{Rb}_4\text{SiW}_{12}\text{O}_{40} \cdot 10\text{H}_2\text{O}$

respectively). Upon further increase in the content of crystal water, the dioxonium ions are further hydrated and incorporated in the network of the hydrate structure.

Proton conductivity of acidic salts is an order of magnitude higher than that of similar neutral salts. At the same time, the activation energies of conductivity ( $E_a$ ) for acidic and neutral



salts with the same cations are close. It can be explained by the increasing numbers of the charge carriers in acidic salts in comparison with neutral ones while their mobilities are close.

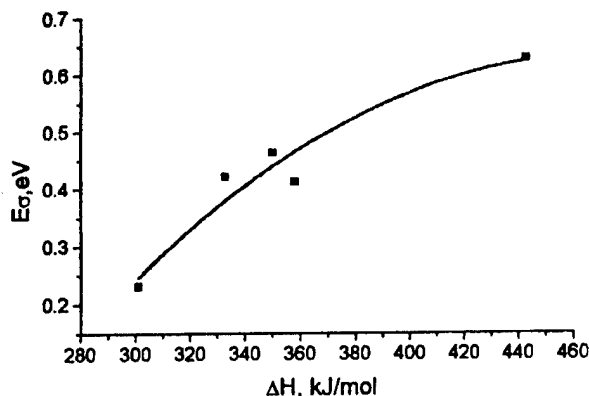


*Fig. 2. The activation energy of conductivity of highly hydrated neutral silicotungstates versus hydration heat of the outer cation.*

The conductivities and activation energies of the salts are strongly dependent on the identity of outer-shell cation (Fig. 1). The activation energies of conductivity correlate with hydration heat of the outer cation (Fig. 2) and elevated conductivity of the ammonium salt (having high  $E_a$ ) can be explained by the contribution of ammonium proton in ionic charge transfer, similarly to ammonium phosphotungstates [2].

The work is supported by the Russian Fundamental Research Foundation, Grant 98-03-32580a.

[1] E.A.Ukshe, L.S.Leonova, A.I.Korosteleva, Solid State Ionics **36**, 219 (1989)

[2] V. Steinberg, B.Shumm, L.Erofeev, ect. Solid State Physics (in Russian) **31**, 128 (1989)

## THE PROTON CONDUCTIVITY OF THE DEHYDRATED $\text{SnO}_2$ AT LOW TEMPERATURES

Leonova L.S., Dobrovolsky Yu.A., Ukshe A.E., Domashnev D.I.  
Institute for New Chemical Problems RAS, Chernogolovka, Russia

Many oxide systems have a heightened proton conductivity at a high temperature [1, 2]. Nevertheless during decreasing the temperature an ionic conductivity considerably falls. At this work we have study the behavior of the electrochemical calls:



in the temperature range from  $-60$  to  $+60$  °C in air with controlled contents of water vapor.

If the water is absent, under heightened temperature the interface  $\text{Ag} | \text{SnO}_2$  is the ohm's contact and tin dioxide behaves as the semiconductor of n-type. The activation energy of electron conductivity is 1.5 eV; that value is considerably more than the wide of foul band. It is mean, that the conductivity is surface as advantage. At room temperature there are the deviations from Ohm law. The conductivity measures at high frequencies give a value of resistance about 2 GOhm/cm.

If there is a water in the air, the cell's behavior changes considerably. The electronic conductivity of specimen, measured at direct current increases up to 4 or 4 orders of value, and the high ionic conductivity arises.

The typical impedance hodograf of the cell  $\text{Ag} | \text{SnO}_2 | \text{Ag}$  is shown at fig.1.

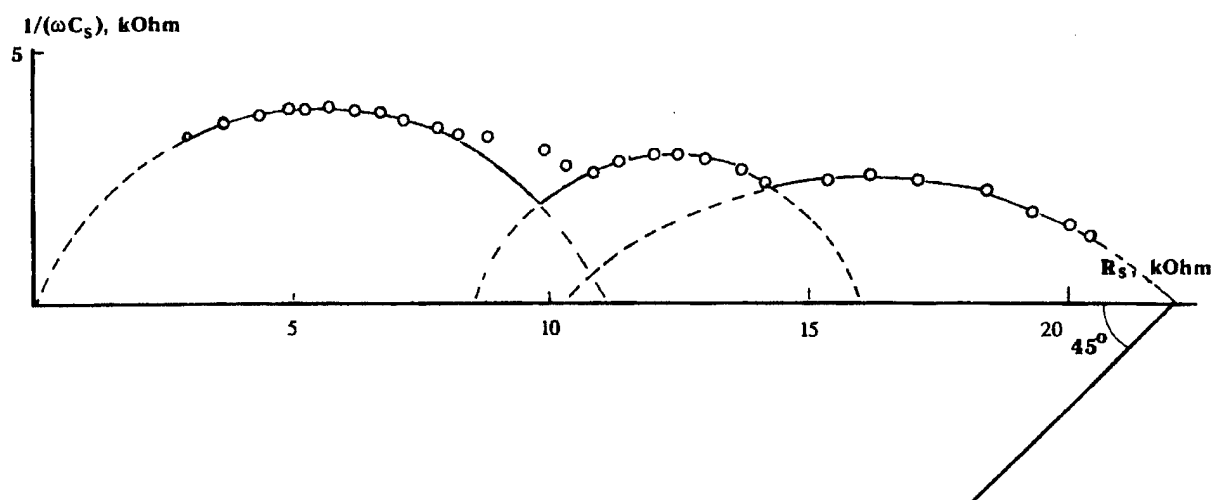


Fig.1. The typical impedance hodograf of the cell  $\text{Ag} | \text{SnO}_2 | \text{Ag}$ .  
The temperature  $+20$  °C, humidity 84% rel.

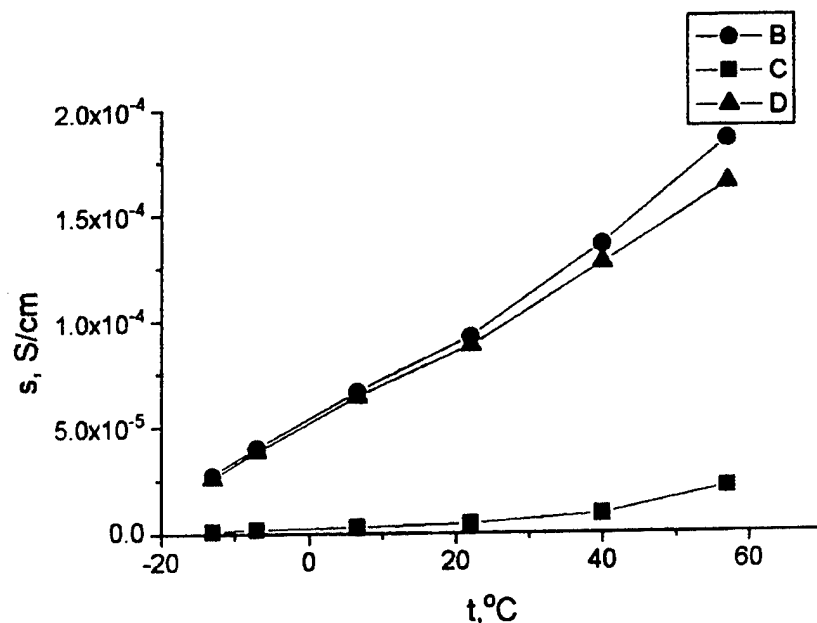


Fig.2. The dependence of total, electronic and ionic conductivity on temperature. B - total, C - electronic, D - ionic conductivity. Humidity 84%rel.

Both electronic and ionic parts of conductivity depend on the temperature (fig.2), and on the humidity of environment. At low temperature and high humidity of environment SnO<sub>2</sub> behaves as ionic conductor (the part of ionic in full conductivity of specimen reaches 95%). The temperature dependencies of impedance parameters testify the complex character of ionic conductivity with the diffusion transport of negative carriers (electrons or, maybe,

OH<sup>-</sup>-groups) attended with fast protonic transport.

The work is supported by the Russian Fundamental Research Foundation, Grant 98-03-32580a.

#### References

- [1] H.Iwahara, T.Esaka, H.Uchida et al., Solid State Ionics 3/4, 359 (1981)
- [2] Y.Larring, T.Norby, Solid State Ionics 77, 147 (1995)

## LATTICE-ASSISTED PROTON MOTION IN PEROVSKITE OXIDES

A.L. Samgin,

Institute of High-Temperature Electrochemistry,  
Russian Academy of Sciences, 620219, Ekaterinburg, Russia

In understanding of migration of such light ions as protons, it is important to know in detail the role played by a thermal reservoir. A treatment based on the Kramers diffusion has been used advantageously along this line [1]. We start from approach [2], which treats of the dynamical properties of a carrier on the basis of an idealized model of hopping motion of particle, specifically, re-expresses the small polaron theory in terms of observables for the "dressed" particle without regard to full details of the interaction between particle and reservoir.

To examine the part of phonons, a formal theory may be used, in which the proton is viewed as the small polaron rather than the proton. Properties of proton motion from site to site near the oxygen ions can be expressed in terms of phenomenological parameters representing activated jumps (probabilities) [2], as well as in terms of frequencies of all involved phonons (such as vibrations of oxygen octahedra or OH-bond), proton transfer integral  $J$  and proton-phonon coupling  $u^2$ . Application of this approach to some oxides seems to be less formal than had been suspected. This is due to the fact that in H-bonded chain the formation of small proton polaron can be really possible owing to the proton-phonons interaction [3]. It is interesting that the Kramers diffusion and the ART theory also can be viewed in a similar manner to hopping of small proton polarons.

Our purpose is to look at a treatment of reservoir in the context of the proton polaron idea with application to  $\text{SrTiO}_3$ ,  $\text{SrZrO}_3$  and  $\text{SrCeO}_3$ -based oxides, and, second, to point out that a proton polaron effects may be large enough in these oxides.

Consider for example the temperature dependence of proton mobility in  $\text{SrCe}_{1-x}\text{Yb}_x\text{O}_3$ . Using an average frequency  $\omega = 6 \cdot 10^{13} \text{ s}^{-1}$  and the known expression for polaronic activation energy

$$E = 2kT u^2 \tanh(\hbar \omega / 4kT), \quad (1)$$

one obtains after substitution of the experimental activation energy  $E=0,63 \text{ eV}$  [4] in eq.(1) the value  $u^2 \sim 30$ . We get  $J = 3,2 \cdot 10^{-21} \text{ J}$ , in that case we obtained values of about  $5,4 \cdot 10^{-6}$ ,  $1,1 \cdot 10^{-5}$ ,  $1,9 \cdot 10^{-5}$  and  $2,9 \cdot 10^{-5} \text{ cm}^2 \text{ s}^{-1} \text{ V}^{-1}$  for the jumping mobility of protons at 600, 700, 800 and 900 °C. These values are very close to that reported in ref.[5] at  $T = 600\text{-}800 \text{ °C}$ . For the same parameters we have calculated the time between proton jumps to be about  $3 \cdot 10^{-11} \text{ s}$  at 600 °C. This value agrees with the experimental value  $2,8 \cdot 10^{-11} \text{ s}$  [6]. To explain the decrease in  $E$  with increasing average hopping distance  $d$ , we invoke the explicit expression, which is a natural extension of the electron polaron theory to the proton

$$E \sim 1/d - 1/R_{pp}, \quad (2)$$

where radius of proton polaron  $R_{pp}$  is equal to 3,45 Å [7]. This suggests that the ratio of activation energies for  $d = 2,83 \text{ Å}$  and  $d = 3,02 \text{ Å}$  is the same as the experimental ratio 3/2 [4].

A consequence of this approach is that the proton motion in H-bonded oxide networks changes from thermally activated jumps to tunneling at  $T < T_c$ , because the polaron mobility comprises the tunneling part and the hopping part. While this conclusion is in a sense parallel to that of ref.[8], a description in terms of proton polarons is able to readily evaluate  $T_c$ . To

evaluate  $T_c$  wherein proton tunneling predominates, consider  $\text{SrTiO}_3$ . In this oxide the proton is located in the site between the O-O ions (this distance is evaluated to be 1,2 Å) as if it forms the hydrogen bond [9]. Taking  $J = u\hbar\omega\pi^{-1/2}$ , we obtain  $T_c \sim \hbar\omega/2k$ . It follows that for the OH-stretching vibration in heavily doped crystal (which is about 2500  $\text{cm}^{-1}$  [9])  $T_c \sim 270$  K. One finds with phonon frequency  $6 \cdot 10^{13} \text{ s}^{-1}$ ,  $T_c \sim 217$  K. Thus,  $T_c$  appears to be sensitive to the frequency of oxygen vibrations and the proton-phonon coupling, or to properties of the reservoir which interacts with an assembly of protons. This temperature correlates with  $T_c$  for proton hopping between potential wells on the H-bond which may be written as [10]

$$T_c \approx \hbar(V/2mb^2)^{1/2}, \quad (3)$$

where  $V$  is the barrier height,  $b$  is the barrier width. Taking  $b = 1,2$  Å and  $V = 0,42$  eV [8], we obtain  $T_c = 269$  K. This is in general agreement with the tunneling mechanism for proton motion observed in doped  $\text{SrZrO}_3$  between 5 and 300 K [11].

- [1] A.S.Nowick, A.V.Vaysleyb, *Solid State Ionics* **97**, 17 (1997).
- [2] G.L.Sewell, *Phys. Rev.* **129**, 597 (1963).
- [3] V.V.Krasnogolovets et al., *Int.J.Quant.Chem.* **33**, 340 (1980).
- [4] T.Scherban et al., *Solid State Ionics* **8**, 585 (1988).
- [5] H.Uchida et al., *Solid State Ionics* **3**, 89 (1989)
- [6] R.Hempelmann et al., *Solid State Ionics* **77**, 152 (1995).
- [7] A.L.Samgin, *The XI Conf. phys.chem. and electrochem. molten and solid electrolytes, Abstracts, Ekaterinburg* **2**, 111 (1998).
- [8] E.Matsushita, A.Tanase, *Solid State Ionics* **97**, 45 (1997).
- [9] N.Sato et al., *Phys.Rev.* **B54**, 15795 (1996).
- [10] M.I.Klinger, A.O.Asisyan, *Fizika i tehnika poluprovodnikov* **13**, 1873 (1979).
- [11] H.Yugami et al., *Solid State Ionics* **77**, 195 (1995).

## CHARGE TRANSFER IN Nb<sup>V</sup>, Ta<sup>V</sup>, Mo<sup>VI</sup> AND W<sup>VI</sup> - BASED CRYOLITES OF ALKALI-EARTH METALS

Arkady Neiman, Irina Animitsa, Denis Dildin and Albert Sharafutdinov

Inorganic Chemistry Department, Ural State University, 620083, Ekaterinburg, Russia

Some perovskites with impurity stimulated or internal oxygen deficiency exhibit high proton conductivity (the typical examples are MeCeO<sub>3</sub>-based phases and Ba<sub>3</sub>Ca<sub>1.18</sub>Nb<sub>1.82</sub>O<sub>9</sub>, correspondingly). There is another family of matrixes considered as potential proton conductors [1,2], namely double oxides with cryolite (double-perovskite) structures containing the so-called structural (constitutional) vacancies (V<sup>S</sup>) in oxygen sublattice. The last represent itself the normal crystallographic sites unoccupied in the structure of stoichiometric compound. The transport properties and water uptake for the stoichiometric Sr<sub>6</sub>Nb<sub>2</sub>O<sub>11</sub>{V<sup>S</sup>}<sub>1</sub> - phase and its solid solutions were firstly described in [1,2].

Phases of this type (with structural vacancies either in oxygen or in metal sublattices) are well known for Nb<sup>V</sup>, Ta<sup>V</sup>, Mo<sup>VI</sup>, W<sup>VI</sup> and Alkali-Earth Metals based complex oxides with similar structures. The present investigation was performed to study the role of structural vacancies in origin of hydrogen transfer phenomenon.

Some phases belonged to (A)-(E) related structures were investigated at the temperatures 100...1300°C and H<sub>2</sub>O-activity - 10<sup>-5</sup>...10<sup>-2</sup> by use of the following techniques: TG, *ac*- and *dc*-conductivity measurements, EMF and Tubandt transport numbers determination, tracer diffusion and Raman spectroscopy.

### A. Cryolites with structural vacancies in oxygen sublattices:

- $\text{Me}^{\text{II}}_6\text{M}^{\text{V}}_2\text{O}_{11}\{\text{V}_\text{o}^{\text{S}}\} \equiv \text{Me}^{\text{II}}(\text{Me}^{\text{II}}_{0.5}\text{M}^{\text{V}}_{0.5})\text{O}_{2.75}\{\text{Vo}^{\text{S}}\}_{0.25}$  Me=Ca, Sr, Ba; M=Nb, Ta;
- $\text{Me}^{\text{II}}_4\text{A}^{\text{I}}_2\text{M}^{\text{VI}}_2\text{O}_{11}\{\text{V}_\text{o}^{\text{S}}\} \equiv \text{Me}^{\text{II}}_{0.5}\text{A}^{\text{I}}_{0.5}(\text{Me}^{\text{II}}_{0.5}\text{M}^{\text{VI}}_{0.5})\text{O}_{2.75}\{\text{Vo}^{\text{S}}\}_{0.25}$  M=Mo, W; A<sup>I</sup>=Na, K;
- $\text{Me}^{\text{II}}_5\text{A}^{\text{I}}\text{M}^{\text{V}}_2\text{O}_{10.5}\{\text{V}_\text{o}^{\text{S}}\}_{1.5} \equiv \text{Me}^{\text{II}}_{0.75}\text{A}^{\text{I}}_{0.25}(\text{Me}^{\text{II}}_{0.5}\text{M}^{\text{V}}_{0.5})\text{O}_{2.625}\{\text{Vo}^{\text{S}}\}_{0.375}$  M=Mo, W; A<sup>I</sup>=Na, K.

### B. Perovskites with structural vacancies in A-metal sublattice:

- $\text{LnM}^{\text{V}}_3\text{O}_9 \equiv \text{Ln}_{1/3}\{\text{V}_{\text{Ln}}^{\text{S}}\}_{2/3}\text{M}^{\text{V}}\text{O}_3$  M=Nb, Ta.

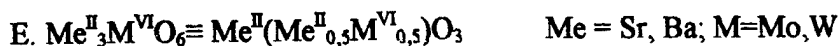
### C. Perovskites with structural vacancies in B-metal sublattice:

- $\text{Me}^{\text{II}}_5\text{M}^{\text{V}}_4\text{O}_{15} = \text{Me}^{\text{II}}(\text{Me}_{0.2}\text{M}^{\text{V}}_{0.8}\{\text{V}_{\text{M}}^{\text{S}}\}_{0.2})\text{O}_3$
- $\text{Me}^{\text{II}}_3\text{M}^{\text{V}}_2\text{O}_8 = \text{Me}^{\text{II}}(\text{Me}_{1/8}\text{M}^{\text{V}}_{6/8}\{\text{V}_{\text{B}}^{\text{S}}\}_{1/8})\text{O}_3$

### D. Cryolites contained 3d-transition metals with structural vacancies in oxygen sublattices:

- $\text{Me}^{\text{II}}(\text{R}^{\text{II}}_{0.5}\text{M}^{\text{V}}_{0.5})\text{O}_{2.75}\{\text{Vo}^{\text{S}}\}_{0.25}$  R- Mn, Co;

The properties of (A)-(D) phases were compared then with characteristics of the cryolite-type phases with complete structures:



The main conclusions are as follows:

1. The TG and conductivity responses upon the change of H<sub>2</sub>O-activity were observed for compounds of all types (A)-(E). We noticed, that the conductivity response was negative for  $\text{Ln}_{1/3}\{\text{V}_{\text{Ln}}^{\text{S}}\}_{2/3}\text{Nb}^{\text{V}}\text{O}_3$  - (A) and  $\text{Ba}_3\text{Nb}_2\text{O}_8=\text{Ba}(\text{Ba}_{1/8}\text{Nb}_{6/8})\{\text{V}_{\text{B}}^{\text{S}}\}_{1/8}\text{O}_3$  - (B), i.e. the total conductivity diminished with rise of H<sub>2</sub>O-activity. The relative magnitude of responses increased with decrease of temperature.
2. Water loss and uptake (500 and 850°C-averaged temperatures) by two stages were reliably determined for the compositions of (A) and (D) types with the oxygen structural vacancies. For  $\text{Sr}_3\text{Nb}_4\text{O}_{15}=\text{Sr}(\text{Sr}_{0,2}\text{Nb}_{0,8})\{\text{V}_{\text{Nb}}^{\text{S}}\}_{0,2}\text{O}_3$  - (A-type) only 500°C-stage was observed.
3. It seems insufficient to regard the water uptake on the base of quasichemical approach only (as an interaction of water molecule with the oxygen vacancy). In general case these processes have to be considered as a chemical interaction between the complex (perovskite, cryolite) and binary oxide (water). The chemical nature of the bulk and surface phases formed (oxyhydrates, intercalation phases) have to be investigated and taken into account too. Thus, both thermodynamics and kinetics aspects for such kind of interactions would be studied using the convenient approach to "gas-solid"-reactions.
4. The phases with fast mixed hydrogen-electron conductivity as well as with hydrogen-oxygen-electron transfer may be produced on the base of complex oxides belonged to (D)-type. In this case the interaction between the electronic subsystem and hydrogen mobile species would be taken into account too.

- [1] A.Neiman, I.Animitsa, T.Norby and R.Glockner, 11-th Int. Conf. Solid State Ionics, Honolulu, Hawaii, USA, November 16-21, 1997, Extended Abstracts, p.96-97.
- [2] R.Glöckner, A.Neiman, T.Norby, Y.Larring. 9-th Int.Conf. on Solid State Protonic Conductors, Bled, Slovenia, August 17-21, 1998, Extended Abstracts, p. 13-14

## **H<sub>2</sub>Ti<sub>3</sub>O<sub>7</sub> AS A POTENTIAL PROTON CONDUCTING FUEL CELL ELECTROLYTE**

Derek J.D. Corcoran and John T.S. Irvine  
University of St. Andrews, School of Chemistry  
St. Andrews, Fife, KY16 9ST, U.K.

Li<sub>2</sub>Ti<sub>3</sub>O<sub>7</sub> with the ramsdellite structure is known to be a fast Li-ion conductor with a conductivity of  $4.62 \times 10^{-4} \text{ S cm}^{-1}$  at 200 °C [1]. In this study, ramsdellite Li<sub>2</sub>Ti<sub>3</sub>O<sub>7</sub> was used as a basis for Li<sup>+</sup>/H<sup>+</sup> exchange to give the hydrogen titanate analogue, H<sub>2</sub>Ti<sub>3</sub>O<sub>7</sub> to investigate its conducting properties for the possible use as a proton conducting electrolyte in solid oxide fuel cells.

X-ray diffraction data and peak refinement analysis confirms Li<sub>2</sub>Ti<sub>3</sub>O<sub>7</sub> to have an orthorhombic unit cell in the Pnma space group,  $a = 9.5337(5)$ ,  $b = 2.9407(1)$ ,  $c = 5.0081(4)$ . After H<sup>+</sup> exchange using 5 M nitric acid refluxing for 12 hrs, the hydrogen titanate, H<sub>2</sub>Ti<sub>3</sub>O<sub>7</sub> was obtained. X-Ray diffraction analysis revealed a similar orthorhombic cell as to before with  $a = 9.7388(0.0019)$ ,  $b = 2.9410(6)$ ,  $c = 4.7247(0.0023)$ , with a total change in unit cell volume (shrinkage) on proton exchange of 3.62 % ( $5.09 \pm 0.13 \text{ Å}^3$ ).

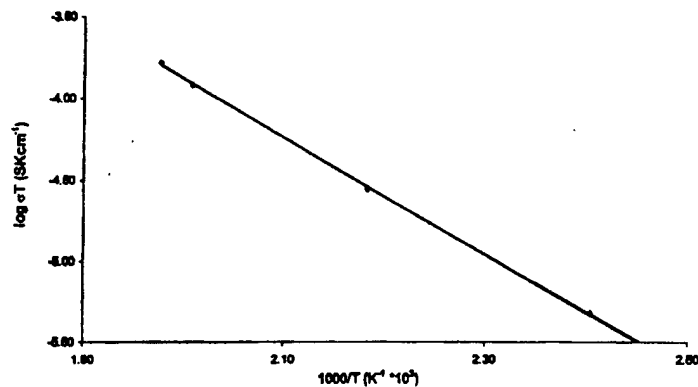
<sup>6</sup>Li-MAS-NMR studies (at 73.599 MHz), on Li<sub>2</sub>Ti<sub>3</sub>O<sub>7</sub> showed that only one type of structural lithium ion exists, with one single sharp peak of approx. 200 Hz base-width showing. It seems that the signal cannot be resolved to reveal the lithium ions in the edge-sharing (Ti,Li)O<sub>6</sub> distorted octahedra and the Li in two tetrahedral sites close to the centre of the open pseudo-rectangular channels having the same chemical shift, resulting in one sharp peak.

Upon Li<sup>+</sup>/H<sup>+</sup> exchange on Li<sub>2</sub>Ti<sub>3</sub>O<sub>7</sub>, the <sup>6</sup>Li-MAS-NMR showed no signal. However, <sup>1</sup>H-MAS-NMR with the H<sub>2</sub>Ti<sub>3</sub>O<sub>7</sub> ramsdellite showed two overlapping (but resolvable) peaks, integrating to 55% and 45%. These may relate to tetrahedral sites in the channels between the TiO<sub>6</sub> octahedra chains, and octahedral sites in the framework.

Previous work has shown that α-H<sub>2</sub>Ti<sub>3</sub>O<sub>7</sub>, the initial product here, is only structurally stable from room temperature up to 202 °C. Structure and space group changes take place up to about 237 °C, above which protons will depart from the channels. Conversion to TiO<sub>2</sub> rutile is achieved above 400 °C [2]. The conductivity (protonic or otherwise) of this compound was therefore examined in the temperature range 140 °C to 233 °C.



(a)



(b)

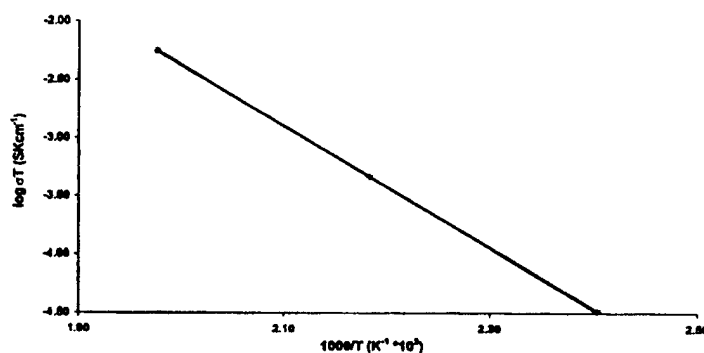


Fig 1. Grain Boundary (a) and Bulk Conductivity (b) Arrhenius plots for  $\text{H}_2\text{Ti}_3\text{O}_7$  (140-233 °C) in wet-air flow.

For conductivity measurements, samples were pressed at 2 tons uniaxial pressure, and both surfaces (1.42 cm<sup>2</sup> each) coated with Au paste, and Au leaf strip electrodes attached. A.c. impedance spectra were taken on  $\text{H}_2\text{Ti}_3\text{O}_7$  under a wet-air gas flow in the range 10 GHz to 0.1 Hz, with gold acting as blocking electrodes. Grain boundary conductivity was found to be  $1.08 \times 10^{-7} \text{ S cm}^{-1}$  at 200 °C with an activation energy of 0.71 eV in the temperature range studied. The bulk response conductivity was found to be  $2.24 \times 10^{-6} \text{ S cm}^{-1}$  at 200 °C, with an activation energy of 1.04 eV in the same temperature range. This compares poorly with  $4.62 \times 10^{-4} \text{ S cm}^{-1}$  for  $\text{Li}^+$  conductivity in  $\text{Li}_2\text{Ti}_3\text{O}_7$  ramsdellite at 200 °C with an activation energy of 0.46 eV [1].

[1] J.B. Boyce, J.C. Mikkelsen Jr., Solid State Comm., **31** 741-745 (1979)

[2] A. le Bail, J.L. Fourquet, Mat. Res. Bull., **27** 75-85 (1992)

## PROTON CONDUCTING MEMBRANES BASED ON VINYLPHOSPHONIC ACID POLYMERIC DERIVATIVES

Z. Florjańczyk, W. Bzducha, E. Wielgus

Warsaw University of Technology, Faculty of Chemistry,  
ul. Noakowskiego 3, 00-664 Warsaw, Poland

Intense research is being carried out during the recent years on the synthesis of proton conducting membranes due to the potential possibility of their practical application as electrolytes in fuel cells. Membranes comprising poly(perfluorosulfonated acids) plasticized with water, exhibiting ionic conductivity of the order of  $10^{-2} \text{ S}\cdot\text{cm}^{-1}$ , are tested now. However, such type of materials, taking into account economic and technological aspects, have many disadvantages, which precludes the commercialization of them.

In the work presented attempts have been made to obtain alternate proton conducting membranes with the use of vinylphosphonic acid polymeric derivatives. The possibility of immobilizing poly(vinylphosphonic acid) in polybenzimidazole (PBI) membranes has been studied and the conducting properties of such systems were determined. It was found that after 48 h imbibition of the polybenzimidazole membrane with 5 M aqueous solution of vinylphosphonic acid, then polymerization of the immobilized acid in the membrane and storing in water, 2.5 vinylphosphonic acid monomeric units fall per one benzimidazole monomeric unit. The ionic conductivity of such systems increases from ca.  $3 \times 10^{-4} \text{ S}\cdot\text{cm}^{-1}$  at room temperature to ca.  $10^{-3} \text{ S}\cdot\text{cm}^{-1}$  at  $90^\circ\text{C}$ .

Studies have been carried out also on the possibility of synthesis of membranes based on poly(vinylidene fluoride) (PVdF) and the copolymer of vinylphosphonic acid with *N,N'*-methylenediacrylamide. Optimization of the composition of such membranes was performed in view of their mechanical and conducting properties. The membranes exhibited good mechanical properties up to ca. 60 wt. % of the copolymer in the membrane. Water imbibition of such membranes was 40 wt. % and the conductivity was of the order of  $10^{-3} \text{ S}\cdot\text{cm}^{-1}$ .

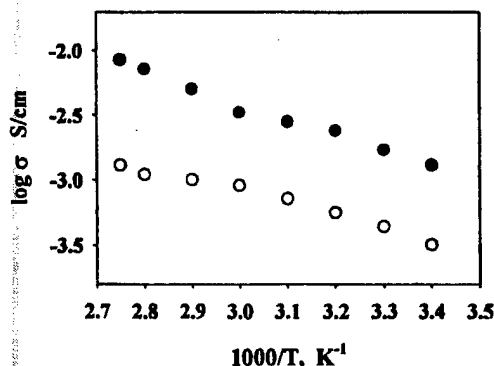


Figure: Ionic conductivity as a function of inverse temperature for membranes containing: (●) – 50 wt. % of PVdF and 50 wt. % of poly[(vinylphosphonic acid)-co-*N,N'*-methylenediacrylamide]; (○) – PBI and poly(vinylphosphonic acid) at mole ratio equal 1 : 2.5.

*This work was financially supported by the Polish State Committee for Scientific Research within the grant no. 8 T10B 075 15.*

## ELECTRONIC TRANSPORT PROPERTIES AND ELECTRONIC STRUCTURE OF $\text{InO}_{1.5}$ -DOPED $\text{CaZrO}_3$

Shu YAMAGUCHI<sup>a</sup>, Kiyoshi KOBAYASHI<sup>b</sup>, Toru HIGUCHI<sup>c</sup>, Shik SHIN<sup>d</sup>, and Yoshiaki IGUCHI<sup>a</sup>

<sup>a</sup>Department of Materials Science and Engineering, Nagoya Institute of Technology

Gokiso-Cho, Showa-Ku, Nagoya 466-8555, Japan

<sup>b</sup>National Institute of Materials and Chemical Research, Higashi 1-1, Tsukuba 305-8565, Japan

<sup>c</sup>Faculty of Science, Science University of Tokyo, Kagurazaka 1-3, Shinjuku, Tokyo 162-0825, Japan

<sup>d</sup>Institute of Solid State Physics, University of Tokyo, Tanashi 188-8501, Japan

### 1. INTRODUCTION

After the discovery of perovskites with proton conductivity at elevated temperatures, various investigations have been made, in order to clarify the origin and its nature of proton conductivity. However, only few information has been available on the transport properties and its electronic structure of those oxides. In the present study, we employed simultaneous measurements of conductivity and thermoelectric power, in order to evaluate the electric transport properties of  $\text{InO}_{1.5}$ -doped  $\text{CaZrO}_3$  (CZ). In addition, the X-ray absorption spectroscopy (XAS) was employed to observe the electronic structure near the band gap.

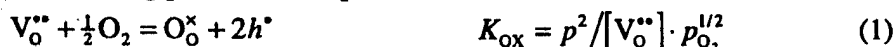
### 2. EXPERIMENTAL

The sample with the nominal composition of  $\text{CaZr}_{0.99}\text{In}_{0.01}\text{O}_{2.995}$  were prepared by a conventional solid state reaction method. The total conductivity was measured by a four-probe dc method under dehydrated (dry) and humidified (wet) atmosphere (at the fixed partial pressure of  $\text{H}_2\text{O}$  ( $p_{\text{H}_2\text{O}}$ ) of 0.037 atm) using  $\text{Ar}+\text{O}_2$  and  $\text{CO}+\text{CO}_2$  gas mixtures. Thermoelectric power was measured by a two-probe method with Pt/gas reversible electrode under the transient state condition. Details of the experimental procedures were reported previously [1].

The XAS measurement was carried out for CZ samples doped with 0, 0.01, 0.02 mol% of  $\text{InO}_{1.5}$ , at the Photon Factory in High Energy Accelerator Research Organization (Tsukuba, Japan). Details of the experimental procedure is published in a separate paper [2].

### 3. RESULTS AND DISCUSSION

Both ionic and hole conductivities were observed in the conductivity measurement under both dry and wet conditions. The defect chemical model employed here is identical to those proposed for other proton conducting perovskites doped with trivalent cations, as shown below.



Overall electrical neutrality condition is written as follows.

$$2[\text{V}_\text{O}^{\bullet\bullet}] + p + [\text{H}_\text{i}^+] = [\text{In}'_\text{Zr}] \quad (3)$$

Since  $2[\text{V}_\text{O}^{\bullet\bullet}] \approx [\text{In}'_\text{Zr}] \gg p$  under the dry condition and the partial conductivity of electrons can be neglected, the total conductivity ( $\sigma_\text{t}$ ) is expressed as,

$$\sigma_\text{t} = \sigma_\text{i} + \sigma_\text{p} \cdot p_{\text{O}_2}^{1/4}, \quad (4)$$

where  $\sigma_\text{p}$  and  $\sigma_\text{i}$  are the partial conductivity of holes at unit  $p_{\text{O}_2}$  and ions. The latter is expressed by the partial conductivity of protons ( $\sigma_\text{H}_\text{i}^+$ ), oxygen vacancy ( $\sigma_\text{V}_\text{O}^{\bullet\bullet}$ ), and their transference numbers ( $t_\text{H}_\text{i}^+$  and  $t_\text{V}_\text{O}^{\bullet\bullet}$ ) as;  $\sigma_\text{i} = t_\text{H}_\text{i}^+ \cdot \sigma_\text{H}_\text{i}^+ + t_\text{V}_\text{O}^{\bullet\bullet} \cdot \sigma_\text{V}_\text{O}^{\bullet\bullet}$ . Under the wet condition,  $[\text{H}_\text{i}^+]$  can be also approximated to be independent of  $p_{\text{O}_2}$  under a fixed  $p_{\text{H}_2\text{O}}$  condition. From the least square analysis using eq'n (4),  $\sigma_\text{i}$ ,  $\sigma_\text{p}$ , and the transference numbers of ion and holes were evaluated.

The total Seebeck coefficient ( $Q_\text{t}$ ) can be expressed, in terms of partial Seebeck coefficients of ion ( $Q_\text{ion}$ ) and holes ( $Q_\text{p}$ ) at unit  $p_{\text{O}_2}$ , by the following equation.

$$Q_\text{t} = t_\text{ion} \left( -\frac{R}{4F} \ln p_{\text{O}_2} + Q_\text{ion}^* \right) + t_\text{p} \left( -\frac{R}{4F} \ln p_{\text{O}_2} + Q_\text{p}^* \right) \quad (5)$$

As  $Q_\text{p}^*$  is further related to the hole concentration ( $p^\circ$ ) at unit  $p_{\text{O}_2}$  and density of state of the valence band ( $N_\text{v}$ ), and transport coefficient ( $A_\text{p}$ ) through the equation below.

$$Q_p^{\circ} = \frac{R}{F} \left( \ln \frac{N_v}{p^{\circ}} + A_p \right) \quad (6)$$

Since the hopping conduction of small polaron was the most probable mechanism for this system and the valence band is composed of O2p orbital, we assume  $A_p=0$  and the value of  $N_v$  being equal to the concentration of oxide ions, in order to estimate  $p^{\circ}$ .

Figures 1 and 2 show the temperature variation of  $p^{\circ}$  and the mobility of hole ( $\mu_p$ ). In this calculation, we assumed that all the oxygen vacancy were equivalent and capable to be occupied. Decrease in  $p^{\circ}$  by the dissolution of proton is clearly observed. The excellent agreement of  $\mu_p$  in dry and wet conditions shows the consistency of the present estimation.

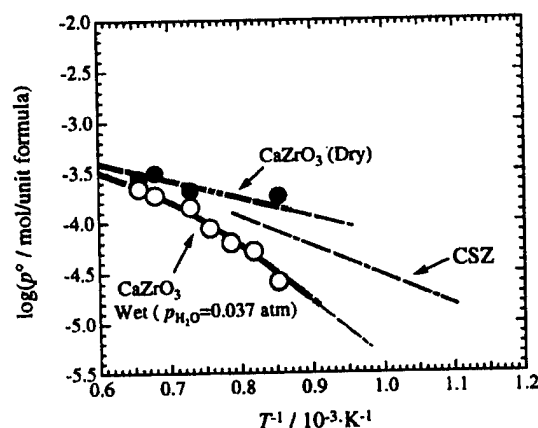


Fig. 1 Temperature variation of concentration of holes at unit oxygen pressure.

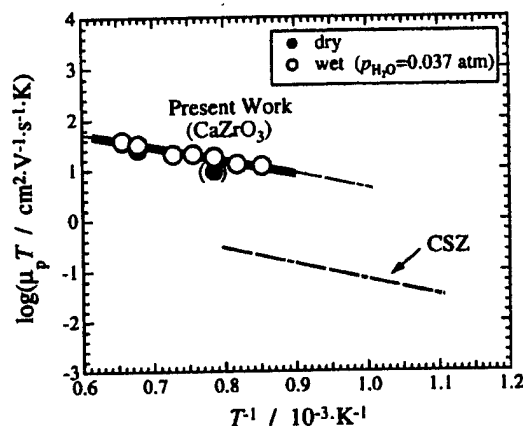


Fig. 2 Arrhenius plot of the mobility of holes.

The equilibrium constants for the quasi-chemical reactions were estimated by fitting eq'ns (1) and (2) to  $p^{\circ}$  shown in Fig. 1, and are expressed as;

$$K_{OX} = 4.20 \times 10^{-3} \exp(-68,069/RT)$$

$$K_{H^+} = 14.9 \times 10^{-3} \exp(112,850/RT)$$

The present results suggest that the concentration of proton saturates at about 900 K and  $p_{H_2O}=0.037$ . Figure 3 shows Arrhenius plot of the mobility of oxide ions and protons, calculated from the partial conductivity, transference numbers, and the concentration of respective carriers.

The heat of transport of oxide ion and protons were also estimated from the present results, and are compared with the activation energy of respective ion conductivity.

By the O1s XAS measurement, the presence of holes at the top of the valence band (O2p) was identified on the samples annealed in dried pure O<sub>2</sub> atmosphere. The hole concentration, showing increase with the increase of doped In content, decreased markedly by the heat treatment under dehydrated CO+CO<sub>2</sub> atmosphere. On the dissolution of protons, the hole state splitted into two with the decrease in the intensity, suggesting the presence of the weakly hydrogen-bonded oxide ions. This observation is also in good agreement with the present defect chemical analysis that the concentration of protons is not negligibly small.

## REFERENCES

- [1] K. Kobayashi, S. Yamaguchi, and Y. Iguchi: Solid State Ionics, 108, 355 (1998).
- [2] T. Higuchi et al.: This Conference.

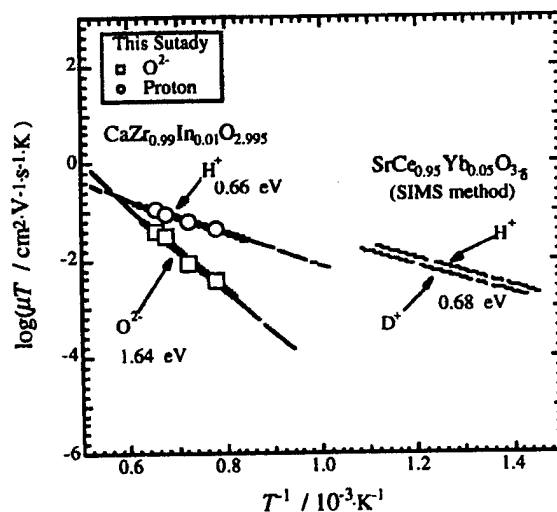


Fig. 3 Arrhenius plot of the mobility of protons and oxide ions.

## CHLORIDE- AND FLUORIDE-BASED ELECTROLYTES AND RELEVANT CERAMIC FUEL CELL TECHNOLOGY

Bin Zhu

Department of Chemical Engineering & Technology  
Royal Institute of Technology (KTH)  
S-100 44 Stockholm  
Sweden

Chlorides, e.g.,  $MCl_x$  ( $M = Na, Ba, Sr, x = 1, 2$ ) and fluorides,  $MF_x$  ( $M = Na, K, Ca, Ba, Sr, Pb, Ce, Bi, La, x = 1-3$ ), based materials and their composites with an oxide  $Al_2O_3$ ,  $CeO_2$  and  $ZrO_2$  have shown high proton and oxygen ion conduction and successful applications in intermediate temperature fuel cells very recently [1-3]. Oxygen ion and proton conduction in the chloride and fluoride-based materials has thus significant importance for both fundamental and applied fields, which has made a new interesting subject for Solid State Ionics. This paper reviews recent progress and achievements on this subject.

It is well known that chlorides are either cationic or chlorine ionic conductors, and fluorides are anionic  $F^-$  conducting materials. The study of the intrinsic conductivity for these ions is not the purpose for the new subject. Instead the unusually high proton or oxygen ion conduction in the materials is focused on. Oxygen ionic conduction had been actually discovered in a number of fluorides but it may be negligible compared with  $F^-$  conductivity [4-6]; on the other hand, proton conduction in these materials is a completely new discovery, and has been investigated very recently.

In the chloride materials, a classical example is  $NaCl$ , which has both cationic and anionic defects, the conductivity of the  $NaCl$  is mainly caused by cationic vacancies; while  $SrCl_2$  and  $BaCl_2$  are predominately anionic conductors. These materials as composting phases used for ceria-based oxide electrolytes can efficiently suppress electronic conduction and enhance fuel cell performances, e.g., higher cell voltages and power outputs, which has provided a new feasibility to develop advanced ceria-based electrolyte SOFC technology. These improvements and benefits from the chlorides may be provided by the proton or oxygen ion conducting property. In addition, these chlorides have also shown promising fuel cell applications [1]. The electrical properties of the  $NaCl$ -based materials can be calculated precisely. A theoretical model and calculation have been performed for the  $NaCl$ -based materials in good agreements with the experimental results.

Among many of fluorides, the alkaline earth fluorides have attracted a special attention, where  $BaF_2$  and  $CaF_2$ -based materials are more promising, since they have shown a strong potential to develop advanced ceramic fuel cell technology at intermediate temperatures.

Doping and composite effects have strong impacts on the electrical properties of the chloride and fluoride based materials, e.g., i) enhanced conductivity, usually 2 to 9 orders of the magnitude higher than the nominally pure materials that are not doped and formed composites, and ii) the ionic transport in the doped and composite materials has a reduced activation energy accompanied by a significant low temperature shift for the high ionic conducting phases. Various doping and composite behaviours in these materials indicate the presence of different defects. Related to the defect structures and chemistry the transport mechanisms for oxygen ions and protons in the chloride and fluoride-based electrolytes have been discussed. The defect structure provides a reasonable explanation for the observed phenomena. Oxygen ions and protons may form various dipoles/pairs and associates with anions,  $Cl^-$  and  $F^-$ , or ionic vacancies, e.g., cationic vacancy in

NaCl, anionic vacancies in fluorides, resulting in unusually high mobilities and conductivities in the materials. Many of the defects may be possible, e.g.,  $M_{M^{y+}}^z, V_{ClorF}, H_i, Cl_i', F_i', O_{ClorF}', O_i''$  ( $M^{y+}$  is the cation;  $y = 1-3$ ;  $z = ' \text{ or } ''$ ; V, vacancy; i, interstitial). These defects can become actually oxygen ion or proton carriers by forming various pairs, e.g.,  $H^+ - Cl^-$ ,  $H^+ - F^-$  dipoles or  $(H^+V_M)^*$  and  $(O_{ClorF}'V_{ClorF}')^*$  associates. Both vacancy and interstitial mechanisms are possible for the oxygen ion and proton transport. Typical examples are in the NaCl-based materials proton or oxygen ion conduction via ionic vacancies is highly possible; while the interstitialcy process for oxygen ions:  $O_F' + F_i' \leftrightarrow O_i'' + F_F^x$ , or for protons:  $H_i + F_i' \rightarrow H_i' + F_i''$ , seems more reasonable for the anion excess chloride or fluoride solid solutions.

Based on the high proton or oxygen ion conduction the chloride and fluoride-based electrolytes have been demonstrated successfully for fuel cell applications, which may meet the requirements on high performance fuel cells at intermediate temperatures. In order to reach this target a wide range of the electrode materials have also been developed. Among many candidates, oxides with a layered rock salt structure, e.g.,  $MNO_2$  ( $M = Li, Na, K, N = Ni, Co, Mn$ ) for both FC anode and cathode, have held promise for success. Various dense and porous ceramic membrane technology via soft chemical routes are under developing for the new systems. It is expected that new advanced ceramic fuel cell technology based on the chloride- and fluoride-based electrolyte materials will provide new opportunities for commercialisation.

## REFERENCES

- [1] B. Zhu, I. Albinsson, B.-E. Mellander, G.-Y. Meng, "Intermediate temperature proton conducting fuel cells – present experience and future opportunities", presented at "9th International Conference on Solid State Protonic Conductors", August 17-21, 1998, Bled, Slovenia.
- [2] B. Zhu, "Intermediate temperature proton conducting salt-oxide composites", *ibid*.
- [3] B. Zhu, G.-Y. Meng, B.-E. Mellander, "Non-conventional fuel cells: new concepts and development", submitted to *J. Power Sources*.
- [4] Donald R. Franceschetti, *Solid State Ionics*, 5, 613 (1981).
- [5] Donald R. Franceschetti, J. Schoonman, J. Ross Macdonald, *Solid State Ionics*, 5, 617 (1981).
- [6] J.-M. Réau, S. Matar, G. Villeneuve and J.-L. Soubeyroux, *Solid State Ionics*, 9/10, 563 (1983).

## FORMATION REACTION AND THERMODYNAMIC PROPERTIES OF $\text{M}\text{Ce}_{1-y}\text{Eu}_y\text{O}_{3-x}$ (M=Sr and Ba)

Toshihide TSUJI, Hirokazu KURONO\* and Yasuhisa YAMAMURA

The Center for New Materials, Japan Advanced Institute of Science and Technology, Hokuriku  
1-1 Asahidai, Tatsunokuchi, Ishikawa 923-1292 Japan

\*Department of Nuclear Engineering, Graduate School of Engineering, Nagoya University,  
Furo-cho, Chikusa-ku, Nagoya 464-8603 Japan

### 1. Introduction

Attractive candidates for protonic conductors at high temperatures are the perovskite-type oxides based on  $\text{ABO}_3$  (A=Ca, Sr, Ba and B=Zr, Ce, Hf) where some trivalent cations are partially substituted for B ions at normal sites. Electrical properties of perovskite-type protonic conductor have been studied by many investigators, but the studies on their reaction mechanism in synthesis are lacking. In this study, the reaction mechanism in synthesis of  $\text{M}\text{Ce}_{1-y}\text{Eu}_y\text{O}_{3-x}$  (M=Sr and Ba) was studied by TG-DTA and high temperature X-ray diffractometry. The results are discussed in the relation of  $\log p(\text{CO}_2)$  versus  $1/T$ .

### 2. Experimental

Starting materials were analytical reagent-grade strontium carbonate(or barium carbonate), cerium dioxide and europium sesquioxide. The powders in the required proportion were mixed in an agate mortar. The sample of (A)  $\text{SrCO}_3$ , (B)  $\text{SrCO}_3 + \text{CeO}_2$ , (C)  $\text{SrCO}_3 + 0.9\text{CeO}_2 + 0.05\text{Eu}_2\text{O}_3$ , (D)  $\text{BaCO}_3$ , (E)  $\text{BaCO}_3 + \text{CeO}_2$  or (F)  $\text{BaCO}_3 + 0.9\text{CeO}_2 + 0.05\text{Eu}_2\text{O}_3$  was put into a platinum cell in TG-DTA apparatus. The weight change and temperature difference were measured in the temperature range from room temperature to 1623 K at the heating rates of 120, 300, 600 and 1200 K/h under various  $\text{CO}_2$  atmospheres. The starting materials and reaction products were analyzed by high temperature X-ray diffractometry.

### 3. Results and discussion

TG-DTA curves for the mixture (C)  $\text{SrCO}_3 + 0.9\text{CeO}_2 + 0.05\text{Eu}_2\text{O}_3$  at the heating rate of 600 K/h under various  $\text{CO}_2$  atmospheres are shown in Fig.1. As seen in TG curves, the initial decomposition temperatures are increased with increasing  $\text{CO}_2$  partial pressures, indicating that the decomposition reaction of  $\text{SrCO}_3$  is depressed due to  $\text{CO}_2$  gas formed by decomposition of  $\text{SrCO}_3$ . It is also seen in DTA curves that two endothermic reactions (1) and (2) were observed at temperatures  $T_1$  and  $T_2$ , respectively. The endothermic reaction (1) is independent of the  $\text{CO}_2$  partial pressures, whereas the endothermic reaction (2) depends on the  $\text{CO}_2$  atmosphere. Both endothermic reactions (1) and (2) were increased with increasing the heating rate. The transition

temperatures for endothermic reactions (1) and (2) were determined to be 1198 and 1309 K by extrapolating to zero heating rate in the relation between  $T_1$  (or  $T_2$ ) and the heating rate, respectively.

In order to know the origin of two phase transitions, high temperature X-ray diffractometry was carried out before and after two endothermic reactions. Only  $\text{SrCO}_3$  and  $\text{CeO}_2$  peaks for starting materials were observed at room temperature below  $T_1$ , although  $\text{Eu}_2\text{O}_3$  was not detected because of small amounts of doped contents. At 1223 K between  $T_1$  and  $T_2$ , a part of  $\text{SrCeO}_3$  changed from orthorhombic to hexagonal phase at high temperatures, and some of  $\text{SrCO}_3$  and  $\text{CeO}_2$  reacted to form  $\text{SrCe}_{0.9}\text{Eu}_{0.1}\text{O}_{3-x}$ . Therefore, the endothermic reaction (1) corresponds to crystal structural phase transition from orthorhombic to hexagonal phase, irrespective of  $\text{CO}_2$  partial pressure. Although  $\text{SrCO}_3$  sample was completely decomposed at 1473 K above  $T_2$ , diffraction peaks of  $\text{SrO}$ ,  $\text{CeO}_2$  and  $\text{SrCe}_{0.9}\text{Eu}_{0.1}\text{O}_{3-x}$  were observed, indicating that formation reaction of  $\text{SrCe}_{0.9}\text{Eu}_{0.1}\text{O}_{3-x}$  was not completely finished at 1473 K.

The reactions for the sample (A),  $\text{SrCO}_3 = \text{SrO} + \text{CO}_2$ , and for the mixture (B),  $\text{SrCO}_3 + \text{CeO}_2 = \text{SrCeO}_3 + \text{CO}_2$ , were calculated by using the chemical thermodynamic data and their results are plotted in the dotted and solid lines in the relation between  $\log p(\text{CO}_2)$  and  $1/T$  in Fig. 2, where the experimental data in this study together with the results reported by Scholten et al.[1] are also shown. Both reaction temperatures determined for the samples (A) and (B) experimentally agree well, but are higher than the calculated curves in constant  $\text{CO}_2$  pressure. The reaction temperatures in this study deviate from the calculated values in lower  $\text{CO}_2$  partial pressure. These factors may be caused by the heating rate,  $\text{CO}_2$  atmospheres, etc. It may be considered from Fig. 2 that the doped  $\text{SrCeO}_3$  sample is less stable than undoped sample in  $\text{CO}_2$  atmosphere at constant temperature.

It can be concluded from our results for the reactions (C) and (F) that  $\text{BaCe}_{0.9}\text{Eu}_{0.1}\text{O}_{3-x}$  sample was less stable than  $\text{SrCe}_{0.9}\text{Eu}_{0.1}\text{O}_{3-x}$  sample in  $\text{CO}_2$  atmosphere at constant temperature.

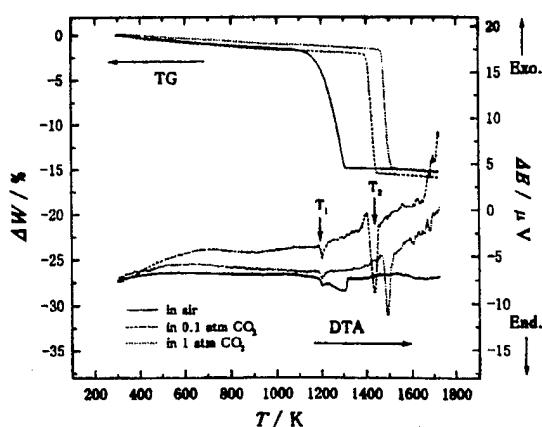


Fig. 1 TG-DTA curves for the mixture (C)

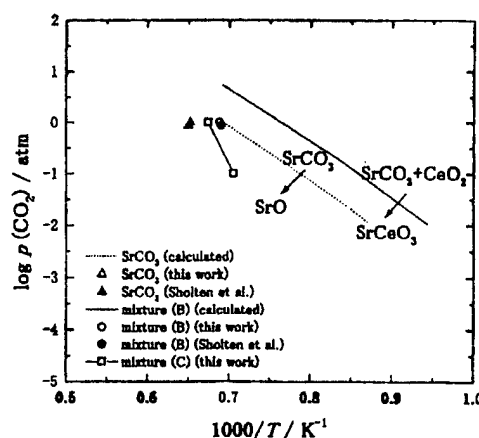


Fig. 2 Stability of  $\text{SrO}$  and  $\text{SrCeO}_3$  in  $\text{CO}_2$  atmospheres

#### 4. References

- [1] M.J.Scholten et al., Solid State Ionics 61, 83 (1993).



## "TOWARDS A NEW GENERATION OF PROTON-CONDUCTING POLYMERS: POLY-4-VINYLMIDAZOLE AS SOLVENT FOR ACIDIC PROTONS"

U.Meister<sup>a</sup>, M.Ise<sup>b</sup>, K.D.Kreuer<sup>b</sup>, W.H.Meyer<sup>a\*</sup>

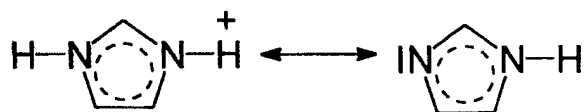
<sup>a</sup> Max-Planck-Institut für Polymerforschung, Ackermannweg 10, D-55021 Mainz

<sup>b</sup> Max-Planck-Institut für Festkörperforschung, Heisenbergstr. 1, D-70569 Stuttgart  
Germany

The proton conductivity in polymers which are applied as separator membranes in fuel cells usually is based on the presence of liquid water, since water acts as a vehicle for the proton transport. This imposes constraints on the maximum operational temperature of such systems. Waterfree polymers with sufficient proton conductivity at temperatures above 100°C still are rather unknown. The proton conductivity of blends of polymers with phosphoric acid is based on phosphoric acid as vehicle and suffers from the formation of polyphosphoric acids at elevated temperatures and loss of acid under fuel cell operation.<sup>1</sup> This is also true for other polymer/oxoacid blends.<sup>2</sup>

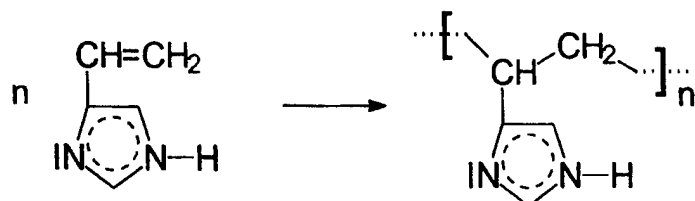
There is a strong demand for polymers which offer a distinctly different chemical environment and allow for fast proton conduction at temperatures above 100°C. For a Grotthuss-type mechanism these must enable the formation of protonic defects and provide strongly fluctuating proton donor and acceptor functions.

Heterocycles such as imidazole are promising candidates as mediator for proton transport. The properties of imidazole and other heterocycles as a solvent for acidic protons has recently been investigated by Kreuer et al.<sup>3</sup> The creation of protonic defects and the mobility of protons in liquid imidazole was found to be similar to the situation in corresponding water systems. The temperature stability is increased and imidazole is a stronger Bronstedt base compared to water. The rather isometric molecules are advantageous for extended local dynamics, and their protonated and unprotonated nitrogens may act as donors and acceptors in fast proton transfer reactions while the ring itself is non-polar.



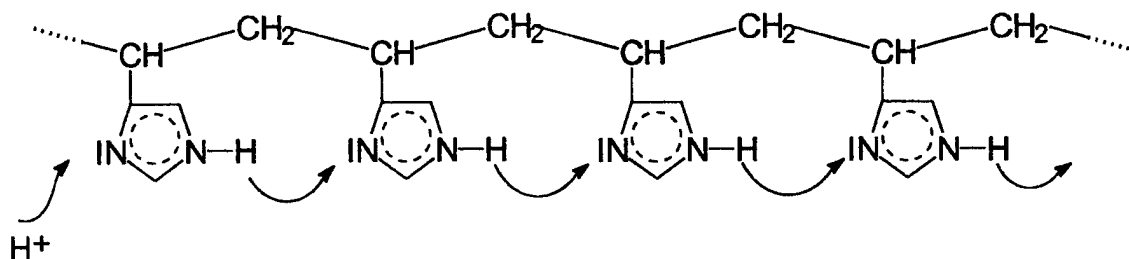
Proton transfer in imidazole

In order to fully suppress any vehicle-type transport mechanism it is necessary to pin the "proton solvent" while allowing for sufficient local dynamics in order to enhance fast proton exchange. This can be materialized when imidazole is bound to a polymer backbone such as in poly(4-vinyl-imidazole) ["P4VI"].

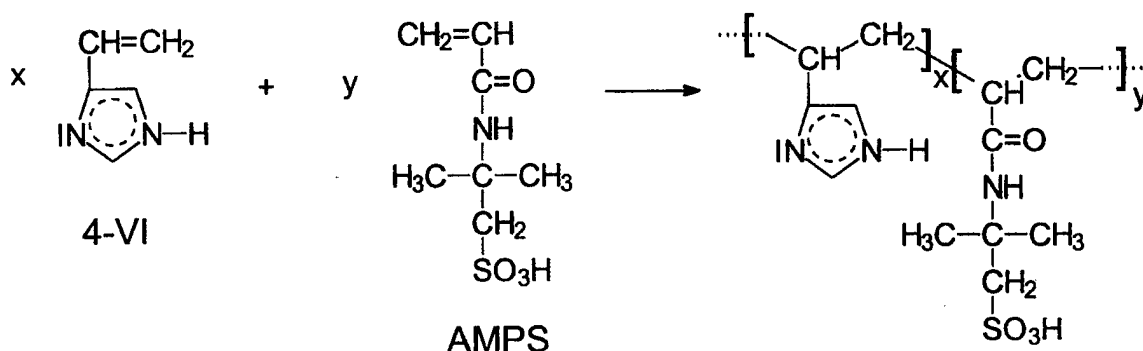


Polymerization of 4-Vinylimidazole

The proton transport along the arrays of imidazole units in poly(4-vinylimidazole) is expected to depend strongly on the dynamics of the imidazole rings and on the ratio of "solvent" molecules, i.e. imidazole units per proton. It may be sketched as follows:



In order to optimize the ratio  $x/y$  of solvent molecules and protons and to allow for a proper mixing of both, statistical copolymers from 4-vinylimidazole as proton solvent ( $x$ ) and acrylamidopropanesulfonic acid (AMPS) as proton source ( $y$ ) have been prepared by us in which  $x/y$  is systematically varied between 1:10 and 10:1 :



The temperature dependent conductivity of dry films prepared from 4VI-AMPS-copolymers will be reported. The proton conductivity diffusion coefficient will be compared with the proton self diffusion coefficient obtained by PFG-NMR analysis as a function of the composition ( $x/y$ ).

Other polymers with heterocyclic Bronstedt bases as proton solvents are being prepared as well as blends from appropriate homopolymers with oxoacids.

This project is financially supported by the Deutsche Forschungsgemeinschaft, contract # ME 1495/2-1.

<sup>1</sup> J.S.Wainright, J.T.Wong, R.F.Savinell, M.Litt, H.Moadell, Proc. ECS **94** / **23**, 255 (1994)

A.Bozkurt, M.Ise, K.D.Kreuer, W.H.Meyer, G.Wegner, Proc. SSPC-9, to be publ.

<sup>2</sup> J.C.Lassegues in: Proton Conductors (Ph. Colomban Ed.), Cambridge University press, p. 311 (1992)

<sup>3</sup> K.D.Kreuer, A.Fuchs, M.Ise, M.Spaeth, J.Maier, Electrochim. Acta, **43**(10/11), 1281 (1998)

# AN INELASTIC NEUTRON SCATTERING STUDY OF THE PROTON DYNAMICS IN MIXED CONDUCTING CERAMICS BASED ON $H_xYBa_2Cu_3O_{7-\delta}$ OXIDE

R. Baddour-Hadjean<sup>1</sup>, Yu. M. Baikov<sup>2</sup>, Ph. Colomban<sup>1</sup>, S. F. Parker<sup>3</sup>

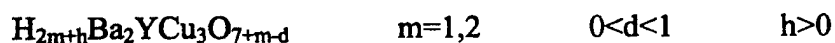
1- LADIR, CNRS, 2 rue Henri Dunant, 94320, Thiais, France.

2- A. F. Ioffe Physico-Technical Institute, Russian Academy of Science, St Petersburg, 194021, Russia.

3- Rutherford Appleton Laboratory, Chilton, Didcot, OX 0QX, U. K.

Yttrium baryum cuprates (YBCO) with the stoichiometric formula  $YBa_2Cu_3O_{7-\delta}$ , belonging to the  $ABO_3$  perovskite structure group, have been at first synthesized in 1987 as compound oxides with superconducting properties below 92K. It is the most popular oxide among the great number of the superconducting oxides and therefore the most studied one. However while studying the influence of hydrogen on the physical and chemical properties of YBCO [1], some of us have discovered the high proton mobility in this oxide and related compounds with the substitution for Y rare-earth elements [2].

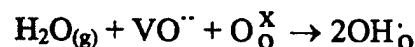
The extended formula of this material can be written :



Hydrogen containing perovskites may be used as proton conductors over  $\sim 700K$  [3-5]. The variety of properties of perovskites structures can be related to the easiness of doping on the A site. No matter how extensive are the substitutions of cations of various valence, the oxygen excess or deficiency or the variations of the A/B ratio, the resulting lattice defects preserve layers of essentially ideal perovskite structure. The following model is generally used to describe the defect : the dominant compensations defects in acceptor-doped perovskites are extrinsic oxygen vacancies. Electron holes are created by the oxidation reaction in which oxygen ions fill the oxygen vacancies in the p-type region [4]. The protons have been considered to be produced by the process of water-vapor reacting with oxygen vacancies :



It is usually assumed that proton enters the valence shell of oxygen atoms :



Hydrogen is known to affect the superconducting properties of  $YBa_2Cu_3O_7$  strongly, and many investigations have been undertaken in order to ascertain the nature of the effect [6-14]. However, the exact nature of hydrogen bonding in high temperature proton conductors remains quite unknown. Hydroxyl groups free of H-bonds are excluded due to the broadness and the low frequency of the IR band. Due to the small amount of hydrogen content, the IR spectra intensity remains low and consequently perturbation by (acid) surface water is likely for powders.

Kreuer et al [15] have recently proposed a conduction mechanism comprising rotational diffusion of hydroxide ions and proton transfer between adjacent oxygens. Thus proton

diffusion would be assisted by the local oxygen dynamics. The recent preparation by Baïkov et al of YBaCuO derivatives with a high hydrogen content makes it possible to study the vibrational spectrum of hydrogen containing perovskites with more success, using inelastic neutron scattering (INS).

INS is particularly well suited to study the proton dynamics in YBCO. Because the scattering cross section of hydrogen atoms is very large compared to those of Y, Ba, Cu and O atoms, the spectra are dominated by signals due to protons. The vibrational frequencies are sensitive to the local potential experienced by the hydrogen atoms. Different sites or distinct chemical bonds for the proton give separate bands with intensities depending on the relative amounts of each species. Furthermore, many experiments not focused on H-problems have been previously made on this family of materials, with different contents of hydrogen, which allows to compare the evolution of the spectrum with the H-content. The INS spectra should then allow to distinguish the nature and the environment of the protonic defects in YBCO (bound or free protons, OH entities, interstitial H species).

The present INS experiments reveal an alternative explanation which is that proton diffusion is not coupled to the oxygen motion. The INS spectra of YBCO show a striking similarity with those of the intermetallic hydrides. In these systems, protons occupy octahedral or tetrahedral sites, with cubic symmetry, in the metal lattice. The proton dynamics corresponds to the isotropic oscillator with a three-fold degenerate transition at around  $1000\text{ cm}^{-1}$ . By analogy with these hydrides, the hydrogen atoms in YBCO are found to occupy interstitial oxygen sites with "hydrogen bonding" with all the neighbouring oxygen. Such sites can be seen at the center of the Ba<sub>4</sub>Cu<sub>2</sub> and Y<sub>4</sub>Cu<sub>2</sub> octahedra.

### References

- [1] T. Hirata, *Phys. State . Sol (a)* 156 (1196) 227-250 and references there in.
- [2] Y. M. Baikov, *Solid State Ionics*, 97 (1997) 471-476
- [3] T. Tokahashi, H. Iwahara, *Rev. Chim. Minérale* 17 (1980) 243-253
- [4] H ; Iwahara, in *Proton Conductors*, Ph. Colomban ed. , Cambridge University Press, 1992, Cambridge.
- [5] N. Bonanos, *Solid State Ionics* 53-56 (1992) 967-974.
- [6] Ph. Colomban, *Ann. Chim. Sciences des Matériaux* (1998).
- [7] S. Kapptan, *Adv. Ceram., The American Ceram. Soc., Vol 23* (1987) 379-386
- [8] F. Freund ch9, in *Proton conductors*, Ph. Colomban ed. , Cambridge University Press, 1992, Cambridge.
- [9] S. Shin, H. H. Huang, M. Ishigame, H. Iwahara, *Solid State Ionics* 40/41 (1990) 910-913
- [10] H. Yugami, Y. Shibayama, T. Hattori , M. Ishigame, *Solid State Ionics* 79 (1995) 171-176.
- [11] H. Yugami, Y. Shibayama, S. Matsua, M. Ishigame, S. Shin, *Solid State Ionics* 85, (1996) 319-32.
- [12] T. Scherban, Y. M. Baikov, E. K. Shalkova, *Solid State Ionics* 66 (1993) 159-164.
- [13] A. S. Nowick, Y. Du, *Solid State Ionics*, 77 (1995) 137.
- [14] K. D. Kreuer, W. Munch, I. Ise, A. Fuchs, U. Traub, J. Maier, *Ber. Bunsenges Phys. Chem.* 101 (1997) 1344.
- [15] K. D. Kreuer, A. Fuchs, J. Maier, *Solid State Ionics*, 77 (1995) 157.

## TRIVALENT ION CONDUCTING SOLID ELECTROLYTES

N. Imanaka, Y. Kobayashi, S. Tamura, and G. Adachi

Department of Applied Chemistry, Faculty of engineering, Osaka University, 2-1 Yamadaoka,  
Suita, Osaka 565-0871 Japan

The mono and divalent ions have been commonly well known to possess a relatively high ionic conductivity with the association of their low activation energies. In contrast, it has been generally regarded that trivalent cations are extremely poor migrants because of their high electrostatic interaction between the trivalent charged ion species and the anions constituting framework structure, like  $O^{2-}$ . Only a few papers have reported the trivalent ion conduction; e.g.  $Ln^{3+}$ - $\beta''$ -alumina,  $\beta$ - $LaNb_3O_9$ ,  $LaAl_{11}O_{18}$ , and  $LaAl_{12}O_{18}N$ . However, no direct and quantitative demonstration of the trivalent ionic conduction in the solids has not been mentioned. In order to realize the trivalent ion conduction in solids, a suitable structure was chosen by the consideration of the mobile trivalent ion route. Furthermore, the mobile trivalent ion candidates need to be stable enough to hold the valency with having a relatively smaller ionic radius. In our research, the  $Sc_2(WO_4)_3$ -type structure was selected since it has a larger tunnel size for ion migration and the electrostatic interaction between the mobile ions and framework of the structure is effectively reduced. Here, aluminum and rare earth ions are chosen as the mobile trivalent ion. In the  $Sc_2(WO_4)_3$ -type structure, the hexavalent tungsten ion,  $W^{6+}$ , functions to weaken the interaction between the trivalent ions and the oxide ions, because the  $O^{2-}$  ions are strongly bonded to  $W^{6+}$ . In these years, we have made a direct and clear demonstration of the trivalent ion migration such as rare earth ions and aluminum.

Here, the clarification of the dependencies of the individual trivalent ion species on both the trivalent ion conductivity and the  $Sc_2(WO_4)_3$ -type structure was accomplished and also the mobile trivalent ion species was explicitly identified. The details of the experimental procedure are described in our previous paper.<sup>1</sup>

The three lattice parameters increase with the increase of the trivalent ionic radius. The expansion ratio was equivalent and an isotropic expansion was observed. Among the tungstates with the  $Sc_2(WO_4)_3$ -type series,  $Sc_2(WO_4)_3$  shows the highest conductivity ( $6.5 \times 10^{-5} \text{ S} \cdot \text{cm}^{-1}$ ) at  $600^\circ\text{C}$  and the lowest activation energy ( $44.1 \text{ kJ} \cdot \text{mol}^{-1}$ ). In order to examine the electrical conducting species in the tungstates, the time dependencies of the dc conductivity variation was measured and compared with the ac conductivity. An abrupt conductivity decrease to the ac one was similarly observed and reached to the steady value. The steady dc conductivities were 2 – 3 orders of magnitudes smaller than ac ones. This clear polarization phenomenon definitely indicates that the predominant conducting species are neither holes nor electrons but only ions and the ionic transference number estimated is higher than 0.99 for scandium tungstate.

A clear polarizing phenomenon of an abrupt decrease of the ratio ( $\sigma_{dc}/\sigma_{ac}$ ) from unity, was equally observed in the both atmospheres (oxygen ( $P_{O_2}$ :  $10^5 \text{ Pa}$ ), helium ( $P_{O_2}$ :  $4 \text{ Pa}$ )). Here,  $\sigma_{dc}$  and  $\sigma_{ac}$  denote dc and ac conductivity, respectively. In the case that  $O^{2-}$  ions are the dominant mobile ionic species, no polarization appears in the oxygen atmosphere. Therefore, the same polarization behaviors in the two atmospheres explicitly deny the oxide ion conduction in the tungstate solid.

In order to directly determine the mobile ionic species in scandium tungstate, an electrolysis was performed by sandwiching the tungstate between two platinum electrodes. Many needle shape deposits were observed on the cathodic surface. In contrast, the color of the anodic surface of the pellet varied from white before the electrolysis to yellow after the electrolysis and plate shape accumulations were also recognized. From EPMA measurements, the needle-shape deposits were found to include Sc and W and that the Sc/W ratio in the deposits considerably

increased to about 6 compared to that of the tungstate bulk (2/3) before the electrolysis. In contrast, the plate-shape accumulations appeared on the anodic surface were identified to contain only W. The XRD measurements were conducted and the deposits of cathodic and anodic surface after the electrolysis were identified to  $\text{Sc}_6\text{WO}_{12}$  and  $\text{WO}_3$ , respectively. The Sc/W ratio (6) of the  $\text{Sc}_6\text{WO}_{12}$  deposits on cathodic surface was in an excellent accordance with that measured by EPMA. From the cross-sectional EPMA line analysis results for  $\text{Sc}_2(\text{WO}_4)_3$  after the electrolysis, the Sc segregation at the cathodic surface of the electrolyte was observed, while W content is equivalent except for the cathodic surface where the W amount considerably decreased. These results explicitly indicate that trivalent  $\text{Sc}^{3+}$  ion conducts macroscopically from anode to cathode direction and that scandium segregates on the cathodic surface and reacted with  $\text{Sc}_2(\text{WO}_4)_3$  bulk to form  $\text{Sc}_6\text{WO}_{12}$ . By the  $\text{Sc}^{3+}$  macroscopic migration, tungsten trioxide was left on the anodic surface.

Further electrolysis (3V, 360h, 1000°C) was carried out by setting two tungstate pellets between two Pt electrodes. One is  $\text{Al}_2(\text{WO}_4)_3$  to the anodic side and the other is  $\text{Sc}_2(\text{WO}_4)_3$  of the  $\text{Sc}^{3+}$  ionic conductor to the cathodic side. After the electrolysis, lots of round shape cluster deposits (as indicated Fig. 1) were recognized in addition to the  $\text{Sc}_6\text{WO}_{12}$  deposits (needle shape) on the Al-free  $\text{Sc}_2(\text{WO}_4)_3$  pellet cathodic surface where Pt cathode was kept in contact. The round shape cluster deposits were analyzed to contain only Al element without any Sc or W element from EPMA. The result of the cross-sectional EPMA line analysis for the two  $\text{Al}_2(\text{WO}_4)_3$  and  $\text{Sc}_2(\text{WO}_4)_3$  pellets after the electrolysis is depicted in Fig. 2. A certain amount of aluminum equally appears inside the  $\text{Sc}_2(\text{WO}_4)_3$  pellet. This phenomenon definitely means that  $\text{Al}^{3+}$  ions in the  $\text{Al}_2(\text{WO}_4)_3$  pellet ionically migrate inside the  $\text{Sc}_2(\text{WO}_4)_3$  pellet and deposit on the cathodic  $\text{Sc}_2(\text{WO}_4)_3$  surface by the  $\text{Al}^{3+}$  macroscopic migration in the  $\text{Sc}_2(\text{WO}_4)_3$  solid. No such a deposition was observed for the cell depicted in Fig. 1 without any dc electrolysis.

The results described above definitely indicate that the trivalent ions are the dominant ionic mobile species in the scandium tungstate type solid.

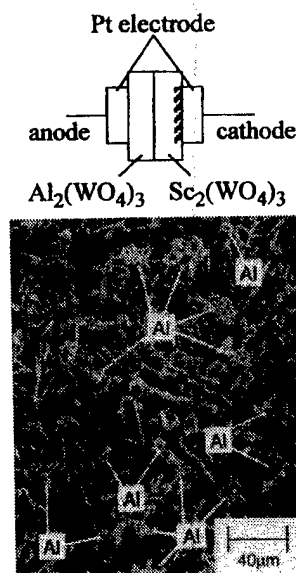


Fig.1. The SEM photograph of the  $\text{Al}_2(\text{WO}_4)_3$ - $\text{Sc}_2(\text{WO}_4)_3$  after the electrolysis.

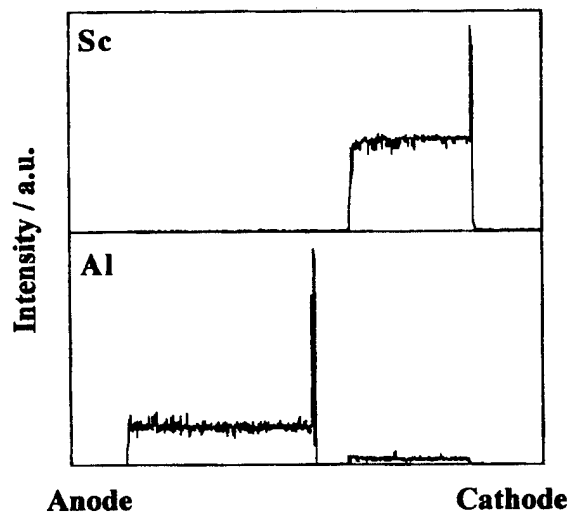


Fig.2. The cross-sectional EPMA line analysis of the  $\text{Al}_2(\text{WO}_4)_3$ - $\text{Sc}_2(\text{WO}_4)_3$  after the electrolysis.

HEAT TRANSFER AND ION MIGRATION IN THE SYSTEM  $\text{Li}_2\text{SO}_4\text{-Na}_2\text{SO}_4$ 

Bashir M. Suleiman, Arnold Lundén and Ernest Karawacki

Department of Physics, Chalmers University of Technology, S-412 96 Göteborg, Sweden

The system  $\text{Li}_2\text{SO}_4\text{-Na}_2\text{SO}_4$  has three high temperature phases, see Figure 1. The phase on the  $\text{Na}_2\text{SO}_4$ -rich side is hexagonal, while  $\text{Li}_2\text{SO}_4$  is fcc [1] and  $\text{LiNaSO}_4$  is bcc [2]. Førlund and Krogh-Moe pointed out that there was a large excess of cation positions in these cubic phases, and that strong rotational orientations must be expected for sulphate ions. The electrical conductivity was found to be of the order of 0.9 S/cm at 823 K [3], while diffusion studies showed that all mono- and divalent cations are very mobile in the cubic phases [4]. These phases can actually be considered as both solid electrolytes and plastic crystals [5]. The cation mobility is enhanced by a strong coupling to the rotation of the otherwise translationally immobile sulphate ions [4,5]. Actually, all possible kinds of transport mechanisms are enhanced. This phenomenon is depicted as the "paddle-wheel" or "cogwheel" model which was first presented in 1972 [4,6,7]. The model is consistent with three neutron scattering studies *viz* powder diffraction [8], single crystal diffraction [9] and total scattering evaluated by the reverse Monte Carlo technique [10], and furthermore with molecular dynamics simulations [11]. A study is in progress by means of coherent quasi-elastic neutron scattering [12].

We considered it of interest to study heat transfer in the system  $\text{Li}_2\text{SO}_4\text{-Na}_2\text{SO}_4$  for two reasons. Firstly, such data are needed if solid sulphates are used for some application, e. g. for high-temperature batteries, fuel cells or heat storage devices. Secondly, it is of interest to see whether the phase transitions that cause dramatic changes of the electrical conductivity, etc. also have some influence on heat transfer. We started with a study of pure  $\text{Li}_2\text{SO}_4$  [13,14], and we went on with pure  $\text{Na}_2\text{SO}_4$  and two mixtures with the compositions  $\text{LiNaSO}_4$  and  $\text{Li}_{1.55}\text{Na}_{0.45}\text{SO}_4$ , respectively [15]. The temperature dependence of the thermal conductivity and diffusivity of pure  $\text{Li}_2\text{SO}_4$  is shown in Figure 2, where the monoclinic-cubic phase transition is marked  $T_C$ . Both parameters are significantly higher in the cubic phase. The most remarkable feature is, however,

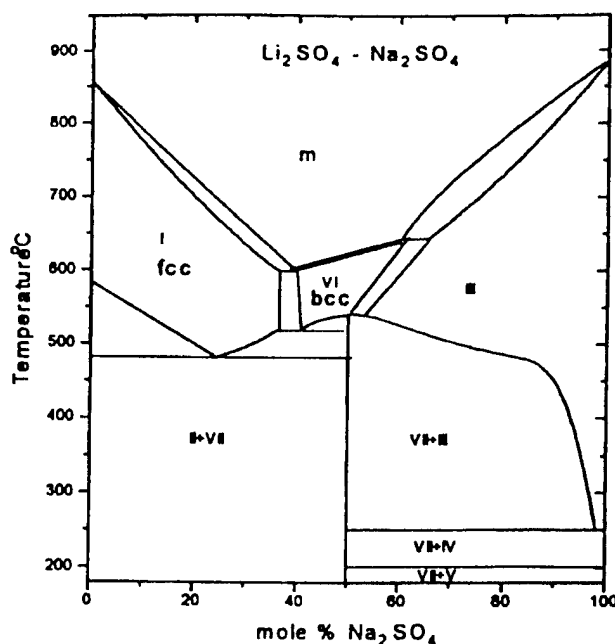


Figure 1. Phase diagram of the system  $\text{Li}_2\text{SO}_4\text{-Na}_2\text{SO}_4$  [15].

the drastic change at about 645 K. The temperature gradient is slightly negative all the way up to this point, where it shifts abruptly and becomes positive. This remarkable behaviour near 645 K is observed also for  $\text{LiNaSO}_4$  and  $\text{Li}_{1.55}\text{Na}_{0.45}\text{SO}_4$ . On the other hand, the situation is completely different for  $\text{Na}_2\text{SO}_4$  where the temperature gradient decreases monotonously over the whole range from slightly above room temperature up to well beyond the transition to the hexagonal "high-temperature" phase. – We have also studied silver iodide from 295 and 640 K. There is a slight decrease in both the thermal conductivity and the diffusivity at the transition at 420 K [15].

Work is in progress on the further interpretation. *Inter alia*, comparisons are made with the line broadening for Raman scattering.

## References

- [1] T. Førland and J. Krogh-Moe, *Acta Chem. Scand.* **11**, 565 (1957).
- [2] T. Førland and J. Krogh-Moe, *Acta Cryst.* **11**, 224 (1958).
- [3] A. Kvist and A. Lundén, *Z. Naturforsch.* **20a**, 235 (1965).
- [4] R. Tärneberg and A. Lundén, *Solid State Ionics* **90**, 209 (1996).
- [5] A. Lundén and J. Thomas, in T. Takahashi, ed.: *High Conductivity Solid Ionic Conductors*, World Scient. Publ. Co., Singapore 1989, p. 45.
- [6] A. Lundén, in B. Scrosati, A. Magistris, C. M. Mari and G. Mariotto, eds.: *Fast Ion Transport in Solids*, NATO ASI Series E:250. Kluwer, Dordrecht, 1993, p. 181.
- [7] A. Lundén, *Z. Naturforsch.* **50a**, 1067 (1995).
- [8] L. Nilsson, J. O. Thomas and B. C. Tofield, *J. Phys. C: Solid St. Phys.* **13**, 6441 (1980).
- [9] R. Kaber, L. Nilsson, N. H. Andersen, A. Lundén and J. O. Thomas, *J. Phys.: Condensed Matter* **4**, 1925 (1992).
- [10] L. Karlsson and R. L. McGreevy, *Solid State Ionics*, **76**, 301 (1995).
- [11] M. Ferrario, M. L. Klein and I. R. McDonald, *Molecular Physics*, **86**, 923 (1995).
- [12] D. Wilmer, Priv. Com.
- [13] A. Lundén, in B. V. R. Chowdari, M. A. K. L. Dissanayake and M. A. Careem, eds: *Solid State Ionics: New Developments*, World Scient. Publ. Co, Singapore 1996, p. 23.
- [14] B. M. Suleiman, M. Gustavsson, E. Karawacki and A. Lundén, *J. Phys. D: Appl. Phys.* **30**, 2553 (1997).
- [15] A. Lundén, B. M. Suleiman and E. Karawacki, in H. A Øye and A. Wærnes, eds: *International Terje Østfold Symposium, Røros - Norway, Nov. 2-3 1998*, Inst. Inorg. Chem., Norwegian Inst. Technology, Trondheim, Norway, in press.

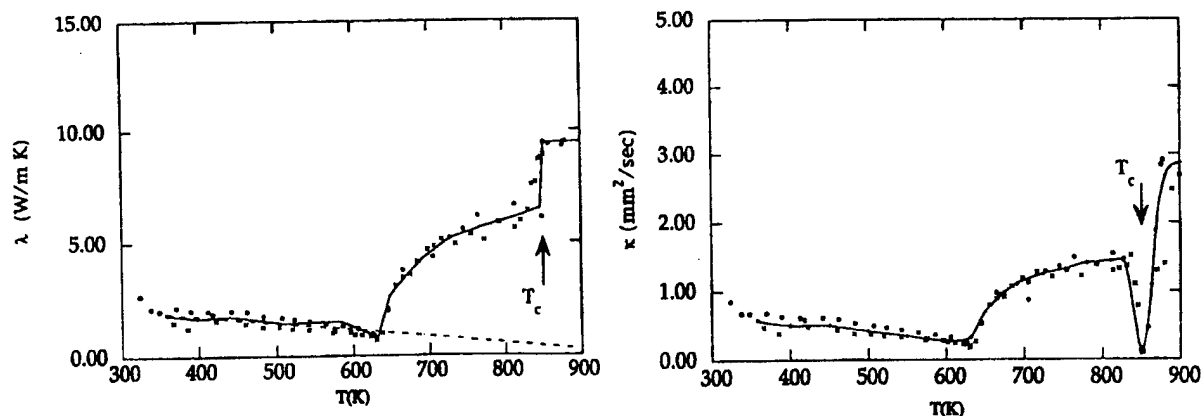


Figure 2. Temperature dependence of the thermal conductivity and diffusivity for  $\text{Li}_2\text{SO}_4$  [14].



## New Lithium Ionic Conductor, Thio-LISICON

Ryoji Kanno, Michihiko Irie, Takayuki Hata, and Yoji Kawamoto,

Department of Chemistry, Faculty of Science, Kobe University  
Nada, Kobe, Hyogo, 657 Japan

Lithium ionic conductors are of technological importance for future applications as solid electrolyte for all-solid lithium battery. A wide variety of materials have been synthesized in the LISICON [ $\text{Li}_{14}\text{Zn}(\text{GeO}_4)_4$ ] family<sup>1</sup>, where the framework is related to the  $\gamma$ - $\text{Li}_3\text{PO}_4$  structure, and are formed by  $\text{GeO}_4$ ,  $\text{SiO}_4$ ,  $\text{PO}_4$ ,  $\text{ZnO}_4$ ,  $\text{VO}_4$  tetrahedra or  $\text{LiO}_6$  octahedra. A wide range of solid solutions can be formed by aliovalent substitutions and interstitial lithium ions or lithium vacancies that contribute their high ionic conductivities at higher temperatures. However, its ionic conductivity is still rather low ( $\approx 10^{-6} \text{Scm}^{-1}$ ) at room temperature. From the conductivity standpoint, the highest value of  $10^{-3} \text{Scm}^{-1}$  at room temperature was obtained for the sulfide glasses in the  $\text{Li}_2\text{S-SiS}_2\text{-Li}_3\text{PO}_4$ <sup>2</sup> system. Sulfides have an advantage in the construction of ionic conductors; larger and more polarizable sulfide ions make the conduction species more mobile.

Crystalline materials might have higher conductivity than the corresponding glasses, if their crystal structure is designed for high ionic conduction. For example, the highest ionic conductive solids,  $\text{Rb}_4\text{Cu}_{16}\text{I}_7\text{Cl}_{13}$  and  $\text{RbAg}_4\text{I}_5$ , have much higher ionic conductivity than any copper and silver conducting glasses. Only a few materials have been investigated previously in the crystalline sulfides;  $\text{Li}_3\text{PS}_4$ <sup>3</sup>,  $\text{Li}_2\text{SiS}_4$ , and  $\text{Li}_4\text{SiS}_4$ <sup>4</sup> were reported to have conductivities of  $10^{-7} - 10^{-9} \text{Scm}^{-1}$  at room temperature and no systematic materials search has been made. Here we report the new materials family of ceramic lithium ionic conductors.

Our materials search has been made for a system based on the germanium sulfides ( $\text{Li}_2\text{S-GeS}_2$ ,  $\text{Li}_2\text{S-GeS}_2\text{-ZnS}$ ,  $\text{Li}_2\text{S-GeS}_2\text{-Ga}_2\text{S}_3$ ). Table 1 summarizes materials of the new thio-LISICON family synthesized in this study. There are seven compounds; six of these are new materials found in this study. Among these materials, the new solid solution,  $\text{Li}_{4+x+\delta}(\text{Ge}_{1-\delta'-x}\text{Ga}_x)\text{S}_4$ , synthesized in the ternary  $\text{Li}_2\text{S-GeS}_2\text{-Ga}_2\text{S}_3$  system showed the highest conductivity. The new phase was found to have an orthorhombic cell with  $a = 6.88$ ,  $b = 6.17$ ,  $c = 7.94 \text{\AA}$ . A wide range of solid solutions were determined to be  $0.2 \leq x \leq 0.6$  in  $\text{Li}_{4+x+\delta}(\text{Ge}_{1-\delta'-x}\text{Ga}_x)\text{S}_4$ . The behavior of the impedance plots show characteristics of a pure ionic conductor composed of bulk and electrode contributions with the bulk resistivity values were calculated from the intercept of the spike. Figure shows the temperature dependence of the conductivity for the  $\text{Li}_2\text{S-GeS}_2\text{-Ga}_2\text{S}_3$  system. The conductivity increases with decreasing  $x$  and the highest conductivity was observed for the

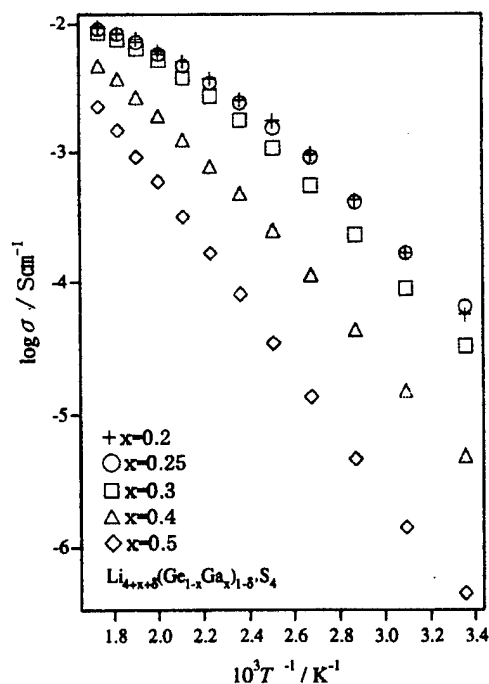
sample with  $x = 0.25$  in  $\text{Li}_{4+x+\delta}(\text{Ge}_{1-\delta'-x}\text{Ga}_x)\text{S}_4$ . The conductivity value at 25°C was  $6.5 \times 10^{-5} \text{ Scm}^{-1}$ . The activation energy decreases with increasing  $x$  at both high temperatures and low temperatures. The gradual slope changes are characteristics for typical high-ionic conductors and these correspond to gradual disorder formation in the mobile ion sublattice.

The conductivities of the new sulfide LISICON are much higher than the oxide LISICON ( $\text{Li}_{14}\text{Zn}(\text{GeO}_4)_4$ )<sup>1</sup> by two or three orders of magnitude. With the discovery of thio-LISICON, a wide variety of new materials formed by  $\text{MS}_4$ , tetrahedra and  $\text{LiS}_6$  octahedra are expected besides the materials synthesized in this study. Further studies on electrochemical properties and all solid lithium cells using thio-LISICON electrolyte will be presented.

Table 1 Materials of the new thio-LISICON family.

compound	reference	crystal system	lattice parameters $a/\text{\AA}, b/\text{\AA}, c/\text{\AA}$	structure type	conductivity(25°C) $\sigma/\text{Scm}^{-1}$
$\text{Li}_2\text{S}-\text{GeS}_2$	new	ortho	5.90, 17.95 6.81	—	$9.7 \times 10^{-9}$ (125°C)
$\text{Li}_2\text{GeS}_3$					
$\text{Li}_4\text{GeS}_4$					
$\text{Li}_2\text{S}-\text{GeS}_2-\text{ZnS}_2$	new	ortho	7.83, 6.53, 6.21	$\beta\text{-Li}_3\text{PO}_4$	$1.4 \times 10^{-9}$ (50°C)
$\text{Li}_2\text{ZnGeS}_4$					
$\text{Li}_{4-x}\text{Zn}_x\text{GeS}_4$					
$\text{Li}_2\text{S}-\text{Ga}_2\text{S}_3$	42-1267	ortho	6.51, 7.87, 6.22	$\beta\text{-NaFeO}_2$	—
$\text{LiGaS}_2$					
$\text{Li}_5\text{GaS}_4$					
$\text{Li}_2\text{S}-\text{GeS}_2-\text{Ga}_2\text{S}_3$	new	ortho	6.89, 6.20, 7.96	—	$5.1 \times 10^{-8}$ (100°C)
$\text{Li}_{4+x+\delta}(\text{Ge}_{1-\delta'-x}\text{Ga}_x)\text{S}_4$					
			(at $x = 0.25$ )		$6.5 \times 10^{-5}$

Figure Temperature dependence and of the conductivity for  $\text{Li}_{4+x+\delta}(\text{Ge}_{1-\delta'-x}\text{Ga}_x)\text{S}_4$ .



#### References

1. H. Y-P. Hong, *Mater. Res. Bull.*, **13**, 117 (1978).
2. S. Kondo, K. Takada, and Y. Yamaura, *Solid State Ionics*, **53-56**, 1183 (1992).
3. M. Tachez, J-P. Malugani, R. Mercier, and G. Robert, *Solid State Ionics*, **14**, 181 (1984).
4. B. T. Ahn and R. A. Huggins, *Mater. Res. Bull.*, **24**, 999 (1989).

## ELECTROTRANSPORT IN SEMICONDUCTING OXIDES

M. Martin

Institute of Physical Chemistry  
Darmstadt University of Technology  
Petersenstr. 20, 64287 Darmstadt, Germany

In a semiconducting oxide the mobile ions are migrating in an external electric field despite of their very small ionic transference number (typically  $t_{\text{cation}} \approx 10^{-4}$ ). This electrotransport phenomenon is interesting in two respects: (i) it gives insight into the microscopic mass and charge transport mechanisms in the oxide, and (ii) due to the directed ionic fluxes, macroscopic phenomena such as demixing of the initially homogeneous oxide, polarization and formation of new phases can be studied. We report on different types of electrotransport experiments.

In homogeneous transition metal oxides, such as  $\text{Fe}_3\text{O}_4$ , or in heterovalently doped oxides, such as  $(\text{Co}_{1-x}\text{In}_x)\text{O}$ , radioactive tracers can be used to measure the drift velocities of the cations. The results can be interpreted in terms of effective charges of the ions. If the mobile ions exist in different charge states the effective charge is an average charge. However, if there are strong defect-defect interactions the effective charges can differ drastically from the formal charges of the cations.

The external electric field can also cause demixing of an initially homogeneous oxide solid solution, e.g.  $(\text{Co}_{1-x}\text{Ni}_x)\text{O}$ . The electric field induces defect fluxes as a result of which ionic fluxes of A and B will occur. Due to the different mobilities a concentration gradient will build up, and the material becomes enriched in A or B on one crystal side. A formal analysis of the demixing phenomenon in an external electric field using the random alloy model for diffusion in a solid solution will be given. The theoretical results are discussed and compared with experimental results. A similar analysis will be presented for doped oxides, where the five-frequency model for impurity diffusion is used. Finally, polarization effects during demixing and the formation of new phases will be discussed.

e-mail: martin@e-chemie.tu-darmstadt.de

# STOICHIOMETRIC CHANGES IN LITHIUM CONDUCTING MATERIALS BASED ON $\text{Li}_{1.3}\text{Al}_{0.3}\text{Ti}_{1.7}(\text{PO}_4)_3$

A. S. Best<sup>a</sup>, M. Forsyth<sup>a</sup> and D. R. MacFarlane<sup>b</sup>.

<sup>a</sup> Department of Materials Engineering and <sup>b</sup> Department of Chemistry  
Monash University, Clayton, Victoria, Australia. 3168.

Ceramic electrolytes are currently plagued by poor sintering and impurity phases. This inhibits the production of a single phase material with good total conductivity for use in electrochemical applications.[1] Lithium Aluminium Titanium Phosphate (LATP) has been shown to have several impurity phases, some of which may inhibit grain boundary conductivity.

Recent studies have shown that LATP has a bulk conductivity of between  $2 \times 10^{-3}$  and  $3 \times 10^{-3} \text{ S.cm}^{-1}$ . However, total conductivity is limited by a grain boundary conductivity of  $10^{-5}$  to  $10^{-7} \text{ S.cm}^{-1}$  due to porosity and poor sintering.[2,3] We have shown in earlier work that the addition of extra starting materials, with the intention of forming glassy phases, and varying sintering temperatures influences the amount of impurity phases present in the material.[4] This influences the grain boundary and bulk conductivities due to a variation in the "real stoichiometry" of the material.[5]

It is hypothesised that by varying the amount of Ti in the material, the amount of residual  $\text{TiO}_2$  (rutile) and possibly  $\text{AlPO}_4$ , both impurity phases, will be decreased. This may increase the overall sinterability of the material and hence the grain boundary conductivity. In this study, therefore, we have systematically varied the relative amounts of Li, Ti and P in the ceramic.

The synthesis method is as per previous work.[4,5] The most interesting changes made to the composition are of the form  $\text{Li}_{1.3+4x}\text{Al}_{0.3}\text{Ti}_{1.7-x}(\text{PO}_4)_3$  and the effect on conductivity is shown in Figure 1. The grain boundary conductivity of Li substituted system increases to a maximum of  $5 \times 10^{-5} \text{ S.cm}^{-1}$  at  $x = 0.1$ . This result suggests that the prevention of impurity phase formation increases the sinterability and therefore the total conductivity in these systems. However, at no time is the bulk conductivity higher than that of  $\text{Li}_{1.3}\text{Al}_{0.3}\text{Ti}_{1.7}(\text{PO}_4)_3$ , suggesting that this value represents the maximum obtainable for this system.

Analysis of the XRD showed that the presence of impurity phases changes depending upon the stoichiometry of the ceramic made as shown in Table 1.

	Composition	$\text{AlPO}_4$ T/B	$\text{TiO}_2$ (rutile)	$\text{TiP}_2\text{O}_7$
A	$\text{Li}_{1.3}\text{Al}_{0.3}\text{Ti}_{1.7}(\text{PO}_4)_3$	T/B	Y	Y
B	$\text{Li}_{1.3}\text{Al}_{0.3}\text{Ti}_{1.65}(\text{PO}_4)_3$	T	Y	Y
	$\text{Li}_{1.3}\text{Al}_{0.3}\text{Ti}_{1.6}(\text{PO}_4)_3$	T	Y	Y
C	$\text{Li}_{1.3}\text{Al}_{0.3}\text{Ti}_{1.65}(\text{PO}_4)_{2.95}$	T	Y	Y
	$\text{Li}_{1.3}\text{Al}_{0.3}\text{Ti}_{1.6}(\text{PO}_4)_{2.9}$	T	Y	Y
	$\text{Li}_{1.3}\text{Al}_{0.3}\text{Ti}_{1.6}(\text{PO}_4)_{2.8}$	T	N	Y
D	$\text{Li}_{1.5}\text{Al}_{0.3}\text{Ti}_{1.65}(\text{PO}_4)_3$	N	N	Y
	$\text{Li}_{1.7}\text{Al}_{0.3}\text{Ti}_{1.6}(\text{PO}_4)_3$	N	N	Y
	$\text{Li}_{1.9}\text{Al}_{0.3}\text{Ti}_{1.55}(\text{PO}_4)_3$	N	N	Y
	$\text{Li}_{2.1}\text{Al}_{0.3}\text{Ti}_{1.5}(\text{PO}_4)_3$	N	N	Y

T = Tridymite, B = Berlinite, N = Not present, Y = Present

From Table 1, it can be seen that increasing the amount of lithium by decreasing the titanium content of the ceramic, assists in reducing the amount of  $\text{TiP}_2\text{O}_7$  and removes peaks attributable to the  $\text{AlPO}_4$  (both the tridymite and berlinite polymorphs) and the  $\text{TiO}_2$  phase. Decreasing the Ti and P content appears to strengthen the peaks attributable to the tridymite phase.

XRD analysis has shown that decreasing the Ti and increasing the Li content of the material decreases the unit cell volume of the material. This correlates with impedance studies, which show the bulk conductivity of the material to increase. However, with a decrease in the unit cell volume, phases such as  $\text{AlPO}_4$ ,  $\text{TiO}_2$  are also present in increased amounts. This affects the grain boundary conductivity also.

SEM has been used to investigate the morphology of the ceramic particles and the effect of sintering. No distinct improvement has been seen in the sintering of the various samples studied in this work. EDX studies have been used qualitatively to study the homogeneity of the samples.

### References:

1. G.-Y. Adachi, N. Imanaka and H. Aono, *Adv. Mater.* 8 (1996) 127.
2. H. Aono, E. Sugimoto, Y. Sadaoka, N. Imanaka and G.-Y. Adachi, *J. Electrochem Soc.*, 140 (1993) 1827.
3. A. S. Best, P. J. Newman, K.M. Nairn, M. Forsyth and D. R. MacFarlane, Abstract p. C51 in *Extended Abstracts 11<sup>th</sup> International Conference on Solid State Ionics* (1997).
4. A. S. Best, S. Wong, K. M. Nairn, D. R. MacFarlane and M. Forsyth, *J. Aust. Ceram. Soc.*, 143 No. 2 (1998)
5. S. Wong, P.J. Newman, A.S. Best, K.M. Nairn, D. R. MacFarlane and M. Forsyth *J. Mater. Chem.*, (1998)

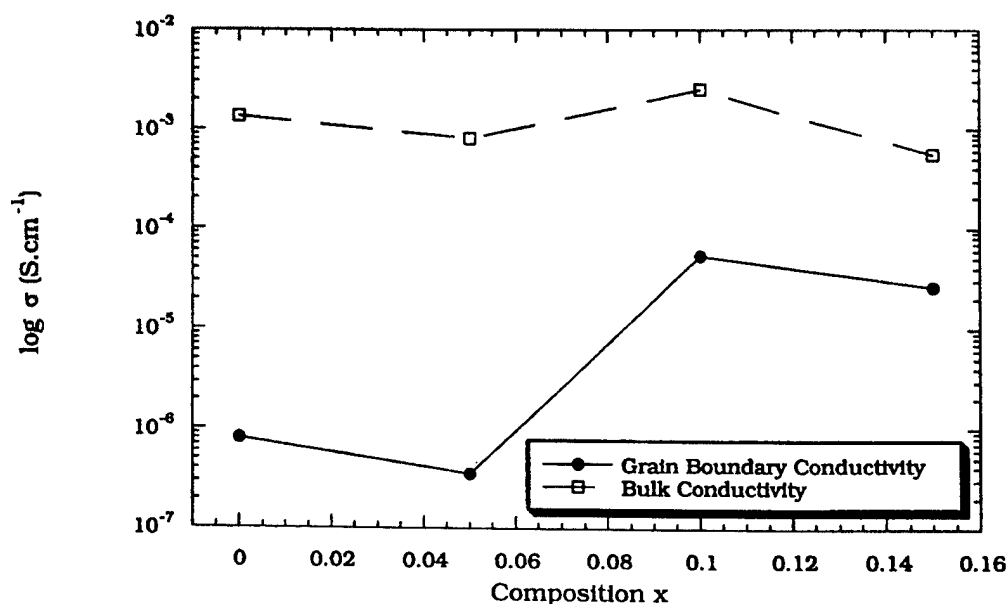


Figure 1: Grain boundary and bulk conductivity of substituted ceramics based on  $\text{Li}_{1.3+4x}\text{Al}_{0.3}\text{Ti}_{1.7-x}(\text{PO}_4)_3$ .

**HIGH IONIC CONDUCTIVITY IN  $\text{Li}_2\text{CaHfF}_8$** 

A. P. Ayala, I. Guedes, P.T.C. Freire, J.M. Sasaki and J. Mendes Filho  
Departamento de Física, Universidade Federal do Ceará  
CP 6030, 60455-760 Fortaleza (CE) Brazil.

R. L. Moreira  
Departamento de Física, ICEx, Universidade Federal de Minas Gerais  
C.P. 702, 30123-970 Belo Horizonte, MG, Brazil

J-Y. Gesland  
Université du Maine - Cristallogénèse, 72025 - Le Mans CEDEX 09 - France.

In 1973, Védrine *et. al.* [1] presented a new family of compound derived from  $\text{LiYF}_4$ , one of the more used host for solid state lasers. In these new compounds the yttrium ions are replaced by a bivalent element ( $\text{M}^{\text{II}} = \text{Ca}, \text{Cd}$ ) and a tetravalent one ( $\text{M}^{\text{IV}} = \text{Th}, \text{U}, \text{Ce}, \text{Tb}, \text{Zr}, \text{Hf}$ ) originating materials of the type  $\text{Li}(\text{M}^{\text{II}}_{0.5}\text{M}^{\text{IV}}_{0.5})\text{F}_4$ . The X-ray diffraction diagrams show that this compounds presents a body centered tetragonal structure, similar to that of  $\text{LiYF}_4$  and  $\text{LiLnF}_4$  ( $\text{Ln}$  : lanthanides) [2]. However, the presence of reflections which are absent in  $\text{LiYF}_4$  suggest the existence of an additional order between the  $\text{M}^{\text{II}}$  and  $\text{M}^{\text{IV}}$  cations. In consequence a double molecule is necessary to describe this structure:  $\text{Li}_2\text{M}^{\text{II}}\text{M}^{\text{IV}}\text{F}_8$ . To determine the actual structure of this compounds Védrine *et. al.* studied  $\text{Li}_2\text{CaUF}_8$  crystals by x-ray diffraction [3]. Their results confirmed that the crystalline structure is tetragonal, with space group  $I-4m2$  ( $D_{2d}^9$ ). The sublattice formed by Li, Ca and U cations is equivalent to that found in  $\text{LiYF}_4$ , while the number of fluorine sites is duplicate and half-occupied. Due to the presence of intrinsic fluorine vacancies, those authors suggest that, if the disorder is dynamic, a high ionic conductivity would be observed in the tetragonal axis direction, since the structure presents possible conduction channels in this direction.

Due to the possibility of observing high ionic conductivity in this family of compounds, we decide to study  $\text{Li}_2\text{CaHfF}_8$  using complex impedance spectroscopy between room temperature and 800 K. In spite of Védrine *et. al.* predictions, the conductivity measured along the *c* direction at 800 K was lower than  $10^{-8} \Omega^{-1} \text{cm}^{-1}$ . This is a very low value for an ionic conductor, specially if we consider the existence of intrinsic fluorine vacancies. Contrarily to what it was observed in the *c* direction, our complex impedance spectroscopy measures show a high ionic conductivity in the *a-b* plane.

In order to investigate this contradiction, we carried out additional investigations by means of x-ray diffraction (powder method), Raman spectroscopy and differential scanning calorimetry (DSC) in the crystal  $\text{Li}_2\text{CaHfF}_8$ . The analyses of our data allow us to propose a new structure for this crystal. This structure is well compatible with the conductivity (complex impedance spectroscopy) and thermal (DSC) behaviors of our system. The conduction mechanisms are discussed in terms of the different conduction pathways for the fluorine and lithium vacancy motion in the crystal.

Financial support : CNPq, FUNCAP, FINEP and FAPEMIG

[1] A. Védrine, L. Baraduc and J-C. Cousseins. *Mat. Res. Bull.* **8**, 581 (1973).

[2] E. Garcia and R. R. Ryan, *Acta Crystallogr C* **49**, 2053 (1993).

[3] A. Védrine, D. Trottier, J.C. Cousseins and R. Chevalier, *Mat. Res. Bull.* **14**, 583 (1979).

## EFFECTS OF THE PEROVSKITE FRAMEWORK ON LITHIUM ION CONDUCTIVITY IN ADPESSs (A-SITE DEFICIENT PEROVSKITE SOLID SOLUTIONS)

Yasuhiro Harada, Jun Kuwano and Yasukazu Saito

Department of Industrial Chemistry, Faculty of Engineering, Science University of Tokyo,  
1-3 Kagurazaka, Shinjuku-ku, Tokyo 162-8601, JAPAN

We have previously reported several kinds of A-site deficient perovskite solid solution (ADPESS) with high Li ion conductivity [1-3]. The bulk conductivity ( $\sigma_b$ ) depended on the primitive cell volume ( $V$ ), the degree of ordering of the A-site ions, the concentrations of Li ions and vacancies, and the kind of the framework ( $fw$ ). For ADPESSs with the  $\text{Ln}_{0.56}\text{M(IV)}\text{O}_3$   $fw$  and disorder arrangement of the A-site ions, a maximum  $\sigma_b$  of  $1.5 \times 10^{-3} \text{ Scm}^{-1}$  at  $25^\circ\text{C}$  was found at  $V^{1/3} \approx 387 \text{ pm}$  for  $\text{M}=\text{La}$ , as Fig. 1 shows. In this study, we prepared the disordered Li-ADPESSs with the  $\text{Ta}_{0.775}\text{M(III)}_{0.225}\text{O}_3$   $fw$  and the  $\text{M(II)}$  and Li concentrations fixed at  $\text{M(II)}_{0.56}\text{Li}_{0.33}$ . The relationship between  $\alpha_b$  and  $V^{1/3}$  and the effects of  $fw$  were discussed.

The compositions of the samples were  $(\text{Sr}_x\text{Ca}_{1-x})_{0.56}\text{Ta}_{0.775}\text{M(III)}_{0.225}\text{O}_3$  [ $\text{M(III)}=\text{Co, Ga, Cr, Fe}$ ]. Mixtures of raw materials were heated initially at  $650^\circ\text{C}$  for 2 h to expel  $\text{CO}_2$  gas and calcined at  $800^\circ\text{C}$  for 12 h on Au-boats. The reground products were cold-pressed at 250 MPa into pellets (12 mm in diameter, 1-2 mm in thickness), which were sintered at  $1300^\circ\text{C}$  or  $1350^\circ\text{C}$  and quenched into liq.  $\text{N}_2$  to form a high-temperature, disordered  $\alpha$ -form as perfect as possible. The crystalline products were characterized by powder X-ray diffraction (XRD). The ac impedance data were collected over a frequency range,  $f=5 \text{ Hz}-13 \text{ MHz}$ , and analyzed using the complex impedance plots and electric modulus spectra.

The samples were a single phase of a simple cubic perovskite except a few samples containing small amounts of extra phases. Fig. 1 shows the relations between  $V^{1/3}$  and  $\sigma_b$  at  $25^\circ\text{C}$ . All the series show dome-shaped dependence with a maximum at a  $V^{1/3}$  value of about 394-395 pm, which is much larger than the optimal value  $\sim 387$  for the  $\text{Ln}_{0.56}\text{M(IV)}\text{O}_3$   $fw$ . The highest  $\sigma_b$  value of  $2.0 \times 10^{-4} \text{ Scm}^{-1}$  was found for  $\text{M(III)}=\text{Cr}$ ,  $x=0.9$ . The incorporation of Sr expands the cell, while increases the electron density on the oxide ions in the  $fw$ . The later is dominant; this calls for a larger optimal  $V^{1/3}$  value of about 394-395 pm for fast Li conduction in the  $\text{Ta}_{0.775}\text{M(III)}_{0.225}\text{O}_3$   $fw$ .

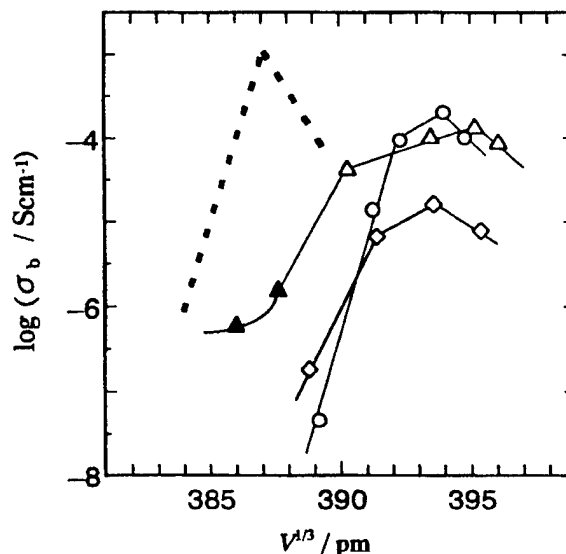


Fig. 1. Relationship between  $V^{1/3}$  and  $\sigma_b$  at  $25^\circ\text{C}$ ;  $\text{M(III)}=\text{Cr}(\bigcirc), \text{Fe}(\triangle), \text{Ga}(\diamond)$ . Closed symbols; distorted perovskite cell. Dotted line; dome-shape dependence for  $\text{Ln}_{0.56}\text{M(IV)}\text{O}_3$   $fw$ .

- [1] H. Kawai et al., J. Electrochem. Soc. **141** (1994) L78.
- [2] H. Watanabe et al., J. Power Sources. **68/2** (1997) 416.
- [3] Y. Harada et al., Solid State Ionics. **108** (1998) 407.

## IONIC CONDUCTIVITY AND STRUCTURE OF HALOCOMPLEX SALTS OF GROUP 13 ELEMENTS

Yasumasa TOMITA, Hiroshi OHKI, Koji YAMADA, and Tsutomu OKUDA

Department of Chemistry, Faculty of Science, Hiroshima University,  
Kagamiyama, Higashi-Hiroshima 739-8526, Japan

Ionic conductivities for the complex salts between monohalides of Li, Cu and Ag, and trihalides of the group 13 elements (Al, Ga and In) were studied by means of NMR, NQR, powder X-ray diffraction, DTA and AC conductivity measurements.

Crystal structures of  $\text{CuAlCl}_4$ ,  $\text{CuAlBr}_4$  and  $\text{CuGaBr}_4$  were determined by Rietveld analysis of the X-ray powder diffraction data. These crystals belong to a tetragonal system in which both Al and Cu atoms are surrounded by four halogens tetrahedrally. In consistent with the structure, a  $^{63}\text{Cu}$  NMR experiment using a single crystal indicated that the principal axis of the  $e^2Qq/h$  tensor is parallel to the  $c$ -axis for  $\text{CuAlCl}_4$  and  $\text{CuMBr}_4$  ( $\text{M}=\text{Al, Ga}$ ). The cation diffusion in  $\text{CuAlX}_4$  ( $\text{X}=\text{Cl, Br}$ ) and  $\text{MGaBr}_4$  ( $\text{M}=\text{Li, Cu}$ ) was confirmed by measuring the temperature dependence of the  $^7\text{Li}$  and  $^{63}\text{Cu}$  NMR linewidths and it was found that these compounds are cationic conductors. The activation energies for the cation diffusion were 36, 51 and 44  $\text{kJmol}^{-1}$  for  $\text{LiGrBr}_4$ ,  $\text{CuAlBr}_4$  and  $\text{CuGaBr}_4$ , respectively. The activation energies for the reorientation of the  $\text{MBr}_4$  ( $\text{M}=\text{Al, Ga}$ ) anions in  $\text{AgAlCl}_4$  and  $\text{CuMBr}_4$  were evaluated from  $^{27}\text{Al}$  and  $^{71}\text{Ga}$  NMR. The rates of these reorientation are much slower than those of the cation diffusion in  $\text{CuAlX}_4$  and  $\text{MGaBr}_4$  ( $\text{M}=\text{Li, Cu, Ag}$ ). As expected from the results for NQR and NMR experiments, the ionic conductivities of  $\text{AgAlBr}_4$  and  $\text{AgGaBr}_4$  were one order higher than those of  $\text{CuAlBr}_4$  and  $\text{CuGaBr}_4$ , respectively. It is considered that this finding may be due to the difference in crystal structure. The ionic conductivity of  $\text{MGaBr}_4$  ( $\text{M}=\text{Li, Cu, Ag}$ ) was higher than that  $\text{MAlBr}_4$  at room temperature. It was found that the ionic conductivity is mainly governed by the ration of the cationic radius to the anionic one.

The satellite spectra of the  $^{63}\text{Cu}$  and  $^{27}\text{Al}$  NMR varied anomalously with temperature. The quadrupole coupling constant,  $e^2Qq/h$ , of  $^{63}\text{Cu}$  and the asymmetric parameter,  $\eta$ , of  $^{27}\text{Al}$  changed linearly with decreasing temperature and  $e^2Qq/h$  of Al did not change so much. From the calculation of electric-field-gradient tensors using the point charge model, it was confirmed that these temperature dependencies are not due to the variation of the lattice constants. The  $\text{Cu}^+$  ion diffusion path in  $\text{CuAlBr}_4$  was decided by NMR experiments so that the  $\text{Cu}^+$  ions jump between the normal sites via interstitial sites and diffuse along the  $ab$  plane. The ionic conductivity was evaluated by use of the parameters obtained from NMR by assuming the diffusion mechanism. Its values was consistent with the observed conductivity.

$\text{Li}_3\text{InBr}_6$  has a phase transition at 314K on heating and 270K on cooling. From  $^7\text{Li}$  NMR and conductivity measurements, it was confirmed that  $\text{Li}_3\text{InBr}_6$  is a superionic conductor due to lithium ions in the high-temperature phase. The ionic conductivity in the high-temperature phase is  $10^{-3}\text{Scm}^{-1}$  at 297K. When  $\text{CaBr}_2$  was doped into  $\text{Li}_3\text{InBr}_6$ , an additional phase transition occurred and the ionic conductivity varied with the amounts of  $\text{CaBr}_2$ . From the substitution effect of the cation, it is considered that the high ionic conductivity results from the considerably disordered state of the cationic sublattice.



# LITHIUM INSERTION AND ELECTROCHROMISM IN POLYCRYSTALLINE MOLYBDENUM OXIDE FILMS

F. F. Ferreira, M.C. A. Fantini, M.H. Tabacniks<sup>1</sup>, Tersio G. Souza Cruz, Sandra C. deCastro and A. Gorenstein<sup>2</sup>

<sup>1</sup> IFUSP, CP 66318, 05315-970, SP, Brasil - mfantini@if.usp.br

<sup>2</sup> Universidade Estadual de Campinas, Instituto de Física "Gleb Wataghin" CP 6165, CEP 13081-970, Campinas, SP, Brasil - annette@ifi.unicamp.br

In this work, we investigated the conditions in which polycrystalline molybdenum oxide films with distinct compositions and microstructures can be obtained by r.f. reactive sputtering. The oxygen flow ( $\phi$ ) during deposition was varied, and the substrates were heated during deposition (300 °C). All other deposition parameters were maintained at constant values. The films were studied by X-Ray Diffraction (XRD), Rutherford Backscattering Spectrometry (RBS), Spectrophotometry and X-Ray Photoelectron Spectroscopy (XPS). Local order of as-grown and intercalated films was investigated by X-Ray Absorption Spectroscopy (XAS) at the L-edge and the valence band was studied by Photoelectron Spectroscopy. These last experiments were performed using synchrotron radiation, at the LNLS (beamline SXS and TGM, Campinas, Brazil).

Table I shows the RBS [O]/[Mo] ratio. Films deposited at low  $\phi$  present a Mo<sup>4.68+</sup> mean oxidation state; for high  $\phi$ , this value approaches that of MoO<sub>3</sub> (Mo<sup>6+</sup>). By XRD, it was concluded that the film deposited at the lowest  $\phi$  is polycrystalline MoO<sub>2</sub>. With the increase of  $\phi$ , the following microstructures were obtained: amorphous  $\rightarrow$  (MoO<sub>2.8</sub> +  $\alpha$ -MoO<sub>3</sub>)  $\rightarrow$   $\beta$ -MoO<sub>3</sub>  $\rightarrow$  (MoO<sub>2.8</sub> +  $\beta$ -MoO<sub>3</sub>). The absorption coefficient for the blue films deposited at low  $\phi$  presented a band centered at 1,5 – 1,6 eV, characteristic of oxygen vacancies [1]. Core level spectra of these samples presented broad Mo 3d lines, indicating the presence of Mo<sup>6+</sup>, 5+ and 4+. Data obtained on high oxygen flow samples (transparent films) show narrow Mo 3d lines, with binding energies characteristic of the 6+ state. The different techniques of analysis provided consistent results.

**Table I**  
*O/Mo ratio, for the different films*

O <sub>2</sub> flow (sccm)	[O]/[Mo] ratio
0.5	2.343 $\pm$ 0.013
0.6	2.902 $\pm$ 0.016
0.7	2.837 $\pm$ 0.022
1.0	2.906 $\pm$ 0.025
2.0	2.875 $\pm$ 0.023
3.0	2.895 $\pm$ 0.028
4.0	2.872 $\pm$ 0.026

The behavior of the samples upon intercalation was studied in an electrolyte containing Li<sup>+</sup> ions. The transmittance changes ( $\lambda = 632.8$  nm) was followed during the reversible insertion or extraction of ions/electrons in the oxide structure. These results are shown in Figure 1. All samples, with the exception of the MoO<sub>2</sub> film, showed an electrochromic behavior. The transmittance change, for the best sample, was ~70 %. The film having the best optical behavior is mostly formed by the  $\beta$ -MoO<sub>3</sub> phase.

Only the XANES region was analyzed in the XAS results, since the superposition of the L<sub>III</sub> and L<sub>II</sub> did not allow an analysis of the EXAFS region. Metallic Mo and commercial  $\alpha$ -MoO<sub>3</sub> were used as reference compounds. The sample deposited at the lowest  $\phi$ , presented the absorption edge shifted to low energy values, near the Mo metal edge. With the increase of  $\phi$  during deposition the

absorption edge for the other films goes to higher energy values, and approaches that of  $\alpha$ - $\text{MoO}_3$ .  $\text{Mo}^{6+}$ -based compounds shows a splitting of the L-lines related to the d-orbital transitions, which depend on the crystal field, i.e., the Mo site symmetry [2]. Our results showed an octahedral coordination of the Mo sites for the  $\text{MoO}_2$  phase. After electrochemical intercalation, this coordination remains octahedral, but with a distinct number of first neighbors, and distinct distances. The amorphous films did not show significant changes in the symmetry of distribution of ions around the Mo, which can be attributed to structural disorder. The most promising sample, concerning electrochromic applications ( $\phi = 3,0$  sccm) showed a change in symmetry upon intercalation. In the as-grown state only octahedral sites were identified; after lithium insertion, both octahedral and tetrahedral sites were present.

The photoemission spectra obtained at low photon energies ( $\sim 120\text{eV}$ ) for the  $\text{MoO}_2$  sample is shown in Figure 2. A clear signal arising from the core level of intercalated cation can be seen (Li 1s, at  $\sim 58$  eV). The valence band ( $\text{O}2\text{p}$ ,  $\text{Mo}4\text{d}$  and  $\text{Mo}5\text{s}$  lines) of the as grown and intercalated sample differs mainly by the presence of a small peak located near the Fermi level (fig. 2, inset). This peak showed up only for this sample, in spite of the presence of the Li 1s line in the spectra obtained for all intercalated samples. The atomic ratio Li/Mo was estimated from the areas of the Li1s and Mo 4p line (at  $\sim 39$  eV, not shown in fig. 2). The obtained value was 0.5, for all samples.

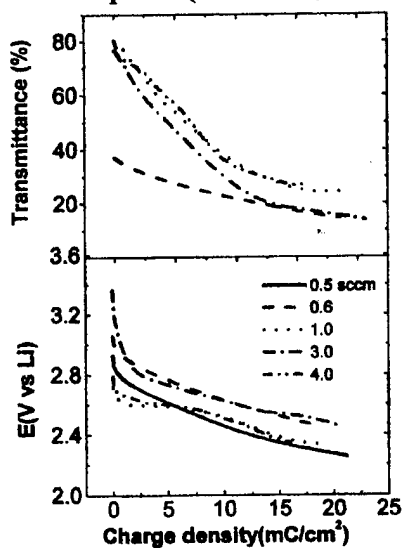


FIGURE 1

Transmittance changes ( $\lambda = 632.8$  nm, upper part) and potential changes (lower part). Galvanostatic intercalation,  $I = 1 \mu\text{A}$

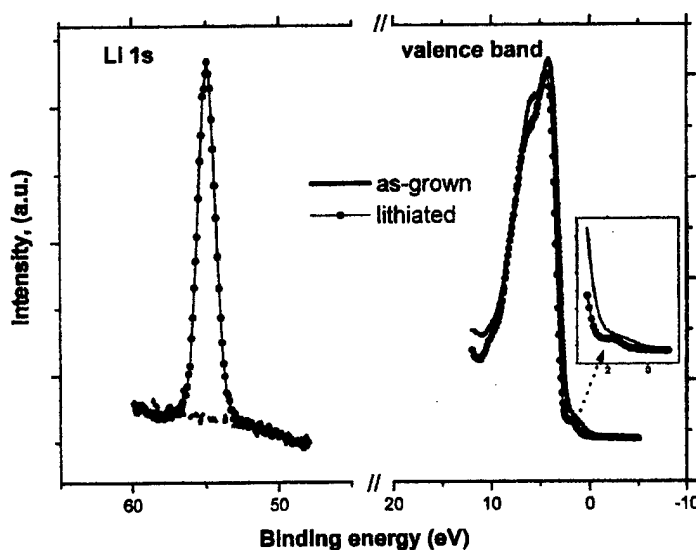


FIGURE 2

Core level Spectra. Photon energy = 120 eV. As grown (full line) and intercalated film (line + circles) Sample deposited at  $\phi = 0.5$  sccm.

## REFERENCES

- [1] M. Anwar, C. A. Hogarth, Phys. Stat. Sol.(a), **109**,469(1998).
- [2] S.R. Bare, G.E. Mitchell, J.J. Maj, G.E. Vrieland and J.L. Gland, J. Phys. Chem. **97**, 6048 (1993).

NMR STUDY OF Na<sup>+</sup> ION MOTION IN Na<sub>3-x</sub>Ru<sub>4</sub>O<sub>9</sub>

Y. Onoda, S.H. Chung, A. Watanabe and T. Mitsuhashi

National Institute for Research in Inorganic Materials, Tsukuba, Ibaraki 305, Japan

Na<sub>3-x</sub>Ru<sub>4</sub>O<sub>9</sub> ( $x \sim 0.9$ ) with 'ruthenium bronze' structure has a large tunnel running parallel to the b-axis, and Na ions locate on three sites in the tunnel as shown in Fig.1<sup>[1]</sup>. This material is expected as an electrode material, since the electronic conductivity is high<sup>[2]</sup> and dc ionic conductivity along the tunnel is thought to be high. To investigate the dynamics of the Na<sup>+</sup> ions and phase transitions in the material, temperature dependence of <sup>23</sup>Na NMR line shape and spin-lattice relaxation time  $T_1^*$  have been measured on powder samples sealed in evacuated silica tubes over the temperature range from 125 K to 909 K.

Line shape below 385 K has two peaks and a shoulder, and it shows a slight change at about 260 K, where a small peak is observed in the specific heat measurement. It was attributed to a change in the occupation number between Na<sub>1</sub> and Na<sub>3</sub> sites using a line shape analysis. At about 390 K, where the specific heat measurement shows a sharp peak, the line shape becomes a single peak with FWHM of about 9 kHz. The width is kept till the maximum measured temperature.

Fig.2 shows temperature dependences of  $T_1^*$  of four powder samples. Sample-1 and sample-2 are different batches, but they were sealed into silica tubes by warming the samples at similar temperatures to eliminate water in the sample. Sample-4 includes much water and  $T_{1\min}^*$  at 250 K is thought due to proton motion. The values of  $T_1^*$  of sample-1 and sample-2 are different but they show similar temperature dependences. A small dip at about 250 K corresponds to the slight change in the line shape. From the linear part of the  $\log(T_1^*)$  vs.  $1/T$  above 270 K, we can get an activation energy of 0.22 eV for the Na<sup>+</sup> ion motion within the channel. The linear decrease of the  $\log(T_1^*)$  above 600 K is thought to be caused by three dimensional Na<sup>+</sup> ion motion.

## References

- [1] J. Darriet, Acta Crystallogr. **B30**, 1459 (1974).
- [2] G. Cao, S. McCall, F. Freibert, M. Shephard, P. Henning and J. E. Crow, Phys. Rev. **B53**, 12215 (1996).

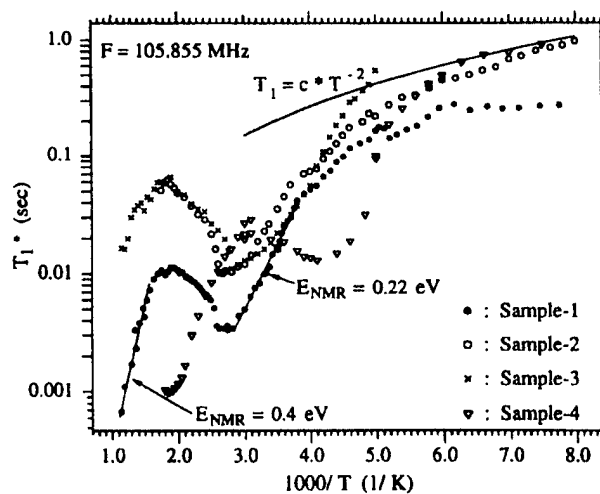
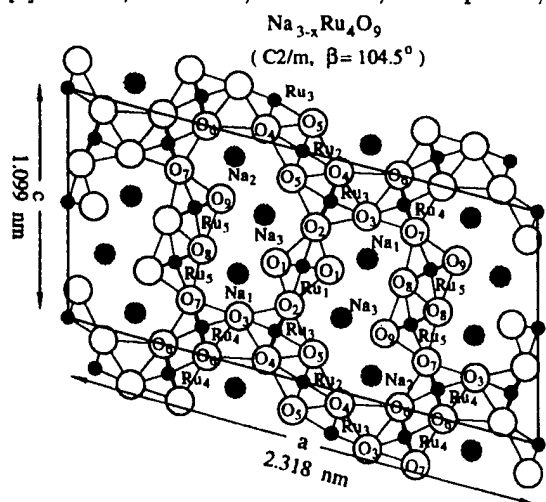


Fig.1 Projection of the structure on the b plane. Fig.2 Temperature dependence of  $T_1^*$

# ION CONDUCTION IN HOLLANDITE-TYPE ONE-DIMENSIONAL SUPERIONIC CONDUCTOR $\text{Na}_x\text{Cr}_x\text{Ti}_{8-x}\text{O}_{16}$ ( $x=1.7$ ) SINGLE CRYSTAL

Shinzo Yoshikado, Yuichi Michiue\*, Yoshito Onoda\*, Mamoru Watanabe\*

Department of Electronics, Doshisha University, Kyotanabe, Kyoto 610-0321, Japan

\*National Institute for Research in Inorganic Materials, Tsukuba, Ibaraki 305-0044, Japan

A one-dimensional (1D) tunnel, which has very weak interaction with neighboring tunnels, has been realized in the system of hollandite-type compounds such as alkali priderites  $\text{A}_x\text{B}_y\text{Ti}_z\text{O}_{16}$  (ABTO,  $\text{A}=\text{K}, \text{Rb}, \text{Cs}$ ,  $\text{B}=\text{Mg}, \text{Co}, \text{Ni}$  ( $y=x/2$ ),  $\text{Al}, \text{Ga}, \text{Cr}$  ( $y=x$ ),  $1.2 < x < 2$ ) and alkali gallotitano-gallates  $\text{A}_x\text{Ga}_y\text{Ga}_{8-x}\text{Ti}_{16-x}\text{O}_{36}$  (AGGTO,  $\text{A}=\text{K}, \text{Rb}, \text{Cs}$ ,  $0.8 \leq x < 1.5$ ). Dynamics of alkali ions in 1-D tunnels has been studied [1, 2]. In this study, the dynamics of sodium ( $\text{Na}^+$ ) ions in single crystal of hollandite-type 1D superionic conductor Na-Cr-priderite,  $\text{Na}_x\text{Cr}_x\text{Ti}_{8-x}\text{O}_{16}$  ( $x=1.7$ ), was studied. Because  $\text{Na}^+$  ions distribute with relatively high density at the bottle necks formed by the nearest neighbor four oxygen atoms, the high direct current ion conductivity is expected [3].

Single crystals were grown by a flux method [3]. Vacuum evaporated gold blocking electrodes were applied to the crystal end faces perpendicular to the c-axis. The sample was loaded between the inner conductor of a 7 mm coaxial line and the shorting plate. The coaxial cell was floated from the ground by an insulator. From 20 Hz to 1 MHz and from 1 MHz to 1.8 GHz, an HP 4284A precision LCR meter and an HP 4291A impedance/material analyzer were used, respectively. Measurements were carried out at the same time using the same coaxial cell in the temperature range between 173 and 453 K in a nitrogen gas atmosphere. At microwave frequencies between 82 and 98 GHz, a standing-wave method was used [1, 2].

Plots in Fig.1 show the measured values of the total complex electrical conductivity  $\sigma_{\text{tot}}$  between 20 Hz and 98 GHz. The frequency dependence was similar to that for AGGTO in spite of the hollandite type structure. In the low frequency region, the frequency-independent conduction process was observed. Figure 2 shows the temperature dependence of the frequency-independent ion conductivity  $\sigma_{\text{fi}}$ . The conduction process was thermally activated and value of the total activation energy was about 2.7 eV. At the present time, it is not concluded that mobile species are  $\text{Na}^+$  ions. The hopping angular frequency  $\omega_p$  of mobile species is shown in the same figure. The  $\omega_p$  also is thermally activated and the value of the activation energy was about 2.3 eV.

In the high frequency region above about 1 MHz, the conduction mechanism could be explained by the motion of  $\text{Na}^+$  ions between two succeeding blocks in the 1D conduction path similar to AGGTO [2]. The conduction process was thermally activated and the value of the activation energy was about 0.05 eV. The mean value of the distance between two blocks was estimated at 6~9 nm.

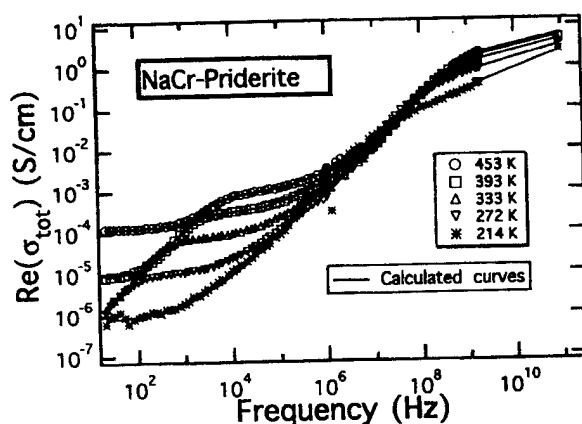


Fig.1 Frequency dependence of the real part of the total complex electrical conductivity  $\sigma_{\text{tot}}$  for Na-Cr-priderite.

[1] S. Yoshikado et al., Solid State Ionics **79**, 34 (1995). [2] S. Yoshikado et al., Solid State Ionics **86-88**, 317 (1996). [3] Y. Michiue et al., J. Solid State Chem. **116**, 296 (1995).

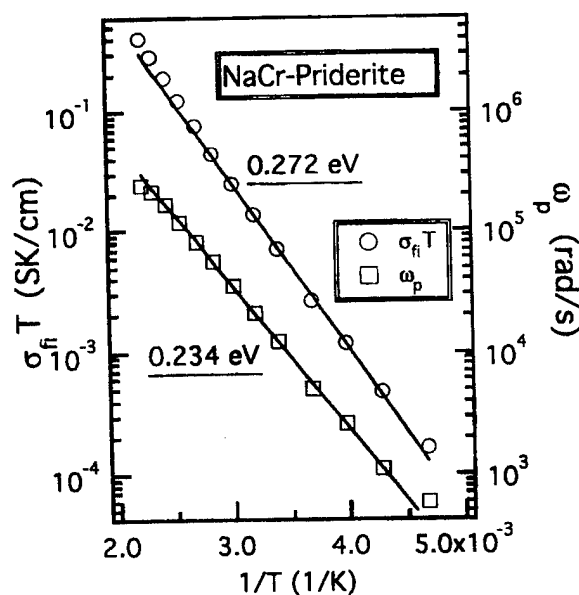


Fig.2 Temperature dependence of  $\sigma_{\text{fi}} T$  and  $\omega_p$  for Na-Cr-priderite.

# THE EFFECT OF HUMIDITY ON THE CONDUCTIVITY PROCESSES IN POLYCRYSTALLINE $\text{Cu}^{2+}$ -STABILIZED $\text{K}^+$ - $\beta$ -FERRITE

M. Karus<sup>1</sup>, O. Kalogirou<sup>2</sup>, W. Gunsser<sup>1</sup> and A. Reller<sup>3</sup>

<sup>1</sup>Institute of Physical Chemistry, University of Hamburg, Bundesstr. 45,  
20146 Hamburg, Germany

<sup>2</sup>Third Laboratory of Physics, Dept. of Physics, Aristotle University of Thessaloniki,  
54006 Thessaloniki, Greece

<sup>3</sup>Solid State Chemistry, University of Augsburg, Universitaetsstr. 2  
86135 Augsburg, Germany

$\text{K}^+$ - $\beta$ -ferrites with the  $\beta$ -alumina type structure (space group  $R\bar{3}m$ ) have been studied for their high ionic conductivity and humidity sensing properties [1-5]. In this work the conductivity of polycrystalline  $\text{Cu}^{2+}$ -stabilized  $\text{K}^+$ - $\beta$ -ferrite was investigated in the temperature range between 20 and 500 °C in atmospheres with variable water vapor partial pressure. The samples, prepared by the standard ceramic technique, were characterized by means of X-ray powder diffraction (XRD) and electron microprobe analysis (EDAX). Combined thermogravimetric – mass spectroscopic (TG-MS) measurements were carried out, additionally.

Impedance spectroscopic measurements revealed differences in the conductivity processes when the samples were measured directly after preparation and after being exposed in a wet atmosphere for a longer period. Hereafter, the different samples are denoted as “as-prepared” and “aged” samples, respectively. The samples were pressed to cylindrically formed pellets, and measured in an ion blocking two-electrodes arrangement, thus allowing exchange of gaseous species through the mantle surface only. In the as-prepared samples the dominating conductivity processes were found to take place only on the mantle surface and in the region near the mantle surface. In the latter region bulk conductivity, conductivity through grain boundaries and processes at the sample-electrode interface were separated. Aged samples were found to present the same conductivity processes, which now take place throughout the entire volume of the material. In the latter case, a conductivity process along the grain boundaries was found, additionally.

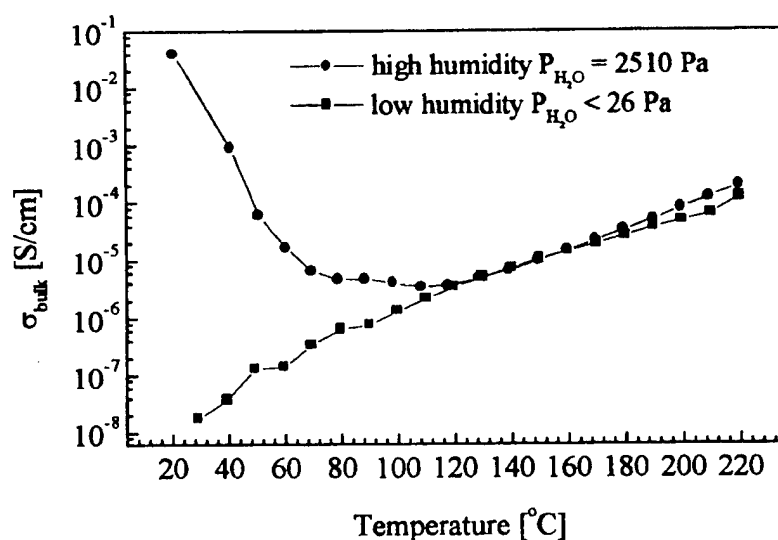


Fig. 1 Bulk conductivity versus temperature measured in different atmospheres.

An Arrhenius type conductivity behavior was observed for all processes in the temperature range between 100 and 500 °C. The conductivity and activation energy values were determined as a function of the water vapor partial pressure in the surrounding atmosphere of the measurement cell. A strong humidity depended increase in the conductivity was observed when cooling the samples below 100 °C down to room temperature. In Fig. 1 the bulk conductivity versus temperature measured in two different atmospheres is plotted, i.e., under low humidity conditions [ $P(\text{H}_2\text{O}) < 26 \text{ Pa}$ ] and under high humidity conditions [ $P(\text{H}_2\text{O}) = 2510 \text{ Pa}$ ], respectively. It is characteristic that the conductivity under high humidity conditions is about seven orders of magnitude higher than that under low humidity conditions. Transference number measurements give strong indication for the presence of high protonic conductivity at temperatures below 100 °C.

Thermogravimetric analysis in a wet flowing atmosphere showed a reversible uptake and loss of weight in the temperature range between 20 and 250 °C, due to water absorption and desorption, respectively, as found by means of mass spectroscopy. Additionally, a loss of  $\text{CO}_2$  was detected during the first heating cycle in the case of the aged samples only.

It is proposed that the above-mentioned differences in the conductivity processes are due to a two step local mechanism. In a first step the potassium ions located in the conduction layers between the spinel blocks of the  $\beta''$ -alumina type structure are exchanged by  $\text{H}_3\text{O}^+$  from the humidified atmosphere at the grains surface. A  $\text{K}^+\text{OH}^-$  complex is then located near the exchanged cation site and becomes hydrated at temperatures below 100 °C. In a second step the reaction of this complex with  $\text{CO}_2$  out of the flowing atmosphere leads to the formation of  $\text{KHCO}_3$  identified by XRD. It seems that these aging reactions in the case of the as-prepared samples take place only on, and near the surface of the whole pellet. This might be caused by a non-uniform depth profile of the water vapor partial pressure throughout the entire pellet volume. In the case of the aged samples it is suggested that these reactions took place at the surfaces of each grain, which were kept in wet air for a longer period, thus leading to a homogeneous conductivity behavior after being pressed to pellets.

## References

- [1] S. Ito, H. Kawase, S. Nariki, N. Koura and N. Yoneda, *Hyomen Gijutsu (J. Surface Finishing Soc. Japan)* **40(12)**, 1443 (1989).
- [2] H. Kawase, S. Ito, S. Nariki, N. Koura and N. Yoneda, *Solid State Ionics* **40/41**, 448 (1990).
- [3] H. Takamura, T. Kagotani, M. Okada and M. Homma, *Mater. Trans. JIM* **34(3)**, 197 (1993).
- [4] O. Kalogirou, M. Karus and U. Sazama, *Ionics* **2(2)**, 97 (1996).
- [5] A. Priese, M. Karus, O. Kalogirou and K.-H. Klaska, *Zeitschrift f. Kristallographie, Suppl. Iss.* **12**, 214 (1997).

## MECHANO CHEMICAL SYNTHESIS OF SILVER ION CONDUCTOR IN THE SYSTEM AgI-Ag<sub>3</sub>PO<sub>4</sub>

Nobuya MACHIDA\*, Shigefumi NISHIDA\*, Toshihiko SHIGEMATSU\*, Hiroshi SAKAI\*, Masahiro TATSUMISAGO\*\*, and Tsutomu MINAMI\*\*

\*Department of Chemistry, Faculty of Science, Konan University

\*\*Department of Functional Materials Science, Osaka Prefecture University

**Introduction** Crystalline superionic conductors and superionic glasses have much attention for fundamental studies of the ion transport mechanism and for their technological applications. Among them, AgI-containing phosphate systems have been extensively investigated as model ionic conductors because of their high ionic conductivities at room temperature and their good stability against atmosphere. In the system AgI-Ag<sub>3</sub>PO<sub>4</sub>, a crystalline compound Ag<sub>7</sub>I<sub>4</sub>PO<sub>4</sub> was reported as superionic phase which show silver ion conductivity  $1.9 \times 10^{-1} \text{ Scm}^{-1}$  at 298K by Takahashi et al. [1]. Minami et al. reported that glasses have been able to be obtained in the same system and these glasses show high ion conductivities in the range of  $10^{-3}$  to  $10^{-5} \text{ Scm}^{-1}$  at 298 K depending on their composition[2]. High-energy ball milling processes are powerful methods to obtain amorphous phases, non-equilibrium compounds and so on[3]. Most of reported studies on mechanical milling dealt with metals and intermetallic compounds, and there are few papers on ionic conductors prepared with the mechanical milling. In this study we report the preparation of silver ion conductors in the system AgI-Ag<sub>3</sub>PO<sub>4</sub> by use of the ball-milling process and their ion conducting properties.

**Experimental**  $\beta$ -AgI and Ag<sub>3</sub>PO<sub>4</sub> crystals were used as raw materials. Desired amounts of the raw materials were weighted and sealed in a stainless steel container with TZP(tetragonal zirconia polycrystals) balls dry Ar atmosphere. The ball-to-powder ratio was 20 : 5 (about 5g of powder) and a rotation rate of ball milling was 380 rpm. The ball-milled powders were characterized by X-ray diffraction measurements and thermal analysis. The ball-milled powders was pressed into a pellet with 8 mm diameter and gold electrodes were evaporated on both sides of the pellet. The pellet was used for electrical conductivity measurements. The electrical conductivity measurements were carried out in dry N<sub>2</sub> atmosphere 20Hz to 1MHz with a impedance meter(HP-4284A) in the temperature range of 240 to 320 K. The conductivities were determined by employing complex impedance analysis.

**Results and Discussion** Figure 1 shows the X-ray diffraction patterns of ball-milled 60AgI•40Ag<sub>3</sub>PO<sub>4</sub> (mol%) sample. The X-ray diffraction patterns of raw materials  $\beta$ -AgI and Ag<sub>3</sub>PO<sub>4</sub> crystals are also shown in the figure. In the figure MM denotes milling time, and the peaks with open circles are attributable to characteristic peaks of  $\gamma$ -AgI phase. The phase transition of  $\beta$ -phase to  $\gamma$ -phase of AgI is occurred in the 5hr ball-milled sample and the diffraction peaks attributed to  $\beta$ - and  $\gamma$ -AgI are disappeared in the samples ball-milled more than 80hr. The diffraction peaks attributed to Ag<sub>3</sub>PO<sub>4</sub> crystals broaden with an increase in the milling time. These results indicate that the samples ball-milled more than 200hr consist amorphous phase and crystalline Ag<sub>3</sub>PO<sub>4</sub> phase, and the amorphous phase includes AgI and Ag<sub>3</sub>PO<sub>4</sub> contents.

Figure 2 shows the X-ray diffraction patterns of ball-milled 80AgI•20Ag<sub>3</sub>PO<sub>4</sub>(mol%) sample. The phase transition of  $\beta$ -AgI to  $\gamma$ -AgI is also

occurred with the ball-milling. In the samples with ball-milling time up to 70hr, the diffraction peaks of  $\gamma$ -AgI and  $\text{Ag}_3\text{PO}_4$  crystalline phase broaden with an increase in the milling time. On the other hand, the samples with ball-milling time more than 190hr show new diffraction peaks which are different from the peaks of  $\beta$ -AgI,  $\gamma$ -AgI,  $\text{Ag}_3\text{PO}_4$  and  $\text{Ag}_7\text{I}_4\text{PO}_4$  phases. These results suggest that the samples ball-milled more than 190 hr comprises an unknown phase.

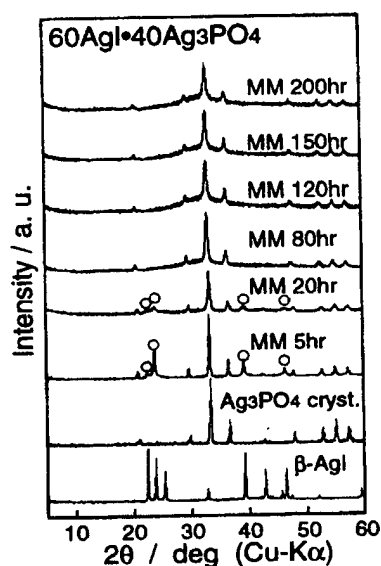


Fig.1 X-ray diffraction spectra of the ball-milled 60AgI·40Ag<sub>3</sub>PO<sub>4</sub> sample.

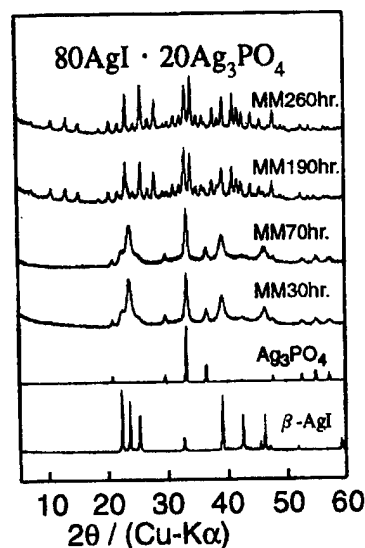


Fig.2 X-ray diffraction spectra of the ball-milled 80AgI·20Ag<sub>3</sub>PO<sub>4</sub> sample.

Figure 3 shows the silver ion conductivities of the ball-milled 60AgI·40Ag<sub>3</sub>PO<sub>4</sub> and 80AgI·20Ag<sub>3</sub>PO<sub>4</sub> samples at 298 K. In this figure closed triangle shows the ion conductivity of 60AgI·40Ag<sub>3</sub>PO<sub>4</sub> glass prepared by melt quenching methods, and the closed circle shows that of Ag<sub>7</sub>I<sub>4</sub>PO<sub>4</sub> crystals reported by Takahashi et al.[1]. The conductivity of the ball-milled 60AgI·40Ag<sub>3</sub>PO<sub>4</sub> sample show a maximum at a milling time 80hr. The maximum of the conductivity is higher than that of the melt quenched glass. The conductivity of the sample ball-milled more than 80 hr decreases with an increase in the milling time, and the conductivity closes to that of the melt quenched glass. The X-ray diffraction pattern of the ball-milled samples shows that AgI are dissolved in to the amorphous phase with ball milling and that the AgI content of the amorphous phase also show a maximum at the milling time 80hr. These results suggest that the AgI containing amorphous phase causes the high ion conductivity of the ball-milled sample.

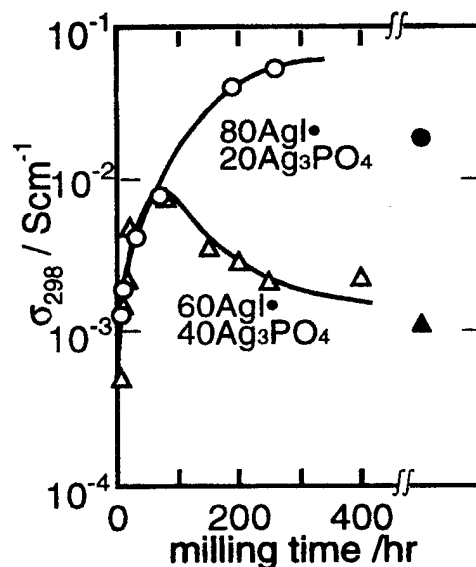


Fig.3 Milling time dependence of  $\sigma_{298}$  of the ball-milled samples.

On the other hand, the conductivity of the 80AgI·20Ag<sub>3</sub>PO<sub>4</sub> sample increases with an increase in the milling time, and saturation of the conductivity is observed. The 260hr ball-milled sample show the conductivity  $6 \times 10^{-2} \text{ Scm}^{-1}$  at room temperature, and the conductivity is higher than that of the Ag<sub>7</sub>I<sub>4</sub>PO<sub>4</sub> phase which is reported as only one high-ion-conducting phase in the system AgI-Ag<sub>3</sub>PO<sub>4</sub> by Takahashi et al.[1]. These result suggests that the unknown new crystalline phase is produced in the sample ball-milled more than 190 hr and that the new phase shows high ion conductivity more than Ag<sub>7</sub>I<sub>4</sub>PO<sub>4</sub> phase.

#### Reference

- [1] T. Takahashi, et al., J. Electrochem. Soc., **119**, 477(1972).
- [2] T. Minami, et al., J. Electrochem. Soc., **124**, 1659 (1977).
- [3] C.C. Koch et al., Appl. Phys. Lett., **43**, 1017 (1983).



## PHASE DIAGRAM AND STRUCTURAL FEATURES OF COMPOUNDS $\text{Ag}_x\text{ZrSe}_2$

N.N. Biccurova, Z.A. Yagafarova, M.J. Gareeva, R.R. Gimadeev

Sterlitamak State Pedagogical Institute

Address: 453103, Russia, Bashkortostan, Sterlitamak, Lenin-street, 37,  
general physics department

Zirconium diselenide is a structural analog of good studied compound  $\text{TiSe}_2$ , has hexagonal crystal structure, class  $P\bar{3}m1$ , in that the layers  $\text{ZrSe}_2$  are connected with each other by weak van der Waals' interaction. The distance between the layers  $\text{ZrSe}_2$  is quite large, and this compound can be considered as a material with quasi-two measured structure, and the possibility of vacant positions filling between the layers  $\text{ZrSe}_2$  with metal atoms makes perspective the synthesis of different materials based on this dichalcogenide.

The research of the phase diagram and the structure  $\text{Ag}_x\text{ZrSe}_2$  was performed with the methods of metrical titrating and x-ray structure analysis.

The patterns for this research was obtained by the ampule synthesis method.

For the synthesis the suspension substances were soldered into the quartz ampules pumped to  $10^{-5}$  mm mercury column and were burnt down at temperature 200–800 °C for 2–3 weeks. Then the obtained composition was pounded in the agat cap and pressed in the tablet and then soldered into the ampules and was burnt down for one month at temperature 500 °C.

The homogeneity and one-phase of obtained patterns were tested by the x-ray structure research was performed on the diffractometer ДРОН 4-07 with  $\text{CuK}_\alpha$  - radiation. For silver intercalation within  $\text{ZrSe}_2$  was used the koolon metrical titrating with element  $\text{Ag}/\text{AgI}/\text{Ag}_x\text{ZrSe}/\text{Pt}$ . The curve for koolon metrical titrating was obtained at temperature 200°C, one-phase field was discovered for  $\text{Ag}_x\text{ZrSe}_2$  at  $0,15 < x < 0,27$ . At room temperature this compound is the mixture of two phases:  $\text{Ag}_2\text{Se}$  and  $\text{Ag}_{0,25}\text{ZrSe}_2$ .

The powder roentgenogram of zirconium diselenide that was intercalated by silver  $\text{Ag}_{0,18}\text{ZrSe}_2$  is indexed in the space group  $P\bar{3}m1$  with the parameters  $a=3.7579\text{Å}$  and  $c=6.1248\text{Å}$ , that points to the sequencing of silver ions in the super-structure  $2a_0\cdot 2b_0\cdot c_0$ , where  $a_0$ ,  $b_0$  and  $c_0$  are the lattice parameters. The silver ions allocation is qualified in depending upon the composition and temperature.

# IONIC PHOTOCONDUCTIVITY - NEW PHYSICAL PHENOMENON IN SUPERIONIC CRYSTALS

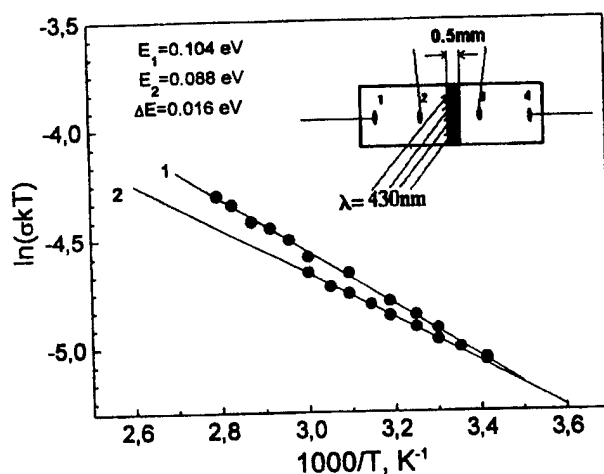
Sergei Bredikhin

Institute of Solid State Physics, Russian Academy of Science,  
142432 Chernogolovka, Moscow Region, Russia

Investigations of superionic conductors attract a lot of attention because they have several unusual and even paradoxical properties. The distinctive feature of superionic crystals is the presence of two types of charge carriers, namely electrons and ions. Interaction between the electronic and ionic systems results in several fundamentally novel phenomena being observed in superionic crystals [1,2]. In the present work we represent our investigations of one manifestation of interaction between the ionic and electronic subsystem - the effect of excited electronic centers on the ionic transport in superionic crystals.

A new effect of illumination by light on the ionic conductivity and activation energy of migration of mobile  $\text{Ag}^+$  cations in  $\text{RbAg}_4\text{I}_5$  superionic crystals has been detected and studied. Measurements were taken using the four-terminal technique and an alternating current. The ionic

conductivity was derived from the slope of the current-voltage characteristic at a frequency  $\sim 10^4$  Hz. An optical system collect light passing through the monochromator and focused it into a spot with dimension of  $\sim 0.5 \times 3$  mm in the region between the potential contacts (Fig. 1). It was shown that irradiation of  $\text{RbAg}_4\text{I}_5$  superionic crystals by light with wavelength  $\lambda = 430$  nm exciting electronic centers leads to reversible changes in the ionic conductivity. Figure 1 shows the logarithm of the ionic conductivity versus reciprocal temperature in the initial state of a  $\text{RbAg}_4\text{I}_5$



sample (1) and after irradiation by light with wavelength  $\lambda = 430$  nm (2). It clearly demonstrates that during the irradiation the activation energy of silver cation migration is lower. After switching off the light, the initial activation energy is restored.

Ionic conductivity in superionic materials can be formally describe by the model of simple hops:

$$\sigma_i = \frac{n_i (Ze)^2 v_0 a_0^2}{kT} \exp\left(\frac{S_m}{k}\right) \exp\left(-\frac{E_m}{kT}\right) \exp\left(-\frac{P\Delta V_m}{kT}\right), \quad (1)$$

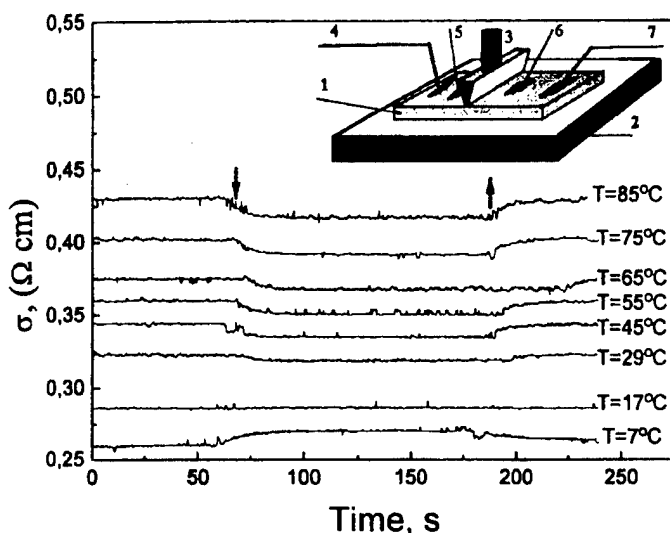
where  $E_m$  is the defect migration energy,  $\Delta V_m$  is the activation volume for the defect migration,  $v_0$  - is the frequency of ion oscillation at a lattice, and  $a_0$  is the hop length. It follows from the expression (1) that the activation energy  $E_a$  measured in experiments includes the migration energy  $E_m$  of mobile cations and a fraction due to the activation volume  $\Delta V_m$  for the defect migration:

$$E_a = E_m + P\Delta V_m. \quad (2)$$

Previously [2] we observed an effect of photoinduced changes in the local concentration of mobile  $\text{Ag}^+$  cations in the local region of superionic crystal irradiated by light with wavelength

$\lambda=430\text{nm}$ . It was shown that generation of silver cation vacancies  $[V]_{Ag}^-$  and holes in the illuminated region of the sample results in the formation of color centers  $h^+[V]_{Ag}^-$  in  $\text{RbAg}_4\text{I}_5$  superionic crystals. Our analysis indicates that photoinduced changes in the ionic conductivity and decrease in the activation energy are due to elastic strain fields generated surround the color centers in the local irradiated region of the sample. As can be seen in Fig. 1, irradiation of  $\text{RbAg}_4\text{I}_5$  superionic crystal by light with wavelength  $\lambda=430\text{nm}$  results in an activation energy for migration of silver cations approximately 0.01 eV lower. Simple estimates indicate that  $\sim 0.01$  eV decrease in the activation energy corresponds to an elastic stress of about  $P_{el} \approx 5 \times 10^8 \text{ Pa}$  in the illuminated sample region.

In order to check the mechanism of the effect of local elastic strain on ionic transport, we have studied the effect of local elastic stress applied to the sample on the ionic conductivity and activation energy for diffusion of mobile



silver ions in  $\text{RbAg}_4\text{I}_5$  crystals. The experimental configuration in local strain studies (Fig. 2) was identical to that of experiments on the photoinduced ionic conductivity (Fig. 1). The sample was placed on the surface of a sapphire substrate (2). Strain was produced by a sapphire prism (3) with a  $0.1 \times 3 \text{ mm}^2$  pressing surface. External stress was applied to a sample region between the two potential contacts (5)-(6). The measurements demonstrated that the local strain in the crystal leads to the reversible change in the ionic conductivity (Fig. 2). When the external stress

was lifted, the ionic conductivity recovered. Figure 2 shows that at temperature higher than room temperature, local strain leads to a reversible decrease in ionic conductivity, and the amplitude  $\Delta\sigma/\sigma_0$  drops with decreasing the temperature. At temperature of about  $17^\circ\text{C}$ , external stress has a little effect on ionic conductivity, and at temperature below  $17^\circ\text{C}$  it results in an increase in ionic conductivity. It was shown that the applied stress  $P \approx 1 \times 10^8 \text{ Pa}$  leads to a similar decrease in activation energy for diffusion of mobile silver cations ( $\Delta E \approx 0.008 \text{ eV}$ ) as in  $\text{RbAg}_4\text{I}_5$  sample irradiated with light  $\lambda=430 \text{ nm}$ . Our measurements indicate that the variation of the value of the activation energy  $E_a$  and of the logarithm of the preexponential factor,  $\ln(AD_0)$ , of the ionic conductivity are correlated in accordance with the compensation law or the Meyer-Neldel rule:  $\ln(AD_0) = (43 \pm 3)E_a - (3.6 \pm 0.1)$ .

Thus, our testing experiments on the effect of external local stress confirm our assumption that the ionic photoconductivity is due to elastic stress  $P_{el}$  generated in the sample region irradiated with light and changes in the ion diffusion coefficient caused by the change in the activation energy of the diffusion ( $E_a = E_m + P_{el}\Delta V_m$ )

[1] S.Bredikhin, T.Hattori and M.Ishigame, *Physical Review B*, **50**, 2444 (1994).

[2] S.Bredikhin, T.Hattori and M.Ishigame, *Solid State Ionics*, **67**, 311 (1994).

# VARIATION OF ELECTRONIC STATE OF AgI-BASED SUPERIONIC CONDUCTORS WITH MOVEMENT OF Ag IONS

Yoshiyuki Kowada<sup>A</sup>, Yoshinobu Yamada<sup>A</sup>, Masahiro Tatsumisago<sup>B</sup>,  
Tsutomu Minami<sup>B</sup>, and Hirohiko Adachi<sup>C</sup>

<sup>A</sup>Hyogo University of Teacher Education, Yashiro-cho, Kato-gun, Hyogo 673-1494, Japan

<sup>B</sup>Department of Applied Materials Science, Osaka Prefecture University, Sakai, 599-8531, Japan

<sup>C</sup>Department of Materials Science and Engineering, Kyoto University, Kyoto 606-01, Japan

AgI-based superionic conductors have very high ionic conductivity, compared with the other monovalent cation conductors, though the ionic radius and mass of Ag ion are larger than those of, for example, Li ion. This interesting behavior of Ag ion may be due to bonding interaction with surrounding atoms being present near conduction paths. Then it is very useful to calculate the electronic state of Ag ion in Ag ion conductors in order to understand such high conductivity. In the present work, we have calculated the electronic state of the several model clusters for the AgI-based superionic conductors and discuss about the change of bonding state of the mobile Ag ion with the surrounding atoms.

We have used the DV-X $\alpha$  cluster method to calculate the electronic state of the AgI-based superionic conductors. This method is one of the linear combination of atomic orbital (LCAO) molecular orbital methods. In this method the exchange potential  $V_{XC}$  is described as,

$$V_{xc\uparrow}(r) = -3\alpha \left[ \frac{3}{4\pi} \rho_{\uparrow}(r) \right]^{\frac{1}{3}} \quad (1)$$

where  $\rho_{\uparrow}$  is the electron density of the cluster and  $\alpha$  is a constant.  $\alpha$  is fixed to be 0.7, which was found empirically as the most appropriate, throughout the present work. The Mulliken population analysis was used for the evaluation of the net charge of each atom and the bond overlap populations of each cluster.

Fig. 1 shows an example of model clusters used in the present work. The structure of this cluster was adopted from the  $\alpha$ -AgI crystal, since

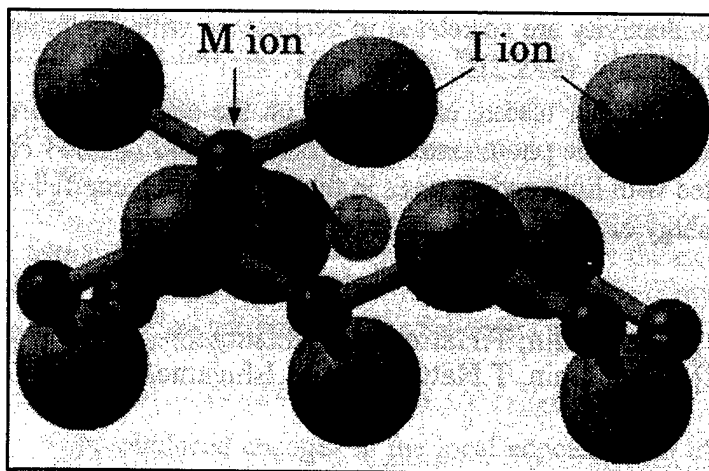


Fig. 1  $M_6I_{10}$  model cluster

the short-range structure around mobile Ag ions in the AgI-based superionic conductors should be similar to that in the  $\alpha$ -AgI crystal. One M ion in this cluster displayed with a large arrow is moved from a tetrahedral site to a neighboring octahedral site through the center of a triangle plane. Na ion, which has almost the same ionic radius as Ag ion, was also adopted as the M ion in the cluster for comparison in the electronic state with the result of Ag ion.

Fig. 2 shows the variation of the total bond overlap population of M ion in the  $M_6I_{10}$  cluster with the position, where M means Ag and also Na as mentioned above. Since the M ion should move in the interaction with all of the surrounding atoms, the sum of all the bond overlap populations of the moving M ion with surrounding atoms is shown in the figure. In this figure, the results of the Ag and Na ions are displayed by open squares and triangles, respectively. The position of M ion is shown as a relative value, that is, the value of zero means the center of the initial tetrahedral site and 1.2 means the center of the final octahedral site. In the case of the Ag ion, the total bond overlap population is 1.14 at the center of the tetrahedral site and is decreased with the movement. The population of the Ag ion has a minimum around the center of the octahedral site. Though the population of the Na ion is also decreased with the movement and has a minimum around the center of the octahedral site, the difference between the minimum and the initial value for the Ag ion is much smaller than that for the Na ion. This decrease of the bond overlap population is corresponding to the decrease of covalent interaction between the M ion and surrounding atoms. Then at the center of the octahedral site, both Ag and Na ions become more unstable than at the center of the tetrahedral site. The unstableness of the Ag ion, however, is much smaller than that of the Na ion. This result means that the Ag ion can much easily move from the tetrahedral site to the neighboring octahedral site than the Na ion. This smaller change of the bond overlap population in the movement of the Ag ion should be one of the origin of the fast movement of Ag ions in AgI-based superionic conductors.

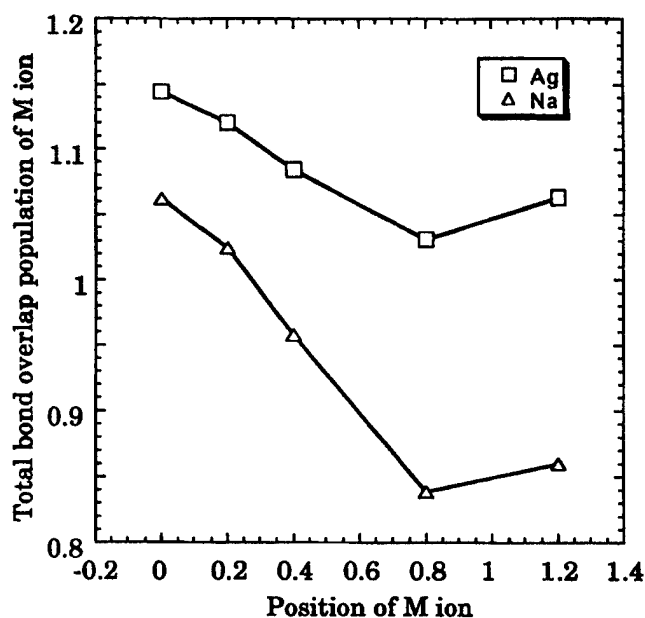


Fig. 2 Variation of the total bond overlap population of M ion in the  $M_6I_{10}$  cluster with the position.

# TEMPERATURE DEPENDENCE OF DIELECTRIC AND PHONON PROPERTIES IN SUPERIONIC CONDUCTOR CuI

K.Wakamura and H.Hiraoka

Graduate School of Applied Science, Okayama Science University,  
1-1 Ridai-cho, Okayama 700, Japan

Intimate relation between dielectric(D) property and high ionic conduction has been suggested through the characteristic electronic energy states and optical phonons[1-3]. Unreasonable behaviors of those temperature dependence are recently pointed out in comparison with semiconducting(S) and ionic(I) crystals [4]. Concerning these results, we are interested in CuI since it exhibits intermediate D-properties between S- and I-crystals. The reststrahlen band of CuI also shows rapid broadening between low and room temperatures[5] but detailed temperature dependence of it has not been reported. In this presentation, we investigate D-properties of CuI from far-infrared spectra as function of temperature T. From the frequencies of longitudinal and transverse phonon modes, we evaluate an effective charge  $Z^*e$ , the long-range and the short-range forces and investigate the role of those on the ionic conduction.

A pellet of CuI was prepared by sintering of powdered sample for 30 minutes under 180 C and the pressure of 2500 Kg/cm<sup>2</sup>. The same X-ray diffraction pattern was obtained before and after the sintering. The sample was polished with optically flat and the reflectivity R was measured near normal incidence with the resolution of 1 cm<sup>-1</sup> in the frequency range from 15 cm<sup>-1</sup> to 900 cm<sup>-1</sup> in the temperature below 300K. For the measurements of T, a Au(0.07 Fe)-Constantan thermocouple was used. A reststrahlen band shows a drastic broadening even below 300 K.

From the R value, we determine the phonon and mobile ion parameters by using the dispersion relation including the mobile ion term derived by Bruesh et al[6]. Obtained  $\epsilon_\infty$  and  $Z^*$  are shown as function of T in Fig.1. The  $\epsilon_\infty$  increases and  $Z^*$  increases with increasing T. These are however unreasonable in comparison with those of normal S- and I-crystals. The  $\epsilon_\infty$  is related to averaged gap  $E_{AV}$  as

$$\epsilon_\infty = 1 + A(\hbar\omega_p/E_{AV})^2.$$

$E_{AV}$  also concerns with the  $E_g$  value as  $E_{AV} = E_g + B$ . Therefore the increase of  $\epsilon_\infty$  is connected with the decrease of  $E_{AV}$  and  $Z^*$  values. By considering the effect of defects on  $E_g$ , we understand the unreasonableness.

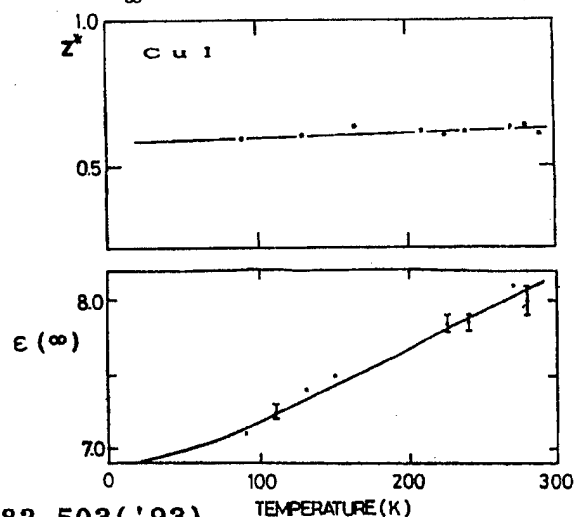


Fig.1

$\epsilon_\infty$  and  $Z^*$  values  
of CuI as function  
of temperature.

## References

- [1] K.Wakamura, Solids State Commun. 82, 503 ('93).
- [2] K.Wakamura, J. Phys. Chem. Solids 59, 591 ('98).
- [3] K.Wakamura, Phys. Rev B 56, 11539 ('97)
- [4] K.Wakamura, unpublished.
- [5] J.N.Plendel et al., Appl. Opt. 5, 397 ('66).
- [6] P.Bruesch et al, Phys. Stat. Sol. a 31, 217 ('75)

# VIBRATIONAL SPECTRA AND PHASE TRANSITIONS OF Cu<sub>8</sub>MX<sub>6</sub> (M=Si, Ge; X=S, Se) AND Cu<sub>4</sub>GeS<sub>4</sub>

M. Ishii<sup>1</sup>, M. Onoda<sup>1</sup>, Xue-an Chen<sup>1</sup>, H. Wada<sup>1</sup> and K. Shibata<sup>2</sup>

<sup>1</sup>National Institute for Research in Inorganic Materials,  
1-1 Namiki, Tsukuba-shi, Ibaraki, 305-0044, Japan

<sup>2</sup>Department of Technology Development, Japan Science and Technology  
Corporation, 4-1-8, Honmachi, Kawaguchi-shi, Saitama, 332-0012, Japan

As for each of Cu<sub>8</sub>MX<sub>6</sub> (M=Si, Ge; X=S, Se) and Cu<sub>4</sub>GeS<sub>4</sub>, one or two phase transitions take place in the temperature range from 320K to 360K [1, 2, 3]. Infrared absorption spectra of the high- and low-temperature phases of these compounds have been measured mainly in the M-X (M=Si, Ge; X=S, Se) stretching regions of the nearly isolated MX<sub>4</sub> units. The frequencies and the relative intensities of the infrared active modes of these compounds have been calculated based on the simple lattice dynamical models and the relations between the phase transitions and the vibrational spectra have been studied.

In the high- and low-temperature phases, each of Cu<sub>8</sub>SiS<sub>6</sub>, Cu<sub>8</sub>SiSe<sub>6</sub> and Cu<sub>8</sub>GeS<sub>6</sub> crystallizes in the cubic and orthorhombic space groups, respectively [1, 4]. The temperature dependences of the spectra of these compounds have been explained based on the structure variations. The half widths of the bands due to  $\nu_3(\text{MX}_4)$  type modes observed in the high temperature phase are two or three times as large as those observed in the low temperature phase for each compound. The results suggest that the copper atoms are disordered and ionic conduction caused by the copper ions are expected in the high temperature phases.

Cu<sub>8</sub>GeSe<sub>6</sub> crystallizes in the hexagonal space groups in both high- and low-temperature phases (T<sub>c</sub>: 328K). Three (P6<sub>3</sub>mc, z=2) and seven (P6<sub>3</sub>cm, z=6) infrared active Ge-Se stretching modes are expected for high- and low-temperature phases, respectively. As shown in Fig. 1, strong peaks observed at about 300 cm<sup>-1</sup> in the spectra of both high- and low-temperature phases, are assigned to  $\nu_3(\text{GeSe}_4)$  type modes, and the results of the calculation correspond satisfactorily with the observed ones.

The features of the infrared spectra due to Ge-S stretching modes of Cu<sub>4</sub>GeS<sub>4</sub> have also varied discontinuously at the transition temperature.

**References:** [1] W. F. Kuhs, et al., Mater. Res. Bull., 14, 241 (1979). [2] S. Jaulmes et al., Acta Crystallogr. C47, 1799 (1991). [3] Xue-an Chen et al., J. Solid State Chem. (to be published). [4] M. Ishii et al., Solid State Ionics (in press).

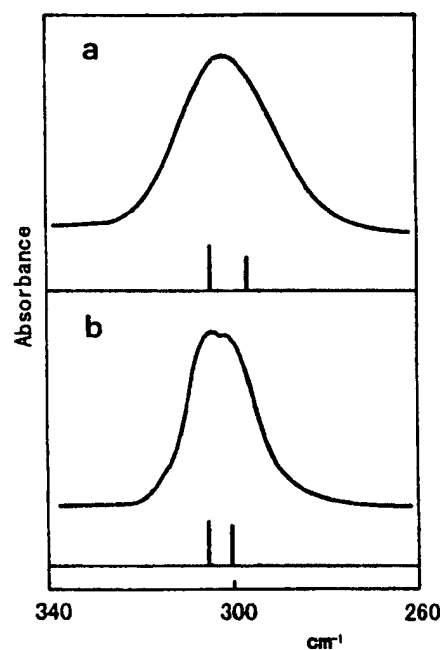


Fig. 1. Infrared spectra of Cu<sub>8</sub>GeSe<sub>6</sub> at 350K (a) and 300K (b). Calculated frequencies and relative intensities are denoted by vertical bars.

# SPECTRAL HOLE-BURNING IN $\text{Eu}^{3+}$ ION EXCHANGED $\beta''$ -ALUMINA

Takeshi HATTORI, Ryotaro YAGI, Kazuhiro ASO and Mareo ISHIGAME

Research Institute for Scientific Measurements, Tohoku University

Katahira, Sendai, 980-8577, JAPAN

Spectral hole-burning, especially persistent one, spectroscopy has been established as a powerful tool to investigate the structural and electronic properties of disordered materials[1]. Superionic conductors are prototype of the disordered materials. Therefore, spectral hole-burning spectroscopy is one of the useful methods for analysis of the disorder natures of superionic conductors. The elemental migration process of proton in perovskite-type proton conducting oxides was discussed first by one of the authors of this work (M.I.)[2].

In this work, persistent spectral hole-burning in  $\beta''$ -alumina, which is one of the typical superionic conductors and belong to the family of  $\beta$ -alumina-type superionic conductors, is studied in order to identify hole-burning spectra and then to get an information about the conduction mechanism, namely, elementary migration process of conduction ion in  $\beta''$ -alumina.

The transition between the energy levels of  $\text{Eu}^{3+}$  ions, mainly  $F_0 \rightarrow {}^5D_0$  transition, which were exchanged in the sample was used for detection of hole spectra.

Two types of holes in  $\text{Eu}^{3+}$  ions exchanged Na  $\beta''$ -alumina at different burning wavelengths were observed at 10K as shown in Fig. 1: One is a transient hole which is overlapped a persistent hole and the other pure persistent one. This pure persistent hole can be burnt up to 110 K. Moreover, this hole with the same shape was also observed after some hours from the switch-off the burning. FWHM of this band at 4.2 K is 0.13 GHz, which is broader than that burned at 577.6 nm. It is concluded from these experimental results that this persistent hole observed is caused by light-induced local-structure change surrounding  $\text{Eu}^{3+}$  ions. The barrier height (potential energy) for the light-induced local motion of ions, which related to the local-structure change surrounding  $\text{Eu}^{3+}$  ions, was determined from the analysis of thermal decay-profile of the persistent hole, which was obtained from the so-called temperature cycling experiment. Two potential energies with Gaussian distribution were obtained. Two potential energies with Gaussian distribution for the light-induced local motion of ions surrounding  $\text{Eu}^{3+}$  ions may be concerned in the elementary migration of the conduction ions in Na  $\beta''$ -alumina.

[1] *Persistent Spectral Hole-Burning: Science and*

*Applications*, ed. W.E. Morener, (Springer-Verlag, Berlin, 1988).

[2] S. Matsuo, H. Yugami, and M. Ishigame, *Solid State Ionics: New Developments*, ed. B.V.R.Chowdari et al (World Scientific, Singapore, 1996) p.277.

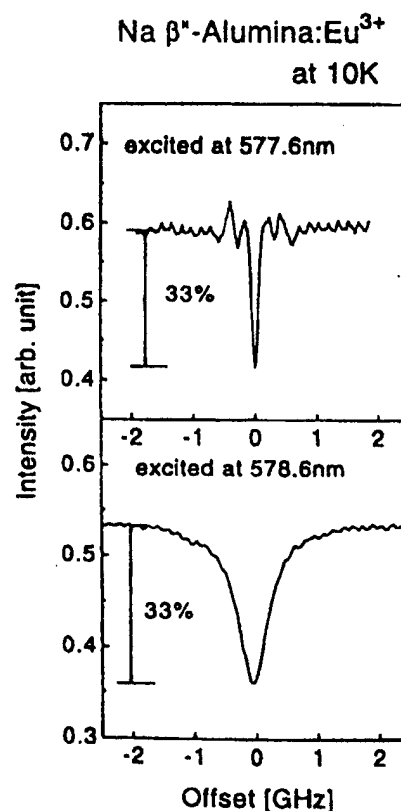


Fig. 1 Hole spectra burned at 577.6 nm and 578.6 nm in  $\text{Eu}^{3+}$  ions exchanged Na  $\beta''$ -alumina.



## DIVALENT MAGNESIUM ION CONDUCTION IN THE PHOSPHATE BASED COMPOSITES

N. Imanaka, Y. Okazaki, and G. Adachi

Department of Applied Chemistry, Faculty of engineering, Osaka University,  
2-1 Yamadaoka, Suita, Osaka 565-0871 Japan

Solid electrolytes with divalent anion, oxide ion( $O^{2-}$ ), have been commercially applied as the main constituent of oxygen sensors in various industrial fields. In contrast, for divalent cations,  $Mg^{2+}$ , alkaline earth cations such as  $Ca^{2+}$ ,  $Sr^{2+}$ ,  $Ba^{2+}$  and transition metal ions like  $Cd^{2+}$ ,  $Zn^{2+}$ ,  $Mn^{2+}$  with  $\beta$ "-alumina type structure, have been reported to become ion conductors. Among various types of divalent cations, magnesium ion has such an advantage of holding a relatively small ionic size and stably maintaining the divalent state. In addition, its metal state is appreciably stable compared with the alkali metal series. However, the  $Mg^{2+}$  ion conductivity of the reported electrolytes is too low to apply as practical electrolytes. In addition to the ion conducting properties, the electrolyte materials should be enduring in various atmospheres. By the consideration of the above mentioned points, the phosphate based compounds with divalent magnesium ions as a mobile species were selected as the candidates for the practical solid electrolytes and its  $Mg^{2+}$  ion conducting characteristics were investigated.

In this study, a sophisticated synthesis technique was applied to obtain the  $Mg^{2+}$  ion conducting solid composites in such a way to simultaneously disperse the secondary insulating phase during the preparation process by heating various types of the starting material mixture with a nonstoichiometric ratio.

The mixture of ammonium hydrogen phosphate, magnesium hydrogen phosphate, and zirconium oxide nitrate was heated initially at 300°C for 5 h and then 1200°C for 12 h in air. By this treatment, zirconium oxide phosphate appears and is microscopically dispersed as a secondary phase and form a composite. The composite powder was pressed and reheated at 1200°C for 12 h in air.

The various types of the composite with the different  $Mg_{1+x}Zr_4P_6O_{24+x}$  and zirconium oxide phosphate( $Zr_2O(PO_4)_2$ ) ratio were obtained. By reducing the amount of both ammonium hydrogen phosphate and zirconium oxide nitrate from the stoichiometric ratio of the  $MgZr_4P_6O_{24}$  single phase preparation reported, the intensities of  $Zr_2O(PO_4)_2$  increased. The conductivity monotonously increased with the increase of the  $Zr_2O(PO_4)_2$  content in the composite and a maximum value( $6.92 \times 10^{-3} \Omega^{-1} \cdot cm^{-1}$  at 800°C) was obtained for the  $Mg_{1+x}Zr_4P_6O_{24+x} + xZr_2O(PO_4)_2$ ( $X=0.4$ ) composite. Further  $Zr_2O(PO_4)_2$  deposition deteriorates its conducting characteristics due to the increase of the insulating volume in the composite.

Figure 1 shows the temperature dependencies of the electrical conductivity for the composite of  $Mg_{1+x}Zr_4P_6O_{24+x} + xZr_2O(PO_4)_2$ ( $x=0.4$ ), which shows the highest conductivity among the composites series. The electrical conductivity results for the  $Mg^{2+}$  ion conductors reported so far are also plotted in the same figure. The electrical conductivity of the present composite shows 10 times higher compared with the single phase reported, in the whole temperature range examined. Even compared to the  $Mg_{1.15}Zr_4P_{5.7}Si_{0.3}O_{24}$  solid electrolyte, which has been described to hold the highest  $Mg^{2+}$  ion conductivity in the phosphate based solid electrolytes reported so far, the conductivity of the present composite prepared by a nonstoichiometric mixing method, is 2.3 times still higher. The conductivity of  $Zr_2O(PO_4)_2$  was also examined and depicted in the same figure. The conductivity of the oxide phosphate is considerably lower compared with that of the composite and this explicitly means that the  $Zr_2O(PO_4)_2$  particles appear as insulating secondary

grains in the composite. The formation of the insulating  $\text{Zr}_2\text{O}(\text{PO}_4)_2$  secondary phase in the composite contributes considerably to increasing the conductivity of the composite and the composite was found to show the highest conductivity among the  $\text{Mg}^{2+}$  ion conductors prepared.

An abrupt decrease in the  $\sigma_{\text{dc}}/\sigma_{\text{ac}}$  ratio was equivalently observed in both oxygen ( $\text{Po}_2$ :  $10^5$  Pa) and helium ( $\text{Po}_2$ : 4 Pa) atmosphere by the measurements of the time dependencies of the ratio. Here,  $\sigma_{\text{dc}}$  and  $\sigma_{\text{ac}}$  denote the conductivity obtained by dc and by ac measurements, respectively. The same polarizing behavior clearly excludes the possibility of oxide ion conduction in the composites. In addition, the considerable polarization phenomenon indicates that the mobile species in the composite are neither electrons nor holes.

In order to identify the mobile species in the composite, the dc electrolysis of the composite sample was carried out with two platinum electrodes. A lot of round shape cluster deposits were recognized on the cathodic surface where the Pt electrode was kept in contact. From the EPMA spot analysis (Fig. 2), the elements identified were Mg, P, Zr and the ratio of  $\text{Mg}/(\text{P}+\text{Zr})$  and  $\text{P}/\text{Zr}$  are 1.44 and 3.36, respectively. In the bulk composite before the electrolysis, the observed ratios of  $\text{Mg}/(\text{P}+\text{Zr})$  and  $\text{Mg}/\text{Zr}$  were 0.12 and 1.41, respectively. The appreciable high amount of Mg segregation, that is, 12.4 times higher in the  $\text{Mg}/(\text{P}+\text{Zr})$  ratio is observed, while the enhancement of the  $\text{P}/\text{Zr}$  peak ratio is only 2.38 times on the cathodic surface. These phenomena definitely indicate that the predominant segregation species is magnesium element.

From the above mentioned polarization and electrolysis results, the predominant mobile species in the  $\text{Mg}_{1+x}\text{Zr}_4\text{P}_6\text{O}_{24+x} + x\text{Zr}_2\text{O}(\text{PO}_4)_2$  ( $x=0.4$ ) composite is explicitly determined to be the divalent magnesium cation in the composite and the conductivity enhancement is predominantly attributed to the microscopic dispersion of the secondary  $\text{Zr}_2\text{O}(\text{PO}_4)_2$  phase in the composite.

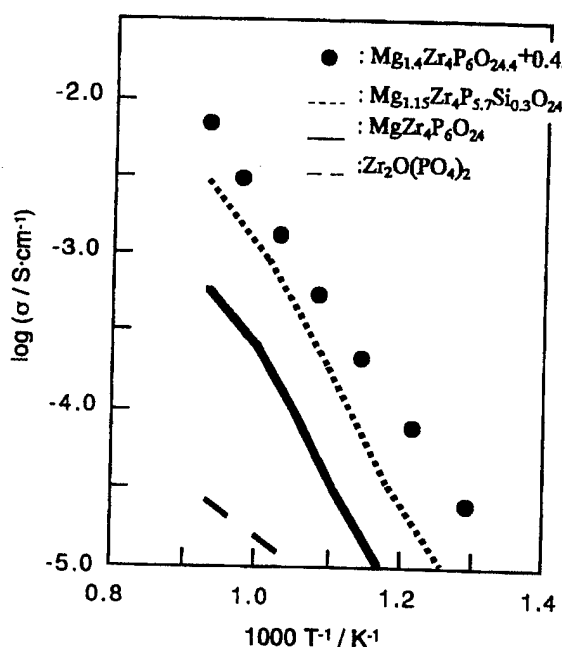


Fig.1 Temperature dependencies of the electrical conductivity for  $\text{Mg}_{1.4}\text{Zr}_4\text{P}_6\text{O}_{24.4} + 0.4\text{Zr}_2\text{O}(\text{PO}_4)_2$  composites.

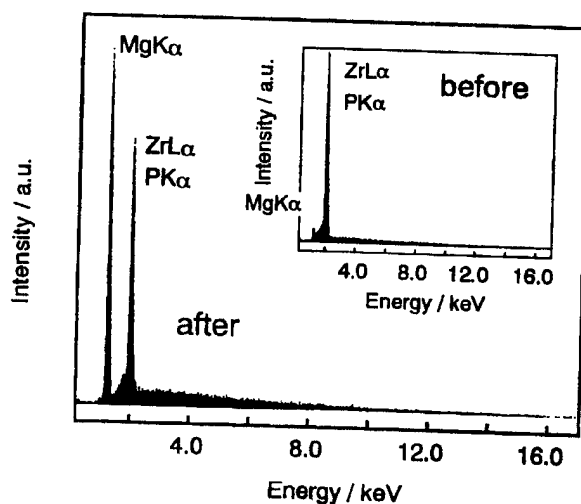


Fig.2 EPMA spot analysis result of the deposite on the cathodic surface after electrolysis.

## INFLUENCE OF IONS AND MOLECULES ON SINGLE CRYSTAL ZEOLITE CONDUCTIVITY UNDER IN SITU CONDITIONS

O. Schäf<sup>1,3</sup>, H. Ghobarkar<sup>2</sup>, W.F. Zhang<sup>1</sup> and U. Guth<sup>1,3</sup>

<sup>1</sup> Sensor Research Center, Greifswald, Germany <sup>2</sup> Free University of Berlin, Institute for Mineralogy, Berlin, Germany <sup>3</sup> University of Greifswald, Institute of Chemistry and Biochemistry, Greifswald, Germany.

Zeolites are materials with structure inherent nanoporous channels and cage systems. Within the class of zeolites, some aluminosilicate based structure types show ion conducting properties which make them interesting as solid electrolytes. Zeolites are also commonly known as materials with specific catalytic and sorptive properties. Therefore, the development of a chemical sensor system based on the combination of these different zeolite properties is interesting with respect to potential application fields.

Earlier investigations showed the conductivity of polycrystalline zeolite materials [1-4]. Results on conductivity measurements of both, polycrystalline specimens and single crystalline materials [5-8] however made clear that only with single crystal material under equilibrium water vapor pressure conditions reproducible results can be obtained. On the other hand, the maximum catalytic activity as well as the "activation" of the zeolite lattice for sorption purposes takes place at temperatures of about 300°C, temperatures where an irreversible alteration of almost all zeolite lattices has occurred [9]. Therefore, basic investigations for possible sensor applications of zeolites have been done in a temperature interval between 60°C and 105°C using single crystal zeolites.

The results obtained show that the interaction of zeolites single crystals under in situ conditions (with equilibrium water content) with water and organic molecules is different from the behavior of polycrystalline materials in the high temperature activated state as water molecules are still present in the cavity system interacting with cations as well as with foreign molecules accessing this system. The reversible expansion behavior of polycrystalline zeolites at low temperatures makes it difficult to obtain reproducible conductivity results.

Experiments made with single crystal zeolites in the gas phase have been compared to equilibrium measurements in aqueous solutions under variation of ion concentration in both, solution and cavity system of zeolite. The results are discussed based on changes in activation energy in the cavity system by the change in occupation, dielectric constant and kinetic diameter of the interacting species.

- [1] E. Krogh Andersen, I.G. Krogh Andersen and E. Skou in: Proton Conductors, P. Columban (ed.), Cambridge University Press, Cambridge (1992) 210-223
- [2] K. Alberti, F. Fetting, Sensors and Actuators B 21 (1994) 39-50
- [3] P. Kurzweil, W. Maunz, C. Plog, Sensors and Actuators B 24-25 (1995) 653-656
- [4] C. Plog, W. Maunz, P. Kurzweil, E. Obermeier, C. Scheibe, Sensors and Actuators B 24-25 (1995) 403-406
- [5] O. Schäf, H. Ghobarkar and U. Guth: Ionics 3 (1997) 282-288

- [6] O. Schäf, H. Ghobarkar and U. Guth in: Proceedings 3<sup>rd</sup> Dresdener Sensor-Symposium, 8.-10.12. 1997, Dresden-Radebeul, Dresdner Beiträge zur Sensorik Bd. 5, 43-46
- [7] O. Schäf, H. Ghobarkar and U. Guth:: Polycrystalline Zeolite Layers for Low Temperature Gas Sensor Applications. Paper presented at the 10<sup>th</sup> German Zeolite-Conference, Bremen 9.-11. 3. 1998, Abstracts KV6
- [8] O. Schäf, H. Ghobarkar and U. Guth: Effect of Water and Combustibles on Single Crystal Zeolite Conductivity. Paper presented at the 5<sup>th</sup> Euroconference on Solid State Ionics, Malaga, Spain 13.-19. 9. 1998, to be published in Ionics
- [9] G. Gottardi, E. Galli: Natural Zeolites. Springer Verlag, Heidelberg, N.Y., Tokyo (1985)

# MULTIPLE-TWINNED CRYSTAL OF THE ROOM-TEMPERATURE PHASE OF $\text{Cu}_8\text{GeS}_6$

Mitsuko ONODA, Xue-an CHEN, Motohiko ISHII & Hiroaki WADA

*National Institute for Researches in Inorganic Materials*

*Namiki 1-1, Tsukuba, Ibaraki, 305-0044, Japan*

The structure of the orthorhombic room-temperature phase of  $\text{Cu}_8\text{GeS}_6$  (phase II) has been refined successively on the basis of X-ray diffraction data from a 12-fold twinned crystal applying a six-dimensional twin refinement technique. The symmetry operations and the unit cell of the pseudo-cubic expression are  $(0,0,0; 1/2, 1/2, 0) + x, y, z; y, x, z; 1/4-x, 3/4-y, 1/2+z; 3/4-y, 1/4-x, 1/2+z; a=b=9.907\text{\AA}, c=9.870\text{\AA}, \alpha=\beta=90^\circ, \gamma=90.64^\circ$ , whose standard settings are  $\text{Pmn}2_1$ ;  $A=7.045, B=6.966, C=9.870\text{\AA}$ . The bounded projections along pseudo-cubic  $[111]$  of some twin domains adopted in our refinement are shown in Fig. 1. Among the twin domains 1-6, the  $\text{GeS}_6$  frameworks can be superposed to each other in principle, and only Cu-Cu network directions differ. The minor twin domains 7-12 are respectively related to the major domains 1-6 by a two-fold rotation on  $[111]$ . The high-temperature phase (phase I) of  $\text{Cu}_8\text{GeS}_6$  is considered to crystallize in the same type as  $\text{Ag}_8\text{GeTe}_6(\gamma)$ . Chalcogen atoms pattern two kinds of almost regular tetrahedral sites, one for Ge atoms and the other empty, and four kinds of distorted tetrahedrons. In  $\text{Cu}_8\text{GeS}_6$  I, Cu ions are expected to distribute statistically over many sites in S-S distorted tetrahedrons and S-S triangular faces. On cooling through the phase-transition temperature, the crystal can be converted into a multiple twin of phase II. Cu ions are transferred to five kinds of independent sites from the statistical distribution state, while Ge and S arrangements are essentially retained.

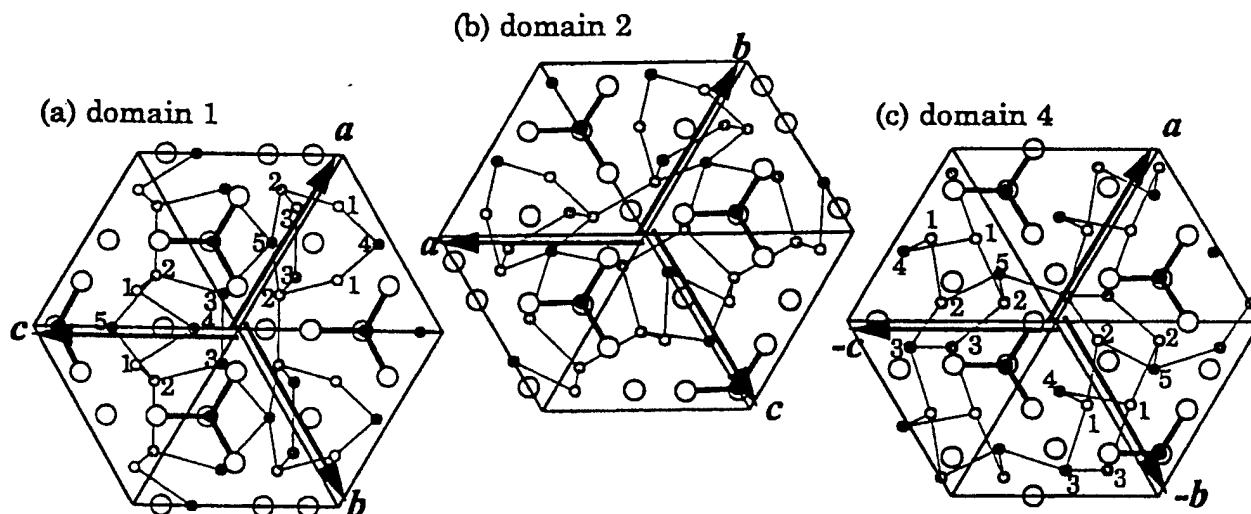


Fig. 1. Bounded projection ( $0.77 < x+y+z < 1.1$ ) of  $\text{Cu}_8\text{GeS}_6$  II along the pseudo-cubic  $[111]$ . (a), (b), (c) correspond to twin domains 1, 2, 4 respectively. Ge ions are joined with thick rods to the nearest S ions, and Cu-Cu distances less than  $2.9\text{\AA}$  are shown by thin rods. Small numbers 1, 2...5 indicate Cu1, Cu2...Cu5 respectively.

# CHEMICAL BOND AND IONIC TRANSPORT

## IN THE $\text{CuCr}_{1-x}\text{V}_x\text{S}_2$ ( $0 \leq x \leq 0.3$ ) COMPOUNDS

R.F.Almukhametov, R.A.Yakshibayev, E.V.Gabitov and A.R.Abdullin.

Department of Physics, Bashkir State University,

450074, Ufa, ul.Frunze 32, Russia

The chromium dichalcogenides  $\text{MCrX}_2$  ( $\text{M}=\text{Cu}, \text{Ag}; \text{X}=\text{S}, \text{Se}$ ) have the X-Cr-X-M-X-Cr-X type layered structure and belong to the hexagonal system. The strong bonds within the X-Cr-X triple layers and the relatively weak bonds in the gaps between triple layers are observed. Therefore Cu and Ag atoms display a high mobility in the interlayer gaps. The ionic transport parameters depending on chemical bond nature are of great interest. Samples of composition  $\text{CuCr}_{1-x}\text{V}_x\text{S}_2$  ( $x = 0; 0.1; 0.15; 0.2; 0.25; 0.3$ ) were synthesized by the solid state reaction method in quartz tubes at 950 °C. The X-ray analysis showed that the  $\text{CuCr}_{1-x}\text{V}_x\text{S}_2$  samples are single phase at  $x \leq 0.15$ . At  $x \geq 0.2$  a small amount of the outside phase  $\text{Cu}_3\text{VS}_4$  appears. The  $a$  and  $c$  unit cell parameters weakly change on linear law with increase of  $x$  in  $\text{CuCr}_{1-x}\text{V}_x\text{S}_2$ . This happens because of the similarity of the atomic sizes and testifies to the isomorphic substitution of Cr by V.

The magnetic susceptibility was measured from 20 to 400 °C and follows the Curie-Weiss law. The effective magnetic moments were determined from the susceptibility measurements. In order to study the chemical bond character, the effective magnetic moments for  $\text{CuCr}_{1-x}\text{V}_x\text{S}_2$  were calculated. The orbital magnetic moments were taken to be quenched by the crystal field; this is correct for the atoms included in  $\text{CuCr}_{1-x}\text{V}_x\text{S}_2$ . Curve 1 (fig1) was calculated when the Cr and V

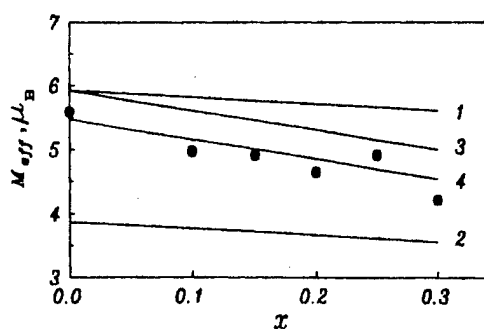


Fig.1 Experimental and calculated (lines) effective magnetic moments as a function of V-content in  $\text{CuCr}_{1-x}\text{V}_x\text{S}_2$

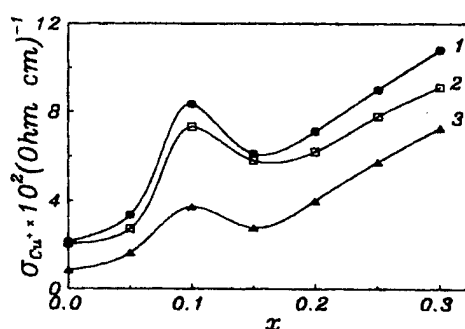


Fig.2 Compositional dependence of the ionic conductivity for  $\text{CuCr}_{1-x}\text{V}_x\text{S}_2$  (1)  $T=415$  °C; (2)  $T=390$  °C; (3)  $T=360$  °C

atoms give one valence-electron to the 3p shell of each S atom. One valence-electron of Cu transfers into the 3p shell of S. The curve 2 shows the magnetic moment versus composition when three Cr and V valence-electrons transfer into the 3p shell of S (1-electron - to the first S atom and

2-electrons - to the second). Curve 3 shows the effective magnetic moments when two Cr valence-electrons and two V valence-electrons transfer into the 3p shell of S. The good agreement between the calculated and experimental effective magnetic moments was observed when two Cr valence-electrons and three V valence-electrons transfer into the 3p shell of S. About 10 percent of Cr transfers its 3 valence-electrons to the 3p shell of S also (curve 4).

According to the magnetic study results, we think that in  $\text{CuCr}_{1-x}\text{V}_x\text{S}_2$  compounds V exhibits a high oxidation state than Cr. This agrees with the low electronegativity of V comparatively to Cr. The sulfur atoms, disposed on the planes above and below the Cu-plane, display different states of oxidation,  $\text{S}^{1-}$  and  $\text{S}^{2-}$ . When Cr is substituted by V the oxidation degree of these atoms becomes equal.

The ionic conductivity was measured from 100 to 450°C. The temperature dependences  $\ln(\sigma_{\text{Cu}} + T) = f(1/T)$  display two straight-line branches. The activation energy values were determined from the slope of these curves.

The activation energy for the low-temperature phase  $\text{CuCr}_{1-x}\text{V}_x\text{S}_2$  displays relatively high values. This is caused by the fact that it includes the activation energy of migration and the energy of defect formation in the Cu-sublattice. The high-temperature activation energy shows low values, that is explained by including the activation energy of the migration only. This is confirmed the following: the high-temperature activation energy values are comparable with the heats of  $\text{Cu}^+$  transport, obtained from our Seebeck effect measurements.

The high-temperature activation energy shows a weak compositional dependence. We believe that this is connected with slight changing of the potential barrier nature when Cr is substituted by V. On the contrary, the low-temperature activation energy shows a strong compositional dependence, indicating a considerable influence of the V-substitution on the defect formation energy in the Cu - sublattice.

The compositional dependences of the ionic conductivity display a complicated nature (fig.2). The anomaly of  $\sigma_{\text{Cu}}(x)$  at  $x \sim 0.10 \div 0.15$  may not be related to the appearance of slight  $\text{Cu}_3\text{VS}_4$  phase. We connect it with the redistribution of the Cu-atoms. The qualitative explanation of the growth of the Cu-cationic conductivity with Cr substitution by V may be given in the following way. The oxidation degree of the sulfur atoms, disposed on the planes above and below the Cu-plane, becomes equal when Cr is substituted by V. A simple calculation with the consideration of the coulomb interaction of the  $\text{Cu}^+$  ions with the nearest-neighbor atoms only shows that the activation energy values must decrease when Cr is substituted by V.

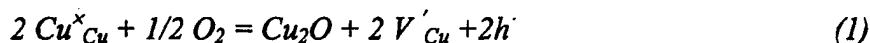
# FORMATION AND TRANSPORT OF MINORITY CARRIERS IN THE SOLID ELECTROLYTE $RbCu_4Cl_3I_2$ .

Gennady I. OSTAPENKO, *Institute of Radio Engineering and Electronics of Russian Academy of Sciences, Ulyanovsk Branch; 48, Goncharov str., Ulyanovsk 432011, Russia;*  
Fax: +7-8422-314504; E-mail: ufire@MV.ru.

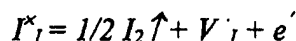
Lyudmila G. VESELOVA, *Ulyanovsk State Agricultural Academy;*  
1, Novy Venets str., Ulyanovsk 432601, Russia.

A superionic conductor  $RbCu_4Cl_3I_2$  have a conductivity of  $0,4 \text{ S} \cdot \text{cm}^{-1}$  due to a high structural disorder cationic sublattice of  $Cu^+$  [1,2].

During preparation of  $RbCu_4Cl_3I_2$ , including melting and sealing [1,2], because of chemical instability a portion of  $Cu^+$  ions is oxidized to  $Cu^{2+}$  ions. From the crystal chemistry position this reaction should be written as follows:



$Cu^{2+}$  ion can be represented as  $Cu^+$  ion with an electron hole  $h^{\cdot}$  localized on it. A competing reaction reducing the number of holes can be evaporation of iodine:



Excessive electrons  $e^{\cdot}$  can recombine with the holes forming according to the reaction (1). After finishing of preparation the number of vacancies and electron defects is "quenched" [3] and determines the type of minority carrier conduction. Obviously, the reaction (1) prevails because  $RbCu_4Cl_3I_2$  have hole conduction. The increase of vacancy concentrations is negligible and doesn't change the value of superionic conductivity. High spread of values of hole conductivity of  $RbCu_4Cl_3I_2$  [1,4] is caused by some differences in conditions of preparation.

A cell:



have OCV  $\varphi_0$  about  $0,5 \text{ V}$ , due to different concentration of  $Cu^{2+}$  ions near copper and vitreous carbon. Concentration of  $Cu^{2+}$  ions (or holes) near copper  $[h]_{Cu}$  is determined by an equilibrium of:



chemical reaction. A calculation by thermodynamic data for this reaction [5], gives  $[h]_{Cu} = 2.5 \cdot 10^{11} \text{ cm}^{-3}$ . Taking (2) as a electrochemical concentration cell it is possible to obtain the number of holes near vitreous carbon  $[h]_C = 1.2 \cdot 10^{20} \text{ cm}^{-3}$  according to Nernst equation:

$$\varphi_0 = (kT/e) \ln ([h]_C / [h]_{Cu})$$

This concentration corresponds to  $Cu^{2+}$  ions content about one percent as to the total copper in  $RbCu_4Cl_3I_2$ .

Wagner reports [6] that in the range of voltages  $0 \dots \varphi_0$  the ion conduction in the cell of (2) - type is blocked. Therefore, the horizontal section of volt - ampere characteristic of electrodes (Fig.) represents a limiting diffusion hole current  $i_{lim}$ , equal to  $3 \cdot 10^{-8} \text{ A} \cdot \text{cm}^{-2}$ .



A hole conductivity :

$$\sigma_h = eLi_{lim}/kT$$

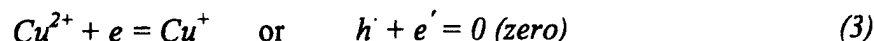
is  $1.2 \cdot 10^{-7} \text{ S} \cdot \text{cm}^{-1}$ , where  $L$  is a thickness of  $\text{RbCu}_4\text{Cl}_3\text{I}_2$  layer in the cell (2), equal to 1 mm.

Assuming that at such negligible hole current the concentration of holes in  $\text{RbCu}_4\text{Cl}_3\text{I}_2$  near electrodes changes slightly, the diffusion coefficient of holes:

$$D = \sigma_h(kT/e^2) (1/[h]_C - [h]_{Cu})$$

will be  $1.6 \cdot 10^{-10} \text{ cm}^2 \cdot \text{s}^{-1}$ . This value coincides well with  $D$  for the other  $\text{Cu}^+$  solid electrolyte [7].

During the flowing of the hole current on the electrodes of the cell (2) the reaction takes place:



from the left to the right on the vitreous carbon electrode and from the right to the left on copper one. In the case a open circuit the electrode reaction (3) is in a dynamic equilibrium: the number of holes  $n_o$ , generating on the electrode is equal to the number of holes  $n_o$ , associating with the electrons. In the given case the equilibrium exchange flux:

$$n_o = (kT/e^2)(\partial i / \partial \varphi)_{\varphi^{\circ}_{Cu} \text{ or } C}$$

(where  $\varphi^{\circ}_{Cu}$  or  $C$  is a nulling current voltage for copper and carbon electrodes (Fig)) for copper electrode is of the order  $10^{12} \text{ s}^{-1} \cdot \text{cm}^{-2}$  and for vitreous carbon -  $10^{11} \text{ s}^{-1} \cdot \text{cm}^{-2}$ .

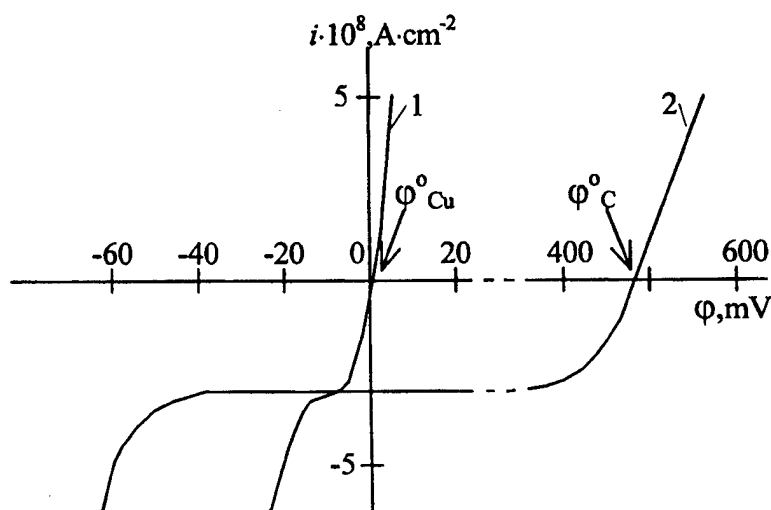


Fig. Volt - ampere characteristic of copper (1) and vitreous carbon (2) electrodes relative to copper probe in  $\text{RbCu}_4\text{Cl}_3\text{I}_2$ .

#### REFERENCES

1. T. Takahashi, O. Yamamoto, H. Yamada and S. Hayashi, *J. Electrochem. Soc.* 126, 1654 (1979).
2. S. Geller, J. Akridge and S. Wilber, *Phys. Rev. B* 19, 5396 (1979).
3. A. Shmidt and J. Bazan, *Electrochim. Acta* 31, 227 (1986).
4. C. Chaney, D. Shriver and D. Whitmore, *Solid State Ionics* 5, 505 (1986).
5. A. Mikhailova and E. Ukshe, *Electrochemistry USSR* 22, 702 (1986).
6. C. Wagner, *Z. Elektrochem.* 60, 4 (1956).
7. R. Armstrong, T. Dickinson and K. Taylor, *J. Electroanal. Chem.* 64, 155 (1975).

## PHASE TRANSITION OF $\text{CuBrTe}_x\text{Se}_{1-x}$

Masaji Arai<sup>a</sup>, Takashi Sakuma<sup>a</sup>, Haruyuki Takahashi<sup>b</sup>  
and Yoshito Onoda<sup>c</sup>

<sup>a</sup> Department of Physics, Faculty of Science, Ibaraki University,  
Mito 310-8512, Japan

<sup>b</sup> Applied Physics Group, Faculty of Engineering, Ibaraki University,  
Hitachi 316-8511, Japan

<sup>c</sup> National Institute for Research in Inorganic Materials,  
Tsukuba 305-0044, Japan

CuBrTe exhibits essentially ionic conductivity that may be two orders of magnitude greater than that of the parent copper halide at room temperature [1]. Structural phase transitions at 230 K ( $\gamma$ - $\beta$ ) and 351 K ( $\beta$ - $\alpha$ ) were confirmed in CuBrTe [2]. One main characteristic of the crystal structure of  $\alpha$ -CuBrTe is the infinite fourfold tellurium helices arranged parallel to the crystallographic  $c$ -axis.

The phase transitions of tellurium substituted CuBrTe,  $\text{CuBrTe}_x\text{Se}_{1-x}$  solid solutions, were investigated by specific heat and X-ray diffraction measurements in the temperature range between 10 K and 523 K. Te atoms are substituted by Se atoms in the range of  $0.7 \leq x \leq 1$ . An anomaly with the heat of transition about 100 cal/mol was observed in the  $\beta$ - $\alpha$  phase transition in the range of  $0.7 \leq x \leq 1$ . The existence of the low temperature  $\gamma$ -phase was confirmed only in the range of  $0.9 \leq x \leq 1$ . The strong X-ray reflection around  $2\theta = 44^\circ$  in the  $\beta$ -phase split into three lines in the  $\gamma$ -phase.

[1] U. V. Alpen, J. Fenner, J. D. Marcoll and A. Rabenau, *Electrochimica Acta*, **22**, 801 (1977).

[2] T. Sakuma, T. Kaneko, H. Takahashi and K. Honma, *J. Phys. Soc. Japan* **60**, 1136 (1991).

## ON THE ELECTRICAL CONDUCTIVITY AND DEFECT STRUCTURE OF COPPER DOPED NICKELOXIDE

Th. Buhrmester, F. Haaß, M. Martin

Institute of Physical Chemistry, Darmstadt University of Technology  
Petersenstraße 20, 64287 Darmstadt, Germany

For the investigation of the defect structure and to evaluate a valid conductivity model of copper doped Nickeloxide  $(\text{Ni}_{1-x}\text{Cu}_x)_{1-\delta}\text{O}$  conductivity measurements were performed. Therefore it was necessary to prepare samples of high density and of high purity. From literature [1] it is known that the single phase region of this Fm3m structured oxide exists between  $x=0$  and  $x=0.33$  in air at  $T=1273$  K.

The preparation we chose was a modified Pechini [2,3] method. This precursor based method starts with aqueous solutions of the cation nitrates and citric acid, leading to a homogeneous product after combustion. The following sintering step of the preparation lead to the desired oxide.

Impedance spectroscopy was applied as a probe for the electronic defects in this p-type semiconductor. The conductivity  $\sigma$  was extracted from the frequency independent part of the impedance spectrum. It was found that conductivity is increasing with temperature and oxygen partial pressure  $a_{\text{O}_2}$ . Surprisingly the conductivity exhibits a maximum at a dopant level  $x$  of approximately 0.02. The exponent of the  $a_{\text{O}_2}$  dependence was found to be approximately 1/5.

To model this behaviour it is necessary to develop a defect structure model of the system, which is introduced in this work. A simple model, assuming an electron hole jump mechanism, consisting of  $\text{Ni}_{\text{Ni}}^x, \text{Ni}_{\text{Ni}}^\bullet, \text{Cu}_{\text{Ni}}^x, \text{Cu}_{\text{Ni}}^\bullet, \text{Cu}_{\text{Ni}}^{\text{I}}, V_{\text{Ni}}^{\text{II}}, \text{Cu}_{\text{Ni}}^x, \{\text{Cu}_{\text{Ni}} / \text{Cu}_{\text{Ni}}\}^x, \{\text{Cu}_{\text{Ni}} / \text{Cu}_{\text{Ni}}\}^\bullet$  can describe the observed maximum in the experimentally obtained conductivity curve.

Further information about the dominant occupation site of copper can be deduced from x-ray absorption measurements. The K-edge x-ray absorption near edge structure (XANES) of the matrix cations was compared with those of the dopant ions. The results of the experiments and the predictions for the conductivity model will be discussed.

All related experiments were performed in situ, varying either the oxygen activity or the temperature for different dopant levels  $x$ .

[1] N.G. Schmahl, F. Müller, Z. anorg. allgemein. Chem. **332** 217 (1964)

[2] M. P. Pechini, U.S. Patent Number 3 330 697, 11. July 1967

[3] Lone-Wen Tai, P. A. Lessing, J Mat. Res., **7** No.2 (1992)

## A NEW TRIVALENT CATIONIC CONDUCTING SOLID ELECTROLYTE WITH NASICON TYPE STRUCTURE

S. Tamura, N. Imanaka, and G. Adachi

Department of Applied Chemistry, Faculty of Engineering, Osaka University, 2-1 Yamadaoka,  
Suita, Osaka 565-0871, Japan

The  $R_2(WO_4)_3$  ( $R$  : Al, Sc, Lu–Y) solid electrolytes with the  $Sc_2(WO_4)_3$  type structure have been directly and quantitatively demonstrated to be trivalent cationic conductors. The tungstates contain hexavalent tungsten ions,  $W^{6+}$ , which reduce the interaction between the trivalent R cation and the oxide anions, because of the strong W–O bondings. Furthermore, this structure also has a large tunnel size which is suitable for the ion migration. However, the trivalent cationic conductivity is considerably low and the hexavalent tungsten ion tends to be reduced, resulting in the partial electronic conduction.

For the purpose of developing a new trivalent cationic conductor, which exhibits high conductivity and high stability,  $Sc_{1/3}Zr_2(PO_4)_3$  with the NASICON type structure was selected as the new trivalent cationic conductor. The three dimensional network of this structure is suitable for cationic migration and also contains pentavalent phosphorus,  $P^{5+}$ , and tetravalent zirconium,  $Zr^{4+}$ , in the structure. These highly charged cations are strongly bonded to the  $O^{2-}$  anions similar to the case for the tungsten ions in the tungstate. In addition to this, the solid electrolyte is expected to exhibit high durability for the reducing atmosphere because of containing phosphorus and zirconium ions and free from  $W^{6+}$ .

$Sc_{1/3}Zr_2(PO_4)_3$  was prepared by a sol-gel method, using  $Sc_2O_3$ ,  $ZrOCl_2 \cdot 8H_2O$  and  $NH_4H_2PO_4$  as starting materials.  $Sc_2O_3$  and  $ZrOCl_2 \cdot 8H_2O$  were individually solved in nitric acid, and mixed each other afterwards. Then  $NH_4H_2PO_4$  solution was poured into the mixed solution. After white precipitations were obtained, the solution was heated at 75 °C for 24h and then 300°C for 24h. The resulting white powder was pelletized and sintered at 850 °C for 36h. Pt electrodes were sputtered on both center surfaces of the sample pellet. The ac conductivity of the sample was measured by a complex impedance method in the frequency range between 20 Hz and 1MHz at the temperature range from 350 to 600 °C in air. In order to identify the conducting species, the polarization behavior was investigated by measuring the time dependence of the  $\sigma_{dc}/\sigma_{ac}$  ratio. The electrolysis of the sample pellet was carried out by applying a dc 10 V at 750 °C for 400 h.

Figure 1 shows the temperature dependencies of the conductivity for  $Sc_{1/3}Zr_2(PO_4)_3$ . The conductivity at 600 °C is about  $1.06 \times 10^{-5} \text{ S} \cdot \text{cm}^{-1}$ . This value is higher than that ( $4.27 \times 10^{-6}$

$\text{S}\cdot\text{cm}^{-1}$ ) of  $\text{Al}_2(\text{WO}_4)_3$ . The abrupt decrease in the  $\sigma_{dc}/\sigma_{ac}$  ratio was observed, indicating that the conducting species in the phosphate based solid electrolyte is not electron nor hole but ion.

The SEM photograph of the cathodic surface of the sample after electrolysis is presented in Fig. 2, showing the deposits can be recognized on the surface. Figures 3(a) and (b) show the EPMA results of the deposits on the cathodic surface after electrolysis and that of the sample before electrolysis, respectively. The Sc content in the deposits considerably increased with respect to that of the original composition. This result clearly means that the  $\text{Sc}^{3+}$  migration occurs in the  $\text{Sc}_{1/3}\text{Zr}_2(\text{PO}_4)_3$  sample and the Sc segregation was observed on the cathodic surface. From the electrolysis results mentioned above,  $\text{Sc}_{1/3}\text{Zr}_2(\text{PO}_4)_3$  is identified to be a  $\text{Sc}^{3+}$  ion conductor.

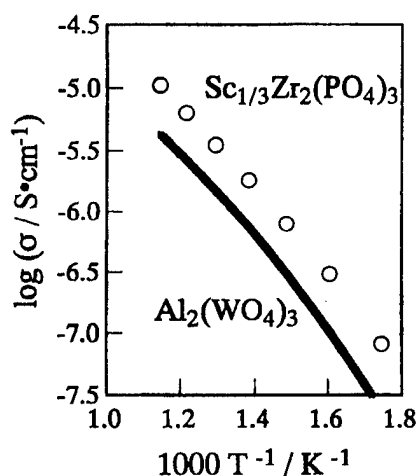


Fig. 1. The temperature dependencies of the conductivity for  $\text{Sc}_{1/3}\text{Zr}_2(\text{PO}_4)_3$ .

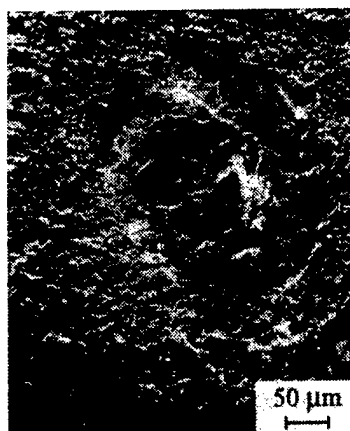


Fig. 2. The SEM photograph at the cathodic surface after the electrolysis.

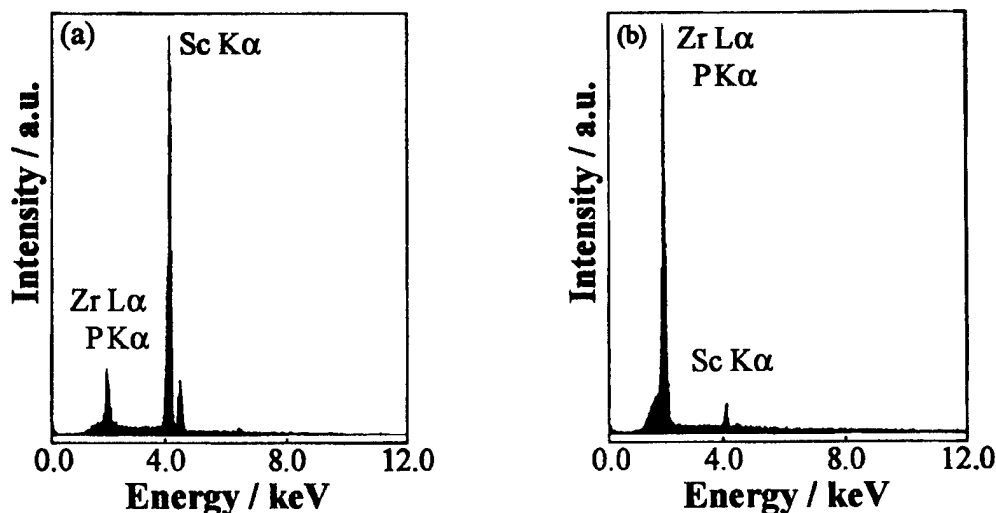


Fig. 3. The EPMA result of (a) the deposits on the cathodic surface after the electrolysis and (b) the bulk before the electrolysis.

# SINGLE CRYSTAL GROWTH OF TRIVALENT ION CONDUCTING ALUMINUM TUNGSTATE-SCANDIUM TUNGSTATE SOLID SOLUTION

M. Hiraiwa, S. Tamura, N. Imanaka, and G. Adachi

Department of Applied Chemistry, Faculty of Engineering, Osaka University,  
2-1 Yamadaoka, Suita, Osaka 565-0871 Japan

and

H. Dabkowska and A. Dabkowski

Brockhouse Institute for Materials Research  
1280 Main Street West, Hamilton, Ontario, Canada

In these years, the trivalent ion in the  $\text{Sc}_2(\text{WO}_4)_3$  type structure has been directly demonstrated to be a predominant mobile species in the tungstates. The ion conducting characteristics of the tungstate series have been mainly investigated in polycrystalline forms. However, in order to clearly identify the ion conducting properties in solid electrolyte crystal lattice, it is necessary to investigate the ion conducting behaviors with single crystal where no grain boundary exists.

Recently, we have succeeded in growing single crystals of  $\text{Al}_2(\text{WO}_4)_3$  by the Czochralski (CZ) method [1]. Trivalent ionic migration to the b-axis direction was found to be most preferential among the three different directions in the  $\text{Sc}_2(\text{WO}_4)_3$  type structure. In addition, the trivalent ion conducting properties in the  $\text{Sc}_2(\text{WO}_4)_3$  crystal structure were also demonstrated to change systematically with the variation of both the mobile trivalent ion size and the lattice volume of the tungstate structure as described in our previous paper [2]. For the purpose of exactly identifying the most suitable lattice size for the individual trivalent ion transport in the crystal lattice, it is indispensable to grow single crystals whose lattice volume can be intentionally controlled.

In this research, the single crystals of the  $\text{Al}_2(\text{WO}_4)_3$ - $\text{Sc}_2(\text{WO}_4)_3$  solid solution were successfully grown by using the modified Czochralski (CZ) method.

$\text{Al}_2\text{O}_3$ ,  $\text{Sc}_2\text{O}_3$ ,  $\text{WO}_3$  were used as starting materials and thoroughly mixed in a molar ratio of 15.3:1.7:83. The mixture was mounted in a Pt crucible and the Pt crucible was heated to melt by the CZ single crystal growth apparatus. The platinum wire (0.5 mm in diameter) was fixed at the one end of alumina ceramic rod and immersed in the melt with rotating the rod in 15-20 rpm. The pull rate was controlled at 0.1-0.15 mm/h.

By the modified single crystal growth, transparent crystals were obtained as shown in Fig. 1 and single crystallinity of the crystals was investigated by the polarization microscope observation. Despite of crossing the polarization direction, the area where single crystal exists is transparent, while the place without single crystal becomes dark. From this phenomenon, it becomes clear that the crystallinity of the single crystals was satisfactory.

The single crystals grown were also ground to carry out the X-ray powder diffraction analysis and the peaks were compared with those of  $\text{Al}_2(\text{WO}_4)_3$  and  $\text{Sc}_2(\text{WO}_4)_3$  polycrystals. The number and the peak profile are identical among those three samples, indicating that all of the three

sample hold the same crystal structure. The angle of the peaks of the  $\text{Al}_2(\text{WO}_4)_3\text{-Sc}_2(\text{WO}_4)_3$  solid solution single crystal grown shifts to lower than that of  $\text{Al}_2(\text{WO}_4)_3$  polycrystal and higher than that of  $\text{Sc}_2(\text{WO}_4)_3$  polycrystal. This result explicitly means that the formation of the solid solution of the  $\text{Al}_2(\text{WO}_4)_3\text{-Sc}_2(\text{WO}_4)_3$  single crystal was also identified. The single crystals were found to contain both Al and Sc elements by the electron probe microanalysis (EPMA) measurements. For the purpose of estimating the ratio of Al : Sc in the single crystal solid solution, the lattice constant data obtained by X-ray powder diffraction (XRD) analysis with the ground single crystal solid solution, were compared with those of the various polycrystalline  $\text{Al}_2(\text{WO}_4)_3\text{-Sc}_2(\text{WO}_4)_3$  solid solution data and the results are presented in Fig. 2. The lattice parameter values (☆) obtained from the single crystal solid solution were exactly the same as the data extrapolated to the polycrystalline solid solution of 8.5 : 1.5 in the ratio of Al : Sc.

From the results obtained above, the  $\text{Al}_2(\text{WO}_4)_3\text{-Sc}_2(\text{WO}_4)_3$  single crystals grown by the present CZ method are exactly clarified to be single crystals of the  $(\text{Al}, \text{Sc})_2(\text{WO}_4)_3$  solid solution with the Al : Sc ratio of 8.5 : 1.5.

By the success of the single crystal growth of the  $\text{Al}_2(\text{WO}_4)_3\text{-Sc}_2(\text{WO}_4)_3$  solid solutions, it is further expected that anisotropic electrical conducting behavior of trivalent ion within the grain bulk of the single crystal solid solution becomes clear.

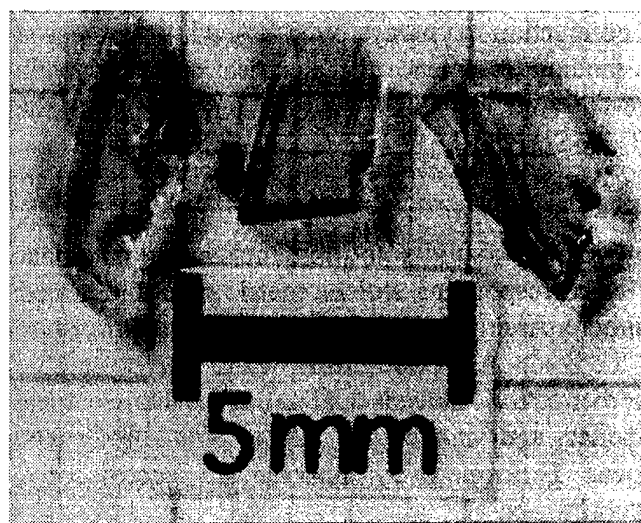


Figure 1 Typical single crystals obtained by the modified CZ method.

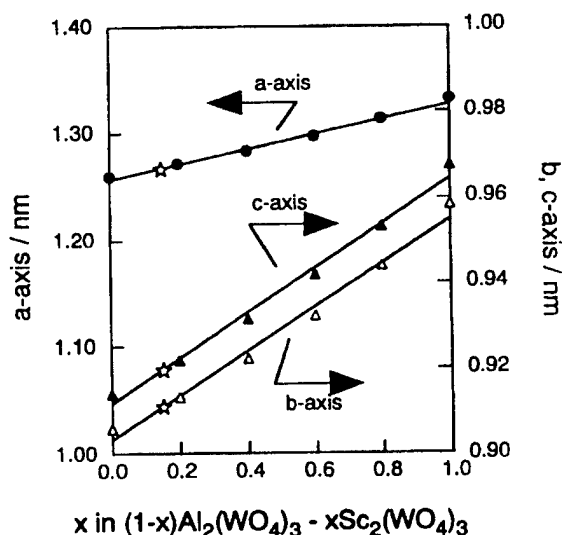


Figure 2 The lattice parameter variation for the polycrystalline  $\text{Al}_2(\text{WO}_4)_3\text{-Sc}_2(\text{WO}_4)_3$  solid solutions. ☆ indicates the parameter values obtained from the single crystal of the  $\text{Al}_2(\text{WO}_4)_3\text{-Sc}_2(\text{WO}_4)_3$  solid solution.

- [1] N. Imanaka et al., *Chem. Mater.*, **10**, 2542 (1998).
- [2] N. Imanaka et al., *Chem. Mater.*, **10**, 2006 (1998).

## ENHANCED $\text{Al}^{3+}$ CONDUCTION IN $\text{Al}_2(\text{WO}_4)_3\text{-Sc}_2(\text{MoO}_4)_3$ SOLID SOLUTIONS

J. Köhler, N. Imanaka and G. Adachi

Department of Applied Chemistry, Faculty of Engineering,  
Osaka University, 2-1 Yamadaoka, Suita, Osaka 565-0871, Japan

### Introduction

The tungstates  $\text{M}_2(\text{WO}_4)_3$  ( $\text{M} = \text{Gd} - \text{Lu}, \text{Sc}, \text{Al}, \text{In}$ ) which crystallize in the  $\text{Sc}_2(\text{WO}_4)_3$  type structure are known for their trivalent  $\text{M}^{3+}$  cationic conducting properties [1-3]. Among these compounds,  $\text{Al}_2(\text{WO}_4)_3$  exhibits the lowest electrical conductivity ( $3.4 \cdot 10^{-6} \text{ Scm}^{-1}$  at  $600^\circ\text{C}$ ) and the highest corresponding activation energy (93.6 kJ/mol) [3]. The small ionic radius of  $\text{Al}^{3+}$  causes a low polarizability and restricts this charge carrier to drastically reduced mobilities due to the high electrostatic interactions with the surrounding anionic host lattice. However, for the practical application in technical devices the conduction properties of the  $\text{Al}^{3+}$  cations need to be drastically improved. Recently, corresponding efforts have been performed by using either homogeneous or heterogeneous doping. In the latter method, fine insulating  $\text{Al}_2\text{O}_3$  particles are embedded into the ion conducting  $\text{Al}_2(\text{WO}_4)_3$  matrix and increased conductivities of about 1-2 orders have been observed [4]. In homogenous doping experiments, the  $\text{Al}^{3+}$  cations are partly replaced by larger  $\text{M}^{3+}$  cations to open the conduction pathways which lead to increased conductivities [5-7]. Here, we report on a new method to enhance the electrical conductivity in  $\text{Al}_2(\text{WO}_4)_3$  by substituting both the cationic and the anionic part of the crystal structure by the formation of solid solutions in the system  $\text{Al}_2(\text{WO}_4)_3\text{-Sc}_2(\text{MoO}_4)_3$ .

### Experimental

For the preparation of  $(\text{Al}_2(\text{WO}_4)_3)_{1-x}(\text{Sc}_2(\text{MoO}_4)_3)_x$  solid solutions, the starting materials  $\text{Al}(\text{OH})_3$ ,  $\text{Sc}_2\text{O}_3$ ,  $\text{WO}_3$  and  $\text{MoO}_3$  are mixed in the corresponding stoichiometric ratio and heated to  $800\text{-}850^\circ\text{C}$  for 24h in a flowing oxygen atmosphere. After grinding, a second heating procedure at  $850\text{-}900^\circ\text{C}$  was applied in order to complete the reaction. The resulting white polycrystalline materials were characterized by X-ray powder diffraction analysis (XRD). For the electrical measurements, the samples were pressed into pellets and sintered for 12h at  $850\text{-}900^\circ\text{C}$ . The electrical characterization of these samples was performed by impedance spectroscopy, polarization measurements and DC electrolysis experiments.

### Results and Discussion

Solid solutions in the system  $(\text{Al}_2(\text{WO}_4)_3)_{1-x}(\text{Sc}_2(\text{MoO}_4)_3)_x$  can be formed over the whole composition range ( $x = 0\text{-}1$ ). Because the ionic radii of  $\text{W}^{6+}$  (0.056nm [8]) and  $\text{Mo}^{3+}$  (0.055nm [8]) are almost identical, the extension of the crystallographic unit cell in these compounds mainly depends on the ionic radius of the trivalent cations. The incorporation of larger  $\text{Sc}^{3+}$  (0.0885nm [8]) cations in  $\text{Al}_2(\text{WO}_4)_3$  ( $r_{\text{Al}^{3+}} = 0.0675\text{nm}$  [8]) leads to a continuous expansion of the cell volume. The resulting opened pathways reduce the electrostatic interactions between the mobile cations and the anionic host lattice leading to increased mobilities. This is shown in Figure 1, where the electrical conductivities ( $\log \sigma$ ) of  $(\text{Al}_2(\text{WO}_4)_3)_{1-x}(\text{Sc}_2(\text{MoO}_4)_3)_x$  at  $600^\circ\text{C}$  are displayed in dependence on the  $\text{Sc}_2(\text{MoO}_4)_3$  content. By replacing the Al site with Sc, the conductivity linearly increases up to  $x=0.6$ . At this composition, the conductivity ( $\sigma = 7.7 \cdot 10^{-5} \text{ Scm}^{-1}$  at  $600^\circ\text{C}$ ) is enhanced by about 22 times with regard to the data of pure aluminum tungstate. A further Al replacement leads to a discontinuity in the electrical conductivity versus composition



relationship, similar to the observation in the  $(\text{Sc}_2(\text{WO}_4)_3)_{1-x}(\text{Lu}_2(\text{WO}_4)_3)_x$  system [7]. This behavior can be interpreted in terms of changing the predominant conducting species from  $\text{Al}^{3+}$  (for  $x < 0.6$ ) to  $\text{Sc}^{3+}$  ( $x > 0.7$ ). Also a comparison of the activation energies ( $E_a$ ) for the electrical conduction in  $(\text{Al}_2(\text{WO}_4)_3)_{1-x}(\text{Sc}_2(\text{MoO}_4)_3)_x$  supports the assumption for an altered conduction mechanism. The corresponding  $E_a$  data are displayed in Figure 2 in dependence on the composition. In the solid solutions with  $x < 0.6$ ,  $E_a$  only slightly decreases (83.9 - 76.0 kJ/mol) and remains similar to the data of pure  $\text{Al}_2(\text{WO}_4)_3$  (93.6 kJ/mol) whereas for compounds with  $x > 0.6$ ,  $E_a$  is significantly decreased (64.4 - 53.11 kJ/mol), approximating the value for pure  $\text{Sc}_2(\text{MoO}_4)_3$  (42.3 kJ/mol). Finally, the corresponding mobile charge carrying cations have been directly determined for different compositions by electrolysis experiments. Conductivity measurements in various atmospheres (differing in the oxygen partial pressure) as well as polarization experiments indicate that other theoretically possible charge carriers, like  $\text{O}^{2-}$  anions or electrons are absent in  $(\text{Al}_2(\text{WO}_4)_3)_{1-x}(\text{Sc}_2(\text{MoO}_4)_3)_x$ . Thus, these solid solution compounds are shown to be mixed cationic conductors with an enhanced  $\text{Al}^{3+}$  migration in comparison to pure  $\text{Al}_2(\text{WO}_4)_3$ .

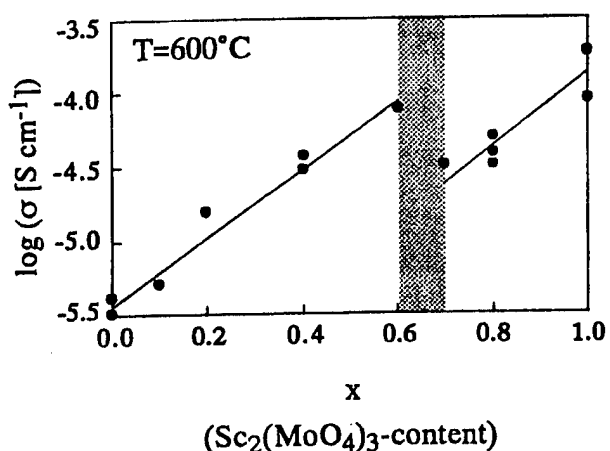


Fig. 1: Ionic conductivity ( $\log \sigma$ ) in dependence on the  $\text{Sc}_2(\text{MoO}_4)_3$  content ( $x$ ) in  $(\text{Al}_2(\text{WO}_4)_3)_{1-x}(\text{Sc}_2(\text{MoO}_4)_3)_x$

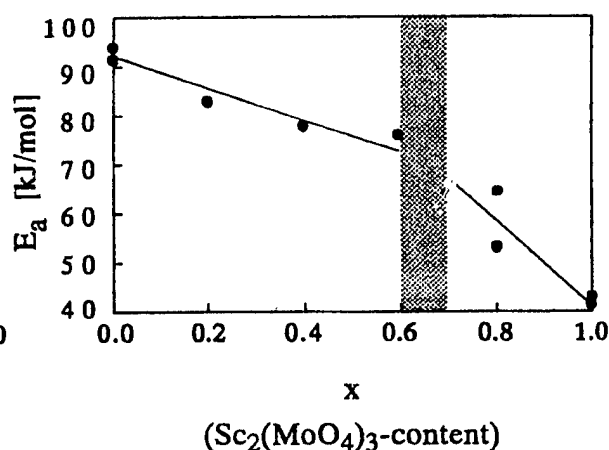


Fig. 2: Activation energy ( $E_a$ ) in dependence on the  $\text{Sc}_2(\text{MoO}_4)_3$  content ( $x$ ) in  $(\text{Al}_2(\text{WO}_4)_3)_{1-x}(\text{Sc}_2(\text{MoO}_4)_3)_x$

- [1] N. Imanaka, Y. Kobayashi, G. Adachi, Chem. Lett. 433 (1995).
- [2] Y. Kobayashi, T. Egawa, S. Tamura, N. Imanaka, G. Adachi, Chem. Mater. 9, 1649 (1997).
- [3] N. Imanaka, Y. Kobayashi, K. Fujiwara, T. Asano, Y. Okazaki, G. Adachi, Chem. Mater. 10, 2006 (1998).
- [4] J. Köhler, Y. Kobayashi, N. Imanaka, G. Adachi, Solid State Ionics (1998), in press.
- [5] S. Tamura, T. Egawa, Y. Okazaki, Y. Kobayashi, N. Imanaka, G. Adachi, Chem Mater. 10, 1958 (1998).
- [6] Y. Kobayashi, T. Egawa, Y. Okazaki, S. Tamura, N. Imanaka, G. Adachi, Solid State Ionics 111, 59 (1998).
- [7] Y. Kobayashi, T. Egawa, S. Tamura, N. Imanaka, G. Adachi, Solid State Ionics (1998), in press.
- [8] R.D. Shannon, Acta Cryst. A32, 751 (1976).

## TRIVALENT $\text{Sc}^{3+}$ ION CONDUCTION IN THE $\text{Sc}_2(\text{WO}_4)_3$ - $\text{Sc}_2(\text{MoO}_4)_3$ SOLID SOLUTION

Y. Okazaki, T. Ueda, S. Tamura, N. Imanaka, and G. Adachi

Department of Applied Chemistry, Faculty of engineering, Osaka University,  
2-1 Yamadaoka, Suita, Osaka 565-0871 Japan

The trivalent cation has been regarded as an ionically poor conducting species in solid electrolytes, due to the high electrostatic interaction of the trivalent cation with the surrounding framework of anions such as  $\text{O}^{2-}$ . To realize the trivalent ion conduction in solids, the  $\text{Sc}_2(\text{WO}_4)_3$ -type structure which effectively acts to reduce the electrostatic interaction, was selected and the trivalent ion conduction in  $\text{R}_2(\text{WO}_4)_3$  ( $\text{R}=\text{Sc}$ ,  $\text{Y}$ ,  $\text{Er-Lu}$ ,  $\text{Al}$ ) has been directly demonstrated. The highest trivalent ion conduction and the lowest activation energy was attained by  $\text{Sc}_2(\text{WO}_4)_3$ [1]. The  $\text{Sc}^{3+}$  ion was found to have the most suitable ionic size for the migration in the  $\text{Sc}_2(\text{WO}_4)_3$ -type structure.

In this study, the suitable lattice size for  $\text{Sc}^{3+}$  ion migration in the  $\text{Sc}_2(\text{WO}_4)_3$ -type structure was examined in order to enhance the  $\text{Sc}^{3+}$  ion conductivity and to make it clear the relationship between the lattice size and the ion conduction. The lattice size was controlled by means of replacing  $\text{W}^{6+}$  ion in  $\text{Sc}_2(\text{WO}_4)_3$  for  $\text{Mo}^{6+}$  ion (0.055nm) which has a smaller ion size than  $\text{W}^{6+}$  ion (0.056nm), and the trivalent ion conduction in the  $\text{Sc}_2(\text{WO}_4)_3$ - $\text{Sc}_2(\text{MoO}_4)_3$  system was investigated.

The solid solutions of the  $(1-x)\text{Sc}_2(\text{WO}_4)_3$ - $x\text{Sc}_2(\text{MoO}_4)_3$  system were prepared by the conventional solid-state reaction. An appropriate amount of  $\text{Sc}_2\text{O}_3$ ,  $\text{WO}_3$  and  $\text{MoO}_3$  was mixed in a mortar and calcinated at  $700^\circ\text{C}$  for 5h and then at  $1100^\circ\text{C}$  for 12h. From the X-ray powder diffraction analysis, the  $\text{Sc}_2(\text{WO}_4)_3$ - $\text{Sc}_2(\text{MoO}_4)_3$  system is found to possess the  $\text{Sc}_2(\text{WO}_4)_3$  type structure in all compositional range examined. The angle of the diffraction patterns is shifted to higher by substituting the  $\text{W}^{6+}$  ion for the smaller  $\text{Mo}^{6+}$  ion. The resulting powder was pelletized and sintered at  $1100^\circ\text{C}$  for 12h. Electrical conductivity of the sintered pellet was measured by ac complex impedance method with two platinum electrodes in air ( $200^\circ\text{C}$  to  $600^\circ\text{C}$ ). Figure 1 shows the compositional dependencies of the electrical conductivity and the activation energy. In the  $(1-x)\text{Sc}_2(\text{WO}_4)_3$ - $x\text{Sc}_2(\text{MoO}_4)_3$  system, the conductivity increased and the activation energy decreased linearly with increasing the Mo content. Among the samples prepared,  $\text{Sc}_2(\text{MoO}_4)_3$  ( $x=1$ ) exhibits the highest electrical conductivity,  $1.84 \times 10^{-4} \text{S}\cdot\text{cm}^{-1}$ , and the lowest activation energy, 44.4 kJ $\cdot\text{mol}^{-1}$  in the  $(1-x)\text{Sc}_2(\text{WO}_4)_3$ - $x\text{Sc}_2(\text{MoO}_4)_3$  system.

The oxygen partial pressure dependencies of the electrical conductivity were studied for  $0.6\text{Sc}_2(\text{WO}_4)_3$ - $0.4\text{Sc}_2(\text{MoO}_4)_3$  and  $\text{Sc}_2(\text{MoO}_4)_3$ . Generally, the electrical conductivity of the ion conducting materials is independent of the oxygen partial pressure, contrary to the electronic conducting materials. The electrical conductivity of both  $0.6\text{Sc}_2(\text{WO}_4)_3$ - $0.4\text{Sc}_2(\text{MoO}_4)_3$  and  $\text{Sc}_2(\text{MoO}_4)_3$  is constant in the oxygen partial pressure range of  $10^{-10}$ - $10^5$ Pa, including the partial pressure of air. From this result, the conducting species is predominantly ionic. At low  $\text{Po}_2$  range, the conductivity enhanced by the increase of the n-type electronic conduction appeared by the reduction of Mo.

To examine the possibility of  $\text{O}^{2-}$  conduction, the dc conductivity was measured at  $700^\circ\text{C}$  in two different atmospheres ( $\text{O}_2$  ( $\text{Po}_2=10^5$ Pa) and  $\text{He}$  ( $\text{Po}_2=4$ Pa)). The time dependencies of the ratio,  $\sigma_{\text{dc}}/\sigma_{\text{ac}}$  in the atmosphere of  $\text{O}_2$  and  $\text{He}$  are shown in Figs.2(a) ( $0.6\text{Sc}_2(\text{WO}_4)_3$ - $0.4\text{Sc}_2(\text{MoO}_4)_3$ ) and 2(b) ( $\text{Sc}_2(\text{MoO}_4)_3$ ). If the predominant mobile ion species is an  $\text{O}^{2-}$  ion, the polarization would

be clearly observed in He, while in O<sub>2</sub> the dc conductivity should be equal to the ac conductivity. For both 0.6Sc<sub>2</sub>(WO<sub>4</sub>)<sub>3</sub>-0.4Sc<sub>2</sub>(MoO<sub>4</sub>)<sub>3</sub> and Sc<sub>2</sub>(MoO<sub>4</sub>)<sub>3</sub>, the same polarization was observed in O<sub>2</sub> and He. Therefore, the O<sup>2-</sup> ion is excluded from the mobile ion species in the Sc<sub>2</sub>(WO<sub>4</sub>)<sub>3</sub>-Sc<sub>2</sub>(MoO<sub>4</sub>)<sub>3</sub> system.

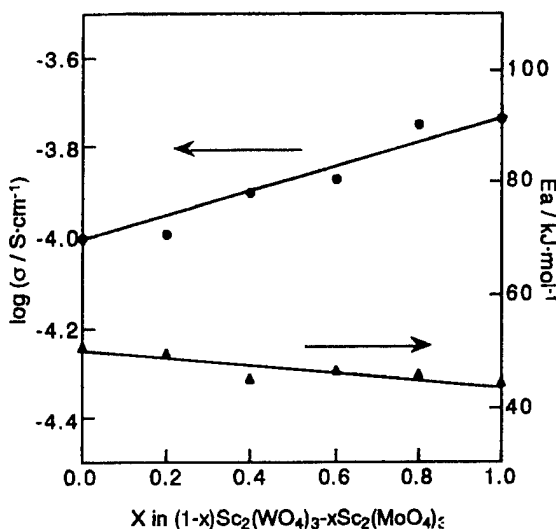


Fig.1 The compositional dependencies of the electrical conductivity and the activation energy for the Sc<sub>2</sub>(WO<sub>4</sub>)<sub>3</sub>-Sc<sub>2</sub>(MoO<sub>4</sub>)<sub>3</sub> system.

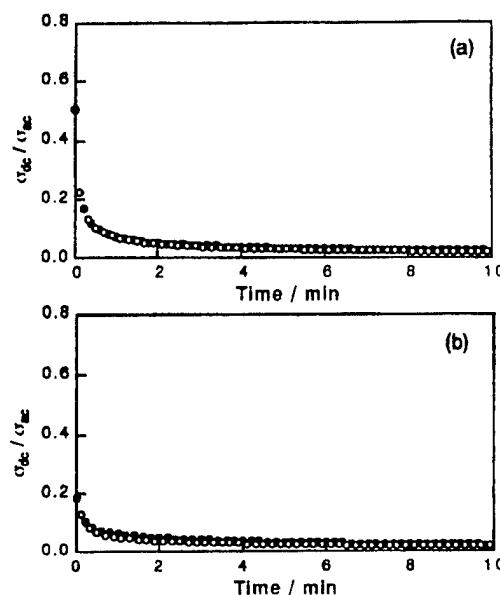


Fig.2 The time dependencies of the ratio,  $\sigma_{dc}/\sigma_{ac}$  in O<sub>2</sub>(●) and He(○) for (a) 0.6Sc<sub>2</sub>(WO<sub>4</sub>)<sub>3</sub>-0.4Sc<sub>2</sub>(MoO<sub>4</sub>)<sub>3</sub> and (b) Sc<sub>2</sub>(MoO<sub>4</sub>)<sub>3</sub>.

To investigate the relationship between the conductivity and the lattice size, Rietveld analysis was done for both Sc<sub>2</sub>(WO<sub>4</sub>)<sub>3</sub> and Sc<sub>2</sub>(MoO<sub>4</sub>)<sub>3</sub>. Table 1 shows the lattice parameter and the scandium-oxygen average distance in Sc<sub>2</sub>(WO<sub>4</sub>)<sub>3</sub> and Sc<sub>2</sub>(MoO<sub>4</sub>)<sub>3</sub>. Because of the smaller ion size of Mo<sup>6+</sup> ion, all lattice parameters of Sc<sub>2</sub>(MoO<sub>4</sub>)<sub>3</sub> are shorter than those of Sc<sub>2</sub>(WO<sub>4</sub>)<sub>3</sub> and therefore the cell volume of Sc<sub>2</sub>(MoO<sub>4</sub>)<sub>3</sub> becomes smaller than that of Sc<sub>2</sub>(WO<sub>4</sub>)<sub>3</sub>. On the contrary, the Sc-O average distance of Sc<sub>2</sub>(MoO<sub>4</sub>)<sub>3</sub> was longer than that of Sc<sub>2</sub>(WO<sub>4</sub>)<sub>3</sub>. This can be easily understood by the fact that the hexavalent cation-oxygen average distance in Sc<sub>2</sub>(MoO<sub>4</sub>)<sub>3</sub> (Mo-O:0.1745nm) is shorter than that in Sc<sub>2</sub>(WO<sub>4</sub>)<sub>3</sub> (W-O:0.1794nm), which caused by the difference of ion size and ionicity between Mo<sup>6+</sup> ion and W<sup>6+</sup> ion. The longer Sc-O average distance of Sc<sub>2</sub>(MoO<sub>4</sub>)<sub>3</sub> leads to reduce the electrostatic interaction between Sc and O which dominates the Sc<sup>3+</sup> ion conduction, and as a result, the Sc<sup>3+</sup> ion conduction in Sc<sub>2</sub>(MoO<sub>4</sub>)<sub>3</sub> was enhanced compared with that in Sc<sub>2</sub>(WO<sub>4</sub>)<sub>3</sub>.

Table 1 The lattice parameters, the cell volume and the scandium-oxygen average distance in Sc<sub>2</sub>(WO<sub>4</sub>)<sub>3</sub> and Sc<sub>2</sub>(MoO<sub>4</sub>)<sub>3</sub>.

	lattice parameter (nm)	cell volume (nm <sup>3</sup> )	Sc-O average distance (nm)
Sc <sub>2</sub> (WO <sub>4</sub> ) <sub>3</sub>	A=1.333, b=0.958, c=0.968	1.236	0.2077
Sc <sub>2</sub> (MoO <sub>4</sub> ) <sub>3</sub>	A=1.325, b=0.955, c=0.964	1.220	0.2100

# K<sup>+</sup>-CONDUCTING SOLID ELECTROLYTES. CRYSTAL CHEMISTRY OF RARE EARTH POTASSIUM SILICATES

O.S. Filipenko\*, L.S. Leonova\*\*, N.S. Tkacheva\*\*, V.I. Ponomarev\*\*\*,  
O.V. Dimitrova\*\*\*\*, A.E. Ukshe\*, L.O. Atovmyan\*

\*Institute for Chemical Physics Research, RAS, Russia,  
\*\*Institute of New Chemical Problems, RAS, Russia,

\*\*\*Institute of Structural Macrokinetics and Materials Science, RA S, Russia,  
\*\*\*\*Moscow State University, Moscow, Russia

In order to obtain new potassium-conducting solid electrolytes with high chemical stability and electric conductivity, we have analyzed the complex oxide compounds having a skeleton structure and containing potential mobile alkaline ions or being solid electrolytes. Based on the heterodesmism principle, a conception of the most favourable skeleton for every conducting alkaline ion has been developed [1]. Under the most favourable transport conditions (high concentration of charge carriers, structural disorder of cations, three-dimensional channel system and most suitable sizes of bottle-necks), the best skeleton ensuring the mobility of potassium ions should consist of two types of functional fragments: discrete lanthanoid octahedra and condensed silicon-oxygen tetrahedra. The crystals with the new skeleton type  $K_6Ln_2Si_6O_{18}$  (I) [2-5] structure comply with these requirements. Solid electrolytes I were prepared by multistage solid-phase synthesis. Electric conductivity was measured using ceramic samples with density 3-3.2 g/cm<sup>3</sup> on symmetric cells Ag/SEL/Ag and impedance spectroscopy technique in the frequency range 10<sup>2</sup> to 2·10<sup>6</sup> Hz. Table 1 gives conductivity data for synthesized electrolytes. Doping of SEL with Zr<sup>4+</sup> and Hf<sup>4+</sup> ions leads to a sufficient decrease in the conductivity activation energy. For pure SEL it is 0.51-0.53 eV, for doped Zr<sup>4+</sup> and Hf<sup>4+</sup> it is 0.35-0.37 eV. As in the case of electrolytes of the Na<sub>5</sub>LnSi<sub>4</sub>O<sub>12</sub> type, these additives improve markedly mechanical and chemical durability of ceramics.

Table 1

structural formula of electrolyte	$\sigma \cdot 10^2$ , S/cm		
	200°C	300°C	400°C
$K_6La_2Si_6O_{18}$	0.39	3.6	11
$K_6Gd_2Si_6O_{18}$	0.32	2.0	10
$K_6Ho_2Si_6O_{18}$	0.50	2.6	17
$K_{6.5}Sm_{1.6}La_{0.4}Si_6O_{18}$	0.45	4.5	14
$K_{5.5}Sm_{1.5}Hf_{0.5}Si_6O_{18}$	1.4	4.6	10
$K_{5.5}Ho_{1.5}Zr_{0.5}Si_6O_{18}$	1.25	5.1	12.5
$K_{5.8}Ho_{1.8}Zr_{0.2}Si_6O_{18}$	0.72	3.3	6.9

The layer structure of  $K_3HoSi_3O_8(OH)_2$  (A) [2-3] is a good potassium ions conductor as it is composed of single octahedra and triortho groups  $Si_3O_8(OH)_2$ . Based on these structural type we succeeded in preparing new solid electrolytes  $K_6Ln_2Si_6O_{18}$ . Ln=La - Yb with high conductivity via K<sup>+</sup> ions [4]. An X-ray study of topotaxial conversion of A crystal at 880 K gave the structure of its dehydration product  $K_3HoSi_3O_9$  (B) [2]. Single crystals of both potassium (A and B) silicate types with Tm, Yb, Lu were

obtained using a hydrothermal synthesis on a  $K_2O-Ln_2O_3-SiO_2-H_2O$  system in the silica-rich region and with high KOH concentration (tabl.2). Their crystal structures were found[3,5]. Based on the solid-phase synthesis data and hydrothermal synthesis, including a paper on the synthesis of  $K_3NdSi_3O_8(OH)_2$  [6] both the isostructural series were full. In the compounds  $K_6Ln_2Si_6O_{18}$ ,  $Ln = Ho, Tm, Lu$  the K atoms distributed over 5 crystallographical positions occupy one (K1) general position in the cavities with octahedral cross section, the rest are on the mirror planes in the through channels parallel to the short  $c$  period. Oxygen atoms surround  $K^+$  ions at distances 2.645 to 3.507 Å, not forming closed polyhedra about them.

Table 2. Crystal data for compounds A and B structural type

Ln	A				B			
	space group $Pmnb$ , $Z=4$				space group $Pm2_1n$ , $Z=2$			
	a, Å	b, Å	c, Å	d g/cm <sup>3</sup>	a, Å	b, Å	c, Å	d g/cm <sup>3</sup>
Ho	13,534	13,175	5,880	3.37	13,874	12,804	5,853	3.29
Tm	13,503	13,127	5,853	3.43	14,053	12,955	5,864	3.22
Yb	13,484	13,095	5,828	3.48				
Lu					14,01	12,919	5,853	3.28

The K - K distances lie in the narrow region of 3.73 to 4.01 Å and allow a 3-D ionic transport. Noted is some disordering of  $K^+$  ions in positions K2 and K3, for positions K3 and K4 a small incomplete occupancy is observed. The difference between Tm and Lu structures are connected with variation in the occupancy of these positions. Decrease in  $E$  with an introduction of additives is associated with the structural disordering of  $K^+$  ions in zeolite-like channels (fig.1). The work is supported by the RBRF, Grant 98-03 -32557a.

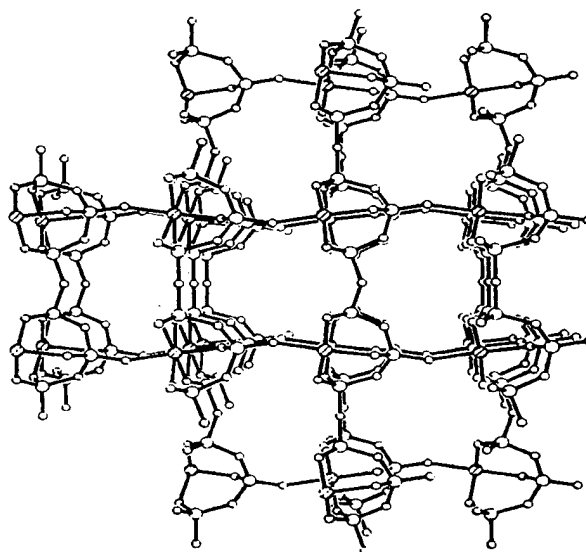


Fig.1. Projection of  $K_6Lu_2Si_6O_{18}$  along [001]

- [1] O.S. Filipenko, L.O. Atovmyan, V.I. Ponomarev, B.N. Litvin, O.V. Dimitrova, L.S. Leonova, N.S. Tkacheva, E.A. Ukshe. Dokl. AN SSSR 283,430(1985).
- [2] V.I. Ponomarev, O.S. Filipenko, L.O. Atovmyan, Dokl. AN SSSR 298,1134(1988).
- [3] V.I. Ponomarev, O.S. Filipenko, L.O. Atovmyan, Kristallogr. 33,98(1988).
- [4] O.S. Filipenko, L.O. Atovmyan, L.S. Leonova, B.N. Litvin, V.I. Ponomarev, N.S. Tkacheva, E.A. Ukshe, USSR Inventors certificate N 3273816/07 of July 16, 1981.
- [5] O.S. Filipenko, O.V. Dimitrova, L.O. Atovmyan, V.I. Ponomarev, Kristallogr. 33,1122(1988).
- [6] S.M. Haile, B.J. Wuensch, T. Siegrist, R.A. Laudise, Solid State Ionics 53-56, 1292(1992)

# MIXED ALKALI EFFECT IN THE $K_{4-4x}Na_{4x}P_2O_7$ AND $K_{4-4x}Rb_{4x}P_2O_7$ SYSTEMS

G.Sh.Shekhtman, N.B.Smirnov, E.I.Burmakin  
Institute of High-Temperature Electrochemistry  
Russian Acad.Sci. Ekaterinburg 620219, Russia.

Alkali ion conductivity of pyrophosphates  $A_4P_2O_7$  ( $A=Na,K,Rb$ ) is  $\approx 10^{-4} \text{ S cm}^{-1}$  at  $400^\circ\text{C}$  and  $\approx 10^{-2} \text{ S cm}^{-1}$  at  $800^\circ\text{C}$  [1]. According to our preliminary data high temperature modifications of this three compounds have similar crystal structure, so one can expect that these compounds forms rather wide ranges of solid solutions in the  $A_4P_2O_7 - A'_4P_2O_7$  ( $A,A'=Na,K,Rb$ ) systems. This assumption is confirmed by X-ray analysis: in the  $K_{4-4x}Rb_{4x}P_2O_7$  system there is the bontinuuous range of solid solutions having structure of high -temperature  $K_4P_2O_7$ . In the  $K_{4-4x}Na_{4x}P_2O_7$  system the range of the similar solid solutions is restricted by  $x=0,3$ . In the  $Na_{4-4x}Rb_{4x}P_2O_7$  system ranges of solid solutions are rather narrow because of large difference in ionic radii Na and Rb.

Results of the electrical measurements are listed in the table.

Electrical properties of the solid solutions in the  $K_{4-4x}Rb_{4x}P_2O_7$   
and  $K_{4-4x}Na_{4x}P_2O_7$  systems.

X	$K_{4-4x}Rb_{4x}P_2O_7$			$K_{4-4x}Na_{4x}P_2O_7$	
	$\sigma_{400^\circ\text{C}} 10^{-5},$ $\text{S cm}^{-1}$	E, kJ mol <sup>-1</sup>	$\Delta E$	E, kJ mol <sup>-1</sup>	$\Delta E$
0,0	40,0	40	1,00	40	1
0,1	17,4	50	1,18	62	1,33
0,2	13,8	59	1,31	81	1,50
0,3	8,9	62	1,33	103	1,69
0,4	7,1	70	1,40	—	—
0,5	5,0	80	1,52	—	—
0,6	4,0	86	1,57	—	—
0,7	4,4	76	1,32	—	—
0,8	5,0	70	1,18	—	—
0,9	8,7	66	1,06	—	—
1,0	21,0	65	1,00	—	—

Here  $\Delta E = E/E_{\text{add}}$  is a parameter characterising the mixed alkali effect where E - actual value of activation energy,  $E_{\text{add}}$  - activation energy for additive change of properties. As one can see, there is minimum of conductivity and maximum of activation energy at  $x=0,6$  in the  $K_{4-4x}Rb_{4x}P_2O_7$  system, i.e. in this system the mixed alkali effect (MAE) takes place. In the  $K_{4-4x}Na_{4x}P_2O_7$  system there are no extremums on concentration dependences of conductivity and activation energy. It may be becaufe of more narrow range of solid solutions compared with previous system. However, deviation from additivity as result of substitution of  $K^+$  for  $Na^+$  in  $K_4P_2O_7$  takes place too and is very similar with K-Rb system for the same compositional range. That is in agreement with results of investigation of MAE in glasses [2]: the more difference of alkali ion radii, the stronger MAE (in one case  $r_{\text{Rb}^+} - r_{\text{K}^+} = 0,14 \text{ \AA}$ ,  $r_{\text{K}^+} - r_{\text{Na}^+} = 0,36 \text{ \AA}$ ).

This research was carried out with support of Russian Fundamental Research Foundation. Project № 98-03-32350a.

[1] G.Sh.Shekhtman, M.A.Mescherjakova, E.I.Burmakin, N.O.Esina, Elektrokhimia  
29, 1414 (1993).

[2] J.O.Isard, J.Non-cryst Solids 1, 235 (1969).

CONDUCTIVITY OF POTASSIUM ORTHOPHOSPHATE  
MODIFYING BY  $M^{2+}$  CATIONS.

G. Sh. Shekhtman, D. N. Mosin, E. I. Burmakin

Institute of High Temperature Electrochemistry, Russian Academy of Sciences, Ekaterinburg,  
620219 Russia.

Solid solutions based on  $\gamma$ - $\text{Na}_3\text{PO}_4$  have rather high cationic conductivity [1]. High temperature form of potassium orthophosphate have similar structure [2], therefore  $\text{K}_3\text{PO}_4$  may be prospective compound for synthesis of new potassium-conducting solid electrolytes. In this work the results of investigations of the systems  $\text{K}_{3-2x}\text{M}_x\text{PO}_4$  ( $M=\text{Ca}, \text{Sr}, \text{Cd}, \text{Ba}, \text{Pb}$ ) are described.

Without additives the conductivity of  $\text{K}_3\text{PO}_4$  is  $\approx 10^{-5} \text{ S cm}^{-1}$  at  $300^\circ\text{C}$ . At the point of phase transition ( $530 \pm 10^\circ\text{C}$ ) conductivity increases sharply ( $\approx 2$  times), the activation energy in this point decreases from 77 to 41  $\text{kJ mol}^{-1}$ . The introduction of  $M^{2+}$  additives leads to sharp increasing of conductivity as result of both potassium vacancies formation and decreasing of phase transition temperature. The values of activation energy of conductivity in the systems with  $M=\text{Ca}, \text{Sr}, \text{Cd}$  are similar ( $\approx 35 \text{ kJ mol}^{-1}$ ), in the systems with  $\text{Ba}^{2+}$  and  $\text{Pb}^{2+}$  these values are higher (40-45  $\text{kJ mol}^{-1}$ ). Monophase ranges of solid solutions based on  $\text{K}_3\text{PO}_4$  in the systems with  $\text{Ca}^{2+}$  and  $\text{Sr}^{2+}$  correspond to  $0 < x \leq 0,125$ , in the system with  $\text{Cd}^{2+}$  this range correspond to  $0 < x \leq 0,35$ . Owing to higher solubility of additive in the system  $\text{K}_{3-2x}\text{Cd}_x\text{PO}_4$  the conductivity values are maximum in this system.

The high values of conductivity of investigated materials ( $1,25 \cdot 10^{-2} \text{ S cm}^{-1}$  at  $300^\circ\text{C}$ ,  $2,25 \cdot 10^{-1} \text{ S cm}^{-1}$  at  $700^\circ\text{C}$  for  $\text{K}_{2,3}\text{Cd}_{0,35}\text{PO}_4$ ) show that  $\text{K}_3\text{PO}_4$  based solutions are a promising class of solid electrolytes with potassium-cationic conductivity.

[1] A.Hooper, P.Mc.Geehin, K.T.Harrison, B.C.Tofield. J.Solid State Chem. **24**, 265 (1978).

[2] A-W.Kolsi, Rev. Chim. Miner. **13**, 416 (1976).

# CRYSTALLOGRAPHIC STUDY OF HYDRATED POLYCRYSTALLINE M-β/β"-FERRITES (M = K<sup>+</sup>, Mg<sup>2+</sup>, Ca<sup>2+</sup>)

P. Keklikoglou, A.C. Stergiou and O. Kalogirou

Section for Applied and Environmental Physics, Dept. of Physics, Aristotle University of  
Thessaloniki, 54 006 Thessaloniki, Greece

β- and β"-ferrites (K<sub>1+x</sub>Fe<sub>11</sub>O<sub>17</sub>) are non-stoichiometric compounds with high ionic conductivity. K<sup>+</sup> ions located on the conduction layers present high mobility and can be substituted by a number of cations by means of ionic exchange reactions thus forming new metastable β- and β"-ferrites. β-ferrite crystallises in the hexagonal system (P6<sub>3</sub>/mmc) [1] whereas β"-ferrite in the rhombohedral one (R $\bar{3}$ m) [2]. Due to the structural relationship between β- and β"-ferrite, synthesis of the parent compound and ionic exchange results to the formation of both phases. It is well known that these materials incorporate either hydronium ions or water molecules when exposed to moist air, which affect strongly their electrical and magnetic properties [3,4]. In this work a complete crystallographic study and the ionic distribution in the conduction layers, including H<sub>2</sub>O, of the Cd<sup>2+</sup>-stabilised K<sup>+</sup>-β/β"-ferrite and the divalent M<sup>2+</sup>-β/β"-ferrites, M<sup>+</sup> = Mg<sup>2+</sup>, Ca<sup>2+</sup>, prepared by ion exchange [5], is presented. The parent compound was prepared from a mixture of nominal composition K<sub>2</sub>CO<sub>3</sub>;5.25Fe<sub>2</sub>O<sub>3</sub>;0.75CdO by the standard ceramic technique. The mixture was heated at 940°C for two hours. X-ray powder diffraction showed the formation of β"-ferrite and of β-ferrite as a secondary phase. The overall composition as determined by electron microprobe (EDAX), was K<sub>1.38</sub>Fe<sub>10.1</sub>Cd<sub>0.87</sub>O<sub>16.7</sub>. Powder of K<sup>+</sup>-β"-ferrite (≈1 g) was soaked into molten eutectic mixtures of M(NO<sub>3</sub>)<sub>2</sub>/NaNO<sub>3</sub> (M<sup>+</sup> = Mg<sup>2+</sup>, Ca<sup>2+</sup>) for 1 hour at 200 °C for Mg<sup>2+</sup>, and 4 hours at 330 °C for Ca<sup>2+</sup>, respectively. The K<sup>+</sup> substitution reached almost 90% in the case of Mg<sup>2+</sup> and 100% in the case of Ca<sup>2+</sup>, as determined by EDAX. Powders of the parent compound and the ionic exchange products were measured in a θ-2θ diffractometer using CoKα radiation.

TABLE I

Ion	Chemical formula (EDAX)	Chemical formula (Rietveld)	a, b (Å)	c (Å)	Phases (%)	R <sub>p</sub> (%)
K <sup>+</sup>	K <sub>1.38</sub> Fe <sub>10.1</sub> Cd <sub>0.87</sub> O <sub>16.7</sub>	K <sub>1.57</sub> Fe <sub>9.97</sub> Cd <sub>1.03</sub> O <sub>16.77</sub> ·0.65H <sub>2</sub> O	5.979(6)	35.875(3)	75.9 β"	5.10
		K <sub>1.41</sub> Fe <sub>10.52</sub> Cd <sub>0.48</sub> O <sub>17</sub> ·0.33H <sub>2</sub> O	5.983(3)	23.851(5)	24.1 β	
Mg <sup>2+</sup>	Mg <sub>0.56</sub> K <sub>0.18</sub> Fe <sub>10.24</sub> Cd <sub>0.76</sub> O <sub>17.33</sub>	Mg <sub>0.67</sub> K <sub>0.18</sub> Fe <sub>9.97</sub> Cd <sub>1.03</sub> O <sub>16.83</sub> ·1.59H <sub>2</sub> O	5.976(1)	36.045(4)	65.9 β"	5.02
		Mg <sub>0.43</sub> K <sub>0.57</sub> Fe <sub>10.41</sub> Cd <sub>0.59</sub> O <sub>17</sub> ·1.0H <sub>2</sub> O	5.978(2)	23.850(2)	27.2 β	
		MgFe <sub>2</sub> O <sub>4</sub>	8.4412(2)		6.9 spinel	
Ca <sup>2+</sup>	Ca <sub>0.89</sub> Fe <sub>10.16</sub> Cd <sub>0.84</sub> O <sub>17.04</sub>	Ca <sub>0.79</sub> Fe <sub>10.17</sub> Cd <sub>0.88</sub> O <sub>16.85</sub> ·1.51H <sub>2</sub> O	5.964(1)	35.655(3)	80.6 β"	5.18
		CaFe <sub>10.09</sub> Cd <sub>0.91</sub> O <sub>17</sub> ·1.0H <sub>2</sub> O	5.971(2)	23.706(4)	19.4 β	



The unit cell parameters, the atom sites and the percentage of the two phases,  $\beta$  and  $\beta''$ , were determined by the powder profile analysis method (Rietveld). The same temperature factors were used for all atoms ( $B = 0.6 \text{ \AA}^2$ ). This analysis showed that both the parent compound and the ionic exchange products are not single phase but present a mixture of the  $\beta''$  and  $\beta$  phases. In the case of  $\text{Mg}^{2+}$  a small amount of Mg-spinel, 7%, was detected. In TABLE I the cell parameters, phase composition and the chemical formulae, as determined by two different methods (EDAX and Rietveld analysis) are given. The weight percent of the water molecules calculated from the Rietveld analysis is 0.96% for  $\text{K}^+$ , and 2.41% for  $\text{Mg}^{2+}$  and  $\text{Ca}^{2+}$ , in good agreement with the weight losses measured by means of thermogravimetric analysis [6], being 1.5%, 2.2% and 3%, respectively. For the first time, the site occupancy of the  $\text{M}^{2+}$  cations on the conduction layers of  $\text{Mg}^{2+}$ - and  $\text{Ca}^{2+}$ - $\beta/\beta''$ -ferrites is determined. In Table II the ionic distribution on the conduction layers for both phases,  $\beta$  and  $\beta''$ , for the compounds under study, is given.

TABLE II

Phase	Atom	Site	Occupation	x	y	z
$\text{K}^+-\beta''$	K	18h	0.784	0.065(6)	x/2	0.172(1)
	$\text{OH}_2$	9d	0.216	1/2	1/2	1/2
	K(1)	2d	0.331	2/3	1/3	1/4
$\text{K}^+-\beta$	K(2)	6h	0.247	0.923(6)	2x	1/4
	$\text{OH}_2$	2d	0.669	2/3	1/3	1/4
$\text{Mg}^{2+}-\beta''$	K	6c	0.09	0	0	0.178(15)
	Mg	6c	0.335	0	0	0.178(15)
	$\text{OH}_2$	9d	0.53	1/2	1/2	1/2
$\text{Mg}^{2+}-\beta$	K	2d	0.57	2/3	1/3	1/4
	Mg	2d	0.43	2/3	1/3	1/4
	$\text{OH}_2$	6h	0.333	0.924(40)	2x	1/4
$\text{Ca}^{2+}-\beta''$	Ca	6c	0.397	0		0.170(1)
	$\text{OH}_2$	9d	0.504	1/2	1/2	1/2
$\text{Ca}^{2+}-\beta$	Ca(1)	2d	0.4	2/3	1/3	1/4
	Ca(2)	6h	0.2	0.942(33)	2x	1/4
	$\text{OH}_2(1)$	2d	0.6	2/3	1/3	1/4
	$\text{OH}_2(2)$	6h	0.133	0.942(33)	2x	1/4

## References

- [1] S. Nariki, S. Ito, K. Kozawa, T. Uchida and N. Yoneda, *Solid State Ionics* **40/41**, 95 (1990).
- [2] J.P. Boilot, P. Colomban, G. Collin and R. Comes, *Solid State Ionics* **1**, 69 (1980).
- [3] G.S. Rohrer, J.O. Thomas and G.C. Farrington, *Chem. of Materials* **3**, 325 (1991).
- [4] S. Nicolopoulos, H. Vincent, M. Anne and J.C. Joubert, *J. Sol. State Chem.* **87**, 298 (1990).
- [5] O. Kalogirou, *J. Sol. State Chem.* **102**, 318 (1993).
- [6] O. Kalogirou, G. Bonsdorf, G. Stoikos, W. Gussner and H. Papadimitraki-Chlichlia, *Solid State Ionics* **74**, 205 (1994).

**ELECTROCHEMICAL AND MORPHOLOGICAL PROPERTIES OF TIN OXIDE****ELECTRODES****G.Savi, S.Panero & B.Scrosati****Dipartimento di Chimica, Università "La Sapienza", 00185 Rome, Italy**

Various classes of lithium intercalation materials have been characterized in the most recent years. Very successful and popular examples are the carbonaceous electrodes used as anodes in lithium ion cells. In alternative to an intercalation process also lithium alloying may be considered as a favourable approach to develop electrodes of importance in the modern electrochemical technology. However, the alloying process is generally accompanied by large volume variations which affect the electrode integrity upon cycling. A way to control this effect is that of using a compound, such as an oxide, as the starting material with the idea that the first electrochemical process may produce a metal dispersed in the oxide matrix in order to accommodate the volume variation associated to the following lithium alloying process. In our laboratory we have prepared low particle size tin oxide electrodes and characterized their electrochemical and morphological properties.

## SOLID STATE LITHIUM ION CONDUCTION IN PYRROLIDINIUM IMIDE SALTS

Junhua Huang<sup>1</sup>, Jiazeng Sun<sup>1</sup>, Pavla Meakin<sup>1</sup>, D. R. MacFarlane<sup>1</sup>, Shan Wong<sup>2</sup>, and Maria Forsyth<sup>2</sup>

Department of Chemistry<sup>1</sup> and Department of Materials Engineering<sup>2</sup>  
Monash University, Clayton, Victoria 3168, Australia

Molten salts of the bis(trifluoromethanesulfonyl) imide anion have been studied widely in recent years. [1] In our previous work, a new family of salts, based on the N,N-methyl alkyl pyrrolidinium cation and the bis(trifluoromethanesulfonyl) imide anion, has been synthesised. [2] Their properties, such as melting point, glass transition temperature, conductivity and electrochemical stability, were studied. It was found that some salts of the family exhibit multiple crystalline phases below their melting points, and that these show significant conductivity in their higher temperature crystal phase. It was proposed that this may be the result of the appearance of plastic crystal phases.

In this work, we have studied the binary systems formed from the pyrrolidinium imides salts mixed with lithium salts. In the N,N-methyl ethyl pyrrolidinium bis(trifluoromethanesulfonyl) imide (P12) - lithium imide system, the lowest melting point observed was 23°C, at lithium concentration of 33 mol% (Figure 1). The details of the phase diagram are not yet sufficiently clear for this to be unambiguously assigned as a eutectic. Figure 2 shows conductivity as a function of inverse temperature for various compositions. The maximum solid state conductivity was also obtained when the lithium concentration was around 33%. All compositions shown here show:

- i) significant conductivity below 23°C,
- ii) a distinct knee around 23°C,
- iii) in some cases, a further knee at higher temperatures, corresponding to the melting point of the sample.

The fact that all compositions show a knee at or near 23°C leads further support to the hypothesis that this represents a eutectic temperature. Above this temperature, samples having significantly higher liquidus points possess an increasingly large liquid domain as the temperature approaches the liquidus. Below this 23°C knee, we believe the sample to be completely solid (crystalline). However the conductivity reached is as high as  $10^{-4}$  S.cm<sup>-1</sup> just below this transition. The pure P12 salt also exhibits solid state conductivity but at a significantly lower level ( $10^{-8}$  S.cm<sup>-1</sup> at 20°C). [2] These results are similar to those reported by Angell for a family of methoxy trialkyl ammonium compounds mixed with Li<sup>+</sup> salts. [3]

Low temperature <sup>7</sup>Li NMR has been employed to probe the <sup>7</sup>Li dynamics of this system. The results appear to support the hypothesis that either the Li<sup>+</sup> itself or its immediate neighbours are highly mobile in the solid state well below 23°C.

## REFERENCE

- [1] J. Sun, M. Forsyth and D. R. MacFarlane, *J Physical Chemistry B* **102**, 8858 (1998).
- [2] D. R. MacFarlane, P. Meakin, J. Sun, N. Amini, M. Forsyth, *J Physical Chemistry*, submitted.
- [3] E. I. Cooper and C. A. Angell, *Solid State Ionics* **18 & 19**, 570 (1986).

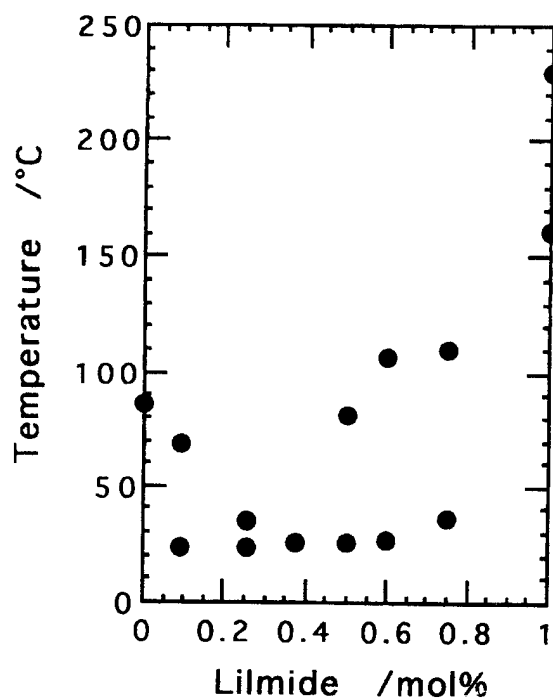


Figure 1. Phase Diagram of the P12 - Li imide system.

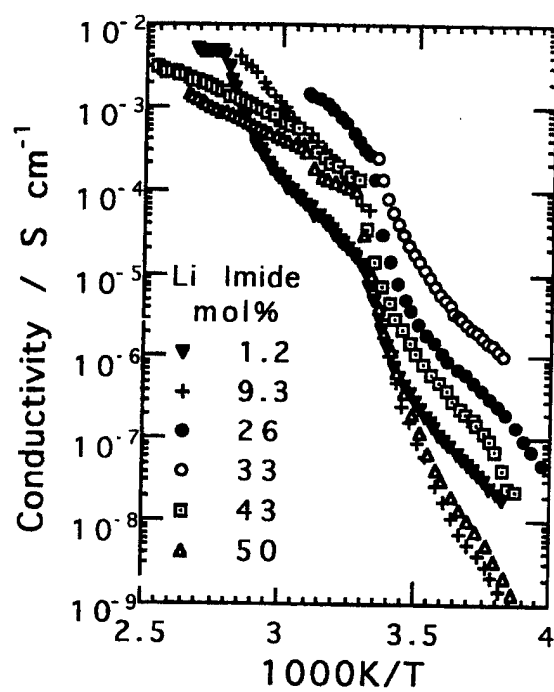


Figure 2. Conductivity of the P12 - Li imide system.

## Ionic conductivity of silica gels and dynamic properties of their pore liquids studied by impedance spectroscopy and polarized-light spectrofluorimetry

M. Wasiucione<sup>1</sup> and M. W. Breiter<sup>2</sup>

<sup>1</sup> Institute of Physics, Warsaw University of Technology, Koszykowa 75, 00-662 Warsaw, Poland

<sup>2</sup> Institut für Technische Elektrochemie, TU Wien, Getreidemarkt 9, 1060 Wien, Austria

Solid-like hybrid ionic conductors based on silica gels exhibit ionic conductivity as high as  $10^{-1} \text{ S}\cdot\text{cm}^{-1}$  (for proton conduction) [1] and  $10^{-2} \text{ S}\cdot\text{cm}^{-1}$  (for  $\text{Li}^+$  conduction) at room temperature [2,3]. These values are close to the conductivity of their respective pore liquids. It has been established that ionic conduction of these systems occurs solely within the liquid phase [4-6]. It has been also pointed out that the ionic transport within gel is influenced by effects due to entrapment of pore liquid in the gel matrix.

On the other hand wet silica gels have recently attracted many investigators as model bi-phasic systems in which the liquid-phase is confined inside the porous, fractal structure formed by a solid framework - gel skeleton. High porosity (exceeding 50% vol.) and narrow, technologically adjustable, pores of nanoscale dimensions are major factors which permit systematic studies of the dynamic behavior of molecules of liquids entrapped inside pores. Up to now most of these studies have applied NMR techniques. Their results reveal important modifications of the rotational and translational dynamics of molecules of pore liquids (mostly water) due to the confinement effects and the interactions of these molecules with highly developed surfaces of pore walls [7].

In this work we report the results of our studies of time dependence of ionic conductivity of silicate sols/gels and local mobility of the molecules of pore liquid using impedance spectroscopy and polarized-light spectrofluorimetry with pyranine as a photoprobe. The latter method (with photoprobes other than pyranine) has proved to be an informative source of data on changes of local molecular dynamics of the liquid phase during the sol-gel process [8].

The sols/gels were prepared from tetramethoxy orthosilicate (TMOS) using a single-step acid-catalyzed procedure described in Ref. [2]. Initial sol compositions corresponded to the formula  $\text{TMOS}:\text{H}_2\text{O}:\text{MeOH}:\text{HCl}=1:4:3:5\cdot 10^{-4}$ . Additionally  $10^{-5} \text{ M}$  of pyranine (HPS) was added to each batch. Impedance spectra were measured at room temperature in 2-probe configuration in 5 Hz - 10 MHz frequency range.

In spectrofluorimetric experiments vertically polarized excitation light at wavelength  $\lambda_{\text{exc}}=390 \text{ nm}$  was used. Emission spectra were taken in the range 400-600 nm at both vertical and horizontal polarizations.

It was found that ionic conductivity of the system under study slowly decreased as the sol-gel process went on. No abrupt change at gelation point was observed. Also emission spectra of the samples underwent polarization-dependent modifications during this process. Both time dependencies are discussed on assumption of correlation between long-range ionic transport and local molecular dynamics.

### Bibliography

- [1] M. Tatsumisago, H. Honjo, Y. Sakai, T. Minami, *Solid State Ionics*, **74**, 105 (1994).
- [2] M. Wasiucionek and M. W. Breiter, *J. Appl. Electrochem.*, **27**, 1106 (1997).
- [3] P.-W. Wu, S.R. Holm, A.T. Duong, B. Dunn and R.B. Kaner, *Chem. Mater.*, **9**, 1004 (1997).
- [4] M. W. Breiter, H. Durakpasa, B. Dunn, *Electroanal. Chem.*, **428**, 141 (1997).
- [5] M. Wasiucionek and M. W. Breiter, *J. Electroanal. Chem.*, **443**, 117 (1998).
- [6] M. Wasiucionek and M. W. Breiter, *Solid State Ionics*, in print.
- [7] J.-P. Korb, Xu. Shu, L. Malier, J. Jonas, *J. Chem. Phys.*, **107**, 4044 (1997).
- [8] R. Winter, D. W. Hua, X. Song, W. Maniutulin, and J. Jonas, *J. Phys. Chem.* **94**, 2706 (1990).

**DIFFUSION AND DIELECTRIC STUDIES OF THE SYSTEM PPG4000-NH<sub>4</sub>CF<sub>3</sub>SO<sub>3</sub>****G. Orädd<sup>1</sup>, M. Furlani<sup>2</sup>, A. Ferry<sup>1</sup>**<sup>1</sup>Dept. of Physical Chemistry/Physics -Umeå University - 90187 Umeå - Sweden<sup>2</sup>Physics and Engineering Physics -Chalmers University of Technology and Göteborg University  
41296 Göteborg - Sweden

Polymer electrolyte materials (PEs) intended for use in electrochemical applications such as high-energy-density batteries must exhibit a high ionic conductivity coupled with an efficient *cationic* transport. Cationic transference numbers are, however, generally low,[ 1] and solid PEs only display sufficiently high conductivities at elevated temperature. Most notably, fundamental details related to the exact nature of the ion-transport mechanisms still remain elusive.

In the present paper, we present a combination of pfg-NMR diffusion studies and dielectric measurements in an attempt to shed further light on the ion-migration processes in a model polymer electrolyte. By following separately the diffusive motion of <sup>19</sup>F and <sup>1</sup>H nuclei, respectively, we can correlate the diffusion of anions (CF<sub>3</sub>SO<sub>3</sub><sup>-</sup>) and cations (NH<sub>4</sub><sup>+</sup>) to ionic conductivity data. These studies we hope will provide an insight into the interplay of correlated ionic motion and net charge transport in typical polymer electrolytes. The particular PPG4000-NH<sub>4</sub>CF<sub>3</sub>SO<sub>3</sub> system was chosen since it is known to exhibit a pronounced composition dependence of its equivalent ionic conductivity, [2] which has been related to composition dependent ionic interactions in the electrolyte [3].

In conclusion, our results show that the Nernst-Einstein relation between ionic diffusion coefficients and net charge migration fails. We suggest that this behavior may be attributed to local inhomogeneities in these materials involving salt-rich microdomains, and consequently strongly correlated motions of ions, in accordance with previous reports on related systems [4, 5].

This work was supported by NFR, and the Wenner-Gren foundation. Partial support from stiftelsen Lars Hiertas Minne is also gratefully acknowledged.

## References

---

- <sup>1</sup> A. Ferry, M.M. Doeff and L.C. De Jonghe, *J. Electrochem. Soc.*, **145**(5), 1586 (1998).
- <sup>2</sup> I. Albinsson, B.-E. Mellander, and J. R. Stevens, *Solid State Ionics* **72**, 177 (1994).
- <sup>3</sup> A. Ferry, P. Jacobsson, and J.R. Stevens, *J. Phys. Chem.*, **100**, 12574 (1996).
- <sup>4</sup> A. Ferry, *J. Chem. Phys.*, **107**, 9168 (1997).
- <sup>5</sup> A. Ferry, G. Orädd, and P. Jacobsson, *J. Chem. Phys.*, **108**, 7426 (1998).

## CATION STABILIZED $\gamma$ -AgI THIN FILMS

*P. Babu Dayal, P. Senthil Kumar and C. S. Sunandana*

School of Physics, University of Hyderabad, Hyderabad 500 046. INDIA

Our interest in the study of formation of AgI layers (thin films) was stimulated by their application potential as hollow IR wave-guides for optical communication systems [1], particularly the  $\gamma$ -form of AgI. At ambient temperature and pressure, the well-known superionic conductor AgI exists in two polymorphic forms, a stable wurtzite phase ( $\beta$ -AgI) and a metastable zincblende phase ( $\gamma$ -AgI). The presence of excess of iodine (I<sup>-</sup>) ions produces the  $\beta$ -phase, whereas an excess of Ag<sup>+</sup>-ions always stabilizes the  $\gamma$ -phase.

Thin films of AgI were prepared conventionally by the iodization of silver films deposited onto a suitable substrate. In our effort to stabilize  $\gamma$ -AgI in thin film form, the silver films used were doped with small amounts of copper so as to form a single phase crystalline structure. The composition of silver and copper (weight ratio = 3:1) and the substrate temperature (300 K) were chosen such that neither an 'amorphous' phase nor a Ag-Cu alloy formation takes place. As the atomic sizes of Ag and Cu atoms are nearly equal, both the atoms are homogeneously mixed in the as-deposited film and the surface mobility of the adatoms allows only limited rearrangements which determine the microstructure of the film and hence its stability. Also, these minority cations act as "seed sites" and play a 'determinative structure role' in the iodization reaction leading to the formation of  $\gamma$ -AgI as in [2] and force the structure into a greater degree of face sharing of the iodine coordination polyhedra required for the stabilization of 'long-term'  $\gamma$ -AgI thin films.

In this paper, the preparative conditions of the thin films are discussed. The structure of the copper substituted silver films was indexed to be a metastable single silver-based fcc phase, with a near-random distribution of Cu<sup>+</sup>-ions among the available Ag<sup>+</sup>-sites. The XRD parameters of the Cu-substituted Ag-films and the as-coated pure Ag-films are analyzed. The diffraction patterns of the long-term stable  $\gamma$ -AgI thin films are compared with the standard JCPDS data. Optical absorption spectrum of these thin films also clearly shows the formation of  $\gamma$ -AgI. From the  $(\alpha h\nu)^2$  vs.  $h\nu$  plot, the band-gap of  $\gamma$ -AgI obtained is found to be in good agreement with the reported values. Electrical and dielectric behaviour of Ag |  $\gamma$ -AgI | Ag structures are under investigation.

### References:

- [1] R. J. Dahan, J. Dror and N. Croitoru, *Mat. Res. Bull.* **27** 761 (1992).
- [2] P. Senthil Kumar and C. S. Sunandana, *Thin Solid Films* **323** 110 (1998).



## THERMAL EXPANSION STUDIES ON AgI AND CuI

*P. Senthil Kumar<sup>†</sup>, N. S. Kini<sup>‡</sup>, A. M. Umarji<sup>‡</sup> and C. S. Sunandana<sup>†</sup>*

*<sup>†</sup>School of Physics, University of Hyderabad, Hyderabad - 500 046. INDIA.*

*<sup>‡</sup>Materials Research Centre, Indian Institute of Science, Bangalore - 560 012. INDIA.*

Tetrahedrally bonded semiconductors such as Si, Ge, GaAs and ZnS exhibits unusual and anomalous (negative) thermal expansion behavior. This effect is observed to increase with increasing ionicity and AgI (ionicity = 0.770) is found to have the most negative value among all the above materials in the same family, while CuI has a positive value despite its high ionicity (= 0.692). It is the aim of this present study to investigate thoroughly the thermal expansion of both AgI and CuI, which when compared with other related measurements and models could throw light on their superionic conduction and phase transition mechanisms.

Thermal Dilatometric measurements on these well-known cationic conductors AgI and CuI are reported over an extended temperature range of 300 - 900 K. The coefficient of linear thermal expansion ' $\alpha$ ' obtained are compared with the available data in the literature. The closely related crystal structures of  $\beta$ - and  $\gamma$ -AgI are discussed to account for their similar phase transition behaviors characterized by sharp anomalies with ' $\alpha$ ' going considerably negative at the transition temperature. This negative thermal expansion in AgI is explained on the basis of a defect model and is also in accordance with the recent molecular dynamics (MD) calculations. But, in the case of CuI, the thermal expansion is always positive owing to the less drastic structural rearrangement of ions. The thermal hysteresis anomalies corresponding to the phase transitions in these type of superionic conductors are thermodynamically viewed. These thermal expansion measurements are correlated to the analogous specific heat and X-ray diffraction data and it is suggested that a model, more fundamental than the one invoking simple Frenkel disorder, is necessary to account for these anomalies. The cumulant expansion procedure of EXAFS and the application of the recent 'bond valence model' to the thermal expansion of these superionic conductors are highlighted.

Thus, these observations lead us to conclude that there is a subtle interplay of vibrational anharmonicity and structural disorder which triggers the anomalies in thermal expansion and is expected to arise from the fluctuating p-d matrix elements between metal and iodine ions because of the thermal fluctuations in interatomic distances.

IONIC CONDUCTIVITY IN Cu-SUBSTITUTED  $\text{Ag}_3\text{SBr}$ 

R. B. Beeken and E. M. Beeken

Department of Physics and Astronomy

University of Wisconsin – Stevens Point

Stevens Point, Wisconsin 54481 U.S.A

$\text{Ag}_3\text{SBr}$  is a fast ion conductor first prepared and characterized in 1965. Since that time, the compound has been synthesized by solid state reaction, crystallization from the melt, and precipitation from aqueous solution. It is generally recognized that  $\text{Ag}_3\text{SBr}$  is extremely difficult to prepare in stoichiometric proportion. Typically, investigators report the presence of small quantities of unreacted  $\text{AgBr}$  even under the most carefully controlled conditions. Over the past twenty years, a number of investigations have been conducted to explore the effect of monovalent anion substitution on the ionic mobility of the silver cation in this compound. The present investigation provides complementary information on the effect of monovalent cation substitution in  $\text{Ag}_3\text{SBr}$ .

Nominally pure polycrystalline samples of  $\text{Ag}_{3-x}\text{Cu}_x\text{SBr}$  in the composition range  $x = 0 \rightarrow 0.25$  were prepared from the melt and annealed at 473 K for 6 months. In nominally pure  $\text{Ag}_3\text{SBr}$ , faint lines of unreacted  $\text{AgBr}$  can readily be observed in the x-ray diffraction pattern (Figure 1). As composition parameter  $x$  increases in the copper substituted compounds, the cubic structure of  $\text{Ag}_3\text{SBr}$  is gradually lost while the proportion of unreacted silver halide grows. Throughout the composition range investigated in this study, the lattice parameters of both the  $\text{Ag}_3\text{SBr}$  structure and the  $\text{AgBr}$  structure remain essentially unchanged.

The effect of Cu substitution on the ionic conductivity of  $\text{Ag}_3\text{SBr}$  is illustrated in Figure 2. With only small quantities of Cu replacing Ag in this compound, one observes a large reduction in the size of the conductivity jump associated with the  $\beta$ - $\gamma$  phase transition at 126 K. From the slopes of these Arrhenius plots, one further concludes that the activation energy governing  $\text{Ag}^+$  migration is increased in both the high temperature  $\beta$  phase and the low temperature  $\gamma$  phase with increasing Cu substitution. These results suggest that the  $\text{Cu}^+$  cation is much less mobile in the  $\text{Ag}_3\text{SBr}$  lattice and also acts to lower the mobility of the  $\text{Ag}^+$  cation as well.

FIGURE 1

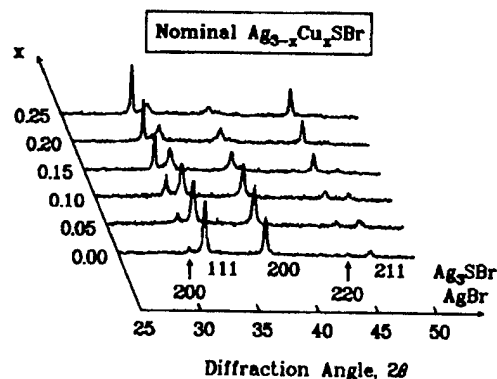
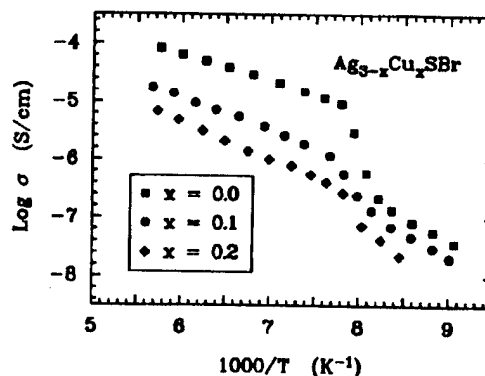


FIGURE 2



## CATHODIC SILVER DEPOSITION ON SILVER CHLORIDE USING IN-SITU ATOMIC FORCE MICROSCOPY AND KELVIN PROBE FORCE MICROSCOPY

Annett Spangenberg, Jürgen Fleig and Joachim Maier

Max-Planck-Institut für Festkörperforschung  
Heisenbergstraße 1, 70569, Stuttgart, Germany  
email: aspange@chemix.mpi-stuttgart.mpg.de

Since the development of the scanning tunneling microscope (STM) it has been mainly used to obtain topographical and structural information. Recently, several attempts have been made not only to determine the topography of surfaces, but to use scanning probe methods as a tool for the fabrication of nanometer scale structures on surfaces. Various techniques have been employed to obtain such nano- and microstructures. For example, Ullmann *et al.* [1] predeposited copper onto a tip of an STM and then deposited it onto a flat Au (111) surface, whereas Craston *et al.* [2] obtained Ag structures by means of transport of  $\text{Ag}^+$  through a Nafion substrate followed by reduction to metallic silver at the tip / ionic conductor interface. It has been stated that there are advantages using atomic force microscopy (AFM) rather than STM, especially when working on electronically insulating or weak conducting substrates [3].

In this study, silver deposition on silver chloride substrates was investigated using AFM and Kelvin probe force microscopy (KFM). In a TOPOMETRIX TMX 2000 Discoverer setup, a conductive tip as used for AFM and KFM is employed as a working electrode. When applying a bias voltage between the tip (negative) and a silver counter electrode on the backside of the crystal (positive) a faradaic current passes when establishing contact with the surface of the silver chloride. Thereby, Ag from the electrode crossing the crystal as  $\text{Ag}^+$  is reduced back to metallic silver at the interface between tip and ionic conductor.

The deposition process was studied in dependence of several parameters such as applied bias, time, surface preparation and current density. The possibilities of fabricating structures by moving the tip over the silver chloride surface will be discussed. Additionally, the dissolution process of silver back into the crystal has been investigated.

In contrast to Ref. [1] the deposited silver structures were observed using the working electrode tip in the force scanning mode. To enhance the information about the deposited metal structures, not only the topography is imaged with AFM, but also surface potentials are scanned simultaneously using the Kelvin probe technique.

[1] R. Ullmann, T. Will and D.M. Kolb, Ber. Bunsenges. Phys. Chem. **99** (1995) 1414.

[2] D.H. Craston, Charles W. Lin and A.J. Bard, J. Electrochem. Soc. **135** (1988) 785.

[3] H.C. Day and D.R. Allee, Appl. Phys. Lett. **62** (1993) 2691.

## ELECTROCHEMICAL AND STRUCTURAL CHARACTERIZATION OF SILVER HAFNIUM SULFIDE CATHODES

Hiroaki Wada, Kenji Sakamaki and Motohiko Ishii  
National Institute for Research in Inorganic Materials  
1-1 Namiki, Tsukuba-shi, Ibaraki 305-0044 Japan

Sulfide compounds with layered and/or framework structures have been expected as one of the candidates of cathode materials in Li cell and a lot of fundamental researches have been done on them for more than twenty years. However, nothing was known concerning ternary sulfides of Ag-Hf-S system. Cubic  $\text{Ag}_4\text{Hf}_3\text{S}_8$  was investigated in this study on the premise that it has 3D rigid framework structure and lithium can be easily inserted by *n*-BuLi [1]. Studies were conducted to more fully characterize the cathodic behavior and structural change of  $\text{Ag}_4\text{Hf}_3\text{S}_8$  in lithium cells.

Electrochemical cells were constructed with lithium metal anodes and  $\text{Li}_x\text{Ag}_4\text{Hf}_3\text{S}_8$  cathodes in non-aqueous organic solvent. Three types of electrolytes used were (1) 1M LiI + propylene carbonate (PC), (2) 1M  $\text{LiClO}_4$  + PC and (3) 1M  $\text{LiPF}_6$  + PC. All the experiments were carried out in a glove box under high-purity argon atmosphere at ambient temperature.

In the case of an electrolyte type (2) the cathodic behavior was examined by using compact  $\text{Ag}_4\text{Hf}_3\text{S}_8$  pellet which was embeded in epoxy resin. Only outside part of pellet (radius: 6.35mm) was reacted. At several discharge stages its crystal structure was checked by X-ray powder diffraction and compared with that of chemical lithiation by *n*-BuLi. Figure 1 shows a low rate discharge curve of  $\text{Li}_x\text{Ag}_4\text{Hf}_3\text{S}_8$  at a current density of  $8 \mu\text{A}/\text{cm}^2$ . The cell voltage varied from 2.4V to 1.3V. The flat cell voltage profiles of two-phase mixture appeared at the first steps of Li-insertion. Figure 2 gives XRD patterns of cathodes at the corresponding discharge stage (a) and (b) in Fig. 1. The phase (a) is cubic  $\text{Ag}_4\text{Hf}_3\text{S}_8$  with the lattice constant of  $a=10.91 \text{ \AA}$  [2]. The phase (b) is cubic  $\text{Li}_x\text{Ag}_4\text{Hf}_3\text{S}_8$  with the lattice constant of  $a=10.43 \text{ \AA}$  whose XRD pattern is similar to that of the cubic  $\text{Li}_5\text{Ag}_2\text{Hf}_3\text{S}_8$  obtained by topochemical lithiation reaction of  $\text{Ag}_4\text{Hf}_3\text{S}_8$  with *n*-BuLi. However, it should be noted that no native silver occurred in the electroinsertion of lithium but small amount of monoclinic phase (c) appeared. Sometimes polarization phenomena was observed less than 1.9V.

In the case of other systems similar electrochemical and structural characterization was performed using XRD, IR, a.c conductivity measurement and charge-discharge cycle behavior.

References: [1] H. Wada et al., Solid State Ionics (in press).

[2] O. Amiel & H. Wada, J. Solid State Chem. 115, 112 (1995).

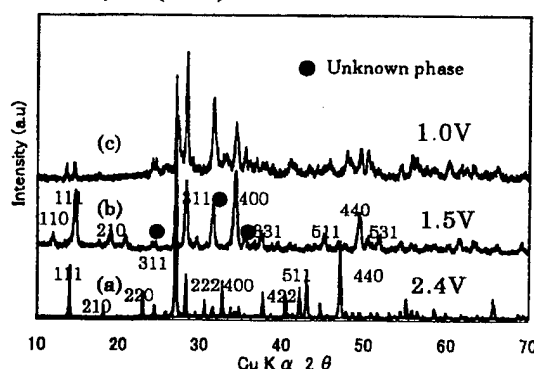
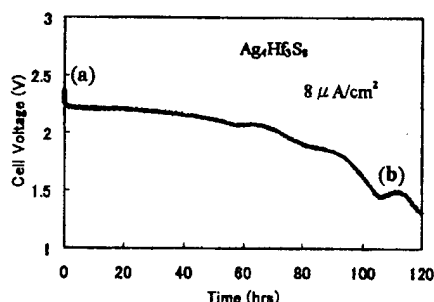


Fig. 1 Discharge curves of Li/1.0M  $\text{LiClO}_4$  +PC/ $\text{Ag}_4\text{Hf}_3\text{S}_8$

Fig. 2 XRD patterns of  $\text{Ag}_4\text{Hf}_3\text{S}_8$  cathode before and after discharge

CHARACTERIZATION OF BASIC TRANSPORT PARAMETERS IN A NEW FAST  $\text{Ag}^+$  ION  
CONDUCTING COMPOSITE ELECTROLYTE SYSTEM :  $(1-x)[0.75\text{AgI}:0.25\text{AgCl}]:x\text{ZrO}_2$

R.C. Agrawal,<sup>\*</sup> R.K. Gupta, Mohan L. Verma, S. Thaker<sup>+</sup>

Solid State Ionics Research Laboratory, School of Studies in Physics,

Pt. Ravishankar Shukla University, Raipur - 492010, M.P., INDIA

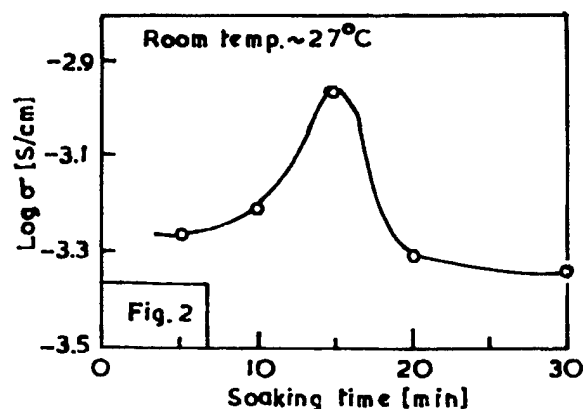
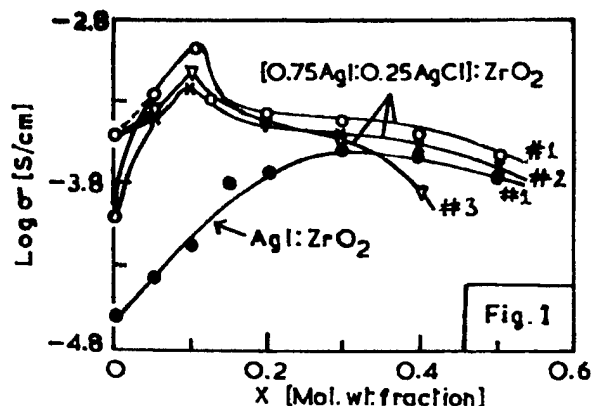
<sup>+</sup> Govt. Science College, Raipur - 492010, M.P., INDIA

Studies on ionic transport property of a new fast  $\text{Ag}^+$  ion conducting 2-phase composite electrolyte system :  $(1-x)[0.75\text{AgI}:0.25\text{AgCl}]:x\text{ZrO}_2$ , where  $0 \leq x \leq 0.5$  (in molar weight fraction), are reported. An alternate compound : 'a quenched/annealed  $[0.25\text{AgI}:0.25\text{AgCl}]$  mixed system/solid solution', recently investigated in the present laboratory [1], has been used as first phase host matrix salt in place of the conventional salt  $\text{AgI}$ . The average size particles ( $\leq 5 \mu\text{m}$ ) of the insulating second phase compound  $\text{ZrO}_2$  were dispersed into the first phase. Homogeneous mixtures of I<sup>st</sup> & II<sup>nd</sup> phase in different compositions were synthesized adopting following routes of preparation :

- #1. Heated  $\sim 700^\circ\text{C}$  for 15 min (soaking time) then quenched rapidly to  $\sim 10^\circ\text{C}$ ;
- #2. Heated  $\sim 700^\circ\text{C}$  for 15 min then left to cool itself to room temperature in air;
- #3. A simple homogeneous mixture thoroughly ground at room temperature.

Fig. 1 shows the compositional dependence of room temperature conductivity. Similar variation for composite electrolyte system :  $(1-x)\text{AgI}:x\text{ZrO}_2$ , prepared by route #1 using conventional host salt  $\text{AgI}$ , is also drawn for direct comparison. The composition :  $0.9[0.75\text{AgI}:0.25\text{AgCl}]:0.1\text{ZrO}_2$ , prepared by route #1 exhibited highest enhancement ( $\sim 10^1$ ) in the room temperature conductivity ( $\sigma_{27^\circ\text{C}} \sim 1.1 \times 10^{-3} \text{ S.cm}^{-1}$ ) as compared to annealed host. This is referred to as 'optimum conducting composition' (OCC). The new host resulted into a better electrolyte system. The soaking time i.e. the time for which the sample mixture is heated at  $\sim 700^\circ\text{C}$ , plays a crucial role as regards to attaining optimum conductivity. Fig. 2 shows 'room temperature conductivity vs soaking time' variation for the OCC. The ionic transport property characterization as a function of temperature was studied on the OCC employing various techniques such as electrical conductivity ( $\sigma$ ) by impedance spectroscopy, ionic mobility ( $\mu$ ) by transient ionic current (TIC) technique, ionic transference number ( $t_{\text{ion}}$ ) by Wagner's dc polarization method etc.; subsequently, mobile ion concentration ( $n$ ) was evaluated from  $\sigma$  and  $\mu$  data and ionic drift velocity ( $v_d$ ) from the Wagner's 'current vs time' plot. The ion transport mechanism in this system has been explained on the basis of existing models on 2-phase composite electrolyte systems.

[1] R.C. Agrawal, R.K. Gupta, R. Kumar and A. Kumar, J. Mater. Sci. 29, 3673 (1994).



# LOCAL ORDER OF Ag IN AgI-Ag<sub>2</sub>MoO<sub>4</sub> GLASSES: AN EXAFS STUDY

Paolo Ghigna, Melissa Di Muri, Piercarlo Mustarelli, Corrado Tomasi, Aldo Magistris  
Dipartimento di Chimica Fisica and CSTE-CNR, Via Taramelli 16  
27100 Pavia, Italy

Silver iodomolybdate glasses are a good model system to investigate the structure/transport relationships in highly disordered systems. Recently, the debate on this topic

has been enriched by both theoretical and experimental contributions which are summarized in [1]. In particular, the picture is emerging that the cation transport is not related to the existence of AgI clusters, but rather to the combined effect of: i) glass network expansion, and ii) formation of preferential pathways connected to the different oxygen/iodine coordination spheres that are experienced by the silver ions. In this frame, it is important to study the local order around Ag<sup>+</sup>. Here, we present a preliminar EXAFS study of some silver iodomolybdate glasses.

Figure 1 shows the EXAFS spectrum at the Ag-K edge of a 0.66AgI:0.33Ag<sub>2</sub>MoO<sub>4</sub> glass at 77 K. The spectrum analysis was performed by means of the GNXAS package [2]. Although the spectrum is noisy ( $N \sim 5 \times 10^{-4}$ ), the model used for the fitting procedure leads to unambiguous conclusions.

Figure 2 shows the EXAFS Fourier Transform of the spectrum of Figure 1. From the scattering amplitudes and phase shifts, the peaks at  $\sim 1.9$  Å and  $\sim 2.6$  Å are attributed to oxygen and iodine atoms, respectively. After correction for the phase shifts the bond distances reported in Table 1, together with the other fitting parameters, are found. The coordination number,  $n$ , found for iodine is in agreement with the <sup>109</sup>Ag NMR results previously reported by our group [3].

Further work is in progress to investigate the structural modifications which can take place above the glass transition and in correspondence of the devitrification.

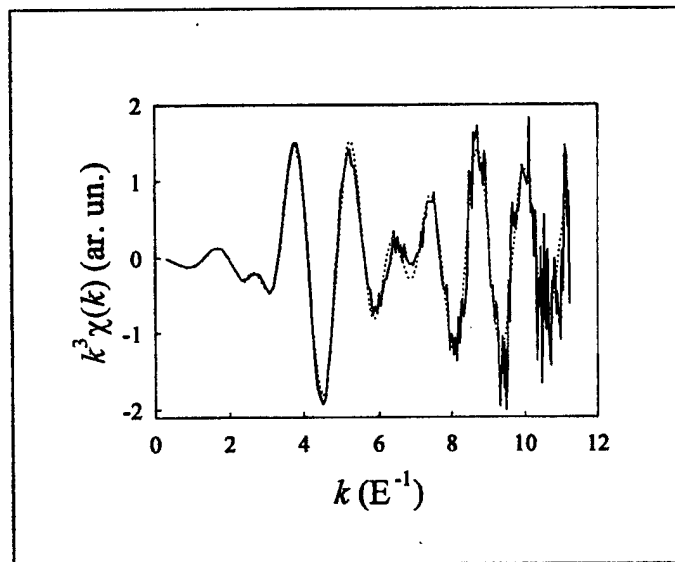


Figure 1 - Continuous line: spectrum; dotted line: fit; dashed line: difference.

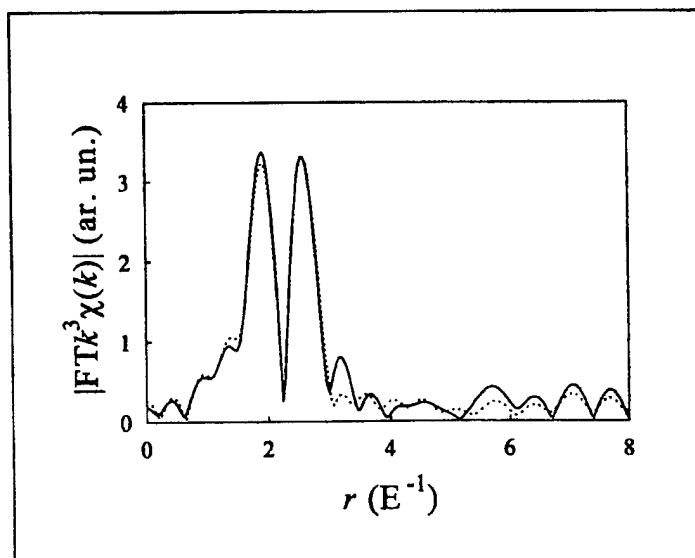


Figure 2 - Continuous line: FT of the spectrum; dotted line: fit; dashed line: difference.

TABLE 1

Shell	Atom	$n$	$r$ (Å)	$\sigma^2$ (Å <sup>2</sup> )
1	O	1.5(2)	2.38(1)	0.01(3)
2	I	1.5(2)	2.830(5)	0.096(9)

- [1] A. Magistris, P. Mustarelli, C. Tomasi, Proceedings of the Sixth Asian Conference on Solid State Ionics, Surajkund, India, 29 Novembre-4 December 1998.
- [2] A. Filipponi, A. Di Cicco, C.R. Natoli, Phys.Rev. B **52**, 15122 (1995); A. Filipponi, A. Di Cicco, Phys.Rev. B **52**, 15135 (1995).
- [3] P. Mustarelli, C. Tomasi, E. Quartarone, A. Magistris, M. Cutroni and A. Mandanici, Phys. Rev. B, **58**, 9054 (1998).

## LOCAL RELAXATION, IONIC MOTION AND ELECTRONIC STRUCTURE OF SILVER OR COPPER ION CONDUCTING CRYSTALS AND GLASSES

Teruyoshi Awano

Department of Applied Physics, Tohoku Gakuin University, Tagajo 985, Japan

There seems to be a relation between local relaxation and ionic motion, because the relaxation process is motion of surrounding ions. Local relaxation has relation also with electronic structure[1]. Relation among these is discussed in this paper.

In organic-inorganic mixed glasses of  $(\text{CH}_3)_4\text{NI}-(\text{C}_2\text{H}_5)_4\text{NI-AgI}$  (TMAI-TEAI-AgI) and its derivatives organic ion radicals were induced by irradiation coloration[2]. They were not affected by ionic conductivity. On the contrary,  $\text{Ag}^{2+}$ ,  $\text{Ag}^0$  and aggregated  $\text{Ag}^0$  were observed in inorganic glasses of  $\text{AgI-AgPO}_3$ ,  $\text{AgI-Ag}_2\text{O-B}_2\text{O}_3$ ,  $\text{AgI-Ag}_2\text{MoO}_4$ ,  $\text{AgI-Ag}_2\text{WO}_4$ .  $\text{Ag}^{2+}$  was induced in all of these inorganic glasses. Some difference seems to be due to the difference of the framework structure of these glasses. These color centers in inorganic glasses were affected by ionic conductivity. Coloration efficiency and thermal stability of induced color centers decreased when the ratio of AgI increased in inorganic superionic glasses. Coloration efficiency also decreased as irradiation temperature increased. These seem to be due to the high ionic mobility, which increase recombination probability of the hole on a silver ion and an electron anywhere else. In this paper, quantitative simulation calculation of this process is reported.

There were far-infrared absorption band around  $100\text{cm}^{-1}$  ( $130\text{cm}^{-1}$  in cuprous glasses), submillimeter band around  $30\text{cm}^{-1}$  and millimeter wave band around  $7\text{cm}^{-1}$  ( $9\text{cm}^{-1}$  in cuprous glasses) in far-infrared and millimeter wave spectra of these superionic glasses[3]. The millimeter wave band is due to a sort of translation motion of conduction ions. In this paper, quantitative simulation of these results is reported.

Previously, color centers and far-infrared and millimeter wave spectra of alkali-silver/cuprous-halide superionic conducting crystals of  $\text{AM}_4\text{X}_5$  (A=alkali metal; M=Ag or Cu; X=halogen) and their derivatives were reported[4,5]. Both of trapped hole centers and trapped electron centers were induced by irradiation at low temperature in silver conductors. The hole was trapped on a silver ion vacancy. It was strongly influenced by the increase of ionic conductivity. On the contrary, a hole trapped on a copper ion ( $\text{Cu}^{2+}$ ) was induced in the copper ion conductor. This seems to be due to the difference of their electronic energy band structures. In this paper, effect of electronic band structure to relaxation process is discussed. In  $\text{AM}_4\text{X}_5$  crystal, a structure by "ionic plasmon" was observed in the spectral region below  $10\text{cm}^{-1}$  in silver ion conductors or  $30\text{cm}^{-1}$  in copper ion conductors in energy loss function spectra at temperatures of superionic conducting phase. Relation between such ionic motion and relaxation is discussed.

## References

- [1]T. Awano, T. Nanba, M. Ikezawa, T. Matsuyama and H. Yamaoka, J. Phys. Soc. Jpn. **58**, 2570 (1989).
- [2]K. Handa, N. Sasaki, T. Awano and T. Matsuyama, SSI-11, D42.
- [3]N. Sasaki, K. Handa, and T. Awano, SSI-11, D41.
- [4]T. Awano, M. Ikezawa, T. Matsuyama and H. Yamaoka, Solid State Ionics, **40/41**, 324 (1990).
- [5]T. Awano, T. Nanba and M. Ikezawa, Solid State Ionics, **53-56**, 1269 (1992).



## PREPARATION OF AMORPHOUS SOLID ELECTROLYTES IN THE SYSTEM $\text{Li}_2\text{S}-\text{SiS}_2-\text{Li}_4\text{SiO}_4$ BY MECHANICAL MILLING

Masahiro Tatsumisago, Hideyuki Morimoto, Hideki Yamashita  
and Tsutomu Minami

Department of Applied Materials Science, Osaka  
Prefecture University, Sakai, Osaka 599-8531, Japan

Amorphous materials are one of the most promising candidates for solid electrolytes utilized for lithium secondary batteries. We have prepared a variety of oxysulfide glasses with high performance as solid electrolytes by using melt quenching procedures [1]; very high conductivities over  $10^{-3} \text{ Scm}^{-1}$  at room temperature and high stability against crystallization have been obtained in the melt quenched glasses [2]. However, when these glasses are utilized as solid electrolytes for lithium secondary batteries, they should be ground to fine powders in order to have a good contact with electrode materials [3].

Very recently we have demonstrated that the lithium ion conductive materials in the oxysulfide systems can be synthesized by use of a new procedure of mechanical milling [4,5]. This procedure is basically a room-temperature process and useful to obtain fine powders directly for solid lithium secondary batteries.

In the present paper, reported are the formation, electrical properties, morphologies, and local structure of the amorphous materials in the system  $\text{Li}_2\text{S}-\text{SiS}_2-\text{Li}_4\text{SiO}_4$  obtained by use of a high energy ball milling technique.

Crystalline raw materials of  $\text{Li}_2\text{S}$ ,  $\text{SiS}_2$  and  $\text{Li}_4\text{SiO}_4$  were used as starting materials for mechanical milling. The treatment was carried out to a mixture of the raw materials using a planetary ball mill at room temperature; alumina pots and balls were mainly used.

Figure 1 shows the X-ray diffraction patterns of the powder samples of a nominal composition of  $95(0.6\text{Li}_2\text{S}-0.4\text{SiS}_2)-5\text{Li}_4\text{SiO}_4$  with different milling periods as an example. Diffraction peaks due to  $\text{Li}_2\text{S}$ ,  $\text{SiS}_2$  and  $\text{Li}_4\text{SiO}_4$  are observed in the powder mixture without mechanical milling. After milling for 1 h the peaks due to  $\text{SiS}_2$  and  $\text{Li}_4\text{SiO}_4$  almost disappear and halo pattern overlaps to the peaks due to  $\text{Li}_2\text{S}$ . As the milling periods are increased, the intensity of the  $\text{Li}_2\text{S}$  peaks is decreased and the halo pattern becomes dominant, indicating that the amorphous part in the mixture is increased with an increase in the milling period.

Figure 2 shows the temperature dependence of electrical conductivity of the powder samples of  $95(0.6\text{Li}_2\text{S}-0.4\text{SiS}_2)-5\text{Li}_4\text{SiO}_4$  prepared with different milling periods. In all the cases of milling period, conductivities follow the Arrhenius type equation. The conductivity of the as-mixed sample is as low as an order of  $10^{-9} \text{ Scm}^{-1}$ . On the other hand the conductivities of the mechanically milled samples are increased with an increase in the milling periods. The conductivities of the samples milled for more than 5 h are higher than  $10^{-4} \text{ Scm}^{-1}$  at room temperature, which is comparable to the conductivity values of the corresponding melt-quenched glasses. Activation energies for conduction are decreased from 78 to 32  $\text{kJmol}^{-1}$  with an increase in the milling periods. It is interesting to notice that the mechanical milling for only 1 h drastically enhances the conductivity by more than three orders of magnitude although the intense diffraction peaks due to low conductive  $\text{Li}_2\text{S}$  crystals are observed in the XRD patterns as shown in Fig.1.

In order to clarify the formation process of the high lithium ion conductive phase during mechanical milling, the structure change of the mixture with milling was investigated by means of MAS NMR technique. Figure 3 shows the  $^{29}\text{Si}$  MAS NMR spectra of the powders of  $95(0.6\text{Li}_2\text{S}-0.4\text{SiS}_2)-5\text{Li}_4\text{SiO}_4$  prepared with different milling periods. The peak at around -20 ppm observed in the as-mixed sample is due to the  $\text{SiS}_4$  tetrahedral units with two edge sharing (E(2)), which corresponds to the presence of  $\text{SiS}_2$  crystals. After mechanical milling for only 1 h, the peak at around -20 ppm almost disappears and two peaks at around -3 and 5 ppm appear. These peaks are attributable to the  $\text{SiS}_4$  tetrahedral units with one edge sharing (E(1)) and no edge sharing (E(0)), respectively. By the mechanical milling for only 1 h, all the  $\text{SiS}_2$  crystals

probably react with a part of  $\text{Li}_2\text{S}$  and/or  $\text{Li}_4\text{SiO}_4$ . SEM observation also showed that all the  $\text{SiS}_2$  crystal particles disappeared after milling for 1 h. The powders mechanically milled for more than 5 h exhibit three new peaks at around -25, -60 and -110 ppm. These peaks are attributable to  $\text{SiS}_2\text{O}_2$ ,  $\text{SiSO}_3$ , and  $\text{SiO}_4$  tetrahedral units, respectively. The NMR pattern for the powder after milling for 20 h is very similar to that of the corresponding melt-quenched glass, indicating that the local structure of the amorphous  $95(0.6\text{Li}_2\text{S}-0.4\text{SiS}_2)-5\text{Li}_4\text{SiO}_4$  powder prepared by mechanical milling is close to that of corresponding glass.

### References

- [1] M. Tatsumisago, K. Hirai, T. Hirata, M. Takahashi, and T. Minami, *Solid State Ionics*, **85-88**, 487 (1996).
- [2] M. Tatsumisago, K. Hirai, T. Minami, K. Takada, and S. Kondo, *J. Ceram. Soc. Jpn.*, **101**, 1315 (1993).
- [3] K. Iwamoto, N. Aotani, K. Takada, and S. Kondo, *Solid State Ionics*, **79**, 228 (1995).
- [4] H. Morimoto, H. Yamashita, M. Tatsumisago, and T. Minami, *J. Am. Ceram. Soc.* (1999), in press.
- [5] H. Morimoto, H. Yamashita, M. Tatsumisago, and T. Minami, *J. Ceram. Soc. Jpn.*, submitted for publication.

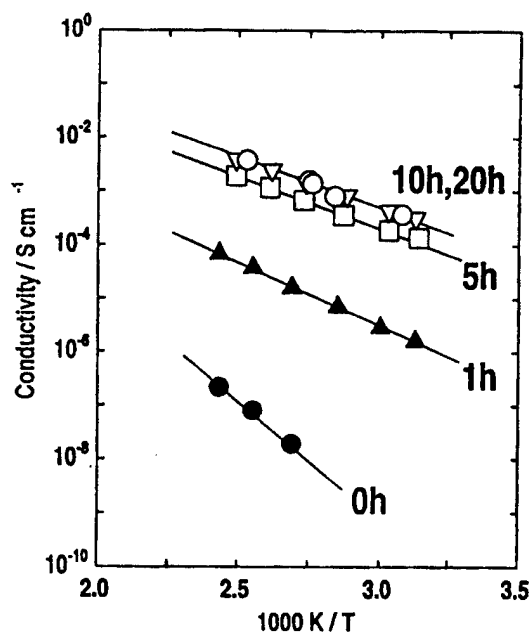


Fig. 2 Temperature dependence of electrical conductivity of the powder samples of  $95(0.6\text{Li}_2\text{S}-0.4\text{SiS}_2)-5\text{Li}_4\text{SiO}_4$  prepared with different milling periods.

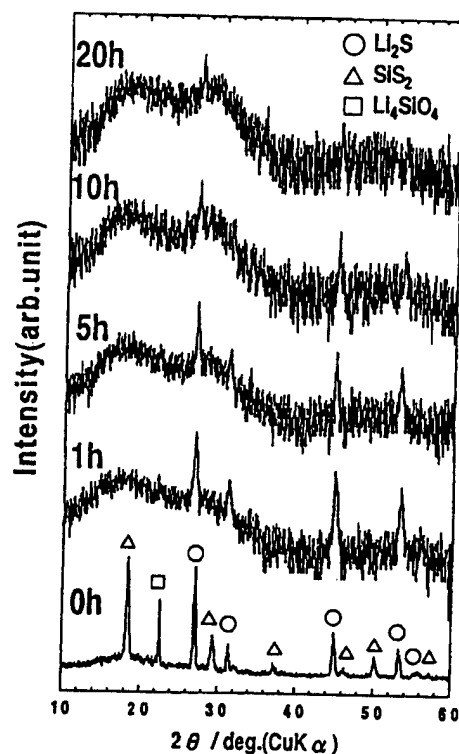


Fig. 1 X-ray diffraction patterns of the powder samples of a nominal composition of  $95(0.6\text{Li}_2\text{S}-0.4\text{SiS}_2)-5\text{Li}_4\text{SiO}_4$  with different milling periods.

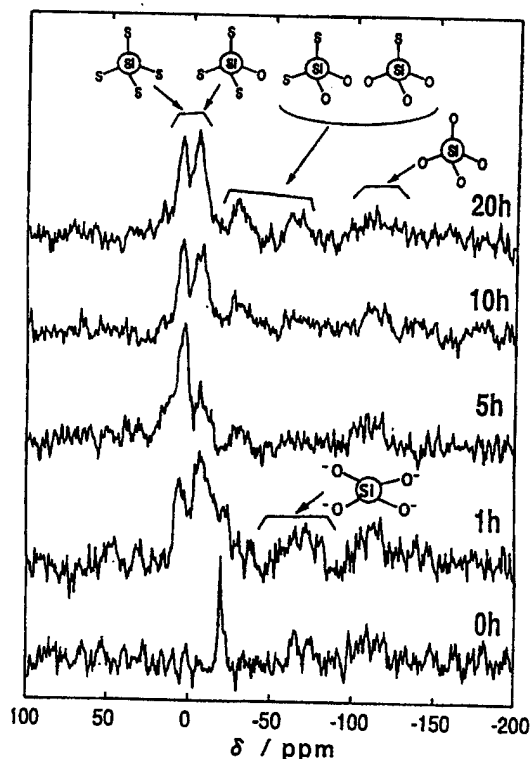


Fig. 3  $^{29}\text{Si}$  MAS NMR spectra of the sample of  $95(0.6\text{Li}_2\text{S}-0.4\text{SiS}_2)-5\text{Li}_4\text{SiO}_4$  prepared with different milling periods.

LITHIUM COORDINATION AND ORDERING IN TRICLINIC  $\text{LiZr}_2(\text{PO}_4)_3$  NASICON:  
A NEUTRON DIFFRACTION STUDY

Michele Catti and Sonia Stramare

Dipartimento di Scienza dei Materiali, Università di Milano II, via Cozzi 53, 20126 Milano, Italy

Within the Nasicon family of ionic conductors, sodium-containing compounds have been thoroughly investigated both from the structural and from the electrical point of view. Much less is known about the detailed structural features of lithium and hydrogen phases, mainly because such atoms are poor X-ray scatterers. On the other hand, a full knowledge of the  $\text{Li}^+$  and  $\text{H}^+$  atomic environments is essential to understand the mechanisms of ionic mobility in these materials [1-3]. The phase of  $\text{LiZr}_2(\text{PO}_4)_3$  synthesized by solid state reaction at 1200 °C is reported to have the rhombohedral  $R\bar{3}c$  Nasicon structure above 50 °C, and to be monoclinic  $C2/c$  at room temperature, on the basis of conventional X-ray diffractometry [1]. We have prepared this phase and studied it carefully by X-ray powder diffraction at variable temperature (Siemens diffractometer with Buehler high-temperature attachment,  $\text{CuK}\alpha$  radiation), and by high-resolution powder neutron diffraction at the ISIS facility of the Rutherford Appleton Laboratory, Chilton, U.K. At first, the room-temperature X-ray diffraction pattern could be indexed according to a monoclinic  $C2/c$  unit-cell, but at closer inspection the  $hkl$  and  $h\bar{k}l$  reflections appeared to be splitted indicating a triclinic  $C\bar{1}$  symmetry. The phase transition to rhombohedral Nasicon structure was confirmed to occur above 50 °C, and the kinetics of the transformation was studied by following the time and temperature evolution of the intensity of significant Bragg peaks.

Neutron diffraction data were collected by the time-of-flight High Resolution Powder Diffractometer (HRPD) at  $2\theta=168.3^\circ$ , in the  $d_{hkl}$  ranges 0.7 to 2.5 Å (12 h) and 2.4 to 4.0 Å (5 h), at room temperature. As in the X-ray case, the true unit-cell appeared to be unambiguously triclinic. Correspondingly, attempts to refine the structure in the  $C2/c$  space group failed ( $R_p=0.23$ ), but confirmed the presence of a monoclinic pseudo-symmetry in a slightly distorted triclinic lattice. Thus the isotropic Rietveld refinement converged successfully in space group  $C\bar{1}$  for 4226 data and 105 variables, with final agreement factors  $R_p=0.0672$ ,  $wR_p=0.0929$ ,  $R(F^2)=0.0617$ . In Fig. 1, the experimental, calculated and difference profiles are shown. The following lattice constants were obtained:  $a=15.0717(1)$ ,  $b=8.8555(1)$ ,  $c=9.1234(1)$  Å,  $\alpha=89.662(1)$ ,  $\beta=123.913(1)$ ,  $\gamma=90.428(1)^\circ$ . All of the 18 atoms in the asymmetric unit but two (Li and P2) are related in pairs by the pseudo-twofold axis, with average shifts of 0.0126, 0.0197 and 0.0115 for the x, y and z fractional coordinates, respectively, with respect to the -x, y, 1/2-z operation. The average e.s.d.'s of atomic coordinates are 0.0004 (x), 0.0006 (y), 0.0007 (z), and relevant interatomic distances are given in Table 1. The Li atom could be located by Fourier difference maps in a site tetrahedrally coordinated by four O atoms, plus a fifth one interacting weakly at a longer distance (Table 1). This contrasts with the position in octahedral coordination (six Li-O distances of 2.50 Å) reported for Li in the  $R\bar{3}c$  phase of  $\text{LiZr}_2(\text{PO}_4)_3$  [1]. Indeed, a careful comparison of the low- ( $C\bar{1}$ ) and high- ( $R\bar{3}c$ ) temperature structures shows that, in the former case, lithium orders with double multiplicity in half of the channels available in the Nasicon framework, thus achieving a less favourable configuration for hopping; this accounts for the lower ionic conductivity of the room-temperature phase. Thus, relevant implications for the  $\text{Li}^+$  mobility and transport mechanism vs. temperature ensue.

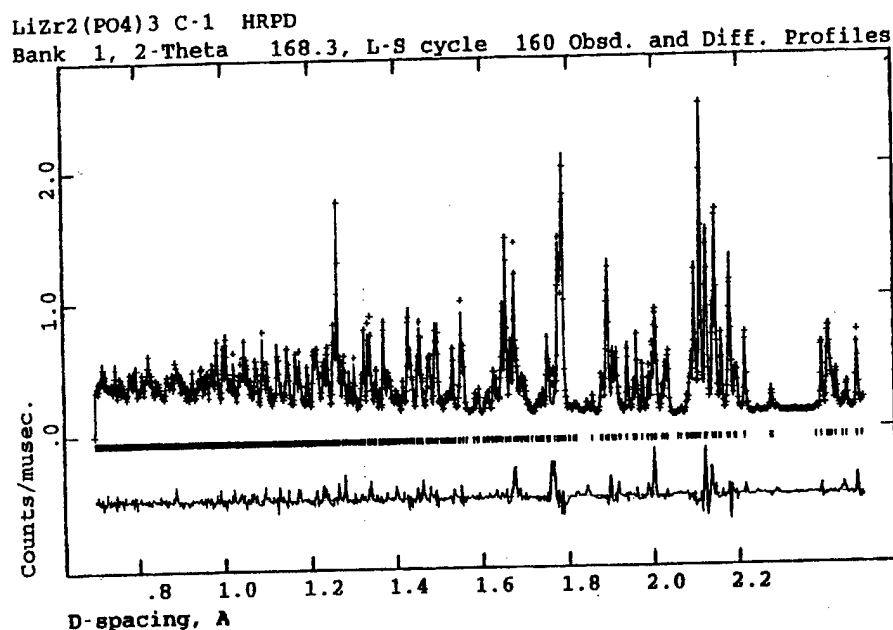


Fig. 1. Experimental, calculated and difference profiles of LiZr<sub>2</sub>(PO<sub>4</sub>)<sub>3</sub>.

Table 1. Interatomic distances (Å) of LiZr<sub>2</sub>(PO<sub>4</sub>)<sub>3</sub>. E.s.d.'s are given in parentheses.

Li - O2	1.891(21)	P1 - O1'	1.524(7)	P1' - O1	1.497(7)
O3	2.137(18)	O2	1.499(7)	O2'	1.555(7)
O5'	2.083(19)	O4'	1.585(7)	O4	1.574(7)
O6'	2.272(20)	O5	1.477(6)	O5'	1.546(7)
<Li-O>	2.096	<P1-O>	1.521	<P1'-O>	1.543
Li - O4'	2.672(20)				
P2 - O3	1.499(7)	Zr1 - O1	2.032(6)	Zr1' - O1'	2.017(7)
O6	1.557(8)	O2	2.192(6)	O2'	2.029(7)
O3'	1.525(8)	O3	2.122(7)	O3'	1.988(8)
O6'	1.576(7)	O4	2.043(7)	O4'	2.102(7)
<P2-O>	1.539	O5	2.082(7)	O5'	2.122(7)
		O6	2.015(6)	O6'	2.072(6)
		<Zr1-O>	2.081	<Zr1'-O>	2.055

## References

- [1] D. Petit, Ph. Colomban, G. Collin and J.P. Boilot, Mat. Res. Bull. **21**, 365 (1986).
- [2] P.R. Rudolf, M.A. Subramanian, A. Clearfield and J.D. Jorgensen, Solid State Ionics **17**, 337 (1985).
- [3] F. Sudreau, D. Petit and J.P. Boilot, J. Solid State Chem. **83**, 78 (1989).

## STUDY THE TRANSPORT PROPERTIES OF CRYSTALLINE SUPERIONIC CONDUCTOR - $\text{Li}_2\text{B}_4\text{O}_7$

Aliev A.E., Krivorotov V.F., Kholmanov I. N.  
Thermal Physics Department, Uzbek Academy of Sciences,  
Katartal str.28, Tashkent 700135, Uzbekistan

Lithium ion conducting superionic conductors are paid much attention, because of their application in solid batteries. Unusual physical properties of these materials, observed in various experimental measurements are mainly caused by their structural peculiarity.

One of the high temperature Li ion conducting material is lithium tetraborate. It is well known, that lithium tetraborate single crystal is a quasi-1D superionic conductor along the crystalline axis (001), which is clearly observed in the temperature dependence of conductivity. To study the mechanism of lithium sublattice disordering process in detail, we have investigated the thermoelectric power of lithium tetraborate in the temperature range of 300-700 K. Obtained experimental results are discussed in the following two considerations:

- 1). In the range 300-530 K the thermoelectric power linearly grows with increasing of the temperature, with the change of the slope of the thermoelectric power versus  $1000/T$  at about 390 K. The similar behavior is observed in the temperature dependence of conductivity. It enables us to assume the appearance of collective effects arising due to the correlated motion of the lithium ions as a result of which the activation enthalpy of conductivity decreases from 0.56 eV in range 300-390 K to 0.38 eV in 390-530 K.
- 2). Above 530 K the decrease of thermoelectric power has been observed. To explain the reason of anomalous behavior of thermoelectric power along ion conducting axis (001) were carried out additional measurements along another crystallographic axes. Negligible small magnitude of conductivity along axes [100], [010] can essentially affect to the value of thermoelectric power. Above 530 K has been observed the abruptly increase of thermoelectric power along [100], [010]. This effect can be explained by the assumption, that lithium ions in lithium tetraborate are located in two energetic nonequivalent positions caused by the noncentrosymmetric location of Li ions in O-Li-O bounds, that can lead to formation of two-level potential system.

At the low temperature there are high probability of the jumps to such positions situated along [001] with vacancy formation in an initial position. In one's turn, the formation of vacant sites along conductive canals in quasi-1D superionic conductors leads to motion of the chain of several ions. With the increasing of the temperature the jump of ions to the positions which was inaccessible at low temperatures is thermally activated. The structural peculiarities of the crystal lattice of lithium tetraborate also shows the energetic and space nonequivalent arrangement of the lithium atoms.

Further, in addition, there has been defined the heat of transfer of lithium ions in all measured temperature range and it is compared with the activation enthalpy of conductivity. The experimental results compared with the theoretical calculations based on Fokker - Plank equation.

## **EFFECT OF IONIC RADII ON SILVER BASED SUBSTITUTIONAL COMPOUNDS**

**B.Nalini and S.Selvasekarapandian**

**Department of Physics**

**Bharathiar University**

**Coimbatore 641 046**

**Tamil Nadu**

**INDIA**

### **ABSTRACT**

A great deal of attention has been paid in recent years on solid electrolytes which exhibit high ionic conductivity. The recipe for fast ionic transport is known to have atleast three ingredients : (i) a high degree of disorder in the mobile ion sublattice, (ii) a high concentration of weakly bonded mobile ions and (iii) suitable structure which permits macroscopic motion of the ion with a low activation energy. One way of tailoring the character of any solid electrolyte is the substitutional approach. Either one or a combination of the following may occur on substitution namely : a new mechanism may begin with the introduction of the foreign entity or the concentration of the mobile ion may increase or the mobility of the mobile ion may be changed. Further more, a double substitution with homovalent and heterovalent ions would also change the behaviour of transport in relation with the enthalpy of formation and enthalpy of migration brought about by the resulting lattice strain. A trial on this view point has been undertaken on silver iodide with  $\text{PbI}_2$ ,  $\text{CuI}$  and  $\text{CsI}$ . The pure lattice has been disturbed by individual entry as well as combined entries of the abovesaid iodides. (i.e)  $\text{AgI-PbI}_2$ ,  $\text{AgI-CuI}$ ,  $\text{AgI-CsI}$ ,  $\text{AgI-PbI}_2\text{-CuI}$ ,  $\text{AgI-PbI}_2\text{-CsI}$  and  $\text{AgI-CuI-CsI}$  are experimented and the comparison has been made on the various compositions of these compounds. For any substitutional compound, ionic radii and structural matching play a vital role in determining the transport property of those materials. Focusing on the factor of ionic radii, a general notion would be that, higher the ionic radii more will be the hindrance caused on the transport. Further analysis on this line shows that if the structural matching is effective irrespective of the ionic radii a

better transport property could be expected. The aspect of structural matching includes the factor of lattice strain caused in the system. Compatibility of structural matching along with the ionic radii could bring a favourable transportation in the system. The facilitation of transport in these compounds are visualised through the number of potentially mobile ions present.

As an innovative approach (based on the theory of Debye), the number of potentially mobile ions ( $n$ ), the mean free path and relaxation time are calculated from the peak relaxation frequency. The correlation of the number of potentially mobile ion and the conductivity paves the way to understand the mechanism of conduction and the causes of any alteration in conductivity phenomena. It is highly interesting to note that relatively conductivity is not influenced much by the cesium ion when incorporated individually in AgI lattice which is a homovalent substitution. In contrary, the lead ions (a heterovalent substitution) employ much of lattice strain pulling down the conductivity which may be attributed to the structural mismatching. On comparison generally in a silver lattice, the conductivity is of the order of  $10^{-3} \Omega^{-1}\text{cm}^{-1}$  corresponding to  $n$  equal to  $10^{23}/\text{cm}^3$ . This condition is observed with the AgI-CuI system, a homovalent substitution having optimum ionic radii and less lattice strain caused due to the copper ions. Mean while, the strain caused with the  $\text{Pb}^{2+}$  ions is greater and comparatively the  $n$  value becomes less of the order of  $10^{18}/\text{cm}^3$  in turn reducing the conductivity. Looking into the double substitutional compounds, the lead incorporated compounds show less  $n$  and less conductivity except in the case of sample having 90-05-05% of AgI-PbI<sub>2</sub>-CuI where the lead entity is observed to precipitate due to the domination of copper ions (observed through XRD). For the surprise, the system with copper and cesium incorporated in silver iodide, cesium influence the transport property greatly and pulls down the conductivity. This shows that in the homovalent substitution the ionic radii plays a versatile role wherein the case is reversed towards the structural compatibility in the case of a heterovalent substitution.

## AC IMPEDANCE SPECTROSCOPY STUDIES OF THE FAST IONIC CONDUCTOR - $\text{AgI-PbBr}_2\text{-Ag}_2\text{O-B}_2\text{O}_3$ .

**S.Selvasekarapandian and R.Chithra Devi**

**Department of Physics, Bharathiar University**

**Coimbatore - 641 046, INDIA**

### ABSTRACT

Solid electrolytes of practical importance are frequently polycrystalline and have lead to many studies of its basic physical properties. Study of such solid ionic materials paves the way to many technological applications such as electrochromic devices, solid state cells, fuel cells etc.,. The research effort in this area has increased quite dramatically over last few years. One of the important method of characterising solid electrolyte is that the ac conductivity measurement in which the measured electrical response is frequency dependent and contains contribution from the whole electrode/electrolyte assembly. This method provides valuable information of the sample under investigation like bulk resistance, grain boundary resistance and interfacial capacitance. In the present work, a new material  $\text{AgI-PbBr}_2\text{-Ag}_2\text{O-B}_2\text{O}_3$  has been synthesized characterised using AC impedance analysis. The pelletised form of the sample has been subjected to the frequency varying from 100Hz to 100kHz over the temperature from room temperature to 573K. The conductivity of the sample is found to be  $2.48 \times 10^{-3} (\Omega\text{cm})^{-1}$  at 443K and the activation energy is calculated to be 0.085 eV at 10 kHz. In the impedance plane plot, the depression of semicircle is due to the distribution of relaxation time present in the sample. The high value of the capacitance has been indicated by the low value of modulus at lower frequencies. The superposition or coincidence of normalised modulus spectra at various temperatures may be attributed to the distribution of relaxation time is independent of temperature. The equivalent circuit analysis has been made on the basis of ac impedance analysis.



## ELECTRIC CONDUCTIVITY IN $\text{Zn}^{2+}$ SUBSTITUTED LITHIUM SULFATE - ALUMINA CERAMICS

Guangyao Meng, Shanwen Tao and Dingkun Peng

USTC Lab. For Solid State Chemistry and Inorganic Membrane

Department of Materials Science and Engineering, University of Science and Technology of  
China, Hefei, Anhui 230026, China

$\text{Li}_2\text{SO}_4$  as a well known fast ionic conductor has been extensively studied by doping various cations, e.g.  $\text{Na}^+$ ,  $\text{K}^+$ ,  $\text{Ag}^+$ ,  $\text{Mg}^{2+}$ ,  $\text{Ca}^{2+}$ ,  $\text{Sr}^{2+}$ ,  $\text{Ba}^{2+}$ ,  $\text{Zn}^{2+}$ ,  $\text{Y}^{3+}$ ,  $\text{La}^{3+}$  etc. Two mechanisms, "paddle-wheel" and "percolation" of ionic conduction in  $\alpha\text{-Li}_2\text{SO}_4$  and other related compounds, such as,  $\text{LiNaSO}_4$ ,  $\text{LiAgSO}_4$  and  $\text{Li}_4\text{Zn}(\text{SO}_4)_3$ , were proposed in order to interpret the influence of the different cations on the conductivity[1]. Experimental results support the validity of these mechanisms, but there has been some conflicting opinions due to the different situations. To prove the effects of the two mechanisms, the dopant cations,  $\text{M}^{n+}$ , should meet the requirements as

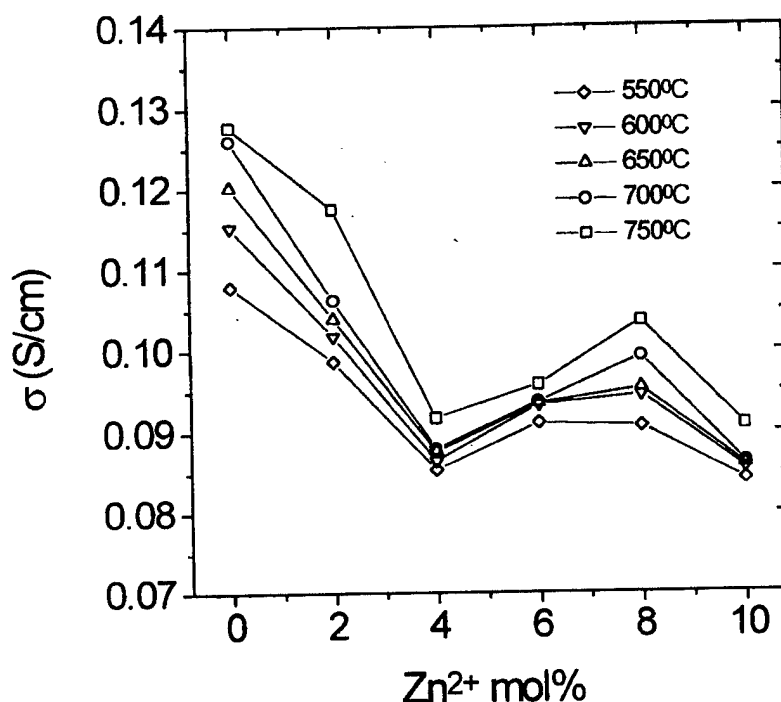
- (1)  $\text{M}^{n+}$  ions pose higher valence than  $\text{Li}^+$ , so that they may create additional ionic vacancies
- (2)  $\text{M}^{n+}$  can fill into the tetrahedron coordination position close to  $\text{SO}_4^{2-}$  ions in the lattice, so that they may restrict the "paddle-wheel" mechanism, and
- (3)  $\text{MSO}_4\text{-Li}_2\text{SO}_4$  may form solid state solution in a wide  $\text{MSO}_4$  content range, so that the both "paddle-wheel" and "percolation" mechanism can be both in function.

Among the normal cations,  $\text{Zn}^{2+}$ , exhibit higher solubility in  $\alpha\text{-Li}_2\text{SO}_4$  because they tend to adopt the tetrahedral anion coordination and occupy tetrahedral positions. And therefore they meet the requirements described above for investigation of the conduction mechanism of  $\alpha\text{-Li}_2\text{SO}_4$ . In addition, study on the conductivity of  $\text{Li}_2\text{SO}_4$  so far was about the samples with large amount of  $\text{ZnSO}_4$ , at least 10mol%. It is of significance, therefore, to investigate the effect of  $\text{Zn}^{2+}$  doping less than 10mole % for both the materials system and the conduction mechanism. This work is aimed at this subject. The samples were made by conventional solid state reaction method. In order to improve the mechanic strength and make it possible to measure the conductivity above the melting point of the salt,  $\alpha\text{-Al}_2\text{O}_3$  was added in the molar ratio of salt to  $\alpha\text{-Al}_2\text{O}_3$  equal to 57:43, to form two phase composite electrolyte.

The results indicated that the conductivity of all  $\text{Zn}^{2+}$ -contained samples is higher than  $\beta\text{-Li}_2\text{SO}_4$  ( $\text{Al}_2\text{O}_3$ ) below 500°C. This may be resulted from the existence of phase V and IV, which are likely high conduction phase. While at the temperatures between 550-750°C, the conductivity of all the samples doped with  $\text{Zn}^{2+}$  ions to form a solid solution with the structure of  $\alpha\text{-Li}_2\text{SO}_4$  is lower than the un-doped ones. This result appear due to the decrease of relative concentration of  $\text{Li}^+$  ions which have a much higher diffusion coefficient than  $\text{Zn}^{2+}$  ( $1.59 \times 10^{-5} \text{cm}^2/\text{s}$  and  $0.05 \times 10^{-5} \text{cm}^2/\text{s}$  at 550°C for  $\text{Li}^+$  and  $\text{Zn}^{2+}$ , respectively [2]). But this phenomenon could also be interpreted by "paddle-wheel" mechanism because the possible occupation of tetrahedral positions near  $\text{SO}_4^{2-}$  ions by large  $\text{Zn}^{2+}$  ions would restrict the rotation of  $\text{SO}_4^{2-}$  ions and cause the decrease of ionic conductivity. On the contrary, according to the "percolation" mechanism which involves vacancy mechanism, the dissolution of  $\text{Zn}^{2+}$  ions in  $\alpha\text{-Li}_2\text{SO}_4$  would create additional vacancies based on the formation of  $\text{Li}_{2-x}\text{Zn}_x\text{V}_x\text{SO}_4$ , where V represents vacancies, which should result in the increase of conductivity. Does "percolation" mechanism not take effect for  $\alpha\text{-Li}_2\text{SO}_4$  phase? It is not so simple. It can be reasonably deduced that the conductivity of samples should monotonously decrease with the increasing amount of  $\text{Zn}^{2+}$  ions in  $\alpha\text{-Li}_2\text{SO}_4$  solid solution according to the "paddle-wheel" mechanism because the more  $\text{Zn}^{2+}$  ions exist, the more difficult for rotation of  $\text{SO}_4^{2-}$  ions. However, as shown in the attached figure, the conductivity decreases first when  $\text{Zn}^{2+}$  ions is less than 4mol% but increases again and

exhibit a maximum point around 7mol%  $\text{Zn}^{2+}$  or, 7mol% vacancies according to formula  $\text{Li}_{2-x}\text{Zn}_x\text{V}_x\text{SO}_4$ . For most of the investigated solid solutions, the maximum conductivity occurs when vacancy concentration is of the order of 7mol% [3]. Therefore, the behavior of the conductivity variation for 4-10mol%  $\text{Zn}^{2+}$  content is a typical characteristic of vacancy mechanism. In other words, the "percolation" mechanism does effect, too. The conductivity of  $\text{Zn}^{2+}$  doped samples for  $\alpha\text{-Li}_2\text{SO}_4$  solid solution is expected higher than undoped one and reaches maximum around 7mol% if the classical vacancy mechanism, or "percolation" mechanism other than "paddle-wheel" mechanism for ionic migration in  $\alpha\text{-Li}_2\text{SO}_4$  solution. It might be difficult to explain the fact that all  $\text{Zn}^{2+}$  doped  $\alpha\text{-Li}_2\text{SO}_4$  exhibit lower conductivity than undoped ones which is opposed to reported results for solid solution of  $\beta\text{-Li}_2\text{SO}_4$ ,  $\text{Na}_2\text{SO}_4$  and  $\text{Ag}_2\text{SO}_4$ . Especially, the conductivity of the samples with 2mol% and 4mol%  $\text{Zn}^{2+}$  decreases, instead increases according to the normal vacancy mechanism. Actually, this may be attributed to the "paddle-wheel" mechanism. In brief, both "paddle-wheel" and "percolation" mechanisms may take effects for the ionic migration in  $\alpha\text{-Li}_2\text{SO}_4$  solid solution phase.

The  $\text{H}_2/\text{O}_2$  fuel cell with zinc dope  $\text{Li}_2\text{SO}_4$  as electrolyte showed an open circuit voltage of 1.02V and maximum current density of 300mA/cm<sup>2</sup> at 775°C. But the long-term performance is not good owing to the chemically unstability of  $\text{Li}_2\text{SO}_4$  in hydrogen at high temperature [4].



#### Acknowledgment

The financial support from Chinese Natural Science Foundation for this work is much acknowledged.

#### References

- [1] L. Karlsson, R.L. McGreevy, *Solid State Ionics* **76**, 301 (1995).
- [2] R. Tarneberg, A. Lunden, *Solid State Ionics* **90**, 209 (1996).
- [3] A. Lunden and M.A.L.K.L Pissanayake, *J. Solid State Chem.* **90**, 171 (1991).
- [4] S.W. Tao, Z.L. Zhan, P. Wang, G.Y. Meng, *Solid State Ionics*, in press.

## GROWTH AND CHARACTERIZATION OF LITHIUM-SUBSTITUTED PEROVSKITE TYPE IONIC CONDUCTOR.

A. K. Ivanov-Schitz <sup>a</sup>, V. V. Kireev <sup>a,b</sup>,  
A. M. Balbashov <sup>c</sup>, N. G. Chaban <sup>b</sup>.

<sup>a</sup>Institute of Crystallography, Russian Academy of Science, Moscow, Russia;

<sup>b</sup>General Chemical Technology Department, Moscow State Academy of  
Fine Chemical Technology, Moscow, Russia;

<sup>c</sup>Moscow Energy Institute, Moscow, Russia.

Lithium-substituted phases based on  $\text{Ln}_{0.66}\text{TiO}_3$  are of great interest because of their extremely high ionic conductivity at room temperature. The many materials are studied previously. The most of investigations were carried out on polycrystalline samples.

Single crystals in the system of  $\text{Li}_2\text{O-La}_2\text{O}_3\text{-TiO}_2$  were grown by floating zone method. For the crystal growth we used infrared heating furnace heated by one 3000 W xenon lamp. Initial polycrystalline rods were prepared by a conventional solid state reaction. Raw materials were  $\text{Li}_2\text{CO}_3$ ,  $\text{TiO}_2$ ,  $\text{La}_2(\text{CO}_3)_3 \cdot 6\text{H}_2\text{O}$ . Calcinated mixture of starting materials was pressed at 200–300 MPa and then fired at 1180°C. The growth was performed in air at a rate of 5 to 10 mm/h. Some loss of lithia and titania was occurred during growth due to evaporation. Phase identification was carried out by a powder X-ray ( $\text{Cu K}\alpha$ ) diffraction method. The obtained boules were ~5mm in diameter. They consist of few blocks, that's why polarisation microscope study was used for single crystal domains selection. Ionic conductivity was measured on cut and polished samples using complex impedance spectroscopy method with graphite electrodes over the frequency range 100 Hz to 500 kHz and over the temperature range 298 to 583 K. The value of ionic conductivity for the best crystals reached to  $1.4 \cdot 10^{-4}$  S/cm at room temperature with activation energy 0.42 eV.

## SURFACE MODIFICATION OF TUNGSTEN OXIDE THIN FILMS

**Ali E. Aliev**

Heat Physics Department of Uzbek Academy of Sciences  
Katartal str.28, Tashkent 700135 Uzbekistan

**Chul Park**

LG Corporate Institute of Technology  
16Woomyeon-Dong, Seocho-Gu, Seoul 137-724, Korea

**Jin-Ho Choy, Young -Il Kim**

Department of Chemistry and Center for Molecular Catalysis  
Seoul National University. Seoul 151-742, Korea

Materials for electrochromic display devices (ECDs) have been extensively studied because of their potential application. The electrochemical behaviors of tungsten trioxide ( $\text{WO}_3$ ) have the most attracted increasing attention recently because of the greatest coloration efficiencies. It is well known, that the high electrochromic reversibility and the short response time of thermally evaporated tungsten oxide layers are the consequence of the open xerogel structure in contrast to the poor electrochromic response of amorphous oxide layers with a glassy structure of high density. Therefore, enlargement of the active surface area compared with a smooth surface may provide much higher activity for heterogeneous reaction taking place at the tungsten trioxide/electrolyte interface. In this paper we report an attempt for application of the opal-like porous structure to the surface modification of tungsten oxide thin films.

The opal-like nanostructured medium has a regular packed array of silica spheres ( $d = 200\div 250\text{nm}$ ). Voids between the spheres, which can be treated as a kind of pore, take up approximately 26% of the sample volume and form a regular three-dimensional thorough interconnected network. The internal surface of silica spheres reach  $500\text{m}^2/\text{g}$ .

We used sol-gel method for deposition of hydrophilic silica nanoparticles  $\text{SiO}_2$  ( $d=40\text{nm}$ ) mixed with Peroxotungstic acid (PTA). The preparation method of spin-coated  $\text{WO}_3$  using PTA on indium-thin oxide (ITO) covered glasses has been described elsewhere [1]. The crucial stage is selective chemical etching of silica nanoparticles. Extraction of the  $\text{SiO}_2$  balls from the  $\text{WO}_3$  layer (using aqueous HF) resulted to significant enlargement of exterior surface. Fig.1. illustrated schematically the surface of inverse opals filled with tungsten oxide.

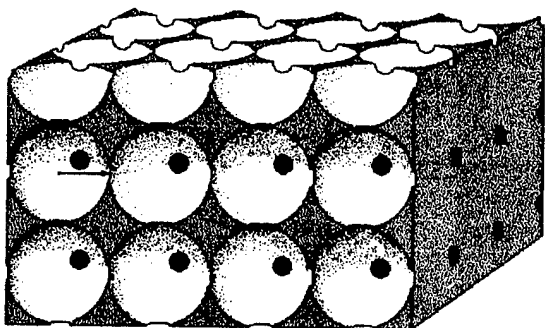


Fig. 1.

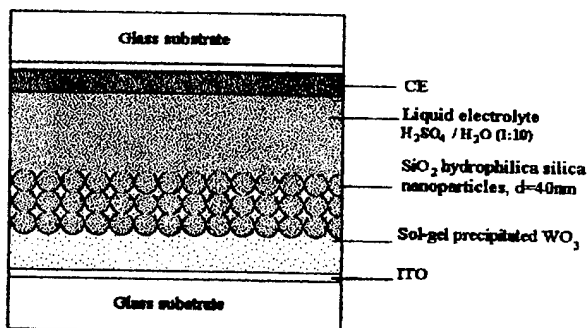


Fig. 2.

The electrochemical cell for testing the coloration and bleaching modified  $\text{WO}_3$  layer is shown schematically in Fig.2. A sulfuric acid solution  $\text{H}_2\text{SO}_4/\text{H}_2\text{O}$  (1:10) was used as the electrolyte.

Scanning electron microscope images show that  $\text{SiO}_2$  particles is dispersed not homogeneously. The ultrasound treatment significantly enhanced the homogenous dispersion of particles. However, wide distribution of particles by size and agglomeration result to the cluster structure of  $\text{SiO}_2$  particles (Fig.3, [A]). As shown in Fig. 3 [B], the extraction of the silica spheres using aqueous HF (1:20) occur quite irregular. Nevertheless, as a result of such surface modification the coloration current and optical density were increased two times. It means that only surface bolls is extracted. More substantial increasing of interior surface may be rich only in crystalline arrangement of silica spheres with extended inter-sphere interface through which the  $\text{SiO}_2$  can be removed by etching.

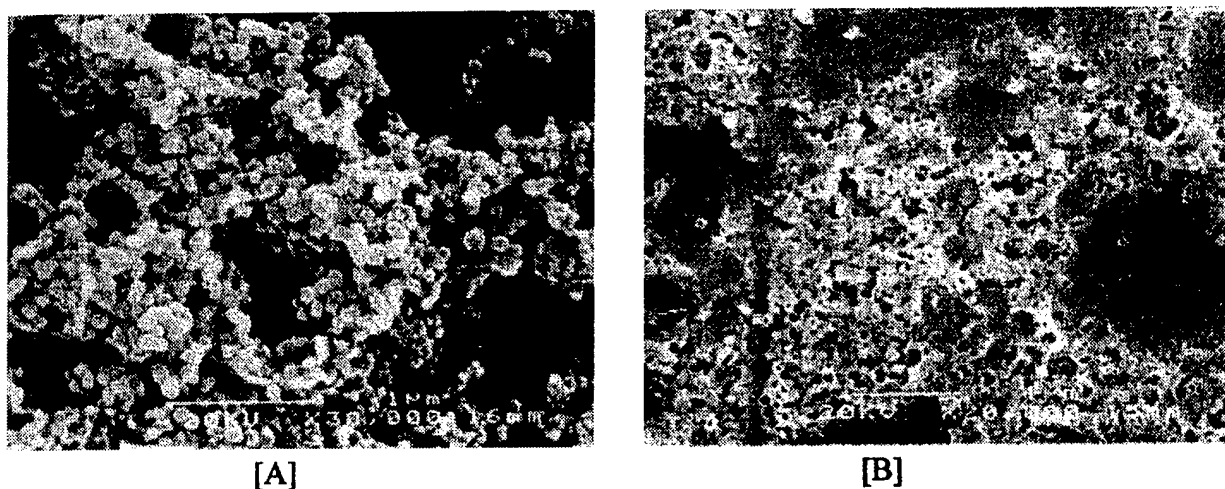


Fig. 3. SEM micrograph of spin-coated hydrophilic silica nanoparticles  $\text{SiO}_2$  ( $d=40\text{nm}$ ) mixed with PTA before [A], and after [B] etching.

Very important consequence of such modification is the shape change of electrochromic response during application of square wave voltage to electrochemical cell.

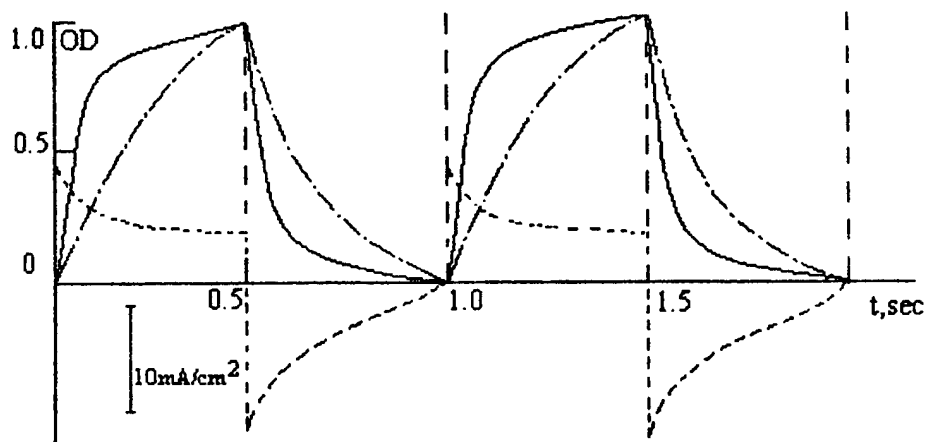


Fig.4. Normalized optical density (OD) vs. time for square wave excitation ( $U^+ = 1\text{V}$ ,  $U^- = 2.5\text{V}$ ). The solid line is for modified surface.

1. K.Yamanaka, H.Oakamoto, H.Kidou and T. Kudo. Japanese J. of Applied Physics, V.25, N9, 1986, pp.1420-1426.

## THE ELECTROCHROMIC PROPERTIES OF TUNGSTEN OXIDE THIN FILMS DEPOSITED BY SOLUTION THERMOLYSIS

P.R. PATIL, S. H. PAWAR AND P.S. PATIL

DEPARTMENT OF PHYSICS,  
SHIVAJI UNIVERSITY, KOLHAPUR - 416 004, INDIA

### ABSTRACT :

Electrochromism is a multifaceted phenomenon exhibited by a number of inorganic materials. It is a reversible and persistent change in optical properties of a material caused by an applied potential. The most widely used electrochromic (EC) material is tungsten oxide ( $\text{WO}_3$ ). The EC activity exhibited by  $\text{WO}_3$  thin films is well known. EC properties of these films vary, depending on the methods used for their preparation.  $\text{WO}_3$  films are usually prepared by techniques such as evaporation, sputtering, chemical vapour deposition, sol-gel, anodically grown and spray pyrolysis [1]. Thin film preparation by spray pyrolysis can offer a cost effective way to form EC coatings. Solution thermolysis (ST), analogous to spray pyrolysis, involves the application of a fine mist of very small droplets containing the reactants on to a hot substrate. During the deposition process, the precursor solution is pulverized on to the substrate. The droplets undergo evaporation, solute condensation and thermal decomposition which results in to the film formation.

Previously, precursor solutions were prepared, mainly by using  $\text{WCl}_6$  in ethanol or N, N dimethyl formamide and aqueous solutions of metatungstic acid ( $\text{H}_6\text{W}_{12}\text{O}_{36}$ ). This paper reports the preparation of  $\text{WO}_3$  thin films by solution thermolysis from ammonium tungstate precursor solution. These  $\text{WO}_3$  films were deposited on to fluorine doped tin oxide (FTO) coated glass substrates (maintained at  $300^\circ\text{C}$  and annealed at  $500^\circ\text{C}$  for 3 hrs.) which then used as working electrodes in a three electrode EC cell, with SCE as a reference electrode and graphite as a counter electrode. The electrochemical and spectroscopic measurements were carried out.

Cyclic voltammetry (C-V) was carried out in  $\text{H}_2\text{SO}_4$  electrolyte. The configuration of EC cell was as follows: FTO /  $\text{WO}_3$  / 0.1 N  $\text{H}_2\text{SO}_4$  / C, SCE. For C-V, a cyclic potential sweep is imposed on an electrode and the current response is observed. The result of this experiment as the voltage is cycled in the range from -0.7 to +0.7 V (SCE) at different scan rates ranging from 10 mV/Sec to 200 mV/Sec is shown in fig. 1. The magnitudes of colorations and bleaching currents found to be increased with the scan rates. The C-V recorded for our film is consistent with the generally accepted mechanism of electrochromism for well defined EC  $\text{WO}_3$  films made by usual methods. From the values of peak currents ( $i_p$ ), diffusion coefficients were calculated to be of the order of  $10^{-11} \text{ cm}^2/\text{sec}$ . Variation of peak currents with the scan rate ( $v$ ) was studied by plotting the graph of  $\log i_p$  versus  $\log v$  and shown in Fig. 2. The slope of the graph is 0.63, suggesting a mixed diffusion-adsorption peak in C-V.

Chronoamperometric studies were carried out and the variation of coloration and bleaching current with respect to time at different fixed potentials is shown in Fig. 3. The nature of variation indicates that bleaching is faster than coloration. The coloration time was about 4 seconds and bleaching time was 2.5 seconds. The  $\text{WO}_3$  films were found to be stable for  $10^3$  cycles. The coloured and bleached  $\text{WO}_3$  thin films were further characterized by transmission and X-ray diffraction studies.

**References:** [1] C.G. Granqvist, Handbook of Inorganic electrochromic Materials, Elsevier, The Netherlands, 1995.

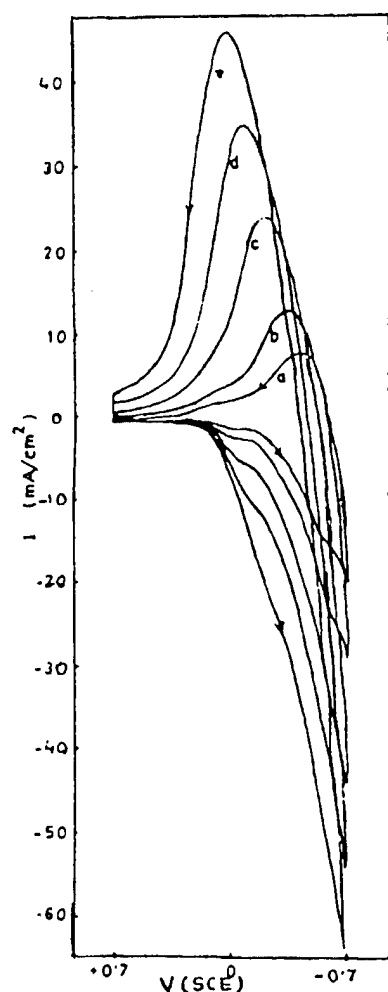


Fig. 1 : Cyclic voltammogram of  $\text{WO}_3$  film in  $0.1 \text{ N H}_2\text{SO}_4$  at different scan rates ( $v$ ).  
a) 10, b) 20, c) 50, d) 100 and e) 200  $\text{mV}/\text{sec}$ .

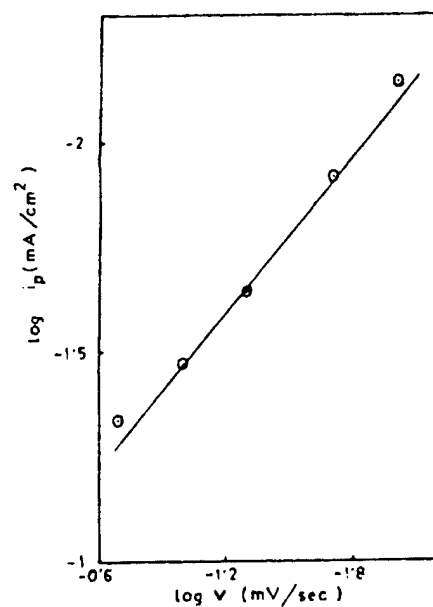


Fig. 2 : Variation of  $\log i_p$  V/s  $\log v$  (scan rate)

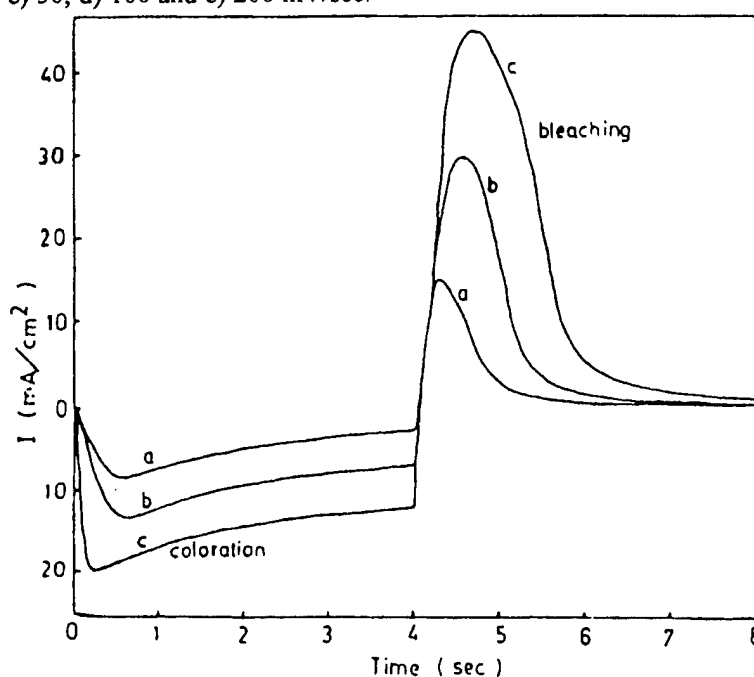


Fig. 3 : Chronoamperometry of  $\text{WO}_3$  film in  $0.1 \text{ N H}_2\text{SO}_4$  at different potential steps  
a) 0.3, b) 0.5 and c) 0.7 versus (SCE)

# CRYSTAL STRUCTURE OF NON-STOICHIOMETRIC $\beta''$ K-Ba-Na MIXED FERRITE, $K_{0.30}Na_{0.62}Ba_{0.62}Fe_{10.44}Mg_{0.29}O_{17}$

A. C. Stergiou<sup>1</sup> - D. K. Giourelis<sup>1</sup>, D. Samaras<sup>2</sup> - G. Litsardakis<sup>2</sup>

<sup>1</sup> Department of Physics

<sup>2</sup> Department of Electrical Engineering.

Aristotle University, 54006 Thessaloniki, Greece.

Crystals of non-stoichiometric K-Na-Ba ferrite, with  $\beta''$ -alumina structure type and chemical formula  $K_{0.30}Na_{0.62}Ba_{0.62}Fe_{10.44}Mg_{0.29}O_{17}$ , were prepared by a partial ionic exchange from a K-Na- $\beta''$ -ferrite. The exchange was performed in a  $Ba(NO_3)_2$ - $KNO_3$  eutectic melt at 650°C for 15min. A single crystal was selected and studied with X-ray diffraction ( $MoK_\alpha$  radiation), using 379 independent reflections. The systematic absences of reflections resulted in the  $R\bar{3}m$  space group, with unit cell constants  $a=b=5.9436(7)\text{\AA}$ ,  $c=35.743(7)\text{\AA}$ , as refined by CELREF [1], and  $Z=3$ . The structure determination was based on the  $\beta''$ -alumina structure model ( $Na_{1-x}Al_{1-x}Mg_xO_{17}$ ), using as initial atom coordinations the ones given by Koeler and Urland [2]. The Na atom sites are occupied by (Ba, K, Na) and the Al ones by Fe. The atom coordinations and thermal parameters were refined using the program SHELX-93 [3]. Investigation of the electron density on the conduction plane ( $z=1/6$ ) gave trigonal distribution around the middle position (0,0,1/6) for (K-Na-Ba) atoms. This distribution can be described by a partial occupation of two sites (18h) with coordinations 0.056, 0.028, 1/6 and 0.26, 0.13, 1/6, by (K, Na, Ba) atoms with an analogous decrement of the site occupation factors. Refinement of population, positional and anisotropic thermal parameters for all atoms, resulted in the final residual factor  $R_1=0.057$ .

Similar description of the Na -  $\beta''$  structure is given by Boilot et. al. [4] and Jorgensen et. al. [5], while some deviations of the alumina and ferrite structure, regarding the position of the stabilizing element, is mentioned by Dunn et. al. [6] and Nariki et. al. [7].

In table I the final atom coordinations, the population parameters and the isotropic thermal parameters ( $\text{\AA}^2$ ) are given. In fig. 1 the ions arrangement on the conduction plane ( $z=1/6$ ) is shown.

Table I. Final atom coordinations, population parameters and thermal parameters.

Atom	Site	x	y	z	pp	B( $\text{\AA}^2$ )
Ba(1)	18h	0.0689(35)	0.0345(18)	0.1700(2)	0.08	0.570(9)
Ba(2)	18h	0.2743(34)	0.1372(17)	0.1667	0.06	0.387(3)
Fe(1)	3a	0	0	0	1	0.058(1)
Fe(2)	6c	0	0	0.3503(1)	0.95	0.049(1)
Fe(3)	18h	0.3351(2)	0.1676(1)	0.0699(1)	0.97	0.045(1)
Fe(4)	6c	0	0	0.4499(1)	0.94	0.042(1)
O(1)	18h	0.1562(5)	0.3125(11)	0.0343(2)	1	0.081(1)
O(2)	6c	0	0	0.2952(2)	1	0.045(1)
O(3)	6c	0	0	0.0967(2)	1	0.038(1)
O(4)	18h	0.1626(4)	0.3252(8)	0.2345(2)	1	0.049(1)
O(5)	3b	0	0	1/2	1	0.303(3)



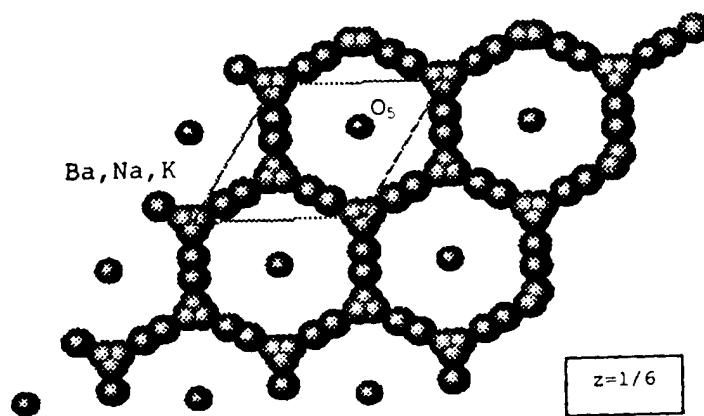


Fig. 1. Ion arrangement on the conduction plane ( $z = 1/6$ )

#### References.

- [1] J. Laugier and A. Filhol, (CELREF), Institute Laue-Langevin, Grenoble, France, (1978).
- [2] J. Koehler and W. Urland, Zeitschrift fuer Anorganische und Allgemeine Chemie, **622**, 191 (1996).
- [3] G Sheldrick, SHELX-93 Program for Crystal Structure Refinement, Institut für Anorganische Chemie der Universität, Tammanstrasse 4, D-3400 Gottingen, Germany, (1993).
- [4] J. P. Boilot, G. Collin, P. Colombari and R. Comes, Physical Review B-Condensed matter, **22**, 5912 (1980).
- [5] J. D. Jorgensen, F. J. Rotella and W. L. Roth, Solid State Ionics, **5**, 143 (1981).
- [6] B. Dunn, B. B. Schwarz, J. O. Thomas and P. E. D. Morgan, Solid State Ionics, **28**, 301 (1988).
- [7] S. Nariki, S. Ito, K. Kozawa, T. Uchida and N. Yoneda, Solid State Ionics, **40/41**, 95 (1990).

## ON THE WAY FROM METAL HYDRIDE FILMS TO SOLID-STATE SWITCHABLE MIRRORS

Anna-Maria Janner and Paul van der Sluis

Philips Research Laboratories, Prof. Holstlaan 4, 5656 AA Eindhoven, The Netherlands

Thin films of hydrides of rare-earth metals can reversibly be switched from non-transparent to transparent upon hydrogen intercalation and deintercalation [1]. Even more drastic optical changes can be obtained by varying the hydrogen concentration for the magnesium rare-earth alloys, since they can switch between a *reflective* and *transparent* state with a contrast up to  $10^5$  [2]. This exceptionally large contrast offers new possibilities for certain interesting applications. The way we are working towards a solid-state switchable mirror device will be discussed.

In order to arrive to a solid-state device the following crucial points have to be fulfilled:

- (i) a counter electrode with high storage capacity is needed.
- (ii) the electrolyte has to have a good ion conductivity and a negligible electric conductivity.
- (iii) the whole stack has to be chemical compatible.

These three points will be discussed with the emphasis on the search for a proper ion conducting solid-state electrolyte. Hydrogen insertion by electrochemical loading in an alkaline-water electrolyte has already successfully been achieved [3], but slow degradation due to the water occurs. Currently we are working with organic ionic liquids, which can be made into a gel with a polymer. The first results look promising.

[1] J.N. Huibers, R. Griessen, J.H. Rector, R.J. Wijngaarden, J.P. Dekker, D.G. de Groot, and N.J.P. Koeman, *Nature* **380**, 231 (1996).

[2] P. van der Sluis, M. Ouwerkerk, and P.A. Duine, *Appl. Phys. Lett.* **70**, 3356 (1997); *Appl. Phys. Lett.* **73**, 1826 (1998); M. Ouwerkerk, *Solid State Ionics*, to be published 1998-1999.

[3] P.H.L. Notten, M. Kremers, and R. Griessen, *J. Electrochem. Soc.* **143**, 3348 (1996).

## TRENDS IN THE DEVELOPMENT OF SOLID STATE AMPEROMETRIC AND POTENTIOMETRIC HIGH TEMPERATURE SENSORS

Wolfgang Göpel

Institute of Physical and Theoretical Chemistry and Center of Interface Analysis and Sensors,  
Auf der Morgenstelle 8, D-72076 Tübingen, Germany

## INTRODUCTION

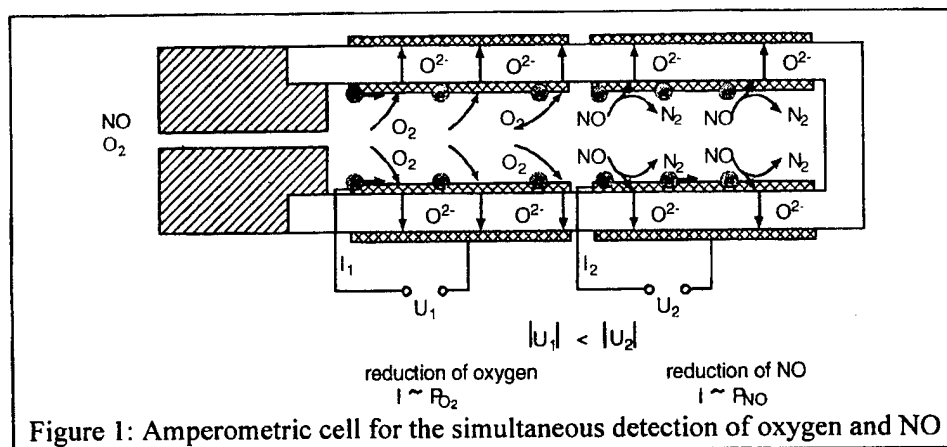
High temperature sensors based on solid electrolytes are well established in several specific applications like the determination of the oxygen content in exhaust gases ( $\lambda$ -probe) or molten steel. In most practical applications, stabilized zirconia, a well-known oxygen ion conductor, is used as the solid electrolyte since it is inert against most chemical and thermal attacks and offers a wide range of oxygen partial pressures and temperatures with predominant ion conduction. Besides its classical application as an oxygen probe in either potentiometric or amperometric operation mode, stabilized zirconia may be applied successfully in the detection of other exhaust gas components or environmentally relevant gases like  $\text{NO}_x$ , CO or various hydrocarbons. These applications utilize signal generation due to specific electrode reactions with certain gases such



or they utilize the kinetically adjusted chemical potential of surface oxygen in a catalytic reaction at the electrode. For all of these new applications, the control of electrode materials and electrode microstructures as functions of temperature, partial pressures, and (in amperometric devices) voltage is of key importance to successfully operate these sensors. Hence, extensive work was done related to the development of new electrode materials, to the optimization of existing electrode materials, and in particular to the in-situ spectroscopic and microscopic characterization of interfaces under sensor operation conditions.

## AMPEROMETRIC SENSORS

Amperometric sensors operate under externally applied voltages which drive the electrode reactions in voltage-dependent directions. Common amperometric sensors contain a diffusion barrier and operate in the gas diffusion limiting mode. Here each molecule passing the diffusion barrier reacts immediately at the electrode and hence, the corresponding limiting current is a unique function of the geometric parameters of the diffusion barrier. This concept was successfully applied since several years in the detection of oxygen over a wide pressure range. Several attempts have been made to extend this principle to the determination of other gases. The most promising concepts are based on amperometric multi electrode cells [1]. The basic idea for the latter is to separate the electrode reaction with the desired gas component from the electrode reaction with oxygen. This can be achieved by using an amperometric cell with one diffusion barrier and a set of consecutive electrodes. The basic principle of a sensor used for the simultaneous detection of oxygen and NO is shown in figure 1. Oxygen is reduced at the first electrode. This leads to a current representative for the oxygen content. The remaining gas reaching the second electrode is thus free of oxygen and NO may there be reduced selectively. In a similar way, hydrocarbons together with oxygen have been detected [2].



### POTENTIOMETRIC SENSORS

Besides the classical zirconia-based oxygen sensors following the Nernst law, new sensors based on the kinetics of different electrode reactions become of increasing interest to monitor other gases. Since the signal in this case is not determined by the Nernst law, corresponding sensors are called non-Nernstian or mixed potential sensors. In this case, electrodes are chosen which are electroactive and hence sensitive to monitor components like  $\text{CH}_x$  or  $\text{NO}_x$  but not oxygen. These devices either use a Nernstian reference electrode exposed to gas (air) or they use the difference in potentials of two electrodes with apparent electrochemical activities occurring in the same gas atmosphere.

In this context, gold and its alloys have been used for the detection of combustible gases in the temperature range between 300 and 700 °C. The sensitivity to reducing gases disappears above 700°C and leads to Nernstian behaviour [3,4,5]. Besides noble metals, a huge amount of oxide-based electrodes have been investigated to detect hydrogen,  $\text{H}_2\text{S}$ , CO [6], hydrocarbons and  $\text{NO}_x$  with increasing numbers of papers appearing in this field. However, stable signals over long times and under various operation conditions are still not obtained and hence a major task for future development. The mixed potentials depend strongly on the catalytic and electrocatalytic properties at and near the 3-phase boundary line electrode/electrolyte/gas. Interface reactions including also sintering effects and surface poisoning by other gaseous components do influence critically the sensor performance because they shift the catalytic and electrocatalytic properties through a shift in the apparent chemical potentials of the different adsorbed species at the potential generating interfaces.

Systematic studies are finally discussed to overcome these problems in a combined approach to investigate the spectroscopic, microscopic, and phenomenological sensor properties [7].

### REFERENCES

- [1] S.I. Somov, G. Reinhardt, U. Guth and W. Göpel, *Sens. Actuators B* **35-36**, 409 (1996).
- [2] S.I. Somov, G. Reinhardt, U. Guth and W. Göpel, *Conf. Proc. 7th IMCS, Beijing (China)* **7**, 443 (1998) and S.I. Somov and U. Guth, *Sens. Actuators B* **47**, 131 (1998).
- [3] R. Hartung, R. Schröder and H.-H. Möbius, *Z. Phys. Chemie (Leipzig)* **262**, 961 (1981).
- [4] R. Hartung, *Z. Chem.* **22**, 153 (1982).
- [5] A. Vogel, G. Baier and V. Schüle, *Sens. Actuators B* **15-16**, 147 (1993).
- [6] N. Miura, T. Raisen, G. Lu and N. Yamazoe, *Sens. Actuators B* **47**, 84 (1998) and references therein.
- [7] W. Zipprich, H.-D. Wiemhöfer, U. Vohrer and W. Göpel, *Ber. Bunsenges. Phys. Chem.* **99**, 1406 (1995); W. Göpel and G. Reinhardt, in H. Baltes, W. Göpel and J. Hesse (Eds.), *Sensors Update Sensor Technology-Applications-Markets* **1**, 49 (1996) and M. Röscher, G. Reinhardt and W. Göpel, Contribution to this conference.

## MECHANISMS AND DYNAMIC RESPONSES OF SOLID ELECTROLYTE „INTELLIGENT“ SENSORS

W. Weppner

Chair for Sensors and Solid State Ionics  
Technical Faculty, Christian-Albrechts University zu Kiel  
Kaiserstr. 2, D-24143 Kiel, Germany

Surface modifications have immensely increased the applicability of solid electrolytes for sensing gases and dissolved chemical species [1]. Chemical energies of virtual and real galvanic cell reactions are converted into electrical energy and vice versa. In spite of well-defined thermodynamic relationships it is often the kinetics of the more favorable galvanic cell reaction which determines the cell voltage even in potentiometric sensors. This results in cross sensitivities, slow responses and aging. The mechanisms depend on the morphology of the surface, catalytic processes and a variety of different polarization effects. Results will be presented for the surface interaction of alkaline solid electrolytes with CO<sub>2</sub>, CO and other interfering gases.

Kinetic principles show several important advantages, compared to thermodynamic devices. The kinetics of the galvanic cell reaction is employed for improving the selectivity and response time. The magnitude of the galvanic cell voltage is a very selective driving force for specific chemical species. Amperometric sensors were demonstrated for selective sensors based on the formation of surface depositions [2]. Theta sensors make use of the dynamics of cell reactions controlled by redox and transport processes.

“Intelligent“ sensors take advantage of learning processes by employing micro-electronics to predict equilibrium or steady state values by analyzing the kinetic performance and to choose the most selective response conditions.

The possibilities for the measurement of neutral and ionized species will be also briefly discussed.

[1] W. Weppner and R.A. Huggins, Solid State Ionics 1, 3 (1980)

[2] J. Liu and W. Weppner, Sensors and Actuators B 6, 270 (1992)

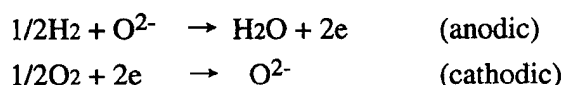
## Mixed Potential Type Solid Electrolyte Devices for Sensing Redox Gases at High Temperature

N. Yamazoe and N. Miura

*Department of Molecular and Material Sciences,  
Graduate School of Engineering Sciences, Kyushu University,  
Kasuga-shi, Fukuoka 816-8580, Japan  
TEL : +81-92-583-7537, FAX : +81-92-583-7539*

Gas sensors using solid electrolytes have been explored extensively in recent years, especially from growing concerns to environmental issues. The gas sensor devices are classified into three main groups based on the principles used for gas detection, as shown in Table 1. The group of devices based on equilibrium potential are further classified into Types I, II and III from the relation between the main solid electrolyte and the gas in problem. Type III devices among them derived by combining a typical solid electrolyte with an auxiliary phase containing oxyacid salt have been proven to be particularly important for detecting oxidic gases such as CO<sub>2</sub>, NO<sub>2</sub>, and SO<sub>2</sub>. The group of devices based on electrochemical pumping are represented by a limiting current type O<sub>2</sub> sensor using YSZ. This group now includes water vapor sensor using YSZ (Type I) and NO<sub>2</sub> sensor using NASICON/NaNO<sub>2</sub> combination (Type III). Compared with these groups, the groups of devices based on mixed potential have been paid less attention so far. However, these devices, if designed properly, exhibit high sensitivity to reducing or oxidizing gases in oxygen -containing atmospheres even at high temperature, showing promise of being applied for combustion exhaust monitoring.

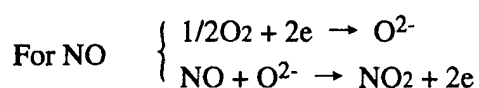
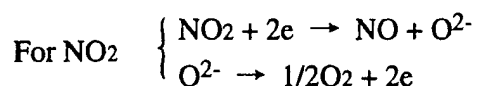
Mixed potential (MP) appears when electrochemical reduction and oxidation reactions take place simultaneously on the same (sensing) electrode. When a potentiometric oxygen sensor using YSZ is exposed to air containing H<sub>2</sub>, for example, the following reactions can take place concertedly on the sensing electrode.



MP is the potential at which the rates of the two reactions are equal to each other. With the reference electrode potential set in equilibrium with the oxygen partial pressure, the device generates an EMF as a function of hydrogen concentration under a mixed oxygen concentration. Obviously MP depends very much on the chemical and electrochemical properties of the sensing electrode. If the electrode is catalytically active for gas phase equilibrium ( $\text{H}_2 + 1/2\text{O}_2 \rightarrow \text{H}_2\text{O}$ ), then the concentration of H<sub>2</sub> arriving at the three-phase-contacts would decrease accordingly. This seems to explain why the conventional Pt sensing electrode fails to give significant MP at high temperature. In contrast, it has been found that some oxide, when used as a sensing electrode, show fairly large MP to reducing or oxidizing gases and, in addition, the MP obtained is fairly gas-selective depending on the oxide used. For example, a device sensitive and fairly selective to H<sub>2</sub> at 600°C is provided with a ZnO sensing

electrode. A sensitive and selective device to CO at 600°C is given when CdO and SnO<sub>2</sub> sensing electrodes are paired. In the latter example, each sensing electrode is sensitive to H<sub>2</sub>, but their H<sub>2</sub> sensitivities are cancelled out by pairing. The advantages of such oxide electrodes seem to be (1) far less active for catalytic gas-phase equilibrium than Pt and (2) probably more specific to the kind of target gas in electrocatalytic activity than Pt.

Probably NO and NO<sub>2</sub> will be among the most important target gases for the mixed potential type devices. So far WO<sub>3</sub> and CdCr<sub>2</sub>O<sub>4</sub> have been found to give fairly promising performances to NO<sub>2</sub> and NO at 600°C and 550°C, respectively. Especially the sensitivity to NO<sub>2</sub> is high enough to be capable of detecting reliably NO<sub>2</sub> down to 10 ppm or less in air. The reaction couples responsible for MP to NO<sub>2</sub> and NO are as follow.



NO<sub>2</sub> is reduced electrochemically, while NO is oxidized. As a result, NO<sub>2</sub> and NO give positive and negative MP, respectively. At the same time, this fact suggests that this device is hardly suited for detecting NO<sub>2</sub> or NO out of their mixtures: The mixture should be converted into NO<sub>2</sub> or NO prior to contacting device. As an alternative method to meet the mixture of NO and NO<sub>2</sub>, it has been shown that the devices can be modified into an NO-selective amperometric one by applying an appropriate external voltage. Prospects and problems of mixed potential type gas sensors will be mention in more detail in the lecture.

Table 1. Classification of solid electrolyte gas sensors.

Sensing principle	Typical cell structure	Gas sensing reaction
Equilibrium potential Type I Type II Type III	(RE) (SE) O <sub>2</sub> , Pt   YSZ   Pt, O <sub>2</sub> CO <sub>2</sub> + O <sub>2</sub> , Au   K <sub>2</sub> CO <sub>3</sub>   Au, CO <sub>2</sub> + O <sub>2</sub> O <sub>2</sub> , Au   NASICON   NaNO <sub>2</sub>   Au, NO <sub>2</sub> + O <sub>2</sub> Au   Na <sub>2</sub> O - TiO <sub>2</sub>   Na β-alumina   Na <sub>2</sub> CO <sub>3</sub>   Au, CO <sub>2</sub> + O <sub>2</sub>	$1/2\text{O}_2 + 2e \rightleftharpoons \text{O}^{2-}$ $2\text{K}^+ + \text{CO}_2 + 1/2\text{O}_2 + 2e \rightleftharpoons \text{K}_2\text{CO}_3$ $2\text{Na}^+ + \text{CO}_2 + 1/2\text{O}_2 + 2e \rightleftharpoons \text{Na}_2\text{CO}_3$ $\text{Na}^+ + \text{NO}_2 + e \rightleftharpoons \text{NaNO}_2$
Mixed potential Type I	(RE) (SE) O <sub>2</sub> , Pt   YSZ   ZnO(Pt), H <sub>2</sub> + O <sub>2</sub> O <sub>2</sub> , Pt   YSZ   WO <sub>3</sub> (Pt), NO <sub>2</sub> + O <sub>2</sub>	$2\text{H}_2 + \text{O}^{2-} \rightarrow \text{H}_2\text{O} + 2e$ $1/2\text{O}_2 + 2e \rightarrow \text{O}^{2-}$ $\text{NO}_2 + 2e \rightarrow \text{NO} + \text{O}^{2-}$ $\text{O}^{2-} \rightarrow 1/2\text{O}_2 + 2e$
Electrochemical pumping Type I Type III	(CE) (WE) O <sub>2</sub> , Pt <sup>⊕</sup>   YSZ   Pt <sup>⊖</sup>   GDL   O <sub>2</sub> Au <sup>⊕</sup>   NaNO <sub>2</sub>   NASICON   NaNO <sub>2</sub>   Au <sup>⊖</sup>   GDL   NO <sub>2</sub>	$1/2\text{O}_2 + 2e \rightarrow \text{O}^{2-}$ $\text{Na}^+ + \text{NO}_2 + e \rightarrow \text{NaNO}_2$

YSZ : Yttria stabilized zirconia (O<sup>2-</sup> conductor), NASICON : Na<sub>3</sub>Zr<sub>2</sub>Si<sub>2</sub>PO<sub>12</sub> (Na<sup>+</sup> conductor), GDL : Gas diffusion layer  
RE : Reference electrode, SE : Sensing electrode, CE : Counter electrode, WE : Working electrode

## MULTI-ELECTRODE ZIRCONIA ELECTROLYTE AMPEROMETRIC SENSORS

S. I. Somov<sup>a</sup>, G. Reinhardt<sup>b</sup>, U. Guth<sup>c</sup> and W. Göpel<sup>b</sup>

<sup>a</sup>Institute of High Temperature Electrochemistry, Ekaterinburg, 620219, Russia

<sup>b</sup>Institute of Physical and Theoretical Chemistry, University of Tübingen, Auf der Morgenstelle 8, D-72076 Tübingen, Germany

<sup>c</sup>Institute of Physical Chemistry, University of Greifswald, Soldtmannstr. 16/23, D-17489 Greifswald, Germany

### INTRODUCTION

During several years we have conducted research and development in the field of solid electrolyte amperometric sensors, intended for real-time measurements of main contaminants of combustible exhaust. The basic principles of our conception are: an application of the cell with sufficient number of working electrodes for extension of the number of parallel informational channels; a correlation of measured gas components with certain electrochemical reactions; an optimization of the cell design and working parameters for controlling of reactions at each electrode, in respect to obtain the highest electrode selectivity to certain components [1,2]. The optimization is based on knowledge on thermodynamics and electrochemical kinetics.

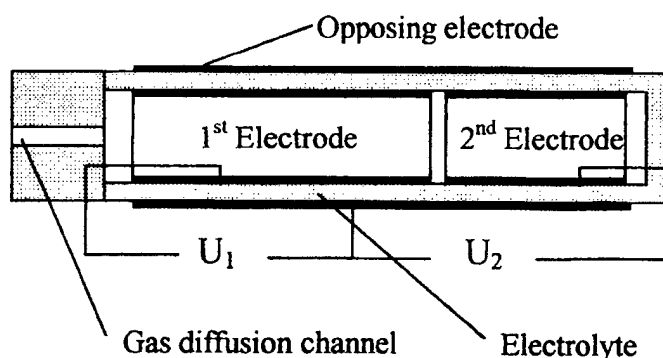


**Figure 1.** Schematic view of a tubular type amperometric cell with two working electrodes

### EXPERIMENTAL

Amperometric sensors based on stabilized zirconia solid electrolyte with two working electrodes have been studied experimentally with respect to the simultaneous measurements of oxygen and nitrogen oxides, or oxygen and combustible compounds in gas mixtures. In our experimental studies we usually used tubular type sensors which are shown schematically in figure 1. Typical tubes are about 4 cm long with outer diameter of 3 mm.

Sensors with different types of working electrodes have been optimized for specific gas analytical task. Sensors for the simultaneous detection of NO and oxygen contain two platinum electrodes, sensors for the simultaneous detection of oxygen and combustibles contain gold as first and platinum as a second electrode. Computer-controlled mass flow controllers have been used to generate the appropriate gas mixtures. All sensors have been characterized in controlled gas mixtures, i.e. O<sub>2</sub>/NO - sensors in N<sub>2</sub>/O<sub>2</sub>/NO-mixtures and oxygen/combustible - sensors in N<sub>2</sub>/O<sub>2</sub>/combustible mixtures with methane, propene, propane, H<sub>2</sub> and CO as the combustible component. In addition, the cross-sensitivities of the sensors to other exhaust gas components such as H<sub>2</sub>O, CO<sub>2</sub>, NO, SO<sub>2</sub> and combustible gas components were also measured. The response itself is based on the oxidation or reduction of the gas component leading to a positive or negative flux of oxygen ions in the solid electrolyte. In general, these sensors are very flexible gas analytical instruments. However, an optimum adjustment of all parameters is necessary for each specific problem. This includes the choice of the cell design, materials for working electrodes, and operation parameters, i.e.



temperature and potentials at each electrode [2]. An almost complete separation of the sensor's signals to defined gas components has been achieved by optimization of the working parameters of the electrodes. These cells show a linear output signal as a function of the concentration, a high accuracy, a high stability even in hazardous environmental conditions, and a good long-term stability of their response characteristics [2-4]. Solid electrolyte amperometric sensors are hence particularly suitable for applications in the control of combustible gases and for monitoring of car exhausts. Tests on cross-sensitivity to different components of car exhausts are particularly important in this context.

## RESULTS AND DISCUSSION

The response of an optimized O<sub>2</sub>/NO<sub>x</sub> sensor in oxygen rich gas had been shown earlier [2,3]. The signals are well separated. Oxygen is reduced completely at the first electrode and NO at the second electrode. A linear correlation between the gas concentrations of O<sub>2</sub> and NO and the current signals exist. Cross-sensitivities to oxygen-containing and to combustible gas components have been measured. The cross-sensitivity of this sensor to H<sub>2</sub>O and CO<sub>2</sub> is based on the reduction to H<sub>2</sub> and CO at the second electrode and appears only at high cathodic potentials. Cross-interference effects from CO<sub>2</sub> and H<sub>2</sub>O at O<sub>2</sub>/NO<sub>x</sub> sensors were minimized by properly adjusting the electrode potentials. Combustible components are oxidised catalytically at the first electrode and hence reduce the current at the first electrode. Combustibles in oxygen rich gases do not affect the signal at the second electrode.

The current response of the sensor to different combustible components has been studied as well [4]. Oxygen is determined at the 1st electrode, and burning component at the 2nd one. A separation of signals from oxygen and the combustible component has been achieved up to oxygen concentrations of 20%. At higher oxygen concentrations, oxygen may reach even the second electrode and leads to cross effects. No significant cross-sensitivities of electrodes were found for the combustible sensor except for H<sub>2</sub> and CO. Both components are partially oxidized at the gold electrode. The lack of oxidation currents in pure nitrogen indicates a predominant catalytic oxidation with gas phase oxygen at the surface of the gold electrode. Cross-effects on O<sub>2</sub>/HC<sub>x</sub>-sensors to gaseous oxides have been found to be even lower than to O<sub>2</sub>/NO<sub>x</sub> sensor.

## CONCLUSIONS

Results of our studies demonstrate the validity of proposed conception based on multi-electrode solid electrolyte amperometric sensors. These sensors are suitable for the analysis of industrial and car exhausts. These cells offer important advantages which make them very attractive for exhaust gas analysis: the high selectivity of the signals to detect the desired gas components, the linear signal characteristics which allows for simple calibration procedures, long-term stability, resistance to hard environmental conditions.

## ACKNOWLEDGMENTS

This work is supported by the Federal Ministry of Education and Research, BMBF.

## REFERENCES

- [1] S.I. Somov, Proceedings of 5th International Meeting on Chemical Sensors. Rome 2, 20 (1994).
- [2] S. I. Somov, G. Reinhardt, U. Guth, U. Schönauer and W. Göpel. *Ionics* 1, 514 (1995).
- [3] S. Somov, G. Reinhardt, U. Guth, W. Göpel. *Sensors and Actuators B* 35-36, 409 (1996).
- [4] S.I. Somov, and U. Guth. *Sensors and Actuators B* 47, 131 (1988).

## ENGINEERING POLYMER ELECTROLYTES WITH ENHANCED IONIC CONDUCTION

A. R. Kulkarni

Department of Metallurgical Engineering and Materials Science  
Indian Institute of Technology - Bombay 400 076, INDIA

Solvent free polymer electrolytes with high ionic conductivity are materials of interest for all solid-state-batteries. However, their commercial use is limited to high temperatures due to low ionic conductivity at ambient temperatures. Engineering the material to a given application has been the goal of materials scientists and developing polymer electrolytes for solid state batteries is an interesting problem. Key to the design of highly conducting polymers is to maximise the content of amorphous phase. The major activity of our group is to tailor these polymer-salt complexes to achieve high ambient temperature conductivity while retaining a desirable combination of mechanical and thermal properties. This paper describes our strategies to engineer these amorphous polymer-salt complexes to enhance the ionic conductivity.

In the first approach, semicrystalline polymer POE was plasticised by amorphous POPG in the presence of sodium salts. For the first time, these systems were considered as three component glass-forming systems as practiced in the field of glass science and technology to investigate glass-forming range. Nature of the complexes was determined from optical microscopy, X-ray diffraction and differential scanning calorimetry for the above ternary system. The polymer salt-complexes revealed a well-defined *glass formation region* in which all the compositions were amorphous and exhibited unusually high ionic conductivity  $\sim 10^{-4} (\Omega\text{-cm})^{-1}$  at ambient temperature. The Flory-Huggins theory which predicts the equilibrium miscibility of polymers and solvents, was extended to polymer-polymer-salt ternary system. Interaction parameters of the polymer1-polymer2, polymer1-salt and polymer2-salt were calculated and used to obtain free energy contours of the ternary systems. The results were applied to POE-POPG-NaI ternary system to obtain spinodal curves that gave an idea of the phases in the system. This region lied within the miscibility window obtained by the thermodynamic relationship. The results suggested that the miscibility limits could be predicted by extending the existing Flory-Huggins theory to the ternary polymer electrolyte systems.

In the second approach, amorphous polymers were used as starting materials to synthesis electrolytes. The polymers chosen were MEEP and Polysiloxane. Both polymers being glutinous, minimum quantity of high molecular weight POE was added to achieve dimensional stability and free standing films so engineered showed high ionic conductivity at room temperature. Electrical properties for these systems were studied. The first approach of engineering reduction in crystalline phases appeared more effective in enhancing ionic conductivity.

SIZE AND LIFETIME LIMITS TO SEMICONDUCTOR DEVICES DUE TO  
DOPANT DIFFUSION AND DRIFTDavid Cahen, Shachar Richter <sup>a</sup>*Weizmann Institute of Science, Rehovot 76100 Israel*

Igor Lubomirsky

*Dept. of Electrical Engineering, UCLA, Los Angeles, CA, 90024, USA*

A doped semiconductor can be viewed as a mixed electronic-ionic conductor, with the dopants as mobile ions [1]. In principle dopant mobility is relevant for all devices in integrated circuits that contain p/n homo- and heterojunctions, incl. most field effect transistors. This is so because such junctions result from gradients in the concentration of one or more dopant species in the semiconductor. The existence of concentration gradients in a single-phase system implies that such structures are thermodynamically unstable, i.e., that they persist only because of slow interdiffusion kinetics [2].

Normally the conditions under which dopant mobility becomes significant are far from where the (opto)electronic properties of the material are of interest and it is generally thought that elemental and III-V based devices are immune to this problem. Indeed, the lifetime of most electronic devices, which we define as the period over which no significant changes in their properties occur, is today some 20 years and generally is not connected to their kinetic stability. However, even today notable exceptions exist, not only in materials such as Si:Li, well-known from its use in radiation detectors, but also in Si:Cu and in compound semiconductors, ranging from II-VI's (as can be understood from problems with ZnSe-based lasers, and (Hg,Cd)Te-based detectors) to high temperature semiconductors, and conducting polymers, such as those used in organic optoelectronic devices. The issue will become progressively more important, as miniaturization of semiconductor devices, one of the main directions of their development during the last 30 years continues. At the same time the search for dopants, that combine desired electrical activity and low room temperature diffusivity will become harder and harder.

By using systems in which dopants can be made to electromigrate under conditions that are not far from ambient (based on CuInSe<sub>2</sub>, (Hg,Cd)Te and Si:Li), we have explored physical limits to **space-charge controlled** device creation. We argue and prove that we can use the Debye lengths of the materials to give us a very simple estimate of a lower limit on the size of such type of devices. To prove this we used conducting tip AFM, both for device creation and for its characterization with scanning spreading resistance. The results [2] show that indeed the smallest device structure that we can make fits this limit.

As noted above, a logical result of dopant mobility is that it can limit device lifetime, because a p-n junction presents a thermodynamically unstable situation for the dopants that create the junction. This is in contrast to the situation for the electronic charge carriers, which are in thermodynamic equilibrium. Thus, p-n junctions persist only because of kinetic stability. As long as device size is large, compared to  $\sqrt{(D.t)}$  (D, dopant diffusion coefficient; t, expected life time), junction degradation is sufficiently slow so that it can be ignored. While not a real problem for Si in the foreseeable future (assuming efficient Cu-

diffusion barriers are in place and no diffusion anomalies in SiGe), it needs to be considered for other systems.

We show how Fick's law dictates a general *chemical* (kinetic) *limit to miniaturization*, due to dopant diffusion & drift (electromigration), across a p-n junction. To this end we analyze dopant flux in a semiconductor p/n junction, due to chemical diffusion and electromigration of charged dopants, as a possible determining factor for device life expectancy at room temperature [4]. We can derive simple relations to allow estimates of life times for cases of both normal and interstitial-substitutional (IS) diffusion [5], for zero, forward or reverse bias. All other factors being equal (assuming identical numerical diffusivity values) we find differences of more than 4 orders of magnitude between the most and least stable situations. We apply our analyses to III-V heterojunction bipolar transistors of the type (Al,Ga)As, doped with Be. We find excellent agreement between our model and lifetime results from the literature [6].

Normally, in calculations involving diffusion, full intermixing is assumed. If we consider some modern types of device structures, with very thin undoped layers sandwiched between doped ones, it is clear that even 1% intermixing can be critical. This decreases lifetime by close to a factor of 100 and leads to the conclusion that for structures containing a critical dimension of 10 nm, none of the components can have  $D \geq 10^{-24}$  cm<sup>2</sup>/sec, averaged over the lifetime, for a desired  $t \sim 3$  yr [6].

The question then arises if this limitation can be overcome or mitigated.

We have found two types of encouraging answers. In the first one we take advantage of the so-called substitutional-interstitial diffusion mechanism. Dopants that move in this way can convey extra kinetic stability to the structure. This is illustrated by Zn diffusion and drift in InP [5].

Alternatively thermodynamically stable junctions are needed [7]. This can be achieved if the n- and p- types are separate phases. We show this to be possible, at least in a model system, viz. Ag : (Cd,Hg)Te, where phase separation at ultra-low concentrations occurs [8].

We conclude that dopant intermixing needs to be considered as a lifetime limiting factor for compound semiconductor devices, as their dimensions shrink.

**Keywords:** dopant; diffusion, drift, electromigration; stability; life time, degradation

## References

<sup>a</sup> Present address: Lucent Technol., Bell Labs, Murray Hill, NJ, USA

- [1] D.Cahen, L.Chernyak, *Adv. Mater.*, **9**, 861(1997).
- [2] J. F. Guillemoles et al., *J. Phys. Chem.* **99**, 14486(1995)
- [3] S. Richter et al., *Appl. Phys. Lett.*, **73**, 1868-1870 (1998);  
S. Richter et al., *Phys. Rev. B*, submitted.
- [4] I. Lubomirsky et al., *J. Appl. Phys.*, **83**, 4678(1998)
- [5] I.Lyubomirsky et al., *Appl. Phys. Lett.*, **70**, 613 (1997)
- [6] D. Cahen, I. Lubomirsky, *Electrochem. Sci. Solid State Lett.*, submitted.
- [7] I.Lyubomirski et al., *Appl. Phys. Lett.* **67**, 3132 (1995)
- [8] I. Lubomirsky et al, *Europhys. Lett.*, in press.

SPECIAL ZrO<sub>2</sub> OXYGEN SENSOR STRUCTURES  
FOR AUTOMOTIVE APPLICATIONS

E. M. Logothetis, R. E. Soltis and T. Wang  
Ford Motor Company  
P.O. Box 2053  
Dearborn, Michigan 48121

Electrochemical-type ZrO<sub>2</sub> oxygen sensors (known as HEGO or lambda sensors) have been used successfully on vehicles for many years for stoichiometric air-to-fuel ratio (A/F) control. However, new or more demanding automotive emission control and monitoring systems require oxygen sensors with improved or special characteristics. This paper describes a number of special ZrO<sub>2</sub>-based oxygen sensor structures which have been developed at Ford to address these needs.

The first structure was developed for the purpose of obtaining a stoichiometric A/F sensor with very fast light-off time (i.e. time to operation), for example, less than 5 seconds. The simplest approach in developing such a sensor is to substantially reduce the mass of the ZrO<sub>2</sub> electrochemical cell which can be more easily achieved by the elimination of the air reference. One method for accomplishing this is to construct an internal reference. Another method which is described here utilizes two dissimilar "electrode structures", both exposed to the exhaust gas. The device shown schematically in Fig. 1 consists of a thin ZrO<sub>2</sub> plate with porous Pt electrodes on the two sides. The two electrodes are covered with porous layers having different thickness or porosity. When the air-to-fuel ratio is changed through stoichiometry, the Pt electrode with the more gas permeable overlayer senses the change faster than the other electrode. It is apparent that the emf output of such a device to changes in the A/F through stoichiometry is in the form of positive and negative pulses. Figure 2 compares the output of this sensor with that of the conventional HEGO sensor when the air-to-fuel ratio is ramped back and forth through the stoichiometric value. The output of the sensor of Fig. 1 can be made to look similar to that of the HEGO sensor by using a simple electronic circuit. Under certain conditions, it is also possible to obtain a device of this type by employing two dissimilar electrode materials. The device shown in Figure 1 can be fabricated using ceramic tape technology or Si-based microfabrication techniques [1].

A second device, called "catalytic/non-catalytic" (C/NC), has the same structure as the conventional HEGO sensor, except that the exhaust gas electrode of the sensor has limited catalytic activity [2]. Depending on the properties of this electrode, the emf of the device depends on the degree of equilibration of the exhaust gas. Figure 3 shows laboratory results on the response of an experimental device with a Au/Pt exhaust gas electrode to simulated exhaust gas. The sensor emf is plotted as a function of the inverse redox ratio  $R'$  (the ratio of the concentration of oxygen over that of the reducing species) for various degrees of gas equilibration from 100% to 0%. When the gas is fully equilibrated, the sensor emf shows the familiar well-defined step near stoichiometry; as the degree of gas equilibration decreases, the step becomes smaller and broader. When placed in the exhaust gas after the three-way-catalyst, a device of this type could be used for the on-board monitoring of the efficiency of the catalytic converter [2]. The behavior of this device was analyzed

using the gas sensor model developed at Ford [3] and was found to vary widely depending on the electrode properties and the details of the structure. It is noted that the device can also be made without the air-reference compartment and in a planar configuration.

A third type of devices to be discussed here employs a combination of  $\text{ZrO}_2$  electrochemical cells operated in the amperometric mode together with special diffusion layers to obtain simple proportional A/F sensors. Several configurations will be described and their operation will be discussed.

- [1] E.M. Logothetis and R.E. Soltis, U.S. Patent No. 4,790,924, Dec. 13, 1988.
- [2] D.R. Hamburg, E.M. Logothetis, J.H. Visser and R.E. Soltis, U.S. Patent No. 5,268,086, Dec. 7, 1993; D.R. Hamburg and A. Kotwicki, U.S. Patent No. 5,363,091, 1994.
- [3] A.D. Brailsford, M. Yussouff, and E.M. Logothetis, Sensor and Actuators B13, 135 (1993).

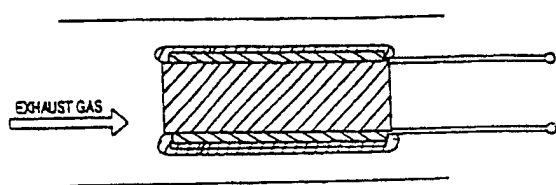


Figure 1. Schematic of the fast light-off HEGO sensor

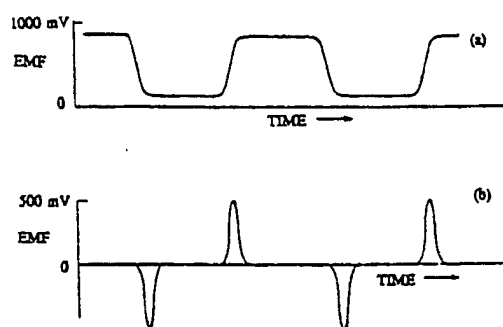


Figure 2. Comparison of the responses of a conventional HEGO sensor (a) and of the sensor in Fig. 1 (b) to changes in the air-to-fuel ratio through stoichiometry.

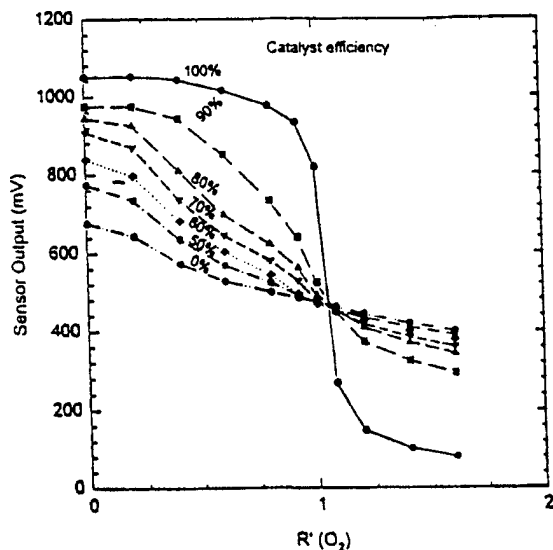


Figure 3. The emf output of a C/NC sensor as a function of the inverse redox ratio of simulated exhaust gas for various degrees of gas equilibration.

## PHASE TRANSITIONS IN OXIDATION CATALYSTS

L. Rieker

Institut für Chemische Verfahrenstechnik  
der Universität Karlsruhe

Oxides of transition metals are extensively used as active components in catalysts for selective oxidation. In these reactions oxygen from the lattice of the catalyst is consumed through reaction with the educt E as oxygen acceptor and replenished through uptake of molecular oxygen from the gas-phase. At steady state the net rate of oxygen loss or uptake must be zero, the oxidation state of the catalyst then being determined by the kinetics of oxygen transfer to and from the solid, which in turn determines the phase-composition of the catalyst under working conditions. It can be oxygen-rich (e.g. NiO) or oxygen-lean (e.g. Ni), depending on the thermodynamic activity  $a_0$  of oxygen in the solid.

In contact with pure oxygen the oxygen-activity  $a_0$  may be defined as the square-root of the oxygen-pressure  $(p_{O_2})_{eq}$  in equilibrium with the solid

$$a_0^2 = (p_{O_2})_{eq} \quad (1)$$

If  $p_{O_2}^*$  is the oxygen partial-pressure where two phases can coexist at a given temperature, then the oxygen-rich phase will be stable if  $a_0 > \sqrt{p_{O_2}^*}$  and the oxygen-lean phase if  $a_0 < \sqrt{p_{O_2}^*}$ . The situation is different when a catalytic reaction takes place, that is under nonequilibrium conditions, where oxygen is continuously removed from the solid. The oxygen-content of the solid at steady state will then be less than at the same  $p_{O_2}$  under equilibrium conditions and we must have

$$a_0 = a_0 \{p_{O_2}, p_E\} < \sqrt{p_{O_2}} \quad (2)$$

The transition between phases of different oxygen content should then take place at a higher oxygen pressure  $(p_{O_2})_{trans} > p_{O_2}^*$  than in the absence of the oxygen-consuming educt E. Two patterns of phase transitions are to be expected in this case, depending on the relative position of the lines of  $a_0 \{p_{O_2}\}$  in the  $a_0$  vs.  $p_{O_2}$ -plane at given  $p_E$ , as has been deduced by Wagner [1]. His predictions were substantiated experimentally by observation of phase transitions in oxidation catalysts through discontinuities in steady-state kinetics [2]. The theoretical treatment of these phenomena hinges on a quantity which cannot be observed from kinetics, i.e. the thermodynamic activity of oxygen in the catalyst under nonequilibrium conditions. The definition of chemical potential and activity applies strictly only to matter at equilibrium. Nevertheless an oxygen activity can be observed in working catalysts by solid electrolyte potentiometry (SEP) based on Nernst's equation. As will be shown in a separate contribution the results of SEP-measurements agree essentially with conclusions drawn from kinetic observations, suggesting that the notion of oxygen activity can be applied in principle also in the case of the nonequilibrium systems considered.

#### References:

- [1] C. Wagner, Ber. Bunsenges. Phys. Chem. 74 (1970) 401
- [2] M. Greger and L. Riekert, Ber. Bunsenges. Phys. Chem. 91 (1987) 1007



## Towards a new solid state ionic polymeric based electorchromic device : A case study of conducting polymer composites

A.TALAE<sup>\*,1,2</sup>, Y. K. LEE<sup>3</sup>, J. JANG<sup>1</sup>

1. Physics Department, Kyung Hee University, Dongdaemoon-ku, Seoul, KOREA

2. Chemical Engineering Department Sydney University, Sydney NSW 2006, Australia

3. Information Display Department, Kyung Hee University, Dongdaemoon-ku, Seoul, KOREA

Polyaniline exhibit electrochromic behavior such that low potentials or small change in the pH of the solution could create colour and conductivity changes on the surface of the polymer. Polyaniline is green in the oxidised state and is transparent yellow in the reduced states. It has violet colour in very acidic and yellow brownish in very basic media. (Figure 1).

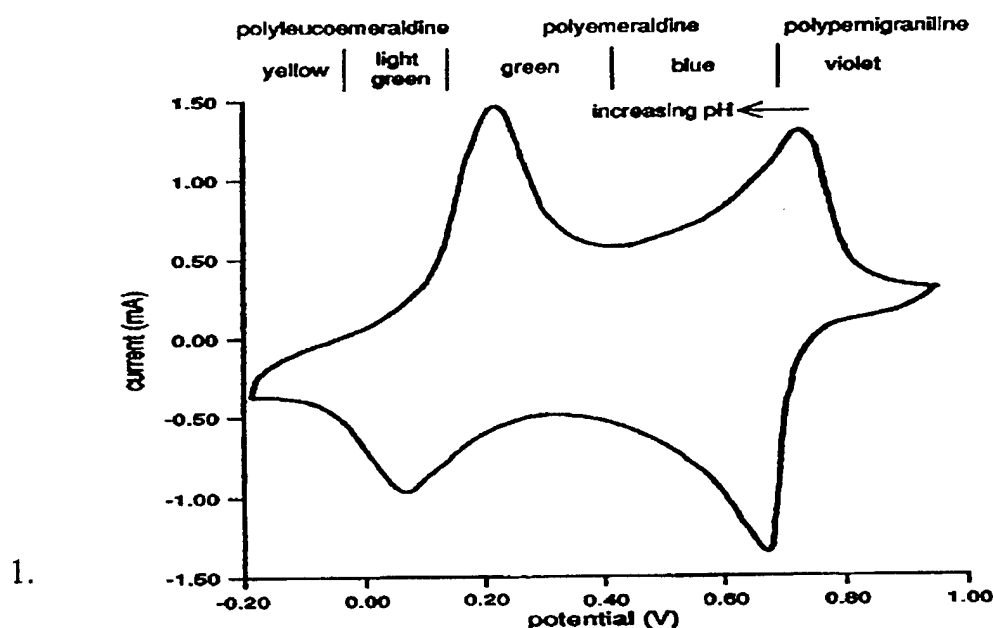


Figure  
Color

dependency of polyaniline with the applied potential

A composite of two conducting polymers, polyaniline and polypyrrole, could result in much improved physical properties with respect to their applications in electrochromic devices. However, the composite has time dependant properties that made the use of dynamic computational algorithms necessary to control its behavior. We used a platinum-modified electrode as an electrochromic display device (shown in Figure 2), which was integrated with a pre-trained computer for data processing and knowledge discovery. Since there is a direct relationship between the colour of the composite and its conductivity, detection of conductivity/colour has been used for prediction of pH. We have found that different parameters within the used computer algorithms can affect the performance of modeling that results in a more reliable device.

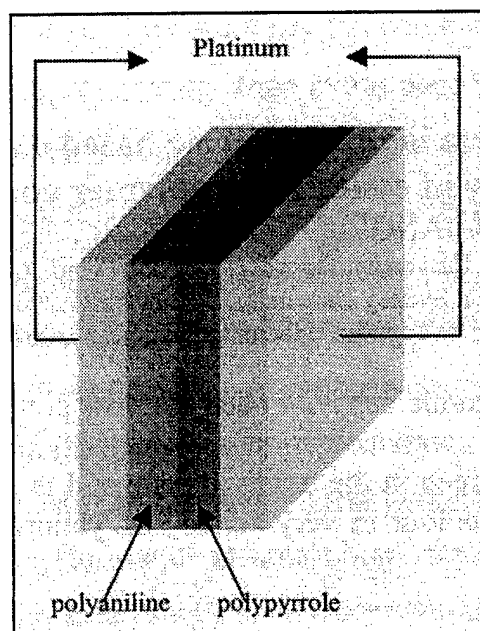


Figure 2. Configuration of the polymeric based electrochromic device.

#### REFERENCES

- 1) S. Bruckenstein and S. Swathirajan, *Electrochim Acta*, **30**, 851 (1985).
- 2) J.R. Reynolds, N.S. Sundaresaan, M. Pomerantz, S. Basak and C. K. Baker, *J. Electroanal. Chem.*, **250**, 355 (1988).
- 3) A. Talaie, *Polymer*, **38**, 1145 (1997).
- 4) K. Naoi, M. Lien and W. H. J. Smyrl, *Electrochem. Soc.*, **138**, 440 (1991).

\* Corresponding author E-mail : [talaie@tflcd.kyunghee.ac.kr](mailto:talaie@tflcd.kyunghee.ac.kr)

# GAS ELECTRODE REACTION WITH METAL-ION CONDUCTING SOLID ELECTROLYTE: CO<sub>2</sub>-O<sub>2</sub>, Au / DOPED-Li<sub>2</sub>CO<sub>3</sub> SYSTEM

Junichiro MIZUSAKI, Shigeki TERUI, Tatsuya KAWADA,  
Kenichi KAWAMURA, Yutaka NIGARA, Atsushi KAIMAI and Hiroaki TAGAWA\*  
*Research Institute for Scientific Measurements, Tohoku University,  
Katahira, Aoba-ku, Sendai 980-8577, Japan*  
\*Prof. Emeritus, Yokohama National University

## 1. Background and Purpose

Much attention has been focused on the kinetics of gas-electrode reaction on solid electrolyte cells with oxide ion or proton conducting electrolytes, expecting the application such as to solid oxide fuel cells and high temperature electrochemical gas sensors. In these electrochemical cells, the gas-electrode reaction is expected to involve little microscopic variation at the electrolyte/electrode interface, because the mobile ionic species only pass through the electrolyte from one electrode / electrolyte interface to another.

On the other hand, when a gas electrode reaction takes place with a metal-ion conducting electrolyte, the electrolyte decomposes at one electrode /electrolyte interface and is formed at another, moving toward the negative electrode as illustrated in Fig. 1. With the proceeding of the reaction, the morphology is expected to vary continuously at the triple phase boundary (TPB) of gas / porous electrode / electrolyte. Even in potentiometric application, small current does flow resulting in the variation of the electrode morphology in a long time operation.

In spite of the disadvantage mentioned above, application of metal-ion conductors is considered for chemical sensors, such as SO<sub>2</sub>, NO<sub>x</sub>, and CO<sub>2</sub> sensors with alkali-ion solid electrolytes. This paper aims to clarify how the electrode morphology varies and the effect of the variation on the electrochemical properties, using Au electrode and doped Li<sub>2</sub>CO<sub>3</sub> electrolyte with CO<sub>2</sub>-O<sub>2</sub> gas-mixtures.

## 2. Experimental

As a working electrode, a spherical Au electrode (2 mm in diameter) was placed on a pellet (3 mm thickness and 7 mm in diameter) of doped Li<sub>2</sub>CO<sub>3</sub> electrolyte (Li<sub>2.05</sub>(CO<sub>3</sub>)<sub>0.95</sub>(PO<sub>4</sub>)<sub>0.05</sub> + 9 wt% LiAlO<sub>2</sub> supplied from Akebono Brake R & D Center, Ltd. [1]). Au mesh was applied as a reference and a counter electrode. All the electrodes were exposed to the same atmosphere of controlled CO<sub>2</sub>-O<sub>2</sub> gas mixtures. Measurements were made on the electrochemical impedance over the frequency range of 1 mHz-100 kHz and polarization current at 773-823K. The microscopic variation of TPB was observed by means of SEM.

## 3. Results and Discussion

### 3.1. Features of the impedance spectrum

In the frequency range studied, a large arc (resonance frequency,  $f_r$ , of 0.1-0.01 Hz) is generally observed, which depends on  $P(\text{CO}_2)$  and  $P(\text{O}_2)$  and is attributed to the electrode reaction impedance at the TPB. The electrode interface conductance,  $\sigma_E$  ( $= 1/R_E$ ;  $R_E$ : the real part of the electrode interface impedance), can be empirically expressed with constants A and B by

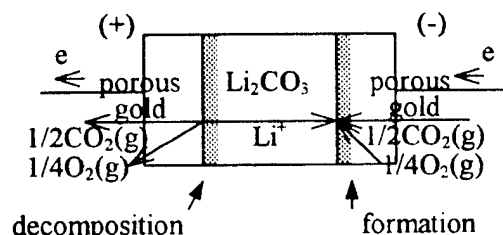


Fig. 1. Schematic example of the gas electrode reaction with metal-ion conducting solid electrolyte.

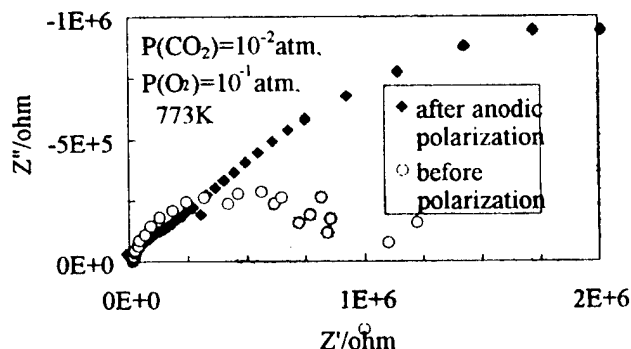


Fig. 2. Impedance plot before and after anodic polarization measurements.

$$\sigma_E = P(O_2)^{1/2} P(CO_2)^{1/4} / \{AP(CO_2)^{1/2} + BP(O_2)^{1/2}\}$$

Another arc is often observed at the higher frequency range with  $f_T$  of 10-100 kHz, which is almost independent of the gas phase composition and is considered due to grain-boundary effects in the electrolyte. The bulk impedance is observed as the converging point of the high frequency arc to the real axis at its high frequency limit.

### 3.2. Variation of impedance spectrum with current

As shown in Fig. 2, after polarization current was applied,  $R_E$  tends to increase and the impedance arc does not converge on the real axis at the lowest frequency region studied in this work, suggesting that the length of TPB changes with current.

### 3.3. Cathodic polarization current

Current decay curves under potentiostatic polarization to the cathodic direction (overall half cell reaction:  $CO_2 + (1/2)O_2 + 2Li^+ + 2e \rightarrow Li_2CO_3$ ) are shown in Fig. 3. After a rapid decay within the time period observed by impedance spectroscopy ( $<1000$  s), the decay of current continues upto  $3000-10^4$  s, suggesting the continuous decrease in the length of TPB. However, with the longer polarization measurements, the current decay is negligibly small.

### 3.4. Anodic polarization

Fig. 4 shows the change in the anodic polarization current at  $\eta = 50$  mV just after the cathodic polarization of different magnitude. After the initial rapid decay due to the relaxation of the reaction kinetics, the current ones increases, suggesting the increase in TPB during the anodic polarization. After the maximum observed at around  $3000-10^4$  s, the current decreases to a stationary value. This increase in current is observed only just after the cathodic polarization.

### 3.5. SEM observation and the effect of Li-ion conduction:

The results of SEM observation is schematically shown in Fig. 5. After a) after cathodic polarization, formation of thin and dense polycrystalline layer of  $Li_2CO_3$  is observed on Au surface extending from the original TPB. That is, the TPB moves from the original position to the surface of Au and the thin  $Li_2CO_3$  film gradually extends on the Au surface. After anodic polarization, the  $Li_2CO_3$  layer on Au becomes porous and Au surface becomes open to the gas phase through the grain-boundaries, suggesting that the reaction of  $Li_2CO_3 \rightarrow 2Li^+ + 2e + CO_2 + (1/2)O_2$  proceeds not only at the obvious TPB but also apparently closely contacted  $Li_2CO_3$  / Au interface around the grain-boundaries to decompose  $Li_2CO_3$  at the site. The increase in current during the anodic polarization may be attributed to the increase in the TPB by the formation of open pores around the grain-boundary. After long-time anodic polarization, islands of  $Li_2CO_3$  are left on the Au surface. The TPB length becomes the original one.

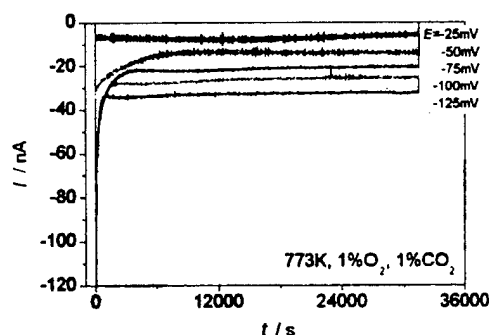


Fig.3. Time change in cathodic polarization current.

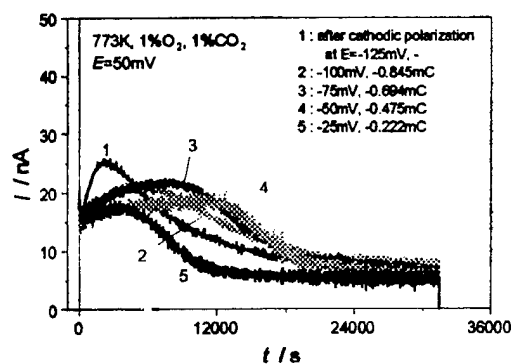
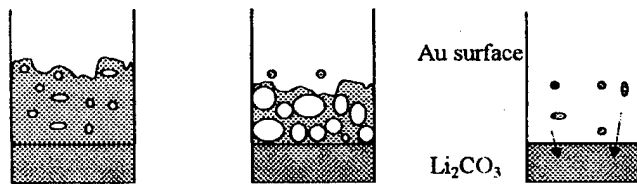


Fig. 4. Time change in anodic polarization current at  $\eta = 50$  mV after cathodic polarization measurements shown in the figure.



[1] Y.C. Zhang, H. Tagawa, S. Asakura, J. Mizusaki, and H. Narita, J. Electrochem. Soc., 144, 4345 (1997).

# ELECTROCHEMICAL CHARACTERISATION OF A JUNCTION BETWEEN PROTON CONDUCTOR AND OXIDE ION CONDUCTOR

N. Bonanos

Materials Research Department, Risø National Laboratory  
DK-4000 Roskilde, Denmark. nikolaos.bonanos@risoe.dk.

Passing a current across the junction between a proton conductor and an oxide ion conductor can cause electrochemical reactions, moreover and the electrical characteristics of such a junction should be interesting for a fundamental electrochemical viewpoint. Junctions have been prepared by forming thin layers of  $\text{SrZrO}_3$  on zirconia [1] giving, among other effects, current rectification. For the present work, junctions were prepared by contacting pellets of a  $\text{SrCeO}_3\text{:Y}$  proton conductor [2] (SCY) and a zirconia oxide ion conductor (YSZ) as shown in Fig.1. The assembly was exposed to controlled atmospheres of  $\text{O}_2/\text{N}_2/\text{H}_2\text{O}$  or  $\text{H}_2/\text{N}_2/\text{H}_2\text{O}$  at temperatures of 600 to 800°C. Contact impedances were measured as a function of junction bias in the range  $\pm 300\text{mV}$ . Interfacial capacitances were of the order of  $100\mu\text{F cm}^{-2}$  and were strongly dependent on bias. The current-voltage curves showed weak rectifying characteristics and were depended on the gas atmosphere, as shown for example in Fig.2. To identify the true electrochemical effects in these observations, complementary experiments were performed on junctions between conductors of the same type.

## Acknowledgements

This work was supported by the Materials Research Department, Risø, and by the New Energy Development Organisation (NEDO) of Japan under the project *Advanced Ceramics for Protonics*.

## References

1. T. Shimura, G. Egusa, H. Iwahara, K. Katahira and K. Yamamoto, *Solid State Ionics* **97**, (1997) 477-482.
2. E.O. Ahlgren, J.R. Hansen, N. Bonanos, F.W. Poulsen and M. Mogensen, *Proc. 17<sup>th</sup> Risø Intl. Symp. on Materials Science: High Temperature Electrochemistry: Ceramics and Metals*, September 2-6 (1996), pp.161-166.

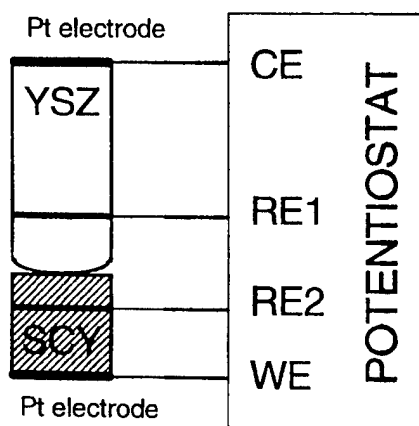


Fig.1 Schematic diagram of proton conductor /oxide ion conductor junction and its connection to electrochemical measuring equipment.

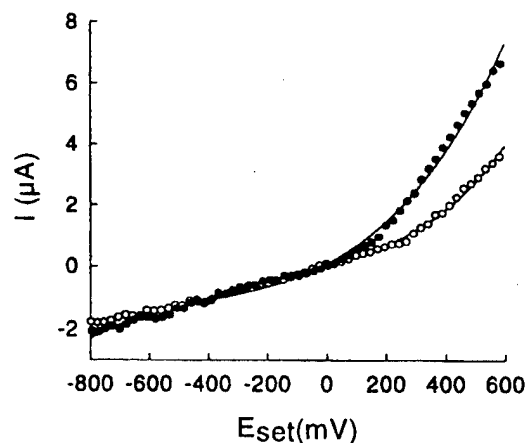


Fig.2 Cyclic voltamogram obtained on the junction at 600°C in atmospheres of  $\text{N}_2/5\%\text{H}_2$  containing controlled amounts of water vapour: (●) 1%  $\text{H}_2\text{O}$ , (○) 0.05%  $\text{H}_2\text{O}$ .

IMPORTANT MATERIALS ASPECTS FOR SENSORS BASED ON Na  $\beta$ -ALUMINAJ. Vangrunderbeek<sup>1</sup>, F. Vandecruys<sup>1</sup> and R.V. Kumar<sup>2</sup><sup>1</sup>VITO – Process Technology, Boeretang 200, B-2400 Mol, Belgium<sup>2</sup>Department of Materials Science and Metallurgy, University of Cambridge, CB2 3QZ, Cambridge, UK**Extended abstract**

The objective of this paper is to give a critical view on the feasibility and reliability of electrochemical sensors combining Na  $\beta$ -alumina solid electrolyte material with an auxiliary phase. Thermodynamic information on the stability of Na- $\beta$ -alumina ( $\text{Na}_2\text{O} \cdot x\text{Al}_2\text{O}_3$ ) and the activity of  $\text{Na}_2\text{O}$  in Na  $\beta$ -alumina is critical in applications for sensors, and especially in situations where the operating temperatures are high and the oxygen pressures are low and where the  $\beta$ -alumina phase is used as a part of the electrode providing reference potentials in galvanic cells.

Over the last two decades several different types of galvanic cells have been used to determine the thermodynamic stability of  $\beta$ -alumina and the activity of  $\text{Na}_2\text{O}$  in the  $\text{Na}_2\text{O} \cdot x\text{Al}_2\text{O}_3$  binary system. In another paper [1], we have demonstrated that in the  $\text{Na}_2\text{O} \cdot x\text{Al}_2\text{O}_3$  binary system, for all compositions from  $5.5 < x < 19$ ,  $\beta''$ -alumina can coexist with  $\beta$ -alumina in the range  $5.5 < x < 8.5$  and with  $\alpha$ - and  $\beta$ -alumina at  $x > 8.5$  in samples prepared by sintering at temperatures above 1900K. This is reflected in the  $\text{Na}_2\text{O}$  activity in the  $\text{Na}_2\text{O} \cdot x\text{Al}_2\text{O}_3$  binary system to decrease with increasing value of alumina for  $5.5 < x < 8.5$  and to remain almost stable only for  $8.5 > x < 19$ .

The main requirement for the reference electrode is to maintain a perfectly constant potential drop at the interface between solid electrolyte and reference system. Therefore, it should have excellent stability and reversibility at least to the component to be measured and the response time should be as fast as required by the process. The most evident reference material, liquid sodium is not applicable due to the very low melting and boiling temperature. Even most of the binary systems suffer from the same disadvantage and require perfect sealing from the surrounding atmosphere. Ternary systems based on oxides, although more complex equilibria have to be established, have the advantage of being open to the air. In the literature, powder mixtures of  $\alpha$ -,  $\beta$ - and  $\beta''$ -alumina are applied as a sodium reference electrode in  $\beta$ -alumina based sensors. However, using the above mentioned thermodynamic data, it is concluded that  $\beta''$ -alumina is not an equilibrium phase in the  $\text{Na}_2\text{O} \cdot x\text{Al}_2\text{O}_3$  ( $5.5 < x < 19$ ) binary system, but that in fact it is invariably present within the  $\beta$ -alumina phase as a region of disorder or intergrowth. It has been shown [2-4] that hematite-sodium ferrite powder mixture are more reliable reference systems since this is a stoichiometric double phase material wherein the  $\text{Na}_2\text{O}$ -activity is independent of the composition. However, a phase transformation at 1033K causes the  $\text{Na}_2\text{O}$ -activity to change its slope (but retaining its linear behaviour).

It has finally been demonstrated that particularly under low oxygen operating conditions Na  $\beta$ -alumina offers excellent potential for in-situ creation of stable auxiliary phases [5]. Reliable  $\text{H}_2\text{S}/\text{H}_2$  sensitive measuring electrodes for reducing atmospheres could be formed by in-situ catalytical exchange of the oxygen ions in the conduction plane of the Na  $\beta$ -alumina surface by sulphur ions during the long-term pre-conditioning of the solid electrolyte surface in a  $\text{H}_2\text{S}/\text{H}_2$  reducing gas mixture. The real nature of the exchange reaction depends on the temperature and the gas composition, eventually resulting in an offset voltage when another phase is incorporated with Na  $\beta$ -alumina instead of the one expected on stoichiometric

considerations. But nevertheless, such a sensing mechanism avoids the need for a macroscopic auxiliary layer and thus the risk for drift on the long term.

### References

- [1] F. Vandecruys, E. Brauns, R.V. Kumar and J. Vangrunderbeek, submitted to J. Materials Science.
- [2] L. Zhang, D.J. Fray, J.C. Dekeyser and F. De Schutter, Met. Trans. B **24**, 794 (1996).
- [3] R.V. Kumar and D.J. Fray, in "Extractive Metallurgy '89" (Institute of Mining and Metallurgy, London 1989) p. 315.
- [4] F. Vandecruys, E. Brauns, M. Mertens, I. Thijs and J. Vangrunderbeek, submitted to Solid State Ionics.
- [5] J. Vangrunderbeek, F. Vandecruys and R.V. Kumar, submitted to Sensors and Actuators B.

### **Li<sup>+</sup> conducting gel electrolyte for Electrochromic Windows**

S.A. Agnihotry, Nidhi, Pradeep, S.S. Sekhon\*

National Physical Laboratory, Dr. K.S. Krishnan Road, New Delhi, 110012, INDIA.

Guru Nanak Dev University, Amritsar, INDIA.

Polymeric gel electrolytes provide a convenient medium with high ionic conductivity and high viscosity. In addition, if they offer high transmission in the visible region they are most attractive for electrochromic (EC) window applications. Polymethylmethacrylate (PMMA), well known for its high transmissive properties is the most suitable polymer immobilizing liquid electrolytes, in preparing gel electrolytes for EC windows. In this paper we report preparation and properties of PMMA based Li<sup>+</sup> ion conducting gels. In order to attain high conductivity at room temperature we have prepared liquid electrolytes of Lithium salt LiN(CF<sub>3</sub>SO<sub>2</sub>)<sub>2</sub> in plasticizing solvents with differing dielectric constants. Using Propylene Carbonate (PC), Ethylene Carbonate (EC) and  $\gamma$ -Butyrolactone ( $\gamma$ -BL) and their mixtures, maximum room temperature conductivity exceeding 10<sup>-2</sup> Scm<sup>-1</sup> could be attained for the liquid electrolyte. Addition of PMMA in different proportions has resulted in increasing the viscosity considerably without lowering the conductivity significantly. Further our Fourier Transform Infra-Red (FTIR) investigations have revealed that the addition of PMMA up to an optimized proportion also has not influenced the complexation between the salt and the solvent system. Thus highly viscous gels with liquid electrolyte like properties with high room temperature conductivity could be prepared. Observed moderate conductivity variations of these gels with temperature are typical of viscous electrolytes and are advantageous for using them in EC windows. Incorporation of these gels in EC devices show excellent performance characteristics making them very promising for EC window applications.



## CATION AND ANION MOBILITY IN POLYPYRROLE

Steen Skaarup and Keld West

Department of Chemistry, Technical University of Denmark, DK-2800 Lyngby, Denmark

L.M.W.K. Gunaratne, K.P. Vidanapathirana and M.A. Careem

Department of Physics, University of Peradeniya, Peradeniya, Sri Lanka

Some of the properties of electronically conducting polymers depend on the oxidation state of the polymer backbone: Electronic conductivity, optical absorbance and also mechanical properties such as volume and elastic constants. This opens the possibility of controlling a given property by the application of a potential. The change in mechanical characteristics forms the basis for the recent interest in electro-chemo-mechanical actuators ("artificial muscles") based on conducting polymers. The goal is the precise control of position and force by the application of a small (0-5 V) potential. However, the properties may drift with time, sometimes even reversing the direction of force, perhaps because of a switch from cation to anion mobility. This destroys the one-to-one correspondence between force/position and potential, and points to the importance of a more complete understanding and control of molecular mechanisms in the polymer

The oxidation/reduction process can be performed by the reversible doping with ions that counterbalance the charges on the one-dimensional polymer chains. Earlier work has shown that this process is wholly analogous to the insertion process in intercalation electrode materials [1]. In highly conjugated forms, the inserted ions may occupy well-defined sites along the chain giving rise to sharp peaks in cyclic voltammograms [2]. The shift in peak positions of these well-defined forms as a function of electrolyte concentration has been used to elucidate the nature of the moving ion.

The nature of the mobile ion turns out to depend critically on finely balanced interactions between the ions, the polymer and the electrolyte solvent: In the system  $\text{LiClO}_4/\text{PPy}$  in propylene carbonate, the perchlorate anion is the dominant mobile species, whereas changing the solvent to acetonitrile causes the lithium cation to be intercalated reversibly.

When a large anion (dodecyl benzene sulphonate, DBS) is used, the results show that, as expected, the sodium cation is the major mobile countercharge. The insertion of the ions has also been studied by correlating cyclic voltammograms with the mass change measured by a quartz crystal microbalance, yielding the same conclusion for sodium DBS/PPy. Measurement of the changes in force, position and stiffness on insertion/ejection of sodium ions reveal that most of the force is obtained in a restricted potential range.

## References:

- [1] K. West, B. Zachau-Christiansen, T. Jacobsen and S. Skaarup, *Mater. Sci. Eng. B13*, 229 (1992)
- [2] K. West, T. Jacobsen, B. Zachau-Christiansen, M. A. Careem and S. Skaarup, *Synth. Met.* 55-57, 1412 (1993)

ALTERNATIVE APPROACHES TO ELECTROCHROMIC  
DEVICES FOR OPTICAL APPLICATIONS

S. Papaefthimiou, G. Leftheriotis and P. Yianoulis

Department of Physics, University of Patras, Patras 26500, GREECE.

Tel: ++30-61-997449. Fax: ++30-61-997472. E-mail: spapaef@physics.upatras.gr

The development of durable electrochromic devices has gained increased attention in recent years [1], [3-6]. The major applications of these devices are in smart windows that can regulate the solar gains of buildings and also in glare attenuation in automobile rear view mirrors. For such applications, devices based on proton and lithium ions have been extensively studied, the latter having attracted attention due to their environmental stability. A typical electrochromic device has a five layer structure : TC/EC/IC/IS/TC, where TC, EC, IC and IS represent the transparent conductor, electrochromic material, ion conductor and ion storage layer, respectively [1]. The systematic study of various electrochromic devices that is presented in this work is mainly focused on the study of different materials as TC, EC, IC and IS layers and the optimisation of the fabricated devices. All the used layers were prepared in the laboratory using thermal evaporation and electron gun deposition.

We have used  $\text{WO}_3$  and  $\text{MoO}_3$  thin films as the basic EC layers, as their favourable behaviour in electrochromic devices has already been proven in many previous works. In Figure 1 the coloration results for an electrochromic device incorporating a  $\text{MoO}_3$  film as EC layer is shown. Furthermore, the use of mixtures of the above two oxides was investigated in order to prepare samples with improved colour and performance characteristics. The results show that the mixed  $\text{WO}_3\text{-MoO}_3$  electrochromic films exhibit similar coloration performance but have an aesthetically more pleasant colour compared to the plain  $\text{WO}_3$  or  $\text{MoO}_3$  films [3-5].

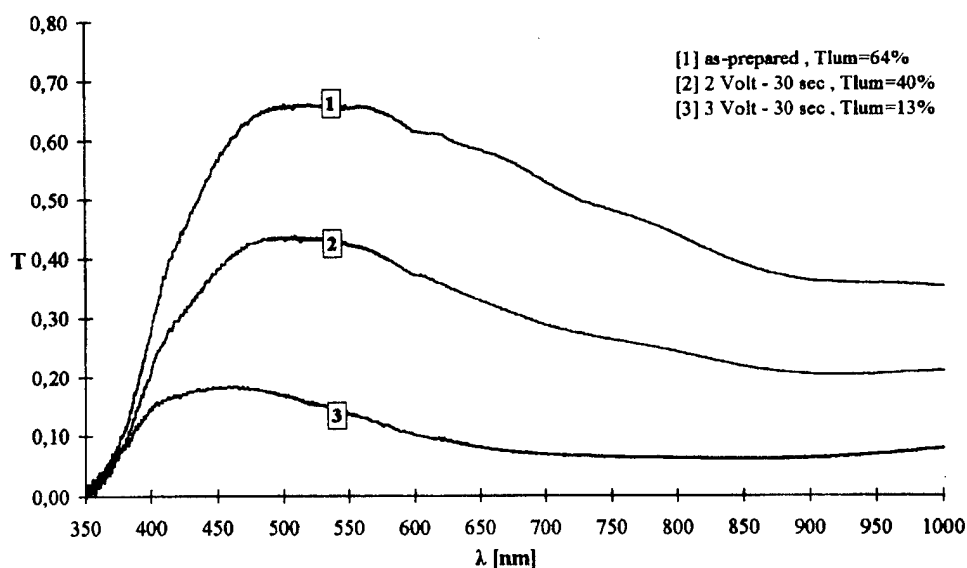


Figure 1

In our electrochromic devices we have mainly used liquid electrolytes as IC layers. The use of highly conductive polymer electrolytes in gel form [6] was also investigated. In such polymer-solvent-salt systems, the polymer serves as a stiffener for the solvent, which dissolves the salt and acts as a conducting medium. These materials may then exhibit conductivity very close to

that observed in liquid electrolytes and with their gel form they can serve as the means to keep together the two separate parts of the whole assembly.

Li<sup>+</sup> doped V<sub>2</sub>O<sub>5</sub> thin films were incorporated in the constructed electrochromic devices serving as IS layers. Because of their layered structure, these films can serve as ion reservoir layer ameliorating the performance of the whole electrochromic device. The use of Li<sup>+</sup> doped V<sub>2</sub>O<sub>5</sub> layers instead of plain V<sub>2</sub>O<sub>5</sub> films was found to significantly improve the performance of the electrochromic device.

The optimised electrochromic devices exhibited excellent characteristics with fast response time ( $\approx 5$  sec for full coloration or bleaching), very low luminous transmittance ( $T_{lum}$ ) values in the coloured state (deep blue colour with  $T_{lum} \approx 13\%$ ) and long term stability

Although the TC is the least studied part of an electrochromic device, it has a dominant role in the effective performance of the whole assembly. We have fabricated electrochromic devices with optimised ZnS/Ag/ZnS films as TC in order to ameliorate their performance. The use of multilayer ZnS/Ag/ZnS films was found to improve the electrical characteristics and to lower the emittance of the TC layer [2].

## References

1. C.G. Granqvist, "Handbook of inorganic electrochromic materials", Elsevier, Amsterdam, (1995).
2. G. Leftheriotis, P. Yianoulis and D. Patrikios, Thin Solid Films 306, 92, (1997).
3. S. K. Deb and J. A. Chopoorian, Journal of Applied Physics 37, 4818, (1966).
4. S. K. Deb, Appl. Opt. Suppl. 3, 193, (1969).
5. J. Zhang et al., Journal of Electrochemical Society 141, 2795, (1994).
6. G. Frand, C. Rousselot and O. Bohnke, Proc of SPIE, 1728, 157, (1992).

# DIELECTRIC PROPERTIES OF CERIA AND YTTRIA STABILIZED ZIRCONIA THIN FILMS GROWN ON SILICON SUBSTRATES

M. Hartmanová and K. Gmucová

Institute of Physics, Slovak Academy of Sciences, 84228 Bratislava, Slovakia

In recent years there has been a growing interest in ceria and yttria stabilized zirconia (YSZ) as an interface material for silicon-on-insulator (SOI) structures, stable capacitors for ULSI (ultralargescale integration) and buffer layers of superconducting materials due to the fact that the mismatch factor for lattice parameters between YSZ and mainly  $\text{CeO}_2$  and silicon is negligible low. The capacitors must have appropriate dielectric properties while operating at low voltages to be useful for this application. Ceria is one of the most attractive insulating materials from this point of view.

This contribution represents a complement to our study of structural and electrical properties of  $\text{CeO}_2$  and YSZ thin films grown on silicon substrates by electron beam evaporation [1, 2].

YSZ and  $\text{CeO}_2$  thin films were deposited on n-doped Si(100) substrates by electron beam evaporation of  $(\text{YO}_{1.5})_{0.18}(\text{ZrO}_2)_{0.82}$  pellet (YSZ) and the fused cerium (IV) oxide pieces (3-6 mm, 99.9% Aldrich Chem.Co.) at 200°C [3, 4]. The thicknesses of oxide layers are estimated using Talystep equipment to be : YSZ - 60 nm,  $\text{CeO}_2$  - 125 nm.

In general, the value of bulk capacitance ( $C_p$ ) measured at room temperature and at 1 MHz is quite constant as a function of frequency and independent on the temperature at 500 mV. The relative dielectric constant  $\epsilon_r$  of YSZ and  $\text{CeO}_2$  can be obtained directly from this high frequency limiting capacitance  $C_p$ , consistent with the geometric factor  $K$  of the sample and with values found in the order of tens of pF.

$\epsilon_r$  values were calculated by using the usual formula  $\epsilon_r = C_p K / \epsilon_0$  where  $K$  is the cell constant (thickness of dielectric layer / area of the gate electrode) and  $\epsilon_0$  is the permittivity of the free space ( $8.845 \times 10^{-14} \text{ F.cm}^{-1}$ ) and at 1 MHz were determined to be :  $\epsilon_r$  (YSZ) = 16.8 and  $\epsilon_r$  ( $\text{CeO}_2$ ) = 2.8, respectively.

The MIS structure (Al / YSZ,  $\text{CeO}_2$  / Si / Au), based on n-type of semiconductor, can be swept from the depletion to the accumulation by applying negative to positive d.c. bias to the top Al electrode. The dielectric constants of YSZ and  $\text{CeO}_2$  can be therefore determined from the measured value of accumulation capacitance ( $C_{acc}$ ) using the relation  $C_{acc} = \epsilon_0 \epsilon_r K^{-1}$ .  $\epsilon_r$  values of both YSZ and  $\text{CeO}_2$  thin layers were estimated from the accumulation capacitances of the C-V curves (Fig. 1, YSZ; Fig. 2,  $\text{CeO}_2$ ) at 1 MHz to be :  $\epsilon_r$  (YSZ) = 18.3 and  $\epsilon_r$  ( $\text{CeO}_2$ ) = 3.4. The similar values of the dielectric constants have been published in [5, 6].

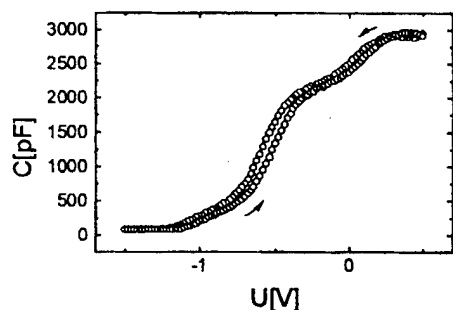


Fig. 1.

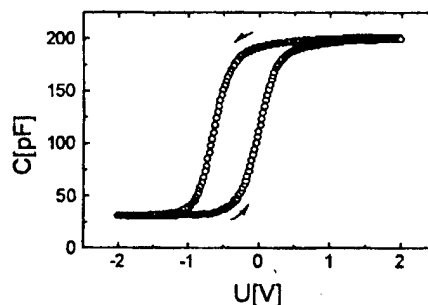


Fig. 2.

**Acknowledgements.** The work was partially supported by the research grants No.2 / 5081 / 98 and 2 / 5040 / 98 of the Slovak Grant Agency.

## References

- [1] M. Hartmanová, I. Thurzo, M. Jergel, J. Bartoš, F. Kadlec, V. Železný, D. Tunega, F. Kundracik, S. Chromik and M. Brunel, *J. Mater. Sci.* **33**, 969 (1998).
- [2] M. Hartmanová, K. Gmucová, M. Jergel, I. Thurzo, F. Kundracik and M. Brunel, *Thin Solid Films*, in print
- [3] S. Chromik, B. Wuyts, I. Vávra, A. Rosová, F. Hanic, S. Beňačka and Y. Bruynseraede, *Physica C* **226**, 153 (1994).
- [4] M. Španková, S. Gaži, S. Chromik, A. Rosová, I. Vávra and S. Beňačka, *J. Low Temp. Physics* **106**, 439 (1997).
- [5] W.-Ch. Tsai and T.-Y. Tseng, *J. Mater. Sci.: Mater. in Electr.* **8**, 313 (1997).
- [6] Y. Miyahara, *J. Appl. Phys.* **71**, 2309 (1992).

LOCAL DISTRIBUTION OF MOBILE SPECIES UPON  
VOLTAGE POLARIZATION ON SEMICONDUCTORS

M. Klingler, W.F. Chu, P. Press and W. Weppner

Chair for Sensors and Solid State Ionics  
Technical Faculty, Christian-Albrechts University zu Kiel  
Kaiserstr. 2, D-24143 Kiel, Germany

Transport properties of pure ionic conductors such as AgI and  $\text{Li}_{0.23}\text{La}_{0.69}\text{Fe}_{0.3}\text{Ti}_{0.7}\text{O}_3$  as well as predominantly electronically conducting semiconductors such as  $\text{LiNbO}_3$ ,  $\text{SrTiO}_3$ ,  $\alpha\text{-Ag}_2\text{S}$  and  $\text{Ag}_x\text{WO}_3$  were investigated by the application of voltages smaller than the decomposition limits between two ionically blocking electrodes or between one blocking and one reversible electrode in the case of  $\text{SrTiO}_3$ . This means that the mobile ionic as well as the mobile electronic species shift from one electrode side to the other within the sample. The change in the stoichiometric composition within the sample as a result of this transport process causes the formation of local inhomogeneities leading to the change of the electrical and optical properties.

The experimental results also showed that Nernst's law has the validity not only to ionic conductors, but to semiconductors as well if a steady state is reached for ionically blocking electrodes.

## Oxygen Cycle in Nickel Metal Hydride Batteries: Modeling and Experimental Validation

**Bor Yann Liaw and Russell Owens**

University of Hawaii

Hawaii Natural Energy Institute, School of Ocean & Earth Science & Technology

Honolulu, HI 96822, USA

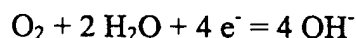
**Wen-Bin Gu and Chao-Yang Wang**

Pennsylvania State University

Department of Mechanical Engineering

University Park, PA 16802, USA

The presence of oxygen cycle in the nickel metal-hydride (Ni-MH) batteries affects battery performance and its cycle life greatly. The interaction of oxygen with the battery system is particularly important in the process of recharging such batteries. The oxygen cycle involves the following reaction:



in both electrodes. During discharging, the oxygen is generated at the negative (MH) electrode while recombined at the positive (Ni) electrode. It is vice versa in the charging process. At high rates, the oxygen side reactions could significantly change the hydroxide concentration in the cell and affect the equilibrium of the active species transport, thus result in significant changes in charge acceptance, efficiency, available capacity, cell pressure and cycle life. More importantly, the interplay of microstructure, surface morphology, active surface area, and porosity through the process of aging and deterioration and their effects on the exchange current density of the oxygen reaction could defy the predefined charging algorithm and cause unsafe operation of the battery. It is therefore critical to understand the oxygen cycle in the Ni-MH battery for better control of the battery performance and cycle life.

Although possible, to conduct quantitative analysis of the oxygen cycle is a challenge. To adequately assess both oxygen generation and recombination in the cycle, combined numerical modeling and experimental validation can provide insightful information about the process. More importantly, quantitative information regarding charge acceptance, charging efficiency, available capacity of the battery can be predicted from the model for charging and operation guidance. It is also possible to determine the maximum cell potential and pressure

change correlated to the exchange current density of the oxygen reaction, providing a precise control of the charging process to avoid overcharging and subsequent effects on the cell cycle life.

The understanding of the oxygen cycle will also help the development of rapid charging algorithm for the Ni-MH battery. The cell potential, pressure and temperature changes at different charging rates can be precisely predicted along with the charge input during the charging process and be validated through experiments. The results can be used in the development of an optimized algorithm that can work with the state of charge of the battery. The effect of the interfacial mass transfer coefficient can profoundly change the cell pressure with the charge input during the charging process. It would be possible to adequately determine the cell pressure to ensure a safe operation, directly assisting in the cell design of the battery. The understanding of the oxygen cycle can also help researcher to evaluate and reduce cell self discharge rate.

Additional thermal modeling capability in our approach can predict thermal behavior of the battery system. Coupled thermal generation from electrochemical process and heat transfer through the package can be simulated to provide temperature profiles during charging and discharging cycles, an very important aspect for the thermal management of the Ni-MH battery systems.

In conclusion, the coupled electrochemical behaviors and thermal processes in the Ni-MH system can be modeled and validated to provide a first-principle model to predict the battery system performance. This capability offers a tremendous advantage to assist understanding battery performance characteristics, including voltage, current, power, temperature and pressure excursions during dynamic charging and discharging cycles. The understanding provides a powerful tool in assisting the design, operation and management of the Ni-MH battery system.



NEW CO<sub>2</sub> SENSOR BASED ON A SOLID STATE OXYGEN CONCENTRATION CELL

H. Näfe

Max-Planck-Institut für Metallforschung, Pulvermetallurgisches Laboratorium  
Heisenbergstraße 5, D-70569 Stuttgart, Germany

Since, under certain circumstances, the employment of Na-beta-alumina as electrolyte of a potentiometric CO<sub>2</sub> sensor may cause problems due to the influence of electronic transference, a new type of such a sensor has been developed that is based on an oxygen ion conductor, e.g. yttria stabilized zirconia (YSZ), as solid electrolyte. Thus, any impact of the electronic conduction is overcome. The set-up of the sensor, the mechanism of operation, the measuring properties and possible pitfalls in using the sensor are discussed.

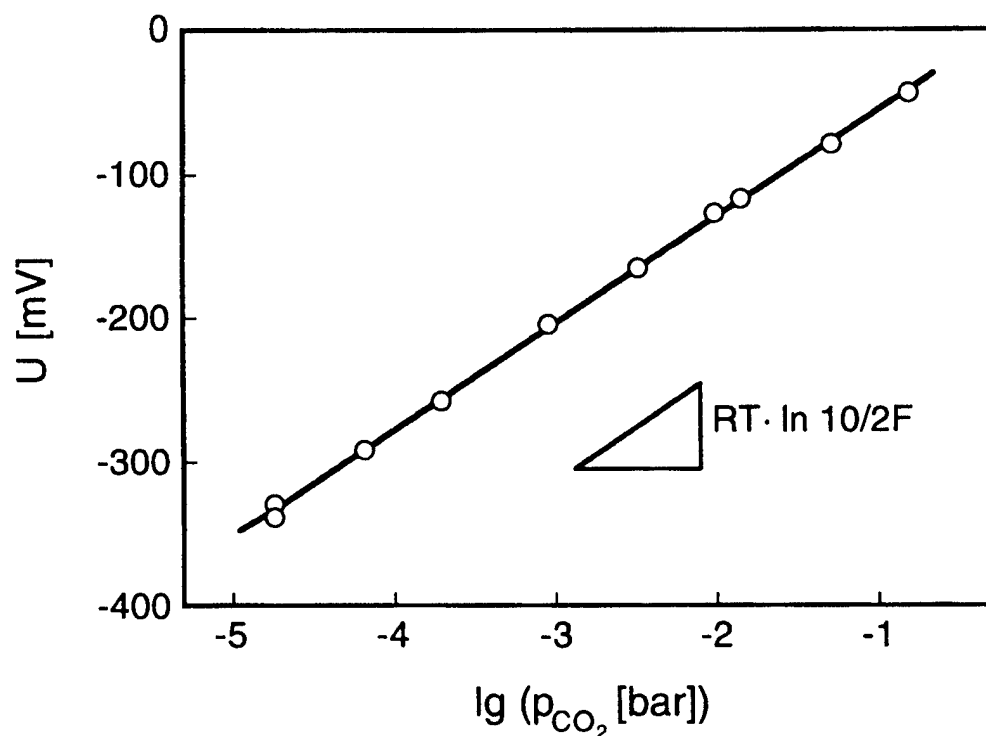


Figure 1:

Voltage response of the sensor to changes of the CO<sub>2</sub> partial pressure in the ambient CO<sub>2</sub>-O<sub>2</sub>-Ar gas atmosphere (T = 500 °C)

## SODIUM ION CONDUCTOR-BASED AMPEROMETRIC SENSOR FOR DETECTION OF TOTAL NO<sub>x</sub> IN ATMOSPHERIC ENVIRONMENTS

Masaki ONO, Kengo SHIMANOE, Norio MIURA, Noboru YAMAZOE

Department of Molecular and Material Sciences, Graduate School of Engineering Sciences, Kyushu University, Kasuga-shi, Fukuoka 816-8580, Japan

Nitrogen oxides of NO and NO<sub>2</sub> usually abbreviated NO<sub>x</sub> are known as typical air-pollutants which cause acid rain and photochemical smog. NO<sub>x</sub> is produced mainly from combustion furnaces and automobile engines. Most of NO<sub>x</sub> is first emitted as NO into environments, NO being gradually converted to NO<sub>2</sub>, a thermodynamically more stable form at room temperature under usual partial pressure of O<sub>2</sub>. However, the ratio of NO<sub>2</sub> to NO is variable, depending on the conditions of atmospheric environments. In fact, the ratio is usually larger than unity in the night time but less than unity in the daytime in urban area. Several solid electrolyte based-NO<sub>x</sub> sensors using metal salt auxiliary phases or metal oxide electrodes have been reported so far.[1,2] However, there had been no report on the sensors which can detect total NO<sub>x</sub> in sub-ppm level concentration. Until we reported the amperometric sensor based on NASICON (Na<sup>+</sup>-super-ionic-conductor) detect NO<sub>2</sub> in ppb range.[3,4] However, this device is unable to detect NO. Therefore, in this study, we attempted to make the device also sensitive to NO by attaching layers of NO oxidation catalysts. The resulting device turned out to work as an amperometric sensor to detect total NO<sub>x</sub>, as described below.

The sensor was fabricated by using a disc (9 mm<sup>φ</sup> × 0.7 mm<sup>t</sup>) of NASICON (Na<sub>3</sub>Zr<sub>2</sub>Si<sub>2</sub>PO<sub>12</sub>), as shown in Fig. 1. The NASICON was synthesized by calcining a powder mixture of ZrSiO<sub>4</sub> and Na<sub>3</sub>PO<sub>4</sub> at 1125°C for 11 h, followed by milling in a zirconia-ball-mill for 24 h, pressing into a disc at 200 MPa and sintering at 1220°C for 14 h in air. A commercial gold paste was applied on both sides of the disc, as a sensing-, counter- or reference-electrode, respectively, followed by annealing at 700°C for 30 min. Each Au electrode was confirmed to be porous. An aqueous paste of (NH<sub>4</sub>)<sub>10</sub>W<sub>12</sub>O<sub>41</sub>·5H<sub>2</sub>O was first applied on the Au sensing-electrode and heated at 600°C for 5 h to form a WO<sub>3</sub> layer. Then, a layer of 0.5 wt% Pt-loaded SiO<sub>2</sub> was stacked on the WO<sub>3</sub> layer. The thicknesses of the Au electrode, the WO<sub>3</sub> layer and the Pt-SiO<sub>2</sub> layer were ca. 10, ca. 50 and ca. 300 μm, respectively. In order to avoid the direct contact with the sample gas, the Au reference-electrode was coated with an inorganic adhesive. The Au counter-electrode was covered with a layer of NaNO<sub>2</sub> (ca. 200 μm thick).

NO<sub>x</sub> sensing experiments were carried out in a conventional gas flow apparatus equipped with a heating facility. Sample gases were allowed to flow over the sensor device at a rate of 100 cm<sup>3</sup>·min<sup>-1</sup>. The sensing electrode was polarized at -150 mV by means of a potentiostat (Hokuto Denko, HA-301), referring to the Au reference-electrode, and then the electric current flowing between the sensing and counter electrodes was measured as a sensing signal.

The polarization curves of the present device attached with the oxide layers were measured in air and in the sample gases containing various concentration of NO<sub>2</sub> (or NO) at 150°C. A clear limiting current involving the reduction of NO<sub>2</sub> was observed over a sensing-electrode potential range of 0 ~ -300 mV and the limiting current increased with increasing NO<sub>2</sub> concentration. Almost the same polarization curves were observed for NO. The current responses to NO<sub>2</sub> (or NO) were measured at a constant sensing-electrode potential of -

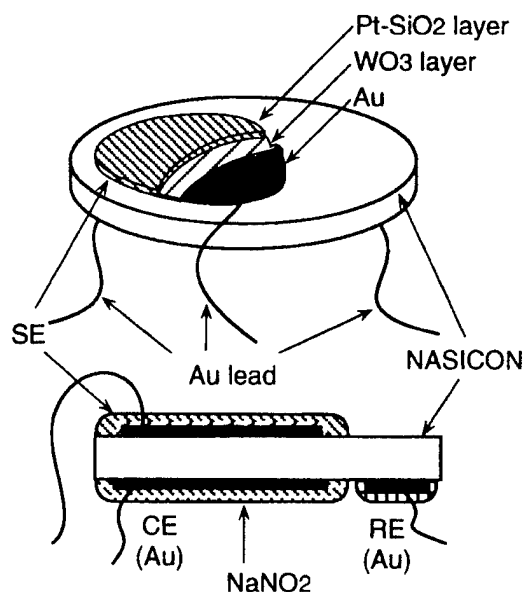


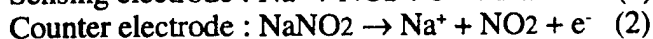
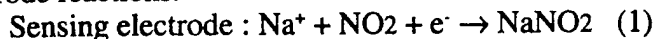
Fig. 1 Configuration of amperometric NO<sub>x</sub> sensor.

150 mV at 150°C were perfectly proportional to the concentration of NO<sub>2</sub> (or NO) up to 1 ppm, as shown in Fig. 2. In addition, the proportionality constants (sensitivity) were almost the same to both NO and NO<sub>2</sub>. This suggests that the double catalyst-layers of WO<sub>3</sub> and Pt-SiO<sub>2</sub> can function well as an NO oxidation catalyst. It is noted that a monolayer of catalyst (WO<sub>3</sub> or Pt-SiO<sub>2</sub>) gave insufficient results. That is, the NO sensitivity was lower than the NO<sub>2</sub> sensitivity when only the WO<sub>3</sub> layer was attached and the current responses to NO and NO<sub>2</sub> became too small when only the Pt-SiO<sub>2</sub> layer was used.

The sensing behavior of the device using the double catalyst layers to 0.5 ppm NO<sub>x</sub> at various NO<sub>2</sub>/NO ratios was tested. Indifferent of the NO<sub>2</sub>/NO ratios, the response current to 0.5 ppm NO<sub>x</sub> was kept almost constant, as shown in Fig. 3. This indicates that the present device can be applied for monitoring of total-NO<sub>x</sub> in air.

It was confirmed that the cross-sensitivities to 100 ppm CO, 1000 ppm CO<sub>2</sub> and 2.50 vol.% H<sub>2</sub>O were much lower than that to 1 ppm NO<sub>2</sub> (or NO). The current response to 0.5 ppm NO<sub>2</sub> (or NO) was hardly affected by changes in the concentration of CO<sub>2</sub> or H<sub>2</sub>O coexistent. With such sensing characteristics, the present device appears to be promising as a total-NO<sub>x</sub> sensor for environmental applications.

As for the sensing mechanism, the present device is considered to involve the following electrode reactions.



At the sensing electrode polarized at -150 mV, an electrochemical reaction (1) is assumed to take place in the NO<sub>2</sub> gas flow. In the case of NO, NO is oxidized to NO<sub>2</sub> by the catalyst layers for being subjected to the same cathodic process. A reverse reaction (2) takes place at the counter electrode. The sodium ions, consumed and produced at the respective electrode, migrate through the NASICON disc from the counter electrode side to the sensing electrode one. This is accompanied by an electric current flow in an external electric circuit as a sensing signal. The porous multi layers of catalysts and electrode may also act as a gas diffusion barrier to provide the current response linear to NO<sub>x</sub> concentration.

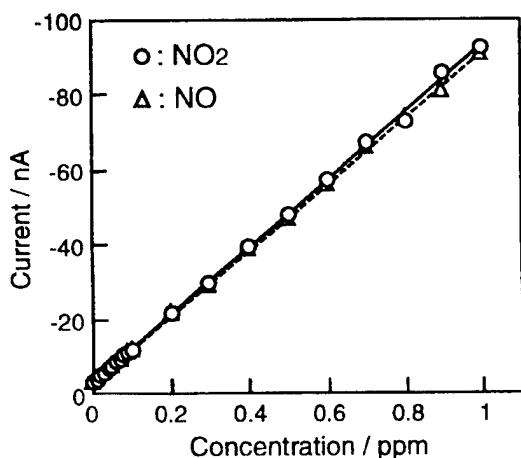


Fig. 2 Dependence of response current on the concentration of NO<sub>2</sub> or NO.  
(SE potential : -150 mV vs. RE, 150°C)

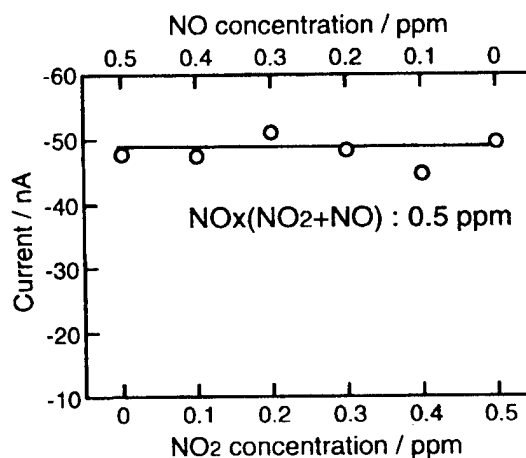


Fig. 3 Response current to 0.5 ppm NO<sub>x</sub> of various NO<sub>2</sub>/NO ratios.  
(SE potential : -150 mV vs. RE, 150°C)

## References

- [1] N. Miura, S. Yao, Y. Shimizu, N. Yamazoe, *Solid State Ionics*, **70/71** (1994) 572-577.
- [2] Y. Shimizu, K. Maeda, *Chem. Lett.*, **1996**, 117-118.
- [3] N. Miura, M. Ono, K. Shimanoe, N. Yamazoe, *Digest of Tech. Papers, Transducers '97, Chicago*, p.951 (1997)
- [4] N. Miura, M. Ono, K. Shimanoe, N. Yamazoe, *Sensors and Actuators B*, **49** (1998) 101-109.

## A NEW APPLICATION OF ZrO<sub>2</sub> SOLID ELECTROLYTE

Xiaojun Hu, Li Xiao, Fushen Li, Xionggang Lu, Lifan Li and K-C. Chou  
 Laboratory on Solid Electrolytes and Metallurgical Testing Techniques  
 Department of physical chemistry, University of Science and Technology Beijing  
 Beijing, 100083 People's Republic of China

Utilizing solid electrolyte cell oxygen can be pumped out from the melt[1-3]. U. B. Pal and K-C. Chou et al.[4-6] have conducted successful deoxidation experiment using a short-circuited solid oxide electrochemical cell. In this work, solid electrolyte, short-circuited materials and aluminium as deoxidizer are integrated to form a deoxidation unit. This unit is directly immersed in melt for deoxidizing. The deoxidation product is removed with the unit, so that this way does not pollute the melt and is simple.

### Principle

If there exists different oxygen potential on both sides of solid electrolyte, because of the electrode reaction, an electric field stopping the diffusion of oxygen ions is formed. When both sides were short-circuited with electronic conductor, the charges accumulated will transfer through conductor and neutralize. The electric field is destroyed and oxygen ions will continuously diffuse until the thermodynamic equilibrium.

### Experimental

The structure of deoxidation unit is shown in Fig.1. The shell of unit is a magnesia-stabilized zirconia (MSZ) tube. Aluminium as deoxidizer is placed inside the MSZ tube and sealed with conductible cermet.

The units are immersed in copper melt contained in an alumina crucible at 1453K, and oxygen concentrations in melt are measured by the oxygen sensor.

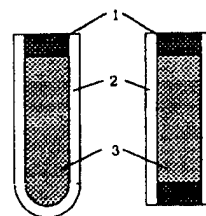


Fig.1 Schematic diagram of deoxidation unit  
 1 Electronic conductor, 2 Solid electrolyte  
 3 Deoxidizer

### Results and Discussion

The experimental results are shown in Fig.2. Within twenty to thirty minutes, the oxygen concentration in melt decreases to 20 ppm, so far as to less than 10 ppm.

According to theory [4-6] of the short-circuited deoxidation,

$$\frac{dI_{ion}}{dt} = \frac{-\frac{I_{ion}M_O \cdot 10^6}{2FM_{melt}}}{\frac{2C_rFR_{total}}{RT} \exp\left(\frac{2FI_{ion}R_{total}}{RT}\right) + \frac{M_O \cdot 10^6}{2\alpha AF\rho_{melt}} + \frac{dC_r}{dI_{ion}} \exp\left(\frac{2FI_{ion}R_{total}}{RT}\right)} \quad (1)$$

Due to the strong deoxidation ability of aluminium,  $C_r=0$  and  $dC_r=0$ , Eq.1 can be simplified.

$$\frac{dI_{ion}}{dt} = -\alpha A \frac{\rho_{melt}}{M_{melt}} \cdot I_{ion} \quad (2)$$

Integrating Eq.2 and substituting to the mass balance equation.

$$\frac{dC_b}{dt} = \frac{-I_{ion}M_O \cdot 10^6}{2FM_{melt}} \quad (3)$$

Eventually, the following equation can be obtained

$$C_b = (C_b^0 - C_r) \cdot \exp\left(-\alpha A \frac{\rho_{melt}}{M_{melt}} \cdot t\right) + C_r \quad (4)$$

Where  $C_b$  is oxygen concentration in the bulk melt,  $C_b^0$  is the initial oxygen concentration in melt,  $C_r$  is the equilibrium concentration,  $\alpha$  is oxygen mass-transfer coefficient in melt,  $A$  is the deoxidation unit/melt interfacial area,  $\rho_{melt}$  is density of the melt,  $M_{melt}$  is mass of the melt,  $t$  is time,  $I_{ion}$  is the oxygen ionic current through solid electrolyte,  $M_o$  is atomic mass of oxygen,  $F$  is the Faraday constant,  $R_{total}$  is the total system resistance,  $T$  is absolute temperature.

Eq.4 shows that the oxygen mass-transfer in copper melt is a rate controlling on the process.

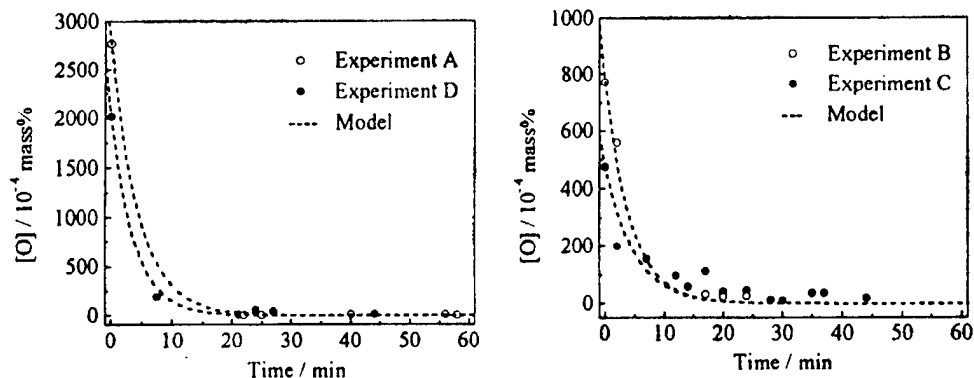


Fig.2 The relationship between oxygen concentration and time

The selection of the parameters in Eq.4 is shown in Table 1. The calculations of each experiment are also shown in Fig.2. Compared the calculation and experimental values, both are identifiable, as also proves the model is correct.

### Summary

This deoxidation way is totally new. Compared with using deoxidizer directly and the previous short-circuited deoxidation method, its advantages are as follows: no pollution, higher efficiency, simple operation, and so on.

Table 1 Selection of the model parameters

xp.	Weight of Cu melt $M_{melt}$ (kg)	Electrolyte/Cu melt interfacial area $A$ ( $\times 10^{-4} \text{m}^2$ )	$k = \alpha A \frac{\rho_{melt}}{M_{melt}}$ (1/s)
A	0.20	$3.7 \times 3 = 11.1$	0.22
B	0.20	$3.8 \times 3 = 11.4$	0.23
C	0.20	$3.3 \times 3 = 9.9$	0.20
D	0.18	$3.9 \times 3 = 11.7$	0.26

$$\rho_{melt} = 7.98 \times 10^3 \text{ kg/m}^3, D = 10 \times 10^{-9} \text{ m}^2/\text{s},$$

$$\delta = 2 \times 10^{-6} \text{ m}, \alpha = \frac{D}{\delta} = 5 \times 10^{-3} \text{ m/s}$$

### References

- [1] W. A. Fischer and D. Janke, *Scr. Metall.* **6**, 923 (1972).
- [2] K. E. Oberg, L. M. Friedman, W. M. Boorstein and R. A. Rapp, *Metall. Trans.* **4B**, 75 (1973).
- [3] M. Iwase, M. Tanida, A. Mclean and T. Mori, *Metall. Trans.* **12B**, 517 (1981).
- [4] Shi Yuan, U. B. Pal and K-C. Chou, *J. Electrochem. Soc.* **141**(2), 467 (1994).
- [5] Zain Hasham, U. B. Pal, K-C. Chou and W. L. Worrell, *J. Electrochem. Soc.* **141**(2), 469 (1995).
- [6] Shi Yuan, U. B. Pal and K-C. Chou, *J. Am. Ceram. Soc.* **79**(3), 641 (1996).

# A FUNDAMENTAL STUDY OF A NOVEL DYNAMIC ELECTROCHEMICAL TECHNIQUE FOR THE MEASUREMENT OF TRACE AMOUNTS OF ARSENIC AND ANTIMONY IN MOLTEN ZINC

T.E. Warner and D.J. Fray

Department of Materials Science and Metallurgy, University of Cambridge, Cambridge CB2 3QZ

The vast majority of electrochemical sensors based upon solid electrolytes are of the potentiometric type. The technique involves the measurement of the open-circuit potential which enables the concentration of the electroactive species to be determined through the use of the Nernst equation. Unfortunately, when used in molten metals for the detection of a minor impurity, the response time can be several minutes. An alternative dynamic approach has been recently described by Liu and Weppner [1] where a symmetrical cell is constructed comprising sodium  $\beta''$ -alumina electrolyte with two identical electrode coatings of sodium carbonate and platinum. a sinusoidal potential was applied across this cell in a controlled gas environment, containing carbon dioxide, whilst the resulting current was recorded. From this current-potential profile a relationship was observed between the current peak and the concentration of carbon dioxide in the gas. This dynamic/symmetric cell technique had the major advantage over conventional potentiometric sensors in that a separately sealed reference electrode was not required thus, enormously simplifying the construction of the device.

In the present work this dynamic electrochemical approach was used for the measurement of trace elements in molten metal. The sodium-arsenic-antimony-zinc intermetallic system was selected for study since sodium ion solid electrolytes are readily available, zinc has a modest melting point of 693 K and, because sodium should react with the dissolved elements in molten zinc to form binary compounds.

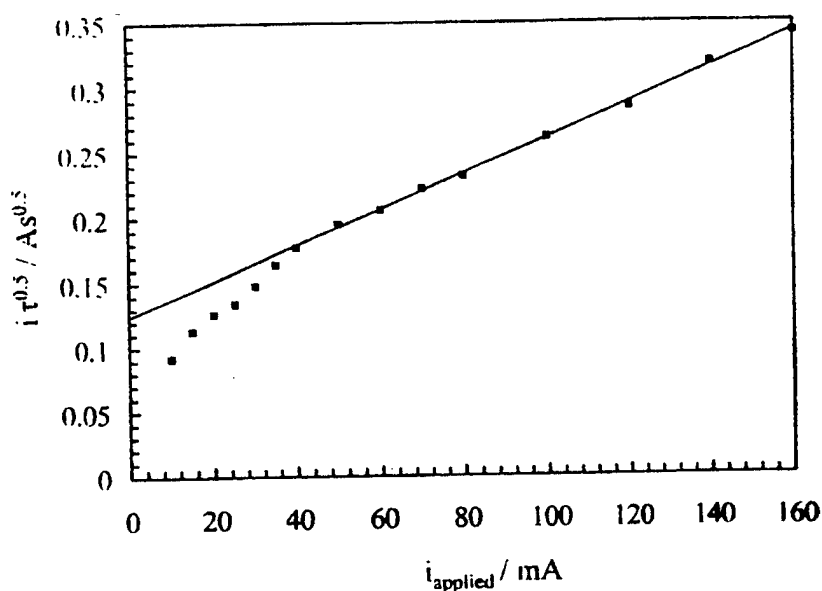


Figure 1. A plot of a test for Sand equation various currents were driven through the cell such that the polarity of the zinc electrode was made cathodic. From the chronopotentiometric waves, the transition times were used to plot a diagnostic test for the Sand equation. From this graph (Figure 1), it can be seen that the product,  $i\tau^{1/2}$ , is current dependent and therefore the reaction is not purely diffusion controlled. However, the linearity of this function at higher applied currents suggests that a diffusion process coupled with a chemical reaction is the rate determining mechanism when the cell reaction is driven at high rates of reaction. Intermittent galvanostatic polarisation was used to elucidate the reaction mechanism. The transient potential was independent of the arsenic content and from the potential it was concluded that the phase that formed was  $\text{NaZn}_{13}$ .

One fundamental difference between this work and that of Liu and Weppner [1], is that molten metals are electronic conductors and, therefore, the cell design was changed. In one cell, a sodium  $\beta''$ -alumina tube was coated with  $\text{Na}_{0.67}\text{CoO}_2$  on the inside, which acted as a reversible sodium electrode as well the counter electrode [2]. This tube was then introduced into a reservoir of zinc. In the second cell, the sodium  $\beta''$ -alumina tube was filled with zinc and immersed in molten zinc, with both compartments being at the same level and from an identical source, thus creating as near as possible a symmetrical cell. With the first design of cell,

With the symmetric cell, linear sweep voltammetry showed a qualitative response to arsenic concentration (Figure 2). This symmetric cell approach was also used to investigate the response upon adding antimony to one of the zinc electrodes whilst maintaining pure high grade zinc at the other electrode. A progressive increase in the current are clearly observed upon antimony additions (Figure 3).

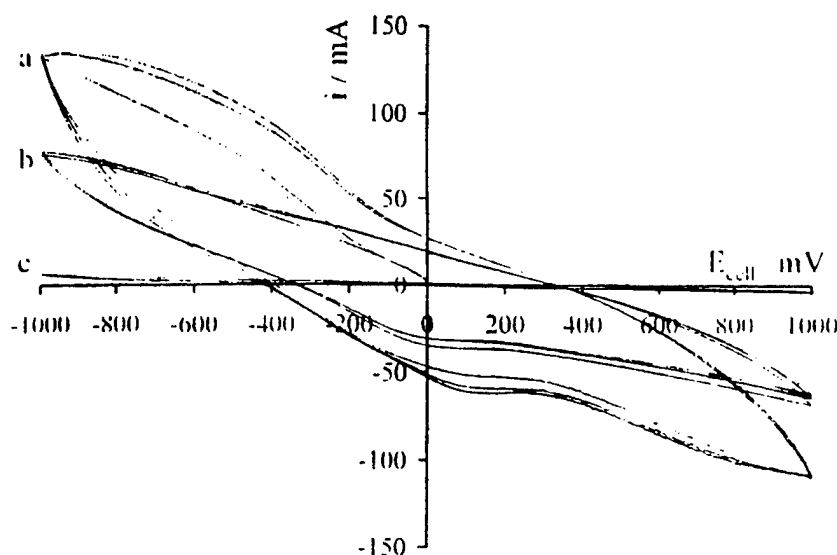


Figure 2. Cyclic voltammograms for the symmetric cell: was As(Zn)|Naβ''alumina|As(Zn). Arsenic concentrations (a) 400 ppm (b) 151 ppm (c) <1ppm

exists between the current generated during cyclic voltammetry and the arsenic and antimony concentrations in the molten zinc. However, the peak potentials could not be resolved to allow distinction between arsenic and antimony. By this method very fast response time to arsenic and antimony is possible. In principle at the scan rate of 500 mVs<sup>-1</sup> this would be less than 2 seconds which can be compared to minutes in the case of potentiometric determinations.

The collective results from a variety of electrochemical experiments performed in this work has shown that there are two "potential-windows" of interest accompanying the electrochemical introduction of atomic sodium into molten zinc, namely, the potential regions above and below approximately -1 V vs. Na<sub>0.67</sub>CoO<sub>2</sub>. Under the more severe polarisation conditions it was shown that atomic sodium generated at the zinc electrode reacts with zinc to form a sodium-zinc intermetallic compound in the vicinity of the electrode which is assumed to be NaZn<sub>13</sub>.

Under less severe polarisation it found by employing a symmetric cell a qualitative relationship

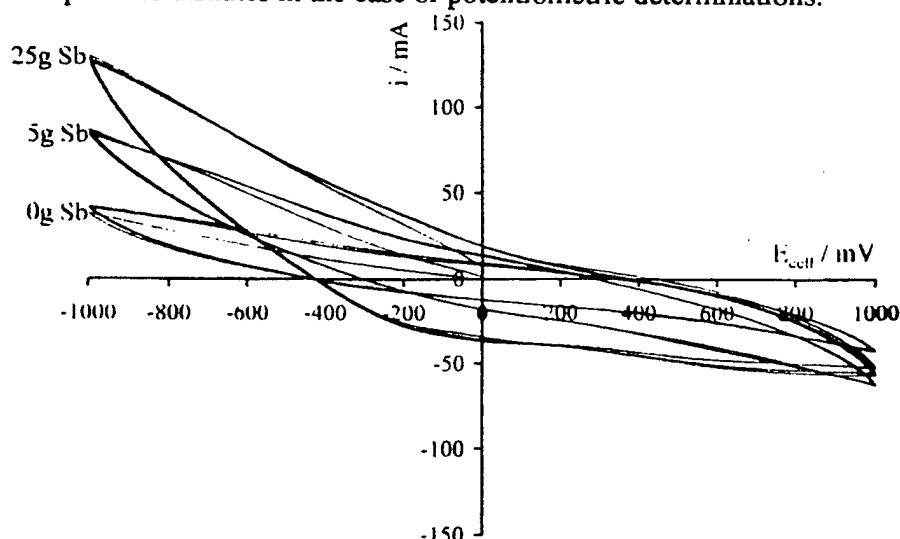


Figure 3. Cyclic voltammogram for the asymmetric cell: Sb(Zn)|Naβ''alumina|Sb(Zn) Initially high grade zinc at both electrodes with subsequent antimony additions to left hand electrode containing 200g zinc.

#### References

1. L.Liu and W. Weppner, Applied Physics, A55, 250 (1992)
2. P.C. Yao and D.J. Fray, J. App. Electrochem., 15, 379 (1985)

## SPUTTERED THIN FILMS OF CuBr AS ELECTRO-CHEMICAL MICROSENSORS FOR NH<sub>3</sub> GAS : STRUCTURE, SENSITIVITY, SELECTIVITY AND AGEING EFFECTS.

P. Lauque\*, M. Bendahan\*, J.-L. Seguin\*, M. Pasquinelli\*\*, P. Knauth\*\*\*

\*Laboratoire Electronique et Physicochimie des Couches Minces, Service 152,

\*\*Laboratoire Défauts dans les Semiconducteurs et leurs Oxydes, Service 231,

\*\*\*Laboratoire EDIFIS (UMR 6518 CNRS), Service 511,

Faculté des Sciences de Marseille-St Jérôme, 13397 Marseille Cedex 20.

The development of chemical microsensors is an important challenge, because « intelligent systems », combining microsensors, microelectronic data processing and microactuators, will be essential in many domains. Ionic and mixed conductors are capable of transforming a change of chemical potential into an easily measurable and processable electrical signal.

Copper halides are model mixed conductors with an important contribution of Cu<sup>+</sup> ion conduction at reduced temperature. By analogy with aqueous solution chemistry, we expect a particular high sensitivity to molecules known to form strong complexes with copper ions in solution : ammonia NH<sub>3</sub> is such a molecule. One can then assume the formation of an interfacial layer in contact between the gas phase and the copper halide ; copper ions are fixed by interaction with the gas molecules. A space charge layer enriched in copper vacancies with enhanced ionic conductivity at reduced temperature may result. In a thin film with small mean grain size and high porosity, a measurable electrical signal should result. However, interfacial effect may also be important at intergranular boundaries and the overall electrical response of the films after a change of gas atmosphere is difficult to predict.

Starting from these theoretical expectations, we prepared porous CuBr thin-films by RF sputtering [1] and studied the sensor characteristics for NH<sub>3</sub> gas [2,3]. The response time is very short, of the order of seconds, which makes the CuBr films a very attractive candidate for sensor applications. The relation between film resistance and NH<sub>3</sub> partial pressure is reported. We have also studied the selectivity using different other gases, O<sub>2</sub>, N<sub>2</sub>, H<sub>2</sub>O, H<sub>2</sub>S etc. and the ageing and hysteresis effects after heat and high vacuum treatments and after application of different partial pressures of ammonia.

[1] J.-L. Seguin, M. Bendahan, G. Lollmun, M. Pasquinelli, P. Knauth, *Thin Solid Films*, 323, 31-36 (1998).

[2] J.-L. Seguin, M. Bendahan, P. Lauque, C. Jacolin, M. Pasquinelli, P. Knauth, *Sensors and Actuators A*, (1998), sous presse.

[3] P. Lauque, M. Bendahan, J.-L. Seguin, M. Pasquinelli, P. Knauth, *J. Europ. Ceram. Soc.*, (1999), sous presse.



## OPTICAL HUMIDITY SENSING USING TRANSITION METAL OXIDE FILMS

Yoshiyuki Sato, Masanori Ando and Tetsuhiko Kobayashi

Osaka National Research Institute, AIST, Midorigaoka 1, Ikeda, Osaka 563-8577, Japan

Thin films of transition-metal oxides, such as iron oxide ( $\text{Fe}_2\text{O}_3$ ), cobalt oxide ( $\text{Co}_3\text{O}_4$ ), nickel oxide ( $\text{NiO}$ ) and iridium oxide ( $\text{IrO}_x$ ) show electrochromism (EC) [1]. Recently, we have reported the humidity-sensitive absorbance change of  $\text{Co}_3\text{O}_4$  [2],  $\text{CuFe}_2\text{O}_4$  [3],  $\text{NiO}$  [4] and  $\text{IrO}_x$  [5], which might be based on a mechanism different from EC. Thus, those oxide films can be used for optical humidity sensors, which give optical transmittance/reflectance changes as a function of humidity in the air. We have prepared those oxide films either by spin-coating of organic solutions of metal salts, followed by pyrolysis in the air [2, 3] or by the oxidation of carbon and metal films (OCAM) process [4, 5]. The  $\text{Co}_3\text{O}_4$  films showed a drawback that the optical humidity sensitivity was small; an absorbance change ( $\Delta\text{Abs}$ ) of  $\sim 0.006$  was observed for the humidity change between 10% and 90% RH in air at RT, which corresponds to a transmittance change of  $\sim 1\%$  [2]. On the other hand, the  $\text{NiO}$  and  $\text{IrO}_x$  films prepared by the OCAM process exhibited higher optical humidity sensitivity compared with  $\text{Co}_3\text{O}_4$ ; a  $\Delta\text{Abs}$  of  $\sim 0.016$ , which was  $\sim 3$  times larger than that of  $\text{Co}_3\text{O}_4$ , for the humidity change between 0% and 90% RH in air at RT [4, 5].

So far, we explained a possible mechanism of the humidity-sensitive absorbance changes of those films qualitatively: increases in the absorbance of the films with increasing the values of RH might be due to the adsorption and capillary condensation of water in the small pores in the films, which results in an increase in the refractive index of the films, as water has a large refractive index compared with air.

In the present paper, we have measured the optical constants of the films and discussed the relation between the microstructure of the films and their optical properties in order to obtain a guiding principle in choosing materials and in tuning their thicknesses.

$\text{NiO}$  and  $\text{IrO}_x$  films were prepared by the OCAM process [4-7]. Glass (Corning 7059), fused silica (2 mm thick) and soda-lime glass (18 mm x 18 mm x 0.1 mm) were used as substrates. The Ni-C films were converted to the  $\text{NiO}$  films either by the plasma oxidation [4] or by heating them at  $400^\circ\text{C}$  for 20 min in the air [6]. The Ir-C films were converted to the  $\text{IrO}_x$  films by heating them at  $250^\circ\text{C}$  or  $350^\circ\text{C}$  for 10 min in the air [5, 7]. The thicknesses and structures of the films were also measured in a similar manner described elsewhere [4-7]. *In-situ* optical transmittance measurements were performed in a quartz cell (200 ml) at  $25^\circ\text{C}$  with a spectrometer (Shimadzu UV-3100PC) equipped with optical fibers. Air of controlled RH ranging from 0% RH to 90% RH was supplied with a humidity generator (SRH-1MS-SP1, Shinyei Co., Ltd.), and passed through the quartz cell at a constant flow rate of 100 ml/min [2]. *Ex-situ* optical measurements were carried out with a spectrometer (Shimadzu UV-2100) and with an ellipsometer (Mizojiri DVA-36L) with an incident angle and wavelength of  $70^\circ$  and 633 nm, respectively.

Figure 1 depicts typical time-response curves of the absorbance of an  $\text{IrO}_x$  and  $\text{NiO}$  film in air with periodically changing humidity between 0% RH and 30% RH, between 0% and 60% RH, and between 0% RH and 90% RH, respectively, at a wavelength of 550 nm. From the XRD measurements the structures of the  $\text{IrO}_x$  and  $\text{NiO}$  film were amorphous and poly-crystalline, respectively. The thermally-oxidized  $\text{NiO}$  film shows smaller value of  $\Delta\text{Abs}$  compared with the plasma-oxidized  $\text{NiO}$  film [4] and the  $\text{IrO}_x$  film.

Figure 2 shows the ellipsometric results for a 70 nm-thick  $\text{IrO}_x$  film on the fused silica substrate. In order to discuss the relation between the microstructure of the oxide films and their optical properties, we assumed the film to be a composite of film and surrounding medium (air or water). The general expression for the dielectric function of the two-composite is given by the following equation [9]

$$f \frac{\epsilon_f - \epsilon}{\epsilon_f + 2\epsilon} + (1-f) \frac{\epsilon_0 - \epsilon}{\epsilon_0 + 2\epsilon} = 0 \quad (1)$$

where  $f$  is the volume fraction of the film, and  $\epsilon$ ,  $\epsilon_f$  and  $\epsilon_0$  being the composite, film and

surrounding medium dielectric constants, respectively.

The density of the  $\text{IrO}_x$  film ranged from 4.7 to 5.4  $\text{g/cm}^3$ , which was about 40% of the bulk  $\text{IrO}_2$  (11.68  $\text{g/cm}^3$ ). We assumed the index of the  $\text{IrO}_x$  film,  $1.79+0.35i$  to be that for the film-air system and calculated  $\epsilon$  in film-water system by putting  $\epsilon_0 = 1.33$ . Table 1 compares the values of transmittance  $T$  for film-air system and for film-water system. We also calculated the values of  $\epsilon$  and  $T$  for various materials with  $f = 0.4$ . As shown in Table 1, the larger the real part of dielectric constant, the larger the transmittance change ( $T$  (film-air) -  $T$  (film-water)) is. We will report the optical properties of other transition metal oxide films and discuss the effect of the thickness and microstructure of the films on their optical humidity sensitivity.

Table 1. Comparison of dielectric constant  $\epsilon$  and transmittance  $T$  in film-air system and in film-water system for various materials. Volume fraction of the film  $f$  and thickness are assumed to be 0.4 and 70 nm, respectively.

	$f$	$\epsilon_f$	$\epsilon$ in film-air system	$T$ (film-air)	$\epsilon$ in film-water system	$T$ (film-water)
$\text{IrO}_x$ film	0.4		$(1.79+0.35i)^2$	0.51	$(1.90+0.40i)^2$	0.45
$\text{SiO}_2$ film	0.4	$1.46^2$	1.38	0.99	1.91	0.98
$\text{Al}_2\text{O}_3$ film	0.4	$1.63^2$	1.53	0.99	2.09	0.97
$\text{ZrO}_2$ film	0.4	$2.0^2$	1.87	0.98	2.51	0.93

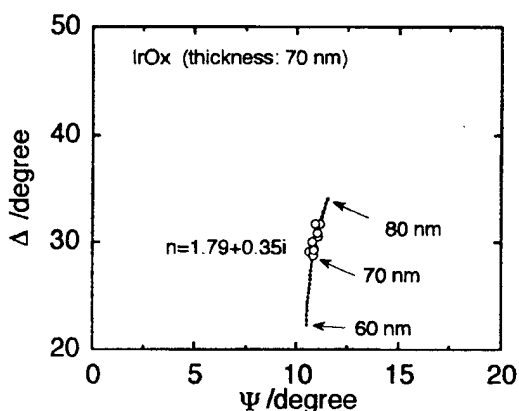
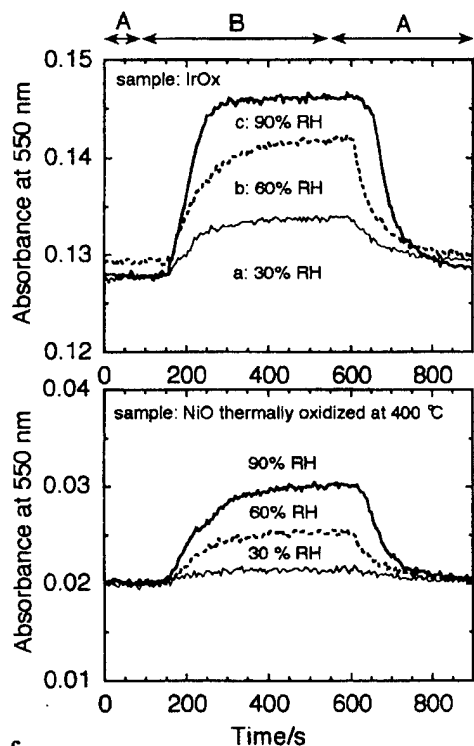


Fig. 1. (left) Time-response of the absorbance of  $\text{IrO}_x$  and  $\text{NiO}$  film with atmosphere periodically changing from (A) dry air (0% RH) to (B) humidified air ((a) 30% RH; (b) 60% RH; (c) 90% RH).  $\lambda=550$  nm.  $T=25^\circ\text{C}$ .

Fig. 2. (right) Ellipsometry results for a 70-nm-thick  $\text{IrO}_x$  film

#### References

- [1] C.G. Granqvist, Handbook of Inorganic Electrochromic Materials, Elsevier Science, Amsterdam, Netherlands, 1995. [2] M. Ando, T. Kobayashi and M. Haruta, Sens. Actuators B **32**, 157 (1996). [3] M. Ando, S. Tsujioka, T. Iwasaki and T. Kobayashi, Extended Abstr. 192nd Meet. Electrochem. Soc. Paris, France, Aug. 31- Sept. 5, 1997. p. 927. [4] M. Ando, Y. Sato, S. Tamura and T. Kobayashi, SSI-11, Honolulu, HI, Nov. 16-21, 1997. [5] Y. Sato, M. Ando and T. Kobayashi, Technical Digest of 7th International Meeting on Chemical Sensors, Beijing, China, 1998, p. 456. [6] Y. Sato, S. Tamura and K. Murai, Jpn. J. Appl. Phys. **35**, 6275 (1996) [7] Y. Sato, K. Ono, T. Kobayashi, H. Wakabayashi and H. Yamanaka, J. Electrochem. Soc. **134**, 570 (1987) [8] D.E. Aspnes, Thin Solid Films **89**, 249 (1982).

## IONIC SENSORS BY LASER ABLATION

M. Morcrette<sup>1,2</sup>, P. Barboux<sup>1</sup>, J. Perrière<sup>2</sup>, A. Laurent<sup>2</sup>, J. P. Boilot<sup>1</sup>

<sup>1</sup> Physique de la Matière Condensée, Ecole Polytechnique, 91128 Palaiseau, France;

<sup>2</sup> Groupe de Physique des Solides, Université Pierre et Marie Curie, 4 Place Jussieu, 75252 Paris, France

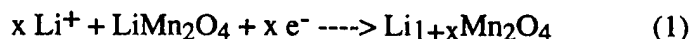
Thin films of  $\text{LiMn}_2\text{O}_4$  and  $\text{LiCoO}_2$  have been deposited in order to study their applications in the domain of electrochemical ionic sensors. Laser ablation was performed with a pulsed Nd:YAG laser (2J with a pulse duration of 7 ns and a repetition rate of 5Hz) quadrupled at 266 nm. The operating oxygen pressure was from  $10^{-6}$  to 1 millibar. Films were deposited onto Si (001), MgO (001) and polycrystalline Pt heated in the temperature range  $500^\circ\text{C}$ - $750^\circ\text{C}$ . The average thickness of the films is of the order of hundred nanometers.

Compositional analysis were obtained from Rutherford Backscattering spectrometry (RBS). The lithium and oxygen content were obtained by Nuclear Reaction Analysis (NRA) using the  $^7\text{Li}(p,\alpha)^4\text{He}$  reaction at energy of 1.5 MeV for lithium and the  $^{16}\text{O}(d,p)^{17}\text{O}$  at 850 keV for oxygen.

For a substrate temperature of  $500^\circ\text{C}$  stoichiometric films of  $\text{LiCoO}_2$  and  $\text{LiMn}_2\text{O}_4$  have been obtained at oxygen pressures above 0.1 mbar from a stoichiometric target. The films are polycrystalline when deposited onto Si or Si/Pt substrates whereas an epitaxial growth is obtained onto MgO. Moreover, MgO induces the successive epitaxial growth of multilayers, Platinum electrode/  $\text{LiMn}_2\text{O}_4$  or  $\text{LiCoO}_2$ . This is confirmed by rocking curves and Phi-Scans.

### $\text{LiMn}_2\text{O}_4$ films:

The potential of  $\text{LiMn}_2\text{O}_4/\text{Pt}/\text{MgO}$  multilayers (referenced to a SCE electrode) has been measured as a function of the lithium concentration in the solution (Fig.1). A Nernst-like behaviour is observed for concentrations above  $5 \cdot 10^{-4} \text{ mol.l}^{-1}$  in good agreement with the half cell reaction:



If we assume that the change of Li (x) is too small to affect the activity of the solid phase, the EMF only depends on the Li concentration with the following relation:

$$E = E_0 + \frac{RT}{F} \log(\text{Li}^+) \quad E_0 = 685 \text{ mV vs calomel electrode}$$

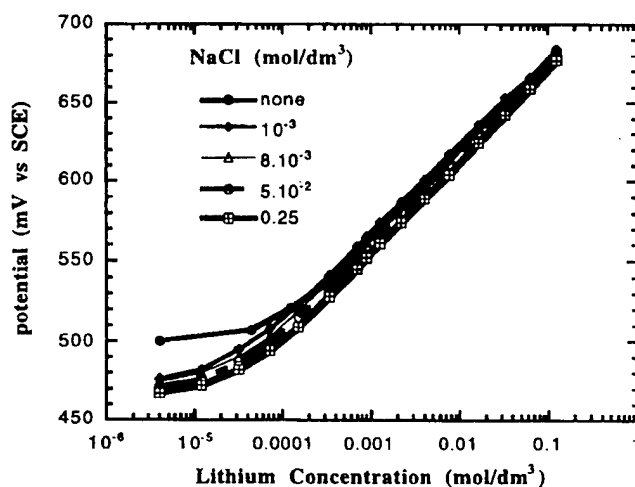


Fig1. Potential of a  $\text{LiMn}_2\text{O}_4$  electrode versus a calomel electrode (SCE) at  $25^\circ\text{C}$  as a function of Li concentration for different NaCl concentrations.

There is no effect of sodium on the potential and this is related to the selective insertion of lithium by the  $\text{LiMn}_2\text{O}_4$  spinel structure [1]. Such sensors show a very rapid response ( $<2\text{s}$ ) but they require to be covered by a solid state electrolyte in order to operate in a larger pH range. Therefore we have deposited the ionic conductor  $\text{Li}_2\text{NiGe}_3\text{O}_8$  recently reported by H. Kawai et

al.[2]. The spinel structure of this ionic conductor fits the  $\text{LiMn}_2\text{O}_4$  structure and allows the epitaxial growth of the complete multilayer  $\text{MgO/Pt/LiMn}_2\text{O}_4/\text{Li}_2\text{NiGe}_3\text{O}_8$  along the [111] direction. Films have been electrochemically cycled in water (Fig. 2 a). X ray diffraction (Fig. 2 b) cannot distinguish in the discharged state between the two layers because of the close lattice parameters ( $8.17\text{\AA}$  for  $\text{Li}_2\text{NiGe}_3\text{O}_8$  and  $8.22\text{\AA}$  for  $\text{LiMn}_2\text{O}_4$ ) whereas two diffraction peaks appear in the charged state ( $8.02\text{\AA}$  for  $\lambda\text{MnO}_2$ ). The selectivity and the potential versus Li of such sensors are not affected by the protective layer although the response time increases ( $\approx 20\text{s.}$ ) due to the low ionic conductivity of  $\text{Li}_2\text{NiGe}_3\text{O}_8$  at room temperature.

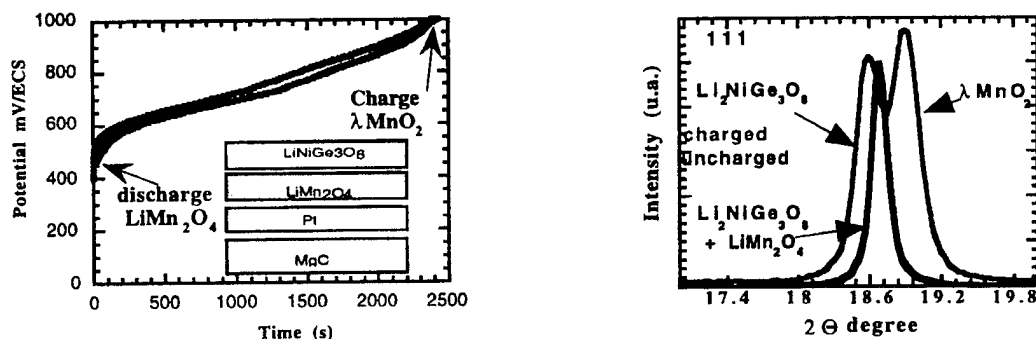
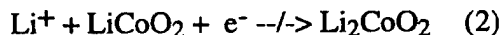


Fig. 2a: Galvanostatic charge and discharge of the multilayered structure

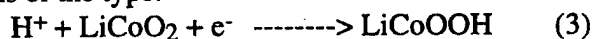
Fig.2 b: X-ray diffraction of the [111] peak of the the multilayer structure in the charge and discharge state.

#### LiCoO<sub>2</sub> Films:

$\text{LiCoO}_2$  films deposited at  $500^\circ\text{C}$  exhibit the rock-salt structure of the low temperature phase[3]. To the contrary of the  $\text{LiMn}_2\text{O}_4$  films, the Li concentration has no effect on the e.m.f (Fig. 3). This  $\text{LiCoO}_2$  structure is a compact NaCl-type structure with ordering of Li and Mn in octahedral 16c and 16d sites. Therefore, the following reaction (2) is rather difficult and probably explains the absence of answer to the lithium concentration.



However, the potential strongly depends on the pH. This correspond to the insertion of protons corresponding to reactions of the type:



The pH dependence could be ascribed to different reaction mechanisms.

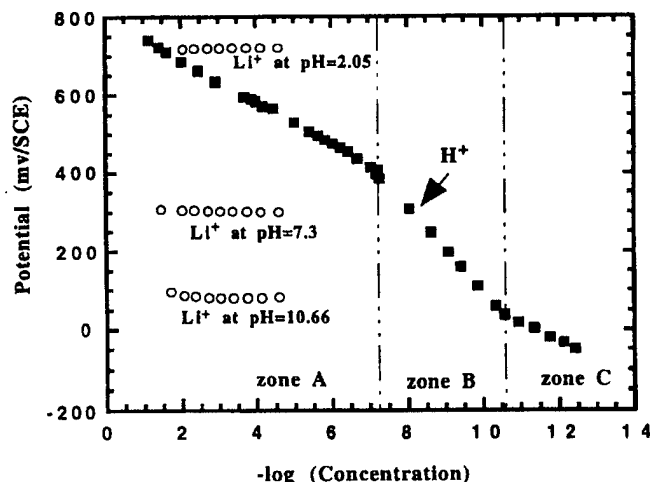


Fig 3: emf of a  $\text{LiCoO}_2$  electrode for different Li concentrations at fixed pH (○) and as a function of pH (—).

- [1] H. Kanoh, W. Tang and K. Ooi, *Electrochemical and Solid-State Letters*. 1 (1998) 17.
- [2] H. Kawai, M. Tabuchi, M. Nagata, H. Tukamoto, A. West, *J. Mat. Chem.* (1998) 8, 1273
- [3] M. Antaya, K. Cearns, J.S. Preston, J.N. Reimers and J.R. Dahn, *J. Appl. Phys.* 76 (1994).

## REDUCTION OF PULSE-INJECTED NITRIC MONOXIDE USING A ZIRCONIA OXYGEN PUMP-GAUGE

Hiroyuki KANEKO, Hitoshi TAIMATSU, Hidefumi ISAJI and Koji SUGANO

Department of Materials Science and Engineering, Faculty of Engineering and Resource Science,  
AKITA University, AKITA 010-8502, JAPAN

### Introduction

Oxygen-ion conducting zirconia electrolyte is used for oxygen sensors and oxygen pumps. A combination of a zirconia oxygen pump and a zirconia oxygen sensor, named a zirconia oxygen pump-gauge, is an intelligent device in which a flowing gas is quantitatively oxidized or reduced by pumping-in or -out oxygen through the pump and the oxygen pressure of the gas is precisely detected by the oxygen sensor following the pump [1,2]. In addition, zirconia oxygen pump has an electrochemically stimulated catalytic activity, as stressed by Vayenas et al. [3,4]. Several researchers [5-7] applied zirconia oxygen pump to investigate the reduction of harmful NO. Also, the authors have developed a titration technique of gases using this type oxygen pump-gauge [8] and the technique has been applied to oxidize or reduce a flowing gas containing CO [8], CH<sub>4</sub> [9] or NO [10]. As a further application of this device, it is important for the device to respond quickly to an abrupt change of a gas composition. In this study, therefore, this technique is applied to reduce NO pulse-injected into a carrier gas and the response of the device is investigated.

### Experimental

A schematic diagram of the oxygen pump-gauge is shown in Fig. 1. A detail was described elsewhere [8]. Platinum pastes were smeared on the both sides of two parts of a stabilized zirconia tube (YSZ, ZrO<sub>2</sub>-8 mol% Y<sub>2</sub>O<sub>3</sub>) and two parts worked as an oxygen sensor and an oxygen pump, respectively. The oxygen pump was operated at 1073 K, and the oxygen sensor at 973 K. A He-516ppm NO gas is pulse-injected into a He gas flowing at a rate of 75 cm<sup>3</sup> s<sup>-1</sup> using a gas-injector. The gas was injected by 1 cm<sup>3</sup> for 1 s into a He gas. The pump potential of the oxygen pump is maintained at a given value using a potentiostat, before and after the pulse-injection in the carrier gas. The current needed to maintain the pump potential of the oxygen pump is monitored. The oxygen pressure of the gas passed through the oxygen pump is determined by the oxygen sensor.

### Results and Discussion

A polarization curve for a He-516 ppm NO gas is shown in Fig. 2, where positive current means oxidizing the gas. As the reducing pump current is increased, pump potential is gradually increased, that is, oxygen pressure is decreased. At the critical pump current, pump potential abruptly increased, because oxygen runs out of the gas. The value corresponds to TOD (total oxygen demand) for the measuring gas and the concentration of NO is calculated from this value, according to the reaction, N<sub>2</sub> + O<sub>2</sub> = 2NO. Calculated and analyzed values agreed with each other. When NO is injected into a flowing He gas, oxygen pressure would be increased because of

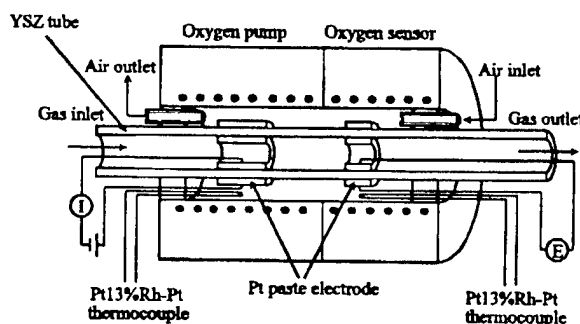


Fig.1 Schematic diagram of the oxygen pump-gauge.

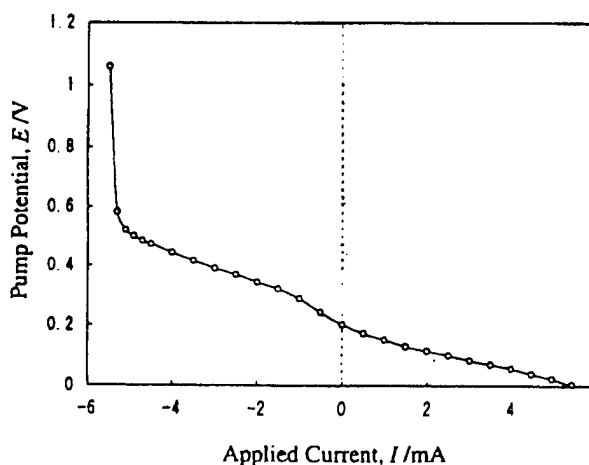


Fig.2 Polarization curve of the oxygen pump in a He-516ppm NO gas at 1073K.

the decomposition of a part of NO, and the pump potential would be decreased. Nevertheless, since the pump potential is maintained with a potentiostat at a given potential, an expected potential difference could be compensated by the real reducing pump current. The catalytic activity of the device can be estimated from electric charge through the oxygen pump and the amount of remaining oxygen measured by the oxygen sensor. Responses of the pump and resultant oxygen pressure change are shown in Fig. 3. Pump potential at zero pump current was 261 mV, where reduction of NO was incomplete. As the pump potential is increased, the reducing pump current is increased and the resultant oxygen pressure change becomes smaller. This shows that NO is reduced more effectively at higher pump potentials. Injected NO was perfectly reduced at a pump potential higher than 400 mV. When the gas passed through the oxygen pump-gauge was analyzed by gas chromatography, it is confirmed that the remaining amount of NO decreased with increasing the pump potential.

As an more realistic case, when the device was maintained at an appropriate pump potential for NO injected intermittently into a flowing He gas, its response was so good as to completely reduce each injected NO. This device will be useful as an intelligent device to control the reduction and oxidation of gases and to evaluate its redox activity.

### Conclusion

NO injected intermittently in a flowing He gas was automatically reduced using the oxygen pump-gauge, in which the pump potential was maintained at an appropriate value with a potentiostat. The reduction of NO proceeded completely when the pump potential was higher than 400 mV. The zirconia oxygen pump-gauge can work as a device to control and estimate the redox state of a gas with a fluctuating composition.

### References

- [1] D. Yuan and F.A. Kröger, *J. Electrochem. Soc.*, **116**, 594 (1969).
- [2] Y. Agrawl, D.W. Short, R. Grunke and R.A. Rapp, *J. Electrochem. Soc.*, **121**, 354 (1974).
- [3] C.G. Vayenas, *Solid State Ionics*, **28-30**, 1521 (1988).
- [4] S. Bebelis and C.G. Vayenas, *J. Catal.*, **118**, 125 (1989).
- [5] S. Pancharatnan, R.A. Huggins and D.M. Mason, *J. Electrochem. Soc.*, **122**, 869 (1975).
- [6] T.M. Gur and R.A. Huggins, *J. Electrochem. Soc.*, **126**, 1067 (1979).
- [7] M.A. Gessner, S.G. Nagy and J.N. Michaels, *J. Electrochem. Soc.*, **135**, 1294 (1988).
- [8] H. Taimatsu, H. Kaneko and M. Kawagoe, *Solid State Ionics*, **34,25** (1989).
- [9] H. Taimatsu, H. Kaneko, and T. Sasaki, *J. Appl. Electrochem.*, **20**, 775 (1990).
- [10] H. Kaneko, N. Mikami and H. Taimatsu, *Denki Kagaku*, **59**, 478 (1991).

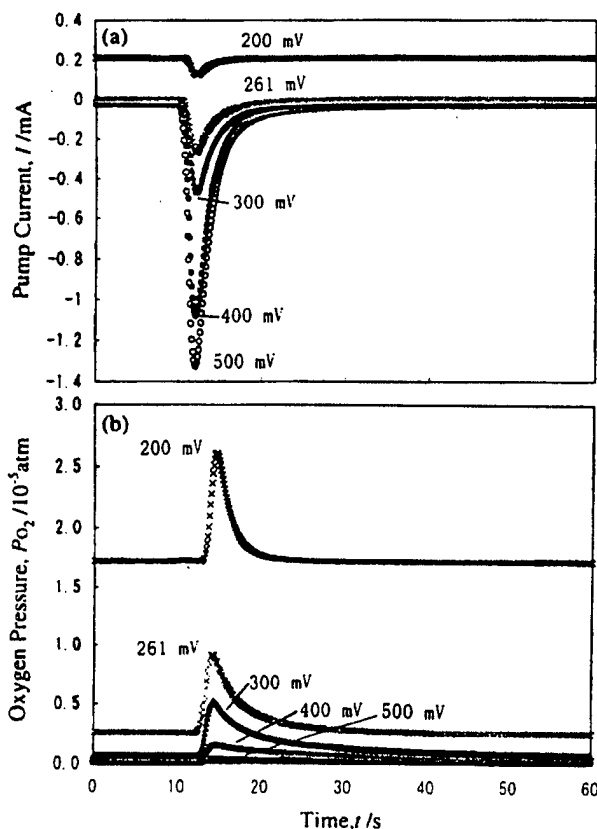
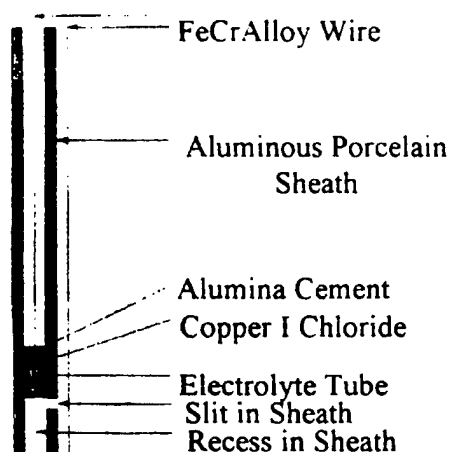


Fig.3 Responses of the oxygen pump (a) and the sensor (b) at various pump potentials (1cm<sup>3</sup> of a He-516ppm NO gas injected for 1s).

## MEASUREMENT OF HIGH COPPER CONCENTRATIONS IN MOLTEN PHASES

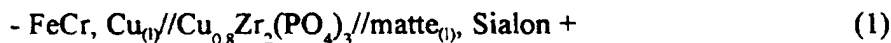
A.J. Davidson<sup>1</sup> and D.J. Fray<sup>2</sup><sup>1</sup>Department of Mining and Mineral Engineering, University of Leeds, Leeds LS2 9JT<sup>2</sup>Department of Materials Science and Metallurgy, University of Cambridge, Cambridge CB2 3QZ

Copper occurs at high concentrations in most alloys and in some of the phases during its reduction from the sulfide. Copper conducting electrolytes have been synthesised and have been shown to respond in accordance with the Nernst equation when separated by solutions containing different amounts of copper [1,2]. However, at high concentrations, the potential only changes slightly with change in copper concentration. For example, a change in the copper content of molten Fe-Cu-S from 56 wt% to 60 wt% at 1423 K results in the change in the potential of only 8 mV which may fall within the scatter of the readings. A similar problem exists in the monitoring of some gas mixtures that are oxygen rich. This has been overcome by using an amperometric approach whereby the transport of oxygen to the surface of the electrolyte is diffusion limited by either applying a porous coating or having a barrier containing a pin hole [3]. Under these conditions and an applied potential, the measured current is proportional to the flux of oxygen which, in turn, is proportional to the concentration of oxygen in the bulk phase. As this method has been proved to be successful, it was decided to observe whether it could be applied to the determination of copper in molten phases.



Cusicon electrolyte ( $\text{CuZr}_2(\text{PO}_4)_3$ ) prepared by firing cuprous oxide, ammonium di-hydrogen orthophosphate and zirconium dioxide and fabricated into tubes by isostatically pressing and firing at 1500 K for 12 hours. Amperometric measurements were made by packing the sintered tubes of electrolyte with copper powder and inserting a FeCrAlloy lead wire. The assembly was cemented into an aluminous porcelain sheath, recessed by approximately 1cm, with a slot cut in the sheath adjacent with the tip of the electrolyte tube. The purpose of the recess was to allow a stagnant volume of the molten phase to be in contact with the electrolyte and the slit in the sheath was to allow escape of air when the recess was filled with the molten phase. The sensor is shown above.

The cell can be represented as:



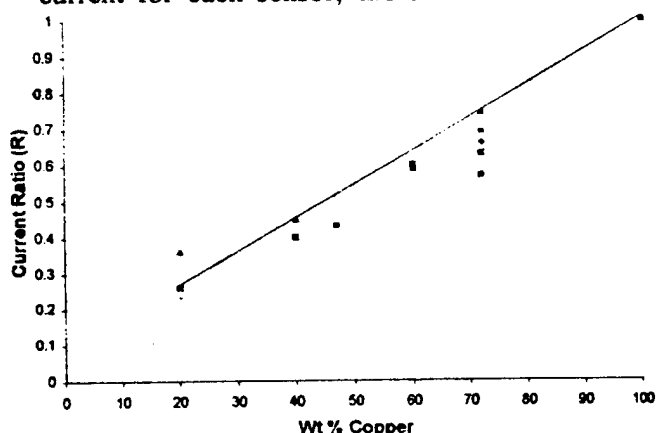
On insertion into molten copper-tin alloys at 1023 K, it was found that the current increased linearly with applied potential. No plateau was observed indicating that the sensor was not operating in the current limited mode. However, the sensor responded instantaneously to changes in copper concentration and very much faster than the equivalent Nernstian sensor. Under the conditions of the experiment, the measured current (I) is given by the following:

$$I = \frac{E_{\text{applied}} - \left( - \left( \frac{RT}{zF} \ln \frac{a_{\text{Cu}}}{a_{\text{Cu}^0}} \right) \right)}{R_{\text{electrolyte}}} + R_{\text{leads}} \quad (2)$$

where  $E_{\text{applied}}$  is the applied voltage,  $R$  is the gas constant,  $T$  is the temperature,  $Z$  is the charge carried,  $F$  is Faraday's constant,  $a_{\text{Cu}}$  is the activity of copper in the alloy,  $a_{\text{Cu}}^{\circ}$  is the activity of pure copper,  $R_{\text{electrolyte}}$  is the resistance of the electrolyte and  $R_{\text{leads}}$  is the resistance of the leads. The conductivity of the electrolyte [3] and the activity of copper in tin at 1023 K is known [2] and, therefore, a theoretical value of the current versus wt % copper can be calculated, assuming negligible resistance in the leads. Reasonable agreement with equation 2 was obtained, given the uncertainties in the conductivity of the electrolytes and the thickness of the electrolyte and the surface areas offered to the metal by each sensor.

When similar measurements were attempted in a sulfide based system, Cu-Fe-S, it was found that although there was a linear dependence between the applied potential and the measured current for each sensor, there was little correlation between sensors due to the differences in

geometry of the individual sensors. In order to overcome this problem it was decided to reverse the potential so that the copper flowed from the copper reference, through the electrolyte as copper ions, into the copper matte and to measure the current. By taking the ratio of the currents a very much better correlation was observed as is shown in the figure above.



Under these conditions, the two individual currents are given by:

$$I_1 = \frac{E_{\text{applied}} - \left( -\left( \frac{RT}{zF} \ln \frac{a_{\text{Cu}}}{a_{\text{Cu}}^{\circ}} \right) \right)}{R_{\text{electrolyte}}} + R_{\text{leads}} \quad (3) \quad I_2 = \frac{E_{\text{applied}} + \left( -\left( \frac{RT}{zF} \ln \frac{a_{\text{Cu}}}{a_{\text{Cu}}^{\circ}} \right) \right)}{R_{\text{electrolyte}}} + R_{\text{leads}} \quad (4)$$

Taking the ratio gives:

$$\frac{I_1}{I_2} = \frac{E_{\text{applied}} - \left( -\left( \frac{RT}{zF} \ln \frac{a_{\text{Cu}}}{a_{\text{Cu}}^{\circ}} \right) \right)}{E_{\text{applied}} + \left( -\left( \frac{RT}{zF} \ln \frac{a_{\text{Cu}}}{a_{\text{Cu}}^{\circ}} \right) \right)} \quad (5)$$

In this case, as expected, the resistance term disappears which makes the current ratio independent of the resistivity of the electrolyte, thickness of the electrolyte and the surface area exposed to the sulfide phase. From values of the activity of copper in the sulfide phase, it is possible to calculate the theoretical dependence of the current ratio on the atom fraction of copper. A close correlation was observed. From equation (5), it can be seen that by altering the applied potential the sensitivity of the sensor can be increased and, furthermore, the dependence of the current ratio is approximately linear as opposed to being logarithmic as in the case of sensors based upon the simple Nernst equation.

In conclusion, a novel sensing technique for the determination of high concentrations of elements has been developed which responds considerably faster and is more sensitive than the approach based upon the Nernst equation. In addition, by alteration of the applied potential to close to that of the Nernst potential the sensitivity can be greatly increased.

#### References

1. J.A. Little and D.J. Fray, Trans. IMM **88**, C229 (1979)
2. P.C. Yao and D.J. Fray, Solid state Ionics, **8**, 35 (1983)
3. T. Takeuchi, Proc. Second International Meeting on Chemical Sensors (Bordeaux, France 1986) 69



### Solid electrolyte electrochemical sensor for studying the behaviour of a partial oxidation catalyst

D Barth, M Sahibzada, IS Metcalfe\*

School of Chemical Engineering  
University of Edinburgh  
Edinburgh EH9 3JL, UK

\* tel: +44 131 6508553, fax: +44 131 6506551, email: i.metcalfe@ed.ac.uk

In industrial control a lack of effective on-line sensors is often a limitation. As a result electrochemical sensors are employed for continuous in situ measurements of process variables whenever possible. The e.m.f. or open circuit voltage (OCV) of an electrochemical sensor with an oxygen ion conductive electrolyte is related to the oxygen content of the electrodes. In a selective oxidation reaction, the catalyst selectivity and activity are similarly affected by the oxygen content or degree of reduction of the catalyst. Comparing OCV values with simultaneously measured reaction rate data gives detailed information about catalyst state, activity and selectivity during oxidation reactions.

Solid electrolyte potentiometry (SEP) was used to monitor the thermodynamic activity of oxygen adsorbed on and absorbed into a mixed oxide catalyst surface under reaction conditions while reaction rate data was measured simultaneously by recording the outlet gas stream concentration using GC and MS techniques. A solid state electrochemical cell consisting of an oxygen ion conductive yttria-stabilised zirconia ( $\text{Y}_2\text{O}_3\text{-ZrO}_2$ ) electrolyte placed between a platinum 'reference' electrode and the mixed oxide 'working' electrode was used as a sensor. For the first time the selective oxidation of propene to acrolein over  $\text{Fe}_2\text{O}_3\text{-Sb}_2\text{O}_4$  surfaces was studied in an electrochemical cell under atmospheric pressure conditions at 400 °C and 450 °C.

Experiments were performed under oxidising and reducing conditions. The steady-state, transient and dynamic behaviour of the catalyst-electrode were analysed. Due to oxygen uptake and removal from the electrode surface, changes of the sensors OCV were observed and the OCV data then correlated with reaction rate data. The results have been interpreted within the framework of a mechanistic description. Additionally a number of experiments were carried out after different pretreatments (pre-reduced

or pre-oxidised) of the electrode to evaluate if 'catalyst history' played a role in determining the catalytic behaviour of the system. The  $\text{Fe}_2\text{O}_3\text{-Sb}_2\text{O}_4$  oxide did not show hysteresis in observed reaction rate for the production of the total oxidation product, carbon dioxide, or the partial oxidation product, acrolein. It was shown that the OCV of the sensor appeared to be most sensitive to the more reactive adsorbed oxygen species on the surface and not to lattice oxygen species. This reactive adsorbed oxygen species was seen to be selective for the formation of carbon dioxide. Hence the catalyst favoured acrolein formation when activities of this adsorbed oxygen were low, i.e. when the OCV is more negative (this can be seen in Figure 1).

Based on these results we can conclude that a potentiometric sensor may provide important information for catalytic partial oxidation process monitoring. The possibility that such sensors are most sensitive to more reactive forms of oxygen species on the surface or in the bulk could lead to a wide range of catalytic applications.

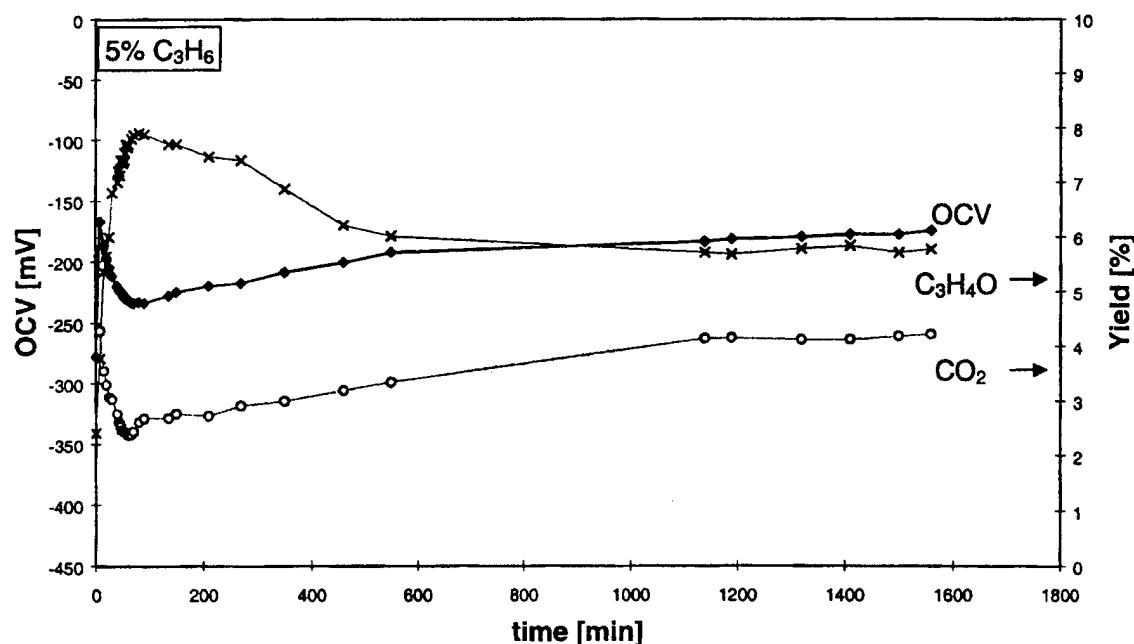


Figure 1: Transient behaviour (OCV and yields versus time) on exposure to 19% oxygen and 5% propene at 400 °C after a prereducing step

ALL SOLID STATE  $\text{Cu}^{2+}$  ION SENSORS BASED ON ISE AND ISFET TRANSDUCERS.

O. Valls\*, G.Taillades\* A. Pradel\*, M.Ribes\*.  
A.Bratov\*\*, C. Dominguez\*\*.

\*Laboratoire de Physicochimie de la Matière Condensée UMR 5617, Université Montpellier II  
34095 Montpellier cedex 5, France.

\*\*Centro Nacional de Microelectronica, Campus UAB, Bellaterra 08193 Barcelona Spain.

To date, quality control of superficial and ground waters results from reliable but expensive analytical measurements carried out in laboratory. Chemical microsensors based on thin films produced by methods compatible with planar silicon technology are essential primary devices for integrated analytical microsystems capable of continuous and in situ measurements. Chalcogenide glasses are well established materials for sensors selective to heavy metal ions ( $\text{Cu}^{2+}$ ,  $\text{Pb}^{2+}$ ,  $\text{Cd}^{2+}$ ...) in liquid media [1]. They are more chemically stable than the corresponding crystalline membrane and a considerable glass forming ability makes possible to adjust the composition to the analytical properties required.

The preparation and the characterisation of potentiometric and modified ISFET microsensors for the detection of copper in solution are presented in this paper.

Ge-Sb-Se thin films highly doped with copper were deposited by RF co-sputtering from the host glass and metal copper assembled as a composite target. A typical micrograph obtain by SEM (figure 1) confirm the good adhesion of the columnar film on the  $\text{Si}/\text{Si}_3\text{N}_4/\text{Al}$  substrate. As prepared potentiometric sensors based on this membrane exhibited fast  $\text{Cu}^{2+}$  ion response. The response obeyed the Nernst's law with a slope of 30 mV/pCu above pCu=5.5. After conditioning, the limit of detection was close to  $6 \cdot 10^{-6} \text{ mol.l}^{-1}$  (figure 2). The sensor showed long term stability and a high selectivity in the presence of alkali, alkaline earth and heavy metal ions.

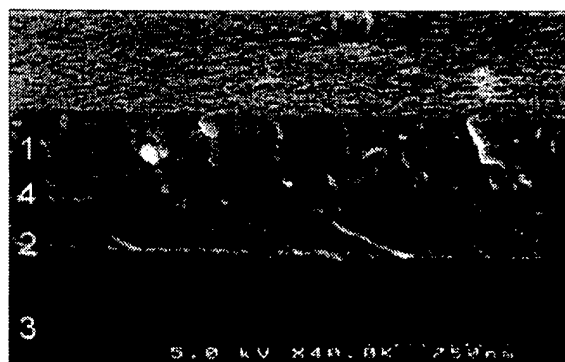


Figure 1 : Micrograph of a Cu-Ge-Sb-Se thin film. (1) sensitive membrane, (2)  $\text{Si}_3\text{N}_4$ , (3) Si substrate, (4) Al.

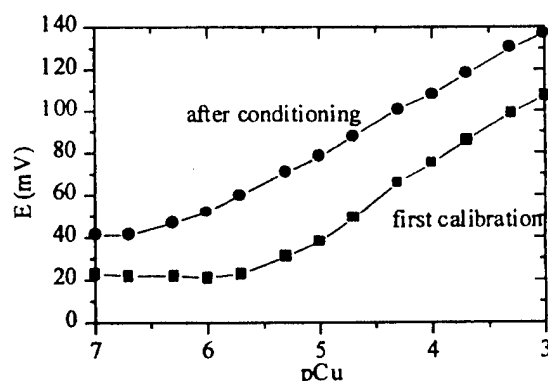


Figure 2 : Potentiometric response before and after conditioning.

The ISFET used for the fabrication of the microsensors were initially designed for pH measurement [2]. Several steps were added to the original production procedure in order to adapt them to their new use. In particular, the Al current collectors were protected by an epoxy layer previous to the deposition of the chalcogenide film on the whole surface of the wafer. The

film was then selectively removed from the wafer (excepted in the gate region) using a photolithographic process specifically developed for this purpose.

ISFET were characterized by measuring the variation of the gate voltage while dipping the sensors in solutions containing different concentrations of copper. A Nernstian response was obtained, the sensitivity are similar to those obtain for potentiometric sensors.

The goal of this work was to obtain the mastery of the fabrication of modified ISFET for the detection of heavy ions in solution. Use of similar processes concerning the deposition method and the photolithography process should help us in building an integrated multisensor system for environmental monitoring and process control.

[1] Yu G. Vlasov and E.A. Bychkov, Ion-selective Electrode Rev. **9**, 5 (1987).

[2] S. Alegret, J. Bartoli, C. Jimenez, M. del Valle, C. Dominguez, E. Cabruja and A. Merlos, Electroanalysis **3**, 355 (1991).

## APPLYING POLARIZED ELECTROCHEMICAL VAPOR DEPOSITION (PEVD) FOR SOLID STATE IONIC DEVICES

Eric Z. Tang\* and Thomas H. Etsell\*\*

\*Global Thermoelectric Inc., Calgary, Alberta, Canada

\*\*Department of Chemical and Materials Engineering, University of Alberta, Edmonton, Canada

In the past 30 years, solid state ionic devices have been developed rapidly in order to serve ever-growing energy and environmental demands. In spite of the great promise they offer, few commercial successes have been reported to date. The major problems faced today in the field of solid state ionic devices are still material related. At present, the key technical challenge is development of reliable and cost-efficient techniques to synthesize solid state ionic materials to serve as solid electrodes and electrolytes. The present availability of numerous types of solid state ionic materials allows for electrochemical reactions to be carried out with the surrounding vapor phase to form products of interest. This recent interfacing of vapor deposition and electrochemistry has led to the development of polarized electrochemical vapor deposition (PEVD).

Generally speaking, PEVD utilizes a solid state electrochemical cell, which can transport one reactant in the ionic state. Thus, under an electrochemical potential gradient, which is mainly provided by a dc electrical potential, an ionic reactant travels from the source side of a solid substrate to the sink side and reacts with the surrounding vapor electrochemically to form a desired solid product. The significance of this new technique is that PEVD applies solid state ionic techniques to modify the widely accepted CVD technique under controlled conditions in a solid electrochemical cell. Compared with other solid state ionic techniques, PEVD takes advantage of not only energy transformation but also material transport itself during ionic and electronic transport in solids to form desired products. Thus, PEVD has brought Wagner's electrochemical tarnishing theory to a new field for making man-made products under well-defined thermodynamic and kinetic conditions. The immediate advantages of using a closed-circuit electrochemical cell in PEVD include easy control and monitoring through applied dc potential and external current, respectively. Furthermore, the PEVD product is capable of modifying the solid electrolyte/electrode interface both physically and chemically due to its unique crystallization and growth behavior. Investigations show that PEVD is the most suitable technique to improve solid electrolyte/electrode contact, and subsequently, the performance of those solid state ionic devices. In this paper, the current applications of PEVD for solid state ionic devices will be discussed in detail.

PEVD was developed initially in the course of fabricating type III potentiometric sensors for gaseous oxide ( $\text{CO}_x$ ,  $\text{SO}_x$  and  $\text{NO}_x$ ) detection. Three kinds of PEVD products ( $\text{NaNO}_3$ ,  $\text{Na}_2\text{CO}_3$  and  $\text{Na}_2\text{SO}_4$ ) were deposited as the auxiliary phases at the working electrode of  $\text{NO}_2$ ,  $\text{CO}_2$  and  $\text{SO}_2$  sensors, respectively. Because of PEVD's ability to control the deposition process and its unique product phase growth behavior, it is possible to prepare, by means of PEVD, a working electrode with the ideal microstructure. For instance, our studies indicated that the response behavior of a potentiometric  $\text{CO}_2$  sensor depends on the thickness of the auxiliary phase and the aspect ratio of the working electrode surface. As shown in Figure 1, a potentiometric  $\text{CO}_2$  sensor can be made by PEVD with a response time of less than 1 min and a recovery time of less than 3 min, for a  $\text{CO}_2$  partial pressure at the working electrode varying from 30 to 300 ppm at  $500^\circ\text{C}$ . This is about 10 times lower than the previously reported value under the same sensing conditions.

PEVD has also been applied to deposit a thin layer of yttria stabilized zirconia at a pure metallic anode to form composite anodes for solid oxide fuel cells. After a critical review of previous investigations of SOFC anodes, several criteria regarding anode materials and microstructure can be

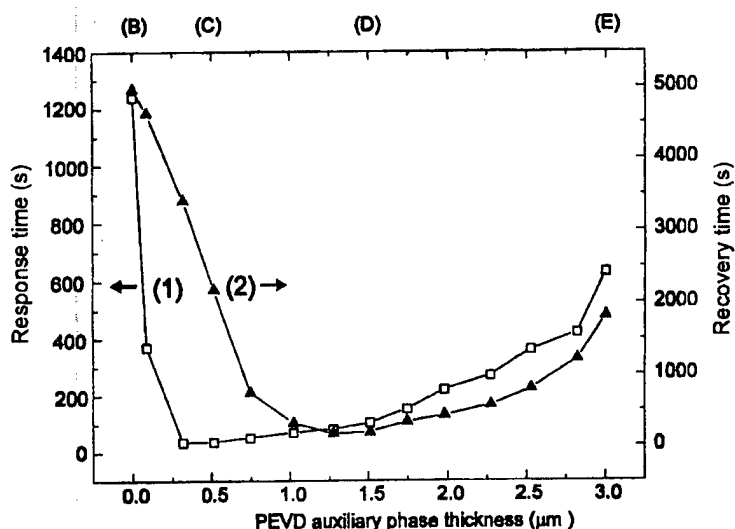


Figure 1. Response and recovery times vs. the thickness of the auxiliary phase of a PEVD potentiometric CO<sub>2</sub> sensor.

summarized, and a theoretically ideal SOFC composite anode can be proposed as shown in Figure 2. It appears that the emergence of the PEVD technique for ceramic phase deposition on high aspect ratio and very irregularly shaped metallic electrodes has made possible the successful fabrication of composite anodes similar to the theoretically ideal one. Consequently, SOFCs with PEVD composite anodes should have higher electrical conductivity, lower overpotential loss, and exhibit better long-term stability.

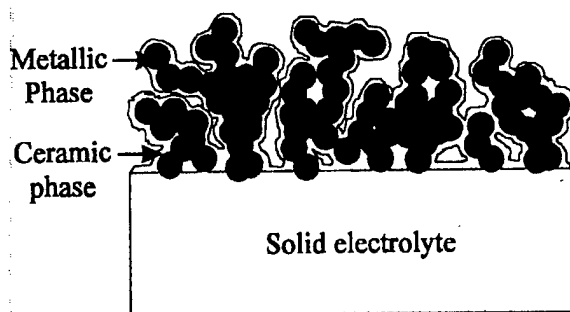


Figure 2. Two dimensional schematic of the microstructure of the theoretically ideal composite anode of solid oxide fuel cells.

In conclusion, these applications of PEVD have shown that PEVD is the most suitable technique to improve solid electrode / electrolyte contact and, consequently, the performance of those solid state ionic devices. Furthermore, the "active" use of material transport through the solid by PEVD offers more interesting opportunities not only for forming deposition products but also for studying the physical properties of the products under well-defined thermodynamic and kinetic conditions. It has been more than sixty years since Wagner's electrochemical tarnishing theory was developed. Finally, the two parallel suggestions of material transport and energy transformation in the theory are interconnected, and the newly developed PEVD will make solid state ionic devices to better serve today's ever-growing energy and environmental demands.

## PROPERTIES AND MORPHOLOGY OF AgCl BASED COMPOSITES AND HIGHLY POROUS AgCl

Amita Chandra\*, Annett Spangenberg and Joachim Maier

\* Department of Physics, Banaras Hindu University, Varanasi-221 005, INDIA  
Max-Planck-Institute for Solid State Research, Heisenberg Strasse 1, 70569 Stuttgart,  
GERMANY

Composites of Frenkel disordered AgCl with Schottky disordered solids such as KCl, CsCl and RbCl have been prepared and investigated. In accordance with the concept of heterogeneous doping, there was no significant conductivity anomaly to be observed. However, the morphological properties offer interesting aspects. If AgCl:KCl eutectics have been treated with H<sub>2</sub>O and KCl, thus, has been leached out, a coherent highly porous AgCl network was obtained. It is shown that this morphology can be used (i) to sense ammonia with a reasonably low response time and (ii) to soak up liquid electrolytes to combine conductivity properties of the liquid and mechanical stability of the solid.

## **SOLID STATE MIXED POTENTIAL GAS SENSORS: THEORY, EXPERIMENTS AND CHALLENGES**

**Fernando Garzon, Eric Brosa and R. Mukundan,  
Electronic and Electrochemical Materials and Devices Group, Los  
Alamos National Laboratory, USA**

Solid state electrochemical devices that sense reducing or oxidizing gases via the generation of a mixed potential due to gas-solid redox reactions have been extensively developed for the last two decades. These electrochemical devices typically consist of two or more dissimilar electrodes deposited onto a solid ionic conductor -typically a zirconia based solid electrolyte. These sensor devices have a variety of possible applications in: combustion control, catalytic converter monitors and in environmental safety systems. Many prototype devices have been fabricated but few if any have been developed into useful commercial devices.

A significant impediment to widespread mixed potential device implementation has been their long-term drift in response characteristics. Electrode aging phenomena such as recrystallization is responsible for much of this drift. Improved devices require development of stable electrode structures. Also the cross-sensitivity of these devices to interference gases must also be improved for practical device development.

The theory of mixed potential devices has been well developed, but it has not been of great developmental use as it requires knowledge of many electrokinetic reaction rates. These reaction rate parameters are difficult, if not impossible, to measure independently in two electrode type device configurations. We have developed three and four electrode devices containing one or two reference electrodes respectively to measure electrokinetic rates of relevant reactions for carbon monoxide and hydrocarbon mixed potential sensors. Careful attention to appropriate test gas mixtures is also important in establishing useful experimental results. Our experimental data demonstrates the importance of the oxygen reduction reaction in determining the mixed potential of a given electrode on an oxygen ion conductor. We have also developed new ceramic and metal electrode materials that offer high response levels and good response stability over thousand of hours of testing. These sensor devices have a variety of potential applications in combustion control, catalytic converter monitors and in environmental safety systems.



## THICK/THIN FILM SULPHUR DIOXIDE CHEMICAL SENSOR

C. D. Eastman, DB Robinson and Associates, Edmonton, Alberta and T.H. Etsell, Department of Chemical and Materials Engineering, University of Alberta

A three part sulphur dioxide (SO<sub>2</sub>) gas sensor consisting of a working electrode fabricated with Li<sub>2</sub>SO<sub>4</sub>-Ag<sub>2</sub>SO<sub>4</sub> and coated with a platinum thin film in combination with a thick film reference electrode was constructed and tested. The working electrode was constructed of Li<sub>2</sub>SO<sub>4</sub>-Ag<sub>2</sub>SO<sub>4</sub> via a sintering process resulting in a pellet approximately 2mm thick. A thin film of platinum 1000 Angstroms thick was deposited onto the sintered pellet. The reference electrode consisted of thick film of Ag / Li<sub>2</sub>SO<sub>4</sub>-Ag<sub>2</sub>SO<sub>4</sub> between 20-30 microns in thickness.

The sensor was exposed to gas concentrations of between 1 to 2400 ppm of SO<sub>2</sub> in air. The experimental results displayed correlation's between cell voltage and the log of SO<sub>2</sub> concentration close to 1. Different ratios of Ag to Li<sub>2</sub>SO<sub>4</sub>-Ag<sub>2</sub>SO<sub>4</sub> in the reference electrode were found to be related to the longevity of the gas sensor. Further work is to be performed in the development of improved fabrication techniques so as to enhance its suitability for miniaturization.

## Methane Detection in Oxygen Poor Atmospheres Using a Catalytic Asymmetric Sensor

L.N. van Rij, R.C. van Landschoot, and J. Schoonman

Laboratory for Inorganic Chemistry, Faculty of Applied Sciences, Delft University of Technology, Julianalaan 136, 2628 BL, Delft, The Netherlands, e-mail: L.N.vanRij@stm.tudelft.nl

### Introduction

The detection principle of the methane sensor is based on a difference in catalytic activity of two electrodes for the CO<sub>2</sub>-reforming reaction of methane (1). Methane is converted into water vapour or hydrogen via reforming reactions<sup>[1,2]</sup>. Since the catalytic activity of both electrodes is different, different partial pressures will be established at the electrodes. This partial pressure difference creates a potential difference across the cell which is a measure of the methane concentration. Hence, the sensor behaves as a Nernst-type sensor, where the water vapour or hydrogen is produced *in-situ* out of methane and CO<sub>2</sub>.

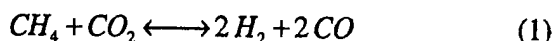
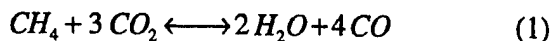
### Experimental

The solid electrolyte, SrCe<sub>0.95</sub>Yb<sub>0.05</sub>O<sub>3-α</sub> (SCYb5), was synthesised according to the method reported by Iwahara *et al.*<sup>[3]</sup>. As catalytic electrode ruthenium was chosen, because of the high catalytic activity of this metal for the CO<sub>2</sub>-reforming of methane<sup>[1,2]</sup>. As counter electrode platinum was used. The sensor system was tested in a set-up with separated compartments, in which the same gas mixture is applied to both sides. The experiments were carried out at 500°C and a constant CO<sub>2</sub> concentration of 10 vol.%. The gas flow was set at 2.1 ml·min<sup>-1</sup> (4.2 cm·min<sup>-1</sup>) and 2.7 ml·min<sup>-1</sup> (5.4 cm·min<sup>-1</sup>), respectively, while the methane partial pressure was varied from 1 to 90 vol.%. The gas flow from the ruthenium compartment was analysed using a gas chromatograph (HP 5890 series II, column: porepack Q, 80/100 Mesh).

In all experiments a current of 50 μA·cm<sup>-2</sup> was applied to the cell (potentiostat: Gamry, PC3), flowing from the catalytic electrode (ruthenium) to the counter electrode (platinum), in order to create an extra driving force for proton conduction through the cell.

### Results and Discussion

The response of the sensor after a constant potential difference has been reached, is shown in figure 1. A maximum in the potential difference of the sensor is observed. This maximum can be attributed to a change in the reactions occurring at the electrodes. It is assumed that at low methane partial pressures methane reacts with CO<sub>2</sub> to form water and CO (reaction 1).



At higher methane partial pressures, when the ratio of CH<sub>4</sub> and CO<sub>2</sub> is increased to a value higher than 1 (>10 kPa), the CO<sub>2</sub>-reforming reaction (2) takes place.

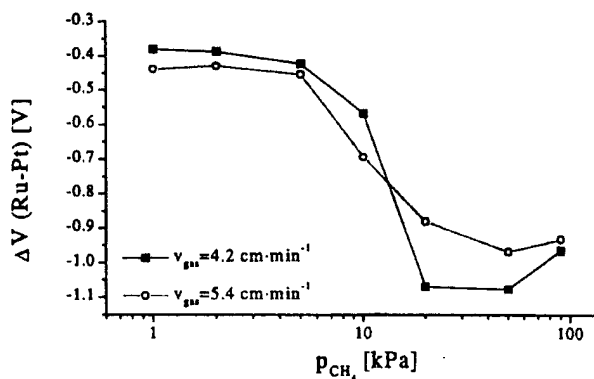


Figure 1: Sensor response to methane at 500°C and 10 vol.% CO<sub>2</sub>.

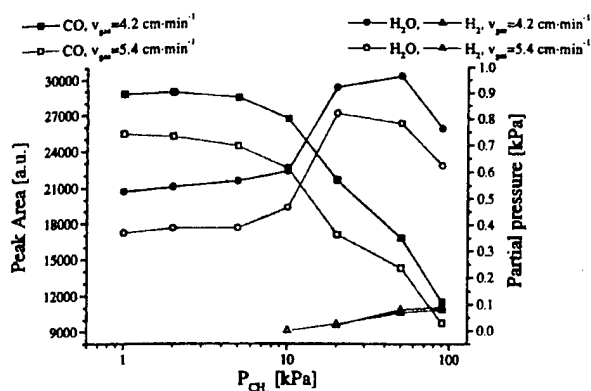
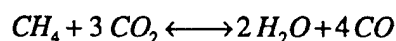


Figure 2: The detected reaction products at 500°C and 10 vol.% CO<sub>2</sub>.

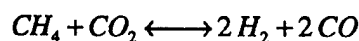
The production of hydrogen at methane partial pressures higher than 10 kPa can easily be explained by a change in the reaction path from reaction 1 to reaction 2. This reaction change also predicts a change in the reaction coefficient for CO from +4 to +2 and, therefore, a decrease in the CO production is expected. The sudden increase in the measured water partial pressure can be explained by the maximum incorporation of water as  $OH_o^*$  in  $SrCe_{0.95}Yb_{0.05}O_{3-\alpha}$ <sup>[4,5]</sup>, which occurs at a gas phase concentration of about 0.5 vol.%. The sudden increase in the measured water concentration takes place at around 0.5 vol.% and is, therefore, in agreement with literature.

## Conclusions

The catalytic asymmetrical Nernst-type sensor shows a clear decrease in the cell potential difference with increasing methane partial pressure. A maximum is observed in the measured potential difference. This maximum could be attributed to a change in the electrode reaction. At low methane partial pressures the following gas phase reaction takes place:



At high methane partial pressures the CO<sub>2</sub> reforming reaction of methane takes place:



To ensure a good response, the sensor has to be operated at a sufficiently high CO<sub>2</sub> concentration. The sensor system studied has been shown to have the potential to be used for the detection of methane in oxygen poor atmospheres. However, to improve the sensor response it might be an advantage to use different electrode materials, in order to catalyse only one reaction at the electrodes.

## References

1. P.D.F. Vernon, M. L. H. Green, A. K Cheetham, and A. T. Ashcroft, Partial oxidation of methane to synthesis gas, and carbon dioxide as an oxidising agent for methane conversion, *Cat.Today*, **13**, (1992) 417-426.
2. D. Qin and J. Lapszewicz, Study of mixed steam and CO<sub>2</sub> reforming of CH<sub>4</sub> to syngas on MgO-supported metals, *Cat.Today*, **21**, (1994) 551-560.
3. H. Iwahara, H. Uchida, and S. Tanaka, High temperature-type proton conducting solid oxide fuel cells using various fuels, *J.Appl.Electrochem.*, **16**, (1986) 663-668.
4. T. Yajima and H. Iwahara, Studies on behavior and mobility of protons in doped perovskite-type oxides: (I) In situ measurements of hydrogen concentration in  $SrCe_{0.95}Yb_{0.05}O_{3-\alpha}$  at high temperature, *Solid State Ionics*, **50**, (1992) 281-286.
5. F. Krug, T. Schober, and T. Springer, In situ measurements of the water uptake in Yb doped SrCeO<sub>3</sub>, *Solid State Ionics*, **81**, (1995) 111-118.

## INTERFACIAL STRUCTURE OF POTENSIOMETRIC CO<sub>2</sub> SENSOR DEVICE ATTACHED WITH Li<sub>2</sub>CO<sub>3</sub>-CaCO<sub>3</sub> AUXILIARY PHASE

Tetsuya KIDA, Kengo SHIMANOE, Norio MIURA, Noboru YAMAZOE

Department of Molecular and Material Sciences, Graduate School of Engineering Sciences,  
Kyushu University, Kasuga-shi, Fukuoka 816-8580, Japan

Solid electrolyte CO<sub>2</sub> sensors have been studied intensively for monitoring indoor air quality as well as control of bio related processes. We have shown that CO<sub>2</sub> sensors, for which NASICON (Na<sub>3</sub>Zr<sub>2</sub>Si<sub>2</sub>PO<sub>12</sub>) is combined with a binary carbonate auxiliary phase such as Li<sub>2</sub>CO<sub>3</sub>-BaCO<sub>3</sub> and Li<sub>2</sub>CO<sub>3</sub>-CaCO<sub>3</sub>, exhibit attractive sensing performances[1,2], and that some can be candidates for the practical applications. For these CO<sub>2</sub> sensors, the hetero-junction between carbonate and NASICON plays an important role in sensing performances. However, actual junction structure has remained yet to be investigated. In this study, we investigated interfacial structure for the hetero-junctions of Li<sub>2</sub>CO<sub>3</sub>-CaCO<sub>3</sub>/ NASICON, and its relevance to the CO<sub>2</sub> sensing properties of the devices.

A schematic drawing of sensor device is shown in Fig. 1. A gold mesh (sensing electrode) was mechanically pressed on NASICON disk. On top of it, a small quantity of metal carbonate (Li<sub>2</sub>CO<sub>3</sub>-CaCO<sub>3</sub>) was placed. The assembly was heated up to 950°C for 5 min and subsequently cooled to room temperature, to have a layer of the carbonate phase coated on the gold mesh and NASICON surface through melting and solidifying. Measurements of CO<sub>2</sub> sensing properties were carried out in a conventional gas-flow apparatus equipped with a heating facility. The electromotive force (EMF) of the device was measured with an electrometer at 300-500°C. Interfacial structures between Li<sub>2</sub>CO<sub>3</sub>-CaCO<sub>3</sub> and NASICON were analyzed by SEM connected with EPMA.

As shown in Fig. 2, the EMF response of the sensor attached with Li<sub>2</sub>CO<sub>3</sub>-CaCO<sub>3</sub> (1:2) followed the Nernst equation well at 350°C, which was more sensitive to CO<sub>2</sub> than the sensor attached with Li<sub>2</sub>CO<sub>3</sub>-CaCO<sub>3</sub> (1:1). Fig. 3 shows that an excessive addition of CaCO<sub>3</sub> was effective for improving the CO<sub>2</sub> sensing capability at lower temperatures. The sensor using Li<sub>2</sub>CO<sub>3</sub>-CaCO<sub>3</sub> (1:2) is seem to allow normal sensing operation down to 350°C. Analyses of fractured surfaces by means of SEM and EPMA indicated the formation of an interfacial layer between carbonate and NASICON (Fig.4), the thickness and morphology of which depended on the carbonate composition used. As revealed by X-ray diffraction analysis, CaZrO<sub>3</sub> was found to be formed between Li<sub>2</sub>CO<sub>3</sub>-CaCO<sub>3</sub> and NASICON, suggesting its relevance to the lower temperature sensing capability.

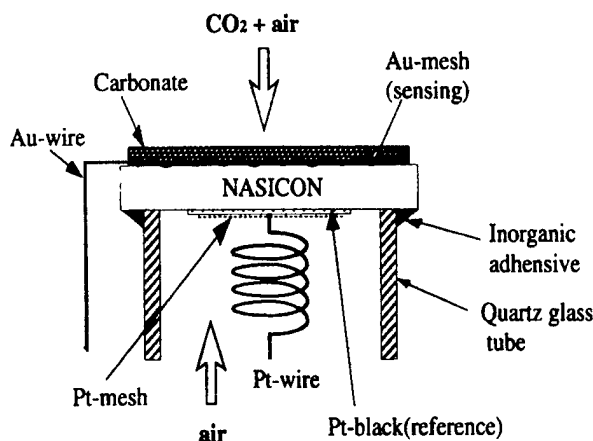


Fig.1 Schematic view of the structure of CO<sub>2</sub> sensor.

## References

- [1] S. Yao, Y. Shimizu, N. Miura, N. Yamazoe, J. Appl. Phys., **31** (1992) L197.  
 [2] S. Yao, Y. Shimizu, N. Miura, N. Yamazoe, Appl. Phys. A, **57** (1993) 25.

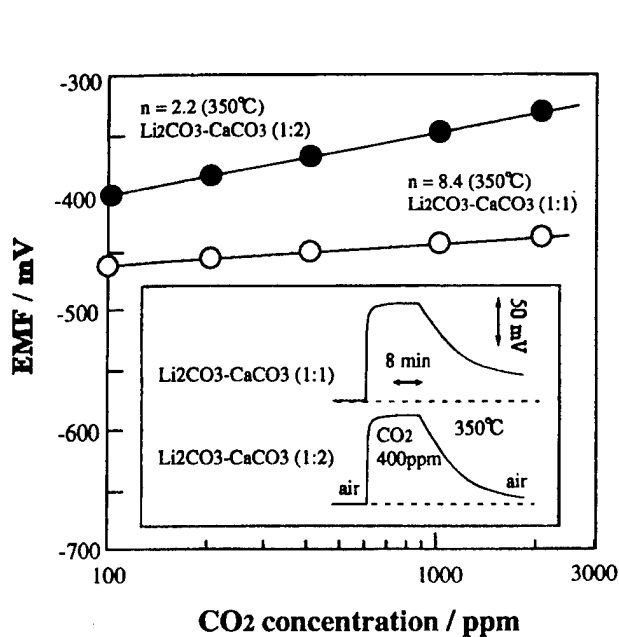


Fig. 2 CO<sub>2</sub> sensing performances of the devices attached with Li<sub>2</sub>CO<sub>3</sub>-CaCO<sub>3</sub> at 350°C.

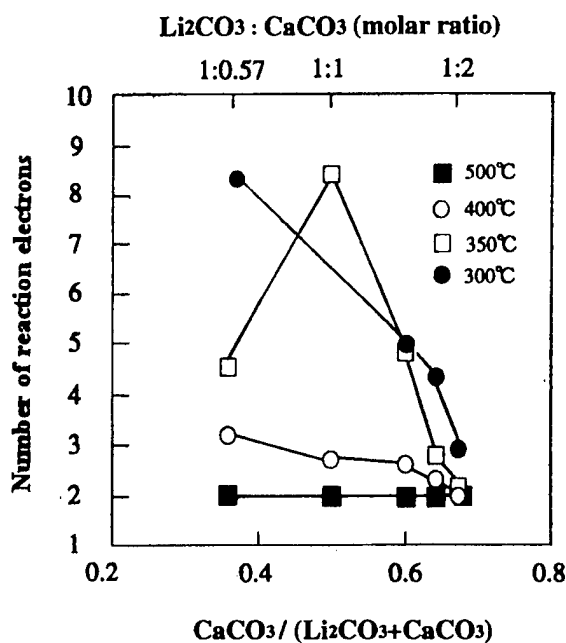


Fig. 3 Number of reaction electrons as correlated with CaCO<sub>3</sub> composition.

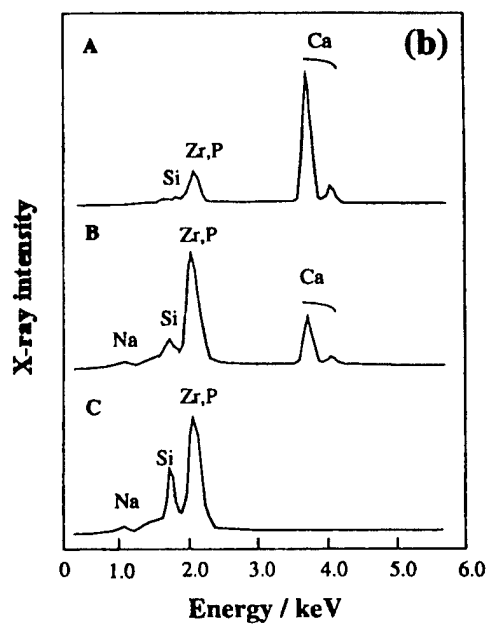
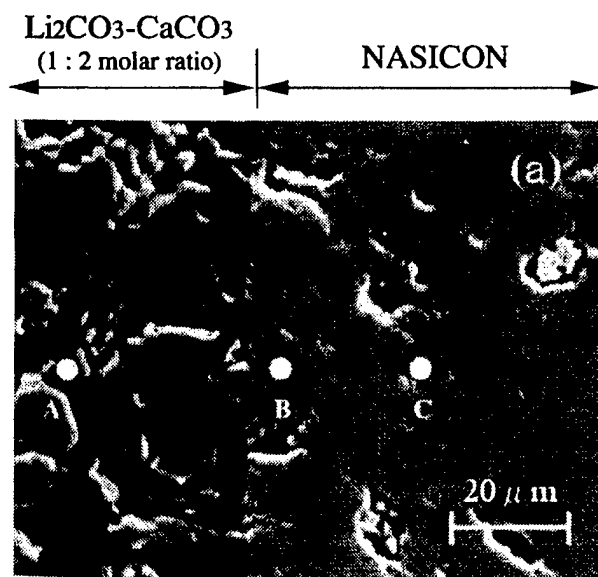


Fig. 4 SEM photograph (a) and EPMA analysis (b) of selected points on fractured surface for Li<sub>2</sub>CO<sub>3</sub>-CaCO<sub>3</sub> (1:2) / NASICON.

## Development of multilayer transparent conductive coatings

G. Leftheriotis and P. Yianoulis

Department of Physics, University of Patras, Patras 26500, GREECE.

Tel: ++30-61-997449. Fax: ++30-61-997472. E-mail: gleftther@physics.upatras.gr

Transparent conductive coatings are an integral part of many thin film devices, such as electrochromic, electroluminescent and photovoltaic cells. They are used as electrodes to convey electrical signals which are crucial for the operation of such devices. They have many other applications as optical filters, heat mirrors, low emittance films for advanced glazing, protective and decorative coatings.

The most common materials used for the production of transparent conductive films are doped metal oxides, for example:  $\text{SnO}_2\text{:F}$ ,  $\text{In}_2\text{O}_3\text{:Sn}$  (also called ITO) and  $\text{ZnO:Al}$  [1-3]. These films are substantially transparent (luminous transmittance: 0.85 to 0.90), were resistant and adhere equally well on many types of substrates (glass, PVC, silicon). They have however, several drawbacks: They exhibit relatively high electrical resistance (sheet resistivity: 20-200  $\Omega/\text{square}$ ), considerable emittance (about 0.20 or more) and significant absorption in the spectral region 1-2  $\mu\text{m}$ , in which transition from high transmittance to high reflectance takes place. Furthermore, these coatings do not block the solar thermal radiation (0.7 to 3  $\mu\text{m}$ ) which may cause overheating problems to devices such as electrochromics and photovoltaics.

In an effort to improve the properties of transparent conductors we have developed a range of multilayer coatings consisting of three to five alternating layers of metals and high refractive index dielectrics.

For the design and optimization of these coatings we have written and implemented a computer program for thin film optics, using the equations for electromagnetic fields propagating in these structures and the characteristic matrix formulation [4-5]. With this program we have predicted the optimum thickness of each film layer and located the most suitable materials [6]: ZnS was chosen to be used as a dielectric because of its high refractive index, ease of deposition and low cost. Of the metals tested, Ag was found to perform best due to its low absorption in the visible, with Cu being a close second.

We have used Physical Vapor Deposition techniques in order to prepare these coatings in our laboratory. An electron beam gun system was used for the deposition of the ZnS layers. The metal layers were thermally evaporated. All coatings were deposited on crown glass. The thickness of each film was monitored during deposition by a quartz crystal thickness measuring device.

The properties of the coatings designed and prepared by the procedures described above are presented next.

**ZnS/Ag/ZnS.** Typical properties of the prepared films are: Luminous transmittance: 0.84, emittance: 0.05, IR reflectance above 0.93, transition to high reflectivity at 0.8  $\mu\text{m}$ , sheet resistance: 6 to 10  $\Omega/\text{square}$ . The films can withstand the scotch tape test and heating up to 250  $^\circ\text{C}$  in air. In figure 1, the transmission spectra of the ZnS layer, the Ag/ZnS stack and the complete ZnS/Ag/ZnS multilayer are shown for an optimized coating deposited on glass. Comparison of the ZnS/Ag/ZnS coatings with the doped metal oxides reveals that the former exhibit a considerable improvement of all relevant properties apart from luminous transmittance, which is marginally lower.

**ZnS/Cu/ZnS.** Cu was used as a metal alternative to Ag. The optical characteristics of the Cu-based films are: Luminous transmittance: 0.672, emittance: 0.045. Compared to

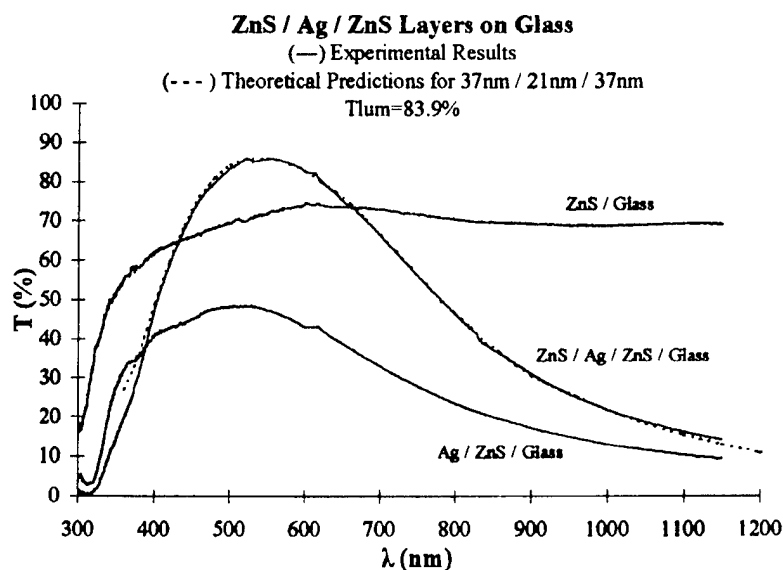


**Figure 1:** Layer build-up of a ZnS / Ag / ZnS film. Effect of each layer on the film transmittance.

equivalent ZnS/Ag/ZnS films, the Cu-based tandems exhibit inferior luminous transmittance due to the higher absorption of Cu in the visible and better emittance possibly due to better homogeneity of the metal lattice. The Cu-based films could be used in applications where the requirement for low emittance prevails and a moderate reduction in transmittance can be tolerated.

**ZnS/Cu/Ag/ZnS.** A thin layer of Cu (~2 to 5 nm) was added onto the Ag layer to test the hypothesis that combination of the two metals could also combine favorably their properties. The characteristics of the 4-layer films are: Luminous transmittance: 0.79, emittance: 0.04. Compared to equivalent ZnS/Ag/ZnS films, the 4-layer tandems exhibit inferior luminous transmittance and better emittance, possibly due to bridging of voids in the Ag lattice by the Cu layer. These films perform better than the Cu-based 3-layer ones, and can also be used in similar applications, ie where low-e is required and a small reduction in transmittance is acceptable.

**ZnS/Ag/ZnS/Ag/ZnS.** We have prepared 5-layer coatings with luminous transmittance equal to 0.67 and very low emittance: 0.02. These coatings exhibit a narrow band of high transmission (0.45 to 0.65 nm) and intense color ranging from blue to green. They can be used in applications where nearly zero emittance is required.

We also plan to prepare coatings incorporating alloys of metals such as Ag-Cu in various ratios of the two elements to investigate possible improvements in the film properties.

#### Acknowledgments

This work has been partially funded by the Commission of the European Communities, as part of the Joule Project: "Durable Peak Performance Evacuated Glazing", Contract No: JOR3-CT95-0038 (DG12 WSME).

#### References

1. Frank G., Kauer E., Kostlin H., *Thin Solid Films*, **77** (1981) 107-117.
2. Hamberg I. and Granqvist C. G., *J. Appl. Phys.*, **60**, 11 (1988) R123-R159.
3. Barlow F. Et. al., *Sol. Energy Mater. Sol. Cels*, **33** (1994) 63-71.
4. H. A. Macleod, *Thin Optical Filters*, Adam Hilger Ltd, (1969).
5. M. Rousseau (Ed.), *Problems in Optics*, Pergamon Press, (1973).
6. G. Leftheriotis, P. Yianoulis and D. Patrikios, *Thin Solid Films*, **306** (1997) 92-99.

## Estimation of the oxidation degree of vanadium in electrode materials on the basis of the $\text{NaV}_6\text{O}_{15}$

O.A.Smirnova, A.M.Mikhailova, M.A.Chernova, I.E.Shpach

Saratov State Technical University

Russia, Saratov

Vanadium bronzes are used as electrochemical active materials for different arrangements, for example, in current sources and solid state sensors. The technology of the preparation of active material and the choice electron conducting and binding materials has the major importance.

The stability of the electrode compositions (initial components and products of the electrochemical reaction) in time in dependence upon external conditions is more interesting.

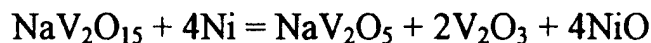
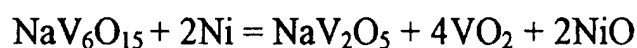
The scheme division of the phases and following determination of vanadium having the oxidation degree 3+, 4+ and 5+ in the vanadium bronzes is offered. The method is founded on the full solubility vanadium (5+) oxide in the 10% solution of the sodium hydroxide, limited solubility of the of the  $\text{VO}_2$  and full insolubility of the  $\text{V}_2\text{O}_3$ . The ion  $\text{V}^{5+}$  is determined by titration with  $(\text{NH}_4)_2\text{Fe}(\text{SO}_4)_2 \cdot 6\text{H}_2\text{O}$  salt, the ion  $\text{V}^{4+}$  is determined by titration with  $\text{KMnO}_4$  solution. The insoluble in the  $\text{NaOH}$  part of  $\text{VO}_2$  is determined as difference between the contents of  $\text{V}^{3+}$  and  $\text{V}^{4+}$  and contents of the  $\text{V}^{3+}$  in the precipitation. The contents of the  $\text{V}^{3+}$  is evaluated by titration with ammonium metavanadate solution in inert atmosphere. The summary contents of both  $\text{V}^{3+}$  and  $\text{V}^{4+}$  is determined by titration with  $(\text{NH}_4)_2\text{Fe}(\text{SO}_4)_2 \cdot 6\text{H}_2\text{O}$  salt after preliminary oxidation of the  $\text{V}^{3+}$  to  $\text{V}^{4+}$ .

How the X-ray analysis showed, the sodium-vanadium bronzes (with electron conducting and binding components) after thermic working up ( $T=823^\circ\text{K}$ ) in the argon atmosphere completely changed the structure.



The chemical analysis of such bronze shows presence of the ions  $V^{4+}$  and  $V^{5+}$  in equal proportion. The  $V^{3+}$  is absent. One is aware that compound of the type  $\beta$ - $M_xV_2O_5$  processes by ion and electron conductivity's. The last prevails and depends on concentrations of the vanadium (5+). The ion's conductivity of the  $\beta$ -phase is relatively low, equals to  $10^{-11} \Omega^{-1} \cdot m^{-1}$ . The chemical analysis of such bronzes consists of defining of the vanadium in the oxidation's degree  $V^{4+}$  and  $V^{5+}$ .

In the bronzes (with 30% carbonyl's nickel) after thermic working up the formation of compounds including the vanadium (3+) is possible:



The chemical analysis of the bronze, dissolved in the sulfur acid, shows the presence of the vanadium (3+) when the total and vanadium (4+) contents are defined. The investigations was carried out to adapt the method of solid state phase's polarographie (with carbon electrode) to defining of the degree of the oxidation of the vanadium in the bronzes. The working electrode was prepared by successive introduction in the carbon electrode of the components with different oxidation's degree. On the basis of the Volt-Ampere's dependencies the caliber's curve was formed.

However, we have failed in receiving of the reproduced peaks of the currents and the potentials for the phases with definite oxidation's degree, corresponding to caliber's curve. The absence of the maximums on the Volt-Ampere's curve shows the presence in the examined sample of co-presented phases with different oxidation's degrees and shows the influence of the carbonyl nickel (possessing the electrons conductivity) and of the liquid electrolyte.

## **Solid State batteries based on some Silver Bromide Solid Electrolytes**

**R.Chithra Devi and S.Selvasekarapandian**  
**Department of Physics, Bharathiar University**  
**Coimbatore - 641 046, INDIA**

### **ABSTRACT**

Development of new materials supports innovation of new technologies. A growing emphasis on energy conversion and alternative energy sources led to a good deal of research, especially to find better materials for batteries and electrochemical cell applications. High conductivity Solid Electrolytes appear to form the best among these new materials since these Solid electrolytes are devoid of corrosion, leakage and possess long shelf-life and can be operated over the extremes of temperature i.e., above boiling point and below freezing point temperatures of the liquid electrolytes. In this present study, a battery has been fabricated with newly synthesised materials based on Silver bromide solid electrolytes. The material selected for this study is  $\text{AgBr-PbX}_2\text{-Ag}_2\text{O-B}_2\text{O}_3$  where  $\text{X}=\text{Br}$  (a),  $\text{I}$  (b). The compound  $\text{AgBr-PbX}_2$  has been added as a dopant in the expectation of increasing the vacancies due to  $\text{Pb}^{2+}$  ions. The conductivity of the sample (a) and (b) are observed to be  $2.58 \times 10^{-4}$  and  $3.67 \times 10^{-4} \Omega^{-1} \text{cm}^{-1}$  with the activation energy of 0.61 and 0.14 eV at 10kHz respectively. Solid state cell have been constructed using these compounds and the open circuit voltage has been measured immediately after the construction of the cells and are found to be 632mV and 613mV and the short circuit current of 3.5  $\mu\text{A}$  and 55  $\mu\text{A}$  respectively at room temperature. Polarization studies have been carried out over the constructed cells for different load resistances 1 k $\Omega$ , 10 k $\Omega$  and 100 k $\Omega$  at room temperature. The variation is found to be linear one. The self-discharge and discharge under various loads have also been carried out over the cell and it has been found that the output voltage remains constant i.e., 616mV and 608mV for 30 days and then slowly reduced reaching the value of about 605mV and 595mV respectively. The drop in potential has been measured for every 60 minutes interval.

# PREPARATION, CHARACTERISATION AND APPLICATION OF FERRITES FOR GAS SENSORS.

C.V.Gopal Reddy, S.V.Manorama, V.J.Rao and P. Kanta Rao  
Materials Science Group,  
Indian Institute of Chemical Technology,  
Hyderabad 500007. India.

## Abstract:

The ever increasing need to check pollutants has increased the demand for development of sensors to monitor and detect several toxic and obnoxious gases. There is also an urgent need to control the ambients in mines, agriculture, chemical processes etc. Solid state devices based on semiconducting oxides play a vital role for this purpose, not only in terms of sensitivity to the gases but also in terms of reliability and cost effectiveness. Tin dioxide has been well studied as a sensor material to detect most of the reducing gases[1-3]. But the major problem associated with this material is its total lack of selectivity. Several novel materials are being tried with distinct and extraordinary gas sensing capabilities. It is our endeavor to prepare different ferrites ( $AFe_2O_4$ ) where A is Zn, Cu, Co, Ni etc. and study the gas sensing behavior with special emphasis to detect potentially toxic and not so well studied gases like chlorine etc.

The above compounds Ni, Cu and Co ferrites are soft ferrimagnetic materials with inverse spinel (trevorite) structure[4]. Where the application of these ferrites are for catalytic, magnetic or electrical[5] applications, high density materials are prepared by high temperature solid state reactions between finely the dispersed and ground constituent powders. Most of these applications demand ferrites in the form of ceramic materials with very high density. On the other hand, other applications like in the present as materials for gas sensors, for which lower density and higher surface area are preferred, there are several routes which have been adopted to prepare these spinels.

The present paper reports the results of our work pertaining to the preparation of ferrites for suitable gas sensing applications. The corresponding amounts of Zinc, Copper, Cobalt and nickel and Iron nitrates are taken in a 1:2 mole ratio along with 3 moles of citric acid and dissolved in de-ionised water with continuous stirring. This mixture was slowly evaporated and then dried in an oven at 120°C overnight. The dried material was crushed and calcined. The calcination temperature was different for each of the ferrites. In case of Nickel ferrite the crystalline single phase is formed above 550°C. So the material was calcined at 600°C whereas for Cobalt and Zinc ferrites the crystalline single phase formed started formation from 600°C but we had to go up to 900°C, for the completion of phase formation for cobalt ferrite and up to 800°C for Zinc ferrite. In case of Copper ferrite we got the single phase at 750°C. X-ray diffraction studies were used to confirm the structure and calculate the crystallite size using the Scherrer formula[6]. The homogeneity of the compound was also confirmed by XRD. The X-ray diffractograms were recorded on a Siemens/D.5000 X-ray diffractometer (Cu  $K_{\alpha}$  radiation  $\lambda=1.5406 \text{ \AA}$ ). The calculated crystallite size for the above compounds using the Scherrer formula are,

~275 Å for nickel ferrite, 196 for cobalt ferrite, 243 for zinc ferrite, and 200 Å for copper ferrite. Each of these materials was used to fabricate sensor elements in the following way. 2 wt% Poly-vinyl alcohol (PVA) was used as a binder to form a paste and the material was coated onto alumina tube substrates provided with platinum wire electrodes for electrical contacts. Finally, the sensor element was sintered at 600°C for 2h, to make it rigid and impart it ceramic properties. The electrical resistance of the element was measured in the presence and absence of the different test gases. For gas sensing measurements the sensor element was provided with a heater fixed inside the alumina tube coated with the sensor material. The schematic of the sensor assembly has been already described earlier[7]. The sensitivity,  $S$  is defined as the ratio of change in resistance of the sensor in presence of gas,  $\Delta R$  to the value of resistance in air,  $R_a$ .

$$S = \Delta R/R_a = |R_g - R_a|/R_a$$

It is observed that  $\text{NiFe}_2\text{O}_4$  shows a maximum sensitivity to chlorine up to 100ppm level at an operating temperature of 300°C. The cross sensitivity with other interfering, oxidising gases like  $\text{O}_2$ ,  $\text{Br}_2$  vapour and reducing gases like  $\text{H}_2\text{S}$ ,  $\text{H}_2$ ,  $\text{CO}$ ,  $\text{NH}_3$  and LPG are also studied. It is seen that this material shows very little response to reducing gases. The similar trend is followed in cobalt ferrite which also senses chlorine but at 350°C, in addition it also senses  $\text{H}_2\text{S}$  at 225°C. It is to be noted that each of these sensitivities are in reverse way because the former is an oxidising gas and the latter a reducing gas. In the case of Zinc and Copper ferrites it is seen that only reducing gases are detected. Different noble metals and metal oxides are added to these materials to improve the sensitivity and selectivity to the different test gases.

An attempt is being made to understand the exact mechanism of sensing in these different ferrites and to establish if there is any role of structure which is playing a role in the gas sensing behavior of these materials.

#### References:

- [1] Noboru Yamazoe, *Sensors and Actuators B*; 5, 7-19 (1991).
- [2] W.Gopel, K.D.Schierbarm, *Sensors and Actuators B*; 26-27, 1-12, (1995).
- [3] G.Sberveglieri, Ed. *Gas sensors: Principles, operation Developments*: Kluwer: Dordrecht, 1992.
- [4] V.P.M.Shafi Kurikka, Yuri Koltypin, Aharon Gedanken, R.Prozorou, J.Balogh, J.Lendvai, I.Felner, *J. Phys. Chem.*, **101**, 6409 (1997).
- [5] G.R.Dube and V.S.Darshane, *J. Mol. Catal.*, **79**, 285 (1993).
- [6] H.P.Klug, L.E. Alexander, *X-ray Diffraction Procedures for Polycrystalline & Amorphous Materials* (John Wiley, New York; Chapman & Hall, London), (1974), pp.491-492.
- [7] L. Satyanarayana, C.V.Gopal Reddy, S.V.Manorama and V.J.Rao, *Sensors and Actuators B*; **46**, 1-7 (1998).

# STRUCTURE AND PROPERTY OF $\text{MNi}_5$ SYSTEM WITH TIN SUBSTITUTION

Qin Lin, Shuang Zhao, Dajian Zhu, Ning Chen

(University of Science and Technology Beijing, Beijing 100083, China)

The structure and property of  $\text{MNi}_{5-x}\text{Sn}_x$  hydrogen storage alloy used for rechargeable batteries were studied to improve its performance and reduce cost.

## 1. Structure and hydriding properties

X-ray diffraction analysis indicates that  $\text{MNi}_{5-x}\text{Sn}_x$  ( $x \leq 0.5$ ) alloys present a hexagonal  $\text{CaCu}_5$  crystal structure without secondary phase. The cell volume  $V$  is a linear function of the Sn content.

$$V = (85.41 + 9.280x) \text{ nm}^3$$

The desorption plateau pressure ( $P_d$ ), enthalpy ( $\Delta H^\circ$ ), entropy ( $\Delta S^\circ$ ) and maximum hydrogen storage capacity ( $H/M$ ) of hydrogen storage alloys are listed in Table 1, which indicates that substitution of Sn for Ni in  $\text{MNi}_5$  or  $\text{LaNi}_5$  results in decrease of  $P_d$ ,  $\Delta H^\circ$ ,  $\Delta S^\circ$  and  $H/M$ .

Table 1. Thermodynamic Properties of  $\text{LaNi}_4.9\text{Sn}_{0.1}$  and  $\text{MNi}_{5-x}\text{Sn}_x$  (298K)

Alloy	H/M	$P_d$ (MPa)	$-\Delta H^\circ$ (kJ/mol)	$-\Delta S^\circ$ (kJ/mol)
$\text{MNi}_5$	5.7	0.22	28.1	90.8
$\text{MNi}_{4.9}\text{Sn}_{0.1}$	5.3	0.12	28.3	90.9
$\text{MNi}_{4.8}\text{Sn}_{0.2}$	5.1	0.10	29.4	94.3
$\text{MNi}_{4.7}\text{Sn}_{0.3}$	4.9	0.08	31.0	99.2
$\text{MNi}_{4.6}\text{Sn}_{0.4}$	4.8	0.06	32.5	103.8
$\text{LaNi}_{4.9}\text{Sn}_{0.1}$	5.8	0.09	31.7	106.1
$\text{LaNi}_5^{[2]}$	6.0	0.16*	30.10	105.0
$\text{LaNi}_{4.8}\text{Sn}_{0.2}^{[3]}$	—	0.048	34.50	109.7

\* 293K

Based on atomic parameters (electronegativity  $\Delta X$ , atomic size  $\delta$  and electron concentration  $e/a$ , et al.) of element and experimental data of plateau pressure of  $\text{LaNi}_{5-x}\text{M}_x$ , a calculation model of standard enthalpy of hydride formation ( $\Delta H^\circ$ ) was established by stepwise regression method. The model is given following

$$\Delta H^\circ = -1.611 \times 10^5 - 4.485 \times 10^5 (\Delta X)^2 + 3.617 \times 10^6 \delta^2 + 1.151 \times 10^4 (e/a)^{2/3}$$

It shows that both of lower electron concentration and atomic size and larger average difference of electronegativity all make the enthalpy of hydride formation more negative which means the hydride more stable. The calculated enthalpy of hydride formation of  $\text{LaNi}_{4.9}\text{Sn}_{0.1}$  is  $-30.6 \text{ kJ/mol}$ , which consists with experimental value  $-31.7 \text{ kJ/mol}$ .

According to the model the main influence factor on  $\Delta H^\circ$  is average electron concentration related to the outer orbit electrons of atoms in the alloys. The lower electron concentration, when Ni is substituted by Sn in  $\text{LaNi}_5$  (or  $\text{MnNi}_5$ ), leads to lower Fermi energy<sup>[4]</sup>, which plays essential role in the performance of alloys.

## 2 Electrochemical Characteristics

The electrochemical performance was tested with plate cells. Charge and discharge were carried out with current  $180 \text{ mA/g}$  ( $0.5 \text{ C}$  rate) or  $360 \text{ mA/g}$  ( $1 \text{ C}$  rate) and cut off voltages  $1.7 \text{ V}$  and  $0.9 \text{ V}$  respectively.

The results show that maximum discharge capacity decreases and cycle life increases with Sn content increase in  $\text{MnNi}_{5-x}\text{Sn}_x$  alloy. In lower Sn content, such as  $x = 0.2$ , the cycle life increases by  $52\%$  ( $0.5 \text{ C}$ ) or  $42\%$  ( $1 \text{ C}$ ), but maximum discharge capacity decreases only by  $3\%$  and  $3.5\%$  respectively. The increase of the cycle life was explained by considering the increase in the unit cell volume of  $\text{MnNi}_{5-x}\text{Sn}_x$  caused by Sn substitution<sup>[5]</sup>

## References

- [1] Lin Qin, Li Rong, Ye Wen, Chen Ning, Liu Renmin.  
*Acta Metallurgica Sinica*, **32**, 624 (1996).
- [2] C. E. Lundin, F. E. Lynch and C. B. Magee  
*Journal of the Less—Common Metals*, **56**, 19 (1977).
- [3] R. C. Bowman, C. H. Luo, C. C. Ahn, C. K. Witham, B. Fultz  
*J. Alloys Comp.*, **217**, 185 (1995).
- [4] Xiao Jimei, "The subject of Alloy Energy"  
Metallurgy Industry Press, Beijing, 1990, 256.
- [5] J. J. G. Willems, *Journal of the Less—Common Metals*  
**129**, 13 (1987).

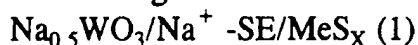
# THE LOW TEMPERATURE SOLID-STATE SENSOR OF H<sub>2</sub>S BASED ON SOLID ELECTROLYTES.

Yu.Dobrovolsky, L.Leonova, N.Tkacheva, A.Levchenko<sup>†</sup>

Institute for New Chemical Problems RAS, Chernogolovka, Russia

<sup>†</sup>Moscow State University, Moscow, Russia

Was earlier shown [1], that the solid electrochemical cells with Na-conducting electrolytes and sulphide semi-conductor electrodes are capable selectively respond to change of H<sub>2</sub>S concentration in air. In the given work the behavior of cells



(where Na<sup>+</sup>-SE Na-conducting solid electrolytes such as NASICON, b-alumina and silicate of rare-earth metals, MeS<sub>x</sub> - semi-conductor sulphide) in air containing H<sub>2</sub>S at natural temperatures (-50 - +60°C) is investigated.

Is shown, that all investigated solid electrolytes can be used as ion membrane in electrochemical cells such as (1). The nature of the solid electrolyte does not render essential influence on sensitivity of the cell and response time at change of H<sub>2</sub>S

concentration, however relaxation speed of the cell depends on their chemical stability. Most chemically steady in damp air containing environment and H<sub>2</sub>S has appeared NASICON, which was used in the further investigations.

As sensitive electrodes the materials were investigated on the basis of semi-conductor sulphide of metals with a various type

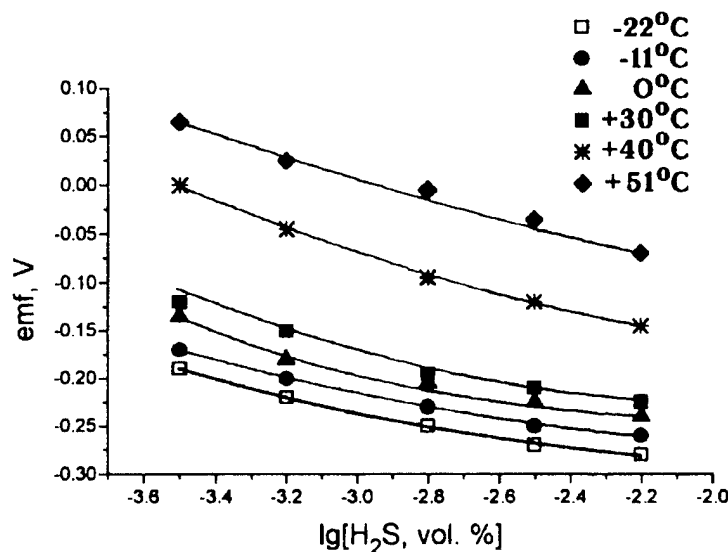


Fig 1. The dependence of the emf of the cell (1) on H<sub>2</sub>S concentration at different temperatures.

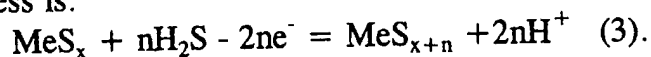
of conductivity. Is shown, that sulphide with n-type conductivity is tolerant to the contents of H<sub>2</sub>S, whereas sulphide p-type semiconductors with wide area of homogeneity change their potential at presence of H<sub>2</sub>S. Optimum on speed and sensitivity there were electrodes on a PbS p-type basis, which were used at study of the sensor structure characteristics.

The optimized sensor cells are sensitive to change of H<sub>2</sub>S concentration in air from 1 up to 100 ppm. The dependence of sensor emf from concentration of the H<sub>2</sub>S in air has no-Nerstian character and is described by logarithmic second order polinoma:

$$E = E_0 + a \cdot \lg[H_2S] + b \cdot (\lg[H_2S])^2 \quad (2).$$

The factors E<sub>0</sub>, a and b of this equation are determined by chemical structure and specific surface of a working electrode and can be received by calculation of the adsorption factors in chemical activity [2].

On the basis of the carried out investigations it is possible to assume, that the potential defining process is:



Relaxation of the such sensor emf on change of the H<sub>2</sub>S concentration in air has diffusion character and is determined by chemisorption processes on a surface of an electrode. Temperature dependence of the emf sensor (fig. 1) has complex character and also, probably, is determined by chemisorption processes.

This work was supported by the Russian Foundation for Basic Research (Projects N 96-03-33123a).

#### References.

- [1]. L.Leonova, Yu.Dobrovolsky, E.Ukshe, Metrologiya (in Russian) **6**, 45 (1991)
- [2]. Yu.Dobrovolsky, L.Leonova, A.Vakulenko, Solid State Ionics **86-88**, 1017 (1996)



# IMPEDANCE SPECTROSCOPY INVESTIGATIONS ON POLY-(N,N-DIMETHYLPROPARGYLAMINE) AS HUMIDITY SENSOR

E. Quartarone, P. Mustarelli, A. Magistris

Department of Chemistry, University of Rome 'La Sapienza', P.le A. Moro, 5  
00185 - Rome, Italy

M.V. Russo, I. Fratoddi, A. Furlani

Department of Physical Chemistry, University of Pavia, Via Taramelli, 16-27100- Pavia, Italy

Recently, many researchers have investigated the use of organic polymeric membranes for sensors, because of their promising performances and their low-cost processing [1]. In particular  $\pi$ -conjugated polymers, as poly-thiophene, poly-pyrrole, polyaniline, seem to show a wide range of sensitivity, with a fast and reproducible response, upon their exposure to various gases [2], but mostly to the moisture [3]. In particular, water content causes relevant effects on the electrical response of these types of polymers, and such property can be used in the preparation of humidity sensors, based on polymeric thin films.

The influence of the degree of moisture on the electrical conductivity is a measure of the sensor "goodness". It is strictly related to parameters like their chemical structure and surface morphology, which involve the adsorption/desorption process of  $H_2O$  molecules [4, 5]. Studies on both inorganic [5, 6] and polymeric sensors [7] have related the dependence of the impedance from moisture to the presence of protons/ hydroxyl ions on their surface. Impedance Spectroscopy is a powerful technique to understand the conduction mechanisms in the sensors and to define equivalent circuit models for the behaviour of these devices.

In this work we present an Impedance Spectroscopy study of a thin film of poly(N,N-dimethylpropargylamine) (PDMPA) between ~0% and 92% of relative humidity. PDMPA has been obtained from N,N-dimethylpropargylamine by reaction with a 1/100 catalyst/monomer ratio in a ethanol/chloroform mixture. The deposition of the thin film has been carried out by spin coating at 2000 r.p.m. for 30 seconds on a silicon substrate, where interdigitated electrodes were previously photolithographically defined. The humidity control has been obtained by using saturated solutions of salts at 20 °C in a glass vessel, where the circuit was placed and let to equilibrate before the impedance measurements. The resulting Nyquist plots, collected in the frequency range of 100 kHz-10 mHz consist of a regu-

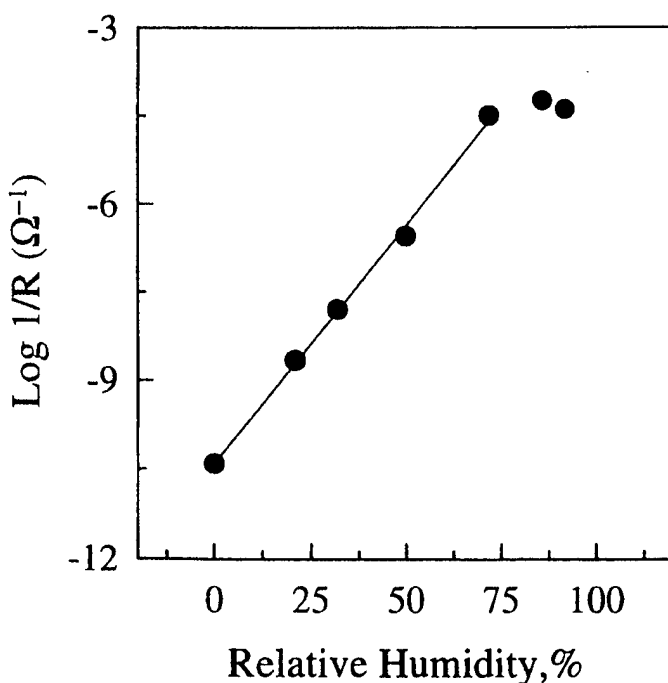


Fig. 1 - Dependence of log of the conductance as a function of the relative humidity for a PDMPA-based thin film sensor

lar semicircle and a straight line at each relative humidity value.

The measurements have proved a well reproducible and linear dependence of the impedance logarithm from the moisture content over a wide range of R.H., whereas the sensor capacity remains constant in the whole range of humidity. This effect results in a current increase of about 6 orders of magnitude, as reported in Fig. 1. In the R.H. range from 0 to 70%, thin films of PDMPA present good performances as humidity sensors. Higher moisture contents cause a sensitivity loss due to saturation effects.

- [1] G. Harsányi, "Polymer Films in sensor applications" Technomic Publishing AG, Switzerland 451 pages (1995).
- [2] J. P. Blanc, N. Derouiche, A. El Hadri, J.P. Germain, C. Maleysson, H. Robert, *Sensor and Actuators B* **1** 130 (1990).
- [3] J.P. Travers, M. Nechtschein, *Synth. Met.* **21** 135 (1987).
- [4] A. Boyle, E.M. Geniès, M. Lapkowski, *Synth. Met.* **28** C769 (1989).
- [5] P. Altamura, A. Bearzotti, A. d'Amico, V. Foglietti, I. Fratoddi, A. Furlani et al., *Mat. Sci. and Eng. C* **5** 217 (1998).
- [6] M. J. Hogan, A. W. Brinkman, T. Hashemi, *Appl. Phys. Lett.* **72** 3077 (1998).
- [7] MR. Yang, KS. Chen, *Sensors and Actuators B-Chemical*, **49** 240 (1998).

# A NEW FAMILY OF GAS-SENSITIVE IONIC CONDUCTORS WITH RESISTIVITY AGAINST A SOLUBLE GAS

O. Glumov, I. Murin,

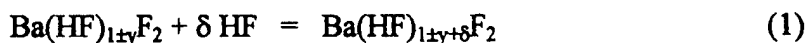
*St. Petersburg State University, Universitetskij pr. 2, 198904 St. Petersburg, Russia*

H.-D. Wiemhöfer

*Westf. Wilhelms-University, Inorg.-Chem. Institute, Wilhelm-Klemm-Str. 8, D-48149 Münster*

There is a tremendous interest in electrochemical sensors for environmental, technological and scientific reasons. Sensors are divided by their mode of measurement into potentiometric, amperometric, and conductometric. In most chemical sensor devices, interfaces play an essential role. Whereas the dependence of the bulk defect concentration on the component activity may be used at high temperature to sense the latter quantity, at lower temperature the partial electronic contact equilibrium, and thus enrichment or depletion of electronic-charge carriers, can be used to measure activity of redox-active species in the neighbouring phases. Accordingly, in commercially available  $\text{SnO}_2$  sensors the decrease (increase) of n-type-conductivity in the boundary regions reveals the presence of oxidizing (reducing) gaseous species [1]. The analogy of electronic and ionic conductors suggests the use of ionophilic (ionophobic) interactions of gas molecules to detect the partial pressure of the interacting gas species via the change of ionic boundary conductance [2].

Many fluorides with high F<sup>-</sup> mobility have been investigated with regard to their potential applications in electrochemical devices, particularly in low temperature sensors [3]. In this contribution, the sensor properties of the solid electrolyte  $\text{Ba}(\text{HF})\text{F}_2$  are studied. The change of the concentration of dissolved dipolar HF molecules changes the concentration and/or mobility of the ionic defects in the solid electrolyte  $\text{Ba}(\text{HF})\text{F}_2$  and therefore its electric resistance. The equilibrium of HF molecules between the gas atmosphere and the solid electrolyte is described by:



The appearance of additional neutral HF molecules with high dipole moment changes the electrostatic interaction between HF,  $\text{Ba}^{2+}$  and  $\text{F}^-$  ions and explains relaxation of the electrostatic bond between  $\text{Ba}^{2+}$  and  $\text{F}^-$  ions in  $\text{Ba}(\text{HF})\text{F}_2$  crystals. Thus, if reaction (1) is reversible, the change of the HF concentration in the gas phase results in a corresponding change of the electric resistance (or ionic conductivity) of  $\text{Ba}(\text{HF})\text{F}_2$ .

$\text{Ba}(\text{HF})\text{F}_2$  was prepared nominally pure and  $\text{Gd}^{3+}$ -doped, i.e.  $\text{Ba}(\text{HF})\text{F}_{2-x}\text{GdF}_3$  ( $x = 0.1$  mol.%; 1 mol.%). The impedance spectra of the polycrystalline membranes were studied with gas-tight reversible electrodes based on  $\text{Sn}, \text{SnF}_2$  in the temperature range between 20°C and 130°C. The bulk conductivity of the solid electrolyte membranes was calculated from the analysis of impedance spectra (see Figure) which is predominated by the electrolyte bulk resistance. The activation enthalpy was obtained from an Arrhenius plot of the conductivity. The ionic conductivity of as-prepared and pressed pure  $\text{Ba}(\text{HF})\text{F}_2$  is of the order  $10^{-9}$  S/cm at room temperature and exceed values of  $10^{-6}$  S/cm at temperatures above 130 °C. The activation enthalpy of conductivity is  $\Delta H_a = 0.55$  eV. The doping of  $\text{Ba}(\text{HF})\text{F}_2$  by  $\text{GdF}_3$  resulted in an increase of conductivity by a factor of ~4. Impedance spectra of  $\text{Ba}(\text{HF})\text{F}_2$  membranes were studied in an inert  $\text{N}_2$  atmosphere with various HF concentrations in the range  $10^{-5}$ – $10^{-3}$  mol./l. The bulk resistance of  $\text{Ba}(\text{HF})\text{F}_2$  membranes decreased in HF atmospheres. Impedance spectra of

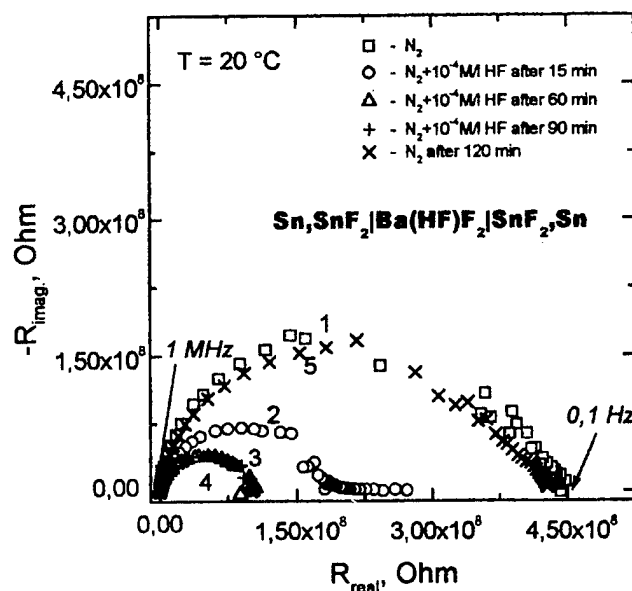


Figure: Impedance spectra of the cell  $\text{Sn,SnF}_2|\text{Ba(HF)F}_2|\text{SnF}_2,\text{Sn}$  at room temperature for pure  $\text{N}_2$  and HF-containing  $\text{N}_2$  gas atmospheres.

bonds. The time dependence of impedance of  $\text{Ba(HF)F}_2$  is explained by bulk diffusion of HF-molecules in the membrane. The reproducibility of the impedance spectra before and after exposing the membrane to HF confirms reversibility of the proposed reaction (1).

The obtained results demonstrate, that the investigated solid electrolyte material  $\text{Ba(HF)F}_2$  can be considered as a member of a new family of complex ionic sensor materials. We will give a brief outlook on applications.

This work was supported by DAAD.

$\text{Ba(HF)F}_2$  membranes are shown in the Figure as a function of the gas composition ( $\text{N}_2 \rightarrow \text{N}_2 + 10^{-4} \text{ mol./l HF} \rightarrow \text{N}_2$ ).

The HF molecules are expected to interact with the  $\text{Ba}^{2+}$ -cations by electrostatic charge-dipole interaction. This may weaken the interaction to surrounding  $\text{F}^-$  ions and thus increase their mobility. However, further investigations have to be carried out to check out the relative role of molecular HF or HF dissociation with accompanying proton mobility on the ion conductivity and the HF transport. The latter, dissociation of HF and movement of the resulting ions, would be an example for a Grotthuss mechanism being favored by the tendency of HF to form hydrogen

[1] J. Janata, Principles of Chemical Sensors, Plenum Press, New York, 1989.

[2] J. Maier, Solid State Ionics **62**, (1,2), 105 (1993).

[3] S. Harke, H.-D. Wiemhöfer and W. Göpel, Sensors and Actuators, **B1**, 188 (1990).

## POST-MORTEM CHARACTERISATION OF ONE YSZ OXYGEN SENSOR

C.M. Rodrigues<sup>(1)</sup>, J.A. Labrincha<sup>(2)</sup>, F.M.B. Marques<sup>(2)</sup><sup>1</sup>ESTG, Polytechnic Institute of Viana do Castelo, Apt. 574, 4900 Viana do Castelo, Portugal<sup>2</sup>Dept. of Ceramics and Glass Engineering, UIMC, University of Aveiro, 3810 Aveiro, Portugal

The use of oxygen sensors based on yttria stabilised zirconia (YSZ) is common in many industrial processes, where the oxygen partial pressure might affect some properties and/or processing steps. In glass-making furnaces, the control of combustion efficiency and of the colour of the glass might require the use of these devices. The aggressive working conditions inside the furnace require a careful placement of the sensor in protected zones, but even in this case the average lifetime is normally short (a maximum of about 6 months). Early detection of sensor failure might prevent difficulties in the process control.

The present work includes the analysis of a zirconia-based sensor after a long exposure to the atmosphere of an industrial glass-making furnace. The final goal was the identification of the causes for sensor failure and possible correlation between the results obtained with these post-mortem tests and previous information obtained from laboratory-scale experiments. These experiments, performed on the degradation of the electrolyte included the study of intimate mixtures of YSZ and glass powders, and the study of YSZ pellets covered by a layer of glass, in all cases submitted to different annealing treatments. Impedance spectroscopy (IS) proved to be a useful technique to monitor the electrolyte degradation process. In fact, after attack by the glassy phase, new interfaces develop inside the electrolyte (YSZ/glass), with specific electrical responses. IS measurements evidenced a large increase in the intermediate frequency arc (usually ascribed to the grain boundary contribution) and a shift in the relaxation frequency of this arc to lower values [1,2].

Figure 1 shows a schematic view of the commercially available oxygen sensor used in the present study, including one closed-end YSZ tube and one open-end alumina tube, the latter used for protection. The selected portions of the tube used in this study (and their distance from the hot-end part) are shown as shadowed areas. Pt electrodes (from nr. 1 to 12) were painted in these areas to perform impedance spectroscopy (IS) measurements. XRD and SEM/EDS analysis were also performed to detect phase transitions and/or the presence of new compounds. Two different regions were observed, defined by clear differences in colour and by the presence (or absence) of cracks. The boundary between these two zones was close to the 10<sup>th</sup> electrode. From that point to the hottest and most exposed part (electrode nr. 1), formation of monoclinic grains and the presence of a glassy phase were clearly observed (Figure 2). The cubic/tetragonal → monoclinic phase transformation induces strong stresses in the material and is responsible for the formation of cracks in the sintered body. In the colder zone, no cracks were found and the formation of monoclinic grains is incipient.

Electrical degradation of the sensor in the attacked zone is also clearly evidenced in the impedance spectra shown in Figure 3. From the 12th to the 2nd electrode (moving from the sensor cold-end to the hot-end) a strong increase in (specific) resistance was observed as well as a shift in relaxation frequency towards lower values. This could be partly attributed to the formation of the less conductive monoclinic phase, but mainly to the presence of cracks and glass in the intergrain region. Both effects are known to cause significant changes in the impedance spectra, namely in the low-intermediate frequency range [1-3]. IS spectroscopy can thus be used to check the sensor condition, with the specific advantage that these tests can be performed in-situ, with only some cooling of the sensor electroded area.

[1] C.M.S. Rodrigues, J.A. Labrincha, F.M.B. Marques, *J. Eur. Ceram. Soc.*, 18 (1998) 95.

[2] C.M.S. Rodrigues, J.A. Labrincha, F.M.B. Marques, *J. Electrochem. Soc.*, 144, 12 (1997) 4303.

[3] L. Dessemond, *Impedance Spectroscopy of Cubic-Zirconia with Cracks*, Ph.D. Thesis, INP Grenoble (1992)

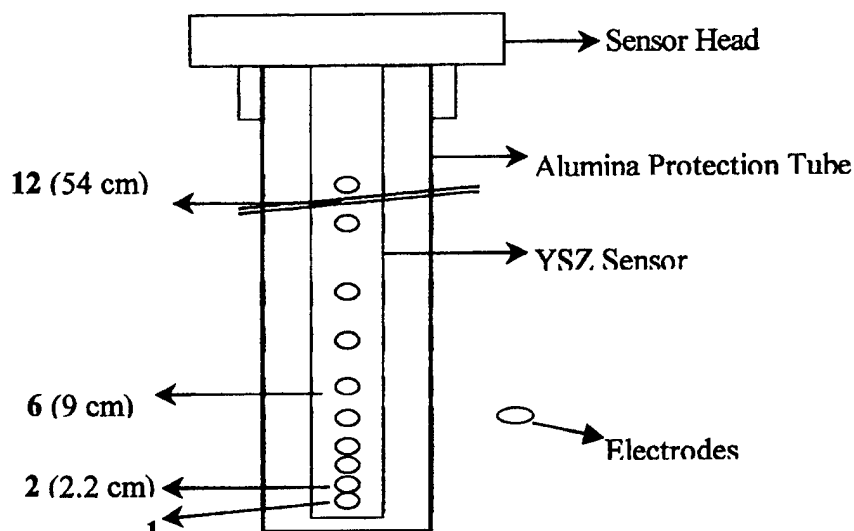


Figure 1 – Schematic view of the sensor and protection tubes, including the relative position of several painted Pt electrodes used for electrical characterisation (between brackets there is the distance from the hot end extreme of the sensor).

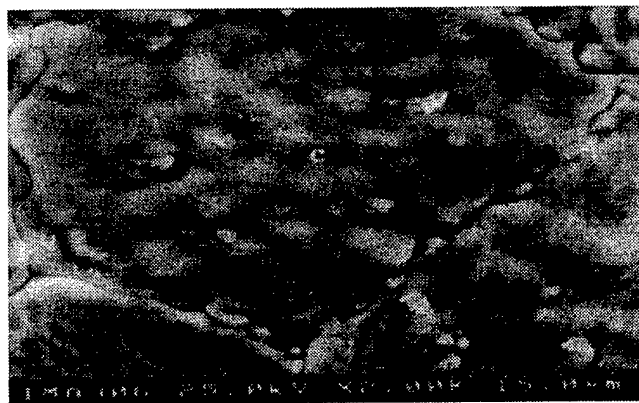


Figure 2 – SEM analysis of electrode 8, showing large cubic grains (C), small monoclinic grains (M), and a glassy-phase (V).

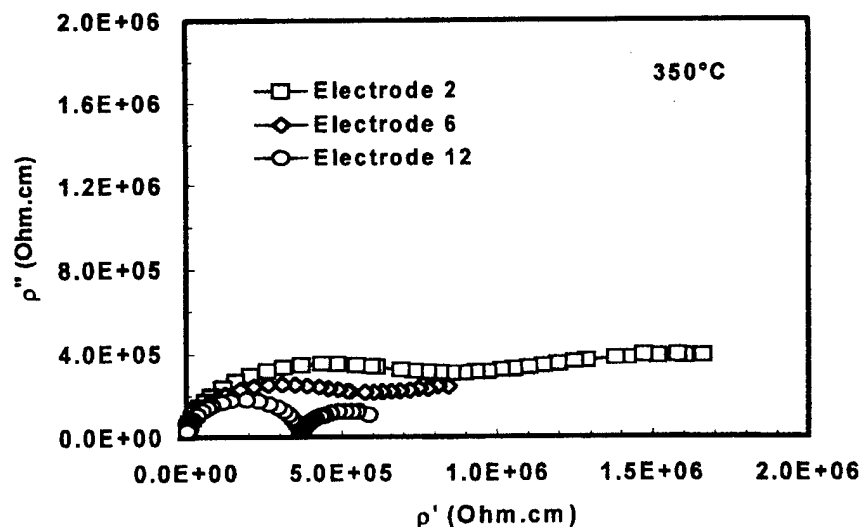


Figure 3 – Impedance spectroscopy (20-10<sup>6</sup> Hz) obtained at 350°C for electrodes placed in different positions along the sensor tube (see Figure 1).

## RECENT STUDIES OF ELECTROCHEMICAL PROMOTION USING ALKALI ION CONDUCTORS

**Richard M. Lambert**

Chemistry Department, Cambridge University  
Cambridge CB2 1EW England

The NEMCA phenomenon, also referred to as electrochemical promotion (EP), discovered, developed and discussed extensively by Vayenas and his school has been applied to a wide variety of catalytic systems, including reactions taking place in solution. These studies have illuminated many important aspects of the underlying phenomena and laid the basis for a fundamental understanding of the NEMCA effect. The present paper has two principal aspects, as follows. On the one hand we describe the applications of NEMCA to catalytic systems that are of particular interest in pure or applied chemistry. Among other things, these observations illustrate the diversity of the catalytic chemistry that can be explored by electrochemical promotion. They also show how such promotion leads to major beneficial changes in catalytic performance and how such findings can aid the design and development of practical catalytic systems. In addition, we present the results of pertinent spectroscopic experiments on NEMCA catalysts and of related measurements on single crystal specimens under conditions of ultra high vacuum. The single crystal measurements enable us to examine specific issues raised in the study of electrochemical modified systems. These investigations are aimed at improving our knowledge of the phenomena involved in the electro-pumping of promoter species to the surface of a working electrode; they also shed light on the chemical state of these species under reaction conditions. Thus, as described below, we have examined the surfaces that develop on working electrodes under reaction conditions by means of XPS, SEM, STM, XANES and time-resolved photoelectron microscopy. All our work has involved the use of either Na- $\beta$ " alumina or K- $\beta$ " alumina as solid electrolytes; much of it is aimed at applying electrochemical promotion to the reduction of NO by CO or propene, reactions that are of major importance with respect to emissions abatement and environmental protection. The following examples illustrate the versatility and utility of electrochemical promotion; fundamental aspects of the phenomenon are also addressed.

1. The Pt-catalysed reduction of NO by CO exhibits strong electrochemical promotion (EP) by backspillover Na supplied from  $\beta$ " alumina under appropriate conditions of temperature, gas composition, and catalyst potential. At high CO partial pressures ( $P_{CO}$ ) the EP effect is attenuated by CO island formation and limited availability of chemisorbed NO. At low  $P_{CO}$ , the CO+O reaction is limited by the low coverage of CO and the EP effect is again relatively small. In the intermediate  $P_{CO}$  regime, Na pumping strongly accelerates the reaction: rate gains in excess of one order of magnitude for  $N_2$  production, relative to the unpromoted rate are observed. This can be understood in terms of Na-induced dissociation of chemisorbed molecular NO, which is thought to be the reaction initiating step. The overall kinetic behaviour and the dependence of  $N_2/N_2O$  selectivity on catalyst potential are in good accord with this hypothesis. Thus the EP system also provides direct information about the nature of the reaction mechanism under conditions of elevated pressure.

2. Metal-catalysed reduction of NO by propene is a more demanding reaction. Furthermore, it is more important from a technical point of view with respect to the abatement of  $NO_x$  emissions. Once again, the system exhibits strong electrochemical promotion by spillover Na supplied from a  $\beta$ " alumina solid electrolyte. In the promoted regime, large rate increases are observed. At sufficiently high loadings of Na the system exhibits poisoning, and excursions between the promoted and poisoned regimes are fully reversible. Reaction kinetic data obtained as a function of catalyst potential, temperature and gas composition indicate that Na increases the strength of NO chemisorption relative to propene. This is accompanied by weakening of the N-O bond, thus facilitating NO dissociation which process is again proposed as the critical reaction initiating step. XPS data confirm that electrochemical promotion of the Pt film does indeed involve reversible pumping of Na to or from the solid electrolyte. They also show that under reaction conditions the promoter phase consists of a mixture of Na nitrite and Na nitrate and that the promoted and poisoned conditions of the catalyst correspond to low and very high

loadings of these sodium compounds. Under all reaction conditions, a substantial fraction of the promoter phase is present as 3D crystallites.

3. The interpretation of the EP effect offered above depends on the Na-induced dissociation of chemisorbed NO. In effect, we argue that EP causes Pt (a poor NO dissociation catalyst) to behave like Rh (a good NO dissociation catalyst). This hypothesis has been tested by appropriate Monte Carlo simulations, as follows. An irreversible surface reaction lattice-gas model for the reaction of carbon monoxide and nitric oxide on a Na-modified Pt(111) surface was investigated. The effect of Na adatoms on the reaction kinetics was examined in terms of a "local" (i.e. short-range) model for alkali-promoted NO dissociation. Within this framework we also studied the effects of extending the range of alkali-induced NO dissociation from nearest neighbour to next nearest neighbour sites. The influence of varying amounts of sodium on overall catalytic activity, reaction kinetics, and on the  $N_2/N_2O$  selectivity were then investigated. It was found that the principal features of the experimental data for electrochemical promotion by Na of the CO+NO reaction over Pt are satisfactorily accounted for in terms of this model.

The insight into reaction mechanism and mode of promoter action provided by the above studies has stimulated the development of new, non-Rh, dispersed catalysts for NO reduction by hydrocarbons. Thus we have shown that conventional Na promotion of Pd particles supported on yttria-stabilised zirconia leads to large gains ( $\sim \times 10$ ) in catalytic activity accompanied by substantial gains in  $N_2/N_2O$  selectivity. In the case of Na-promoted Pt particles on  $\gamma$ -alumina, the results are even more spectacular. Rate gains of two orders of magnitude and huge increases in  $N_2/N_2O$  selectivity. In both cases, the activity and selectivity response to Na promotion of the conventional catalysts mirrors that of the relatively well understood EP catalysts.

4. As might be anticipated, the chemical state of the electrochemically supplied Na promoter depends on the gas environment. As noted above, in NO/propene atmospheres, the Na is present on the surface of the working electrode as a mixture of nitrate and nitrite. Thus while the catalytic combustion of propene by oxygen also shows strong EP effects (promoted and poisoned regimes) the Na surface compounds present are quite different. The formation, chemical identity, stability and electrochemical decomposition of these Na surface compounds produced in the promoted and poisoned regimes have been explored using post-reaction XPS, AES, and, for the first time, post-reaction Na K-edge XAFS. The results indicate that thick layers consisting of sodium carbonate are responsible for catalyst poisoning, whereas the promoter phase consists of smaller amounts of sodium carbonate and much of this material is present as three dimensional crystallites. These promoter and poisoning phases are stable at reaction temperature, but rapidly destroyed by electro-pumping Na away from the catalyst surface. Their direct participation in the electrochemically promoted reaction is thereby demonstrated.

5. Finally, the applicability of electrochemical promotion (EP) has been extended to an investigation of the Pt-catalysed hydrogenation of acetylene to ethylene and ethane, the first example of the use of EP in catalytic selective hydrogenation. The system exhibits strong promotion by spillover Na supplied from a  $\beta$ -alumina solid electrolyte. In the hydrogen-rich regime, reversible, potential-dependent, increases in ethylene selectivity of an order of magnitude are achievable under the influence of  $\sim 0.02$  monolayers Na, while maintaining high acetylene conversion. Butenes, butadiene and benzene are observed as minor products whose formation is also promoted by Na. The principal findings can be accounted for in terms of a simple reaction model based on the destabilising effect of charge transfer from Na to adsorbed ethylene: by weakening the chemisorption of the latter, desorption is favoured over further hydrogenation to ethane. Thus EP by Na induces Pt, normally a poor selective hydrogenation catalyst, to behave like Pd. Similar data obtained using K- $\beta$  alumina as the solid electrolytes enable one to address whether the chemical identity of the



# ELECTROCHEMICAL PROMOTION OF MO<sub>2</sub>-CATALYSTS FOR THE GAS PHASE COMBUSTION OF C<sub>2</sub>H<sub>4</sub>

S. Wodiunig, J. Nicole, E. Varkaraki and C. Comninellis

Institute of Chemical Engineering, Swiss Federal Institute of Technology, CH-1015 Lausanne, Switzerland

The combustion of volatile organic compounds (VOC) is still of high interest to comply with the emission limits into the environment. Emission sources are wide spread and vary from industrial waste air to motor vehicle exhaust fumes and oil heating systems. The research of new and more efficient catalysts is still the most common way to reduce the emission. The non-Faradaic electrochemical modification of catalytic activity (NEMCA) which was discovered at the end of the 80ies by Vayenas et al. [1] opens new possibilities for the reduction of such emissions.

The electrochemical promotion (EP) of metal oxides has been studied since the beginning of the 90th in our laboratories. More exactly, it has been studied with IrO<sub>2</sub> [2-5] and RuO<sub>2</sub> [6-8] catalysts for the gas phase combustion of ethylene.

The catalyst films were prepared by thermal decomposition of the corresponding chloride dissolved in 2-propanol. Ytria stabilised zirconia (YSZ) plates were used in all cases as electrolyte and as catalyst support. The optimal decomposition temperature was found to be at 550°C. The catalyst films were characterised by XRD, XPS, SEM. The counter and pseudo reference electrode consisted in all cases of pure gold deposited onto the YSZ-plate on the other side of the catalyst which is used as working electrode.

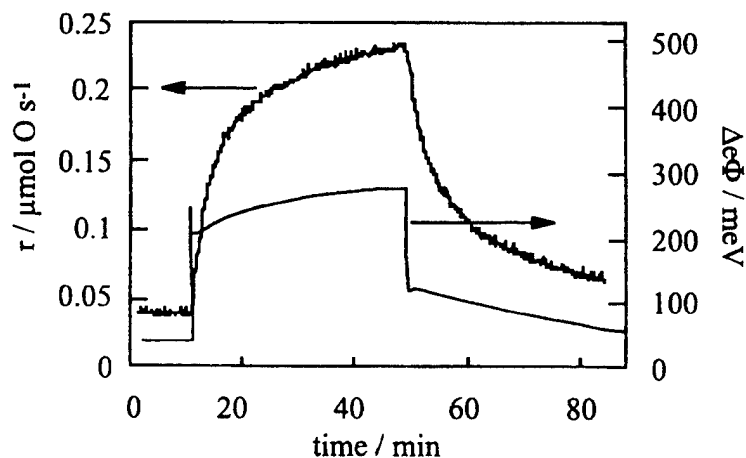
The electrochemical promotion was studied in a constant flow stirred tank reactor (CSTR). The reactor and the experimental setup are described elsewhere [2, 6, 8].

The origin of the EP was studied by work function measurements using the Kelvin Probe method [4, 6] (Fig.1), temperature programmed desorption (TPD) of oxygen [7], measurements of the voltammetric charge [2] and kinetic steady state measurements [8]. The importance of these measurements for the understanding of the mechanism of the EP and the differences between IrO<sub>2</sub> and RuO<sub>2</sub>-catalysts will be discussed.

Recently Nicole and Comninellis [3] proposed a two step mechanism for the EP of IrO<sub>2</sub> catalysts. In a first step the IrO<sub>2</sub>/YSZ interface is polarised and an electrochemical double layer is formed at the interface. Under these conditions O<sup>2-</sup>-ions are discharged according to eq. 1.

Fig. 1:

Temporal evolution of the change of the work function ( $\Delta\phi$ ) and the catalytic rate ( $r$ ) during a galvanostatic step of 100  $\mu$ A during 40 minutes.  $P_{C_2H_4}=0.114$  kPa,  $P_{O_2}=17.7$  kPa,  $V=175$  ml min<sup>-1</sup> STP,  $T=386^\circ$ C.





The  $\text{O}^-$ -ions then migrate over the gas exposed catalyst surface (backspillover oxygen) causing an increase of the catalyst work function. The increase of the work function affects the catalytic activity of the  $\text{IrO}_2$ -film. This first step can also be described as a two step mechanism with a electrochemical activation due to the polarisation and a physical activation due to the backspillover of oxygen ions.

In a second step the backspillover oxygen ions might react with the catalyst forming a higher oxide as shown in eq. 2.



The permanent promotion which was observed for  $\text{IrO}_2$ -catalyst [3] is explained by the formation of this higher oxide.

The influence of the formation of backspillover oxygen ions on the catalyst work function during a galvanostatic transient and the correlation between the work function and the ohmic drop free catalyst potential will be discussed. The effect of the observed work function changes on adsorbed oxygen was studied by TPD measurements. It will be shown that the polarisation of the catalyst/YSZ interface induce a change in the binding strength of adsorbed oxygen which was measured via the desorption activation energy. The importance of the formation of the electrochemical double layer at the catalyst/YSZ interface was studied by cyclic voltammetry measurements. The dependence of the film thickness on the voltammetric charge and the correlation between catalytic rate and charge will be discussed.

The mechanism of the ethylene oxidation must be studied to understand more properly the EP. Questions as the influence of the backspillover oxygen ions on the reaction rate constants or the introduction of new terms in the kinetic model must be solved. First attempts in this direction will be presented.

## References

- [1] C. G. Vayenas, S. Bebelis and S. Neophytides, *J. Phys. Chem.* **92**, 5083 (1988).
- [2] E. Varkarakis, J. Nicole, E. Plattner and C. Comninellis, *J. Appl. Electrochem.* **25**, 978 (1995).
- [3] J. Nicole and C. Comninellis, *J. Appl. Electrochem.* **28**, 223 (1998).
- [4] J. Nicole, D. Tsiplakides, S. Wodiunig and C. Comninellis, *J. Electrochem. Soc.* **144**, L312 (1997).
- [5] D. Tsiplakides, J. Nicole, C. G. Vayenas and C. Comninellis, *J. Electrochem. Soc.* **145**, 905 (1998).
- [6] S. Wodiunig, C. Comninellis and C. Mousty, *The Electrochemical Society Proceedings Series*, Paris '97, W. A. Adams, L. J. J. Janssen, E. J. Rudd, J. Thonstad and C. W. Walton, Editors, Pennington, 147.
- [7] S. Wodiunig and C. Comninellis, *J. Europ. Cer. Soc.*, *in press*.
- [8] S. Wodiunig and C. Comninellis, 5<sup>th</sup> European Symposium on Electrochemical Engineering, Exeter '99, *in press*.

## SOLID ELECTROLYTE AIDED STUDY OF NO-CO REACTION ON Pd

Soonho Kim and Gary L. Haller  
Department of Chemical Engineering  
Yale University  
New Haven, CT 06520-8286 USA

Introduction

The catalytic properties of solid catalysts can be modified by doping the active phase or by metal-support interactions. It is frequently accepted that such modifications of catalyst properties result from changes in the binding energies of chemisorbed species although geometric considerations often play an important role. It has been reported that the catalytic activity and selectivity of metals can be altered dramatically and reversibly by supplying or removing oxide anions at the metal surface by interfacing the catalyst with an  $O^{2-}$  conductor. This novel effect has been termed non-Faradaic electrochemical modification of catalytic activity (NEMCA) by Vayenas et al. [1].

Experimental

The NO-CO reaction was studied in a flow reactor at a total pressure of 1 atm. Streams of pure He, premixed 0.99% NO in He and 1.90% CO in He were passed separately through mass flowmeters. A porous but continuous thin Pd film was placed both inside and outside of a  $Y_2O_3$ -stabilized  $ZrO_2$  (YSZ) tube by using a thin coating of Engelhard Pd A2985 paste so that the reactor could be operated in a fuel-cell configuration. The flow stream was analyzed before and after passing over the catalyst by a gas chromatograph. Our studies required the analysis of a mixture of NO, CO,  $CO_2$ ,  $N_2$  and  $N_2O$ .

Results and Discussion

The electrochemical promotion of the catalytic activity and the selectivity to  $N_2O$  is reversible and this system showed both electrophilicity and electrophobicity, depending on the direction of oxygen ion pumping. In the electrophilic (NEMCA) regime, a negative current enhances the reaction rate and a positive current reduces the reaction rate. In contrast, the reaction rate increased in proportion to the oxygen ionic current in the electrophobic (electrocatalysis) regime. In a typical experiment, the enhancement of reaction rate is 100 times greater than the rate of oxygen ion removal from the catalyst electrode. Rate enhancement,  $\rho$ , which is defined as the ratio of the reaction rate under an applied potential to the rate at open circuit, was observed to be  $\rho_{CO_2} = 2.2$ ,  $\rho_{N_2O} = 2.2$  and  $\rho_{N_2} = 4.2$  measured at  $V_{WR} = -1.8$  V and 370 °C. One should also note that  $S_{N_2O}$  is dependent on  $V_{WR}$ . In the NEMCA regime, the change in  $S_{N_2O}$  was purely induced by means of electrochemical oxygen pumping and the mass balance is closed, within experimental error, as a result of slow oxygen ion transport through the YSZ comparing to the NO-CO reaction rate at this temperature. In this particular experiment, it was possible to reduce  $S_{N_2O}$  to zero by NEMCA alone.

The electrochemical promotion was sensitive to inlet partial pressures of NO and CO and showed a maximum when  $1 < P_{NO}/P_{CO} < 2$ . The formation of  $N_2$  and  $N_2O$  for the NO-CO reaction over Pd|YSZ appeared to occur in parallel and thus electrochemical promotion of  $S_{N_2O}$  should be interpreted as modification of catalytic active sites rather than increase in site density.

[1] C. G. Vayenas, S. Bebelis and Ladas, S., Nature (London) **343**, 625 (1990).

## Spatially resolved measurements of electrochemically induced spillover on microstructured Pt/YSZ catalysts

*R. Imbihl*

Institut für Physikalische Chemie und Elektrochemie, Universität Hannover,  
Callinstr. 3-3a, D-30167 Hannover, Germany

A very efficient electrochemical promotion of heterogeneously catalyzed reactions has been achieved by deposition of porous metal films on solid electrolytes [1,2]. Although this so-called NEMCA effect (= Non-Faradaic Electrochemical Modification of Catalytic Activity) pioneered by Vayenas et al. has up to now been demonstrated for over 40 reactions employing different solid electrolytes and a variety of different metal electrodes a detailed mechanistic picture is still lacking. In particular, the nature of the spillover species which has been postulated to explain the observed changes in work function and catalytic activity has not been clarified unambiguously.

Our aim was to employ spatially resolved techniques to study the spreading of the electrochemically produced oxygen spillover species on Pt/YSZ (YSZ = yttrium stabilized zirconia) catalysts. In order to have the three-phase-boundary (tpb) of the Pt/YSZ samples accessible to direct observation we prepared microstructured Pt/YSZ catalysts with 500 Å thick Pt films employing optical lithography. As spatially resolving techniques we used photoemission electron microscopy (PEEM) and scanning photoelectron microscopy (SPEM). PEEM images the local work function with a resolution of ca. 1 μm but yields no or only indirect information about the chemical identity of the imaged species. To obtain the chemical information we used SPEM - a technique in which an x-ray beam (≈ 600 eV) is focused into a spot of ≈ 0.15 μm. Photoelectrons from a specific core level are collected while the sample is rastered. Besides the microstructured catalysts also samples with porous catalysts prepared in our lab or supplied from the Patras group were studied. All investigations with surface sensitive techniques were conducted in an UHV environment.

In measurements of the integral work function (WF) (conducted with a Kelvin probe) we found that the variation of the work function in a range from -2 V to + 2V follows indeed the potential  $V_{WR}$  between reference and working electrode as postulated before [1,2]. We observed, however, that the behavior of the sample with porous Pt films was strongly dependent on the preparation. Only the samples supplied from the Patras group exhibited this strong WF variation whereas the samples prepared in our lab showed no WF changes at all upon electrochemical pumping [3]. Both types of samples exhibited an electrocatalytic effect in catalytic CO oxidation but again the qualitative and quantitative effects were strongly dependent on the preparation of the samples. Under the low pressure condition ( $p < 10^{-4}$  mbar) under which we studied catalytic CO oxidation the rate increase was always Faradaic within the accuracy of our measurements.

In PEEM measurements of the microstructured Pt/YSZ samples we observed upon electrochemical pumping work function changes of the Pt surface which we can attribute to the formation of a spillover species [4]. In PEEM a darkening of the Pt surface upon applying a positive voltage  $V_{WR}$  and a brightening with a negative voltage  $V_{WR}$  was seen. No time dependent spatial concentration profiles were registered which would have been indicative of the slow diffusional spreading of a spillover species.

In SPEM measurements with the microstructured Pt/YSZ samples a strong increase of the O1s signal on the Pt was observed upon electrochemical pumping with a positive voltage [5]. The shift of the O1s binding energy is comparable to that seen with chemisorbed oxygen at high coverages. At the tpb dynamic change in the oxygen concentration profiles could be resolved. A mechanistic picture for the spillover effects is discussed on a tentative basis.

## References

- [1] C. G. Vayenas, S. Bebelis and S. Ladas, *Nature* **343** (1990) 625.
- [2] C. G. Vayenas, M. M. Jaksic, S. I. Bebelis and S. G. Nephytides, in *Modern Aspects of Electrochemistry* **29**, eds. J. O. M. Bockris et al, Plenum Press, New York 1996, p. 57
- [3] S. Völkening, Diploma Thesis, Hannover 1996.
- [4] J. Poppe, A. Schaak, J. Janek and R. Imbihl, *Ber. Bunsenges. Phys. Chem.* **102** (1998) 1019; 1718.
- [5] B. Luerssen, S. Günther, H. Marbach, M. Kiskinova, J. Janek and R. Imbihl, in preparation.

## On the Electrochemistry of Metal/YSZ Single Contact Electrodes

By R. J. Aaberg,<sup>a</sup> R. Tunold,<sup>a</sup> and R. Ødegård<sup>a,b</sup>

<sup>a</sup>Institutt for materialteknologi og elektrokjemi, Noregs teknisk-naturvitskaplege universitet,  
N-7034 Trondheim, Norway.

<sup>b</sup>Statoil forskningscenter, postuttak, N-7005 Trondheim, Norway.

The electrochemistry of the Ni/YSZ and Pt/YSZ single contact electrodes has been investigated at 1273 K by potential step measurements and impedance spectroscopy in various hydrogen and water vapour mixtures. The apparent reaction orders with respect to H<sub>2</sub> and H<sub>2</sub>O were obtained from the potential step measurements, but due to time and potential dependent variations in electrode morphology and catalytic activity [1], only semi-steady state results could be acquired. A theoretical impedance model has been developed and fitted to the measured spectra in order to extract the inverse charge transfer resistance at the open circuit potential,  $1/R_{ct}^o$  [2]. For both electrodes, the impedance spectra suggest that chemical processes, such as adsorption, desorption and reaction between adsorbed species, dominated the impedance response of the electrodes. Any rate limiting diffusion could not be detected from the impedance spectra. The value of  $1/R_{ct}^o$ , which is proportional to the exchange current density, was evaluated as a function of  $p(H_2)$  and  $p(H_2O)$ . From these results, in combination with the measured reaction orders, the value of the charge transfer coefficient,  $\alpha$ , could be estimated. For the Pt/YSZ electrode,  $\alpha$  was found to be about 0.7 at anodic overpotentials, and about 1.0 at cathodic overpotentials. It is believed that the high values for  $\alpha$  are related to an electrochemical ion transfer process [3]. The results were less conclusive with respect to the Ni/YSZ electrode, suggesting that the reaction mechanism is more complicated than for the Pt electrode. Polarization induced electrode activation, a phenomenon which may give rise to variations in the electrode kinetics by orders of magnitude, was observed for both types of electrodes. It is assumed that such changes are due to modifications of the electrolyte surface.

Since the impedance model accounts for the current constriction around the TPB, the extension of the Faradaic reaction zone could be estimated both for the Ni/YSZ and the Pt/YSZ electrode. The current constriction seems to have a measurable effect on the shape of the impedance spectra of metal/YSZ point electrodes.

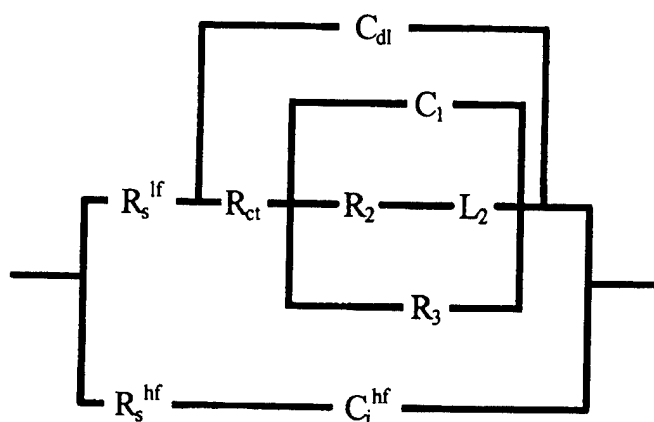


Fig. 1. Equivalent circuit for the theoretical electrode impedance.

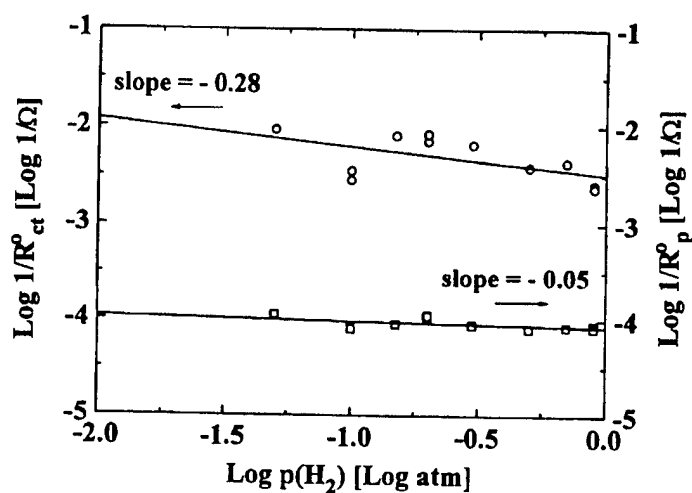


Fig. 2.  $\text{Log}\{1/R_{ct}^o\}$  and  $\text{Log}\{1/R_p^o\}$  versus  $\text{Log}\{p(\text{H}_2)\}$  for the Ni/YSZ electrode. Constant  $p(\text{H}_2\text{O}) = 0.10$  atm. The parameter  $R_p^o$  is the overall polarization resistance at OCV.

## References

- [1] R. J. Aaberg, R. Tunold, M. Mogensen, R. W. Berg and R. Ødegård, *J. Electrochem. Soc.*, **145**, 2244 (1998).
- [2] R. J. Aaberg, R. Ødegård og R. Tunold, to be submitted to *J. Electrochem. Soc.*.
- [3] R. J. Aaberg, *Thesis*, Doktoringeniøravhandling 1998:122, NTNU, Trondheim, Norway (1998).

## NEMCA isomerization of 1-butene: A mechanistic study

E. Smotkin

Illinois Institute of Technology  
Department of Chemical and Environmental Engineering  
IL 60613, USA

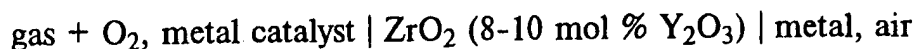
The non-Faradaic electrochemically modified catalysis of 1-butene isomerization to cis- and trans-2-butene at polymer electrolyte porous gas diffusion cathodes has recently been reported. Further isotopic studies with a deuterium anode and D<sub>2</sub>O saturated anode and cathode feeds have permitted determination of the rate-limiting step and confirmed the proposed mechanism. Isotope studies were performed in a Nafion electrolyte fuel cell assembly. The mechanism was determined through use of mass spectroscopy (MS) and Fourier Transform infrared spectroscopy (FTIR). Additionally, kinetic studies revealed substantially reduced NEMCA isomerization rates for deuterium in comparison to the previously published hydrogen data indicating that abstraction of H<sub>ads</sub><sup>+</sup> is the rate determining step.



# EFFECT OF NON-FARADAIC ELECTROCHEMICAL MODIFICATION OF CATALYTIC ACTIVITY

V.D. Belyaev, T.I. Politova, V. A. Sobyenin  
Boreskov Institute of Catalysis, 630090 Novosibirsk, Russia  
Fax: +7(383)2-34-30-56; E-mail: belyaev@catalysis.nsk.su

Recently much attention has been paid [1,2] to the study of oxidative conversion of gases (CO, CH<sub>4</sub>, C<sub>2</sub>H<sub>4</sub>, CH<sub>3</sub>OH) over metal electrode-catalysts in a solid oxide electrolyte cell:

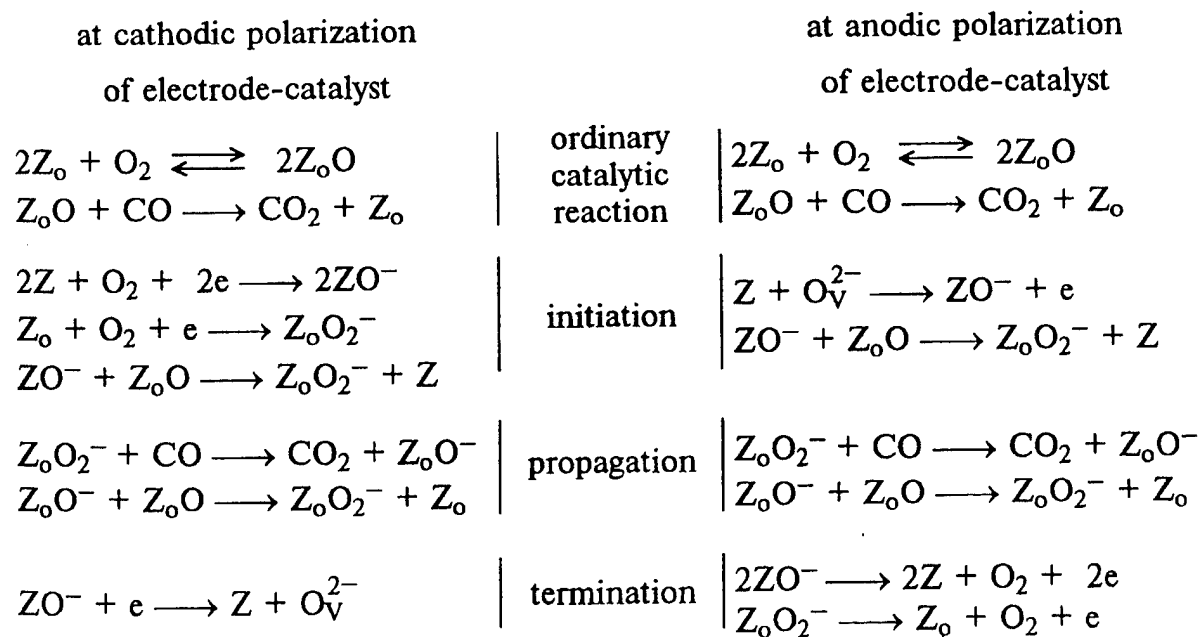


The current passing through the cell (a flow of O<sup>2-</sup> ions through the electrolyte) was found to change remarkably and reversibly the activity of the metal catalyst. The induced change in the catalytic rate exceeded by several orders of magnitude the rate of oxygen flow through the yttria-stabilised zirconia (YSZ) electrolyte. This effect has been termed non-Faradaic Electrochemical Modification of Catalytic Activity (NEMCA effect).

The NEMCA effect is of interest for heterogeneous catalysis, since current passing through the cell or electrode potential is an additional parameter that can be applied to control catalytic properties of electrode-catalyst.

Here we briefly summarize our previous data and current research activity on the NEMCA studies. In particular, the origin of the NEMCA effect for carbon monoxide oxidation over Pt [3], Au [4] and Ag-Pd alloy [5] electrodes is discussed on the basis of chain reaction mechanisms involving electrochemically generated oxygen species [6].

As an example, the simplest chain mechanism of CO oxidation under the NEMCA conditions might be as follows:



where  $Z_o$  is a catalytically active site on the gas-exposed surface of the metal electrode;  $Z_oO$  is atomic oxygen species on the catalytically active site;  $Z_oO^-$  and  $Z_oO_2^-$  are charged oxygen species on the catalytically active site;  $Z$  is an electrochemically active site on the three-phase boundary gas-metal-YSZ;  $ZO^-$  and  $ZO_2^-$  are charged oxygen species on the electrochemically active site;  $O_V^{2-}$  is the oxygen anion in the bulk of YSZ.

As example Fig. 1 shows the experimental data on CO oxidation over Ag-Pd alloy electrode-catalyst under the NEMCA conditions and results of the calculation at realistic rate constants of steps for above chain reaction mechanism. The experimental data are seen to fit satisfactorily the theory.

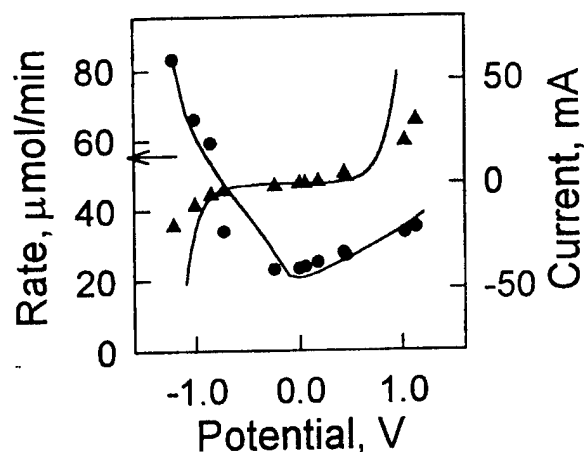


Fig. 1. Effect of potential on current and on the rate of  $CO_2$  formation over Ag-Pd alloy electrode.  $T = 500^\circ C$ ;  $[CO]_0 = 5 \text{ vol\%}$ ;  $[O_2]_0 = 25 \text{ vol\%}$ . Points - experiment [5]; lines - theory

In conclusion note that if under the NEMCA conditions reaction rate changes is due to a chain process than enhancement factor ( $\Lambda$ ), which reflects the change in the reaction rate relative to the oxygen flow rate through the electrolyte, can be as large as the chain length.

#### References:

- [1] C.G.Vayenas, S.Bebelis, S. Ladas, *Nature*, **343**, 625(1990).
- [2] C.G.Vayenas, M.M.Jaksic, S.I.Bebelis, S.G.Neophytides, *Modern Aspects of Electrochemistry*, No 29, Plenum Press, N.-Y., 1996, pp. 57-202.
- [3] I.V.Yentekakis, C.G.Vayenas, *J.Catal.*, **111**, 170 (1988).
- [4] O.A.Mar'ina, V.A.Sobyanin, *Catal.Lett.*, **13**, 61 (1992).
- [5] T.I.Politova, V.V.Gal'vita, V.D.Belyaev, V.A.Sobyanin, *Catal. Lett.*, **18**, 153 (1993).
- [6] V.A.Sobyanin, V.D.Belyaev, *React.Kinet.Catal.Lett.*, **51**, 373 (1993).

**SEP aided study of reactions on oxidic catalysts - results and perspectives**

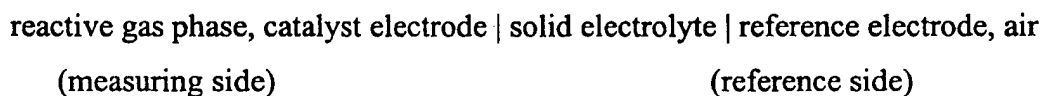
H.-G. Lintz

Institut für Chemische Verfahrenstechnik, Universität (TH) Karlsruhe, Kaiserstraße 12,  
D-76128 Karlsruhe, Germany  
and

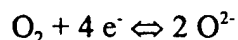
Laboratoire des Sciences du Génie Chimique, CNRS-ENSIC, 1, rue Grandville, BP 451,  
F-54001 Nancy, France

The transfer of oxygen via oxidic catalyst, i.e. in the partial oxidation of an organic compound, is a function of the phase composition of the solid, its oxidation state. Under operating conditions this oxidation state is not only determined by the oxygen partial pressure in the gas phase but results from the rates of oxygen transfer to and from the solid. Thus there is a mutual interaction of the gas phase and the solid catalyst, depending on the nature of the oxygen donor, i.e. O<sub>2</sub> or a nitrogen oxide and the oxygen acceptor, i.e. a hydrocarbon or ammonia.

The phase composition of the oxidic catalyst under working conditions is characterized by its oxygen activity. According to a suggestion of C. Wagner [1], this oxygen activity can be determined by means of an electrochemical method, called Solid Electrolyte Potentiometry (SEP). It is based on the use of an ion conducting solid and the catalytically active oxide is one electrode of the galvanic cell:



If the potential determining reaction is unambiguously given by



the oxygen activity in the catalyst  $a_{\text{O}}^2$  is related to the reference partial pressure  $P_{\text{O}_2}^{\text{R}}$  of oxygen according to a Nernst equation

$$\Delta E = \frac{R \cdot T}{4F} \ln \frac{a_{\text{O}}^2}{P_{\text{O}_2}^{\text{R}}}$$

where  $\Delta E$  designs the potential difference measured under working conditions simultaneously with the rate of the catalyzed reactions. As such combined measurements are meaningful only in the temperature domain of interest in the catalyzed reaction, special care must be given to the adequate preparation of the catalyst electrode. The latter should show:

- good adherence to the solid electrolyte;
- high porosity, that is a high value of the boundary line catalyst - electrolyte - gas phase;
- sufficient electric conductivity.

The results of the combined kinetic and potentiometric measurements will be exemplified by three oxidic catalysts of increasing complexity:

- copper oxide in the oxidation of propene to acrolein;
- vanadia/titania in the oxidation of o-xylene to phthalic acid anhydride;
- a multicomponent catalyst containing mainly molybdenum, vanadium and copper oxides in the oxidation of acrolein to acrylic acid.

In the 1<sup>st</sup> case we observe abrupt phase transitions accompanied by dramatic changes in the kinetic behaviour. In the 2<sup>nd</sup> case a smooth phase transition parallels a continuous variation of activity and selectivity. The 3<sup>rd</sup> example demonstrates the existence of a „buffer effect“ due to the multicomponent system: The oxygen activity remains nearly constant as long as the conversion of the reactant is less than 90% but its value changes by several orders of magnitude as soon as acrolein has disappeared.

Using the examples the possibilities and limitations of the experimental method are discussed.

[1] C. Wagner, Adv. Catal. 21 (1970) 323

## Electrocatalytic And Catalytic Activity As The Interionic And Polarization Effects

Milan M. Jaksic

University of Belgrade, Yugoslavia

Ever since Sabatier principle became stated and related the chemisorptive bonding strength of intermediates in the rate determining steps (rds) with the overall activity in heterogeneous catalytic reactions, the search for the Balandin type of volcano plots along various energetic axis, such as the enthalpy of adsorption, has been the search and criteria for the existence of synergism in catalytic reactions. The same search from the earliest 1950s until now characterizes the plots of logarithm of exchange current density ( $\log i_0$ ) versus the enthalpy of H-atom chemisorption accompanied with theoretical predictions for optimal activity in accordance with the Sabatier principle in catalysis.

Thorough theoretical and experimental investigation of plentiful data so far gathered for the hydrogen evolution reaction (her) have unambiguously shown that there always results the straight line dependence instead of volcano plot. In other words, the plot of  $\log j_0$  virtually means the plot of enthalpy of activation versus the enthalpy of adsorption and, therefore, there unavoidably results the linear dependence. Since there exists linear dependence amongst various type of energies, such as cohesive and surface free energy, Gibbs free energy of metal bonding, energy of sublimation and fusion, and since Fermi energy represents the elementary type of bonding energy also in linear correlation with above mentioned and various other type of energies, there has been shown that the Fermi wave vector plots various physical and chemical properties into reasonable straight line dependencies. In other words, there certainly exists some "common denominator" of universal significance to plot these and other physical parameters along various straight line dependencies. In such a context, the square of Fermi wave vector plots ionic radius and interionic distances of individual metals along fairly nice straight lines, too, and shows the linearity for lattice wave properties.

Meanwhile, there exists another, Gschneidner type of volcano curve dependence, when one plots various features along the Periodic Table. Such volcano plots show the same shape for cohesive and surface free energy, work function and bulk modulus, electrocatalysis for hydrogen evolution and catalysis for hydrodesulphurization of oil, energy of vaporization of liquid metals to their ground state atoms and Pauling d-character, etc. Such state of experimental facts testifies that volcano plots along transition series reflect physical and chemical features of elements directly associated with electronic configuration and as the direct result of the latter. In the essence volcano plots along the Periodic Table virtually describe the periodic properties of elements resulting from the same origin and the same causes. Since the d-orbital represents the bonding band for interionic interaction in the metallic lattice and for chemisorptive bonding of intermediates at the surface or the property of surface free energy of metals, such volcano plots define the d8-electronic configuration for optimal in the her, or d6-structure for chemical hydrodesulphurization. Such conclusions resulting from volcano plot analysis are expected, since two H-atoms need two "seats" at d-orbitals of individual transition metals to produce one  $H_2$ -molecule, at least by following the Volmer-Heyrovsky mechanism, while sulphuric ions need four such "seats" for their intermediate chemisorption.

The Brewer intermetallic bonding theory thermodynamically predicts the extrastrong bonding and extrahigh stability of intermetallic phases produced by the interaction of hypo-hyper-d-electronic combinations of transition elements, which in its essence represents a Lewis type of acid-base interionic interaction. This paper shows that such Brewer

intermetallic hypo-hyper-d-electronic (interionic) interaction results in the property that their phase diagrams behave as the part of Periodic Table between each two constituents in various features, such as electrocatalytic activity, work function, cohesive energy, Gibbs free energy of bonding, etc. In other words, that there always exist typical volcano plots characteristic for the part of Periodic Table, which indicates the synergism in various physical properties. The stronger the intermetallic bonding, the shorter their interionic distance and, as the result, the higher the electronic density of states.

Meanwhile, the higher the electronic density, the stronger the chemisorptive bonding of electron accepting intermediates ( $M=O$ ), while the weaker the adsorptive bonding of electron donating species ( $M-H$ ). Thus, besides the optimal d-electronic configuration, the electronic density of states defines another accompanying factor for catalytic and electrocatalytic activity, which can be advanced by proper interatomic (interionic) combinations and their resulting bonding effectiveness. The shorter the interionic lattice distance, and the higher the electronic density, and thereby, the faster the Volmer-Tafel reaction for the her. There exist three types of such interionic catalytic and electrocatalytic improvements:

(a) Typical Brewer intermetallic interaction, (b) The interaction of ions of various salts even upon noble metal surfaces (for example, tungstenate and/or molybdate upon Pt surface), and (c) The interionic interaction of various combinations of hypo-hyper-d-electronic salts (typically the combinations of Mo and Ni sulphides, polytungstenates and Ni salts, etc.) upon various metallic substrates. In the same such a context it should be mentioned that several intermetallic combinations in their highly dispersed state represent now the most promising electrocatalytic systems for mobile fuel cells for cars, like  $MoPt_3$ ,  $HfPd_3$ ,  $WPt_3$ , etc., that are the main breakthroughs and achievements communicated in the present paper. There should be inferred that hypo-hypo-d- an/or hyper-hyper-d-electronic combinations or their interionic interactions never produce any synergetic catalytic effect and their phase diagrams consist from smooth lines in any physical properties from one to another constituent, such as, first of all the melting point along the atomic percentage axis.

However, there exists another substantial improvement of catalytic properties: the non-Faradaic promotion or NEMCA. The latter virtually consists in the programmed change of electronic density of states of catalytic substrates by external polarization, resulting in dramatic increases of heterogeneous reaction rates. In such a respect, anodic polarization decreases electronic density of Pt substrate and thereby reduces the  $M=O$  bonding strength, which results in dramatic increase of the reaction rate for hydrogen oxidation upon Pt. In the same context, anodic polarization of highly or saturated hydridic  $Ti_2Ni$  with proper electrocatalyst upon its surface dramatically increases the rate of aldehyde hydration reaction, such as production of sorbitol from D-glucose or xylitol from D-xylose.

## GAS-PHASE ELECTROCATALYSIS: METHANE OXIDATION TO SYNGAS IN A SOLID OXIDE FUEL CELL REACTOR

V.A.Sobyanin, V.D.Belyaev

Boreskov Institute of Catalysis, 630090 Novosibirsk, Russia

Fax: +7(383)2-34-30-56; E-mail: sobyanin@catalysis.nsk.su

Electrocatalytic methane oxidation in a solid oxide fuel cell (SOFC) reactor

CH<sub>4</sub>, electrode-catalyst | ZrO<sub>2</sub> (8-10 mol% Y<sub>2</sub>O<sub>3</sub>) | air electrode

is a new way for syngas production. The studies in this field are interesting both for elucidating feasibility of electrocatalytic conversion of methane to syngas and for developing the natural gas fueled SOFC.

At electrocatalytic oxidation of methane in the SOFC reactor methane flow does not contain oxygen. It is fed directly into the reaction zone by passing anodic current through the cell. In this case oxygen ions O<sup>2-</sup> form at the air electrode (cathode). Then, these ions transfer to the electrode-catalyst (anode) through the YSZ electrolyte. On the anode they oxidize methane:



This way provides a number of advantages over the catalytic oxidation of methane to syngas. The electrocatalytic oxidation of methane enables to produce simultaneously syngas and electricity. It diminishes explosion of the reaction mixture, since CH<sub>4</sub> and O<sub>2</sub> (air) are separated by the YSZ electrolyte. When air is used as an oxidant, no nitrogen accumulates in the reaction zone, since oxygen is separated from nitrogen at the stage of its feeding to the reaction zone.

Recently we have shown that Pt and Ni electrodes are highly effective for electrocatalytic oxidation of methane to syngas in the SOFC reactor [1-5]. Here we summarize our previous data and describe further studies on electrocatalytic oxidation of methane to syngas. In contrast to the previous investigations, experiments were done using methane without diluent. The effect of varying the process conditions has been examined.

As an example Fig. 1 shows the plots of electric power generated and of syngas productivity versus methane flow rate at electrocatalytic methane oxidation over Pt electrode-catalyst. The experiment was performed at a constant ratio of methane and oxygen flows (CH<sub>4</sub>/O<sub>2</sub> ≈ 1.8), so that an increase in methane flow rate was equivalent to an increase in the current (oxygen flow). Variations in the current are also plotted in Fig. 1.

Syngas productivity is seen to increase linearly with the CH<sub>4</sub> flow rate (or current), whereas electric power is passing through a maximum. The observed linear dependence of syngas productivity results from the fact that methane conversion (X<sub>CH<sub>4</sub></sub>), CO selectivity (S<sub>CO</sub>) and [H<sub>2</sub>]/[CO] ratio are dependent on the inlet ratio of methane and oxygen flows and independent of their absolute values. In fact, it was found that X<sub>CH<sub>4</sub></sub> ≈ 96%, S<sub>CO</sub> ≈ 95% and [H<sub>2</sub>]/[CO] ≈ 2. The maximum in the plot of electric power versus current is typical for a power-product fuel cell. It is due to the Ohmic losses, cathodic and anodic overpotentials of the SOFC reactor.

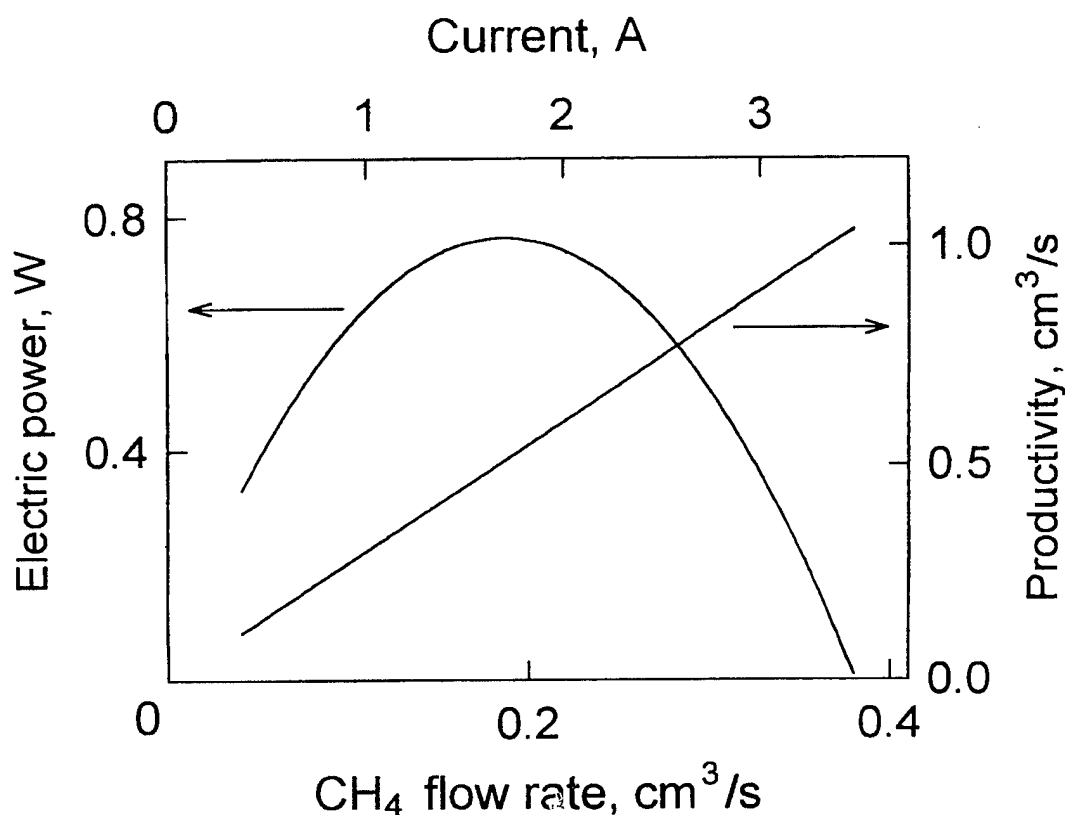


Fig. 1. Effect of methane flow rate (or current) on generated electric power and syngas productivity at electrocatalytic oxidation of methane over Pt electrode-catalyst.  $T = 800^{\circ}\text{C}$ ,  $\text{CH}_4/\text{O}_2 = 1.8$ .

The results obtained over Pt- and Ni-based electrode-catalysts allow us to analyze reaction pathways, problem of carbon formation, electrode-catalyst stability, possibility of cogeneration of syngas and electricity, the outlook of the SOFC reactor application for development of energy-saving and environmentally friendly technology of methane utilisation.

#### References

- [1] V.V.Gal'vita, V.D.Belyaev, V.N.Parmon, V.A.Sobyanin, *Catal. Lett.*, **39**, 209 (1996).
- [2] V.V. Gal'vita, V.D.Belyaev, V.A.Sobyanin, *Kinetika i kataliz*, **38**, 736 (1997) (in Russian).
- [3] V.V. Gal'vita, V.D.Belyaev, A.K.Demin, V.A.Sobyanin, *Appl. Catal. A*, **165**, 301 (1997).
- [4] V.A.Sobyanin, V.D.Belyaev, V.V.Gal'vita, *Catal. Today*, **42**, 337 (1998).
- [5] G.L.Semin, V.D.Belyaev, V.A.Sobyanin, *Appl. Catal. A*, (1998) to be published.



ROLE OF Rh ANODE IN THE YSZ-AIDED CH<sub>4</sub> OXIDATION INTO SYNGAS

K. Sato,<sup>a</sup> J. Nakamura,<sup>a\*</sup> T. Uchijima,<sup>a</sup> T. Hayakawa,<sup>b</sup> S. Hamakawa,<sup>b</sup> T. Tsunoda,<sup>b</sup> T. Shishido<sup>c</sup> and K. Takehira<sup>c\*</sup>

<sup>a</sup>Institute of Materials Science, University of Tsukuba, 1-1-1 Tennoudai, Tsukuba, Ibaraki 305, Japan

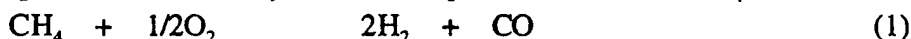
<sup>b</sup>National Institute of Materials and Chemical Research, Tsukuba Research Center, AIST, 1-1 Higashi, Tsukuba, Ibaraki 305, Japan

<sup>c</sup>Department of Applied Chemistry, Faculty of Engineering, Hiroshima University, 1-4-1 Kagami Yama, Higashi Hiroshima 739, Japan

Recently intensive study has been carried out on the catalytic partial oxidation of CH<sub>4</sub> into synthesis gas [1-3]. Usually the reaction proceeds *via* two steps mechanism, *i.e.*, complete oxidation of CH<sub>4</sub> into CO<sub>2</sub>/H<sub>2</sub>O followed by reforming of CH<sub>4</sub> with CO<sub>2</sub>/H<sub>2</sub>O into CO/H<sub>2</sub>. Schmidt *et al.* [4] suggested the possibility of the direct partial oxidation of CH<sub>4</sub> into CO/H<sub>2</sub> by using a Rh- or Pt- coated monolith catalyst at a short residence time. Some attempts to produce CO/H<sub>2</sub> directly from CH<sub>4</sub> were also made by reaction of CH<sub>4</sub> with adsorbed oxygen species on the surface of the catalysts. That is, adsorbed oxygen species on Rh/SiO<sub>2</sub> catalyst [5] or Pd/Y zeolite catalyst [6] can oxidize CH<sub>4</sub> directly into CO/H<sub>2</sub>.

For purpose of supplying continuously atomic oxygen onto the Rh catalyst to produce the adsorbed oxygen species, an Rh/YSZ/Ag membrane reactor was used for the partial oxidation of CH<sub>4</sub> into CO/H<sub>2</sub>. A membrane reactor was constructed from an YSZ disk (Y<sub>2</sub>O<sub>3</sub>, 8mol%) as reported previously [7]. Thin electrodes of Rh (thickness *ca.* 0.5 μm) and Ag were prepared as the anode and cathode, respectively, by vacuum evaporation on each face of disk. The oxidation of CH<sub>4</sub> was carried out at 773K with the 0.4 % CH<sub>4</sub> in N<sub>2</sub> gas at a total flow rate of 1000 ml·hr<sup>-1</sup> in the anode chamber, and O<sub>2</sub> gas at a flow rate of 1000 ml·hr<sup>-1</sup> in the cathode chamber. The components in the effluent gas from the anode chamber, O<sub>2</sub>, CH<sub>4</sub>, H<sub>2</sub>, CO and CO<sub>2</sub>, were analyzed by gas chromatography. The anode surface was characterized by SEM and XRD.

When the Rh anode was treated with oxygen species pumped through the YSZ, the rate of CO/H<sub>2</sub> formation increased, while that of CO<sub>2</sub> formation slightly decreased. Thus, the oxygen pre-pumping improves the selectivity to CO/H<sub>2</sub> formation. The molar ratio of CO/H<sub>2</sub> was *ca.* 1/2, corresponding to the stoichiometry of the direct partial oxidation of CH<sub>4</sub> (1). We have proposed



a model of reaction sites, where two sites exist on the Rh anode surface [7]. One is triple-phase boundary, Rh/YSZ/gas phase, where oxygen pumped through the YSZ appears and reacts with CH<sub>4</sub> to produce CO<sub>2</sub> and H<sub>2</sub>O. Another is the surface of the Rh metal anode on which some oxygen species migrates from the triple-phase boundary to form adsorbed oxygen species, and then reacts with CH<sub>4</sub> to form CO and H<sub>2</sub>.

When the Rh anode was treated by oxygen pre-pumping, the amounts of CO and H<sub>2</sub> increased with the pumping time and attained to a constant level at 5 min, although the amount of CO<sub>2</sub> increased linearly with oxygen pre-pumping time over 30 min. The saturated level in the amount of CO produced (*ca.* 0.2×10<sup>-2</sup> mmol) corresponds to a monolayer of adsorbed oxygen on the Rh surface. Thus, the surface area of Rh was roughly estimated to *ca.* 1200 cm<sup>2</sup> assuming that a surface oxygen is bound to a single rhodium atom and the density of surface rhodium is

$1 \times 10^{15}$  atoms  $\cdot$  cm<sup>-2</sup> as follows:  $0.2 \times 10^{-5}$  (mol)  $\times 6 \times 10^{23}$  (molecules  $\cdot$  mol<sup>-1</sup>)  $\times 10^{-15}$  (cm<sup>2</sup>  $\cdot$  molecule<sup>-1</sup>). Considering the geometric surface area of the membrane disk (8.0 cm<sup>2</sup>), Rh should have some specific structure to show the high surface area on the YSZ.

XRD analyses of the surface of Rh anode showed that only the surface of Rh was oxidized by the oxygen pumping treatment. The fresh anode surface showed metallic luster, while the surface of the used sample had no metallic luster and brittle nature of black color. It is suggested that the Rh anode suffered chemical or physical alteration during the oxygen pumping treatment. The SEM image of the Rh anode surface of fresh sample is composed of small particles or domain even in the bulk. When the Rh anode was calcined in air at 773 K, followed by reduction with 20 % H<sub>2</sub> at 773K, the Rh particles grew slightly large (0.1-0.3  $\mu$ m) by sintering. Apparent macroscopic morphology is not significantly changed by the oxidation-reduction treatment. After oxygen was pumped at 5 mA for 20 min, three-dimensional network appeared consisting of Rh particles with a size of 0.1-0.3  $\mu$ m, which is characteristic of the samples after oxygen pumping treatment. It is considered that oxygen species migrated from the triple-phase boundary to Rh particles creates the network. As a result, the Rh lines grow three-dimensionally and the brittle nature should be due to the formation of the network. The high surface area (ca. 1200 m<sup>2</sup>) estimated by assuming the monolayer adsorption of oxygen may also be due to the network structure. Thus, the morphological change, *i.e.*, the formation of three dimensional network, is probably related to the change in activity upon oxygen pre-pumping.

It is considered that the migration of oxygen requires a good contact between Rh particles on the YSZ surface. This can be achieved by the formation of the three dimensional network probably due to a bridging between Rh particles by forming rhodium oxides. Thus, the partially oxidized Rh surface promotes the migration of oxygen species, resulting in the effective production of CO/H<sub>2</sub> from CH<sub>4</sub>.

## References

- [1] A. T. Ashcroft, A. K. Cheetham, J. S. Foord, M. L. H. Green, C. P. Grey, A. J. Murrell and P. D. F. Vernon, *Nature*, **344**, 319 (1990); D. Dissanayake, M. P. Rosynek, K. C. C. Kharas and J. H. Lunsford, *J. Catal.*, **132**, 117 (1991).
- [2] J. Nakamura, K. Sato, K. Aikawa, K. Kunimori and T. Uchijima, *Shokubai (catalyst)*, **35**, 84 (1993).
- [3] T. Hayakawa, H. Harihara, A. G. Andersen, A. P. E. York, K. Suzuki, H. Yasuda and K. Takehira, *Angew. Chem., Int. Ed. Engl.*, **35**, 192 (1996).
- [4] D. A. Hickman and L. D. Schmidt, *J. Catal.*, **138**, 267 (1992); D. A. Hickman and L. D. Schmidt, *Science*, **259**, 343 (1993).
- [5] J. Nakamura, K. Kubusiro and T. Uchijima, *Stud. Surf. Sci. Catal.*, **77**, 373 (1993).
- [6] H. Matsumoto and S. Tanabe, *J. Chem. Soc. Faraday Trans.*, **90**, 301 (1994); H. Matsumoto, *J. Phys. Chem.*, **98**, 5180 (1994).
- [7] K. Sato, J. Nakamura, T. Uchijima, T. Hayakawa, S. Hamakawa, T. Tsunoda and K. Takehira, *J. Chem. Soc. Faraday Trans.*, **91**, 1655 (1995); K. Takehira, T. Hayakawa, S. Hamakawa, T. Tsunoda, K. Sato, J. Nakamura and T. Uchijima, *Catal. Today*, **1996**, **29**, 397.

## METHANE CONVERSION INTO SYNTHESIS GAS USING AN ELECTROCHEMICAL MEMBRANE REACTOR

S. Hamakawa<sup>1</sup>, T. Hayakawa<sup>1</sup>, K. Suzuki<sup>1</sup>, K. Murata<sup>1</sup>, K. Takehira<sup>2</sup>, S. Yoshino<sup>3</sup>, J. Nakamura<sup>3</sup> and T. Uchijima<sup>3</sup>

<sup>1</sup> National Institute of Materials and Chemical Research, 1-1 Higashi, Tsukuba, Ibaraki 305-8565 Japan

<sup>2</sup> Hiroshima University, 1-4-1 Kagamiyama, Higashi Hiroshima, Hiroshima 739-8527 Japan

<sup>3</sup> University of Tsukuba, 1-1-1, Tennoudai, Tsukuba, Ibaraki 305-0004, Japan

Recently, partial oxidation of CH<sub>4</sub> to the synthesis gas, a mixture of CO and H<sub>2</sub>, has been pointed out as one of the most promising candidates for the effective utilization of natural gas. In the recent few years, an intensive effort has been also made to realize the use of CH<sub>4</sub> gas as a fuel in the research field of the solid oxide fuel cell (SOFC) [1,2]. A problem of the SOFC to develop the efficient energy converter is the investigation of the anode materials which have the ability to inhibit the coke formation, because the coke formation from CH<sub>4</sub> occurs easily on the anode catalyst at high temperature around 1000°C and this phenomenon leads to the drop of the electric power and stability. In a course of work with respect to the heterogeneous catalyst for the CH<sub>4</sub> conversion to synthesis gas, we have developed the Ni metal supported on the perovskite type oxide based on CaTiO<sub>3</sub>, which has a high catalytic activity to form the synthesis gas and an ability to inhibit the coke formation over the catalyst [1]. Although there are some applications of high temperature type membrane reactor to partial oxidation of CH<sub>4</sub> into synthesis gas, no attempt has so far made to apply the anode catalyst with the inhabitation effect of the carbon deposition to the electrochemical membrane reactor. In this presentation, we report the application of the Ni metal catalyst supported on the perovskite type oxide for an anode material of an electrochemical membrane reactor for the CH<sub>4</sub> conversion.

An electrochemical reactor was constructed from an 8 mol% yttria-stabilized zirconia (YSZ) disk. Porous Au and Pt electrodes were used as anode and cathode, respectively. The Ni/Ca<sub>0.8</sub>Sr<sub>0.2</sub>TiO<sub>3</sub> and Ni/Ca<sub>0.8</sub>Sr<sub>0.2</sub>Ti<sub>1-x</sub>Fe<sub>x</sub>O<sub>3-α</sub> were used as the anode catalyst. Their preparation methods were described in detail elsewhere [3]. A mixture of a prepared perovskite powder and Au paste was painted on the Au anode, and fired 10 min at 1100°C. The reaction temperature was 900°C. The flow rates of the 5% CH<sub>4</sub> diluted with N<sub>2</sub> into anode and the pure oxygen into cathode were 1.8 and 1.0 l/hr, respectively. Product analysis was carried out using TCD-gas chromatography.

On applying the direct current to the membrane reactor with Ni/Ca<sub>0.8</sub>Sr<sub>0.2</sub>TiO<sub>3</sub> used as an anode catalyst, the formation rates of CO and H<sub>2</sub> were enhanced drastically and their formation rates increased linearly with increasing the electric current. CO selectivity was almost 100 % under the oxygen pumping conditions, and highest CH<sub>4</sub> conversion was about 40 %. The amount of surface carbon decomposition over the Ni/Ca<sub>0.8</sub>Sr<sub>0.2</sub>TiO<sub>3</sub> was 10 times smaller than that of typical catalysts for the CH<sub>4</sub> conversion, namely Ni-YSZ cermet and Ni/α-Al<sub>2</sub>O<sub>3</sub>, indicating that Ni/Ca<sub>0.8</sub>Sr<sub>0.2</sub>TiO<sub>3</sub> is useful for the anode catalyst for the partial oxidation of CH<sub>4</sub> into synthesis gas. However, the maximum power density of this cell was 14.5 mW/cm<sup>2</sup> at 900°C and its value was so low, when this cell was regarded as the SOFC using CH<sub>4</sub> as a fuel. This may be due to the low ionic and electronic conduction of the anode catalyst, mainly Ca<sub>0.8</sub>Sr<sub>0.2</sub>TiO<sub>3</sub>. Therefore, in this presentation, we will also report the preparation of the partial substitution by Fe<sup>3+</sup> for Ti<sup>4+</sup> site in the perovskite type crystal Ca<sub>0.8</sub>Sr<sub>0.2</sub>TiO<sub>3</sub> in order to increase of the oxide ionic and electronic conduction in the perovskite type oxide and the application them as the support of the anode catalyst in the electrochemical membrane system.

### References

- [1] K. Eguchi, Y. Kunisaka, M. Kayano, K. Sekizawa, S. Yano and H. Arai, DENKI KAGAKU, **64**, 597 (1996).
- [2] Y. Hiei, T. Ishihara and Y. Takita, Solid State Ionics, **86-88**, 1267 (1996).
- [3] T. Hayakawa, H. Harihara, A. G. Andersen, A. P. E. York, K. Suzuki, H. Yasuda and K. Takehira, Angew. Chem. Int. Ed. Engl., **35**, 192 (1996).

## **IN SITU CATALYTIC, ELECTROCATALYTIC AND ELECTROCHEMICAL STUDIES OF FUEL PROCESSING ANODES IN SOLID OXIDE FUEL CELLS RUNNING ON NATURAL GAS**

Caine M. Finnerty, Robert H. Cunningham and R. Mark Ormerod

Birchall Centre for Inorganic Chemistry and Materials Science, Department of Chemistry, Keele University, Staffordshire, ST5 5BG, United Kingdom

Fuel cells offer tremendous potential as a more efficient and cleaner method of electricity generation than conventional methods. Solid oxide fuel cells (SOFCs) offer advantages over other fuel cell systems because the high operating temperatures allow both flexibility in the choice of fuel, and the possibility of running the cell directly on natural gas and other liquid hydrocarbon fuels, internally reforming the fuel within the fuel cell, which leads to increased operational efficiency. However, several major operational problems remain to be solved before such cells can ever be routinely run using hydrocarbon fuel. These include the problem of carbon deposition at the anode or internal reforming catalyst, and the subsequent deactivation which leads to a loss of cell performance and poor durability, anode sintering, problems associated with the strongly endothermic nature of steam reforming, and problems of start-up and operation at low power.

In turns of studying internal reforming in SOFCs and evaluating optimum anode formulations and process operating conditions, one of the key problems is the design of a suitable test system to study the fuel processing catalysis and surface chemistry of the fuel cell, as well as evaluate the electrical performance and durability of the fuel cell. The design and construction of such a system is not straightforward. In particular the problems of rapid heating of the cell to operating temperature, thermal cycling, sealing, obtaining gas tight connections and being able to make both electrochemical and gas analysis measurements all have to be overcome; a particular problem with planar-type devices.

We have developed a test system, based on a thin-walled extruded yttria-stabilised zirconia tubular reactor, which can be used to investigate the fuel processing catalysis in the fuel cell, the chemistry occurring at the anode or reforming catalyst surface, as well as the durability and performance of the SOFC, under actual working conditions [1]. In particular the system permits simultaneous monitoring of the catalytic activity and surface chemistry, and the cell performance, allowing a direct correlation to be made between the fuel cell performance and its reforming characteristics [1]. In addition, the test system can be readily used to study the problems of carbon deposition and poor durability in operation. The particular benefits of this test cell are that it can be rapidly assembled, heated and cooled, and it has no sealing and leakage problems, which many test devices suffer from. The test cell inlet is linked to a gas manifold which allows complete flexibility in the choice of fuel and fuel/steam ratio, enabling evaluation over a full range of operating conditions and fuel compositions. The reactor outlet is directly linked to a continuously sampling on-line mass spectrometer which permits the fuel processing reactions at the anode to be directly studied in an actual SOFC under operating conditions, and allows the chemistry occurring at the anode surface to be

investigated using temperature programmed measurements. These have been used to study the reduction characteristics of the anode, hydrocarbon activation, methane steam reforming and the reaction pathways occurring at the anode surface, the process of carbon deposition, and the nature and extent of carbon deposition following reforming [REFS]. The same system and identical experimental arrangement can be used to carry out electrochemical measurements on the same cell, allowing a direct correlation to be made between the reforming characteristics of the anode and the fuel cell performance.

In this paper we shall describe this test system and show how the system has been used to study a range of different nickel/zirconia cermet anode formulations in tubular SOFCs, and internal reforming in SOFCs. Carbon deposited following high temperature reforming has been characterised using temperature programmed oxidation. The effect of methane/steam ratio, the influence of operating temperature, and the effect of adding small quantities of dopants to the anode, have all been investigated in terms of their influence on the methane reforming activity, the surface chemistry, and the nature and level of carbon deposition, as well as on the cell performance.

- [1] C.M. Finnerty, R.H. Cunningham, K. Kendall and R.M. Ormerod, *J. Chem. Soc., Chem. Commun.*, (1998) 915.
- [2] R.H. Cunningham, C.M. Finnerty, K. Kendall and R.M. Ormerod, in: *Proc. 5th Int. Symp. on Solid Oxide Fuel Cells*, (The Electrochemical Society) (1997) 965.
- [3] R.H. Cunningham, C.M. Finnerty and R.M. Ormerod, in: *Proc. 5th Int. Symp. on Solid Oxide Fuel Cells*, (The Electrochemical Society) (1997) 973.
- [4] C.M. Finnerty, R.H. Cunningham and R.M. Ormerod, in: *Proc. 3rd European Solid Oxide Fuel Cell Forum*, Vol. 1 (1998) 217.
- [5] C.M. Finnerty, R.H. Cunningham and R.M. Ormerod, in: *Proc. 3rd European Solid Oxide Fuel Cell Forum*, Vol. 1 (1998) 227.
- [6] C.M. Finnerty, R.H. Cunningham and R.M. Ormerod, *Catalysis Today*, **46**, 137 (1998).

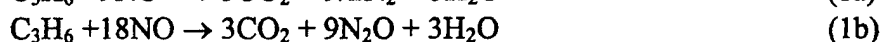
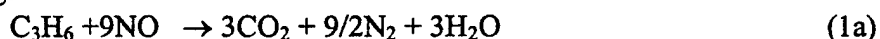
# ELECTROCHEMICAL PROMOTION OF NO REDUCTION BY C<sub>3</sub>H<sub>6</sub> ON Rh/YSZ CATALYST - ELECTRODES

C. Pliangos, C. Raptis, Th. Badas and C.G. Vayenas

University of Patras, Department of Chemical Engineering, Patras GR 26 500, GREECE

## ABSTRACT

The effect of Electrochemical Promotion (or Non-faradaic Electrochemical Modification of Catalytic Activity – NEMCA) [1, 2] was used to promote the NO reduction by Propylene, in the presence of excess oxygen. The particular reactions which take place on the Rh catalyst-electrode are the following:



In very high excess of oxygen, the oxidation of NO to NO<sub>2</sub> also takes place. This reaction system is very important from the environmental point of view, due to the need of designing effective catalysts for lean burn or diesel engines. Lean burn engines offer considerable, up to 15% enhancement in fuel efficiency.

It is well established [3] that Rh-based catalysts exhibit a superior behaviour in NO reduction reactions. Therefore, Rh polycrystalline films interfaced with Ytria – stabilized – Zirconia were used in this investigation, in galvanic cells of the type:



The reactor used in this study was of the "single - pellet" configuration [1, 2], where both the Rh working electrode and the Au reference and counter electrodes are all exposed to the reaction mixture. This design is more promising for practical applications, than the classical fuel cell type design used also in NEMCA studies [1].

It was found that both the catalytic activity and the selectivity of the Rh catalyst-electrode is affected dramatically upon varying its potential with respect to the Au pseudoreference electrode. The rates of CO<sub>2</sub> and N<sub>2</sub> production are enhanced dramatically both with positive and with negative potentials or currents, i.e., the system exhibits electrophobic behaviour at positive potentials and electrophilic behaviour at negative ones. The induced changes in catalytic rates are typically 3 orders of magnitude higher than the rate  $I/2F$  of O<sup>2-</sup> supply or removal to or from the Rh catalyst electrode. Thus, the Faradaic efficiency,  $\Lambda$ , defined from

$$\Lambda = \Delta r / (I/2F) \quad (2)$$

was found to take values as high as 4000 and as low as -6000. The rate enhancement ratios,  $\rho$ , for the three main products CO<sub>2</sub>, N<sub>2</sub> and N<sub>2</sub>O were also found to take very high values. These parameters are defined from:

$$\rho_{\text{CO}_2} = r_{\text{CO}_2} / r_{\text{CO}_2}^0 ; \rho_{\text{N}_2} = r_{\text{N}_2} / r_{\text{N}_2}^0 ; \rho_{\text{N}_2\text{O}} = r_{\text{N}_2\text{O}} / r_{\text{N}_2\text{O}}^0 \quad (3)$$

where  $r_{\text{CO}_2}^0$ ,  $r_{\text{N}_2}^0$  and  $r_{\text{N}_2\text{O}}^0$  are the open-circuit, i.e., unpromoted rate values and  $r_{\text{CO}_2}$ ,  $r_{\text{N}_2}$  and  $r_{\text{N}_2\text{O}}$  are the electrochemically promoted values. Positive current (or potential) application leads to  $\rho_{\text{CO}_2}$  and  $\rho_{\text{N}_2}$  values up to 150 and 60 respectively, i.e., there is up to 150-fold enhancement in the rate of CO<sub>2</sub> production and an up to 60-fold enhancement in the rate of N<sub>2</sub> production. The  $\rho_{\text{CO}_2}=150$  value is the highest reported so far in NEMCA studies utilizing YSZ.

A typical galvanostatic NEMCA experiment is shown in Figure 1, which shows the transient effect of a constant positive current application on the rates of formation of CO<sub>2</sub>, N<sub>2</sub> and N<sub>2</sub>O, on the NO conversion and on the catalyst potential,  $V_{\text{WR}}$ . The open-circuit (unpromoted) rates correspond to  $t < 0$  in the figure. At  $t=0$  the galvanostat is used to apply a constant current

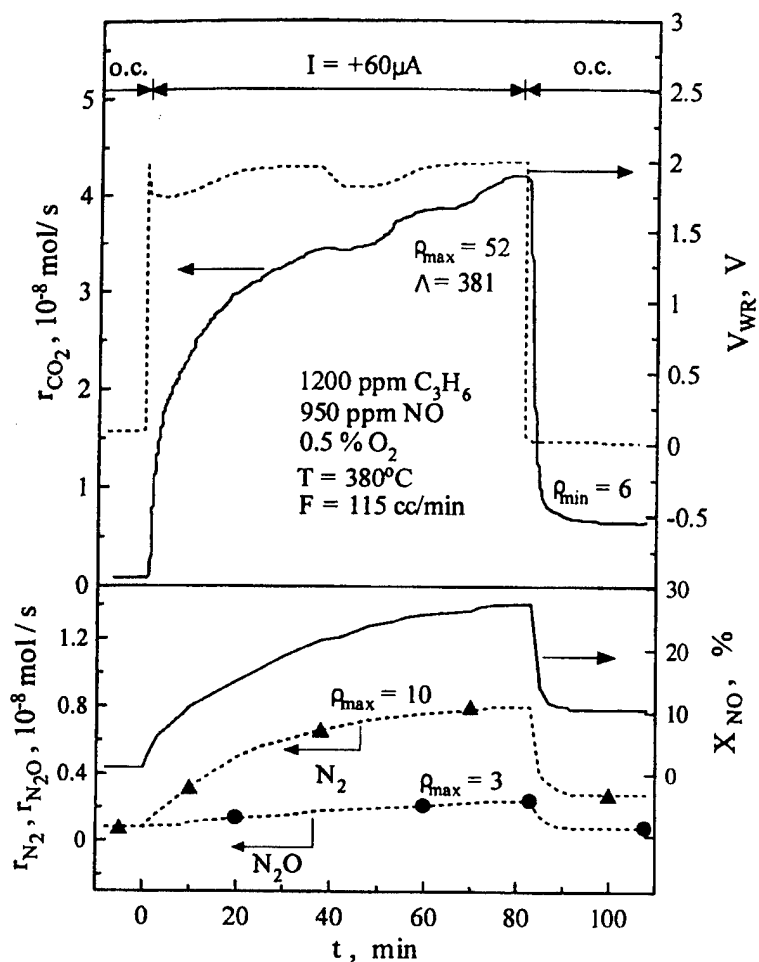


Fig. 1. Transient effect of a constant applied current on the catalytic rates of CO<sub>2</sub>, N<sub>2</sub> and N<sub>2</sub>O production, on NO conversion (X<sub>NO</sub>) and on catalyst potential (V<sub>WR</sub>).

$I=60\mu\text{A}$  between the working and counter electrode. At the new steady state, reached after 80 min, the catalyst-electrode performance has changed dramatically. There is a 1300% increase in NO conversion and a 5200%, 1000% and 300% enhancement in the rates of CO<sub>2</sub>, N<sub>2</sub> and N<sub>2</sub>O formation ( $\rho_{\text{CO}_2}=52$ ,  $\rho_{\text{N}_2}=10$ ,  $\rho_{\text{N}_2\text{O}}=3$ ). The increase,  $\Delta r_{\text{CO}_2}$ , in the rate of CO<sub>2</sub> formation is 380 times larger than the rate,  $I/2F$ , of supply of O<sup>2-</sup> to the Rh catalyst. The product selectivity to N<sub>2</sub> (vs N<sub>2</sub>O) is also significantly enhanced.

It is worth noting in Fig. 1, that after current interruption the effect is not totally reversible, since the catalytic rates do not return to their initial open circuit values (i.e., there is a 6-fold permanent enhancement of the catalytic activity for CO<sub>2</sub> production and a 3-fold permanent enhancement in NO conversion). This is a manifestation of the so called "permanent NEMCA" studied by Comninellis and coworkers [4]. We found that the initial rates can be restored after treating the catalyst with C<sub>3</sub>H<sub>6</sub> for a few minutes in absence of O<sub>2</sub> and NO.

The observed pronounced promotional phenomena can be rationalized by taking into account the effect of changing the potential, and thus work function [1,2], on the chemisorptive bond strength of oxygen, NO and propylene. In particular, it appears that the pronounced weakening in the Rh=O bond, induced at high potentials [1], enables NO to adsorb and dissociate even in presence of significant amounts of gaseous oxygen. This may be of significant practical importance. Also the significant weakening in the C<sub>3</sub>H<sub>6</sub> chemisorptive bond at negative potentials, may again enhance NO adsorption and dissociation, causing the observed electrophilic behaviour.

#### References:

- [1] "The Electrochemical Activation of Catalysis", C.G. Vayenas, M.M. Jaksic, S. Bebelis and S.G. Neophytides, in "Modern Aspects of Electrochemistry" (J.O'M. Bockris, B.E. Conway and R.E. White eds) Vol. 29, pp. 57-202 Plenum Press, NY, (1995).
- [2] C.G. Vayenas and I.V. Yentekakis, Electrochemical modification of catalytic activity, in "Handbook of Heterogeneous Catalysis" (G. Ertl, H.Knözinger, J. Weitkamp, Eds.). VCH, Weinheim, New York (1996).
- [3] J.N. Armor, in "Environmental Catalysis", (Armor J.N. eds), Amer. Chem. Soc., Symp. Ser., No 552, 90 - 93, Washington, DC (1994).
- [4] J. Nicole and Ch. Comninellis, *J. Electrochemical Soc.*, in press (1998).

## ELECTROCATALYTIC REDUCTION OF NO<sub>x</sub> ON La<sub>1-x</sub>A<sub>x</sub>B<sub>1-y</sub>B'<sub>y</sub>O<sub>3-δ</sub>; EVIDENCE OF ELECTRICALLY ENHANCED ACTIVITY

Eric D. Wachsman  
Department of Materials Science and Engineering  
University of Florida  
Gainesville, FL 32611-6400

Palitha Jayaweera, Gopala Krishnan, and Angel Sanjurjo  
Materials Research Center  
SRI International  
Menlo Park, CA 94025

Solid-state electrochemical cells can be used to sense and reduce NO<sub>x</sub> from combustion exhaust gases. The solid-state electrocatalytic reduction of NO to N<sub>2</sub> and O<sub>2</sub> was first demonstrated by Pancharatnam et al [1] and subsequently investigated for combustion emission reduction [2-5]. In the early work on NO<sub>x</sub> reduction [1-3] the cathode was porous Pt, similar to the O<sub>2</sub> sensor, where the reduction reaction is limited to the three-phase (Pt-zirconia-gas) interface. A major theme in these earlier studies was the promotion of NO<sub>x</sub> reduction by F-center type defects (electron occupied oxygen vacancies) in the oxide surface.

In general, metal oxides of the form ABO<sub>3</sub> (perovskite), where A and B are metal cations have the desirable properties of electronic and ionic conductivity so that the reduction reaction can occur across the entire cathode surface. Moreover, perovskites can also have F-center type defects and are known to be catalytically active and potentially selective, depending on the nature of the B-site cation and the degree of aliovalent substitution on the A-site.

Therefore, a series of La<sub>1-x</sub>A<sub>x</sub>B<sub>1-y</sub>B'<sub>y</sub>O<sub>3-δ</sub> perovskites were prepared and systematically evaluated for NO and O<sub>2</sub> reduction activity and relative selectivity. Temperature programmed reaction (TPR) experiments were used to evaluate the catalytic activity and selectivity of these materials. In general, the more readily reducible the catalyst, the more active it was toward NO reduction. For example, in a series of B-site substitution of first row transition metals in LaBO<sub>3</sub>, it was observed that those metals with near half full d-orbitals are the most active.

A potential electrocatalyst was selected based on these catalytic studies. Yttria stabilized zirconia (YSZ) tubes were coated internally (cathode) with the electrocatalyst, and externally (anode) with a Pt electrode. The cells were evaluated in simulated combustion exhaust streams (500 ppm NO, 0 to 5% O<sub>2</sub>, 2.4% CO, 9% CO<sub>2</sub>, balance N<sub>2</sub>/He) under catalytic (no applied current) and electrocatalytic (applied current) conditions.

The conversion of NO<sub>x</sub> as a function of O<sub>2</sub> concentration in the cell feed and applied current was determined using a chemiluminescence detector. In these experiments the cell was bypassed to establish feed gas composition. The feed gas was then switched through the cell and allowed to equilibrate in order to determine purely catalytic "three-way like" (CO oxidation, NO reduction, no hydrocarbons) conversion. A current was then applied stepwise (100 mA increments) and the cell allowed to equilibrate at each step.

With no applied current the electrocatalyst is an effective catalyst with >90 % conversion of NO<sub>x</sub> when the O<sub>2</sub> concentration is stoichiometric with the CO concentration ( $\lambda=1$ ). Typical of a three way catalyst, the NO<sub>x</sub> conversion decays with increasing O<sub>2</sub> concentration. Application of a



few 100 mA current extends the NO<sub>x</sub> conversion into excess O<sub>2</sub> conditions ( $\lambda > 1$ ). Moreover, complete (100 %) conversion of NO<sub>x</sub> is achieved at O<sub>2</sub> concentrations exceeding 3%.

Catalytic (no applied current) and electrocatalytic (400 mA) data are plotted in Figure 1. The catalytic data shifted by 1.5 % O<sub>2</sub> is also plotted in Figure 1. Under the experimental conditions, 400 mA corresponds to removal of 1.5 % O<sub>2</sub> from the gas stream. The higher NO<sub>x</sub> conversion achieved at 400 mA as compared to the shifted catalytic data demonstrates an "electrocatalytically enhanced" three-way catalyst effect. This effect is more than just electrochemical pumping of O<sub>2</sub> out of the gas stream and provides evidence for electrically enhanced activity.

Vayenas has reported extensively on enhanced electrocatalytic activity, or Non-Faradaic Electrochemical Modification of Catalytic Activity (NEMCA), see for example [6]. The majority of these studies focused on oxidation or partial oxidation reactions. To this body of work we add our results on the enhanced electrocatalytic reduction of NO<sub>x</sub>. Further fundamental investigations of this effect could lead to development of new lean NO<sub>x</sub> catalysts and electrocatalysts.

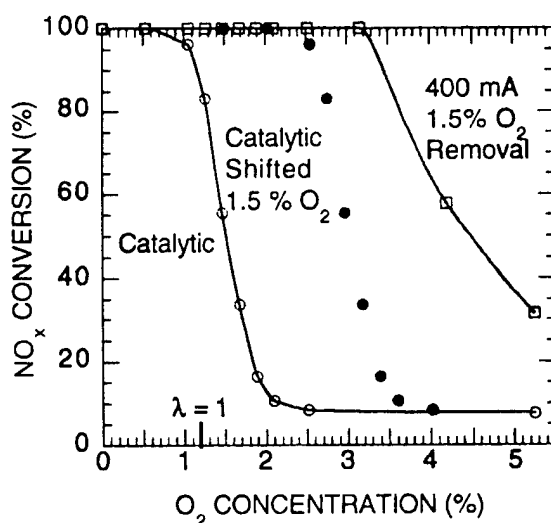


Figure 1. Conversion of NO<sub>x</sub> as a function of O<sub>2</sub> concentration, for catalytic, electrocatalytic (400 mA) and equivalently shifted (1.5% O<sub>2</sub>) catalytic reduction; 500 ppm NO, 2.4% CO, 9% CO<sub>2</sub>, balance N<sub>2</sub> and He, 700°C.

- [1] S. Pancharatnam, R.A. Huggins, and D.M. Mason, *J. Electrochem. Soc.* **122**, 869 (1975).
- [2] T.M. Gur and R.A. Huggins, *J. Electrochem. Soc.* **126**, 1067 (1979).
- [3] E. D. Wachsman, T. A. Lin, N. Jiang, C. Ming, and D. M. Mason, DOE/PETC Final Technical Report, Contract No. DE-FG22-86PC90501 (1989).
- [4] E. D. Wachsman, G. N. Krishnan, B. G. Pound, P. Jayaweera, N. Jiang, D. Lowe, J. G. McCarty, and A. Sanjurjo, GRI Final Technical Report, Contract No. 5091-254-2226 (1998).
- [5] E. D. Wachsman, P. Jayaweera, G. Krishnan, and A. Sanjurjo, *SAE Technical Paper No.* 982513 (1998).
- [6] C. G. Vayenas, S. Bebelis, I.V. Yentekakis, and H.-G. Lintz, *Catalysis Today*, **11**, 303 (1992).

REDUCTION OF OXYGEN AT Pt/ZrO<sub>2</sub>-Y<sub>2</sub>O<sub>3</sub> ELECTRODE IN PRESENCE OF NO

S.I. Somov, A.N. Ezin

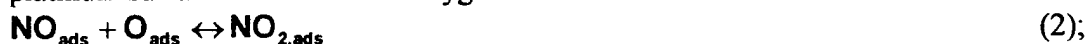
Institute of High Temperature Electrochemistry  
Ul. S. Kovalevskoi 20, Ekaterinburg, 620219 Russia

A number of experimental facts have shown that a presence of NO in gas mixture accelerates the oxygen reaction rate at platinum electrode of zirconia electrolyte cell [1]. Herewith, NO is not reduced noticeably at potentials,  $E \geq -350$  mV, vs. the air reference electrode [2,3]. From experimental data and knowledge about electrode process we can formulate the following model for mechanism of current generation. It is illustrated at fig.1. The principal propositions of the model are follow:

- a dissociative adsorption of oxygen takes place at a gas/platinum interface;
- oxygen is diffused to TPB (triple phase boundary);
- a reduction of oxygen takes place at TPB



- if NO is presented in the gas phase, then it is adsorbed at platinum surface;
- at the platinum surface NO react with oxygen



- NO<sub>2,ads</sub> diffuse to TPB, as well;
- at TPB NO<sub>2,ads</sub> is reduced to NO<sub>ads</sub>, and the rate of reaction (3) is very high



- NO molecules diffuse back, then they disrobe or a react with oxygen again.

Equation (4) is derived from this model:

$$I = \sinh \tilde{\eta} \cdot 4e \sqrt{\frac{1}{3} J_{\text{O}_2}^0 Z D_{\text{O}} \Theta_{\text{O}}^0 P_{\text{O}_2}^{3/4} [e^{6\tilde{\eta}} - 3e^{2\tilde{\eta}} + 2]} +$$

$$+ 3 \frac{D_{\text{NO}} K_{\text{NO}}}{D_{\text{O}} \Theta_{\text{O}}^0} P_{\text{O}_2}^{-1/2} P_{\text{NO}} (\varphi + 1) \left[ 2\varphi \ln \frac{\varphi + 1}{\varphi + e^{2\tilde{\eta}}} + \frac{(e^{2\tilde{\eta}} - 1)^2 + 2\varphi(e^{2\tilde{\eta}} - 1)}{\varphi + e^{2\tilde{\eta}}} \right]^{1/2} \quad (4)$$

Where:  $\varphi = \frac{D_{\text{NO}}}{D_{\text{NO}_2} K_{\text{NO/NO}_2} \Theta_{\text{O}}^0} P_{\text{O}_2}^{-1/2}$ ;  $\tilde{\eta} = \frac{F}{RT} \eta$ ;

$D_{\text{NO}}$ ,  $D_{\text{NO}_2}$ ,  $D_{\text{O}}$  – diffusion coefficients of NO, NO<sub>2</sub>, and O at the platinum surface;  $K_{\text{NO}}$ ,  $K_{\text{NO/NO}_2}$  – equilibrium constants for NO adsorption and reaction (3), respectively.  $J_{\text{O}_2}^0$  – is an exchange rate of oxygen at Pt/gas interface;  $\Theta_{\text{O}}^0$  – oxygen coating ratio;  $Z$  – a density of adsorption centres.

In the absence of NO this equation is transformed to the known equation (5), derived from model of the diffusion extension of reaction zone near TPB [4]:

$$I = \sinh \tilde{\eta} \cdot 4e \sqrt{\frac{1}{3} J_{\text{O}_2}^0 Z D_{\text{O}} \Theta_{\text{O}}^0 P_{\text{O}_2}^{3/4} [e^{6\tilde{\eta}} - 3e^{2\tilde{\eta}} + 2]}^{1/2} \quad (5)$$

Equation (4) show the possibility for increasing of the rate of oxygen reduction at platinum cathode. Despite of two reactions are occurred at TPB, the general electrode reaction is the oxygen reduction only. The couple NO<sub>ads</sub>/NO<sub>2,ads</sub> plays the role of catalyst in this process.

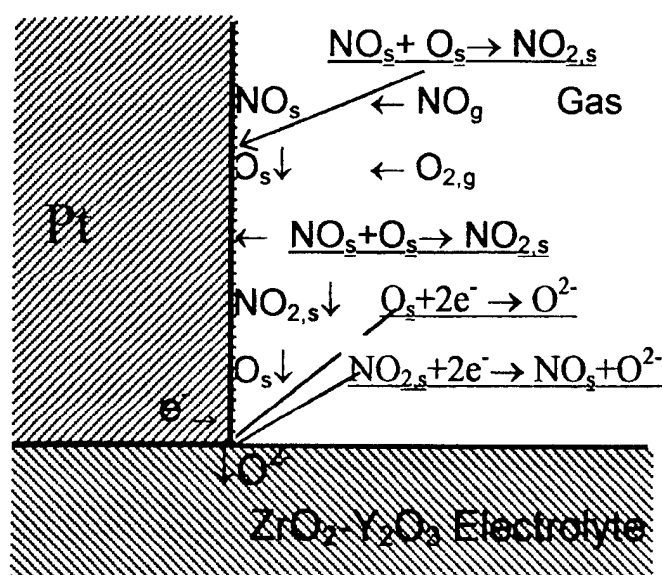


**Fig. 1.** Scheme of reactions at Pt/ZrO<sub>2</sub>-Y<sub>2</sub>O<sub>3</sub>- electrode in gas mixtures containing oxygen and nitrogen oxide.

Nitrogen oxides are carriers, which realise additional mechanism of oxygen transportation from gas/platinum interface to TPB. Approximations for small and high cathodic overvoltage have been derived from equation (4). We have carried out the numerical simulation of the equations depending on model parameters, O<sub>2</sub> and NO concentrations. Promotion coefficient of oxygen reduction rate, K<sub>p</sub>, may be defined as:

$$K_i = \frac{I(P_{NO})}{I(P_{NO} = 0)} \quad (6)$$

It is equal:

$$K_i = \left\{ 1 + 3 \frac{D_{NO}}{D_O} \frac{K_{NO}}{\Theta_O^0} P_{O_2}^{-1/2} P_{NO} (\varphi + 1) \times \right. \\ \left. \frac{2\varphi \ln \frac{\varphi + 1}{\varphi + e^{2\tilde{\eta}}} + \frac{(e^{2\tilde{\eta}} - 1)^2 + 2\varphi(e^{2\tilde{\eta}} - 1)}{\varphi + e^{2\tilde{\eta}}}}{e^{6\tilde{\eta}} - 3e^{2\tilde{\eta}} + 2} \right\}^{1/2} \quad (7)$$

K<sub>i</sub> is increased with increasing of the cathodic overpotential and NO concentration. An increasing of oxygen content in gas mixtures decrease the K<sub>i</sub>.

Thus, the proposed model explains unusual behaviour of oxygen reaction at platinum cathode in presence of NO. It is an example of catalysis of electrochemical reaction by means of gaseous molecules.

#### REFERENCES:

- [1] S.I. Somov, G. Reinhardt, H.-D. Wiemhöfer and Göpel. *Ionics* **1**, 136 (1995).
- [2] S.I. Somov, G. Reinhardt, U. Guth, U. Schönauer and Göpel. *Ionics* **1**, 514 (1996).
- [3] Kenneth L. Walsh, Peter S. Fedkiw. *Solid State Ionics* **93**, 17 (1997).
- [4] M.V.Perfil'ev, S.F. Paluev Trudy Institute of Electrochemistry UFAN USSR **8**, 157 (1968).

# SUCCESSFUL APPLICATION OF ELECTROCHEMICAL PROMOTION TO THE DESIGN OF EFFECTIVE CONVENTIONAL CATALYST FORMULATION

I.V. Yentekakis and M. Konsolakis

Dept of Chemical Engineering, University of Patras and ICE/HT-FORTH, GR-26500, Patras, Greece.

R.M. Lambert, A. Palermo and M. Tikhov

Dept of Chemistry, University of Cambridge, Cambridge CB2 1EW, UK

Electrochemical promotion (EP), discovered and developed by Vayenas and co-workers [1, 2] provides a novel in situ reversible and high controllable means of catalyst promotion. We have found that Pt-group metal catalysts exhibit strong electrochemical promotion by sodium during reactions related to emission control catalysis, such as NO reduction by hydrocarbons [3, 4]. Close similarities are found between the performance of Pt-film catalyst promoted electrochemically with highly dispersed on large surface area carriers (e.g.,  $\gamma$ -Al<sub>2</sub>O<sub>3</sub>) Pt promoted by conventional means (impregnation). These similarities include (i) the overall kinetic behaviour and (ii) the dependence of the activity and selectivity on Na loading. For example, using both methods of Na-promotion, the catalytic reduction of NO by propene exhibited rate enhancements as high as 1 to 2 orders of magnitude accompanied by very pronounced increases of the system selectivity towards N<sub>2</sub> (Figure 1).

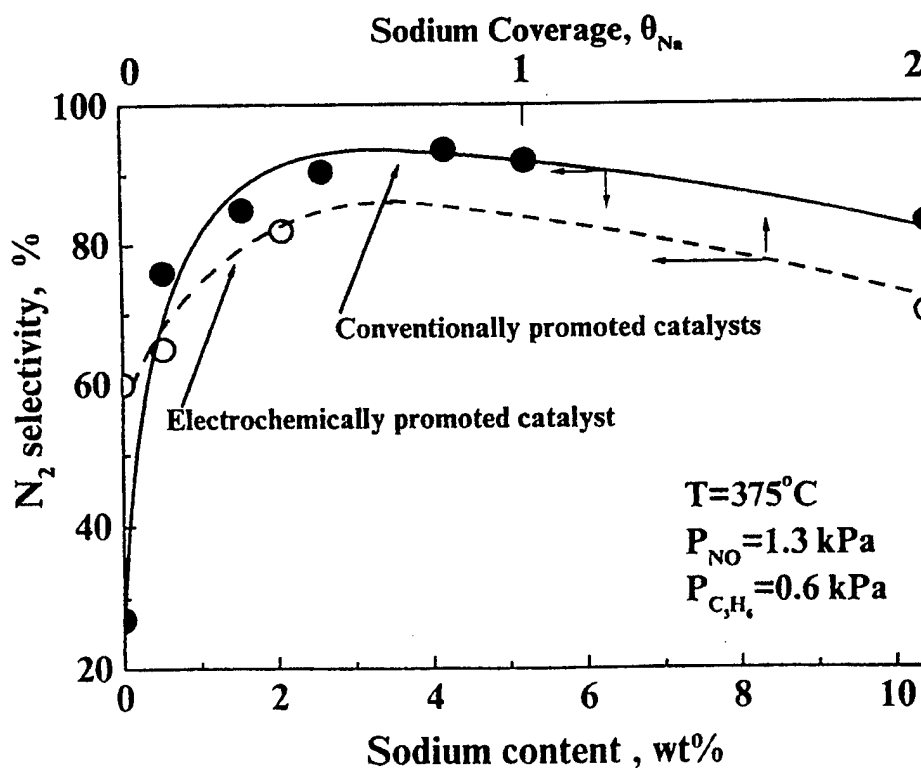


Figure 1: Comparison of electrochemically promoted and conventionally promoted Pt with respect to N<sub>2</sub>-selectivity during the NO+propene reaction. Conditions: T=375°C, P<sub>NO</sub>=1.3kPa, P<sub>prop.</sub>=0.6kPa.

Among other things, our results serve to validate further the interpretation offered for the EP (or NEMCA) phenomenon. More importantly, they demonstrate that the insight obtained from EP studies can be used to design conventional type effective catalyst formulations that were previously untried, thus opening up new areas for investigation in the frontiers between catalysis and electrochemistry.

#### References

- [1] C. G. Vayenas, S. Bebelis, I.V. Yentekakis and H.-G. Lintz, *Catalysis Today*, **11**, 303 (1992).
- [2] C.G. Vayenas, S. Bebelis, and S. Ladas, *Nature*, **343**, 625 (1990).
- [3] I.V. Yentekakis, A. Palermo, N. Filkin, M. Tikhov and R. M. Lambert, *J. Phys. Chem. B*, **101**, 3759 (1997).
- [4] I.V. Yentekakis, A. Palermo, N. Filkin, M. Tikhov and R. M. Lambert, *Stud. Surf. Sci. Catal.*, **116**, 255 (1998).

## IN SITU SPECTROSCOPIC INVESTIGATIONS OF SILVER ELECTRODES ON STABILIZED ZIRCONIA

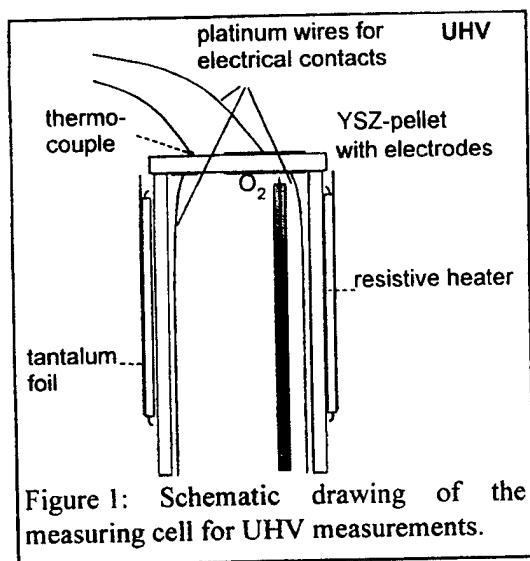
Martin Rösch, Götz Reinhardt, Wolfgang Göpel

Institute of Physical and Theoretical Chemistry and Center of Interface Analysis and Sensors,  
Auf der Morgenstelle 8, D-72076 Tübingen, Germany

### INTRODUCTION

The investigation of the nature of surface oxygen species on electrodes of solid oxygen ion conductors like zirconia is important to understand the mechanisms of catalytic and electrode reactions in electrocatalysis, solid electrolyte sensors and solid oxide fuel cells. In several studies work function changes [1,2,4] and spillover oxygen species [3,4] were observed during oxygen pumping. We developed a new setup for in-situ photoelectron spectroscopic and mass spectrometric investigations under ultra high vacuum (UHV), which allows to operate the electrochemical cell under well-defined thermodynamic conditions. In situ ultraviolet and x-ray photoelectron spectroscopic (UPS and XPS) studies have been performed on silver electrodes on yttria stabilized zirconia under applied potentials. In addition, impedance spectroscopic investigations have been performed in the same setup.

### EXPERIMENTAL



A new electrochemical setup operating with a gaseous oxygen reference was developed to perform in situ spectroscopic investigations under thermodynamically well defined conditions (figure 1). The setup consists of an yttria stabilized zirconia pellet sealed gas tight to a zirconia tube by a glass. The use of pellets allows to prepare well-defined electrodes by different techniques like vacuum evaporation or screen printing. A three-electrode arrangement is realized with the working electrode positioned at the UHV side of the pellet. Counter- and reference-electrodes are exposed to pure oxygen under reduced total pressure conditions. According to the results of numerical calculations [5], working- and counter-electrode of the same shape were placed exactly opposite to each other to achieve a homogeneous

potential distribution at the electrode/electrolyte interface. Pellet and tube are heated by two different heating systems: a xenon lamp inside the tube and a resistive platinum heater at the outside of the tube. The temperature of the pellet is detected by a Ni/NiCr-thermocouple. The whole electrochemical cell is integrated into a manipulator connected to the UHV system.

First investigations were performed on evaporated silver electrodes with thicknesses of 2  $\mu\text{m}$  at a temperature of 550°C and an oxygen pressure inside the tube of  $10^{-1}$  mbar. Under these conditions, the base pressure in the UHV system was about  $5 \cdot 10^{-9}$  mbar and open circuit potentials of the order of -1400 mV were observed. UPS was performed using He I (21.2 eV) and He II (40.8 eV), XPS using Mg  $K_{\alpha}$  (1253.6 eV) radiation. Potentials were applied by a Jaissle 1002 T-NC potentiostat. The working electrode was connected to ground during XPS studies. For UPS studies the working electrode was biased to -6V with respect to the ground.

## RESULTS

Potential-dependent measurements were performed for anodic potentials ranging from the open circuit potential (-1400 mV) to +100 mV. A significant oxygen current was observed for anodic potentials larger than -250 mV.

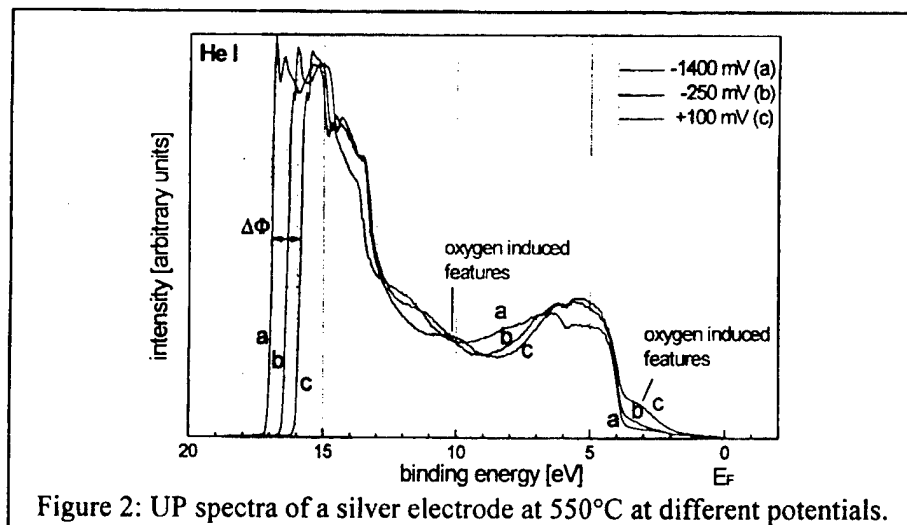


Figure 2: UP spectra of a silver electrode at 550°C at different potentials.

As a typical result, figure 2 shows UP(He I) spectra. Additional features at 3 eV and 10 eV binding energy appear in the spectra during oxygen pumping. These features are attributed to surface oxygen species. The work function increases from 4.25 eV at -1400 mV, which is close to the literature value for polycrystalline silver [6], to 5.35 eV at +100 mV. The correlation between change in work function and change in applied potential is non-linear. A large change in work function occurs in a comparatively narrow potential region between -250 mV and +100 mV. In this region large changes in the current were observed.

XP spectra of the O1s emissions show an increase in intensity and shift of the O1s signal in the direction to lower binding energies during oxygen pumping.

## DISCUSSION

The results show the possibilities of our new setup to perform in situ UHV spectroscopic investigations under well defined conditions. Its major advantages are the use of a gaseous reference with quasi-infinite amount of available oxygen for pumping and the use of pellets which permits proper and reproducible electrode preparation conditions. Significant changes in work function and oxygen induced features during oxygen pumping were observed in the UP spectra. Similar oxygen induced features were found in adsorption experiments on polycrystalline [7] and single crystalline [8] silver at high temperatures. A model is finally presented to explain the change in work function and the UPS and XPS results as a function of temperature and potential.

## REFERENCES

- [1] C.G. Vayenas, S. Bebelis and S. Ladas, *Nature* **343**, 625 (1990).
- [2] S. Ladas, S. Bebelis and C.G. Vayenas, *Surf. Sci.* **251/252**, 1062 (1991).
- [3] S. Ladas, S. Kennou, S. Bebelis and C.G. Vayenas, *J. Phys. Chem.* **97**, 8845 (1993).
- [4] W. Zipprich, H.-D. Wiemhöfer, U. Vohrer and W. Göpel, *Ber. Bunsenges. Phys. Chem.* **99**, 1406 (1995).
- [5] G. Reinhardt and W. Göpel, *Proc.-Electrochem. Soc.* **97-24**, 610 (1998).
- [6] H.B. Michaelson, *J. Appl. Phys.* **48**, 4729 (1977).
- [7] C. Rehren, M. Muhler, X. Bao, R. Schlögl and G. Ertl, *Z. Phys. Chemie* **174**, 11 (1991).
- [8] X. Bao, M. Muhler, Th. Schedel-Niedrig and R. Schlögl, *Phys. Rev. B* **54**, 2249 (1996).

## **XPS CHARACTERIZATION OF THE ELECTROCHEMICALLY GENERATED O SPECIES ON A Au ELECTRODE EVAPORATED ON Y<sub>2</sub>O<sub>3</sub> STABILIZED ZrO<sub>2</sub>(100).**

S.G. Neophytides, S. Zafeiratos, and S. Kennou

Institute of Chemical Engineering & High Temperature Chemical Processes  
P.O. Box 1414, Patras, GR-26500, Greece

The electrochemically induced modification of the surface properties of metal electrodes deposited on solid electrolytes, has been proved to be of high significance in catalysis and electrocatalysis [1]. Their catalytic properties can be considerably and reversibly affected by electrochemical variation of catalyst-electrode potential and work function. This is accomplished by the electrochemically controlled supply and adsorption of ionic species onto the catalyst-electrode surface. The existence of these ionic species was confirmed by XPS [2] and TPD [3] for polycrystalline Pt electrodes deposited on Ytria Stabilized Zirconia (YSZ) and by STM for Pt on  $\beta''$ -Al<sub>2</sub>O<sub>3</sub> [4]. These backspillover ionic adsorbates induce reversible alterations on the catalyst-electrode electronic properties, thus affecting the catalytic reaction rates.

In the present work, for the first time, XPS was used to investigate O species which are electrochemically generated onto a Au electrode surface, evaporated in UHV on YSZ(100) an O<sup>2-</sup> conductor. The present study is turned out to be quite helpful so as to clarify the origin of the promotional effect of applied current on the catalytic and electrocatalytic properties of Au surface.

The Au working electrode was evaporated in UHV on an YSZ single crystal (100) at 400°C by a resistively heated gold source. A Pt counter electrode was deposited on the other site of the crystal. Thus oxygen ions (O<sup>2-</sup>) could be supplied at the Au/YSZ interface by potential application between the counter and the working electrodes. The XPS measurements were performed at about 400°C, were the YSZ crystal was conductive, using a SPECS LHS 10 analyzer and the MgK $\alpha$  excitation source.

The electrochemical supply of oxygen ions (O<sup>2-</sup>) onto the Au film, via current application between the Pt counter and Au working electrodes, caused the creation of two distinct oxygen adsorption states at 530.0 eV and 532.4 eV, the area of which is progressively increased with increasing current application. This experimental evidence supports the observation of the two oxygen states on gold which were detected during TPD experiments following electrochemical O<sup>2-</sup> adsorption on Au electrode surface deposited on polycrystalline YSZ [5].

### **REFERENCES**

1. C.G. Vayenas and S.G. Neophytides, «Catalysis series of Royal Soc. Of Chem.», **12**, 199 (1996).
2. S. Ladas, S. Kennou, S. Bebelis and C.G. Vayenas, J. Phys. Chem., **97**, 8845 (1993).
3. S.G. Neophytides and C.G. Vayenas, J. Phys. Chem., **99**, 17063 (1995).
4. M. Makri, C.G. Vayenas, S. Bebelis, K.H. Besocke, C. Cavalia, Surf. Sci, **369**, 351 (1996)
5. D. Tsiplakides, S. Neophytides and C.G. Vayenas, Ionics, **3**, 201 (1997).



# OXYGEN ELECTRODE REACTION ON STABILIZED ZIRCONIA UNDER HIGH OXYGEN PRESSURE (up to 100 bar)

C. Drevet, M. Hénault, J. Fouletier\*

Laboratoire d'Electrochimie et de Physicochimie des Matériaux et des Interfaces (L.E.P.M.I.),  
E.N.S.E.E.G.-I.N.P. Grenoble, BP 75, 38402 Saint Martin d'Hères Cedex, (France)

Very few investigations have been carried out on the electrode reaction mechanism on stabilized zirconia at oxygen pressure higher than 1 bar.

The oxygen electrode reaction has been studied by impedance spectroscopy in the range 0.2 up to 100 bar (in the 50 kHz - 10<sup>-3</sup> Hz frequency range using a Frequency Response Analyzer). Three electrode materials have been tested : a metal dissolving no oxygen, i.e. platinum, a metal dissolving high oxygen content, i.e., silver, and an oxide with perovskite structure (doped lanthanum manganite).

With platinum (paste, Degussa 308 A), whatever the oxygen pressure and temperature, the impedance diagrams can be deconvoluted into one single semicircle. The variation of the polarization resistance with the oxygen pressure we have obtained is given in figure 1 a.

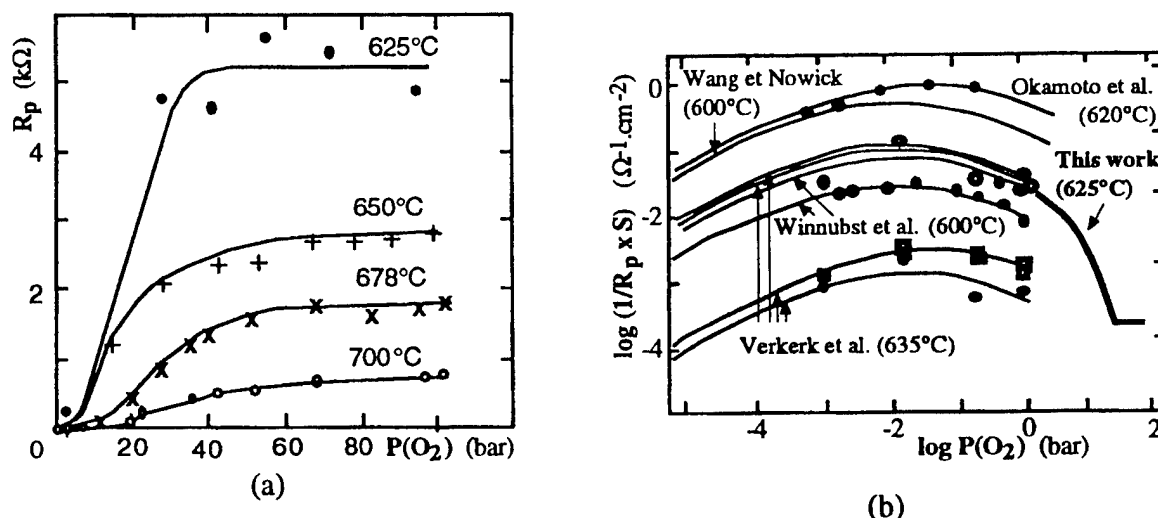


Figure 1 : Polarization resistance variation of platinum electrode as a function of oxygen pressure.

(a) Our results, in the range 0.2 to 100 bar

(b) Comparison of our work around 600°C with published results (from Mizuzaki et al. [1]).

The polarization resistance increases with oxygen pressure and then remains constant. The oxygen pressure corresponding to the maximum of the  $R_p = f[P(O_2)]$  curves increases with the oxygen pressure, i.e., 30 bar at 650°C and 90 at 750°C. Generally, an increase of the reciprocal polarization resistance is observed with the oxygen pressure at low oxygen pressure, as shown in fig. 1 b. In this oxygen pressure range, reported polarization resistances vary as  $P(O_2)^{-n}$  with  $n$  equal to 0.25 or 0.5 according to the limiting step of the electrode reaction. In spite of disagreements in the polarization resistance values, the published results show similar oxygen pressure dependence, with a maximum of  $\sigma_E$  around 10<sup>-2</sup> bar at 600°C. As shown in fig. 1 b, our results are in good agreement with the published results obtained at oxygen pressure lower than 1 bar.

This behaviour appears reversible after oxygen pressure cycles. Moreover, the calculated electrode capacitance values are low (of the order of 1  $\mu F \cdot cm^{-2}$ ).

\* to whom correspondence should be addressed

These results have been attributed to platinum oxide formation at high oxygen pressure. Such superficial platinum oxide formation has been suggested previously for oxygen pressures lower than 1 bar.

With sputtered silver electrode, the variation of the polarization resistance with the oxygen pressure is given in fig. 2 a. For oxygen pressure lower than 30 bar, at 500°C, the polarization resistance decreases with the oxygen pressure, corresponding to an increase of the electrode reversibility. At very high oxygen pressures, a sharp increase of the polarization resistance was observed. This behaviour has been explained by the formation of silver oxide, Ag<sub>2</sub>O.

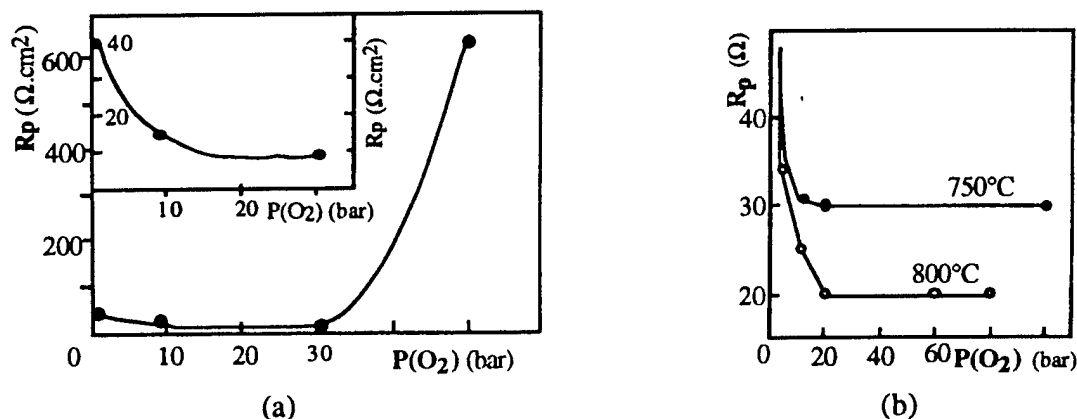


Figure 2 : Polarization resistance variation of silver and doped lanthanum manganite electrodes as a function of oxygen pressure.

(a) Sputtered silver (500°C), (b) Doped lanthanum manganite (LSM<sub>35</sub>) deposited from a slurry.

Examples of impedance diagrams as a function of the oxygen pressure, with doped lanthanum manganite (La<sub>0.65</sub>Sr<sub>0.35</sub>MnO<sub>3</sub>, referred to as LSM<sub>35</sub>) is given in fig. 3. At low frequency the diagram shape is characteristic of a diffusion limiting process.

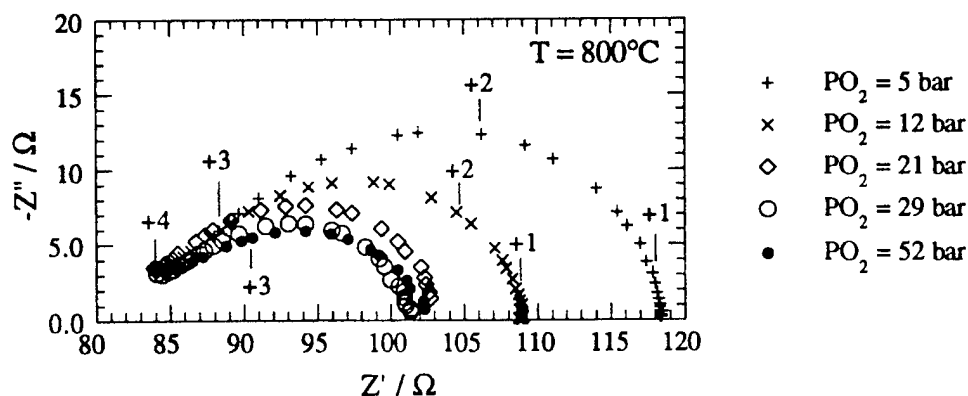


Figure 3 : Examples of impedance diagrams obtained at 800°C with LSM<sub>35</sub> electrode.

As shown in fig. 2 b, a decrease of the electrode polarization with the oxygen pressure was observed. This behaviour can be ascribed to a change of the electrode stoichiometry with the oxygen pressure.

This work was supported by Cryotechnologie S.A. (Blagnac, France) and C.N.E.S. (Centre National d'Etudes Spaciales, Toulouse, France).

#### Reference

- [1] J. Mizusaki, K. Amano, S. Yamauchi and K. Fueki, Solid state Ionics **22**, 313 (1987).

ELECTROCHEMICAL PROMOTION OF RuO<sub>2</sub>-CATALYSTS  
FOR THE GAS PHASE COMBUSTION OF C<sub>2</sub>H<sub>4</sub>S. Wodiunig<sup>1</sup>, V. Patsis<sup>2</sup>, F. Roubani-Kalantzopoulou<sup>2</sup> and C. Comninellis<sup>1</sup><sup>1</sup>Institute of Chemical Engineering, Swiss Federal Institute of Technology, CH-1015 Lausanne,  
Switzerland<sup>2</sup>Departement of Chemical Engineering, National Technical University of Athens,  
GR-15780 Zografou, Greece

The electrochemical promotion (EP) or NEMCA-effect opens new dimensions in heterogeneous catalysis. It allows a reversible *in-situ* modification of catalytic properties compared with the well known irreversible modifications by doping of the catalyst, by catalyst-support interaction or by gas phase promoters.

The EP was studied for the combustion of C<sub>2</sub>H<sub>4</sub> as a model substance for volatile organic compounds (VOC) over thin RuO<sub>2</sub>-catalyst films. The electrochemical cell consisted of a yttria stabilised zirconia plate (YSZ) which was used as well as solid electrolyte and as support for the electrodes. The working electrode or catalyst (RuO<sub>2</sub>) was deposited on one side of the plate and the gold counter and reference electrode on the opposite side. The catalyst films were prepared by thermal decomposition of ruthenium (III) chloride dissolved in 2-propanol. The optimal decomposition temperature was found to be at 550°C. The catalyst films were characterised by XRD, XPS and SEM measurements. The EP measurements were carried out in a constant flow stirred tank reactor (CSTR-type).

The behaviour of pure ruthenium dioxide catalysts were studied under open circuit condition and during galvanostatic polarisation. A kinetic model which takes the ethylene and the oxygen partial pressure into consideration was proposed by Wodiunig et al. [1] for RuO<sub>2</sub> catalysts. The model assumes a dissociative oxygen adsorption in two steps. The reaction between ethylene from the gas phase and atomically adsorbed oxygen is considered to be irreversible forming a highly reactive intermediate in the gas phase. It will be shown that both the adsorption of oxygen and the reaction of ethylene from the gas phase with adsorbed oxygen are influenced by the EP. This can be explained by the lowering of the binding strength of adsorbed oxygen during anodic polarisation of the catalyst. The influence of the anodic polarisation on the desorption activation energy of oxygen was studied in an earlier work [2]. It was found that the desorption activation energy of adsorbed oxygen is decreasing with increasing potential.

The increase of the reactivity of adsorbed oxygen is explained by a backspillover of oxygen ions over the gas exposed catalyst surface [3, 4]. The influence of the backspillover oxygen ions on the work function of RuO<sub>2</sub>-catalyst films were measured *in-situ* using the Kelvin Probe method by Wodiunig et al. [5]. It was found that the work function is increasing during anodic polarisation. The influence of the polarisation time led to the assumption that backspillover oxygen ions are formed at the three phase boundary (tpb) which are then slowly migrating over the gas exposed catalyst surface changing the catalyst work function.

The influence of the thickness of the catalyst film was studied by cyclic voltammetry measurements. The voltammetric charge was found to be independent on the thickness of the catalyst film (Fig.1). The catalytic reaction rate after anodic polarisation was also found to be independent of the voltammetric charge (Fig.2). These two results are in good agreement and show that the voltammetric charge of ruthenium dioxide catalysts interfaced with YSZ is mainly

located at the interface between the catalyst and the solid electrolyte which explains also the relatively low measured charge.

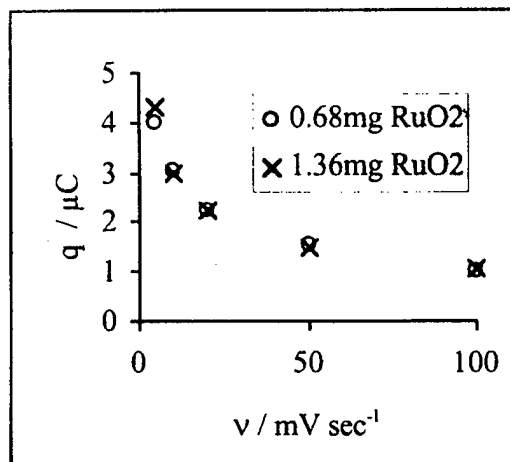


Fig.1: Dependence of the catalyst amount on the voltammetric charge for different sweep rates.  $P_{\text{C}_2\text{H}_4}=0.1\text{kPa}$ ,  $P_{\text{O}_2}=12\text{kPa}$ ,  $T=380^\circ\text{C}$ ,  $V=175\text{mlmin}^{-1}$  STP.

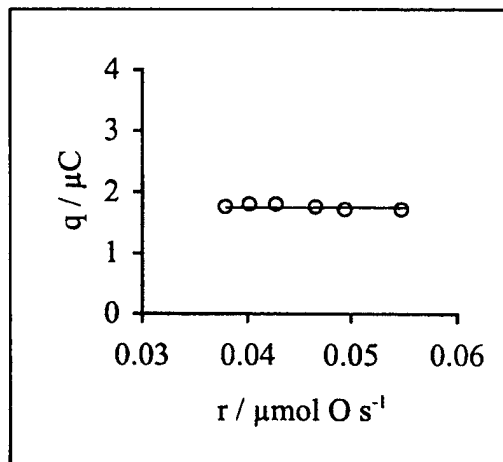


Fig.2: Dependence of the catalytic reaction rate on the voltammetric charge after polarisation. Sweep rate  $v=20\text{mVs}^{-1}$ ,  $P_{\text{C}_2\text{H}_4}=0.1\text{kPa}$ ,  $P_{\text{O}_2}=12\text{kPa}$ ,  $T=380^\circ\text{C}$ ,  $V=175\text{mlmin}^{-1}$  STP.

- [1] S. Wodiunig and C. Comninellis, 5<sup>th</sup> European Symposium on Electrochemical Engineering, Exeter '99, *in press*.
- [2] S. Wodiunig and C. Comninellis, *J. Europ. Cer. Soc.*, *in press*.
- [3] Vayenas, C. G., Jaksic, M. M., Bebelis, S. and Neophytides, S. G., *Modern Aspects of Electrochemistry*, Bockris, J. O'M., Conway, B. E. and White, R. E., Editors, Plenum Press, New York, 29, 1995.
- [4] J. Nicole and C. Comninellis, *J. Appl. Electrochem.* **28**, 223 (1998).
- [5] S. Wodiunig, C. Comninellis and C. Mousty, *The Electrochemical Society Proceedings Series*, Paris '97, W. A. Adams, L. J. J. Janssen, E. J. Rudd, J. Thonstad and C. W. Walton, Editors, Pennington, 147.

# EFFECTS OF ACOUSTIC WAVES GENERATED ON POLARIZED FERROELECTRIC SUBSTRATES UPON SELECTIVITY CHANGES IN ETHANOL DECOMPOSITION OVER Ag and Cu THIN FILMS

H. Saito, H. Nishiyama, K. Sato, and Y. Inoue\*

Department of Chemistry, Nagaoka University of Technology,  
Nagaoka 940-2188, Japan

The design of a catalyst which has artificially controllable functions for chemical reactions is among important issues. We have demonstrated that surface acoustic waves (SAWs) and resonance oscillation (RO) of bulk acoustic waves, generated on a poled ferroelectric support by applying radio frequency electric power, are useful for the artificial control of catalysis [1,2]. In the present work, the effects of different vibrational mode resonance oscillation and of polarized ferroelectric substrates on the selectivity of catalytic ethanol decomposition were studied.

A X-cut  $\text{LiNbO}_3$  single crystal with a thickness-shear mode vibration and a Z-cut  $\text{LiNbO}_3$  single crystal with a thickness-extensional mode vibration were employed as ferroelectric substrates. These crystals have a resonance frequency of 3.5 MHz as the primary line. On the front and back planes of the crystal, a 100 nm thin Ag or Cu film, which works as a catalyst as well as an electrode, was deposited by resisting heating of a Ag or Cu metal in high vacuum. Temperature of the catalyst surfaces was measured by a radiation thermometer and by the shift of resonance frequency, and controlled by an outer electric furnace. Radio frequency power was generated from a network analyzer, amplified and introduced to the catalyst after impedance adjustment. The catalytic decomposition of ethanol vapor was carried out in a gas-circulating reaction system, and the products were analyzed by gas chromatograph connected to the reaction system.

Ethanol decomposition over Ag deposited on the  $\text{LiNbO}_3$  substrates produced ethylene as dehydration and acetaldehyde as dehydrogenation. When a shear mode RO was generated with Ag/X-cut  $\text{LiNbO}_3$  at a frequency of 3.5 MHz by a rf power of 3 W, no activity enhancement of the Ag catalyst was observed. On the other hand, the thickness-extensional mode RO (TERO) of Ag/Z-cut  $\text{LiNbO}_3$  caused the enhancement of activity for ethylene production by a factor of 10 at 573 K, whereas the acetaldehyde production was not accelerated. The increased activity for ethylene production was maintained until the power was turned off. Similar selective activity increase for ethylene production, compared to acetaldehyde production, was observed for Cu/Z-cut  $\text{LiNbO}_3$  with TERO-on.

A Z-cut  $\text{LiNbO}_3$  single crystal has polarization axis normal to the surface and exposes a positively and a negatively polarized surface at the front and back side of the crystal. In order to see the effects of the polarized surfaces on the catalyst activation, either of the polarized surfaces was deposited by Ag, and the opposite was covered with a catalytically inactive Al metal, as shown in Fig. 1. The activity enhancement for ethylene production showed polarization dependence of the ferroelectric support. Fig. 2 shows ethylene and acetaldehyde production with reaction time. With TERO-on, the production of ethylene increased remarkably for Ag deposited on a positively polarized Z-cut  $\text{LiNbO}_3$  substrate ( (+)Ag ), whereas the activity for acetaldehyde production was not enhanced. For Ag

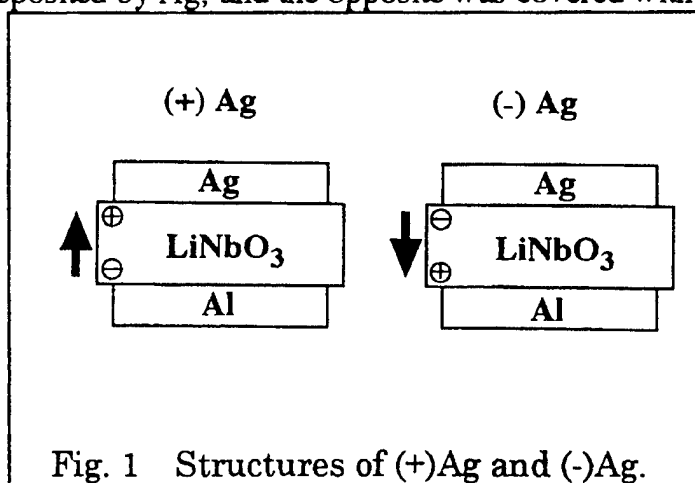


Fig. 1 Structures of (+)Ag and (-)Ag.

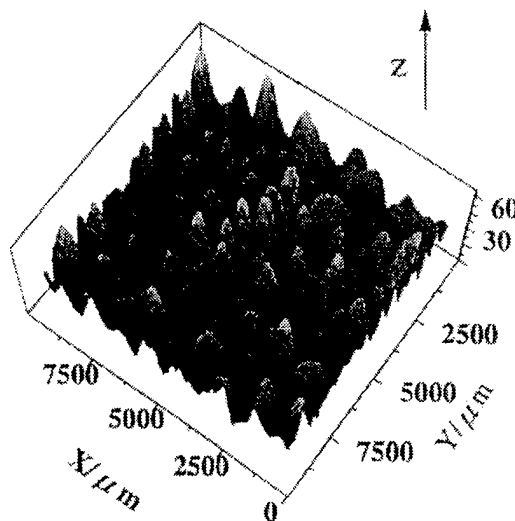
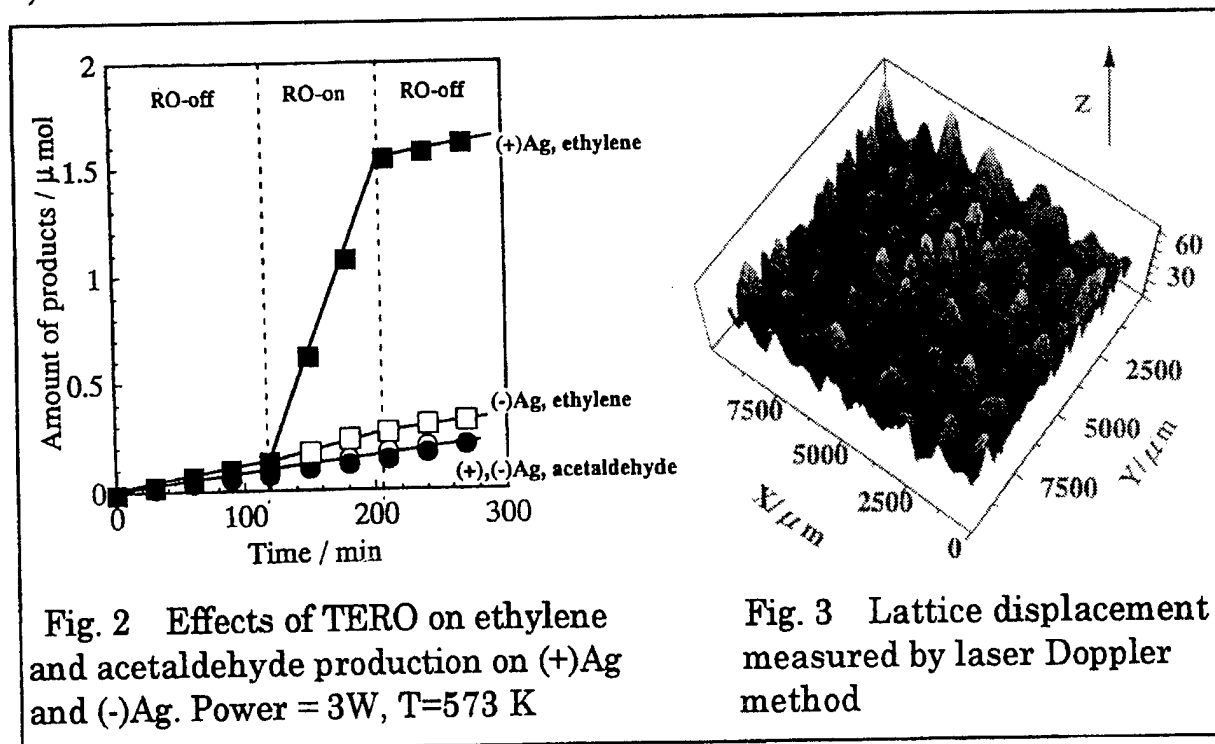
deposited on a negatively polarized Z-cut LiNbO<sub>3</sub> substrate ( (-)Ag ), only a small increase in the activity for ethylene production was observed with TERO-on, and little increase in acetaldehyde production was the same as observed for (+)Ag. At a power of 3 W, the selectivity for ethylene production increased from 47% without TERO to 86% for (+)Ag, but remained at a low level of 60 % for (-)Ag. Furthermore, for (+)Ag, the activation energy of ethylene formation decreased from 156 kJ mol<sup>-1</sup> with TERO-off to 103 kJ mol<sup>-1</sup> with TERO-on but that of acetaldehyde production, 95 kJ mol<sup>-1</sup>, remained unchanged. On the other hand, for (-)Ag, the activation energy of ethylene formation slightly decreased from 156 kJ mol<sup>-1</sup> to 145 kJ mol<sup>-1</sup>.

The thickness mode vibration of TERO is supposed to exhibit uniform movement over a whole surface. As shown in Figure 3, however, three dimensional laser Doppler measurements have demonstrated that the TERO of Z-cut LiNbO<sub>3</sub> produced irregular standing wave patterns of dynamic lattice displacement and that the vibration is composed of many parts with different amplitudes ranging from 20 to 70 nm. This irregular pattern of the standing waves indicates that surface lattice of the catalyst at some parts is more significantly distorted than that at the others.

Surface potential measurements showed that the potential varied in an opposite way between the polarized surfaces: a negative voltage was generated for (+)Ag, and vice versa. In contrast, X-cut LiNbO<sub>3</sub> caused neither significant lattice displacement nor changes in the surface potential. These results indicate that the thickness-extensional mode RO which causes large lattice displacement vertical to the surface is effective for changing the selectivity. A mechanism is proposed in which the (+)Ag surface results in electron enrichment and the (-)Ag surface in an electron deficient state with TERO-on.

The TERO effects are proved to be useful for the artificial control of selectivity of Ag catalysts for ethanol decomposition, and it would be possible to apply the effects to any metal and even oxide catalysts. Although a variety of catalytic systems must be further examined, the present results suggest the development of a catalyst which has artificially controllable functions for the selectivity of chemical reactions.

- 1) N. Saito, Y. Ohkawara, Y. Watanabe, Y. Inoue, Appl. Surf. Sci., 121/122 (1997) 343.
- 2) Y. Ohkawara, N. Saito, K. Sato, Y. Inoue, Chem. Phys. Lett., 286 (1998) 502.



## THE INFLUENCE OF POINT DEFECTS ON THE RESISTANCE OF CERIA TO CARBON DEPOSITION IN HYDROCARBON CATALYSIS

E. Ramirez-Cabrera<sup>1</sup>, A. Atkinson<sup>1</sup> and D Chadwick<sup>2</sup>

<sup>1</sup> Department of Materials and <sup>2</sup> Department of Chemical Engineering  
Imperial College of Science Technology and Medicine  
London SW7 2BP, UK

Cerium oxide is used in a wide variety of reactions involving the oxidation, or partial oxidation, of hydrocarbons (e.g. automotive catalysis). The reason for this is that the ceria lattice can contain a high concentration of highly mobile oxygen vacancies and can thus act as a local source or sink for oxygen involved in reactions taking place on the ceria surface or on other catalytic materials supported on the ceria. There is now increasing interest in using ceria in more reducing conditions, such as in methane reforming at the anodes of solid oxide fuel cells, where the potential for deactivation through carbon deposition is much greater. Consequently we have been studying the deposition and oxidation of carbon on ceria by temperature programmed reaction techniques.

Ceria powders, doped with either 10 cation % Gd, 0.8 cation % Nb or undoped were prepared by co-precipitation from aqueous solutions and calcined at 1000 °C for 1 h in air. Temperature programmed reactions were studied using small (up to 100 mg) powder specimens in a microreactor system. Premixed gases were passed into the microreactor and after reaction at the specimen were analysed using either a flame ionisation detector or mass spectrometer. Temperature programmed reduction (TPR) was first carried out in a mixture of 5 % hydrogen in argon to establish a standard reduced starting condition. Carbon deposition on the cerias from a mixture of helium and methane was then studied by both isothermal exposure and temperature programmed reaction (TPRx). Deposition was studied on both pre-oxidised and pre-reduced surfaces. Finally the subsequent oxidation of deposited carbon was investigated by temperature programmed oxidation (TPO) in a mixture of 10 % oxygen and helium. The surface condition of the ceria specimens was characterised at different stages in these processes by XPS. The results are interpreted in terms of the known point defect properties of ceria and how the concentrations of oxygen vacancies and electronic carriers change with temperature, dopant and oxygen activity. The behaviour of ceria is compared with that already established for Ni supported on zirconia [1, 2] and doped lanthanum chromite [3].

- [1] R.T. Baker and I.S. Metcalfe, *Ind. Eng. Chem. Res.* 34, 1558 (1995).
- [2] R.H. Cunningham, C.M. Finnerty and R.M. Ormerod, *Electrochem. Soc. Proc.* 97-40, 973 (1997).
- [3] R.T. Baker and I.S. Metcalfe, *Appl. Cat. A*, 126 297 and 319 (1995).

## ELECTROCHEMICAL PROMOTION OF ETHYLENE AND PROPYLENE OXIDATION ON Pt DEPOSITED ON YTTRIA-TITANIA-ZIRCONIA

P. Beatrice, AAAS Defense Policy Fellow, W.L. Worrell, U. Penn.;  
C. Vayenas U. Patras

### Introduction

The electrochemical promotion of the oxidation of ethylene and propylene was investigated on a Pt catalyst film deposited on 4.5 mol% yttria-10 mol% titania-zirconia electrolyte. Propylene oxidation was enhanced by a factor of 2 upon the application of -2V in an oxidizing environment for temperatures between 350 and 500°C. In the same environment, the system showed a smaller rate increase under the application of positive voltage. Ethylene oxidation using similar temperatures, oxygen-rich gas conditions, and flowrates, showed oscillatory reaction behavior under both open circuit and applied voltage conditions. Upon application of -2V, the oxidation rate was enhanced by a factor of 2. The modest enhancement factors, compared to similar systems using a yttria stabilized zirconia electrolyte, is presumably due to the lower ionic conductivity resulting from the titanium dopant.

### Experimental

The 4.5 mol% yttria-10 mol% titania-zirconia (YZTi10) powder was produced using a co-precipitation process. The powder was isopressed into discs (1 mm thick) that were sintered at 1600°C for 12 hours in air. The Pt working electrode and the Au counter and reference electrodes were prepared by standard procedures described elsewhere [1]. The sample was mounted in a continuous flow "single-pellet" reactor and exposed to reactant gases of pure He and mixtures of O<sub>2</sub>/He, C<sub>2</sub>H<sub>4</sub>/He, and C<sub>3</sub>H<sub>6</sub>/He. Gas flow rates between 150 to 200 cm<sup>3</sup>/min were used. A Perkin-Elmer Sigma 300 Gas Chromatograph with a Porapak N column was used to analyze the reactant and product gases. In addition, the CO<sub>2</sub> concentration was monitored with an Anarad IR Gas Analyzer.

### Results

The Pt/YZTi10/Au cell was characterized to determine the open circuit behavior, current-voltage relationship, and NEMCA behavior. The extent of electrochemical promotion (NEMCA) was quantified using the non-Faradaic efficiency factor

$$\Lambda = \Delta r / (I/2F) \quad (1)$$

where  $\Delta r$  is the difference between the reaction rate under an applied voltage and the reaction rate under open circuit conditions,  $I$  is current, and  $F$  is Faraday's constant and the enhancement ratio,  $\rho$ , which is the ratio of the reaction rate under applied voltage to the reaction rate under open circuit conditions.

#### 1) PROPYLENE OXIDATION

Under open circuit conditions at 450°C, the effect of varying the P<sub>O<sub>2</sub></sub> with constant P<sub>C<sub>3</sub>H<sub>6</sub></sub> shows that the reaction rate increases with increasing oxygen throughout the measured range of 0 to 8 kPa O<sub>2</sub>. The effect of varying the partial pressure of C<sub>3</sub>H<sub>6</sub> under constant P<sub>O<sub>2</sub></sub> shows a maximum at approximately 1.5 kPa C<sub>3</sub>H<sub>6</sub>. The fact that there is a rate maximum with respect to propylene but not with respect to oxygen indicates that the propylene is more strongly adsorbed on the Pt surface.

The current-potential behavior was measured in an atmosphere of 9.7 kPa O<sub>2</sub> and 2.1 kPa C<sub>3</sub>H<sub>6</sub> for temperatures between 400 and 500°C. The activation energies of the anodic and cathodic exchange currents are 29 and 21 kcal/mol, respectively, in good agreement with the 26.6 kcal/mol value found for propylene oxidation on Pt/YSZ/Au. [3] At 450°C, the cell shows electrophilic behavior with a  $|\Lambda|$  factor of 92 and a  $\rho$  value of 2 upon the application of -2V. Enhancement of the rate is also seen at 450°C with the application of a positive potential, but with a smaller  $\Delta r$  and a



lower  $\Lambda$  value of 49 at +2V applied voltage. NEMCA behavior was observed only under oxidizing conditions.

## 2) ETHYLENE OXIDATION

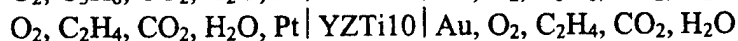
The current-voltage behavior for ethylene oxidation in 9 kPa O<sub>2</sub> and 2.1 kPa C<sub>2</sub>H<sub>4</sub> shows that the oxidation of ethylene is faster than that of propylene. The upper temperature for evaluation was limited to 475° C because the reaction and conversion rates increased dramatically above this temperature.

Under oxidizing conditions oscillatory reaction behavior was observed. Several heterogeneous catalytic reaction systems exhibit isothermed kinetic oscillations, including oxidation of CO, hydrogen, and hydrocarbons on noble metals. The oscillations under P<sub>O2</sub>=13 kPa and P<sub>C2H4</sub>=2kPa are confined within stable high and low activity rates over a time period of 35 minutes. Each individual oscillation has a period of approximately 50 seconds. At the higher P<sub>O2</sub> of 17 kPa the oscillation pattern destabilizes with time showing increasing range of activity and an extending period.

The oxidation rate is enhanced with the application of -2V. A potentiostatic transient under stoichiometric conditions (where reaction conditions were nonoscillating) shows an enhancement ratio of 2 and a non-Faradaic efficiency of 250. Under oxidizing conditions and a corresponding oscillating reaction rate, the application of -2V doubles the reaction rate but the increase is not sustained over time.

## CONCLUSIONS

The solid oxide fuel systems



both exhibit NEMCA behavior. Propylene oxidation showed both electrophobic and electrophilic behavior with an enhancement ratio,  $\rho$ , of 2 and a non-Faradaic efficiency,  $\Lambda$ , of -92 upon the application of -2V and a  $\rho$  of 2.4 and a  $\Lambda$  of 49 under +2V. Ethylene oxidation exhibits oscillatory kinetics under both open circuit and applied voltage conditions in an oxidizing environment, and its catalytic rate doubled with an applied voltage of -2V. The rate oscillations grew more unstable with increasing P<sub>O2</sub>.

1. C.G. Vayenas, M.M. Jaksic, S.I. Bebelis and S.G. Neophytides in *Modern Aspects of Electrochemistry*, J.O'M. Bockris, B.E. Conway and R.E. White, Eds., Vol. 29, Plenum Press, NY, 57 (1995).
2. C. Pliangos, I.V. Yentekakis, S. Ladas and C.G. Vayenas, *J. Catalysis* **159**, 189 (1996).
3. A. Kaloyiannis and C.G. Vayenas, *J. Catalysis* **182**, 37 (1999).

# APPLICATION OF SOLID OXIDE ELECTROLYTE AMPEROMETRIC CELLS FOR STUDIES OF COMPLEX REACTION KINETICS

S.I. Somov\*, U. Guth†

\*Institute of High Temperature Electrochemistry, Ekfeterinburg, 62219, Russia

†Institute of Physical Chemistry of the University of Greifswald, , Soldtmannstr. 16/23,  
D-17489 Greifswald, Germany

A separation of concurrent reactions in a complex chemical process is a common problem in electrochemistry and catalysis. This question could be considered from different angles. One task is a separation of competing reactions taking place simultaneously at the same place. Usually, it is necessary to measure or to control the individual rates of constituent reactions. The purpose may consist in obtaining of the certain product or in preventing of the undesirable chemical process. It is nontrivial task, which needs a special approach for each case. A necessary information may be extracted from analysis of reaction products, thermal energy flux, or from signals of sensors incorporated in the reactor. Then, a pattern of reactions may be reconstructed through solution of the inverse problem. A weakness of the method based on analysis of products is that it gives an indirect information and a gas composition may be changed at the way from reactor to analytic instrument. Methods based on high temperature solid electrolyte cells provide the means for studies of complex reactions in situ [1]. An application of amperometric cells gives a way for precise distinguishing between competing reactions [2]. Such kind of cell has been used for separation of CO reduction to carbon from reduction of CO<sub>2</sub> to CO [3]. The steady state rate of the last reaction has been totally controlled by diffusion barrier. The rate of former reaction has been measured in two ways: as excess current comparing to limiting one, or by means of oxidation of an accumulated carbon. The rate of the last reaction is much faster, but this reaction result in the carbonising of electrodes and a damage of the device. A similar problem takes place for a fuel cell anode, when it works with a natural gas feeding in the internal reforming mode.

A more complicated problem is an exploration of space distributed composite reactions. It may be necessary to determine a distribution of certain reaction flows in the space, or to control the overall process such a way that a needed space separation of different reactions is realised. Such task takes place in applications of multi-electrode amperometric sensors for parallel measurement of gas components in a complex mixture [4]. In this sensor electrochemical reactions at working electrode give signals on concentrations of electrochemically active gas components. A complete information about distribution of constituent reactions is necessary for measurement of gas composition. A theory based on conditions of mass and charge balance in the cell connects sensor's signals and gas composition. If N is a number of electrochemically active components, and it is equal to number of working electrodes, then:

$$x_j = \frac{I_{j,lim}}{I_j^{(0)}} = \frac{1}{I_j^{(0)}} \left( \sum_{i=1}^N \beta_{ji} \cdot I_i \right) \quad (1).$$

Here:  $x_j$  - the mole fraction of component j in the analysed environment,  $I_{j,lim}$  the limiting current of the reduction/oxidation of component j,  $I_j^{(0)}$  - the limiting current constant of component j, and matrix  $\hat{\beta}_{ji}$  is the reciprocal matrix of the matrix selectivity  $\hat{\alpha}_{ij}$ . The last matrix is derived easily from a series of N tests with different gas compositions. Theory operates with

linear matrix equations, and its application is limited to linear systems. It is valid to amperometric sensors because of small concentrations of reactive gases in the working space of the cell. The method has been applied for parallel measurements of oxygen, nitrogen oxides and combustible components in exhaust gases. Solid electrolyte amperometric sensors are very flexible instrument because of opportunity for regulation of sensor's functions and characteristics. This control is based on optimization of a sensor's structure, selection of electrode materials, temperature regime, and working potentials.

In kinetic studies this approach opens an effective ways for comparative studies of reaction kinetics at different catalyst materials and electrodes under different working conditions (gas composition, temperature, and electrode potential). Theory, developed for multi-electrode sensors, gives a simple formal way for extraction of complete information about distribution of reaction rates in working space of chemical or electrochemical reactor. Elements of matrix selectivity  $\hat{\alpha}_{ij}$  are fractions of the certain electrochemical reactions at the each individual electrode. So, in parallel with development of amperometric sensors information on specific reaction kinetics have been accumulated. This knowledge may be applied in techniques for control of the complex reaction process.

A double electrode amperometric cell has been used for investigation of NO decomposition in presence of oxygen. The cell with noncatalytic electrode has been used in investigations of oxidation reaction kinetics for such components as: CO, H<sub>2</sub> and some hydrocarbons. Subsequent development has given a means for separation not only electrochemical reactions but catalytic reaction rates in chemically non-equilibrium mixtures.

#### REFERENCES

1. C. Wagner. *Adv. Catalysis* **21**, 323 (1970).
2. S.I. Somov, U. Guth. The 1997 Join International Meeting of Electrochemical Society and International Society of Electrochemistry. Paris. Abstracts 2557 (1997).
3. S.I. Somov, M.V. Perfil'ev. *J. Russian Electrochimia* **16**, 1246 (1980).
4. S.I. Somov, G. Reinhardt, U. Guth, U. Schönauer and Göpel. *Ionics* **1**, 514 (1996).

## INVESTIGATION OF ELECTROCHEMICAL PROMOTION USING TPD AND WF MEASUREMENTS

D. Tsiplakides, S. Neophytides\* and C.G. Vayenas

Department of Chemical Engineering, University of Patras, Patras GR-26500, Greece

\* Institute of Chemical Engineering and High Temperature Chemical Processes, P.O. Box 1414,  
Patras GR-26500, Greece

### INTRODUCTION

The catalytic activity and selectivity of metal films in contact with electrolytes, both solid state and aqueous, can be varied in situ in a very pronounced and reversible manner. This is accomplished via electrical potential application (typically  $\pm 1-2$  V) between the catalyst film and a counter electrode also in contact with the electrolyte. The catalytic rates can thus be varied by up to a factor of 200 while their induced steady-state change is up to five order of magnitude larger than the steady-state rate of electrochemically supplied ionic species from the solid electrolyte onto the catalyst surface. This novel effect of Electrochemical Promotion (EP) or non-Faradaic Electrochemical Modification of Catalytic Activity (NEMCA) has been studied for over 45 catalytic reactions on Pt, Ag, Ph, Pd, Ni, IrO<sub>2</sub> and RuO<sub>2</sub> catalyst-electrodes using a variety of solid electrolytes (O<sup>2-</sup>, F<sup>-</sup>, Na<sup>+</sup>, H<sup>+</sup> conductors), mixed ionic-electronic conductors and aqueous alkaline solutions [1]. The physicochemical origin of the EP effect has been explored using a variety of techniques including work function measurements, XPS, UPS, TPD, cyclic voltammetry, STM and ab initio quantum mechanical investigations [1].

In present study the origin of the EP effect was investigated using Y<sub>2</sub>O<sub>3</sub>-stabilized-ZrO<sub>2</sub> (YSZ), an O<sup>2-</sup> conductor as a solid electrolyte. Two different techniques were utilized:

- a) Temperature Programmed Desorption (TPD) of oxygen from polycrystalline Pt and Ag films under high-vacuum conditions.
- b) Work function measurements of a Pt film under reaction conditions in atmospheric pressure.

### EXPERIMENTAL

The TPD experiments were carried out in a vacuum chamber equipped with a mass-spectrometer in order to follow the oxygen adsorption from the catalyst films. Three modes of oxygen adsorption on the catalyst surface were used for the thermal desorption experiments: (i) gaseous oxygen adsorption by exposure to oxygen atmosphere, (ii) electrochemical oxygen adsorption, by application of positive current between the catalyst and a Au counter electrode and (iii) mixed gaseous and electrochemical adsorption. For the work function investigations an electrochemical reactor of novel design was used in which work function measurement could be carried out in situ during kinetic measurements of the ethylene oxidation reaction. For measuring the catalyst work function a Kelvin probe was used which was entirely independent of the solid electrolyte cell circuit.

### RESULTS AND DISCUSSION

After exposure of the Pt and Ag catalyst films to gaseous oxygen for several temperatures and exposures times, two different behaviors were observed as depicted from the corresponding oxygen thermal desorption spectra. In the case of Pt, under all experimental conditions, a single oxygen desorption peak with a peak temperatures at  $445 \pm 59^\circ\text{C}$ , attributed to the dissociatively chemisorbed oxygen species. The situation is more complex in the case of the Ag catalyst film. At low temperature a single peak is obtained, attributed to the same oxygen species as in the case of Pt. When the adsorption temperature is raised to  $350^\circ\text{C}$ , two oxygen species are present, at

400°C and 500°C. The low temperature peak is again assigned to chemisorbed oxygen species while the high temperature one corresponds to the sub-surface oxygen.

Electrochemical  $O^{2-}$  supply to the Pt-catalyst film through the solid electrolyte leads to the creation of two oxygen peaks. The low temperature peak corresponds to the atomic oxygen while the high temperature peak is attributed to the strongly bonded "ionic" or "backspillover" oxygen. The latter does not form via gas-phase adsorption. Electrochemical adsorption on Ag causes also the formation of the two oxygen species, namely the weakly bound atomic and the strongly bonded anionic oxygen. In both cases the two oxygen species coexist on the surface.

Electrochemical  $O^{2-}$  pumping to Pt and Ag catalyst film in the presence of preadsorbed oxygen (mixed adsorption) creates strongly bonded "backspillover" anionic oxygen, with a concomitant pronounced lowering of the desorption temperature of the more weakly bound preadsorbed atomic oxygen (Figure 1). The lowering of  $T_p$  is about 500°C for Pt and  $\sim 30^\circ\text{C}$  for Ag. This pronounced weakening in the metal-oxygen bond causes the observed dramatic catalytic rate enhancement in NEMCA studies, while the strongly bonded oxygen state acts as a sacrificial promoter.

In order to measure the desorption activation energy of oxygen,  $E_d$ , the modified Redhead analysis of Falconer and Madix [2] was applied. In both cases it was found that  $E_d$  decreases linearly with increasing catalyst potential (Figure 2). This decrease implies a pronounced increase in the desorption rate of adsorbed oxygen at any fixed temperature and thus an increase in the reactivity of adsorbed oxygen for catalytic oxidation reactions.

The work function of the Pt catalyst film was measured under different reaction mixtures and temperatures. A strong relationship between the oxygen to ethylene ratio was observed. The effect of catalyst potential on catalyst work function was also investigated. Small deviations from the equality between changes in catalyst potential and changes in catalyst WF were observed, strongly depending on the reaction mixture.

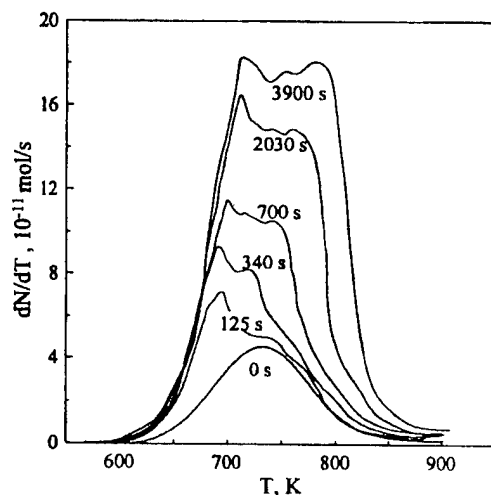


Fig. 1: TPD spectra after gaseous oxygen adsorption on Pt at 673 K and  $P_{O_2} = 4 \times 10^{-6}$  Torr for 1800 s followed by electrochemical  $O^{2-}$  supply ( $I = +15 \mu\text{A}$ ) for various time periods.

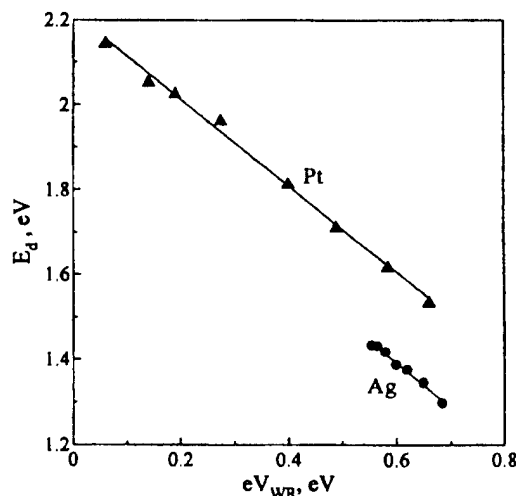


Fig 2: Effect of catalyst potential on the desorption activation energy.

## REFERENCES

- [1] C.G. Vayenas, M.M Jaksic, S. Bebelis and S. Neophytides, in: *Modern Aspects of Electrochemistry*, No 29, (J.O. 'M. Bockris, B.E. Conway and R.E. White, Eds, Plenum Press, New York, 1996) pp. 57-202 and references therein.
- [2] J.L. Falconer and R.J. Madix, *Surf. Sci.* **48**, 393 (1975)

## NO REDUCTION BY CO OVER Ag-Pd ALLOY ELECTRODE IN A SOLID OXIDE ELECTROLYTE CELL

T.I. Politova, V.D. Belyaev, V.A. Sobyenin

Boreskov Institute of Catalysis, Novosibirsk 630090, Russia

Fax: +7(383)2-34-30-56; E-mail: sobyanin@catalysis.nsk.su

The reduction of NO by CO catalyzed by noble metals has been investigated extensively because of its importance for automotive exhaust emission control. Recently the CO + NO reaction over a Pd electrode in a solid oxide electrolyte cell was studied [1]. The NEMCA phenomenon for this system was observed upon application of cathodic current. To our knowledge, there are as yet no report in the literature of the effect of electrochemical oxygen pumping on reduction of NO by CO over Ag-Pd alloy electrodes in a solid oxide electrolyte cell.

This presentation is devoted to investigation of the influence of both cathodic and anodic currents on NO reduction by CO over Ag-25 at.% Pd alloy electrode-catalyst in the cell with YSZ electrolyte:



The electrochemical cell design was similar to that used in Ref. [2]. The experiments were performed at 500-600°C, atmospheric pressure and a fixed rate of CO + NO + He flow of ca. 1 cm<sup>3</sup>/s. The inlet concentrations of CO and NO were varied in the ranges 2.4 ÷ 12.6 vol.%, and 7 ÷ 10.7 vol.%, respectively. The electrode characterization was performed by XRD, SEM and XPS techniques.

It was shown that:

- i) under open-and closed circuit conditions the main reaction pathway is  $2\text{CO} + 2\text{NO} = 2\text{CO}_2 + \text{N}_2$ . In particular the N<sub>2</sub>O formation rate is one order of magnitude lower than the N<sub>2</sub> formation rate, and there is no effect of electrochemical oxygen pumping on the rate of N<sub>2</sub>O formation;
- ii) a small change in the CO + NO reaction rate under electrochemical oxygen pumping from the Ag-Pd alloy electrode is observed at high values of cathodic potential ( $\varphi < -1.7$  V). This effect is not reproducible;
- iii) electrochemical oxygen pumping to the Ag-Pd alloy electrode leads to reversible enhancement of the CO<sub>2</sub> formation rate.

The results obtained are discussed on the base of the current knowledge on the NEMCA effect.

### References

- [1] M. Marwood, C.G.Vayenas, J.Catal, **170**, 275 (1997)
- [2] T.I. Politova, V.V. Galvita, V.D. Belyaev, V.A. Sobyenin, Catal. Lett., **44**, 75 (1997).

AC IMPEDANCE SPECTROSCOPY CHARACTERIZATION OF THE Pt/ $\beta$ "-Al<sub>2</sub>O<sub>3</sub> INTERFACE UNDER POLARIZATION CONDITIONSS. Bebelis <sup>a</sup> and G. Reinhardt <sup>b</sup><sup>a</sup>Department of Chemical Engineering, Univ. of Patras, GR-26500, Greece<sup>b</sup>Institut für Physicalische und Theoretische Chemie, Universität Tübingen, Germany**Introduction**

Sodium  $\beta$ "-Al<sub>2</sub>O<sub>3</sub> is a solid electrolyte with sodium ion conductivity [1]. Besides its wide application in the sodium-sulphur battery [2] or the sodium-metal chloride battery [3], sodium  $\beta$ "-Al<sub>2</sub>O<sub>3</sub> has found application in electrochemical promotion studies [4] as active catalyst support for in situ and reversible electrochemical sodium dosing of metal catalysts. The electrochemically induced and controlled backspillover of sodium species onto a Pt(111) single crystal interfaced to  $\beta$ "-Al<sub>2</sub>O<sub>3</sub> has been recently verified using Scanning Tunneling Microscopy [5].

In order to investigate the electrochemical phenomena involved in electrochemical promotion experiments using  $\beta$ "-Al<sub>2</sub>O<sub>3</sub>, we carried out AC impedance spectroscopy measurements under conditions of polarization of a polycrystalline platinum film interfaced to  $\beta$ "-Al<sub>2</sub>O<sub>3</sub>, i.e. under conditions similar to the ones in electrochemical promotion studies.

**Experimental**

A single pellet type reactor configuration was used [4], i.e. a  $\beta$ "-Al<sub>2</sub>O<sub>3</sub> pellet (17mm O.D., 4mm thickness) was suspended in the interior of a quartz tube, surrounded by the gas mixture. The porous Pt catalyst-working electrode film was deposited on  $\beta$ "-Al<sub>2</sub>O<sub>3</sub> by application of thin coatings of a Pt-paste (Engelhard A1121), followed by calcining in air at 830 °C for 20 min, as described in detail elsewhere [4]. Pt counter and reference electrodes were also similarly deposited on the other side of the  $\beta$ "-Al<sub>2</sub>O<sub>3</sub> pellet, opposite to the Pt catalyst-working electrode.

AC impedance measurements were carried out in the frequency range 1mHz-30Hz, applying a 20mV sinusoidal stimulus superimposed on different DC polarization potentials and using a Solartron 1255 Frequency Response Analyzer combined with a 1286 Electrochemical Interface. L'Air Liquide synthetic air and ultrapure N<sub>2</sub> were used as reference gases.

**Results and discussion**

Figure 1 shows complex impedance spectra (Nyquist plots) taken at 300 °C in synthetic air atmosphere and in a sequence of negative polarization potentials corresponding to different sodium coverages on the Pt catalyst surface.

At low sodium coverages (low polarization potential absolute values) the main feature of the Nyquist complex impedance plot is an inclined line at low frequencies. This line is related to the electrode/electrolyte interface, in agreement with literature [6]. The extrapolation of this line to the real axis can give a good estimation of the resistivity of the electrolyte (including bulk and grain boundary resistivity) [6]. Increasing catalyst potential to more negative values causes a decrease in the magnitude  $|Z|$  of the complex impedance, when comparing impedance values at the same frequency, as shown clearly in Figure 2a, where the frequency dependence of  $|Z|$  is presented (Bode plot). This is equivalent to a shift of the frequency spectrum to the right of the Nyquist plot (Figure 1), where also an additional semicircle at the higher frequencies is partly resolved. At highly negative catalyst potential values, i.e. higher than -350 mV, the main feature in the Nyquist plot is a depressed semicircle, which becomes smaller, i.e. the apparent polarization resistance  $R_{app}$  of the interface decreases, with absolutely increasing polarization potential. This is also shown in the corresponding Bode plot (Figure 2a) by the appearance of a low frequency plateau at potentials more negative than -350 mV, corresponding to gradually decreasing  $|Z|$  by absolutely increasing catalyst potential value.

Besides polarization the gas phase composition also affects the complex impedance characteristics of the platinum/ $\beta''$ - $\text{Al}_2\text{O}_3$  interface. In Figure 2b is compared the frequency dependence of  $|Z|$  at different catalyst potentials when the Pt catalyst film is exposed to ultrapure  $\text{N}_2$  or synthetic air. At catalyst potentials more negative than -100 mV  $|Z|$  is in the case of  $\text{N}_2$  higher over all the frequency range. As shown in Fig. 2b this difference becomes higher by absolutely increasing negative catalyst potential.

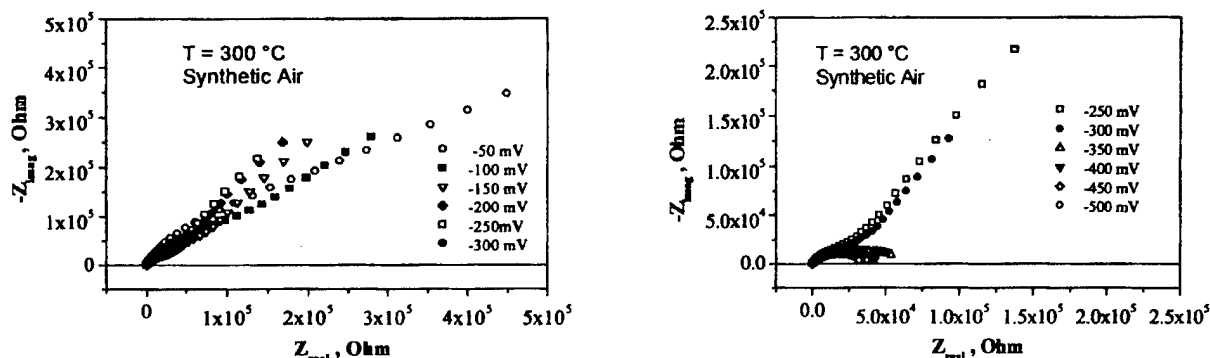


Figure 1: Complex impedance spectra (Nyquist plots) of Pt/ $\beta''$ - $\text{Al}_2\text{O}_3$  under synthetic air and at different platinum catalyst-electrode potentials and;  $T=300\text{ }^\circ\text{C}$ .

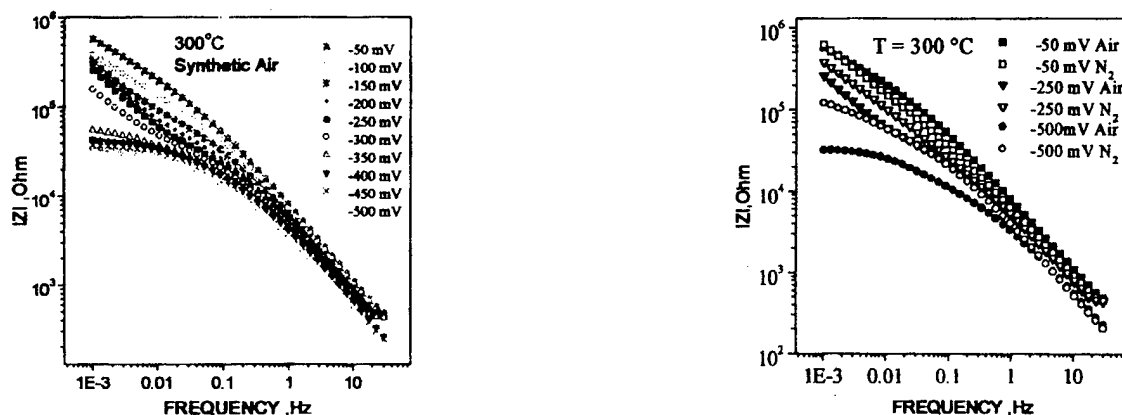


Figure 2: Frequency dependence of the magnitude  $|Z|$  of the impedance (Bode plot) of Pt/ $\beta''$ - $\text{Al}_2\text{O}_3$  at different platinum catalyst-electrode potentials and under synthetic air (a). Effect of gas phase composition (b);  $T=300\text{ }^\circ\text{C}$ .

### References

- [1] B. Dunn and G. C. Farrington, *Solid State Ionics* **5**, 223 (1983).
- [2] 'The sodium-sulphur battery', J. L. Sudworth and A. R. Tilley, Eds., Chapman and Hall, London (1985).
- [3] K. T. Aldendorff and M. H. Thackeray, *J. Electrochem. Soc.*, **135**, 2121 (1988).
- [4] C.G. Vayenas, M.M. Jaksic, S. I. Bebelis and S. G. Neophytides, S.G., "The Electrochemical Activation of Catalytic Reactions" in *Modern Aspects of Electrochemistry* (Bockris, J.O.'M. et al., Ed.) **29**, pp. 57-202, Plenum Publ. Co., New York (1995) and references therein..
- [5] M. Makri, C. G. Vayenas, S. Bebelis, K. H. Besocke and C. Cavalca, *Surface Sci.*, **369**, 351 (1996).
- [6] E. Butcereit, M. Schreiber and J. Schoonman, *Solid State Ionics* **69**, 1 (1994).



# CHANGE OF THE STRUCTURE OF ELECTRICAL DOUBLE LAYER ON THE INTERFACE ELECTRODE /SOLID ELECTROLYTE BY ADDITION OF THE SOLVENTS INTO THE SYSTEM AND INFLUENCE OF MECHANICAL CHARGES.

A. M. Mikhailova, I. E. Shpuck, L. V. Nickitina

SARATOV STATE TECHNICAL UNIVERSITY, RUSSIA

The changing of electrical double layer (e.d.l.) on the interface boundary metal/solid state electrolyte (s.e.) was investigated by estimating low-frequency and high-frequency impedance in the range from 0,1 to 100 kHz ( $T=298\pm5^{\circ}\text{K}$ ).

Impedance dependence upon frequency corresponds equivalent scheme represented on the figure. This equivalent circuit corresponds to E. A. Uckshe's and N. G. Buckun's double layer's relaxation model [1].

High-frequency capacity ( $C_1$ ) is nearly changeless if the dipolar aprotic solvents or the water is introduced in the s.e. ( $0,4\ldots0,45\ \mu\text{F}\cdot\text{cm}^{-2}$ ), however one is notably lower, if nonpolar solvent (for ex. benzol) is added ( $C_1=0,27\ \mu\text{F}\cdot\text{cm}^{-2}$ ). Relaxation's low-frequency capacity ( $C_2$ ) meanwhile is monotonically reduced in the row:  $\text{C}_2\text{H}_5\text{OH}>\text{H}_2\text{O}>\text{CH}_3\text{COCH}_3>\text{C}_6\text{H}_6$ . The values  $C_2$  are practically equal if acetone ( $\epsilon=21,4$ ) or benzol ( $\epsilon=2,29$ ) are in the s.e. ( $C_2=12,5$  and  $11$ , correspondingly).

Capacity ( $C_1$ ) dependence for the cell  $\text{Ag}|\text{RbAg}_4\text{I}_5|\text{Ag}$  from external pressure is found to be practically linear in the range of pressures from  $17,5$  to  $100\ \text{M}(\text{N}\cdot\text{m}^{-2})$ . High-frequency capacity ( $C_1$ ) depends on the state of electrode surface, dispersion degree and activity of fresh-electrodeposited silver.

The value ( $C_1$ ) for the cell  $\text{Au}|\text{RbAg}_4\text{I}_5||\text{Ag}$  equals to  $4,78\ \mu\text{F}\cdot\text{cm}^{-2}$ . The value ( $C_1$ ) increases up to  $13,44\ \mu\text{F}\cdot\text{cm}^{-2}$  after passing through cathode  $5\ \text{mC}$  quantity of the electricity. The value  $C_1$  is lowered to initial meaning after 24-hours storing at indoor temperatures. The capacity  $C_1$  is lowered to  $1,02\ \mu\text{F}\cdot\text{cm}^{-2}$  after electrolytical dissolution of the silver. Low-frequency capacity ( $C_2$ ) by changing surface state by the silver plating increases from  $42,7$  to  $800\ \mu\text{F}\cdot\text{cm}^{-2}$ . After removing it, the capacity ( $C_2$ ) is reduced to  $670\ \mu\text{F}\cdot\text{cm}^{-2}$ .

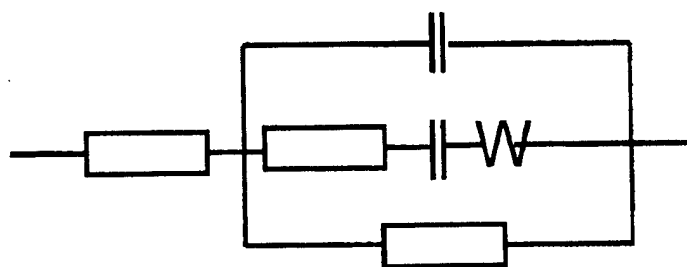


Fig. The equivalent circuit for the cell  $\text{Ag}|\text{Ag}^+\text{-s.e.}|\text{Ag}$

The contact difference of potentials corresponding to zero-charge potential, is determining (on condition that solvent is absent), consequently e.d.l. is analogy to transition layer in Mott-Shottky's model and high-frequency capacity ( $C_1$ ) is corresponded to the capacity of the model flat condenser. It follows from Frumkin's equation [2]:

$$\varphi_0 = W_0 - \psi_{H_2O},$$

where  $\varphi_0$  – the difference of zero-charges potentials,  $W_0$  – the difference of works of electron's emission,  $\psi_{H_2O}$  – difference of Volta-potentials on the interfaces metal/solution. Consequently, the molecules of polar solution are out of contact layer and they are distributed out of Helmholtz's plane into relaxation's diffusion part, connected with participation nonbasic bearers of the charge  $\Gamma$ .

Quantitative estimation of the capacity e.d.l. interface  $Ag|RbAg_4I_5$  gives the value  $0,45 \mu F \cdot cm^{-2}$  that is near in order to value high-frequency capacity  $C_1$  under conditions that zero-charge potential (or contact's difference of potentials) may be interpreted as difference of chemicals potentials of the electrons on the interface metal/solid electrolyte. The last is formed by mobile ions of silver ( $Ag^+$ ).

#### REFERENCES

1. E. A. Uckshe, N. G. Buckun. Solid Electrolytes. Moscow. "Science", 176, (1977).
2. A. N. Frumkin. Electrode Processes. Moscow. "Science", 37, (1987)

## Catalytic and Electrocatalytic oxidation of Ethanol over $\text{La}_{0.6}\text{Sr}_{0.4}\text{Co}_{0.8}\text{Fe}_{0.2}\text{O}_3$ Perovskite-type Catalyst.

S. Douvartzides and P. Tsiakaras\*

Department of Mechanical and Industrial Engineering, University of Thessaly

Pedion Areos, 383 34, Volos, Greece. E-mail: [tsiak@uth.gr](mailto:tsiak@uth.gr)

### Abstract

The catalytic and electrocatalytic behavior of the perovskite-type  $\text{La}_{0.6}\text{Sr}_{0.4}\text{Co}_{0.8}\text{Fe}_{0.2}\text{O}_3$  catalyst was investigated during gas-ethanol oxidation reaction. Saturated air-ethanol mixtures, at ambient temperature and pressure conditions, were found to lead to significant yields of acetaldehyde and formaldehyde. Experiments were carried out at atmospheric total pressure in a fully Yttria-Stabilized-Zirconia (YSZ) continuous stirred tank reactor (CSTR) at a temperature range between 300-700°C. The perovskite-type catalytic material  $\text{La}_{0.6}\text{Sr}_{0.4}\text{Co}_{0.8}\text{Fe}_{0.2}\text{O}_3$  exhibited high yields of formaldehyde for temperatures under 400°C, where purely catalytic behavior was observed. Above this temperature gas phase oxidation phenomena were predominant leading to high formation rates of acetaldehyde and also providing 100% ethanol conversion at about 700°C. Moreover, the electrochemical characteristics of ethanol oxidation reaction have been examined using the specific material as anode electrocatalyst of an ethanol-fueled solid oxide electrochemical cell.

---

\* Corresponded author

# ELECTROCHEMICAL PROMOTION OF Pd, Fe and DISTRIBUTED Pt CATALYST - ELECTRODES

S. Balomenou, G. Pitselis, D. Polydoros, A. Giannikos, A. Frenzel<sup>1</sup>, C. Pliangos, H. Pütter<sup>1</sup>  
and C.G. Vayenas

Department of Chemical Engineering, University of Patras, Patras, GR-26500 Greece

<sup>1</sup>BASF AG, D-67056 Ludwigshafen, Germany

## ABSTRACT

The effect of non-faradaic electrochemical modification of catalytic activity (NEMCA) or Electrochemical Promotion (EP) in catalysis has been studied for more than 50 different catalytic systems using a variety of metal or metal-oxide catalysts, solid electrolytes and catalytic reactions [1,2]. Work in this area has been extensively reviewed [1,2]. In brief it has been found that the catalytic and chemisorptive properties of polycrystalline metal films interfaced with solid electrolytes can be altered *in situ* in a very pronounced and reversible manner by electrically polarizing the metal-solid electrolyte interface with the application of currents or potentials between the catalyst film and a counter electrode in a three-electrode electrochemical cell.

In this communication we summarize and discuss some of the first attempts to induce the NEMCA effect on the following systems:

- $C_2H_4$  oxidation on electronically isolated Pt catalysts on YSZ, where NEMCA is induced via potential application between two terminal Au electrodes also supported on the solid electrolyte (wireless configuration, [3]).
- $NH_3$  decomposition on Fe catalyst electrodes interfaced with  $CaZr_{0.9}In_{0.1}O_{3-\alpha}$ , a proton conducting solid electrolyte support (single pellet configuration, [2]).
- Selective  $C_2H_2$  hydrogenation on Pd catalyst electrodes interfaced with  $\beta''-Al_2O_3$ , a  $Na^+$  conductor (multi-pellet configuration, [4]).

In all the cases the reactor configurations constitute electrochemical cells, where the metal electrodes are all exposed to the reaction mixture.

*i. Electrochemical Promotion of  $C_2H_4$  oxidation using electronically isolated Pt catalysts.* The present study is a first step in an ongoing research to extend NEMCA to systems with dispersion comparable with industrial catalysts [3]. The active catalyst area consists of Pt polycrystalline films deposited on the YSZ in the form of stripes or dots. It was found that significant enhancement of the catalytic rate can be obtained upon potential application between the two

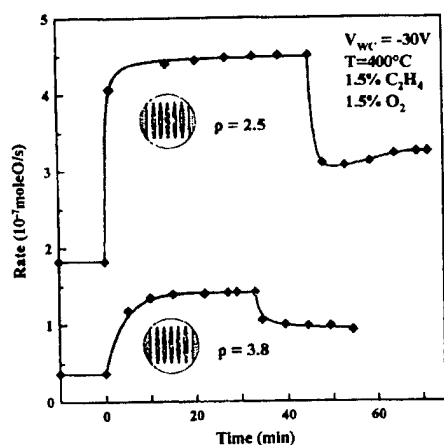


Fig. 1: Transient effect of the applied potential (-30 V) on the catalytic rate (expressed in mol O/s) for two different platinum configurations.

terminal gold electrodes. Such a behaviour is shown in Figure 1. The rate enhancement ratio  $\rho$ , defined from  $\rho = r/r^0$ , where  $r$  is the electrochemically promoted catalytic rate and  $r^0$  is the open-circuit (unpromoted) catalytic rate, ranges between 2.5 and 3.8. The increase of the catalytic rate  $\Delta r = r - r^0$  was in any case higher than the rate of  $O^{2-}$  ion transfer between the two gold electrodes as calculated from Faraday's law ( $I/2F$ ). This "wireless" NEMCA appears to be due to the "bipolar" electrode function of the electronically isolated catalyst located between two other electrodes which are electrically biased via a potentiostat. Part of the platinum film is therefore polarized with a positive charge while the other part is polarized with a negative charge. In this way one part of the catalyst acts as an anode and the other as a cathode. Thus there is not a uniform catalyst work function as in the case when platinum

is used as the working electrode. The resulting effect is a combination between the activity of negatively and positively polarized catalyst surfaces.

ii. *Electrochemical Promotion of  $\text{NH}_3$  decomposition on Fe catalyst electrodes interfaced with  $\text{CaZr}_{0.9}\text{In}_{0.1}\text{O}_{3-x}$*  This study shows that NEMCA can affect remarkably the catalytic activity of the industrially used Fe catalysts for the  $\text{NH}_3$  synthesis or decomposition. The experiments were carried out in atmospheric conditions and at a temperature range of 500 to 600°C. At the higher temperatures, the catalytic rate was found to increase significantly with increasing the catalyst potential (or equivalently, its work function [1,2]). Upon positive potential application up to 5-fold increases in the decomposition rate were observed. The magnitude of EP is larger at the lower  $\text{NH}_3$  concentration region. The effect of backspillover proton ions on the catalytic activity is discussed in terms of the theory of NEMCA by considering the effect of varying the catalyst work function on the coverages and chemisorptive bond strengths of  $\text{NH}_3$ , N and H.

iii. *Electrochemical Promotion of the selective acetylene hydrogenation on  $\text{Pd}/\beta''\text{-Al}_2\text{O}_3$*  The present study shows that Electrochemical Promotion can be used to enhance the performance of

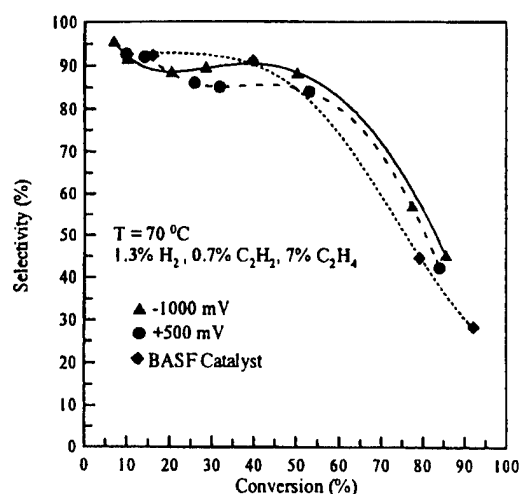


Fig. 2: Dependence of selectivity on the  $\text{C}_2\text{H}_2$  conversion for various catalyst potentials. Dashed line shows the behaviour of a state-of-art BASF catalyst for similar operating conditions.

hydrogenation catalysts at temperatures lower than those used in previous NEMCA studies and under conditions simulating industrial practice, i.e. reactant conversions exceeding 90%. It was found that both the acetylene conversion and the hydrogenation selectivity can be affected significantly by means of externally applied potentials, i.e., by supplying or removing  $\text{Na}^+$  to or from the catalyst surface. Such a case is presented in Fig. 2, which depicts the dependence of selectivity on acetylene conversion at 70°C for a Na free ( $V_{\text{WR}} = +0.5\text{V}$ ) and a Na promoted ( $V_{\text{WR}} = -1\text{V}$ ) catalyst surface. The overall catalytic behaviour is compared with a state-of-art

industrial catalyst of BASF for similar operating conditions (dotted line). The BASF catalyst exhibits similar selectivity values in the low conversion region, while the "NEMCA" catalyst exhibits higher selectivity in the high conversion region (up to 30% enhanced selectivities). The corresponding maximum conversion and

selectivity values are 90% and 85%, respectively.

The results presented above create new possibilities for the practical utilization of Electrochemical Promotion. Significant modification of the catalytic behaviour can be obtained even with electrode configurations closer to the commonly used dispersed systems (i.e., classical supported catalysts) and with experimental conditions (temperature, conversion, GHSVs) comparable with those used in industrial practice.

#### References:

- [1] C.G. Vayenas, M.M. Jaksic, S. Bebelis and S.G. Neophytides, *The electrochemical activation of catalytic reactions* in "Modern Aspects of Electrochemistry" (J.O.'M. Bockris, B.E. Conway, and R.E. White, Eds.), Vol. 29, pp. 57-202, Plenum, New York, (1996).
- [2] C.G. Vayenas, S. Bebelis, I.V. Yentekakis, and H.-G. Lintz, *Catal. Today* **11**, 303 (1992).
- [3] M. Marwood and C.G. Vayenas, *J. Catal.* **168**, 538 (1997).
- [4] A. Giannikos, P. Petrolekas, A. Frenzel, C. Pliangos, C.G. Vayenas and H. Pütter, *Ionics* (1998), in press.

## ELECTROCHEMICAL PROMOTION OF METHANE OXIDATION ON Pd/YSZ

A. D. Frantzis, S. Bebelis and C. G. Vayenas

Department of Chemical Engineering, University of Patras, GR-26500, Greece

**Introduction**

Palladium is the most attractive catalyst for complete oxidation of methane as it exhibits high catalytic activity at temperatures above ca 250°C, lower than that needed with other noble metals, while its price is relatively low [1]. In the present work we examine the possibility of using  $\text{ZrO}_2(\text{Y}_2\text{O}_3)$  (or YSZ), an oxygen ion conducting solid electrolyte, as active catalyst support in order to increase the activity of Pd for catalytic combustion of methane in galvanic cells of the type:  $\text{CH}_4$ ,  $\text{O}_2$ ,  $\text{CO}_2$ , Pd/YSZ/Au,  $\text{CH}_4$ ,  $\text{O}_2$ ,  $\text{CO}_2$ , via the effect of non-Faradaic electrochemical modification of catalytic activity (NEMCA) [2] or electrochemical promotion [3]. In parallel to the measurement of polarization induced catalytic rate changes, we investigated, using AC impedance spectroscopy, the polarization characteristics of the Pd/YSZ interface.

**Experimental**

A "single pellet" type [3] continuous flow atmospheric pressure reactor configuration was used, i.e. an YSZ disk (3/4" O.D., 2 mm thickness) was suspended in the interior of a quartz tube of volume 40 cm<sup>3</sup>, surrounded by the gas mixture. A porous Pd catalyst-working electrode film was deposited on the one side of the YSZ disk, while inert Au counter and reference electrodes were deposited on the other side of the YSZ pellet, opposite to the Pd electrode. Details on electrode preparation procedure can be found elsewhere [3,4], along with details concerning the gas analysis system [3,4]. The only products detected were  $\text{CO}_2$  and  $\text{H}_2\text{O}$ . AC impedance measurements were carried out in the frequency range 0.1Hz-1MHz, applying a 20mV sinusoidal stimulus superimposed on different DC polarization potentials and using a Solartron 1255 Frequency Response Analyzer combined with an 1286 Electrochemical Interface.

**Results and Discussion**

Figure 1 shows for catalyst film C1 (true surface area  $4.7 \times 10^{-7}$  mol Pd) a typical NEMCA potentiostatic transient, i.e., the response of the rate  $r$  of  $\text{CH}_4$  oxidation and current  $I$  to a step change in potential between the Pd catalyst and the Au reference electrode. Initially ( $t < 0$ ) the circuit is open ( $I=0$ ), the open-circuit catalytic rate,  $r_o$ , is  $2.73 \times 10^{-9}$  mol O/s and the catalyst potential is -140 mV. At  $t=0$ , a potential  $V_{\text{WR}}$  of 2V is imposed and  $\text{O}^{2-}$  are pumped to the catalyst surface. The rate increases gradually, reaching a steady state value 29 times larger than the open circuit rate ( $p=r/r_o=29$ ). The steady state rate increase  $\Delta r=7.64 \times 10^{-8}$  mol O/s is 48 times larger than the rate of  $\text{O}^{2-}$  supply  $I/2F$ , thus the system exhibits NEMCA behavior with corresponding enhancement factor or faradaic efficiency  $\Lambda=\Delta r/(I/2F)$  equal to 48. The observed changes in catalytic rate are quite reversible. As shown in Figure, upon current interruption the catalytic rate and potential tend to relax to their open circuit values.

Figure 2 shows, for the same catalyst film, the steady state effect of varying ohmic-drop free catalyst potential  $V_{\text{WR}}$  on the catalytic rate and corresponding work function change  $\Delta(e\Phi)=e\Delta V_{\text{WR}}$  [2,3]. Under the conditions of Fig. 2 (400 °C,  $P_{\text{O}_2}=1.9$  kPa and  $P_{\text{CH}_4}=2.6$  kPa) the catalytic rate is nearly first order in  $\text{CH}_4$  and zero order in  $\text{O}_2$  [4]. As shown in Figure,  $\text{CH}_4$  oxidation on Pd is both an electrophobic and an electrophilic reaction, i.e. the catalytic rate increases (by up to 1200%) both with positive current application ( $\text{O}^{2-}$  supply to the catalyst) and, to a lesser extend, with negative current application ( $\text{O}^{2-}$  supply from the catalyst), respectively. The enhancement factor  $\Lambda$  takes here absolute values up to 150. Even larger rate increases (up to 9000%) have been reported for positive current application in a recent similar study [4], where,

however, neither subtraction of the parasitic working-reference ohmic drop nor negative polarization experiments were carried out.

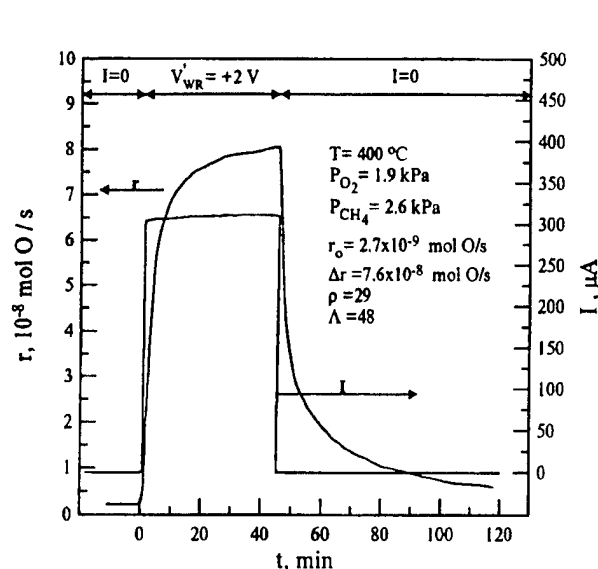


Fig. 1. Rate  $r$  and current  $I$  response to a step change in applied potential  $V_{WR}$ ; see text for discussion

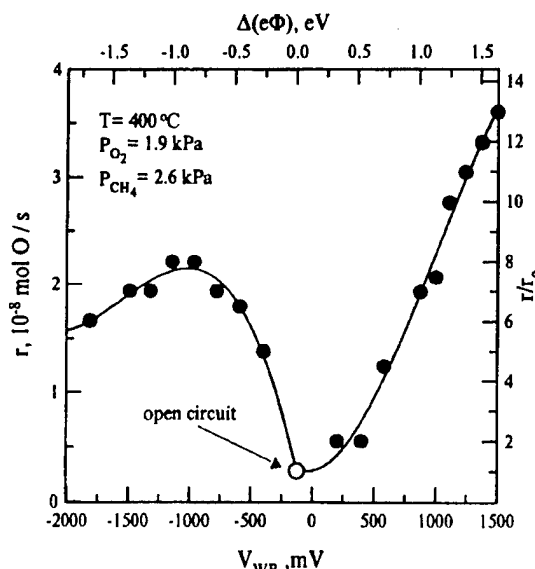


Fig. 2. Effect of applied ohmic-drop free catalyst potential  $V_{WR}$  on the rate of  $\text{CH}_4$  oxidation

Figure 3 shows complex impedance spectra (Nyquist plots) corresponding to selected experimental points in Fig.2. Near open circuit conditions the main feature of the Nyquist plot is an inclined line at low frequencies, which is actually part of a semicircle corresponding to the Pd/YSZ interface. Indeed, by increasing  $V_{WR}$  to highly positive or negative values a depressed semicircle is clearly formed, while the frequency spectrum is shifted to the right of the Nyquist plot. This semicircle becomes smaller with absolutely increasing polarization potential, i.e. the apparent polarization resistance  $R_{app}$  of the interface decreases, while the oxidation state of the Pd electrode seems to remain unaltered.

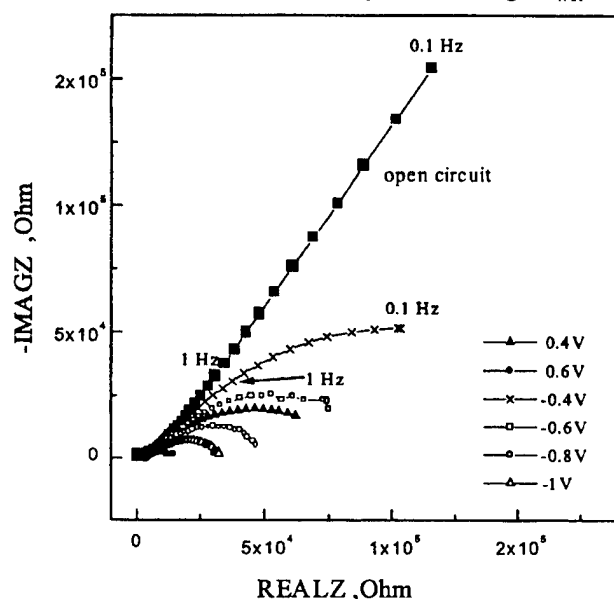


Fig. 3. Complex impedance spectra of Pd/YSZ at different Pd catalyst-electrode potentials. Conditions as in Fig. 2;  $V_{WR}^0 = -0.13\text{V}$ .

As in previous electrochemical promotion studies the present results can be rationalized on the basis of the theoretical considerations invoked to explain electrochemical promotion behavior, i.e. the promotional action of back-spillover oxide ions which migrate from the YSZ solid electrolyte onto the catalyst surface under the influence of the applied potential [2-5]. The back-spillover oxide ions are less reactive with  $\text{CH}_4$  than normally chemisorbed  $\text{O}_2$  and act as promoters by affecting the binding strength of chemisorbed  $\text{O}_2$  and  $\text{CH}_4$ .

## References

- [1] R.F. Hicks, H. Qi, M. L. Young and R.G. Lee, *J.Catal.* **122**, 280 (1990)
- [2] C.G. Vayenas, S. Bebelis and S. Ladas, *Nature (London)* **343**, 625 (1990).
- [3] C.G. Vayenas, M.M. Jaksic, S.I. Bebelis and S.G. Neophytides, "The Electrochemical Activation of Catalytic Reactions" in *Modern Aspects of Electrochemistry*, Vol. 29, eds. J.O.'M. Bockris, B. E. Conway and E. White (Plenum Publ. Co., New York, 1995), Ch. 2, pp. 57-202.
- [4] A. Giannikos, A. D. Frantzis, C. Pliangos, S. Bebelis and C. G. Vayenas, *Ionics*, in press (1998)

ELECTRODE POLARIZATION AT THE O<sub>2</sub>(g), Pd/YSZ INTERFACE

C. Athanasiou, G. Karagiannakis, S. Zisekas and M. Stoukides  
 Chemical Engineering Department  
 and Chemical Process Engineering Research Institute,  
 University Box 1517, University Campus, Thessaloniki 54006, Greece

The steady state current-overpotential characteristics of the O<sub>2</sub> - Pd/YSZ interface have been studied as a function of oxygen partial pressure and temperature in a three electrode cell, using the current interruption technique. The experimental setup has been described in previous works [1].

The electrode kinetics of the oxygen exchange between the gas phase and the electrolyte can be modelled into a form of the Butler-Volmer equation [2]:

$$I = I_0 [ \exp( \alpha_a F \eta / RT ) - \exp( \alpha_c F \eta / RT ) ] \quad (1)$$

where  $\alpha_a$  and  $\alpha_c$  are the anodic and the cathodic charge transfer coefficients, respectively,  $F$  is Faraday's constant,  $R$  is the ideal gas constant,  $I_0$  is the exchange current and  $\eta$  is the overpotential, which is defined as:

$$\eta = V_{WR} - V_{WR}^0 - IR_{drop} \quad (2)$$

where  $V_{WR}^0$  is the open circuit potential and  $IR_{drop}$  is the ohmic potential difference through the system. Equation (1) assumes negligible mass transfer effects. In case, however, the charge transfer reaction rate is in competition with the rate of mass transfer, the current will approach a limiting value  $I_l$ . In this case the high field approximation of the Butler-Volmer equation becomes:

$$|\eta| = ( RT / \alpha F ) \{ \ln[ |I| / ( I_l - |I| ) ] + \ln( I_l / I_0 ) \} \quad (3)$$

where  $\alpha$  is either  $\alpha_a$  or  $\alpha_c$  depending whether the working electrode is the anode or the cathode.

The current - overpotential data of the O<sub>2</sub>(g), Pd/YSZ interface were studied using equation (3). The charge transfer coefficients,  $\alpha_a$ ,  $\alpha_c$ , and the exchange current density,  $I_0$ , were found from the slope and intercept respectively of the  $\ln[|I| / ( I_l - |I| )]$  vs  $|\eta|$  curves at temperatures between 400 and 550°C and oxygen partial pressures between 0.2 and 4 kPa. At the above conditions, the equilibrium state of the working electrode at open circuit, was palladium oxide, as indicated by Solid Electrolyte Potentiometry (SEP) measurements. The



SEP technique is essentially based on Nernst's equation and allows monitoring of the thermodynamic activity of atomically absorbed oxygen on the electrode surface by simply measuring the EMF of the solid electrolyte cell. The measured oxygen activity values can be compared to those theoretically predicted for equilibrium between metal and its oxide in order to determine the oxidation state of the electrode. Details on the SEP technique have been described in previous works [3]. For cathodic conditions, and temperatures higher than 500°C, the  $I - \eta$  curves indicate a possible decomposition of PdO to metallic Pd, which does not, however, seem to affect the values of exchange current densities and charge transfer coefficients. The calculated values of the anodic and cathodic charge transfer coefficients varied between 0.5 - 0.7 and 0.3 - 0.5, respectively, without exhibiting any clear dependence on temperature or oxygen partial pressure. The values of anodic limiting and exchange currents were generally higher than the corresponding cathodic values. The  $I_l$  and  $I_0$  apparent activation energies were both about 12 kcal/mol and they are not significantly affected by the oxygen partial pressure. The exchange current density,  $I_0$ , was found to increase with  $P_{O_2}$  according to the relationship:

$$\ln I_0 \propto m \ln P_{O_2} \quad (4)$$

The value of  $m$  varied between 0.3 and 0.4.

Considering  $\alpha_a = \alpha_c = 0.5$ , a model for the reaction mechanism is proposed, in which the single charge transfer to  $O_{ad}$  is the rate determining step.

#### REFERENCES

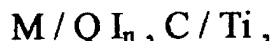
- [1] P. Tsiakaras, G. Marnellos, C. Athanasiou, M. Stoukides, J. E. ten Elshof, H. J. M. Bouwmeester, H. Verweij, *Solid State Ionics* **86-88**, 1451-1456(1996).
- [2] J.O' M. Bockris and A. K. N. Reddy, *Modern Electrochemistry* (Plenum Press, New York, 1977)
- [3] C. Athanasiou, G. Marnellos, P. Tsiakaras and M. Stoukides, *Ionics* **2**, 353, (1996).

Electrochemical behavior of solid-state short-circuite systems  
alkaline metal-organic semiconductor

by A. Mikhailova, W. Efanova, H. Bukun, B. Goffman  
Saratov State Technical University

Russia, Saratov.

Organic semiconductors: iodine complexes of phenothiazine  $2\text{Ph}\cdot\text{nI}_2$  with  $n=3$  and  $5$ , and complex of benzofulvalen  $\text{BF}\cdot\text{I}_3$  are the donor-acceptor with interior intermolecular charge transfer leading to formation of chemical bond. The ionicity of such compounds is determined with the character and extent of charge transfer. The differences between the charge-transfer characteristics and crystal structures determine the properties of the charge-transfer complexes (CTC). In particular most of polyiodides of molecular CTC and ion-radical salts have high electronic conductivity. We have studied the electrochemical cells:

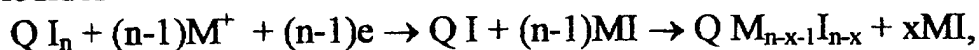


where  $\text{M}=\text{Li}, \text{Na}$ ;  $\text{Q}=\text{Ph}, \text{BF}$ , and  $n=3,5$ .

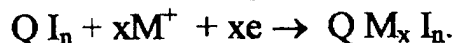
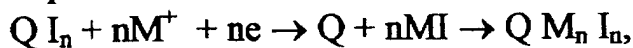
The phases which have been found upon interfaces of  $\text{Li}$  or  $\text{Na}$  and  $2\text{Ph}\cdot 3\text{I}_2$  or  $\text{BF}\cdot\text{I}_3$  contain  $\text{Li}^+$ ,  $\text{Na}^+$  but they differ from  $\text{LiI}$ ,  $\text{NaI}$ .

The study of electrode reactions products have been made with linear sweep voltammetry, IR and UF Spectroscopy, X-ray and chemical analysis.

All these methods lead to conclusion that the cation-radicals take part in formation of the transitional layers. We propose next mechanisms for elections: for polyiodides



and for molecular complexes:



The velocity of consecutive chemical reaction can be determined with cyclic voltammetry. The velocity is equals to  $2,3 \cdot 10^{-3} \text{ cm}\cdot\text{s}^{-1}$  for  $\text{BF}\cdot\text{I}_3$ . In case of the complex  $2\text{Ph}\cdot 5\text{I}_2$ , which is a hole conductor, when cathodic potential is imposed the hole conductivity is diminished owing to injection of electrons from the external circuit. But simultaneous ion injection from anode  $\text{Li}$ ,  $\text{Na}$  provides a large ionic conductivity. So the cell resistance is kept near  $10 \text{ Ohm}$  without appreciable changes. The electronic and ionic conductivities of final products are  $10^{-3}\text{-}1^{-1} \text{ Sm}\cdot\text{cm}^{-1}$ . Thus cathodic reduction upon interfaces of organic semiconductors and alkaline metal developer, according to their electrical properties, irreversibility and with simultaneous alterations of ionic and electronic conductances. These processes can be carried out by means of double injection of electrons and ions if the iodine complex has an appreciable initial conductivity to realize the cathodic process consists in the phase transitions and formation of superionic phases.

The work was carried out by finance supporting of RFFI (96-03-33648a).

## ION BEAM TECHNIQUES AND THEIR APPLICATION TO OXYGEN TRANSPORT MEASUREMENTS.

J.A. Kilner

Centre for Ion Conducting Membranes,  
Department of Materials,  
Imperial College of Science, Technology and Medicine,  
London SW7 2BP,  
UK.

Ion beam techniques are useful in the characterisation of a whole range of solid state materials, including semiconductors and ionic conductors. Many of these techniques have been applied to ionic conductors, yielding a wealth of varied information such as: bulk chemical composition; structural perfection; surface structure and composition; and depth profiles of chemical and isotopic composition. Of particular interest for ionic conductor studies are the techniques of Secondary Ion Mass Spectrometry (SIMS), Rutherford Backscattering (RBS), Nuclear Reaction analysis (NRA) and the Ion Scattering techniques such as Low Energy Ion Scattering (LEIS) and Medium Energy Ion Scattering (MEIS). This presentation will focus on the application of ion beam based techniques to the study of oxygen transport in ionic conductors, and in particular to the study of isotopic oxygen exchange.

The first part of the talk will discuss the use of conventional SIMS analysis in the Isotope Exchange Depth Profiling (IEDP) technique, to measure the oxygen self diffusivity and surface exchange coefficient in single crystal and polycrystalline oxides. The main topics to be discussed are the limits to this technique in terms of the lowest and highest diffusivities that can be measured. For example the physical phenomenon of ion beam mixing imposes limits as to how deep an isotope penetration profile must be before it can be measured with some accuracy [1]. This places a lower limit on the diffusivity that can be measured by the direct depth profiling technique of  $10^{-17}$  to  $10^{-18}$  cm<sup>2</sup>/sec. The upper limit to the measurement of diffusivity is imposed by the limitations of line-scanning. This is an instrumental problem, however the longest line scans that can be reasonably measured by SIMS are in the mm range, giving an upper limit to the diffusivity in the region of  $5 \times 10^{-6}$  cm<sup>2</sup>/sec. Examples of the type of data obtainable with the line-scanning technique are shown in Figure 1 for Ytria Stabilised Zirconia (YSZ) single crystals [2].

The newer technique of high lateral resolution SIMS will also be discussed. The advent of high resolution SIMS instrumentation has enabled the imaging of the lateral distribution of isotopes and impurities down to a sub-micron scale. This type of imaging has proven to be very useful for the observation of grain boundary diffusion and segregation in a range of ceramic materials [3]. Newer focused ion beam instruments can also micro-machine selected areas of sample to reveal the internal grain structure of a desired area. This combined technique of imaging and milling presents the opportunity of isolating and examining the transport properties of single grains within a polycrystalline matrix.

Finally the technique of Ion scattering will be discussed. LEIS is finding increasing application with ceramic materials due to the unparalleled sensitivity of the technique to the outermost atomic layers. The atomic composition of the immediate surface layer can be

determined, yielding information about the surface structure and chemistry. LEIS has recently been applied to the fluorite electrolyte ceria gadolinia (CGO) [4], where it has shown the extent of dopant segregation in these materials and how this segregation can be related to grain boundary impedances of ceramic materials. Similar studies of the perovskite mixed conductor  $\text{Sm}_{1-x}\text{Sr}_x\text{CoO}_{3-\delta}$  [5] have shown the likely surface structure of this material, and the extent of surface segregation, both of which have large implications for the surface exchange of oxygen.

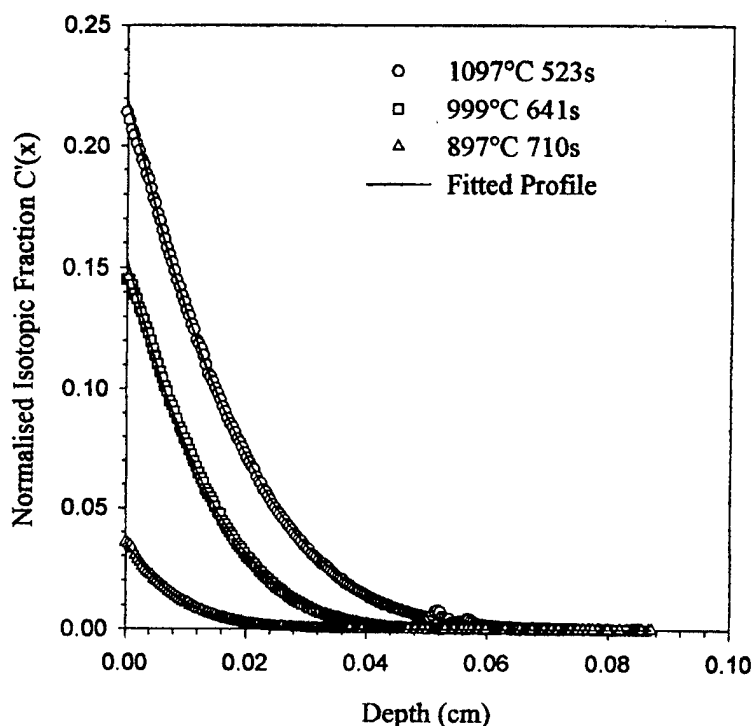


Figure 1 Line-scan data for isotope exchanged YSZ single crystals. from ref. [2]

### References

- [1] J.A.Kilner and R.A.De Souza, Proceedings of the 17<sup>th</sup> Riso International Symposium on Materials Science: High Temperature Electrochemistry: Ceramics and Metals. Eds Poulsen F.W., Bonanos N., Lideroth S., Mogensen M, and Zachau-Christiansen B. Riso National Laboratory, Denmark 1996, pp 41-54.
- [2] P.S. Manning, J.D. Sirman, J.A. Kilner, Solid State Ionics, **93**, 125, (1997)
- [3] T. Kawada, T. Horia, N. Sakai, H.Yokokawa, and M.Dokiya Solid State Ionics **79**, 210, (1995).
- [4] P.J. Scanlon, R.A.M. Bink, F.P.F. van Berkel, G.M. Christie, L.J. van Ijzendoorn, H.H. Brongersma and R.G. van Welznis, Solid State Ionics **112**, 123, (1998).
- [5] I.C. Fullarton, J-P. Jacobs, H.E. van Benthram, J.A. Kilner, H.H. Brongersma, P.J. Scanlon, and B.C.H. Steele, Ionics **1**, 51, (1995).

## LOCAL STRUCTURE AND IONIC MOTION IN SUPERIONIC CONDUCTORS STUDIED BY SOLID STATE NMR TECHNIQUES

<sup>1</sup>Hans-Martin Vieth, <sup>2</sup>Sergei V. Dvinskikh, <sup>1</sup>Milo Hindennach, <sup>2</sup>Igor V. Murin, <sup>3</sup>Alexei F. Privalov

<sup>1</sup> Freie Universität Berlin, Institute of Experimental Physics, Arnimallee 14, D-14195 Berlin

<sup>2</sup> St. Petersburg University, Universitetskii pr. 2, 198904 St. Petersburg, Russia

<sup>3</sup> Universität Dortmund, Fachbereich Physik, Otto-Hahn-Str. 4, D-44221 Dortmund, Germany

Nuclear Magnetic Resonance spectroscopy is well suited to provide detailed information on microscopic structural and motional properties of superionic conductors, since NMR observables are sensitive to the local environment of spins and its dynamical changes. Among the characteristic advantages of NMR are its selectivity with respect to a particular ionic species (<sup>1</sup>H, <sup>7</sup>Li, <sup>17</sup>O, <sup>19</sup>F, <sup>23</sup>Na etc.), its ability to differentiate between structurally inequivalent ions, and between dynamically inequivalent ions of the same structural type, and thus to analyze static and motional disorder. The sensitive time scale is very wide, when different NMR techniques are combined. It extends from below 10<sup>-9</sup>sec in relaxation time analysis to more than 10sec in 2D exchange spectroscopy. Typical examples of one- and multidimensional spectroscopy and of spin-lattice relaxometry are presented with particular emphasis on structural changes in the crystalline lattice due to temperature variation and heterovalent ionic substitution and on the resulting changes in the ionic mobility.

For such a study monocrystals of several F<sup>-</sup> conducting materials with fluorite and tysonite structure, Ba<sub>1-x</sub>La<sub>x</sub>F<sub>2+x</sub>, and La<sub>1-x</sub>Sr<sub>x</sub>F<sub>3-x</sub> and Ce<sub>1-x</sub>Sr<sub>x</sub>F<sub>3-x</sub>, resp., have been investigated by <sup>19</sup>F NMR in the temperature range between 30K and 1200K and for various values of x. Structural changes are most clearly seen in CeF<sub>3</sub> because of the large paramagnetic line shift due to the Ce 4f electron and the resulting wide separation of spectral lines. While at low temperatures its tysonite structure has three distinct fluorine sublattices, F<sub>1</sub>, F<sub>2</sub> and F<sub>3</sub>, with intensity ratio 6:2:1, around 350K two of them, F<sub>2</sub> and F<sub>3</sub>, become magnetically equivalent. As is seen from changes in the NMR linewidth ionic diffusion starts within the F<sub>1</sub> sublattice (below 300K), while ionic exchange between the different sublattices on the NMR timescale has an onset temperature around 500K.

Here, as in all other crystals of this study, clear evidence for disorder of the ionic motion is detected in the spectra. Since we deal with crystal lattices with well defined atomic positions, the motional disorder is not induced by heterogeneities of the local geometry as is typical for ionic glasses. The hopping among F<sub>1</sub> sites can be well described by a model based on a distribution of correlation times with approximately log-Gaussian shape. A second log-Gaussian distribution characterizes the exchange between F<sub>1</sub> and F<sub>2,3</sub>. The center and width of the distribution are changing with dopant concentration x and temperature; when increasing x the distribution becomes broader and the motional process is shifted to lower temperatures. The same model also describes the frequency dependent NMR spin-lattice relaxation times, T<sub>1</sub>(ω), which are sensitive to much shorter correlation times in comparison with the spectral analysis and thus allow to monitor the ionic motion at higher temperatures. Since the motional disorder reflects the distribution of interionic potentials, its analysis can be utilized to study the influence of heterovalent substitution on the potential landscape and to test theoretical approaches to modeling this behavior.

## STRUCTURAL STUDIES ON THE OPTIMISATION OF FAST OXIDE ION TRANSPORT

John T.S. Irvine, Alan J. Feighery and Duncan P. Fagg

School of Chemistry, University of St. Andrews, St Andrews, Fife KY16 9ST,  
Scotland, UK

The structure of a solid can be investigated using a wide range of diffraction and spectroscopic techniques; however, it is important to realise that different techniques probe different length scales. The structural methods that we are most familiar with, that is neutron and X-ray diffraction, generally reflect length scales of the order of microns; whereas techniques such as electron diffraction and especially spectroscopic techniques such as EXAFS tend to reflect much shorter length scales. In the consideration of the role of structure in determining ionic conduction properties, it is the local structure that is most important. This effect is well illustrated by the zirconia-based fluorite systems where the average structure appears as simple cubic when the local structure is generally dominated by microdomain formation.

X-ray diffraction is very insensitive to local order in these systems, with the cubic fluorite structure being observed over the entire range of fluorite-related phase formation in the  $\text{Y}_2\text{O}_3\text{-ZrO}_2\text{-TiO}_2$  and  $\text{Y}_2\text{O}_3\text{-ZrO}_2\text{-Nb}_2\text{O}_5$ . In the  $\text{Gd}_2\text{O}_3\text{-ZrO}_2\text{-TiO}_2$  system; however, an extensive range of pyrochlore phase formation is observed, although in this case the defect ordering is uniform throughout the lattice. The insensitivity of X-ray diffraction to local ordering in fluorites reflects the fact the effect of local order is much more pronounced in the anion sublattice.

Neutron diffraction is much more sensitive to oxygen than X-ray diffraction and, indeed there is clear evidence of local ordering in the form of diffuse peaks in the neutron diffraction patterns throughout the fluorite region of the  $\text{Y}_2\text{O}_3\text{-ZrO}_2\text{-TiO}_2$  and  $\text{Y}_2\text{O}_3\text{-ZrO}_2\text{-Nb}_2\text{O}_5$  systems. For compositions close to  $\text{ZrO}_2$ , the diffuse peaks disappear on increasing temperature. This loss of diffuse peaks indicates a breakdown of short-range order and correlates with a decrease in activation energy for ion transport of 0.15 eV. At higher degrees of doping the diffuse peaks persist to the highest temperatures.

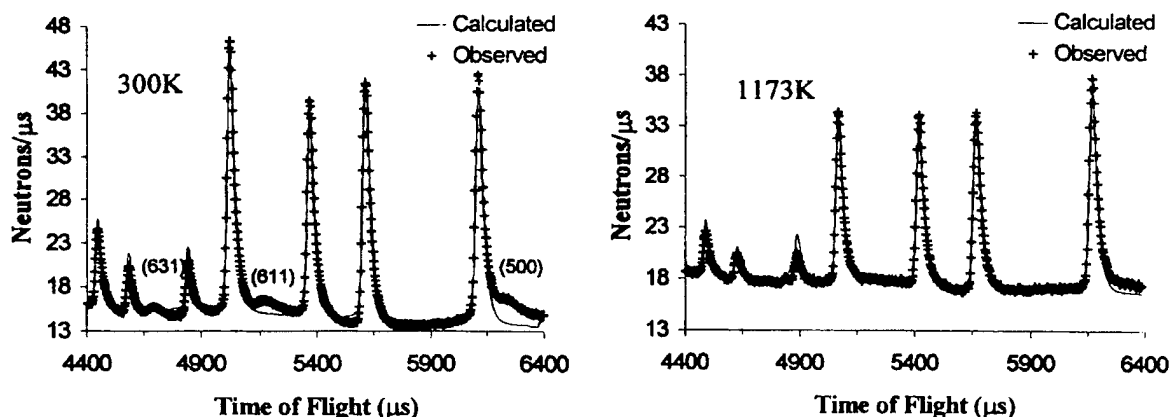


Figure 1 Neutron Powder Diffraction patterns of  $\text{Y}_{0.15}\text{Zr}_{0.85}\text{O}_{1.925}$

The presence of microdomains also affects the average structure, increasing the temperature factors (ITFs) associated with the oxygen atoms in particular. For low doping levels, there is a change in the temperature dependence of the ITFs at the same temperature as that associated with the disappearance of diffuse peaks, which is attributed to the breakdown of microdomains. By examining the temperature dependence of the Oxygen ITF values, an estimate of the intrinsic (0K) contribution of the local disorder within microdomains can be obtained. This value is seen to correlate with the conductivity prefactor (figure 2), clearly indicating that the extent of microdomain formation may relate to the number of ions available for ion migration.

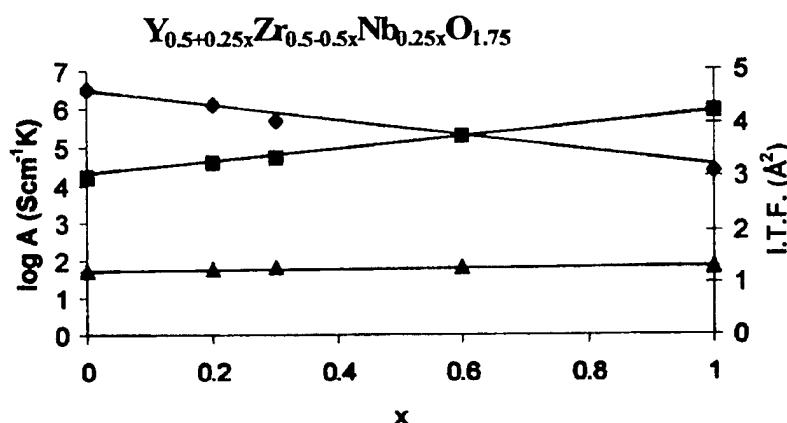


Figure 2 Plot of log conductivity prefactor (◆), Oxygen ITF (■) and Metal ITF (▲) against composition for a solid solution series exhibiting constant activation energy.

EXAFS clearly shows that the preferred co-ordination of the Yttrium ion is 8-fold; whereas the smaller Zr, Ti and Nb ions prefer 6- or 7-fold. This would indicate that the local ordering in the microdomains is likely to involve 3-dimensional ordering of 6- and 8- co-ordinate ions as in the pyrochlore structure or 1-dimensional order as in the orthorhombic  $Y_3TaO_7$  phase[1]. Electron diffraction patterns from Nb-rich phases show unusual incommensurate features indicative of local ordering of the 1-dimensional  $Y_3TaO_7$  type.

In summary, results from a wide range of diffraction and spectroscopic techniques will be analysed and compared to conductivity data and a model describing the conductivity behaviour of a wide range of zirconia-based fluorite compositions will be presented.

1. H.J.Rossell, J.Solid.State.Chem. 27(1979)115.

## LOCAL CATIONIC ENVIRONMENT IN LITHIUM NICKEL-COBALT OXIDES USED AS CATHODE MATERIALS FOR LITHIUM BATTERIES

C. Julien

<sup>a</sup>Laboratoire des Milieux Désordonnés et Hétérogènes, UMR 7603, Case 86,  
Université Pierre et Marie Curie, 4 place Jussieu, 75252 Paris cedex 05, France

$\text{LiNi}_{1-y}\text{Co}_y\text{O}_2$  compounds are currently used as positive electrodes in lithium-ion cells because they provide high specific energy density, high voltage, and remarkable reversibility for lithium intercalation-deintercalation process. They are isostructural with the layered oxide end-members, i.e.,  $\text{LiCoO}_2$  and  $\text{LiNiO}_2$  [1-2].

In this paper, we report on the vibrational spectra of  $\text{LiNi}_{1-y}\text{Co}_y\text{O}_2$  solid solution. Studies were carried out by Raman and FTIR spectroscopies on samples grown by solid state reaction and wet-chemistry techniques. Lattice dynamics of oxides were investigated using the factor group analysis and the local environment model. The local environment of cations against oxygen neighboring atoms has been determined by considering polyhedral units building the lattice. Structural modifications induced by intercalation-deintercalation process, by cation substitution, and by low-temperature preparation route are examined.

Vibrational spectroscopies, i.e., Raman scattering (RS) and Fourier transform infrared (FTIR), are sensitive to the short-range environment of oxygen coordination around the cations in oxide lattices. Since RS and FTIR techniques can solve the problem of phase determination when various environments are present. As a first approximation, spectra consist of a superposition of the components of all local entities. The frequencies and relative intensities of the bands are sensitive to coordination geometry and oxidation states [3]. Thus, spectra are less affected by the grain size or the degree of long-range order of the lattice.

In the process of studying the lattice vibrational properties of the  $\text{LiNi}_{1-y}\text{Co}_y\text{O}_2$  solid solution, we have examined the compositional dependence of the Raman-active modes. Fig. 1 shows the shift of the Raman mode frequencies plotted against the Co composition. The frequencies of the modes  $A_{1g}$  and  $E_g$  shift continuously from those of  $\text{LiNiO}_2$  to those of  $\text{LiCoO}_2$  without the appearance of new branch. The  $A_{1g}$  and  $E_g$  modes show the general features of vibrational properties in mixed compounds exhibiting an optical phonon behavior traditionally classified as one-mode type behavior. The one-mode behavior has been defined by the occurrence of one strong optical mode over the entire composition range. The oscillator strength of the phonon modes vary continuously between those of the end members. This experimental results explain satisfactorily on the basis of the atomic displacements for each mode. The FTIR spectra of  $\text{LiNi}_{1-y}\text{Co}_y\text{O}_2$  samples exhibit the four infrared bands according to the theoretical group analysis. The IR-active vibrations are separated into two groups; so,  $\text{LiO}_6$  and  $\text{MO}_6$  octahedra exhibit a large difference between their vibrational frequencies. Vibrational modes of  $\text{LiO}_6$  octahedra at 200-300  $\text{cm}^{-1}$  are well separated from those of  $\text{MO}_6$  octahedra at 400-700  $\text{cm}^{-1}$ . However, the small shift in the frequency of the  $\text{LiO}_6$  vibrations is not surprising since  $\text{LiO}_6$  octahedra are interlinked by common oxygen atoms.

The frequency shift of both bending and stretching modes are attributed to the evolution of the hexagonal cell parameters and to the modification of the  $c/a$  ratio of the mixed  $\text{LiNi}_{1-y}\text{Co}_y\text{O}_2$  phases. The increase of the inner slab bond covalency in  $(\text{Ni}_{1-y}\text{Co}_y\text{O}_2)_n$  with increasing cobalt



content explains the decrease of the metal-metal intralayer distance, which induces a frequency shift of the Raman-active modes. The partially disordered cation distribution appearing in lithium nickelate materials can also explain the observed broadening of the Raman spectrum.

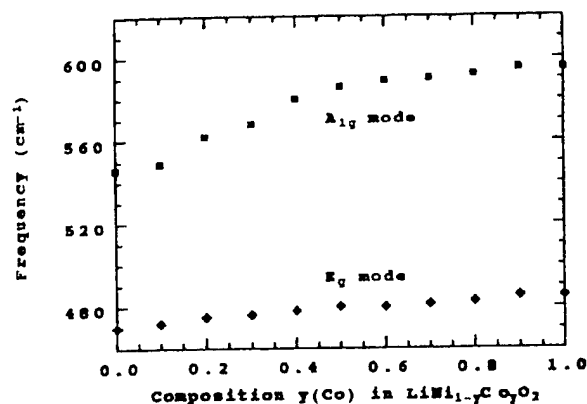


Fig. 1. Frequency shift of the Raman modes against the composition  $y$  in  $\text{LiNi}_{1-y}\text{Co}_y\text{O}_2$  phases.

Two important aspects have been studied in  $\text{LiNi}_{1-y}\text{Co}_y\text{O}_2$  solid solution using vibrational spectroscopies, i.e., the cation mixing occurring in the predominantly Li layers and the disordered distribution occurring in the  $(\text{Ni}, \text{Co})\text{O}_2$  layers. They can be viewed by the frequency shift of the stretching modes of either  $\text{MO}_6$  and  $\text{LiO}_6$  octahedra. Figs. 2 and 3 show such diagrams for samples of the  $\text{LiNi}_{1-y}\text{Co}_y\text{O}_2$  system prepared by a wet-chemistry method using oxalic-acid as a reducing agent.

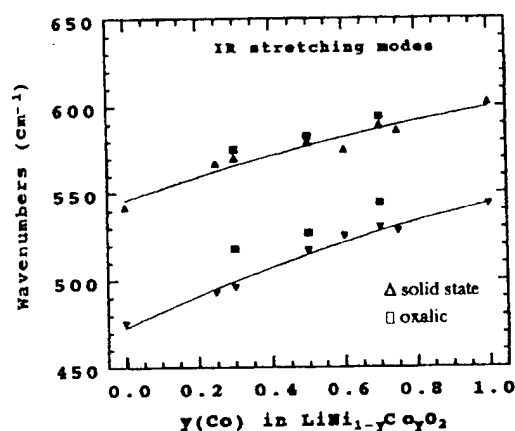


Fig. 2. Frequency shift of the IR stretching modes,  $\nu(\text{MO}_6)$ , in LT- $\text{LiNi}_{1-y}\text{Co}_y\text{O}_2$  samples showing the disorder in the  $(\text{MO})_2$  slabs.

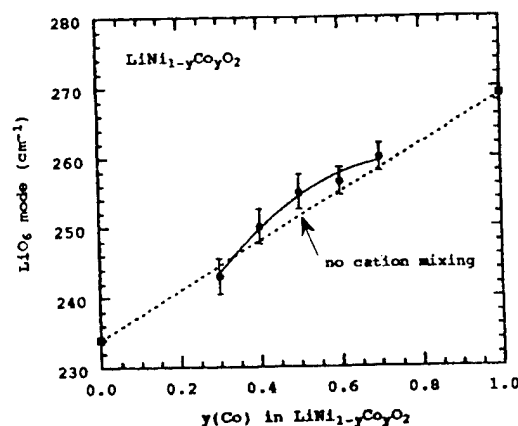


Fig. 3. Frequency shift of the IR stretching modes,  $\nu(\text{LiO}_6)$ , in LT- $\text{LiNi}_{1-y}\text{Co}_y\text{O}_2$  showing the cation mixing effect.

#### References

- [1] C. Delmas and I. Saadoune, *Solid State Ionics* **53-56**, 370 (1992).
- [2] T. Ohzuku, A. Ueda and M. Kouguchi, *J. Electrochem. Soc.* **142**, 4033 (1995).
- [3] C. Julien, M. Massot, C. Perez-Vicente, E. Haro-Poniatowski, G.A. Nazri and A. Rougier, *Mater. Res. Soc. Symp. Proc.* **496**, 415 (1998).

## Defect Formation in Lithium Based Complex Oxides by means of High Temperature Kelvin Probe

Michio Yamawaki, Atsushi Suzuki, Toshihiko Yokota and Kenji Yamaguchi

Graduate School of Quantum Engineering and Systems Science, School of Engineering, the University of Tokyo  
7-3-1 Hongo, Bunkyo-ku, Tokyo 113-8656, JAPAN

### Abstract

Lithium based complex oxides are considered to be promising candidates for tritium breeder materials to be used in the blanket of fusion reactors. Defect structures and ionic transport properties of these materials have been little investigated yet, though those properties are highly important on account of their close relationship with the recovering rate of bred tritium there-from.

In this study, defect formation properties of lithium-based complex oxides,  $\text{Li}_4\text{SiO}_4$ ,  $\text{Li}_2\text{ZrO}_3$  and  $\text{Li}_2\text{TiO}_3$ , together with that of  $\text{Li}_2\text{O}$ , have been studied by using the high temperature Kelvin probe [1,2]. The contact potential differences (CPD) of the specimens were measured by changing the atmosphere gas composition to know the oxygen potential effect.

$\text{Li}_4\text{SiO}_4$  showed decrease of CPD as much as about 200 mV when the oxygen potential dropped from 102 to 10-15 Pa by changing the atmosphere from helium gas to  $\text{He}+0.25\%\text{H}_2$  mixed gas. Such a CPD change was attributed to oxygen vacancy formation.  $\text{Li}_2\text{ZrO}_3$  showed the oxygen vacancy formation property similar to  $\text{Li}_4\text{SiO}_4$ .

On the other hand,  $\text{Li}_2\text{TiO}_3$  did not exhibit such a change of CPD to be attributable to the oxygen vacancy formation. The behavior of  $\text{Li}_2\text{O}$  was similar to that of  $\text{Li}_2\text{TiO}_3$ .

The behaviors of  $\text{Li}_4\text{SiO}_4$  and  $\text{Li}_2\text{ZrO}_3$  can be explained from the mid-temperature electron energy level distribution of oxide semiconductors, where EF can be related with the oxygen partial pressure according to the defect equilibrium.

### References

- (1) J. Nowotny, M. Sloma and W. Weppner, J. Am. Ceram. Soc. 72 (1989) 564.
- (2) A. Suzuki, M. Shibata, K. Yamaguchi, M. Yamawaki, J. Alloys Comp. 262-263 (1997) 185.

## MOTIONAL DISORDER IN SUPERIONIC CONDUCTORS VIA NMR SPIN-LATTICE RELAXATION DISPERSION

A. F. Privalov, S. Dvinskikh<sup>1</sup>, F. Fujara, I. V. Murin<sup>2</sup> and H.-M. Vieth<sup>3</sup>

Department of Physics, Dortmund University, D-44221 Dortmund, Germany

<sup>1</sup>Department of Physics, St. Petersburg University, St. Petersburg, Russia<sup>2</sup>Department of Chemistry, St. Petersburg University, St. Petersburg, Russia<sup>3</sup>Institute of Experimental Physics, Free University of Berlin, D-14195 Berlin, Germany

NMR spin-lattice relaxation times  $T_1$  contain valuable information on the spectral density of the local field fluctuations and thus on the motional processes in superionic conductors (SIC) on a microscopic scale. Until now most  $T_1$  studies on SIC have been done at fixed NMR frequency  $\langle\nu\rangle$  by varying the temperature thus matching all motional processes with  $\langle\nu\rangle$ . The temperature scan in these studies has to be done over a wide enough range to get dynamic processes much slower than  $\langle\nu\rangle$  at low temperature and much faster than  $\langle\nu\rangle$  at high temperature. Apart from the fact that some substances cannot be heated high enough because of thermal damage, such data can be correctly interpreted only if the nature of the relevant dynamic processes does not change with temperature. This is a serious limitation and to avoid it the frequency dependence of  $T_1(\nu)$  at fixed temperatures can be analyzed [1]. Likewise the NMR frequency range has to be significantly wider than the spectrum of the dynamic processes in the material at the chosen temperature. For this purpose, the  $T_1$  values usually have been measured at various magnetic fields using spectrometers with variable field or several spectrometers at fixed field. These studies are limited by poor NMR sensitivity below 5 MHz. Experiments on relaxation in the rotating frame, so called  $T_{1\rho}$ , usually cannot provide data in a frequency range wider than one decade around 100 kHz. Nowadays the problem can be solved by applying the fast field-cycling NMR technique which has been used in the studies of dynamics in polymers, liquid crystals and biological systems [2]. This method allows one to investigate the frequency dependence of the spin-lattice relaxation at magnetic fields ranging from 2 T down to the intrinsic local fields without loss of detection sensitivity. The combination of field cycling with the standard relaxometry at high fields allows one to measure  $T_1$  dispersion in the frequency range from a few kHz to several hundred MHz, thus making NMR sensitive to motions with correlation times ranging from  $10^{-9}$  s to  $10^{-4}$  s and overlapping with the time scale of neutron scattering and optical methods. The  $T_1(\nu)$  technique is applicable to the study of dynamic heterogeneities in SIC as well [3].

In this contribution the study of motional disorder in crystalline superionic conductors with tysonite and fluorite structure by  $T_1$  dispersion is demonstrated. To extend the frequency range we used field-cycling NMR in combination with standard NMR relaxometry. As an example, the experimental  $^{19}\text{F}$   $T_1$  dispersion dependencies measured in the frequency range from 90 kHz to 370 MHz for single crystals of  $\text{La}_{1-x}\text{Sr}_x\text{F}_{3-x}$  ( $x=0; 0.03$ ) are shown in Fig. 1. From the NMR line shape analysis it is known that for both compounds only one dynamic process, exchange over  $\text{F}_1\text{-F}_1$  sublattices, dominates in the frequency range under investigation [4]. Nevertheless, for both compounds the relaxation dispersion shows a complicated behavior with additional fast relaxation processes characterized by correlation times around  $10^{-9}$  s. In Fig. 1 this extra process can be clearly distinguished in the upper frequency decade. Since these fast relaxational processes are not found in the NMR line shape analysis, we conclude that they are not induced by ionic hopping but rather by paramagnetic impurities.

At low frequencies the relaxation in tysonite is induced mostly by fluctuations of dipole-dipole interactions due to ionic hopping within the  $F_1$  sublattice. In periodic potentials of a crystalline lattice the relaxational behavior usually can be well described by the standard BPP model, which assumes a monoexponential correlation function. Nevertheless, the measured  $T_1(\nu)$  dependencies deviate from this model, reflecting a dynamic disorder, which is obviously not caused by static structural disorder. NMR line shape results have been well described by a model with a log-Gaussian distribution of correlation times for diffusing ions [4]. With relaxation dispersion, profiting from its possibility to access even much shorter correlation times, we support the existence of a log-Gaussian distribution at higher temperatures. The model assuming a log-Gaussian distribution of correlation times has been found to be suitable for the description of the NMR  $T_1$  relaxation dispersion also in fast ionic conductors with fluorite structure, such as  $Ba_{1-x}La_xF_{2+x}$ .

Thus, we can conclude that the NMR relaxation dispersion  $T_1(\nu)$  is applicable to the investigation of peculiarities of dynamic processes in superionic conductors in the range of correlation times from  $10^{-9}$  s to  $10^{-5}$  s. The method is sensitive to motional disorder in the superionic state, which reflects the distribution of interatomic potentials and can be used for analyzing the influence of heterovalent substitutions on the potential energy landscape.

### References

- [1] F. Noack. *Progr. NMR Spectr.* **18**, 171 (1986)
- [2] R. Kimmich. *NMR Tomography, Diffusometry, Relaxometry*. 1997, Springer-Verlag, Berlin
- [3] A. F. Privalov, S.V. Dvinskikh, F. Fujara and H.-M. Vieth. *Appl. Magn. Res.* **15**, 353 (1998)
- [4] A. F. Privalov, A. Cenian, F. Fujara, H. Gabriel, I. V. Murin, H.-M. Vieth. *J. Phys. Condens. Matter* **9**, 9275 (1997)

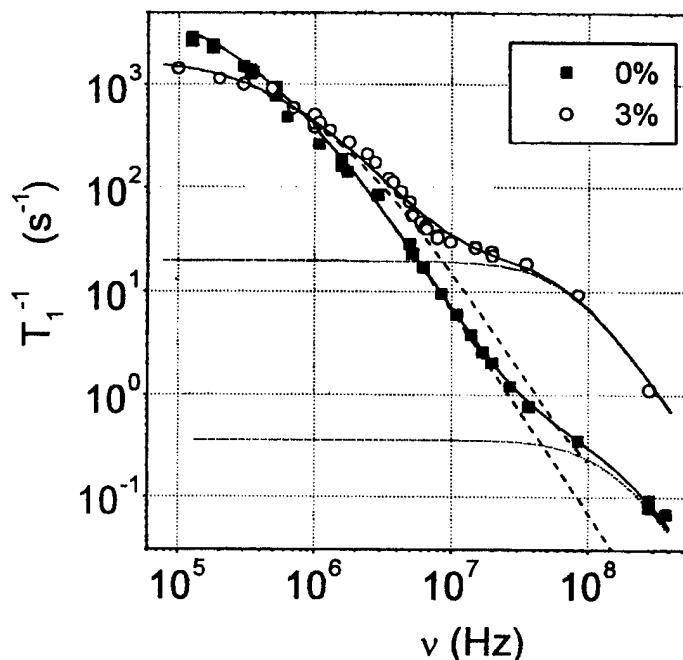


Fig. 1.  $^{19}\text{F}$   $T_1^{-1}$  frequency dependencies in  $\text{LaF}_3$  at 373K and in  $\text{La}_{0.97}\text{Sr}_{0.03}\text{F}_{2.97}$  at 290K. Dashed curves - log-Gaussian fit, dotted curves - high frequency contribution fitted with BPP model; full lines - sum of both processes.

## ADVANCES IN THE CONDUCTIVITY RELAXATION TECHNIQUE

M.W. den Otter, L.M. van der Haar, B.A. Boukamp, H.J.M. Bouwmeester, H. Verweij  
Laboratory of Inorganic Materials Science, Department of Chemical Technology,  
University of Twente, PO Box 217, 7500 AE Enschede, the Netherlands

Mixed conduction oxides with high oxygen ion conductivity, *e.g.* the cobaltate and cobaltate/ferrate based perovskites, are receiving increasing attention due to their prospective use in membranes for oxygen separation and as fuel cell electrodes. Measurement of the diffusion and exchange of oxygen in these mixed conducting materials is non-trivial. Imposing an electrochemically induced gradient in the oxygen activity along one dimension in the mixed conducting samples can lead to serious bypass currents through the ambient (due to fast exchange between lattice oxygen and the ambient). The only alternative is the stepwise change in the oxygen partial pressure in the ambient, either in a fixed volume containing the sample [1, 2] in which the oxygen flux and activity are measured simultaneously, or by measuring the change in oxygen concentration in the sample in a flow through system. The latter can be accomplished using a micro balance or by measuring a quantity related to the oxygen content, *e.g.* the change in the electronic conductivity. This method, known as the conductivity relaxation experiment, has lately found increasing interest [3], because of the simple experimental arrangement. In this presentation the technique and subsequent data analysis are critically evaluated and improvements to the standard methods are proposed.

The experimental set-up is schematically presented in Fig. 1. A polished sample with known dimensions is provided with two electrical contacts at both ends. The sample is placed in a cell with a minimised internal volume in order to decrease the influence of its 'dead volume'. The cell is flushed with a gas mixture in which the oxygen partial pressure can be changed quickly. Upon a change in the ambient  $PO_2$ , oxygen will be absorbed by (or removed from) the sample. Depending on the defect chemistry, the electronic conductivity changes slightly in response. For improved signal to noise ratio the conductivity change is measured using a 'Wheatstone bridge' type of arrangement, which is driven with an AC-voltage. A lock-in amplifier, connected to a PC, is used for signal detection.

Data analysis can be performed either in the time domain, or, after a Fourier transformation of the data, in the frequency domain. The advantage of the frequency domain is the ease of analysis in terms of 'equivalent circuits' using standard CNLS-fit programs [4], the disadvantage is the need for an extra transformation procedure.

The time domain solution of Fick's laws in this boundary value problem is well known (see *e.g.* Crank[5]), but involves the numerical evaluation of the 'eigenvalue' problem

$$\beta_n \tan \beta_n = \frac{lK_{ex}}{\tilde{D}} = L, \quad (1)$$

where the  $\beta_n$  are the roots which have to be calculated;  $l$  is the sample thickness,  $K_{ex}$  the oxygen transfer rate at the surface and  $\tilde{D}$  is the chemical diffusion coefficient of oxygen. A precise evaluation of the eigenvalues  $\beta_n$  is critical for obtaining reliable  $K_{ex}$  and  $\tilde{D}$  values. Recently a fast and precise method has been developed, which easily can be incorporated in any time domain fitting procedure [6].

An important parameter in the relaxation experiments is the rate at which the oxygen partial pressure changes in the sample chamber. Although a stepwise change in the  $PO_2$  is implemented at the feed line of the experimental cell, the CISTR characteristics of the sample chamber will cause a gradual change in the gas phase composition (in our set-up the cell is flushed in the order of seconds, typically). For the short time data set ( $t \leq \tau_{CISTR}$ ) this will cause

significant deviations from the model function. In order to obtain insight in the rate of change of the  $PO_2$  in the sample chamber measurements were performed with a specially developed sensor with a very short response time ( $\tau < 0.1$  s). This sensor consists of a thin film of  $La_{0.5}Sr_{0.5}CoO_{3-8}$  (50LSC) deposited by laser ablation on a  $SrTiO_3$  single crystal substrate. The thus measured CISTR characteristics of the sample chamber are used as input for an improved fitting procedure of actual relaxation experiment data.

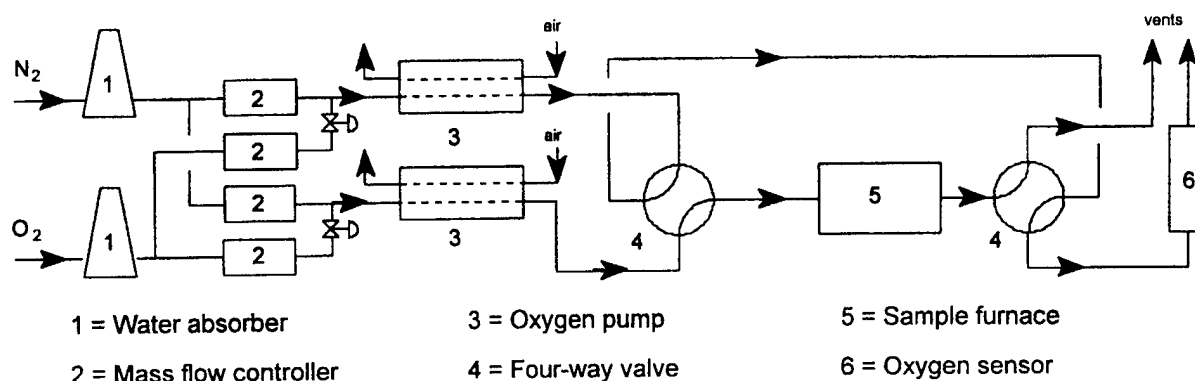


Figure 1 Conductivity relaxation experimental set-up.

### References

- [1] M.H.R. Lankhorst *et al.*, Phys. Rev. Lett. **77** 2989 (1996).
- [2] K.Lade, T. Jacobsen, Solid State Ionics **72** 218 (1994).
- [3] Isamu Yasuda and Tomoji Hikita, J.Electrochem. Soc. **141**, 1268 (1994); I. Yasuda and M. Hishinuma, Solid State Ionics **80**, 141 (1995); B. Ma, *et al.*, Solid State Ionics **83**, 65 (1996).
- [4] B.A. Boukamp, Solid State Ionics **18-19**, 136 (1986) & **20**, 31 (1986).
- [5] J. Crank, 'The mathematics of diffusion', 2<sup>nd</sup> ed., pp. 60, Clarendon press, Oxford (1975).
- [6] M.W.den Otter, B.A. Boukamp, H.J.M. Bouwmeester, H. Verweij, to be published.

OXYGEN TRANSPORT AT THE INTERFACE OF  $\text{La}_{0.92}\text{MnO}_{3-x}$  FILM /  $\text{Y}_{0.15}\text{Zr}_{0.85}\text{O}_{1.925}$  SINGLE CRYSTAL

Teruhisa Horita, Katsuhiko Yamaji, Hideyuki Negishi, Natsuko Sakai, Harumi Yokokawa, and Tohru Kato\*

National Institute of Materials and Chemical Research (NIMC)

\* Electrotechnical laboratory

Oxygen reduction at the interface of electrode/electrolyte is one of the most important reactions in solid electrolyte devices because it mainly determines the performance. For understanding the oxygen reduction mechanism, the oxygen transport at the cathode/electrolyte interface must be clarified. So far, many studies have investigated the electrochemical behaviors of the interface by the observation of electron movements, such as DC polarization and AC impedance spectroscopy. However, there still remains uncertainty about the reaction process or reaction mechanism. One reason for the uncertainty is the "indirect observation" of movements of oxygen.

In order to clarify the oxygen reduction at the electrode/electrolyte interface, a new technique has been adopted by using secondary ion mass spectrometry (SIMS) for samples with isotope oxygen exchange ( $^{16}\text{O}/^{18}\text{O}$  exchange). This "direct observation" of the movements of oxygen has already been examined at the interface of the mesh shaped  $\text{La}_{0.9}\text{Sr}_{0.1}\text{MnO}_{3-x}$  (LSM) on a substrate of  $\text{Y}_{0.15}\text{Zr}_{0.85}\text{O}_{1.925}$  (YSZ)[1]. In the previous work, the active sites for oxygen reduction have been determined by SIMS imaging analysis. However, the oxygen transport has not been clarified at the interface of LSM/YSZ. The purpose of the present study is to clarify the oxygen transport at the electrode/electrolyte interface. To reduce chemical reaction between electrode and electrolyte, A-site deficient  $\text{LaMnO}_3$  ( $\text{La}_{0.92}\text{MnO}_3$ , LM) was used, because of their low chemical reactivity with electrolyte. The LM film was fabricated by rf-sputtering technique, with a smooth surface. Also, the single crystal of  $\text{Y}_{0.15}\text{Zr}_{0.85}\text{O}_{1.925}$  (YSZ) was used as a substrate to eliminate the effect of the grain boundary.

Figure 1 shows diffusion depth profiles of  $^{18}\text{O}$  at the LM film/YSZ interface for different annealing temperatures by SIMS. The annealing treatments give continuous concentration profiles of  $^{18}\text{O}$  at the LM/YSZ interface, whereas the profile for the sample as deposition shows discontinuous curve at the interface. With increasing the annealing temperature, diffusion of  $^{18}\text{O}$  inside the LM film became smaller. Lower diffusivity of  $^{18}\text{O}$  in the LM film can come from the composition change of LM film.

## References

- [1] T. Horita, K. Yamaji, M. Ishikawa, N. Sakai, H. Yokokawa, T. Kawada, and T. Kato, *J. Electrochem. Soc.*, **145**, No.9, 3196, (1998).

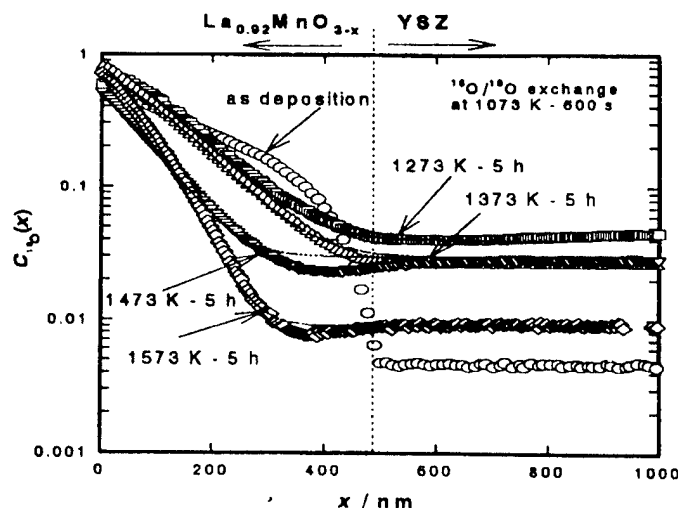


Fig. 1 Diffusion depth profiles of  $^{18}\text{O}$ -concentration at LM film/YSZ interface.

# SPATIALLY RESOLVED MEASUREMENTS OF SINGLE GRAIN BOUNDARIES USING MICROCONTACT IMPEDANCE SPECTROSCOPY

J. Fleig, S. Rodewald, and J. Maier

Max-Planck-Institut für Festkörperforschung  
Heisenbergstr. 1, 70569 Stuttgart, Germany

Impedance spectroscopy is an important tool to investigate the electrical properties of *blocking grain boundaries* in polycrystalline materials. However, conventional impedance measurements average over thousands of grain boundaries and recent finite element calculations on the impedance of electroceramics showed that such averaged values may be difficult to interpret [1],[2]. Consequently, it can be useful not only to determine the influence of grain boundaries on the overall properties but also to measure the properties of single grain boundaries within polycrystalline samples. Measurements of single grain boundaries in ZnO have been reported [3]-[5]. However, most of these studies applied dc-techniques which do neither allow

for a simple separation of electrode, grain boundary and bulk resistance nor the determination of the grain boundary capacitance. Thus, impedance spectroscopic studies using microcontacts on two adjacent grains are highly desired to overcome these restrictions.

In this contribution we present microcontact impedance measurements of single grain boundaries in acceptor-doped SrTiO<sub>3</sub> which demonstrate the applicability and power of this method in characterising single grain boundaries. The measurement principle as well as a microelectrode pattern applied by lithography and impedance spectra with and without a grain boundary are shown in Figs. 1 and 2. Measurements on more than 50 grain boundaries allowed for a statistical analysis of grain boundary resistivities. The spatial variations and the temperature and bias dependencies of the grain boundary properties in SrTiO<sub>3</sub> are discussed.

Furthermore finite element calculations demonstrate in how far a quantitative analysis of the impedance is possible and show the

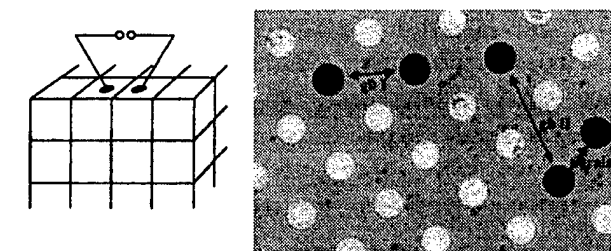


Fig. 1: Sketch of the measurement principle and image of microcontacts (20  $\mu\text{m}$ ) on SrTiO<sub>3</sub>

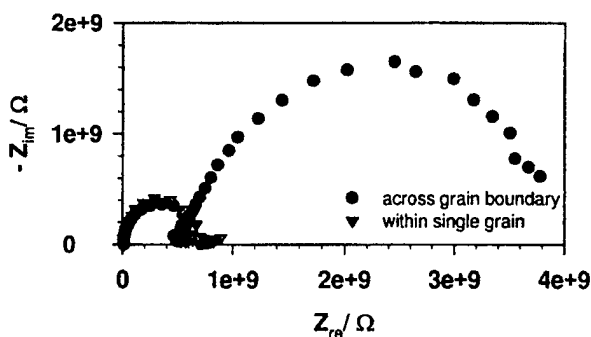


Fig. 2: Impedance spectra between two microcontacts with and without grain boundary

potentials and limits of the method. In particular, these calculations reveal the influence of neighboring grain boundaries on the measured single grain boundary impedance. The knowledge of the frequency distribution and hence impedance spectroscopy is indispensable for a quantitative, grain size independent determination of grain boundary resistivities.

The situation complicates for *highly conducting grain boundaries* since they do not yield an additional semicircle in the complex impedance plane. It is even difficult to decide whether the d.c. resistance is determined by the bulk or by highly conducting paths. Hence, a method



would be very helpful which allows to unambiguously distinguish between grain boundary conductance and bulk conductivity.

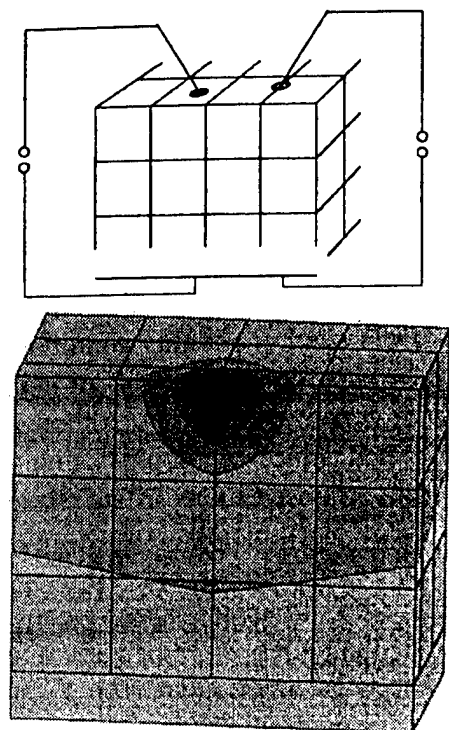


Fig. 3: Sketch of the measurement set-up and potential distribution in a polycrystal with highly conducting grain boundaries.

For this purpose we modified the microcontact impedance spectroscopy just described to tackle this problem. The applicability of the method is demonstrated by proving highly conducting grain boundaries in AgCl-polycrystals. Using finite element calculations we show how the grain conductivity and the grain boundary conductance can be estimated from microcontact measurements and whether or not the obtained values represent local conductances of single grain boundaries. A sketch of the set-up and a calculated potential distribution in one half of an idealized polycrystal is shown in Fig. 3 Furthermore, possible applications in investigations of composites (solubility effects, enhanced conductivity at interfaces, etc.) are discussed.

#### References:

- [1] J. Fleig and J. Maier, Solid State Ionics, in press.
- [2] J. Fleig and J. Maier, J. Europ. Ceram. Soc., in press.
- [3] M. Tao, Bui Ai, O. Dorlante and A. Loubiere, J. Appl. Phys., **61**, 1562 (1986).
- [4] R. Einzinger, Advances in Ceramics **1**, 359 (1981).
- [5] E. Olsson and G.L. Dunlop, J. Appl. Phys. **66**, 3666 (1989)

DEFECT STRUCTURES IN DOPED CeO<sub>2</sub> STUDIED BY USING XAFS SPECTROSCOPY

Tsuneo Matsui, Toyo Ohashi, Satoshi Yamazaki and Yuji Arita  
 Dept. of Quantum Engineering, Graduate School of Engineering,  
 Nagoya University, Chikusa-ku, Nagoya 464-8603, Japan

Ceria doped with trivalent cations has been known to exhibit high oxygen ion conductivity due to the presence of oxygen vacancies introduced by doping from electroneutrality condition. At low dopant contents, the ionic conductivity increases with increasing dopant content. At high dopant contents, to the contrary, the conductivity decreases with dopant content [1]. Although oxygen vacancies are generally considered to be preferentially located adjacent to dopant cations, it has been reported that oxygen vacancies were located adjacent to host cations in stabilized zirconia [2].

In the present study, the local structures in Ce<sub>1-x</sub>Ln<sub>x</sub>O<sub>2-x/2</sub> (Ln=Sc, Y, Nd, Sm, Gd, Yb, X=0-0.30) were studied by using EXAFS (extended X-ray absorption fine structure) spectroscopy. The powdered samples of Ce<sub>1-x</sub>Ln<sub>x</sub>O<sub>2-x/2</sub> were prepared by heating the pellets made of a mixture of CeO<sub>2</sub> and M<sub>2</sub>O<sub>3</sub> powders at 1723K in air for a week and then pulverizing them. The X-ray diffraction patterns of the doped samples indicated the presence of a single fluorite phase except for Sc<sub>2</sub>O<sub>3</sub>-doped CeO<sub>2</sub>. The X-ray absorption measurements near Ce-L3, Y-K and Gd-L3 edges were made at room temperature with synchrotron radiation by use of the EXAFS facilities on the beam line 7C of 2.5 GeV storage ring at Photon Factory of the High Energy Accelerator Research Organization (KEK, Tsukuba).

From the XANES spectrum, the Ce atoms in Ce<sub>1-x</sub>Ln<sub>x</sub>O<sub>2-x/2</sub> were seen to be as the tetravalent Ce ions. The Ce-O distances in doped CeO<sub>2</sub> obtained from EXAFS analysis are plotted as a function of dopant concentration in Fig.1. Except for the Ce-O distance in Sc-doped CeO<sub>2</sub>

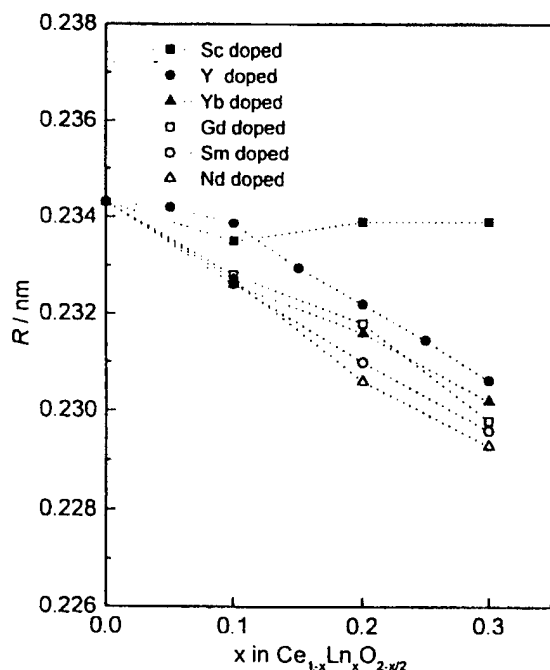


Fig.1 The Ce-O distances of Ce<sub>1-x</sub>Ln<sub>x</sub>O<sub>2-x/2</sub> (Ln=Sc, Yb, Y, Gd, Sm, Nd)

showing the presence of two-phases, those in CeO<sub>2</sub> doped with Y, Nd, Sm, Yb and Gd are seen to decrease with increasing dopant concentration, suggesting that oxygens surrounding oxygen vacancies around Ce are relaxed toward their adjacent vacancies, and as a result, Ce-O distances become short. Due to the overlapping of the X-ray absorption spectrum between Ln-K or Ln-L3 and Ce-L3, the Y-O and Gd-O distances were only determined. The Gd-O distances decreased with dopant content, but the Y-O distances were seen almost constant. The several complex defect structures composed of Ce, Gd or Y and oxygen atoms were proposed to explain these dependences of Ce-O, Gd-O and Y-O distances on dopant content.

[1]H. Inaba and H. Tagawa, Solid State Ionics, **83**, 1(1996).

[2]C.R.A.Catlow, A.V.Chadwick, G.N.Greaves and L.M.Moroney, J.Am.Ceram.Soc., **69**, 272(1986).

## **PREPARATION OF OXIDE THIN FILMS BY CONTROLLED DIFFUSION OF OXYGEN ATOMS.**

Z. Rosenstock and I. Riess

Physics department, Technion -- Israel Institute of Technology.  
Haifa 32000, Israel.

A new method for preparing thin oxide films is described. It makes use of slow diffusion of oxygen through a protecting layer, towards the metal to be oxidized. We have used this method to oxidized copper. The permeable layer is a dense silver film. Diffusion time and temperature have been varied in order to study the influence of these parameters on the oxide thickness and on the oxide growth rate. The formation of the layer was followed in situ by measuring the resistance of the cell.

A second method that allows a controlled preparation of oxide thin film is an electrochemical one.

Copper oxide films prepared by the two methods are compared.

## OXYGEN SURFACE EXCHANGE ON GADOLINIA DOPED CERIA.

J.A. Lane and J.A. Kilner

Centre for Ion Conducting Membranes, Dept. of Materials,  
Imperial College of Science, Technology and Medicine,  
London SW7 2BP, UK.

### Abstract

Gadolinia doped ceria (CGO) is the focus of an increasing amount of attention as an electrolyte material for applications such as solid oxide fuel cells (SOFC) and oxygen separators. The vast majority of work completed to date on the oxygen ion transport properties of electrolyte materials has been undertaken using AC impedance spectroscopy or other electrical testing techniques. In general, these electrical tests are excellent methods for measuring the oxygen mobility of materials such as CGO due to their negligible electronic conductivity. However, it is also useful to measure the oxygen ion diffusivity of materials directly using instruments such as secondary ion mass spectrometers (SIMS) to verify these conductivity results. The added advantage of a technique such as SIMS is that it also provides data on the kinetics of oxygen exchange on the surface of the material as well as the oxygen diffusion in the bulk. However, there is very little work published to date on the measurement of oxygen ion diffusivity using SIMS on this type of electrolyte material.

Recently, work conducted in our research laboratory has measured the oxygen diffusion and oxygen surface exchange behaviour in polycrystalline  $\text{Ce}_{0.9}\text{Gd}_{0.1}\text{O}_{1.95}$  [1] and other related fluorite materials such as polycrystalline and single crystal YSZ [2] and single crystal  $\text{Ce}_{0.69}\text{Gd}_{0.31}\text{O}_{1.845}$  [3,4]. The oxygen surface exchange properties of these materials are as important as the bulk diffusion properties but are often not considered in the literature. This is, in part, due to the difficulty in performing tracer experiments on electronically insulating ceramics. The mechanism for the incorporation of oxygen into these materials is of particular importance with regard to the performance of these materials as electrolytes. More recently there has been interest in the use of composite electrodes, mixtures of an ionic conducting and an electronic conducting ceramic, to improve electrode performance. The performance of such a mixed conducting electrode is dependent on its surface exchange behaviour [5] and data from our laboratory is reported in a corresponding paper in these proceedings [6].

This paper will concentrate on the oxygen diffusion and oxygen surface exchange behaviour of  $\text{Ce}_{0.9}\text{Gd}_{0.1}\text{O}_{1.95}$  measured by isotope exchange and SIMS. Data will be presented for the dependence of the tracer diffusion coefficient,  $D_T$ , and the oxygen surface exchange coefficient,  $k$ , both as functions of temperature and oxygen partial pressure,  $p\text{O}_2$  (Figure 1). These results will provide the basis for determining the mechanism for the incorporation of oxygen into these materials.

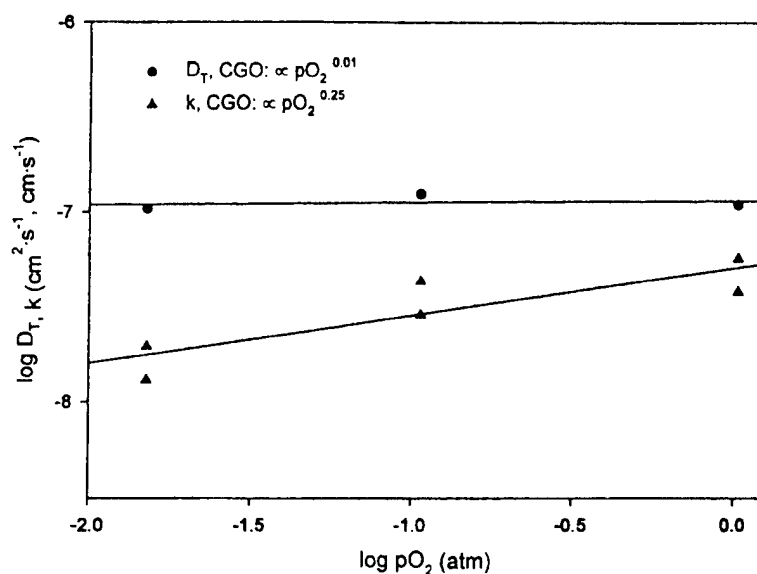


Figure 1. Oxygen partial pressure dependence at 800°C of the oxygen tracer diffusion coefficient,  $D_T$ , and oxygen surface exchange coefficient,  $k$ , for a  $\text{Ce}_{0.9}\text{Gd}_{0.1}\text{O}_{1.95}$  ceramic sample.

- [1] P.S. Manning, J.D. Sirman and J.A. Kilner, Solid State Ionics, **93** (1997) 125-132.
- [2] P.S. Manning, J.D. Sirman, R.A. De Souza and J.A. Kilner, Solid State Ionics, **100** (1997) 1-10.
- [3] J.D. Sirman, Ph.D. Thesis, University of London (1998).
- [4] E. Ruiz-Trejo, J.D. Sirman, Yu. M. Baikov and J.A. Kilner, to be published in the Proc. of the XI<sup>th</sup> Conference on Solid State Ionics, Honolulu (1997).
- [5] S.B. Adler, J.A. Lane and B.C.H. Steele, J. Electrochem. Soc., **143** (11), 1996, p.3554-3564.
- [6] V.J. Dusastre, J.A. Lane, and J.A. Kilner, these proceedings.

## ELECTROLYTE DEGRADATION CAUSED BY POINT CONTACT ELECTRODES ON $\text{Sr}(\text{Zr,Dy})\text{O}_{3-\delta}$

B.Gharbage, F.M.B.Marques, J.R.Frade

Ceramics and Glass Engineering Department, UIMC, University of Aveiro, 3810 Aveiro, Portugal

Pt point contact electrodes were used to characterise the cathodic processes occurring at the  $\text{Sr}(\text{Zr,Dy})\text{O}_{3-\delta}/\text{Pt}$  contacts. Cathodic polarisation was performed in a potentiostatic mode, with the Autolab Frequency Response Analyser, by superimposing an ac signal on a dc bias. Impedance spectra in the range  $10^{-3}$  to  $10^5$  Hz were thus used to separate the ohmic resistance of the strontium titanate based protonic conductor from electrode process contributions.

This type of measurements provided interesting features of electrode processes taking place at the surface of  $\text{Sr}(\text{Zr,Dy})\text{O}_{3-\delta}$  in atmospheres containing  $\text{H}_2$  and  $\text{H}_2\text{O}$  [1]. However, the ohmic losses obtained under cathodic polarisation were significantly lower than for zero dc bias, and the difference increases with the applied voltage. Post-mortem EDS analysis showed Sr-segregation at the point contact electrode, probably because the electric field is relatively high near the point contact electrode even for moderate applied voltages (typically 1 V or lower).

One may thus propose an explanation for the changes in ohmic resistance by assuming that Sr-segregation yields a significant concentration of negatively charged strontium vacancies ( $\text{V}_{\text{Sr}}''$ ). This concentration may then be compensated by enhanced concentrations of the expected positively charged carriers in high temperature protonic conductors (protons and/or oxygen ion vacancies). Electron holes are less likely in the actual reducing conditions.

A sudden interruption of the dc bias yield a slow recovery of the ohmic resistance, which tends to the initial value obtained before application of the dc bias. The time dependence of the changes in ohmic resistance is nearly described by a  $t^{1/2}$  law, thus indicating a diffusion controlled recovery.

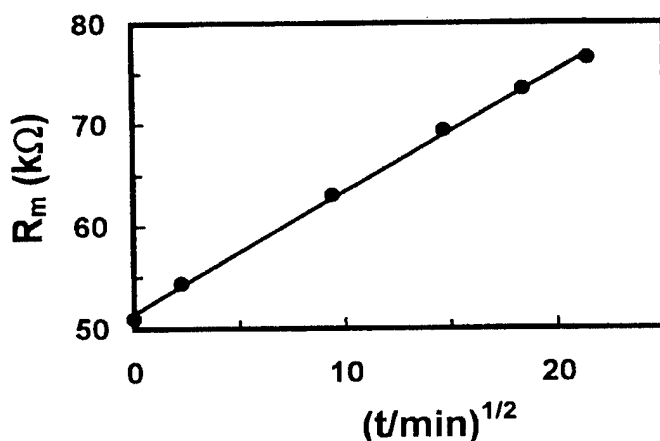


Figure 1: Change of ohmic resistance after interruption of a dc bias of 1.4V.

STRUCTURE AND THERMODYNAMICS  
OF ZIRCONIA – NIOBIA CERAMIC ALLOYS

J.R. Sellar

Department of Materials Engineering

Monash University

Clayton 3168 Victoria Australia

e-mail: [jeff.sellar@eng.monash.edu.au](mailto:jeff.sellar@eng.monash.edu.au)

As an engineered oxygen-conducting ceramic, zirconia is usually stabilized in a room-temperature phase which is (on average) of cubic structure by the addition of oxides of metals of valency lower than four. Though these anion-deficient alloys are currently still an active field of ceramics research, considerable interest has also recently been expressed (see e.g. [1]) in the consequences of “stabilizing” zirconia to comparable doping levels with oxides of metals with valency greater than four (eg.  $\text{Nb}_2\text{O}_5$ ,  $\text{Ta}_2\text{O}_5$ ) in particular because of their wide solid-solution range, their seemingly anomalous behaviour, and for the light they may shed on the operation of the anion-deficient alloys.

The alloys are structurally complex, so some explanation of the current incomplete state of our understanding of them is in order. The description of the structures of these anion-excess alloys has in fact undergone considerable change with time in the last twenty-five years or so. Early diffraction experiments showed that the results of such anion-excess doping were alloys with structures very different from the familiar cubic zirconias mentioned above. The main consequence of doping with niobia ( $\text{Nb}_2\text{O}_5$ ) appeared to be the production of orthorhombic long-period superlattices with very sharp electron diffraction spots and an apparently continuous distribution of dopant-dependent superlattice wave-vectors within the composition limits  $5:1 \leq \text{ZrO}_2:\text{Nb}_2\text{O}_5 \leq 8:1$  i.e. a continuous series of alloys with formula  $\text{Nb}_2\text{Zr}_{x-2}\text{O}_{2x+1}$  ( $x = 7-10$ ) such that each phase with non-integral  $x$  was a single superlattice structure rather than an intergrowth of two adjacent phases each with integer values for  $x$ . The average metal subcell is still roughly cubic, but the early single crystal x-ray studies of two “integral  $x$ ” phases with simple stoichiometries,  $\text{Nb}_2\text{Zr}_6\text{O}_{17}$  and  $\text{Ta}_2\text{Zr}_8\text{O}_{21}$ , resulted in apparent eightfold and tenfold superlattices in the [100] direction. In 1974 a radical new interpretation appeared furnishing an efficient description of the mechanism by which this alloy series could accommodate continuous non-stoichiometry. According to [2], the orthorhombic niobia-zirconia alloys could best be described as having periodic, approximately face-centered cubic metal positions with periodic two-dimensional nets of oxygen atoms alternating smoothly between  $3^6$  locally hexagonal nets and  $4^4$  locally tetragonal nets in the superlattice direction and arrayed in antiphase in the [010] direction of the orthorhombic superlattice structures, needing only small rotations of the oxygen nets in order to change gradually between the two net types.

Recently [1], it has been suggested that the zirconia-niobia alloys are more appropriately described as incommensurate compositely-modulated structures, but this viewpoint is limited by the existence of an irreproducible canting of the oxygen superlattice away from the  $a$ -axis of the composite. Widespread disorder has also been detected on the oxygen lattice.

In the present paper electron microscope evidence is produced suggesting that the alloys are not strictly crystalline and that several aspects of their behaviour as a function of temperature may be interpreted as proper to a frustrated two-dimensional XY model where the distinctive planes of

oxygen atoms in the alloys form a lattice of planar XY "spins". Evidence is presented for the existence of frustration, which produces superlattice canting in the model including electron microscope evidence for the existence of domains of staggered Ising-type chirality in the alloys, as predicted earlier for the frustrated two-dimensional XY model.

- [1] Thompson, J.G., Withers, R.L., Sellar, J., Barlow, P.J. and Hyde, B.G., *J. Solid State Chem.*, 88, 465, (1990)
- [2] Hyde, B.G., Bagshaw, A.N., Andersson, S. and O'Keeffe, M., *Ann. Rev. Mater. Sci.*, 4, 43, (1974)



# FIRST OBSERVATION OF $^{109}\text{Ag}$ - $^{107}\text{Ag}$ DOUBLE RESONANCE BY DIPOLAR-DEPHASING DIFFERENCE NMR EXPERIMENT ON A SILVER ION CONDUCTOR $\text{Ag}_9\text{GaSe}_6$

Masataka Tansho<sup>1,2</sup>, Colin A. Fyfe<sup>2</sup>, Hiltrud Grondey<sup>2</sup>, Tom Markus<sup>2</sup> and Hiroaki Wada<sup>1</sup>

<sup>1</sup>National Institute for Research in Inorganic Materials (NIRIM),  
1-1 Namiki, Tsukuba, Ibaraki 305-0044, Japan

<sup>2</sup>Department of Chemistry, University of British Columbia,  
2036 Main Mall, Vancouver, B.C., V6T 1Z1, Canada

$^{109}\text{Ag}$ - $^{107}\text{Ag}$  double resonance of a silver compound has been measured for the first time. It is known that because of the quite small gyromagnetic ratios of silver nuclei, usually quite long  $T_1$  values of the order of 1000s are expected for silver compounds. However, in many silver ion conductors, the  $T_1$  minimum was actually found to be of the order of 100ms, and a large scalar coupling between silver nuclei has been suggested for the relaxation mechanism in these systems [1, 2]. To detect interactions between silver nuclei, we have carried out a  $^{109}\text{Ag}$ - $^{107}\text{Ag}$  double resonance measurement. Using the dipolar-dephasing difference NMR method[3], the signal from  $^{109}\text{Ag}$ - $^{107}\text{Ag}$  resonance is observed for  $\text{Ag}_9\text{GaSe}_6$ .

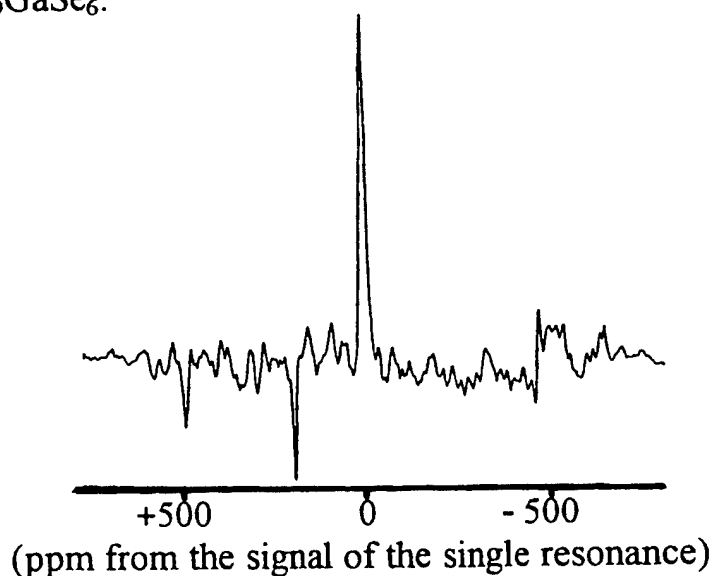


Fig. 1  $^{109}\text{Ag}$ - $^{107}\text{Ag}$  double resonance spectrum on  $\text{Ag}_9\text{GaSe}_6$

[1] M. Tansho, H. Wada, M. Ishii, and Y. Onoda, *Solid State Ionics* **86-88**, 156 (1996).

[2] M. Tansho, H. Wada, M. Ishii, and Y. Onoda, *J. Phys. Chem. B* **102**, 5047 (1998).

[3] C.A.Fyfe, K.T.Mueller, H.Grondey, and K.C.Wong-Moon, *J. Phys. Chem.* **97**, 13484 (1993).

# HIGH-TEMPERATURE X-RAY STUDY FOR A SINGLE CRYSTAL OF THE HOLLANDITE-TYPE ONE-DIMENSIONAL IONIC CONDUCTOR, $\text{Na}_x\text{Cr}_x\text{Ti}_{8-x}\text{O}_{16}$ ( $x=1.7$ )

Yuichi Michiue, Mamoru Watanabe and Shinzo Yoshikado\*

National Institute for Research in Inorganic Materials, 1-1 Namiki, Tsukuba, Ibaraki 305-0044, Japan \* Department of Electronics, Doshisha University, Tanabe, Kyoto 610-0321, Japan

In the hollandite structure, pseudo-cuboctahedral cavities are linearly connected to form one-dimensional (1-D) tunnels available for ion transport. Distribution and dynamics of  $\text{K}^+$  ions in this 1-D pathway have been extensively studied so far. In recent years, we have studied the isostructural  $\text{Na}^+$ -salt  $\text{Na}_x\text{Cr}_x\text{Ti}_{8-x}\text{O}_{16}$  ( $x=1.7$ ) and clarified the structural properties of the tetragonal form (22 °C) [1,2] and the monoclinic form (-50 °C). In the present study, X-ray diffraction measurement for a single crystal of  $\text{Na}_x\text{Cr}_x\text{Ti}_{8-x}\text{O}_{16}$  ( $x=1.7$ ) has been performed at 500 °C. The Maximum Entropy Method (MEM) has been applied in order to obtain electron density maps in the tunnel.

Single crystals were grown by the slow-cooling method using a  $\text{Na}_2\text{CO}_3$ - $\text{MoO}_3$  flux melt [1]. Crystallographic data and experimental conditions for the structure refinement are summarized in the table below. For the MEM analysis (program: MEED [3]), the unit cell is divided into  $64 \times 64 \times 32$  pixels. The set of electron densities satisfying  $C/N < 1$  was obtained after 1191 iterations from the flat distribution, where  $C = \sum_k |F_c(k) - F_o(k)|^2 / \sigma_F(k)^2$ , and  $N$  is the number of reflections, 620.

The  $\text{Na}^+$  ions are located at three positions Na1:(0.072, 0.014, 0.5), Na2:(0, 0, 0.203) and Na3:(0, 0, 0) at room temperature. The Na1 is a little deviated from the cavity center (0,0,0.5) toward the tunnel wall. This cavity is so large that a  $\text{Na}^+$  ion is unstable at the center position. The Na2 is shifted from the cavity center along  $z$ , the direction of the tunnel axis. The boundary of adjacent cavities, the Na3 site, is also available for a Na position, where the  $\text{Na}^+$  ion forms the square-planar coordination with four oxygens. At 500 °C, electron density distribution obtained from the MEM is naturally more broad than that at room temperature as shown in Fig. 1. It should be noted that the density peak at (0,0,0) clearly observed at 22°C has almost disappeared at 500 °C.

## Crystallographic data and experimental conditions for $\text{Na}_x\text{Cr}_x\text{Ti}_{8-x}\text{O}_{16}$ ( $x=1.7$ )

Temperature	773 K
Crystal system	tetragonal
Space group	$I4/m$
$a$ (Å)	10.099(2)
$c$	2.971(2)
$V$ (Å <sup>3</sup> )	303.4(2)
$Z$	1
$D_x$ (g/cm <sup>3</sup> )	3.7
$\mu(\text{MoK}\alpha)$ (cm <sup>-1</sup> )	54.8
Crystal size (mm)	$0.15 \times 0.15 \times 0.25$
Radiation	$\text{MoK}\alpha(0.71069 \text{ Å})$
$2\theta_{\text{max}}$ (°)	90
Reflection used	620
Final $R$ , $wR$ (%)	3.34, 3.08

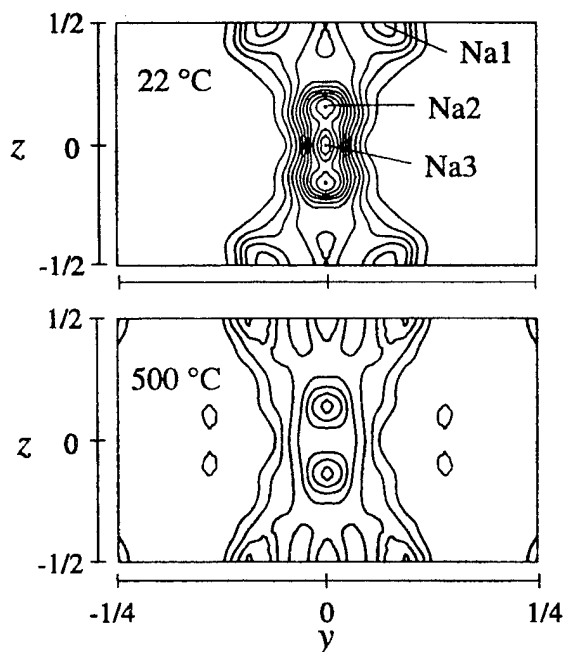


Fig. 1 Electron density maps at the section  $x=0$  drawn by the maximum-entropy method. Contour intervals are  $0.4 \text{ e/Å}^3$ .

[1] Y. Michiue et. al., J. Solid State Chem. **116**, 296 (1995). [2] Y. Michiue et. al., Solid State Ionics **79**, 116 (1995). [3] S. Kumazawa et.al., J. Appl. Crystallogr. **23**, 526 (1990).

## ELECTRON CRYSTALLOGRAPHY OF BIMEVOX

P. Pongratz, P. Kurek<sup>a</sup>, G. Fafilek<sup>b</sup>

Institute of Applied and Technical Physics, Vienna University of Technology  
Wiedner Hauptstr. 8-10, A-1040 Vienna, Austria

<sup>a</sup>Institute of Physics, Warsaw University of Technology  
Koszykowa 75, 00-662 Warsaw, Poland

<sup>b</sup>Institute of Technical Electrochemistry, Vienna University of Technology  
Getreidemarkt 9, A-1060 Vienna, Austria

It is a well known fact that the high ionic conductivity of the  $\gamma$  phase in the BIMEVOX family depends on the disorder of oxygen ions within the anion deficient perovskite-like layers [1]. Doping strategies have been developed to maximize the effect and structural refinements by X-ray and neutron techniques have been performed in order to get a clear explanation for the elementary process which is responsible for this property. Two activation energies for ion conductivity are observed, which are related to the  $\gamma'$  and  $\gamma$  phase regions. This fact could be related to the qualitative result of electron diffraction experiments showing a superlattice ordering process of oxygen ions [2]. The superlattice, indicating the presence of some long range order was also found by other groups using X-ray or neutron diffraction [3]. In spite of the fact that many investigations in the past have tried to find out a good structure model which should also explain the different activation energies of the mobile ions at high temperatures, the problem has not been solved yet.

That is why we think that a new method, called electron crystallography, may be suited to quantify the nature of local order-disorder of oxygen ions and their tendency to form extended coherent long range order superlattice domains within the average structure.

In principle, TEM and electron diffraction can contribute to this task with higher sensitivity than other diffraction methods, because of the stronger interaction of electrons with matter. The situation is favourable in comparison to X-ray or neutron diffraction techniques, since there is no need to integrate over a large crystalline sample volume. However, electron crystallography as a quantitative method has not been developed in comparison to X-ray crystallography, because the image intensities could not be digitised in a convenient way. Now HRTEM images and diffraction patterns with high intensity dynamics can be quantified with a modern TEM-CCD camera. The application of computer processing techniques to the image data combined with fast Fourier transforms and filtering, provide new possibilities to find out the differences between local structural image details and the average structure information within a sample[4].

The experimental procedure, the power of the method and its limits will be discussed. First results of a local structure refinement using this method when applied to single crystal data of BIMEVOX samples (Me=Cu, Ni) will be presented in our paper. Superlattice quantification after various heat treatments of crystals is of main interest in the context of the new possibilities.

### References

- [1] F. Abraham, J. C. Boivin, G. Mairesse, G. Nowogrocki, Solid State Ionics, 40-41 (1990) 934.
- [2] P. Kurek, P. Pongratz, M. W. Breiter, Solid State Ionics 113-115 (1998) 665.
- [3] C. Muller, M. Anne, M. Bacmann, Solid State Ionics 111 (1998) 27.
- [4] X. Zou, Y. Sukharev, S. Hovmöller, Ultramicroscopy 52 (1993) 436.

## X-RAY ABSORPTION NEAR EDGE STRUCTURE (XANES ) AND IONIC CONDUCTIVITY STUDIES OF CERIA BASED SOLID ELECTROLYTES

J. Hormes <sup>1</sup>, M. Pantelouris <sup>1</sup>, Bryan Balazs <sup>2</sup> and B. Rambabu <sup>\*\*</sup>

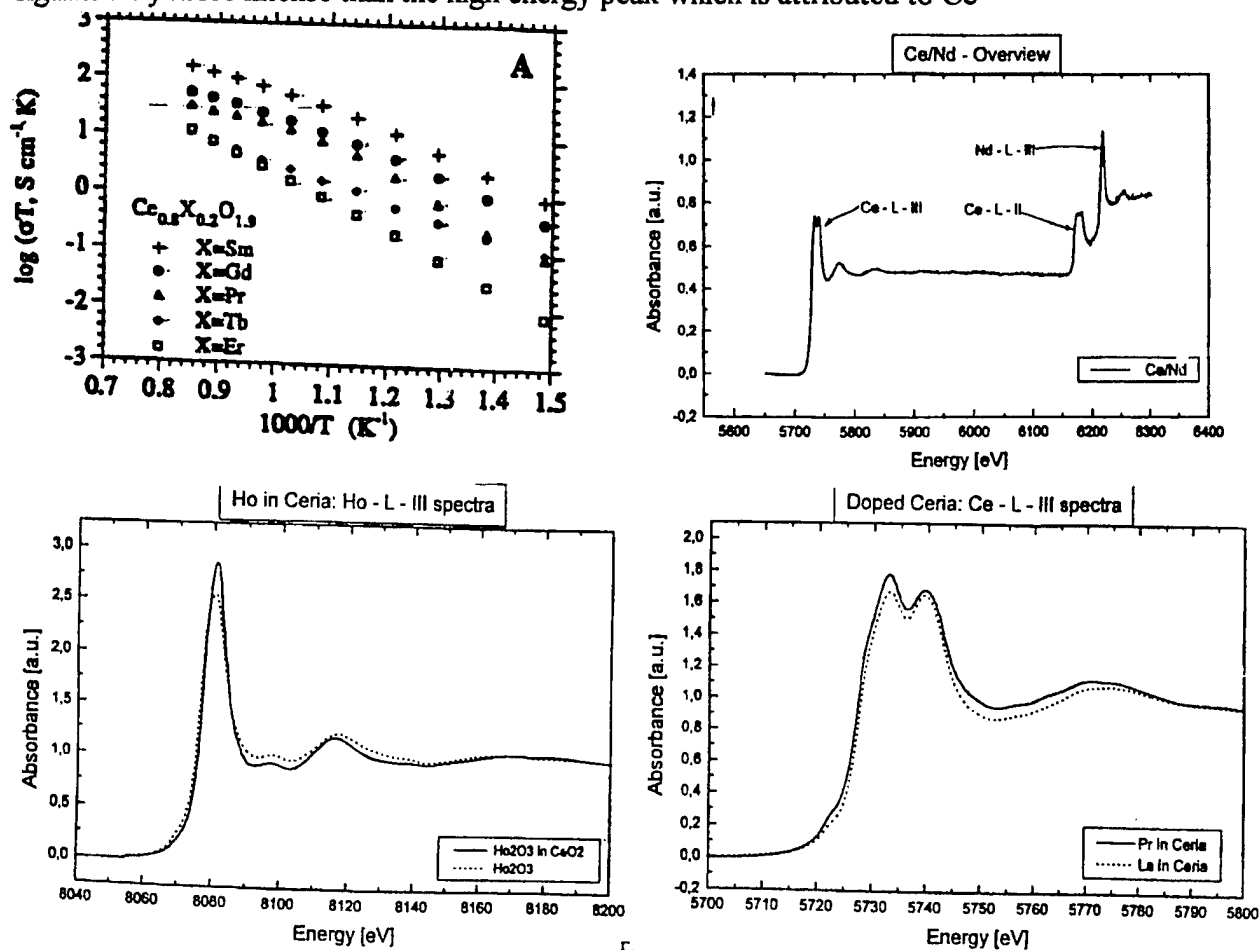
<sup>\*</sup>Surface Science, Spectroscopy and Solid State Ionics Laboratory  
Department of Physics, Southern University, Baton Rouge, Louisiana 70813

1. Physikalisches Institut, Universitat Bonn, Nussallee 12, D-53115, Bonn
2. Lawrence Livermore National Laboratory, Livermore, CA -94550

CeO<sub>2</sub> based solid electrolytes have stable defect structure at elevated and intermediates temperatures and pressures and showed great potential for fuel cells and gas phase sensor applications. Trivalent rare earth ion doping increases the concentration of oxygen vacancies and enhance its ionic conductivity. In recent years, doped ceria systems have become increasingly popular for their role as an electrolyte or an electrode for solid oxide fuel cells ( SOFCs ) because of their relatively high ionic and electronic conductivity. A CeO<sub>2</sub> electrolyte doped with a rare earth like gadolinium exhibits higher ionic conductivity in air than zirconia. An ionic conductivity of  $8.3 \times 10^{-2}$  S/cm has been reported for (CeO<sub>2</sub>)<sub>0.8</sub>(GdO<sub>1.5</sub>)<sub>0.2</sub> at 800 °C, which is approximately four times that of Y<sub>2</sub>O<sub>3</sub> doped ZrO<sub>2</sub>, at the same temperature. Among the trivalent cations, anomalous behavior has been reported for Y<sup>3+</sup>, Sm<sup>3+</sup>, Gd<sup>3+</sup>, and La<sup>3+</sup>, where as Sc<sup>3+</sup> doped ceria showed much smaller ionic conductivity compared to their counter parts. The dopant ionic radie and its effect on the host lattice structure are a major factor in providing mixed ionic and electronic conductivities which are desirable in some applications. In order to understand the precise role the dopant plays in modifying the properties of the oxide, the primary information that is required is the exact location of the dopant in the host lattice. However, in many systems this problem can not be resolved by conventional diffraction techniques. For example, the concentration of the dopant may be very low, the dopant may be indistinguishable from the host, the dopant may introduce complex disorders into the lattice or the material may be amorphous. It is therefore import to use the experimental techniques like Extended Absorption Fine Structure Spectroscopy ( EXAFS ) for obtaining the information on the electronic structure as well as the local geometric structure. In this work, we used X-ray absorption near edge spectroscopy ( XANES ) which is a sensitive probe for investigating the electronic properties e.g. the valency, the symmetry of the unoccupied electronic states, and the effective charge of a chosen atom within a molecule or in a solid but also for the coordination geometry of the excited atom. In this paper, we present XANES measurements of ceria doped with 10 mole % of the elements of the entire lanthanide series. Also, we have attempted to correlate our new results with the data obtained from ionic conductivity measurements shown in Figure 1 [ G.B. Balazs et al, 185<sup>th</sup> The ECS meeting, San Fransisco, 1994 ].

The objective of this present study is to verify the local structure and short range order around a defect or dopant in order to explain the variations in conductivities. The rare earth doped ceria samples were prepared at Lawrence Livermore National Laboratory (LLNL). The cations of different ionic radie (over sized and under sized) than that of Ce<sup>4+</sup> were chosen for XANES study

and compared with the ac impedance measurements. XANES measurements have been performed at the DCM beamline of the storage ring of the Center for Advanced Microstructure and Devices (CAMD) in Baton Rouge. For all the measurements the ring was operated at an electron energy of 1.3 GeV with an average current of 100 mA. Synchrotron radiation was monochromatized by a modified Lemmonier type double crystal X-ray monochromator equipped with Ge (220) crystals. The monochromator flux was about  $10^{10}$  photons per sec. The spectra were obtained in transmission mode with ionization chambers measuring the incident beam intensity before and the transmitted beam intensity after the sample cell. The ionization chambers were filled with air with a pressure optimized for the corresponding energy range. We have measured the Ce- L<sub>111</sub> edge and the L<sub>111</sub> edge XANES of the trivalent rare earth dopants (lanthanide series) in ceria and compared with the data obtained from non trivalent impurities. As reference spectra the corresponding oxides of the dopants have been included in our investigation. The structural parameters for the solid solutions obtained from the best fit were then compared with various defect models and the structures of the next nearest neighbours (cation-cation pairs) are analyzed. Figure 2 show the typical XANES spectra of ceria doped with Nd. Figure 3 show the L<sub>111</sub> XANES spectra of trivalent dopant Ho and is compared with that of Ho<sub>2</sub>O<sub>3</sub>. Figure 4 show the L<sub>111</sub> edge of Ce doped with La and Pr. For the Pr doped sample, the low energy peak is significantly more intense than the high energy peak which is attributed to Ce<sup>3+</sup>



**B.Rambabu** acknowledge the US.DOE Office of Energy Research and the RCS program for HBCUs at LLNL for supporting this work through a grant GE FG 05-95ER45549 and a LLNL subcontract

## WHAT CAN CALORIMETRY CONTRIBUTE TO THE UNDERSTANDING OF VITREOUS AND COMPOSITE SOLID ELECTROLYTES ?

J. Rogez\*, O. Schäf\*\*, P. Knauth\*\*\*

\*Centre de Thermodynamique et de Microcalorimétrie du CNRS, F-13331 Marseille Cedex 3,

\*\*Forschungszentrum Sensorik Greifswald, D-17489 Greifswald, \*\*\*Laboratoire EDIFIS-

CNRS, Faculté des Sciences de Marseille-St Jérôme, F-13397 Marseille Cedex 20.

In recent years, significant progress has been achieved in the preparation of solid electrolytes for applications in the domains of energy storage and conversion and intelligent sensor technology. In the future, glassy and composite solid ionic conductors may not only offer enhanced ionic conductivity, but also superior mechanical and thermal properties, long-time stability and low cost.

Fundamentally, a major centre of interest is related to the mechanisms of ionic conduction in disordered (glassy) or multiphase (composite) materials. In this respect, a study of the energetics is worthwhile with the objective to correlate the ionic conductivity with the particular energetic interactions in the material. In this contribution, we present calorimetric investigations on  $\text{Li}^+$  ion conducting glasses ( $\text{Li}_2\text{O}-\text{Al}_2\text{O}_3-\text{SiO}_2$  system) and two-phase mixtures of two  $\text{Ag}^+$  ion conductors with very limited solid solubility ( $\text{AgCl}-\text{AgI}$  system).

Solution calorimetry was performed in a rotating calorimeter built in the laboratory. Samples of about 50 mg were dissolved in 50 ml solvent :  $\text{HF}/\text{HNO}_3$  mixtures for the  $\text{Li}_2\text{O}-\text{Al}_2\text{O}_3-\text{SiO}_2$  system and a mixture of  $\text{Na}_2\text{S}_2\text{O}_3$  solution with ammonia for the silver halides. The preparation of phase-pure  $\text{Li}^+$  ion-conducting glassy materials was described elsewhere [1]. For calorimetric experiments, the glasses were first ground to powder and the absence of crystalline phases verified by X-ray diffraction. To investigate the  $\text{AgCl}-\text{AgI}$  system, pure silver halide powders were compressed to pellets, which were annealed during 24 h at  $200^\circ\text{C}$  to eliminate transient defects and stresses due to compression. Composite pellets were prepared in the same way, but  $\text{AgI}$  and  $\text{AgCl}$  powders were first thoroughly mixed during 8 h. The structure was verified by X-ray diffraction ; mean grain sizes were determined from the line broadening using Scherrer's relation and confronted with SEM micrographs.

Calorimetric measurements were successful to determine the enthalpies of crystallisation of  $\text{Li}^+$  ion conducting glasses. Furthermore, calorimetry can be used to determine the amount of crystalline phases in partially crystallised glassy samples.

In the  $\text{AgCl}-\text{AgI}$  system, a concentration dependence of the enthalpies of dissolution was observed ; therefore, the enthalpy was extrapolated to infinite dilution for the calculations. The small enthalpy of formation of the composites may be correlated with the interface area.

[1] O. Schäf, Ph. D. Thesis, Free University of Berlin, 1995.

## TWO-DIMENSIONAL SILVER FAST-ION CONDUCTION IN (LaO)AgS

D. Wilmer<sup>1</sup>, J.D. Jorgensen<sup>2</sup> and B.J. Wuensch<sup>3</sup><sup>1</sup>University of Münster, Institute of Physical Chemistry, Schloßplatz 4/7, D-48149 Münster<sup>2</sup>IPNS, Argonne National Laboratory, Argonne, IL<sup>3</sup>Department of Materials Science and Engineering, MIT, Cambridge, MA

In 1980, Palazzi et al. [1] reported a new crystalline silver fast-ion conductor, (LaO)AgS, which had been obtained by solid state reaction of a mixture of La<sub>2</sub>O<sub>2</sub>S and Ag<sub>2</sub>S at 580 °C to 640 °C in the presence of a small amount of iodine. Conductivity measurements (ac impedance, dc using blocking electrodes) indicated that the conductivity is mainly ionic, with an activation energy of  $(0.195 \pm 0.05)$  eV. The structure was solved by the same group [2]: the tetragonal cell (S.G. P4/nmm, with  $a = 4.050$  Å and  $c = 9.039$  Å) contains two formula units.

The structure of (LaO)AgS, shown in Fig. 1, consists of eight-coordinated La ions (position  $2c \frac{1}{4} \frac{1}{4} z$ , with  $z = 0.1356$ ) between a sheet of oxygen ions ( $2a \frac{3}{4} \frac{1}{4} 0$ ) and a sheet of sulfur ions ( $2c \frac{1}{4} \frac{1}{4} z$ , with  $z = 0.6929$ ) linked to form a layer of composition LaO<sub>2</sub>S. The silver ions ( $2b \frac{3}{4} \frac{1}{4} \frac{1}{2}$ ) are situated in tetrahedral coordination between a pair of sulfur layers. The AgS<sub>4</sub> tetrahedra share four of their six edges to form a second type of polyhedral layer of composition AgS. Each sheet of S ions is common to a LaO<sub>2</sub>S layer and an AgS layer; the O layer is shared between a pair of LaO<sub>2</sub>S layers. The sequence of layers along  $c$  is thus O-La-S-Ag-S-La-O. The layered nature of the (LaO)AgS structure, with edge-sharing tetrahedral layers separated by two intervening LaO<sub>2</sub>S slabs, suggests a two-dimensional enhancement of silver mobility within (001).

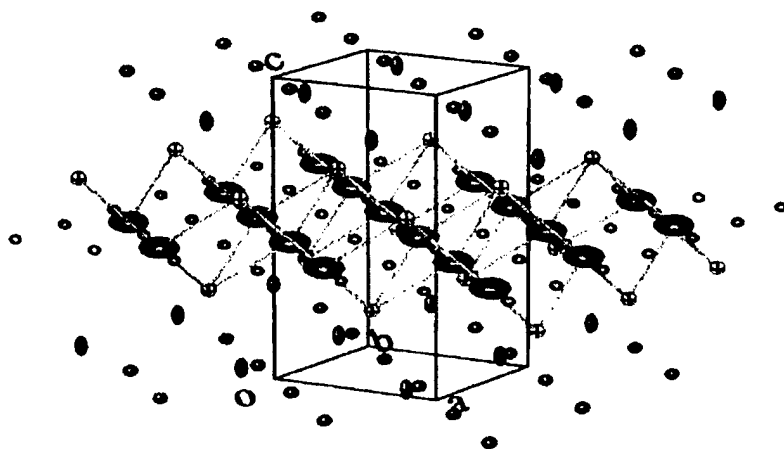


Figure 1: Structure of (LaO)AgS. Large ellipsoids: silver ions. Bonds visualize AgS<sub>4</sub> tetrahedra. Thermal ellipsoid sizes are taken from 673 K data. Tiny spheres at  $z = \frac{1}{2}$  depict interstitial positions 4e.

A few years later, Ishikawa et al. [3] re-examined the electrical properties of (LaO)AgS. They reported difficulties in obtaining pure samples when using Palazzi's method and used a sulfur atmosphere instead of iodine. The total conductivities they determined showed an activation energy of 0.30 eV and, at about 100 °C, were more than two orders of magnitude lower than the values previously reported [1]. In addition, both their ionic and total conductivities exhibited a stepwise increase at about 180 °C which was not explained. (LaO)AgS was classified as an *n*-type mixed conductor.

In 1995, the same group published new results for (LaO)AgS [4], now giving an activation energy for the ionic conductivity of 0.107 eV. Although the data in their Arrhenius-type plots of

ionic and total conductivities are very close together, their results from two different measurements of the silver transference number yield values of 0.066 and 0.48, respectively. Moreover, an excess of  $\text{La}_2\text{O}_2\text{S}$  had to be added in order to suppress the stepwise increase of conductivities at around 180 °C.

The main goal of the present study was to examine the structural properties which determine the silver ion transport mechanism in  $(\text{LaO})\text{AgS}$ . We, therefore, have performed neutron time-of-flight diffraction experiments on  $(\text{LaO})\text{AgS}$  at five different temperatures in order to use changes in site occupancies and thermal vibration amplitudes to gain information on preferred conduction paths and their dimensionality. Diffraction data were collected at five temperatures between 300 K and 773 K with the Special Environment Powder Diffractometer (SEPD) at the Intense Pulsed Neutron Source (Argonne National Laboratory).

The refined values of the anisotropic temperature factor coefficients,  $u_{ij}$ , are considerably larger for silver than for all other ions in the system. In addition,  $u_{11}(\text{Ag}) > u_{33}(\text{Ag})$ , supporting the view that silver ions reside in a potential that is shallower in a direction normal to  $c$  and that they move preferentially in the  $a$ - $b$ -plane.

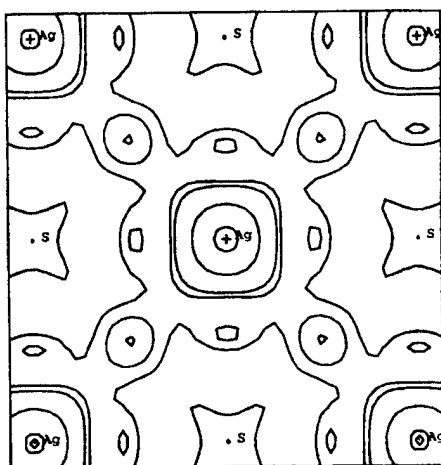


Figure 2: Fourier section ( $F_{obs}$ ) of  $(\text{LaO})\text{AgS}$  at 673 K for  $z = \frac{1}{2}$ . The silver ions at the center of the diagram is located at position  $\frac{3}{4}\frac{1}{4}\frac{1}{2}$ . Contour values are 0.10, 0.20, 0.30, 1.0, 2.0.

Fourier sections at  $z = \frac{1}{2}$  exhibit silver ion density not only at the regular lattice sites, but also at interstitial positions  $4e$  ( $\frac{1}{2}\frac{1}{2}\frac{1}{2}$ ), see Fig. 2. At higher temperatures, there is continuous silver density from a regular  $2b$  via a  $4e$  to a neighboring  $2b$  site. Obviously, the mobile silver ions move preferentially along  $\langle 110 \rangle$  via interstitial  $4e$  sites, located at the mid point of the shared edge between neighboring  $\text{AgS}_4$  tetrahedra. Silver ion conduction in  $(\text{LaO})\text{AgS}$  is performed in two dimensions.

Since the published conductivity data [1, 3, 4] are not consistent with each other, we also include a preliminary report on conductivity measurements that we have performed.

## REFERENCES

1. M. Palazzi, C. Carcaly, and J. Flahaut, *J. Solid State Chem.* **35**, 150 (1980).
2. M. Palazzi and S. Jaulmes, *Acta Cryst.* **B37**, 1337 (1981).
3. K. Ishikawa et al., *J. Electrochem. Soc.* **138**, 1166 (1991).
4. K. Ishikawa, A. Kumagai, O. Kohichi, S. Yamada, and Y. Suzuki, *Solid State Ionics* **78**, 41 (1995).



# BASIC PRINCIPLES AND GROWTH MECHANISMS OF POLARIZED ELECTROCHEMICAL VAPOR DEPOSITION

Eric Z. Tang\* and Thomas H. Etsell\*\*

\*Global Thermoelectric Inc., Calgary, AB, Canada

\*\*Department of Chemical and Materials Engineering, University of Alberta,  
Edmonton, AB, Canada

The ionic and electronic transport within solids suggested by Wagner's electrochemical tarnishing research in the 1930's has two sets of implications [1]. First of all, since material transport through solids involves both ionic and electronic current flow, conversion between electrical and chemical energy in a solid electrochemical cell is possible. In the past 60 years, a variety of energy conversion applications based on the energy transformation capability of solids has been identified. Many solid state ionic devices, such as sensors, fuel cells and batteries, have been developed in order to serve ever-growing energy and environmental demands [2]. Secondly, ionic and electronic transport within solids permits material transport through solids in a controlled manner. However, this implication has not been applied as extensively as the first one [3].

The present availability of numerous types of solid electrolytes permits transport control of various mobile ionic species through them in solid electrochemical cells under well-controlled conditions, and permits electrochemical reactions to be carried out with the surrounding vapor phase to form products of interest. This interfacing of modern vapor deposition technology and solid state ionic technology has led to the recent development of polarized electrochemical vapor deposition (PEVD) in our laboratory [4]. Generally speaking, PEVD is a modified form of chemical vapor deposition (CVD). A comparison between PEVD and conventional CVD is shown schematically in Figure 1 for a product (D) formed from reactants (A) and (B). In a CVD process, both reactants (A) and (B) are supplied through a vapor phase at the same side of a solid substrate (E). They react chemically at the surface of the solid substrate (E), aided by some type of catalytic effect, to form a desired product (D). In a PEVD process, one reactant (A) is transported from one side (source) of a solid substrate (E) to the other side (sink) under well-controlled thermodynamic and kinetic conditions. At the sink side, reaction with (B) occurs to form (D). Further growth of (D) into a continuous thin film with the desired thickness in a PEVD process also relies on (A) transported in the solid state but now through (D) to react with (B).

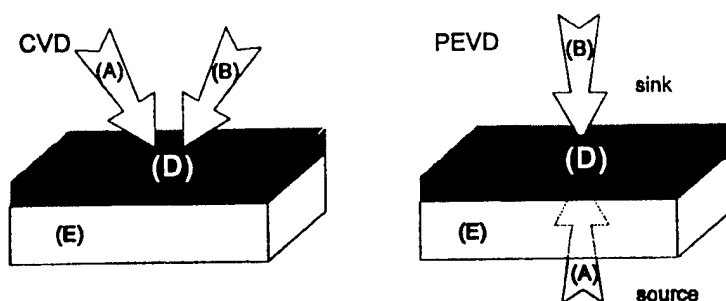


Figure 1. Comparison of PEVD and CVD processes. (A) and (B) are reactants; (D) is a deposit; (E) is a solid substrate.

The reason that reactant (A) can be transported through the solid substrate (E) and the solid deposited phase (D) is because both (E) and (D) are solid state ionic materials [5], in which the ionic state of reactant (A) is mobile. Thus, reactant (A) will be transported as a combination of

corresponding ionic and electronic carriers under the mixed influence of chemical potential gradients and electric fields in the solids. The characteristic feature of PEVD is that deposit (D) growth is driven by the presence of a chemical potential gradient of reactant (A) across deposit (D). Deposit (D) growth follows Wagner's electrochemical tarnishing theory and is parabolic in nature. Unlike the initial applications of Wagner's theory in corrosion, solid-state transport of the reactant in PEVD is under well-controlled thermodynamic and kinetic conditions, mainly through dc electric potential control via a solid electrochemical cell. In the current study, it was found that the electrochemical potential of the mobile ionic species at the interface between substrate and deposit is floating in a PEVD system. Thus, the driving force for mass and charge transport in a PEVD system can be effectively provided via a dc source through an external electrical circuit. Furthermore, the solid electrochemical cell in a PEVD system effectively separates the transport paths of ionic and electronic charged carriers from the source to the sink side. Accordingly, a PEVD process can be monitored through the electronic current in the external circuit. In an ideal condition, a linear relation between the applied dc potential and deposition rate can be expected. However, due to overpotential, the linear relationship is altered.

Since the reaction of the solid-state transported reactant (A) and the vapor phase reactant (B) to form a deposit (D) is electrochemical in nature in PEVD, the product growth in PEVD follows its unique electrocrystallization behavior [6]. Consequently, PEVD holds promise for a wide range of potential applications. Investigations have shown that PEVD is the most suitable technique to improve solid electrode/electrolyte contact and, consequently, the performance of solid state ionic devices, such as ceramic sensors [7] and solid oxide fuel cells [8]. In ceramic sensor applications, PEVD has been applied to deposit an auxiliary phase, for instance,  $\text{Na}_2\text{CO}_3$ , at the working electrode of a type III potentiometric  $\text{CO}_2$  sensor. During the PEVD process,  $\text{Na}^+$  ions have been transported through a  $\text{Na}^+$ - $\beta$ -alumina substrate to react with vapor phase reactants,  $\text{O}_2$  and  $\text{CO}_2$ , to deposit the auxiliary phase with an ideal microstructure at the cathode. In solid oxide fuel cell applications, a composite anode with the ideal microstructure was formed by driving  $\text{O}^{2-}$  ions through a Y(Yb)SZ substrate to react with  $\text{ZrCl}_4$  and  $\text{YCl}_3$  at the anode. A thin layer of YSZ was deposited upon a pure metallic anode. Furthermore, the "active" use of material transport through the solid by PEVD offers interesting opportunities not only for forming deposition products but also for studying the physical properties of the products under well-defined thermodynamic and kinetic conditions [9].

It has been more than 60 years since Wagner's electrochemical tarnishing theory was developed. Finally, the two parallel suggestions of material transport and energy transformation in the theory overlap, and the newly developed PEVD technique will make solid state ionic devices to better serve today's ever-growing energy and environmental demands. In the hope of promoting future research in PEVD and extending its application to other potential areas, the basic principles and product growth mechanisms of PEVD are discussed in the current paper.

1. Wagner, C., *Z. Phys. Chem. B* 21 (1933) 25.
2. Tillement, O, *Solid State Ionics*, 68 (1994) 9.
3. Choudhury, N.S. and Patterson, J.W., *J. Electrochem. Soc.*, 118 (1971) 1389.
4. Tang, E.Z. and Etsell, T.H., *Solid State Ionics*, 91 (1996) 213.
5. Hladik, J. in: *Physics of Electrolytes*, ed. J. Hladik, (Academic Press, London, 1972) 35.
6. Tang, E.Z., Etsell, T.H. and Ivey, D.G., in: *Electrochemically Deposited Thin Films III, The Electrochemical Society Proceeding Series*, Pennington, NJ. PV96-19 (1996) 71.
7. Tang, E.Z., Etsell, T.H. and Ivey, D.G., *Sensors and Actuators B*, 45 (1997) 131.
8. Tang, E.Z., Etsell, T.H. and Ivey, D.G., *J. Am. Ceram. Soc.*, submitted for publication (1998).
9. Tang, E.Z., Ivey, D.G. and Etsell, T.H., *Micron*, 29 (1998) 251.

**Estimation of the charge carrier concentration in NaCl single crystals  
from analysis of the frequency dependent conductivity**

E.F.Hairetdinov, N.F.Uvarov

*Institute of Solid State Chemistry, Siberian Branch of Russian Academy of Science  
Kutateladze 18, Novosibirsk-128, 630128, Russia*

Up to date it is recognized that analysis of the frequency dependences of conductivity allows to extract information on hopping rate and concentration of free charge carriers in superionic crystals and glasses. In particular, the values of charge carrier concentration in Na<sub>2</sub>S-B<sub>2</sub>S<sub>3</sub> glasses [1] or some fluorite-type solid solutions [2] obtained by fitting of Almond-West equation [3] to the experimental ac-conductivity data agrees well with those found using independent chemical, structural or spectroscopic methods.

Other method for determination of charge carrier parameters is classical Schottky - Wagner technique [4] based on the analysis of the temperature dependences of dc-conductivities for pure crystal and the crystal doped with known concentration of heterovalent dopant. As a rule, the use of this technique is limited by low concentrations of the additive. Usually concentration of the defects is, indeed, due to low solubility of the dopant. In some systems, like fluorite-type salts, the solubility range is wide, however, in this case, at high concentration of the dopant strong defect-defect interaction takes place leading to formation of associates, clusters and Schottky-Wagner concept does not work. Earlier [2] we have undertaken a first attempt to estimate charge carriers concentration in single crystals (1-x)SrF<sub>2</sub>-xLaF<sub>3</sub> over a wide range of the LaF<sub>3</sub> concentrations ( 0.001 < x < 0.4). It was shown that Almond West approach gives reasonable estimates for hopping rates and defects concentration in the limit of low concentrations of the dopant.

In this work ac-conductivity was analyzed of NaCl single crystals doped low concentrations (0.01 - 0.1 mol % ) of bivalent additives (Co<sup>2+</sup>, Ca<sup>2+</sup>). The ac-conductivity measurements were carried out on the crystals of different geometry with various electrodes. For the analysis of the ac-conductivity a theoretical expressions have been used which took into account contributions of dielectric relaxation of both the dipoles (vacancy - impurity cation pair associates) and charge carriers (cation vacancies). Influence of electrode effects was also taken into consideration. Results of the analysis show that high-frequency ac-conductivity of doped NaCl is completely due to the dipole relaxation. Parameters of the dipole reorientation agrees with the data reported earlier [5]. As no appreciable contribution of the charge carrier relaxation was detected, high limit of the concentration of unbounded vacancies was estimated as  $x < 10^{-7} - 10^{-4}$  at temperature range 120 - 220°C. It agrees well with data reported in literature [4]. Therefore, Almond West approach seems to be applicable not only to systems with high concentration of charge carriers, but also to classical ionic salts with Schottky disorder.

#### References

- [1] E.F.Hairetdinov, N.F.Uvarov, H.K.Patel, S.W.Martin, Phys. Rev. **B50** 13259 (1994).
- [2] N.F.Uvarov, E.F.Hairetdinov, Solid State Ionics **36** 29 (1989).
- [3] D.P.Almond, A.R.West, Solid State Ionics **9&10** 277 (1983).
- [4] A.Lidiard, Handbuch der Physik **20**, Springer Verlag, Berlin (1957) p.246.
- [5] J.A.Chapman, E.Lilley, J. Phys. **34** C9-455 (1973).

## IN SITU INVESTIGATIONS ON THE OXIDATION OF INTERMETALLIC COMPOUNDS IN THE SYSTEM COBALT-GALLIUM

Ulrich Koops, Manfred Martin  
Institute of Physical Chemistry  
Darmstadt University of Technology  
Petersenstrasse 20, 64287 Darmstadt, Germany

In the metallic system of cobalt and gallium two intermetallic compounds are formed. The Pm3m-structured CoGa possesses a large range of stability while the P-4n2-structured CoGa<sub>3</sub> possesses only a very small range of stability [1]. During the oxidation of these intermetallic compounds the main product observed is monoclinic Galliumoxide Ga<sub>2</sub>O<sub>3</sub> in both cases. Only traces of the cobalt-gallium-spinel CoGa<sub>2</sub>O<sub>4</sub> are formed. Fig. 1 shows a x-ray-powderdiffraction pattern of the in situ oxidation of CoGa<sub>3</sub> in air at 800°C for product identification. Due to the formation of galliumoxide one observes the decomposition of the CoGa<sub>3</sub>-Phase to form the adjacent CoGa-phase. The same happens during the oxidation of CoGa in air at 800°C, where the decomposition leads to the adjacent cubic Co-Phase containing 16.5at% gallium.

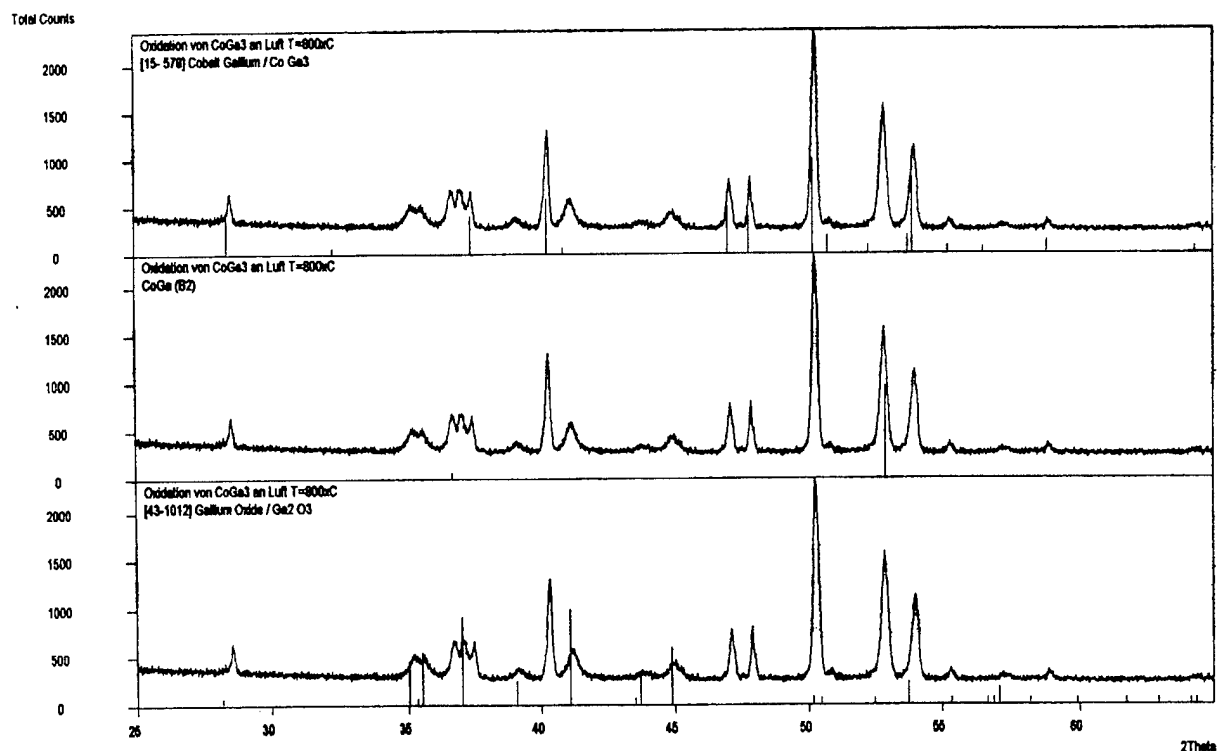
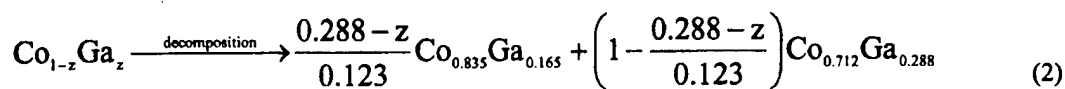
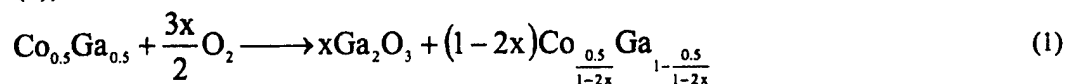


Figure 1: Oxidation of CoGa<sub>3</sub> in air at 800°C, identification of the products

To determine the pseudokinetics of the reaction in situ time resolved XRD is used. Fig. 2 and 3 show the kinetic evolution of the observed phases for the oxidation of CoGa and CoGa<sub>3</sub>. The induction period before decomposition occurs is much longer for CoGa than for CoGa<sub>3</sub>. The oxidation and decomposition of CoGa are describable with the following reaction scheme (eq. (1) and (2)):



where  $z < 0.288$  (according to the phasediagram)

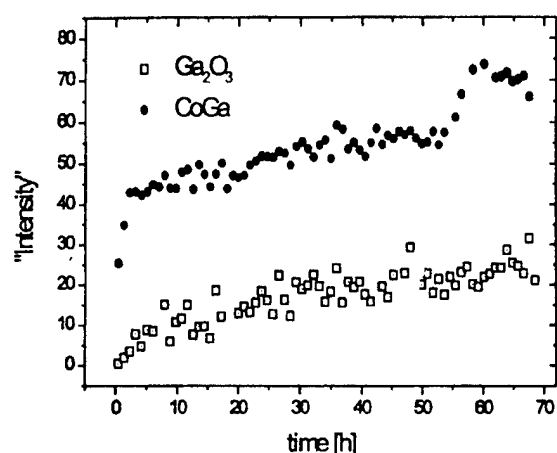


Figure 2: Pseudokinetics of the oxidation of CoGa<sub>3</sub> in air at 800°C

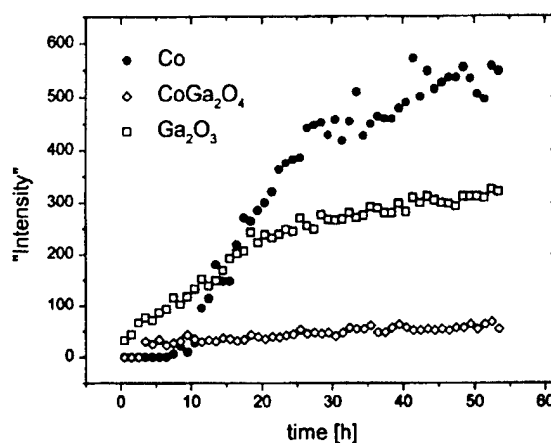


Figure 3: Pseudokinetics of the oxidation of CoGa in air at 800°C

[1] P. Feschotte, P. Eggimann, J. less common metals **63**, 15 (1974)

# PHASE BEHAVIOUR OF RbH<sub>2</sub>AsO<sub>4</sub> ABOVE ROOM TEMPERATURE

E. Torijano, R.A. Vargas, J.E. Diosa, R. Cataño\* and B.-E. Mellander\*\*

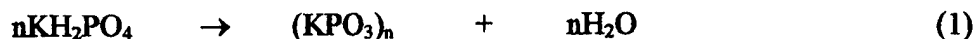
Departamento de Física, Universidad del Valle, AA 25360, Cali-Colombia

\*Departamento de Química, Universidad del Valle, AA 25360, Cali-Colombia.

\*\*Department of Physics, Chalmers University of Technology, S-412 96 Gothenburg-Sweden.

Several phase transitions in crystals of the KH<sub>2</sub>PO<sub>4</sub> (KDP) type well above room temperature, known as a high-temperature phase transitions (HTPT), have been reported around a characteristic temperature T<sub>p</sub>.

Although there is a large number of publications about it, there are significant disparities between the results obtained [1]. The reported values of T<sub>p</sub> for various KDP salts vary according to experimental probes and experimental conditions. The old paper of Kiehl and Wallace [2] suggests that a chemical reaction takes place in the sample:



However, there are many studies in the field of inorganic and structural chemistry which claim that the MH<sub>2</sub>RO<sub>4</sub> (R = P, As) compounds eliminate water upon heating to form the corresponding metaphosphates and metaarsenates [3,4]. It has also been reported [5] that when MH<sub>2</sub>RO<sub>4</sub> is heated, it tends to lose water according to the reaction:



where n is the number of molecules participating in the thermal decomposition. The letters s or v denote solid or vapor state respectively.

NMR studies suggest that only two compounds of this family, RbH<sub>2</sub>PO<sub>4</sub> and KD<sub>2</sub>PO<sub>4</sub>, undergo non-destructive high temperature transitions from tetragonal to a monoclinic crystal form [6].

In special, for the RbH<sub>2</sub>AsO<sub>4</sub> (RDA) the experimental studies on the high temperature behaviour are scarce. NMR studies revealed that RDA begins to decompose at 129 °C [6]. However, Zhigarnovskii et al [7] reported polymorphous transformations at 170 °C with formations of a phase apparently monoclinic, not manifested on DTA curves but only detected by high-temperature X-ray diffraction analysis.

The thermal decomposition was studied by thermogravimetry (TG) and evolved gas analysis (EGA) and it was detected stepwise weight loss at 199°C as an indication of various polymeric intermediates products [3].

Here we present the results of study of phase behaviour of RDA above room temperature by using differential scanning calorimetry (DSC), thermogravimetric (TG) and high-temperature X-rays diffraction analysis in order to obtain more information on high temperature phase behaviour and to compare with that observed for the KDP compounds.

In the Fig. 1 the DSC thermogram for a fresh sample of RDA shows several endothermic peaks at 70, 120, 155 and 245 °C on the first heating run, but not thermal anomalies are observed on the subsequent cooling run.

The thermogravimetric curve in Fig. 2 shows stepwise weight loss at around the same temperatures as the DSC peaks and our X-ray diffraction results reveal changes in the crystalline phases above and below these temperatures.

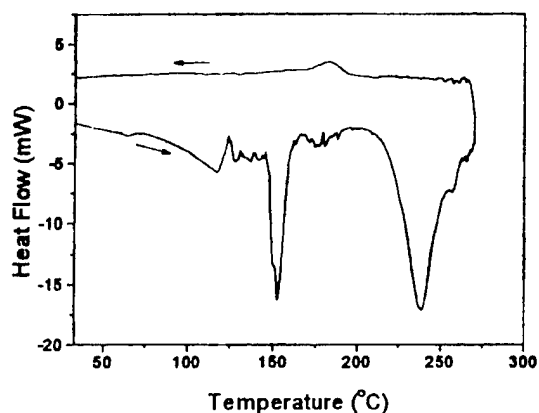


Fig. 1. DSC heating and cooling trace of fresh RDA under a dry nitrogen flux of 50 ml/min and temperature rate of 5 °C/min.

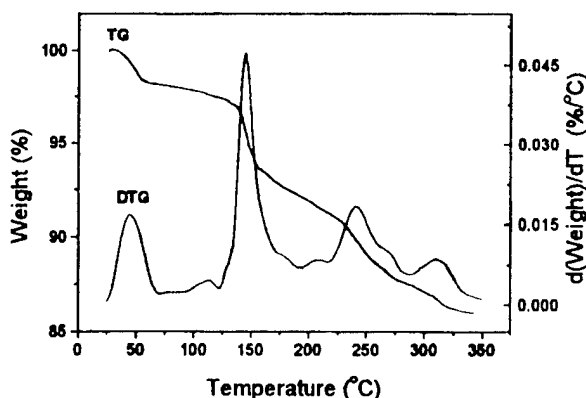


Fig. 2. TG and DTG curves of fresh RDA showing the water weight loss when the sample is first heated at 5 °C/min under a dry nitrogen atmosphere.

Our results confirm that RDA behave like KDP-type compounds, that is, polymerization occurs when the water is depleted from the salt according to Eq. 2. However in RDA, four regions of rapid weight loss occur around 70, 120, 155 and 245 °C, respectively, indicating the possibility of a sequence of partial polymerizations when RDA is heated.

The authors gratefully acknowledge the support of the Colombian Research Agency, COLCIENCIAS, and the International Program in the Physical Science, IPPS, of Uppsala University, Sweden.

#### References

- [1] K.S. Lee, J. Phys. Chem. Solids 57, N° 3, 333 (1996).
- [2] S.J. Kiehl and Wallace, J. Amer. Chem. Soc. 49, 375 (1927).
- [3] P.K. Gallagher, Thermochimica Acta 14, 131 (1976).
- [4] B.M. Nirsha, E.N. Gudinitza, A.A. Fakeev, V.A. Efremov, B.V. Zhadanov and V.A. Olikova, Zh. Neorg. Khim. 27, N° 6, 1366 (1982).
- [5] E. Thilo, "Condensed Phosphates and Arsenates", in *Advances in Inorganic Chemistry and Radiochemistry*, Vol. 4, edited by H.J. Emeleus and A.G. Sharpe, (Academic Press, New York, 1962), pp. 1-75.
- [6] J.Y. Nicholson and J.F. Soest, J. of Chem.-Phys. 60, N° 2, 715 (1974).
- [7] B.M. Zhigarnovskii et al, Inorganics Materials, 20, N° 7, 1074 (1984).

HIGH-TEMPERATURE PHASE TRANSITIONS IN  $K_{1-x}(NH_4)_xH_2PO_4$ 

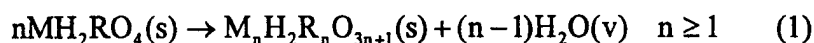
J.F. Jurado\*, A. García y R.A. Vargas.

\*Departamento de Física Universidad Autónoma de Occidente, A.A 2790, Cali.

Departamento de Física Universidad del Valle, A.A 25360, Cali.

The binary salts families,  $MHRO_4$  and  $MH_2R'O_4$  ( $M = K, Rb, Cs$  and/or  $NH_4$ ;  $R = S, Se$ ;  $R' = P, As$ ;  $H =$  Hydrogen or Deuterium) have received much attention on the way to understand their interesting properties and to develop new materials.[1,2]. For example, ammonium dihydrogen phosphate,  $NH_4M_2PO_4$  (ADP) was found to be antiferroelectric under  $T_N=148$  K while, potassium dihydrogen phosphate,  $KH_2P_4O$  (KDP) was found to be ferroelectric under  $T_c=123$  K. Proton-glass phase are found in mixtures of ferroelectric and antiferroelectric phase for intermediate concentrations and low temperatures[3,4]. The  $Rb_{1-x}(NH_4)_xH_2PO_4$  (RADP)<sub>x</sub> is the system more studied; a similar system but less studied is  $K_{1-x}(NH_4)_xH_2PO_4$  (KADP)<sub>x</sub>.

On the other hand, the KDP-type compounds for different heating cycles show a high temperature phase transitions (HTPT) at a characteristic temperature  $T_p$ . There are, however, large discrepancies in the literature concerning the nature of this transition, as well as regarding the number of additional transitions at higher temperatures. For example, a structural phase transition from tetragonal to monoclinic symmetry has been proposed for KDP at 180 °C [2]. Other researchers have proposed that when the KDP-type compounds are heated above room temperature, loss of water will take place. The thermal dehydration can be described by [2]



where  $n$  is the number of molecules participating in the thermal decomposition,  $s$  and  $v$  denote solid or vapor state respectively.

According to Lee[2], the term HTPT at  $T_p$  should be replaced by the term *onset of partial polymerization at reaction sites on the surface*.

Recently, Boukhris et al.[7], have shown for X-ray diffraction studies on (KADP)<sub>x</sub> ( $0.0 < x < 1.0$ ) that the thermal vibration of the phosphate group as well as the cell parameters, vary considerably with composition  $x$ . These observations below room temperature may be due to a static disorder because of the large difference between cell parameters of KDP and ADP, or to fluctuations of their concentration throughout the system (KADP)<sub>x</sub>.

At higher temperature we, then, expect a higher degrade of disorder and other phase transitions related to it.

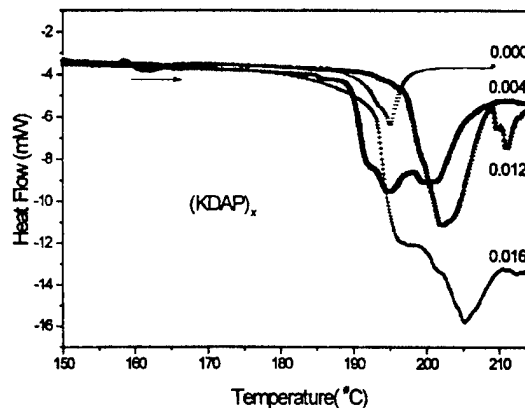


Fig.1 DSC termogram of freshly grown mixed crystal of KDP with ADP impurities up to a concentration of  $x < 0.02$ , under a dry nitrogen flux of 80 ml/min



In order to investigate if partial polymerization could be the cause of the HTPT, reported for different KDP-type compounds, we have used thermogravimetric analysis and differential scanning calorimetry (DSC) to study these transition in mixed crystal of KDP with ADP impurities up to a concentration  $x < 0.02$  and grown by slow evaporation of aqueous KDP solution with ADP impurities.

The thermal analysis of polycrystalline fresh sample, heated at 5 °C/min in 80 ml/min of gas nitrogen gas, are shown in Fig.1. The DSC curve for KDP ( $x = 0$ ) shows an endothermic peak at  $T_p \approx 180$  °C but above approximately 220 °C, the curve bends downwards indicating thermal decomposition of the sample. However, DSC curves for sample with ADP impurities show at a temperature  $T_p \geq 180$  °C (few degrees above 180 °C, depending on  $x$ ), a downward bend that include an endothermic peak indicating decomposition of the sample immediately after the transition at  $T_p$ .

Our thermogravimetric measurements have shown for  $(\text{KADP})_x$  for various concentration  $x$ , that there is a small weight loss at temperatures close to  $T_p$ . Fig.2 shows the TG curves of powdered  $(\text{KADP})_x$  samples showing the time dependence of the water weight loss for sample that were previously annealed at 120 °C for 30 min, the data were taken during the following temperature program: the sample is first heated from 120 °C at 5 °C/min and then arrested at 240 °C.

Our results, then show that a thermal dehydration takes place for  $T \geq T_p$ . Already at  $T_p$  a small weight loss occurs even for pure KDP, indicating the possibility of a partial polymerization on the surface of the KDP grains, however, when the impurities ADP are added to KDP, the thermal dehydration propagates faster toward the whole sample at lower temperatures than that for the  $x = 0$  sample.

## REFERENCES

- [1] Rapaport E., J. Chem., Phys. **53**, 311(1971).
- [2] K. Lee, J. Phys. Chem. Solids, **57**, 33(1996), and references there in.
- [3] Fukami T, Akahoshi S, Hukuda K and Yagi T., J. Phys. Soc. Japan **56**, 2223 (1987).
- [4] Sook-II K, Jong-Gul Y and Donghan L., Japanese J. of Applied Physics, **24**, 966(1985).
- [5] Kiehl S.J. and Wallace G. H., J. Amer. Chem. Soc. **49**, 375(1927).
- [6] Thilo E., "Condensed Phosphates and Arsenates", in Advances in Inorganic Chemistry and Radiochemistry, Vol. 4, edit. By H.J.E. and A.G. Sharpe, (Academ. Press. N.Y., 1966). pp. 1-75.
- [7] A. Boukhris, M. Souhassou, C. Lecomte, B. Wyncke, and A. Thalal, J. Phys.: Condens. Matter **10**, 1621(1998).

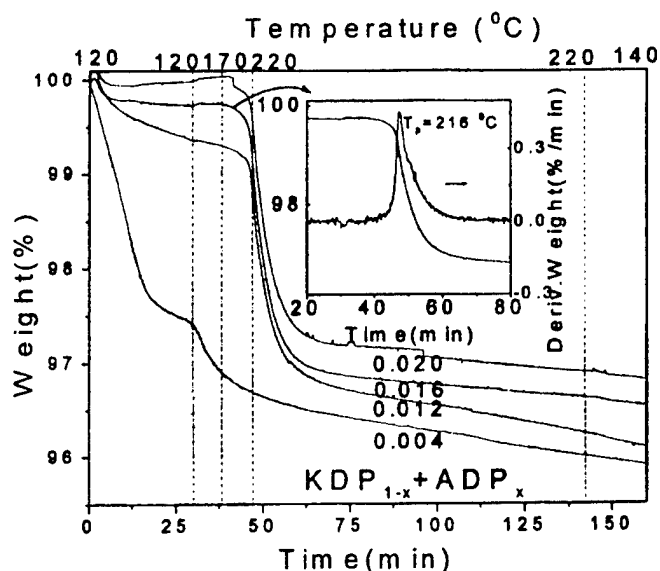


Fig.2 Thermogravimetric analysis (TGA) of a freshly grown mixed crystal of KDP with ADP impurities up to a concentration of  $x < 0.02$ , under a dry nitrogen flux of 10 ml/min.

## **A SIMPLE METHOD FOR DETERMINING SURFACE EXCHANGE AND BULK TRANSPORT KINETICS FOR OXYGEN-ION CONDUCTING MATERIALS UNDER REDUCING CONDITIONS**

M. Sahibzada\*, W. Morton, A. Hartley, D. Mantzavinos, I.S. Metcalfe

School of Chemical Engineering, University of Edinburgh,

King's Buildings, Edinburgh EH9 3JL, United Kingdom

\* tel: +44 131 6507254, fax: +44 131 6506551, email: m.sahibzada@ed.ac.uk

### **Extended abstract**

Oxygen conducting solid oxide materials find applications as the electrolyte/ electrodes in solid oxide fuel cells (SOFCs), catalysts for oxidation processes, component materials in solid state oxygen sensors, and membranes in ceramic oxygen generators (COGs). The performance of these materials is dependent upon the kinetics of oxygen take up from the gas phase, reflected in the surface exchange coefficient ( $k^*$ ), and the kinetics of oxygen-ion transport in the solid, reflected in the self-diffusion coefficient ( $D^*$ ). In the case of SOFC cathodes and solid oxide membranes for COGs, perovskite materials are being investigated [1,2]. The long term aim to reduce the operating temperature of SOFCs [3,4] requires the kinetic properties ( $k^*$  and  $D^*$ ) of these materials to be optimised.

Screening the array of perovskite materials by measurement of  $k^*$  and  $D^*$  is generally carried out by Isotope Exchange Depth Profiling – Secondary Ion Mass Spectrometry (IEDP-SIMS) [1,2]. In the present study we are developing a simple method for determining the surface and bulk kinetic parameters using powdered oxide materials and normal oxygen. The system makes use of zirconia electrochemical oxygen pumps to control and monitor oxygen release/uptake. **This allows the materials to be conditioned under gas phase atmospheres necessary to simulate the reduced oxide state which exists under cathodic bias. Hence we are able to measure the appropriate kinetics for these materials under working conditions.**

Experimental data is obtained as follows. Perovskite materials are pre-conditioned at temperatures between 600-900°C, and with oxygen pressures down to  $10^{-5}$  atm controlled by oxygen pumping through a solid electrolyte membrane. A small perturbation in the temperature or oxygen pressure is introduced. The uptake/release of oxygen is monitored by solid electrolyte coulometry.

The surface exchange and ionic transport of oxygen in the porous oxide cathode material is modelled here using the equivalent geometry of dense spheres. The diffusion of oxygen in the solid lattice can be described by Fick's 2<sup>nd</sup> law, here in spherical polar co-ordinates with purely radial diffusion. The surface exchange boundary condition is also given below.

$$\frac{\partial C}{\partial t} = \frac{D^*}{r} \frac{\partial^2}{\partial r^2}(rC)$$

$$D \frac{\partial C}{\partial r} = k^*(C_{eq} - C)$$

The kinetic coefficients  $k^*$  and  $D^*$  are obtained by fitting the experimental transients to the solution of the above equations using a non-linear parameter optimisation method. Data will be presented showing the effect of temperature and oxygen pressure on the kinetics of surface exchange and lattice oxygen diffusion for a range of doped  $\text{LaCoO}_3$  materials.

## References

- [1] HJM Bouwmeester, H Kruidhof, AJ Burggraaf, Solid State Ionics 72 (1994)
- [2] JA Kilner, Electrochem Soc Proc 94-12 (1994) 174
- [3] BCH Steele in: Brit Ceram Proc, Institute of Materials, London (1997)
- [4] M Sahibzada, BCH Steele, K Zheng, RA Rudkin, IS Metcalfe, Catal Today 38 (1997) 1

## MEASURING OXYGEN DIFFUSION AND OXYGEN SURFACE EXCHANGE BY CONDUCTIVITY RELAXATION.

J.A. Lane and J.A. Kilner

Centre for Ion Conducting Membranes, Dept. of Materials,  
Imperial College of Science, Technology and Medicine,  
London SW7 2BP, UK.

### Abstract

Measurements of oxygen diffusion and oxygen surface exchange have primarily been performed employing isotope exchange techniques with analysis of the exchanging gas phase [1] or secondary ion mass spectrometry (SIMS) analysis of the exchanged ceramic sample [2]. However, not everyone has access to these techniques and alternative methods must be employed.

For materials that are predominantly electronic conductors and possess a materials property that changes with oxygen partial pressure then a 'relaxation' technique may be used. Perhaps the simplest to implement is the conductivity relaxation technique [3, 4]. For many mixed conducting materials a change in the oxygen partial pressure will result in a corresponding change in the electrical conductivity of the material due to, primarily, a change in the concentration of charge carriers. If the ionic conductivity of a material is significantly less than its electronic conductivity then the time for this change to propagate throughout the material is almost exclusively controlled by the movement of ionic species. This change or 'relaxation' can be modelled (Figure 1) and oxygen diffusion coefficients and surface exchange coefficients can be extracted from the data.

This paper will discuss the measurement of oxygen transport in mixed-conducting ceramic oxides using the conductivity relaxation technique. Particular emphasis will be placed on the analysis of the 'relaxation' profile and the problems associated with determining oxygen diffusion coefficients and oxygen surface exchange coefficients simultaneously. Results obtained using the conductivity relaxation technique will be contrasted with diffusion and surface exchange coefficients obtained at equilibrium using the more conventional isotope exchange/SIMS technique.

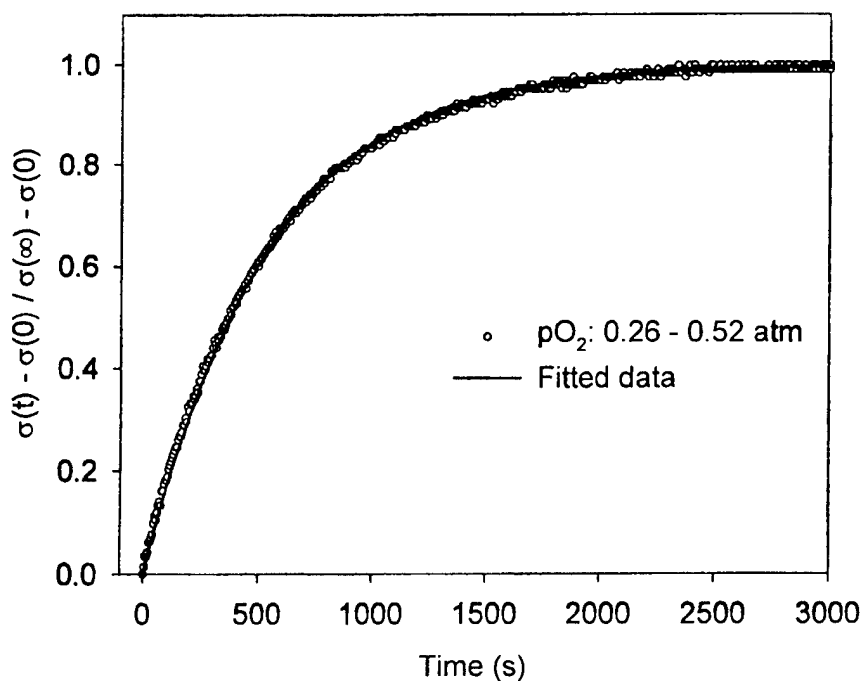


Figure 1. Normalised conductivity relaxation plot for  $\text{La}_{0.6}\text{Sr}_{0.4}\text{Co}_{0.2}\text{Fe}_{0.8}\text{O}_{3-\delta}$  at  $800^\circ\text{C}$  for oxidation from  $p\text{O}_2$ : 0.26 to 0.52 atm with the fitted data to the theoretical behaviour.

[1] Boukamp paper

[2] S.J. Benson, R.J. Chater and J.A. Kilner, in Proc. of the 3<sup>rd</sup> International Symposium on Ionic and Mixed Conducting Ceramics, the 192nd Meeting of The Electrochemical Society, Inc. and the 48th Annual Meeting of the International Society of Electrochemistry August 31<sup>st</sup> - September 5<sup>th</sup>, Paris, France, (1997).

[3] I. Yasuda and M. Hishinuma, J. Solid State Chem., **123**, (1996) 382-390.

[4] J.E. ten Elshof, M.H.R. Lankhorst and H.J.M. Bouwmeester, Solid State Ionics, **99**, (1997) 15-22.

## HIGH TEMPERATURE BIAXIAL FATIGUE OF THIN ZIRCONIA ELECTROLYTE MATERIAL IN OXIDISING AND REDUCING ATMOSPHERES.

C. Leach, N. Richet.

Manchester Materials Science Centre,  
University of Manchester and UMIST,  
Grosvenor Street, Manchester, M1 7HS.

Fatigue induced crack growth has been carried out on yttria doped zirconia using pre-cracked samples loaded under conditions of biaxial flexure. The experimental method adopted was based on a modification of the method used by Liu and Chen [1] for uniaxial fatigue and has also been used to study crack growth rates in bioceramics [2].

For these tests, an indentation was made in the sample using a micro-indenter using a suitable load to generate small cracks at the corners of the indentation. The test piece was then placed in a custom built silicon-nitride ring-on-ring biaxial test rig and subjected to fatigue cycle loading at room and elevated temperatures, using R values of 0.5 and 0.01. The stress intensity at the crack tips was calculated using the appropriate equation from reference [3] and other standard equations. The peak stress and the number of cycles were adjusted to provide an overall crack growth of around 200 $\mu$ m during each test. On completion of cycling the actual crack growth was established by measuring the mean growth of the four cracks extending from the indent. From these data graphs of crack growth rate versus  $\Delta K$  could be plotted.

Tests were carried out at room temperature and at 900°C in air and under reducing conditions using a 10% hydrogen in nitrogen mixture. Strength, fracture toughness and fatigue data corresponding to crack growth rates in the range  $10^{-8}$  to  $10^{-5}$  m/cycle were established. The magnitude of the Paris law exponent, n, was found to be lower than that generally calculated for zirconia under conditions of uniaxial flexure. Additional data will be presented showing the effect of R, temperature and atmosphere on the fatigue induced crack growth rate in yttria doped zirconia.

### References:

- [1] S.Liu, I.Chen. J.Amer.Ceram.Soc 71, 1206, (1991).
- [2] T.Hussain, A.Gholinia, C.Leach. Proc. 5<sup>th</sup> Euro. Ceramics, Key Engineering Materials 132-136, 577, (1997).
- [3] D.K.Shett, A.R.Rosenfield, P.McGuire, G.K.Bansal, W.H.Duckworth. Ceramic Bulletin 29, 1193, (1980).

# HIGH TEMPERATURE PHASE TRANSITION OF $\text{Ce}_{0.80}\text{Ln}_{0.20}\text{O}_{1.90-y}$ ( $\text{Ln} = \text{La}, \text{Gd}, \text{Y}$ ) STUDIED BY HEAT CAPACITY MEASUREMENTS

Satoshi Yamazaki, Toyo Ohashi, Yuji Arita and Tsuneo Matsui

Nagoya University, Graduate School of Eng., Dept. of Quantum Eng., Nagoya 464-8601, Japan

Ceria doped with lower-valent cations has been known to exhibit high oxygen ion conductivity due to the presence of oxygen vacancies introduced by doping from electroneutrality condition. The phase equilibrium for nonstoichiometric  $\text{Ce}_{0.818}\text{Gd}_{0.182}\text{O}_{1.909-y}$  has been determined from heat capacity measurements in the temperature range of 300-1250 K and compositional range,  $y$ , of 0–0.178 using a controlled adiabatic scanning calorimeter [1]. The presence of the phase transitions for the samples with the compositional range  $0.050 \leq y \leq 0.178$  originating from the disordering of the ordered defects with oxygen vacancies and  $\text{Ce}^{3+}$  has been revealed. The association of two Gd ions and one oxygen vacancy has been proposed in  $\text{Ce}_{1-x}\text{Gd}_x\text{O}_{2-x/2}$  [2].

In the present study, the heat capacity measurements of ( $\text{Ln} = \text{La}, \text{Gd}, \text{Y}$ ) were made in order to investigate the mechanism of the phase transition related to the association of dopant cations and oxygen vacancies.

The heat capacity measurements were made with an adiabatic scanning calorimeter in the temperature range 300-953 K. The stoichiometric samples were made by heating the pellets made of a mixture of  $\text{CeO}_2$  and  $\text{Ln}_2\text{O}_3$  powders at 1723 K in air for one week and then pulverising them. The nonstoichiometric samples were prepared by heating the stoichiometric samples at 1173 K in a flowing hydrogen gas for one day. The reduced samples were sealed in a silica tube with 150 torr-helium for heat capacity measurements.

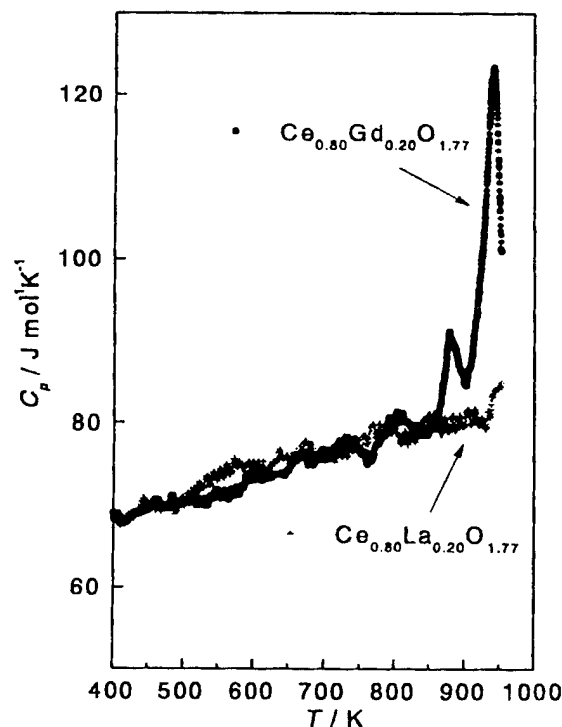


Fig. 1 Heat capacities of  $\text{Ce}_{0.80}\text{Ln}_{0.20}\text{O}_{1.90-y}$  ( $\text{Ln} = \text{La}, \text{Gd}$ ).

No anomaly was found in the heat capacity curves of stoichiometric  $\text{Ce}_{0.80}\text{Ln}_{0.20}\text{O}_{1.90}$  ( $\text{Ln} = \text{La}, \text{Gd}$ ) samples. The heat capacities of reduced samples of  $\text{Ce}_{0.80}\text{Gd}_{0.20}\text{O}_{1.77}$  and  $\text{Ce}_{0.80}\text{La}_{0.20}\text{O}_{1.77}$  are shown in Fig. 1. The  $\lambda$ -type peak is found at about 940 K in the heat capacity curve of  $\text{Ce}_{0.80}\text{Gd}_{0.20}\text{O}_{1.77}$ . It seems that this peak is due to the order-disorder transition, that is from the ordered phase formed by the association of  $\text{Ce}^{3+}$  ions and oxygen vacancies to the disordered phase. On the other hand, no peak is found in the curve of  $\text{Ce}_{0.80}\text{La}_{0.20}\text{O}_{1.77}$ , indicating that no phase transition exists. Since the ionic radius of  $\text{La}^{3+}$  is close to that of  $\text{Ce}^{3+}$ , oxygen vacancies and trivalent-cations ( $\text{La}^{3+}$  and  $\text{Ce}^{3+}$ ) are thought to be distributed at random in the structure of  $\text{Ce}_{0.80}\text{La}_{0.20}\text{O}_{1.77}$ .

[1] N. Stelzer and J. Nölting, *J. Solid State Chemistry* **117**, 392 (1995).

[2] T. Ohashi, S. Yamazaki, T. Tokunaga, Y. Arita, T. Matsui, T. Harami and K. Kobayashi, *Solid State Ionics*, in print.

## NEUTRONGRAPHICUL RESEARCH $\text{Cu}_{2-x}\text{Se}$ BY NEUTRONS' NON-ELASTIC SCATTERING

N.N. Biculova, Z.A. Yagafarova, S.A. Danilkin,  
L.E. Jdrovski, V.A. Semjenov, M.J. Gareeva, Ponosov J.S.  
Sterlitamak State Pedagogical Institute  
United institute of nuclear researchings, Dubna  
Adress: 453103, Russia, Bashkortostan, Sterlitamak, Lenin-street, 37,  
general physics department

Copper selenide deals with the conductors with mixed ion-electronic conductivity.

Copper selenide choice as the subject of research is conditioned by the fact that for this research the compounds parameters of ion and electron transmittion are well known, and structure simplicity and monocrystal receiving possibility makes this compound the suitable subject for super-ionic conductivity nature studying.

The results of research  $\text{Cu}_2\text{Se}$  and  $\text{Cu}_{1.75}\text{Se}$  are presented in this report by method of non-elastic neutron scattering.



## THE ROLE OF HYDRATION IN DIELECTRIC PROPERTIES OF POLYCRYSTALLINE ROCKS

A. Kyritsis<sup>1,2</sup>, M. Siakantari<sup>1</sup>, A. Vassilikou – Dova<sup>1\*</sup>, P. Varotsos<sup>1</sup>, P. Pissis<sup>2</sup>

1. Athens University, Physics Department, Section of Solid State Physics, Panepistimiopolis, 15 784 Zografos, Greece
2. Physics Department, National Technical University of Athens, 157 80 Zografou, Greece

Rocks are a special category of inhomogeneous materials, whose dielectric behavior seems to be highly dependent on the hydration level [1]. Complex impedance investigations in sandstone revealed the frequency and the water saturation dependence of the dielectric constant in the frequency range 60kHz to 4MHz [2], which suggests a conductive or Maxwell – Wagner type of mechanism. In theoretical modeling of water-wet rocks, whatever the composition or geometry of pores, is concluded that the dielectric response is governed by the wetted matrix values [3]. Dielectric measurements on natural and artificial rock samples, in the range 5Hz to 13MHz, exhibit very high permittivities (up to  $10^6$ ) for the lowest frequencies, which do not depend significantly on the sample thickness [4]. These permittivities are attributed to diffusion effects at the solid-liquid interface.

In the present work we report results from a dielectric study of natural polycrystalline granite and marble in the frequency range  $10^{-2}$  to  $10^6$  Hz, at room temperature. Even small changes in samples' hydration resulted in a remarkable increase of the dielectric constant, especially in the low frequencies. It should be pointed out that the hydration achieved is always lower than 1%. The absorbed water is found to be proportional to the sample's volume thus suggesting that the hydration is a bulk effect. The water diffusion process obeys to the Fick's law and the diffusion coefficient has been calculated.

- [1] R. Knight and A. Nur, Log. Anal. 28, 513, 1987
- [2] R. Knight and A. Nur, Geophysics 52, 644, 1987
- [3] R. Knight and A. Endres, Geophysics 55, 586, 1990
- [4] B. Nettelblad and G. Niklasson, Solid State Comm. 90, 201, 1994

\* corresponding author, e-mail : avasilik@atlas.uoa.gr

## STRUCTURAL AND TRANSPORT PROPERTIES OF THE TERNARY SYSTEM $\text{CdI}_2$ - $\text{Ag}_2\text{O}$ - $\text{MoO}_3$

S.A. Suthanthiraraj and A.C. Ganeshkumar

Department of Energy, University of Madras  
Guindy Campus, Chennai - 600 025, India.

Synthesis and characterisation of new solid electrolytes form an essential component of research activity in the emerging area of solid state Ionics [1-4]. This paper deals with the preparation of the mixed system  $\text{CdI}_2$  -  $\text{Ag}_2\text{O}$  -  $\text{MoO}_3$  and study of its structural and transport properties over a wide range of compositions.

Analard grade chemicals of  $\text{CdI}_2$ ,  $\text{Ag}_2\text{O}$  and  $\text{MoO}_3$  were used as starting materials for the synthesis of various specimens. Polycrystalline samples of the mixed system  $(\text{CdI}_2)_a [(\text{Ag}_2\text{O}) (\text{MoO}_3)]_{100-a}$  where  $a = 20, 30, 35, 40, 45, 50, 55, 60, 70$  and  $80$  mole % respectively were prepared by annealing the mixture of appropriate quantities of the starting materials in ceramic boats at  $873\text{K}$  for  $5\text{ h}$  and quenching the molten mixture using an ice bath. The powdered samples were analysed using a Philips X-ray generator model 1140 with  $\text{FeK}\alpha_1$  radiation ( $\lambda = 1.936\text{\AA}$ ). Also, impedance measurements were carried out as a function of frequency ( $20\text{Hz}$  to  $1\text{ MHz}$ ) and temperature ( $299$  to  $447\text{K}$ ) using a Hewlett-Packard Model 4284A Precision LCR meter.

These studies have shown that all the observed XRD data contain d-spacings different from that of the starting materials and that such compositions are polycrystalline in nature consisting of a multiphase mixture of  $\gamma\text{AgI}$  and/or other phases. From the room temperature electrical conductivity data it is found that the best conducting composition  $(\text{CdI}_2)_a [(\text{Ag}_2\text{O}) (\text{MoO}_3)]_{100-a}$  where  $a = 45$  mole % shows the room temperature conductivity of  $4.57 \times 10^{-5} \text{ Scm}^{-1}$ . The activation energy values evaluated from the slopes of  $\log(\sigma T)$  versus  $1000/T$  plots have shown that the best conducting composition  $45\% (\text{CdI}_2)$   $55\% [(\text{Ag}_2\text{O}) (\text{MoO}_3)]$  has the lowest activation energy of  $0.19\text{ eV}$ .

X ray diffraction studies appears to suggest that  $\text{AgI}$  may be the major content in this material and therefore it is expected that this composite system would behave very much like  $\text{AgI}$  in its electrical properties. The electrical conductivity results have shown that the typical composition  $45\% \text{ CdI}_2$  -  $27.5\% \text{ Ag}_2\text{O}$  -  $27.5\% \text{ MoO}_3$  exhibits the highest conductivity value of  $4.57 \times 10^{-5} \text{ Scm}^{-1}$  at room temperature.

### References

- [1] M.Z.A. Munshi (Ed.), 'Handbook of Solid State Batteries and Capacitors', World Scientific, Singapore (1995).
- [2] A.M. Sureshini and K. Hariharan, Mater. Res. Bull., **27** (1992) 9.
- [3] A. Viswanathan and S.A. Suthanthiraraj, Solid State Ionics, **58** (1992) 89 ; 62.
- [4] R. Suresh Kumar and K. Hariharan, Bull. Electrochem., **12** (1996) 665.

## PREPARATION AND ELECTRICAL CHARACTERISATION OF THE MIXED SYSTEM $\text{CdI}_2$ - $\text{Ag}_2\text{O}$ - $\text{CrO}_3$

S.A. Suthanthiraraj and A.C. Ganeshkumar

Department of Energy, University of Madras  
Guindy Campus, Chennai - 600 025, India.

Among the various ionic solids those having electrical conductivities of the order of  $10^{-5}$  to  $10^{-1} \text{ Scm}^{-1}$  at room temperature are widely being used in batteries, fuel cells, etc. Such varied applications of these materials have led to a lot of research interest in the development of new solid electrolyte materials in recent years [1-6]. This work deals with the synthesis of a new mixed system  $\text{CdI}_2$ - $\text{Ag}_2\text{O}$ - $\text{CrO}_3$  and its electrical characteristics.

Analar grade chemicals of  $\text{CdI}_2$ ,  $\text{Ag}_2\text{O}$  and  $\text{CrO}_3$  were used as starting materials for the synthesis of various specimens. Polycrystalline samples of the mixed system  $(\text{CdI}_2)_a [(\text{Ag}_2\text{O})(\text{CrO}_3)]_{100-a}$  where  $a = 20, 30, 35, 40, 45, 50, 55, 60, 70$  and  $80$  mole % respectively were prepared by annealing the mixture of appropriate quantities of the starting materials in ceramic boats at  $873\text{K}$  for  $5\text{h}$  and quenching the molten mixture using an ice bath. Impedance measurements were carried out on pressed pellets as a function of frequency ( $20\text{Hz}$  to  $1\text{MHz}$ ) and temperature ( $294$  to  $442\text{K}$ ) using a Hewlett - Packard model 4284A Precision LCR meter. From the room temperature electrical conductivity data it is found that the best conducting composition  $55\% \text{ CdI}_2$  -  $22.5\% \text{ Ag}_2\text{O}$  -  $22.5\% \text{ CrO}_3$  has a room temperature conductivity of  $1.31 \times 10^{-5} \text{ Scm}^{-1}$ . The activation energy values calculated from the slopes of  $\log(\sigma T)$  versus  $1000/T$  plots have shown that the best conducting composition  $55\% \text{ CdI}_2$  -  $22.5\% \text{ Ag}_2\text{O}$  -  $22.5\% \text{ CrO}_3$  exhibits the lowest activation energy of  $0.10\text{eV}$ .

### References

- [1] T. Takahashi and A. Kozawa, (Eds.), "Applications of Solid Electrolytes", JEC Press, Ohio (1980).
- [2] B.V.R. Chowdari and S.Radhakrishna, (Eds.) "Materials for Solid State Batteries", World Scientific, Singapore ((1986).
- [3] B.V.R. Chowdari and S. Radhakrishna, (Eds.) "Solid State Ionic Devices", World Scientific, Singapore (1988).
- [4] A.L. Laskar and S. Chandra, (Eds.) "Superionic Solids and Solid Electrolytes - Recent trends", Academic press, San Diego (1989).
- [5] T. Takahashi, (Ed.) "High conductivity Solid Ionic Conductors - Recent Trends and Applications", World Scientific, Singapore (1989).
- [6] B.V.R. Chowdari, M. Yahaya, I.A. Talib and M.M. Salleh, (Eds.) - "Solid State Ionic Materials", World Scientific, Singapore (1994).

## SPATIAL DISTRIBUTION AND BONDING OF MOBILE IONS IN SINGLE- AND MIXED ALKALI GLASSES: RESULTS FROM SOLID STATE NMR.

Hellmut Eckert, Michael Janssen, Eva Ratai, and Jerry C.C. Chan,  
Institut für Physikalische Chemie, Westfälische Wilhelms-Universität Münster, Schloßplatz 7,  
D48149 Münster.

Attaining knowledge about the local environments and spatial distributions of network modifier species is an important task for developing an improved understanding of cation transport in glassy solid electrolytes. In the area of silicate glasses much of the information has come from EXAFS data [1] and molecular dynamics simulations [2], suggesting that the modifier cations are far from uniformly distributed [3]. Furthermore, conflicting hypotheses have been put forward with respect to the structural origin of the mixed-alkali effect [4-6]. As recently demonstrated, solid state NMR is a powerful new experimental approach for addressing such issues. A variety of modern complementary techniques are available, which are capable of exploring and characterizing cation-cation and cation-framework interactions in oxide glasses. Most of these methods are based on selective measurements of internuclear dipole-dipole interactions [4], which can be related to internuclear distance distributions. We will describe these techniques, discuss their informational contents, and present results for a series of alkali-borate based glass systems.

In discussing appropriate NMR approaches for characterizing cation-cation interactions, it is necessary to differentiate between interactions of like nuclei and interactions among unlike nuclei. Spatial correlations among *like cations* can be probed selectively by measuring homonuclear dipole-dipole interactions via spin echo decay spectroscopy [7]. In this method, the height of a  $90^\circ$ - $t_1$ - $180^\circ$ - $t_1$  spin echo is measured as a function of the time increment  $t_1$ . As previously discussed, these measurements yield a dipolar second moment characterizing an average internuclear coupling strength, which can be compared to calculated values for different atomic distribution scenarios [7]. Spatial correlations among *unlike cations* (eg.  $^7\text{Li}$ - $^{23}\text{Na}$ ) can be probed by spin echo double resonance (SEDOR) spectroscopy [8,9], in an analogous fashion. In order to measure the dipolar interaction strength between two nuclear types S and I one measures the height of a  $90^\circ$ - $t_1$ - $180^\circ$ - $t_1$  spin echo for the S-nuclei, while a  $180^\circ$  pulse is applied to the spin system of the I-nuclei. The extra decay of S-magnetization observed in this experiment allows quantitative assessment of the I-S coupling and hence comparison with scenarios relating to the distribution of both cation species relative to each other.

EXAFS measurements have shown [1] that the cations in glasses tend to possess distinct oxygen environments that are cation-specific and appear to be rather independent on the glass composition. As previously shown, NMR chemical shift measurements are able to resolve additional detail on the kind of cation binding in glasses. In principle, chemical shifts can be measured selectively by means of the magic-sample spinning (MAS) technique. Since most of the cations of interest ( $^7\text{Li}$ ,  $^{23}\text{Na}$ ,  $^{133}\text{Cs}$ ) possess quadrupolar nuclei, accurate measurements require that MAS is combined with field dependent measurements and/or multiple quantum transitions [10,11]. Cation-framework interactions can also be probed on the basis of dipole-dipole couplings measurable between the corresponding nuclei. To this end, the rotational echo double resonance (REDOR) experiment [12], a spinning variant of the SEDOR technique, has

been particularly successful, since it combines the selectivity of heterodipolar coupling measurements with the benefits of magic-angle-spinning.

Using a combination of the solid state NMR approaches discussed above, the local chemical environments and spatial distributions of the sodium cations have been examined. The compositional trends of the  $^{23}\text{Na}$  chemical shifts and the  $^{23}\text{Na}$ - $^{23}\text{Na}$  dipolar second moments suggests that the sodium species appear to be more or less homogeneously distributed at higher cation contents, whereas there appears to be a slight tendency towards Na clustering at low cation concentrations (below 16 mole%  $\text{Na}_2\text{O}$ ) [13]. Further information on the issue of cation clustering is available from the magnitude of the  $^{23}\text{Na}$ - $^{11}\text{B}$  dipole-dipole interaction. It is well known that in the presence of  $\text{Na}_2\text{O}$  the trigonal  $\text{BO}_3$  units present in the framework are transformed into negatively charged tetrahedral  $\text{BO}_4$  units, and both framework species can be well-discriminated by  $^{11}\text{B}$  MAS-NMR. In the presence of strong clustering effects, one would expect the sodium nuclei to interact much more strongly with the  $\text{BO}_4$  units than with the remaining  $\text{BO}_3$  sites. Indeed,  $^{11}\text{B}\{^{23}\text{Na}\}$  REDOR studies carried out with this objective reveal that in the region of low  $\text{Na}_2\text{O}$  concentrations the  $\text{BO}_4$  units interact more strongly with the  $^{23}\text{Na}$  spins than the  $\text{BO}_3$  units do, while at higher cation contents there is no discernable spectroscopic differentiation. The results reveal the ability of solid state NMR for detecting subtle cation clustering effects in sodium borate glasses.

To investigate the cation distribution in mixed-alkali systems, heterodipolar interactions and chemical shifts were measured for a series of (Na,Li)-, (Na,K)-, and (Na,Cs)-borate glasses with fixed overall cation contents. The compositional trends of the cation chemical shifts, the heterodipole-dipole couplings measured in  $^{23}\text{Na}\{^7\text{Li}\}$  and  $^{23}\text{Na}\{^{133}\text{Cs}\}$  SEDOR experiments, as well as an analysis of detailed  $^{11}\text{B}\{^{23}\text{Na}\}$  REDOR measurements reveal consistently that the two types of cations are statistically mixed. Thus, the NMR experiments provide clear evidence against like-cation phase separation previously proposed for silicate glass systems [6,8]. Conversely, they also argue against the idea of preferred unlike-cation interactions previously proposed for other systems [5].

- [1] G.N. Greaves, *J. Noncryst. Solids* **71**, 203 (1985)
- [2] C. Huang and A. N. Cormack, *J. Chem. Phys.* **95**, 3634 (1991).
- [3] S. J. Gurman, *J. Noncryst. Solids* **125**, 151 (1990)
- [4] A. Bunde, M. D. Ingram, and P. J. Maass, *J. Noncryst. Solids* **172-174**, 1222 (1994).
- [5] M.D. Ingram, *Phys. Chem. Glasses* **28**, 215 (1987).
- [6] J. F. Emerson and P. J. Bray, *J. Noncryst. Solids* **169**, 87 (1994).
- [7] B. Gee and H. Eckert, *Solid State Nucl. Magn. Reson.* **5**, 113 (1995).
- [8] A.T.W. Yap, H. Förster, and S.R. Elliott, *Phys. Rev. Lett.* **75**, 3946 (1995)
- [9] B. Gee and H. Eckert, *J. Phys. Chem.* **100**, 3705 (1996)
- [10] L. Frydman and J. S. Harwood, *J. Am. Chem. Soc.* **117**, 5367 (1995)
- [11] C. Fernandez and J. P. Amoureux, *Chem. Phys. Lett.* **242**, 449 (1995).
- [12] T. Gullion and J. S. Schaefer, *J. Magn. Reson.* **81**, 196 (1989).
- [13] E. Ratai, M. Janssen, and H. Eckert, *Solid State Ionics* **105**, 25 (1998)

## PREPARATION AND CHARACTERIZATION OF LITHIUM ION CONDUCTING OXYSULFIDE GLASSES

Tsutomu Minami, Akitoshi Hayashi, and Masahiro Tatsumisago

Department of Applied Materials Science, Osaka Prefecture University,

Sakai, Osaka, 599-8531, Japan

The  $\text{Li}_2\text{S}-\text{SiS}_2$  based lithium ion conducting glasses have recently attracted much attention as one of the most promising candidates of solid electrolytes utilized for solid-state lithium secondary batteries because of their high conductivities of  $10^{-4}$ - $10^{-3} \text{ S cm}^{-1}$  at room temperature, wide electrochemical window, and easy preparation without vacuum sealing [1-3]. The structure of these glasses has been analyzed using several spectroscopic techniques such as solid-state NMR and X-ray photoelectron spectroscopy (XPS) [4,5].

In this paper, we review the properties and structure of the lithium ion conducting  $\text{Li}_2\text{S}-\text{SiS}_2-\text{Li}_x\text{MO}_y$  ( $\text{Li}_x\text{MO}_y$ : lithium ortho-oxosalt) oxysulfide glasses prepared by using a twin-roller quenching technique. The effects of the addition of  $\text{Li}_x\text{MO}_y$  to the  $\text{Li}_2\text{S}-\text{SiS}_2$  system on the properties and structure of the glasses are reported. The relationship between properties and structure of these oxysulfide glasses are discussed. Furthermore, the solid-state batteries with these oxysulfide glasses as solid electrolytes are prepared and the performance as lithium secondary batteries is characterized.

Thermal, electrical, and electrochemical properties for the  $(100-x)(0.6\text{Li}_2\text{S} \cdot 0.4\text{SiS}_2) \cdot x\text{Li}_x\text{MO}_y$  ( $\text{M}=\text{Si}, \text{P}, \text{Ge}, \text{B}, \text{Al}, \text{Ga}$  and  $\text{In}$ ) oxysulfide glasses were examined. The difference between the crystallization temperature  $T_c$  and glass transition temperature  $T_g$ ,  $T_c-T_g$ , was used as one of the measures of glass stability against crystallization. The value of  $T_c-T_g$  ranged from 23 to 150 °C. In all the systems the value of  $T_c-T_g$  exhibited a maximum at the composition added with small amounts of  $\text{Li}_x\text{MO}_y$  (about 5 mol%  $\text{Li}_x\text{MO}_y$ ). The highest value of about 150 °C was obtained for  $T_c-T_g$  in the  $\text{Li}_4\text{SiO}_4$  added system. Further addition of  $\text{Li}_x\text{MO}_y$  lowered the glass stability against crystallization in all the oxysulfide systems. The oxysulfide glasses added with 5 mol% of  $\text{Li}_x\text{MO}_y$  exhibited the high conductivity of  $10^{-3} \text{ S cm}^{-1}$  at room temperature in all the systems. The conductivity of  $10^{-3} \text{ S cm}^{-1}$  obtained in these oxysulfide glasses is considerably high as solid electrolytes. The glasses added with large amounts of  $\text{Li}_x\text{MO}_y$  exhibited low conductivity of about  $10^{-5} \text{ S cm}^{-1}$ . The electrochemical stability of these oxysulfide glasses against Li electrode was examined by using cyclic voltammetry. The cyclic voltammogram of the glass added with 5 mol%  $\text{Li}_4\text{SiO}_4$  revealed that no reactions except for lithium dissolution / deposition reactions were observed up to 10 V vs.  $\text{Ag}/\text{Ag}^+$ , suggesting that this glass has a wide electrochemical window. Furthermore, this glass had good chemical and electrochemical stability in contact with Li metal and withstood high voltage application without decomposition. Further addition of  $\text{Li}_4\text{SiO}_4$  lowered the electrochemical stability of the oxysulfide glasses. The addition of small amounts of  $\text{Li}_x\text{MO}_y$  was the most effective to improve the glass properties as solid electrolytes.

Structure of these oxysulfide glasses were analyzed in detail by means of solid-state NMR and XPS measurements. We report in this study the structural analysis of the  $(100-x)(0.6\text{Li}_2\text{S}\cdot 0.4\text{SiS}_2)\cdot x\text{Li}_4\text{SiO}_4$  oxysulfide glasses as the representative ones among those many oxysulfide glasses.  $^{29}\text{Si}$  MAS-NMR spectra of the glass added with 5 mol%  $\text{Li}_4\text{SiO}_4$  suggested that large amounts of silicon structural units coordinated with both sulfur and oxygen atoms were present; such structural units have not been observed in crystalline compounds. Further addition of  $\text{Li}_4\text{SiO}_4$  decreased those structural units. Since large amounts of those unique silicon structural units were present in the glass with 5 mol%  $\text{Li}_4\text{SiO}_4$ , large structural change was needed during the crystallization. Therefore, the oxysulfide glass at this composition exhibited high glass stability against crystallization.

XPS spectra revealed that most of sulfur atoms were present as nonbridging ones and most of oxygen atoms were present as bridging ones in the oxysulfide glass added with 5 mol%  $\text{Li}_4\text{SiO}_4$ . With an increase in the content of  $\text{Li}_4\text{SiO}_4$  the relative amounts of  $\text{S}^{2-}$  units increased and those of nonbridging sulfur atoms decreased. On the other hand, the relative amounts of nonbridging oxygen atoms increased while those of bridging ones decreased with an increase of  $\text{Li}_4\text{SiO}_4$  added. The glass with 5 mol%  $\text{Li}_4\text{SiO}_4$  exhibited high conductivity at room temperature because bridging oxygen atoms worked as a weaker trap of lithium ions compared to nonbridging ones. The presence of large number of  $\text{S}^{2-}$  units and nonbridging oxygen atoms lowered the conductivity and electrochemical stability in the oxysulfide glasses added with 20 mol%  $\text{Li}_4\text{SiO}_4$ .

Electrochemical cells were constructed with the oxysulfide glasses as a solid electrolyte,  $\text{LiCoO}_2$  as a positive electrode, and indium as a negative electrode. Charge and discharge behaviors of the cell at a constant current with a density of  $127\text{ }\mu\text{A}/\text{cm}^2$  were examined. The cell with the oxysulfide glasses added with 5 mol%  $\text{Li}_4\text{SiO}_4$  exhibited excellent cycling properties with no decrease of charge-discharge capacity and the charge-discharge efficiency was almost 100 %.

## References

- [1] J. H. Kennedy, *Mat. Chem. Phys.*, **23**, 29 (1989).
- [2] M. Tatsumisago, K. Hirai, T. Hirata, M. Takahashi, and T. Minami, *Solid State Ionics*, **86-88**, 487 (1996).
- [3] K. Takada, N. Aotani, K. Iwamoto, and S. Kondo, *Solid State Ionics*, **86-88**, 877 (1996).
- [4] K. Hirai, M. Tatsumisago, M. Takahashi, and T. Minami, *J. Am. Ceram. Soc.*, **79**, 349 (1996).
- [5] A. Hayashi, M. Tatsumisago, T. Minami, and Y. Miura, *Phys. Chem. Glasses*, **39**, 145 (1998).

## ION DYNAMICS IN SUPERIONIC CHALCOGENIDE GLASSES

Michel Ribes, Renaud Belin, Gilles Taillades and Annie Pradel

Laboratoire de Physicochimie de la Matière Condensée UMR 5617 Université Montpellier II  
34095 Montpellier cedex 5 France

The general problem of non Debye, i. e. non exponential, relaxation in ionic conductive glasses was extensively discussed over the last 25 years. A non-Debye relaxation is often expressed by the Kolrausch-Williams-Watts function in the time domain

$$\phi(t) = \phi(0) \exp.[-(t/\tau)^\beta] \quad (1)$$

with  $0 < \tau < 1$ .

The study of the frequency dependence of the electrical conductivity,  $\sigma(\omega)$ , in glasses is commonly used to analyse this behaviour. Electrical conductivity was usually described by the so-called "universal law" first proposed by Jonscher :

$$\sigma(\omega) = \sigma_{dc} + A\omega^s \quad (2)$$

with  $0 \leq s \leq 1$ .

Several models were proposed to account for this behaviour :

- the Coupling Model (CM) developed by Ngai [1] who invokes the concept of correlated states between mobile ions (a correlation between ions would take place after a critical time  $t_c$ ). For  $t < t_c$  (very short time) the relaxation rate would be constant and for  $t > t_c$  the model predicts a power law dependence.

- the Jump Relaxation Model (JRM) proposed by Funke [2] is based upon the existence of correlated forward-backward ion hops due to the retarded response of neighbouring ions. This model leads, as the previous one, to the frequency dependence of conductivity given by equation 2 in the low frequency range while a plateau should be observed in the high frequency region.

- the Diffusion Controlled Relaxation Model (DCR) proposed by Elliott [3], based on an interstitialcy mechanism, predicts a dispersive behaviour of conductivity with  $s = 0.5$ .

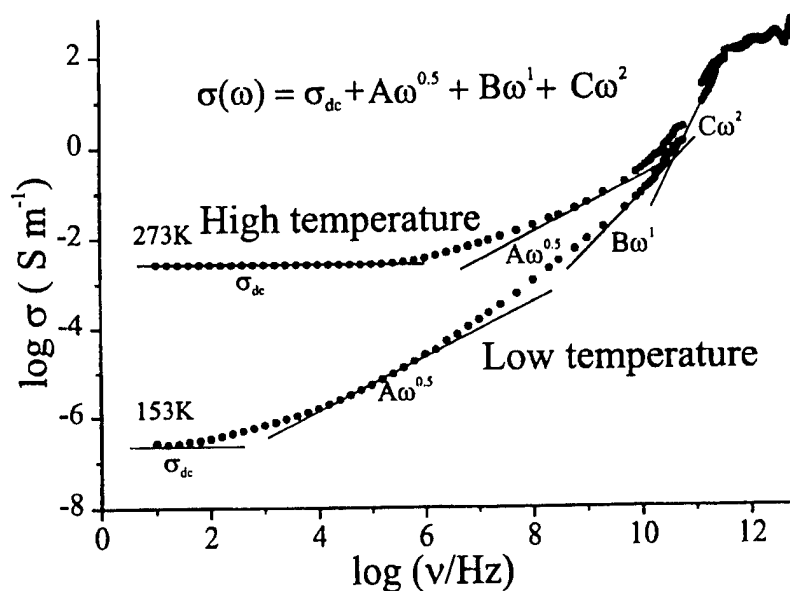
- the Lattice Gas Model (LGM) developed by Maass et al [4] based upon the Monte Carlo simulation of ion movement in a disordered structure leads to a dispersive behaviour of  $\sigma(\omega)$  with a sub-linear frequency exponent.

According to all these models the two contributions to conductivity, i. e.  $\sigma_{dc}$  and  $A\omega^s$  (equation 2), arise from the same relaxation process. A is thermally activated with an activation energy  $E_{ac}$  related to the activation energy from  $\sigma_{dc}$ , i. e.  $E_{dc}$ , by  $E_{ac} = (1-s)E_{dc}$ .

Recently conductivity measurements at high frequency, i. e. in the GHz region, have shown an additional contribution with a superlinear frequency dependence. The Unified Site Relaxation Model (USRM) [5] explains the two dispersive regimes. As an alternative to the USRM, Hsieh and Jain [6] postulated that the superlinear regime has some link with the relaxation process known to exist at low temperature and described by the Asymmetric Double Well Potential Model.

Partial experimental results, i.e. obtained in rather narrow frequency ranges and/or narrow temperature domains, were generally used as the basis of the proposed models. In this work complete conductivity spectra from  $\sigma_{dc}$  to IR optical conductivity in a large temperature range for the glass  $0.5\text{Ag}_2\text{S}-0.5\text{GeS}_2$  were obtained using different instruments depending upon the temperature and frequency ranges investigated. Two typical spectra are shown in figure 1.





Which conclusions could be drawn from these experimental results?

- The results could be described using the following equation :

$$\sigma(\omega) = \sigma_{dc} + A\omega^{0.5} + B\omega^1 + C\omega^2 \quad (3)$$

While  $\sigma_{dc}$  and  $A$  are thermally activated with activation energies  $E_{dc} \sim 0.3$  eV and  $E_{ac} \sim 0.13$  eV respectively,  $B$  and  $C$  are not or very weakly temperature dependent.

The use of the third term ( $B\omega^1$ ) on the right hand-side of equation 3 is not useful anymore for spectra taken at temperatures larger than 200K.

- Therefore there is no need for an additional superlinear frequency dependent contribution to account for the conductivity at high frequency below the IR domain as it was previously reported. Such a result was probably an artefact due to an incomplete data set.

- No plateau can be seen in the high frequency part of the spectra which is a main difference with results obtained for crystalline superionic conductors.

- In agreement with Hsieh and Jain, we conclude that the linear frequency contribution visible at high frequency in the low temperature spectra corresponds to an unique additional regime to be seen in between the dispersive region with a dependence  $A\omega^{0.5}$  and the vibration regions.

All these results will be described in details and consequences on the validity of the proposed models discussed.

[1] K.L. Ngai, J. Phys. Coll. C2, 2, 61 (1992).

[2] K. Funke, Prog. Solid State Chem., 22, 111 (1993).

[3] S. R. Elliott, P. Owens, Phil. Mag. 60, 777 (1989).

[4] P. Maass, J. Peterson, A. Bunde, W. Dieterich and H. E. Roman, Phys. Rev. Lett. 66, 52 (1991).

[5] A. Bunde, K. Funke, M. D. Ingram, Solid State Ionics 86-88, 1311 (1996).

[6] C. H. Hsieh, H. Jain, J. Non-Cryst. Solids 203, 293 (1996).

## SPECTROSCOPIC INVESTIGATION OF AgI-DOPED BORATE GLASSES

C.P. Varsamis, E.I. Kamitsos and G.D. Chrysikos

*Theoretical and Physical Chemistry Institute, National Hellenic Research Foundation,  
48 Vass. Constantinou Ave., Athens 116 35, Greece*

AgI-containing borate glasses  $x\text{AgI}-(1-x)[\text{Ag}_2\text{O}-n\text{B}_2\text{O}_3]$  have received particular attention as models of fast ion conducting (FIC) glasses. The special interest to these materials is due to the fact that they are stable, with relatively high glass transition temperature, high ionic conductivity and can be prepared easily in a wide glass-forming region [1,2]. Despite the numerous studies devoted to such FIC glasses, their structure and the ion conduction mechanism are still a matter of debate [2-6].

The purpose of this work is to investigate the structure of the borate glass network and its dependence on the AgI doping salt, as well as the nature of sites occupied by the charge carrying silver ions. Glasses were obtained in bulk and thin film forms for  $n=2$  (diborate) and  $n=0.5$  (pyroborate), and their infrared spectra were measured by the specular reflectance and transmission techniques.

The analysis of the mid-infrared profiles of diborate bulk compositions showed that the short-range order of the glass network consists of borate triangles ( $\text{B}\emptyset_2\text{O}^-$  and  $\text{B}\emptyset_3$ ) and tetrahedra ( $\text{B}\emptyset_4^-$ ), where  $\emptyset$ =oxygen atom bridging two boron centers. Spectral deconvolution was performed to quantify the glass structure by calculating the mole fractions of the local borate structural units. It was found that the fractions of  $\text{B}\emptyset_2\text{O}^-$  triangles and  $\text{B}\emptyset_4^-$  tetrahedra depend on the AgI content of the glass, and this effect was explained in terms of the isomerisation reaction  $\text{B}\emptyset_4^- \rightleftharpoons \text{B}\emptyset_2\text{O}^-$ . A quasi-equilibrium constant of this reaction was calculated from the spectroscopic data, and found to decrease with increasing the AgI content of the glass. It was concluded that the AgI-induced transformation of  $\text{B}\emptyset_2\text{O}^-$  triangles into  $\text{B}\emptyset_4^-$  tetrahedra leads to a better packing of the borate backbone and thus to an improvement of the medium-range order of the glass. Therefore, the influence of AgI on the diborate structure appears to be indirect and can be attributed to its plasticizing effect on the glass transition and fictive temperatures at which the structure of the supercooled liquid is frozen into the glassy state.

Similarly, it was shown that the network structure of pyroborate glasses can be understood on the basis of the disproportionation of pyroborate dimers ( $\text{B}_2\text{O}_5^{4-}$ ) to orthoborate monomers ( $\text{BO}_3^{3-}$ ) and metaborate tetrahedra, i.e.  $\text{B}_2\text{O}_5^{4-} \rightleftharpoons \text{BO}_3^{3-} + \text{B}\emptyset_4^-$ . The spectroscopic data indicate that AgI favors this disproportionation reaction, and thus explain glass formation in the silver-pyroborate system, despite the fact that the  $\text{Ag}_2\text{O}-0.5\text{B}_2\text{O}_3$  composition does not vitrify nor forms a crystalline phase.

The study of the infrared transmission spectra of thin films in the diborate family showed that the relative intensity of the absorption envelope due the borate tetrahedra decreases with increasing film thickness, and approaches the behaviour of the corresponding bulk glass. It was demonstrated that the main origin of this trend is traced to optical effects, and in particular to the strong dependence of the period and amplitude of the background interference wave on film thickness. Besides optical effects, thin films and bulk glassy samples may exhibit differences in thermal history that can lead to structural variations and thus to additional spectral differences. The present results suggest that direct comparison of infrared data of thin films and bulk glasses should be avoided, since it may lead easily to erroneous conclusions.

The far-infrared absorption spectra of AgI-doped pyroborate glasses showed that, besides the presence of the two bands at *ca* 40 and 175  $\text{cm}^{-1}$  arising from the vibration of silver ions in oxide sites [7], a third band develops at *ca* 100  $\text{cm}^{-1}$  as AgI is added to the glass. This new

feature was assigned to the localized vibration of silver ions in primarily iodide sites [5]. The intensity and resonance frequency of this band was found to increase with AgI content and this was taken to indicate the progressive aggregation of silver-iodide sites into disordered AgI-like microdomains. In contrast to pyroborates, the far-infrared profiles of diborate glasses could be simulated with only two silver ion motion bands. The resonance frequency of the stronger component was found to decrease from 146 to 128  $\text{cm}^{-1}$  as the AgI content increases from  $x=0$  to  $x=0.65$ . It was found that this trend can be described better by a model involving two bands, one at *ca* 110  $\text{cm}^{-1}$  (silver-iodide sites) and the other at 146  $\text{cm}^{-1}$  (silver-oxide sites), rather than by the progressive formation of mixed silver-oxyiodide sites with effective force constant and reduced mass of vibration varying with AgI content.

The far-infrared spectroscopic data for both glass series investigated in this work are supportive of the models proposing the formation of AgI microdomains, which provide diffusion pathways for silver ion transport [8]. In addition to this mechanism, the network expansion induced by AgI doping leads to more open structures between the borate segments and this process favors also ion conduction in AgI-containing glasses [9].

## References

- [1] A. Magistris, G. Chiodelli and A. Schiraldi, *Electrochim. Acta* **23**, 585 (1978).
- [2] T. Minami, Y. Ikeda and T. Tanaka, *J. Non-Cryst. Solids* **52**, 159 (1982).
- [3] G. Chiodelli, A. Magistris, M. Villa and J.L. Bjorkstam, *J. Non-Cryst. Solids* **51**, 143 (1982).
- [4] G. Carini, M. Cutroni, M. Frederico, G. Galli and G. Tripodo, *Phys. Rev. B* **30**, 7212 (1984).
- [5] E.I. Kamitsos, J.A. Kapoutsis, G.D. Chryssikos, J.M. Hutchinson, A.J. Pappin, M.D. Ingram and J.A. Duffy, *Phys. Chem. Glasses* **36**, 141 (1995).
- [6] J.J. Hudgens and S.W. Martin, *Phys. Rev. B* **53**, 5348 (1996).
- [7] J.A. Kapoutsis, E.I. Kamitsos and G.D. Chryssikos, in *Borate Glasses, Crystals and Melts*, A.C. Wright, S.A. Feller and A.C. Hannon, Eds., Soc. Glass Technology, Sheffield, U.K. (1997), p. 303.
- [8] T. Minami, *J. Non-Cryst. Solids* **73**, 273 (1985).
- [9] J. Swenson and L. Borjesson, *Phys. Rev. Lett.* **77**, 3569 (1996).

# IONIC MOTION AND STRUCTURAL PROPERTIES IN OPTIMIZED SILVER THIO-BORATE GLASSES

<sup>1</sup>A. Matic, <sup>1</sup>J. Swenson, <sup>2\*</sup>T. Akai, <sup>1</sup>L. Börjesson and <sup>2</sup>S. W. Martin

<sup>1</sup>Department of Applied Physics, Chalmers University of Technology, S-41296 Göteborg, Sweden

<sup>2</sup>Department of Material Science and Engineering, Iowa State University of Science and Technology, Ames, Iowa, 50011, USA

In the search for new ion conducting materials to be used as solid electrolytes in various electrochemical applications the silver thio-borate glasses are one of the more remarkable systems developed in recent years. When designing this glass all known relationships between glass chemistry and conductivity were applied to increase the conductivity. Using different glass formers based on sulphides, having polarizable Ag-ions as charge carriers and finally doping the host matrix with a halide salt, the resulting glass,  $\text{AgI-Ag}_2\text{S-B}_2\text{S}_3\text{-SiS}_2$ , showed record high room temperature ionic conductivity [1]. The glass not only has a high conductivity, but is also relatively stable in ambient atmosphere, a problem for e. g. Li-analogs, and hence more suitable for applications. Another interesting feature is the deviation from Arrhenius behaviour in the conductivity below  $T_g$  [1]. For the silver thio-borate glasses with the highest conductivity, this effect sets in far below  $T_g$  and it has been suggested that this perhaps indicates a upper limit for the ionic conductivity in glasses.

Apart from the chemical implications for the high ionic conductivity, used in the design of the glass, little is known about the microscopic conduction process which is of importance for the understanding and further developments of improved electrolytes which may be able to overcome the conductivity limiting non-Arrhenius behaviour. In this work we present results from both dynamical and structural studies on this glass system both being of importance for getting insight in microscopic conduction mechanisms. With neutron diffraction, Raman, IR and NMR spectroscopy, we have probed the glass structure from the local environment of the cations to the intermediate range order of the host glass network. Using Quasi-Elastic Neutron Spectroscopy (QENS), we are able to directly probe the ionic motion within the host structure.

The neutron diffraction results are shown in fig. 1 and the obtained inter atomic distances and coordination numbers are summarised in table I. From previous IR [2] and NMR [3] studies of these and related alkali thio-silicate [4] glasses, it is proposed that the glass network is built up by three different structural units: trigonal  $\text{BS}_3$  units,  $\text{BS}_4^-$  and  $\text{SiS}_4$ -tetrahedra. These three different coordinating structures will provide at least three distinctly different  $\text{Ag}^+$  sites. From  $^{109}\text{Ag}$  NMR data indeed three chemically different  $\text{Ag}^+$  species are observed with the possible explanation that these are Ag-ions coordinating to these three different units. Upon doping with AgI, the host structure is expanded to accommodate the salt. This is observed by the appearance of a new diffraction peak at very low Q. A similar peak is also observed e. g. in AgI-doped silver borate and phosphate glasses and is related to an increase of the intermediate range order in the system [5,6]. The position of this first diffraction peak (FSDP) is  $Q_1=0.55 \text{ \AA}^{-1}$  and corresponds to a real space length scale of  $2\pi/Q \approx 11 \text{ \AA}$ .

**Table I** Inter atomic distances and coordination numbers obtained from neutron diffraction experiments on the  $x\text{AgI-(1-x)[0.525Ag}_2\text{S-0.475(B}_2\text{S}_3\text{-SiS}_2\text{)]}$  glasses.

Correlation	x=0	x=0.2
B-S	$r=1.83 \text{ \AA}$ (trigonal) $r=1.99 \text{ \AA}$ (tetrahedral)	$r=1.83 \text{ \AA}$ (trigonal) $r=1.94 \text{ \AA}$ (tetrahedral)
Si-S	$r=2.15 \text{ \AA}$	$r=2.15 \text{ \AA}$
Ag-S	$r=2.53 \text{ \AA}$ $N_{\text{Ag-S}}=4.87$	$r=2.47 \text{ \AA}$ $N_{\text{Ag-S}}=2.59$
Ag-I	-	$r=2.71 \text{ \AA}$ $N_{\text{Ag-I}}=2.14$
Ag-Ag	$r=3.10 \text{ \AA}$	$r=3.04 \text{ \AA}$
S-S	$r=3.62 \text{ \AA}$	$r=3.68 \text{ \AA}$

\* On leave from Osaka National Research Institute, Osaka, Japan

Using QENS, we are able to investigate the ionic motion on a microscopic level. The random movement of the ions within the static host structure results in a broadening of the elastic line. Information regarding the nature of the ionic motion can be then obtained from the momentum transfer dependence of the intensity and width of this quasi-elastic contribution. Fig. 2 shows the results from these experiments. The results are analysed within the simple Chudley-Elliot model [7] which is able to describe the momentum transfer dependence of the half-width. The agreement between the model and the data indicates that the ionic motion is of jump-diffusion type. The parameters within this model are the average residence time  $\tau$  and the average jump distance  $l$ , and from the fits we obtain an average jump distance which is in agreement with the average Ag-Ag distance obtained from the neutron diffraction data. We also observe that the jump distance is not affected by temperature while the average relaxation time decreases with increasing temperature, see fig. 2. The conductivity calculated from these parameters is an order of magnitude larger than the estimated DC-conductivity (conductivity data is not available at these elevated temperatures). This may indicate a considerably higher local conductivity, where ions have a larger mobility in domains of the structure, which contribute to the QENS spectrum but not to the long range DC-conductivity.

The optimised silver thio-borate glasses are highly complicated materials both regarding structural and dynamical properties. By applying a range of different experimental techniques we are however able to extract valuable information e. g. regarding the microscopic structure and the high mobility of the Ag-ions. The results will be discussed in connection to the glass structure and the high conductivity of the glasses.

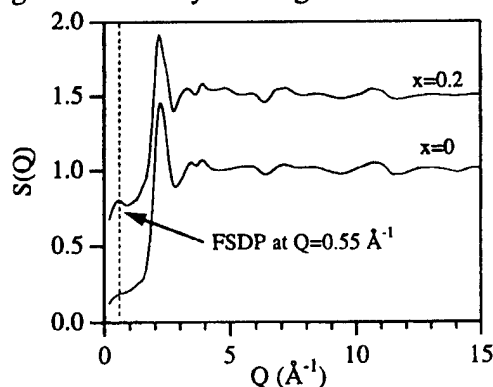


Fig. 1 Results from the neutron diffraction experiments on  $x\text{AgI}-(1-x)[0.525\text{Ag}_2\text{S}-0.475(\text{B}_2\text{S}_3-\text{SiS}_2)]$  with  $x=0$  and  $0.2$ . The major effect of the salt doping is the appearance of a peak at low  $Q$  in the doped sample indicates the presence of intermediate range order in the structure.

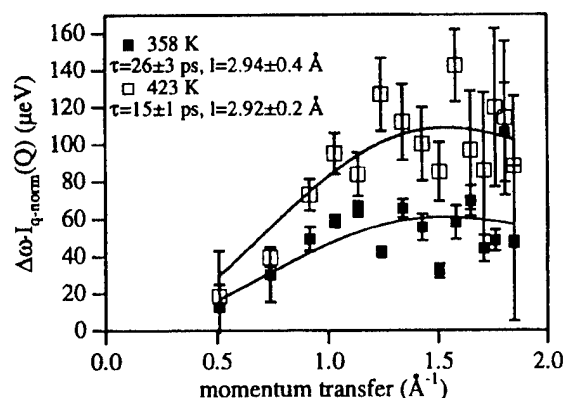


Fig. 2 Momentum transfer dependence of the half-widths of the quasi-elastic contribution in the QENS experiment. The solid line is a fit to the Chudley-Elliot model and the parameters obtained from the fit are shown in the figure.

## References

- [1] J. Kincs and S. W. Martin, Phys. Rev. Lett. 76, 1 (1996)
- [2] A. Burns, S. W. Martin, to be published
- [3] J. A. Sills, S. W. Martin and D. R. Torgeson, J. Non-Cryst. Sol., 175, 270 (1995)
- [4] S. W. Martin and J. A. Sills, J. Non-Cryst. Sol., 135, 171 (1991)
- [5] J. Swenson, L. Börjesson, R. L. McGreevy and W. S. Howells, Phys. Rev. B 55, 11236 (1997)
- [6] J. D. Wicks, L. Börjesson, G. Bushnell-Wye, W. S. Howells and R. L. McGreevy, Phys. Rev. Lett. 74, 726 (1995)
- [7] C. T. Chudley and R. J. Elliot, Proc. Phys. Soc. 77, 353 (1961)

## Neutron diffraction studies of $\text{Ag}_2\text{S}-\text{As}_2\text{S}_3$ glasses in percolation and network-controlled domains

E. Bychkov<sup>1</sup> and D.L. Price<sup>2</sup>

<sup>1</sup> *Université du Littoral, 59140 Dunkerque, France*

<sup>2</sup> *Argonne National Laboratory, Argonne, IL 60439, USA*

Electrical [1] and  $^{110}\text{Ag}$  tracer diffusion [2] measurements show two distinctly different transport regimes at low (0.001-2 at.%) and high (15-30 at.%) silver concentrations for homogeneous  $x\text{Ag}_2\text{S}-(1-x)\text{As}_2\text{S}_3$  glasses. Power-law composition dependencies of the ionic conductivity  $\sigma_i(x)$  and silver tracer diffusion coefficient  $D_{\text{Ag}}(x)$  at low  $x$  are associated with percolation in the critical region just above the percolation threshold. A nearly exponential increase of  $\sigma_i(x)$  and  $D_{\text{Ag}}(x)$  at high  $x$  is indicative of a network-controlled ion transport. These two composition domains are also distinguished by thermal properties of the glasses. In particular, the glass transition temperature  $T_g(x)$  decreases rapidly in the percolation domain but remains nearly constant at  $x \geq 10$  at. % Ag. The observed trends suggest structural differences between the two domains which were examined in the present work using high resolution neutron diffraction experiments ( $Q_{\text{max}} = 40 \text{ \AA}^{-1}$ ) [3,4].

The neutron diffraction measurements show significant changes in the first sharp diffraction peak (FSDP) at  $Q \approx 1.2-1.3 \text{ \AA}^{-1}$  (Fig. 1). First, the intensity of the peak decreases with  $x$  quite rapidly, and it disappears almost completely in the network-controlled region at  $x = 25$  at. % Ag. A gradual displacement of the FSDP towards higher  $Q$  values is also observed.

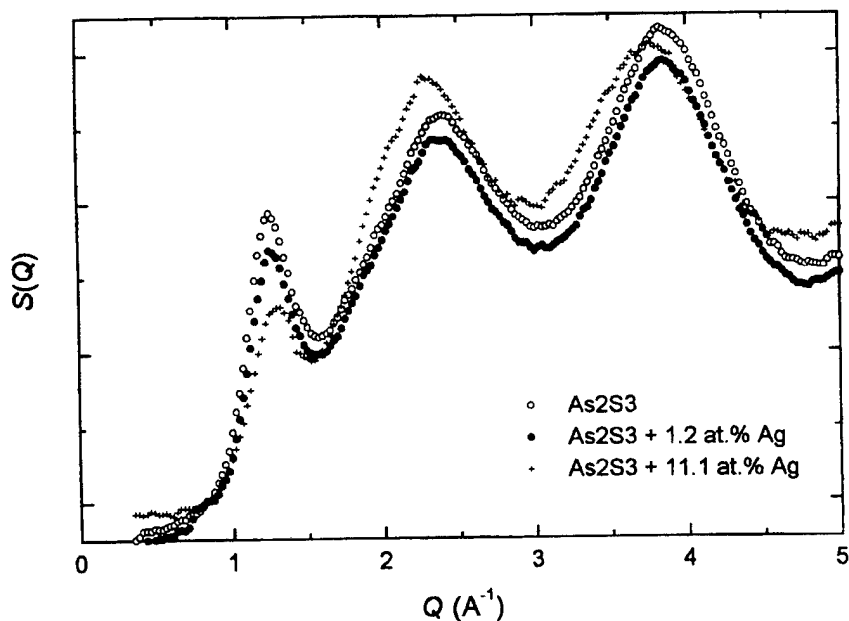


Fig. 1. Structure factors  $S(Q)$  at low  $Q$  values for selected  $\text{Ag}_2\text{S}-\text{As}_2\text{S}_3$  glasses.

Additionally, the total pair correlation functions  $T(r)$  exhibit remarkable changes in the shape of the 1st ( $r \approx 2.3$  Å) and 2nd ( $r \approx 3.5$  Å) peaks. These changes would be expected at high  $x$  where correlations involving silver become significant. Nevertheless, distinct changes in the shape of these peaks are observed at low  $x$  (Fig. 2) when the silver concentration itself is not high enough and, respectively, the intensity of the Ag-based correlations. In other words, it means that the silver additions in the percolation domain modify markedly the short- and intermediate-range order of the host  $\text{As}_2\text{S}_3$  glass network. Possible structural interpretations of the observed phenomena will be discussed.

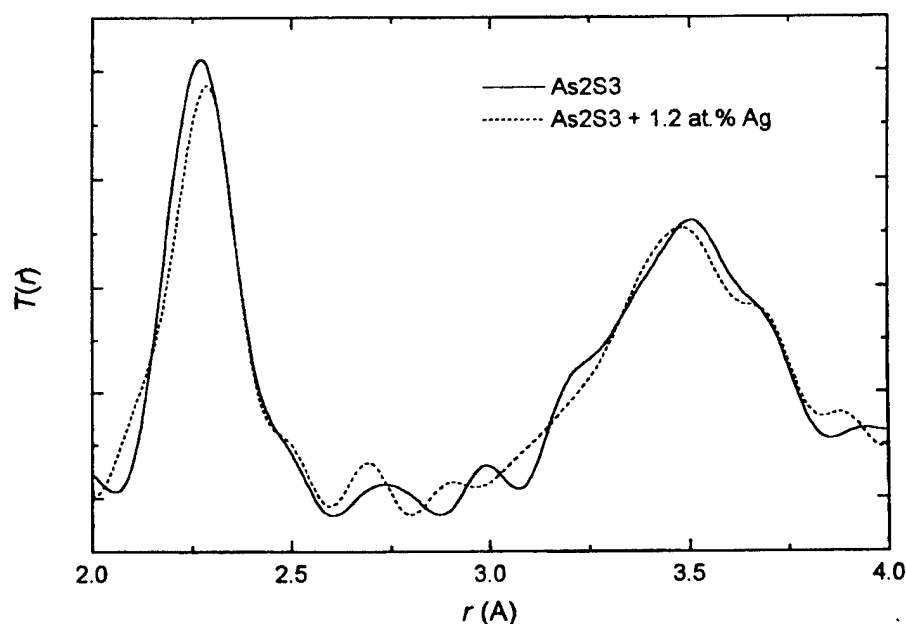


Fig. 2. Total pair correlation functions  $T(r)$  for pure  $\text{As}_2\text{S}_3$  and the  $\text{Ag}_2\text{S}$ - $\text{As}_2\text{S}_3$  glass with 1.2 at.% Ag.

## References

- [1] E. Bychkov, A. Bychkov, A. Pradel, M. Ribes, *Solid State Ionics* (1998), in press.
- [2] Yu. Drugov, A. Bolotov, Yu. Vlasov, E. Bychkov, *this conference*.
- [3] A.J.G. Ellison, R.K. Crawford, D.G. Montague, K.J. Volin, D.L. Price, *J. Neutron Res.* 1 (1993) 61.
- [4] K. Suzuya, D.L. Price, C.K. Loong, S.W. Martin, *J. Non-Cryst. Solids* 232-234 (1998) 650.

# IONIC CONDUCTIVITIES OF Na<sup>+</sup>-ION IMPLANTED SILICO-PHOSPHATE GLASS-CERAMICS

TOSHINORI OKURA and KIMIHIRO YAMASHITA\*

Department of Applied Chemistry, Faculty of Engineering, Kogakuin University, 1-24-2, Nishi-shinjuku, Shinjuku-ku, Tokyo 163-8677, Japan

\*Division of Inorganic Materials, Institute for Medical and Dental Engineering, Tokyo Medical and Dental University, 2-3-10, Surugadai, Kanda, Chiyoda-ku, Tokyo 101-0062, Japan

The glass-ceramics of the phosphorus containing Na<sub>3</sub>RSi<sub>4</sub>O<sub>12</sub>-type (R=rare earth) Na<sup>+</sup>-superionic conductors (Narpsio-V) have been developed by crystallization of glasses with the composition Na<sub>3-3x</sub>R<sub>1-x</sub>P<sub>y</sub>Si<sub>3y</sub>O<sub>9</sub>. These materials have been reported as being comparable to the conventional ceramic Na<sup>+</sup>-conductors such as NASICON, β- and β''-Aluminas. The R elements have a significant effect on the crystallization of glasses, as well as on the conduction properties. To date, polycrystalline Narpsio-V has been obtained with Sc, Y, Gd or Sm as the R element. These Narpsio-V compounds will be referred to as Nascpsio-V, Naypsio-V, Nagpsio-V and Naspsio-V, respectively, in the following. The size of the R ions has been expected to have a significant effect on the crystallization of the phase. Although the precise structure analysis of the silicophosphate Narpsio-V has not yet been completed, it is currently assumed from the analogy with Na<sub>3</sub>RSi<sub>4</sub>O<sub>12</sub> that all the R ions can be octahedrally coordinated with the non-bridging oxide ions of the (SiO<sub>4</sub>, PO<sub>4</sub>)-tetrahedra of the 12-membered rings. The reported results on the silicate ceramics show that the conductivity of Narpsio-V increases with increasing size of its R ions, giving the order Naspsio-V>Nagpsio-V>Naypsio-V>Nascpsio-V. It can be expected that Naspsio-V is the most conductive. However, this order was not always true in glass-ceramics. Although most of the Narpsio-V compounds were obtained as uncracked bulky glass-ceramics, Naspsio-V was difficult to prevent from cracking during crystallization. It was found that uncracked Nagpsio-V with larger Gd<sup>3+</sup> ions was the most conductive; however, Naspsio-V with the largest Sm<sup>3+</sup> ions was less conductive than Naypsio-V with medium Y<sup>3+</sup> ions. In the present study, the Naspsio-V ionic conductors were prepared by crystallization of glasses. The optimum conditions for crystallization were discussed with reference to the conduction properties and the preparation of uncracked glass-ceramic Naspsio-V. We consider that a material processing technique to introduce a large amount of mobile Na<sup>+</sup> ions into samples is required to realize superionic conduction in Narpsio-V compounds. Here we report that a large enhancement of electrical conductivity, probably due to Na<sup>+</sup> ions, has been obtained in the glass-ceramic Naspsio-V by ion implantation of Na<sup>+</sup> ions.

The uncracked glass-ceramic Naspsio-V superionic conductors were successfully produced by crystallization of glasses with the composition Na<sub>3-3x</sub>Sm<sub>1-x</sub>P<sub>y</sub>Si<sub>3y</sub>O<sub>9</sub>. The crystallization of the single-phase glass-ceramic Naspsio-V was dependent strongly on the concentrations of both [R] and [P] and the temperature employed for crystallization of glass specimens. The ionic conductivity of the glass-ceramic Na<sub>3</sub>Sm<sub>0.6</sub>P<sub>0.4</sub>Si<sub>2.7</sub>O<sub>9</sub> was  $2.38 \times 10^{-2}$  S/cm at 300°C. The Naspsio-V was less conductive than Naypsio-V as the grain sizes of the presented specimens were very small. Although grain growth may cause high conductivity, it was difficult to prevent the sample heated for a long time from cracking during crystallization. Large enhancement of electrical conductivity has been observed in the glass-ceramics by ion implantation of Na<sup>+</sup> ions at 200 keV to a fluence of  $1 \times 10^{15}$  cm<sup>-2</sup>. Upon implantation ionic conductivity at 300°C was drastically increased from  $2.38 \times 10^{-2}$  S/cm to  $7.15 \times 10^{-2}$  S/cm.



## EXPERIMENTAL INSIGHT INTO THE MIXED MOBILE ION EFFECT IN GLASSES

J. Swenson<sup>1</sup>, A. Matic<sup>1</sup>, A. Mandanici<sup>2</sup>, C. Gejke<sup>1</sup>, M. Cutroni<sup>2</sup> and L. Börjesson<sup>1</sup>

<sup>1</sup>Department of Applied Physics, Chalmers University of Technology,  
S-412 96 Göteborg, Sweden.

<sup>2</sup>Dipartimento di Fisica dell' Università di Messina and Istituto Nazionale per la Fisica della Materia,  
Unità di Ricerca di Messina, Salita Sperone 31-98166, Messina, Italy

An interesting phenomenon observed for ion conducting glasses is that large changes in many dynamic properties occur when a fraction of the mobile ions is substituted by another type of mobile ions. These changes are often referred to as the mixed mobile ion effect (also called the mixed alkali effect, since the effect is usually largest for alkali glasses), a topic extensively reviewed by Isard [1] and Day [2]. The largest deviations from linearity, when the concentration ratio between the two mobile ions is changed, are observed in those properties which are related to ionic transport, such as ionic conductivity, ionic diffusion, dielectric relaxation and mechanical loss and internal friction. The ionic conductivity of a mixed alkali glass may be as low as five orders of magnitude lower than that of either single alkali glass [2]. Macroscopic properties such as molar volume and density, refractive index, thermal expansion coefficient and elastic moduli usually change linearly or only slowly with composition.

Several models (see Isard [1] and Ingram [3] for reviews) have been proposed to explain the "anomalous" conductivity behaviour during the mixing of two monovalent cations. None of the models is, however, able to quantitatively explain all the properties of mixed alkali glasses, and the mixed mobile ion effect in glass remains therefore only poorly understood. In this paper we present a comprehensive series of experimental results on the mixed alkali metaphosphate glasses  $(A_2O)_x(B_2O)_{1-x}P_2O_5$ , where A and B are Li, Na or Rb. The experimental techniques we have used include neutron diffraction, Raman and IR spectroscopy, mechanical relaxation and high frequency conductivity measurements. Furthermore, we have used the reverse Monte Carlo (RMC) method [4] to produce three dimensional structural models which are quantitatively consistent with the neutron data and applied physical constraints. In this way we have been able to probe both the total atomic structure and the interactions between the network atoms and their local cationic environments.

The results (see Fig. 1 and table I for a few examples) show that the  $Li^+$ ,  $Na^+$  and  $Rb^+$  ions have distinctly different local environments and that these environments remain effectively the same for all compositions. There is a large difference between the nearest Li-O, Na-O and Rb-O distances (about 2.0, 2.4 and 2.9 Å, respectively), and also the corresponding coordination numbers are slightly different. It is therefore likely that the different sizes and characters of the chemical bondings of the different ions cause considerable mismatch energies for  $A^+$  ions on  $B^+$  sites and vice versa. In fact, *ab initio* molecular orbital calculations on mixed lithium and sodium silicate glasses have shown that the site mismatch energies are so large that jumps to dissimilar sites are unlikely to occur [5]. Furthermore, the  $A^+$  and  $B^+$  ions appear to be uniformly distributed and there are no indications for any preferred correlation between similar or dissimilar pairs of cations. Due to the uniform distribution of sites the mixed alkali effect is still present at very high frequencies (see Fig. 1(b)). This implies that the average jump distance increases and the number of energetically favourable sites decreases when a fraction of the mobile ions is substituted by another type of mobile ions. Thus, the mobility of each kind of mobile ion depends effectively on its concentration and when the two mobilities are added together the sum is producing the experimentally observed conductivity behaviour.

With the present results we are able to qualitatively understand the mobile ion effect on a purely static structural basis. We therefore propose a very simple "random distribution model", where there is no preferred correlation between similar or dissimilar pairs of cations, and no structural or dynamical alterations other than what is expected for a statistical mixing of two different ions with distinctly different local environments. The consequence of the model is that the ionic conductivity for a mixed  $A_xB_{1-x}$  glass is effectively determined by the sum of the conductivities for the corresponding single  $A_x$  and  $B_{1-x}$  glasses.

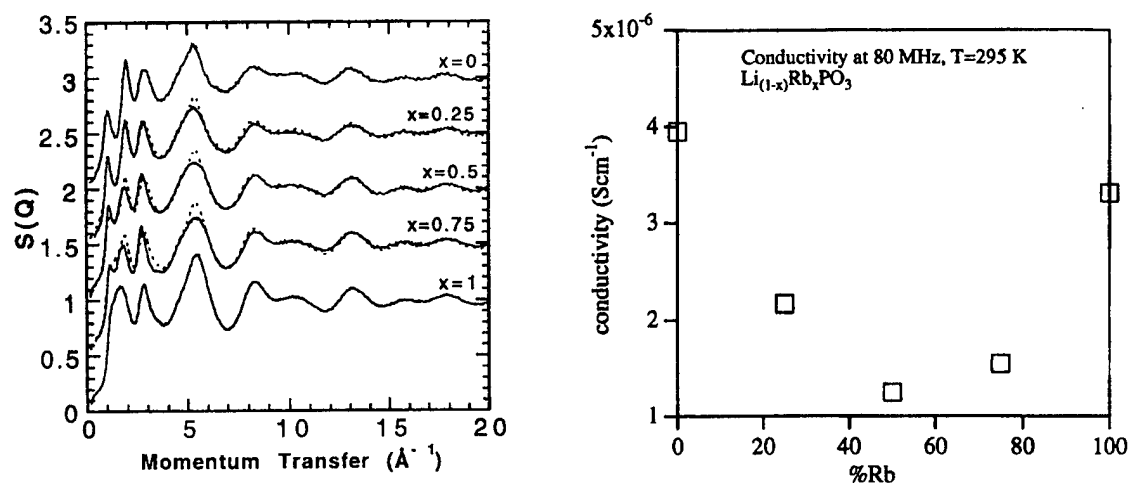


Fig. 1. (a) Experimental neutron structure factors,  $S(Q)$ , of  $\text{Li}_x\text{-Rb}_{1-x}\text{-PO}_3$  ( $x=0, 0.25, x=0.5, x=0.75, x=1$ ) glasses (solid curves) and correspondingly weighted sums from the  $S(Q)$  of the single alkali glasses (dashed curves). Consecutive curves are shifted vertically by 0.5, for clarity. The figure is taken from Ref. 6. (b) Ionic conductivity at 80 MHz and room temperature for the same glass compositions.

Table I. Peak positions and average coordination numbers for the first Li-O and Rb-O distances. The values are obtained from the experimental radial distribution functions,  $J(r)$ , see Ref. 6.

Glass composition	Distance Li-O (Å)	Coordination number Li-O	Distance Rb-O (Å)	Coordination number Rb-O
$\text{LiPO}_3$	$2.03 \pm 0.04$	$4.0 \pm 0.4$		
$\text{Li}_{0.75}\text{Rb}_{0.25}\text{PO}_3$	$2.00 \pm 0.06$	$4.5 \pm 0.6$	$3.0 \pm 0.2$	$6.1 \pm 1.5$
$\text{Li}_{0.5}\text{Rb}_{0.5}\text{PO}_3$	$1.97 \pm 0.08$	$3.4 \pm 1.0$	$2.9 \pm 0.1$	$4.7 \pm 1.1$
$\text{Li}_{0.25}\text{Rb}_{0.75}\text{PO}_3$	$1.96 \pm 0.1$	$3.2 \pm 1.8$	$2.9 \pm 0.1$	$5.3 \pm 0.8$
$\text{RbPO}_3$			$2.9 \pm 0.1$	$5.0 \pm 0.6$

## References

- [1] J. O. Isard, *J. Non-Cryst. Solids* **1**, 235 (1969).
- [2] D. E. Day, *J. Non-Cryst. Solids* **21**, 343 (1976).
- [3] M. D. Ingram, *Phys. Chem. Glasses* **28**, 215 (1987).
- [4] R. L. McGreevy and L. Pusztai, *Mol. Simul.* **1**, 359 (1988).
- [5] T. Uchino, T. Sakka, Y. Ogata and M. Iwasaki, *J. Non-Cryst. Solids* **146**, 26 (1992).
- [6] J. Swenson, A. Matic, A. Brodin, L. Börjesson and W. S. Howells, *Phys. Rev. B* **58**, 11331 (1998).

## Ag-109 NMR STUDY OF AgI-BASED GLASSES CONTAINING FROZEN $\alpha$ -AgI NANOCRYSTALS

Naoaki Kuwata<sup>1</sup>, Junichi Kawamura<sup>1</sup>, Yoshio Nakamura<sup>1</sup>,  
Kazuhiro Okuda<sup>2</sup>, Masahiro Tatsumisago<sup>2</sup>, Tsutomu Minami<sup>2</sup>

<sup>1</sup> Graduate School of Science, Hokkaido University, Sapporo 060, Japan

<sup>2</sup> Department of applied Materials Science, Osaka Prefecture University, Sakai, Osaka 599, Japan

Recently AgI-based glasses  $\text{AgI-Ag}_2\text{O-M}_x\text{O}_y$  ( $\text{M}_x\text{O}_y=\text{B}_2\text{O}_3, \text{GeO}_2$ ) containing frozen  $\alpha$ -AgI nanocrystals have been reported to show high ionic conductivity of  $10^{-2}$  to  $10^{-1} \text{ Scm}^{-1}$  at room temperature [1]. In this study the structure and ionic transport in glasses with  $\alpha$ -AgI nanocrystals were investigated by Ag-109 MAS-NMR spectroscopy. Samples were prepared by twin roller rapid quenching. Figure 1 shows the NMR spectra of  $\text{AgI-Ag}_2\text{O-B}_2\text{O}_3$ ,  $\text{AgI-Ag}_2\text{O-GeO}_2$  systems, and crystalline AgI at room temperature. For  $82\text{AgI} \cdot 13.5\text{Ag}_2\text{O} \cdot 4.5\text{B}_2\text{O}_3$  and  $79\text{AgI} \cdot 14\text{Ag}_2\text{O} \cdot 7\text{GeO}_2$ , the three NMR peaks labeled as peak ①, peak ②, and peak ③ appear at 670 to 680 ppm, 695 to 705 ppm, and 775 ppm respectively. It can be deduced that peak ①, peak ② and peak ③ can be mainly ascribed to the glass matrix,  $\alpha$ -AgI nanocrystals and crystalline  $\beta$ -AgI respectively, from a comparison with the results of X-ray diffraction and FE-SEM measurements. It is conjectured that silver ion is exchanging between glass matrix sites and  $\alpha$ -AgI sites with the exchange time about 10 ms, from the results of NMR hole-burning spectra. Therefore, it is confirmed that frozen  $\alpha$ -AgI nanocrystals in the glasses have a high ionic conductivity at room temperature. The integrated intensity of peak ② increased with increasing temperature, while that of peak ① decreased. This is consistent with the X-ray diffraction results, and can be explained as the softening of the glass matrix results the growth and the aggregation of  $\alpha$ -AgI[2].

[1] M. Tatsumisago, Y. Shinkuma and T. Minami, *Nature* **354**, 217 (1991)

[2] N. Torata, T. Saito, M. Tatsumisago and T. Minami, *J. Mater. Sci. Lett.* **16**(12), 1012 (1997)

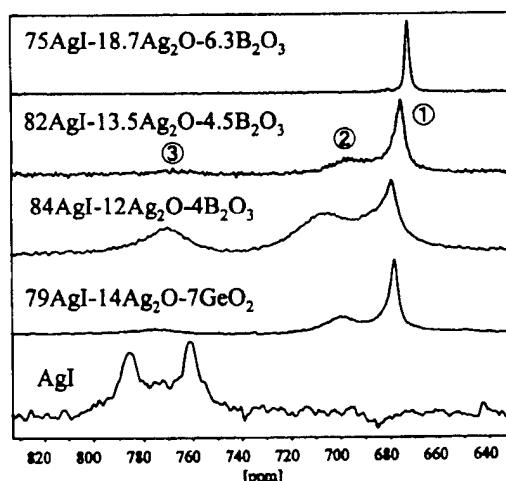


Fig. 1 Ag-109 MAS NMR spectra at room temperature.

## GENERAL FEATURES IN THE COMPOSITION DEPENDENCE OF IONIC MOBILITIES IN MIXED CATION GLASSES

B. Roling

Institut für Physikalische Chemie, Westfälische Wilhelms-Universität Münster,

Schloßplatz 4/7, 48149 Münster, Germany

Ionic mobilities in mixed alkali alkaline-earth glasses of general composition  $x A_2O \cdot (3 - x) MO \cdot n (SiO_2 \text{ or } B_2O_3)$  with  $A = Li, Na, K$  and  $M = Mg, Ca, Sr, Ba$  are studied by mechanical loss and electrical conductivity spectroscopy. For the mechanical loss experiments, we use a dynamic mechanical thermal analyser (DMTA) [1] providing a frequency range of five decades. From our experimental results, we derive general features in the composition dependence of the ionic mobilities. These features are compared with those observed for mixed alkali glasses of composition  $y A'_2O \cdot (1 - y) A''_2O \cdot n (SiO_2 \text{ or } B_2O_3)$  with  $A', A'' = Li, Na, K, Rb, Cs$  [2-6]. We, thereby, find some characteristic common features as well as some characteristic differences. The common features are the following.

- (i) For a given set of ions  $A, M, A', A''$ , the mobility of the faster ionic species (i.e. the majority species in the mixed alkali glasses and the alkali ions in the mixed alkali alkaline-earth glasses, respectively) increases with its relative concentration.
- (ii) For given relative concentrations (i.e. for given values of  $x$  and  $y$ ), the mobility of the slower species is largest, when the radius ratio  $r_{\text{slower ions}}/r_{\text{faster ions}}$  is close to unity.

The following differences are observed.

- (iii) For a given set of ions  $A, M, A', A''$ : In mixed alkali glasses, the mobility of the slower species (minority species) increases with its relative concentration. In mixed alkali alkaline-earth glasses, the mobility of the slower alkaline-earth ions decreases with increasing relative concentration.
- (iv) For given relative concentrations: In mixed alkali glasses, the mobility of the faster species increases with the radius ratio  $r_{\text{slower ions}}/r_{\text{faster ions}}$ . In mixed alkali alkaline-earth glasses, the mobility of the faster alkali ions decreases with increasing radius ratio  $r_{\text{slower ions}}/r_{\text{faster ions}}$ .

Features (ii) and (iii) point to the influence of faster ions on the mobilities of slower ions in glass. Van Ass et al. argue that within the time window of the slower ion transport process, the faster ions act as an electrical fluid so that the slower ions diffuse in a conducting medium [6]. Thus, the slower transport process can be considered an interdiffusion process between faster and slower ions, the interdiffusion coefficient being determined by the diffusion

coefficient of the slower ions. This viewpoint is confirmed by feature (ii). Interdiffusion in a static glassy network will be facilitated if the radii of the dissimilar ions are similar.

Features (i) and (iii) indicate the stronger network modifying character of alkali oxides as compared to alkaline-earth oxides. Both features can be explained by the assumption that during the glass preparation process, the glassy network adapts to the structural and chemical requirements of the mobile ions [7,8]. Therefore, in mixed alkali glasses, the network structure favors the diffusion of the majority species. On the other hand, in mixed alkali alkaline-earth glasses, the alkaline-earth ions are more tightly bound to the glassy network, and the Coulomb repulsion between them is strong. Thus, they need the dynamic assistance of faster alkali ions to become mobile. Accordingly, the mobility of both the alkali ions and the alkaline-earth ions increases with the alkali oxide content.

An explanation for feature (iv) is presently not available. We show that standard models, like e.g. free volume models or models considering the electronic polarizability of the glassy network, do not account for this feature.

## References

- [1] B. Roling, M. D. Ingram, *Solid State Ionics* **105**, 47 (1998).
- [2] H. Rötger, *Glastechnische Berichte* **31**, 54 (1958).
- [3] J. E. Shelby, D. E. Day, *J. Am. Ceram. Soc.* **52**, 169 (1969).
- [4] J. E. Shelby, D. E. Day, *J. Am. Ceram. Soc.* **53**, 182 (1970).
- [5] G. L. McVay, D. E. Day, *J. Am. Ceram. Soc.* **53**, 508 (1970).
- [6] H. M. J. M. van Ass, J. M. Stevels, *J. Non-Cryst. Solids* **16**, 27 (1974).
- [7] A. Bunde, P. Maass, *Physica A* **200**, 80 (1993).
- [8] A. Bunde, M.D. Ingram, P. Maass, *J. Non-Cryst. Solids* **172-174**, 1222 (1994).

## STUDIES ON $\text{Li}_2\text{O}-\text{Al}_2\text{O}_3-(\text{TiO}_2 \text{ OR } \text{GeO}_2)-\text{P}_2\text{O}_5$ GLASS-CERAMICS

B.V.R. Chowdari<sup>1,2</sup>, G.V. Subba Rao<sup>2</sup> and G.Y.H. Lee<sup>1</sup>

<sup>1</sup>Department of Physics, <sup>2</sup>Institute of Materials Research and Engineering  
National University of Singapore  
Singapore 119260

### Abstract

Recently there is an heightened interest in the study of fast lithium-ion conductors because of their use as solid electrolytes for an all solid lithium-rechargeable battery. Studies done so far have shown that glasses and sintered polycrystalline materials exhibit great potential as solid electrolytes. Glass-ceramics is another category of materials which may be of great potential as solid electrolytes. Lithium ion conducting glass-ceramics were obtained by heat-treatment of glasses in the systems  $\text{Li}_2\text{O}-\text{Al}_2\text{O}_3-\text{MO}_2-\text{P}_2\text{O}_5$  ( $\text{M} = \text{Ti}$  and  $\text{Ge}$ ) by Fu. The glass-ceramics are mainly composed of the crystalline conducting phase  $\text{LiM}_2(\text{PO}_4)_3$  in which the  $\text{M}^{4+}$  ions are partially substituted by  $\text{Al}^{3+}$  ions (Li-analogue of NASICON) as indicated by X-ray diffraction studies. Presently, we report the preparation and characterization of the above glass-ceramics using thermal (DSC), ionic conductivity and XPS techniques. XPS studies on the as-prepared and stress-annealed glasses and the glass-ceramics have been carried out. Results show that the O 1s spectra for all the glasses and glass-ceramics in the two systems could be deconvoluted into two peaks mainly corresponding to the non-bridging oxygen (NBO) and bridging oxygen (BO) atoms. The binding energies of other ions (Li, Ti, Ge, Al and P) have also been measured and listed. In the  $\text{Li}_2\text{O}-\text{Al}_2\text{O}_3-\text{TiO}_2-\text{P}_2\text{O}_5$  system, the Ti 2p spectra could also be deconvoluted to indicate the existence of two oxidation states of titanium, namely the +3 and the +4. The colour change that occurred during the annealing process of the  $\text{Li}_2\text{O}-\text{Al}_2\text{O}_3-\text{TiO}_2-\text{P}_2\text{O}_5$  glasses was explained using the XPS studies. Results indicate that the extent of the  $\text{Ti}^{3+}$  to  $\text{Ti}^{4+}$  oxidation process increases during annealing. The Ti 2p core levels are also characterized by high binding energies, suggesting that the  $\text{Ti}^{4+}-\text{O}$  bonds are highly ionic in character. The electrical conductivity of the systems  $\text{Li}_2\text{O}-\text{Al}_2\text{O}_3-\text{MO}_2-\text{P}_2\text{O}_5$  ( $\text{M} = \text{Ti}$  and  $\text{Ge}$ ) studied over a wide frequency and temperature range indicates good agreement with those reported in the literature. Using the glass-ceramics as solid electrolytes, Li-ion cells have been fabricated and performance tests carried out.

# DECOUPLING OF LITHIUM IONIC CONDUCTIVITY IN ORGANIC-INORGANIC COMPLEXED GLASSES

Junichi Kawamura, Takayuki Maki, Eichi Shudo and Yoshio Nakamura

Division of Chemistry, Graduate School of Science, Hokkaido University,  
Sapporo, 060-0810, Japan

Ionic conduction in organic polymer solid electrolytes is coupled to the structural  $\alpha$ -relaxation of the polymer chains; this causes the poor ionic conductivity below the glass transition temperature  $T_g$ . On the other hand, it is decoupled from the structural relaxation in inorganic fast ion conductor glasses even below  $T_g$  [1]. Present authors have been seeking for the decoupled glasses composed of inorganic salts and organic substances and reported some fast ion conductor glasses of silver and copper halides and alkylammonium iodides [2,3]. In this report, some recent results will be presented on fast lithium ionic conduction in similar glasses made of lithium halides and organic ions.

Glass forming regions were investigated in the system of LiI and some different alkylammonium iodides. In comparison with glasses containing silver or copper halides, those of lithium salts showed poor solubility and lower glass transition temperatures. However, some glass compositions were found to show rather high lithium ion conductivity even below  $T_g$  [4]. On the other hand, lithium salts were found to be easily solved in alkylamines to form glasses, although their ionic conductivity was found very small at  $T_g$  [5].

In figure 1 is shown a typical example of ionic conductivity of two glass forming salts, (i)  $\text{LiNO}_3$ -diamminopropane (DAP) and (ii) LiI-tetraethylammonium iodide (TEAI) - tetrapropylammonium iodide (TPAI), through the liquid to the glassy states.

Their ionic conductivities are almost the same at high temperature liquid state, however they are significantly different in 7 or more orders of magnitude below  $T_g$ . The relatively high conductivity in the latter is due to the lack of direct coordination bond between lithium and organic ions. The details of the glass formation and conduction mechanisms will be discussed.

## References

1. C. A. Angell, *Ann.Rev.Phys.Chem.* 43 (1992) 693./ M. McLin and C. A. Angell, *J.Phys.Chem.* 92 (1988) 2083.
2. J. Kawamura and S. Hiyama, *Solid State Ionics* 53-6 (1992) 1227-1231.
3. J. Kawamura, N. Kuwata, and Y. Nakamura, *Solid State Ionics* (1998) in press.
4. J. Kawamura, T. Maki and Y. Nakamura, to be published.
5. H. Hayashi, E. Shudo, J. Kawamura and Y. Nakamura, *J. Non-Cryst. Solids*, in press.

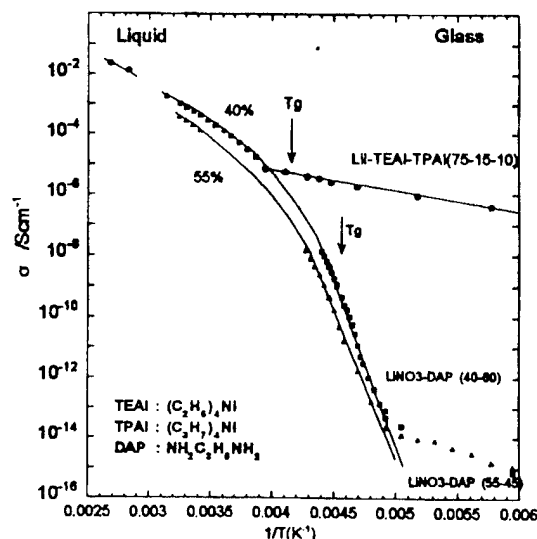


Fig. 1. Arrhenius plot of the conductivity of LiI-TEAI-TPAI system and  $\text{LiNO}_3$ -DAP in liquid and glassy states.

## EFFECT OF LOW TEMPERATURE SYNTHESIS ON IONIC TRANSPORT AND STRUCTURAL PROPERTIES OF LITHIUM SILICATE DRIED GELS

N. Satyanarayana<sup>1</sup>, Xiaogang Xie<sup>2</sup>, Steve Noding<sup>3</sup>, Rhonda Johnson<sup>1</sup>, and B. Rambabu<sup>\*1</sup>

<sup>\*</sup>Surface Science, Spectroscopy and Solid State Ionics Laboratories  
Department of Physics, Southern University, Baton Rouge, Louisiana 70813

2. Department of Geology and Geophysics, LSU, Baton Rouge, Louisiana 70802

3. Process Analytical Division, Dow Chem Company, Plaquemine, Louisiana

Lithium ion conducting silicate gels are becoming popular and increasingly useful materials as electrolytes for Li- based high energy density batteries. Recently many techniques have been developed to synthesize different types of new materials for electrochemical applications, of which sol-gel process has been gaining prominence due to its versatility in preparing electrochemical systems at low temperature with high ionic conductivity, homogeneity, purity, etc. In general, the glasses, with less dense, can be prepared by sol gel technique compared to the other conventional methods. Sol-gel process involves the transition of a system from a liquid "sol" (mostly colloidal) into a solid "gel" phase. The dried gels prepared at ambient temperature contain water molecules in which protons of the water molecule contribute to the transport and hence, the conductivity is high. However, the use of organic solvents instead of water to prepare silicate xerogels and dried xerogels at low temperature could enhance its ionic conductivity and reduce the proton conductivity. The objective of this study is to understand the effect of low temperature sol gel synthesis on the ionic transport and structural properties of Li- silicate gels in order to improve the ionic conductivity. In this work, we have prepared and characterized the Li-silicate [ $x \text{ Li}_2\text{O} - (1-x) \text{ SiO}_2$ ;  $x = 0.1$  to  $0.9$  in steps of  $0.1$ ] gels using XRD, XANES, FTIR, SEM, EDS, WDS and impedance spectroscopy techniques.

Tetraethylorthosilicate (TEOS), lithium nitrate, ethylalcohol and nitric acid precursor chemicals were used for the sol gel synthesis of lithium silicate (LS) system in different compositions. Two (A and B) different solutions were prepared independently and mixed to obtain various compositions of compounds of LS system. Solution A was prepared by dissolving the TEOS in ethylalcohol and stirred. The required amount of double distilled water was added to the solution A was prepared by dissolving the TEOS in ethylalcohol and stirred. The required amount of double distilled water was added to the solution A under continuous stirring for about 3 hours. Required amount of lithium nitrate was dissolved in distilled water to form solution the solution B and the same was added to the solution A under continuous stirring for about 2 hours, until a clear solution (SOL) was formed. The sols were cast in a beaker and allowed to form a gel at  $40^\circ\text{C}$ . A clear transparent gels were obtained within 96 hrs and were allowed to dry at  $40^\circ\text{C}$  to obtain dried gels.

All the compositions of the compounds were made into fine powders for measuring the structural and ionic transport properties of the LS system. To begin with we have measured the XANES spectra of crystalline and amorphous  $\text{SiO}_2$ . The XANES measurements were performed at the DCM beamline of the storage ring of the Center for Advanced Microstructure and Devices (



CAMD) in Baton Rouge. Figure 1 shows the typical Si-K - XANES spectra of SiO<sub>2</sub>. At the high energy of the white line where shape resonance as e.g. in crystalline quartz are expected and the absorbance is absolutely structureless indicating that the samples are to a high degree amorphous i.e. they have no medium range order.

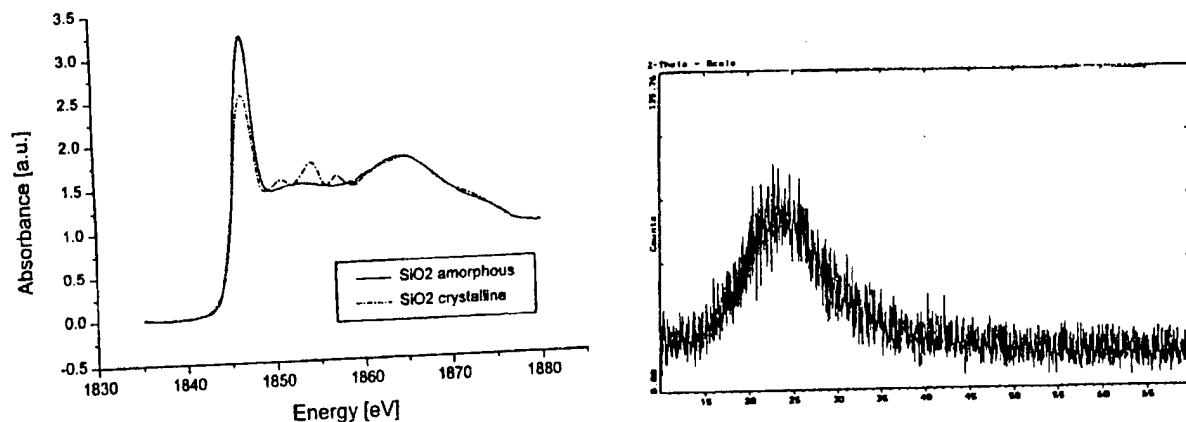
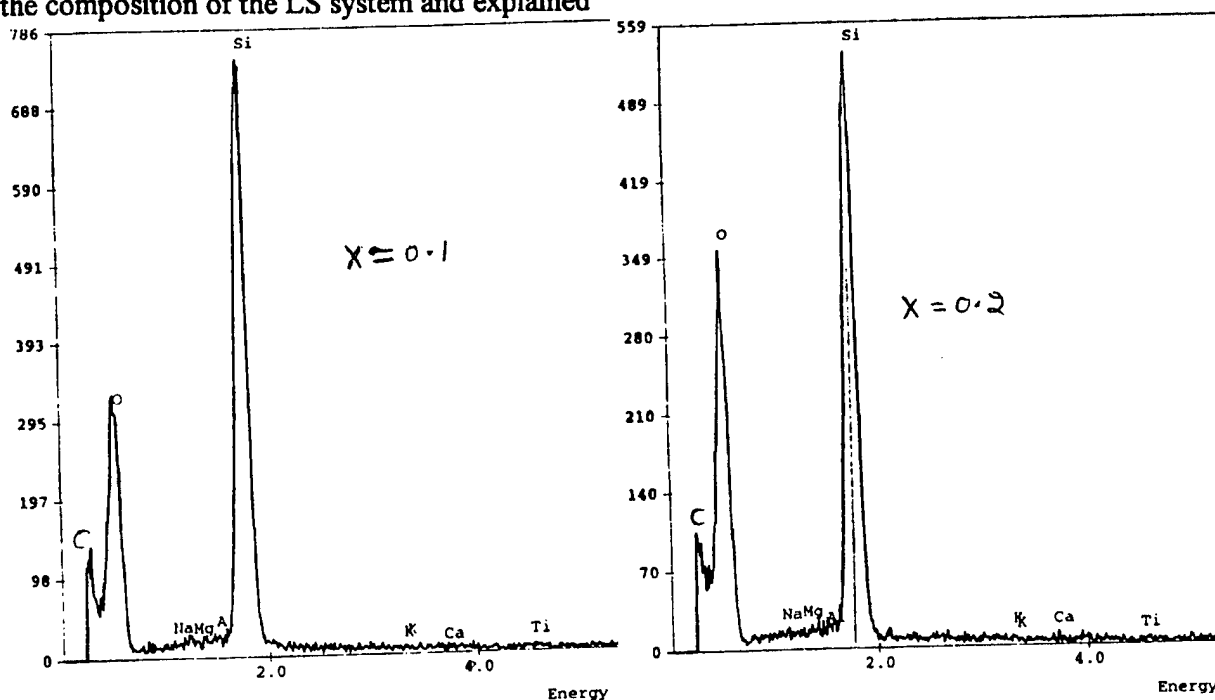


Figure 2 shows the XRD of  $x$  Li<sub>2</sub>O - (1- $x$ ) SiO<sub>2</sub>;  $x = 0.1$  reveal the amorphous nature. Figure 3 shows the EDS spectra of the LS ( $x = 0.1$  and  $0.2$ ). The chemical composition of the Si of LS system was estimated. The electrical behavior and ionic transport of the LS system were estimated by measuring the impedance spectra. Structural and ionic transport properties were correlated with the composition of the LS system and explained.



**B.Rambabu** acknowledge the US.DOE Office of Energy Research, the RCS program for HBCUs at LLNL, and the HBCU PV program at NREL for supporting this work through a grant GE FG 05-95ER45549 and subcontracts. NS thanks University of Pondicherry, India for allowing him to avail the exchange visitor program opportunity at Southern University, USA.

EFFECT OF MIXED GLASS FORMERS ON IONIC CONDUCTIVITY OF A NEW  $\text{Ag}^+$  ION  
CONDUCTING SUPERIONIC GLASS :  $0.7[0.75\text{AgI}:0.25\text{AgCl}]:0.3[\text{Ag}_2\text{O}:\{xB_2\text{O}_3:(1-x)\text{MoO}_3\}]$

R.C. Agrawal<sup>\*</sup>, R. Kumar<sup>1</sup>, M.L. Verma<sup>2</sup>

Solid State Ionics Research Laboratory, School of Studies in Physics,  
Pt. Ravishankar Shukla University, Raipur - 492010, INDIA

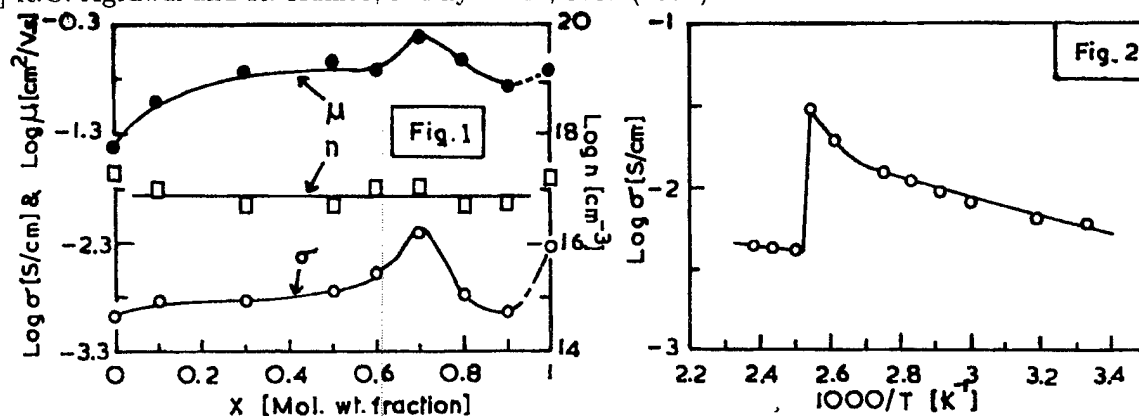
<sup>1</sup> Department of Physics, Dr. H.S. Gaur Univ., Sagar - 470003, INDIA

<sup>2</sup> Govt. D.B. Girls P.G. College, Raipur - 492001, INDIA

Preparation of a quaternary fast  $\text{Ag}^+$  ion conducting glass system :  $0.7[0.75\text{AgI}:0.25\text{AgCl}]:0.3[\text{Ag}_2\text{O}:\{xB_2\text{O}_3:(1-x)\text{MoO}_3\}]$  by rapid quenching method is reported. A new compound : 'a quenched  $[0.25\text{AgI}:0.25\text{AgCl}]$  mixed system/solid solution', recently investigated as a better alternate to the conventional salt  $\text{AgI}$ , has been used as host matrix salt [1]. The effect of 'mixed formers' on the conductivity, was studied by mixing two glass formers  $\text{B}_2\text{O}_3/\text{MoO}_3$  in different compositions ( $0 \leq x \leq 0.9$ ) and keeping  $\text{Ag}^+$  ion salt concentration constant. Fig. 1 shows the variation of electrical conductivity ( $\sigma$ ), ionic mobility ( $\mu$ ) and mobile ion concentration ( $n$ ) as a function of  $x$ . The conductivity increases as  $x$  increases from 0, attains a peak value at  $x = 0.7$ , then decreases afterwards for  $x = 0.8$  &  $0.9$ . The composition :  $0.7[0.75\text{AgI}:0.25\text{AgCl}]:0.3[\text{Ag}_2\text{O}:\{0.7\text{B}_2\text{O}_3:0.3\text{MoO}_3\}]$  exhibited highest conductivity ( $\sigma_{27^\circ\text{C}} \sim 6 \times 10^{-3} \text{ S.cm}^{-1}$ ), and is referred to as 'optimum conducting composition (OCC)'. The conductivity value of the OCC is very close to that of pure borate glass system :  $0.7[0.75\text{AgI}:0.25\text{AgCl}]:0.3[\text{Ag}_2\text{O}:\text{B}_2\text{O}_3]$ , discovered recently in the present laboratory [2]. The enhancement in the room temperature conductivity of the pure molybdate glass system :  $0.7[0.75\text{AgI}:0.25\text{AgCl}]:0.3[\text{Ag}_2\text{O}:\text{MoO}_3]$  as a result of substitution of second glass former ( $\text{B}_2\text{O}_3$ ) is certainly a 'mixed glass formers effect'. According to model suggested, mixing the two glass formers results into structural changes of the glass network which in turn gives rise to more opening for mobile  $\text{Ag}^+$  ions. Hence,  $\mu$  increases while  $n$  remains unaltered. The reason for conductivity increase in the present system can clearly be attributed to the increase in  $\text{Ag}^+$  ion mobility ( $\mu$ ), as obvious from Fig. 1.  $\mu$  varied analogously as  $\sigma$ , having maxima at  $x = 0.7$  while  $n$  remained almost constant. Fig. 2 shows the ' $\log \sigma$  vs  $1/T$ ' variation for the OCC.  $\sigma$  increases linearly with temperature upto  $90^\circ\text{C}$  then decreased sharply. This temperature probably corresponds to the glass transition temperature ( $T_g$ ) of the system which would be confirmed by DTA(DSC) studies. Activation energy  $E_a \sim 0.109 \text{ eV}$ , computed from the linear portion of the ' $\log \sigma$  vs  $1/T$ ' plot, is very low and hence, indicative of easy ion transport in this system.

[1] R.C. Agrawal, R.K. Gupta, R. Kumar and A. Kumar, J. Mater. Sci. 29, 3673 (1994).

[2] R.C. Agrawal and R. Kumar, J. Phys. D 27, 3431 (1994).



## STUDIES OF SILVER-VANADATE-PHOSPHATE GLASSES BY IMPEDANCE, EPR AND RAMAN SPECTROSCOPY METHODS

J.E.Garbarczyk, P.Machowski, M.Wasiucionek, L.Tykowski, R.Bacewicz, A.Aleksiejuk  
Institute of Physics, Warsaw University of Technology, Koszykowa 75, 00-662 Warsaw,  
Poland

Glasses of the  $\text{AgI-Ag}_2\text{O-V}_2\text{O}_5\text{-P}_2\text{O}_5$  system are a family of interesting materials exhibiting, in general, mixed electronic-ionic electrical conduction. Compositions of high content of AgI and low content of  $\text{V}_2\text{O}_5$  exhibit pure ionic conduction. However in our last papers [1,2] we have shown, that by an appropriate choice of proportions of the glass constituents it is possible to prepare a whole range of electrical conductors: from purely ionic, through mixed electronic-ionic to almost purely electronic. Such a possibility is interesting from the point of view of both basic research and perspectives of practical applications.

In this paper reported are the results of studies of glasses of new compositions described by the formula  $x\text{AgI} \cdot (1-x)[0.15\text{Ag}_2\text{O} \cdot 0.70\text{V}_2\text{O}_5 \cdot 0.15\text{P}_2\text{O}_5]$  for  $0 \leq x \leq 0.30$ . Electronic component of electrical conduction in these glasses is due to the presence of aliovalent vanadium ions  $\text{V}^{4+}$  and  $\text{V}^{5+}$ , which serve as centers for electron hopping. The presence of a glass modifier  $\text{Ag}_2\text{O}$  and a dopant - AgI is responsible for the ionic part of electrical conduction (via  $\text{Ag}^+$  ions).

The glasses were prepared by *press-quenching* method. X-ray diffraction patterns confirmed the amorphous state of the samples. The characteristic temperatures of glass transition  $T_g$  and recrystallization  $T_c$  determined by DTA scans depend on the composition and lie in the following temperature ranges:  $230^\circ\text{C} \leq T_g \leq 244^\circ\text{C}$  and  $250^\circ\text{C} \leq T_c \leq 295^\circ\text{C}$ .

The EPR studies have revealed the existence of a strong spectral line, at a  $g$  value of 1.97, due to unpaired  $3d^1$  electrons of  $\text{V}^{4+}$  centers. The line intensity depends on the  $\text{V}_2\text{O}_5$  content in the glasses under study. The line exhibits superfine splitting which is the most pronounced in glasses characterized by  $x = 0.20$  (Fig.1).

Raman scattering studies have shown the presence of broad bands characteristic for disordered (amorphous) solids (Fig. 2). Observed Raman spectra show features typical for vanadate chains ( $600 - 950 \text{ cm}^{-1}$ ), orthophosphate groups (around  $1000 \text{ cm}^{-1}$ ) and mixture of metavanadate and phosphate species [3].

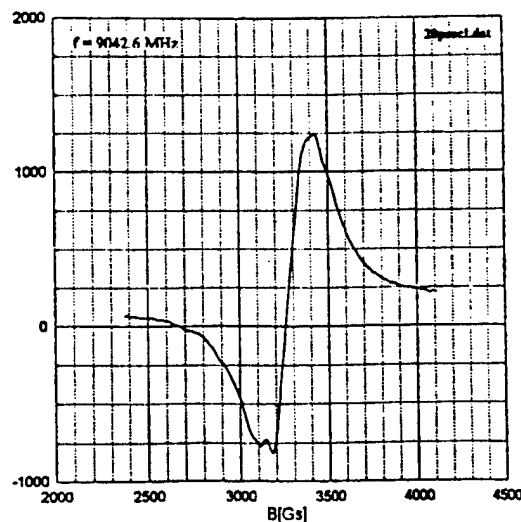


Fig. 1. EPR line of the glass of composition  $20 \text{ AgI} \cdot 12 \text{ Ag}_2\text{O} \cdot 56 \text{ V}_2\text{O}_5 \cdot 12 \text{ P}_2\text{O}_5$

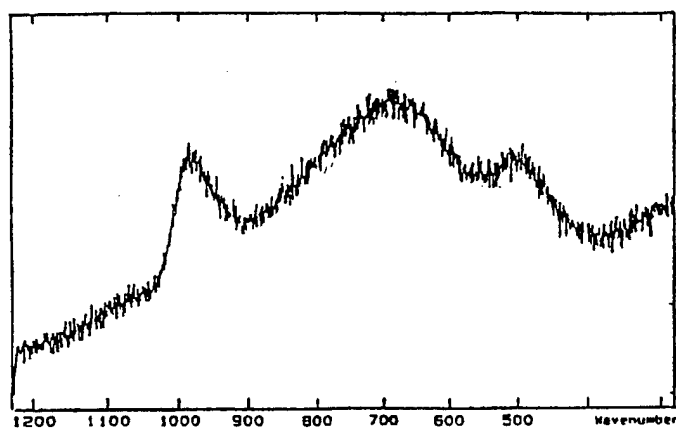


Fig. 2. Raman spectrum of the glass of composition 30 AgI·11 Ag<sub>2</sub>O·49 V<sub>2</sub>O<sub>5</sub>·10 P<sub>2</sub>O<sub>5</sub>

tact effects at the metallic electrode - glass interface [4]. We have shown that these side-effects can be reduced by extensive polishing of glass surfaces before applying the electrodes or appropriate annealing of the samples at about 200°C for several hours (Fig.3).

It seems that annealing improves contact between sample and electrode by decrease of glass viscosity and/or by diffusion of metallic electrode species into the glass surface. Contact effects can also be reduced if impedance spectra are measured using 4-probe instead of 2-probe configuration.

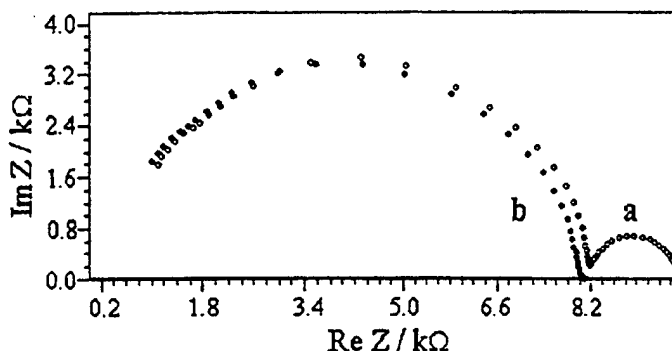


Fig. 3. Impedance spectrum of the electronic-conductive glass 80 V<sub>2</sub>O<sub>5</sub>·20 P<sub>2</sub>O<sub>5</sub>: a) before annealing, b) after annealing (frequency range: 1 mHz - 10 MHz)

The interpretation of impedance, EPR and Raman data will be given in the full paper.

### References

1. M.Wasiucioneck, J.E.Garbarczyk, B.Wnętrzewski, P.Machowski, W.Jakubowski, *Solid State Ionics*, **92**, 155 (1996).
2. J.E.Garbarczyk, M.Wasiucioneck, P.Machowski, W.Jakubowski, *Solid State Ionic* (1999), accepted for publication.
3. R.Lewandowska, K.Krasowski, R.Baciewicz, J.Garbarczyk, *Solid State Ionics* (1999), accepted for publication.
4. Jin-Ha Kwang, K.Kirkpatrick, T.Mason, E.Garboczi, *Solid State Ionics*, **98**, 93 (1997).

## AVERAGE ELECTRONEGATIVITY, MEDIUM-RANGE-ORDER AND IONIC CONDUCTIVITY IN SUPERIONIC GLASSES

Masaru ANIYA

Department of Physics, Faculty of Science, Kumamoto University,  
Kumamoto 860-8555, Japan

Superionic conducting glasses have attracted considerable interest for the last several years. Investigation of ionic conductivity in vitreous materials is interesting from both academic and practical points of view. The practical aspect results from their use as key materials for solid state electrochemical technology. Superionic conducting glasses have several advantages over crystalline electrolytes such as physical isotropy, the absence of grain boundaries, continuously variable composition, and good workability. The academic interest arises from the fact that the mechanism of ion transport in glasses remains poorly understood. In particular, the evolution of parameters such as concentration and mobility of free carriers, as a function of composition and temperature, have not been definitively established. Furthermore, the role of the medium range order on the ionic conductivity is not clear yet. In the present contribution, the following two topics will be discussed in order to understand the behavior of superionic conducting glasses.

### 1) Average electronegativity and chemical scaling of the ionic conductivity

The elemental parameters such as valence, atomic size, electronegativity, and ionicity are directly associated with the character of the chemical bond. The use of these parameters has provided a mean for classifying many basic properties of molecules and solids. Based on the idea that the ionic transport properties depend on the nature of the chemical bond of the materials, a parameter that describes the average electronegativity of a glass is introduced. Such a parameter that is defined as a generalization of the principle of electronegativity equalization [1], is written in terms of the chemical composition and the atomic nodal radii of the constituent elements of the glass. When the ionic conductivity of the glasses are plotted as a function of the average electronegativity and scaled, a universal behavior as shown in Fig.1 is found [2]. The same average electronegativity provides also a universal behavior of the network expansion by doping. This finding has much in common with the recent work showing the correlation between the free volume and the ionic conductivity in superionic glasses [3].

### 2) Correlation between medium range structure and ionic conductivity

The presence of the intermediate range order in glasses is demonstrated for instance, through characteristic signatures such as first sharp diffraction peak (FSDP) in the neutron and X-ray diffraction patterns. Recently, the author has found an interesting correlation between the ionic

conductivity and the position of the FSDP as shown in Fig.2. By analyzing such correlation, the role of the medium range structure on the ionic conductivity can be isolated. The analysis shows that the medium range structure influences primarily the activation energy for the ionic transport.

### References

- [1] R.T.Sanderson: *Chemical Bonds and Bond Energy* (Academic Press, 1976).
- [2] M.Aniya: *Solid State Ionics* **79** (1995) 259.
- [3] J.Swenson and L.Borjesson: *Phys.Rev.Lett.* **77** (1996) 3569.

**Fig. 1** Normalized ionic conductivity as a function of the normalized average electronegativity of the glass.

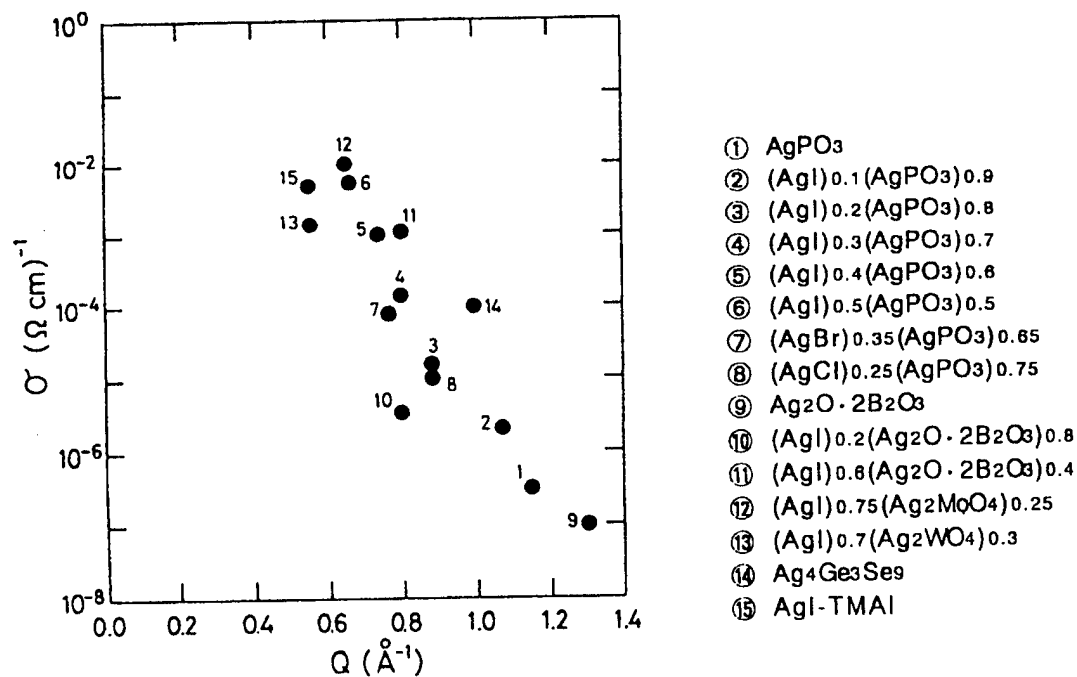
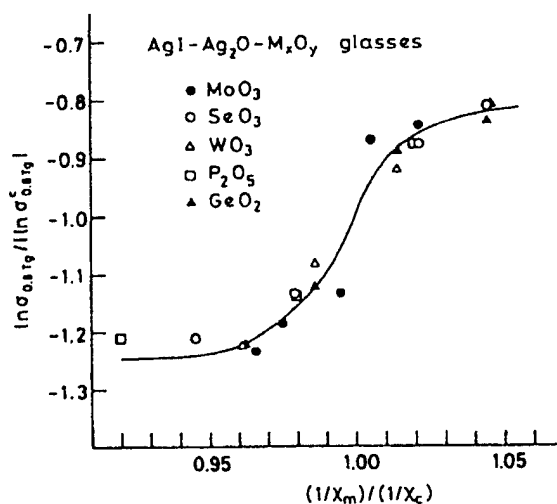


**Fig. 2** Relationship between the ionic conductivity of glasses at room temperature and the position of the First Sharp Diffraction Peak.

## Percolation transition in Ag<sub>2</sub>S-As<sub>2</sub>S<sub>3</sub> glasses: a <sup>110</sup>Ag tracer diffusion study

Yu. Drugov<sup>1</sup>, A. Bolotov<sup>1</sup>, Yu. Vlasov<sup>1</sup> and E. Bychkov<sup>2</sup>

<sup>1</sup> St. Petersburg University, 199034 St. Petersburg, Russia

<sup>2</sup> Université du Littoral, 59140 Dunkerque, France

Recently, two distinctly different transport regimes at low and high silver concentrations were found for a number of homogeneous Ag<sup>+</sup> ion-conducting chalcogenide glasses using <sup>110</sup>Ag tracer diffusion experiments and conductivity measurements [1,2]. At low concentrations ( $x < 3$  at.% Ag), a power-law composition dependence of the ionic conductivity  $\sigma_i(x)$  and silver tracer diffusion coefficient  $D_{Ag}(x)$

$$\sigma_i(x) \propto x^t \text{ and } D_{Ag}(x) \propto x^{t_D} \quad (t_D = t - 1, \text{ according to the Nernst-Einstein relation})$$

with temperature-dependent power law exponent  $t \propto T_0/T$ , was found to describe precisely the conductivity and diffusion data over 2-2.5 orders of magnitude in the silver concentration and 3-5 orders of magnitude in the ionic conductivity (2-3 orders of magnitude in the  $D_{Ag}$ ). This transport regime can be explained by modified classical percolation in the critical region just above the percolation threshold and/or by the dynamic structure model [3]. Conductivity measurements on homogeneous Ag<sub>2</sub>S-As<sub>2</sub>S<sub>3</sub> glasses were undertaken [2] to distinguish between these two approaches. It was found that the critical exponent  $t$  is markedly lower for the arsenic sulphide glasses with reduced network dimensionality caused by quasi-2D AsS<sub>3</sub> pyramidal units compared to that for Ag<sub>2</sub>S-GeS-GeS<sub>2</sub> glasses whose 3D network is formed by distorted GeS<sub>4</sub> tetrahedra. This result was expected in the modified classical percolation model but not predicted in the dynamic structure approach. Nevertheless, the conductivity results could lead to incorrect conclusions because of possible influence of the residual electronic conductivity at low and extremely low Ag concentrations. To complete these measurements, <sup>110</sup>Ag tracer diffusion experiments were performed in a wide composition range from  $4 \times 10^{-4}$  to 33.3 at.% Ag.

Typical <sup>110</sup>Ag tracer diffusion isotherm in the percolation domain (0.01 – 3 at.% Ag) is shown in Fig. 1 for the investigated arsenic sulphide glasses plotted together with that for the germanium sulphide system [1]. In accordance with the conductivity data [2] ( $t < 1$  above the room temperature), the diffusion critical exponent  $t_D = t - 1 < 0$ . In contrast, the  $t_D$  values are positive for the Ag<sub>2</sub>S-GeS-GeS<sub>2</sub> glasses which are characterised by  $t > 1$  at  $T < 550$  K [1].

Comparison of the conductivity and tracer diffusion results distinctly shows that the Ag<sub>2</sub>S-As<sub>2</sub>S<sub>3</sub> glasses in the percolation domain are nearly pure Ag<sup>+</sup> ion conductors. The silver ion transport number  $t_{Ag^+} \approx 0.8$  for the most diluted glass ( $x = 0.012$  at.% Ag) in this region. The Haven ratio decreases monotonically from  $H_R \approx 1$  to  $H_R \approx 0.8$  with increasing Ag content from 0.012 to 1.2 at.% Ag (Fig. 2). On the contrary, concentrated homogeneous glasses in the network-controlled domain ( $x = 20$ -33.3 at.% Ag) are characterised by essentially constant values of  $H_R = 0.25$ -0.30.

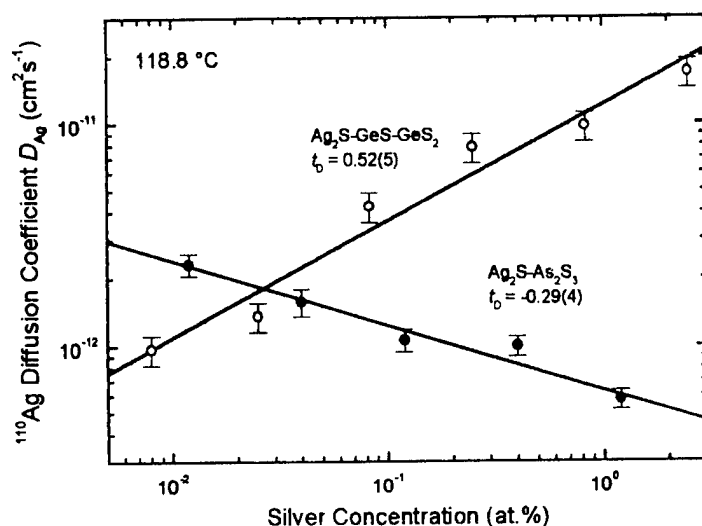


Fig. 1.  $^{110}\text{Ag}$  tracer diffusion isotherm at 118.8 °C for the  $\text{Ag}_2\text{S-As}_2\text{S}_3$  (present work) and  $\text{Ag}_2\text{S-GeS-GeS}_2$  [1] glasses in the percolation domain.

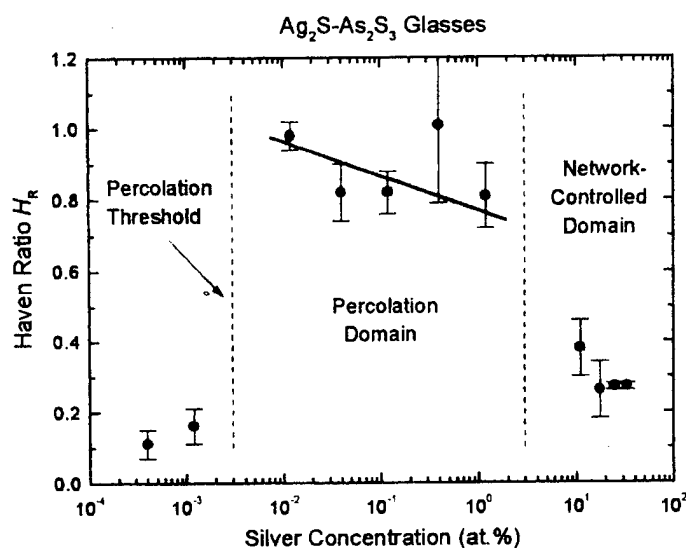


Fig. 2. Haven ratio  $H_R$  for the  $\text{Ag}_2\text{S-As}_2\text{S}_3$  glasses.

The percolation threshold in the  $\text{Ag}_2\text{S-As}_2\text{S}_3$  system is found to be at ca.  $3 \times 10^{-3}$  at.% Ag. Below this percolation threshold, the glasses are predominantly hole conductors with  $t_{\text{Ag}^+} \approx 0.1\text{-}0.2$ .

## References

- [1] E. Bychkov, V. Tsegelnik, Yu. Vlasov, A. Pradel, M. Ribes, *J. Non-Cryst. Solids* **208** (1996) 1.
- [2] E. Bychkov, A. Bychkov, A. Pradel, M. Ribes, *Solid State Ionics* (1998), in press.
- [3] A. Bunde, M.D. Ingram, P. Maass, *J. Non-Cryst. Solids* **172-174** (1994) 1222.



## Mixed anionic effect in the glasses of the system

### $\text{Pb}(\text{F},\text{Cl})_2 - \text{PbO} \cdot \text{SiO}_2$

Sokolov I.A.\*, Murin I.V.\*, Wiemhöfer H.-D.\*\* and Pronkin A.A.\*

\*St. Petersburg State University, Universitetsky pr. 2, Petrodvoretz, 198904 Russia.

\*\*Münster University, Münster, 148149 Germany

A large amount of publications is devoted to the investigation of mutual influence of different alkali ions upon the physico-chemical properties of oxide glasses - so called mixed alkali effect. But up to now there does not exist unified theory of this phenomenon. There are a number of hypotheses explaining different "sides" of this effect.

The investigation of anionconducting glasses was started by the experimental proof of fluorine ionic nature of the conductivity of the glasses based on  $\text{BeF}_2$  [1]. The mutual influence of different halogen ions on the physico-chemical properties of halogen-containing oxyphosphate glasses was investigated for the first time in [2]. The study of the dependence of electrical properties of glasses of the system  $(0.2-x)\text{BaF}_2 \cdot x\text{BaCl}_2 \cdot 0.8\text{Ba}(\text{PO}_3)_2$  on  $\beta_2$  (where  $\beta_F = [\text{F}]/[\text{F}] + [\text{Cl}]$ ) showed the existence of the minimum at the dependence  $\lg\sigma = f(\beta_F)$  and of the maximum at  $E_\sigma = f(\beta_F)$ . In accordance with mixed alkali effect this effect was named mixed anionic effect. The interpretation of mixed anionic effect in halogen-containing phosphate glasses is rather difficult because the transfer of electric current in them is fulfilled simultaneously by the fluoride, chloride ions and protons which are the current carriers in alkali-free phosphate glasses of the type  $\text{Me}_x\text{O}_y \cdot \text{P}_2\text{O}_5$ .

In halogen-containing lead silicate glasses already the addition of ~20mol% of  $\text{Pb}(\text{Hal})_2$  (where Hal - F,Cl) brings to the situation that only the fluoride and chloride ions take part in the electric current transfer. Thus, the glasses of the system  $\text{Pb}(\text{F},\text{Cl})_2 - \text{PbO} \cdot \text{SiO}_2$  with the overall content of the halogenides of lead 23.4mol% were chosen as the subjects of investigation. It will allow to estimate the influence of the equimolar exchange of  $\text{PbF}_2$  for  $\text{PbCl}_2$  upon the physico-chemical properties of glasses, which is not being complicated by the existence of proton conductivity. Total bulk concentration of halogen ions in the glasses of the systems under consideration is practically constant and is  $2.05 \cdot 10^{-2} \text{ mol/cm}^3$ . At the same time there appears a minimum at the dependence  $\lg\sigma = f(\beta_F)$ , and a maximum at the dependence  $E_\sigma = f(\beta_F)$ . For all the investigated compositions  $\eta_F + \eta_{\text{Cl}} = 1.00$ , where  $\eta$  is the true transport number of the corresponding ion (within the limits of experimental error this does not exceed ~5%). Unlike the glasses of the system  $(0.2-x)\text{BaF}_2 \cdot x\text{BaCl}_2 \cdot 0.8\text{Ba}(\text{PO}_3)_2$  the mixed anionic effect in halogen-containing lead silicate glasses (at the temperature 200°C) is much less. Thus, for halogen-containing phosphate glasses with the bulk concentration of fluoride and chloride ions  $\sim 7 \cdot 10^{-4} \text{ mol/cm}^3$  the drop of electroconductivity (in comparison to chlorine-containing glasses) is  $\Delta \lg\sigma \approx 3$ , and  $E_\sigma \approx 0.6 \text{ eV}$  (transport numbers of the anions of fluoride in fluorophosphate glasses are equal to 0.81, and in chlorine-containing glasses is 0.34). The change of these values in halogen-containing lead silicate glasses comprises  $\Delta \lg\sigma \approx 1$ , and  $\Delta E_\sigma \approx 0.15 \text{ eV}$ . Such serious differences in the value of mixed anionic effect in halogen-containing phosphate and silicate glasses can be explained by the fact that in phosphate glasses three types of current carriers participate in the current transfer. The ions formed with the dissociation of structurally bonded water influence strongly the electric conductivity of halogen-containing phosphate glasses. This fact explains that electric conductivity of chloride-containing glass is higher than that of fluoride-containing. The content of structurally bonded hydrogen in phosphate glasses is higher than that

in the silicate and it is confirmed by the values of the transport numbers. The lead halogenides form easily the double salts of the type  $x\text{PbF}_2 \cdot y\text{PbCl}_2$  in which the strength of bonds for fluoride and chloride ions does not differ significantly. The participation of fluoride and chloride ions in the processes of the ionic conductivity is defined according to the experimentally obtained concentration dependence  $\eta_F = f(\beta_F)$ .

This work was supported by INTAS-RFBR 95-0090.

### References

1. K.K. Evstrop'ev, B.S. Kondrat'eva, G.T. Petrovsky Dokl. Acad. Nauk, USSR, (Russian) **169**, 382 (1966).
2. A.A.Pronkin, K.K. Evstrop'ev Glass Physics and Chemistry (Russian) **4**, 240, (1978).
3. I.A.Sokolov, I.V.Murin, H.-D.Wiemhöfer and A.A.Pronkin Glass Physics and Chemistry (Russian) **24**,509 (1998).

# FREE VOLUME AND DISSOCIATION EFFECTS IN FAST ION CONDUCTING GLASSES

J. Swenson, A. Matic, C. Gejke and L. Börjesson

Department of Applied Physics, Chalmers University of Technology, S-412 96 Göteborg, Sweden.

By adding 19%  $\text{PbI}_2$  to the  $\text{AgPO}_3$  glass the conductivity of the mobile  $\text{Ag}^+$  ions increases by more than four orders of magnitude to nearly  $10^{-2}$  S/cm [1]. Thus, it is evident that the immobile  $\text{Pb}^{2+}$  and I ions affect the microscopic structure of the glass in a way that leads to an increased mobility of the silver ions. By studying the structural changes induced by  $\text{PbI}_2$  we aim to find structural properties associated with high ionic conductivity.

In this paper we have investigated the fast ion conducting glasses  $(\text{PbI}_2)_{0.1}-(\text{AgPO}_3)_{0.9}$  and  $(\text{PbI}_2)_{0.1}-(\text{AgI})_{0.1}-(\text{AgPO}_3)_{0.8}$  using neutron and x-ray diffraction and Raman and infrared experiments. Furthermore, we have applied the reverse Monte Carlo (RMC) modelling method [2] to produce structural models in quantitative agreement with both the x-ray and the neutron data, as well as with the experimental density and applied physical constraints. The structural results have been compared with corresponding results for  $\text{AgPO}_3$  [3] as well as for AgI doped phosphate, borate and molybdate glasses [3-6].

Figure 1 shows the experimental neutron and x-ray structure factors for  $\text{AgPO}_3$  [3],  $(\text{PbI}_2)_{0.1}-(\text{AgPO}_3)_{0.9}$  and  $(\text{PbI}_2)_{0.1}-(\text{AgI})_{0.1}-(\text{AgPO}_3)_{0.8}$ . It is particularly useful to combine neutron and x-ray diffraction results for the present glasses due to that the various pair correlations are very differently weighted in the neutron and x-ray data. The neutron data is dominated by internal P-O correlations, whereas in the x-ray data the total scattering from the salt ions is strongly weighted. The almost identical high Q range of the neutron data of the glasses in Fig. 1(a) indicates that the short range P-O structure is basically unaffected by the introduced salt ions. However, from the changes in the low Q range it is evident that the salt ions affect the intermediate range order of the P-O network. The x-ray data in Fig. 1(b) show significant changes on doping. However, this is expected even for minor structural changes, due to the large x-ray scattering coefficients for Pb, I and Ag correlations. A detailed analysis of the neutron and x-ray data shows that both the  $\text{Pb}^{2+}$  and I ions affect the coordination of the  $\text{Ag}^+$  ions. The coordination of  $\text{Pb}^{2+}$  to oxygen is also confirmed by the Raman measurements where bands associated with symmetric stretching P-O vibrations of the network change in both position and intensity due to the replacement of some  $\text{Ag}^+$  by  $\text{Pb}^{2+}$  at the non-bridging oxygen sites.

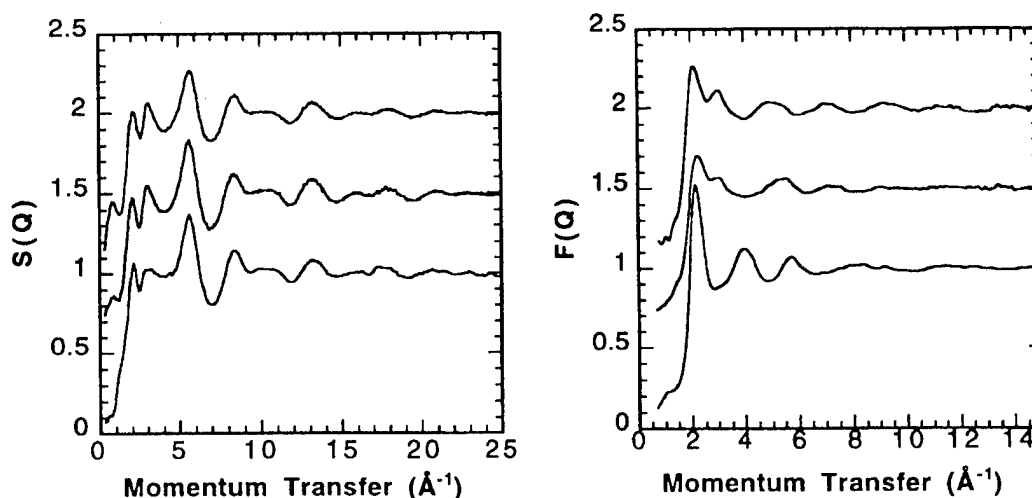


Fig. 1. Experimental neutron (a) and x-ray (b) structure factors for (in ascending order)  $\text{AgPO}_3$  [3],  $(\text{PbI}_2)_{0.1}-(\text{AgPO}_3)_{0.9}$  and  $(\text{PbI}_2)_{0.1}-(\text{AgI})_{0.1}-(\text{AgPO}_3)_{0.8}$ .

The RMC results show that the  $\text{Pb}^{2+}$  and  $\text{I}^-$  ions expand the  $\text{PO}_4$ -network, which opens doorways and creates new pathways in the structure suitable for ion conduction. Furthermore, the main part of the  $\text{Pb}^{2+}$  ions coordinate to oxygens and in that way reduces the average Ag-O coordination number (see Fig. 2). The  $\text{I}^-$  ions play a similar role by expanding the host glass and coordinating to  $\text{Ag}^+$  ions, leading to a further decrease of the Ag-O coordination. The introduced  $\text{Pb}^{2+}$  and  $\text{I}^-$  ions promote an increased free volume and a dissociation of  $\text{Ag}^+$  ions from oxygens, which are likely to decrease both the strain energy and the electrostatic binding energy of the  $\text{Ag}^+$  ions and thereby also the total activation energy for  $\text{Ag}^+$  migration. The present study confirms the earlier findings [7] that an open structure, with a large accessible free volume for the mobile ions, is a key parameter (direct or indirect) for high ionic conductivity.

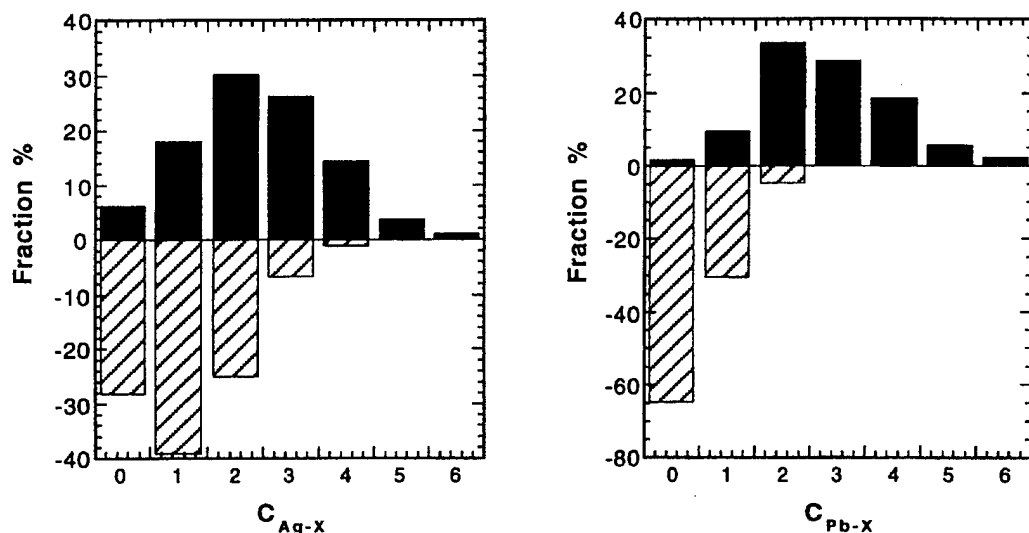


Fig. 2. Distributions of Ag-X and Pb-X coordination numbers calculated from the RMC configuration of  $(\text{PbI}_2)_{0.1}-(\text{AgI})_{0.1}-(\text{AgPO}_3)_{0.8}$ . The positive bars are coordinations to O, whereas the negative bars (for clarity) are coordinations to I. Note that the  $\text{Pb}^{2+}$  ions seem to have a larger tendency of coordinating to O than the  $\text{Ag}^+$  ions.

## References

- [1] J. P. Malugani, R. Mercier and M. Tachez, *Solid State Ionics* **21**, 131 (1986)
- [2] R. L. McGreevy and L. Pusztai, *Mol. Simul.* **1**, 359 (1988)
- [3] J. Wicks, L. Börjesson, R.L. McGreevy, W.S. Howells, and G. Bushnell-Wye, *Phys. Rev. Lett.* **74**, 726 (1995)
- [4] J. Swenson, L. Börjesson, R.L. McGreevy and W. S. Howells, *Phys. Rev. B* **55**, 11236 (1997)
- [5] J. Swenson, R.L. McGreevy, L. Börjesson, J. D. Wicks and W. S. Howells, *J. Phys: Cond. Matter* **8**, 3545 (1996)
- [6] J. Swenson, R.L. McGreevy, L. Börjesson and J. D. Wicks, *Solid State Ionics* **105**, 55 (1998)
- [7] J. Swenson and L. Börjesson, *Phys. Rev. Lett.* **77**, 3569 (1996)

## STRUCTURAL INVESTIGATION OF TIN OXIDE GLASSES

C. Gejke, A. Matic and L. Börjesson

Department of Applied Physics, Chalmers University of Technology, S-412 96 Göteborg, Sweden

Tin-based amorphous composite oxide (TCO) has recently received much attention as the active component in anode materials for rechargeable lithium ion batteries [1]. These materials show up to 50% better reversible capacity compared to the commonly used graphite electrodes. One of the disadvantages with TCO is the large irreversible capacity due to the reaction of lithium with oxygen. It is suggested that the lithium ions, when inserted into the material, react irreversibly with the oxygen in the tin oxide to form  $\text{Li}_2\text{O}$  [2]. Thereby metallic tin is also formed, and it aggregates in clusters which are dispersed in a matrix consisting of  $\text{Li}_2\text{O}$ . The reversible reaction is believed to be the alloying between metallic tin and lithium. Aggregation of tin atoms can be controlled by the voltage range during cycling and the morphology of the material.

Knowledge of the structure and morphology of the tin-based amorphous composite oxide is vital for understanding the behaviour during cycling. This would aid the work to optimise the glass structure so as to minimise the large irreversible capacity by decreasing the size of the tin clusters formed during lithium insertion. The aim of this work is to determine the structure and the changes during lithium insertion.

One glass that can be used besides the original TCO system is  $\text{Sn}_2\text{BPO}_6$ , which has almost the same capacity. The structure of any of these glasses is at present not well understood. The assumption is that the boron oxide and phosphorous oxide form a host network containing dispersed tin oxide. Both boron and phosphorous oxide are known to be excellent glass formers and the coordinating structures of these glass systems are rather well known.

To investigate the structure we have used infrared and Raman spectroscopy. The different structural units in the glass give rise to characteristic vibrational bands that can be probed with these techniques. The interaction with the tin atoms (and lithium in lithiated glasses) will influence the position and intensity of these bands. In this work we present results from infrared and Raman spectroscopy experiments on a series of glasses with various compositions of tin, boron and phosphorous oxides.

### Reference

- [1] Y. Idota, T. Kubota, A. Matsufuji, Y. Maekawa, T. Miyasaka, *Science* **276** (1997) 1395.
- [2] I.A. Courtney and J.R. Dahn, *J. Electrochem. Soc.* **144** (1997) 2045

PREPARATION, CHARACTERIZATION AND IMPEDANCE STUDIES OF SUPERION CONDUCTING AgI-Ag<sub>2</sub>O-CrO<sub>3</sub>-V<sub>2</sub>O<sub>5</sub> GLASSY SYSTEM

N. Satyanarayana<sup>1,3</sup>, R. Patchaammale<sup>1</sup>, P. Muralidharan<sup>1,2</sup>,  
M. Venkateswarlu<sup>1</sup> and B. Rambabu<sup>3</sup>, <sup>1</sup>Department of Physics  
Pondicherry University, Pondicherry 605 014 India,  
<sup>2</sup>Department of Chemistry, Pondicherry University,  
Pondicherry, 605 014, India, <sup>3</sup>Surface Science,  
Spectroscopy and Solid State Ionics Laboratory,  
Department of Physics, Southern University and  
A & M College, Baton Rouge, 70813, LA, USA

Superionic conducting silver glasses are finding promising applications, as solid electrolyte materials in various ionic devices, like solid state batteries, sensors, timers, displays, fuel cells, capacitors, etc. Because, these glasses have high ionic conductivity and stability than that of their crystalline counterparts at ambient temperature [1]. In this paper, we report the preparation, characterization and impedance study of superionic conducting silver chromovanadate (SCV) glassy system.

Different compositions of D%AgI M%Ag<sub>2</sub>O F%[(x)CrO<sub>3</sub> + (1-x)V<sub>2</sub>O<sub>5</sub>] ; D=60%, M/F=2.0 and x= 0.1 to 0.9 in steps of 0.1, system was prepared by melt quenching technique. Analar grade AgI, Ag<sub>2</sub>O, CrO<sub>3</sub> and V<sub>2</sub>O<sub>5</sub> precursor chemicals were ground into fine powders, rinsed with acetone and dried them around 150 °C for few hours. Later, all the precursors were mixed well in a quartz crucible and kept in high temperature furnace. The temperature is raised to its molten state and the melt was stirred to ensure the homogeneity. After 20 minutes, the molten liquid was rapidly quenched in liquid nitrogen to form bulk glassy compounds.

The X-ray diffraction spectra were recorded for all the compositions of the SCV system and confirmed the glassy nature and hence, glass forming island was estimated. Similarly glass transition temperature (T<sub>g</sub>) and formation of ion clusters of Ag<sup>+</sup>, I<sup>-</sup>, chromate and vandate were respectively estimated by recording DSC and IR spectra for all the prepared SCV compounds. Impedance studies were carried out in the frequency range 20Hz to 1MHz at different temperatures and estimated the bulk conductivity and the electrical behavior of the SCV glassy system. The highest conductivity was found to be of the order of 10<sup>-2</sup>

$\text{cm}^{-1} \Omega^{-1}$ . The obtained DSC, IR and conductivity results with the composition of SCV glassy system were correlated and also explained, using the existing theoretical models, the conduction mechanism for the highest conducting SCV system [2]. The detailed results will be presented and discussed.

References :

[1] T. Minami, K. Imazawa, and M. Tanaka, J. Non Cryst. Solids 42, 469 (1980)

[2] M. Glass, J. Applied Physics, 51 3756 (1980)

Acknowledgement : NS acknowledges UGC & DST Govt. of India, for granting research projects and PM, RP & MV are grateful to CSIR for awarding SRFs & RA. Also authors thank Dr. S.C.A.S.V.S.Rao, CWMF, IGCAR for providing IR facilities.

## SYNTHESIS AND CHARACTERISATION OF $\text{CuI} \cdot \text{Cu}_2\text{O} \cdot \text{TeO}_2 \cdot \text{MO}_3$ ( $\text{M} = \text{Mo}$ and $\text{W}$ ) GLASS SYSTEMS

B.V.R. Chowdari<sup>1,2</sup>, K.L.Tan<sup>1</sup> and L.Fang<sup>1</sup>

<sup>1</sup>Department of Physics, <sup>2</sup>Institute of Materials Research and Engineering,  
National Univ. of Singapore, Singapore 119260

### Abstract

Cuprous ion conducting glasses are relatively a new class of solid electrolytes. After having successfully made and studied the  $\text{CuI} \cdot \text{Cu}_2\text{O} \cdot \text{TeO}_2$  glass system, we have directed our efforts to synthesize glasses based on ternary oxide system  $\text{Cu}_2\text{O} \cdot \text{TeO}_2 \cdot \text{MO}_3$  ( $\text{M} = \text{Mo}$  and  $\text{W}$ ) doped with  $\text{CuI}$ . The purpose of our present study is to make glass electrolytes with large amount of amorphous  $\text{CuI}$  phase and, if possible, even with stabilised  $\alpha\text{-CuI}$  crystallites which are believed to have good ionic conductivity.

The glasses were prepared according to the formula  $z\text{CuI} \cdot (1-z)\{x\text{Cu}_2\text{O} \cdot (1-x)[y\text{TeO}_2 \cdot (1-y)\text{MO}_3]\}$  ( $\text{M} = \text{Mo}$ ,  $z = 0.3, 0.4$  and  $0.5$  and  $\text{M} = \text{W}$ ,  $z = 0.3$  and  $0.4$  respectively). The glasses exhibit phase separation and for most glass compositions  $\alpha\text{-CuI}$  crystallites are stabilised at the room temperature. Both XRD and high-resolution transmission electron microscopy confirmed the presence of  $\alpha\text{-CuI}$  crystallites. The highest ionic conductivity at room temperature is  $8.08 \times 10^{-3} \text{ Scm}^{-1}$  for the composition  $0.3\text{CuI} \cdot 0.28\text{Cu}_2\text{O} \cdot 0.21\text{TeO}_2 \cdot 0.21\text{MoO}_3$ . The Arrhenius plots show a break and jump in the temperature range 280-290 K with conductivity in the range  $10^{-4}$ - $10^{-5} \text{ Scm}^{-1}$ . The conductivity behaviour in the low temperature region ( $< 280 \text{ K}$ ) may be due to the electronic conduction and in the high temperature region ( $> 290 \text{ K}$ ) due to mixed (electronic+ionic) conduction. DSC studies do not show any phase transition in the region 280-290 K. FTIR spectroscopic study indicates that the IR bands of glasses are not affected by the presence of  $\text{CuI}$ , and the structural units in the glasses are found to be  $\text{TeO}_3$ ,  $\text{TeO}_4$ ,  $\text{MoO}_4$ ,  $\text{MoO}_6$  (or  $\text{WO}_4$  and  $\text{WO}_6$ ). XPS studies show that both systems ( $\text{M} = \text{Mo}$  and  $\text{W}$ ) contain copper in two oxidation states and the fractional areas  $[\text{Cu}^+ / (\text{Cu}^+ + \text{Cu}^{2+})]$  are in the region 0.36-0.61 as deduced from  $\text{Cu } 2p_{3/2}$  and  $\text{Cu } 2p_{1/2}$  spectra. The average fraction of non-bridging oxygen (NBO) is about 0.59, which is higher than that (0.36) in the corresponding oxide glasses (without  $\text{CuI}$ ). This indicates that the bonds between oxygen and Cu atoms are formed on the interface of oxide glass matrix and amorphous  $\text{CuI}$  phases.



## **EFFECT OF $\text{Na}_2\text{O}$ / $\text{Fe}_2\text{O}_3$ ON THE PHYSICAL PROPERTIES OF A BORATE GLASS SYSTEM**

**K.SHREEKRISHNA KUMAR**

School of Technology and Applied Sciences  
Mahatma Gandhi University, Marmanam. P.O.  
Kottayam, Kerala, India - 686 561.

### **Abstract:**

The cabal glass system ( $\text{CaO}$  -  $\text{B}_2\text{O}_3$  -  $\text{Al}_2\text{O}_3$ ) is characterised by an exceptionally high resistance. Efforts were made to reduce the resistance of this glass system to a reasonable extend by introducing an alkali oxide ( $\text{Na}_2\text{O}$ ) or a transition metal oxide ( $\text{Fe}_2\text{O}_3$ ) as the fourth component. The work also aims at the investigation on the dielectric properties of the glass system so as to explore the possibility of producing a capacitor with variable dielectric constants which may find application in impulse generators.

We also have made an attempt to compare the conductivity behaviour of the alkali containing glass system and the transition metal oxide containing glass system with the help of the existing models for ionic conductivity and polaromic hopping. The results have shown that the conductivity and the structure of the cabal glass system can be changed to a reasonable extend by the incorporation of the alkali / transition metal oxide content.

## Tracer diffusion studies of ion-conducting chalcogenide glasses

E. Bychkov

*Université du Littoral, 59140 Dunkerque, France*

Tracer diffusion measurements allow independent and complementary information on long-range ion transport in glasses to be obtained. These experiments are rather rare for ion-conducting chalcogenide glasses although the existing diffusion data exhibit a lot of interesting examples of the combined (conductivity  $\sigma$  and diffusion  $D$ ) studies and even the phenomena which could not be observed by using the electrical measurements alone. Some selected topics of the tracer diffusion experiments in chalcogenide glasses will be given in the present paper.

### Percolation transition in $\text{Ag}^+$ conducting glasses

$^{110}\text{Ag}$  tracer diffusion experiments and electrical measurements show 2 distinctly different transport regimes at low ( $< 1\text{-}3\text{ at.}\%$ ) and high ( $> 8\text{-}10\text{ at.}\%$ ) silver concentrations for  $\text{Ag}_2\text{S-GeS-GeS}_2$ ,  $\text{Ag-Ge-Sb-Se}$  and  $\text{Ag}_2\text{S-As}_2\text{S}_3$  homogeneous glasses [1-3]. A power-law composition dependence of  $\sigma_i(x)$  and  $D_{\text{Ag}}(x)$

$$\sigma_i(x) \propto x^t \text{ and } D_{\text{Ag}}(x) \propto x^{t-1}$$

with temperature-dependent power-law exponent  $t \propto T_0/T$ , is a characteristic feature of the ion transport in diluted and extremely diluted glasses. The Haven ratio  $H_R$  decreases in this region from  $\approx 1$  to  $0.3\text{-}0.4$  with increasing  $x$  indicating an increased correlation of the ion movement. A remarkably low value of the percolation threshold ( $x_c \approx 3 \times 10^{-5}$ ), modified classical percolation and dynamic structure model [4] approaches will be discussed within the context of the diffusion data. Some evidences of important structural changes in the percolation domain using direct (neutron diffraction [5]) and indirect (Mössbauer spectroscopy) measurements will also be given.

### Degenerated mixed cation effect in $(\text{Cu}^+, \text{Ag}^+)$ conducting glasses

In contrast to usual behaviour of mixed cation glasses (large deviations from additivity with a pronounced minimum at the conductivity isotherms and a diffusivity crossover when guest cations reduce the mobility of ions coming from the host matrix), the  $\text{CuI-AgI-As}_2\text{Se}_3$  [6] and  $\text{Cu-Ag-As-Se}$  glassy systems exhibit exciting differences in the transport properties. First, the ionic conductivity increases monotonically by four orders of magnitude when  $\text{CuI}$  is gradually replaced by  $\text{AgI}$ , without any minimum at intermediate concentrations. Secondly, no diffusivity crossover was observed in the two systems which were studied using both  $^{64}\text{Cu}$  and  $^{110}\text{Ag}$  tracers. Moreover, the  $^{64}\text{Cu}$  tracer diffusion coefficient *increases* by a factor of 20 to 50 when copper is substituted by silver. The obtained results will be discussed from the structural point of view [7,8] as well as taking into account possible electronic structure effects of the two mobile ions.

## Non-Arrhenius vs Arrhenius behaviour of superionic glasses at high temperatures

Recently, a non-Arrhenius temperature dependence of d.c. ionic conductivity was found for a number of superionic glasses [9,10]. It was interesting to prove whether similar phenomena could be observed in a tracer diffusion experiment. The temperature dependence of  $D_{Ag}$  for a  $0.5Ag_2S-0.5GeS_2$  glass, measured using thin-layer absorption method which is particularly useful for highly conducting superionic solids [11], clearly show a nearly perfect Arrhenius-type fit over the entire investigated temperature range (Fig. 1(a) [12]). The observed discrepancies between  $\sigma_i(T)$  and  $D_{Ag}(T)$  will be discussed.

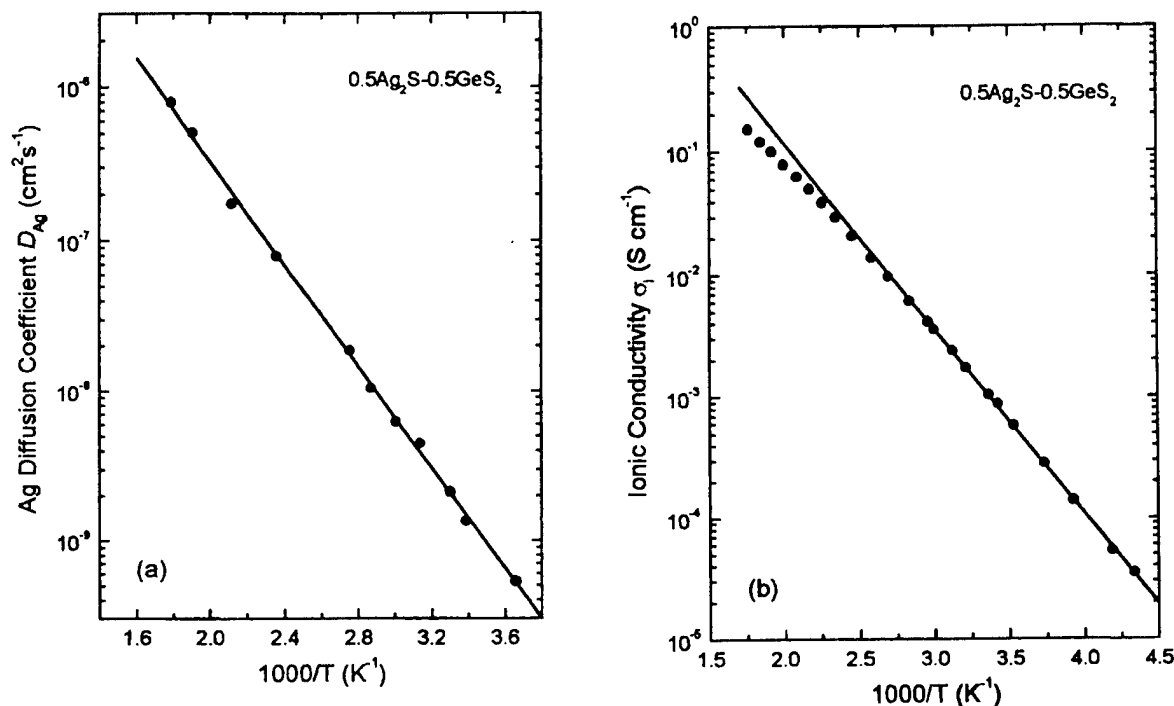


Figure 1. (a) Silver diffusion coefficient  $D_{Ag}$  [12] and (b) ionic conductivity  $\sigma_i$  for  $0.5Ag_2S-0.5GeS_2$  glass.

## References

- [1] E. Bychkov, V. Tsegelnik, Yu. Vlasov, A. Pradel, M. Ribes, *J. Non-Cryst. Solids* **208** (1996) 1.
- [2] E. Bychkov, A. Bychkov, A. Pradel, M. Ribes, *Solid State Ionics* (1998), in press.
- [3] Yu. Drugov, A. Bolotov, Yu. Vlasov, E. Bychkov, *this conference*.
- [4] A. Bunde, M.D. Ingram, P. Maass, *J. Non-Cryst. Solids* **172-174** (1994) 1222.
- [5] E. Bychkov, D.L. Price, *this conference*.
- [6] A. Bolotov, E. Bychkov, Yu. Gavrilov, Yu. Grushko, A. Pradel, M. Ribes, V. Tsegelnik, Yu. Vlasov, *Solid State Ionics* (1998), in press.
- [7] P.S. Salmon, J. Liu, *J. Non-Cryst. Solids* **205-207** (1996) 172.
- [8] E. Bychkov, A. Bolotov, P. Armand, A. Ibanez, *J. Non-Cryst. Solids* **232-234** (1998) 314.
- [9] J. Kincs, S.W. Martin, *Phys. Rev. Lett.* **76** (1996) 70.
- [10] M. Ribes, G. Taillades, A. Pradel, *Solid State Ionics* **105** (1998) 159.
- [11] Yu. Vlasov, E. Bychkov, V. Tsegelnik, Y.M. Ben-Shaban, *Radiokhimiya* **37** (1995) 281.
- [12] V. Tsegelnik, *private communication*.

STUDY OF TERNARY LITHIUM ION CONDUCTING Li<sub>2</sub>O-V<sub>2</sub>O<sub>5</sub>-P<sub>2</sub>O<sub>5</sub> SYSTEM

N.Satyanarayana<sup>1,3</sup>, P.Muralidharan<sup>1,2</sup>, R.Patcheammalle<sup>1</sup>,  
M.Venkateswarlu<sup>1</sup>, P.Sambasiva Rao<sup>2</sup>, and B.Rambabu<sup>3</sup>,

<sup>1</sup>Department of Physics, Pondicherry University, Pondicherry,  
605 014, India, <sup>2</sup>Department of Chemistry, Pondicherry  
University, Pondicherry 605 014, India and <sup>3</sup>Surface Science,  
Spectroscopy and Solid State Ionics Laboratory, Department of  
Physics, Southern University and A & M College, Baton Rouge,  
70813, LA, USA

In recent advances, the fast ion conducting glassy materials are of great interest in the field of Solid State Ionics. The lithium based glassy materials are finding wide range of applications in fabricating solid state batteries and various other electrochemical devices [1]. Hence, we report the preparation, structural and electrical properties of ternary Li<sub>2</sub>O-V<sub>2</sub>O<sub>5</sub>-P<sub>2</sub>O<sub>5</sub> (LVP) system.

Analar grade chemicals were used in the preparation of 60%Li<sub>2</sub>O 40%[(X)V<sub>2</sub>O<sub>5</sub>+(1-X)P<sub>2</sub>O<sub>5</sub>]; X=0.1 to 0.9 in steps of 0.1 (LVP), system by varying formers [X V<sub>2</sub>O<sub>5</sub> + (1-X)P<sub>2</sub>O<sub>5</sub>] composition. The precursors were ground into fine powders, rinsed with acetone and dried around 150°C for few hours. Then all the precursors were mixed well in the platinum crucible and kept in high temperature furnace. The temperature was raised to its molten state and the molten liquid was rapidly quenched on to stainless steel plate to obtain a pure glass.

The prepared compounds were characterised by XRD, IR & DSC techniques and also impedance studies were carried out as a function of frequency and temperature. The XRD results showed that all the compositions of LVP system formed the glass. From IR, DSC and Impedance studies respectively estimated the formation of network, glass transition temperature (T<sub>g</sub>) and the bulk conductivity of the LVP system. The observed variation of conductivity with formers composition was explained using the existing theoretical "RANDOM SITE" model [2]. The obtained results will be presented and discussed in detailed.

References:

- [1].B.V.R.Chowdari and S.Radhakrishna (Eds), Solid State Ionic Devices, World Scientific Co., Singapore (1988)
- [2].M.Glass, J.Applied Physics, 51 3756 (1980)

Acknowledgements: NS acknowledges UGC & DST Govt. of India, for granting research projects, PM, RP & MV are grateful to CSIR for awarding SRFs & RA. Also authors thank Dr. S.C.A.S.V.S.Rao, CWMF, IGCAR for providing IR facilities.

## POLYMERIC MIXED IONIC ELECTRONIC CONDUCTORS

Ilan Riess, Physics Department, Technion-Israel Institute of Technology, Haifa 32000, Israel.

Polymers can be made ionic conductors by doping with salt. Conjugated polymers can be made electron and hole conductors by proper doping. Since many of the larger dopants are usually mobile, a mixed ionic electronic conductor (MIEC) results rather than a pure electron/hole conductor. Enhanced mixed conductivity is obtained by mixing the two types of doped polymers. When applying a voltage on such a MIEC, both the ionic defects and the electrons/holes move.

It is possible to control the electron, hole and mobile ion concentrations and thus their conductivities. It is therefore possible to tailor MIECs that conform to different, interesting defect models. The experimental flexibility when working with polymers allows to examine theories developed for MIECs for which it is difficult to find model inorganic materials. In particular it is possible to prepare MIECs that form, under the applied voltage, pn junctions of rare nature, i.e. locally neutral ones. This type of pn junctions may be optically active and emit light. The whole operation takes place at room temperature.

Two such types of MIECs have been identified for which experimental data exists. In one the mobile ion concentration is high compared to the electron/hole one, in the second it is comparable to the electron/hole concentration. Both may emit light.

Electron injection at the electrodes is an inherent part in the operation and analysis of galvanic cells based on polymers operating at room temperature. To achieve injection thin films and high electric fields are used.

The discussion here will refer to electron/hole conducting, ion conducting and MIEC polymers. It will also discuss galvanic cells based on such polymers, in particular the MIEC ones. The I-V relations of galvanic cells based on polymer MIECs and the distribution of local defects as well as internal electric fields will be discussed in detail for the two model polymers for which experimental data exists.

# ION DIFFUSION AND NETWORK RELAXATION IN POLYMER ELECTROLYTES: A MONTE CARLO STUDY

O. Dürr<sup>1</sup>, W. Dieterich<sup>1</sup> and A. Nitzan<sup>2</sup>

<sup>1</sup>Fakultät für Physik, Universität Konstanz, D-78457 Konstanz, Germany

<sup>2</sup>School of Chemistry, The Sackler Faculty of Science, Tel Aviv University, Tel Aviv 69978, Israel

Certain polymer chain molecules carrying an electronegative atom in their repeat unit are known to dissolve some salts, and the resulting polymer-salt solutions may show significant ionic conductivities. Well-known examples are PEO (polyethylene-oxid)-based electrolytes, where cations tend to bind to the electronegative oxygen atoms. Several experimental studies have revealed a subtle interplay between ionic and polymeric degrees of freedom [1,2]. For example, with increasing ion concentration the polymer network becomes more rigid because of crosslinking of chains via the cations. This manifests itself in an increased glass transition temperature and in a reduction of ionic mobilities.

The aim of our work is to discuss these effects in a lattice model of an ion-polymer mixture. Originally the model has been proposed by Olender and Nitzan for the description of ion solvation and association equilibria [3]. By Monte Carlo simulation we obtain ion and chain diffusion constants, both of which closely follow a Vogel-Tammann-Fulcher (VTF)-law [4,5]. Further emphasis is put on the question of model calculations under constant pressure, an issue which is particularly important when we compare systems with different salt concentrations. Separate Monte Carlo simulations of a constant pressure ensemble are presented, and the resulting equation of state is compared with predictions of the quasi-chemical approximation. Combination of these results with dynamical simulations at constant volume finally leads to a description of diffusion and network relaxation properties at constant pressure. This enables us to discuss the behaviour of ionic mobilities and the salt-induced change in the glass transition temperature, which are found to agree with the experimental trends.

- [1] J. Fan, R. F. Marzke, E. Sanchez and C. A. Angell, *J. Non-Cryst. Solids*, **172-174**, 1178 (1994).
- [2] S. Lascaud, M. Perrier, A. Vallee, S. Besner and J. Prudhomme, *Macromolecules*, **27**, 7469 (1994).
- [3] R. Olender and A. Nitzan, *J. Chem. Phys.*, **100**, 705 (1994); **101**, 2338 (1994).
- [4] P. Pendzig, W. Dieterich and A. Nitzan, *J. Non-Cryst. Solids* **235-237**, 748 (1998).
- [5] W. Dieterich, O. Dürr, P. Pendzig, A. Bunde and A. Nitzan, submitted to *Physica A*.

A SYMMETRY-BASED ANALYSIS OF RAMAN AND INFRARED SPECTRA IN THE  
COMPOUNDS (POLYETHYLENE OXIDE)<sub>3</sub>LiCF<sub>3</sub>SO<sub>3</sub> AND (POLYETHYLENE  
OXIDE)<sub>3</sub>NaCF<sub>3</sub>SO<sub>3</sub>

Christopher Rhodes and Roger Frech  
Department of Chemistry and Biochemistry  
University of Oklahoma

The recent availability of the detailed crystal structures of the two compounds (polyethylene oxide)<sub>3</sub>LiCF<sub>3</sub>SO<sub>3</sub> [1] (space group P2<sub>1</sub>/a) and (polyethylene oxide)<sub>3</sub>NaCF<sub>3</sub>SO<sub>3</sub> [2] (space group P2<sub>1</sub>/c) from x-ray diffraction studies has provided an unprecedented look at the local environment of the ions and the conformation of the poly(ethylene oxide) backbone. These data have led us to a symmetry-based vibrational analysis of the normal modes of each compound. A standard factor group analysis predicts a much larger number of normal modes than are seen in the Raman and infrared spectra of either compound, suggesting that the chains which run through the unit cells are highly vibrationally decoupled. This observation leads, in turn, to a helical group analysis which considers only the vibrations of a single chain.

A number of internal vibrational modes of the CF<sub>3</sub>SO<sub>3</sub><sup>-</sup> anion are especially sensitive to the degree and nature of anion-cation interactions, including the SO<sub>3</sub> symmetric stretching mode,  $\nu_s(\text{SO}_3)$  [3], and the CF<sub>3</sub> symmetric deformation mode,  $\delta_s(\text{CF}_3)$  [4]. There are striking differences between the Raman scattering spectra and the infrared transmission spectra in both spectral regions in each of the two compounds. We will describe the number of  $\nu_s(\text{SO}_3)$  and  $\delta_s(\text{CF}_3)$  normal modes predicted by both a factor group analysis and a helical group analysis in each compound. We will also describe the spectral activities of these modes predicted by the group theory analyses and compare these predictions to Raman scattering and infrared transmission data of each compound.

The group theoretical analyses can be modified to describe the number and spectral activities of polyethylene oxide (PEO) chain modes. Therefore we will also consider the CH<sub>2</sub> rocking modes, since the frequencies of these modes are particularly sensitive to the local conformation of the polymer, specifically the O-C-C-O torsional angle. A helical group analysis establishes that in (PEO)<sub>3</sub>LiCF<sub>3</sub>SO<sub>3</sub> there are twelve rocking modes and in (PEO)<sub>3</sub>NaCF<sub>3</sub>SO<sub>3</sub> there are four rocking modes. These modes are simultaneously infrared and Raman active in each compound. A comparison of the infrared and Raman spectral data will be made for this region and discussed in terms of the group theory predictions.

Our examination of the  $\text{CH}_2$  rocking spectral region in  $(\text{PEO})_3\text{LiCF}_3\text{SO}_3$ ,  $(\text{PEO})\text{NaCF}_3\text{SO}_3$ , and crystalline PEO (for comparison) shows that there are significantly fewer modes present than are expected from a helical group analysis. As an example, the infrared spectra of the three compounds are shown in the accompanying figure. In this paper we will discuss the vibrational decoupling which is suggested by the data shown in the figure and additional spectral data.

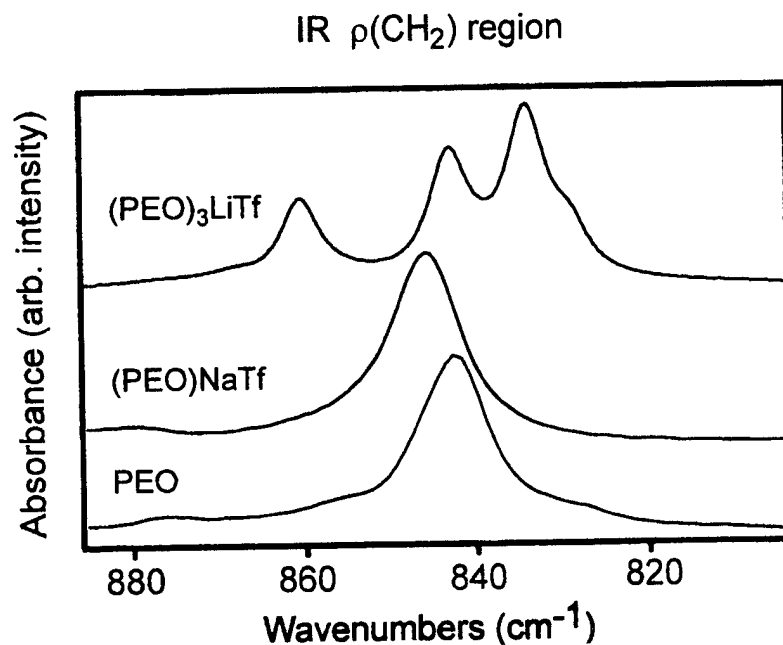


Figure 1. Infrared absorbance spectra of PEO,  $(\text{PEO})_3\text{LiCF}_3\text{SO}_3$  and  $(\text{PEO})\text{NaCF}_3\text{SO}_3$  in the  $\text{CH}_2$  rocking region.

#### References

- [1] P. Lightfoot, M. A. Mehta and P. G. Bruce, *Science*, 262, 883 (1993).
- [2] Y. G. Andreev, G. S. MacGlashan and P. G. Bruce, *Phys. Rev. B* 55, 12011 (1997).
- [3] G. Petersen, P. Jacobsson and L. M. Torell, *Electrochim. Acta* 37, 1495 (1992).
- [4] W. Huang, R. Frech and R. A. Wheeler, *J. Phys. Chem.* 98, 100 (1994).



LITHIUM PLATING/DISSOLUTION PROCESS FROM A  
DRY SOLID POLYMER ELECTROLYTE.

M. Gauthier\*, A. Bélanger\*, Y. Choquette\*, P. Hovington\*, M. Simoneau\*, M. Armand\*\*  
and R. Atanasoski\*\*\*,

\* Institut de recherche d'Hydro-Québec (IREQ), 1800, Boul. Lionel Boulet, Varennes,  
Québec, J3X 1S1, Canada

\*\* Université de Montréal, Département de Chimie, C.P. 6128, Montréal, Québec, H3C 3J7,  
Canada

\*\*\* Minnesota Mining and Manufacturing (3M), 209-2C-26, 3M Center, St-Paul, Mn 55144,  
USA

Lithium metal can be cycled efficiently at high rates from dry solid polymer electrolytes (DSPE) as shown recently from Lithium Polymer Battery successful application to the Electric Vehicle [1-2] and to the Hybrid Electric Vehicle [2]. Furthermore, it has been shown that Li<sup>0</sup>/DSPE-based rechargeable batteries are chemically and thermally stable over long periods of time, e.g. over 10 years at 60-80°C, [3] and are intrinsically less reactive than other liquid electrolyte lithium-based systems [3-4].

The Li<sup>0</sup>/DSPE interface obeys qualitatively the same rules as its liquid-electrolyte based equivalent, such as summarized by Peled recently [5], with the in-situ formation of a Solid Electrolyte Interface (SEI) between the lithium anode and the polymer electrolyte. However, significant differences exist upon cycling the Li<sup>0</sup>/DSPE interface in a practical LPB that makes the solvent-free system unique.

Some factors of importance will be reviewed, including : the SEI formation and its evolution with cycling, the mechanics of the Li<sup>0</sup>/electrolyte separator interface, the operating temperature effect of the Li<sup>0</sup> metal plating process, the effect of the polymer electrolyte transport number on salt concentration gradients ..etc.

Electrochemical tests and extensive electron microscopy techniques, both post-mortem and in-situ, have been used in conjunction to support these observations and to develop a phenomenological model that describes the lithium plating and cycling processes under normal and abnormal conditions.

## References :

- [1] C. Letourneau, M. Gauthier, A. Bélanger, D. Kuller, J. Hoffman. EV-14 Symposium Proceeding, Orlando, Fl. Dec. 12 17 (1997).
- [2] C. Letourneau, A. Bélanger, Y. Choquette, D. Kuller, EV-15 Symposium Proceeding, Bruxelles, Belgium, Oct. 1-3 (1998).
- [3] M. Gauthier, A. Bélanger, M. Armand, M. Simoneau and R. Atanasoski, 9<sup>th</sup> International Meeting Lithium Battery Symposium, Edinburgh, July 12-17 (1998).
- [4] Y. Choquette, M. Gauthier, A. Bélanger and B. Kapfer, 6<sup>th</sup> International Meeting on Lithium Batteries, Munster, Germany, May 10-15, 1992.
- [5] E. Peled, D. Golodnitsky and G. Ardel, J. Electrochem. Soc., 144(8), L208 (1997).

## Structure and molecular mobility studies in novel polyurethane ionomers based on poly(ethylene oxide).

G. Polizos, A. Kyritsis and P. Pissis

National Technical University of Athens, Department of Physics, Zografou Campus, 157 80 Athens, Greece

V.V. Shilov and V.V. Shevchenko

Academy of Sciences of Ukraine, Institute of Macromolecular Chemistry, 253160 Kiev, Ukraine

Ionomers contain charged groups in their molecular chains [1, 2]. They are usually prepared by introduction of pendant acid groups (acid form, protonic conductivity) which can be neutralised with bases (salt form, ionic conductivity). Here we report the results of our studies on segmented polyurethanes based on poly(ethylene oxide) with nonionic hard segments of varying length and flexible segments containing protons or alkali ions. Our interest is focused on studying the effects of structure and morphology on molecular mobility and electrical conductivity.

Acid-containing polyurethanes (APU) were prepared in a two-steps-process on the basis of poly(ethylene oxide), (PEO, MW 1500), 4,4'-diphenylmethane diisocyanate (MDI), 1,4-butanediol (BD) and pyromellitic anhydride (PMA). Samples of different amount of hard segments were prepared and denoted as B0, B1, B2 in the order of increasing hard segments content. The corresponding ion ( $\text{Li}^+$ ,  $\text{Na}^+$ ,  $\text{K}^+$ ) polyurethane (IPU) was prepared by treating the APU sample with an alkali base.

The structure and the properties of the polyurethanes were investigated by means of differential scanning calorimetry (DSC), small-angle X-ray scattering (SAXS), thermally stimulated depolarisation currents (TSDC) techniques and broadband ( $10^{-2}$ - $10^9$  Hz) dielectric relaxation spectroscopy (DRS).

TSDC measurements allow for a quick characterization of molecular mobility as a function of temperature at low frequencies ( $10^{-2}$ - $10^{-4}$  Hz) [3]. Fig.1 shows the TSDC thermogram for the B0Na sample. We observe peaks at about -140 and -90 °C due to secondary  $\gamma$  and  $\beta$  relaxations, respectively, and at about -30 °C due to Maxwell-Wagner-Sillars (MWS) interfacial polarization [4]. The MWS peak reflects properties of the microphase-separated morphology. The primary  $\alpha$  peak, associated to the glass transition of the polyether-rich phase, is here masked by the more intense MWS peak.

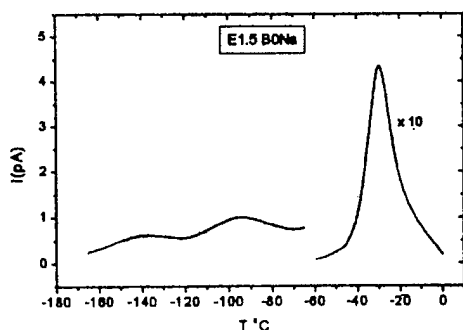


FIGURE 1: TSDC thermogram for sample B0Na

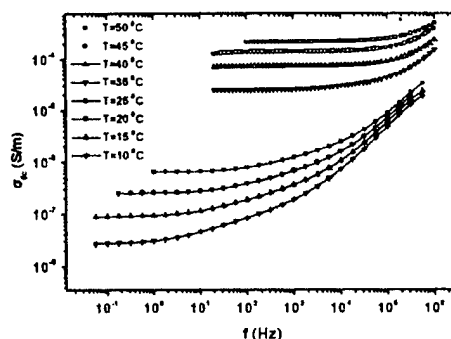


FIGURE 2:  $\sigma_{ac}(f)$  plots for sample B1H at several temperatures indicated on the plot.

Fig.2 shows the frequency dependence of ac conductivity,  $\sigma_{ac}$ , for the B1H sample at several temperatures. We observe dc plateaus which extend to higher frequencies with increasing

temperature. Values of dc conductivity,  $\sigma_{dc}$ , were obtained from these plateaus, as well as from complex impedance (Z) plots. Their dependence on temperature and sample was studied in detail. Interestingly,  $\sigma_{dc}$  was found 1-2 orders of magnitude higher than in similar polyurethane ionomers based on poly (tetramethylene oxide) (PTMO) [5].

#### References

- [1]. A. Eisenberg, B. Hird and R. B. Moore, *Macromolecules* 23, 4098(1998)
- [2]. M. R. Tant, K. A. Mauritz and G. L. Wilkes(Eds), *Ionomers*, Chapman and Hall, London, 1997
- [3]. P. Pissis, A. Anagnostopoulou-Konsta, L. Apekis, D. Daoukaki-Diamanti and C. Christodoulides, *J. Non-Cryst. Solids*, 131-133, 1174(1991).
- [4]. P. Pissis, A. Kanapitsas, Y. V. Savelyev, E. R. Akhramovic, E. G. Privalko, and V. P. Privalco *Polymer* 39, 3431(1998).
- [5]. P. Pissis, A. Kyritsis and V. V. Shilov, *Solid State Ionics*, submitted.

## THE STRUCTURAL PROPERTIES OF AN AMORPHOUS POLYMER ELECTROLYTE, PPO-LiClO<sub>4</sub>, FROM DIFFRACTION EXPERIMENTS AND REVERSE MONTE CARLO SIMULATION.

D. Andersson<sup>1</sup>, P. Carlsson<sup>1</sup>, J. Swenson<sup>2</sup>, L. Börjesson<sup>2</sup>, R.L. McGreevy<sup>3</sup> and L.M. Torell<sup>1</sup>

<sup>1</sup>Department of Experimental Physics and <sup>2</sup>Department of Applied Physics,  
Chalmers University of Technology, S-412 96 Göteborg, Sweden.

<sup>3</sup>Studsvik Neutron Research Laboratory, S-611 82 Nyköping, Sweden.

The structure of an amorphous polymer electrolyte model material, PPO-LiClO<sub>4</sub>, has been investigated on the short and intermediate length scale using x-ray and neutron diffraction experiments in combination with reverse Monte Carlo simulations. The aim is to describe the interplay between the polymer matrix and the ions, and indeed, large changes are observed in the structure of the polymer as the salt is introduced.

Hydrogenous PPO and PPO-LiClO<sub>4</sub> of ether-oxygen/Li concentrations 16:1 and 5:1 were investigated using x-ray diffraction. Corresponding samples with hydrogenous and deuterated polymers were investigated using neutron diffraction. In the neutron diffraction experiment on deuterated samples the scattering is mainly from the polymer chains, while in the x-ray and neutron diffraction experiments on hydrogenous materials the scattering from the salt ions can also be detected. By comparing the results of the different experiments the structure of the polymer matrix, the distribution of the salt and the interplay between the polymer chains and the ions can be studied.

An inspection of the experimental data reveals marked differences in the first sharp diffraction peak (FSDP) of the static structure factors as the salt is introduced in the polymer matrix, see figure 1. The FSDP is related to the intermediate range order and has, for pure PPO, been shown to originate from inter-chain correlations [1], i.e. correlations between segments of (in space) neighbouring chains. The differences observed may therefore be attributed to salt induced changes in the inter-chain correlations.

The FSDP of the static structure factors obtained by x-ray diffraction ( $S_X(Q)$ ) is characterised by a single broad peak for the pure polymer whereas it is split in two peaks for the polymer-salt complexes. As the salt concentration increases, the high- $Q$  peak narrows and shifts to higher- $Q$  values while the low- $Q$  peak becomes more pronounced. Similar characteristics were found in the FSDP of the static structure factor obtained by neutron diffraction on hydrogenous materials ( $S_H(Q)$ ) [2]. The FSDP of the static structure factor obtained by neutron diffraction studies of deuterated samples ( $S_D(Q)$ ) is characterised by a single peak also for the polymer salt complexes. The peak narrows and shifts to higher- $Q$  values with increasing salt concentration. The low- $Q$  peak is however absent in ( $S_D(Q)$ ).

The above experimental data therefore confirm that the salt induces contraction and ordering of the polymer network [2, 3]. The effect can be explained by that cations coordinate to several ether-oxygens in different chains introducing ionic cross links which contract the network. The low- $Q$  peak is however not present in  $S_D(Q)$  which, in light of the different contrasts for the experiments, demonstrate that it cannot be due to correlations between polymer chains only. The previously suggested [2] scenario of the peak being due to correlations between neighbouring chains which are pushed apart by bulky anions, must therefore be discarded. Rather, the results indicate that it originates from the correlations between ions and polymer chains or correlations between ions.

To consistently interpret the different diffraction data sets and to extract information not only from positions and intensities of peaks the reverse Monte Carlo (RMC) simulation method [4] has been employed. The RMC method creates an atomistic model of the ma-

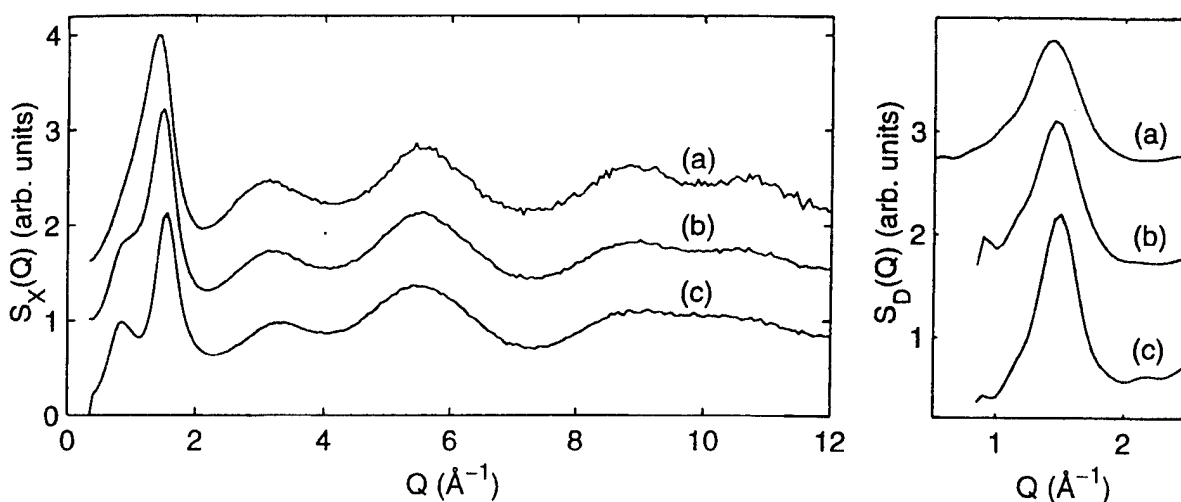


Figure 1: The static structure factors of pure PPO (a), PPO-LiClO<sub>4</sub> of ether-oxygen/Li concentrations 16:1 (b) and 5:1 (c) as obtained from x-ray diffraction (left) and neutron diffraction experiments on deuterated samples (right). The graphs have been vertically shifted for clarity.

terial based on chemical knowledge (number density, bond lengths, coordination numbers etc.) which is consistent with the structure factors obtained through the x-ray and neutron diffraction experiments. Simulations have been performed for PPO and PPO-LiClO<sub>4</sub> of ether-oxygen/Li concentrations 16:1 and 5:1 and will be analysed in terms of salt induced effects on the inter-chain correlations and the local chain conformations. The results of the RMC simulations will be presented and structural properties such as the presence of ionic cross links, the distribution of ions and the coordination of ions to the polymer chains will be discussed.

- [1] P. Carlsson, J. Swenson, L. Börjesson, L.M. Torell, R.L. McGreevy, and W.S. Howells. *submitted*.
- [2] P. Carlsson, B. Mattsson, J. Swenson, L. Börjesson, L.M. Torell, R.L. McGreevy, and W.S. Howells. *Electrochimica Acta*, 43:1545, 1998.
- [3] P. Carlsson, J. Swenson, R.L. McGreevy, B. Gabrys, W.S. Howells, L. Börjesson, and L.M. Torell. *Physica B*, 234-236:231-235, 1997.
- [4] D.A. Keen and R.L. McGreevy. *Nature*, 344:423, 1990.

## DYNAMIC LIGHT SCATTERING INVESTIGATION OF THE MECHANISM OF IONIC CONDUCTIVITY IN A POLYMER BASED GEL ELECTROLYTE

C. Svanberg\*, J. Adebahr\*, H. Ericson\*, L. Börjesson†, L.M. Torell\*, and B. Scrosati‡

\*Department of Experimental Physics and †Department of Applied Physics, Chalmers University of Technology, SE-412 96 Göteborg, Sweden

‡Department of Chemistry, University of Rome "La Sapienza", I-00185 Rome, Italy

Many types of lithium-ion conducting polymers have been prepared and characterised during recent years with the aim of using them as electrode separators in lithium-polymer batteries [1-3]. One family of polymer electrolytes that has been extensively studied consists of poly-ethers, e.g. PEO, mixed with lithium salts. Despite impressive efforts, the ion conduction mechanism in these systems is not completely understood, although there are convincing indications that the conductivity is related to the segmental mobility of the host polymer [2, 4, 5]. Thus, the increase of the conductivity requires an increase of the mobility of the polymer host, which normally has the counteracting effect of decreasing the mechanical stability of the system, unless special approaches are used as that recently proposed by Scrosati and co-workers [6]. Special attention is today paid to another class of electrolytes, i.e. the polymer gel electrolytes, materials which combine high ionic conductivity with good mechanical properties [7]. These electrolytes are generally prepared by the immobilisation of a liquid solution containing lithium salt in a polymer matrix. Typical examples are gels formed by trapping propylene carbonate/ethylene carbonate, PC/EC, solutions of lithium salts in a poly(acrylonitrile) (PAN) or a poly(methyl methacrylate) (PMMA) matrix. Although these gel-type polymer electrolytes have been known for some years [8] the mechanism of their ionic conductivity is still unclear. In this work we report an interpretation of this mechanism based on dynamic light scattering measurements.

The dynamic light scattering (DLS) experiments were performed on a model electrolyte formed by gelling a lithium perchlorate solution,  $\text{LiClO}_4/\text{PC/EC}$ , in a PMMA matrix [7]. The average composition of the  $\text{LiClO}_4:\text{EC}:\text{PC}:\text{PMMA}$  sample was in mole ratio 4.5:46.5:19:30 where the PMMA ratio refers to the monomer.

The DLS experiments reveal three distinctly different relaxation processes. Two of them can be assigned to diffusive motions and one to the local segmental mobility of the polymeric backbone. The fast motion is shown to be caused by the diffusion of the low molecular solvent. A comparison with conductivity results allows to establish that the ionic diffusion is closely related to the fast diffusive motion of the low molecular weight solvent within the gel. This motion is strongly decoupled from the segmental motion of the polymer backbone, in net contrast to the mechanism which controls the ionic conductivity in solvent-free, PEO-based polymer electrolytes [2,4,5]. To our knowledge this is the first investigation that provides a demonstration of the conductivity mechanism of the gel electrolytes.

## References

- [1] Scrosati, B, *Nature*, **373**, 557-558 (1995).
- [2] Gray, F. M. *Polymer Electrolytes* (Royal Society of Chemistry, Cambridge, 1997).
- [3] Scrosati, B. & Neat, R. J. *Lithium polymer batteries*, 182-222 (Chapman and Hall, London, 1993).
- [4] Sandahl, J., Schantz, S., Börjesson, L., Torell, L. M. & Stevens, J. R. *J. Chem. Phys.*, **91**, 655 (1989).
- [5] Bergman, R., Börjesson, L., Fytas, G. & Torell, L. M., *J. Non-Cryst. Solids*, **172-174**, 830 (1994).
- [6] Croce, F., Appetecchi, G.B., Persi, L. and Scrosati, B., *Nature*, **394**, 456-458 (1998).
- [7] Appetecchi, G. B., Croce, F. & Scrosati, B., *Electrochimica Acta*, **40**, 991 (1995).
- [8] Feuillade, G. and Perche, Ph. *J. Appl. Electrochem.*, **5**, 63-69, (1975).

# NEW ALKALI IONOMERS : TRANSPORT MECHANISM FROM TEMPERATURE AND PRESSURE CONDUCTIVITY MEASUREMENTS.

Michel Duclot, Fannie Alloin, Oleg Brylev, Jean Yves Sanchez, Jean Louis Souquet  
 Laboratoire d'Electrochimie et de Physicochimie des Matériaux et des Interfaces (LEPMI)  
 (UMR CNRS INPG N° 5631, associée à l'Université Joseph Fourier Grenoble)  
 ENSEEG BP 75 - 38402 Saint Martin d'Hères - France

New ionomers exclusively cation-conducting were synthesised [1, 2]. This result was obtained by grafting the anion of the solvated salt to a macromolecular polyethylene oxide chain. The first step is the polycondensation reaction between a low mass poly(ethylene glycol) ( $\overline{M}_w$  # 1000) with the 3-chloro-2-chloromethyl-1-propene in a basic medium (KOH). The alkali (Li, Na or K) N,N diallyl amido-1-tetrafluoroethane sulfonate is then grafted to the macromolecular chains by thermal free-radical copolymerization. The vitreous transition temperatures,  $T_g$ , of these ionomers range from -60°C to -30°C. Transport number measurements carried out on the lithium ionomer show an exclusive  $\text{Li}^+$  conductivity.

The experimental set up was designed in order to accurately measure the conductivity versus pressure (1 - 5000 bars) as well as versus temperature (20 - 150°C) [3, 4].

Isobar data correctly verify the following so called V.T.F equation :

$$\sigma T = A \exp - \frac{B}{R(T - T_0)} \quad (1)$$

The ideal transition temperature  $T_0$  was extrapolated from numerical identification for each set of measurements.

The isothermal conductivity variations with pressure lead to the determination of an "apparent activation volume",  $\Delta V_{\text{app}}^*$ , by the relationship :

$$\Delta V_{\text{app}}^* = -RT \left( \frac{\partial \ln \sigma}{\partial P} \right)_T \quad (2)$$

The  $\Delta V_{\text{app}}^*$  values deduced from eq. 2 are higher than those observed for usual solid electrolytes and vary between 20 to 40  $\text{cm}^3 \cdot \text{mol}^{-1}$ . For each composition, these values decrease with temperature.

In these ionomers, the mobility of the charge carriers is interpreted in terms of a free volume mechanism. The available free volume,  $\overline{V}_f$ , should follow the state equation :

$$P \overline{V}_f = R(T - T_0) \quad (3)$$

meaning that the kinetics energy of the charge carrier in its free volume is proportional to the thermal energy received between T and  $T_0$ .

This state equation leads to an expression of the apparent activation volume,  $\Delta V_{app}^*$ , as a function of temperature :

$$\Delta V_{app}^* = \frac{V_f^* T}{(T - T_0)} \quad (4)$$

in which  $V_f^*$  represents the minimal free volume required for an elementary displacement.

The values of  $V_f^*$  calculated using eq. 4 vary from 10 to 20 cm<sup>3</sup>.mol<sup>-1</sup> and are higher than the cationic volumes (0.5 to 6 cm<sup>3</sup>.mol<sup>-1</sup>). This result suggests that the cationic displacement is assisted by the macromolecular chain movements.

[1] D. Benrabah, S. Sylla, F. Alloin, J-Y Sanchez and M. Armand, *Electrochem. Acta* **40**, 2259 (1995).

[2] F. Alloin, D. Benrabah and J-Y. Sanchez, *J. Power Sources* **68**, 372 (1997).

[3] Y. Grincourt, M. Hénault, M. Duclot and J-L Souquet, *Physics and Chemistry of Glasses* **37**, 236 (1996)

[4] F. Alloin, J.Bolton, J-L. Souquet and M. Duclot, *Solid State Ionics* **110**, 15 (1998)



# CONDUCTION PROPERTIES OF PVDF-TYPE POLYMER ELECTROLYTES WITH LITHIUM IMIDE SALTS, $\text{LiN}(\text{CF}_3\text{SO}_2)_2$ AND $\text{LiN}(\text{C}_2\text{F}_5\text{SO}_2)_2$

Claudio CAPIGLIA, Yuria SAITO, Hitoshi YAMAMOTO, Hiroshi ISHIKAWA,  
\*Piercarlo MUSTARELLI

Osaka National Research Institute, 1-8-31 Midorigaoka, Ikeda, Osaka 563-8577 Japan

\*CSTE and Department of Physical Chemistry of University of Pavia,  
Via Taramelli 16, 27100 Pavia Italy

Conduction properties of lithium gel-type electrolytes composed of imide salts such as  $\text{LiN}(\text{CF}_3\text{SO}_2)_2$  and  $\text{LiN}(\text{C}_2\text{F}_5\text{SO}_2)_2$  and poly-vinylidene fluoride (PVDF)-type polymer have been investigated based on the results of ionic conductivities and diffusion coefficients. The gel-electrolyte samples changing the mixing ratio of polymer to lithium salt solution have been prepared for 2M, 1M and 0.5M solutions in order to elucidate the dissociation effect of the salt and the interactive effect between the salt and the polymer chain on the conduction properties. The ionic conductivity increased orderly with the increase of the solution ratio of the gel-electrolyte independent of the solution concentration. In order to confirm the mobility change, self-diffusion coefficients of lithium ( $D_{\text{Li}}$ ) and fluoride ( $D_{\text{F}}$ ) species have been measured using the pulsed field gradient NMR technique (fig. 1). The lower the solution concentration of the gel-electrolytes, the higher the diffusion coefficients. This is due to the viscosity change with the concentration and the change of mobile ion content depending on the dissociation degree of the salt. The  $D_{\text{Li}}$  and  $D_{\text{F}}$  decreased and approached each other with the increase of the polymer ratio of the gel-electrolytes. This indicates that the dissociation degree of the salt is influenced by gelation. Considering the drastic change of the conductivity, the dissociation degree orderly decreases with the increase of the polymer ratio of the gel-electrolyte. It is also characteristic that the  $D_{\text{Li}}$  and  $D_{\text{F}}$  do not change so much in the region of 50 - 60 polymer ratio. This may show the possibility that the polymer segmental motion enhances the migration of carrier in this region. Furthermore, the effect of the anion size difference on the conduction properties would be discussed by the comparison of the results of two kinds of lithium imide salts.

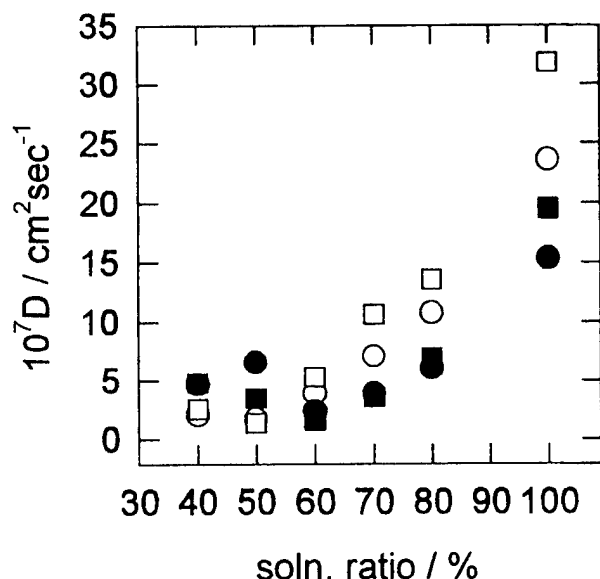


Fig. 1 Diffusion coefficients of lithium (circle) and fluoride (square) species of  $\text{LiN}(\text{CF}_3\text{SO}_2)_2$  - EC/DEC ( occupied : 1M, unoccupied : 0.5M ) in PVDF-HFP gel electrolytes

## HIGH FREQUENCY DIELECTRIC PROPERTIES OF POLY(PROPYLENE OXIDE) - $\text{LiCF}_3\text{SO}_3$ AND $\text{LiN}(\text{CF}_3\text{SO}_3)_2$ SYSTEMS

B.-E. Mellander<sup>a</sup>, Samantha W. A. <sup>b</sup>, H. Eliasson<sup>a</sup>, I. Albinsson<sup>a</sup>, and M. Furlani<sup>a</sup>

<sup>a</sup>Physics and Engineering Physics, Chalmers University of Technology and Göteborg University, 412 96 Göteborg, Sweden

<sup>b</sup>Dept of Physics, University of Peradeniya, Peradeniya, Sri Lanka

### Abstract

Studies of the dielectric properties are commonly used to characterise insulating polymeric materials. However, in the case of ion conducting polymers this type of analysis is more sparse [1, 6]. Given the appropriate frequency range, the dielectric analysis gives information about the dipolar relaxations present in the system. From this information segmental and local polymeric relaxations as well as ion association can be detected.

This high frequency study is performed in the frequency range 1 MHz to 1.8 GHz using a HP 4291A impedance analyzer. Pure atactic poly(propylene oxide) (PPG), which is a completely amorphous polymer, has been studied by Yano [3] in the high frequency range. The present work is to our knowledge the first one involving PPG as polymer host in combination with lithium triflate ( $\text{LiCF}_3\text{SO}_3$ ) and lithium bis(trifluoromethane sulphone) imide ( $\text{LiN}(\text{CF}_3\text{SO}_3)_2$ ) in this frequency range. We have investigated the concentration range  $8 < n < 500$ , where  $n$  is the number of ether oxygens per lithium ion, in the temperature interval -20 to 80 °C.

In the frequency range and temperature interval investigated, two relaxation peaks ( $\alpha$  and  $\alpha'$ ) may be found in the pure polymer. In the polymer-salt systems an additional peak has been observed. This peak may be attributed to the dipolar relaxation of ion pairs or higher aggregates in accordance with similar assignments in silver triflate-PPG [4] and in deuterated and non-deuterated ammonium triflate-PPG [5]. In the PPG-lithium imide system the ion aggregate peak is less predominant as expected, since many studies have shown that ion association is weak in LiTFSI.

The concentration and temperature dependence of the peak positions is examined in order to evaluate the activation energy of the dipole relaxations and their dependence on the salt concentration.

### References

- [1] F. M. Gray, C. A. Vincent and M. Kent, *J. Polym. Sci. B: Polym. Phys.*, (1989), **27**, 2011.
- [2] B.-E. Mellander and I. Albinsson, in *Solid State Ionics: New developments*, edited by B. V. R. Chowdari et al. (World Scientific, Singapore) p 83, 1996.
- [3] S. Yano, R. R. Rahalkar, S. P. Hunter, C. H. Wang and R. H. Boyd, *J. Polym. Sci. B: Polym. Phys.* **14**, 1877 (1976).
- [4] H. Eliasson, I. Albinsson and B.-E. Mellander, *Electrochimica Acta* **43**, 1459 (1998).
- [5] a) I. Albinsson and B.-E. Mellander, in *Fast Ion Transport in Solids* (Edited by B. Scrosati, A. Magistris, C. M. Mari and G. Marriotto) 347, Kluwer Academic Publishers, Dordrecht (1993); b) I. Albinsson, B.-E. Mellander and J.R. Stevens, *Solid State Ionics* **72**, 177 (1994).

# IONIC CONDUCTANCE OF POLYMERIC ELECTROLYTES CONTAINING LITHIUM SALTS MIXED WITH RARE EARTH SALTS

Masayuki MORITA, Fusamori ARAKI, Nobuko YOSHIMOTO, Masashi ISHIKAWA,  
and Hiromori TSUTSUMI

Department of Applied Chemistry and Chemical Engineering, Yamaguchi University,  
Tokiwadai, Ube 755-8611, Japan

Polymeric ion conductors are key materials for developing all-solid electrochemical devices such as batteries and capacitors. We have synthesized and characterized  $\text{Li}^+$ -ion and multivalent cation ( $\text{Mg}^{2+}$ ,  $\text{La}^{3+}$ ,  $\text{Ce}^{3+}$ ,  $\text{Yb}^{3+}$ ) conductors that consist of polymer matrices with cross-linked oligo(ethylene oxide) units and inorganic salts with proper complex forming reagents [1-3]. In the course of the work, a specific feature has been observed that mixing the inorganic salts in polymeric composites improved the ionic conductance [4]. We have examined, in this work, the effects of the rare earth salt mixing on the ionic structure and the conductance behavior of  $\text{Li}^+$  in the polymeric composite.

The preparation procedure of the polymer composite is shown in Fig. 1 [1, 2]. Mono- and di-functional oligo(ethylene oxide)-grafted methacrylates, PEM and PED, were used as prepolymers for the matrix formation. Metal salts ( $\text{MX}_n$ :  $\text{M} = \text{Li}$ ,  $\text{La}$ ,  $\text{Yb}$ ,  $\text{X} = \text{CF}_3\text{SO}_3$ ) were dissolved in the mixture of the prepolymers. Poly(ethylene glycol) dimethylether (PEGDE, MW = 230-400) was added as a complex-forming reagent to the  $\text{MX}_n$ /mixed prepolymer solution. The resulting solution was solidified on an aluminum sheet by photo-induced polymerization to yield cross-linked polymer matrix, poly(ethylene oxide)-grafted poly(methylmethacrylate) (PEO-PMMA) dispersing metal salts (Fig. 1). The obtained polymeric composites were characterized by XRD, DSC, NMR and Raman spectroscopy. The ionic conductivity was measured in an ambient temperature region by an AC method (10 kHz).

Figure 2 shows the temperature dependence of the ionic conductivity for the composite (PEO-PMMA)/PEGDE/( $\text{LiCF}_3\text{SO}_3 + \text{La}(\text{CF}_3\text{SO}_3)_3$ ), where the molar ratios of PEM/PED in the mixed prepolymer and the ethylene oxide (EO) unit in (PEO-PMMA)/PEGDE were 3/1 and 1/1, respectively, and the total concentration of the anion in the composite was kept constant,  $[\text{CF}_3\text{SO}_3^-]/[\text{EO}] = 1/32$ . About  $2 \times 10^{-5} \text{ S cm}^{-1}$  of the conductivity was obtained at room temperature for the composite containing 100% Li salt, while the conductivity of the composite containing 100% La salt was ca.  $10^{-6} \text{ S cm}^{-1}$  at  $30^\circ\text{C}$ . The polymeric composite containing mixed salt ( $\text{LiCF}_3\text{SO}_3 + \text{La}(\text{CF}_3\text{SO}_3)_3$ ) showed higher conductivity than that consisting of each component salt. The variation in the conductivity with the salt composition is shown in Fig. 3. Maximum conductivity was obtained at the salt composition of  $[\text{Li}^+]/3[\text{La}^{3+}]$  being 80/20 (ie. 20% substitution of  $\text{Li}^+$  by  $\text{La}^{3+}$ ). As shown in Fig. 3, the conductivity enhancement by the "cation substitution" was more significant at higher temperature. Similar effects were also observed when the La salt was merely added to the polymeric composite that contains constant concentration of the Li salt.

Substitution of  $\text{Li}^+$  by  $\text{Yb}^{3+}$  (or addition of  $\text{Yb}^{3+}$ ) was also effective to improve the ionic conductivity of the polymeric composite containing the Li salt. The DSC measurements showed that the phase-transition temperature of

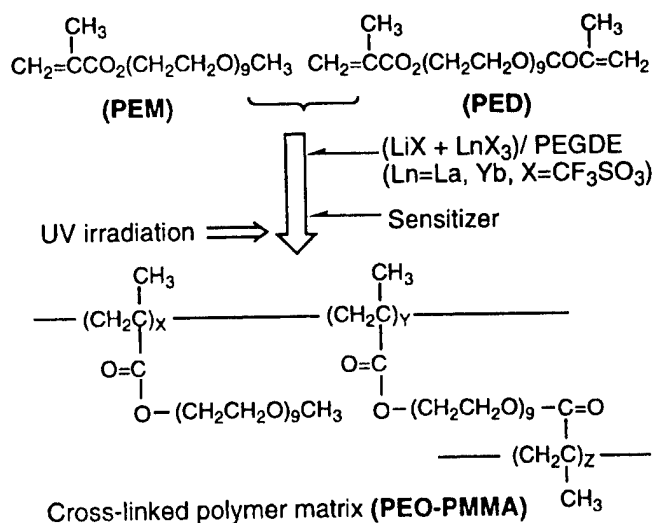


Fig.1 Preparation of the polymer matrix for solid electrolytes from methacrylate-based prepolymers (PEM and PED).

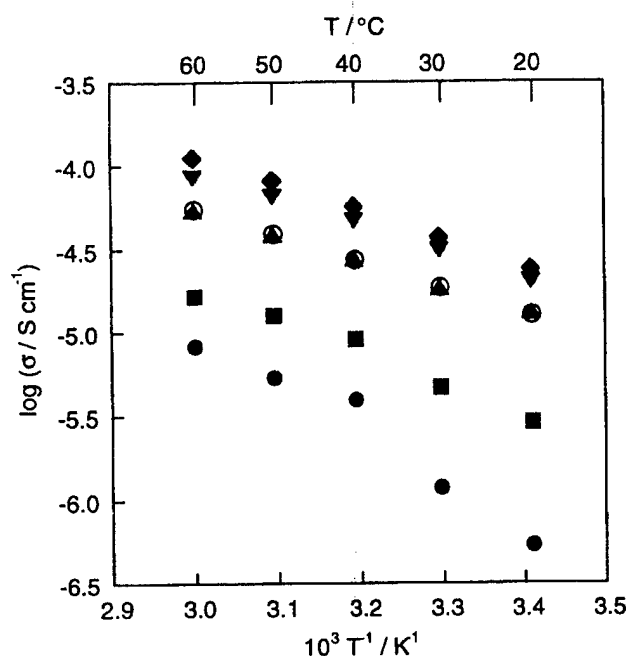


Fig. 2 Temperature dependence of ionic conductivity for (PEO-PMMA)/PEGDE/(LiCF<sub>3</sub>SO<sub>3</sub>+La(CF<sub>3</sub>SO<sub>3</sub>)<sub>3</sub>), (PEO-PMMA)/PEGDE = 1/1, [CF<sub>3</sub>SO<sub>3</sub>]<sup>-</sup>/[EO] = 1/32, [Li<sup>+</sup>]/3[La<sup>3+</sup>] = 100/0 (○), 80/20 (◆), 60/40 (▼), 40/60 (▲), 20/80 (■), and 0/100 (●).

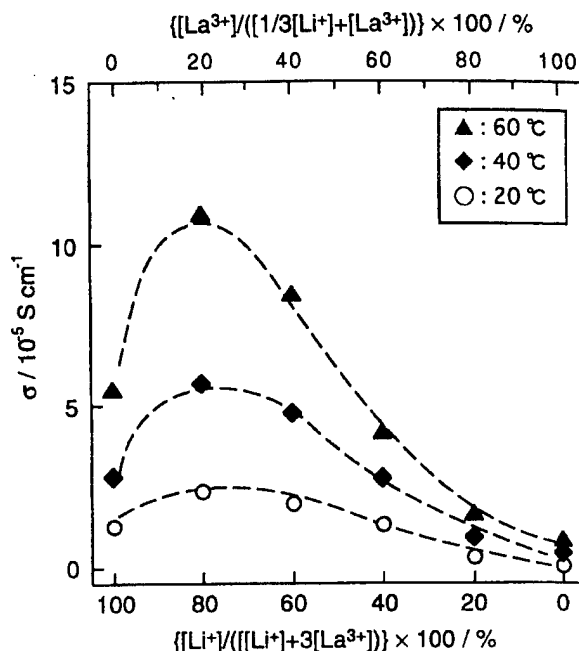


Fig. 3 Ionic conductivity of (PEO-PMMA)/PEGDE/(LiCF<sub>3</sub>SO<sub>3</sub>+La(CF<sub>3</sub>SO<sub>3</sub>)<sub>3</sub>), as a function of the [Li<sup>+</sup>]/[La<sup>3+</sup>] ratio in the salt composition, (PEO-PMMA)/PEGDE = 1/1, [CF<sub>3</sub>SO<sub>3</sub>]<sup>-</sup>/[EO] = 1/32.

the polymer composite is scarcely affected by the substitution of Li<sup>+</sup> by Ln<sup>3+</sup>. The Raman spectra suggested that the ionic structure of the composite is somewhat changed by the cation substitution. From <sup>7</sup>Li NMR results, the mobility of Li<sup>+</sup> in the composite can be enhanced by the addition of La<sup>3+</sup>.

This work was supported by "Research for the Future" Program from the Japan Society for the Promotion of Science (JSPS-RFTF 96P00102), and a Grant-in Aid for Scientific Research (No. 09650907) from the Ministry of Education, Science, Sports and Culture of Japan.

- [1] M. Morita, T. Fukumasa, M. Motoda, H. Tsutsumi, Y. Matsuda, T. Takahashi and H. Ashitaka, *J. Electrochem. Soc.* **137**, 3401 (1990).
- [2] M. Morita, M. Ishikawa and Y. Matsuda, *J. Alloys and Compounds*, **250**, 524 (1997).
- [3] M. Morita, F. Araki, K. Kashiwamura, N. Yoshimoto and M. Ishikawa, submitted to *Electrochim. Acta*.
- [4] F. Araki, M. Ishikawa and M. Morita, *Extended Abstr. 24th SSI Meeting in Japan* (Paper No. 1B05), 1998.

## RESISTANCE OF THE CONDUCTING POLYMER GELS TO THE EXTERNAL HUMIDITY AND THE EFFECT OF WATER ON THE MOLECULAR INTERACTIONS

J. Adebahr, H. Ericson, D. Ostrovskii, P. Jacobsson

*Department of Physics, Chalmers University of Technology, SE-412 96 Göteborg, Sweden*

The development of new polymeric gel electrolyte materials is motivated by their high applicability for the different electrochemical devices such as Li polymer batteries [1] or smart windows [2].

One important demand on the electrolyte is a high processability which will allow an easy assembling of the whole device. This demand requires, in turn, a knowledge about specific characteristics of the material such as its sensitivity to the temperature, humidity, atmosphere *etc.* However, despite a great number of investigations studying the internal properties of the gels (structure, conductivity, interactions between the components), there are very few reports devoted to the stability of the materials with regard to external conditions.

In particular, the presence of water molecules in the material may essentially alter its properties by changing the intermolecular and ionic interactions and, even more serious, cause corrosion on the electrodes. The situation is further complicated by the fact that in a multi-component system each component can have different properties which may vary from "very hygroscopic" (for instance  $\text{LiClO}_4$ ) to "non-hygroscopic" (PMMA). Therefore, in addition to the studies of interaction between water and components of the gel, one needs to investigate the whole system in order to determine its general behavior regarding a humid atmosphere.

In the present work we have investigated the response of several typical gel electrolytes (prepared with use of different solvents and different polymeric matrices) to the external humidity by means of vibrational spectroscopy. A number of systems, from pure liquid solvents to final gels, are systematically studied regarding both hygroscopic properties and the influence of water molecules on the different intermolecular ionic interactions. It is found that the presence of water substantially affects the Li-solvent coordination and that new type of interaction involving the salt anions occurs. In addition, an obvious dependence of the state of water molecules on the type of polymeric host is observed.

*This work was financially supported by the MISTRA program (Sweden).*

### References:

- [1] B. Scrosati, *Nature* **373**, 557 (1995).
- [2] A.M. Grillone, S. Panero, B. Retamal, B. Scrosati, *J. Electrochem. Soc.*, **in press**.

COMPOSITE ELECTROLYTES BASED ON LOW MOLECULAR WEIGHT  
POLYGLYCOLSM. Marcinek, A. Zalewska, G. Żukowska and W. WieczorekFaculty of Chemistry, Warsaw University of Technology, ul. Noakowskiego 3, 00-664  
Warszawa, Poland**INTRODUCTION**

The interest in studies of polymeric electrolytes arises from the possibility of their applications in various electrochemical devices such as batteries, electrochromic windows, displays and fuel cells working from sub-ambient e.g.  $-50^{\circ}\text{C}$  to moderate e.g.  $200^{\circ}\text{C}$  temperatures.[1-2] In spite of intensive search the mechanism of ionic transport in polymeric electrolytes as well as the electrode- electrolyte interfacial behaviour are still under discussion.[3] Due to the low dielectric constant of polymer matrices ion- ion interactions are equally important to polymer- ion interaction in polymer ionic conductors.

It has been demonstrated by several authors that conductivity and ion- polymer or ion- ion interactions can be modified by the addition of inorganic fillers to high molecular weight polyether electrolytes.[4-6] For these semicrystalline systems the increase in conductivity has been attributed to the lowering of their degree of crystallinity resulting in the formation of a highly conducting amorphous phase. Similar effect of the addition of  $\text{Al}_2\text{O}_3$  fillers on conductivity enhancement has recently been observed in amorphous oxymethylene linked poly(ethylene oxide) systems and low molecular weight poly(ethylene glycol) based electrolytes. This conductivity enhancement was attributed to the changes in polymer- ion interactions leading to the increase in the flexibility of the polymer host as well as to the reduction in the fraction of ion-pairs formed in composite systems compared to pristine polymeric electrolytes.

In the present work the ionic conduction is studied in poly(ethylene glycol)- $\text{LiClO}_4$  electrolytes -  $\alpha$ -  $\text{Al}_2\text{O}_3$  over the wide salt concentrations and temperature ranges. Composite electrolytes with  $\alpha$ - $\text{Al}_2\text{O}_3$  containing inert surface groups are examined. Conductivity enhancement was observed compared to poly(ethylene glycol)- $\text{LiClO}_4$  electrolytes in the 0.5-5 mol/kg salt concentration range. Conductivity studies are coupled to viscosity and DSC experiments which helps us to establish the relation between salt concentration and viscosity (flexibility) of polymer host. The ion- polymer and ion- ion interactions are studied on the basis of the FT-IR spectroscopy and particular changes in the intensity of the IR modes characteristic for C-O-C and  $\text{ClO}_4^-$  vibrations. These bands are characteristic for ion- polymer and ion- ion interactions, respectively. Finally, the ionic associations are discussed on the basis of the Fuoss-Krauss formalism [7]. These studies show the reduction in the ion-pair formation for composite polymeric electrolytes in the entire concentration range studied.

**ACKNOWLEDGEMENTS**

This work was financially supported by the President of the Warsaw University of Technology according to the 504/164/853/8 research grant.

**REFERENCES**

- [1] *Applications of Electroactive Polymers*, Scrosati, B., Ed.; Chapman and Hall: London; 1993.
- [2] *Solid State Electrochemistry*, Bruce, P.G. Ed.; Cambridge University Press: Cambridge, 1995;
- [3] Bruce, P.G.; Shriver, D.F.; Gray, F.M. Chapters 5&6 in ref. (2)
- [4] Wieczorek, W.; Florjańczyk, Z.; Stevens, J.R. *Electrochim. Acta* 40, 2251 (1995)

- [5] Gray, F.M. *Solid Polymer Electrolytes-Fundamentals and Technological Applications*; VCH: Weinheim, Germany, 1991.
- [6] Scrosati, B.; Neat, R. Chapter 6 in ref. 1
- [7] Fuoss, R.M.; Accascina, F. *Electrolytic Conductance*; Interscience: NY, 1959.

## COMPARATIVE INVESTIGATIONS CONCERNING THE CHARGE CARRIER TRANSPORT OF VARIOUS TYPES OF GEL ELECTROLYTES

A. Reiche, A. Weinkauff, R. Sandner, B. Sandner, F. Rittig\*, G. Fleischer\*  
Martin-Luther-University Halle-Wittenberg, Institute of Technical and Macromolecular Chemistry,  
Geusaer Str. 88, D-06217 Merseburg, Germany  
e-mail: reiche@chemie.uni-halle.de

\*University of Leipzig, Faculty of Physics and Geosciences, Linne-Strasse 5,  
D-04103 Leipzig, Germany

The relationship between the ionic conductivity and the charge carrier diffusivity is given by the Nernst-Einstein equation which shows discrepancies in the field of polymer electrolytes.

Recently, these discrepancies were described for homogeneous gel electrolytes on basis of poly(ethylene glycol)<sub>23</sub> dimethacrylate and the corresponding liquid electrolytes in terms of a modified Nernst-Einstein equation considering, that only charged ionic species contribute to the conductivity whereas PFG-NMR measures the self-diffusivity of charged as well as non-charged species [1].

Now, a further type of gel electrolytes has been studied. By *in situ* photopolymerization of e.g. tri(ethylene glycol) dimethacrylate ((EG)<sub>3</sub>DMA) in the presence of oligo(ethylene glycol)<sub>11</sub> dimethylether ((EG)<sub>11</sub>DME) as plasticizer and LiCF<sub>3</sub>SO<sub>3</sub>, heterogeneous gel electrolyte films can be prepared, characterized by two glass transition temperatures one related to the (EG)<sub>11</sub>DME salt solution ( $-75 < T_g < -65^\circ\text{C}$ ) and one related to the polymer at temperatures far above the working temperature range of the gel electrolyte.

These electrolytes with a (EG)<sub>11</sub>DME content > 65 wt% show conductivities in the range of  $1 \cdot 10^{-4}$  S/cm at room temperature comparable to that of the liquid electrolyte. Due to weaker interactions between the cations and the polymer in result of the reduced oligo(ethylene glycol) spacer length cationic transference numbers in the range of 0,5 can be achieved. Despite of the high plasticizer content, these materials show high mechanical and thermal stability.

The conductivity of the electrolyte systems clearly depends on the plasticizer content, whereas the self-diffusivity of charge carriers and plasticizer is slightly affected by the composition and comparable with that of the liquid electrolyte system. That means, especially in the case of a low plasticizer content, no or only a weak correlation between conductivity and self-diffusivity can be found. It is assumed for explanation, that PFG-NMR which measures in length scales in the  $\mu\text{m}$  range, records the liquid phase of the heterogeneous system contrary to the conductivity which is a macroscopic quantity.

Additionally, the influence of a higher polarity of the polymer e.g. in gel electrolyte systems on basis of copolymers of (EG)<sub>3</sub>DMA with cyanomethyl methacrylate or on basis of alternating copolymers of maleic anhydride with tetra(ethylene glycol) divinyl ether is discussed.

[1] A. Reiche, T. Cramer, G. Fleischer, R. Sandner, B. Sandner, F. Kremer, J. Kärger, *J. of Phys. Chem.* 102 (1998) 1861



## NMR AND DSC STUDY OF POLYMER ELECTROLYTE / CARBON BLACK COMPOSITES

R.W.A. Franco<sup>1</sup>, J.P. Donoso<sup>1</sup>, C.J. Magon<sup>1</sup>, J.M. Pernaut<sup>2</sup>, P.P. de Souza<sup>2</sup>

<sup>1</sup>Inst. de Física de São Carlos, Universidade de São Paulo, C.P. 369, 13560-970, SP, Brasil

<sup>2</sup>ICEX, Universidade Federal Minas Gerais, CP 702, 31270-901, B. Horizonte, MG, Brasil

Composites polymer electrolytes consisting of poly(ethylene oxide), PEO, a lithium salt and fine fillers have received considerable attention [1]. The composites based on the addition of conductive *carbon black*, CB, has been proposed for applications in solid-state electrochemical capacitors [2]. In this work we present a <sup>1</sup>H nuclear magnetic resonance, NMR, study of the composites based on PEO/CB and PEO<sub>8</sub>LiClO<sub>4</sub>/CB. The composites were prepared by the solvent casting technique described earlier [3] using PEO (M.W. 5×10<sup>6</sup>), LiClO<sub>4</sub> (Aldrich) and *Carbon Black* (Blacks Pearls 2000/Cabot). The composites were prepared with five different weight percentages of CB, from 10% to 70%, and were characterized by DSC (scan rate 10 K/min). Proton NMR line-shapes, spin-lattice (T<sub>1</sub>) and spin-spin (T<sub>2</sub>) relaxation times measurements were carried out on a pulsed spectrometer operating at 36 MHz in the temperature range of 180 K to 360 K.

Figure 1 shows the temperature dependence of the <sup>1</sup>H full width at half intensity of the PEO<sub>8</sub>LiClO<sub>4</sub> (denoted PS) and the composites PEO/20% CB (PC 20) and PEO<sub>8</sub>LiClO<sub>4</sub>/20% CB (PCS 20). Earlier reports have shown that the spectra of the polymer electrolyte consist of one broad component assigned to crystalline PEO present in both PEO and electrolytes and one

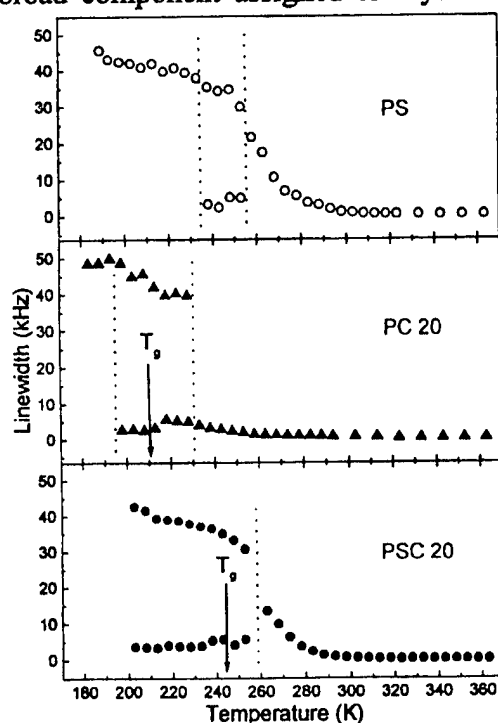


Figure 1: <sup>1</sup>H linewidth vs. temperature.

narrow component assigned to the amorphous PEO-salt phase [4]. The spectra of the composites in Fig. 1 also shows the coexistence of these two phases. The onset of the line-narrowing, which reflect the increase in the polymer chain mobility, is just above the glass transition temperature of the samples, T<sub>g</sub>, as expected for polymer electrolytes [4,5] (T<sub>g</sub> ≈ 210 K for PC and 244 K for PSC 20, as determined by DSC). For the composite PC 20, the mobility of the polymer chain increase in the crystalline phase to producing a substantial line narrowing at 230 K, where the spectrum collapses into a single narrow component. In pure PEO a single narrow line is observed to occur close to the melting point of the crystalline PEO, T<sub>m</sub> = 320-335 K [4,6]. This result suggests that the polymer chain mobility in the composite PC 20 is higher than in the pure PEO.

Figure 2 shows the temperature dependence of the proton spin lattice relaxation rate (T<sub>1</sub><sup>-1</sup>) for the composites PC and PSC with 20% and 30% of CB As reported in a previous work [3], three temperature

regions can be distinguished, according to the behaviour of the magnetization recovery toward equilibrium. In the high and in the low temperature regions the relaxation recovery is well described by a single exponential, but in the intermediate temperature region the data are well fitted by the sum of two exponential curves. The shorter T<sub>1</sub> is attributed to the protons in the high mobility amorphous phase, and the longer T<sub>1</sub> is attributed to the protons in the low mobility, or

crystalline regions. The former  $T_1$  data display a relaxation rate maxima at 317 K-325 K for the PSC and at  $\approx 270$  K for the PC composites. A similar shift ( $\approx 50$  K) in the position of the two rate maxima of the amorphous component was also observed between pure PEO and polymer electrolytes [4,6].

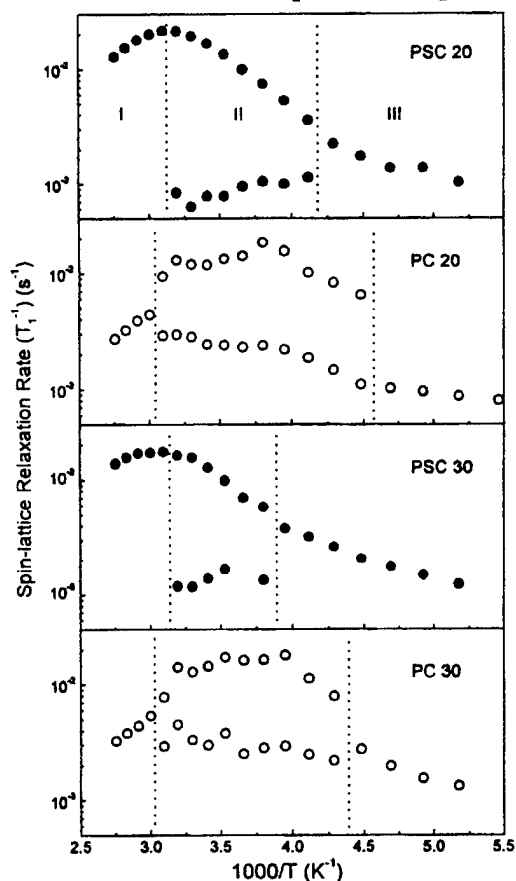


**Figure 2:** Relaxation rate  $T_1^{-1}$  of  $^1\text{H}$  as a function of the reciprocal temperature.

concentration below 50%. However, the relaxation maximum is less pronounced in PSC 50 and PSC 70 composites compared to that shown in Fig. 2. The data shown in Fig. 2 indicates that the long  $T_1$  component, in the PC composites, seems to converge to the short  $T_1$  value as the temperature is increased, contrasting with the PSC samples behavior. This long  $T_1$  is attributed to the proton belonging to polymer chains which are tightly attached to the porous CB particles and those belonging to the crystalline phase in the polymer chain, whereas the short  $T_1$  component is assigned to those belonging to the polymer chains in the amorphous phase, loosely bound to the CB particles [3,7].

This work was partially supported by CNPq, CAPES, Fapemig, Fapesp and Finep (Brazil).

- [1] - E. Quartarone, P. Mustarelli, A. Magistris, *Solid State Ionics* **110**, 1 (1998)
- [2] - J.M. Pernaut, C. Goulart, *J. Power Sources* **55**, 93 (1995)
- [3] - R.W.A. Franco, J.P. Donoso, C.J. Magon, C.B. Rodella, A.O. Florentino, M.J. Saeki, J.M. Pernaut, A.L. Oliveira, *Solid State Ionics* (in press)
- [4] - A. Johansson, J. Tengenfeldt, *J. Chem. Phys.* **104**, 5317 (1996)
- [5] - K.J. Adamic, S.G. Greebaum, K.M. Abraham, M. Alamgir, M.C. Wintersgill, J.J. Fontanella, *Chem. Mater.* **3**, 534 (1991)
- [6] - W. Gorecki. These de Doctorat, Université de Grenoble, France (1984)
- [7] - J. Przyluski, M. Siekierski, W. Wieczorek, *Electrochimica Acta* **40**, 2101 (1995)

## MAGNESIUM-ION CONDUCTING POLYMER ELECTROLYTES BASED ON POLYACRYLONITRILE (PAN)

Kumudu Perera, M.A.K.L. Dissanayake and P.W.S.K. Bandaranayake,  
Department of Physics, University of Peradeniya, Peradeniya, Sri Lanka.

Various types of solid polymer electrolytes such as those formed by complexing lithium salts with poly(ethylene oxide) PEO, have been extensively studied during the last decade. One of the major disadvantages of these electrolytes is that, when their conductivity is enhanced, for example, by the addition of suitable plasticizers, they lose their dimensional stability. To overcome this problem, a number of alternative polymer structures which do not contain the  $\text{CH}_2\text{-CH}_2\text{-O}$  unit either in the backbone or in the side chain have been developed to obtain polymer electrolytes with high room temperature conductivity while retaining dimensional stability. The common concept has been that of trapping a liquid electrolyte solution into a polymer cage. Properties and applications of several different types of polymer electrolytes, prepared based on this concept have been reported by various groups [1-3]. Most of these non-conventional polymer electrolytes reported so far have incorporated lithium salts in a PAN or PMMA network and are being developed as possible electrolyte membranes for lithium polymer batteries. Only a few reports are available on PAN based electrolytes incorporating cations other than  $\text{Li}^+$ . Such studies, especially on systems incorporating multivalent cations, are important in order to understand the conducting mechanism and the role played by the host polymer matrix.

$\text{Mg}^{2+}$  ion conducting polymer electrolytes can be interesting not only for understanding the multivalent cationic conductivity mechanism in the polymer, but also for using as thin film electrolyte membranes in electrochemical devices due to their low cost, ease of fabrication, and low equivalent weight. In this paper, we report conducting properties of hybrid polymer electrolyte films containing  $\text{Mg}(\text{ClO}_4)_2$  in EC/PC, incorporated in a matrix of polyacrylonitrile (PAN) polymer.

Polyacrylonitrile (PAN) and  $\text{Mg}(\text{ClO}_4)_2$  were used as received from Aldrich Chemicals. Propylene carbonate (PC)(Aldrich, 99%) and ethylene carbonate (EC)(Aldrich, 98%) were used as plasticizers. After weighing and magnetically stirring the appropriate composition ratios, the mixture was poured into small aluminium foil cups and baked at  $140^\circ\text{C}$  for 45 minutes. Resulting polymer electrolyte membranes were transparent in colour and free from air bubbles and pin holes. Disc shaped samples were removed from the aluminium cups and dried at  $60^\circ\text{C}$  prior to electrical measurements.

The optimum composition ratio which corresponds to the highest room temperature conductivity was found to be 18mol%PAN / 64mol%EC / 14mol%PC / 04mol%Mg( $\text{ClO}_4$ )<sub>2</sub> where the percentages refer to molar ratios. The results of the polarization tests for these samples taken with stainless steel blocking electrodes at  $70^\circ\text{C}$  is shown in Fig. 1. According to Fig. 1, it is clear that the PAN / EC / PC /  $\text{Mg}(\text{ClO}_4)_2$  electrolyte is predominantly an ionic conductor with negligible electronic conductivity. The ionic transference number,  $t_{\text{ionic}}$  estimated from these data is  $\approx 0.92$  and the electronic transference number  $\approx 0.08$ . According to the polarisation data taken with non-blocking magnesium electrodes, the sample appears to be totally transparent to magnesium ions, suggesting that the material is predominantly a  $\text{Mg}^{2+}$  ion conductor.

The results of the dc polarization tests obtained for liquid solution electrolyte, having identical molar percentage ratios as that used in the PAN based polymer electrolyte and with stainless steel gives the ionic transference number,  $t_{\text{ionic}}$ , to be  $\approx 0.83$  and the electronic

transference number,  $t_{\text{electronic}}$  to be 0.17. It is interesting to note that, as obtained from polarization measurements, the cationic transference number in the polymer electrolyte,  $t_i \approx 0.92$ , is higher than that in the liquid solution electrolyte,  $t_i \approx 0.83$ . Similar results have been reported by other workers for Li ions in PAN based polymer electrolytes. This suggests that the role played by the polymer component (PAN) is much more complex than merely acting as a porous solid support for the liquid solution electrolyte component.

Variation of  $\log(\sigma T)$  with  $1/T$  for the PAN / EC / PC /  $\text{Mg}(\text{ClO}_4)_2$  samples, taken with stainless steel blocking electrodes is shown in Fig.2. It can be seen that the conductivity obeys the Arrhenius behaviour. The room temperature conductivity is  $\sigma_{\text{RT}} = 3.2 \times 10^{-3} \text{ Scm}^{-1}$ . This value is little higher than the room temperature conductivity of  $2.0 \times 10^{-3} \text{ Scm}^{-1}$  reported by Alamgir et al for a similar material[4]. In addition, we have been able to identify  $\text{Mg}^+$  ions as the mobile species in this material from the results of the dc polarization test using magnesium electrodes. The activation energy for cationic migration calculated from Fig. 2 is 0.24 eV.

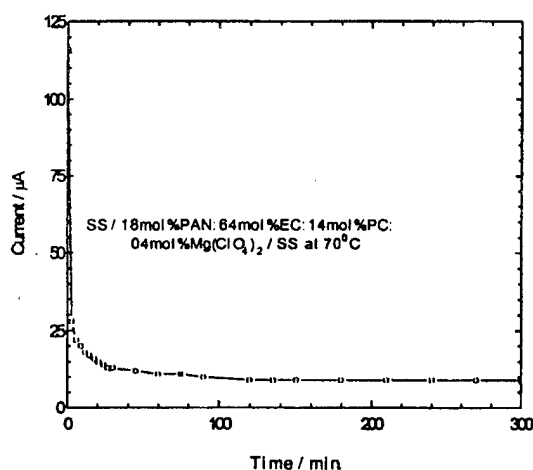


Fig.1

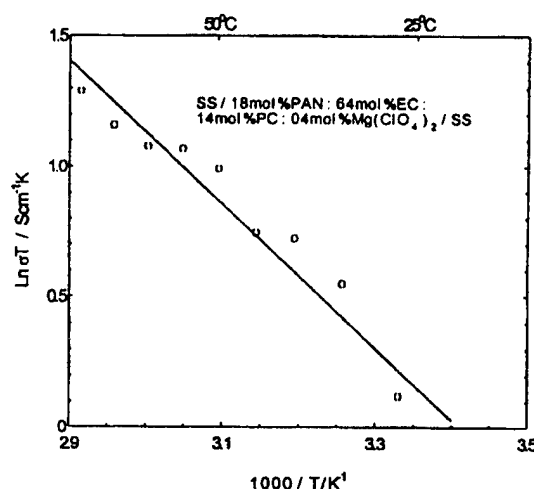


Fig.2

As in the case of lithium salts in PC/EC solutions incorporated into PAN network, the Mg-containing PAN electrolyte also exhibits high conductivity comparable to liquid solutions. The high conductivity can possibly be attributed to the liquid solution electrolyte,  $\text{Mg}(\text{ClO}_4)_2$  in EC/PC, trapped in a matrix of PAN as suggested by other workers [3]. However, the mechanism of ion transport and the role played by the host polymer in this new generation of "hybrid electrolytes" is yet to be understood.

A Research Grant from the National Science Foundation, Sri Lanka is greatly acknowledged. We thank the International Program in the Physical Sciences (IPPS), Uppsala, Sweden for providing equipment and training fellowships for the SSI Project at Peradeniya.

- [1] K.M. Abraham, in : B. Scrosati (Eds.), Applications of Electroactive Polymers, Chapman and Hall Pu., London, 1993.
- [2] B. Scrosati, in : B.V.R. Chowdari et al (Eds.), Solid State Ionic Materials, World Scientific Publishing Co., Singapore, 1994, p.111.
- [3] M. Alamgir and K. M. Abraham, in : G. Pistoia (Eds.), Lithium Batteries - New Materials, Developments and Perspectives, vol.5, Elsevier, 1994, p. 93.
- [4] M. Alamgir, R.D. Moulton and K.M. Abraham, in : K. M. Abraham and M. Salomon (Eds.), Primary and Secondary Lithium Batteries, The Electrochemical Society, Pennington, New Jersey, 1991, p.131.

**SOLVENT EFFECT ON GEL ELECTROLYTES CONTAINING LITHIUM SALTS**

S.S.Sekhon , Deepa , S.A..Agnihotry

Department of Applied Physics, G.N.D.University, Amritsar-143005, INDIA.

National Physical Laboratory, New Delhi-110012, INDIA.

Gel electrolytes of Polymer-Solvent-Salt type are suitable for electrochromic window applications due to their high value of ionic conductivity, good electrode-electrolyte interfacial contacts, good adhesive properties etc.. In the present paper, we report the results on polymeric gel electrolytes with polymethylmethacrylate (PMMA) as the polymer,  $\gamma$ -butyrolactone, propylene carbonate, ethylene carbonate as the solvent and lithium triflate as the salt. The effect of different solvents on the properties of gel electrolytes has been studied and mixed solvents have been found to show better properties. The variation of conductivity with salt concentration and temperature has been studied. The addition of polymer has been found to result in an increase in the viscosity of gel electrolytes accompanied by a small decrease in conductivity value. The room temperature conductivity of these polymeric gel electrolytes is of the order of 1-10 mS/cm and they also have high transmission in the visible region. The stable potential window has been found to be comparable to that of the corresponding liquid electrolytes. The small variation in conductivity value over the operational temperature range has been found to be advantageous for electrochromic device applications.

## NMR AND DSC STUDY OF POLYMER ELECTROLYTES BASED ON PEO/PEG BLENDS

A.C. Bloes<sup>1</sup>, J.P. Donoso<sup>1</sup>, C.J. Magon<sup>1</sup>, J. Schneider<sup>1</sup>, E.C. Pereira<sup>2</sup>

<sup>1</sup>Inst. de Física de São Carlos, Universidade de São Paulo, C.P. 369, 13560-970 SP Brasil

<sup>2</sup>LIEC, Dep. Química, Universidade Federal de São Carlos, CP 676, 13560-970 SP Brasil

Polymer electrolytes based on blends of poly(ethylene oxide) and poly(ethylene glycol) complexed with a lithium salt have received considerable attention because in these materials, the ionic conductivity appears to be enhanced compared to the PEO-salt systems<sup>[1,2]</sup>. In this work we report thermal properties, ionic conductivity and nuclear magnetic resonance (NMR) studies of the polymer electrolytes  $[\text{PEO}_x : \text{PEG}_{1-x}]_8 \text{LiBF}_4$ .

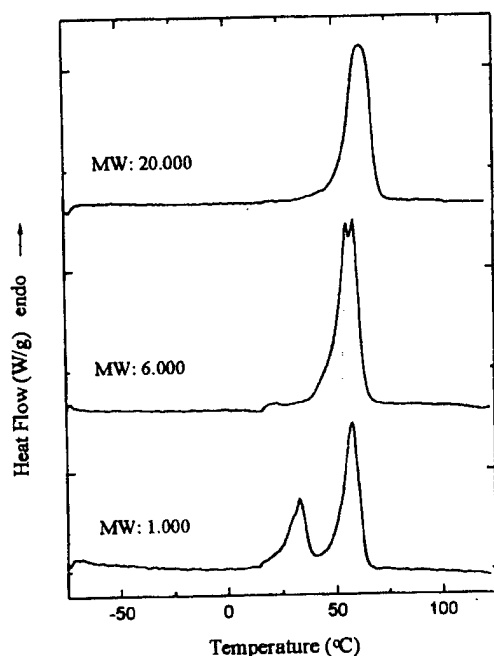


Fig. 1. DSC thermograms of the PEO/PEG blends, of composition 50:50 (without  $\text{LiBF}_4$ ) for PEG molecular weight of 1,000, 6,000 and 20,000.

Samples were prepared by the solvent casting technique<sup>[3]</sup>, using PEO (Aldrich, M.W.  $5 \times 10^6$ ), PEG (Reagen, M.W.  $10^3$ ) and lithium tetrafluoroborate (Aldrich). Differential scanning calorimetry (DSC) measurements were performed in a Du Pont thermal analysis system.  $^1\text{H}$  and  $^{19}\text{F}$  NMR line shape and spin-lattice relaxation times ( $T_1$ ) measurements were carried out on a pulsed spectrometer operating at 36 MHz, in the temperature range 190 to 370 K.  $^7\text{Li}$  NMR was measured at 155.43 MHz with a Varian-400 spectrometer.

Figure 1 presents DSC data for POE/PEG blends at 50 / 50 mol%. It is observed a important change in the behaviour of the endothermic peaks related with crystalline portion fusion. The POE fusion is observed at the 58-60 °C region, as described in the literature<sup>[4]</sup>. Otherwise, a secondary crystalline phase fusion it is observed only for POE/PEG (1.000). Although no effect on the POE crystalline fusion temperature occurs, it is observed an important variation in the heat associated with this process. For this sample, the heat, measured

from the peak area, is  $147,9 \text{ Jg}^{-1}$  while for others samples investigated, namely POE / PEG (6.000) and POE / PEG (20.000), the heat is constant ( $240,0 \text{ Jg}^{-1}$ ). These facts are possibly related with a decrease in the POE crystalline portion due to its interaction with PEG.

Figure 2 shows the temperature dependence of the  $^1\text{H}$  half width at half height (HWHH) line widths and the  $^1\text{H}$  and  $^7\text{Li}$  relaxation rates ( $T_1^{-1}$ ) of the  $[\text{PEO}_{0.5} + \text{PEG}_{0.5}]_8 \text{LiBF}_4$ . The NMR spectrum shows the coexistence of two components in the temperature region between 250 K and 310 K. Line narrowing processes of both components are observed to occur at different temperatures: near the glass transition temperature ( $T_g \approx 231 \text{ K}$ , as determined by DSC) and around 285 K, i.e. below the melting point of the electrolyte ( $T_m \approx 328 \text{ K}$ ). These line narrowing process are associated with ionic or molecular motion on a time-scale comparable to the reciprocal of the NMR linewidth<sup>[4-6]</sup>. Close to  $T_g$ , the mobility of the polymer chain increases enough in the amorphous phase of the electrolyte producing a line narrowing of both components, collapsing into one single narrow line at 310 K. The activation energy in the motional narrowing

regime was found to be around 0.4 eV, a value similar to those obtained from the DC conductivity measurements. The temperature dependence of the nuclear relaxation rate  $T_1^{-1}$  show a rate maximum at  $T \approx 340$  K for the lithium and at  $T \approx 310$  K for the proton. The difference between the  $^7\text{Li}$  and the  $^1\text{H}$  relaxation curves is related to the difference between the Larmor

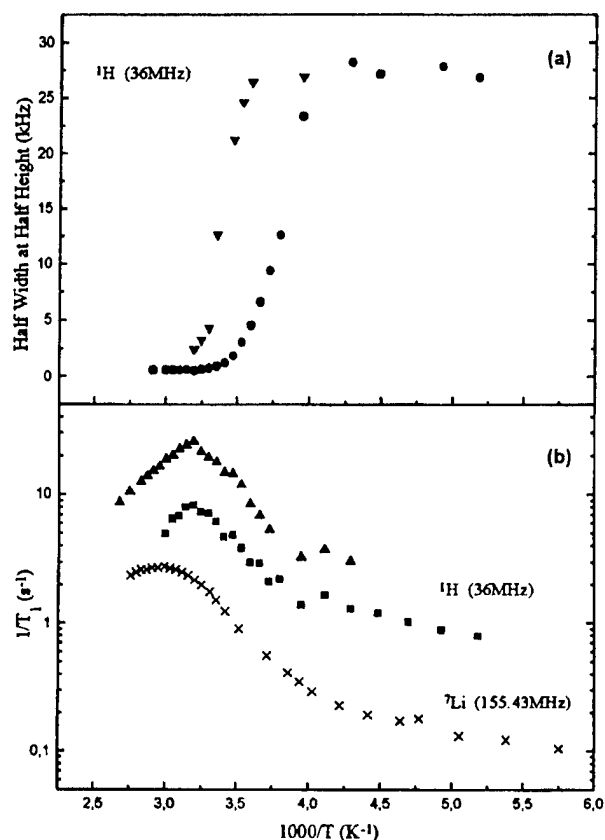


Fig. 2. Temperature dependence of the (a) line width (HWHH) and (b) spin-lattice relaxation rate ( $T_1^{-1}$ ) of  $^1\text{H}$  and  $^7\text{Li}$  in the  $[\text{PEO}_{0.5} + \text{PEG}_{0.5}]_8\text{LiBF}_4$ . Two relaxation times was observed for the  $^1\text{H}$ , indicated

frequency and the interaction strengths, the H-H interaction in the polymer chain being stronger than the intermolecular H-Li interaction<sup>[3]</sup>. The existence of two phases, already observed as separate components in the  $^1\text{H}$  NMR spectrum, is also evident in the spin relaxation data as a clear bi-exponential behavior over most of the temperature range. Further work is in progress to correlationate the observed increase in the conductivity with an enhancement of the the ionic and polymer mobility in the blends.

The  $^{19}\text{F}$  spectra of the  $[\text{PEO}_{0.5} + \text{PEG}_{0.5}]_8\text{LiBF}_4$  electrolyte shows a decrease in the HWHH line width at  $T \approx 260$  K, and the relaxation rate ( $T_1^{-1}$ ) shows a well-resolved maximum around 286 K. These results reflects the mobility associated with reorientational motion of the  $\text{BF}_4$  anion characterized by a single activation energy of  $\approx 0.2$  eV, as obtained from the relaxation data.

This work was partially supported by CNPq, Fapesp and Finep (Brazil).

1 - I. Kelly, J.R. Owen, B.C.H. Steele, J.

Electroanal. Chem. **168**, 467 (1984)

2 - C. Wang, Q. Liu, Q. Cao, Q. Meng, L. Yang, Solid State Ionics **53-56**, 1106 (1992)

3 - J.P. Donoso, T.J. Bonagamba, H. Panepucci, L.N. Oliveira, W. Gorecki, C. Berthier, M. Armand, J. Chem. Phys. **98**, 10026 (1993)

4 - A. Johansson, J. Tengenfeldt, J. Chem. Phys. **104**, 5317 (1996)

5 - K.J. Adamic, S.G. Greebaum, K.M. Abraham, M. Alamgir, M.C. Wintersgill, J.J. Fontanella, Chem. Mater. **3**, 534 (1991)

6 - Y. Dai, Y. Wang, S.G. Greenbaum, S.A. Bajue, D. Golodnitsky, G. Ardel, E. Strauss, E. Peled, Electrochimica Acta **43**, 1557 (1998)

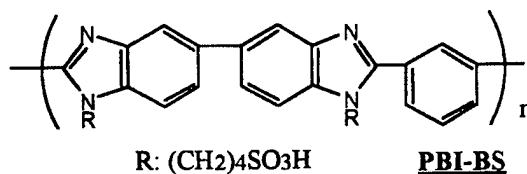
## PROTON CONDUCTION OF SULFOALKYLATED POLY(BENZIMIDAZOLE) FILMS (X)

Masahiro Rikukawa, Mitsuyasu Kawahara, Kohei Sanui, Naoya Ogata  
Department of Chemistry, Sophia University  
7-1 Kioi-cho, Chiyoda-ku, Tokyo 102-8554, Japan

Applications of solid polymer electrolyte fuel cells (SPEFCs) has received much attention in the last few years.[1] The SPEFCs use a polymer membrane as a solid electrolyte, which is an electronic insulator and an excellent proton conductor. Currently, perfluorosulfonate ionomer membranes such as Nafion have been used for their efficient proton conductivity, reliability, and long term chemical stability. However the conductivity decreases above the boiling temperature because of the loss of adsorbed water in the membranes. Thermostable polymers with good water affinity at higher temperature have been strongly desired for SPEFCs with good reliability. In this study, poly(benzimidazole) substituted with butanesulfonic acid group (PBI-BS), propanesulfonic acid group (PBI-PS) were synthesized and the proton conductivity was compared with Nafion under various conditions.

### Experimental

According to the Gielsman et al [2], PBI-BS and PBI-PS were synthesized by a ring-opening reaction of 1,4-butanedisulfone or 1,3-propanedisulfone in a PBI anion solution. The PBI-BS and PBI-PS were analyzed by FT-IR, <sup>1</sup>H, <sup>13</sup>C-NMR, and elementary analysis. The sulfonation level on the NH group of PBI was estimated by elementary analysis and <sup>1</sup>H-NMR. Proton conductivity of samples was evaluated by the complex impedance method with a humidic chamber (YAMATO IW-241). Nafion 115 films were pretreated by boiling in 3 % H<sub>2</sub>O<sub>2</sub>, rinsing in boiling water, boiling in 0.5 M H<sub>2</sub>SO<sub>4</sub>, and finally rinsing in boiling water (at least 1 h for each step).



Scheme 1 Structure of PBI-BS.

### Results and discussion

The PBI-BS and PBI-PS exhibited higher solubility than the parent polymer. The decomposition temperature of PBI-BS and PBI-PS decreased to 350 °C with increasing the sulfonation level. This degradation was attributed to the desulfonation of PBI-BS.

Figure 1 shows the comparison of Arrhenius plots of conductivity for PBI-BS (70.5 mol% sulfonation level) and Nafion 115 in a humidic chamber at 90 %RH. The conductivity of the PBI-BS showed the order of 10<sup>-3</sup> Scm<sup>-1</sup> in the temperature range from 30 °C to 85 °C. The conductivity of PBI-BS at 30 °C was 10 times that of Nafion. The number of adsorbed water for PBI-BS was 23.0 H<sub>2</sub>O per sulfonic acid group, while Nafion 115 was 8 H<sub>2</sub>O per sulfonic acid group. The high proton conductivity and good water affinity of PBI-BS is due to the high sulfonation level and flexible side chains. These results provide useful data for future design



and development of fuel cells based on polymer electrolytes.

### Acknowledge

This study was supported by the Proposal-Based Advanced Industrial Technology R&D Program from NEDO of Japan.

### REFERENCE

- [1] Fiona M. Gray, "Polymer Electrolytes", The Royal Society Chemistry, Cambridge, (1997).
- [2] M. B. Gielsman and J. R. Reynolds, *Macromolecules*, **25**, 4832 (1992).

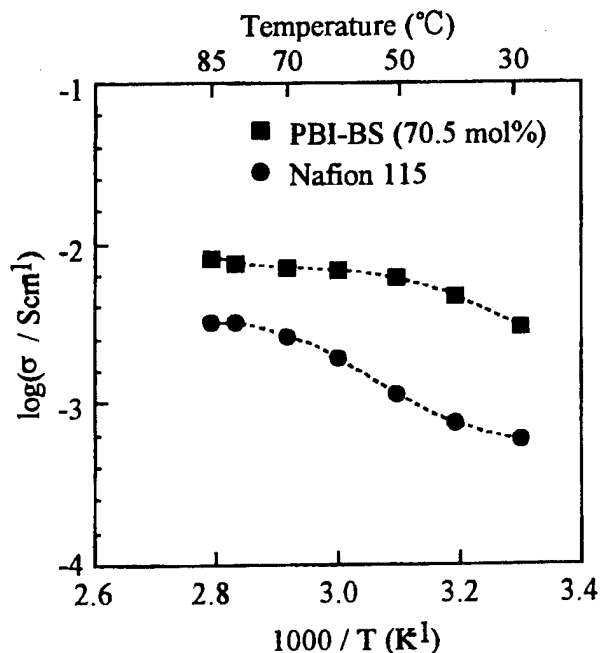


Figure 1 Comparison of Arrhenius plots of conductivity for PBI-BS (70.5 mol%) and Nafion 115 at 90 %RH

## **ELECTRICAL CONDUCTIVITY STUDIES OF POLYVINYL CHLORIDE (PVC) BASED ELECTROLYTES WITH DOUBLE SALT SYSTEM**

**S. RAMESH**

Institute of Postgraduate Studies and Research, University of Malaya, 50603 Kuala Lumpur, Malaysia.

**A.K. AROF**

Physics Division, Center for Foundation Studies in Science, University of Malaya, 50603 Kuala Lumpur, Malaysia.

### **Abstract**

Polyvinyl chloride has a low electrical conductivity of the order  $10^{-8} \text{ S cm}^{-1}$ . It can serve as a host matrix for solvating lithium salts. Conductivity measurements were made for films doped with  $\text{LiBF}_4$  and  $\text{LiCF}_3\text{SO}_3$ . The highest room temperature electrical conductivity of  $5.2 \times 10^{-6} \text{ S cm}^{-1}$  was achieved for the composition 50 wt% PVC, 15 wt%  $\text{LiCF}_3\text{SO}_3$  and 35 wt%  $\text{LiBF}_4$ . Dipole-dipole type attractions occur in PVC. These interactions can be weakened by the presence of plasticizers. The plasticizers increase the flexibility of PVC, reduce its viscosity and thereby increase the mobility of the charge carriers. On addition of suitable mixtures of polyethylene carbonate (PC) and ethylene carbonate (EC), the room temperature electrical conductivity is observed to increase. At room temperature, the conductivity value of  $\sim 2.0 \times 10^{-3} \text{ S cm}^{-1}$  was obtained for a film of concentration 9 wt% PVC, 2.7 wt%  $\text{LiCF}_3\text{SO}_3$ , 6.3 wt%  $\text{LiBF}_4$ , 12 wt% EC and 70 wt% PC.

## PAN BASED GEL ELECTROLYTE WITH LITHIUM SALTS

S.S.Sekhon, Narinder Arora, S.A.Agnihotry

Department of Applied Physics, G.N.D.University, Amritsar-143005, INDIA

National Physical Laboratory, New Delhi-110012, INDIA

Polyacrylonitrile(PAN) based polymer electrolytes containing lithium triflate and by using propylene carbonate(PC), and propylene carbonate and ethylene carbonate in different volume ratios as the solvent have been investigated in the present study. The electrical conductivity of lithium triflate in the single solvent and binary solvent mixtures of propylene carbonate and ethylene carbonate has been determined in the 0-80°C and the optimised binary mixed solvent compositions showing maximum value of room temperature conductivity have been identified. The effect of salt concentration and temperature on conductivity value has also been studied. The addition of PAN has been found to result in gel formation and viscosity increases with the addition of PAN content. The interaction between the salt/solvent/polymer has been investigated by IR spectroscopy. The high value of room temperature conductivity (1 mS/cm) of these gel electrolytes is suitable for use in various solid state ionic devices.

## THE EFFECT OF SOLVENT ON THE CONDUCTIVITY AND PHYSICO-CHEMICAL PROPERTIES OF POLY(VINYLDENE FLUORIDE) BASED PROTON CONDUCTING GEL ELECTROLYTES

G. Żukowska, M. Rogowska, and W. Wieczorek  
Warsaw University of Technology, Faculty of Chemistry,  
ul. Noakowskiego 3, 00-664 Warszawa, Poland

### ABSTRACT

Proton conducting polymer electrolytes have attracted considerable attention due to the possibility of their application in various electrochemical devices, e.g. fuel cells, sensors, electrochromic displays and windows working at ambient and sub-ambient conditions [1]. Various type of proton conducting polymer complexes, polyelectrolytes and hydrogel have been studied to this end [1,2]. Recently a new type of proton conducting systems based on non-aqueous polymeric gels has been developed [3]. These systems exhibit high ambient and sub-ambient temperature conductivities and are colorless in the wide solvent and polymer concentration ranges. Therefore the possibility of their application in electrochromic devices was mentioned. However most of the gels studied so far are based on non-commercial polymer matrices which might limit their commercial application because of the relatively complicated preparation procedure.

In the present work proton conducting gels based on commercially available poly(vinylidene fluoride) (PVdF) system are studied. The polymer and  $\text{H}_3\text{PO}_4$  (used as a proton donor) are dissolved in dimethylformamide (DMF) or dimethyl acetate (DMA) at ambient temperatures and then cast on the flat glass substrate. Highly conducting ( $5 \times 10^{-4} \text{ S/cm}$  at  $20^\circ\text{C}$ ) colorless polymeric membranes are obtained in a relatively narrow PVdF and  $\text{H}_3\text{PO}_4$  concentration ranges. Conductivities measured for systems containing DMF are slightly higher than for DMA based derivatives. The gel electrolytes studied are thermally stable up to  $70\text{--}120^\circ\text{C}$  as shown by the DSC experiments. The interactions between  $\text{H}_3\text{PO}_4$  and solvents used are studied by means of FT-IR spectroscopy.

### Acknowledgements

This work is financially supported by the Polish State Committee for Scientific Research under the 3 TO9B 087 13 research contract.

### References

- [1] J.C. Lasseques in "Proton Conductors: Solids, Membranes and Gel-Materials and Devices" (Ed. P. Colombari), Cambridge University Press, Cambridge, 1992. Ch. 20
- [2] W. Wieczorek and J.R. Stevens, *Polymer* **38**, 2057 (1997)
- [3] D. Raducha, W. Wieczorek, Z. Florjańczyk and J.R. Stevens, *J. Phys. Chem.* **100**, 20126 (1996)

## SYNTHESIS OF PROTON CONDUCTING POLYMER BASED ON POLY(SILAMINE) (VI)

Masahiro Rikukawa, Koji Tsuruhara, Kohei Sanui, Naoya Ogata,  
Yukio Nagasaki\* and Masao Kato\*

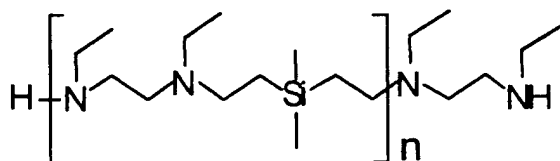
Department of Chemistry, Sophia University  
7-1 Kioi-cho, Chiyoda-ku, Tokyo 102-8554, Japan

\*Department of Material Science and Technology, Science University of Tokyo

Proton conducting polymer electrolytes are being developed for fuel cell applications, electrochromic display, sensor and supercapacitor development. It has reported that complexation of basic polymers with strong acids provides proton conducting polymers.[1] In this study, new proton conducting polymer based on poly(silamine) (PSA) with phosphoric acid ( $\text{H}_3\text{PO}_4$ ) was synthesized and the proton conduction was investigated.

### Experimental

The PSA /  $\text{H}_3\text{PO}_4$  complexes were synthesized by adding  $\text{H}_3\text{PO}_4$  into a 3 wt % methanol solution of PSA at room temperature under  $\text{N}_2$  for 24 h. The thermal stability of PSA /  $\text{H}_3\text{PO}_4$  complexes was measured by using thermogravimetry differential thermal analysis. The conductivity measurement of PSA /  $\text{H}_3\text{PO}_4$  complexes was carried out on a computer-interfaced YHP 4192A impedance analyzer over the temperature range of 20 °C to 160 °C.



Scheme Structure of PSA.

### Results and discussion

The reaction between *N,N'*-diethylethylenediamine( DEDA ) and dimethyldivinylsilane( DVS ) in the presence of *n*-butyllithium gave the PSA which was clear yellow and viscous liquid. The results of  $^1\text{H-NMR}$  analysis for the PSA indicated that the end-group of PSA was amine and the molecular weight was about 2000. The PSA /  $\text{H}_3\text{PO}_4$  complexes were obtained by blending the PSA and  $\text{H}_3\text{PO}_4$  due to the acid-base interaction between amine group of PSA and phosphoric acid molecules. The content of  $\text{H}_3\text{PO}_4$  in PSA /  $\text{H}_3\text{PO}_4$  complexes was controlled by changing the feed ratio of  $\text{H}_3\text{PO}_4$ . The PSA /  $\text{H}_3\text{PO}_4$  complexes were thermally stable up to 200 °C.

The PSA /  $\text{H}_3\text{PO}_4$  complexes exhibited proton conduction at anhydrous state. Figure 1 showed the temperature dependence of conductivity of PSA /  $\text{H}_3\text{PO}_4$  complexes with different  $\text{H}_3\text{PO}_4$  content. The conductivity of the PSA /  $\text{H}_3\text{PO}_4$  complexes increased with increasing  $\text{H}_3\text{PO}_4$  content and did not decrease over 100 °C. The PSA /  $\text{H}_3\text{PO}_4$  complex showed the conductivity of  $10^{-5} \text{ Scm}^{-1}$  at 160 °C at a concentration of 0.8  $\text{H}_3\text{PO}_4$  per repeat unit. Although the conductivity of general proton conducting polymers decreases around boiling

point of water due to evaporation of adsorbed water, the PSA/H<sub>3</sub>PO<sub>4</sub> complexes did not show such a decrease in conductivity. The carrier ion was shown to be proton to investigate H/D isotope effects of conductivity for PSA / H<sub>3</sub>PO<sub>4</sub> and PSA / D<sub>3</sub>PO<sub>4</sub> complex. These results indicate that H<sub>3</sub>PO<sub>4</sub> molecules served as carrier ion and solvent to transport proton in the complex films.

### Acknowledge

This study was supported by the Proposal-Based Advanced Industrial Technology R&D Program from NEDO of Japan.

### REFERENCE

[1] Fiona M. Gray, "Polymer Electrolytes", The Royal Society Chemistry, Cambridge, (1997).

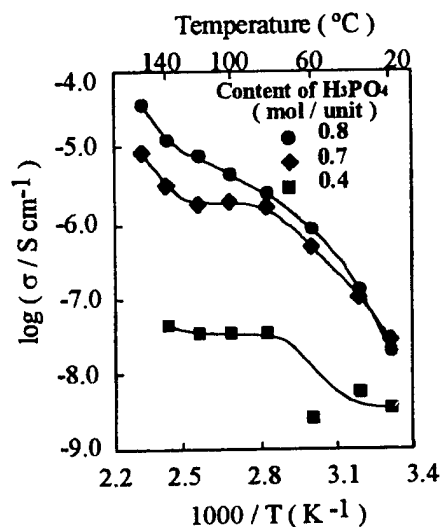


Fig.1 Arrhenius plots of conductivity for PSA / H<sub>3</sub>PO<sub>4</sub> complexes.

# ELECTROCHEMICAL AND STRUCTURAL INVESTIGATIONS ON SOLUTIONS OF MAGNESIUM ORGANO COMPOUNDS IN POLYMER ETHERS

C. Liebenow

Institut für Chemie und Biochemie,  
Ernst – Moritz – Arndt – Universität, Greifswald, Germany

Due to their interesting combination of mechanical and electrochemical properties polymer electrolytes were intensively investigated. Nevertheless there are only little experiences with polymer electrolytes which show a conductivity for multivalent cations. Solutions of simple magnesium salts ( $\text{MgX}_2$ ) in poly ethylene oxide (PEO) have only a little conductivity and behave as pure anion conductors. According to the HSAB – concept the  $\text{Mg}^{2+}$  - ion (hard acid) is tightly bound to the ether oxygen (hard base). In its metal organo compounds the magnesium ion ( $\text{R-Mg}^+$ ) appears to be a softer acid [3]. Therefore we investigated solutions of ethyl magnesium halides ( $\text{EtMgX}$ ) in the polymer ether with regard to their electrochemical and structural properties [4].

For electrolyte preparation PEO was intensively mixed with etheric solutions of  $\text{EtMgX}$ . As monomer ether tetrahydrofuran (THF), dibutylether (DBE) and diethylether (DEE) was used. It was removed from the system by evaporation in vacuum at elevated temperatures. The polymer electrolyte systems still contain one molecule of monomer ether per magnesium ion. Thus solid polymer or gel-like systems were obtained. The composition is given by the formula  $\text{EtMgX} \cdot \text{P}(\text{EO})_n \cdot \text{ether}$ , with  $2 < n < 20$ ,  $\text{X} = \text{Cl}, \text{Br}, \text{I}$ .

In figure 1 the dependence of the conductivity on the composition is shown. Best results were obtained with low EO to Mg – ratios, it means at very high electrolyte concentrations. With DEE as monomeric ether the highest conductivity and a low temperature dependence of conductivity were found. The kind of monomer ether has a influence on the conductivity. The content and kind of monomer ether influence the activation energy of the conducting process and the mechanical properties.

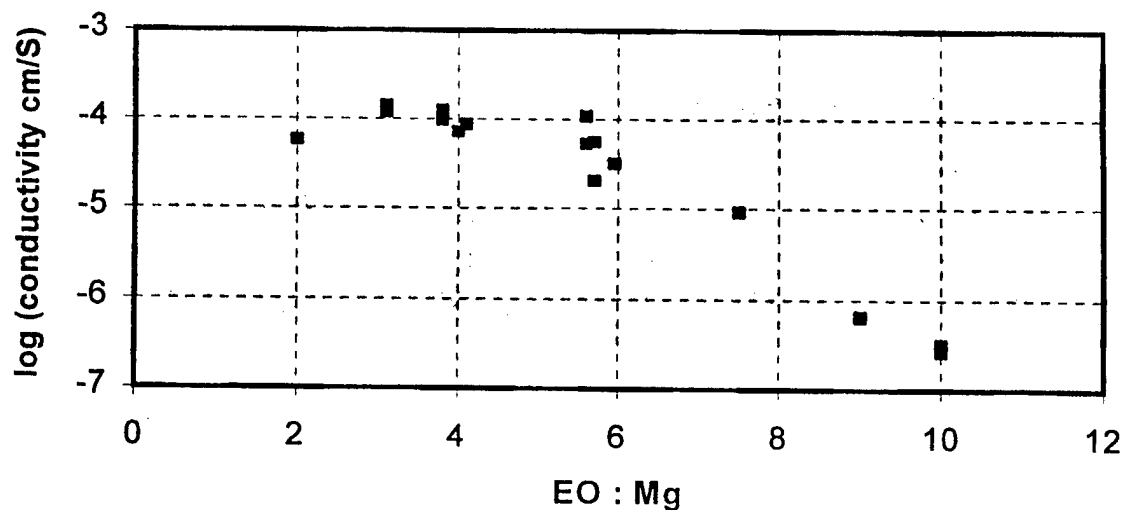


Fig 1: Dependence of conductivity on  $n$  (EO : Mg),  $\text{EthylMgBr} \cdot \text{P}(\text{EO})_n \cdot \text{DEE}$ , 40 °C.

Using these electrolytes the electrochemical magnesium deposition and oxidation is possible (fig.2).

The potential of magnesium electrodes in contact with these electrolytes were measured. For the system Mg/EtMgBr\*P(EO)<sub>6</sub>\*THF a OCV of 1,9 V vs. Ag/AgCl was found. This potential shows no pronounced dependence on the organic group or on the kind of monomer ether.

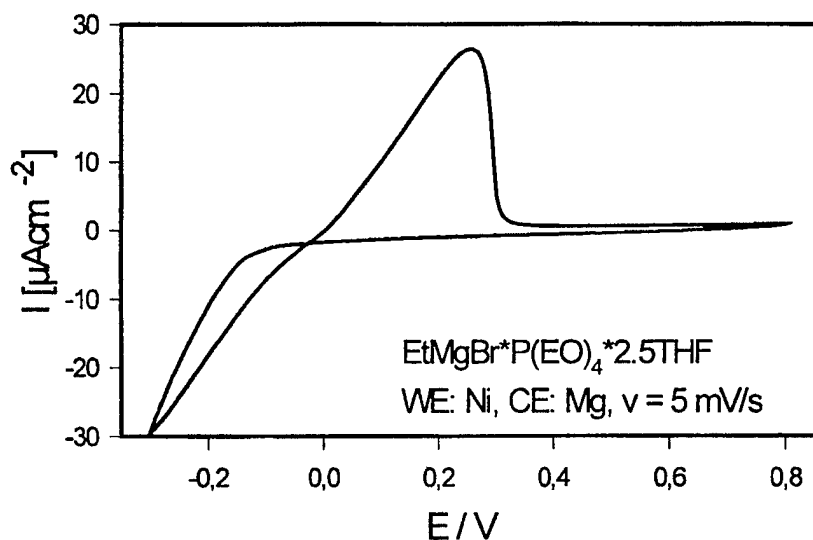


Fig. 2: CV, two-electrode cell, EtMgBr\*P(EO)<sub>4</sub>\*2,5 THF, temperature: 20 °C.

DSC- and X-ray diffraction measurements on the THF-containing electrolytes show a decreasing content of the crystalline phase in the PEO with increasing content of EtMgBr. At a EO to Mg ratio (n) of 4 the PEO - phase of the electrolyte is completely amorph. Furthermore the DSC-traces proof the formation of Mg-PEO complexes (high melting points). It shows, that the magnesium organo compound is at least partly bound to the polymer ether. On the other hand the monomer ether and the organic groups are also bound to the magnesium (IR-spectra). So the magnesium ions are coordinated with the oxygen of polymer ether and with monomer species and should be transported in form of positively charged complexes. This way a motion of magnesium along the polymer chain is understandable. As it was found for the conductivity there is a pronounced dependence of the electrolyte structure on the kind of monomer ether.

- [1] G. C. Farrington, R. G. Linford in J. R. MacCallum and C. A. Vincent, Polymer Electrolyte Reviews **2**, Elsevier Applied Science, London 1989, 271
- [2] C. A. Vincent, Electrochim. Acta **40**, 2035 (1995)
- [3] P. R. Markies, O. S. Akkerman, F. Bickelhaupt, W. J.J. Smeets, A.L. Spek, Adv. Organometal. Chem. **32**, 147 (1991)
- [4] C. Liebenow, Electrochim. Acta **43**, 1253 (1998)



THERMAL AND TRANSPORT PROPERTIES OF P(EO)<sub>n</sub>LiTFSI

Ludvig Edman <sup>1,2</sup>, Marca M. Doeff <sup>2</sup>, Anders Ferry <sup>3</sup>, John Kerr <sup>4</sup>, and L.C. De Jonghe <sup>2</sup>

<sup>1</sup> Department of Experimental Physics, Umeå University, S-901 87 Umeå, Sweden

<sup>2</sup> Lawrence Berkeley National Laboratory, Materials Science Division, University of California, Berkeley, California 94720, USA

<sup>3</sup> Department of Materials Engineering, Monash University, Clayton, 3168 VIC, Australia

<sup>4</sup> Lawrence Berkeley National Laboratory, Environmental Energy Technology Division, University of California, Berkeley, California 94720, USA

The polymer electrolyte system consisting of high molecular weight poly(ethyleneoxide) (PEO) complexed with LiN(CF<sub>3</sub>SO<sub>2</sub>)<sub>2</sub> (LiTFSI) has attracted considerable interest following the discovery of this low lattice energy salt by Armand and coworkers in 1990. [1] An initial report indicated a 'crystallinity gap' in the phase diagram for an O:Li ratio ranging from (8:1) to (10:1) for PEO-LiTFSI. [2] This was indeed a promising observation since, in previously examined systems, pristine PEO forms an eutectic with a stoichiometric polymer/salt compound having a melting point well above room temperature. [3] This had basically excluded the use of PEO based electrolytes at ambient conditions since it has been shown that significant ionic transport only appears in the amorphous regions of these materials. A latter report on a high molecular weight system apparently confirmed this crystallinity gap using repeated differential scanning calorimetry (DSC) measurements. Although small endothermic peaks originating in crystalline fractions did appear in the first heat cycle, all traces of non-conducting regions were gone in the second cycle. [4]

In this article we report a modified phase diagram for this system in which no 'crystallinity gap' or 'almost crystalline-free' concentrations exist near room temperature. Through extensive DSC measurements combined with AC impedance data, it is instead confirmed that the P(EO)<sub>n</sub>LiTFSI system behaves in a similar manner to other studied PEO systems, but that its recrystallization process is *extremely slow*. It is also shown that the eutectic concentration is located in the previously reported 'crystallinity gap', with a melting point close to room temperature. An indication of the very slow kinetics of recrystallization apparent in PEO/LiTFSI electrolytes was also observed by monitoring the crystallinity fraction in several different compositions as a function of temperature. This strongly underlines the importance of a non pre-

heat exposure of PEO based electrolytes in general, and this system in particular, in order to observe true intrinsic properties. The relevance of these observations to accurate measurements of the transport properties of PEO/LiTFSI electrolytes will be discussed.

This work was supported by the Assistant Secretary for Energy Efficiency and Renewable Energy, Office of Transportation Technologies, Office of Advanced Automotive Technologies of the U.S. Department of Energy under Contract No. DE-AC03-76SF00098. L.E. would like to thank Yong Bong Han and Steve Sloop for assistance in the laboratory and J.C. Kempes minnes stipendiefond and Vattenfall Utveckling AB for financial support. A.F. acknowledges support from NFR and the Wenner-Gren foundation.

## References

---

- [1] M. Armand, W. Gorecki and R. Andréani, Second International Symposium on Polymer Electrolytes, Edited by B. Scrosati, Elsevier Applied Science: New York, 91 (1990).
- [2] A. Vallée, S. Besner and J. Prud'homme, *Electrochimica Acta* 37, 1579 (1992).
- [3] C.D. Robitaille and D. Fauteux, *Journal of the Electrochemical Society* 133, 315 (1986).
- [4] W. Gorecki, M. Jeannin, E. Belorizky, C. Roux and M. Armand, *Journal of Physics: Condensed Matter* 7, 6823 (1995).

## INFLUENCE OF NaI ON STRUCTURAL RELAXATIONS IN POLY(ETHYLENE OXIDE).

A. van Zon, G.-J. Bel, B. Mos<sup>†</sup>, P. Verkerk<sup>†</sup> and S.W. de Leeuw  
*Department of Applied Physics, Delft University of Technology,  
Lorentzweg 1, 2628 CJ Delft, The Netherlands.*

<sup>†</sup>*Interfacultair Reactor Instituut, Delft University of Technology,  
Mekelweg 15, 2629 JB Delft, The Netherlands.*

To study the influence of NaI on the structural relaxations in Poly(ethylene-oxide) (PEO), we performed both molecular dynamics (MD) simulations and neutron spin-echo experiments on pure PEO and PEO<sub>x</sub>NaI electrolytes. The general formula of PEO is CH<sub>3</sub>-CH<sub>2</sub>-O-(CH<sub>2</sub>-CH<sub>2</sub>-O)<sub>m</sub>-CH<sub>2</sub>-CH<sub>3</sub>, where the number of monomers *m* is 25 in both simulations and experiments. In the simulations, a realistic model is used to describe the polymer backbone dynamics, using valence angle and torsion angle potentials. For the non-bonded interactions, Lennard-Jones and Coulomb potentials are used, where reduced charges are used to simulate polarization effects. The starting configurations are made by using a Pivot Monte Carlo sampling procedure.

During the MD simulations, we calculated the mean square displacement of the backbone sites and the incoherent part of the intermediate scattering function  $F(k, t)$ , for 400 ps. The latter is calculated in *k*-range between 1.6 nm<sup>-1</sup> and 23 nm<sup>-1</sup>. Neutron spin-echo experiments, performed at the Institut Laue-Langevin (ILL, Grenoble), are used to measure the  $F(k, t)$ , from 4 to 1000 ps and in a *k*-range from 3.71 nm<sup>-1</sup> to 15.30 nm<sup>-1</sup>. The results of these experiments are compared with the results of the simulations.

By studying the mean square displacement, we find a Rouse-like motion, which can be described by  $\langle \Delta R^2(t) \rangle = (D_R t)^\alpha$ , with  $\alpha=0.65$  and independent of the NaI concentration. The "diffusion constant"  $D_R$  depends on the NaI concentration and is decreasing as the concentration is increased, indicating the dynamics is slowed down by the influence of NaI. This is believed to be caused by the cross-linking of two oxygen atoms via a sodium atom.

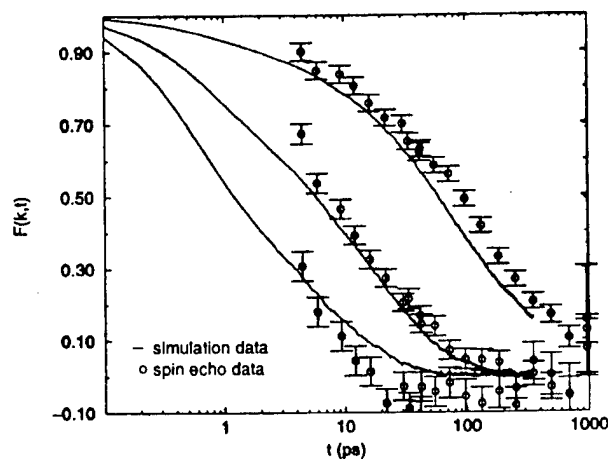


Figure 1:  $F(k, t)$  for pure PEO, for  $k=14.76 \text{ nm}^{-1}$ ,  $k=9.84 \text{ nm}^{-1}$  and  $k=4.92 \text{ nm}^{-1}$  (left to right) at  $T=343\text{K}$

The  $F(k, t)$  is calculated and measured at  $T=343\text{K}$ , at which PEO is in the liquid phase. The results are shown in figure 1 for  $k=4.92\text{ nm}^{-1}$ ,  $9.84\text{ nm}^{-1}$  and  $14.76\text{ nm}^{-1}$ , for pure PEO. It shows that the simulations are in good agreement with the spin-echo experiments, in this  $k$ -range. The relaxation can be described by a stretched exponent,  $F(k, t) = A \exp(-(t/\tau)^\beta)$ , where  $A$ ,  $\tau$  and  $\beta$  can be  $k$ -dependent. The small  $k$  exponent  $\beta=0.65$ , coincides with the exponent  $\alpha$ , obtained from the mean square displacement. This can be understood by realizing that the mean square displacement and the  $F(k, t)$  are related via the Gaussian approximation,  $F(k, t) = \exp(-k^2/6 \langle \Delta R^2(t) \rangle)$ , which is valid for small  $k$ -values.

Using this stretched exponent, the relaxation times  $\tau$  are obtained at different NaI concentrations, in a large  $k$ -region, and are shown in figure 2. Here, as is the case for the mean square displacement, the relaxation times become longer as the NaI concentration is increased. This slowing down occurs at all  $k$ -values. Also, it is clearly visible that, in the simulations, the increase in

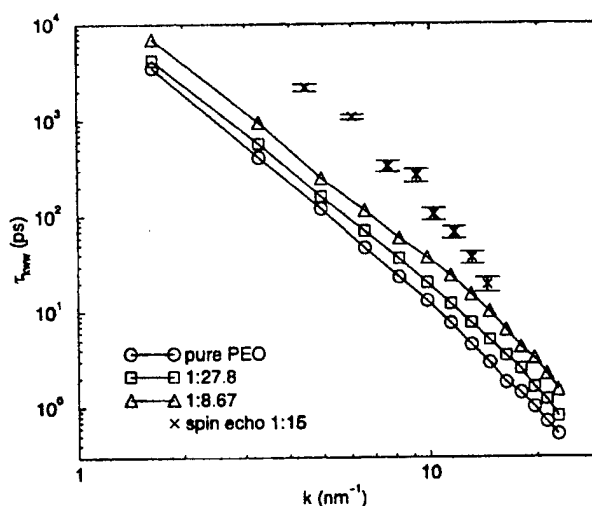


Figure 2: relaxation times  $\tau$  for different NaI concentrations at  $T=343\text{K}$ , obtained from simulation (solid line) and spin-echo experiments (dashed line).

relaxation time is too small as compared to the experimental data. Probably, this is caused by the use of reduced charges, which reduces the interaction between the sodium and the oxygen. It is therefore less likely, that in the simulation two oxygen atoms are cross-linked via a sodium atom.

In summary, we performed MD simulations and neutron spin-echo experiments on PEO and studied the influence of NaI on the structural relaxations. In the pure PEO melt, the results of the simulations are in good agreement with the experiments. When NaI is added, we observe an increase in relaxation times in the entire  $k$ -region measured. However, the influence of NaI is smaller in the case of simulations.

## SOLUTE SEGREGATION, ELECTRICAL PROPERTIES AND DEFECT THERMODYNAMICS OF NANOCRYSTALLINE TiO<sub>2</sub> AND DOPED CeO<sub>2</sub>

P. Knauth\*, H. L. Tuller\*\*

\*Laboratoire EDIFIS-CNRS, Faculté des Sciences de Marseille-St Jérôme, F-13397 Marseille Cedex 20, \*\*Massachusetts Institute of Technology, Department of Materials Science and Engineering, Cambridge, MA 02139.

The development of many suitable preparation techniques for nanocrystalline oxides has created a great deal of interest in these materials, given the likelihood of unique properties resulting from the large proportion of atoms at interface sites. For instance, large increases in electronic conductivity and oxygen deficiency were previously reported for nominally pure CeO<sub>2</sub> [1]. This was tentatively ascribed to the lower enthalpy of formation of oxygen vacancies at interface sites.

Recently, the question of enhanced solubility in nanocrystalline solids was investigated. The apparent solubility of copper in the CeO<sub>2</sub>-Cu<sub>2</sub>O system was found to be about 10 mol% by electrochemical e.m.f. measurements [2]. This exceptionally large increase in solubility compared with coarse-grained ceria, in which copper is nearly insoluble, may be interpreted on the basis of segregation of copper at the high density of interfacial sites. The maximum solubility corresponds approximately to the order of one monolayer of copper segregated onto the ceria particles. This interpretation is corroborated by the high catalytic activity of nanocrystalline copper-doped ceria.

While the CeO<sub>2</sub>-PrO<sub>x</sub> fluorite system already exhibits a large solid solubility, the material with 70 mol% PrO<sub>x</sub>, reported to be two phase when coarse grained, is found to be single phase in nanocrystalline form [3]. In accordance with previous investigations of other nanocrystalline oxides, the oxygen deficiency attains very high values ( $x > 0.1$ ) with evidence for vacancy ordering. Furthermore, the measured chemical diffusivities are quite large, of the order of  $10^{-6}$  cm<sup>2</sup>/s, consistent with the rapid establishment of steady state following change in oxygen partial pressure. The low activation energy of 0.3 eV suggests short circuiting diffusion paths via interfaces.

Studies have also been initiated on nanocrystalline TiO<sub>2</sub> with the low temperature anatase phase, another model mixed conductor with a different intrinsic disorder type (cation Frenkel). Our experiments [4] reveal an uncommon domain of ionic conductivity at high oxygen partial pressures, whereas at low  $P(O_2)$ , the electronic conductivity predominates and increases strongly with a  $P(O_2)^{-1/2}$  dependence. These results are interpreted on the basis of a defect model in which partially ionized titanium interstitials and electrons are generated in the presence of background acceptor impurities.

- [1] Y.-M. Chiang, E. B. Lavik, I. Kosacki, H. L. Tuller, J. Y. Ying, *J. Electroceramics*, **1**, 7 (1997).
- [2] P. Knauth, G. Schwitzgebel, A. Tschöpe, S. Villain, *J. Solid State Chem.*, October 1998.
- [3] P. Knauth, H. L. Tuller, *J. Europ. Ceram. Soc.*, 1999, in press.
- [4] P. Knauth, H. L. Tuller, *J. Appl. Phys.*, January 1<sup>st</sup>, 1999 issue.

NMR AND IMPEDANCE STUDIES OF IONIC MOTION  
IN NANOCRYSTALLINE CERAMICS

Paul Heitjans

Institut für Physikalische Chemie und Elektrochemie, Universität Hannover,  
Callinstr. 3-3A, D-30167 Hannover, Germany  
E-mail: heitjans@mbox.pci.uni-hannover.de

Nanocrystalline materials consist of an assembly of randomly oriented crystallites with an average diameter of typically 10 nm and structurally disordered interfacial regions where as much as 30% of the atoms are located [1]. The main point of interest here is the influence of this heterogeneous structure on ion dynamics and transport.

The nanocrystalline ceramics on which we report here were prepared – partly for the first time – by condensation of the evaporated compound in a noble gas or by mechanical attrition of the coarse-grained starting material in a high-energy ball mill. Most of the nanocrystalline ceramics studied by our group up to now are chemically homogeneous; these include  $\text{CaF}_2$ ,  $\text{LiNbO}_3$ ,  $\text{LiTiS}_2$  and  $\text{LiBO}_2$ . The latter system is also being investigated as a heterogeneous mixture  $\text{Li}_2\text{O}:\text{B}_2\text{O}_3$  at various compositions  $(1-x)\text{Li}_2\text{O}:x\text{B}_2\text{O}_3$  with  $x = 0 \dots 0.9$ . In all cases the normal-crystalline counterparts where the percentage of atoms in the interfaces is negligible and in the cases of  $\text{LiTiS}_2$  and  $\text{LiBO}_2$  also the amorphous/glassy modifications have been studied for comparison. In order to exclude grain boundary relaxation and grain growth in the nanocrystalline samples, measurements had to be restricted to temperatures below about 500 K as a rule.

NMR measurements of the spin-lattice relaxation rate  $T_1^{-1}$  of  $^{19}\text{F}$  and  $^7\text{Li}$ , respectively, in the nanocrystalline samples show the typical rise of  $T_1^{-1}$  with temperature  $T$ , starting partly below room temperature, to the diffusion-induced maximum [2]. The effective activation energy as obtained from the slope of the low-temperature flank in the usual  $\log T_1^{-1}$  vs  $T^{-1}$  plot is in each case considerably smaller than the corresponding value in the polycrystalline counterpart except for  $\text{LiTiS}_2$ . While in layer-structured  $\text{LiTiS}_2$  the moving ions ( $\text{Li}^+$ ) in the layers of the crystallites and the interfacial regions experience essentially the same potential and perform 2D diffusion, in the other ion conductors, having 3D structures, transformation from the normal poly- to the nanocrystalline form leads to a considerable increase of the effective average jump rate. The frequency dependence of  $T_1^{-1}$  on the low-temperature flank was generally found to deviate strongly from that expected from standard theory for uncorrelated jumps.

Measurements of the NMR lineshape of  $^{19}\text{F}$  and  $^7\text{Li}$  (central line), respectively, as a function of temperature revealed that in the nanocrystalline materials the line consists of two contributions centered at the same frequency: a broad component which corresponds to the rigid lattice line of the polycrystalline reference material and superimposed a motionally narrowed component which results from the NMR probe nuclei in the interfacial regions being already mobile at a temperature where the probes in the grains are still at rest. At high  $T$  where the probes in the grains are also mobile and at low  $T$  where the probes in the grain boundaries as well as in the grains are immobile an unstructured line shows up. It is thus possible to differentiate between the ions having different mobilities in the heterogeneous structure of the nanocrystalline materials.

Measurements of the complex conductivity, performed by impedance spectroscopy in the frequency range from 5 Hz to 13 MHz, also allow one to discriminate between contributions from the grain boundaries and the grains. This has explicitly been shown for nanocrystalline  $\text{CaF}_2$ . The d.c. conductivity  $\sigma_{dc}$  is strongly enhanced as compared to single- or polycrystalline

CaF<sub>2</sub> which is attributed to the fast conduction pathways in the structurally disordered grain boundary regions whose volume fraction is largely increased due to the reduction in grain size. This also corresponds to the observation in the case of LiBO<sub>2</sub> that  $\sigma_{dc}$  increases with the milling time to produce the nanocrystalline material.  $\sigma_{dc}$  does, however, not attain the value of the glassy modification. Another interesting effect occurs in the nanocrystalline composite (1-x)Li<sub>2</sub>O:xB<sub>2</sub>O<sub>3</sub>. When the fraction  $x$  of the insulating phase B<sub>2</sub>O<sub>3</sub> is increased,  $\sigma_{dc}$ , starting from the value of the poorly conducting Li<sub>2</sub>O, rises by a factor of about ten to a maximum at  $x \approx 0.5$ . This behaviour is qualitatively similar to that of the classic dispersed ionic conductors discovered by Liang [3]. On the other hand in the polycrystalline composite  $\sigma_{dc}$  monotonously decreases with increasing  $x$ .

[1] H. Gleiter, Progress in Materials Science **33**, 223 (1989)

[2] P. Heitjans and A. Schirmer, in: Diffusion in Condensed Matter, J. Kärger, P. Heitjans, R. Haberland (eds.), Vieweg, Braunschweig/Wiesbaden 1998, p. 116

[3] C. C. Liang, J. Electrochem. Soc. **120**, 1289 (1973)

## Ion and Electron Transport in Two-Dimensional Polymer-Inorganic Nanocomposites of $V_2O_5$ , $MoO_3$ , $MoS_2$ and $RuCl_3$

M. G. Kanatzidis<sup>\*,1</sup>, Lei Wang<sup>1</sup>, J. Schindler<sup>2</sup>, Paul Brazis<sup>2</sup>, Melissa Rocci<sup>2</sup> and Carl Kannewurf<sup>2</sup>

(1) Department of Chemistry and the Center of Fundamental Materials Research, Michigan State University, East Lansing, Michigan 48824 (2) Department of Electrical Engineering and Computer Science, Northwestern University, Evanston, Illinois 60208

Inorganic layered materials exist in great variety. They possess well defined, ordered intralamellar space potentially accessible by foreign species. This ability enables them to act as matrices or hosts for polymers, yielding interesting hybrid nano-composite materials. During the decade we have focused our efforts on creating such materials with conjugated and saturated organic macromolecules. We have developed several general synthetic routes for inserting polymer chains into host structures and have designed many novel nanocomposites. We have now three synthetic strategies at our disposal: (a) *In-situ* intercalative polymerization (ISIP) of a monomer using the host itself as the oxidant. The rationale behind intercalative polymerization is that host matrices with high electron affinity can oxidatively polymerize appropriate monomers in their interior. (b) Monomer intercalation followed by topotactic intralamellar solid state polymerization. This route creates conjugated polymers inside non-oxidizing hosts. (c) *Direct* precipitative encapsulation of polymer chains by colloiddally dispersed *single layers* of a host. This approach gives access to a large variety of nano-composites with many kinds of polymers and hosts. Examples include saturated long molecular weight (MW) polymers such as polyethylene oxide (PEO), nylons, cellulose etc.

Experimental work has generally shown that virtually all types and classes of nanocomposite materials lead to new and improved properties when compared to their macrocomposite counterparts. Therefore, nanocomposites promise new applications in many fields such as mechanically reinforced lightweight components, battery cathodes, solid electrolytes and sensors.

Polymer-inorganic nanocomposites exhibit fast ion conduction and introduction of a polymer with affinity for Li ions between the sheets of  $V_2O_5$ ,  $MoO_3$ ,  $MoS_2$ ,  $LiMnO_2$ ,  $RuCl_3$  etc could improve its performance as intercalative electrode. The host materials must be colloiddally dispersed into single layers in various solvents.

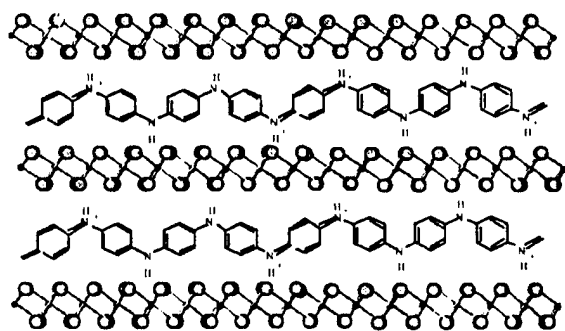
We used the exfoliated suspension method to encapsulate several water-soluble polymers such as poly(vinylpyrrolidone) (PVP), poly(propylene-glycol) (PPG) and methyl-cellulose in  $V_2O_5$  xerogel,  $MoO_3$ ,  $MoS_2$  and  $RuCl_3$ . A detailed account of this work has been published.<sup>1</sup> This methodology is general and suitable for intercalation of very large MW polymers provided these polymers are soluble. The synthesis of  $PEO/V_2O_5 \cdot nH_2O$  compounds is accomplished by mixing aqueous solutions of PEO with aqueous gels of vanadium oxide in various ratios. The  $PEO/V_2O_5 \cdot nH_2O$  films absorb water reversibly and they are capable of ion redox intercalation. For example,  $Li^+$  can be intercalated by reaction with lithium iodide or by occlusion of  $Li^+$  salts. Results on the inclusion of other alkali ions in  $(PEO)_xV_2O_5 \cdot nH_2O$  will be presented. The



(PEO)<sub>x</sub>V<sub>2</sub>O<sub>5</sub>·nH<sub>2</sub>O films are light-sensitive and turn dark-blue upon irradiation. The irradiated samples have dramatically enhanced conductivity at room temperature. The ion and electron transport properties of these materials will be presented.

The lamellar V<sub>2</sub>O<sub>5</sub>·nH<sub>2</sub>O xerogel and its polymer intercalation compounds such as (PEO)<sub>x</sub>V<sub>2</sub>O<sub>5</sub>·nH<sub>2</sub>O are used as the active material for sensing reducing gases such as hydrogen, hydrazine, hydrogen sulfide, mercaptans etc. and oxidizing gases such as N<sub>2</sub>O<sub>4</sub>. The V<sub>2</sub>O<sub>5</sub>·nH<sub>2</sub>O xerogel based materials are fabricated into films which are easily deposited onto electrode arrays of any size and shape. The sensors detect increases in electrical conductivity because electrons from the small molecules are transferred to the conduction band of V<sub>2</sub>O<sub>5</sub>·nH<sub>2</sub>O. This introduces additional charge carriers into the material and gives rise to an increase in conductivity. To bring the (PEO)<sub>x</sub>V<sub>2</sub>O<sub>5</sub>·nH<sub>2</sub>O back to the low conducting state an applied anodic voltage can be applied to remove the added electrons. The sensitivity of these sensors is in the ppb to ppm range.

α-RuCl<sub>3</sub> is an interesting new host material. We have discovered that it can be a suitable host for polymer intercalation particularly PEO, PPO, polyaniline and polypyrrole. The new materials Li<sub>x</sub>(PEO)RuCl<sub>3</sub> will be described in detail. The potential of Li<sub>x</sub>(PEO)RuCl<sub>3</sub> for use as a novel electrode material to perform electrocatalytic reactions will be discussed.



Polymer-RuCl<sub>3</sub> nanocomposite

In this presentation, we will present and discuss the Li transport as well as electron transport properties of these materials as a function of temperature. Solid state <sup>7</sup>Li NMR spectroscopy of the nanocomposites indicates a more versatile chemical environment in the nanocomposites than in the host which leads to higher ionic conductivities in these lamellar systems than otherwise might be attainable.

## References

1. C.-G. Wu, D. C. DeGroot, H. O. Marcy, J. L. Schindler, C. R. Kannewurf, Y.-J. Liu, Hirpo, W., M. G. Kanatzidis, *Chem. Mater.*, **1996**, 8, 1992-2004.
2. Hui-Lien Tsai, Jon L. Schindler, Carl R. Kannewurf and Mercouri G. Kanatzidis, *Chem. Mater.* **1997**, 9, 875-878.
3. Lei Wang, Jon Schindler, Carl R. Kannewurf, Mercouri G. Kanatzidis, *J. Mater. Chem.*, **1997**, 7, 1277-1283.
4. Lei Wang, Paul Brazis, Melissa Rocci, Carl R. Kannewurf, Mercouri G. Kanatzidis, *Chem. Mater.*, **1998**, 10 (11), 3298 -3300.

## ELECTRICAL CONDUCTIVITY AND BAND GAP ENERGY IN NANOCRYSTALLINE CERIA AND ZIRCONIA THIN FILMS

Igor Kosacki, Vladimir Petrovsky and Harlan U. Anderson

Electronic Materials Applied Research Center, University of Missouri-Rolla  
303 MRC, Rolla, MO 65401, USA

A number of studies have shown that the electrical properties of dense oxides becomes microstructural dependent when the grain size decreased to below 100nm. This dependence appears to be primarily due to increased interfacial area and size-dependent defect properties which tend to enhance the electrical conductivity and reaction kinetics what is very important for the application of nanocrystalline materials in electrochemical devices. In order to observe these phenomena, it is necessary to produce dense oxides at sufficiently low temperatures and stabilize their microstructure. This can be achieved using the thin film preparation techniques which allow the formation of dense materials at reduced processing temperatures. Thus our studies have employed a polymeric precursor spin coating technique which allows the preparation of dense nanocrystalline oxide thin films at temperatures about 1000 degrees lower than those to obtain dense microcrystalline sized materials.

Our research has been focused on the obtaining the nanocrystalline thin films of oxygen conductors and study their structural, electrical and optical properties related to the microstructure. In the present work, the results of the preparation of  $\text{ZrO}_2\text{:16\%Y}$  and  $\text{CeO}_2$  thin films will be presented and correlated with the processing parameters such as sintering temperature, the thin film thickness and the type of substrate. Atomic force microscopy and x-ray analyze were used to determine the grain size which has been varied from 1 to 300nm when the sintering temperature was changed in the 350-1400°C range.

The electrical conductivity has been studied by impedance spectroscopy as a function of oxygen activity and correlated with the microstructure and energy gap which was determined from optical absorption measurements. Nanocrystalline thin films are characterized by enhanced electrical conductivity and different stoichiometry comparing with the microcrystalline specimens. For  $\text{ZrO}_2\text{:16\%Y}$  films an anomalous decrease in the electrical conductivity in low oxygen activity range was observed which has been interpreted using a defect pair association model. This model describes the relationship between the electrical conductivity and oxygen partial pressure relative to the band structure and partly ionized defect associates.

The relationship between the band gap and microstructure of  $\text{ZrO}_2\text{:16\%Y}$  and  $\text{CeO}_2$  thin films has been also determined and discussed. In the nanocrystalline range the band gap energy was found to increase with decreasing grain size suggesting agreement with the quantum confinement effect. This observation suggests that the ratio between ionic and electronic conductivity is influenced by material microstructure.

## ELECTRODEPOSITION OF NANOSTRUCTURED METAL FILMS

George S. Attard, Joanne M. Elliott, Philip N. Bartlett and John R. OwenDepartment of Chemistry  
University of Southampton  
Southampton SO17 1BJ, UK.

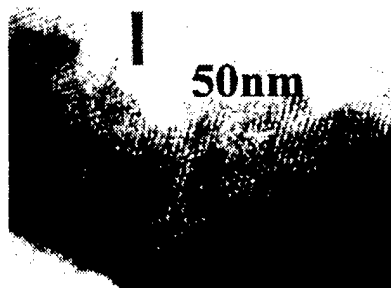
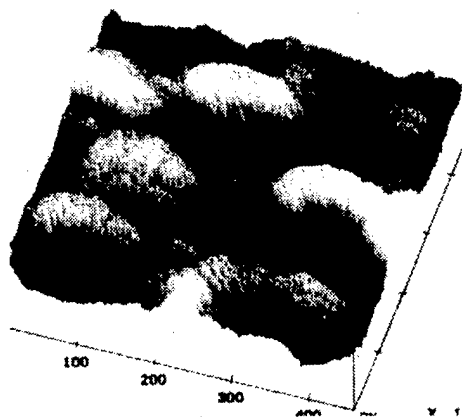
The electrodeposition of nanostructured platinum films from the aqueous environments of lyotropic liquid crystal phases has recently been described as a versatile method of producing mesoporous solids with a high degree of spatial order[1]. This paper will review recent progress in the fabrication of other materials in various new forms with various properties which may have applications in many areas including batteries, supercapacitors, electrochromic devices and sensors.

Characterisation by transmission electron microscopy reveals well-defined, long-range porous nanostructure. Scanning tunneling microscopy confirms the nanoporosity and also shows the electrodeposited film as a macroscopically smooth surface which follows the surface profile of the substrate.

Electrochemical characterisation by cyclic voltammetry in sulphuric acid shows the normal features of polycrystalline platinum and very high specific capacitance consistent with the large internal surface. Impedance measurements indicate that the internal pores are open and that the electronic conduction path is well connected.

Nanostructured platinum has been prepared in hexagonal and cubic forms according to the corresponding regions in the binary phase diagram the amphiphile, C<sub>16</sub>EO<sub>8</sub> and water. The addition of platinum salt usefully extends the stability range of the hexagonal form to temperatures higher than 90°C. The pore sizes can be controlled by addition of heptane to the amphiphile/water mixture. The products are believed to be stable to temperatures of up to 500°C without sintering because the high surface area is associated with a highly concave internal surface.

The technique has been extended to palladium, nickel, cobalt, tin and lead. In the case of tin, the material has shown an increased tolerance to deep lithium cycling over the bulk form.

TEM of H<sub>1e</sub> PtSTM of H<sub>1e</sub>-Pt

[1] G.S. Attard, P.N. Bartlett, N.R.B. Coleman, J.M. Elliott, J.R. Owen and J.H. Wang. *Nature* (1997) **278**, 838-840

# INVESTIGATION OF NANOCRYSTALLINE MAGHEMITE ( $\gamma\text{-Fe}_2\text{O}_3$ )

G. Schimanke, M. Martin

Institute of Physical Chemistry, Darmstadt University of Technology,  
Petersenstraße 20, 64287 Darmstadt, Germany

Nanocrystalline ironoxides were produced by inert gas condensation (IGC). The phase and crystal size analysis were done by x-ray powder diffraction (XRD), x-ray absorption spectroscopy (XAS) and transmission electron microscopy (TEM). All three methods show that only maghemite was formed with crystall sizes of about 20 nm.

The kinetics of the phase transition from maghemite to hematite was observed by in situ XRD measurements at temperatures around 300°C. It is possible to describe the transition by a first order kinetics, with an activation energy of 76 kJ/mol (Fig.1). The sizes of the produced hematite crystals were above 35 nm, but growing of the maghemite crystals was not observed. There are two explanations. First, several maghemite crystals are growing fast and transform above 35 nm to hematite or there is first the transformations and then the fast growing of the hematite crystals.

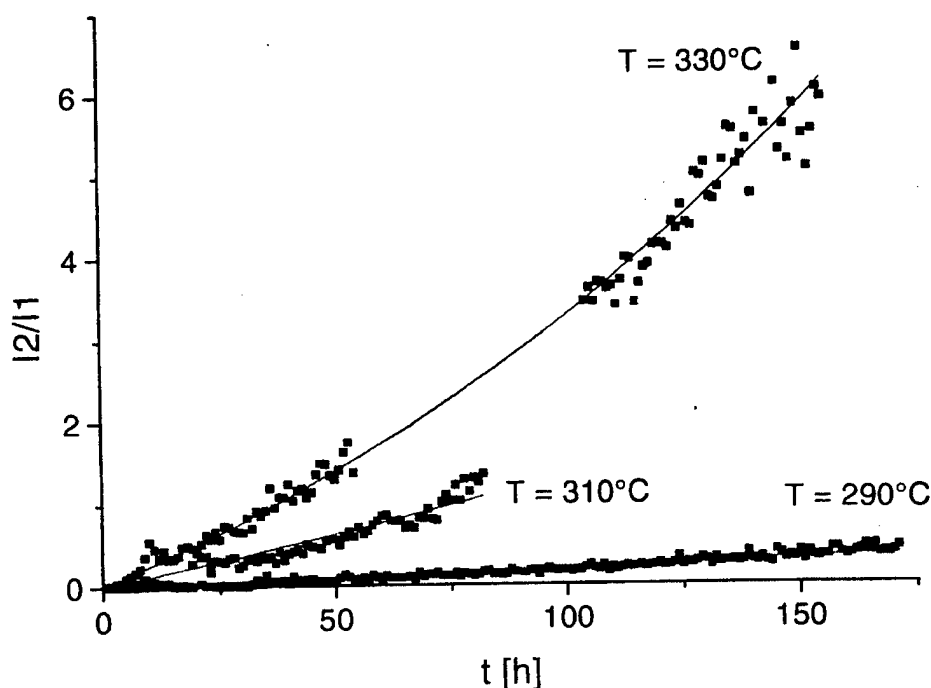


Fig.1 XRD-intensity ratio of maghemite(1) and hematite(2) as a function of time

At temperatures below 280°C the reaction rate is so slow, that no hematite is found after 7 days. So impedance measurements were done below this temperature. It was found, that the resistivity of the sample decreases with increasing water partial pressure and decreasing oxygen partial pressure. These results are discussed using an appropriate defect model for  $\gamma\text{-Fe}_2\text{O}_3$ .

## ELECTRIC AND THERMAL PROPERTIES OF PEO-BASED NANOCOMPOSITE POLYMER ELECTROLYTES

Domenico Marchesini, Piercarlo Mustarelli, Eliana Quartarone, Corrado Tomasi, Aldo Magistris  
C.S.T.E.-C.N.R. and Dipartimento di Chimica-Fisica, Università di Pavia  
Viale Taramelli 16, 27100 Pavia - Italy

Solid state electrolytes based on poly(ethylene oxide) (PEO) complexed with alkali salts are still of great interest for applications in solid-state electrochemical devices [1]. In order to enhance electric and mechanical properties of these solvent-free electrolytes, several studies were addressed on the effect of adding both organic and inorganic fillers [2]. After many works regarding the introduction of fillers in the micrometer range, recently, much attention has been focused on PEO-based composites with nanoscale fillers. For instance, Michael et al. [3] reported conductivity of the order of  $10^{-3} \text{ ohm}^{-1} \text{ cm}^{-1}$  below the PEO melting point, by adding nanoscale  $\gamma\text{-Al}_2\text{O}_3$  to PEO- $\text{LiClO}_4$  plasticised with benzene-based esters.

The aim of the present work is to investigate two solvent-free PEO-based systems, PEO: $\text{LiPF}_6$  and PEO: $\text{LiN}(\text{CF}_3\text{SO}_2)_2$  to search suitable compositions for super-ambient electrolytes, chiefly for applications in electric vehicles. Attention is paid on both electric and thermal properties changes after addition of nanoscale silica. The out-of equilibrium phase diagram of PEO: $\text{LiPF}_6$ , to date non yet reported in the literature, is discussed. This system presents a complex at  $n = 6$ . Electric conductivity measurements as a function of  $\text{LiPF}_6$  content, show a maximum at room temperature located at  $n = 30$  (see Fig. 1). Differential Scanning Calorimetry on 60 days-aged samples highlights, as expected, a higher extent of crystallinity than the one observed on as-prepared samples.

Different amounts of nanoscale silica (ranging from 5 to 20 wt%) have been added to  $n = 30$  sample aliquots. The filler addition enhances the conductivity and it improves the film stability by inhibiting the complex formation in PEO: $\text{LiPF}_6$  up to  $110^\circ\text{C}$ . The stability of the composite electrolytes is also studied by combining thermal and solid-state NMR information. The PEO: $\text{LiN}(\text{CF}_3\text{SO}_2)_2$  system displays higher conductivity values than those collected for PEO: $\text{LiPF}_6$ , but poorer mechanical properties.

- [1] F. Croce, G.B. Appetecchi, L. Persi, B. Scrosati, *Nature* **394**, 456 (1998).
- [2] E. Quartarone, P. Mustarelli, A. Magistris, *Solid State Ionics*, **110**, 1 (1998).
- [3] M.S. Michael, M.M.E. Jacob, S.R.S. Prabaharan and S. Radhakrishna, *Solid State Ionics*, **98**, 167 (1997).

COMPOSITE ELECTRODES FOR LITHIUM-ION BATTERIES CONTAINING  
NANO-SIZED LITHIUM STORAGE METALSMario Wachtler<sup>1</sup>, Ilse Papst<sup>2</sup>, Ferdinand Hofer<sup>2</sup>, Martin Winter<sup>1</sup>, and Jürgen O. Besenhard<sup>1</sup><sup>1</sup> Institute for Chemical Technology of Inorganic Materials, Graz University of Technology,  
Stremayrgasse 16 / III, A-8010 Graz, Austria.<sup>2</sup> Research Institute for Electron Microscopy, Graz University of Technology,  
Steyrergasse 17 / III, A-8010 Graz, Austria.

Li-ion batteries are on the best way to become the most important battery system on the consumer market. Accordingly, a lot of effort is put into the further improvement of the gravimetric and volumetric capacities. One very promising approach is to replace the commonly used carbon anodes with lithium storage metals (LSMs) such as Al, Si, Sn, Sb, Bi, and Ag (e.g., [1]) or with precursor materials to LSMs, such as tin oxides (e.g., [2]). LSMs can readily take up and release Li at reasonable rates, and show theoretical Li storage capacities as high as 948 mAh g<sup>-1</sup> in the case of Sn. A crucial point is the structural integrity of the electrode during charge and discharge: since the volume differences between the unlithiated and the fully lithiated metals are in the order of some 100 % the materials will crumble unless the reaction layer is kept very small.

From our previous works on electroplated [1] and chemically precipitated [3] metals and intermetallics, such as Sn, Sn/SnSb, and Sn/SnAg<sub>3-4</sub>, and from work by other authors, three major strategies have been identified with which it is possible to prolong the cycle life: first, the tailoring of a proper particle morphology, above all a reduction of the particle size; second, the use of phase mixtures, such as Sn/SnSb, instead of single phase materials, such as pure Sn; and third, the choice of active phases, like SnSb, which show complex reversible phase separation reactions during the reaction with Li.

At the centre of interest of this contribution are the morphology of LSM-containing composite electrodes and the changes of the morphology during (galvanostatic) cycling. Apart from the active material, such as Sn/SnSb, the composite electrodes contain PVDF as binder and Ni (containing some B) as conductive additive. The active metal powders as well as the Ni(B) powder were synthesized by reductive precipitation with NaBH<sub>4</sub> in aqueous solution [3]. The morphology was investigated with SEM and TEM (including element mapping). As an example a TEM brightfield image of an uncycled Sn/SnSb composite electrode is reproduced in Fig. 1. It can be seen that the smallest particles of the active material are only about 15 nm in diameter. An electron energy loss (EEL) spectrum of the specimen region, shown in Fig. 2, reveals the overlapping Sn M<sub>4,5</sub>, Sb M<sub>4,5</sub>, and O K edges.

A second point which is addressed is the formation of the so-called 'solid electrolyte inter-phase' (SEI) on the surface of the composite electrode. Stemming from electrolyte decomposition mainly during the first charge/discharge cycles, it prevents the electrolyte from further decomposition. Its formation, however, irreversibly consumes Li (thus contributing to the irreversible capacity) and electrolyte, and it increases the resistance of the electrode. The SEI was investigated with SEM and impedance spectroscopy (cf., for example, also work on Li-Sn and Li-Sn-Cd alloys [4]).

- [1] J. Yang, M. Winter, and J.O. Besenhard, *Solid State Ionics* **90**, 281 (1996).
- [2] I.A. Courtney and J.R. Dahn, *J. Electrochem. Soc.* **144**, 2045 (1997).
- [3] J. Yang, M. Wachtler, M. Winter, and J.O. Besenhard, submitted to *Electrochemical and Solid-State Letters*, (1998/99).
- [4] A.V. Churikov, E.S. Nimov, and A.L. Lvov, *Electrochim. Acta* **42**, 179 (1997).



Fig. 1: TEM brightfield image of an Ar-ion milled Sn/SnSb composite electrode (82 wt % Sn/SnSb, 10 % Ni, 8 % PVDF, on a stainless steel grid).

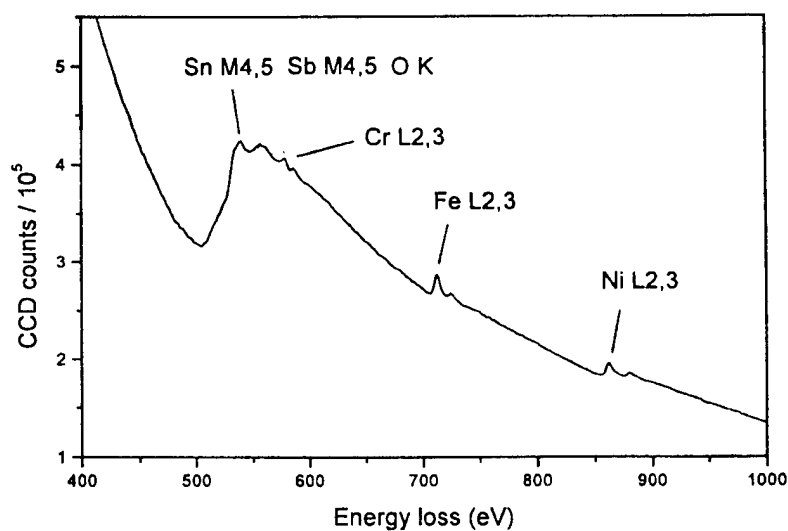


Fig. 2: EEL spectrum of a Sn/SnSb composite electrode (82 wt % Sn/SnSb, 10 % Ni, 8 % PVDF, on a stainless steel grid, the Sn/SnSb contains some oxygen impurities).

The authors acknowledge the financial support through the Austrian Science Fund (FWF) and the Oesterreichische Nationalbank (special research programme: 'Electroactive materials' and project FWF-P12768-CHE) and through Mitsubishi Chemical Corp., Japan.

## PHASE STABILITY OF NANOSTRUCTURED TETRAGONAL POLYCRYSTALLINE ZIRCONIA (TPZ) VERSUS TEMPERATURE AND WATER VAPOUR

E. Djurado, L. Dessemond, C. Roux

Laboratoire d'Electrochimie et de Physico-Chimie des Matériaux et des Interfaces  
LEPMI, BP 75, 38402 St Martin d'Hères Cedex, France, (INPG-CNRS-UJF)

Phone : (33) 04 76 82 66 84 - Fax : (33) 04 76 82 66 70

e-mail : Elisabeth.Djurado@lepmi.inpg.fr

Yttrium doped tetragonal zirconia is expected to be a good ceramic because of its high strength, high toughness and wear resistance. However, the moisture sensitivity of this ionic conductor is a severe problem that has to be solved before any direct application. Several authors [1,2,3,4] observed that the H<sub>2</sub>O vapour accelerated the increasing of grain growth and facilitated the t to m-ZrO<sub>2</sub> transformation. We have recently successfully synthesized two powdered batches of pure tetragonal undoped ZrO<sub>2</sub> (without any stabilizing dopant) characterized by 6.9 (#1) and 13.2nm (#2) averaged crystallite size by spray-pyrolysis and a third t-ZrO<sub>2</sub> batch (#3) consisting of doped containing 2 mol% Y<sub>2</sub>O<sub>3</sub> with 6.3nm averaged crystallite size [5]. The spray-pyrolysis method mainly provided nanocrystallized powders with homogeneity in chemical composition, and good sinterability.

In the present work, the first part is focusing on the influence of temperature on our samples. Quantitative analysis of the m-ZrO<sub>2</sub> amount is done by XRD and Raman spectroscopy. In a second part, we investigate the evolution of both the crystallite size and the content of m-ZrO<sub>2</sub> in a 350°C humid environment. In the last part, the detrimental ageing phenomenon of 2YSZ ceramic is evaluated by impedance spectroscopy in moist environment, at temperatures below 400°C.

### 1. Influence of temperature on TPZ powders

DTA and TGA were carried out in dry air. A 5wt% H<sub>2</sub>O loss was evaluated from two successive endothermal steps, at ≈100°C and ≈450°C for all compounds. Bound OH groups coming from the synthesis (spray-pyrolysis takes place for 8s at 600°C from an aqueous precursor solution) seem to play an important role in the formation process of the tetragonal form. Exothermal effect assigned to the appearance of m-ZrO<sub>2</sub> was determined for batches 1 and 2, on cooling, respectively at ≈980°C and ≈600°C while 2YSZ reversibly remains tetragonal. It shows that the temperature of the tetragonal to monoclinic transition strongly depends on initial crystallite size.

Samples #1 and 2 were annealed at different temperatures and for different times in air in order the crystallite size to be increased. Quantitative determination of m-ZrO<sub>2</sub> content was measured by XRD and Raman spectroscopy versus crystallite sizes [6]. Critical crystallite size, over which m-ZrO<sub>2</sub> transformation is completed, was found < 45nm. This is in good agreement with previous published values on the beginning of this transformation in the 22 to 30nm range [1,7]. Moreover, the t → m-ZrO<sub>2</sub> transformation is completed much more rapidly for batch 2 than for batch 1. Indeed, the appearance of m-ZrO<sub>2</sub> is delayed (only ≈3wt%) for batch 2 where crystallite size increases up to 21.8nm after a 900°C /15min annealing. Beyond this threshold, we observe a huge increase of m-ZrO<sub>2</sub> content (≈80wt%) for only 22nm crystallite size and after a 950°C/1h annealing. The batch 1 contains instantaneously ≈5wt% m-ZrO<sub>2</sub> but after the same annealings, the m-ZrO<sub>2</sub> amount slowly grows up.

### 2. Influence of water vapour on TPZ powders

The three powdered batches were annealed at 350°C for 12h in air with saturated water vapour pressure (P<sub>H<sub>2</sub>O</sub>=2338Pa at 20°C) in order to evaluate the TPZ stability. The averaged crystallite size was evaluated from XRD patterns and the content of m-ZrO<sub>2</sub> from Raman spectra. The results are collected in the following table :



#batch (Crystallite size) m-ZrO <sub>2</sub> amount	#1 (6.9nm) 5.0 wt%	#2 (13.2nm) 1.5 wt%	#3 (6.3nm) 0 wt%
dry air 350°C / 12h	(7.6nm) 23.0 wt%	(14.8nm) 7.4 wt%	(6.6nm) 0 wt%
humid air 350°C / 12h	(7.8 nm) 24.6 wt%	(14.6 nm) 9.3 wt%	(7.1nm) 0 wt%

Increasing TPZ stability

----->

First, 2YSZ is the best stabilized composition of the series in humid air. It could be interpreted in terms of yttria dopant cumulated with small final crystallite size (7.1nm). It is worth to note that the m-ZrO<sub>2</sub> content and crystallite sizes of undoped zirconia (batches 1 and 2) after annealing in humid air compared to the annealing in dry air are in the same order of magnitude. Thus, for undoped zirconia, humidity is neither the controlling factor of crystallite growth, nor the destabilizing factor at least for a 12h annealing time. Besides, for batches 1 and 2, acceleration of the transformation by a factor 5 is significant in dry air annealing by increasing of  $\approx 10\%$  relative crystallite size. It could be concluded that for undoped zirconia, a threshold of m-ZrO<sub>2</sub> content is necessary to block the growing of m-ZrO<sub>2</sub> in large amount in humid environment. We have to remark that only  $\approx 9\text{wt}\%$  m-ZrO<sub>2</sub> were detected in undoped tetragonal zirconia. We selected tetragonal 2YSZ (6.3nm) powder (the most stable one) for in-situ electrical characterization in humid atmosphere.

### 3. Electrical behaviour of 2YSZ ceramic

2YSZ(6.3nm) powders were hydrostatically pressed at 300MPa. The pellet was then sintered in dry air at 1500°C for 2h. Final density of  $\approx 98\%$  was obtained while simultaneously keeping the crystallite size below 100nm. The tetragonal monophase was detected by XRD.

The detrimental aging phenomenon of 2YSZ ceramic has been evaluated by impedance spectroscopy in moist environment, below 400°C. This non destructive technique was proved to be a powerful tool for in-situ monitoring and on line gathering information on the microstructural evolution of this material and of the electrolyte/electrode interface. The overall electrolyte behaviour is clearly distinguished from the electrode characteristic by using silver electrodes deposited by RF sputtering at RT. During aging treatment, a degradation of the electrical properties of the material was studied. It mainly results from an increasing blocking effect relevant to the t  $\rightarrow$  m transformation. The influence of the microstructure on the rate of degradation will be emphasized. Extensive measurements of the aging effect are in progress and all the obtained results will be discussed.

- [1] Y. Murase, E. Kato, J. Am. Ceram. Soc. **66**, 196 (1983)
- [2] T. Sato, M. Shimada, J. Am. Ceram. Soc. **68**, 356 (1985)
- [3] M. Yoshimura, Am. Ceram. Soc. Bull **67** 1950 (1988)
- [4] S. Lawson, J. Eur. Ceram. Soc. **15**, 485 (1995)
- [5] E. Djurado, E. Meunier, J. Solid State Chem. **140**, 000 (1998), in press
- [6] E. Djurado, P. Bouvier, G. Lucazeau, J. Solid State Chem., to be published
- [7] R. C. Garvie, J. Phys. Chem. **69**, 1238 (1965)

## LOW-TEMPERATURE CONFINEMENT OF SIC-SUPERTHIN FILM AND SUPERFINE PARTICLES

Tadao ISHII

Faculty of Engineering, Okayama University, Okayama 700-0082

The phase transition and conductivity involved in a sandwiched ionic conductor superthin film is discussed in terms of lattice liquid model, taking account of ion concentration distribution. Around interface, there exists the depletion layer having a small conductivity, but also exists the highest conductivity layer. The conductivity maximum layer lies at phase transition front. In a thin film, the transition front goes back from the surfaces with temperature to smear out. This is the melting or superionic phase transition of the superthin film, which is possible to occur far below the bulk transition temperature, namely is realized the low-T confinement of SIC-superthin film. The case for low-T confinement of fine particles realized in glasses by Tatsumisago et al. is also discussed.

### Phase Transition Front and Conductivity in Ionic Conductor Thin Film

The phase transitions of a sandwiched ionic conductor superthin film and superfine particles at lower temperatures below the bulk  $T_c$  is discussed. Here, the microscopic studies in terms of the lattice liquid model are tried in which we specifically discuss the sublattice melting of thin films and its effect on the conductivity.

#### 1. Phase transition front and film melting

Consider a bulk consisting of two species of ions, mobile ( $\text{Ag}^+$ ) and immobile ( $\text{I}^-$ ) ions as in  $\beta\text{-AgI}$ . The thin film of this material is sandwiched between insulators as sapphire. Mobile ions in the film then go out to the surface so as to vanish the electrochemical potential difference, which induces the space charge. From the free energy, given by the pair approximation of the cluster variation method, under these charge distributions, we have the transition front of the ordered region near the surfaces. If we raise the temperature, then this front goes back to the center region and finally the sandwiched superthin film becomes melt.

#### 2. Confined superionic phase far below the bulk superionic transition temperature

Let us define the sublattice melting (superionic transition) temperature of the film  $T_M$  by the transition temperature of the whole film. Then we have the phase diagram of Fig.1, where the arrow corresponds to the bulk transition temperature  $\hat{T}_M/\hat{\epsilon} = \hat{T}_C/\hat{\epsilon} \approx 1.22$ . This diagram shows that the smaller the film width becomes,  $\hat{T}_M/\hat{\epsilon}$  gets lower. Since the disordered state corresponds to the superionic phase, one can

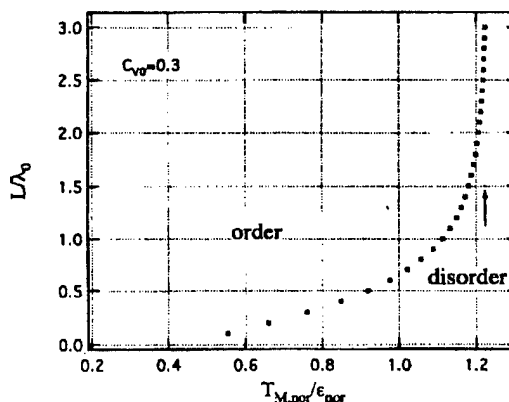


Fig.1 Temperature dependence of the critical film thickness for the sublattice melting. The arrows indicates the value for bulk.

understand this as that the superionic phase is realized at low temperatures far below the bulk  $T_C$ . It has recently been reported that the superionic phase of AgI-fine particles of some ten nm in diameter is frozen at much lower temperatures than  $T_C$ .

### 3. High Ionic Conductivity

The mean dc conductivity can also be obtained, where it takes an optimum value at a film width. This maximum is related to the transition front giving the largest conductivity layer. When the surface has a comparatively large vacancy density, the surface region is in the disordered state. However, the region away from there is in the ordered state. Thus the optimum conductivity layer at the transition front having a critical density in-between exists near the interface or surface.

### References

- 1) M. Tatsumisago, Y. Shinkuma and T. Minami: Nature **354** (1991) 217.
- 2) M. Tatsumisago, T. Saito and T. Minami: Solid State Ionics **86-88** (1996) 415.
- 3) S. Furusawa: Report on 1995 Scientific Research on Priority Area (No.260), (1996) p.111, unpublished.
- 4) T. Ishii and J. Kawamura: J. Phys. Soc. Jpn. **67** (1998) 3517.
- 5) T. Ishii, H. Sato and R. Kikuchi: Phys. Rev. **B34** (1986) 8335.

## **EPR-EXAMINATION OF NICKEL PARTICLES INCLUDED IN X AND Y ZEOLITE CARRIERS**

Chr. Papaioannou and G. Petroustos, National Technical University of Athens, Department of Chemical Engineering, Zografou Campus, 15773 Athens, Greece.

### **EXTENDED ABSTRACT**

Since metal clusters have a high proportion of surface atoms, they are important for heterogeneous catalysis.

In the characterization of the transition metal particles within a zeolite carrier, many questions occur concerning their interaction with the zeolite carrier, the dipole-dipole interaction between the particles, the shape, crystalline and other anisotropies, etc. The special structure of the zeolite carrier limits the particle size in the nm range. For this reason the electronic, magnetic and structural properties of these systems could not be derived from the respective properties of the solid metal.

In order to answer the above questions, the application of the EPR absorption has been chosen, as one of the most appropriate methods. In the resonance equation of the ferromagnetic materials, the effective resonance field includes the coercive force, which depends on the shape (shape anisotropy), as well as on anisotropy fields caused by crystalline or stress or other anisotropies [1, 2].

In the present study EPR measurements were performed on X and Y zeolites containing a nickel metal phase with a superparamagnetic behaviour [3] during the magnetic measurements. The zeolites contained  $\text{Na}^+$  and/or  $\text{Ca}^{2+}$  and  $\text{Ni}^{2+}$  as compensating cations and nickel crystallines received by reduction with hydrogen [4, 5]. The size distribution of the nickel particles were determined by magnetization isotherms [6, 7]. The recorded spectra of the EPR measurements are the first derivatives of the resonance adsorption curves.

The spectra are asymmetrical indicating the presence of anisotropy fields or dipole-dipole interaction which cause a widening and a shifting of the curves [8, 9]. These spectra have been fitted by a set of Lorentzian and Gaussian functions with satisfactory results. The Lorentzian and Gaussian curves are due to superparamagnetic and non-superparamagnetic ("blocked") nickel particles respectively [8].

The fitting results show that all the metal nickel particles included in X and Y zeolite carriers do not behave superparamagnetically in EPR measurements, like in magnetic measurements. Their majority presents anisotropies, which are not described by theoretical models [10, 11]. It is however certain, that these particles appear at least a shape anisotropy and the presence of charge condensing cations  $\text{Ca}^{2+}$  probably favours the appearance of the stress anisotropy.

## REFERENCES

- [1] C. Kittel, Physical Review, **71**, 270 (1947).
- [2] C. Kittel, Physical Review, **73**, 155 (1948).
- [3] P. W. Selwood, "Adsorption and Collective Paramagnetism", Acad. Press, N. York, (1962).
- [4] P. A. Jacobs, Studies in Surface Science and Catalysis **12**, 71 (1982)
- [5] F. Schmidt et. al., in "Proc. of the 4th Conf. on Catalysis", Varna, p. 331 (1979).
- [6] F. Schmidt, T. Bein, U. Ohlerich and P. Jacobs, in "Proc. of 6th Int. Conf. on Zeolites", p.151 (1984).
- [7] W. Romanowski, Zeitschrift für anorganische and allgemeine Chemie, **351**, 180 (1967).
- [8] K.-H. Mader, W. Gunsser, A. Knappwost, Berichte der Bunsen-Gesellschaft für Physikalische Chemie, **74**, 240 (1970).
- [9] E. Schloemann, The Journal of Physical Chemistry, Solids, **6**, 242 (1958).
- [10] S. V. Vonsovskii, in "Ferromagnetic Resonance", (ed. S. V. Vonsovskii), Pergamon Press (1966).
- [11] G. T. Rado, Journal of Applied Physics, **61(8)**, 4262 (1987).

MESOSCOPIC MULTIPHASE EFFECTS IN AgI:Al<sub>2</sub>O<sub>3</sub> COMPOSITE ELECTROLYTES  
VIA A SEVEN-LAYER AgI POLYTYPEJong-Sook Lee<sup>a\*</sup>, Stefan Adams<sup>b</sup>, Joachim Maier<sup>a</sup><sup>a</sup>Max-Planck-Institut für Festkörperforschung, D-70569 Stuttgart, Germany<sup>b</sup>Min.-Kristallographisches Institut, Universität Göttingen, D-37077, Germany

The enhancement of the moderate conductivity of the low-temperature  $\beta$ -AgI [1] by 'heterogeneous doping' [2] e.g., with alumina, turned out to be remarkably successful, giving rise to more than  $10^3$  enhancement at room temperature. In Fig. 1 the conductivity of the AgI:Al<sub>2</sub>O<sub>3</sub> composite with 40 m/o alumina is compared to that of the pristine AgI. While in AgCl and AgBr conductivity enhancement can be quantitatively addressed by the ideal space charge effects [2], and while many aspects qualitatively point towards analogous effects in AgI, the absolute values seem to be at least two orders of magnitude too large to be in accordance with this model. In addition, the defect chemistry is a matter of great disputation, partly due to the anisotropy in wurtzite structure of  $\beta$ -AgI and partly due to the bismorphism of  $\beta$ -AgI and (metastable)  $\gamma$ -AgI at low temperature. Even further, the phase transition behavior to the high-temperature  $\alpha$ -AgI is greatly affected in the AgI:Al<sub>2</sub>O<sub>3</sub>. Large thermal hysteresis in phase transition is consistently observed in conductivity, DSC and in-situ XRD with a superheating by 10°C (T(+)) and an undercooling by 40°C (T(-)) as illustrated in Fig.1.

A close examination of the XRD patterns reveals the existence of a structural modification of AgI in the composites as a seven-layer polytype (7H) in a stacking sequence ABCBCAC. The formation seems triggered by chemical interaction with  $\gamma$ -Al<sub>2</sub>O<sub>3</sub> at the interface and occurs extensively such that all AgI in the composites with alumina more than 30m/o exists as 7H phase. In Fig. 2 the 7H structure was represented by close packed layers of tetrahedral sites occupied by silver ions. As indicated, the stacking arrangement of 7H structure can be regarded as a heterostructure of  $\beta$ -AgI (ABABAB...) and  $\gamma$ -AgI (ABCABC...) in nanoscale. Each phase extends over 2 or 3 times of a close packed layer of length 3.75 Å, which is then comparable to the Debye-length ( $\lambda$ ) of  $\beta$ -AgI of ca. 10 Å. The extreme conductivity enhancement may be thus attributed to a mesoscopic multiphase ionic conductivity effect predicted earlier [2]: Under mesoscopic conditions where the length scale falls below  $4\lambda$ , the sample is charged throughout and an exceeding disorder results. Mixed-phase effect as in AgCl:AgI and AgBr:AgI system was verified in two-polymorph system of  $\beta$ -AgI: $\gamma$ -AgI as shown in Fig. 3. AgI specimens of different  $\beta/\gamma$  contents are prepared by quenching process at different rates and room temperature conductivity is compared as a function of composition.

The observed activation energy of 0.29 eV of the composites is identified with the characteristic migration enthalpy for the transport mode in the close packed planes in AgI system. The large hysteresis can be attributed to the elastic effects in the martensitic transformation between  $\alpha$ -AgI and 7H-AgI.

[1] K. Shahi, J. B. Wagner, Jr., J. Electrochem. Soc., **128**, 6 (1981)

[2] J. Maier, Prog. Solid St. Chem., **23**, 171 (1995).

\*presently at National Creative Research Initiative Center for Microstructure Science of Materials, Seoul National University, Seoul 151-742, Korea

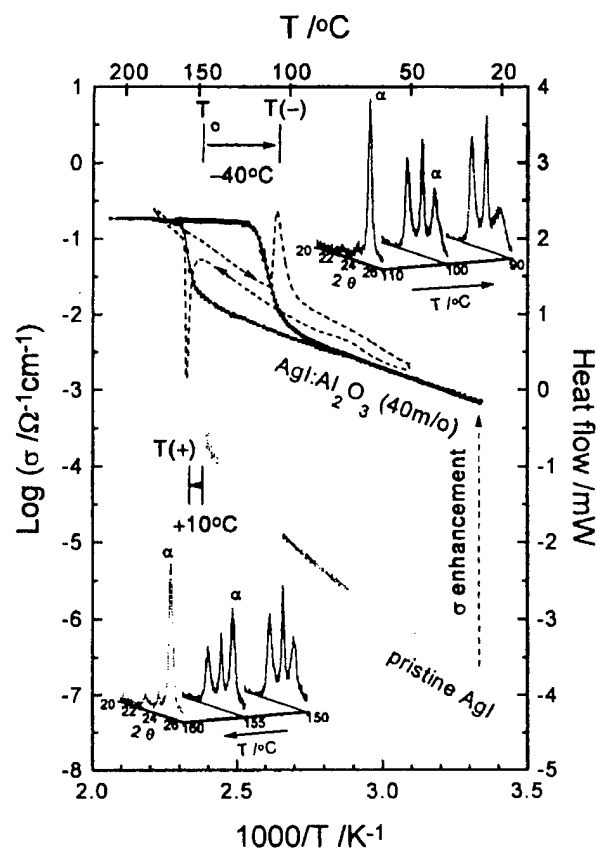


Fig. 1 Conductivity, DSC curve and in-situ XRD for AgI:Al<sub>2</sub>O<sub>3</sub> (40m/o) composite. Large thermal hysteresis in phase transition with superheating by 10°C (T(+)) and undercooling by 40°C (T(-)) is consistently observed. Conductivity enhancement larger than 10<sup>3</sup> with respect to the pristine AgI is to be noted.

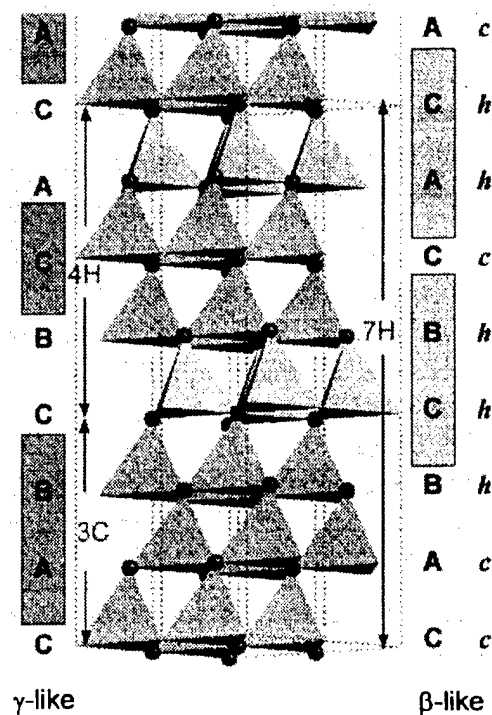


Fig. 2 7H structure represented by close packed tetrahedra occupied by silver ions. Partial stacking sequences like β-AgI (right side) and like γ-AgI (left side) are designated.

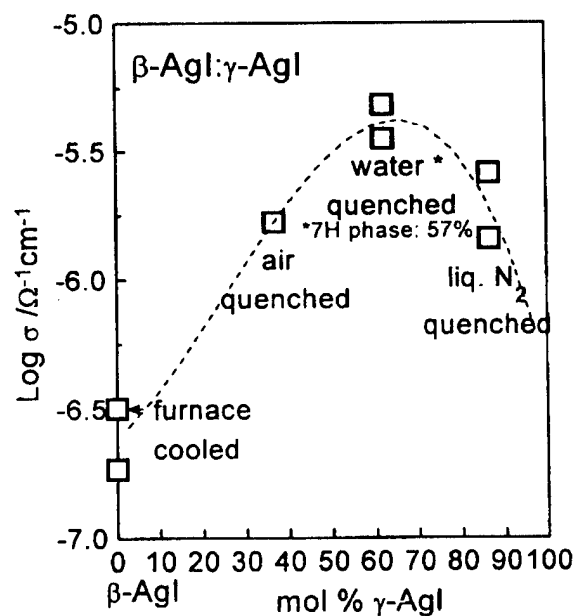


Fig. 3 Room temperature conductivity as a function of phase amounts of β-AgI and γ-AgI in differently quenched AgI specimens.

# Estimation of composites conductivity using a general mixing rule

N. F. Uvarov

*Institute of Solid State Chemistry, Russian Academy of Science  
Kutateladze 18, Novosibirsk-128, 630128, Russia*

New simple methods of calculation of the conductivity in conductor - insulator mixtures are of importance in many applications. Effective medium or percolation models are usually employed [1-4] for such calculations. However, in case of complex morphology of the composite and high concentration of conductive phase the resulting expressions become very complicated. The most difficult problem is the calculation of the conductivity of systems in which strong percolation effects occur and total conductivity sharply changes by several orders of magnitude as a function of the composition.

In early works [5,6] it was shown that conductivity of the two-phase mixture obey a power-law mixing rule:

$$\sigma^\alpha = (1-f) \cdot \sigma_1^\alpha + f \cdot \sigma_2^\alpha \quad (1)$$

where  $\sigma_1, \sigma_2$  are conductivities of the phases;  $f$  is the volume fraction of phase 2;  $\alpha$  is a constant ( $-1 \leq \alpha \leq 1$ ) defined by morphology of the composite. Really this equation cannot be used over whole concentration range as morphology of real composite progressively varies with  $f$ . The change in the morphology can be accounted by the variation of the  $\alpha$  value. In first approximation it can be suggested that  $\alpha$  varies linearly with  $f$ :  $\alpha(f) = \alpha_1 \cdot (1-f) + \alpha_2 \cdot f$ , where  $\alpha_1$  and  $\alpha_2$  are constants specific of the morphology of mixtures in zero concentration limits. Then the mixing rule, Eqn.(1), can be rewritten in a more general form

$$\sigma^{\alpha_1(1-f)+\alpha_2 f} = (1-f) \cdot \sigma_1^{\alpha_1(1-f)+\alpha_2 f} + f \cdot \sigma_2^{\alpha_1(1-f)+\alpha_2 f} \quad (2)$$

Shape of theoretical  $\sigma(f)$  curves is determined by parameters  $\alpha_1$  and  $\alpha_2$  (Fig.1a). If  $\alpha_1$  and  $\alpha_2$  are different in sign then  $\sigma(x)$  curves are typical of percolation systems: at point  $f_c = \alpha_1/(\alpha_1 - \alpha_2)$  the sign of the parameter  $\alpha(f)$  changes and the system "switches" its effective arrangement (or connection of the phases) from parallel to a series one, hence,  $f_c$  may be considered as a percolation threshold for conductivity of the composite.

The mixing rule (2) can be also used for description ionic conductivity of composite solid electrolytes where conductivity occurs through interface. Volume fraction of the high-conducting interface regions can be roughly estimated [7] as  $f_s = \beta \cdot (2\lambda/r_A) \cdot f \cdot (1-f)$ , where  $\beta$  is geometric factor,  $\lambda$  is the thickness of the interface layer;  $f$  and  $r_A$  volume fraction and the grain size of dispersed additive; and for conductivity of composite one finds

$$\sigma^{\alpha_1(1-f)+\alpha_2 f} = (1-f-f_s) \cdot \sigma_1^{\alpha_1(1-f)+\alpha_2 f} + f_s \cdot \sigma_s^{\alpha_1(1-f)+\alpha_2 f} + f \cdot \sigma_2^{\alpha_1(1-f)+\alpha_2 f} \quad (3)$$

where  $\sigma_s$  is the conductivity within the interface region. In most of composite electrolytes  $\sigma_s \gg \sigma_1, \sigma_2$  and Eqn.(2) can be represented in a simpler form

$$\sigma = \sigma_s \cdot [\beta \cdot (2\lambda/r_A) \cdot f \cdot (1-f)]^{1/[\alpha_1(1-f)+\alpha_2 f]} \quad (4)$$

Concentration dependence Eqn.(4) is a curve with a maximum (Fig.1b), its position is determined by morphology of the composite, i.e. parameters  $\alpha_1, \alpha_2$ ; in the case  $\alpha_1 = \alpha_2$  the maximum occurs at  $f = 0.5$ . Theoretical curves (1-3) are compared with conductivity data reported for various composites of the conductor - insulator type and composite solid



electrolytes. Preliminary results are reported elsewhere [8]. It is shown that the general mixing rule satisfactorily describes experimental values in many composites. Also, it agrees with the conductivity values obtained by computer simulation for some model systems exhibiting the percolation behavior [9]. It should be emphasized that obtained expressions qualitatively agree with ones obtained in terms of effective medium models, takes automatically into account percolation effects, are relatively simple and convenient for rough calculation of the dc-conductivity values over whole concentration range.

## References

- [1]. D.A.G. Bruggeman, Ann. Phys. **24**, 636 (1935).
- [2]. R. Landauer, J. Appl. Phys. **23**, 779 (1952).
- [3]. K. Yoshida, Phil. Mag. **B53**, 55 (1986).
- [4]. D. S. McLachlan, M. Blaszkiewicz, R. E. Newnham, J. Amer. Ceram. Soc. **73**, 2187 (1990).
- [5]. K. Lichtenecker, Phys. Z. **37**, 906 (1936).
- [6]. R. E. Newnham, Ann. Rev. Mater. Sci. **16**, 47 (1986).
- [7]. N. F. Uvarov, P. Vanek, Yu. I. Yuzyuk, et. al., Solid State Ionics **90**, 201 (1996).
- [8]. N. F. Uvarov, Doklady Russian Acad. Sci. **353**, 213 (1997) (in Russian).
- [9]. S. Kirkpatrick, Rev. Mod. Phys. **45**, 574 (1973).

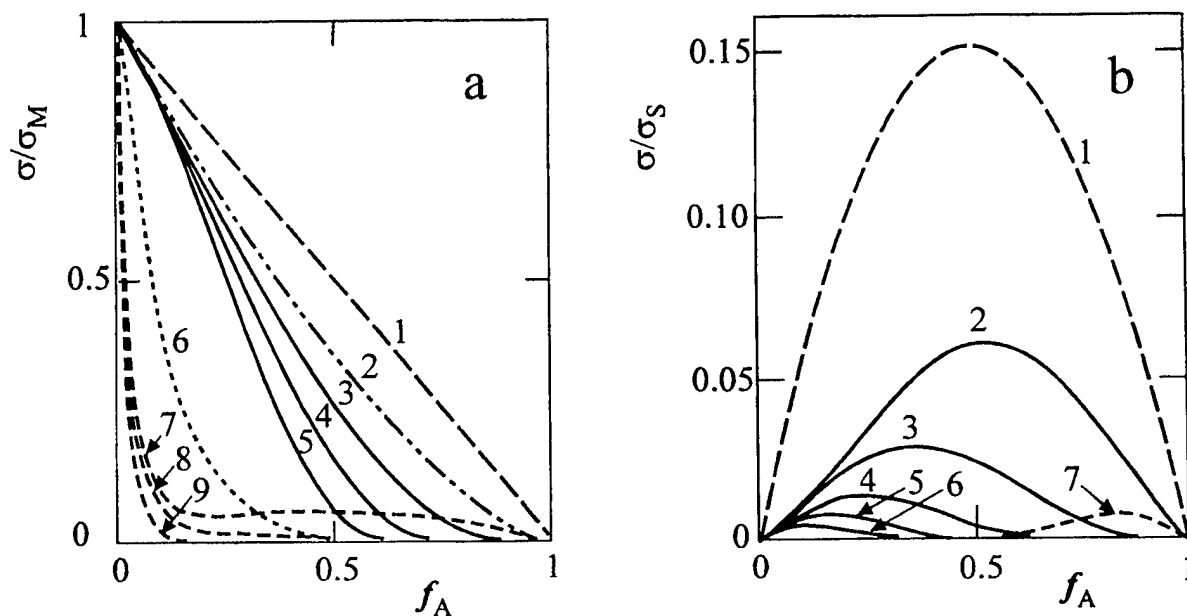


Fig.1. Concentration dependences of conductivity for metal-insulator composites (a) and composite solid electrolytes (b) calculated using Eqn. (2) and Eqn. (4), respectively. Curves are obtained at following parameters  $\alpha_1, \alpha_2$ : (1, 1); (2/3, 2/3); (2/3, 1/3); (2/3, 0); (2/3, -1/3); (0, 0); (-1/3, 2/3); (-1/3, 1/3) and (-1/3, 0), curves 1; 2; 3; 4; 5; 6; 7; 8 and 9, respectively. Theoretical curves for composite solid electrolytes (b) are obtained at  $(\lambda/L) = 0.1$ .

**Effect of nanocrystalline alumina on ionic conductivity and phase transition in CsCl**

N. F. Uvarov, L. I. Brezhneva and E. F. Hairtdinov

*Institute of Solid State Chemistry, Siberian Branch of Russian Academy of Science  
Kutateladze 18, Novosibirsk-128, 630128, Russia*

Cesium chloride is the only alkali halide salt with bcc-structure stable at room temperature. Conductivity of bcc-phase is low and governed by chlorine vacancies  $V_{Cl}^{\bullet}$  formed by Schottky mechanism [1]. At temperature  $T_i = 469^{\circ}\text{C}$  bcc-phase transforms into a high-temperature fcc-phase of NaCl-type. The transition is accompanied by strong decrease in the conductivity. It has been reported [2] that heterogeneous doping of CsCl with alumina leads to the increase in the conductivity. The authors used alumina with specific surface area  $11\text{ m}^2/\text{g}$ . No changes in structure and heat of bcc-fcc phase transition of CsCl in the CsCl- $\text{Al}_2\text{O}_3$  composites have not been detected.

In the present work conductivity, structure and thermodynamic parameters of CsCl in CsCl- $\text{Al}_2\text{O}_3$  composites are investigated. As the heterogeneous dopant, high-dispersed alumina with specific surface area  $210\text{ m}^2/\text{g}$  (mean particle size  $\sim 10\text{ nm}$ ) is used. The composites are prepared by mechanical treatment of initial mixtures in a high-energy planetary ball mill followed by sintering at  $600^{\circ}\text{C}$  for several hours.

In the temperature range, where bcc-phase is stable, conductivity of  $(1-x)\text{CsCl}-x\text{Al}_2\text{O}_3$  composites does not depend on  $x$  at low alumina content,  $x \leq 0.10$ , and sharply raises at  $x > 0.10$ . Maximum conductivity,  $\sigma \sim 5 \cdot 10^{-4}\text{ S/cm}$ , is observed at  $x \sim 0.6-0.7$ . At  $T > T_i$  dependences  $\sigma(x)$  are typical for composite solid electrolytes: conductivity sharply increases at  $x \geq 0.05$ . In composites very strong hysteresis of the phase transition is observed. As  $x$  rises, conductivity of bcc and -fcc phases tend to level-off and at  $x > 0.6$  no conductivity drop occurs, only small change in activation energy is observed. Conductivity data are in a fair agreement with results obtained by differential scanning calorimetry. The heat of the phase transition decreases with  $x$  and at  $x > 0.6$  no bcc-fcc phase transition is detected. Sintering leads to marked broadening and diminishing in integral intensity of all reflections of bcc-CsCl and at  $x > 0.2$  additional reflections attributed to fcc-phase of CsCl appear on the X-ray powder diffraction patterns.

The results obtained can be interpreted as follows: strong interface interaction takes place between  $\text{Al}_2\text{O}_3$  and CsCl and it is energetically favorable for CsCl to spread along alumina surface. Possibly, as a result of the interface interaction, cations shift to the alumina surface forming positively charged layer on the interface, likewise it takes place in AgCl-A composites [3]. The positive surface charge is compensated by negatively charged defects  $V_{Cs}'$  or  $\text{Cl}_i'$  forming diffusive layer and responsible for conductivity of the composites. As these defects have lower mobility than that of  $V_{Cl}^{\bullet}$  vacancies [1], at low  $x$  conductivity can decrease. Moreover, fcc-phase of CsCl is stabilized in the composites, however, it is not clear whether it occurs as a thin intermediate layer located between alumina and bcc-CsCl or it is separate inclusions distributed within the matrix of bcc-phase. At high concentration of alumina after sintering all X-ray diffraction peaks (for both bcc- and fcc-phases) disappear, no heat effects due to bcc-fcc phase transition is detected, no conductivity change at  $T_i$  is observed, Arrhenius  $\sigma(T)$  dependences become non-linear. It is not improbable, that amorphous CsCl-phase is also formed on the CsCl-alumina interface and this phase is responsible for enhanced conductivity of CsCl- $\text{Al}_2\text{O}_3$  composites.

[1] I.M.Hoodless and R.G.Turner, Phys. Stat. Solidi (a) **11** 689 (1972).

[2] A.Kumar and K.Shahi, Solid State Ionics **68** 71 (1994).

[3] J.Maier, J. Phys. Chem. Solids **46** 309 (1985).

**Effect of nanocrystalline alumina on ionic conductivity and phase transition in CsCl**

N. F. Uvarov, L. I. Brezhneva and E. F. Hairtdinov

*Institute of Solid State Chemistry, Siberian Branch of Russian Academy of Science  
Kutateladze 18, Novosibirsk-128, 630128, Russia*

Cesium chloride is the only alkali halide salt with bcc-structure stable at room temperature. Conductivity of bcc-phase is low and governed by chlorine vacancies  $V_{Cl}^{\bullet}$  formed by Schottky mechanism [1]. At temperature  $T_t = 469^{\circ}\text{C}$  bcc-phase transforms into a high-temperature fcc-phase of NaCl-type. The transition is accompanied by strong decrease in the conductivity. It has been reported [2] that heterogeneous doping of CsCl with alumina leads to the increase in the conductivity. The authors used alumina with specific surface area  $11\text{ m}^2/\text{g}$ . No changes in structure and heat of bcc-fcc phase transition of CsCl in the CsCl- $\text{Al}_2\text{O}_3$  composites have not been detected.

In the present work conductivity, structure and thermodynamic parameters of CsCl in CsCl- $\text{Al}_2\text{O}_3$  composites are investigated. As the heterogeneous dopant, high-dispersed alumina with specific surface area  $210\text{ m}^2/\text{g}$  (mean particle size  $\sim 10\text{ nm}$ ) is used. The composites are prepared by mechanical treatment of initial mixtures in a high-energy planetary ball mill followed by sintering at  $600^{\circ}\text{C}$  for several hours.

In the temperature range, where bcc-phase is stable, conductivity of  $(1-x)\text{CsCl}-x\text{Al}_2\text{O}_3$  composites does not depend on  $x$  at low alumina content,  $x \leq 0.10$ , and sharply raises at  $x > 0.10$ . Maximum conductivity,  $\sigma \sim 5 \cdot 10^{-4}\text{ S/cm}$ , is observed at  $x \sim 0.6-0.7$ . At  $T > T_t$  dependences  $\sigma(x)$  are typical for composite solid electrolytes: conductivity sharply increases at  $x \geq 0.05$ . In composites very strong hysteresis of the phase transition is observed. As  $x$  rises, conductivity of bcc and -fcc phases tend to level-off and at  $x > 0.6$  no conductivity drop occurs, only small change in activation energy is observed. Conductivity data are in a fair agreement with results obtained by differential scanning calorimetry. The heat of the phase transition decreases with  $x$  and at  $x > 0.6$  no bcc-fcc phase transition is detected. Sintering leads to marked broadening and diminishing in integral intensity of all reflections of bcc-CsCl and at  $x > 0.2$  additional reflections attributed to fcc-phase of CsCl appear on the X-ray powder diffraction patterns.

The results obtained can be interpreted as follows: strong interface interaction takes place between  $\text{Al}_2\text{O}_3$  and CsCl and it is energetically favorable for CsCl to spread along alumina surface. Possibly, as a result of the interface interaction, cations shift to the alumina surface forming positively charged layer on the interface, likewise it takes place in AgCl-A composites [3]. The positive surface charge is compensated by negatively charged defects  $V_{Cs}'$  or  $\text{Cl}_i'$  forming diffusive layer and responsible for conductivity of the composites. As these defects have lower mobility than that of  $V_{Cl}^{\bullet}$  vacancies [1], at low  $x$  conductivity can decrease. Moreover, fcc-phase of CsCl is stabilized in the composites, however, it is not clear whether it occurs as a thin intermediate layer located between alumina and bcc-CsCl or it is separate inclusions distributed within the matrix of bcc-phase. At high concentration of alumina after sintering all X-ray diffraction peaks (for both bcc- and fcc-phases) disappear, no heat effects due to bcc-fcc phase transition is detected, no conductivity change at  $T_t$  is observed, Arrhenius  $\sigma(T)$  dependences become non-linear. It is not improbable, that amorphous CsCl-phase is also formed on the CsCl-alumina interface and this phase is responsible for enhanced conductivity of CsCl- $\text{Al}_2\text{O}_3$  composites.

[1] I.M.Hoodless and R.G.Turner, Phys. Stat. Solidi (a) **11** 689 (1972).

[2] A.Kumar and K.Shahi, Solid State Ionics **68** 71 (1994).

[3] J.Maier, J. Phys. Chem. Solids **46** 309 (1985).

## EFFECT OF SILICA POROUS STRUCTURE ON THE PROPERTIES OF COMPOSITE ELECTROLYTES BASED ON $\text{MeNO}_3$ ( $\text{Me}=\text{Rb}, \text{Cs}$ )

Ponomareva V.G., Lavrova G.V., Simonova L.G.

*Institute of Solid State Chemistry, Siberian Branch of Russian Academy of Science*

*Kutateladze 18, Novosibirsk-128, 630128, Russia*

*Boriskov Institute of Catalysis, Russian Academy of Sciences, Lavrentieva 5, Novosibirsk-90, 630090, Russia*

One of the most interesting and promising methods for improving the ionic salt conductivity is its heterogeneous doping with inert highly dispersed and electrically isolating oxides. Physico-chemical properties of the ionic crystals may change greatly at the heterogeneous doping process. The conductivity enhancement in composites is due to the space charge layer formation. In some cases in nanocomposites the more intensive surface interface interaction takes place, which may lead to a strong structural distortion in the bulk of the ionic component with the formation of the phases with unusual properties. Such changes may be caused by different factors characteristic of each particular composite. The data are known on dimensional effect in clusters, thin films and confined substance in small pores of solids. Chemical properties of the solid matrix as well as its porosity (specific surface area, pore size and their distribution) may influence the properties of composite electrolytes. The data obtained are very limited, but they are of great importance for understanding the reasons of composite conductivity increase. The first data were obtained for  $\text{CsHSO}_4\text{-SiO}_2$  system.

In this work the influence of silica porous structure on the properties of solid electrolytes  $(1-x)\text{MeHSO}_4\text{-}x\text{SiO}_2$  and  $(1-x)\text{MeNO}_3\text{-}x\text{SiO}_2$ , (where  $\text{Me}=\text{Cs}, \text{Rb}$ ,  $x=0\text{-}0.9$ ) was investigated. Transport, thermal and structural properties of composite solid electrolytes have been studied by complex impedance, differential scanning calorimetry, Raman and NMR-spectroscopy, X-ray diffraction methods. The used silicas are different in their specific surface area ( $13\text{-}580\text{ m}^2/\text{g}$ ), pore size ( $R=14\text{-}1000\text{ \AA}$ ) and pore size distribution.

It was shown that composite conductivity is ca 2-3 orders of magnitude higher than that of the individual salt. It depended on  $\text{SiO}_2$  content, silica pores size and their distribution. The low-temperature phase conductivity is maximum at  $x=0.5\text{-}0.7$ . The composite conductivity increases greatly and was qualitatively determined by the silica specific surface area if  $\text{SiO}_2$  pores size was above  $100\text{ \AA}$ . Such correlation was not observed if pore size was  $\leq 70\text{-}100\text{ \AA}$ . There is the optimum pores size of heterogeneous dopant, which is in a range of  $35\text{-}100\text{ \AA}$ , where the most composite conductivity increase takes place for all investigated salts and thermodynamic and structural properties change markedly ("dimensional effect"). For composites based on these silicas the enthalpies of superionic phase transition and melting considerably decrease. All reflections of the low-temperature phase in all salt become broader at  $x$  increase and a weak halo appears which does not coincide with the halo of  $\text{SiO}_2$  used. Phase transition drops practically disappeared at  $\sigma(T)$  dependencies. The ionic component becomes either partially or completely amorphous. The ionic salt dispersion most likely proceeds in composites based on silica which pore size is  $170\text{ \AA}$ . The salt state does not change when the  $\text{SiO}_2$  pore size is  $1000\text{ \AA}$ . In systems with  $R = 14\text{ \AA}$  both salt low-temperature phase and amorphous state are observed.

Thus the properties of the composite electrolytes are defined not only by specific surface area of inert dopant, but depend on its porous structure (pores radius and their distribution), which should be taken into account in the nanocomposite systems.

**Nanocomposite ionic conductors in the system  $\text{MeNO}_3 - \text{SiO}_2$  ( $\text{Me} = \text{Rb}, \text{Cs}$ )**

Lavrova G.V., Ponomareva V.G., Uvarov N.F.

I

*Institute of Solid State Chemistry, Siberian Branch of Russian Academy of Science  
Kutateladze 18, Novosibirsk-128, 630128, Russia*

Composite electrolytes exhibit high ionic conductivity and good mechanical properties and are promising materials for many applications. Rubidium nitrate is of special interest as it exhibits a series of phase transitions at 346-583 K, accompanied by both orientational disordering of nitrate groups and large changes in the ionic conductivity. Data have been reported on the properties of the  $\text{RbNO}_3\text{-Al}_2\text{O}_3$  composites [1] and nanocomposites prepared using  $\gamma$ -alumina with particle size  $\sim 10\text{-}30$  nm [2].  $\text{RbNO}_3$ - or  $\text{CsNO}_3$ -containing composites with the other heterogeneous dopants have not been investigated yet.

At the present work properties of  $\text{PbNO}_3$  and  $\text{CsNO}_3$  in  $(1-x)\text{MeNO}_3\text{-}x\text{SiO}_2$  nanocomposites ( $x = 0 - 0.8$ ) were studied by X-ray powder diffraction technique, conductivity measurements, differential scanning calorimetry and Raman spectroscopy. The highly dispersed silica (specific surface area  $\sim 300$  m<sup>2</sup>/g) with uniform pores size distribution and average pores size 7 nm was used as chemically inert additive. The composites were prepared by the mechanical mixing of components followed by the heating at temperatures near  $\text{MeNO}_3$  melting point.

The addition of  $\text{SiO}_2$  leads to the sharp increase in conductivity over all the temperature range investigated at  $x < 0.5$ , especially at low temperatures. Conductivity isotherms  $\sigma(x)$  have maximum at silica contents  $x = 0.6\text{-}0.7$ . Powder X-ray diffractograms of the composites correspond to the structure of the low temperature phases  $\text{RbNO}_3$  (IV) and  $\text{CsNO}_3$  (II). As  $x$  increases the conductivity changes due to phase transitions diminish and at  $x > 0.5$  practically disappears. The intensity of the peaks decreases and the reflections become broadened, at  $x > 0.7$  a weak halo appears. This is most likely due to diminishing of the grain size and the salt amorphization on the highly-dispersed silica surface. According DSC data, the enthalpies of all phase transitions decrease sharply with  $x$ . That is connected with the formation of amorphous phases of  $\text{RbNO}_3$  or  $\text{CsNO}_3$  as it takes place in  $\text{RbNO}_3\text{-Al}_2\text{O}_3$  system [1]. Moreover the transport and structural properties of nitrates in the composites with highly dispersed silica are similar to those based on  $\text{Al}_2\text{O}_3$  [1]. The influence of the humidity on the composite properties (ionic conductivity, the type of charge carriers, phase formation and thermal stability) was investigated.

**References**

1. N.F.Uvarov, P.Vanek, Y.I.Yuzyuk et.al., Solid State Ionics **90**, 201 (1996).
2. B.Zhu and B.E.Mellander, Ferroelectrics **167**, 1 (1995).

### Investigation of AgI-Al<sub>2</sub>O<sub>3</sub> interface by luminescence spectroscopy

Politov A. A. and Uvarov N. F.

*Institute of Solid State Chemistry, Siberian Branch of Russian Academy of Science,  
Kutateladze 18, Novosibirsk-128, 630128, Russia*

As it was shown earlier [1-6] transport, structural and thermodynamic properties of silver iodide change due to its heterogeneous doping with nanocrystalline alumina. The reason of the observed effects is the interface interaction between AgI and Al<sub>2</sub>O<sub>3</sub>. As a result of the interaction, during heating silver salt tends to spread along alumina surface. It leads to a strong decrease of AgI grains in size. If nanocrystalline alumina used as an additive and concentration of the dopant in the composite is sufficiently high, then AgI grain size becomes very small and interface interaction strongly affects bulk properties of silver iodide. However, up to date no direct information on the interface interaction has been obtained, it becomes unclear what phases are stabilized on the alumina surface: new crystalline disordered phases [4-6], high-temperature  $\alpha$ -AgI phase, or amorphous state [3].

In this work attempt is made to investigate physical states of AgI located on alumina surface using method of luminescence spectroscopy. Samples for investigation was prepared in different ways: mechanical mixing followed by sintering, precipitation of AgI on alumina surfaces from KI and AgNO<sub>3</sub> water solutions, evaporation of AgI at high temperatures, etc. Luminescence spectra were obtained with luminescence microscope MSFU 6 (LOMO, Russia) at 77K.

Spectroscopic studies show that after treatment the AgI-Al<sub>2</sub>O<sub>3</sub> samples at high temperatures from 450°C up to the AgI melting temperature AgI transforms into new phase with unusual orange luminescence spectra. The half-width of non-structure emission band is 200 nm. We propose the new state may be attributed to either amorphous state or  $\alpha$ -AgI disordered crystals, with broad band resulting from energy spread of recombination centers.

On storage the heated samples in air re-crystallization takes place which proceeds in several stages. At first, a mixture of amorphous phase and highly disordered crystals, mainly polytypes, is detected by luminescence analysis, then  $\beta$ -AgI phase appears. In the samples obtained by evaporation of AgI on alumina from the gas phase the unusual state transforms into  $\beta$ -phase through a series of unusual states which cannot be attributed to 2H or 4H polytypes only. We suggest the AgI interface may be responsible for these effects.

#### References

- [1] K.Shahi, J.B.Wagner, Jr., J. Electrochem. Soc. **128**, 6 (1981).
- [2] A.C.Khandkar, J.B.Wagner, Solid State Ionics **18/19**, 110 (1986).
- [3] N.F.Uvarov, M.C.R.Shastry, K.J.Rao, Rev. Solid State Sci. **4**, 61 (1990).
- [4] N.F.Uvarov, E.F.Hairetdinov, N.B.Bratel, Russ. J. Electrochem. **29**, 1406 (1993).
- [5] N.F.Uvarov, E.F.Hairetdinov, N.B.Bratel, Solid State Ionics **86-88**, 573 (1996).
- [6] J.S.Lee, J.Maier, Proc. Intern. Conf. EUROSOLID-97, 1997, p.115.

## EFFECT OF UV LIGHT IRRADIATION ON THE MORPHOLOGY OF PYROLYZED $\text{Co}_3\text{O}_4$ FILMS

Masanori Ando and Tetsuhiko Kobayashi  
Osaka National Research Institute, AIST, MITI,  
Midorigaoka 1-8-31, Ikeda, Osaka 563-8577, Japan

Metal oxide films such as cobalt oxide and nickel oxide have considerable potential for use as thin film catalysts, gas and humidity sensors [1,2] and optical materials [3]. Several metal oxide films can be prepared by pyrolysis of precursors such as metal alkylcarboxylates coated on substrates. However, a drawback is that in some cases it is difficult to obtain uniform metal oxide films by this method. We found that when UV light is irradiated on the precursor film of cobalt naphthenate before pyrolysis,  $\text{Co}_3\text{O}_4$  films with improved uniformity can be obtained.

Cobalt naphthenate was used as the precursor of  $\text{Co}_3\text{O}_4$  films. The  $\text{Co}_3\text{O}_4$  films were prepared in the following two manners. (1) Cobalt naphthenate was spin-coated on a glass plate substrate from toluene solution, and without UV light irradiation, pyrolyzed at 400°C in air. (2) Cobalt naphthenate was spin-coated on a glass plate substrate from toluene solution, and after UV light irradiation ( $\lambda=185$  nm and 254 nm) by use of a Hg lamp, pyrolyzed at 400°C in air.

Without UV light irradiation (method (1)), as shown in the SEM picture (Fig. 1a), nonuniform  $\text{Co}_3\text{O}_4$  films which comprise uncontinuous small fragments were formed on the substrate. On the other hand, when UV light was irradiated on the precursor film (methods (2)), uniform  $\text{Co}_3\text{O}_4$  films without large cracks were formed on the substrate (Fig. 1b). The size of the  $\text{Co}_3\text{O}_4$  crystals in the pyrolyzed films prepared by methods (1) and (2) were estimated to be almost the same (about 10 nm) from the width of the X-ray diffraction lines. IR spectroscopy suggested that the number of OH groups in the precursor film increased by UV light irradiation. This change is assumed to increase the affinity between the precursor film and the glass plate substrate having OH groups on the surface and bring about the formation of uniform  $\text{Co}_3\text{O}_4$  film after pyrolysis.

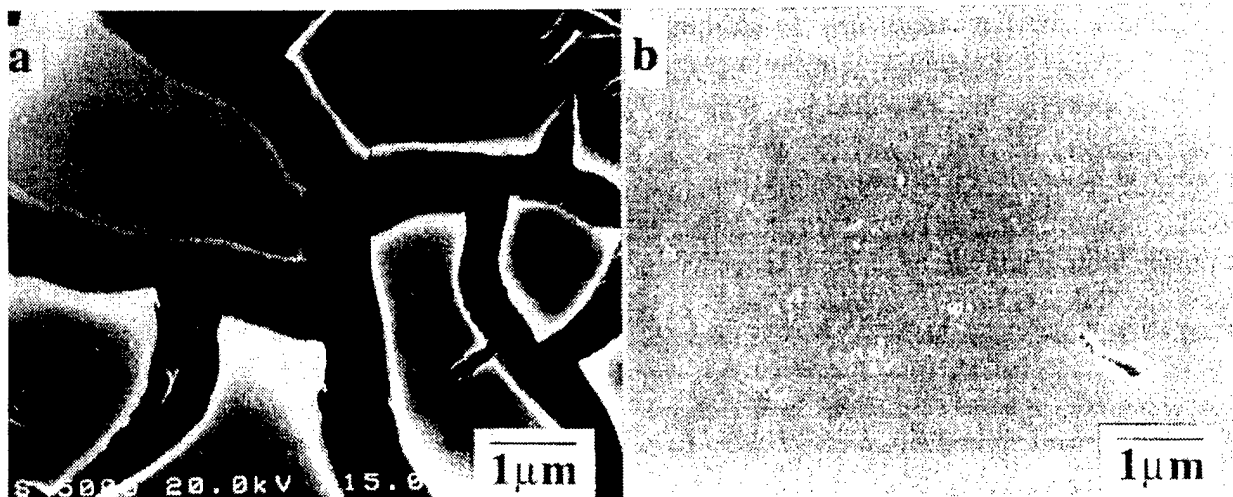


Fig. 1. SEM pictures of the surface of the pyrolyzed  $\text{Co}_3\text{O}_4$  film. a:  $\text{Co}_3\text{O}_4$  film prepared by method (1) (without UV light irradiation). b:  $\text{Co}_3\text{O}_4$  film prepared by method (2) (with UV light irradiation).

### References

- [1] M. Ando, T. Kobayashi and M. Haruta, *Catal. Today* **36**, 135 (1997).
- [2] M. Ando, T. Kobayashi and M. Haruta, *Sensors and Actuators B* **32**, 157 (1996).
- [3] M. Ando, K. Kadono, M. Haruta, T. Sakaguchi and M. Miya, *Nature* **374**, 625 (1995).

## AMORPHOUS POLYMER NANOCOMPOSITE MATERIALS

A. S. Best<sup>a</sup>, M. Forsyth<sup>a</sup>, D.R. MacFarlane<sup>b</sup>

<sup>a</sup>Department of Materials Engineering and <sup>b</sup>Department of Chemistry  
Monash University, Victoria, Australia. 3168.

Polymer composites have recently received much attention for applications in lithium electrochemical devices. Studies have involved the use of lithium conducting ceramics, glasses or insulating fillers dispersed in a conductive polymer matrix. All these materials have been beset by a common problem of low room temperature conductivity, which has hampered their use as electrolytes. [1]

Recently, the effect of finely dispersed particles within a polymer matrix has been investigated. The chosen polymer was either semi-crystalline poly(ethylene oxide) (PEO), or a derivative such as amorphous oxymethylene linked PEO, which was doped with lithium salts. [2,3] It was shown that using micron sized particles of Al<sub>2</sub>O<sub>3</sub>, TiO<sub>2</sub> or SiO<sub>2</sub> increases the conductivity of the system and suppresses the re-crystallisation of PEO. [2]

Recent work however, has looked at the use of nano sized particles of alumina and titania in PEO<sub>8</sub>:LiClO<sub>4</sub>. It was found that the nano-particles increased conductivity by 2 orders of magnitude at room temperature. [4] However, the mechanism by which this increase in conductivity occurs was unclear. Using an amorphous polymer electrolyte material, based on a polyether copolymer triol of MW 5000, with ethylene and propylene oxide units in a 3:1 ratio (3PEG), the ubiquity of this observation has been examined in this work.

The salt concentration of greatest interest was 1.5 mol/kg LiClO<sub>4</sub>, as this is approximately the same ratio of O : Li in PEO, which has shown the greatest increases in conductivity. Degussa P25 TiO<sub>2</sub> powders were dried at 250°C for 24 hours as per previous work. All samples were prepared in a dry box [5] by mixing 10wt% TiO<sub>2</sub> into the polymer/salt mixture followed by the addition of Thorcat<sup>TM</sup> catalyst. The sample was then heated on a hot plate in order to decrease the viscosity of the polymer and reduce the amount of dissolved nitrogen in the mixture. At this point some of the mixture was removed in order to measure the conductivity of the uncured system. Hexamethylene diisocyanate crosslinking agent was then added to the sample followed by vigorous stirring. The mixture was then poured into a mould and compressed before curing for 3 days at 50°C. Impedance measurements were made as a function of frequency on a Hewlett Packard 4192A for four different electrolytes; the uncured polymer/salt, the uncured filled polymer/salt, the cured polymer/salt, and the cured filled polymer/salt systems.

Figure 1 shows the comparison between the work of Croce et al.[4] and this work. The uncured 3PEG 1.5 mol/kg LiClO<sub>4</sub> has a conductivity of  $1.5 \times 10^{-5}$  S.cm<sup>-1</sup> at room temperature and exhibits VTF behaviour over a range of temperatures. The cured 3PEG 1.5 mol/kg LiClO<sub>4</sub> polymer had a room temperature conductivity of  $1.3 \times 10^{-6}$  S.cm<sup>-1</sup> compared to that of 3PEG 1 mol/kg LiClO<sub>4</sub> which has a conductivity of  $5.3 \times 10^{-6}$  S.cm<sup>-1</sup>. [6] Measurements on the uncured electrolytes at approximately 20°C show that the 10 wt% TiO<sub>2</sub> in 3PEG 1.5 mol/kg LiClO<sub>4</sub> polymer is more conductive than the 10 wt% TiO<sub>2</sub> PEO<sub>8</sub>:LiClO<sub>4</sub> sample. As the temperature increases, the conductivity falls below that of the Croce samples due to the settling of the titania in the polymer over time. However, after stirring the sample, the conductivity was recovered.

The cured 10 wt% TiO<sub>2</sub> in 3PEG 1.5 mol/kg LiClO<sub>4</sub> samples had a slightly lower room temperature conductivity than that of uncured samples of the same composition. The effect of TiO<sub>2</sub> on the 1.5 mol/kg LiClO<sub>4</sub> sample is to reduce the conductivity slightly. However, at the lower salt concentration in 3PEG (1 mol/kg), which corresponds to a maximum in conductivity



in this system, there is a barely significant (<10%) improvement in conductivity on the addition of TiO<sub>2</sub>.

It would appear from these results that the TiO<sub>2</sub> has an effect in the PEO electrolyte systems which is not present in the polyether electrolytes studied in this work. It is interesting to note that the effect of the filler is to raise the conductivity of the PEO system to a level comparable to that exhibited by the fully amorphous 3PEG systems. This appears to be true above as well as below  $T_m$  of the PEO, suggesting that the effect relates to disruption of ordered domains even in the molten PEO system. In the highly conductive, fully amorphous 3PEG systems studied here, the TiO<sub>2</sub> filler therefore has no effect other than mechanical property enhancement.

### References:

1. E. Quartarone, P. Mustarelli, A. Magistris, *Solid State Ionics*, 110 (1998) 1–14.
2. W. Wieczorek, Z. Florjanczyk, J. R. Stevens, *Electrochimica Acta*, 40, No 13–14 (1995) 2251–2258.
3. L. Krawiec, L.G. Scanlon, Jr., J.P. Fellner, R.A. Vaia, S. Vasudevan, E.P. Giannelis, *J. Power Sources*, 54 (1995) 310–315.
4. F. Croce, G. B. Appetecchi, L. Persi, B. Scrosati, *Nature*, 394 (1998) 456–458.
5. K. Nairn, A. S. Best, P. J. Newman, D.R. MacFarlane, M. Forsyth, *Extended Abstracts of 11<sup>th</sup> International Conference on Solid State Ionics*, (1997) 308.
6. S. Ng, M. Forsyth, D.R. MacFarlane, *Polymer*, 1998, in press.

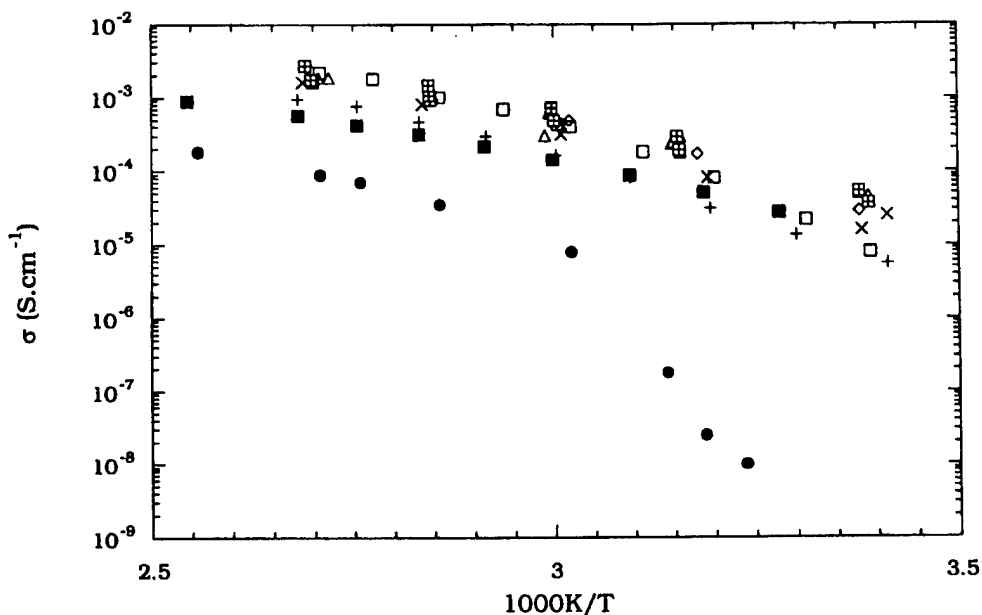


Figure 1: Conductivity of the amorphous materials completed in this work compared to that of Croce et al.[3] Figure symbols: ● PEO<sub>8</sub>:LiClO<sub>4</sub>, □ PEO<sub>8</sub>:LiClO<sub>4</sub> 10wt% TiO<sub>2</sub> added, diamonds: 3PEG 1.5 mol/kg LiClO<sub>4</sub> – uncured, × 3PEG 1.5 mol/kg LiClO<sub>4</sub> 10 wt% TiO<sub>2</sub> – uncured, + 3PEG 1.5 mol/kg LiClO<sub>4</sub> 10 wt% TiO<sub>2</sub> – cured, triangles 3PEG 1 mol/kg LiClO<sub>4</sub> – uncured, boxes 3PEG 1 mol/kg LiClO<sub>4</sub> 10 wt% TiO<sub>2</sub> – uncured, ■ 3PEG 1 mol/kg LiClO<sub>4</sub> 10 wt% TiO<sub>2</sub> – cured.

## ELECTROCHEMICAL LITHIUM INSERTION IN CARBON NANOTUBES \*

C. Bousquet, G. Maurin and F. Henn

LPMC, Université Montpellier II, Place E. Bataillon, 34095 Montpellier cedex 5.

R. Almayrac and P. Bernier

GDPC, Université Montpellier II, Place E. Bataillon, 34095 Montpellier cedex 5.

B. Simon

SAFT, direction de la recherche, route de Nozay, 91460 Marcoussis.

Since many years, carbon materials have been widely studied for their use as intercalation compounds in anodes of accumulator [1,2]. Furthermore, among carbon materials, carbon nanotubes are particularly interesting because they combine structural characteristics of graphite and fullerene [3], and would allow different ways of interaction like intercalation of alkali atoms between the graphitic layers of the multi-walled nanotubes and/or insertion inside the tube in the case of single-walled nanotubes [4].

In this work, we study the electrochemical insertion of lithium in carbon nanotubes. Electrochemical lithium insertion is carried out at room temperature in button cells using carbon nanotubes as cathode and lithium metal foil as anode. The two electrodes are separated by porous polypropylene disks, soaked by electrolyte. Buttons cells are assembled under an argon atmosphere.

Galvanostatic Intermittent Titration Technique (G.I.T.T.) [5] and cycling experiments allow to determine the reversible capacity and kinetic parameters, and so to conclude about the electrochemical performances of our materials used as electrodes.

Structural modifications induced by the lithium intercalation are evidenced by X-ray diffraction and Transmission Electron Microscopy. IR and Raman spectroscopies are used to emphasize the distortion of the carbon rings and to underline the Li-C interactions.

## References:

- [1] K. Tatsumi, N. Iwashita, H. Sakaebe, H. Shioyama, S. Higuchi, A. Mabuchi and H. Fujimoto, *J. Electrochem. Soc.*, **142** (3), 716 (1995).
- [2] Z. X. Shu, R. S. McMillan and J. J. Murray, *J. Electrochem. Soc.*, **140** (4), 922 (1993).
- [3] S. Xie, N. Li, Z. Zhang, W. Liu, G. Wang, S. Qian and C. Fu, *J. Mat. Science*, **30**, 2291 (1995).
- [4] V. A. Nalimova, D. E. Sklovsky, G. N. Bondarenko, H. Alvergnat-Gaucher, S. Bonnamy and F. Béguin, *Synthetic Metals*, **88**, 89 (1997).
- [5] W. Weppner and R. A. Huggins, *J. Electrochem. Soc.*, **124** (10), 1569 (1977).

\* work supported by the CNRS contract 42 PRG "Matériaux" # 98N42/0046

## DEPOSITION OF NANOPHASE DOPED - CERIA SYSTEMS ON CERAMIC HONEYCOMBS FOR AUTOMOTIVE CATALYTIC APPLICATIONS

C. Agrafiotis, A. Tsetsekou and C. J. Stournaras

CERECO S.A.

72<sup>nd</sup> km of Athens - Lamia Ntl. Road

P.O. Box 146

34100, Chalkida

GREECE

Cerium oxide is currently being used as an oxygen ion conductor in solid oxide fuel cells, oxygen sensors and three-way automobile catalysts because of its high ion conductivity. Its ability to act as an oxygen buffer and therefore operate effectively under conditions of oscillating oxygen concentration (rich-lean air/fuel) has promoted its use in automotive catalytic applications [1]. Cerium oxide can provide oxygen by conversion into  $\text{CeO}_{2-x}$ , to oxidize CO and hydrocarbons, and  $\text{CeO}_{2-x}$  can store oxygen from the exhaust gas, to reduce  $\text{NO}_x$  under lean fuel conditions. A remarkable enhancement on the catalytic activity of cerium oxide has been observed when the powder is of nanophase dimensions. The large number of lattice stoichiometric defects such as oxygen vacancies present in nanophase materials, provides a large number of active sites for gas-solid catalysis [2] and in addition increases the rate of oxygen diffusion. These defects can be created by partial substitution (doping) of the cerium atoms in the cerium oxide lattice with other metals atoms of lower oxidation state such as Ca, Nd, Pb or Tb. Because of these properties, nanophase doped cerium oxide supports can act as catalysts themselves, reducing significantly or even eliminating completely the need for precious noble metals [2,3].

In this study, the deposition of calcium-doped cerium oxide on ceramic honeycombs directly from the liquid phase, via the sol-gel technology was investigated. By this approach extremely active nanophase materials can be synthesized through liquid precursor solutions. A further advantage is that doping can take place in the liquid phase and at the molecular level. In addition, by this route the synthesis of dispersible powders and the preparation of slurries can be avoided and the washcoat layer can be formed in situ and adhered upon the monolith walls during calcination. However, problems inherent with the low solids content of the sols employed, can appear. These are the low loading achieved per impregnation, the extent of cracking and subsequent "peeling" of the washcoat layer because of the loss of large amounts of volatile compounds, and the penetration of the sol in the porous structure of the support where it fills the inner pores and makes the precious metals less accessible to the gaseous reactants. A further problem with nanophase cerium oxide powders is that they suffer from severe reduction of specific surface area and pore closure at elevated temperatures [4], where they also exhibit significant grain growth and crystallization. Another potential problem could be the reaction of cerium oxide with the support material at these elevated temperatures. These phenomena deteriorate their catalytic properties and prevent their use as high-temperature catalytic systems.

Inorganic precursor materials such as nitrates and chlorides have been used for the synthesis. Adjustment of the sol viscosity with the addition of organic binders was employed for the deposition of thick, surface washcoat layers on the ceramic support. Multiple impregnations were required for the loading of honeycombs with a total amount of washcoat of the order of 15 wt %.

The loaded honeycombs were characterized with respect to their surface area and pore structure. Treatment of the honeycombs at the high temperatures to be encountered during automotive operation and relevant surface area measurements, have verified a drastic surface

area reduction, especially above 1000 °C. Stabilization of nanophase ceria was attempted, by its dispersion within a  $\gamma$ -alumina washcoat matrix previously deposited upon the surface of the honeycomb substrate. This hybrid technique can provide for maintenance of high surface area and can also prevent the cerium oxide precursor sol from penetrating deep into the porous structure of the support. Experiments on the interaction of cerium oxide powders with various support materials currently employed in high-temperature catalytic applications such as cordierite and aluminum titanate, are also under way, in order to test the suitability of cerium oxide-based materials for high temperature applications.

#### REFERENCES

1. A. Trovarelli, C. de Leitenburg and G. Dolcetti, *Chemtech*, **27** (6), 32, (1997).
2. Y. Zhang, S. Andersson and M. Muhammed, *Applied Catalysis B : Environmental*, **6** (4), 325, (1995).
3. S. Bernal, G. Blanco, M. Cauqui, P. Corchado, J. Pintado and J. Rodriguez-Izquierdo, *Chemical Communications*, 1546, (1997).
4. B. Powl, R. Bloink and C. Eickel, *Journal of the American Ceramic Society*, **71** (2), C-104, (1988).

## EFFECT OF YBCO POWDER CHARACTERISTICS ON THICK COATINGS PREPARED BY ATMOSPHERIC PLASMA SPRAYING

E. Georgiopoulos, A. Tsetsekou, C. Andreouli  
Cereco S.A., P.O.Box 146, 34100 Chalkida, Greece

The discovery of superconducting YBCO oxides with critical temperature above 90K, has been followed by various efforts to obtain high  $T_c$  thin and thick films. For the production of thin films the most promising techniques are the laser ablation and sputtering [1, 2, 3], while one of the methods suitable for the construction of thick films is the plasma spraying technique [4]. The properties exhibited by YBCO thermal sprayed coatings are very promising for applications such as magnetic shielding with a lot of technical and process advantages [5, 6]. This technique is very flexible and has the ability to make components with a large variety of geometries, offering good adherence on the substrates, operation in non-vacuum conditions and large deposition rates.

For the production of the YBCO powdered superconducting material two different routes have been used: a) the solid state reaction using as starting materials  $\text{BaCO}_3$ ,  $\text{Y}_2\text{O}_3$  and  $\text{CuO}$  and b) the spraying drying process using as raw materials  $\text{Ba}(\text{NO}_3)_2$ ,  $\text{Cu}(\text{NO}_3)_2 \cdot 2.5\text{H}_2\text{O}$  and  $\text{Y}(\text{NO}_3)_3 \cdot 5\text{H}_2\text{O}$ .

The conventional solid state reaction mechanism for the production of YBCO powders has extensively studied. The processing parameters as well as the particle size distribution of the starting powders have been found to have a pronounced effect on the reaction kinetics as well as on the reaction sequence [7]. The investigation has shown that the superconducting  $\langle 123 \rangle$  phase is rapidly formed at an early reaction stage at low temperatures, lower than  $830^\circ\text{C}$ . The secondary phases:  $\langle 211 \rangle$  (an intermediate product),  $\langle 202 \rangle$  and  $\langle 011 \rangle$  (intermediate or decomposition products) reduce the reaction rate for the production of pure superconducting  $\langle 123 \rangle$  phase. For this reason the YBCO powder was formed following a multi-step procedure, comprising sintering at  $900^\circ\text{C}$  and grinding for 10 hours. The final YBCO powder is a high purity single-phase superconducting material and exhibits narrow particle size distribution (90% under  $14\mu\text{m}$  and 10% under  $3\mu\text{m}$ ).

Using the spray drying process powders with variable particle size distributions can be produced according to the selected conditions. These powders are spherical in shape, homogeneous with almost perfect stoichiometry exhibiting enhanced rheological characteristics suitable for the thermal spraying technique. The formation of  $\langle 123 \rangle$  superconducting phase that has occurred at even lower temperatures compared to the solid state reaction ( $710^\circ\text{C}$ ) due to the fact that spray dried granules consist of nanosized particles. The final YBCO powder consisted mainly of  $\langle 123 \rangle$  phase after an one-step calcination procedure at  $870^\circ\text{C}$  for 40 hours exhibiting a wide particle size distribution of 90% under  $43\mu\text{m}$  and 10% under  $10\mu\text{m}$ .

The objective of our study was to systematically investigate the effect of the feeding powder characteristics and especially the particle morphology and size distribution on the properties of the produced coatings. For this reason the powders produced from the above-described different routes were used in order to deposit thick YBCO coatings on stainless steel substrates using the APS technique. Various coatings were produced using as starting materials: a) the solid state reaction powder, b) the spray dried powder and c) mixed in various percentages powders from the above two batches.

The coatings were sprayed under optimized conditions (plasma and carrier gas, powder feed rate, spray distance, power supply) and the effect of the feeding powder characteristics (grain size

distribution, mineralogical analysis and homogeneity) was extensively studied. The coating properties were examined using X-ray diffraction analysis, SEM combined with EDS microanalysis and scratching tests in order to characterize the adhesion of the coatings on the substrate, the coating morphology, the thickness and crystalline structure as well as the powder phase transformations during spraying.

It was shown that the adhesion on the substrate and the quality of the coatings are greatly influenced by the feedstock powder characteristics.

#### References

- [1] S.Proyer, E.Stangl, M.Borz, B.Hellebrand, D. Bauerle, *Physica C* **257**, 1 (1996).
- [2] C.Andreouli, S.Christoulakis, T.Efthimiopoulos, A.Tsetsekou, M.Holiastou and C.Panagopoulos, *SPIE* **3423**, 374 (1997).
- [3] A.C. Westerheim, *J. Appl. Phys.* **75**, 393 (1994).
- [4] L. Pawlowski, A.Gross and R. McPherson, *J. Mater. Sci.* **26**, 3803 (1991).
- [5] G.Swaminathan, M. V. T. Dhanajeyan, K.A. Durgaprasad and R. Somasundaram, *Thin Solid Films* **206**, 175 (1991).
- [6] H. Weyten, S. Heusdains, J. Cornelis, F. Lostak and R. Chaouadi, *Silicates Industriels* **7-8**, 123 (1992).
- [7] C.Andreouli, A. Tsetsekou, *Physica C* **291**, 274 (1997).

## EXPLORING THE LOW-TEMPERATURE ELECTRICAL RELAXATION OF CRYSTALLINE OXYGEN-ION AND PROTONIC CONDUCTORS

A. S. Nowick

Columbia University, New York, NY 10027, U.S.A.

Studies of the ac conductivity of highly disordered ionic materials (glasses and highly doped crystals) have shown two distinct phenomena ("universalities"). [1] The first, called the "universal dielectric response" or UDR by Jonscher [2], occurs at high temperatures and/or low frequencies and involves a power-law dependence of the form

$$\sigma(\omega) = \sigma(0) + A\omega^s \quad (1)$$

where  $\sigma(0)$  is the "dc conductivity and the exponent  $s$  generally falls between 0.55 and 0.70. Both  $\sigma(0)$  and  $A$  are strongly temperature dependent, and related to each other. There are a multitude of theories of this effect, involving limitations on ionic motions of carriers caused by interionic interactions. The second phenomenon, occurring at low temperatures and/or high frequencies, involves a power law close to unity, and is therefore known as nearly constant loss, or NCL, behavior. This behavior is only weakly temperature dependent. It has been attributed to a broad distribution of asymmetric double-well potentials, ADWP's (also called "two-level systems"), but its physical origins are not well understood. The present work attempts to gain a better understanding of the NCL behavior by examining materials with a relatively simple defect structure, notably, crystalline materials with low defect concentrations. The materials chosen are the following:

(a)  $\text{CeO}_2:\text{M}^{3+}$  where  $M$  is either Gd or Y. The lower valent  $\text{M}_{\text{Ce}}'$  ion is compensated by oxygen vacancies to make the material an oxygen-ion conductor. Here the defect structure at lower temperatures is well known, involving a network of  $\text{M}_{\text{Ce}}'$  and  $(\text{M}_{\text{Ce}}\text{V}_\text{O})'$  defects [3].

(b)  $\text{CaTiO}_3:\text{Al}^{3+}$ , which also gives rise to oxygen vacancies that compensate  $\text{Al}_{\text{Ti}}'$  defects, and is also an oxygen-ion conductor.

(c)  $\text{BaCeO}_3:\text{Nd}^{3+}$ , which also forms oxygen vacancies to compensate  $\text{Nd}_{\text{Ce}}'$  defects, except that here, after treatment in  $\text{H}_2\text{O}$  vapor, the  $\text{V}_\text{O}$  defects are replaced by protons in the form of  $(\text{OH})_\text{O}$  defects, which results in the material becoming a good protonic conductor. [4]

Measurements were made of the ac conductance and capacitance of the above materials over the frequency range 10Hz to 100 kHz, and the temperature range ~50 to 250 K. The following compositions were studied: (a) For  $\text{CeO}_2$ , the  $\text{Gd}^{3+}$  doping ranging from 1 to 11.3 atomic % (i.e., from low to high defect concentrations), and the same range for the  $\text{Y}^{3+}$  doping. (b) For  $\text{CaTiO}_3$ ,  $\text{Al}^{3+}$  doping from 1.5 to 30 at.%. (c) For  $\text{BaCeO}_3$ , only 5%  $\text{Nd}^{3+}$  doping.

In the first two cases, for the low composition, the low-temperature behavior showed a well defined loss peak for the quantity:  $\tan \delta(\omega) = \epsilon''(\omega)/\epsilon'(\omega)$ . In the cases of  $\text{CeO}_2$  and  $\text{CaTiO}_3$ , the peaks shifted in frequency with increasing temperature in a classical (Arrhenius) manner, showing an activation energy,  $E$ , close to 0.2eV. This is substantially lower than  $E$  for the dc conductivity. With increasing dopant concentration, however, these peaks broaden and decrease, until at high concentration they show very nearly a constant loss. This variation with concentration is shown in Fig. 1 for the case of  $\text{CaTiO}_3:\text{Al}$ .

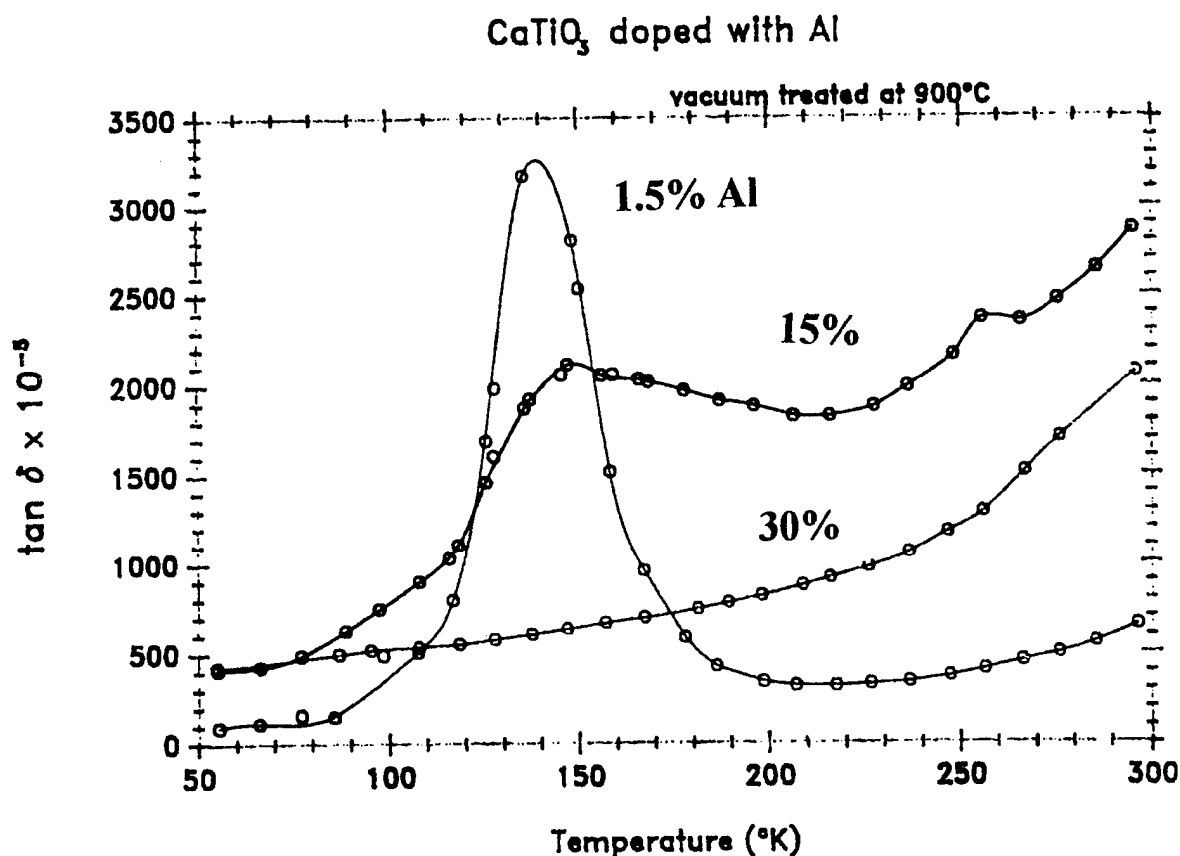
In the case of the protonic conductor  $\text{BaCeO}_3:\text{Nd}$ , a nearly Debye peak is observed. This peak is not classical, and apparently involves quantum-mechanical tunneling of protons.

These low-temperature peaks may be interpreted as due to relatively large atomic configurations which are off-symmetry in the lattice, and therefore, when relaxing due to the electric field, undergo wiggling motions involving small ionic displacements, with corresponding low activation energies. Such processes are discrete at low concentrations, but are spread out into a continuous distribution at high defect concentrations, thus accounting for the NCL behavior.

### References

- [1] A.S. Nowick, A.V. Vaysleyb and W. Liu, *Solid State Ionics* 105, 121 (1998).
- [2] A.K. Jonscher, "Universal Relaxation Law", Chelsea Dielectrics press, London, 1996.
- [3] A.S. Nowick, in "Diffusion in Crystalline Solids", ed. G. Murch and A. Nowick, Academic Press, Orlando, 1984, Chapter 3.
- [4] H. Iwahara et al., *Solid State Ionics* 3/4, 359 (1981).

Fig 1. Variation with temperature of the loss tangent,  $\tan \delta$ , measured at 1 kHz, for three compositions of  $\text{CaTiO}_3:\text{Al}^{3+}$





## A RANDOM RESISTOR NETWORK MODEL TO FORECAST THE ELECTRICAL PROPERTIES OF CRYSTALLINE IONIC CONDUCTOR COMPOSITES

Claudio M. Mari

Dept. of Materials Science, University of Milano, via Emanuelli 15, 20126 Milano, ITALY

Giovanni Dotelli

Dept. of Industrial Chemistry and Chemical Engineering, Polytechnic of Milano, P.zza L. da Vinci 32, 20133 Milano, ITALY

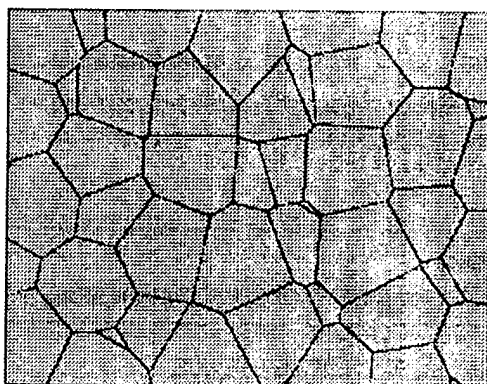
The interest in the electrical properties of ion conducting composites arises from their possible application in the planar SOFC, the electrolyte of which has to own both good ionic conductivity and high bending strength. Generally the dispersed phase used to improve the mechanical properties of the ionic conductor presents poor electrical conductivity and the final electrical properties of the composites are worse than those of the pure electrolyte.

A random resistor network approach was suggested as a possible route to anticipate the electrical properties of the ion conducting composites [1] and some preliminary results were encouraging [2]. Nevertheless experimental results [3] recently showed that the particles size of both electrolyte and dispersed phase play an important role in the final electrical properties of the composites and a more sophisticated model has to be used.

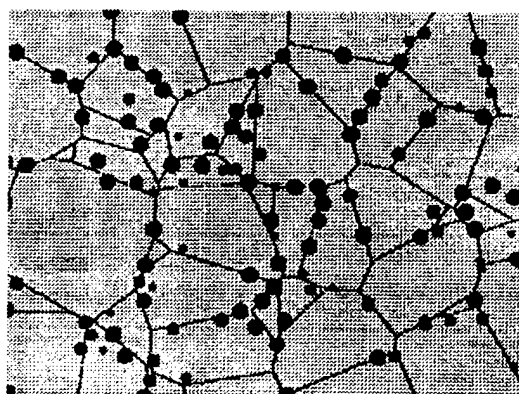
Aim of this work is to present a model that might be able to forecast the electrical properties of crystalline composites in which are present both insulating and ionic conductor phase taking into account the relative size and distribution of the particles.

The model works through two steps: a suitable representation of the material microstructure and its conversion into a 3-D electrical network.

The computer simulation generates the polycrystalline microstructure of the composite using the Voronoi tessellation [4], a well known technique in computational geometry. To reproduce the proper shape and dimension of the ionic conductor grains, a volume is subdivided into a set of convex polyhedra (or hulls), fig. 1a; the insulating phase, dispersed, may be considered as spheres of constant radius and randomly distributed in intergranular and in intragranular positions (fig. 1b).



(a)



(b)

Figure 1. Sections of the simulated polycrystalline microstructure without (a) and with (b) dispersed phase, as generated by the Voronoi tessellation.

Then a 3-D network of cubes was superimposed onto the simulated polycrystalline microstructure and the edges of each cube substituted with discrete impedances (fig.2).

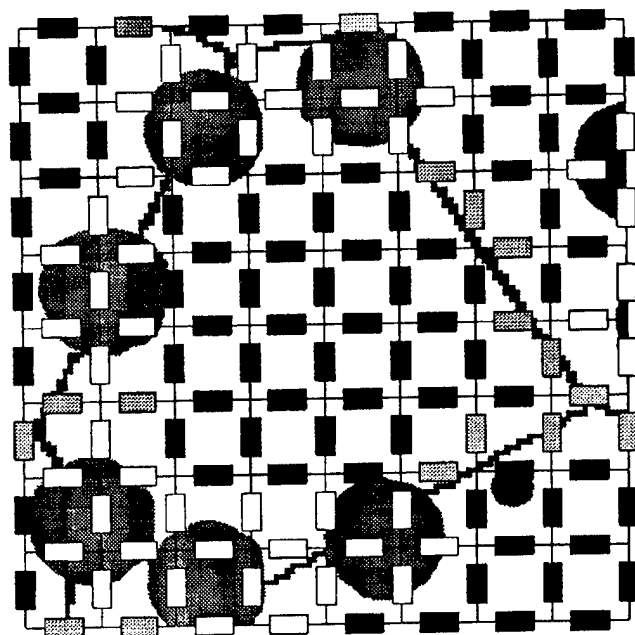


Figure 2. Schematic view of a planar section of the 3-D electrical network: black, grey and white boxes represent bulk, grain boundary and dispersed phase impedances, respectively.

Different values and combination of  $R$  and  $C$  reproduce the bulk and the grain boundary electrical behaviour of the different phases. The electrical impedances were distributed using well defined rules. Bulk contribution was assigned when the edge of the cube is inside the convex polyhedra and the grain boundary in the case the edge crosses two different hulls. This approach permits to take into account the many parameters that influence the electrical behaviour of these composites.

The electrical network thus obtained can be solved by a transfer-matrix method [5] for a range of frequencies and the complex impedance spectra produced.

In principle, this model, with relatively minor variations, might be also used to simulate the electrical behaviour of many different both crystalline and amorphous composites.

## REFERENCES

- [1] G. Dotelli, R. Volpe, I. Natali Sora, C. M. Mari, Solid State Ionics, in press
- [2] G. Dotelli, F. Casartelli, I. Natali Sora, C.M. Mari, in "Modeling and Simulation of Materials", Proceedings of the 9<sup>th</sup> CIMTEC -World Ceramic Congress and Forum on New Materials, vol. XVIII, Florence (ITALY) 14-19 Giugno 1998, in press.
- [3] I. Natali Sora, C. Schmid, G. Dotelli, F. Casartelli, C. M. Mari, submitted to J. Inorg Mater.
- [4] M. de Berg, M. van Kreveld, M. Overmars, O. Schwarzkopf, Computational Geometry, Springer-Verlag, Berlin (1997).
- [5] B. Derrida, J.G. Zabolitzky, J. Vannimenus, D. Taufer, J. Stat. Phys., **36**, 31 (1984).

## REFERENCE ELECTRODES AND THE GIBBS PHASE RULE

Robert A. Huggins

Technical Faculty  
Christian-Albrechts-Universität zu Kiel  
Kaiserstrasse 2  
D-24143 Kiel, Germany

Reference electrodes play an important role in the study of many aspects of electrochemical systems. Experimental work in the literature often involves the use of different reference systems, and it is sometimes difficult to translate between measurements made with one from those made using another.

There are significant differences in both philosophy and practice between the aqueous electrochemistry and the solid state electrochemistry communities.

Reference electrodes that are used in solid state electrochemical systems are based upon the chemical potentials of electrically neutral chemical species. Electrochemical cell voltages can be calculated on the basis of normal chemical thermodynamics. The identity, composition and properties of the electrolyte have no significance, so long as it is predominantly an ionic conductor.

On the other hand, the general practice in aqueous electrochemistry is to use reference electrodes that involve the properties of ions, and to focus attention upon the electrochemical interface. The composition and the pH of the electrolyte are important in some cases, but not in others.

These matters are discussed in terms of the Gibbs Phase Rule, showing the difference between zero-degree-of-freedom (ZDF) electrodes, and those in which an additional parameter, such as the electrolyte pH, must be specified. The interrelationship between these two types is illustrated using potential-pH plots, or Pourbaix diagrams, in which the electronic and ionic components of the chemical potential are separated.

This approach provides a simple understanding of the two major types of references used in aqueous electrochemistry and the glass electrode systems that are used to measure the pH of electrolytes. It will also be shown that in electrodes with a mixed-conducting matrix and an internal ZDF reaction the potential in an electrochemical cell is determined by the internal chemical reaction, rather than the external electrochemical reaction.

## CONCEPT OF MISMATCH AND RELAXATION DERIVED FROM CONDUCTIVITY SPECTRA OF SOLID ELECTROLYTES

K. Funke and D. Wilmer

University of Münster, Institute of Physical Chemistry, Schloßplatz 4/7, D-48149 Münster

In solid electrolytes, conductivity spectra contain relevant information on the hopping dynamics of the mobile ions at times ranging from picoseconds to seconds. To extract this information, it is important to recognize and identify those features which make up the essence of the experimental spectra. To this end, we have plotted normalized conductivities,  $\sigma(\omega)/\sigma(0)$ , versus normalized angular frequencies,  $\omega/\omega_{\text{onset}}$ , for a variety of crystalline and glassy ion conductors in a log-log representation. Remarkably, the resulting master plot displays a very general behaviour combining the Jonscher-type universal dynamic response (UDR) [1] and the nearly constant loss (NCL) [2] frequency regimes in a continuous fashion. As the temperature is decreased, the onset of the dispersion is shifted to lower frequencies and thus the characteristic shape of the master curve becomes visible in an increasingly broad frequency range. Therefore, with decreasing temperature, the UDR is gradually replaced by the NCL behaviour at any given frequency.

The experimental conductivity master curve obtained from crystalline electrolytes including  $\text{RbAg}_4\text{I}_5$ ,  $\beta\text{-AgI}$ , and others is shown to be well reproduced by the following parameter-free model master curve:

$$\ln \left( \frac{\sigma(\omega)}{\sigma(0)} \right) = E_1^{-1} \left( \frac{\omega_{\text{onset}}}{\omega} \right), \quad (1)$$

where  $E_1^{-1}$  is the inverse function of the exponential integral,  $E_1$ . At millimetre-wave frequencies, dispersive conductivities attain high-frequency plateaux [3]. Again the data are well reproduced if Eq.(1) is modified to become:

$$\frac{\omega_{\text{onset}}}{\omega} = E_1 \left( \ln \frac{\sigma(\omega)}{\sigma(0)} \right) - E_1 \left( \ln \frac{\sigma(\infty)}{\sigma(0)} \right). \quad (2)$$

Here,  $\sigma(\infty)$  denotes the high-frequency limiting value of the hopping conductivity. A set of model master curves featuring both low- and high-frequency plateaux is shown in Fig. 1. Note that there is no fixed power-law exponent in the dispersive regime. Rather, the slope in Fig. 1 increases (but does not surpass unity), until the high-frequency plateau is attained.

The particular mathematical structure of Eq. (1) can be exploited to gain new insight into the hopping dynamics of the mobile ions. This is done with the help of two decaying functions of time,  $f(t)$  and  $g(t)$ :

$$f(t) := \ln \frac{D(t)}{D(\infty)} \quad \text{and} \quad g(t) := \exp(-\langle r^2(t) \rangle / a^2). \quad (3)$$

In Eq. (3),  $D(t)$ ,  $\langle r^2(t) \rangle$ , and  $a$  denote the time-dependent coefficient of self-diffusion, the mean square displacement, and a typical hopping distance, respectively. The particular form of the master curve, cf. Eq. (2), implies that  $f(t)$  and  $g(t)$  are proportional to each other. Their negative time derivatives,  $-df(t)/dt$  and  $-dg(t)/dt$ , are readily visualized in the physical picture of the jump relaxation model. In that picture, each hop is supposed to create a local mismatch. Mismatch relaxation is then achieved either by a backward hop of the ion or by rearrangement of its mobile neighbours. Interestingly, the rates of relaxation via those single- and many-particle routes are

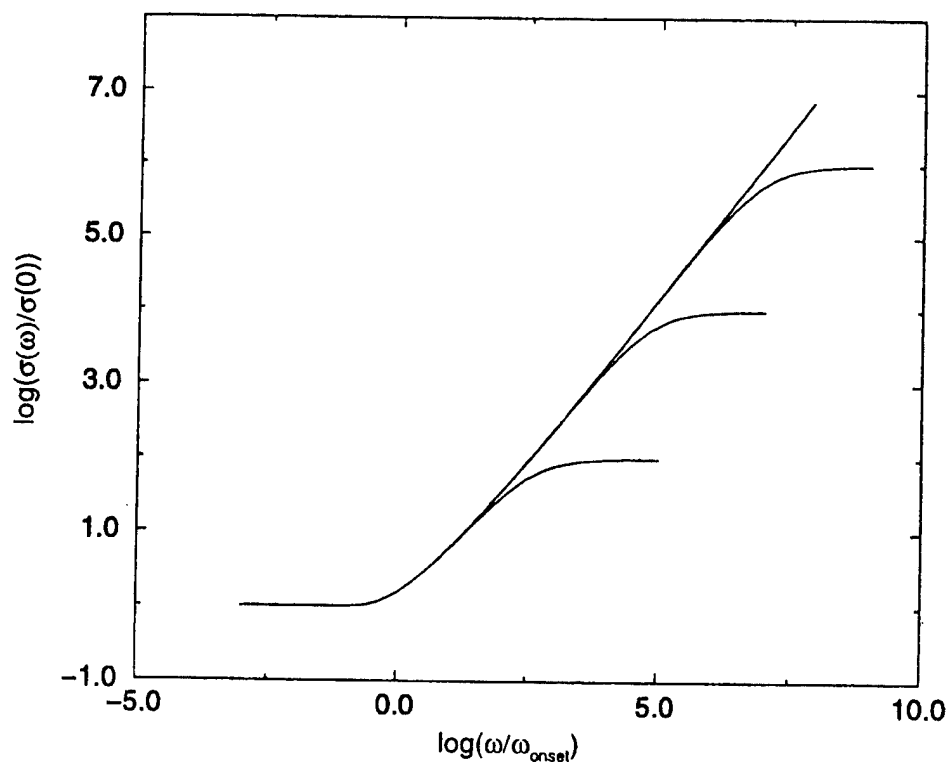


Figure 1: Master curves.

given by  $-df(t)/dt$  and  $-dg(t)/dt$ , respectively. These have been shown to be proportional to one another. We thus arrive at the central statement of the concept of mismatch and relaxation (CMR) which claims that the rates of relaxation via the two competing routes are coupled to each other in a synchronous fashion.

Reversing our line of reasoning, we may now utilize the CMR as a physical basis for model construction. This opens up the possibility to combine the CMR with structure-related traits and thus to explain specific features of experimental conductivity spectra.

## REFERENCES

1. A. K. Jonscher, *Nature* **267**, 673 (1977).
2. W.-K. Lee, J. F. Liu, and A. S. Nowick, *Phys. Rev. Letters* **67**, 1559 (1991).
3. K. Funke, *Prog. Solid St. Chem.* **22**, 111 (1993).

## DIELECTRIC RELAXATION IN IONIC SOLIDS: EXPERIMENTAL EVIDENCES

F.Henn, S.Devautour, J.C.Giuntini, J.V.Zanchetta  
 Laboratoire de Physicochimie de la Matière Condensée, UMR 5617 CNRS  
 Université de Montpellier II  
 Place Eugène Bataillon, F-34095 Montpellier, France  
 H.Schaefer  
 HF-NMR facility, NSR center, University of Nijmegen  
 Toernooiveld, Nijmegen, The Netherlands  
 and  
 J.Vanderschueren  
 Chimie Macromoléculaire et Chimie-Physique  
 Research Associate of the National Fund for Scientific Research  
 Institut de Chimie Sart Tilman. Université de Liège  
 B-4000 Liège, Belgium

The comparison of different experimental methods of dielectric relaxation measurements applied on diverse ionic solids clearly demonstrates that ac conductivity dispersion observed in these solids is of dielectric nature.

The dielectric relaxation measurements were undertaken:

- i) in the frequency domain. The dissimilarity of  $\sigma'_{ac}(\omega)$  (or  $\varepsilon''_{ac}(\omega)$ ) measured with or without the use of blocking insulating films allows a clear separation of the dc and dielectric contributions of the global ac signal [1,2].
- ii) in the time/temperature domain by means of Thermally Stimulated Current including different experimental approaches such as: global depolarisation or polarisation and thermal windowing. Varying the dc electric field of polarisation and the temperature of polarisation [3] enables to decide which among the various contributions of the thermally stimulated response is due to charge migration or dielectric relaxation phenomena.

The qualitative and quantitative treatments of the data obtained from these distinct experimental tools lead to extract from the relaxation spectrum the dc conductivity and related signals (like electrode polarisation) and therefore to access to the pure dielectric response of the ionic material.

Furthermore, the analysis of this dielectric response by means of

- i) Inverse and Ill-Posed Problem[4] or non-linear fitting[5] methods and
- ii) the examination of the variation of Thermally Stimulated Depolarization Currents with the heating rate[6]

shows particularly that the use of distribution of relaxation time function (DRT) is very well adapted for understanding the ac conductivity dispersion and for characterising the physical or chemical properties of some ionic solids.

Experimental results obtained on poorly conductive materials as  $H^+, Li^+, Na^+, K^+$  exchanged zeolites[7] and on superionic conductors of the glassy AgI-AgPO<sub>3</sub> system will be given.

Finally, chemical considerations based on the one hand on electron chemical potential and chemical hardness concepts [8], and on the other hand on ion-ion interactions allow us to explain the different behaviours observed in these ionic solid systems.

#### References :

- [1] F. Henn *et al.*, Phys. Rev., **B48**,573(1993)
- [2] S. Devautour *et al.*, Ionics, **3**, 373 (1997)
- [3] S. Devautour *et al.*, J.Phys.D: Applied Phys., (under press in volume **38** (1998))
- [4] H. Schäfer *et al.*, Phys. Rev. Lett., **76**, 2177 (1996)
- [5] S. Devautour *et al.*, J. Appl. Phys., **82**,5057 (1997)
- [6] F. Henn *et al.*, J. Appl. Phys. (under press in volume **85/4** (1999))
- [7] S. Devautour *et al.*, J. Phys. Chem., **B102**, 3749 (1998)
- [8] S. Devautour *et al.*, J. Phys. Chem., (under press)

## STUDY OF PHONONS AND NORMAL MODE ANALYSIS OF SUPERIONIC CONDUCTORS

M.M.SINHA and K.WAKAMURA\*

Department of Physics,  
Sant Longowal Institute of Engineering and Technology, Longowal  
Sangrur (Punjab) – 148106 INDIA

\*Department of Applied Science, Okayama University of Science  
1-1 Ridai-cho, Okayama 700, JAPAN

A de Launey angular force (DAF) model [1] has been used to calculate the frequency at zone centre and normal modes in the phase-I of CsPbCl<sub>3</sub> and  $\gamma$ -phase of Ag<sub>3</sub>SI and Ag<sub>3</sub>SBr compounds. The phase-I of CsPbCl<sub>3</sub> and  $\gamma$ -phase of Ag<sub>3</sub>SI and Ag<sub>3</sub>SBr are assumed to have ideal perovskite structure.

The analysis involves three central force constants  $\alpha_1$ ,  $\alpha_2$  and  $\alpha_3$  and three angular force constants  $\alpha_1'$ ,  $\alpha_2'$  and  $\alpha_3'$  between Pb-Cl (S-Ag), Cs-Cl (I or Br-Ag) and Cs-Pb (S-I or Br) atoms respectively. The values of force constants are then determined by fitting the experimental values of transverse infrared active phonon frequencies at zone centre. The central force constant  $\alpha_3$  between Cs-Pb (S-I or Br) is found to be strongest among all others in all these compounds. This result is reasonable since the ions compose the cage ions in superionic conducting phase.

The dynamical matrix is then computed at zone centre taking these force constants as input parameters. A set of eigenvectors is calculated corresponding to each frequency and the normal vibrational modes are assigned. The assigned highest mode ( $\nu_1$ ) in present investigation is different from that done by others for perovskites [2]. The present mode analysis interprets reasonably the higher values of  $\nu_2$  and  $\nu_3$  in CsPbCl<sub>3</sub> [3] than those of Ag<sub>3</sub>SX (X=Br,I) [4,5] inspite of its lower value of highest mode ( $\nu_1$ ).

### References:

- [1] J.de Launey, Solid State Physics, 2, 219 (1956)
- [2] I.Nakagawa, A.Tsuchida, T.Shimanouchi, J.Chem. Phys. 47, 982 (1967)
- [3] K.Wakamura et al. 11<sup>th</sup> Int. Conf. on Ternary and Multinary Compounds, 515 (1997)
- [4] K.Wakamura et al. Proc. 3<sup>rd</sup> Int. Conf. Phonon Phys. 1171 (1990)
- [5] K.Wakamura et al. Phys. Rev. B 41, 2758 (1990)



## MODELLING ION CONDUCTION PATHWAYS BY BOND VALENCE PSEUDOPOTENTIAL MAPS

Stefan Adams

MKI Universität Göttingen, Goldschmidtstr.1, 37077 Göttingen (Germany)

Empirical bond length bond valence relations have become a routine tool to check the plausibility of crystal structure determinations or to localise light elements from X-ray data. The extension of this approach to completely model the site dependence of the bond valence sum for a mobile ion throughout a given structure opens a comparatively simple way to determine systematically ion conduction pathways in perfectly crystalline, highly disordered and even amorphous systems [1,2]. In this work a variety of silver ion conducting systems is considered to elucidate the meaningfulness and limitations of the bond valence technique. The resulting models are discussed in the light of independent experimental observations.

For several crystalline  $\text{Ag}^+$  ion conductors of sufficient crystal perfection anharmonic atomic displacement parameters can be determined. The distribution of the Ag probability density in the vicinity of the regularly occupied sites then directly corresponds to the valence sum mismatch [3]. As an example Fig. 1 displays the bond valence model of the  $\text{Ag}^+$  silver ion conduction pathways in  $\text{RbAg}_4\text{I}_5$  based on a recent redetermination of its structure including anharmonic atomic displacement parameters from neutron single crystal data [4]. While experimental observations are limited to the environment of equilibrium sites bond valence models equally include vacancies. Thereby the existence of interstitial pathways may be easily checked. In the case of  $\beta\text{-Ag}_2\text{HgI}_4$  sketched in Fig. 2 pathways connecting the occupied sites via octahedral vacancies are found to be more likely than previously discussed interstitial pathways.

Beyond a description of the conduction pathway topology bond valence pseudopotentials should also provide a simple tool to estimate migration enthalpies and jump probabilities for the mobile ions within the pathways (cf. Fig. 3). Correlations between the quantities determined from the temperature dependence of the ionic conductivity and the valence sum mismatch at the saddle points of the elementary jumps are exemplified for several types of compounds including the polymorphs of  $\text{AgI}$ , and silver iodide- silver oxysalt compounds [1,5,6].

In contrast to modelling techniques that rely explicitly on the crystal symmetry the bond valence approach is well suited to describe the influence of disorder. Since local hops of mobile

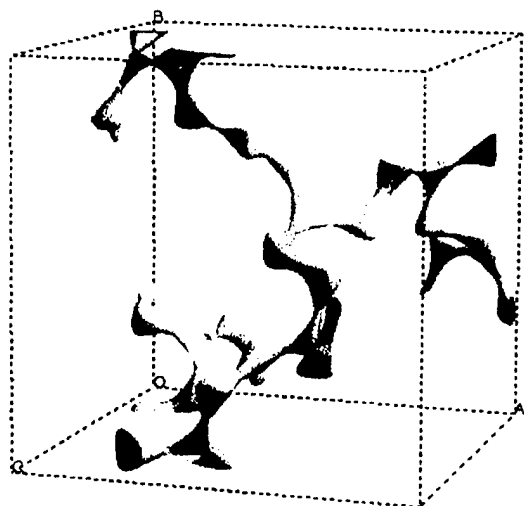


Fig. 1: bond valence model of ion conduction pathways in  $\text{RbAg}_4\text{I}_5$  (cf. [3])

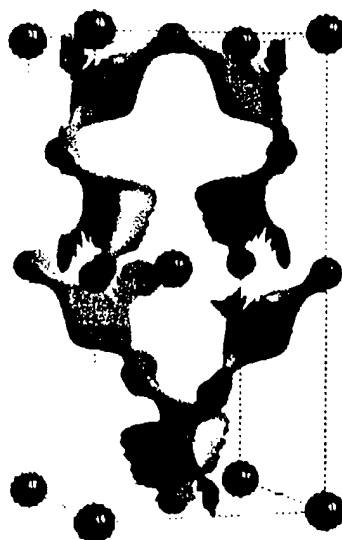


Fig. 2: Pathway model for  $\beta\text{-Ag}_2\text{HgI}_4$ , dark balls: Ag, light balls: Hg

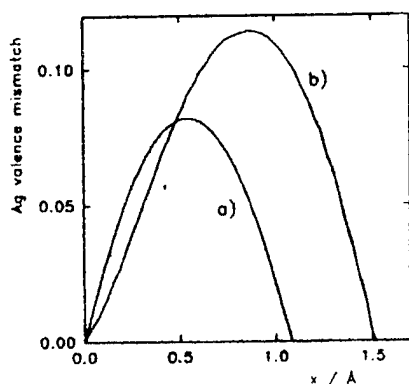
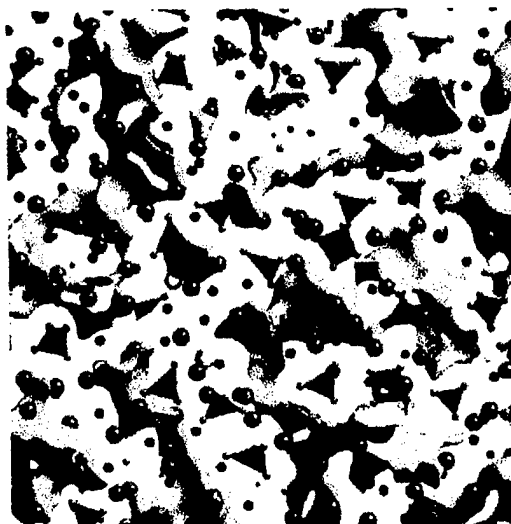


Fig. 3: Valence mismatch barriers in  $\beta$ -AgI for jumps a) from an octahedral interstitial b) from a regular tetrahedral site to adjacent octahedral sites

Fig. 4: Detail from a Ag bond valence isosurface for the glassy silver ion conductor  $\text{AgI}_{0.75}(\text{Ag}_2\text{MoO}_4)_{0.25}$



ions rather depend on the actual local co-ordination than on average structures it becomes necessary to construct chemically meaningful local structure models first. In some cases such as in  $\alpha$ - $\text{Ag}_2\text{HgI}_4$ ,  $\text{Ag}_{26}\text{I}_{18}\text{W}_4\text{O}_{16}$  the crystallographic information about the mean anion displacements can be translated directly into a model of the local displacement. For systems with more complex anion disorder (such as the almost free rotation of  $\text{P}_2\text{O}_7^{4-}$  groups in  $\text{Ag}_{16}\text{I}_{12}\text{P}_2\text{O}_7$ ) molecular mechanics simulations have been employed to ensure the plausibility of the local structural model for the bond valence calculations [1].

The simplicity of the valence sum pseudopotentials permits the modelling of comparatively large model systems and hence also of glassy ion conductors. For the  $\text{Ag}^+$  ion conducting glasses  $(\text{AgI})_{0.6}(\text{Ag}_2\text{O}-\text{B}_2\text{O}_3)_{0.4}$  and  $\text{AgI}_{0.75}(\text{Ag}_2\text{MoO}_4)_{0.25}$  atomic arrangements had were taken from a slightly modified Reverse Monte Carlo (RMC) technique [7]. Bond valence isosurfaces calculated from these RMC models contain complex pathway networks which appear confusing at first sight, but the essential features are quite similar to those of the corresponding crystalline silver iodide-silver oxysalts (cf. Fig. 4). While for crystalline ion conductors the variation of the valence mismatch around all relevant saddle points can be analysed in detail, representative results for glassy systems e.g. on the involvement of differently co-ordinated silver ions in the transport process (Fig. 5) require a statistic evaluation of the percolation of mobile ions along the bond valence sum isosurfaces.

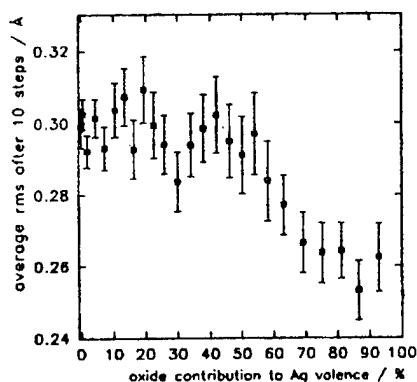


Fig. 5: Relative mobilities of  $\text{Ag}^+$  ions with different co-ordinations along bond valence isosurfaces in  $\text{AgI}_{0.75}(\text{Ag}_2\text{MoO}_4)_{0.25}$  [7]

#### References:

- [1] St. Adams, J. Maier, *Solid State Ionics* **105**, 67 (1998).
- [2] St. Adams, *Z. Kristallogr.* **211**, 770 (1996).
- [3] J.D. Garrett, J.E. Greedan, R. Faggiani, S. Carbotte, I.D. Brown, *J. Solid State Chem.* **42**, 183 (1982).
- [4] St. Adams, W.F. Kuhs, D. Wilmer to appear in *Z. Kristallogr.* (1999).
- [5] St. Adams, J. Lee and J. Maier, *Materials Structure* **5**(1998), 68-98.
- [6] J. Lee, St. Adams and J. Maier, *in preparation*
- [7] J. Swenson, St. Adams, *Proc. Neutrons & Numerical Methods*, Grenoble Dez. 1998.

## DOPE OF TIN OXIDE SURFACE AND PROTON MIGRATION DYNAMIC AS SEEN QUANTUM CHEMISTRY

Zyubina T.S., Dobrovolsky Yu.A., Ukshe A.E.<sup>1</sup>, Domashnev D.I.<sup>2</sup>

Institute for New Chemical Problem RAS, Chernogolovka

<sup>1</sup>Institute for Chemical Physics Problem RAS, Chernogolovka

<sup>2</sup>Moscow State University, Moscow

Clusters  $\text{MO}_2(\text{SnO}_2)_n$  ( $n=0\div 31$ ),  $M=\text{Si, Ge, Sn, Pb, In, Sb}$  are calculated by using PM3-method and SBK(d,p), 6-31G(d,p), LanL2DZ(d,p) basis sets at the Hartree-Fock and density functional levels employing the three-parameter Becke functional B3LYP.

The quantum chemical modeling of migration dynamics for the protons on the surface and in the bulk of the tin oxide was carried out. Cluster approximation was used for determine the geometrical positions and configurations of conductivity channels for protons on the surface of the tin oxide, and interference of migrating protons. The activation barriers for migration of the single proton and proton set was evaluated. The qualitative picture of the correlation transport for proton set on the oxide surface was realized. The energy variations of conductivity channels for cooperative movement of protons and conditions of proton migration from the surface in the bulk was analyzed. The method for modeling the collective phenomena during the proton transport via surface was developed. The method based on an idea of complex description of proton behavior by quantum chemistry and stochastic methods and fractal geometry.

The calculations had shown that protons migrate on the surface quasiindependently if the proton density on the surface is that the average distance between protons is in excess of two size of the unit cell. The part of the protons is moved in the bulk if the average distance between protons is comparable with single size of the unit cell.

Evaluating of  $S_0 \rightarrow S_1$  vertical excitation (at CIS/LanL2DZ(d,p) level) shows that dope of tin oxide by Ge and Pb does not essential influence on proton migration. But dope by Pb leads to increasing of electron conductivity. Proton affinity for  $M=\text{Sb}$  is the greatest one in the row  $M=\text{Ge, Sn, Pb, In, Sb}$ .

Dope of tin oxide by Sb atom influences essentially on the proton migration type. Dope of tin oxide by Sb atom lead to both increasing bulk proton conductivity simultaneously with decreasing surface one.

Collective phenomena during the proton transport via surface we have been modeling by the method of computer simulation. Our method based on the hypothesis, that there are two and only two possible configuration in the system of two protons on the surface of elementary cell. The ion jump is possible only if it lead to change or create of one of possible configurations or to decrement of proton number less than two. Such ideas correspond to our quantum chemistry calculations but was ventilated by M. Kompan [1].



As the result of our simulation we got, that if the number of protons is large (more than 20% sites are occupied), the transport via surface to macroscopic distance is impossible. During the gradual decreasing the number of surface protons, at the electrode area by the drift under electric current for example, at the some moment their distribution becomes non-stochastic. There is the fractal

"coagulation" occurs, and the superstructure with fractal geometry is created. (Fig.)

Ion and electron conductivity of the hydrated polycrystalline tin oxide ( $\text{SnO}_2 \cdot 1.5\text{H}_2\text{O}$ ) with addition of Sb was investigated experimentally. It was shown, that conductivity is mostly ionic one and pass in the bulk of granule. The rider of Sb does not influence on the ion conductivity character, but increases the electron conductivity. Influence of the gaseous atmosphere on Pt/ $\text{SnO}_2$  surface behavior was investigated. In hydrogenless atmosphere the Pt/ $\text{SnO}_2$  surface is slightly reversible for minor charge carrier. In presence of hydrogen, it was shown, that diffusion surface currents increase sharply and stable equilibrium of the proton exchange appears.

The work is supported by the Russian Fundamental Research Foundation, Grant 96-03-33652a and 97-03-32149a.

[1] M.Kompan, G.Venus, J.of Experimental & Theoretical Physics 1, 1424 (1992).

# The Model of the Li-Sb<sub>2</sub>S<sub>x</sub> Direct Contact in the Li/Sb<sub>2</sub>S<sub>x</sub> System.

by N. Arkhipova, A. Mikhailova and T. Arkhipova.

Saratov State Technical University.

Russia, Saratov.

The Li-Sb<sub>2</sub>S<sub>x</sub> interface in the Li/Sb<sub>2</sub>S<sub>x</sub> system one may represent as Schottky's metal-semiconductor barrier's model regarding to classical notions of solid state physics. The Li/Sb<sub>2</sub>S<sub>3</sub> and Li/Sb<sub>2</sub>S<sub>5</sub> voltamperic study [1] showed similar behaviour of both of these systems, moreover by the use of the empiric equation (Fig.1).

$$\log i = a + b \Delta E^{1/2} \quad (1)$$

most satisfactory linear approximation is achieved. It is known that analogic dependence takes place in the thermoelectronic and thermoionic emission of a dielectric with electric field applying [2]. Schottky's equation binds emission current ( $i_e$ ) with electric field strength in a dielectric ( $\Delta E_d$ ):

$$\log i_e = \log AT^{-2} - 0,43 e \varphi / kT + 0,43 / kT \sqrt{(e^3 / 4 \pi \epsilon \epsilon_0 d)} \sqrt{(\Delta E)}, \quad (2)$$

where  $A = 12 \cdot 10^5 \text{ A/m}^2 \text{ K}^{-2}$  – a Richardson's constant,

$e \varphi$  – electron work function,

$\varphi$  – metal-dielectric barrier's height,

$k = 1,38054 \cdot 10^{-23} \text{ J/K}$  – Boltzmann's constant,

$e = 1,602 \cdot 10^{-19} \text{ C}$  – electron charge,

$\epsilon_0 = 8,8542 \cdot 10^{-12} \text{ F/m}$  – the dielectric constant of vacuum,

$\epsilon$  – relative dielectric constant,

$d$  – dielectric film's thickness, m.

In strong electric fields  $\log i - \Delta E$  curves linearity of the Li/Sb<sub>2</sub>S<sub>x</sub> systems is one of Schottky's and Frenkel's currents' indication.

Metal-semiconductor's potential barrier's magnitudes of Li/Sb<sub>2</sub>S<sub>x</sub> system using zero extrapolation of overvoltage ( $\Delta E=0$ ) may be determined. Hence these magnitudes are calculated from the following equation:

$$(\log j)_{\Delta E=0} = \log (AT^{-2}) - 0,43 e \varphi / kT \quad (3)$$

The calculations give magnitudes of Li/Sb<sub>2</sub>S<sub>3</sub> and Li/Sb<sub>2</sub>S<sub>5</sub> systems' potential barrier's heights.  $\phi_1$  and  $\phi_2$  significances found from the calculations:  $\phi_1 = 0,723\text{eV}$  and  $\phi_2 = 0,691\text{eV}$  respectively. Literature data of Li/Sb<sub>2</sub>S<sub>3</sub> system's give the magnitude of potential barrier's height: it is equal  $0,740\text{eV}$ . Schottky's space charge  $dn$  is valued from the angular coefficient (b) of the corresponding linear dependence according to the following equation:

$$b = 0,43/kT \sqrt{e/4\pi\epsilon\epsilon_0 dn} \quad (4)$$

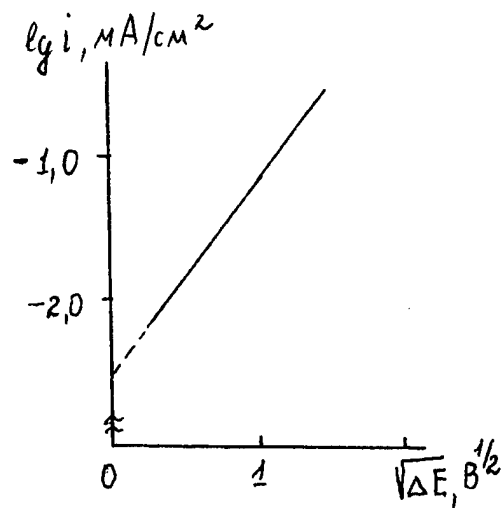


Fig.1 Voltamperic characteristic of Li/Sb<sub>2</sub>S<sub>x</sub> interface (cathodic polarization)

whereby Li/Sb<sub>2</sub>S<sub>3</sub> space charge magnitude ( $dn$ ) equals to  $1,64 \cdot 10^{-8} \text{ m}^{-3}$ .

Thus, the model of the Li – Sb<sub>2</sub>S<sub>x</sub> direct contact in the Li/Sb<sub>2</sub>S<sub>x</sub> system is suggested. It was found, that this model is typical for metal – semiconductor interface with Schottky's barrier lay and it well describes both the equilibrium state and the system's behaviour in the electric fields.

#### Litetature.

1. N. Arkhipova, A. Mikhailova – Elektrokhimiya – 1995 – V. 31, №1. – p.36.
2. P. Oreshkin – Physics of Semiconductors and Dielectrics. – Moscow: Vysshaya Shkola – 1977. – 448p. & ill.

## PERCOLATION ORIGIN OF ANOMALOUS CONDUCTIVITY

BEHAVIOR IN  $\text{BaCe}_{1-x}\text{Er}_x\text{O}_3$  NEAR  $x=0,3$ 

A.L. Samgin,

Institute of High-Temperature Electrochemistry,  
Russian Academy of Sciences, 620219, Ekaterinburg, Russia

The study of the dependence of the conductivity on dopant concentration is important to the development of the theory of protonic conduction. The analysis of this dependence up to the present has been based, for the most part, upon relatively low doping level. Recent experimental study of  $\text{BaCe}_{1-x}\text{Er}_x\text{O}_3$  ceramics at  $0 < x < 0,75$  [1] shows that, in wet air, the conductivity declines considerably at  $x > 0,15$  and undergoes a minimum near  $x=0,3$ , and then strongly increases.

Using percolation theory [2], and taking into account that i) within the region of the anomalous behavior, the growth of a second phase was observed and ii) the relationship between these perovskite-type phases is defined by concentration of Er [1], we may suppose that there the proton conduction is governed by the coexistence of low (with fraction  $1-x$ ) and high (with fraction  $x$ ) conducting phases. With increasing  $x$ , the Er ions block proton paths which cause proton hopping through the lattice. Near percolation threshold, which is about  $x_c=0,31$  for cubic lattice [2], the proton mobility approaches to zero. Inside infinite cluster proton transport occurs along a continuous path involving fractal channels, thus above  $x_c$  the proton conductivity is bound to increase with a power law dependence as  $(x-x_c)^t$ , where  $t$  is a critical exponent ( $t \approx 1,5$  [2]).

Similar percolation effect is found in  $\text{Sr}_3\text{Ca}_{1+x}\text{Nb}_{2-x}\text{O}_{9,5}$ -type oxides [3]. However, in ref. [3] one concludes that the properties of the complex materials are intimately related to their microstructural features in contrast to simple perovskites. Our study shows that doped  $\text{ABO}_3$  oxide seems to be also suitable for application of site percolation theory, but only at high  $x$  values. One would expect that the percolation clusters in perovskite-type protonic conductors may cause not only anomaly of electrical properties, but anomalous set of other properties (e.g., optical or mechanical properties) as well. To test the percolation model, several experiments with particular reference to comparison between mobility power laws with 2D (case of proton conducting thin films) and 3D critical exponents (case of crystals) may be of interest in the future.

[1] N.V.Sharova et al., *Neorganich. mater.* **33**, 1021 (1997).

[2] S.Kirkpatrick, *Rev. Mod. Phys.* **45**, 574 (1973).

[3] Y.Du, A.S.Nowick, *J. Am. Ceram. Soc.*, **78**, 3033 (1995).

MODELING OF PERSISTANCE IN SOLID STATE DIFFUSION  
AND ELECTRICAL RESPONSE

Donald R. Franceschetti and John W. Hanneken  
Departments of Physics and Chemistry  
The University of Memphis  
Memphis, Tennessee 38152 U. S. A.

Deviations of defect motion from classical random walk diffusion has been attributed to a number of causes including: (i) geometric or cooperative effects, (ii) the failure of a the migrating defects to thermalize after each jump, and (ii) the finite time needed for the charge distributions around a displaced defect to return to an equilibrium configuration [1-3]. While such nonclassical motion is inherently a many-body problem, it is naturally highly desirable to have a viable independent-particle description exists for use in interpreting experimental data. In this work three candidate independent particle models: a discrete time correlated random walk, a two-population model governed by coupled differential equations, and a fractional diffusion equation, are compared as to their prediction of behavior in the time and frequency domain and their potential usefulness in modeling electrical response.

In the discrete-time correlated random walk model, for which an exact distribution function has been obtained recently under a broad range of boundary conditions [4], the jumping particle "remembers" the direction of the previous jump and is biased to jump in the same or the opposite direction. In the two-population model the moving defects are divided into two groups based on the direction of their previous motion. The fractional diffusion model is based on the fractional diffusion equation

$$\frac{\partial^\alpha c}{\partial t^\alpha} = D \nabla^2 c$$

for which an exact solution (in one dimension) is known in terms of Fox functions, rather complicated in themselves but which can be expanded to very high accuracy as a sum of gaussians in the scaling parameter  $x^2/Dt^\alpha$  [5].

Behavior in the frequency domain can be obtained from the distribution function through the use of standard integral transform relations or, in the case of the two population model at least, directly from the dynamical equations using linear response theory [2]. Admittance functions for the three models will be displayed in both algebraic and graphical and their representation by networks of differential elements (transmission lines) will be examined, particularly as it can be generalized to the description of diffusion in non-planar geometries. The response to step function signals, effectively creating an asymmetry in the particle distribution function, will also be considered.

- [1] K. Funke, Solid State Ionics, **18/19**, 183 (1985).
- [2] K. Funke, Solid State Ionics, **28-30**, 100 (1988).
- [3] D. R. Franceschetti, Solid State Ionics, **40/41**, 196 (1990).
- [4] J. W. Hanneken and D. R. Franceschetti, J. Chem. Phys. **109**, 6533 (1998).
- [5] J. W. Hanneken, K. L. Harrington, D. M. Vaught and B. N. Achar (to be published).



## DEMIXING PROFILES IN OXIDES UPON THE APPLICATION OF AN ELECTRICAL FIELD

D.P. Korfiatis, S.F. Potamianou, E.D. Tsagarakis and K.A.Th. Thoma  
Physics Department, University of Patras  
Rio 26500, Patras, Greece  
E-mail address: phaethon@physics.upatras.gr

Kinetic demixing is observed in oxide materials, both upon the application of an external applied field and under oxygen partial pressure gradient. Time evolution of concentration profiles leading to steady state demixing is presented in the literature through experimental as well as theoretical studies [1,2].

To our knowledge, theoretical calculations referring to the application of external fields up to now, are based on current density equations of the mobile charged species of the materials. Current densities are dependent upon concentration gradients of the species, as well as applied external fields, taking into account diffusion constants for each of the mobile species.

In this work an one dimensional transient computer model is used assuming a sample of the oxide material under the application of an external field. The model is incorporating, besides current density and continuity equations for each of the mobile charged species, Poisson's equation as well, which relates field gradient to total charge at each point in the sample. Results are discussed in comparison to those found in the literature.

### References :

- [1] D. Monceau, M. Filal, M. Tebtoub, C. Petot, G. Petot-Ervas, Solid State Ionics 73 (1994) 221-225
- [2] T. Ishikawa, S.A. Akbar, W. Zhu and H. Sato, J. Am. Ceram. Soc. 71 (1988) 513-521

## CHARGE CARRIER INTERACTIONS IN IONIC CONDUCTORS: A CLASSICAL MD AND MC STUDY ON AgI

F. Zimmer, P. Ballone, J. Maier, M. Parrinello  
Max-Planck-Institut für Festkörperforschung  
Heisenbergstraße 1, 70569 Stuttgart, Germany

Recently Hainovsky and Maier[1] showed that for various Frenkel disordered materials the anomalous defect concentration at high temperature can be described by a cube root term in the chemical potential of the defects. The model does not only allow one to compute thermodynamic properties of the defective solid, its ionic conductivity and heat capacity, it also leads to a phenomenological understanding of the transition temperatures. In the present study, with the use of classical MD and MC simulations and the effective pair potentials of [2,3], we analyse this approach on the atomistic level for  $\beta$ -AgI [4]. It is shown that the cube-root approximation is indeed well fulfilled even in the case of  $\beta$ -AgI, in which two types of interstitial defects appear in the simulation. The simulation analysis comprises static properties such as defect energies including excess energies, defect concentrations as well as defect correlations and dynamical properties such as the diffusion constants.

### References

- [1] N. Hainovsky and J. Maier, Phys. Rev. B **51**, 15789 (1995).
- [2] M. Parrinello, A. Rahman, and P. Vashishta, Phys. Rev. Lett. **50**, 1073 (1982).
- [3] A. B. Walker, M. Dixon and M. J. Gillan, J. Phys. C: Solid State Phys. **15** (1982) 4061-4073.
- [4] F. Zimmer, P. Ballone, J. Maier, M. Parrinello, Ber. Bunsenges. Phys. Chem. **9**, 1333 (1997).

# HAVEN RATIO, CORRELATION FACTORS AND CONDUCTIVITY OF SOLID STATE IONICS

C. Uebing<sup>1</sup> and V.S. Vikhrenko<sup>2</sup>

<sup>1</sup>Max-Planck-Institut für Eisenforschung, Düsseldorf, Germany

<sup>2</sup>Belarussian State Technological University, Minsk, Belarus

The Haven ratio is given by the expression

$$f_H = D^* q / \mu k T \quad (1)$$

where  $D^*$  is the tracer diffusion coefficient,  $T$  is the temperature,  $k$  is the Boltzmann constant,  $q$  and  $\mu$  are the particle charge and mobility, respectively. The connection between the Haven ratio and the tracer correlation factor  $f_t$  is frequently discussed [1,2]. There are big discrepancies between both factors as is inferred from electrical conductivity and tracer diffusion experiments.

On the basis of modern theories of non-equilibrium processes such as Zwanzig - Mori projection operator techniques or the Zubarev non-equilibrium ensemble method it can be shown that the electrical conductivity and the kinetic diffusion coefficient  $D_K$  can be represented by the same particle velocity time correlation functions. Thus, the equality

$$D_K q = \mu k T \quad (2)$$

holds. On the other hand, the tracer and kinetic diffusion coefficients are represented by the mean square displacements of either a target particle or the center of mass of  $N$  particles at time  $t$  [3]

$$D^* = \lim_{t \rightarrow \infty} \frac{1}{td} \langle (\Delta \mathbf{r})^2 \rangle, \quad (3)$$

$$D_K = \lim_{\substack{t \rightarrow \infty \\ N \rightarrow \infty}} \frac{1}{Ntd} \left\langle \sum_{i=1}^N \Delta \mathbf{r}_i \cdot \sum_{j=1}^N \Delta \mathbf{r}_j \right\rangle, \quad (4)$$

In contrast to  $D^*$  the kinetic diffusion coefficient  $D_K$  contains so-called cross-correlation terms, i.e. products of displacements of different particles. Introducing the multiparticle correlation factor  $f_m$  as the ratio of the cross terms in Eq. (4) to the mean square displacement of a particle we rewrite this equation in the form

$$D_K = D^* (1 + f_m). \quad (5)$$

The tracer correlation factor can be introduced [4] as the ratio of the particle mean square displacement to the number of its jumps multiplied by the square of the lattice parameter. It is evident that in general there is no simple relation between these two correlation factors and Haven ratio cannot be identified with the tracer correlation factor. Only for non-interacting lattice gases Haven ratio is simply connected to the tracer correlation factor.

To clarify the situation in more general cases Monte Carlo simulations for two-dimensional gases on a square lattice with nearest neighbor interactions were carried out. It is shown that Haven ratio as defined by Eq. (1) significantly deviates from the tracer correlation factor. These deviations are especially large for repulsive interactions where the Haven ratio is much lower than the tracer correlation factor and the latter can be much lower its value for Langmuir gas of the same concentration.

[1] H. Sato, Solid State Ionics, 5, 183 (1981).

[2] S. Hoshino, Solid State Ionics, 48, 179 (1991).

[3] R. Gomer, Rep. Progr. Phys. 53, 917 (1990).

[4] C. Uebing, R. Gomer, J. Chem. Phys. 95, 7626, 7636, 7641, 7648 (1991).

## LATTICE-GAS MODEL FOR INTERCALATION COMPOUNDS

V.I. Kalikmanov, M.V. Koudriachova, and S.W. de Leeuw  
 Department of Applied Physics, Computational Physics Section,  
 University of Delft, Lorentzweg 1, 2628 CJ Delft, The Netherlands

Li-metal oxide systems draw attention due to their prospective use as electrode materials in rechargeable batteries [1]. Important characteristics of the batteries are determined by the distribution of intercalated ions over interstitial sites of the host lattice.

As a first step in describing the host-lattice - guest ions system we replace it by an effective one-component medium of equally charged guest ions forming a sublattice of interstitial sites. We assume a short range nearest-neighbor repulsive interaction between the intercalated ions. The presence of the host matrix, taken into account effectively, maintains electro-neutrality of the system.

The proposed lattice-gas model is equivalent to the nearest-neighbor antiferromagnetic Ising model in an external field. Using this analogy we describe the phase diagram of the intercalation compound within the framework of two approximations: the mean field theory and the Bethe approximation [2]. We found the second order phase transition which manifests itself in the divergence of the isothermal compressibility. A singularity indicates a possible fine structure of intercalated ions at corresponding concentrations. Fig. 1 shows the phase diagram for the square lattice (number of nearest neighbors  $q = 4$ ) in the chemical potential-temperature plane. It contains the regions of ordered and disordered states separated by the line of second order phase transitions. We have carried out Monte Carlo simulations which confirm the theoretical predictions.

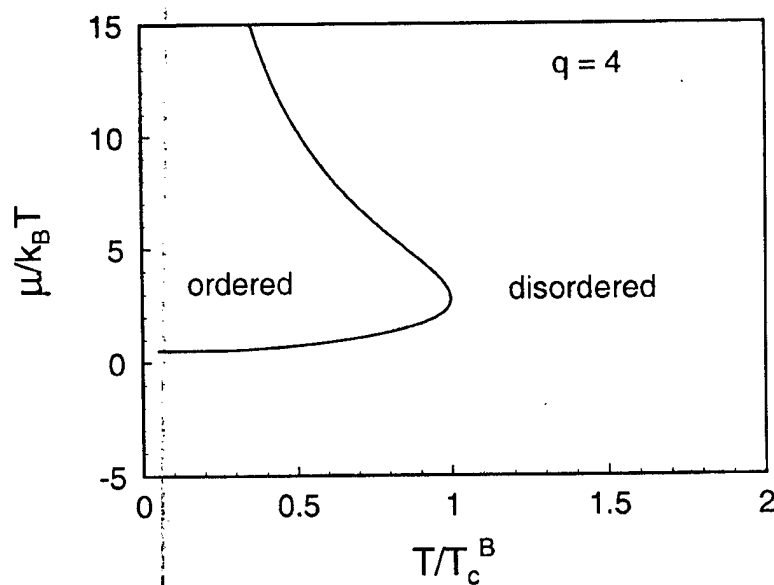


Figure 1: Lattice-gas phase diagram in the Bethe approximation.  $\mu$  is the chemical potential of the intercalated ion,  $T$  the absolute temperature,  $T_c^B$  the critical temperature.

One of the most important features of the batteries is a voltage-discharge curve describing the dependence of the voltage drop  $V$  in the battery on the relative amount  $x$  of the

intercalated material. Experimental studies (see e.g. [3]) provide evidence of a step-like behaviour of  $V(x)$  with possible nonanalytic features at certain ion concentrations. It is explained within the proposed model by the occurrence of the order-disorder transition.

Fig. 2 shows the voltage drop as a function of the intercalated ion fraction  $x$  predicted by the mean-field theory for different values of the mean-field parameter  $qK$ , where  $q$  is a number of nearest neighbors,  $K = qu/(4k_B T)$ ,  $u$  is a short-ranged repulsive interaction energy,  $k_B$  the Boltzmann constant, and  $T$  the absolute temperature. For  $qK < 1$  voltage is a smooth function of  $x$ . If  $qK$  exceeds unity a step-like behavior occurs. Moreover,  $V(x)$  is nonanalytical: two cusps on each curve correspond to the order-disorder transition. Our Monte Carlo simulations are in a good agreement with theoretical results.

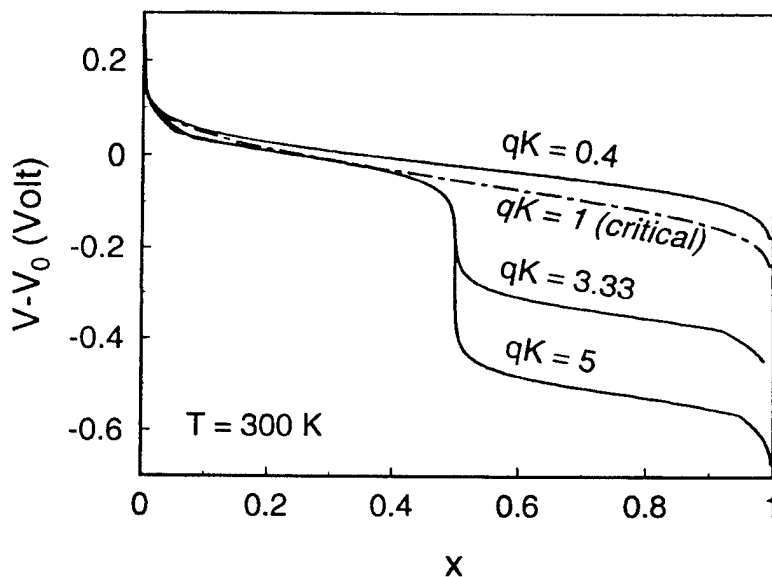


Figure 2: Voltage drop as a function of the intercalated ion fraction: mean-field calculations.

## References

- [1] A.D. Robertson, A.R. West, and A.G. Ritchie, *Solid State Ionics*, **104**, 1 (1997).
- [2] R.J. Baxter, *Exactly solved models in statistical mechanics* (Academic Press, London, 1982).
- [3] P. Rozier, J.M. Savariault, and J. Galy, *Solid State Ionics*, **98**, 133 (1997).

# Authors Index

## A

Aaberg, R.J. I-IN-03  
Aasland, Siv C-17  
Abdullin, A.R. F-02-P  
Abe, Takeshi A-IN-10  
Abeles, B. C-KE-02  
Abiko, Hironobu A-10, A-IN-04  
Abraham, Francis D-07, D-07-P  
Abrahams, Isaac D-08, D-13-P  
Abrantes, J.C.C. C-11-P, B-09  
Abu-Lebdeh, Yaser E-21  
Adachi, Gin-Ya F-KE-01, F-16, F-06-P, F-07-P, F-08-P, F-09-P  
Adachi, Hirohiko F-12  
Adams, Stefan N-03, M-02-P  
Adebahr, Josefina A-25, L-08, L-03  
Adler, Stuart C-IN-04  
Ado, Kazuaki A-17  
Adriansens, W. C-IN-09  
Agnihotry, S.A. L-13, L-04-P, G-02  
Agrafiotis, C. M-11-P  
Agrawal, Rakesh Ch. K-10, F-23-P  
Ahmad-Khanlou, Ariane B-17-P  
Ahn, H. C-12  
Aihara, Y. A-39  
Akai, T. K-01  
Akasaka, N. C-IN-01  
Albinsson, I. L-06  
Aldinger, F. C-05-P  
Aleksiejuk, A. K-11  
Aliiev, Ali E. F-33-P, F-28-P, D-09-P  
Alloin, Fannie L-04  
Almayrac, R. M-10-P  
Almukhametov, R.F. F-02-P  
Amatucci, G.G. A-14-P  
Ammundsen, Brett A-02  
Anderson, Harlan M-01  
Andersson, Anna M. A-38  
Andersson, Daniel L-02  
Ando, Masanori M-08-P, G-13  
Andreouli, M-12-P  
Constantina E-23, E-03-P  
Animitsa, Irina K-12  
Aniya, Masaru B-05  
Antony, M.P. C-10-P  
Arachi, Yoshinori F-04-P  
Arai, Masaji L-07  
Araki, Fusamori D-02, C-IN-08  
Arikawa, Hiroshi B-IN-05  
Arisaka, Shin-ichi J-08-P, J-04  
Arita, Yuji N-02-P  
Arkhipova, N. N-02-P  
Arkhipova, T. L-IN-03  
Armand, Michel L-03-P  
Arof, Abdul-Kariem L-04-P  
Arora, Narinder L-04-P  
Asahi, Yasushi D-06-P  
Asai, T. C-10-P  
Aso, Kazuhiro F-15  
Atake, Tooru D-03  
Atanasoski, L-IN-03  
Radoslav I-07-P  
Athanasίου, Costas I-10  
Atkinson, Alan F-10-P  
Atovmyan, L.O. M-02  
Attard, George S. D-06  
Auchterlonie, G.J. A-07  
Avvakumov, E.G. F-25-P  
Awano, Teruyoshi F-02  
Ayala, Alejandro Pedro B

## B

Bacewicz, R. K-11  
Badas, Thomas I-01

Baddour-Hadjean, Rita E-15-P  
Badwal, Sukhvinder D-12, B-20-P, B-21-P  
Baffier, N. A-22-P  
Baikov, Yurii M. E-15-P  
Bak, T. B-21-P  
Balazs, Bryan J-12  
Balbashov, A.M. F-32-P  
Ballone, P. N-06-P  
Balomenou, Stella I-05-P  
Bandaranayake, Kumara L-12  
Baranov, A.I. E-IN-02  
Barboux, P. G-14  
Bardal, Asgeir C-11  
Barth, D. G-17  
Bartlett, Philip M-02  
Bates, John B. A-KE-03  
Beatrice, Pamela I-12  
Bebelis, Symeon I. I-02-P, I-06-P  
Becker, Klaus C-IN-07  
Dieter F-20-P  
Beeken, Elizabeth M. F-20-P  
Beeken, Robert B. A-29  
Behm, Marten L-09-P  
Bel, G.-J. L-IN-03  
Belanger, Andre K-IN-01  
Belin, Renaud A-29  
Belliard, Frederique I-IN-05, I-IN-08, I-01-P  
Belyaev, Vladimir D. G-12  
Bendahan, M. C-02  
Berckemeyer, F. M-10-P  
Bernier, P. M-05  
Besenhard, Jurgen O. F-01, M-09-P  
Best, Adam B-IN-03  
Bieberle, Anja J-09-P, F-10  
Bikkulova, N.N. E-12  
Bismayer, U. A-03  
Bjork, Helen L-01-P  
Bloes, A.C. B-03-P, B-02-P  
Boersma, Reinder J. D-13-P  
Bogusz, W. A-11-P, A-12-P  
Bohnke, Odile G-14  
Boilot, J.P. D-08-P  
Boivin, Jean-Claude K-01-P  
Bolotov, A. G-IN-08  
Bonanos, Nicholas L-03, K-01, K-03-P, K-04, L-02, K-04-P  
Borjesson, Lars D-10, B-16, J-01  
Boukamp, Bernard M-10-P  
Bousquet, C. J-01, C-19, C-09  
Bouwmeester, Henry B-18-P  
Boysen, Dane B-10-P  
Bradley, J. A-30  
Branci, C. G-18  
Bratov, A. M-IN-01  
Brazis, Paul C-11  
Bredesen, Rune F-11, C-02-P  
Bredikhin, Sergei F-16-P  
Breiter, M.W. M-04-P  
Brezhneva, L.I. B-05-P  
Brichzin, V. E-18  
Brodin, A. D-05  
Bronin, Dimitrij I. G-21  
Brosha, Eric A-IN-09  
Brousse, Thierry A-KE-01  
Bruce, Peter G. L-04  
Brylev, Oleg C-IN-09  
Buekenhoudt, Anita F-05-P, A-18-P  
Buhmester, Thorsten I-08-P  
Bukun, H. E-25  
Bukun, Nadezda G. F-11-P, F-12-P  
Burns, Gary R. A-02

Burnside, Shelly A-04  
Bush, A.J. D-13-P  
Buzare, J.Y. A-11-P, A-12-P  
Bychkov, Eugene K-02, K-08-P, K-01-P  
E-06-P  
Bzwucha, W. C  
Cahen, David G-IN-03  
Camacho-Lopez, M. A-10-P  
Capiglia, Claudio L-05  
Careem, Mohamed G-03  
A. J-03-P  
Catano, R. F-27-P  
Catti, Michele A-KE-02  
Ceder, Gerbrand A-42, F-32-P  
Chaban, N.G. I-10  
Chadwick, D. K-KE-01  
Chan, Jerry C.C. G-20  
Chandra, Amita E-15  
Chandra, Suresh A-03-P, A-15  
Chang, Soon Ho B-01  
Charpentier, Pascale C-10, C-21  
Chen, Chu-sheng A-32, A-33, C-05  
Chen, Ligan B-11-P, B-12-P  
Chen, Ming G-05-P  
Chen, Ning F-01-P, F-14  
Chen, Xue-an G-02-P  
Chernova, M.A. E-13, B-18-P  
Chisholm, Calum R.I. G-03-P, F-30-P  
Chithra Devi, R. A-10-P  
Chitra, S. C-04  
Choi, Gyeong Man L-IN-03  
Choquette, Y. G-10  
Chou, K-C. K-06-P, K-07, A-18  
Chowdari, B.V.R. F-33-P  
Choy, Jin-Ho K-IN-02  
Chryssikos, G.D. G-06  
Chu, Wing Fong A-14, A-06-P, A-07-P  
Chung, Hoon-Taek A-26, A-28, B-13  
Chung, S.H. F-06  
Chung, Tai-Joo D-04  
Ciacchi, F.T. D-12  
Cicka, R. D-IN-01  
Closset, Alexandre C-IN-05  
Colomban, Philippe E-15-P  
Comninellis, I-KE-02, I-08  
Christos A-29  
Connor, Paul A. C-IN-09  
Cooymans, J. E-04-P  
Corcoran, Derek J.D. A-27, A-KE-04  
Croce, F. C-13  
Croft, M. A-16-P  
Croguennec, L. A-IN-09  
Crosnier, O. I-IN-11  
Cunningham, Robert H. K-04  
Cutroni, Maria D  
Dabkowska, H. F-07-P  
Dabkowski, A. F-07-P  
Dalmazio, L. M-11-P  
Danilkin, S.A. J-09-P  
Davalos, J. A-21  
Davidson, A.J. G-16  
Dayal, P. Babu F-18-P  
De Jonghe, L.C. L-08-P  
de Leeuw, Simon N-08-P, L-09-P  
W. L-11  
De Souza, P.P. F-05  
Decastro, Sandra C. L-13  
Deepa A-IN-03, A-16-P  
Delmas, Claude B-19, C-06-P  
Demin, Anatoly K. J-01, C-09  
den Otter, M.W. B-01  
Denos, Y.

Dessemond, L. M-06  
Devautour, S. N-01  
Devyatkina, E.T. A-07  
Dieterich, Wolfgang L-IN-01  
Diethelm, Stefan C-IN-05  
Dildin, Denis E-03-P, E-23  
Dimitrova, O.V. F-10-P  
Diosa, Jesus Evelio E-14, J-03-P  
Dissanayake, L-12  
Malavi

Djurado, Elisabeth M-06  
Dobrovolsky, Yury G-06-P, E-27  
N-01-P, E-26

Dobson, Jeremy B-09-P  
Doeff, Marca M. L-08-P  
Doeff, Marca M. L-08-P  
Doile, Michael A-40  
Domashnev, D.I. N-01-P, E-27  
Dominguez, C. G-18  
Donoso, Jose Pedro L-11, L-01-P, E-16  
Dotelli, Giovanni N-IN-01  
Douvartzides, S. I-04-P  
Drennan, John D-06  
Drevet, C. I-07  
Drugov, Yu. K-01-P  
Du Pasquier, A. A-14-P  
Duclet, Michel L-04  
Dudney, N.J. A-KE-03  
Duerr, O. L-IN-01  
Dunyushkina, Lilya C-06-P  
A.

Dusastre, V. B-21  
Dvinskikh, Sergei V. J-KE-02, J-IN-03  
Dygas, J.R. D-13-P

## E

Eastman, Craig D. G-22  
Eckert, Hellmut K-KE-01  
Edman, Ludvig L-08-P  
Edmondson, C.A. B-13, A-28  
Edstrom, Kristina A-38  
Efanova, W. I-08-P  
Eguchi, Koichi C-IN-01  
Elangovan, S. B-IN-01  
Eliasson, H. L-06  
Elliott, Joanne M-02  
Emery, J. A-11-P, A-12-P  
Endo, A. B-IN-06  
Ericson, Hanna E-18, L-08, L-03  
Esaka, Takao D-KE-01, D-06-P  
Etsell, Thomas H. G-19, J-15, G-22, B-20

Evans, C.D. A-KE-03  
Ezin, A.N. C-03-P, I-03

## F

Faflek, Gunter D-09, J-11  
Fagg, Duncan J-KE-03  
Fang, L. K-06-P  
Fantini, Marcia F-05, A-21  
Farcy, J. A-22-P  
Fattakhova, Dina A-04  
Fedorov, P.P. D-IN-01, D-05-P  
Fee, C.J. B-03-P  
Feighery, Alan J-KE-03  
Ferreira, A.A.L. C-11-P, B-09  
Ferreira, F.F. F-05  
Ferry, A. F-17-P  
Ferry, Anders L-08-P  
Figueiredo, Filipe B-23  
Filipenko, O.S. F-10-P  
Finnerty, Caine M. I-IN-11  
Fleig, Jurgen J-03, F-21-P, B-05-P

Fleischer, G. L-10  
Florentino, A. E-16  
Florian, P. A-12-P  
Florjanczyk, E-06-P, A-15-P  
Zbigniew  
Flot, David M. B-06-P  
Fontanella, John J. A-28, B-13  
Forsyth, Maria F-15-P, F-01, M-09-P, B-12

Fouletier, Jacques B-13-P, I-07  
Fournes, L. A-IN-03  
Fourquet, J.L. A-11-P, A-12-P  
Frade, Jorge C-11-P, J-07, B-23, B-09, B-01, A-IN-09  
Ribeiro N-04-P  
Fragnaud, P. L-11  
Franceschetti, Donald R.  
Franco, Roberto W.A.

Fransson, Linda A-38  
Frantzis, Aristotelis I-06-P  
Fratoddi, I. G-07-P  
Fray, Derek J. G-16, G-11  
Frech, Roger L-IN-02  
Freire, P.T.C. F-02  
Frenzel, A. I-05-P  
Friedrich, J. E-IN-01  
Ftikos, Christos B-15-P, B-16-P  
Fujara, F. J-IN-03  
Fujii, S. B-26  
Fujisawa, Masami E-22  
Fujita, Hirofumi A-19-P  
Fukunaga, H. B-IN-06  
Funke, Klaus N-IN-03  
Furlani, A. G-07-P  
Furlani, Maurizio L-06, F-17-P  
Fyfe, Colin A. J-09

## G

Gabitov, E.V. F-02-P  
Ganeshkumar, A.C. J-11-P, J-12-P  
Garbacz, Jerzy K-11  
E.  
Garcia, A. J-04-P  
Gareeva, M.J. F-10, J-09-P  
Garzon, Fernando G-21  
Gauckler, Ludwig J. C-KE-01, B-14, B-IN-03

Gauthier, Michel L-IN-03  
Gavelin, P. A-25  
Gehain, E. B-01  
Gejke, Cecilia K-04-P, K-03-P, K-04

Georgiopoulos, E. M-12-P  
Georgoussis, G. E-20  
Gesland, J-Y. F-02  
Gharbage, B. J-07  
Ghigna, Paolo F-24-P  
Ghobarkar, H. F-17  
Giannikos, I-05-P

Alexandros  
Gimadeev, R.R. F-10  
Giourelis, D.K. F-35-P  
Giuntini, J.C. N-01  
Glerup, Marianne C-IN-02  
Glumov, Oleg G-08-P, D-KE-02, D-02-P

Gmucova, K. G-05  
Goepel, Wolfgang G-KE-01, G-IN-01, I-05  
I-08-P  
A-26  
B-16

Goffman, B. A-10-P  
Golodnitsky, Diana A-21, F-05  
Gonzalez Cuenca, A-01-P, A-02-P  
Mercedes PL-02  
Gopukumar, S. A-14-P  
Gorenstein, Annette C-14-P  
Gorova, M. A-21-P  
Gottesfeld, Maryline Le  
Shimshon  
Gozdz, A.S. A-04  
Grammatikakis, J. A-41  
Granvalet-Mancini, A-26, A-28, B-13  
Maryline Le  
Gratzel, Michael C-13  
Gray, Melanie A-22-P  
Greenbaum, Steve E-19, E-18  
G. J-09

Greenblatt, Martha C-13  
Gregoire, G. A-22-P  
Grillone, A.M. E-19, E-18  
Grondey, Hiltrud J-09

Gu, Wen-Bin G-07  
Guedes, I. F-02  
Guillodo, M. B-15  
Guindet, J. B-15, B-13-P  
Guizard, C. M-11-P  
Gulbis, Fyodor Ya. B-19  
Gunaratne, G-03  
L.M.W.K.  
Gunsser, Walter F-08  
Gupta, Ravindra K. F-23-P, K-10  
Gustafsson, A-03  
Torbjorn  
Guth, Ulrich G-IN-01, I-13, F-17, D-IN-02, C-08

Guyomard, A-IN-06, A-08-P, Dominique A-09-P

## H

Haass, Frank F-05-P  
Habermeier, H.-U. B-05-P  
Habermeier, H.-U. B-05-P  
Haile, Sossina M. B-18-P, B-02, E-13  
Hairetdinov, E.F. J-01-P, M-04-P  
Haller, Gary I-IN-01  
Hamakawa, Satoshi I-IN-10, I-IN-09  
Han, Kyoo-Seung A-IN-07, A-19-P, A-20-P

A-IN-02  
Han, Wonchull A-IN-02  
Hanneken, John W. N-04-P  
Harada, Yasuhiro F-03  
Hartley, A. D-14-P, J-05-P  
Hartmanova, Maria G-05, D-10-P  
Hartvigsen, J. B-IN-01  
Hata, Takayuki F-IN-02  
Hattori, Takeshi F-15, E-06, PL-04  
Hayakawa, Takashi I-IN-10, I-IN-09  
Hayashi, Akitoshi K-KE-02  
He, Hongpeng C-05  
Heitjans, Paul M-KE-02  
Henault, M. I-07  
Henn, Francois N-01, M-10-P  
Hervieu, M. A-13  
Hibino, Mitsuhiro A-IN-02, A-10, A-IN-04

C-04-P  
Hiei, Yoshiko E-22, C-03, E-07-P, E-05  
Higuchi, Tohru J-KE-02

F-07-P  
Hindennach, Milo A-05, A-17  
Hiraiwa, Masamichi F-13  
Hirano, Atsushi M-05  
Hiraoka, H. C-08, C-IN-02  
Hofer, Ferdinand C-01-P  
Holtappels, Peter B-14  
Holzinger, Michael B-01-P  
Honegger, K. J-02, B-24, B-04  
Hong, Jeong-Oh J-12  
Horita, Teruhisa L-IN-03  
Hormes, J. G-10  
Hovington, P. F-15-P  
Hu, Xiaojun C-20  
Huang, Junhua A-32, A-33, C-05  
Huang, P. N-IN-02  
Huang, Xuejie D-07-P  
Huggins, Robert  
Huve, Marielle

Ichikawa, Takayuki A-31  
Iguchi, Fumitada E-07  
Iguchi, Yoshiaki C-03, E-07-P, E-05

A-34  
Ikuta, H. F-KE-01, F-16, F-06-P, F-07-P, F-08-P, F-09-P  
Imanaka, Nobuhito A-31, C-10-P  
Imanishi, Nobuyuki I-IN-02  
Imbihi, Ronald B-26, A-IN-10  
Inaba, Minoru I-09  
Inoue, Yasunobu F-IN-02  
Irie, Michihiko A-IN-10  
Iriyama, Yasutoshi

Irvine, John T.S. J-KE-03, A-29, B-06-P, B-09-P, B-10-P, E-04-P  
 Isaji, Hidefumi G-15  
 Ise, M. E-14-P  
 Ishida, Tadashi A-08  
 Ishigame, Mareo PL-04, E-22, E-06, F-15  
 Ishihara, Tatsumi C-IN-08, D-02  
 Ishii, Motohiko F-01-P, F-14, F-22-P  
 Ishii, Tadao M-07  
 Ishikawa, Hiroshi L-05  
 Ishikawa, Masashi L-07  
 Ishimoto, Yoko D-01  
 Ivanov-Schitz, A.K. A-42, F-32-P  
 Iwahara, Hiroyasu E-KE-01, E-02

Jacobson, Allan J. C-KE-02  
 Jacobsson, P. A-25, L-08, E-18  
 Jatrovski, L.E. J-09-P  
 Jagafarova, Z.A. F-10, J-09-P  
 Jak, Michiel J.G. A-24  
 Jakobs, Stefan D-IN-02  
 Jaksic, Milan I-IN-07  
 Jamnik, Janko C-08-P  
 Jannasch, P. A-25  
 Janner, Anna-Maria F-36-P  
 Janssen, Michael K-KE-01  
 Jantscher, C-01-P  
 Wolfgang  
 Jayaweera, Palitha I-02  
 Jiang, J. G-IN-06  
 Jiang, M. C-10  
 Jiang, S.P. B-20-P, B-21-P  
 Jiang, S.P. B-IN-04  
 Jiang, Yi A-IN-05  
 Jin, Weihua K-09  
 Johnson, Rhonda B-12  
 Jordan, Larry R. J-14  
 Jorgensen, J.D. B-KE-04  
 Jorgensen, Mette  
 Juhl  
 Jouanneau, S. A-IN-06  
 Julbe, A. M-11-P  
 Julien, Christian J-IN-01, A-12, A-10-P  
 Jung, W. B-16  
 Jurado, J.R. B-IN-08, C-11-P, B-14-P  
 Jurado, Jesus J-04-P  
 Fabian

Kageyama, Hiroyuki A-17, A-08  
 Kaimai, Atsushi B-10, B-11, A-16, G-IN-07  
 Kaiser, Andreas B-10-P  
 Kalhammer, Fritz B-KE-02  
 Kalikmanov, Vitaly I. N-08-P  
 Kalish, R. C-01  
 Kalogirou, Orestis F-08, F-13-P  
 Kalyani, P. A-10-P  
 Kamitsos, Efstratios K-IN-02  
 Kanashiro, Tatsuo A-23  
 Kanatzidis, Mercouri M-IN-01  
 G.

Kaneko, Hiroyuki G-15  
 Kang, Seong-Gu A-15, A-03-P  
 Kannewurf, Carl M-IN-01  
 Kanno, Ryoji F-IN-02, A-17, A-08, A-05, B-22  
 Karagiannakis, G. I-07-P  
 Karawacki, Ernest F-IN-01  
 Karelin, A. E-26  
 Karus, M. F-08  
 Katanosaka, A. A-39  
 Kato, Masao L-06-P  
 Kato, Tohru J-02  
 Kavan, Ladislav A-04  
 Kawada, Tatsuya C-15, E-10, B-10, B-11, A-16, G-IN-07, C-06

Kawahara, Mitsuyasu L-02-P  
 Kawamoto, Yoji F-IN-02, A-05, B-22  
 Kawamura, Junichi K-08, K-05  
 Kawamura, Kenichi A-16, E-10, B-10, B-11, G-IN-07, C-06  
 Kawasaki, Syuji A-05  
 Keklikoglou, P. F-13-P  
 Keklikoglou, P. F-13-P  
 Kelder, Erik M. A-24  
 Kennou, Stella I-06  
 Keppeler, F.M. C-05-P  
 Kerr, John L-08-P  
 Khan, M. Sakib B-07-P  
 Khandkar, Ashok F-IN-01  
 Kholmanov, B-28-P, D-09-P  
 Iskandar N. G-24  
 Kida, Tetsuya A-11, A-09  
 Kikuchi, Masahiro J-KE-01, J-06, J-06-P, B-21, C-16, C-13-P, C-12  
 Kilner, John A. D-04  
 Kim, Doh-Yeon A-06-P, A-07-P  
 Kim, Ho Gi A-06-P, A-07-P  
 Kim, Jin Gyun A-06-P, A-07-P  
 Kim, Moon Kyu C-KE-02  
 Kim, S. I-IN-01  
 Kim, Soonho F-33-P  
 Kim, Young-Il D-06  
 Kimpton, J. F-19-P  
 Kini, N.S. D-07-P  
 Kinowski  
 Christophe  
 Kireev, V.V. F-32-P  
 Kitamura, N. E-06  
 Kleinlogel, B-14, C-KE-01  
 Christoph  
 Klinger, M. C-02-P  
 Klingler, M. G-06  
 Kobayashi, Hironori A-08, A-13-P, A-17  
 Kobayashi, K. E-17  
 Kobayashi, Kiyoshi C-03, E-22, E-07-P  
 Kobayashi, M-08-P, G-13  
 Kobayashi, Tetsuhiko F-KE-01  
 Kobayashi, Yasuyuki B-26  
 Kobune, M. F-08-P  
 Koehler, Joachim E-26  
 Kolesnikova, A. A-35  
 Komaba, Shinichi I-04  
 Konsolakis, Michalis J-02-P  
 Kooops, Ulrich N-05-P  
 Korfiatis, Demetrios P. M-01  
 Kosacki, Hab. Igor A-07  
 Kosova, Nina V. B-15-P, B-16-P  
 Kostoglou, G.Ch. D-02-P  
 Kot, S.A. N-08-P  
 Koudriachova, M.V. F-12  
 Kowada, Yoshiyuki B-03  
 Koyama, Toshiyuki A-35  
 Kozawa, Kazufumi E-KE-03, E-04, E-14-P  
 Kreuer, K.-D. I-02  
 Krishnan, Gopala D-05-P  
 Krivandina, E.A. D-09-P  
 Krivorotov, A.E. F-28-P  
 Krivorotov, V.F. D-13-P, D-08  
 Krok, Franciszek A-04  
 Krtil, Petr A-09, A-11  
 Kubo, Momoji A-06  
 Kucza, W. A-IN-04, A-IN-02, A-10  
 Kudo, Tetsuichi G-IN-02  
 Kulkarni, Ajit A-35  
 Kumagai, Naoaki A-35  
 Kumagai, Nobuko

Kumar, P. Senthil F-18-P, F-19-P  
 Kumar, R. Vasant G-01  
 Kumar, Ranveer K-10  
 Kundracik, F. D-10-P  
 Kuratomi, A-39  
 Kurek, Piotr J-11, D-09  
 Kurioka, Yutaka A-08  
 Kurono, Hirokazu E-11-P  
 Kurumchin, E.Kh. C-03-P  
 Kuwano, Jun F-03  
 Kuwata, Naoaki K-05  
 Kuzin, Boris L. D-05  
 Kveder, V. C-02-P  
 Kyritsis, A. L-01, E-20, J-10-P

Labas, V. D-IN-01  
 Labrincha Batista, B-09, G-09-P  
 Joao Antonio  
 Lakshmi, N. E-15  
 Lambert, Richard I-KE-01, I-04  
 Lane, Jonathan A. J-06, J-06-P  
 Lauque, P. G-12  
 Laurent, A. G-14  
 Lavrova, G.V. M-06-P, M-05-P  
 Le Gal La Salle, A. A-08-P, A-09-P, A-IN-06  
 Leach, Colin J-07-P  
 Lee, Chang Ho C-04  
 Lee, G.Y.H. K-07  
 Lee, Gyejoong A-03-P  
 Lee, Jong-Sook D-04, M-02-P  
 Lee, Y.K. G-IN-06  
 Leftheriotis, G. G-01-P, G-04  
 Legagneur, A-09-P, A-08-P  
 Vanessa  
 Lemal, M. A-10-P  
 Leonhardt, M. C-08-P  
 Leonova, Lyudmila E-27, G-06-P, E-26, F-10-P  
 S.  
 Levchenko, A. G-06-P  
 Leysen, R. C-IN-09  
 Li, Fushen G-10  
 Li, Hong A-33, A-32  
 Li, Jinze A-32  
 Li, Lifan G-10  
 Li, Wenzhao B-IN-04  
 Liaw, Bor Yann G-07  
 Liddicott, K.M. B-18  
 Liebenow, Cornelius L-07-P  
 Lin, Qin G-05-P, A-IN-05  
 Linderth, S. B-15  
 Lintz, Haus I-IN-06  
 Guenther  
 Litsardakis, George F-35-P  
 Liu, Renmin A-IN-05  
 Liu, W. C-21, C-10  
 Logothetis, E.M. G-IN-04  
 Lomonova, E.E. D-10-P  
 Love, J. B-20-P, B-21-P  
 Lu, Xionggang G-10  
 Lu, Zhi-Yi B-11-P, B-12-P  
 Lu, Zigu B-IN-04  
 Lubomirsky, Igor G-IN-03  
 Lunden, Arnold F-IN-01  
 Luyten, Jan C-IN-09

MacFarlane, F-15-P, F-01, M-09-P  
 Douglas R. F-09  
 Machida, Nobuya K-11  
 Machowski, P. C-IN-07  
 Mack, D. A-IN-08, M-04, A-27, F-24-P, G-07-P  
 Magistris, Aldo L-11, L-01-P, E-16  
 Magon, C.J. C-KE-03, E-04, M-02-P, J-03, F-21-P, B-05-P, C-07-P, C-08-P, N-06-P, C-01, G-20  
 Maier, Joachim





**Q**  
 Qiu, Suntai D-03-P  
 Quartarone, Eliana G-07-P, M-04, A-27, A-IN-08

**R**  
 Ramanarayanan, T.A. D-11  
 Rambabu, Bobba K-09, J-12, K-09-P, K-05-P  
 Ramesh, S. L-03-P  
 Ramirez-Cabrera, Elvia I-10  
 Ran, S. C-10  
 Randle, T.H. D-06  
 Randrianantoandro, N. A-11-P  
 Rao, P. Kanta G-04-P  
 Rao, V. J. G-04-P  
 Raptis, Costas I-01  
 Ratai, Eva K-KE-01  
 Raz, Shaul C-01  
 Recio, P. B-14-P  
 Reddy, C.V. Gopal G-04-P  
 Red'kin, B. C-02-P  
 Reiche, Annette L-10  
 Reinhardt, Goetz G-IN-01, I-02-P, I-05  
 Rekas, Mieczyslaw B-20-P, B-21-P  
 Reller, Armin F-08  
 Rhodes, C. L-IN-02  
 Ribes, Michel K-IN-01, A-30, G-18  
 Richet, N. J-07-P  
 Richter, Shachar G-IN-03  
 Riekert, Lothar G-IN-05  
 Riess, Ilan L-KE-01, D-04-P, B-12, J-05  
 Rikukawa, Masahiro L-02-P, L-06-P  
 Rim, H. A-15  
 Ringuede, A. B-13-P  
 Rittig, F. L-10  
 Rocci, Melissa M-IN-01  
 Rodewald, S. J-03  
 Rodionov, V.V. E-25  
 Rodrigues, C.M. G-09-P  
 Rodriguez-Carvajal, Juan A-13, A-20  
 Roesch, Martin I-05  
 Rogalska, Ewa A-15-P  
 Rogez, J. J-13  
 Rogowska, M. L-09, L-05-P  
 Rolling, Bernhard K-06  
 Rom, I. C-01-P  
 Romer, E.W.J. C-19  
 Rosenstock, Zvi J-05  
 Roubani- Kalantzopoulou, F. I-08  
 Rougier, Aline A-12, A-IN-03  
 Rousse, Gwenaelle A-13  
 Roux, C. M-06  
 Roziere, Jacques A-02  
 Runge, Henrico C-18  
 Rutman, Jeremy D-04-P  
 Ryu, Kwang Hyun B-02  
 Ryu, KwangSun A-03-P, A-15

**S**  
 Saeki, M.J. E-16  
 Sahibzada, Mortaza J-05-P, D-14-P, G-17  
 Saiful Islam, M. A-02, B-07-P  
 Saito, H. I-09  
 Saito, Mai A-19  
 Saito, Morihito A-36  
 Saito, Yasukazu F-03  
 Saito, Yuria L-05  
 Sakaabe, Hikari A-17  
 Sakai, Hiroshi F-09  
 Sakai, Natsuko B-24, B-04, J-02, C-07

Sakamaki, Kenji F-22-P  
 Sakuma, Takashi F-04-P  
 Samantha, W.A. L-06  
 Samaras, D. F-35-P  
 Sambasiva Rao, P. K-09-P  
 Samgin, Alexander N-03-P, E-01-P  
 L.  
 Sammes, Nigel B-02-P, D-12-P, C-04-P, B-03-P, C-05-P  
 L-04  
 Sanchez, Jean- Yves B-14-P  
 Sanchez, L. A-21  
 Sanchez, M.A.E. L-10  
 Sandner, B. L-10  
 Sandner, R. I-02  
 Sanjurjo, Angel L-02-P, L-06-P  
 Sanui, Kohel A-IN-06  
 Sarciaux, S. A-30  
 Sarradin, J. A-20-P  
 Sasagawa, Itsuro F-02  
 Sasaki, J.M. C-07-P, B-05-P  
 Sasaki, Kazunari E-06, PL-04, E-22  
 Sata, Noriko I-IN-09  
 Sato, K. I-09  
 Sato, K. A-19, D-01  
 Sato, Mineo G-13  
 Sato, Yoshiyuki K-05-P, K-09-P, K-09  
 Satyanarayana, N. F-14-P  
 Savi, G. E-17  
 Sawada, F. F-17, J-13  
 Schaef, Oliver N-01  
 Schaefer, H. C-02-P  
 Scharner, Sebastian M-03  
 Schimanke, Guido M-IN-01  
 Schindler, J. A-01, A-IN-09, B-01  
 Schleich, Donald M. L-01-P  
 Schneider, J. E-IN-01  
 Schober, Tilman PL-03, G-23, A-24  
 Schoonman, Joop D-10-P  
 Schulz, H. B-19-P  
 Schulz, Olaf A-KE-04, E-18, A-27, L-03, E-19, F-14-P  
 Scrosati, Bruno G-12  
 Seguin, J.-L. E-04  
 Seifert, G. L-13, L-04-P, G-02  
 Sekhon, Satpal A-36  
 Singh J-08, B-08, B-05  
 Sekine, Kyoichi F-30-P, G-03-P, F-29-P  
 Sellar, Jeff R. J-09-P  
 Selvasekarapandian, S. C-IN-09  
 Semenov, V.A. D-03-P  
 Servaes, F. E-03-P  
 Shao, Changgui C-13-P  
 Sharafutdinov, Albert F-11-P, F-12-P  
 Shaw, Cynthia L-01, E-20  
 Shekhtman, Georgiy Sh. C-09-P  
 Shevchenko, V.V. F-14  
 Shevchuk, V.N. F-09  
 Shibata, K. A-17  
 Shigematsu, Toshihiko A-08  
 Shigemura, Hikari L-01, E-20  
 Shikano, Masahiro G-09, G-24  
 Shilov, V.V. E-22, C-03, E-07-P, E-05  
 Shimanoe, Kengo I-IN-09  
 Shin, Shik G-02-P, I-03-P  
 Shishido, T. K-07-P  
 Shpuck, I.E. K-08  
 Shreekrishna- Kumar, K. C-13  
 Shudo, Eichi J-10-P  
 Shuk, Pavel M-10-P  
 Siakantari, Maria  
 Simon, B.

Simoneau, M. L-IN-03  
 Simonova, L.G. M-05-P  
 Singhal, Subhash C. B-KE-01  
 Sinha, M.M. N-02  
 Sinitsyn, Vitaly V. E-IN-02  
 Sitte, Werner C-IN-03, C-01-P  
 Skaarup, Steen G-03  
 Skarmoutsos, D. B-17  
 Skinner, Stephen C-16, C-13-P  
 Slater, P.R. B-10-P  
 Smirnov, N.B. F-11-P  
 Smirnova, O.A. G-02-P  
 Smotkin, Eugene I-IN-04  
 Sobolev, B.P. D-IN-01  
 Sobyenin, Vladimir I-IN-08, I-IN-05, I-01-P  
 Sokolov, I.A. K-02-P  
 Soltis, R.E. G-IN-04  
 Somov, Serguei G-IN-01, I-13, I-03  
 Sone, H. E-06  
 Song, Chang-rock C-IN-06  
 Song, Seung-Wan A-19-P, A-20-P  
 Sorell, C.C. B-21-P  
 Souma, I. A-39  
 Soundan, P. A-22-P  
 Souquet, Jean L-04  
 Louis  
 Souza Cruz, Tersio F-05  
 G.  
 Spangenberg, F-21-P, G-20  
 Annette  
 Stallworth, Philip E. A-28, B-13  
 Stanef, Geoff B-02  
 Starostin, M.Yu. D-IN-01  
 Steele, Brian C.H. B-18  
 Stelzer, N. C-01  
 Stergiou, A.C. F-35-P, F-13-P  
 Stoukides, Michael I-07-P  
 Stournaras, C.J. M-11-P  
 Stoyanova, A-02-P  
 Radostina  
 Stramare, Sonia F-27-P  
 Suard, Emmanuelle D-07-P, A-IN-03  
 Subba Rao, G.V. A-18, K-07  
 Suchanek, Wojciech A-IN-07  
 Sugano, Koji G-15  
 Sukesini, A. Mary A-08, A-13-P  
 Suleiman, Bashir M. F-IN-01  
 Sun, Jiazeng F-15-P  
 Sunandana, C.S. F-18-P, F-19-P  
 Suthanthiraraj, J-11-P, J-12-P  
 S.Austin  
 Suzuki, Atsushi J-IN-02  
 Suzuki, Ken A-11, A-09  
 Suzuki, Kunio I-IN-10  
 Svanberg, Christer L-03  
 Swenson, Jan K-03-P, K-04, K-01, L-02  
 Swierczek, K. A-06

**T**  
 Tabacniks, M.H. F-05  
 Tabuchi, Mitsuharu A-17, A-08, A-13-P  
 Tagawa, Hiroaki G-IN-07  
 Taillades, Gilles K-IN-01  
 Taimatsu, Hitoshi G-15  
 Taji, T. B-26  
 Takahashi, F-04-P  
 Haruyuki  
 Takai, Shigeomi D-06-P  
 Takami, Seiichi A-11, A-09  
 Takamura, Tsutomu A-36  
 Takano, Mikio A-05  
 Takeda, Takashi B-22  
 Takeda, Yasuo A-31, C-10-P, B-22  
 Takehira, Katsuomi I-IN-09, I-IN-10  
 Takeuchi, K. E-KE-01  
 Takita, Yusaku C-IN-08, D-02  
 Talaie, Afshad G-IN-06

Tambelli, C.E.  
Tamura, Shinji

Tan, K.L.  
Tang, Eric Z.  
Tangen, I.L.  
Tansho, Masataka  
Tao, Shanwen  
Tarascon, Jean-Marie  
Tatsumisago, Masahiro  
Teeters, Dale  
Terui, Shigeki  
Thaker, S.  
Thery, Odile  
Thoma, Kallirroe-Adriane Th.  
Thomas, Josh  
Thompson, Scott D.  
Tietz, Frank

Tikhov, M.  
Tkacheva, N.S.  
Toda, Kenji  
Tojo, Takeo  
Tomasí, Corrado

Tomita, Yasumasa  
Tompsett, Geoffrey  
Torijano, Esperanza  
Trnovcova, Viera  
Tsagarakis, Evangelos D.  
Tsetsekou, Athena  
Tsiakaras, Panagiotis  
Tsodikovski, V.I.  
Tsinarakis, G.  
Tsiplakides, Dimitrios  
Tsoga, Anna  
Tsuji, Toshihide  
Tsukamoto, Takeyo  
Tsumura, Tomoki  
Tsunoda, T.  
Tsuruhara, Koji  
Tsutsumi, Hiromori  
Tu, Hengyong  
Tuller, Harry L.  
Tunold, Reidar  
Turaeva, M.S.  
Tykarski, L.

## U

Uchida, Hiroyuki  
Uchijima, T.  
Uebing, C.  
Ueda, A.  
Ueda, T.  
Uematsu, Kazuyoshi  
Ukshe, Alexander

Umarji, A. M  
Ustundag, Ersan  
Uvarov, Nikolai F.

## V

Vakulenko, Alexandra I.  
Valls, O.  
Van Der Haar, L.M.  
Van Der Sluis, Paul  
Van Herle, A.J.  
Van Landschoot, R.C.  
Van Rij, Leen  
Van Tendeloo, G.  
van Zon, Alex  
Vandecruys, F.

E-16  
F-06-P, F-KE-01,  
F-07-P, F-09-P,  
K-06-P  
J-15, G-19  
C-17  
J-09  
F-31-P  
PL-01, A-14-P,  
A-40  
F-26-P, F-KE-02,  
K-05, F-12, F-09  
A-21-P  
G-IN-07  
F-23-P  
D-07-P  
N-05-P

A-KE-06, A-03  
B-12  
C-20, B-16,  
B-17-P  
I-04  
F-10-P  
D-01, A-19  
D-03  
G-07-P, M-04,  
F-24-P, A-IN-08  
F-04  
D-12-P  
J-03-P, E-14  
D-IN-01, D-05-P  
N-05-P

M-11-P, M-12-P  
I-04-P

C-03-P  
B-15-P  
I-14

B-06, B-17  
E-11-P, E-03  
E-22  
A-39  
I-IN-09  
L-06-P  
L-07  
B-25  
M-KE-01  
I-IN-03  
D-02-P  
K-11

B-IN-05  
I-IN-09, I-IN-10  
N-07-P  
A-KE-03  
F-09-P  
A-19  
E-27, N-01-P,  
F-10-P  
F-19-P  
B-02  
M-03-P, M-04-P,  
A-07, M-06-P,  
M-07-P, J-01-P

E-26

G-18  
C-09, J-01  
F-36-P  
C-IN-05  
G-23  
G-23  
D-07-P  
L-09-P  
G-01

Vanderschueren, J.  
Vangrunderbeek, J.  
Vannier, Rose-Noelle  
Vargas, Ruben A.

Varkaraki, Elli  
Varotsos, P.  
Varsamis, C.P.  
Vassilikou-Dova, A.  
Vayenas, Costas G.

Vdovin, G.K.  
Venkateswarlu, M.  
Verkerk, P.  
Verma, Mohan L.  
Vernoux, P.  
Verweij, H.  
Veselova, Lyudmila G.  
Vidanapathirana, Kamal P.  
Vieth, Hans-Martin  
Vikhrenko, Vyacheslav S.  
Vlasov, Yu.  
Vovktoob, E.

## W

Wachsmann, Eric D.  
Wachtler, Mario  
Wada, Hiroaki

Wakamura, Kunio  
Wakihara, M.  
Wakita, Masayuki  
Wang, Chao-Yang  
Wang, Conghua  
Wang, Da-Qian  
Wang, Dazhi  
Wang, Lei  
Wang, Ping  
Wang, S.  
Wang, Shizhong

Wang, T.  
Wang, Wenji  
Wang, Y.  
Wasiucionek, Marek  
Watanabe, Akiteru  
Watanabe, Mamoru  
Watanabe, T.  
Weinkauf, A.  
Wen, C.  
Wen, Ting-Lian

Weppner, Werner

Wesslen, B.  
West, Keld  
Weston, Mike  
Westphal, Dietrich  
Weyten, H.  
Whitehead, Adam  
Wieczorek, Wladyslaw  
Wielgus, Edyta  
Wiemhoefer, Hans-Dieter  
Wiik, K.  
Wilk, P.  
Wilmer, Dirk  
Winter, Martin  
Wintersgill, Mary  
Wissmann, S.  
Wodiunig, Stefan  
Wong, Shan  
Woodman, Rob  
Worrell, Wayne L.  
Wu, Guoliang  
Wu, Q.Y.  
Wuensch, B. J.

N-01  
G-01  
D-08-P, D-07,  
D-07-P  
J-03-P, J-04-P,  
E-14  
I-KE-02  
J-10-P  
K-IN-02  
J-10-P  
I-12, I-01, I-05-P,  
I-14, I-06-P  
C-03-P  
K-09-P, K-05-P  
L-09-P  
K-10, F-23-P  
B-15  
J-01, C-19  
F-03-P

G-03  
J-KE-02, J-IN-03  
N-07-P

K-01-P  
E-23

I-02  
M-05  
F-22-P, F-14,  
F-01-P, J-09  
F-13, N-02

A-34  
A-17  
G-07  
B-KE-03  
B-25  
C-10  
M-IN-01  
E-09  
C-KE-02  
B-10, B-11,  
B-IN-04  
G-IN-04  
A-17-P  
A-28, B-13  
F-16-P, K-11  
D-11-P, F-06  
J-10, F-07  
A-20-P  
L-10  
B-IN-06  
B-25, B-12-P,  
B-11-P  
G-KE-02, C-02-P,  
C-02, G-06

A-25  
G-03  
B-08-P  
C-12-P, D-IN-02  
C-IN-09  
A-41  
L-09, L-05-P  
E-06-P  
C-14, G-08-P,  
K-02-P  
C-17  
A-05-P  
J-14, N-IN-03  
M-05  
A-28, B-13  
C-IN-07  
I-08, I-KE-02  
F-15-P  
B-02  
B-KE-03, I-12  
A-IN-05  
E-24  
J-14

## X

Xiao, Li  
Xie, S.  
Xie, Xiaogang  
Xu, Jiayin

G-10  
C-21  
K-09  
D-03-P

## Y

Yagi, Ryotaro  
Yakshibayev, R.A.  
Yamada, Koichi  
Yamada, Koji  
Yamada, Takashi  
Yamada, Yoshinobu  
Yamaguchi, Kenji  
Yamaguchi, Shu

Yamaji, Katsuhiko  
Yamakawa, T.  
Yamamoto, Hitoshi  
Yamamoto, Osamu

F-15  
F-02-P  
B-IN-06  
D-01-P, F-04  
C-IN-08  
F-12  
J-IN-02  
E-07-P, E-05,  
E-22, C-03  
B-04, B-24, J-02  
B-03  
L-05  
A-31, C-10-P,  
D-03, B-22  
D-03  
E-11-P

Yamamura, Hiroshi  
Yamamura, Yasuhisa  
Yamashita, Hideki  
Yamashita, Kimihiro  
Yamawaki, Michio  
Yamazaki, Nobuyuki  
Yamazaki, Satoshi  
Yamazoe, Noboru

F-26-P  
K-03  
J-IN-02  
A-11, A-09  
J-08-P, J-04  
G-KE-03, G-09,  
G-24  
B-IN-04  
B-25  
A-31  
A-IN-05  
C-KE-02  
B-25  
B-IN-07  
B-03  
D-01  
I-04  
G-04, G-01-P  
A-11, A-09  
B-24, B-04, J-02,  
C-07  
J-IN-02  
C-IN-06, B-01-P  
A-19  
F-07, J-10  
L-07  
A-IN-07, A-19-P,  
A-20-P  
I-IN-10  
B-20  
A-18  
E-07, C-07, C-06

Yan, Jingwang  
Yang, Jianhua  
Yang, Jun  
Yang, Xinhe  
Yang, Y.L.  
Yang, Yong-Ji  
Yao, Takeshi  
Yasuda, Isamu  
Ye, Zuo-Gang  
Yentekakis, Ioannis  
Yianoulis, P.  
Yokoi, Yasuto  
Yokokawa, Harumi

Yokota, Toshihiko  
Yoo, Han-Il  
Yoshida, Kenji  
Yoshikado, Shinzo  
Yoshimoto, Nobuko  
Yoshimura, Masahiro  
Yoshino, S.  
Young, Jason L.  
Yu, Aishui  
Yugami, Hiroo

## Z

Zafeiratos, S.  
Zalewska, A.  
Zanchetta, J.V.  
Zhang, G.G.  
Zhang, S.  
Zhang, W.F.  
Zhang, Yahong  
Zhang, Yurong  
Zhao, Shuang  
Zhecheva, Ekaterina  
Zheng, T.  
Zhu, Bin

I-06  
L-09  
N-01  
C-21  
A-01  
F-17  
B-IN-04  
A-17-P  
G-05-P  
A-01-P, A-02-P  
A-14-P  
B-04-P, E-11,  
E-10-P  
G-05-P  
N-06-P  
C-14  
I-07-P  
L-09, L-05-P  
A-15-P  
N-01-P

Zhu, Dajian  
Zimmer, F.  
Zipprich, Wolfgang  
Zisekas, S.  
Zukowska, G.  
Zygadlo-Monikowska, Ewa  
Zyubina, T.S.